frontiers | Research Topics

Towards sustainable urban development: Use of geographic big data for spatial planning

Edited by
Ying Jing, Jiaxing Cui, Yiyun Chen and Ding Ma

Published in
Frontiers in Environmental Science
Frontiers in Ecology and Evolution
Frontiers in Earth Science

FRONTIERS EBOOK COPYRIGHT STATEMENT

The copyright in the text of individual articles in this ebook is the property of their respective authors or their respective institutions or funders. The copyright in graphics and images within each article may be subject to copyright of other parties. In both cases this is subject to a license granted to Frontiers.

The compilation of articles constituting this ebook is the property of Frontiers.

Each article within this ebook, and the ebook itself, are published under the most recent version of the Creative Commons CC-BY licence. The version current at the date of publication of this ebook is CC-BY 4.0. If the CC-BY licence is updated, the licence granted by Frontiers is automatically updated to the new version.

When exercising any right under the CC-BY licence, Frontiers must be attributed as the original publisher of the article or ebook, as applicable.

Authors have the responsibility of ensuring that any graphics or other materials which are the property of others may be included in the CC-BY licence, but this should be checked before relying on the CC-BY licence to reproduce those materials. Any copyright notices relating to those materials must be complied with.

Copyright and source acknowledgement notices may not be removed and must be displayed in any copy, derivative work or partial copy which includes the elements in question.

All copyright, and all rights therein, are protected by national and international copyright laws. The above represents a summary only. For further information please read Frontiers' Conditions for Website Use and Copyright Statement, and the applicable CC-BY licence.

ISSN 1664-8714
ISBN 978-2-8325-2467-1
DOI 10.3389/978-2-8325-2467-1

About Frontiers

Frontiers is more than just an open access publisher of scholarly articles: it is a pioneering approach to the world of academia, radically improving the way scholarly research is managed. The grand vision of Frontiers is a world where all people have an equal opportunity to seek, share and generate knowledge. Frontiers provides immediate and permanent online open access to all its publications, but this alone is not enough to realize our grand goals.

Frontiers journal series

The Frontiers journal series is a multi-tier and interdisciplinary set of open-access, online journals, promising a paradigm shift from the current review, selection and dissemination processes in academic publishing. All Frontiers journals are driven by researchers for researchers; therefore, they constitute a service to the scholarly community. At the same time, the *Frontiers journal series* operates on a revolutionary invention, the tiered publishing system, initially addressing specific communities of scholars, and gradually climbing up to broader public understanding, thus serving the interests of the lay society, too.

Dedication to quality

Each Frontiers article is a landmark of the highest quality, thanks to genuinely collaborative interactions between authors and review editors, who include some of the world's best academicians. Research must be certified by peers before entering a stream of knowledge that may eventually reach the public - and shape society; therefore, Frontiers only applies the most rigorous and unbiased reviews. Frontiers revolutionizes research publishing by freely delivering the most outstanding research, evaluated with no bias from both the academic and social point of view. By applying the most advanced information technologies, Frontiers is catapulting scholarly publishing into a new generation.

What are Frontiers Research Topics?

Frontiers Research Topics are very popular trademarks of the *Frontiers journals series*: they are collections of at least ten articles, all centered on a particular subject. With their unique mix of varied contributions from Original Research to Review Articles, Frontiers Research Topics unify the most influential researchers, the latest key findings and historical advances in a hot research area.

Find out more on how to host your own Frontiers Research Topic or contribute to one as an author by contacting the Frontiers editorial office: frontiersin.org/about/contact

Towards sustainable urban development: Use of geographic big data for spatial planning

Topic editors

Ying Jing — Zhejiang University, China
Jiaxing Cui — Central China Normal University, China
Yiyun Chen — Wuhan University, China
Ding Ma — Shenzhen University, China

Citation

Jing, Y., Cui, J., Chen, Y., Ma, D., eds. (2023). *Towards sustainable urban development: Use of geographic big data for spatial planning*.
Lausanne: Frontiers Media SA. doi: 10.3389/978-2-8325-2467-1

Table of contents

06 Editorial: Towards sustainable urban development: Use of geographic big data for spatial planning
Ying Jing, Jiaxing Cui, Ding Ma and Yiyun Chen

08 Interaction Between Construction Land Expansion and Cropland Expansion and Its Socioeconomic Determinants: Evidence From Urban Agglomeration in the Middle Reaches of the Yangtze River, China
Liye Wang, Siyu Zhang, Yanfang Liu and Yaolin Liu

22 The Spatiotemporal Characteristics and Rationality of Emerging Megacity Urban Expansion: A Case Study of Zhengzhou in Central China
Enxiang Cai, Qingsheng Bi, Jie Lu and Heping Hou

34 Identification and Analysis of Industrial Land in China Based on the Point of Interest Data and Random Forest Model
Qingsong He and Xinyu Tang

46 A Deep Learning–Based Approach for Moving Vehicle Counting and Short-Term Traffic Prediction From Video Images
Ye Zheng, Xiaoming Li, LiuChang Xu and Nu Wen

56 Road Safety Evaluation Framework for Accessing Park Green Space Using Active Travel
Yuanyuan Luo, Yanfang Liu, Lijun Xing, Nannan Wang and Lei Rao

75 Optimizing Leisure Agriculture by Analyzing Spatial Patterns and Tourists' Perceptions: Evidence From Wuhan, China
Chengcheng Wang, Shaohua Wu, Wei Yang, Haijun Bao, Jinxia Zhu and Xia Wang

88 What Is the Impact of the Establishment of Natural Reserves on Rural Residential Land? An Empirical Study From Hunan Province, China
Yuanlai Wu, Houtian Tang, Ping Jiang and Jinxiu Chen

103 Deep Semantic Segmentation for Rapid Extraction and Spatial-Temporal Expansion Variation Analysis of China's Urban Built-Up Areas
Maoyang Bai, Shiqi Zhang, Xiao Wang, Yu Feng, Juan Wang and Peihao Peng

121 Research on the spatiotemporal distribution and evolution of remote sensing: A data-driven analysis
Yu Liu, Xi Kuai, Fei Su, Shaochen Wang, Kaifeng Wang and Lijun Xing

138 The spatial pattern and influence mechanism of urban vitality: A case study of Changsha, China
Xiaojiang Xia, Yang Zhang, Yue Zhang and Tiechuan Rao

153 Multisource data integration for targeted bus exterior advertising
Meng Huang, Xinchi Li, Wei Tu and Mingchuan Yang

167 Differential characteristics and driving forces of the spatial distribution of heritage trees in Luoyang, an ancient capital of China
Heping Hou, Longchong Zhang, Huitao Bi, Jing He, Enxiang Cai and Wanqian Ren

182 The topological structure of urban roads and its relation with human activities at the street-based community level
Yan Zhang, Yebin Chen, Wei Zhu, Wenwen Wang and Qian Zhang

191 Evaluating civil aviation airport competitiveness in the Yangtze River Economic Belt of China: A lens of spatial-temporal evolution
Yang Zhang, Xue Jin, Meng Li, Rongtian Liu and Ying Jing

205 Research on spatial structure and resilience of complex urban network: A case study of Jing-Jin-Ji Urban Agglomeration
Yang Zhang, Yang Yang, Shaokun Wei, Zijun Ma, Miao Tian, Meng Sun and Jiabin Nie

224 Environmental drivers of the vital urban coastal zones: An explorative case study based on the data-driven multi-method approach
Yuting Yin, Yuhan Shao, Huilin Lu and Yun Han

241 Evaluating the barrier of typical production factor flow in the Chengdu-Chongqing Urban Agglomeration based on multi-source big data
Yang Zhang, Xingping Wang, Mengrong Ji, Yulu Chen and Feng Yan

253 Flood impact on urban roads and commuting: A case study of Wuhan, China
Yaolin Liu, Hongxin Zhang, Huiting Chen and Cuizhen Chen

271 UAV trajectory planning based on an improved sparrow optimization algorithm with multi-strategy integration
Yu Yang, Qing He and Liu Yang

294 Impact of socio-economic and environmental factors on livestock production in Kyrgyzstan
Jiamiao Yang, Yanwen Wang, Hao Zhang, Yuming Su, Xiaoyang Wu, Shuqi Yan and Shuwang Yang

310 Exploration of the regional correlation and network structure characteristics of land prices: A case study of Hebei, China
Can Li, Wei Wei, Yajing Duan, Zhongjiang Feng, Xiaomiao Feng, Chenming Zhu and Pengfei An

334 Influence of spatial scale on the study of access fairness of urban park green space
Shuna Xu and Yinzhen Wang

345 Mapping of nighttime light trends and refugee population changes in Ukraine during the Russian–Ukrainian War
Chaoqing Huang, Song Hong, Xiaoxiao Niu, Qian Wu, Yanmei Zhong, Huan Yang and Haoran Zhang

358 Unraveling the supply-service relationship between high-speed railway and conventional railway: A temporal perspective
Guangxia Zhang, Yanfang Liu, Ying Jing, Huiting Chen, Yiheng Wang and Zhengyu Wang

frontiers | Frontiers in Environmental Science

TYPE Editorial
PUBLISHED 04 May 2023
DOI 10.3389/fenvs.2023.1202661

Check for updates

OPEN ACCESS

EDITED AND REVIEWED BY
Alexander Kokhanovsky,
German Research Centre for Geosciences, Germany

*CORRESPONDENCE
Jiaxing Cui,
cuijiaxing@ccnu.edu.cn

RECEIVED 09 April 2023
ACCEPTED 17 April 2023
PUBLISHED 04 May 2023

CITATION
Jing Y, Cui J, Ma D and Chen Y (2023), Editorial: Towards sustainable urban development: Use of geographic big data for spatial planning.
Front. Environ. Sci. 11:1202661.
doi: 10.3389/fenvs.2023.1202661

COPYRIGHT
© 2023 Jing, Cui, Ma and Chen. This is an open-access article distributed under the terms of the Creative Commons Attribution License (CC BY). The use, distribution or reproduction in other forums is permitted, provided the original author(s) and the copyright owner(s) are credited and that the original publication in this journal is cited, in accordance with accepted academic practice. No use, distribution or reproduction is permitted which does not comply with these terms.

Editorial: Towards sustainable urban development: Use of geographic big data for spatial planning

Ying Jing[1], Jiaxing Cui[2]*, Ding Ma[3] and Yiyun Chen[4]

[1]School of Business, NingboTech University, Ningbo, China, [2]College of Urban and Environmental Sciences, Central China Normal University, Wuhan, China, [3]School of Architecture and Urban Planning, Shenzhen University, Shenzhen, China, [4]School of Resource and Environmental Sciences, Wuhan University, Wuhan, China

KEYWORDS

spatial analysis, geographic big data, spatial planning and design, sustainable development, geographical information science (GIScience)

Editorial on the Research Topic
Towards Sustainable Urban Development: Use of Geographic Big Data for Spatial Planning

Since the introduction of geo-big data, we have been able to observe how its role in social development and human–environment interactions has grown through the years. Multiple examples of geo-big data applications can be found in leisure space optimization, traffic prediction, agricultural planning, air quality monitoring, livelihood improvement, social justice, forest management, interregional development, green space accessibility, and environmental diagnosis. This extensive use of geo-big data facilitates sharing of spatial information and spatial data mining, and it can be applied to geographic assessment, prediction, analysis, and planning. The geo-big data era provides a new opportunity for the transformation of spatial planning and sustainable decision-making by revealing spatial regularity based on geo-big data [see (Jing and Liu, 2018; Jing et al., 2021)].

The goal of this Research Topic is to introduce academic output that adopts geospatial big data to facilitate intelligent urban governance. In the rapid process of urbanization, geo-big data serves as a crucial factor of technological innovation that covers all the aspects of urban systems (i.e., fundamental infrastructures, traffic networks, architectures, energy systems, *etc.*). Based on smart spatial analytical platforms and geospatial artificial intelligence technologies, geospatial big data can be used to empower urban governance in an intelligent and smart way, serving as an engine to monitor, assess, diagnose, and ultimately tackle urban problems, and optimize urban systems towards sustainable development.

This Research Topic has collected 24 publications on sustainable development and smart spatial planning decision-making involving multi-source geo-big data. Wang et al. proposed strategies for leisure agriculture optimization by exploring its spatiality and competitiveness utilizing user-generated content (including leisure agriculture sites) with a case study of Wuhan, China. Cai et al. analyzed the spatial and temporal features of urban expansion during the latest decade based on remote sensing images and socioeconomic statical data and revealed the imbalance and spatial disorder of urban expansion in Zhengzhou, China. Luo et al. proposed a

safety evaluation framework for assessing active travel traffic safety near a park green space (PGS) through POI data and similar and found that the walking mode is safer than the cycling mode in terms of road facilities near a PGS. Wang et al. used spatial analytical techniques to study the tempo–spatial interaction between cropland expansion and urbanization and revealed the socioeconomic determinants via land use data and statical data in the middle section of the Yangtze River. Bai et al. constructed an urban model for extracting urban built-up areas based on nighttime light data, analyzed the spatiotemporal factors of China's urban built-up area expansion, and revealed the agglomeration-to-dispersion trend of urban built-up area expansion. Zheng et al. proposed a packaged method for traffic flow prediction in consideration of weather conditions based on real traffic video data and suggested that the algorithm outperformed the previous solutions (with 10% higher accuracy). He and Tang put forward a new notion and method of large-scale industrial land identification by using POI data and a random forest model and researched the spatial pattern of industrial land in China. Wu et al. explored the distributive characteristics of rural residential land concerning natural reserves and non-natural reserves based on land use data and statistical yearbooks in Hubei. Liu et al. carried out a scientometric analysis of research output on the tempo-spatial distribution and dynamic evolution of remote sensing based on the Web of Sciences database and revealed the global spatial pattern of those academic publications in a significant dispersion. Xia et al. adopted mobile phone data to assess urban spatial vitality and found an evident center–periphery pattern in Changsha, China. Yin et al. explored environmental drivers of vitalizing urban coastal zones based on multi-source geo-big data. Huang et al. used multi-source data (i.e., mobile phone signaling data, GPS data, land use data, and smart card data) for targeted bus exterior advertising. Zhang et al. adopted street network data and Flickr photo location data to measure the heterogeneity of street networks for a better understanding of urban activities and urban space. Hou et al. revealed the spatial patterns and driving mechanisms of heritage trees in an ancient city in China through geospatial analysis methods and a geographically weighted regression model. Zhang et al. measured the competitiveness of civil aviation airports and revealed their spatiotemporal dynamics in the Yangtze River Economic Belt through a series of spatial analytical methods (e.g., spatial auto-correlation, *etc.*) combining POI data and fundamental geographical data and similar. Zhang et al. analyzed the economy-information-coupling connection complex network structure based on Baidu search index data of the Beijing Tianjin Hebei Urban Agglomeration. Xu and Wang researched urban PGS accessibility on different scales (subdistrict, community, and residential quarter) by the Gaussian-based two-step floating catchment area method combining park green data, road networks, residential quarter data, *etc.* Zhang et al. evaluated the barriers of labor flow, technology flow, and capital flow with multi-source big data (e.g., Baidu Migration data) and analyzed how factors influence the barrier of the three typical production flows in the Chengdu–Chongqing urban agglomeration, China. Yang et al. spatialized the impact of environmental and socioeconomic factors on the changes in inventory, self-consumption, and livestock sales in Kyrgyzstan through mainly spatial regression analysis. Huang et al. employed nighttime light images to measure the changes in the refugee population before and after the war in Ukraine. Yang et al. proposed a multi-strategy sparrow search algorithm to deal with the UAV trajectory planning issue for maximizing the UAV efficiency and minimizing the flight distance in a three-dimensional environment. Li et al. took residential land price data and characterized the spatiotemporal network structure and the regional correlation in Hebei Province, China. Liu et al. combined location-based service big data to simulate commuting under floods according to the minimum time–cost principle and found that inconsistent spatial distribution exists among commuting loss, flood exposure hot spots, and road vulnerability. Zhang et al. unraveled the cooperation and competition between the conventional railway and high-speed railway based on railway timetable data and railway location data in China.

We are convinced that this academic output can benefit both the academic community and political decision-makers, targeting smart and sustainable spatial planning development by means of multi-source geographical data and analytical techniques. Moreover, current studies may also inspire information engineers to advance the development of pertinent information system platforms and toolboxes.

The Guest Editors are thankful for the Editorial Team's assistance. We are grateful to the invited reviewers for their professional comments which have helped to improve the articles. Last but not least, we also appreciate the authors; they have believed in and selected this Research Topic to contribute their wisdom for advancing academic progress in this domain.

Author contributions

All the guest editors conceptualize this editorial together. Specifically, YJ and JC are responsible for writing this editorial. DM and YC are responsible for editing the whole editorial.

Conflict of interest

The authors declare that the research was conducted in the absence of any commercial or financial relationships that could be construed as a potential conflict of interest.

Publisher's note

All claims expressed in this article are solely those of the authors and do not necessarily represent those of their affiliated organizations, or those of the publisher, the editors and the reviewers. Any product that may be evaluated in this article, or claim that may be made by its manufacturer, is not guaranteed or endorsed by the publisher.

References

Jing, Y., and Liu, Y. L. (2018). *Quantifying the spatiality of urban leisure venues in Wuhan, Central China-GIS-based spatial pattern metrics*. Sustainable Cities and Society.

Jing, Y., Shu, J. J., Wang, R., and Zhang, X. (2021). Tempo-spatial variability of urban leisure functional zones: An analysis based on geo-big data. *Growth Change A J. Urban Regional Policy* 52, 1852–1865. doi:10.1111/grow.12526

frontiers | Frontiers in Environmental Science

ORIGINAL RESEARCH
published: 12 April 2022
doi: 10.3389/fenvs.2022.882582

Interaction Between Construction Land Expansion and Cropland Expansion and Its Socioeconomic Determinants: Evidence From Urban Agglomeration in the Middle Reaches of the Yangtze River, China

Liye Wang[1], *Siyu Zhang*[2], *Yanfang Liu*[1] *and Yaolin Liu*[1,3]*

[1]School of Resource and Environmental Sciences, Wuhan University, Wuhan, China, [2]College of Public Administration, Huazhong Agricultural University, Wuhan, China, [3]Collaborative Innovation Center of Geospatial Information Technology, Wuhan University, Wuhan, China

OPEN ACCESS

Edited by:
Jiaxing Cui,
Central China Normal University, China

Reviewed by:
Bohan Yang,
Central China Normal University, China
Bangbang Zhang,
Northwest A&F University, China

***Correspondence:**
Yaolin Liu
yaolin610@163.com

Specialty section:
This article was submitted to Land Use Dynamics, a section of the journal Frontiers in Environmental Science

Received: 24 February 2022
Accepted: 14 March 2022
Published: 12 April 2022

Citation:
Wang L, Zhang S, Liu Y and Liu Y (2022) Interaction Between Construction Land Expansion and Cropland Expansion and Its Socioeconomic Determinants: Evidence From Urban Agglomeration in the Middle Reaches of the Yangtze River, China. Front. Environ. Sci. 10:882582. doi: 10.3389/fenvs.2022.882582

Nowadays, both urbanization and cropland expansion are hot issues. However, research related to the spatiotemporal interaction between urbanization and cropland expansion and their socioeconomic determinants remains scarce. Accordingly, this research takes the urban agglomeration in the middle reaches of the Yangtze River (MRUA) as the research area by combining spatial analysis, sensitivity analysis, and the spatial gravity model. To achieve this goal, we identified the area of the construction land expansion and cropland expansion, the sensitivity of cropland expansion to construction land expansion, and the shifting trajectory of gravity centers of construction land expansion and cropland expansion and their interaction during 2000–2020, respectively. Additionally, the geographically weighted regression model was utilized to explore the spatiotemporal heterogeneity of four socioeconomic determinants of the interaction between construction land expansion and cropland expansion. The results are as follows: 1) the area of the expanded construction land and the expanded cropland and the sensitivity of cropland expansion to construction land expansion show an overall increasing pattern; 2) the gravity center of the expanded construction land shifted toward the northeast, whereas that of the expanded cropland moved to the southeast but with similar moving distances (17.83 and 15.37 km, respectively); 3) the GDP has an increasing positive effect on the interaction of the construction land expansion and cropland expansion, whereas the investment in fixed assets shows an increasing negative effect during 2000–2020. The GDP in the agricultural sector and population displays a stable influence. This article offers a solution for decision makers to promote the interaction between construction land and cropland.

Keywords: gravity center, cropland protection, GWR, sensitivity analysis, urban agglomeration

INTRODUCTION

Globally, frequent human interactions with the natural environment have significantly changed Earth's surface (Song et al., 2018; Tesfaw et al., 2018). Only in the second half of the 20th century, human's efforts to develop the social economy have resulted in 24% of Earth's surface conversion into cropland and lost more than 55% of mangroves and coral reefs (Millennium Ecosystem Assessment, 2005). Therefore, land use/land cover change (LUCC) has been a hot issue in recent decades (Ariti et al., 2018; Folberth et al., 2020). Under human demands to attain economic progress, urbanization has unavoidably become one of the most active LUCCs, which then promoted the expansion of the impervious surface and loss of ecological land (Deng et al., 2009; Salerno et al., 2018; Qiu et al., 2019).

The urbanization level worldwide is estimated to reach over 80%, and in developing countries, the quantity of urban areas in 2050 will be far larger than that in 2000 with an increasing

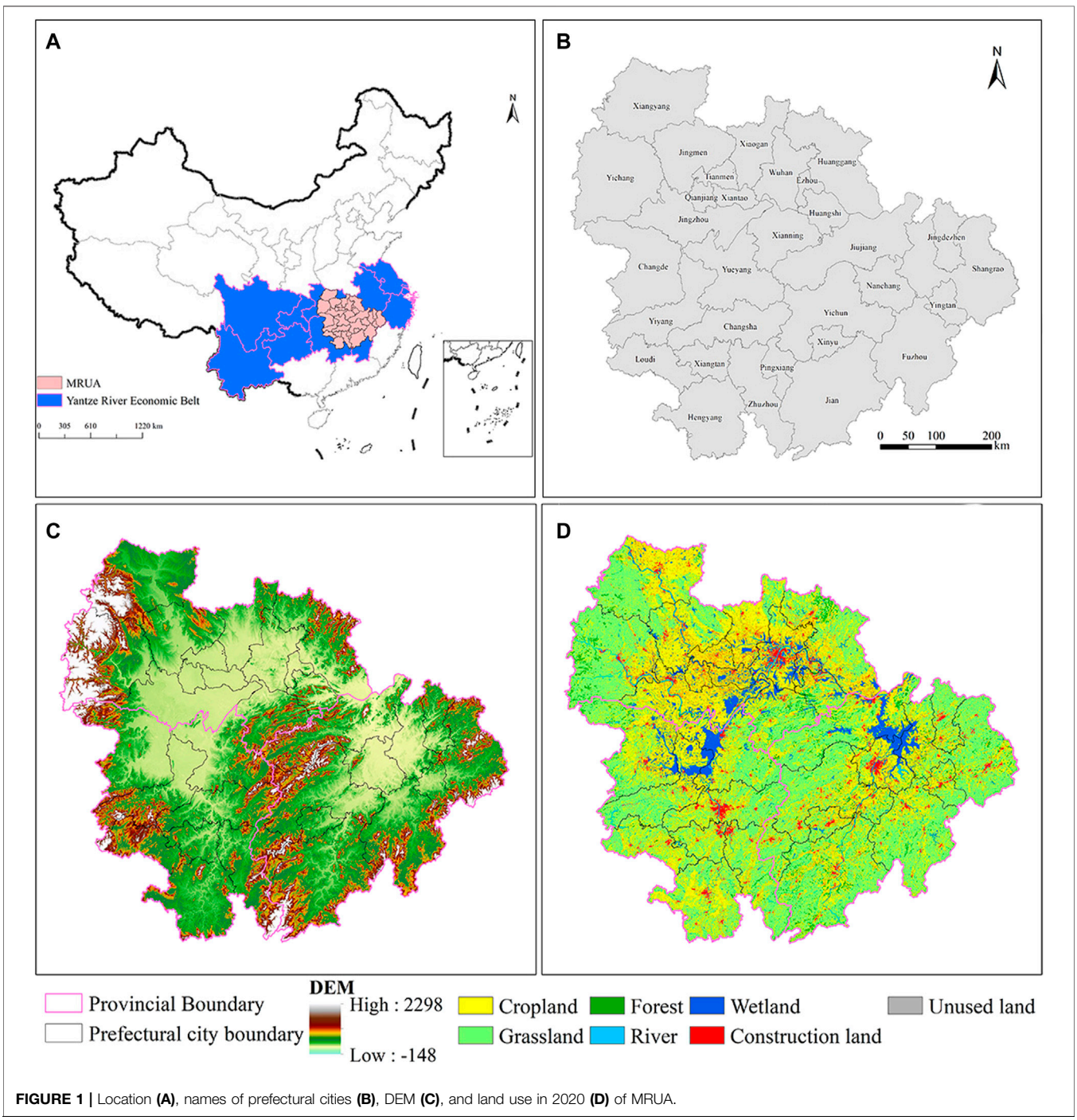

FIGURE 1 | Location **(A)**, names of prefectural cities **(B)**, DEM **(C)**, and land use in 2020 **(D)** of MRUA.

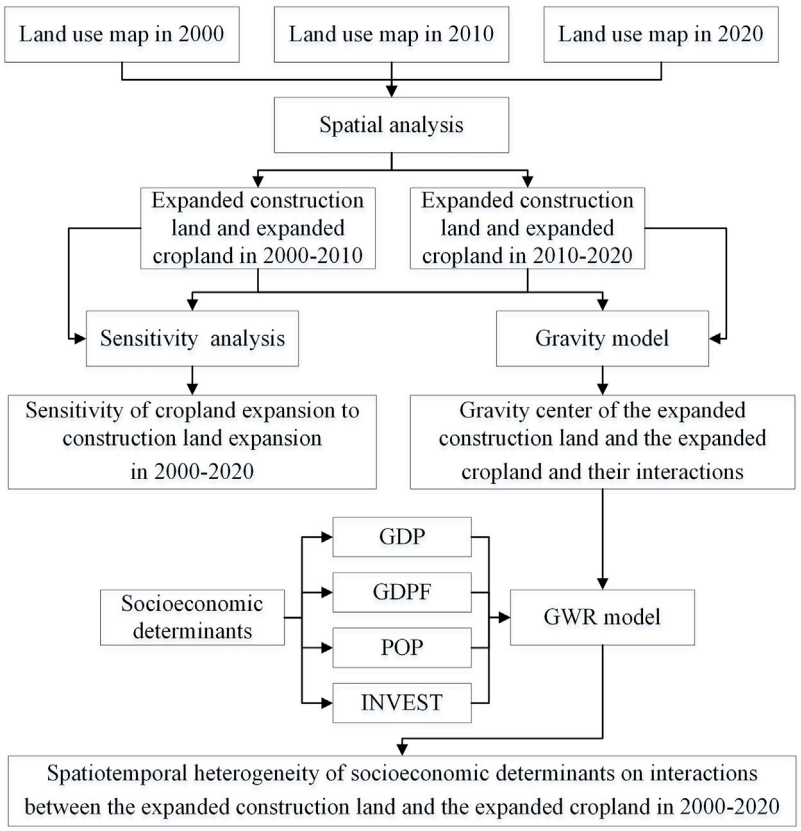

FIGURE 2 | Research framework.

expansion rate (Angel et al., 2011; United Nations, 2018). The increased urban area inevitably takes up a large number of cropland and occupies the space of ecological land (van Vliet et al., 2017; Wang et al., 2020; Wu et al., 2020). The high-quality lives brought by urbanization to the people also lead to the booming population (Shu et al., 2018; Boudet et al., 2019). Facing the pressure from two sides, that is, the reduction of cropland and population growth, the world is under severe food security problems (Foley et al., 2011; Asche et al., 2015).

Cropland, as a scarce resource, holds the key to maintaining food security for a country and the world (Egli et al., 2018; Yang et al., 2020a). To avoid cropland loss and ensure food security, many countries worldwide have promulgated several cropland protection policies in line with their national conditions (Monk et al., 2013). For example, in 1938, the United Kingdom promulgated the "Green Belt Policy" to restrict the growth of urban area and prevent cropland loss (Cullingworth et al., 2014); in 1996, China implemented a series of policies to ensure no net loss of cropland and increase the quality of cropland, such as the "Cropland Balance Policy" and the "Basic Cropland Policy" (Ke et al., 2018; Su et al., 2020; Wang et al., 2021). These policies are not only aimed at preventing cropland loss but can also promote cropland expansion (Ke et al., 2019; Tang et al., 2021). Song and Pijanowski (2014) pointed out that in 1999–2008, due to the "Cropland Balance Policy", 27,677 km^2 of cropland was reclaimed through land consolidation, exploitation, and rehabilitation in China. Additionally, the spontaneous agricultural activities of farmers can increase the area of cropland (He et al., 2021; Zhang et al., 2022). In the future, cropland expansion will play an increasingly important role in maintaining food security.

Both urbanization and cropland expansion are hot research topics at the regional and global scale. Researchers initially focused on the causes and effects of urbanization (Haase et al., 2012; He et al., 2014). At the regional scale, Souza et al. (2016) discussed the effects of urbanization on the microclimate of Manaus. Su et al. (2012) evaluated the urbanization impacts on ecosystem services at the eco-regional scale. Moreover, Liu et al. (2021) examined the characteristics of the urban expansion structure in a city scale. At a global scale, Lambin and Meyfroidt (2011) evaluated the relationships among urbanization, economic globalization, and land scarcity. Seto et al. (2012) projected the global urban area in 2030 and discussed its direct impact on carbon biomass. Li et al. (2022) analyzed the characteristics of global urbanization trend and its related population dynamics. As time goes on, the area of cropland expansion is continuously increasing (Zabel et al., 2019; Eigenbrod et al., 2020; Cheng et al., 2021), consequently gaining considerable attention on its effects. The effects of cropland expansion on ecosystem services (Ke et al., 2019; Tang et al., 2021) and cropland productivity (Song and

Pijanowski, 2014; Song and Liu, 2017), the causes of cropland expansion (Zelaya et al., 2016; He et al., 2021), and the relationships among cropland expansion, cropland intensification, and food security (Mauser et al., 2015; Zabel et al., 2019; Folberth et al., 2020) are all hot issues of the researchers. The interactions between urbanization and cropland change are also explored (Liu L. et al., 2014; van Vliet et al., 2017). For example, Tu et al. (2021) discussed the interactions of urbanization and cropland loss under different rates and patterns of urban expansion. Zhou et al. (2021) applied macro–micro comparative analysis to detect the urbanization-associated cropland loss at different scales. However, all of the aforementioned urban and cropland interaction research works are all based on the analysis of urbanization resulting cropland loss. Research scarcely focused on the interaction between urban expansion and cropland expansion.

Thus, this study attempts to explore the interaction between urban expansion and cropland expansion and its socioeconomic determinants. To this end, taking the urban agglomeration in the middle reaches of the Yangtze River (MRUA), China as the research area, we first identified the expanded construction land and the expanded cropland through spatial analysis during the periods of 2000–2010 and 2010–2020. Then, sensitivity analysis was utilized to detect the sensitivity of cropland expansion to construction land expansion. We also identified the gravity centers of the expanded construction land and expanded cropland, their shifting trajectories, and interaction. Last, the geographically weighted regression (GWR) model was applied to detect the socioeconomic determinants of the interaction between construction land expansion and cropland expansion.

STUDY AREA AND DATA SOURCES

MRUA is located within 110°15′ – 118°30′E and 25°58′ – 32°39′N, covering an area of 3,26,100 km^2, and lying in the middle of the Yangtze River Economic Belt (YREB) (**Figure 1**). YREB is the most complete urban system with the largest population and the largest industrial scale in the world (Pan et al., 2020). As one of the most important urban agglomerations in YREB, MRUA has a population of 125 million and a regional GDP of 7.90 trillion Yuan, creating 9.6% of the total economic output in China using 3.4% of the land area and 9.0% of the population according to the statistical yearbook in 2018. Moreover, MRUA has a large amount of cropland because of the large plains located in the middle and northeast (**Figures 1C,D**) and the abundant precipitation, making it an important rice production base in China. The agricultural activities are active. Therefore, given the pressure from both urbanization and agriculture, MRUA is a perfect area to study the interaction between construction land expansion and cropland expansion.

This research uses two types of data: spatial data and statistical data. The spatial data include the land use maps in 2000, 2010, and 2020 from the Data Center of Resources and Environment, Chinese Academy of Science (http://www.resdc.cn), and were reclassified into seven land use types based on the original land use reclassification system (Liu et al., 2010; Liu et al., 2014a). The statistical data come from the Statistical Yearbook of Hubei, Hunan, and Jiangxi Provinces in 2000–2020.

METHODS AND MATERIALS

Research Framework

In order to detect the interaction between construction land expansion and cropland expansion and explore its socioeconomic determinants, four steps were conducted (**Figure 2**). First, the area of the expanded construction land and cropland in the periods of 2000–2010 and 2010–2020 was evaluated using spatial analysis. Then, by integrating sensitivity analysis, we calculated the sensitivity of cropland expansion to construction land expansion to reflect the relationships between them. Third, the gravity model was chosen to estimate the spatial balance of construction land expansion and cropland expansion, changes of the gravity centers, and the interaction between construction land expansion and cropland expansion in 2000–2020. Finally, four socioeconomic determinants and the GWR model were applied to explore the spatial local effects of the variables on the interaction between construction land expansion and cropland expansion. The spatiotemporal heterogeneity of socioeconomic determinants can be identified by using these steps.

Identification of the Expanded Construction Land and the Expanded Cropland

This research defines the expanded construction land or the expanded cropland as follows: that a parcel is no construction land or no cropland at the beginning of the research period and it is transformed to construction land or cropland at the end of the research period. Therefore, the amount of the expanded construction land and the expanded cropland is calculated as follows:

$$Con_i = \sum_{n1=1}^{m} L_{n1i}, \quad (1)$$

$$Crop_i = \sum_{n2=1}^{m} L_{n2i}, \quad (2)$$

where Con_i and $Crop_i$ denote the amount of the expanded construction land and the expanded cropland in city i, respectively, m represents the number of land use types excluding construction land or cropland, which is six in these two equations, $n1$ and $n2$ represent the land use types, and L_{n1i} is the area of $n1$ land use type in city i. In detail, $n1$ indicates cropland, grassland, forest, river, wetland, and unused land and $n2$ denotes grassland, forest, river, wetland, unused land, and construction land.

Sensitivity Analysis

To evaluate the impact of the expanded construction land on the expanded cropland, the sensitivity analysis model was chosen to assess the sensitivity of cropland expansion to construction land expansion. The sensitivity analysis can reflect the effects of one

TABLE 1 | List of explanatory variables.

Variable	Description	Unit
GDP	Average gross domestic product in the research period	100 million Yuan
GDPF	Average gross domestic product in the agricultural sector in the research period	100 million Yuan
POP	Average population in the research period	10 thousand people
INVEST	Average investment in fixed assets in the research period	10 thousand Yuan

TABLE 2 | Area of the expanded construction land and the expanded cropland in 2000–2020 (km^2).

	2000–2010	2010–2020
Construction land	3,410.92	5103.82
Cropland	1,785.92	7809.46

changing element on another or a group of elements through quantitative analysis (Han et al., 2016; Chai et al., 2019). The sensitivity of cropland expansion to construction land expansion is calculated as follows:

$$\theta_i = \frac{\left(Crop_{t_{2i}} - Crop_{t_{1i}}\right)/Crop_{t_{1i}}}{\left(Con_{t_{2i}} - Con_{t_{1i}}\right)/Con_{t_{1i}}}, \tag{3}$$

where θ_i is the sensitivity of cropland expansion to construction land expansion in city i, $Crop_{t_{1i}}$ and $Crop_{t_{2i}}$ refer to the area of the expanded cropland at the beginning and end of the research period, respectively, and $Con_{t_{1i}}$ and $Con_{t_{2i}}$ denote the area of the expanded construction land at the beginning and end of the research period, respectively.

The sensitivity analysis denotes the reflection of cropland change to construction land expansion, where a positive score indicates that cropland expansion is affected by construction land expansion; whereas a negative score represents that cropland expansion has an inverse relationship with construction land expansion. Notably, this study focuses on the sensitivity of the expanded cropland area to the area of expanded construction land. Thus, the score of sensitivity is positive. A higher value of sensitivity indicates a higher sensitivity of cropland expansion to construction land expansion.

Spatial Gravity Model

In the development process of an element, its quantity, quality, and location continue to change in space, leading to the change in spatial force magnitude (Li et al., 2018; Chai et al., 2019). The concept of gravity center is from physics, which refers to a space point whose forces are relatively balanced in all directions (Zhang et al., 2012; Wang et al., 2018). Therefore, the spatial gravity model can be utilized to analyze the spatial balance of some elements by analyzing the direction and distance changes, such as energy (Zhang et al., 2012), grain production (Chai et al., 2019), and ecological capacity (Cheng et al., 2019). The gravity model can also calculate the interaction or flow between at least two locations (Zeng et al., 2019; Yang et al., 2020b). In this article, the gravity model is first used to calculate the coordinate of the center of the expanded construction land and the expanded cropland. Then, it estimates the interaction between the expanded construction land and the expanded cropland. The coordinates of the gravity center can be calculated according to **Eqs 4**, **5**:

$$\bar{X} = \frac{\sum_{i=1}^{n}(X_i \times V_i)}{\sum_{i=1}^{n} V_i}, \tag{4}$$

$$\bar{Y} = \frac{\sum_{i=1}^{n}(Y_i \times V_i)}{\sum_{i=1}^{n} V_i}, \tag{5}$$

where $(\bar{X}, \bar{Y})$ is the coordinate of the element's gravity center, (X_i, Y_i) represents the coordinate of the element and V_i denotes the attribute value in location (X_i, Y_i). This research calculates two types of gravity center, one is the gravity center in the subresearch area and the other is the gravity center in the entire research area. In the former calculation process, (X_i, Y_i) denotes the coordinate of the location of the focused attribute in city i. For the latter, (X_i, Y_i) is the coordinate of the gravity center of the focused attribute in city i.

The changing direction and distance of the gravity center is evaluated according to the following equations, respectively:

$$\alpha = \left(\frac{k \times \pi}{2} + \left(\arctan\left(\frac{\bar{Y}_{t_2} - \bar{Y}_{t_1}}{\bar{X}_{t_2} - \bar{X}_{t_1}}\right)\right)\right) \times \frac{180°}{\pi}, \tag{6}$$

$$D = \sqrt{\left(\bar{X}_{t_2} - \bar{X}_{t_1}\right)^2 + \left(\bar{Y}_{t_2} - \bar{Y}_{t_1}\right)^2}, \tag{7}$$

where α and D represent the changing direction and distance of the gravity center, respectively, $(\bar{X}_{t_1}, \bar{Y}_{t_1})$ and $(\bar{X}_{t_2}, \bar{Y}_{t_2})$ refer to the gravity center's coordinate at the beginning and end of the research period t, respectively, and k is the coefficient that makes sure α belongs to $[-180°, 180°]$, which equals 0, 1, and 2. We defined east as 0°, and the anticlockwise direction was defined as the positive direction. Owing to the changing distance calculation, all the coordinates in this article are defined as projected coordinates.

The interaction calculated by the gravity model exhibits a positive relationship with the focused elements' attributes and a negative relationship with their spatial distances. The equation is as follows:

$$I_i = \frac{V_{1i} \times V_{2i}}{D_{12i}^2}, \tag{8}$$

where I_i denotes the interaction between the two elements in city i, V_{1i} and V_{2i} represent the attribute values of two elements, and D_{12i} is the spatial distance between the two elements.

Geographically Weighted Regression Model

The GWR model was conducted to investigate the socioeconomic determinants of the interaction between construction land expansion and cropland expansion in MRUA. Regression models are widely used in the driving mechanism analysis (Zhong et al., 2011; Ariti et al., 2015; Mohmmed et al., 2019).

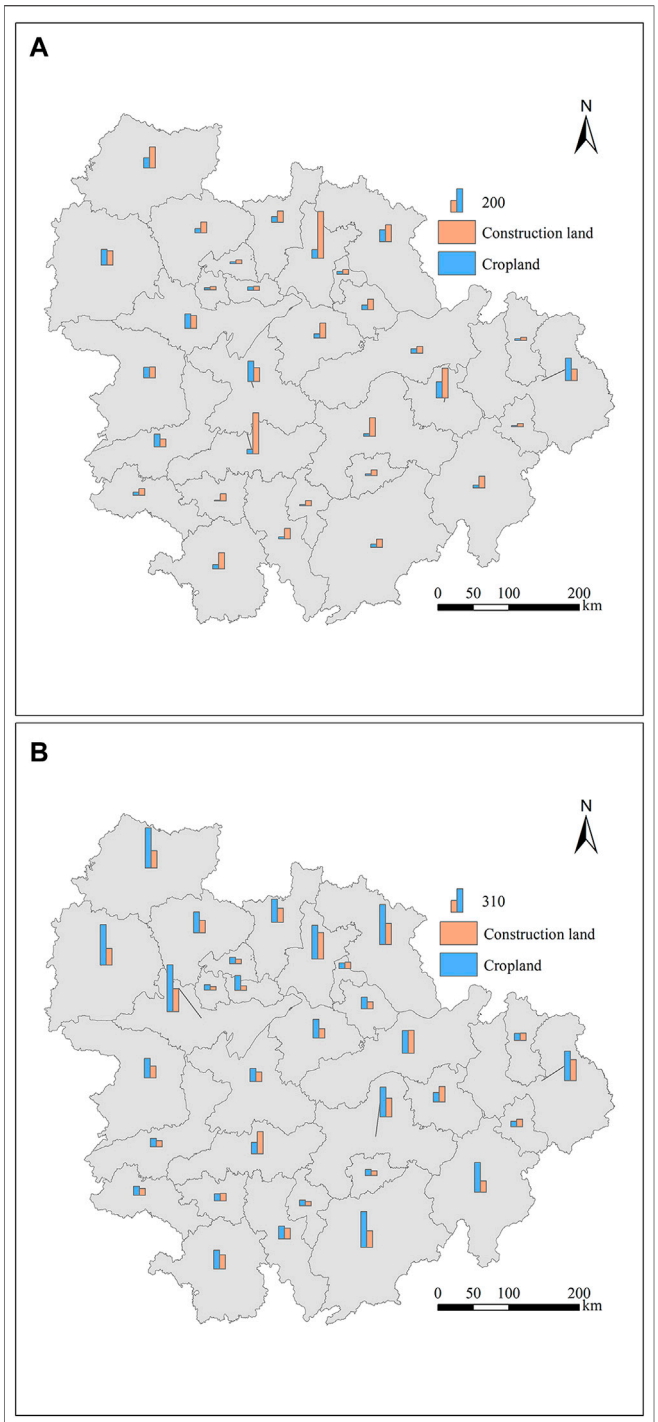

FIGURE 3 | Area of the expanded construction land and the expanded cropland in the subresearch area in the periods of **(A)** 2000–2010 and **(B)** 2010–2020 (km^2).

The GWR model is an extension of the traditional regression model, which considers the spatial effect by integrating the coordinates of the variables into the calculation (Fotheringham et al., 1996; Punzo et al., 2022). Therefore, the GWR model can estimate the coefficients as many as the local research units, thereby better reflecting the local spatial effects of the explanatory variables on dependent variables (Su et al., 2014; Guo et al., 2021). To obtain a better view of the spatially varying relationships between the interaction of construction land expansion and cropland expansion and socioeconomic determinants, the GWR model was used to visualize the spatial heterogeneity. The GWR model is described as follows:

$$y_{it} = \gamma_t(X_i, Y_i) + \sum_k^q \gamma_{kt}(X_i, Y_i)x_{ikt} + \varepsilon_{it} \quad i \in \{1, 2, \ldots, n\}, \tag{9}$$

where y_{it} is the dependent variable at research unit i in period t, γ_t is the intercept, (X_i, Y_i) is the spatial coordinate of the explanatory variable of x_{ikt}, γ_{kt} is the coefficient of the variables, ε_{it} is the error, n and q represent the number of research units and explanatory variables. The dependent variable in this article is the value of the interaction between construction land expansion and cropland expansion at two time periods 2000–2010 and 2010–2020, and the explanatory variables are the socioeconomic determinants selected in **section 3.6**. To avoid the multicollinearity between the selected variables, we transferred all variables into their LN format.

Variable Selection

The interaction between the construction land expansion and cropland expansion is a result of the development of social economy, and its calculations are based on two sides the expanded construction land and the expanded cropland. Thus, it is influenced by the joint effects of socioeconomic factors affecting the construction land and cropland. **Table 1** displays the explanatory variables selected in this study. The GDP and INVEST have been regarded as the factors influencing construction land expansion (Zhang et al., 2020; Wu et al., 2021), while GDPF is the factor affecting the change of cropland (Cheng et al., 2020; Eigenbrod et al., 2020; Tian et al., 2021). In addition, POP can be considered as the socioeconomic factor that influences both construction land and cropland (Sarparast et al., 2020; Uisso and Tanrıvermiş, 2021).

RESULTS

Characteristics of Construction Land Expansion and Cropland Expansion

In the last 20 years, MRUA has experienced massive changes of construction land and cropland expansions. As time goes by, both construction land expansion and cropland expansion display an increasing trend (**Table 2**). In 2000–2010, MRUA experienced the expansion of 3,410.92 km^2 of construction land and 1785.92 km^2 of cropland. Meanwhile, these figures increased to 5,103.82 and 7,809.46 km^2, respectively, in the period of 2010–2020. **Figure 3** provides a detailed view on the amount of the expanded construction land and cropland in each subresearch area. From this figure, we can see that in 2000–2010, as capital cities in their provinces, Wuhan, Changsha, and Nanchang experienced the largest amount of construction land expansion

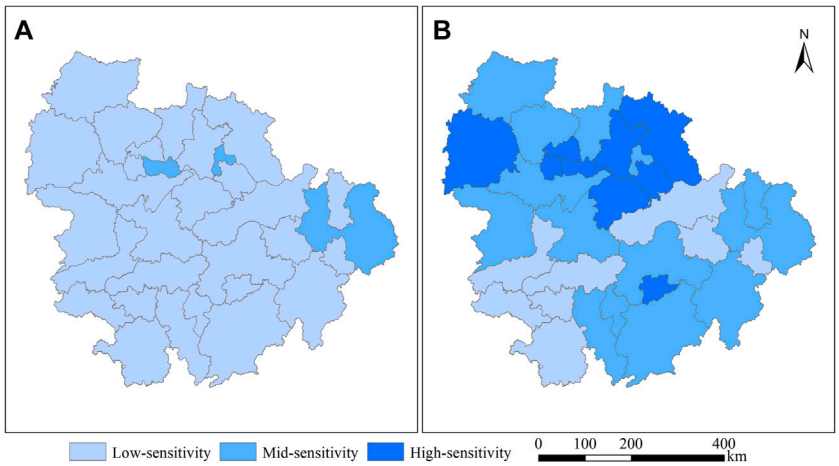

FIGURE 4 | Sensitivity of cropland expansion to construction land expansion in the periods of **(A)** 2000–2010 and **(B)** 2010–2020.

with a number of 407.02, 357.68, and 257.21 km^2, respectively. In 2010–2020, Wuhan was still the city that experienced the largest number of construction land expansion with a number of 351.38 km^2. Meanwhile, the other top two cities with the largest areas of construction land expansion have been changed to Jiujiang and Jingzhou with the area of 305.29 and 302.75 km^2, respectively. As for the area of the expanded cropland, Shangrao, Yueyang, and Nanchang are the top three cities experiencing cropland expansion (194.41, 176.32, and 139.42 km^2, respectively) in 2000–2010; while in 2010–2020, the top three cities with the largest cropland expansion have been changed to Jingzhou, Yichang, and Xiangyang and the areas of the expanded cropland have been increased to 621.41, 537.73, and 531.73 km^2, respectively.

Figure 3 also shows that the difference between the expanded construction land and the expanded cropland indicates a shrinking trend. In 2000–2010, only five cities, namely, Yichang, Jingzhou, Shangrao, Yueyang, and Yiyang showed that the area of the expanded cropland was larger than that of the expanded construction land. The other cities experience more construction land expansion than cropland expansion, especially in fast developing cities, such as Wuhan and Changsha. In 2010–2020, the area of the expanded cropland showed an increasing pattern, and that of the expanded construction land displays a decreasing trend compared with that in 2000–2010. The phenomenon of the area of the expanded cropland which is larger than that of the expanded construction land happens in nearly all the subresearch area and meets the requirement of cropland protection policies.

Sensitivity of Cropland Expansion to Construction Land Expansion

By integrating the area of the expanded construction land and the expanded cropland, the sensitivity of cropland expansion to construction land expansion of each city in MRUA was estimated (**Figure 4**). To gain a clear view of the results, the sensitivity was divided into three levels as follows: low sensitivity ($0 < \theta \leq 0.1$), mid sensitivity ($0.1 < \theta \leq 0.2$), and high sensitivity ($\theta > 0.2$).

Overall, the number of cities denoting the sensitivity of mid and high continuously increased and those with low sensitivity kept decreasing over time. During 2000–2010, only three cities were with mid sensitivity and the other cities in MRUA were all at the level of low sensitivity (**Figure 4A**). In comparison, the number of cities with low sensitivity decreased to eight, whereas the quantity of cities with mid and high sensitivity increased to 14 and nine during 2010–2020, respectively (**Figure 4B**). Additionally, cities with high sensitivity were mainly located in the north of MRUA. The results of sensitivity analysis in MRUA demonstrate that the area of cropland expansion is becoming increasingly related to the area of construction land expansion over time.

Changes of the Gravity Center of the Expanded Construction Land and the Expanded Cropland and Their Interaction

Figure 5 displays the changes of the gravity centers of the expanded construction land and the expanded cropland in 2000–2020, and the change directions and distances of the gravity centers are listed in **Table 3**. Although the gravity centers were all in Xianning during 2000–2020, the gravity center of the expanded construction land has moved toward the northeast, whereas that of the expanded cropland has continuously changed toward the southeast of the research area. Both the gravity centers of the expanded construction land and expanded cropland show a moving trend toward the east. The moving distances of the gravity centers of the expanded construction land and the expanded cropland experienced little difference with distances of 17.83 and 15.37 km, respectively. With respect to the moving directions, the difference between the expanded construction land and the expanded cropland showed substantial changes. During 2000–2020, the change direction of

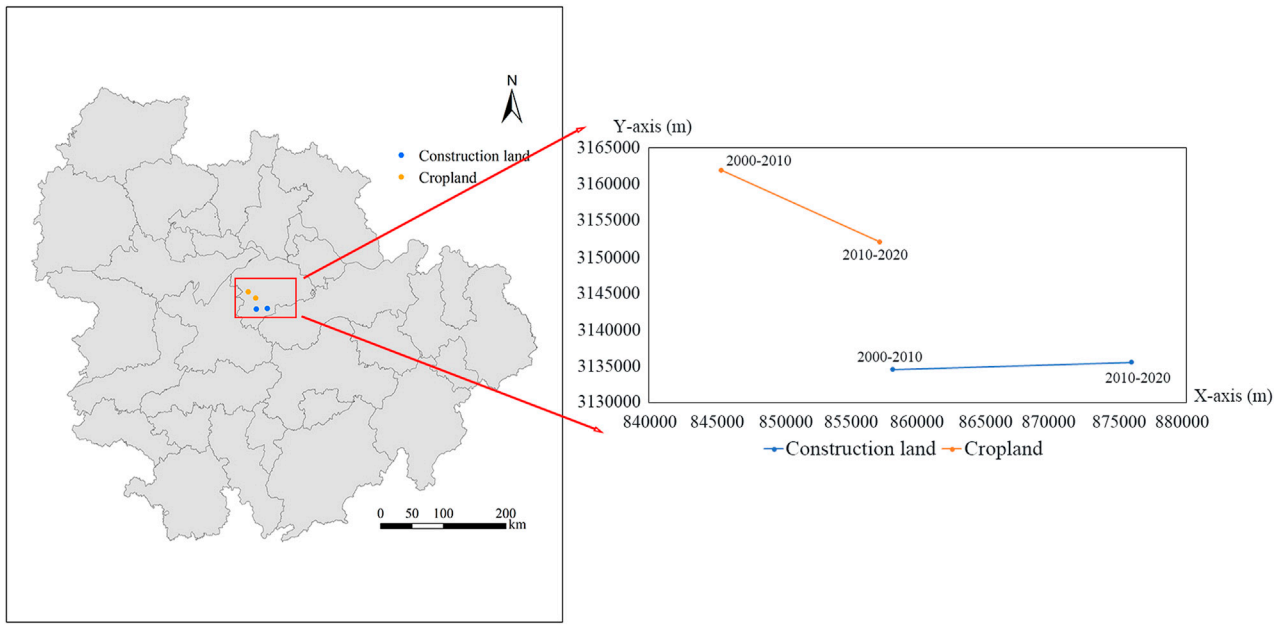

FIGURE 5 | Changes of the gravity center of the expanded construction land and the expanded cropland in 2000–2020.

TABLE 3 | Moving directions and distances of the gravity centers of the expanded construction land and cropland.

Period	Center of the expanded construction land		Center of the expanded cropland	
	Direction (°)	Distance (km)	Direction (°)	Distance (km)
2000–2020	3.24	17.83	−39.74	15.37

the gravity center of the expanded construction land was 3.24°, while that of the expanded cropland changed to −39.74°. In other words, the gravity center of the expanded construction land moved 3.24° and 17.83 km toward the northeast, whereas the gravity center of the expanded cropland shifted −39.74° and 15.37 km toward the southeast.

Figure 6 presents the spatiotemporal characteristics of the spatial interaction between the construction land expansion and cropland expansion in each subresearch area from 2000 to 2020. For a clear view, **Figure 6** presents the LN format of the values of the interactions. From an overall perspective, the values of the interaction show an increasing trend as follows: the minimum and maximum values of the interaction have increased from 5.65 and 8.72 in 2000–2010 to 7.15 and 9.89 in 2010–2020. For a spatial perspective, in 2000–2010, cities with high values mainly locate in the central and north of the research area; meanwhile, the highest values distribute in the central of the research area. Wuhan, Changsha, Xianning, and Jingzhou were the cities with the highest values of interactions. The lowest values distribute in the south of the research areas, such as Zhuzhou, Xiangtan, and Jingdezhen. For the period of 2010–2020, only three cities showed the lowest values, namely, Yichang, Xiangtan, and Zhuzhou. The highest values occured in Tianmen and Wuhan. Most of the cities with the lowest values in 2000–2010 have increased their interaction values, indicating a good phenomenon for balancing the tradeoffs between construction land expansion and cropland expansion.

Spatiotemporal Heterogeneity of Socioeconomic Determinants

The GWR model was utilized to analyze the spatiotemporal heterogeneity of socioeconomic determinants on the interaction between construction land expansion and cropland expansion both in 2000–2010 and 2010–2020. **Table 4** shows the performance of the GWR model in 2000–2010 and 2010–2020. The values of AICc in 2000–2010 and 2010–2020 are 580.84 and 219.26, respectively, and the adjusted R^2 values are 0.92 and 0.6, respectively, indicating that the GWR model can be used to reveal the spatial and temporal differentiations of socioeconomic determinants. From the summary table of the estimated coefficients (**Table 5**), we can see considerable variations in the coefficient of each explanatory variable with different positive and negative effects. The standard deviation of GDP and INVEST shows a decreasing trend over time, changing from 5.15 and 4.66 in 2000–2010 to 3.87 and 3.89 in 2010–2020, respectively, whereas that of GDPF and POP displays an increasing pattern (2.7 and 4.76 in 2000–2010 and 4.28 and 5.25 in 2010–2020, respectively).

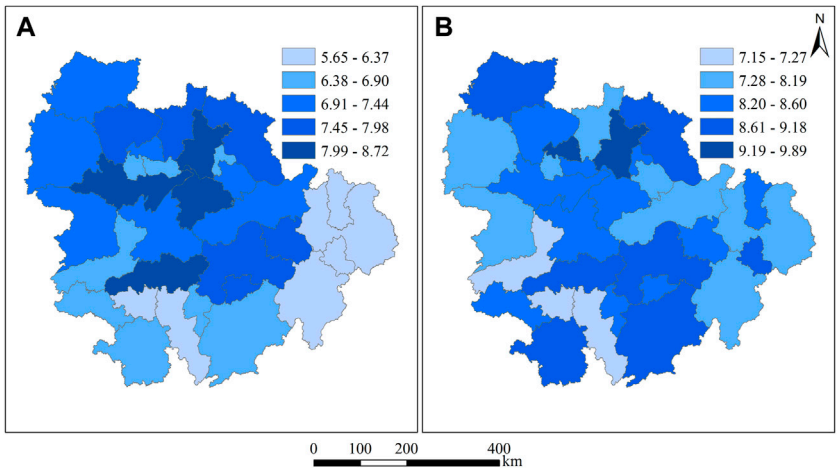

FIGURE 6 | LN format of the interaction between the expanded construction land and the expanded cropland in the periods of **(A)** 2000–2010 and **(B)** 2010–2020.

TABLE 4 | Performance of the GWR model in the periods of 2000–2010 and 2010–2020.

Indicator	2000–2010	2010–2020
AICc	580.84	219.26
Adjusted R^2	0.92	0.6

TABLE 5 | Summary of the estimated coefficients detected by the GWR model.

	2000–2010				2010–2020			
	Min	Mean	Max	SD	Min	Mean	Max	SD
GDP	−11.19	−0.23	11.12	5.15	−2.14	2.21	17.14	3.87
GDPF	−5.93	0.02	6.31	2.7	−12.37	−1.94	3.68	4.28
POP	−6.93	1.48	12.06	4.76	−3.95	2.89	16.82	5.25
INVEST	−11.54	0.09	9.72	4.66	−18.56	−2.49	0.123	3.89

Min, Mean, Max, and SD represent the minimum, mean, maximum, and standard deviation of the estimated coefficients.

Based on the local coefficients estimated by the GWR model and the Natural Breaks Jenks method in ArcGIS 10.2, the coefficients with similar values have been divided in to the same classification level (**Figure 7**). In addition, to distinguish the positive and negative effects, the authors separated the positive and negative coefficients as follows: blue represents the positive values, and yellow denotes the negative values.

The spatiotemporal effects of GDP on the interaction between the construction land expansion and cropland expansion in 2000–2010 and 2010–2020 are shown in **Figure 7A**. Overall, the positive effects of GDP displayed an increasing trend, whereas the absolute values of coefficients showed a shrinking pattern. In 2000–2010, the positive coefficients distributed in the south of the research area, and the negative coefficients were located in the northwest and northeast. In 2010–2020, nearly all the subresearch areas displayed with the positive coefficients whereas negative coefficients could only be seen in northwest and were scattered in the middle. The proportions of positive coefficients increased overtime with a proportion of 45.16% in 2000–2010 to 77.42% in 2010–2020 (**Table 6**).

According to **Figure 7B**, the influence of GDPF on the interaction between construction land expansion and cropland expansion slowly follows the trend of negative effects distributed in the west and positive effects located in the east both in 2000–2010 and 2010–2020. Moreover, the proportions of the positive and negative coefficients are stable in these two time periods (**Table 6**).

The spatiotemporal effects of POP in 2000–2020 are displayed in **Figure 7C**, showing an overall pattern of the positive coefficients located in the west and the negative coefficients distributed in the east. The distribution pattern of the POP's different types of coefficients is nearly reversed with that of the GDPF. Meanwhile, the proportions of the positive and negative coefficients of POP are similar to that of GDPF, with proportions of 58.06 and 41.94% both in 2000–2010 and 2010–2020 (**Table 6**).

Figure 7D presents the spatiotemporal influences of INVEST on the interaction between construction land expansion and cropland expansion, which shows that the overall pattern of the cities with negative coefficients are continuously increasing over time. In 2000–2010, the positive coefficients could be detected in the northwest and southeast of the research area; whereas in 2010–2020, only two cities had positive coefficients. Therefore, the proportion of the negative coefficients showed a sharp increase, with a proportion of 41.94% in 2000–2010 to 93.55% in 2010–2020 (**Table 6**).

DISCUSSION

Taking 31 prefectural cities in MRUA as the case area, this study analyzed the spatiotemporal patterns of the interaction between construction land expansion and cropland expansion and detected their socioeconomic determinants' effects from 2000 to 2020 by integrating the spatial gravity model and the GWR

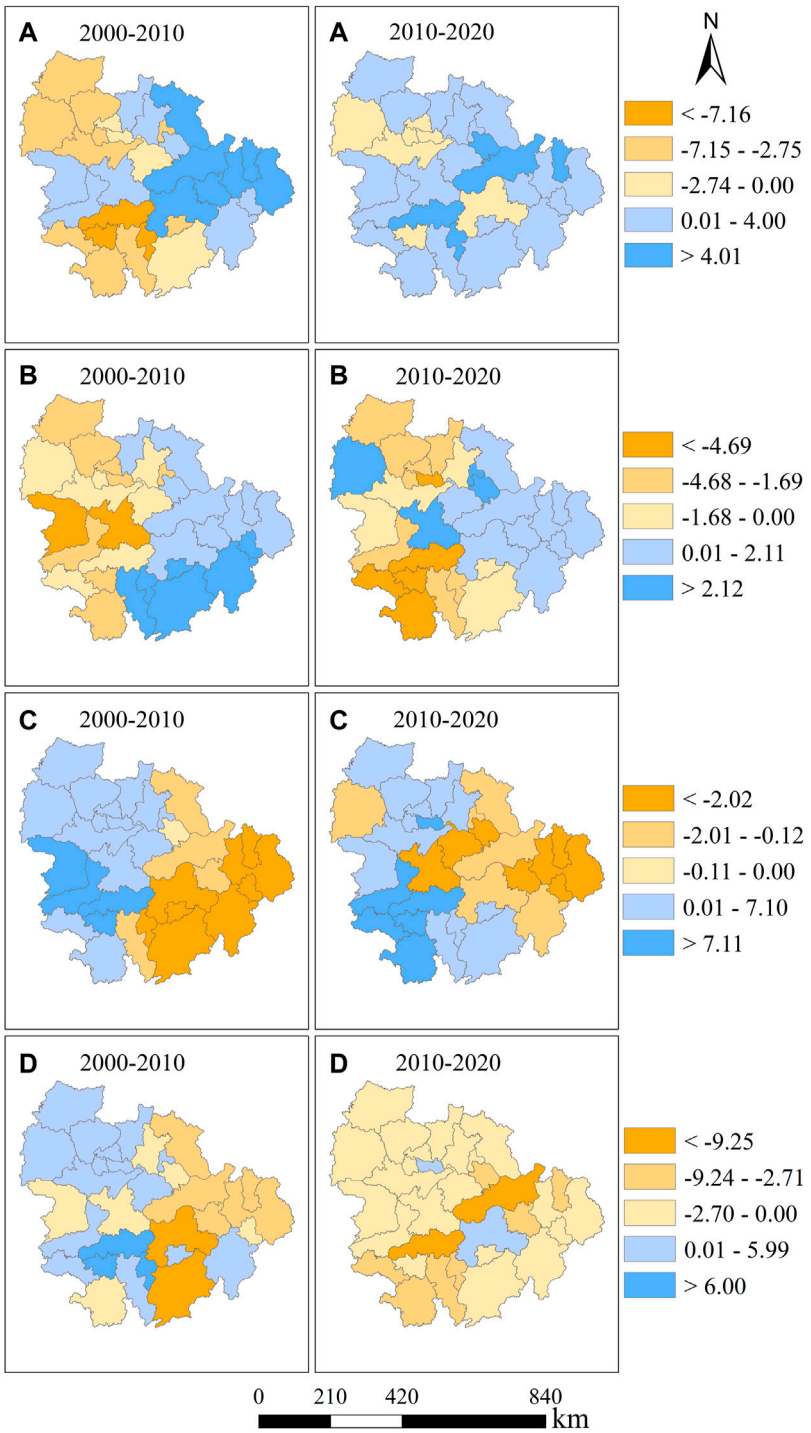

FIGURE 7 | Spatiotemporal distributions of the GWR coefficients of socioeconomic determinants in MRUA from 2000 to 2020: **(A)** GDP, **(B)** GDPF, **(C)** POP, and **(D)** INVEST.

model. The urbanization and cropland expansion are both hot issues for researchers (Badreldin et al., 2019; Zhou et al., 2021; Wang et al., 2022). Since the implication of cropland protection policies, it is important to assess the implication effect and its consequences (Liu et al., 2017; Ke et al., 2018; Ke et al., 2019; Wang et al., 2020). The interaction analysis of construction land expansion and cropland expansion can directly reflect the requirements of cropland protection policies on the cropland area. Owing to one of the cropland protection policies, Cropland Balance Policy, requests that if the development of construction

TABLE 6 | Proportions of the cities with different types of coefficients (%).

	2000–2010		2010–2020	
	Positive	Negative	Positive	Negative
GDP	45.16	54.84	77.42	22.58
GDPF	45.16	54.84	41.94	58.06
POP	58.06	41.94	58.06	41.94
INVEST	58.06	41.94	6.45	93.55

land takes in cropland, the construction land developer must reclaim the same area of cropland as the loss of cropland due to construction land development through land consolidation, exploitation, or rehabilitation (Lichtenberg and Ding, 2008; Song and Pijanowski, 2014; Liu et al., 2017). The results of the characteristics of the expanded construction land and the expanded cropland showed that during 2000–2020 both construction land and cropland expansions displayed an increasing trend. Additionally, the area of the expanded cropland exceeded those of the expanded construction land in 2010–2020. In the subresearch areas, during 2000–2010, only five cities showed that the area of cropland expansion exceeded that of construction land expansion. This phenomenon nearly happened in all subresearch areas. The value of the interaction of construction land expansion and cropland expansion also showed an overall increasing pattern with the minimum and maximum values increased from 5.65 and 8.72 to 7.15 and 9.89, respectively. All of the aforementioned results have proven that the implementation results of the cropland protection policies are progressively improving over time, which is in line with the conclusions of Yu et al. (2018) and Yang et al. (2020a).

We also identified the spatial and temporal sensitivity of cropland expansion to construction land expansion through sensitivity analysis and drew the shifting map of the gravity centers of the expanded construction land and the expanded cropland. The decrease in the sensitivity of cropland expansion to construction land expansion may cause many problems, such as imbalance of regional land use structures and insufficiency of grain production (Xu et al., 2013; Chai et al., 2019). The sensitivity analysis also demonstrated an increasing pattern of sensitivity of cropland expansion to construction land expansion. Moreover, the proportion of high sensitivity cities is progressively expanding over time, showing that cropland expansion is becoming increasingly sensitive to construction land expansion. The results of the gravity center showed that during 2000–2020, the gravity centers of the expanded construction land and the expanded cropland were all located in one prefectural city, but their shifting patterns were different. Both the gravity centers of the expanded construction land and the expanded cropland shifted to the east in the X-axis direction in 2000–2020, which supported the research of Chai et al. (2019) conducted in Hubei Province. In the Y-axis direction, distinct from the research carried out by Wang et al. (2018), the gravity center of the expanded construction land shifted toward the north and that of the expanded cropland moved toward the south. This phenomenon decided by the DEM of the research area (**Figure 1B**). The research area presents a pattern of high in the southeast and low in the northwest. People prefer to use the land with low DEM for developing construction land because of the low cost and high repay (Liu et al., 2005; Su et al., 2020), pushing the expanded cropland to the locations with relatively high DEM. Therefore, the gravity center of the expanded cropland moved to the southeast of the research area.

Existing studies have separately discussed the influence factors of construction land and cropland transitions (Ariti et al., 2015; Zelaya et al., 2016; Zhou et al., 2020). However, these studies did not explore the spatiotemporal impacts of socioeconomic determinants on the interaction between construction land expansion and cropland expansion. Thus, this study explored the spatiotemporal heterogeneity of the socioeconomic determinants of the interaction between construction land expansion and cropland expansion for 2000–2010 and 2010–2020 using the GWR model. Four socioeconomic determinants were chosen, namely, GDP, GDPF, POP, and INVEST. The positive impact of GDP showed an increasing pattern over time. The GDP reflects the overall economic level of a region (Xie and Wang, 2015; Gollin et al., 2016). With the improvement of socio economy, the government began to pay extra attention to the implementation of cropland protection (Liu et al., 2017; Piquer-Rodríguez et al., 2018). Therefore, the more construction land expansion, the larger the area of cropland expansion. Then, it promotes the interaction between them. The impacts of GDPF and POP nearly show an inversed distribution pattern. This finding is due to the fact that the economic development of the west of the research area is better than the east. The high GDPF is more attractive for the people in the east for agricultural activities. Thus, the positive impact of GDPF located in the east. By contrast, people in the economically underdeveloped areas prefers to live in the urban areas and the construction land expansion rate brought by population increase in economic developed areas is higher than that in underdeveloped areas (Li et al., 2019; Li et al., 2022). Therefore, the negative effect of POP distributed in the east. The negative influence of INVEST is continuously increasing during 2000–2020 because the investment in fixed assets concentrates on the urban areas and ignores the development in the agricultural areas. This situation leads the unilateral expansion of construction land instead of the joint expansion of construction land and cropland, thus negatively affecting their interaction.

This research contains some limitations. First, only two time periods of construction land expansion and cropland expansion were identified with a time interval of 10 y. Several LUCC-related studies have chosen the time interval of 5 y to better reveal the detailed change in land use changes (Lang et al., 2018; Wu et al., 2021). The time interval in this article can be improved. Second, construction land expansion can also bring the loss of cropland. Future research could explore the relationships among construction land expansion, cropland expansion, and cropland loss. Last, this article identified the spatiotemporal heterogeneity of four socioeconomic determinants on the interaction between construction land expansion and cropland expansion. Several other socioeconomic determinants may also

affect the interaction between construction land expansion and cropland expansion. Other determinants should be explored in the future.

CONCLUSION

This study first detected the spatial and temporal characteristics of construction land expansion and cropland expansion. Then, the sensitivity analysis was applied to identify the sensitivity of cropland expansion to construction land expansion. Next, the gravity center of the expanded construction land and the expanded cropland and their shifting trajectories were detected by the spatial gravity model. Finally, four socioeconomic determinants were chosen, namely, GDP, GDPF, POP, and INVEST, and their impacts on the interaction between construction land expansion and cropland expansion were explored by the GWR model. The results show that the areas of the expanded construction land and expanded cropland and the sensitivity of cropland expansion to construction land expansion demonstrated an overall increasing trend over time in MRUA. The shift trajectories of the expanded construction land and cropland displayed different patterns, where the gravity center of the expanded construction land moved toward the northeast, whereas that of the expanded cropland shifted toward the southeast. The spatiotemporal heterogeneity of socioeconomic determinants of the interaction between construction land expansion and cropland expansion obviously exists in MRUA. The GDP has an increasing positive effect, whereas the investment in fixed assets displays an increasing negative influence during 2000–2020. The GDP in the agricultural sector and the population show a stable effect with half the proportion of the cities having a negative or positive influence. However, the distribution of the negative or positive influence of these two determinants are almost reversed. This study is not only helpful to understand the regional spatiotemporal interaction of construction land and cropland expansions and their socioeconomic determinants but can also offer solutions for the decision makers to promote this interaction and continue the pursuit of sustainable development.

DATA AVAILABILITY STATEMENT

The original contributions presented in the study are included in the article/Supplementary Material, further inquiries can be directed to the corresponding authors.

AUTHOR CONTRIBUTIONS

LW: writing—original draft preparation, methodology, and writing—reviewing and editing. SZ: writing—reviewing editing and methodology. YL (3rd author): writing—reviewing and editing and methodology. YL (4th author): writing—editing and supervision.

FUNDING

This work was supported by the National Key Research and Development Program of China (Grant No. 2017YFB0503601).

REFERENCES

Angel, S., Parent, J., Civco, D. L., Blei, A., and Potere, D. (2011). The Dimensions of Global Urban Expansion: Estimates and Projections for All Countries, 2000-2050. *Prog. Plann.* 75, 53–107. doi:10.1016/j.progress.2011.04.001

Ariti, A. T., van Vliet, J., and Verburg, P. H. (2015). Land-use and Land-Cover Changes in the Central Rift Valley of Ethiopia: Assessment of Perception and Adaptation of Stakeholders. *Appl. Geogr.* 65, 28–37. doi:10.1016/j.apgeog.2015.10.002

Ariti, A. T., van Vliet, J., and Verburg, P. H. (2018). What Restrains Ethiopian NGOs to Participate in the Development of Policies for Natural Resource Management? *Environ. Sci. Pol.* 89, 292–299. doi:10.1016/j.envsci.2018.08.008

Asche, F., Bellemare, M. F., Roheim, C., Smith, M. D., and Tveteras, S. (2015). Fair Enough? Food Security and the International Trade of Seafood. *World Develop.* 67, 151–160. doi:10.1016/j.worlddev.2014.10.013

Badreldin, N., Abu Hatab, A., and Lagerkvist, C.-J. (2019). Spatiotemporal Dynamics of Urbanization and Cropland in the Nile Delta of Egypt Using Machine Learning and Satellite Big Data: Implications for Sustainable Development. *Environ. Monit. Assess.* 191, 767. doi:10.1007/s10661-019-7934-x

Boudet, F., Macdonald, G. K., Robinson, B. E., and Samberg, L. H. (2019). Rural-urban Connectivity and Agricultural Land Management across the Global South. *Glob. Environ. Change* 60, 101982. doi:10.1016/j.gloenvcha.2019.101982

Chai, J., Wang, Z., Yang, J., and Zhang, L. (2019). Analysis for Spatial-Temporal Changes of Grain Production and farmland Resource: Evidence from Hubei Province, central China. *J. Clean. Prod.* 207, 474–482. doi:10.1016/j.jclepro.2018.10.008

Cheng, C., Liu, Y., Chen, Y., Liu, Y., Zhang, Y., Shen, S., et al. (2019). Diagnosing Cropland's Allowable Range and Spatial Allocation in China's Typical Mountainous Plateau Area: An Evaluation Framework Based on Ecological Carrying Capacity. *Sci. Total Environ.* 685, 1255–1268. doi:10.1016/j.scitotenv.2019.03.200

Cheng, C., Liu, Y., Liu, Y., Yang, R., Hong, Y., Lu, Y., et al. (2020). Cropland Use Sustainability in Cheng-Yu Urban Agglomeration, China: Evaluation Framework, Driving Factors and Development Paths. *J. Clean. Prod.* 256, 120692. doi:10.1016/j.jclepro.2020.120692

Cheng, P., Tang, H., Dong, Y., Liu, K., Jiang, P., and Liu, Y. (2021). Knowledge Mapping of Research on Land Use Change and Food Security: A Visual Analysis Using Citespace and Vosviewer. *IJERPH* 18, 13065. doi:10.3390/ijerph182413065

Cullingworth, B., Nadin, V., Hart, T., Davoudi, S., Pendlebury, J., Vigar, G., et al. (2014). *Town and Country Planning in the UK*. doi:10.4324/9781315742267

Deng, J. S., Wang, K., Hong, Y., and Qi, J. G. (2009). Spatio-temporal Dynamics and Evolution of Land Use Change and Landscape Pattern in Response to Rapid Urbanization. *Landscape Urban Plann.* 92, 187–198. doi:10.1016/j.landurbplan.2009.05.001

Egli, L., Meyer, C., Scherber, C., Kreft, H., and Tscharntke, T. (2018). Winners and Losers of National and Global Efforts to Reconcile Agricultural Intensification and Biodiversity Conservation. *Glob. Change Biol.* 24, 2212–2228. doi:10.1111/gcb.14076

Eigenbrod, F., Beckmann, M., Dunnett, S., Graham, L., Holland, R. A., Meyfroidt, P., et al. (2020). Identifying Agricultural Frontiers for Modeling Global Cropland Expansion. *One Earth* 3, 504–514. doi:10.1016/j.oneear.2020.09.006

Folberth, C., Khabarov, N., Balkovič, J., Skalský, R., Visconti, P., Ciais, P., et al. (2020). The Global Cropland-Sparing Potential of High-Yield Farming. *Nat. Sustain.* 3, 281–289. doi:10.1038/s41893-020-0505-x

Foley, J. A., Ramankutty, N., Brauman, K. A., Cassidy, E. S., Gerber, J. S., Johnston, M., et al. (2011). Solutions for a Cultivated Planet. *Nature* 478, 337–342. doi:10.1038/nature10452

Fotheringham, A. S., Charlton, M., and Brunsdon, C. (1996). The Geography of Parameter Space: an Investigation of Spatial Non-stationarity. *Int. J. Geog. Inf. Sci.* 10, 605–627. doi:10.1080/026937996137909

Gollin, D., Jedwab, R., and Vollrath, D. (2016). Urbanization with and without Industrialization. *J. Econ. Growth* 21, 35–70. doi:10.1007/s10887-015-9121-4

Guo, B., Wang, X., Pei, L., Su, Y., Zhang, D., and Wang, Y. (2021). Identifying the Spatiotemporal Dynamic of PM2.5 Concentrations at Multiple Scales Using Geographically and Temporally Weighted Regression Model across China during 2015-2018. *Sci. Total Environ.* 751, 141765. doi:10.1016/j.scitotenv.2020.141765

Haase, D., Schwarz, N., Strohbach, M., Kroll, F., and Seppelt, R. (2012). Synergies, Trade-Offs, and Losses of Ecosystem Services in Urban Regions: an Integrated Multiscale Framework Applied to the Leipzig-Halle Region, Germany. *E&S* 17. doi:10.5751/ES-04853-170322

Han, Z., Song, W., and Deng, X. (2016). Responses of Ecosystem Service to Land Use Change in Qinghai Province. *Energies* 9, 303. doi:10.3390/en9040303

He, C., Liu, Z., Tian, J., and Ma, Q. (2014). Urban Expansion Dynamics and Natural Habitat Loss in China: A Multiscale Landscape Perspective. *Glob. Change Biol.* 20, 2886–2902. doi:10.1111/gcb.12553

He, X., Yan, J., and Cheng, X. (2021). Household Perspective on Cropland Expansion on the Tibetan Plateau. *Reg. Environ. Change* 21. doi:10.1007/s10113-021-01752-8

Ke, X., van Vliet, J., Zhou, T., Verburg, P. H., Zheng, W., and Liu, X. (2018). Direct and Indirect Loss of Natural Habitat Due to Built-Up Area Expansion: A Model-Based Analysis for the City of Wuhan, China. *Land Use Policy* 74, 231–239. doi:10.1016/j.landusepol.2017.12.048

Ke, X., Wang, L., Ma, Y., Pu, K., Zhou, T., Xiao, B., et al. (2019). Impacts of Strict Cropland Protection on Water Yield: A Case Study of Wuhan, China. *Sustainability* 11, 184. doi:10.3390/su11010184

Lambin, E. F., and Meyfroidt, P. (2011). Global Land Use Change, Economic Globalization, and the Looming Land Scarcity. *Proc. Natl. Acad. Sci. U.S.A.* 108, 3465–3472. doi:10.1073/pnas.1100480108

Lang, Y., Song, W., and Deng, X. (2018). Projected Land Use Changes Impacts on Water Yields in the Karst Mountain Areas of China. *Phys. Chem. Earth Parts A/B/C* 104, 66–75. doi:10.1016/j.pce.2017.11.001

Li, H., Song, Y., and Zhang, M. (2018). Study on the Gravity center Evolution of Air Pollution in Yangtze River Delta of China. *Nat. Hazards* 90, 1447–1459. doi:10.1007/s11069-017-3110-1

Li, M., van Vliet, J., Ke, X., and Verburg, P. H. (2019). Mapping Settlement Systems in China and Their Change Trajectories between 1990 and 2010. *Habitat Int.* 94, 102069. doi:10.1016/j.habitatint.2019.102069

Li, M., Verburg, P. H., and van Vliet, J. (2022). Global Trends and Local Variations in Land Take Per Person. *Landscape Urban Plann.* 218, 104308. doi:10.1016/j.landurbplan.2021.104308

Lichtenberg, E., and Ding, C. (2008). Assessing farmland protection Policy in China. *Land use policy* 25, 59–68. doi:10.1016/j.landusepol.2006.01.005

Liu, J., Zhan, J., and Deng, X. (2005). Spatio-temporal Patterns and Driving Forces of Urban Land Expansion in China during the Economic Reform Era. *AMBIO: A J. Hum. Environ.* 34, 450–455. doi:10.1579/0044-7447-34.6.450

Liu, J., Zhang, Z., Xu, X., Kuang, W., Zhou, W., Zhang, S., et al. (2010). Spatial Patterns and Driving Forces of Land Use Change in China during the Early 21st century. *J. Geogr. Sci.* 20, 483–494. doi:10.1007/s11442-010-0483-4

Liu, J., Kuang, W., Zhang, Z., Xu, X., Qin, Y., Ning, J., et al. (2014a). Spatiotemporal Characteristics, Patterns, and Causes of Land-Use Changes in China since the Late 1980s. *J. Geogr. Sci.* 24, 195–210. doi:10.1007/s11442-014-1082-6

Liu, L., Xu, X., and Chen, X. (2014b). Assessing the Impact of Urban Expansion on Potential Crop Yield in China during 1990-2010. *Food Sec.* 7, 33–43. doi:10.1007/s12571-014-0411-z

Liu, X., Zhao, C., and Song, W. (2017). Review of the Evolution of Cultivated Land protection Policies in the Period Following China's Reform and Liberalization. *Land Use Policy* 67, 660–669. doi:10.1016/j.landusepol.2017.07.012

Liu, J., Jiao, L., Zhang, B., Xu, G., Yang, L., Dong, T., et al. (2021). New Indices to Capture the Evolution Characteristics of Urban Expansion Structure and Form. *Ecol. Indicators* 122, 107302. doi:10.1016/j.ecolind.2020.107302

Mauser, W., Klepper, G., Zabel, F., Delzeit, R., Hank, T., Putzenlechner, B., et al. (2015). Global Biomass Production Potentials Exceed Expected Future Demand without the Need for Cropland Expansion. *Nat. Commun.* 6. doi:10.1038/ncomms9946

Millennium Ecosystem Assessment (2005). *Ecosystems and Human Well-Being: Synthesis*. ISBN: 1-56973-590-5.

Mohmmed, A., Li, Z., Olushola Arowolo, A., Su, H., Deng, X., Najmuddin, O., et al. (2019). Driving Factors of CO2 Emissions and Nexus with Economic Growth, Development and Human Health in the Top Ten Emitting Countries. *Resour. Conserv. Recycl.* 148, 157–169. doi:10.1016/j.resconrec.2019.03.048

Monk, S., Whitehead, C., Burgess, G., and Tang, C. (2013). *International Review of Land Supply and Planning Systems*. London: Joseph Rowntree Foundation, 1–110.

Pan, D., Hong, W., and Kong, F. (2020). Efficiency Evaluation of Urban Wastewater Treatment: Evidence from 113 Cities in the Yangtze River Economic Belt of China. *J. Environ. Manage.* 270, 110940. doi:10.1016/j.jenvman.2020.110940

Piquer-Rodríguez, M., Butsic, V., Gärtner, P., Macchi, L., Baumann, M., Gavier Pizarro, G., et al. (2018). Drivers of Agricultural Land-Use Change in the Argentine Pampas and Chaco Regions. *Appl. Geogr.* 91, 111–122. doi:10.1016/j.apgeog.2018.01.004

Punzo, G., Castellano, R., and Bruno, E. (2022). Using Geographically Weighted Regressions to Explore Spatial Heterogeneity of Land Use Influencing Factors in Campania (Southern Italy). *Land Use Policy* 112, 105853. doi:10.1016/j.landusepol.2021.105853

Qiu, L., Pan, Y., Zhu, J., Amable, G. S., and Xu, B. (2019). Integrated Analysis of Urbanization-Triggered Land Use Change Trajectory and Implications for Ecological Land Management: A Case Study in Fuyang, China. *Sci. Total Environ.* 660, 209–217. doi:10.1016/j.scitotenv.2018.12.320

Salerno, F., Gaetano, V., and Gianni, T. (2018). Urbanization and Climate Change Impacts on Surface Water Quality: Enhancing the Resilience by Reducing Impervious Surfaces. *Water Res.* 144, 491–502. doi:10.1016/j.watres.2018.07.058

Sarparast, M., Ownegh, M., and Sepehr, A. (2020). Investigation the Driving Forces of Land-Use Change in Northeastern Iran: Causes and Effects. *Remote Sensing Appl. Soc. Environ.* 19, 100348. doi:10.1016/j.rsase.2020.100348

Seto, K. C., Güneralp, B., and Hutyra, L. R. (2012). Global Forecasts of Urban Expansion to 2030 and Direct Impacts on Biodiversity and Carbon Pools. *Proc. Natl. Acad. Sci. U.S.A.* 109, 16083–16088. doi:10.1073/pnas.1211658109

Shu, C., Xie, H., Jiang, J., and Chen, Q. (2018). Is Urban Land Development Driven by Economic Development or Fiscal Revenue Stimuli in China? *Land Use Policy* 77, 107–115. doi:10.1016/j.landusepol.2018.05.031

Song, W., and Liu, M. (2017). Farmland Conversion Decreases Regional and National Land Quality in China. *Land Degrad. Develop.* 28, 459–471. doi:10.1002/ldr.2518

Song, W., and Pijanowski, B. C. (2014). The Effects of China's Cultivated Land Balance Program on Potential Land Productivity at a National Scale. *Appl. Geogr.* 46, 158–170. doi:10.1016/j.apgeog.2013.11.009

Song, X.-P., Hansen, M. C., Stehman, S. V., Potapov, P. V., Tyukavina, A., Vermote, E. F., et al. (2018). Global Land Change from 1982 to 2016. *Nature* 560, 639–643. doi:10.1038/s41586-018-0411-9

Souza, D. O. d., Alvalá, R. C. d. S., and Nascimento, M. G. d. (2016). Urbanization Effects on the Microclimate of Manaus: A Modeling Study. *Atmos. Res.* 167, 237–248. doi:10.1016/j.atmosres.2015.08.016

Su, S., Xiao, R., Jiang, Z., and Zhang, Y. (2012). Characterizing Landscape Pattern and Ecosystem Service Value Changes for Urbanization Impacts at an Eco-Regional Scale. *Appl. Geogr.* 34, 295–305. doi:10.1016/j.apgeog.2011.12.001

Su, S., Li, D., Hu, Y. n., Xiao, R., and Zhang, Y. (2014). Spatially Non-stationary Response of Ecosystem Service Value Changes to Urbanization in Shanghai, China. *Ecol. Indicators* 45, 332–339. doi:10.1016/j.ecolind.2014.04.031

Su, Y., Qian, K., Lin, L., Wang, K., Guan, T., and Gan, M. (2020). Identifying the Driving Forces of Non-grain Production Expansion in Rural China and its Implications for Policies on Cultivated Land protection. *Land Use Policy* 92, 104435. doi:10.1016/j.landusepol.2019.104435

Tang, L., Ke, X., Chen, Y., Wang, L., Zhou, Q., Zheng, W., et al. (2021). Which Impacts More Seriously on Natural Habitat Loss and Degradation? Cropland Expansion or Urban Expansion? *Land Degrad. Dev.* 32, 946–964. doi:10.1002/ldr.3768

Tesfaw, A. T., Pfaff, A., Golden Kroner, R. E., Qin, S., Medeiros, R., and Mascia, M. B. (2018). Land-use and Land-Cover Change Shape the Sustainability and Impacts of Protected Areas. *Proc. Natl. Acad. Sci. U.S.A.* 115, 2084–2089. doi:10.1073/pnas.1716462115

Tian, G., Duan, J., and Yang, L. (2021). Spatio-temporal Pattern and Driving Mechanisms of Cropland Circulation in China. *Land Use Policy* 100, 105118. doi:10.1016/j.landusepol.2020.105118

Tu, Y., Chen, B., Yu, L., Xin, Q., Gong, P., and Xu, B. (2021). How Does Urban Expansion Interact with Cropland Loss? A Comparison of 14 Chinese Cities from 1980 to 2015. *Landscape Ecol.* 36, 243–263. doi:10.1007/s10980-020-01137-y

Uisso, A. M., and Tanrıvermiş, H. (2021). Driving Factors and Assessment of Changes in the Use of Arable Land in Tanzania. *Land Use Policy* 104, 105359. doi:10.1016/j.landusepol.2021.105359

United Nations (2018). *World Urban Prospects: The 2018 Revision-Key Facts*. ST/ESA/SER.A/366.

van Vliet, J., Eitelberg, D. A., and Verburg, P. H. (2017). A Global Analysis of Land Take in Cropland Areas and Production Displacement from Urbanization. *Glob. Environ. Change* 43, 107–115. doi:10.1016/j.gloenvcha.2017.02.001

Wang, J., Zhang, Z., and Liu, Y. (2018). Spatial Shifts in Grain Production Increases in China and Implications for Food Security. *Land Use Policy* 74, 204–213. doi:10.1016/j.landusepol.2017.11.037

Wang, L., Ke, X., and Abu Hatab, A. (2020). Trade-offs between Economic Benefits and Ecosystem Services Value under Three Cropland protection Scenarios for Wuhan City in China. *Land* 9, 117–17. doi:10.3390/land9040117

Wang, L., Zheng, W., Tang, L., Zhang, S., Liu, Y., and Ke, X. (2021). Spatial Optimization of Urban Land and Cropland Based on Land Production Capacity to Balance Cropland protection and Ecological Conservation. *J. Environ. Manage.* 285, 112054. doi:10.1016/j.jenvman.2021.112054

Wang, L., Zhang, S., Tang, L., Lu, Y., Liu, Y., and Liu, Y. (2022). Optimizing Distribution of Urban Land on the Basis of Urban Land Use Intensity at Prefectural City Scale in mainland China. *Land Use Policy* 115, 106037. doi:10.1016/j.landusepol.2022.106037

Wu, C., Chen, B., Huang, X., and Dennis Wei, Y. H. (2020). Effect of Land-Use Change and Optimization on the Ecosystem Service Values of Jiangsu Province, China. *Ecol. Indicators* 117, 106507. doi:10.1016/j.ecolind.2020.106507

Wu, R., Li, Z., and Wang, S. (2021). The Varying Driving Forces of Urban Land Expansion in China: Insights from a Spatial-Temporal Analysis. *Sci. Total Environ.* 766, 142591. doi:10.1016/j.scitotenv.2020.142591

Xie, H., and Wang, W. (2015). Exploring the Spatial-Temporal Disparities of Urban Land Use Economic Efficiency in china and its Influencing Factors under Environmental Constraints Based on a Sequential Slacks-Based Model. *Sustainability* 7, 10171–10190. doi:10.3390/su70810171

Xu, S.-w., Wu, J.-z., Song, W., Li, Z.-q., Li, Z. m., and Kong, F.-t. (2013). Spatial-Temporal Changes in Grain Production, Consumption and Driving Mechanism in China. *J. Integr. Agric.* 12, 374–385. doi:10.1016/S2095-3119(13)60236-1

Yang, B., Ke, X., van Vliet, J., Yu, Q., Zhou, T., and Verburg, P. H. (2020a). Impact of Cropland Displacement on the Potential Crop Production in China: a Multi-Scale Analysis. *Reg. Environ. Change* 20. doi:10.1007/s10113-020-01690-x

Yang, J., Zeng, C., and Cheng, Y. (2020b). Spatial Influence of Ecological Networks on Land Use Intensity. *Sci. Total Environ.* 717, 137151. doi:10.1016/j.scitotenv.2020.137151

Yu, Q., Hu, Q., van Vliet, J., Verburg, P. H., and Wu, W. (2018). GlobeLand30 Shows Little Cropland Area Loss but Greater Fragmentation in China. *Int. J. Appl. Earth Obs. Geoinf.* 66, 37–45. doi:10.1016/j.jag.2017.11.002

Zabel, F., Delzeit, R., Schneider, J. M., Seppelt, R., Mauser, W., and Václavík, T. (2019). Global Impacts of Future Cropland Expansion and Intensification on Agricultural Markets and Biodiversity. *Nat. Commun.* 10, 1–10. doi:10.1038/s41467-019-10775-z

Zelaya, K., van Vliet, J., and Verburg, P. H. (2016). Characterization and Analysis of Farm System Changes in the Mar Chiquita basin, Argentina. *Appl. Geogr.* 68, 95–103. doi:10.1016/j.apgeog.2016.02.001

Zeng, C., Song, Y., Cai, D., Hu, P., Cui, H., Yang, J., et al. (2019). Exploration on the Spatial Spillover Effect of Infrastructure Network on Urbanization: A Case Study in Wuhan Urban Agglomeration. *Sustain. Cities Soc.* 47, 101476. doi:10.1016/j.scs.2019.101476

Zhang, Y., Zhang, J., Yang, Z., and Li, J. (2012). Analysis of the Distribution and Evolution of Energy Supply and Demand Centers of Gravity in China. *Energy Policy* 49, 695–706. doi:10.1016/j.enpol.2012.07.012

Zhang, P., Yang, D., Qin, M., and Jing, W. (2020). Spatial Heterogeneity Analysis and Driving Forces Exploring of Built-Up Land Development Intensity in Chinese Prefecture-Level Cities and Implications for Future Urban Land Intensive Use. *Land Use Policy* 99, 104958. doi:10.1016/j.landusepol.2020.104958

Zhang, Y., Wang, W., and Feng, Y. (2022). Impact of Different Models of Rural Land Consolidation on Rural Household Poverty Vulnerability. *Land Use Policy* 114, 105963. doi:10.1016/j.landusepol.2021.105963

Zhong, T.-Y., Huang, X.-J., Zhang, X.-Y., and Wang, K. (2011). Temporal and Spatial Variability of Agricultural Land Loss in Relation to Policy and Accessibility in a Low Hilly Region of Southeast China. *Land Use Policy* 28, 762–769. doi:10.1016/j.landusepol.2011.01.004

Zhou, Y., Li, X., and Liu, Y. (2020). Land Use Change and Driving Factors in Rural China during the Period 1995-2015. *Land Use Policy* 99, 105048. doi:10.1016/j.landusepol.2020.105048

Zhou, B.-B., Aggarwal, R., Wu, J., and Lv, L. (2021). Urbanization-associated farmland Loss: A Macro-Micro Comparative Study in China. *Land Use Policy* 101, 105228. doi:10.1016/j.landusepol.2020.105228

Conflict of Interest: The authors declare that the research was conducted in the absence of any commercial or financial relationships that could be construed as a potential conflict of interest.

The handling editor JC declared a past co-authorship with the author YL.

Publisher's Note: All claims expressed in this article are solely those of the authors and do not necessarily represent those of their affiliated organizations, or those of the publisher, the editors, and the reviewers. Any product that may be evaluated in this article, or claim that may be made by its manufacturer, is not guaranteed or endorsed by the publisher.

Copyright © 2022 Wang, Zhang, Liu and Liu. This is an open-access article distributed under the terms of the Creative Commons Attribution License (CC BY). The use, distribution or reproduction in other forums is permitted, provided the original author(s) and the copyright owner(s) are credited and that the original publication in this journal is cited, in accordance with accepted academic practice. No use, distribution or reproduction is permitted which does not comply with these terms.

frontiers | Frontiers in Environmental Science

ORIGINAL RESEARCH
published: 26 April 2022
doi: 10.3389/fenvs.2022.860814

The Spatiotemporal Characteristics and Rationality of Emerging Megacity Urban Expansion: A Case Study of Zhengzhou in Central China

Enxiang Cai[1], *Qingsheng Bi*[1], *Jie Lu*[1] *and Heping Hou*[2]*

[1]School of Resources and Environment, Henan Agricultural University, Zhengzhou, China, [2]College of Forestry, Henan Agricultural University, Zhengzhou, China

Studies on urban expansion in megacities are essential for managing urban sprawl to promote high-quality development. In this study, we have selected the emerging megacity of Zhengzhou as the research area, used the spatial analysis method to quantify the spatiotemporal characteristics of urban expansion from 1990 to 2020, and evaluated the rationality of urban expansion on the basis of the elasticity index and a comparison with other megacities. Results demonstrated that 1) Zhengzhou experienced great urban expansion from 1990 to 2020 and showed a trend of "steady–fast–slow," with steady expansion from 1990 to 2000, fast expansion from 2000 to 2010, and slow expansion after 2010; 2) Zhengzhou's urban expansion has obvious imbalance and spatial disorder, mainly concentrated in the urban central area, and is characterized by sprawl or a leap in space; 3) the occupation of cultivated land by urban expansion in Zhengzhou has gradually decreased, but the occupation of ecological land such as water areas has increased significantly, which may lead to a series of negative ecological effects; 4) Zhengzhou's urban expansion was inefficient, while the utilization intensity and economic benefits of Zhengzhou's urban construction land have improved, but relatively lower than those of other megacities in China. The findings have important reference that is significant for promoting the sustainable urban expansion of megacities and achieving sustainable regional development.

Keywords: sustainable development, spatiotemporal characteristics, urban expansion, emerging megacity, Zhengzhou

OPEN ACCESS

Edited by:
Ding Ma,
Shenzhen University, China

Reviewed by:
Hao Zhang,
Fudan University, China
Luyi Tong,
China University of Geosciences Wuhan, China
Qingsong He,
Huazhong University of Science and Technology, China

***Correspondence:**
Heping Hou
2009202050027@whu.edu.cn

Specialty section:
This article was submitted to Environmental Informatics and Remote Sensing, a section of the journal Frontiers in Environmental Science

Received: *23 January 2022*
Accepted: *21 March 2022*
Published: *26 April 2022*

Citation:
Cai E, Bi Q, Lu J and Hou H (2022) The Spatiotemporal Characteristics and Rationality of Emerging Megacity Urban Expansion: A Case Study of Zhengzhou in Central China. Front. Environ. Sci. 10:860814. doi: 10.3389/fenvs.2022.860814

1 INTRODUCTION

Rapid economic and population growth have led to an unprecedented increase in urban construction land, and urban expansion has become a global geographic phenomenon in the process of urbanization (Schneider and Woodcock, 2014; Tayyebi et al., 2014). As the carrier of social and economic activities, the expansion of urban construction land not only meets the growing social needs of urban residents but also provides important support for sustainable regional development (Bagan and Yamagata, 2014). However, in recent decades, the rapid urbanization in the world, especially in developing countries, has triggered the disorderly sprawl of urban construction land, which has a profound negative impact on resources (Hu et al., 2017; Lafortezza and Sanesi, 2019), the environment (Hamidi and Ewing, 2014), geographic processes (Liu et al., 2008; Xu et al., 2009),

biodiversity (Kovács et al., 2019), etc. and has become one of the most important factors that hinder sustainable regional and even global development (He et al., 2018). Exploring the mechanism of urban expansion, proposing strategies to prevent urban sprawl, and realizing sustainable development have become core topics of urban research.

In the middle of the twentieth century, many scholars began to conduct systematic research on urban expansion (Dai et al., 2010). A large number of scholars have used spatial analysis tools to conduct quantitative research on urban expansion from a geographic perspective (Buyantuyev et al., 2015; Hecht et al., 2020), mainly focusing on measuring urban expansion from the characteristics of land scale and spatial form, and building a series of index models such as expansion intensity index (Yue et al., 2016), expansion steady state index (Zhao et al., 2017), expansion elasticity index (Rusk, 1993), and sprawl index (Tian et al., 2017). With the technological innovation of geographic information systems and spatial statistics, the driving forces, prediction, and simulation of urban expansion have become research hot spots (Kantakumar et al., 2016; Zhang et al., 2018; Zhong et al., 2020; Liu et al., 2022). With the increasing pressure on resources and the environment, the sustainability of urban expansion needs to be discussed, and the rationality of urban expansion has attracted growing interest from urban planners and managers (Tong, 2020). Urban expansion can cause complex changes in regional natural systems. Whether it will lead to ecological degradation (Chien and Saito, 2021), food security issues (Gren and Andersson, 2018), and climate change (Khamchiangta and Dhakal, 2021) has become an important criterion for judging the rationality of urban expansion. Analyzing the coordination between urban expansion, population growth, and economic development by using the decoupling model (Cai et al., 2020) and the elastic coefficient (Jiao et al., 2016) is an important way of evaluating urban expansion. Although previous research generated an impressive body of work, urban expansion research mainly focuses on mature megacities and less on not well-known emerging megacities that have important regional influence and are undergoing rapid socioeconomic transformation. In addition, the urban expansion evaluation is mainly based on the expansion scale and effects of the city itself, and comparative analysis with similar cities is lacking. These comparisons have an important reference for judging the rationality of urban expansion.

Since the implementation of the reform and opening-up policy, China has made world-renowned urban development achievements, and a number of world-influential megacities such as Beijing, Shanghai, and Shenzhen have emerged. The seventh national census in 2020 shows that 21 megacities in China have a population of more than 5 million in central urban areas (CNBS, 2020). These megacities are not only clusters of job creation and population living but also core areas that support economic development and participate in international competition (Sassen, 1994). However, under the traditional urban development model oriented by economic growth in the past, Chinese megacities have seen a wave of blind expansion, which has caused problems such as loss of arable land, traffic congestion, skyrocketing land prices, and environmental pollution (Chen et al., 2013; Li et al., 2014). Megacities occupy a pivotal position in socioeconomic development, and the resource and environmental problems faced by their urban expansion are more serious than those faced by small- and medium-sized cities. Unlike the urbanization of mature megacities, which has stagnated, the urbanization of emerging megacities is still developing rapidly, and the demand for urban expansion continues to be strong. The expansion of emerging megacities has obvious diversity and differences, and the problems encountered in urban management are more complex (Yao et al., 2009). Therefore, a systematic study needs to be conducted on the characteristics and rationality of urban expansion in China's emerging megacities, and high-quality and sustainable urban expansion needs to be achieved.

This study takes Zhengzhou, a city in central China, as the research area to study the urban expansion of emerging megacities. The main purposes of this work are 1) to measure the spatiotemporal characteristics of urban expansion from 1990 to 2020; 2) to judge the rationality of urban expansion through the coordination of urban expansion, economy, and population, and a comparison with other megacities; and 3) to propose targeted suggestions for urban expansion management and provide a reference for the development of emerging megacities.

2 MATERIALS AND METHODS

2.1 Study Area

Zhengzhou is the capital of Henan Province in central China (34°16′–34°58′N and 112°42′–114°14′), adjacent to the lower Yellow River in the north. Zhengzhou covers an area of 7446.2 km^2, of which the central urban area covers 1181.51 km^2. As the core city of China's central plains urban agglomeration, one of the eight national central cities and an important national comprehensive transportation hub (NDRC, 2017), Zhengzhou is experiencing rapid economic growth and urbanization. In 2020, the permanent population was 12.6 million, of which the non-agricultural population accounted for 78.4%. Furthermore, its GDP was 1200.3 billion RMB (Zhengzhou Bureau of Statistics, 2021). Zhengzhou had a population of 5.34 million in the central urban area in 2020, becoming one of the 21 cities in China with a population in the central urban area exceeding 5 million, and it is an emerging megacity in China. Zhengzhou has 12 administrative districts, including 6 districts [Jinshui (JS), Zhongyuan (ZY), Erqi (EQ), Guancheng (GC), Huiji (HJ), and Shangjie (SJ)], 5 county-level cities [Xinzheng (XZ), Xinmi (XM), Xingyang (XY), Gongyi (GY), and Dengfeng (DF)], and 1 county [Zhongmo (ZM)] (**Figure 1**).

From 1990 to 2020, Zhengzhou's socioeconomic status experienced rapid development. The urban population and GDP increased significantly. The urban population increased from 2.38 million to 9.89 million, an increase of 3.15 times. Meanwhile, the urbanization rate increased from 42.7 to 78.4%, an increase of 35.7 percentage points. GDP increased from 11.64 billion yuan to 1,200 billion yuan, an increase of 102.12 times (**Figure 2**). Furthermore, the urban population and GDP growth

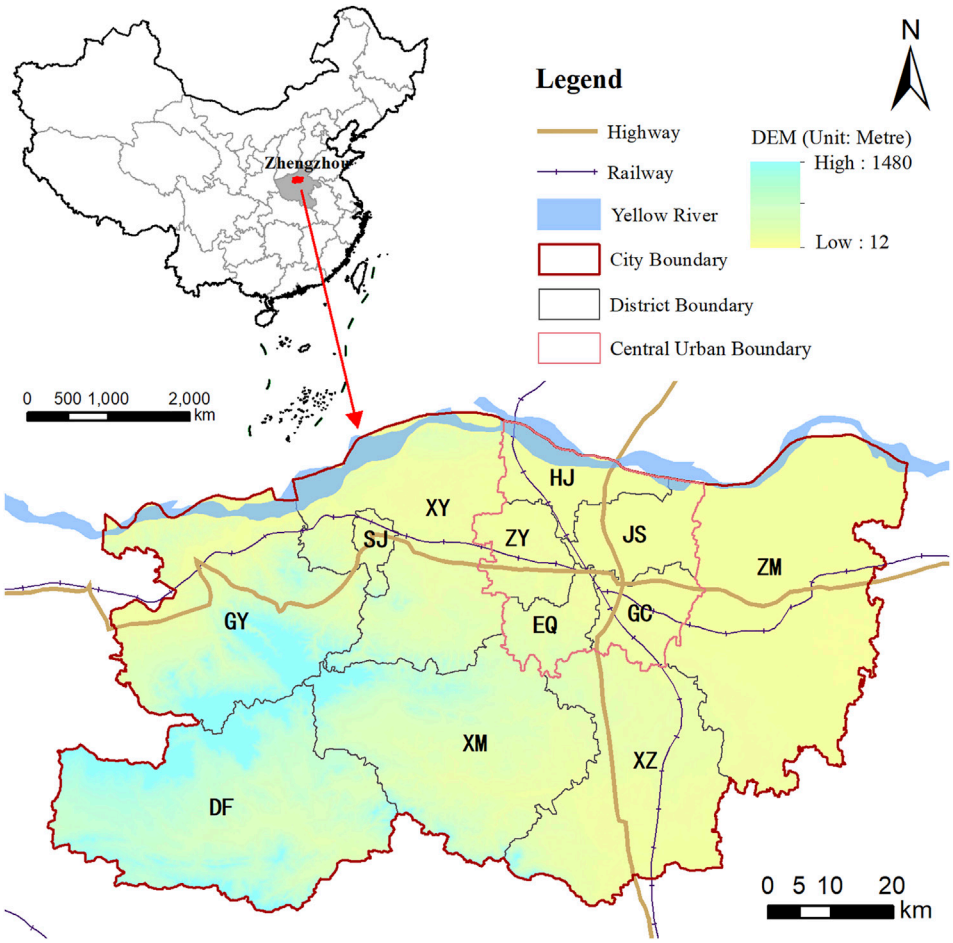

FIGURE 1 | Location and administrative districts of Zhengzhou.

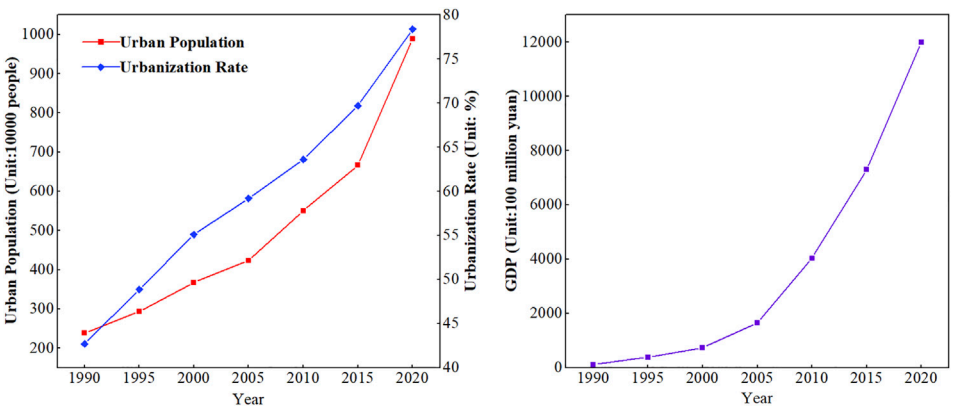

FIGURE 2 | Socioeconomic development of Zhengzhou from 1990 to 2020.

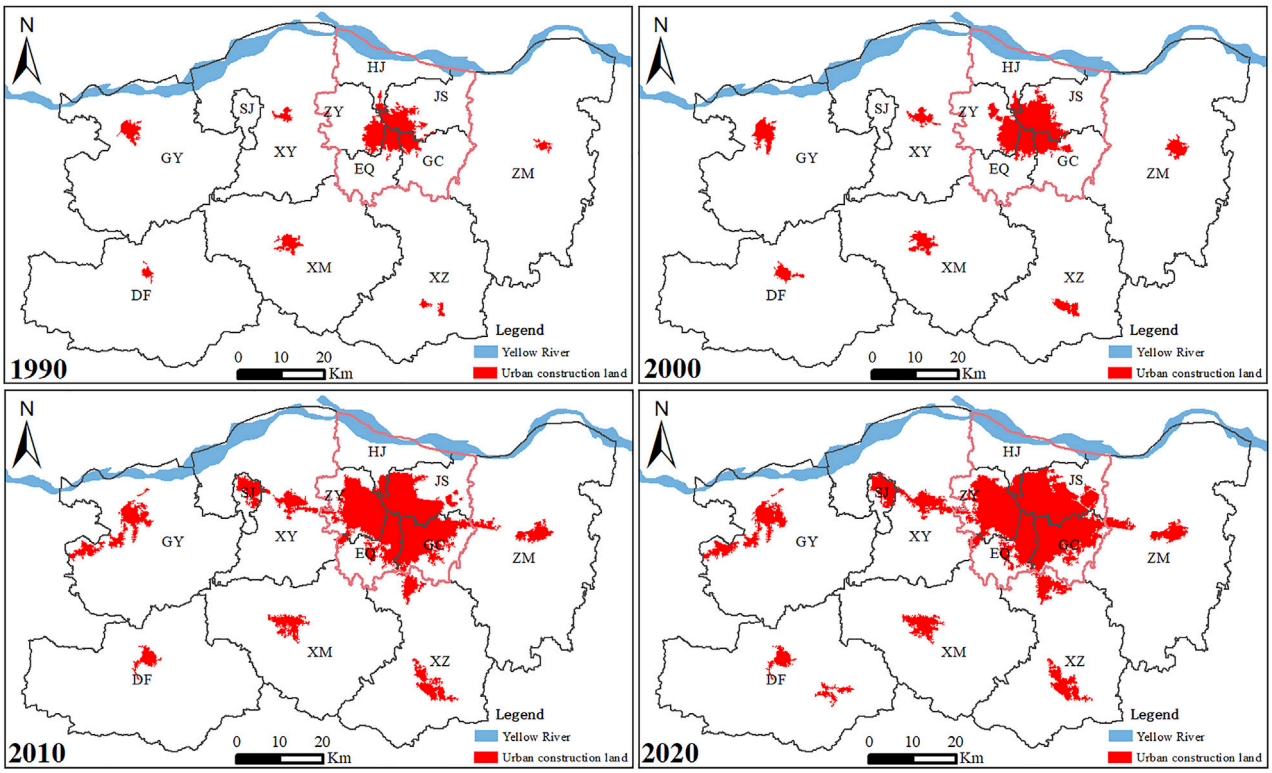

FIGURE 3 | Spatial allocation of urban construction land in 1990, 2000, 2010, and 2020.

continue to accelerate, and Zhengzhou's urbanization is still in the stage of rapid development.

2.2 Data

This study collected multi-temporal remote sensing images (Landsat TM/ETM+) and obtained land use and land cover (LUCC) data at the time nodes of 1990, 1995, 2000, 2005, 2010, 2015, and 2020, with a spatial resolution of 30 m. According to the LUCC classification system proposed by the Institute of Geographic Sciences and Natural Resources Research of the Chinese Academy of Sciences, with the use of supervised classification and human–computer interaction interpretation to extract information, the interpreted land use types were divided into 6 categories and 25 subcategories (Liu et al., 2003). After quality inspection and data integration, the comprehensive evaluation accuracy of land use types reached more than 94.3%. The urban construction land defined by this research refers to the urban land used for construction such as industrial and mining land, residential land, and roads. The urban expansion monitoring process of Zhengzhou was based on LUCC maps from 1990 to 2020 (**Figure 3**). The socioeconomic data used were mainly derived from the annual socioeconomic statistics published by the official websites of the national-, provincial-, and prefecture-level municipal statistical departments.

2.3 Methods

2.3.1 Average Annual Expansion Index

The urban expansion index refers to the percentage of the growth area of urban construction land in its original urban construction land area within a certain period. A large index value corresponds to fast urban expansion. This study uses the average annual urban expansion index (AAEI) to analyze the characteristics of urban expansion in Zhengzhou. The specific calculation formula is as follows:

$$I = \frac{1}{n} \times \frac{U_j - U_i}{U_i} \times 100, \quad (1)$$

where I refers to the AAEI; U_i and U_j represent the area of urban construction land in the base period and the end period of the study period, respectively; and n is the number of years in the period.

The AAEI was used to analyze the three phases of urban expansion in the various districts of Zhengzhou from 1990 to 2000, 2000 to 2010, and 2010 to 2020. According to the urban expansion characteristics of each district, urban expansion was divided into three types: low-, medium-, and high-speed expansion based on the AAEI value ranges of 0–5, 5–10, and >10, respectively.

2.3.2 Urban Expansion Elasticity Index

The urban expansion elasticity index is mainly divided into the man-land elasticity index and the economic-land elasticity

index. Urban construction land is the carrier of urban residents' life and economic activities. The carrying population and economic scale are important indicators to measure the rationality of urban expansion. The urban expansion man-land elasticity index refers to the ratio of the growth rate of the urban construction land area to the growth rate of the urban population during the study period; the urban expansion economic-land elasticity index refers to the ratio of the regional GDP growth rate to the growth rate of the urban construction land area within the study period. The specific calculation formulas are as follows:

$$P_{EI} = \frac{\left(U_j - U_i\right)/U_i}{\left(P_j - P_i\right)/P_i}, \tag{2}$$

$$G_{EI} = \frac{\left(G_j - G_i\right)/G_i}{\left(U_j - U_i\right)/U_i}, \tag{3}$$

where P_{EI} and G_{EI} refer to the man-land elasticity index and the economic-land elasticity index, respectively; P_i and P_j are the number of urban permanent residents in the base and end of the study period, respectively; and G_i and G_j are the GDP in the base and end of the study period, respectively.

2.3.3 Indexes of Urban Expansion Efficiency

The efficiency of urban expansion was mainly analyzed from two aspects: urban construction land intensive use and economic benefits. Per capita urban construction land area and per capita GDP are the most important indicators to measure urban construction land intensive use and economic benefits, respectively, and can also provide an important reference for evaluating whether urban expansion is reasonable. The index's calculation formulas are as follows:

$$PA = UCLA/UP, \tag{4}$$

$$PE = GDP/UCLA, \tag{5}$$

where *PA* and *PE* refer to the per capita urban construction land area and per capita GDP, respectively; *UCLA* is the urban construction land area; *UP* is the urban population; and *GDP* is the gross domestic product.

3 RESULTS

3.1 Spatiotemporal Characteristics of Urban Expansion

3.1.1 Temporal Characteristics of Urban Expansion

According to the statistical results of land use data from Landsat TM/ETM + image interpretation, from 1990 to 2020, the area of urban construction land in Zhengzhou increased from 168.23 to 751.26 km^2, with an increase rate of 346.57% and an average annual increase of 19.43 km^2. During the study period, Zhengzhou's urban construction land showed a "steady-fast-slow" expansion trend (**Figure 4**). The growth rate from 1990 to 2000 was relatively stable, with an average annual growth rate of 5.36%; from 2000 to 2010 was a period of rapid growth, with an average annual growth rate of 14.4%; and from 2010 to 2020, the growth rate gradually slowed down, with an average annual growth rate of 1.91%. Especially during 2015–2020, the average annual growth rate is only 0.38%, which was the lowest in 1990–2020.

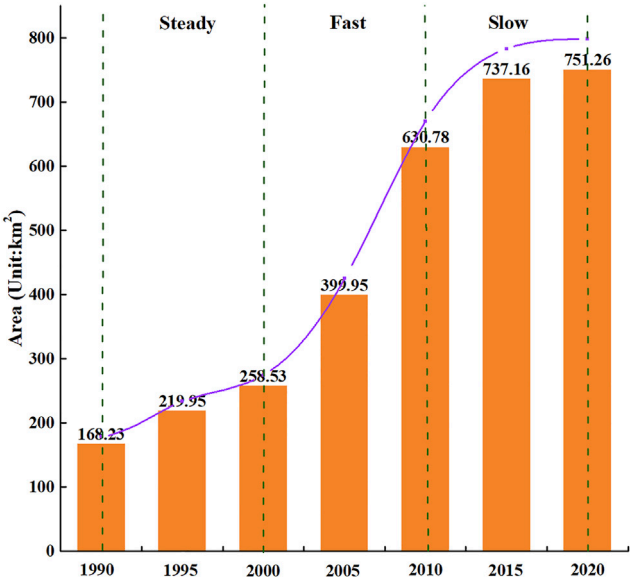

FIGURE 4 | The process of urban construction land expansion from 1990 to 2020.

3.1.2 Spatial Characteristics of Urban Expansion

The data on urban construction land in Zhengzhou in 1990, 2000, 2010, and 2020 were extracted, and the expansion of urban construction land in Zhengzhou from 1990 to 2020 was obtained by the spatial overlay analysis (**Figure 5**). The urban expansion in Zhengzhou has obvious spatial differences. The urban expansion of the central city was mainly in three directions: east, south, and west, with the east and south having a larger expansion and being the main areas of urban development in Zhengzhou. The urban development space was limited, and the expansion was small during the study period because of the obstruction of the Yellow River in the north. In Xinzheng, Xinmi, Xingyang, and Zhongmu, which are adjacent to the central urban area, the urban expansion direction was mainly toward the central urban area, indicating that the urban development in these areas was obviously driven by the central urban area, and their urban development space was gradually integrated with the central urban area. The urban expansion direction of Gongyi in the outer suburbs was mainly to the west. The urban expansion directions were diverse, and new urban spaces appeared in the later stage of the study because of the influence of the mountains in Dengfeng. The north and southwest of the central urban area were difficult to develop because of the restrictions by geological factors such as the Yellow River basin and the mountainous terrain. Most of the available areas in the central urban area have been developed, and the urban expansion space is faced with a shortage.

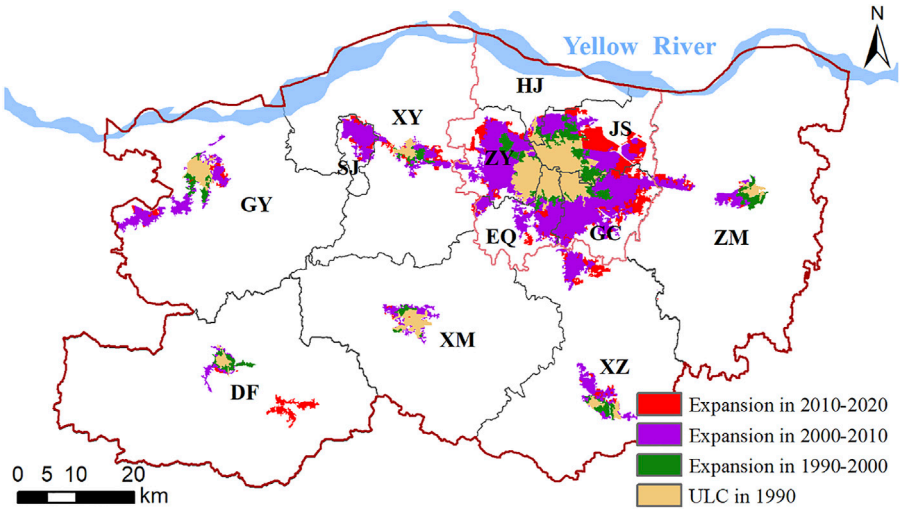

FIGURE 5 | Distribution of urban construction land (UCL) expansion from 1990 to 2020.

TABLE 1 | Characteristics of urban construction land expansion from 1990 to 2020.

Region	1990/km^2	2020/km^2	Growth area/km^2	AAEI	Type
Erqi	19.61	68.89	49.28	8.38	Medium speed
Zhongyuan	28.94	122.97	94.04	10.83	High speed
Guancheng	19.01	135.58	116.57	20.44	High speed
Huiji	5.03	11.15	6.12	4.05	Low speed
Jinshui	40.49	141.78	101.29	8.34	Medium speed
Shangjie	0.00	27.84	27.84	∞	High speed
Xinzheng	6.18	57.97	51.80	27.96	High speed
Xingyang	7.18	36.81	29.63	13.75	High speed
Xinmi	15.13	27.05	11.92	2.63	Low speed
Gongyi	15.85	59.10	43.25	9.10	Medium speed
Dengfeng	4.91	28.52	23.61	16.02	High speed
Zhongmo	5.90	33.60	27.70	15.66	High speed

From 1990 to 2020, Guancheng and Jinshui had the largest urban expansion areas of 116.57 and 101.29 km^2, respectively. Except for Shangjie, the largest average annual expansion indexes were those for Xinzheng and Guancheng, reaching 27.96 and 20.44, respectively. Seven high-speed expansion regions, three medium-speed expansion regions, and two low-speed expansion regions were developed during this period (**Table 1**). The urban expansion rate in the central urban area was generally low, and the areas with a larger expansion rate were mainly in the outer suburbs. Most of the districts experienced rapid urban expansion, among which the central urban area had the largest expansion, and its urban expansion area accounted for 63% of Zhengzhou.

3.1.3 Land Use Effects of Urban Expansion

From 1990 to 2020, the urban expansion area of Zhengzhou was 587.84 km^2. The land occupied by urban expansion was mainly arable land, with an area of 471.88 km^2, accounting for 80.27%; followed by construction land with an occupied area of 77.02 km^2, accounting for 13.1%; and then followed waters, with an occupied area of 20.19 km^2, accounting for 3.44%. Spatially, in addition to arable land, a large amount of waters (mainly rivers and lakes) in the northeast and west of the central urban area is occupied (**Figure 6**). The conversion of rural residential land to urban construction land was mainly concentrated in Shangjie and Gongyi.

Although arable land was the main type of land occupied by urban expansion, its proportion dropped from 88.89% in 1990–2000 to 69.44% in 2010–2020; the proportion of construction land occupied by urban expansion increased from 10.34% in 1990–2000 to 17.62% in 2010–2020. The proportion of occupied waters grew the fastest, from 0.69% in 1990–2000 to 15.8% in 2010–2020. This finding shows that with the strengthening of cultivated land protection, urban expansion reduces the occupation of cultivated land, and more land is converted from village land to urban land (**Table 2**). However, the occupation of water bodies has increased rapidly, indicating that the erosion of ecological land by urban expansion has intensified, and caution needs to be taken to avoid damage to the natural ecology, especially water ecology.

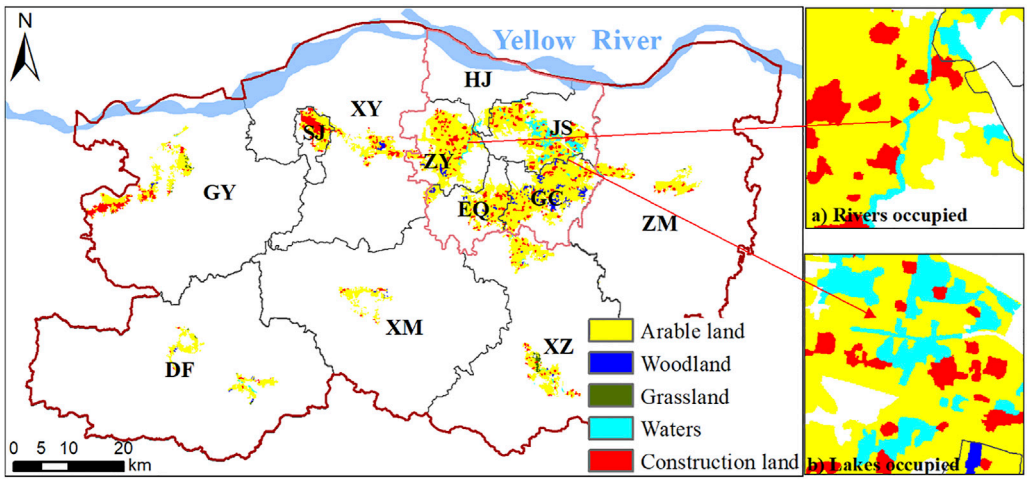

FIGURE 6 | Distribution of the land occupied by urban expansion.

TABLE 2 | Changes in the structure of the urban expansion sources (Units: km^2, %).

Type	1990–2000		2000–2010		2010–2020	
	Area	Proportion	Area	Proportion	Area	Proportion
Arable land	80.27	88.89	286.09	73.61	85.02	69.44
Woodland	0.00	0.00	11.37	2.93	0.00	0.00
Grassland	0.00	0.00	2.61	0.67	0.04	0.04
Waters	0.69	0.76	6.97	1.79	15.80	12.91
Construction land	9.34	10.34	81.62	21.00	21.58	17.62

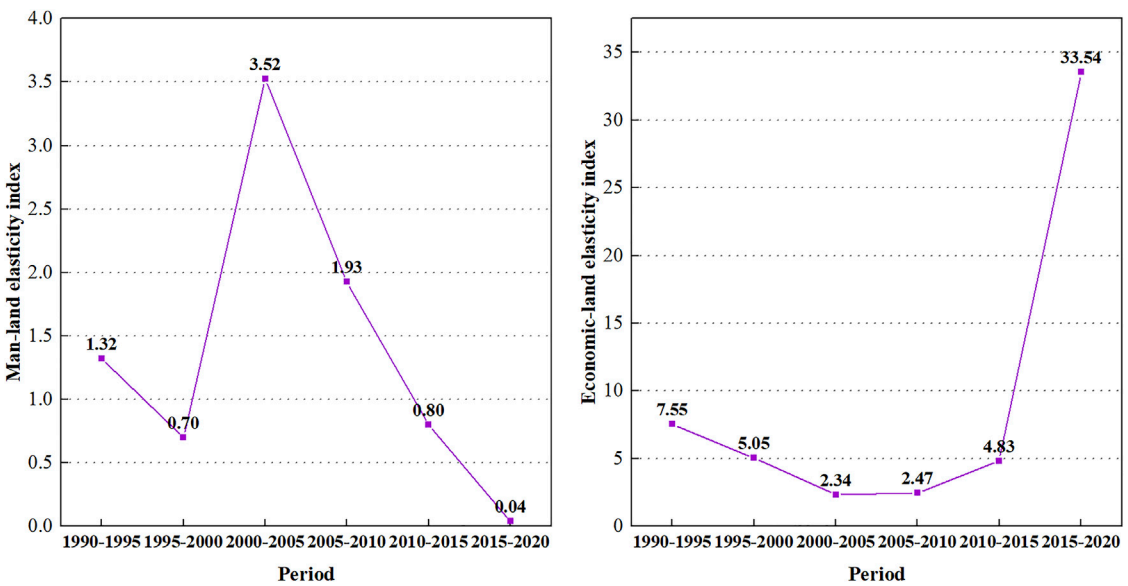

FIGURE 7 | Variation of elastic coefficient of urban expansion from 1990 to 2020.

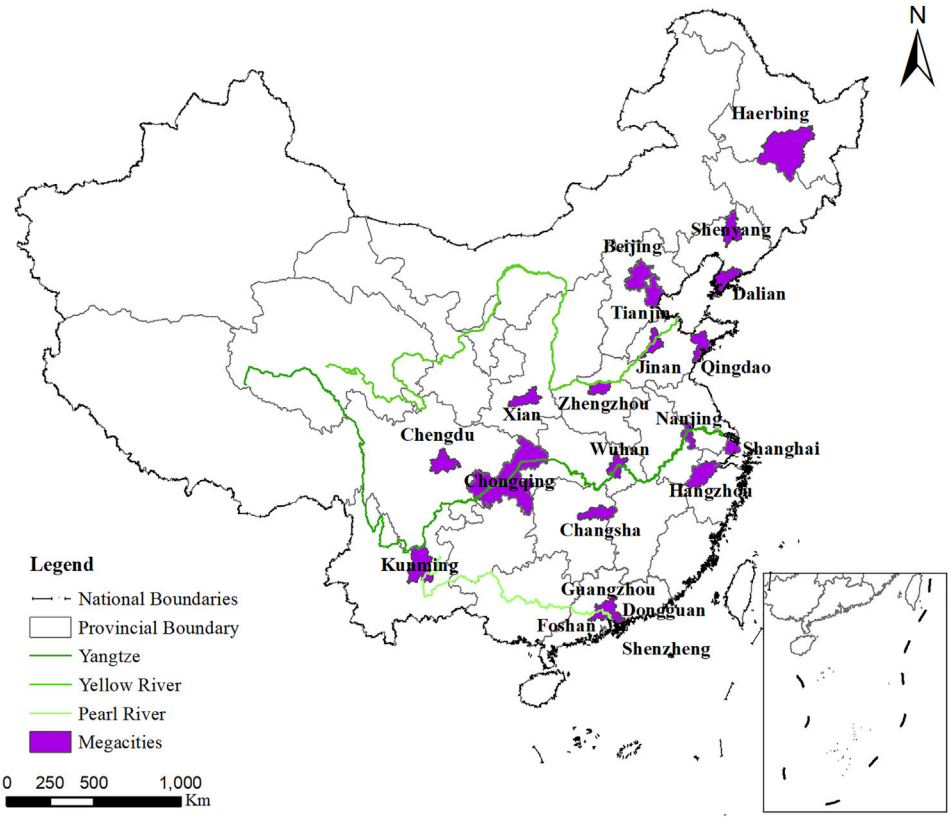

FIGURE 8 | Location of China's megacities.

3.2 Rationality of Urban Expansion in Zhengzhou

3.2.1 Elasticity Indexes of Urban Expansion

As shown in **Figure 7**, the man-land elasticity index of urban expansion increased from 1.32 to the peak of 3.52 in 2000–2005 and then continued to decrease, indicating that Zhengzhou's urban expansion was generally too rapid relative to the population growth from 1990 to 2010, and urban land use was relatively extensive. After 2010, the elasticity index was lower than 1 and reached a very low value of 0.04 in 2015–2020. The urban expansion rate began to be lower than the urban population growth rate, the population density of urban land gradually increased, and land use tended to be intensive. The economic land elasticity index of urban expansion showed a "U" shape. During the study period, Zhengzhou's GDP growth rate was always greater than the urban expansion rate. The elasticity index dropped from 7.55 to 2.34 during 1990–2005 and then began to grow slowly, increasing to 33.54 during 2015–2020. This finding shows that the economic benefits of urban land use continued to improve. Although the rate of improvement declined during 1990–2005, it began to accelerate significantly thereafter, and the economic benefits of urban land use increased significantly in the later period.

3.2.2 Comparative Analysis Among Similar Megacities

According to China's urban classification standards, cities with a population of more than 5 million in the central urban area are considered megacities (SCC, 2014). In 2020, China had 21 megacities, which are mainly located in central and eastern China (**Figure 8**). These megacities account for 7.5% of China's area, but they carry 20.7% of the population and generate 33.1% of the GDP. These megacities are the core force that supports China's economic development and participates in international competition.

3.2.2.1 Area of Urban Construction Land Expansion

From 1990 to 2020, Zhengzhou's urban construction land area has always been in the middle of 21 megacities, but the ranking continues to increase, from 14th in 1990 to 10th in 2020 (**Figure 9**). This finding shows that the growth rate of urban construction land in Zhengzhou is higher than the average growth rate of China's megacities. During the study period, Zhengzhou's urban construction land area increased by 583.03 km^2, which was 13% higher than the average growth area of 515.97 km^2 in megacities. The expansion of urban construction land in Zhengzhou was growing rapidly in megacities.

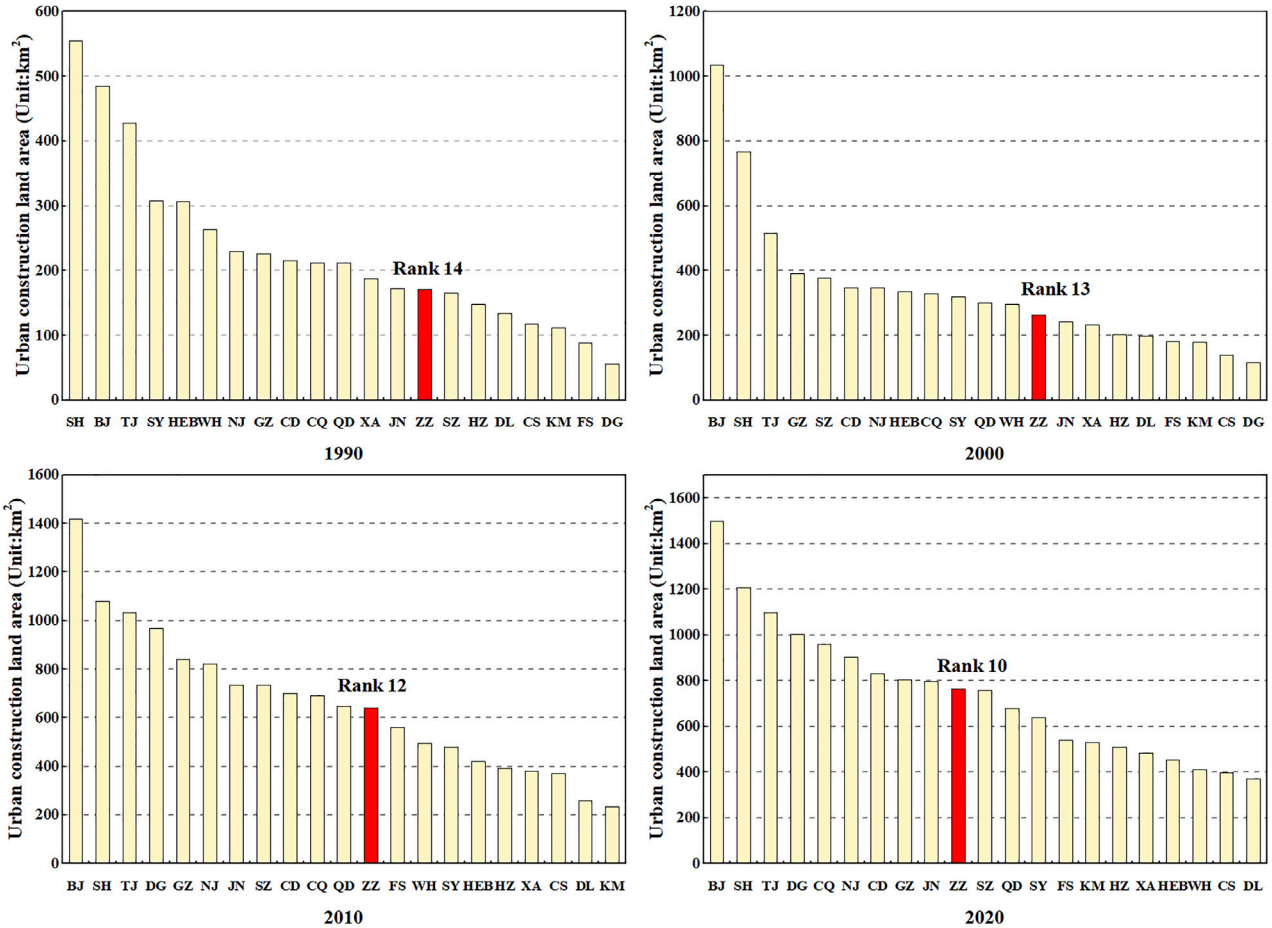

FIGURE 9 | Urban construction land area of China's megacities from 1990 to 2020. BJ, Beijing; SH, Shanghai; GZ, Guangzhou; SZ, Shenzhen; TJ, Tianjin; DG, Dongguan; NJ, Nanjing; CQ, Chongqing; SY, Shenyang; FS, Foshan; JN, Jinan; CD, Chengdu; ZZ, Zhengzhou; XA, Xian; HZ, Hangzhou; WH, Wuhan; QD, Qingdao; KM, Kunming; HEB, Haerbing; DL, Dalian; CS, Changsha.

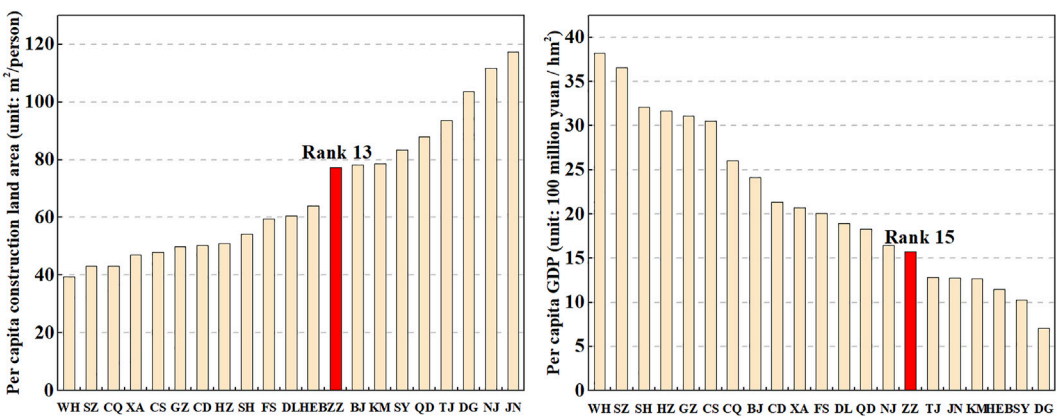

FIGURE 10 | Efficiency of urban construction land of China's megacities in 2020. BJ, Beijing; SH, Shanghai; GZ, Guangzhou; SZ, Shenzhen; TJ, Tianjin; DG, Dongguan; NJ, Nanjing; CQ, Chongqing; SY, Shenyang; FS, Foshan; JN, Jinan; CD, Chengdu; ZZ, Zhengzhou; XA, Xian; HZ, Hangzhou; WH, Wuhan; QD, Qingdao; KM, Kunming; HEB, Haerbing; DL, Dalian; CS, Changsha.

3.2.2.2 Efficiency of Urban Construction Land

In 2020, Zhengzhou's per capita urban construction land area was 77.21 m^2, and the per capita GDP was 1.574 billion yuan/hm^2, ranking 13th and 15th among China's megacities, respectively (**Figure 10**), which are significantly lower than the ranking of construction land area. Although Zhengzhou has experienced relatively rapid expansion among China's megacities, its land use efficiency has lagged behind the average level. The intensive use and economic benefits of urban construction land in Zhengzhou reached only 50.97 and 41.22% of the top megacities in China, respectively, indicating that the urban land use efficiency remains unsatisfactory. Under the increasing pressure of land supply and environmental protection faced by urban development, the urban expansion model of Zhengzhou needs to transform from the past spatial sprawl to one with improved land use efficiency.

4 DISCUSSION

4.1 Climate Effects of Urban Expansion

Previous studies on the negative effects of urban expansion mainly focused on the loss of arable land, landscape destruction, and deterioration of human settlements, often ignoring the climatic lag effects of urban expansion (Camacho-valdez et al., 2014). The occupation of arable land by urban expansion has been curbed because of China's increasingly stringent arable land protection policy. However, wetlands and grasslands were usually regarded as unused land by urban managers without protection and were freely occupied by urban expansion. The spatial analysis of Zhengzhou urban expansion shows that a large number of rivers and lakes in Zhengzhou, especially in the central urban area, have been occupied. The area of waters in the central urban area of Zhengzhou decreased from 95.58 km^2 in 1990 to 66.89 km^2 in 2020, with a reduction rate of 42.89%. The substantial reduction of the water body area has destroyed the urban permeable surface, which not only further aggravates the water shortage in Zhengzhou as a city in arid regions of the northern hemisphere but also weakens the city's ability to withstand floods.

Zhengzhou experienced a historically rare catastrophic rainstorm and urban waterlogging in the summer of 2021, which brought major property losses and casualties (Zhang et al., 2021). In addition to the natural extreme rainstorm factors, the occupation of rivers and lakes by urban expansion made the rainwater unable to be discharged in time, which may also play an important role in the worsening of this disaster. Emerging megacities are still in the stage of rapid urban development, and the negative climate effects of urban expansion may not yet appear. Research on the prediction of climate disasters that may be caused by improper urban expansion should be carried out to take appropriate countermeasures in advance. The climate effects of urban expansion should also attract the attention of managers and planners of other emerging megacities in the world.

4.2 Urban Expansion Evaluation System

Rapid population and economic growth in emerging megacities have driven urban expansion, while also making urban land use more intensive and efficient. Therefore, if the urban expansion is evaluated based on the city's conditions only, then the results of urban expansion evaluation are mostly satisfied, and finding the problem of urban expansion is difficult (Tan et al., 2010). As megacities face greater difficulty with land supply and more severe environmental constraints, there should be higher standards for urban land-use. Comparative analysis with similar or higher-level megacities may have different conclusions from the evaluation based on the city's conditions.

This study adopts an urban expansion evaluation method that combines socioeconomic coupling analysis with a comparison of similar cities. The socioeconomic coupling analysis shows that the economic benefits and intensive utilization of Zhengzhou's urban land use have improved, and urban land use has developed in a positive direction in the process of urban expansion. However, in comparison with other similar megacities in China, Zhengzhou's urban expansion was too fast, and its economic benefits and intensive utilization were relatively low. This comprehensive urban expansion evaluation method facilitates the detection of urban expansion problems and avoids the one-sidedness of the evaluation conclusion, which provides important insights into the urban management of emerging megacities.

4.3 Recommendations for Future Study

By analyzing the spatiotemporal characteristics and rationality of urban expansion in Zhengzhou, this study strengthens the cognition of urban expansion in emerging megacities and provides significant reference for cities undergoing rapid development and growth. However, some problems need to be explored in future research. First, systematic research should be conducted on megacity groups, rather than just a single or a few cities. The expansion of megacities at different development stages shows obvious differences, and the study of the urban expansion of megacity groups is helpful for exploring the urban expansion mechanism of megacities. Second, research on the relationship between urban expansion and meteorological disasters should be strengthened. Unreasonable human activities in the process of urban expansion may be the cause of meteorological disasters. Understanding the relationship between the two can help in the implementation of countermeasures.

5 CONCLUSION

Taking Zhengzhou as an example, this study analyzes the spatiotemporal characteristics of urban expansion in China's emerging megacities and the rationality for urban expansion on the basis of the man-land elasticity index, the economic-land elasticity index, and a comparison with other megacities. It then summarizes urban expansion problems and presents relevant suggestions. These findings have important reference significance for curbing the disorderly sprawl of

megacities, realizing smart management of megacities and promoting regional sustainable development. The main conclusions were as follows:

1) During the study period, the urban expansion of Zhengzhou showed a trend of "steady–fast–slow." From 1990 to 2000, the urban expansion of Zhengzhou was relatively stable, and from 2000 to 2010, it entered a stage of rapid expansion. After 2010, the urban expansion of Zhengzhou entered a slow stage due to the constraints on the expansion of the central urban area.

2) Zhengzhou urban expansion has obvious imbalance and spatial disorder. The growth area of urban construction land in the central urban area, which accounts for only 13.44% of Zhengzhou, accounts for 63% of the city's total. The suburban urban expansion was more disorderly, and the central urban area expansion was limited by the Yellow River in the north and the mountainous areas in the southwest. The space for urban development is insufficient. In the future, urban development should transform from single-core development of the central urban area to coordinated development of the central urban area and the suburbs.
3) Urban expansion has gradually increased the occupation of water bodies, and the ecological problems of urban expansion have become prominent. Although the area occupied by waters was relatively small during the urban expansion of Zhengzhou, its proportion has since increased significantly. With Zhengzhou being a rapidly developing emerging megacity with relative water shortage, the occupation of ecological land such as waters may damage the carrying capacity of urban water resources and cause a series of natural ecological problems.
4) Zhengzhou's urban expansion was inefficient. Although the utilization intensity and economic benefits of Zhengzhou's urban construction land have continued to improve, compared with other megacities in China, Zhengzhou's urban expansion was too fast, and the urban construction land utilization intensity and economic benefits were relatively low.

DATA AVAILABILITY STATEMENT

The original contributions presented in the study are included in the article/Supplementary Material, further inquiries can be directed to the corresponding author.

AUTHOR CONTRIBUTIONS

Conceptualization and writing: EC and HH; methodology and software: EC and QB; data acquisition: QB; and analysis and interpretation of data: JL.

FUNDING

This research was funded by the Henan Philosophy and Social Science Planning Project (no. 2019CHH078), Humanities and Social Sciences Research Projects of Higher Education Institutions in Henan Province (no. 2011-ZZJH-157), Zhengzhou Soft Science Research Project (no. 2020RKXF0104), and Major consulting and research projects of institute local cooperation of Chinese Academy of Engineering(no. 2021HENZDA04).

REFERENCES

Bagan, H., and Yamagata, Y. (2014). Land-cover Change Analysis in 50 Global Cities by Using a Combination of Landsat Data and Analysis of Grid Cells. *Environ. Res. Lett.* 9 (6), 064015. doi:10.1088/1748-9326/9/6/064015

Buyantuyev, A., Wu, J., and Gries, C. (2015). Multiscale Analysis of the Urbanization Pattern of the Phoenix Metropolitan Landscape of USA: Time, Space and Thematic Resolution. *Landscape Urban Plann.* 94 (3-4), 206–217. doi:10.1016/j.landurbplan.2009.10.00.5

Cai, E., Liu, Y., Li, J., and Chen, W. (2020). Spatiotemporal Characteristics of Urban-Rural Construction Land Transition and Rural-Urban Migrants in Rapid-Urbanization Areas of Central China. *J. Urban Plann. Dev.* 146 (1), 05019023. doi:10.1061/(ASCE)UP.1943-5444.0000551

Camacho-Valdez, V., Ruiz-Luna, A., Ghermandi, A., Berlanga-Robles, C. A., and Nunes, P. A. L. D. (2014). Effects of Land Use Changes on the Ecosystem Service Values of Coastal Wetlands. *Environ. Manage.* 54 (4), 852–864. doi:10.1007/s00267-014-0332-9

Chen, M., Liu, W., and Tao, X. (2013). Evolution and Assessment on China's Urbanization 1960-2010: Under-urbanization or Over-urbanization? *Habitat Int.* 38 (4), 25–33. doi:10.1016/j.habitatint.2012.09.007

Chien, H., and Saito, O. (2021). Evaluating Social-Ecological Fit in Urban Stream Management: The Role of Governing Institutions in Sustainable Urban Ecosystem Service Provision. *Ecosystem Serv.* 49, 101285. doi:10.1016/j.ecoser.2021.101285

China National Bureau of Statistics (CNBS) (2020). Major Figures on 2020 Pupulation Census of China. AvaliableAt: http://www.stats.gov.cn/tjsj/pcsj/rkpc/d7c/202111/P020211126523667366751.pdf (Retreved December 22, 2021).

Dai, J., Gao, X., and Du, S. (2010). Expansion of Urban Space and Land Use Control in the Process of Urbanization: An Overview. *Chin. J. Popul. Resour. Environ.* 8 (3), 73–82. doi:10.1080/10042857.2010.10684994

Gren, Å., and Andersson, E. (2018). Being Efficient and green by Rethinking the Urban-Rural divide-Combining Urban Expansion and Food Production by Integrating an Ecosystem Service Perspective into Urban Planning. *Sust. Cities Soc.* 40, 75–82. doi:10.1016/j.scs.2018.02.031

Hamidi, S., and Ewing, R. (2014). A Longitudinal Study of Changes in Urban Sprawl between 2000 and 2010 in the United States. *Landscape Urban Plann.* 128, 72–82. doi:10.1016/j.landurbplan.2014.04.021

He, C., Liu, Z., Gou, S., Zhang, Q., Zhang, J., and Xu, L. (2018). Detecting Global Urban Expansion over the Last Three Decades Using a Fully Convolutional Network. *Environ. Res. Lett.* 14 (3), 034008. doi:10.1088/1748-9326/aaf936

Hecht, R., Behnisch, M., and Herold, H. (2020). Innovative Approaches, Tools and Visualization Techniques for Analysing Land Use Structures and Dynamics of Cities and Regions (Editorial). *J. Geovisualization Spat. Anal.* 4 (2), 1–4. doi:10.1007/s41651-020-00060-9

Hu, X., Zhou, W., Qian, Y., and Yu, W. (2017). Urban Expansion and Local Land-Cover Change Both Significantly Contribute to Urban Warming, but Their Relative Importance Changes over Time. *Landscape Ecol.* 32 (4), 763–780. doi:10.1007/s10980-016-0484-5

Jiao, L., Dong, T., and Yanyan, G. U. (2016). The Spatial Resilience of Prefecture-Level Cities in China from 2000 to 2012. *Resour. ence* 38 (7), 1254–1265. doi:10.18402/resci.2016.07.07

Kantakumar, L. N., Kumar, S., and Schneider, K. (2016). Spatiotemporal Urban Expansion in Pune metropolis, India Using Remote Sensing. *Habitat Int.* 51, 11–22. doi:10.1016/j.habitatint.2015.10.007

Khamchiangta, D., and Dhakal, S. (2021). Future Urban Expansion and Local Climate Zone Changes in Relation to Land Surface Temperature: Case of Bangkok Metropolitan Administration, Thailand. *Urban Clim.* 37, 100835. doi:10.1016/j.uclim.2021.100835

Kovács, Z., Farkas, Z. J., Egedy, T., Kondor, A. C., Szabó, B., Lennert, J., et al. (2019). Urban Sprawl and Land Conversion in post-socialist Cities: The Case of Metropolitan Budapest. *Cities* 92, 71–81. doi:10.1016/j.cities.2019.03.018

Lafortezza, R., and Sanesi, G. (2019). Nature-based Solutions: Settling the Issue of Sustainable Urbanization. *Environ. Res.* 172, 394–398. doi:10.1016/j.envres.2018.12.063

Li, J., Zhang, W., Sun, T., and Zhang, A. (2014). Characteristics of Clustering and Economic Performance of Urban Agglomerations in China. *Acta Geographica Sinica* 69 (4), 474–484. doi:10.11821/dlxb201404004

Liu, G., Li, J., and Nie, P. (2022). Tracking the History of Urban Expansion in Guangzhou (China) during 1665-2017: Evidence from Historical Maps and Remote Sensing Images. *Land Use Policy* 112, 105773. doi:10.1016/j.landusepol.2021.105773

Liu, J., Liu, M., Zhuang, D., Zhang, Z., and Deng, X. (2003). Study on Spatial Pattern of Land-Use Change in China during 1995–2000. *Sci. China* 46, 374–384. doi:10.1360/03yd9033

Liu, M., Tian, H., Chen, G., Ren, W., Zhang, C., and Liu, J. (2008). Effects of Land-Use and Land-Cover Change on Evapotranspiration and Water Yield in China during 1900-20001. *J. Am. Water Resour. Assoc.* 44 (5), 1193–1207. doi:10.1111/j.1752-1688.2008.00243.x

Naitonal Development, and Reform Commission (NDRC) (2017). Reply of the National Development and Reform Commission on Supporting Zhengzhou to Build a National central City. AvaliableAt: https://www.ndrc.gov.cn/xwdt/ztzl/xxczhjs/ghzc/201701/t20170125_972047.html?code=&state=123 (Retreved December 23, 2021).

Rusk, D. (1993). *Cities without Suburbs*. Washington: Woodrow Wilson Center Press.

Sassen, S. (1994). The Urban Complex in a World Economy. *Int. Soc. Sci. J.* 46 (139), 43–62.

Schneider, A., and Woodcock, C. E. (2014). Compact, Dispersed, Fragmented, Extensive? A Comparison of Urban Growth in Twenty-Five Global Cities Using Remotely Sensed Data, Pattern Metrics and Census Information. *Urban Stud.* 45 (3), 659. doi:10.1177/0042098007087340

State Council of China (2014). Circular of the State Council on Adjusting the Classification Standards of the City Size. AvaliableAt: http://www.gov.cn/zhengce/content/2014-11/20/content_9225.htm (Retreved December 29, 2021).

Tan, K. C., Lim, H. S., MatJafri, M. Z., and Abdullah, K. (2010). Landsat Data to Evaluate Urban Expansion and Determine Land Use/land Cover Changes in Penang Island, Malaysia. *Environ. Earth Sci.* 60 (7), 1509–1521. doi:10.1007/s12665-009-0286-z

Tayyebi, A., Perry, P. C., and Tayyebi, A. H. (2014). Predicting the Expansion of an Urban Boundary Using Spatial Logistic Regression and Hybrid Raster–Vector Routines with Remote Sensing and GIS. *InternationaL J. Geographical Inf. Sci.* 28 (3-4), 639–659. doi:10.1080/13658816.2013.845892

Tian, L., Li, Y., Yan, Y., and Wang, B. (2017). Measuring Urban Sprawl and Exploring the Role Planning Plays: A Shanghai Case Study. *Land Use Policy* 67, 426–435. doi:10.1016/j.landusepol.2017.06.002

Tong, L. (2020). A Review on Definitions and Measurements for Urban Expansion. *World Reg. Stud.* 29 (4), 762–772. doi:10.17576/geo-2021-1702-10

Xu, H., Ding, F., and Wen, X. (2009). Urban Expansion and Heat Island Dynamics in the Quanzhou Region, China. *IEEE J. Sel. Top. Appl. Earth Observations Remote Sensing* 2 (2), 74–79. doi:10.1109/JSTARS.2009.2023088

Yao, S., Chen, S., Wu, J., Zhang, Y., and Chan, R. (2009). Spatial Expansion Patterns of Chinese Big Cities the Case of Suzhou. *Scientia Geographica Sinica* 29 (1), 15–21. doi:10.1007/978-3-642-00205-2_9

Yue, W., Zhang, L., and Liu, Y. (2016). Measuring Sprawl in Large Chinese Cities along the Yangtze River *via* Combined Single and Multidimensional Metrics. *Habitat Int.* 57, 43–52. doi:10.1016/j.habitatint.2016.06.009

Zhang, W., Liao, Q., Yang, S., Zhang, X., Zhang, C., Xiang, M., et al. (2021). Thoughts and Inspirations: Urban Flood Risk Management Inferred from Zhengzhou Flood Model. *China Flood Drought Manag.* 31 (9), 1–4. doi:10.16867/j.issn.1673-9264.2021251

Zhang, Z., Liu, F., Zhao, X., Wang, X., Shi, L., Xu, J., et al. (2018). Urban Expansion in China Based on Remote Sensing Technology: A Review. *Chin. Geographical Sci.* 28 (05), 727–743. doi:10.1007/s11769-018-0988-9

Zhao, G., Zheng, X., Liu, Y., and Liu, F. (2017). Urban Expansion Steady-State index of Urban Expansion Based on Remote Sensing and GIS and its Applications. *Trans. Chin. Soc. Agric. Eng.* 33 (11), 272–281. doi:10.11975/j.issn.1002-6819.2017.11.035

Zhengzhou Bureau Of Statistics (2021). Zhengzhou City's Annual Statistics. AvaliableAt: http://tjj.zhengzhou.gov.cn/ndsj/index.jhtml (Retreved December 23, 2021).

Zhong, Y., Lin, A., He, L., Zhou, Z., and Yuan, M. (2020). Spatiotemporal Dynamics and Driving Forces of Urban Land-Use Expansion: A Case Study of the Yangtze River Economic Belt, China. *Remote Sensing* 12 (2), 287. doi:10.3390/rs12020287

Conflict of Interest: The authors declare that the research was conducted in the absence of any commercial or financial relationships that could be construed as a potential conflict of interest.

Publisher's Note: All claims expressed in this article are solely those of the authors and do not necessarily represent those of their affiliated organizations, or those of the publisher, the editors, and the reviewers. Any product that may be evaluated in this article, or claim that may be made by its manufacturer, is not guaranteed or endorsed by the publisher.

Copyright © 2022 Cai, Bi, Lu and Hou. This is an open-access article distributed under the terms of the Creative Commons Attribution License (CC BY). The use, distribution or reproduction in other forums is permitted, provided the original author(s) and the copyright owner(s) are credited and that the original publication in this journal is cited, in accordance with accepted academic practice. No use, distribution or reproduction is permitted which does not comply with these terms.

frontiers | Frontiers in Environmental Science

ORIGINAL RESEARCH
published: 11 May 2022
doi: 10.3389/fenvs.2022.907383

Identification and Analysis of Industrial Land in China Based on the Point of Interest Data and Random Forest Model

*Qingsong He and Xinyu Tang**

College of Public Administration, Huazhong University of Science and Technology, Wuhan, China

The purpose of this study was to provide a new concept and technical method for the large-scale identification of industrial land and analyze the distribution characteristics of industrial land in China. The following research methods are employed using the point of interest data and random forest model based on data accessibility, this study selected 2015 data on Wuhan and Luoyang as training samples to identify the industrial land of China. Then, the proportion of industrial land in all 334 prefecture-level cities on the Chinese mainland was calculated, and the spatial pattern was analyzed. The results show that: 1) by comparing multiple experiments and robustness analysis, the optimal parameter setting of the random forest model is obtained. According to the test of actual industrial land distribution in Wuhan city and Luoyang city, the identification of industrial land in different scale cities by random forest model is accurate and effective. 2) From the perspective of spatial patterns, industrial land shows a "large aggregation and small scattering" distribution. 3) From the perspective of spatial distribution, the proportion of industrial land in these cities shows spatial aggregation. High–high aggregation areas were mainly distributed in North and Northeast China, and low–low aggregation areas were mainly located in West China. 4) From the perspective of related factors, industrial land was close to rivers, highways, and railway stations and had a relatively low correlation with the distribution of airports. Industrial land was located within approximately 10–60 km distance from the municipal government office. In terms of the proportion of industrial land, the proportion of industrial land is higher in the cities where the industrial land was closer to railway stations. However, when the industrial land in cities was closer to four other types of related factors (waters and lakes, major highways, airports, and municipal government stations), the share of industrial land is lower. In conclusion, the method based on the point of interest data and random forest model can accurately and effectively identify large-scale industrial land.

Keywords: POI data, random forest model, industrial land, spatial pattern analysis, associated factor analysis

OPEN ACCESS

Edited by:
Ying Jing,
Zhejiang University, China

Reviewed by:
Zuo Zhang,
Central China Normal University, China
Jiayu Wu,
Zhejiang University, China

****Correspondence:***
Xinyu Tang
2547728639@qq.com

Specialty section:
This article was submitted to Land Use Dynamics, a section of the journal Frontiers in Environmental Science

Received: *29 March 2022*
Accepted: *12 April 2022*
Published: *11 May 2022*

Citation:
He Q and Tang X (2022) Identification and Analysis of Industrial Land in China Based on the Point of Interest Data and Random Forest Model. Front. Environ. Sci. 10:907383. doi: 10.3389/fenvs.2022.907383

1 INTRODUCTION

Industry plays an important role in maintaining a steady growth of the national economy, and industrial land is the most basic natural resource to support industrial development. Industrial land refers to land that carries the production, operation, and service activities of economic entities in urbanized areas (Moomaw, 1978; Louw et al., 2012). With its unique social system, China's economy has developed rapidly and consequently. China has become the world's factory (Liu et al., 2014; Liu et al., 2018a, b). At the same time, China is also the only country that contains the whole industrial chain, which conveys a great advantage in international competition (Jcw et al., 2021). At present, there are two main forms of urban industrial land in China: industrial parks and scattered industrial land. In the context of the new normal economy, China has actively promoted the transformation and upgrading of the secondary industry, but the layout and planning of urban industrial land have not kept pace, resulting in problems such as waste of resources (Lai et al., 2020), destruction of the ecological environment (Yang et al., 2018), and a mismatch between industrial land and space (Zhang et al., 2020). Therefore, the scientific and effective identification and analysis of urban industrial land is of great significance to optimize the layout of urban industrial land, improve the scientificity of urban industrial land planning in the whole region, and promote China's industrial transformation and upgrading.

In the past, the identification of urban industrial land mainly used traditional land data and remote sensing image maps (Myint et al., 2011; Dankoub et al., 2012; Zhang and Du, 2015). The artificial statistical survey, expert qualitative, remote sensing interpretation, and other methods were used for this identification (Murphy and Vance, 1954; Davies, 1959; Eklund et al., 1998); however, all these methods are problematic as they are time-consuming, laborious, and lack timeliness. Single remote sensing image data can only identify urban construction land in the process of large-scale recognition, and cannot further refine the spatial details of urban industrial land. Therefore, its application method must be further improved. The aforementioned identification methods are mostly based on a single city (or region), which cannot reflect the layout of urban industrial land on a larger scale, and different data (including years) and methods cannot enable case comparison. From the perspective of national conditions, although the quality and quantity of socio-economic data of developing countries (represented by China) have improved in recent years (Jean et al., 2016), there is still a lack of unified standard and complete data to conduct efficient research on the identification of industrial land within a country. Therefore, for large-scale industrial land recognition, a more effective method combined with remote sensing image data should be developed.

The development of geographic information technology, especially the application of big data (Toole et al., 2012; Long and Shen, 2015; He et al., 2018; Jo et al., 2020) and machine classification model (Wachtel et al., 2018; Li et al., 2019), provides new ideas for urban industrial land identification. Among big data commonly used in urban land research, point of interest (POI) data offers the advantages of wide coverage, large amount of data, and easy access (Ivan et al., 2016). POI data record the location information of physical point elements of various socio-economic departments, which is a more in-depth representation of the spatial distribution of socio-economic activity intensity and functional composite utilization (Mckenzie et al., 2015). Therefore, these data are widely used for the identification and analysis of urban land use types (Yuan et al., 2012; Zheng et al., 2014; Jiang et al., 2015). At present, research on urban land class recognition using POI data is mainly based on medium and small scales (Zhai et al., 2019), and a few large-scale studies have been conducted in China. Common classifiers include maximum likelihood estimation, support vector machines, decision tree, and random forest (RF) (Lu and Weng, 2006). The RF model has been proposed by Breiman (2001). Because of its high accuracy, good robustness, and practicality (Belgiu and Dragut, 2016), RF has attracted the attention of scholars in the field of land use (Li et al., 2019; Luciano et al., 2019), and has been applied to land use classification (Jamali, 2021; Sun et al., 2021). However, research on the identification of urban industrial land on a national scale has not been conducted, which limits the research on the spatial pattern analysis of urban industrial land in China from the macro level. In recent years, the spatial distribution characteristics of urban industrial land have attracted the attention of many scholars. The methods of spatial autocorrelation (Xie and Wang, 2015; Li et al., 2018), landscape pattern analysis (Lin et al., 2016), and co-location pattern mining (Marcon and Puech, 2009) have been employed. However, there are certain problems, such as small sample data, incompatibility, and spatial heterogeneity (the research conclusions of a single city cannot reflect the overall pattern).

In summary, to compensate for the shortcomings of the earlier research to a certain extent, this study uses large scale data (334 prefecture-level cities in China) and a 1 km × 1 km scale unit. Moreover, the National Land-Use/Cover Database of China with the spatial resolution of 30 m [NLUD-C, made from the Landsat TM image and China–Brazil Earth resource satellite image with a classification accuracy greater than 90% (Lai et al., 2016)] is used to explore the feasibility and scientificity of land class recognition based on POI data and the RF model. The spatial distribution characteristics of urban industrial land and the factors related to the layout planning of urban industrial land in China are clarified. The remainder of this study is structured as follows: **Section 2** describes data source and data processing and introduces the method. **Section 3** describes the results of industrial land identification, spatial pattern analysis, and correlation factor analysis in China. **Section 4** presents the conclusion and discussion.

2 METHODS AND DATA

2.1 Methods and Ideas

The research methods mainly involve RF, landscape pattern analysis, exploratory space data analysis (ESDA), and correlation factor analysis (which is a co-location pattern

TABLE 1 | Model accuracy comparison.

Training models	AUC	CA	F1	Precision
RF	0.965	0.889	0.889	0.889
Artificial neural networks	0.681	0.628	0.628	0.629
Logistic regression	0.552	0.558	0.546	0.558
Support vector machine	0.454	0.475	0.460	0.472

mining method). The four algorithm models of RF, artificial neural networks, logistic regression, and support vector machine were selected for experiments. The reason why these four kinds of analysis models were selected in this study is that they are widely used in the research of various urban land uses. Combined with the previous relevant literature on the classification of urban land use types (Wachtel et al., 2018; Li et al., 2019); as shown by the precision comparison presented in **Table 1**, RF was finally selected for China's industrial land recognition training to obtain an urban industrial land map of China. First, the pattern characteristics of China's urban industrial land were macroscopically grasped through spatial pattern analysis. Then, ESDA was used to explore the regional agglomeration of China's urban industrial land. Finally, the distance relationship between China's urban industrial land and related factors was explored through correlation factor analysis.

The research idea was based on POI data and RF, and by using the city construction map spot, Wuhan and Luoyang were selected as training samples. Employing the principle of data accessibility, the spatial distribution of industrial land under China's 1 km grid unit was identified, and then, the industrial land ratio of 334 prefecture-level cities in Chinese mainland was calculated. Spatial pattern analyses (NP, SPLIT, and CONHESION), ESDA (Moran's I, Local Moran's I), and correlation factor analysis (nearest neighbor distance method) were used. The specific method flow chart is shown in **Figure 1**.

2.1.1 Random Forest Model

RF is a natural nonlinear data algorithm proposed by Breiman (2001), which can be used for regression analysis and data classification (Pal, 2005). RF is based on the single decision tree algorithm and combines the bagging method and the random subspace method. By bootstrap sampling of training samples, a training set is formed, and unselected samples are used to predict and evaluate the error. The decision tree sequence is obtained by a combination of multiple training sets, and the final prediction result is selected by voting (Ham et al., 2005).

From data accessibility perspective, the spatial distribution data of industrial land in Wuhan and Luoyang in 2015 were obtained based on the project cooperation in Wuhan Natural Resources and Planning Bureau and Luoyang Natural Resources and Planning Bureau, respectively. Other cities cannot be obtained publicly because the data of the third land survey have not been made public. Therefore, Wuhan and Luoyang were used as RF training samples. According to the research of Chang and Ke (2020) and the principle of practicality, POI indicators were selected from the perspective of the distribution characteristics of facilities on industrial land. For example, because of the dominant characteristics of functions, there are relatively few entertainment and leisure facilities, education, and medical facilities. Therefore, the following five

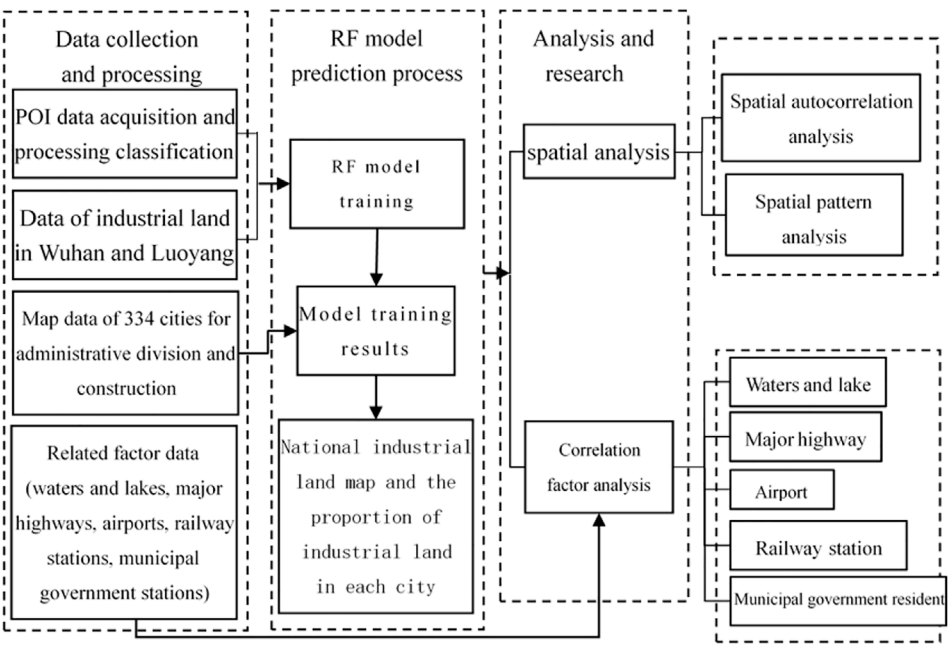

FIGURE 1 | Method flow chart.

TABLE 2 | Descriptions of landscape ecological index.

Index name	Index description
Number of patches (NP)	It reflects the heterogeneity of landscape, and its value is generally positively correlated with the fragmentation of landscape, which can reflect the fragmentation of urban industrial land in China
Splitting index (SPLIT)	It reflects the degree of fragmentation of the landscape, and its value is positively correlated with the degree of fragmentation
Patch cohesion index (COHESION)	It reflects the agglomeration degree of the landscape, ranging from (0.100], and its value is positively correlated with the agglomeration degree. It reflects whether there is a macro agglomeration phenomenon

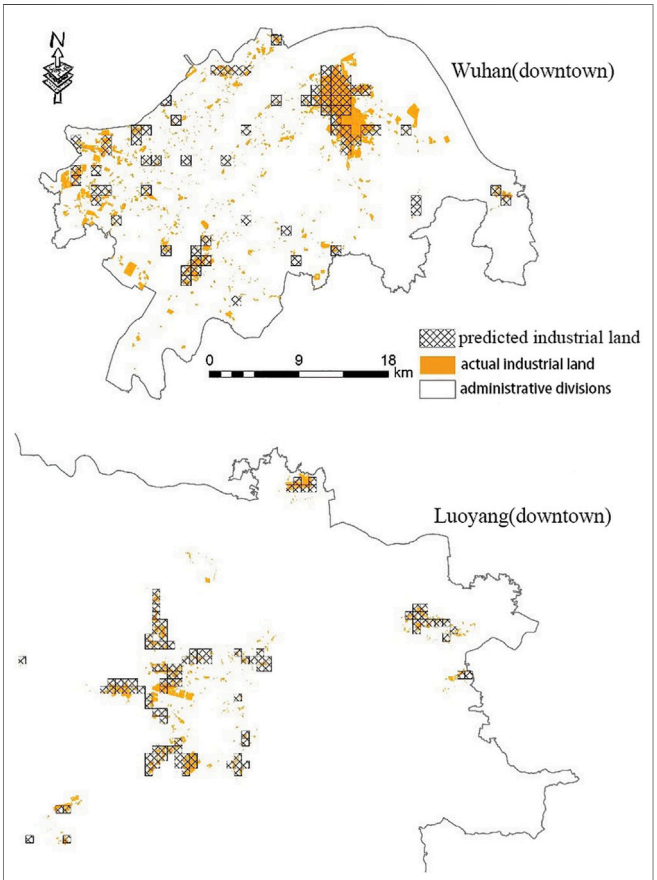

FIGURE 2 | Comparison of predicted and actual industrial land use in Wuhan city and Luoyang city.

variables were selected: the number of POIs (POISUM), the mixing degree of POIs (MIX), the proportion of POIs in industrial enterprises (FRATIO), the number of POI types (POITYPENUM), and the average distance among POIs (MEANDIS); moreover, the number of workers is relatively concentrated on industrial land, and the population density may be different from other urban land types. Therefore, population density (POPD) was selected as an index (POI data itself represent the population). Finally, considering that the roads inside the industrial land mainly serve the transportation vehicles in the plant area, the road network structure is much simpler than that outside of the industrial land; therefore, a seventh variable, that is, the highway node density per unit area (JUNCTIOND) was designed. The

TABLE 3 | Results of the training model.

Training model	AUC	CA	F1	Precision
RF	0.965	0.889	0.889	0.889

TABLE 4 | Predicted actual values of industrial land in Wuhan city and Luoyang city.

Region	Downtown of Wuhan (km^2)	Downtown of Luoyang (km^2)
Actual value	71.04	59.09
Predicted value	73.00	57.00

calculation of the aforementioned seven indicators was completed within the 1 km grid, the reason why this study chose it is that the spatial basic unit scales of various types of urban construction land are different. For example, many industrial lands are concentrated and connected in the form of industrial parks, whose degree of functional mixing is low, and the form of basic spatial units is large and complete. Among them, MIX refers to the mixing degree of different functions in a newly developed plot, and its formula is as follows:

$$MIX = -\sum_{i=1}^{n} (p_i * lnp_i). \quad (1)$$

In **Formula 1**, p_i represents the proportion of the i-th POI type in the total POI records, and n is the total number of POI types.

After the selection of indicators, based on the selected training samples (including a certain amount of industrial land and non-industrial land), the ability of the RF model to identify industrial land is determined through the 10-folds crossover method. In this method, the data are randomly divided into 10 sets, nine of which are used to train the model and one data set is used for the prediction of the RF model. Finally, the distribution of industrial land in China was obtained. The aforementioned steps were completed using orange data mining software (https://orangedatamining.com/), which is often used for classification training and can obtain better classification training results (Naik and Samant, 2016; Ishak et al., 2020).

2.1.2 Spatial Analysis Method

This study used spatial pattern analysis to analyze the overall agglomeration of industrial land in China, and then used

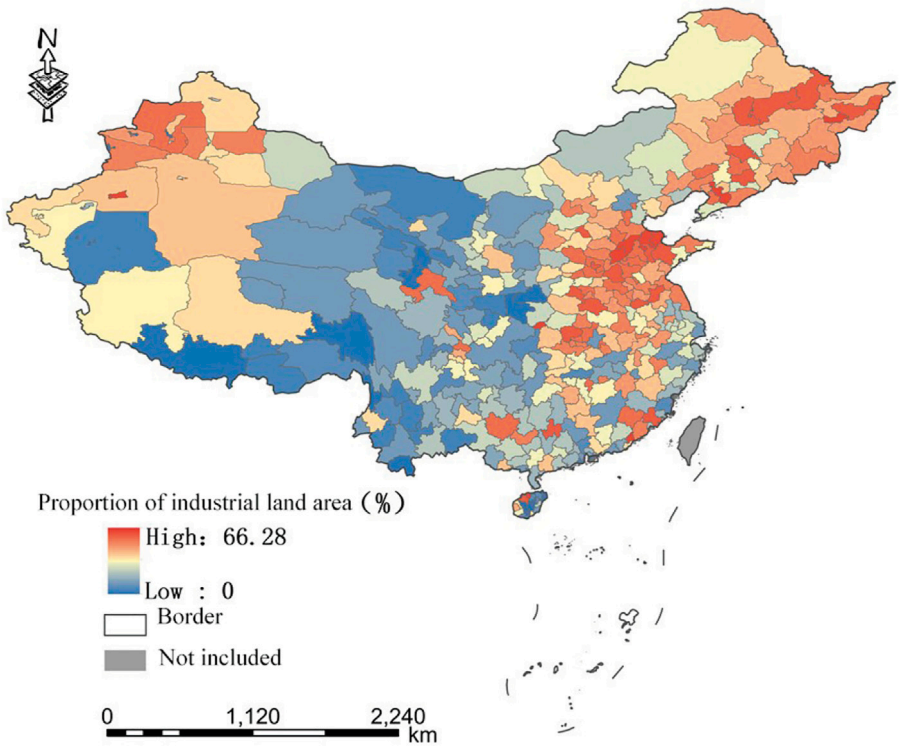

FIGURE 3 | Proportions of industrial land in China's prefecture-level cities.

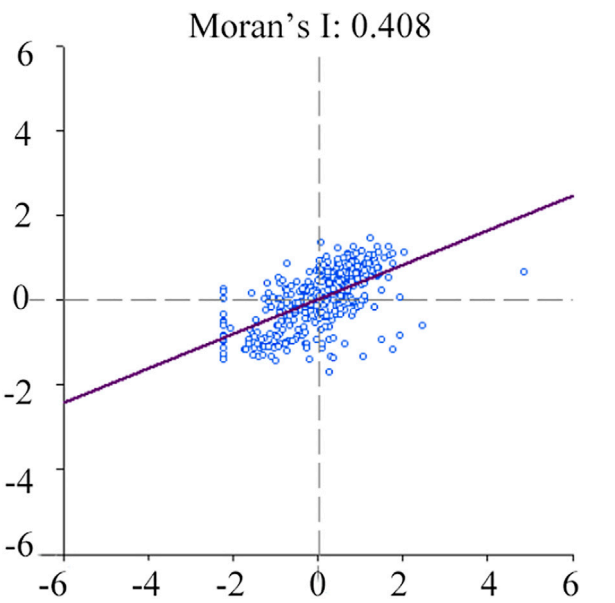

FIGURE 4 | Moran's I of industrial land proportion in 334 prefecture-level cities in China.

exploratory space data analysis to further analyze the spatial agglomeration degree of various internal regions. The two are the logical relationship from the whole to the inside.

2.1.2.1 Spatial Pattern Analysis

Analyzing the pattern of urban industrial land in China can more intuitively and effectively clarify its overall spatial characteristics. NP, SPLIT, and COHESION were selected in the patch type level index of FRAGSTATS for spatial pattern analysis. The three indexes could verify the overall macro and micro characteristics of China's industrial land pattern and provided a reference for subsequent analysis and research. The description of each index is shown in **Table 2** (Gao et al., 2012).

2.1.2.2 Exploratory Space Data Analysis

Global spatial autocorrelation analysis in ESDA is a method of spatial analysis that places spatial variables in the whole research space. Moran's I and local Moran's I are selected for analysis (Anselin, 1995). The formula is as follows:

$$Moran's\ I = \frac{n\sum i\sum jW_{ij}(x_i-\bar{x})\left(x_j-\bar{x}\right)}{\sum i\sum jW_{ij}\sum i(x_i-\bar{x})^2}. \quad (2)$$

In **Formula 2**, the range of calculation result is [−1,1]. A result within [−1,0] indicates that it is spatially negatively correlated, a result of 0 indicates that there is no spatial correlation, and a result in the range of (0,1] indicates that it is spatially positively correlated.

$$Local\ Moran's\ I_i = \frac{(x_i-\bar{x})\sum_{j=1}^{n}W_{ij}(x_i-\bar{x})}{\mathbf{S}^2}. \quad (3)$$

TABLE 5 | Proportion of verified regional prediction.

Verified area	Whole (%)	Area interval (km^2)				
		Predicted proportion				
Downtown of Wuhan	60.09	≤0.050271	(0.050271,0.199545]	(0.199545,0.523040]	(0.523040,1.420785]	(1.420785,3.733991]
		31.29%	44.40%	56.13%	65.92%	67.78%
Downtown of Luoyang	71.34	≤0.027057	(0.027057,0.092730]	(0.09273,0.231727]	(0.231727,0.559674]	(0.559674,1.381397]
		29.11%	63.10%	66.28%	73.18%	78.78%

In **Formula 3**, n represents the number of prefecture level administrative units, x_i and x_j refer to the attribute value of industrial land proportion of each prefecture-level administrative unit, W_{ij} refers to the spatial weight matrix established between research units i and j, and $\mathbf{S}^2$ refers to variance.

2.1.3 Statistical Method of Related Factors

ArcMap was used to calculate the average distance between urban industrial land and main waters and lakes, major highways (both national and provincial highways), airports, railway stations, and municipal government stations in 334 prefecture-level cities. Then, the relationship between these elements was statistically analyzed using SPSS software. According to this analysis, we not only analyze the distance analysis between industrial land and related factors in each city, but also classify cities with different proportions of industrial land, so as to intuitively see the status of urban-related factors with different proportions of industrial land, and finally achieve the purpose of comprehensive and scientific analysis to avoid miscellaneous analysis as far as possible.

2.2 Data Source and Processing

For the data source, the research area explored includes the whole Chinese mainland (Hong Kong, Macao, and Taiwan were excluded because of a lack of specific data). The data used include the urban construction maps and administrative boundaries of 334 prefecture-level cities in China for 2015, which is the base map of the 1 km grid established later. This means the identification of urban industrial land must be established within the scope that the base map is the construction land in the land use classification. The data involved in this study also include the data of industrial land in Wuhan and Luoyang, and the geographical data of China's main waters and lakes, major highways (both national and provincial highways), airports, railway stations, and municipal government stations in 2017. The map spots for urban construction and the map spots of main waters and lakes originate from NLUD-C with a spatial resolution of 30 m of the Chinese Academy of Sciences. These data are interpreted by remote sensing images. Urban construction land is defined by impervious surface and urban vegetation (He et al., 2017). Because of the difficulty to obtain the latest data, the map used shows data of 2015. The original data of construction spots were diagrammatically translated from satellite remote sensing images, rather than using official urban boundaries. The utilized data scale is large, which can compensate for the problem of relatively old data to a certain extent. At the same time, it usually takes 2–3 years for China's urban construction map spots (only extracted map spots) to develop into specific functions; based on data availability, this study selected the industrial land use data of Wuhan and Luoyang (both land use data in 2015). Among them, the land use data of Wuhan in 2015 were only used for training RF data, and the use of historical data in the training is a basic operation. The industrial land data of Wuhan and Luoyang in 2015 are land use survey data accessed from the Wuhan Natural Resources and Planning Bureau and Luoyang Natural Resources and Planning Bureau, respectively. These data were only used for the mapping of a single land type (industrial land), and these data do not involve other land types, and do not include specific coordinate information. These data can be used after being confirmed with the Luoyang natural resources and Planning Bureau. The administrative boundary data originate from China's second land use survey. Also, 54 million POI data of 12 categories in China in 2017 were obtained through web crawler technology based on the Baidu map open interface. These data include shopping centers, transportation facilities, educational facilities, financial institutions, hotels, tourist attractions, community services, entertainment facilities, medical facilities, restaurants, and corporate facilities. These locations reflect the basic activities of local residents in the four aspects of life, work, commuting, entertainment, and leisure. More detailed POI data introduction and processing flow can be found in He et al. (2018). Because the morphological dimension of China's land use map used is 2015, the POI data of 2017 were obtained, and the geographic data of major highways (both national and provincial highways), airports, and railway stations were obtained from the free map service open street map, which offers a large amount of data and strong timeliness.

In terms of data processing, this study used ArcGIS to extract the construction land of 334 prefecture-level cities in China from the land use map. A 1 km × 1 km grid was used as statistical unit to divide the construction land in China, China's construction land was divided and seven types of POI indicators are calculated. Wuhan and Luoyang were used as training samples to identify China's industrial land. After the identification of industrial land of 334 prefecture-level cities in China was completed with the RF model, the area and proportion of industrial land in each city were further counted, and the identified industrial land was extracted again using ArcGIS software. The whole research area was divided into industrial land and non-industrial land, and finally rasterized into the TIFF format.

TABLE 6 | Industrial land landscape fragmentation index.

Type	NP	SPLIT	COHESION
Industrial land	6685	679118	94.32

TABLE 7 | Statistics on the number of cities with different proportions of industrial land.

Proportion of industrial land %	Number of cities	Proportion of cities %
<15	37	11.08
15–30	92	27.54
>30%	205	61.38

3 RESULTS AND ANALYSIS

3.1 Verification and Analysis of Random Forest Identification Results

Based on the availability of data, industrial land and non-industrial land contained in the land use survey data of Wuhan Central Urban Area in 2015 and the land use data of Luoyang in 2015 were extracted, and the two types of land were set as y = 1 and y = 0, respectively. After this setting was completed, data were intersected with the kilometer grid to obtain the data set of two types of land for each grid. Through multiple groups of experiments and combined with robustness analysis, 30% of the grid was extracted from industrial land and non-industrial land for training. After optimizing the experimental adjustment parameters, the training results were obtained using orange data mining software (**Table 3**).

After training with Wuhan and Luoyang, the predicted industrial land was compared with the actual industrial land in the main urban areas of Wuhan and Luoyang in 2015 as shown in **Table 4** and **Figure 2**. The results show that the predicted area of industrial land in the central urban area of Wuhan is 73 km^2, which is close to its actual industrial land area of 71.04 km^2, and the predicted area of industrial land in the central urban area of Luoyang is 57 km^2, which is close to the actual value of 59.09 km^2. The comparison results between the predicted industrial land and the actual industrial land in Wuhan and Luoyang proved that POI data and RF can be used to identify urban industrial land.

To further test the accuracy of urban industrial land prediction, the "intersect" tool of the software ArcGIS10.2 was used to intersect the predicted results of urban industrial land in Wuhan and Luoyang with the actual urban industrial land, which obtained the overlapping area S (i.e., the area with accurate

TABLE 8 | Statistical analysis of distance relationship between industrial land in 334 prefecture-level cities and related factors.

Related factors	Distance/km	Number of cities	Average proportion of industrial land %	Minimum proportion of industrial land %	Maximum proportion of industrial land %
Waters and lake	<2	40	15.33	0	58.75
	2–4	66	33.77	2.44	58.37
	4–6	79	33.72	7.14	60.01
	6–8	60	37.96	12.65	54.83
	8–10	30	34.60	11.28	51.73
	>10	60	30.83	8.65	66.28
Major highways (national and provincial highways)	<1	167	28.11	0	66.28
	1–2	107	35.45	9.87	60.01
	2–3	33	34.65	8.70	56.12
	3–4	6	39.97	11	50.12
	4–5	6	33.15	19.66	45.20
	>5	15	33.73	8.80	58.75
Airport	<25	65	22.05	0	58.37
	25–50	96	32.43	8.66	55.25
	50–75	71	34.08	2.44	60.01
	75–100	56	34.66	7.14	56.29
	100–125	39	37.23	11.28	58.75
	>125	7	33.32	15.18	66.28
Railway station	<10	163	31.00	0	58.37
	10–20	129	34.60	2.44	60.01
	20–30	16	27.79	8.80	44.42
	30–40	7	29.09	10.80	56.29
	40–50	7	28.91	7.14	46.22
	>50	12	26.57	7.47	66.28
Municipal government resident	<20	111	27.72	0	66.28
	20–40	147	34.99	9.87	60.01
	40–60	43	31.48	2.44	50.70
	60–80	17	33.62	9.27	56.29
	80–100	3	30.40	7.14	52.58
	>100	13	29.93	12.28	48.75

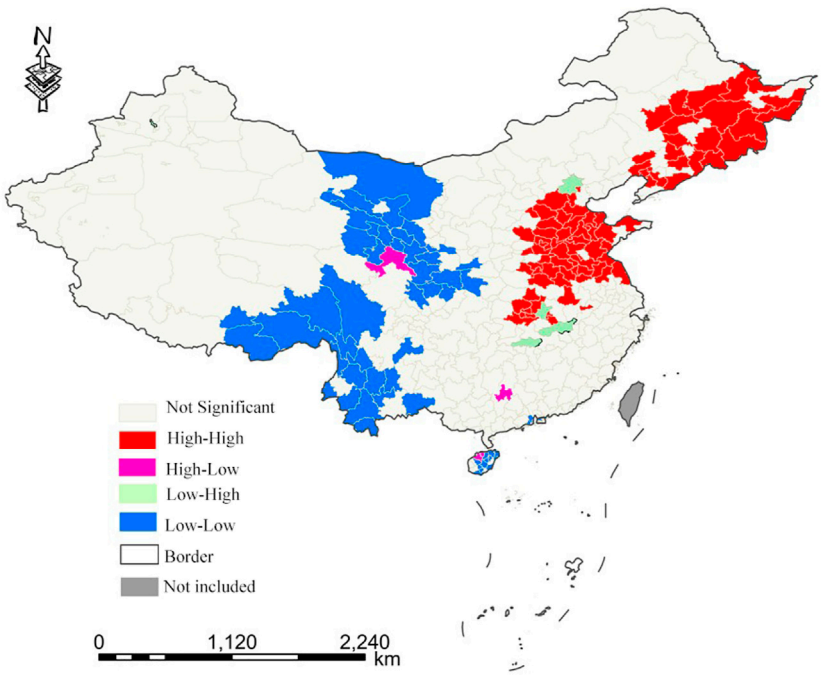

FIGURE 5 | LISA map of industrial land proportion in 334 prefecture-level cities in China.

predicted spatial location). The percentage of S and the actual area were used as a measurement standard to judge the recognition accuracy. The specific results are shown in **Table 5**. The overall recognition accuracy of the two places exceeds 60%, and that of Luoyang is 71.34%. Several of the plots failed to achieve accurate prediction. On the one hand, the prediction unit is a regular grid, but the actual patch is irregular, and intersecting the two will lose part of the area. On the other hand, the data in **Table 4** show that the identification method is more suitable for predicting urban patches over 0.5 km^2, which can capture a large range of urban industrial land, and its accuracy basically exceeds 60%.

3.2 Spatial Characteristics Analysis of Urban Industrial Land in China

3.2.1 Spatial Pattern Characteristics of Industrial Land in China

The numbers of NP, SPLIT, and COHESION in the patch type level index in FRAGSTATS were selected for spatial pattern analysis, to explore the agglomeration degree of industrial land in the national macro scope. The results are presented in **Table 6** showing that the number of industrial land patches in China is 6,685, which is large. The separation index is high and the aggregation index is also high. This shows that the national industrial land presents a distribution trend of "large agglomeration and small dispersion" from the perspective of spatial pattern, that is, it shows strong agglomeration in a large regional scope, while it is relatively scattered in a small regional scope, for example, within a prefecture level administrative division.

3.2.2 Spatial Distribution Characteristics of Urban Industrial Land in China

The industrial land area of each city was assessed, but because the construction land area of each city is different, the area proportion of industrial land in construction land of each city was further assessed as shown in **Figure 3** to analyze spatial characteristics. According to the standard of urban land classification and planning and construction land (GB 50137-2011), the proportion of urban industrial land is in the range of 15%–30%.

According to statistical data shown in **Table 7**, among China's 334 prefecture level administrative units, only 92 cities have this range, and the proportion of cities not in this range is 72.46%, of which 37 have less than 15% and 205 have more than 30%. This indicates that China's 334 prefecture-level administrative units overall invest more in the secondary industry. The analysis results are in line with the national conditions indicating that the proportion of the secondary industry in the three major industries is much higher than that of developed countries. At the same time, the results show that many cities have not adhered to the recommended value of industrial land proportion according to the standards, which implies that the development objectives of various cities in China are diverse and that the development stages are different. This requires further studies at a later timepoint. From the perspective of spatial distribution characteristics, as shown in **Figure 3**, cities with a large proportion of industrial land are mostly concentrated in the north, especially in Shandong, Henan, and Hebei, three eastern provinces, which are located in the North China Plain, as

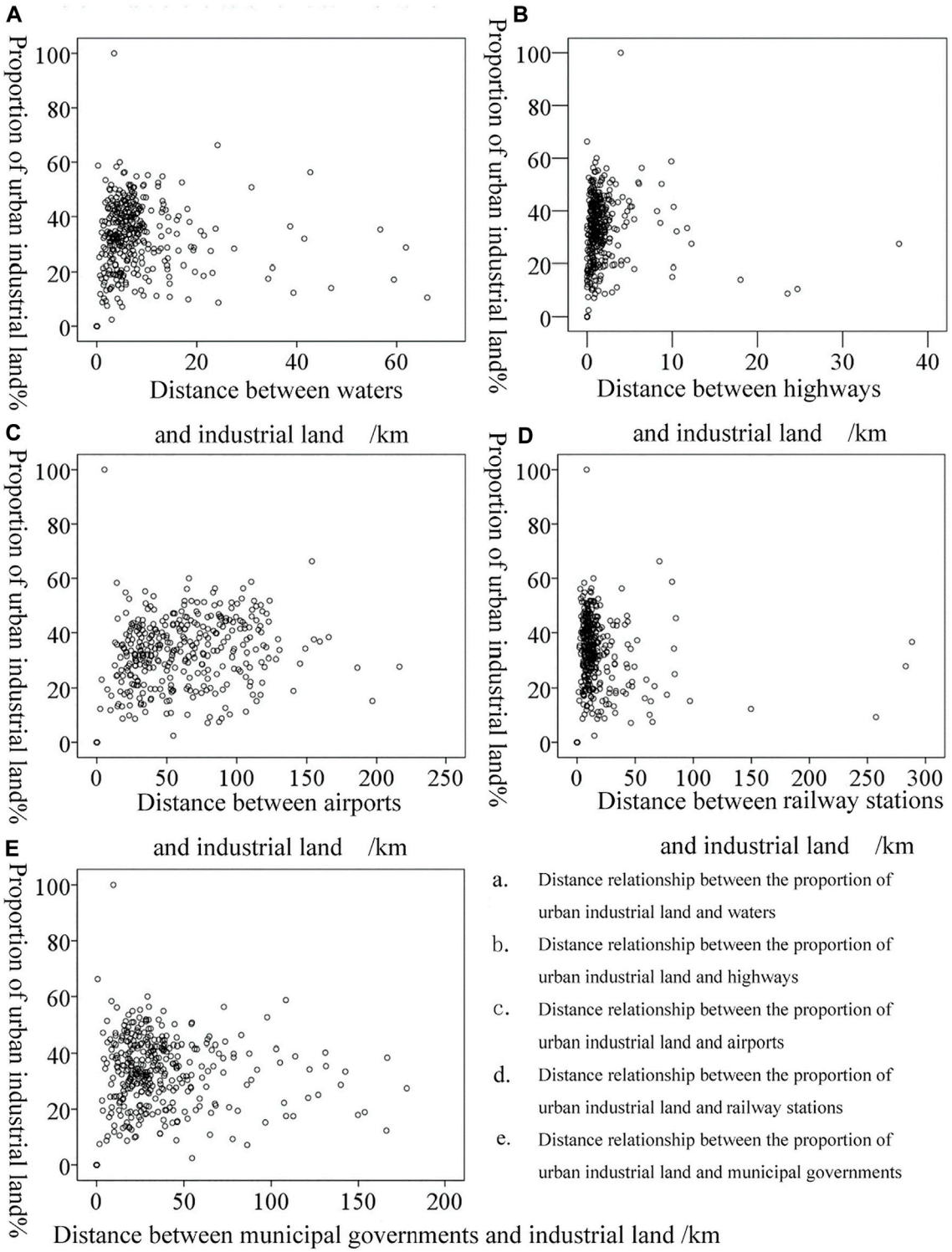

FIGURE 6 | Industrial land proportion in 334 prefecture-level cities in China at different distances from related elements. **(A)** Distance relationship between the proportion of urban industrial land and waters. **(B)** Distance relationship between the proportion of urban industrial land and highways. **(C)** Distance relationship between the proportion of urban industrial land and airports. **(D)** Distance relationship between the proportion of urban industrial land and railway stations. **(E)** Distance relationship between the proportion of urban industrial land and municipal governments.

well as a small part of Xinjiang. Here, the proportion of industrial land is relatively high in certain cities. As the cities with a high proportion of industrial land are concentrated in specific areas, it is necessary to further explore the degree of spatial agglomeration.

Using GeoDa software and using data on the proportion of industrial land area of each prefecture level city, global and local spatial autocorrelation analyses were conducted on the predicted industrial land in China. As shown in **Figure 4**, the Moran's I of the proportion of industrial land in 334 cities in China is 0.408, showing the characteristics of spatial positive correlation. This further shows that cities with a high proportion of industrial land in China have the characteristics of spatial agglomeration. To explore the spatial agglomeration characteristics and dispersion of industrial land in China more intuitively and carefully, further analysis was conducted *via* a LISA diagram in **Figure 5**. In general, there are clear differences in the agglomeration degree of industrial land in China. High–High agglomeration areas are mainly distributed in North China and Northeast China. Low–Low concentration areas are mainly concentrated in Tibet, Qinghai, Western Inner Mongolia, Western Sichuan, Yunnan, and Shaanxi.

3.3 Analysis on Related Factors of Urban Industrial Land in China

In the past, scholars studied the factors affecting the spatial pattern of industrial land in a single city, and often discussed the relationship between the spatial distribution of urban industrial land and the distance to the urban center (McGrath, 2000; Langer and Korzhenevych, 2018), administrative center (Wang et al., 2007), river surface (Wang et al., 2007), highways, and railways (Fan et al., 2017). This research has verified that these factors have a certain correlation with the spatial pattern distribution of urban industrial land in China. Further analysis of the correlation factors of urban industrial land in China at the macro level has important reference significance for the overall understanding of the spatial pattern of urban industrial land in China.

Therefore, China's main waters and lakes, main traffic highways (both national and provincial highways), airports, railway stations, and municipal government stations were used as centers, and the buffer distance was generated using ArcMap. Then, SPSS was used to generate a scatter map to analyze the relationship between the proportion of industrial land in China and the distance of five related factors. As shown in **Figure 6**, the industrial land in most cities in China is located within 10 km from the main waters and lakes (**Figure 6A**), not more than 3 km from the nearest main traffic highway (**Figure 6B**), and not more than 25 km from the nearest railway station (**Figure 6D**). Compared with the aforementioned three related factors, the phenomenon of "urban agglomeration" is not prominent in the distance relationship between industrial land and airport (**Figure 6C**) and municipal government garrison (**Figure 6E**). The distance between most urban industrial land and the nearest airport is about 130 km, but it is relatively scattered in this distance range. The industrial land in many cities is about 10–60 km away from the center of the municipal government.

In **Figure 6**, the relationship between the proportion of urban industrial land and related factors cannot be effectively identified. Therefore, SPSS was used for tabular hierarchical statistics. The results in **Table 8** show that the average proportion of urban industrial land within 2 km from main water bodies and lakes is 15.33%, which is significantly lower than that of other distance sections, and the average value within 1 km from the major highways is 28.11%, which is lower than that of other sections. The average value within 25 km from airports is 22.05%, which is also lower than the proportion of urban industrial land in other distance sections. The number of cities 20 km away from the railway station is not only small, but also the proportion of industrial land is low, which shows that the railway transportation is highly related to the location of industrial land. The industrial land of most cities is located within 100 km from the municipal government, and the proportion of urban industrial land less than 20 km in this distance is significantly lower than that of other distance segments.

In summary, the industrial land of each city is close to the main waters and lakes, major highways, and railway stations, while there is no evident phenomenon of "urban agglomeration" from the airport. It is about 10–60 km from the garrison of the municipal government. The proportion of industrial land is not high in cities where the industrial land is close to the main waters and lakes, major highways, airports, and municipal government stations. However, the proportion of industrial land in cities close to the railway station is high, and the correlation between the two is high. The aforementioned results illustrate the distance relationship between China's urban industrial land and related factors from the macro level, but the mechanism or the driving factors behind the relationship must be further discussed due to the focus and the limited length of the study.

4 CONCLUSION

In this study, POI data and RF are used to identify and analyze China's industrial land. The main conclusions are summarized as follows:

1) By analyzing and comparing several groups of experiments, the result of RF for urban industrial land identification is proved to be scientific and referential. Based on the experimental results, the recognition accuracy of industrial land in industrial parks is greater than that of scattered industrial land.
2) From the perspective of spatial pattern, China's urban industrial land presents the distribution trend of "large agglomeration and small dispersion."
3) From the perspective of spatial distribution characteristics, cities with a high proportion of industrial land are mostly concentrated in the north. The Moran's I of the proportion of industrial land in 334 cities in China is 0.408, which represents the characteristics of spatial agglomeration. High–high concentration areas are mainly distributed in North China and Northeast China, while low–low concentration areas are mainly concentrated in western regions such as Tibet, Qinghai, Western Inner Mongolia, Western Sichuan, Yunnan, and Shaanxi.
4) The industrial land of each city is close to the waters and lakes, highways, and railway stations, while there is no obvious

connection with airports. Also, it is about 10–60 km away from the municipal government. In terms of the proportion of industrial land, the proportion of industrial land is not high in cities where the industrial land is close to waters and lakes, transportation highways, airports, and municipal government stations. The proportion of industrial land is high in cities where the industrial land is close to railway stations.

This study provides a new method and idea for single land type identification in large-scale research range. However, the following points may become the research direction in the future:

1) The POI data are only single period data, which fails to further analyze the temporal and spatial evolution of China's urban industrial land. Also, there is a certain subjectivity in the selection of POI indicators. In the future, more complete time series POI data should be collected and standardized POI index selection standards should be formulated. Finally, this study selected urban industrial land as the research object, but China, as a developing country, has a large number of rural industrial land. An approach to scientifically and effectively identify a wide range of rural industrial land based on big data is a potential research direction.
2) It is necessary to continue to verify the applicability of RF to other types of industrial land.
3) The model used here is more suitable for the prediction of areas larger than 0.5 km^2. Follow-up research will further improve the model method to better identify urban industrial land.
4) This study explores the relationship between urban industrial land and related factors but does not provide an in-depth analysis of the driving factors behind it. For example, industrial land is far away from municipal governments, which may be driven by multiple factors such as the government, enterprises, and the public, which should be explored in future research.

DATA AVAILABILITY STATEMENT

The original contributions presented in the study are included in the article/Supplementary Material, further inquiries can be directed to the corresponding author.

AUTHOR CONTRIBUTIONS

QH contributed to the conception of the study; XT performed the data analyses and wrote the manuscript.

REFERENCES

Anselin, L. (1995). Local Indicators of Spatial Association: LISA. *Geographical Anal.* 27, 93–115. doi:10.1111/j.1538-4632.1995.tb00338.x

Belgiu, M., and Drăguț, L. (2016). Random Forest in Remote Sensing: A Review of Applications and Future Directions. *Isprs J. Photogrammetry Remote Sensing* 114, 24–31. doi:10.1016/j.isprsjprs.2016.01.011

Breiman, L. (2001). Random Forests. *Mach Learn.* 45, 5–32. doi:10.1023/a:1010933404324

Chang, X., and Ke, H. (2020). Urban Impervious Surface Information Extraction Based on Random forest Algorithm: Taking Changchun as an Example. *Bull. Surv. Mapp.* 11, 43–49. doi:10.13474/j.cnki.11-2246.2020.0352

Dankoub, Z., Ayoubi, S., Khademi, H., and Lu, S.-G. (2012). Spatial Distribution of Magnetic Properties and Selected Heavy Metals in Calcareous Soils as Affected by Land Use in the Isfahan Region, Central Iran. *Pedosphere* 22 (1), 33–47. doi:10.1016/S1002-0160(11)60189-6

Davies, D. H. (1959). Boundary Study as a Tool in CBD Analysis: An Interpretation of Certain Aspects of the Boundary of Cape Town's Central Business District. *Econ. Geogr.* 35 (4), 322–345. doi:10.2307/142466

Eklund, P. W., Kirkby, S., and Salim, A. (1998). Data Mining and Soil Salinity Analysis. *Int. J. Geographical Inf. Sci.* 12 (3), 247–268. doi:10.1080/136588198241888

Fan, S., Zhang, L., Zeng, Z., Huang, Y., and Lin, X. (2017). Factors Influencing Land Intensive Use of Development Zone in Regions with Different Levels of Economic Development: A Case Study in Fujian Province. *China Land Sci.* 31 (06), 51–58. doi:10.11994/zgtdkx.20170627.132544

Gao, Y., Wu, Z., Lou, Q., Huang, H., Cheng, J., and Chen, Z. (2012). Landscape Ecological Security Assessment Based on Projection Pursuit in Pearl River Delta. *Environ. Monit. Assess.* 184 (4), 2307–2319. doi:10.1007/s10661-011-2119-2

Ham, J., Yangchi Chen, Y., Crawford, M. M., and Ghosh, J. (2005). Investigation of the Random forest Framework for Classification of Hyperspectral Data. *IEEE Trans. Geosci. Remote Sensing* 43 (3), 492–501. doi:10.1109/tgrs.2004.842481

He, Q., He, W., Song, Y., Wu, J., Yin, C., and Mou, Y. (2018). The Impact of Urban Growth Patterns on Urban Vitality in Newly Built-Up Areas Based on an Association Rules Analysis Using Geographical 'big Data'. *Land Use Policy* 78, 726–738. doi:10.1016/j.landusepol.2018.07.020

He, Q., Song, Y., Liu, Y., and Yin, C. (2017). Diffusion or Coalescence? Urban Growth Pattern and Change in 363 Chinese Cities from 1995 to 2015. *Sustain. Cities Soc.* 35, 729–739. doi:10.1016/j.scs.2017.08.033

Ishak, A., Siregar, K., AspriyatiGinting, R., Ginting, R., and Afif, M. (2020). Orange Software Usage in Data Mining Classification Method on the Dataset Lenses. *IOP Conf. Ser. Mater. Sci. Eng.* 1003 (1), 012113. doi:10.1088/1757-899X/1003/1/012113

Ivan, I., Singleton, A., Horák, J., and Inspektor, T. (2016). *The Rise of Big Spatial Data*. United Kingdom: Springer International Publishing.

Jamali, A. (2021). Land Use Land Cover Mapping Using Advanced Machine Learning Classifiers. *Ekológia (Bratislava).* 40 (3), 286–300. doi:10.2478/eko-2021-0031

Jean, N., Burke, M., Xie, M., Davis, W. M., Lobell, D. B., and Ermon, S. (2016). Combining Satellite Imagery and Machine Learning to Predict Poverty. *Science* 353, 790–794. doi:10.1126/science.aaf7894

Jiang, S., Alves, A., Rodrigues, F., Ferreira, J., and Pereira, F. C. (2015). Mining point-of-interest Data from Social Networks for Urban Land Use Classification and Disaggregation. *Comput. Environ. Urban Syst.* 53, 36–46. doi:10.1016/j.compenvurbsys.2014.12.001

Jo, S. S., Lee, S. H., and Leem, Y. (2020). Temporal Changes in Air Quality According to Land-Use Using Real Time Big Data from Smart Sensors in Korea. *Sensors* 20.21, 6374. doi:10.3390/s20216374

Lai, L., Huang, X., Yang, H., Chuai, X., Zhang, M., Zhong, T., et al. (2016). Carbon Emissions from Land-Use Change and Management in China between 1990 and 2010. *Sci. Adv.* 2 (11). doi:10.1126/sciadv.1601063

Lai, Y., Chen, K., Zhang, J., and Liu, F. (2020). Transformation of Industrial Land in Urban Renewal in Shenzhen, China. *Land* 9, 371. doi:10.3390/land9100371

Langer, S., and Korzhenevych, A. (2018). The Effect of Industrial and Commercial Land Consumption on Municipal Tax Revenue: Evidence from Bavaria: Evidence from Bavaria. *Land Use Policy* 77 (9), 279–287. doi:10.1016/j.landusepol.2018.05.052

Li, C., Liu, M., Hu, Y., Shi, T., Qu, X., and Walter, M. T. (2018). Effects of Urbanization on Direct Runoff Characteristics in Urban Functional Zones. *Sci. Total Environ.* 643, 301–311. doi:10.1016/j.scitotenv.2018.06.211

Li, G., Chang, L., Liu, X., Su, S., Cai, Z., Huang, X., et al. (2019). Monitoring the Spatiotemporal Dynamics of Poor Counties in China: Implications for Global Sustainable Development Goals. *JOURNAL CLEANER PRODUCTION* 227, 392–404. doi:10.1016/j.jclepro.2019.04.135

Lin, T., Sun, C., Li, X., Zhao, Q., Zhang, G., Ge, R., et al. (2016). Spatial Pattern of Urban Functional Landscapes along an Urban-Rural Gradient: a Case Study in Xiamen City, China. *Int. J. Appl. Earth Observation Geoinformation* 46, 22–30. doi:10.1016/j.jag.2015.11.014

Liu, Y., Fang, F., and Li, Y. (2014). Key Issues of Land Use in China and Implications for Policy Making. *Land Use Policy* 40, 6–12. doi:10.1016/j.jag.2015.11.01410.1016/j.landusepol.2013.03.013

Liu, Y., Li, J., and Yang, Y. (2018a). Strategic Adjustment of Land Use Policy under the Economic Transformation. *Land Use Policy* 74, 5–14. doi:10.1016/j.landusepol.2017.07.005

Liu, Y., Zhang, Z., and Zhou, Y. (2018b). Efficiency of Construction Land Allocation in China: an Econometric Analysis of Panel Data. *Land Use Policy* 74, 261–272. doi:10.1016/j.landusepol.2017.03.030

Long, Y., and Shen, Z. (2015). *Geospatial Analysis and Application: A Comprehensive View of Planning Support Issues in the Beijing Metropolitan Area*. Springer International Publishing.

Louw, E., van der Krabben, E., and van Amsterdam, H. (2012). The Spatial Productivity of Industrial Land. *Reg. Stud.* 46, 137–147. doi:10.1080/00343404.2010.530250

Lu, D., and Weng, Q. (2006). Use of Impervious Surface in Urban Land-Use Classification. *Remote Sensing Environ.* 102 (1-2), 146–160. doi:10.1016/j.rse.2006.02.010

Luciano, A. C. d. S., Picoli, M. C. A., Rocha, J. V., Duft, D. G., Lamparelli, R. A. C., Leal, M. R. L. V., et al. (2019). A Generalized Space-Time OBIA Classification Scheme to Map Sugarcane Areas at Regional Scale, Using Landsat Images Time-Series and the Random forest Algorithm. *Int. J. Appl. Earth Observation Geoinformation* 80, 127–136. doi:10.1016/j.jag.2019.04.013

Marcon, E., and Puech, F. (2009). Measures of the Geographic Concentration of Industries: Improving Distance-Based Methods. *J. Econ. Geogr.* 10 (5), 745–762. doi:10.1093/jeg/lbp056

McGrath, D. T. (2000). Urban Industrial Land Redevelopment and Contamination Risk. *J. Urban Econ.* 47 (3), 414–442. doi:10.1006/juec.1999.2147

Mckenzie, G., Janowicz, K., Gao, S., and Gong, L. (2015). How where Is when? on the Regional Variability and Resolution of Geosocial Temporal Signatures for Points of Interest. *Comput. Environ. Urban Syst.* 54, 336–346. doi:10.1016/j.compenvurbsys.2015.10.002

Moomaw, R. L. (1978). An Econometric Analysis of Industrial Land-Use Intensity within an Urban Area. *Urban Stud.* 15, 321–326. doi:10.1080/713702405

Murphy, R. E., and Vance, J. E. (1954). Delimiting the CBD. *Econ. Geogr.* 30 (3), 189–222. doi:10.2307/141867

Myint, S. W., Gober, P., Brazel, A., Grossman-Clarke, S., and Weng, Q. (2011). Per-pixel vs. Object-Based Classification of Urban Land Cover Extraction Using High Spatial Resolution Imagery. *Remote Sensing Environ.* 115 (5), 1145–1161. doi:10.1016/j.rse.2010.12.017

Naik, A., and Samant, L. (2016). Correlation Review of Classification Algorithm Using Data Mining Tool: WEKA, Rapidminer, Tanagra, Orange and Knime. *PROCEDIA COMPUTER SCIENCE* 85, 662–668. doi:10.1016/j.procs.2016.05.251

Pal, M. (2005). Random forest Classifier for Remote Sensing Classification. *Int. J. Remote Sensing* 26 (1), 217–222. doi:10.1080/01431160412331269698

Sun, Z., Jiao, H., Wu, H., Peng, Z., and Liu, L. (2021). Block2vec: An Approach for Identifying Urban Functional Regions by Integrating Sentence Embedding Model and Points of Interest. *Ijgi* 10 (5), 339. doi:10.3390/ijgi10050339

Toole, J. L., Ulm, M., González, M. C., and Bauer, D. (2012). Inferring Land Use from mobile Phone Activity. *Proc. Acm Sigkdd Int. Workshop Urban Comput.*, 1–8. doi:10.1145/2346496.2346498

Wachtel, I., Zidon, R., Garti, S., and Shelach-Lavi, G. (2018). Predictive Modeling for Archaeological Site Locations: Comparing Logistic Regression and Maximal Entropy in north Israel and north-east China. *J. Archaeological Sci.* 92, 28–36. doi:10.1016/j.jas.2018.02.001

Wang, A., Mou, B., and Chen, S. (2007). Spatial Differentiation and Impact Factors of Industrial Land-Use in Guangzhou. *Trop. Geogr.* (02), 132–138.

Wang, J.-C., Jin, Z.-D., Yang, M., and Naqvi, S. (2021). Does Strict Environmental Regulation Enhance the Global Value Chains Position of china's Industrial Sector? *Pet. Sci.* 18 (6), 1899–1909. doi:10.1016/j.petsci.2021.09.023

Xie, H., and Wang, W. (2015). Spatiotemporal Differences and Convergence of Urban Industrial Land Use Efficiency for China's Major Economic Zones. *J. Geogr. Sci.* 25 (10), 1183–1198. doi:10.1007/s11442-015-1227-2

Yang, Q., Li, Z., Lu, X., Duan, Q., Huang, L., and Bi, J. (2018). A Review of Soil Heavy Metal Pollution from Industrial and Agricultural Regions in china: Pollution and Risk Assessment. *Sci. Total Environ.* 642 (15), 690–700. doi:10.1016/j.scitotenv.2018.06.068

Yuan, J., Zheng, Y., and Xie, X. (2012). "Discovering Regions of Different Functions in a City Using Human Mobility and POIs," in The 18th ACM SIGKDD International Conference on Knowledge Discovery and Data Mining (New York, USA.

Zhai, W., Bai, X., Shi, Y., Han, Y., Peng, Z.-R., and Gu, C. (2019). Beyond Word2vec: An Approach for Urban Functional Region Extraction and Identification by Combining Place2vec and POIs. *Comput. Environ. Urban Syst.* 74 (03), 1–12. doi:10.1016/j.compenvurbsys.2018.11.008

Zhang, J., Zhang, X., Zhang, A., and He, S. (2020). Theory, Mechanism and Benefit Loss of Spatial Misallocation of Construction Land:an Empirical Analysis Based on Hubei Province. *China Popul. Resour. Environ.* 30 (04), 42–53. doi:10.12062/cpre.20191103

Zhang, X., and Du, S. (2015). A Linear Dirichlet Mixture Model for Decomposing Scenes: Application to Analyzing Urban Functional Zonings. *Remote Sensing Environ.* 169, 37–49. doi:10.1016/j.rse.2015.07.017

Zheng, Y., Capra, L., Wolfson, O., and Yang, H. (2014). Urban Computing: Concepts, Methodologies, and Applications. *ACM Transaction Intell. Syst. Technol.* 5 (3), 38. doi:10.1145/2629592

Conflict of Interest: The authors declare that the research was conducted in the absence of any commercial or financial relationships that could be construed as a potential conflict of interest.

Publisher's Note: All claims expressed in this article are solely those of the authors and do not necessarily represent those of their affiliated organizations, or those of the publisher, the editors, and the reviewers. Any product that may be evaluated in this article, or claim that may be made by its manufacturer, is not guaranteed or endorsed by the publisher.

Copyright © 2022 He and Tang. This is an open-access article distributed under the terms of the Creative Commons Attribution License (CC BY). The use, distribution or reproduction in other forums is permitted, provided the original author(s) and the copyright owner(s) are credited and that the original publication in this journal is cited, in accordance with accepted academic practice. No use, distribution or reproduction is permitted which does not comply with these terms.

frontiers | Frontiers in Environmental Science

ORIGINAL RESEARCH
published: 11 May 2022
doi: 10.3389/fenvs.2022.905443

A Deep Learning–Based Approach for Moving Vehicle Counting and Short-Term Traffic Prediction From Video Images

Ye Zheng[1], *Xiaoming Li*[2], *LiuChang Xu*[3] *and Nu Wen*[4]*

[1]Faculty of Electrical Engineering and Computer Science, Ningbo University, Ningbo, China, [2]Shenzhen Key Laboratory of Spatial Information Smart Sensing and Services, Shenzhen University, Shenzhen, China, [3]College of Information Engineering, Zhejiang A&F University, Hangzhou, China, [4]Guangzhou Wonping Info-Tech Co., Ltd., Guangzhou, China

The intelligent transportation system (ITS) is one of the effective solutions to the problem of urban traffic congestion, and it is also one of the important topics of smart city construction. One particular application is the traffic monitoring and flow prediction. However, there are still challenges regarding both aspects. On the one hand, the current traffic monitoring relies heavily on the single object detection method that cannot achieve accurate statistics of moving target counting and, meanwhile, has limited speed advantage; on the other hand, the existing traffic flow prediction models rarely consider different weather conditions. Therefore, the present article attempts to propose a packaged solution, which combines a new target tracking and moving vehicle counting method and an improved long short-term memory (LSTM) network for traffic flow forecast with weather conditions. More specifically, the DCN V2 convolution kernel and MultiNetV3 framework are used to replace YOLOv4's conventional convolution kernel and backbone network to realize multi-target tracking and counting, respectively. Subsequently, combined with the temporal characteristics of historical traffic flow, this article introduces weather conditions into the LSTM network and realizes the short-term prediction of traffic flow at the road junction level. This study carries out a series of experiments using the real traffic video data with a 2-month time span at a popular road junction in the downtown of Shenzhen, China. The results suggest that the proposed algorithms outperform the previous methods in terms of the 10% higher accuracy of target detection tracking and about a half reduction of traffic prediction error, when considering weather conditions.

Keywords: multi-target tracking, short-term traffic flow prediction, DCN-MultiNet-YOLO, CLSTM, smart city

OPEN ACCESS

Edited by:
Ying Jing,
Zhejiang University, China

Reviewed by:
Wen Xiao,
Newcastle University, United Kingdom
Ka Zhang,
Nanjing Normal University, China

****Correspondence:***
Nu Wen
wennu1989@126.com

Specialty section:
This article was submitted to Environmental Informatics and Remote Sensing, a section of the journal Frontiers in Environmental Science

Received: *27 March 2022*
Accepted: *11 April 2022*
Published: *11 May 2022*

Citation:
Zheng Y, Li X, Xu L and Wen N (2022) A Deep Learning–Based Approach for Moving Vehicle Counting and Short-Term Traffic Prediction From Video Images. Front. Environ. Sci. 10:905443. doi: 10.3389/fenvs.2022.905443

1 INTRODUCTION

Recent rapid urban development in China has led to increasing car ownership, which has led to more severe traffic congestion and longer commuting times. According to a 2020 investigation on commuting times for the 36 major Chinese cities, by the China Academy of Urban Planning and Design, more than 10 million people (accounting for 13% of total population) have a daily commute of more than 1 h each way. Among those cities, Shenzhen, one of the four "top-tier" cities in Guangdong province, has a population of 17.56 million people (according to bureau statistics

2020) and a GDP of 2.76 trillion yuan (ranking it third in mainland China). As evidenced by the Shenzhen traffic police office, the numbers of registered vehicles and drivers are around 3.36 and 4.39 million, respectively. The resulting traffic density is estimated at more than 500 per km, which is the highest in the country. In the era of information and communication technology, urban transportation at such a large scale cannot function well without the support of intelligent transportation systems (ITSs) (Telang et al., 2021, Zear et al., 2016, Khatoun and Zeadally, 2016, Mckenney and Frey-Spurlock, 2018). For instance, one plausible measure for coordinating urban road traffic could be monitoring the traffic volume using closed circuit television (CCTV) images at each road junction and implementing the prediction based on the historic traffic volume data. In doing so, we could predict the future traffic situation for better traffic management and optimization, thereby partly alleviating traffic congestion. Numerous studies have investigated traffic monitoring and prediction at the junction level spanning a wide range of disciplines. For example, Khekare and Sakhare (2013) introduced a new scheme consisting of a smart city framework that transmits information about traffic conditions to help drivers make appropriate decisions. Marais et al. (2014) devised an approach to deal with the inaccuracy of signal propagation conditions for urban users who demand accurate localization by associating GNSS data and imaging information. Raja et al. (2018) proposed a cognitive intelligent transportation system (CITS) model that provides efficient channel utilization, which is the key to make any application successful in vehicular *ad hoc* networks. Zheng et al. (2020) used an adaptation evolutionary strategy to control arterial traffic coordination for a better passage rate along one single road with several junctions. However, the existing literature may still face challenges regarding the inaccuracy of both car object detection and traffic volume prediction. To be more specific, current detection methods from CCTV images mainly focus on single car object detection and may suffer from the inaccuracy of multiple moving object recognition and tracking (such as omission or false detection) and have a limited speed advantage. Also, the traffic volume prediction models that are based merely on the detection results may be distant from reality as they seldom consider environmental factors such as weather conditions (for example, sunny or rainy days).

The present study is motivated to put forward a two-level traffic flow management system to cope with the abovementioned challenges, which is supported by the deep learning technique and is validated by a 2-month video image series at a popular road junction located at downtown Shenzhen. Specifically, the system is layered with YOLOv4 for car object detection and tracking and is then layered with a modified long short-term memory (LSTM) network embedded with the spatio-temporal characteristics of historic traffic records, as well as corresponding weather information, to build up a short-term traffic flow prediction model. Therefore, the main contributions of this article are twofold. First, regarding moving object detection, we proposed a lightweight DCN-MultiNet-YOLO network for video-based multi-target tracking for the collection of traffic volume statistics at the urban road junction level. Second, for traffic flow forecasts, we proposed an improved LSTM network that is closer to realistic scenarios by considering various weather conditions associated with real traffic flow changes.

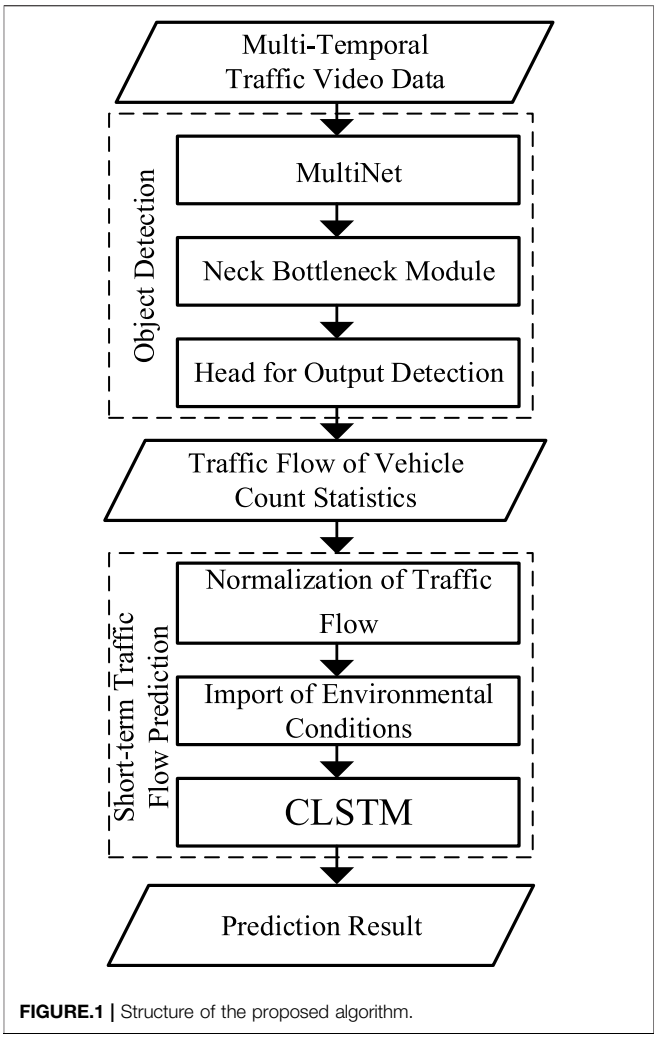

FIGURE.1 | Structure of the proposed algorithm.

The remainder of this article is organized as follows. After introducing the overall structure of our approach, the implementation details of object detection and traffic prediction are described in detail in **Section 2**. **Section 3** provides a case study of the junction level moving car monitoring and traffic flow prediction. Finally, **Section 4** concludes the study and points to potential applications of this research.

2 METHODS

2.1 Overall Structure of the Algorithm

Figure 1 shows the overview of our approach, including two parts. The first part is the vehicle detection and flow extraction from multi-temporal traffic video data, where the core neural network includes the Multi-Net of backbone, neck module for enhancing feature extraction, and head module for detecting the

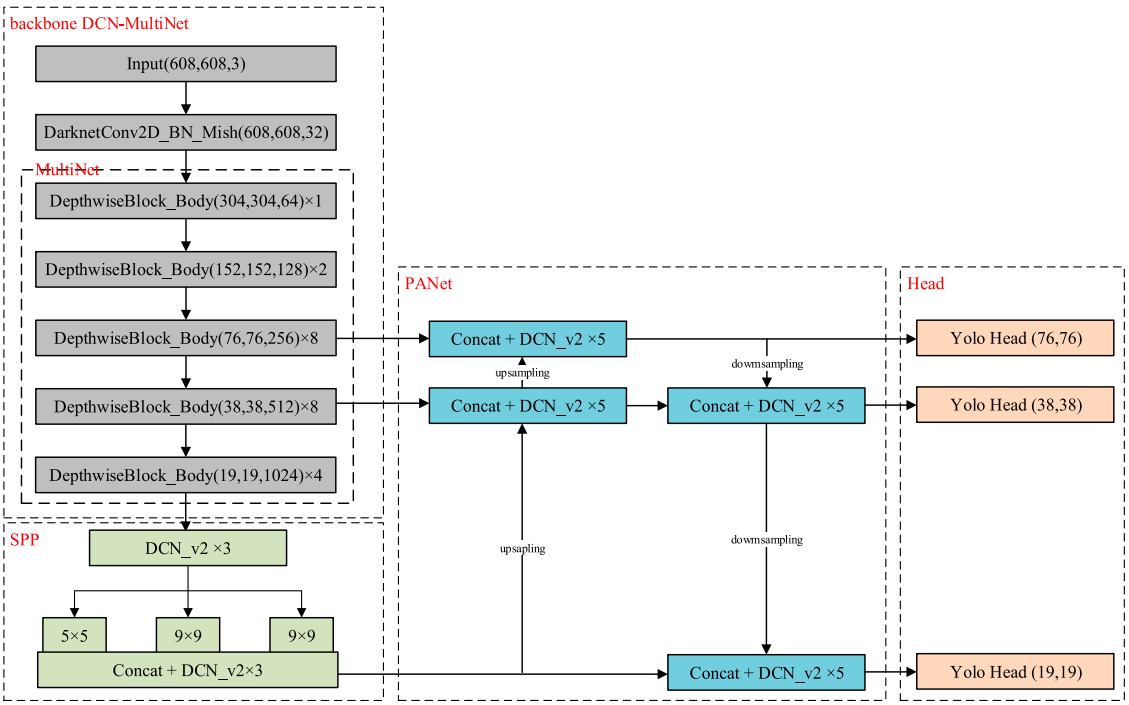

FIGURE 2 | Network architecture of DCN-MultiNet-YOLO.

output. In the second part, after normalizing the traffic data, we extracted the feature vector of environmental factors and imported it into an improved LSTM network to predict the traffic flow data under different weather conditions.

2.2 DCN-MultiNet-YOLO

According to the overall structure, target counting methods can be divided into those based on traditional feature extraction (Zhou et al., 2014; Denimal et al., 2017; Li et al., 2020) and those based on the convolutional neural network (CNN) (Yoo et al., 2016; He et al., 2017; Redmon and Farhadi, 2018). Traditional feature extraction methods include the Haar-like feature, the local binary pattern, and histogram of the oriented gradient. The aforementioned algorithm usually focuses on edge feature extraction to detect and count the individual targets, so it requires a high accuracy of edge detection and is not suitable for the counting of overlapping or dense targets. With the development of deep learning, the mainstream object detection and counting algorithms are realized by extracting target object features based on the CNN. On the basis of the original YOLOv3 target detection architecture, YOLOv4 (Bochkovskiy et al., 2020) is optimized in data processing and enhancement (Mosaic), backbone network (Backbone), network training (self-adversarial training), activation function (Mish), and loss function (Focal Loss), which greatly improve the accuracy of target detection and the training efficiency. In the data processing, YOLOv4 obtains the anchor box by clustering the ground-truth box and then uses the Mosaic data enhancement method to label and train targets with different scales. The backbone of YOLOv4 draws on the advantages of extracting deep feature information from deep residual learning [ResNet (He et al., 2016)]. It also adopts the design idea of a spatial pyramid pooling network [Spatial Pyramid Pooling Net (He et al., 2015) Atrous Spatial Pyramid Pooling Net (Liu and Huang, 2019)] to splice arbitrary size feature maps and convert them into fixed output size feature vectors, which can be output at one time to realize multi-scale object detection. The activation function YOLOv4 adopted is mixed with smooth, non-monotonic, and lack of upper bound characteristics. Although its computational complexity is higher than that of ReLu in YOLOv3, its detection effect is improved. In the final loss function training, YOLOv4 uses the idea of focal loss for reference, that is, redistributing the training weights of easy classification samples and difficult classification samples to achieve the accuracy of the two-level detector without losing the network training and prediction speed. Based on the original YOLOv4 network, our approach modifies the framework of backbone and applies the DCN V2 convolution to expand the receptive field of the feature layer and enhance the accuracy of object detection. As shown in **Figure 2**, the framework of the DCN-MultiNet-YOLO model can be divided into three parts: the backbone of DCN-MultiNet, bottleneck for enhanced feature, and head for detecting output, of which the neck mainly includes the SSP-Net and pyramid attention network. The network parameters of each component are described in detail as follows; the first two units of network parameters in the figure are pixel, and the last is depth. For example, as shown in the figure, the network $608 \times 608 \times 3$ represents an image with a pixel value of 608×608 and three channels.

DCN-MultiNet: DCN-MultiNet follows the darknet network in YOLOv4. In order to reduce the parameters of the network

structure, multi-convolution layers are used as the core hidden layer of the backbone network. All conventional convolutions in the network framework are replaced by deformable convolutions, which avert possible network accuracy degradation caused by separable convolution. Moreover, we introduced the cross-stage partial network to integrate the gradient changes into the feature map. A smoother Mish is applied instead of the original ReLu as the activation function, which obtains the three types of anchor boxes closest to the real frame by clustering the data in the ground-truth box. Finally, according to the input image with a pixel of 608 × 608×3, the neural network outputs three scale feature maps with shapes of 76 × 76, 38 × 38, and 19 × 19.

Neck: The bottleneck module is designed to enhance the ability of network feature extraction. SSP-Net uses three convolution layers with different shapes to expand the perception threshold of the feature map to the front hidden layer, which can enhance the target recognition ability of the network. SSP-Net also introduces a differentiation pooling strategy, which not only avoids the risk of network overfitting but also outputs fixed size image features. Based on the feature pyramid network (FPN), PANet uses downsampling and upsampling methods to fuse different scale feature maps at the same time so that the output layer after mapping and fusion has richer features and improves the expression ability of the network for shallow feature information and deep semantic information.

Head: The output of the feature map corresponds to the last three feature layers of the backbone network, with shapes of 76 × 76 × 75, 38 × 38 × 75, and 19 × 19 × 75, which has the ability to perform multi-feature layer object detection. The first two dimensions represent the size of the feature map grid, which can extract targets of different shapes. The third dimension is related to the dataset used in network training. If the dataset has 20 categories and the dimensions of location information and category information are five, we should set the layer with a shape of 3 × (20 + 5) to adapt to the anchor box.

To test the detection accuracy of the proposed architecture, we compared the mean average precision between other neural network structures. The formula of precision is as follows:

$$P = TP/(TP + FP), \tag{1}$$

where P represents the algorithmic precision, TP indicates that a positive sample is correctly retrieved as a positive sample, and a false positive indicates that a negative sample is incorrectly retrieved as a positive sample. The formula for recall is as follows:

$$R = TP/(TP + FN), \tag{2}$$

where R represents the recall rate of the algorithm, and FN indicates the number of positive samples that were incorrectly retrieved as negative samples. An excellent objection detection model means that the accuracy increases as the recall rate increases. The average precision is obtained by integrating the P–R curves of a class. The formula for the average precision is as follows:

$$AP = \int_0^1 p(r)dr. \tag{3}$$

The mean average precision (mAP) is the average of the area under the P–R curve for all categories. The formula for mAP is as follows:

$$mAP = \frac{1}{n}\sum_{k=1}^{n} AP_k. \tag{4}$$

2.3 Conditional Long Short-Term Memory

The detected traffic flow from video images, as one of the basic parameters of short-term traffic prediction parameters, can be used as the key basis of traffic decision in the intelligent transportation system (Chen and Chen, 2020). Short-term prediction is to provide short-term (usually 5–10 min) or even real-time traffic prediction based on the traffic data close or exact to the current observation (Petkovics et al., 2015; Fu et al., 2016). Short-term traffic flow prediction is very challenging due to the stochastic and dynamic traffic condition. In recent years, scholars from around the world have conducted widespread and thorough research of LSTM or its variants in short-term traffic flow forecasting with excellent achievements. Ma et al. (2015) developed a long short-term memory (LSTM) neural network to predict the travel speed prediction based on RTMS detection data in Beijing city. The proposed model can capture the long-term temporal dependency for time series and also automatically determine the optimal time window. Zheng et al. (2017) put forward a traffic forecast model based on the LSTM network that considers temporal–spatial correlation in the traffic system *via* a two-dimensional network composed of many memory units. Du et al. (2020) proposed a deep irregular convolutional residual LSTM network model called DST-ICRL for the urban traffic passenger flow prediction. Little et al. (1981) proposed an end-to-end deep learning architecture that consists of convolution and LSTM to form a Conv-LSTM module to extract the spatial–temporal information from the traffic flow information. Moreover, Ma et al. (2021 and Zheng et al. (Dai et al., 2019; Zheng et al., 2021) proposed an improved LSTM model to improve the accuracy of short-term traffic flow prediction. However, in addition to the traffic flow statistics itself, weather conditions, emergencies, and other external environmental conditions also have great changes on the flow value, which have received less attention in the aforementioned literature studies. The conditional long short-term memory (CLSTM) proposed in this article inputs the aforementioned environmental conditions and traffic flow to the LSTM network and fully connected layer (FC layer), respectively. Then, the output of them is fed into the feature fusion layer (FF layer) and FC layer, which finally export the predicted traffic flow.

Before introducing the structure of the CLSTM, we first described the problem setting of our traffic scenario. The problem of traffic flow prediction can be formulated as follows. First, we divided the total traffic flow into multiple time periods at every Δ time interval and summarized the traffic flow at each period. Let X_i^c denote the traffic flow of the i

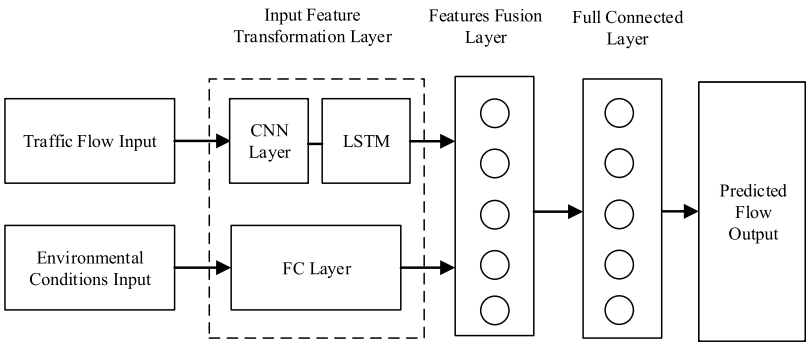

FIGURE 3 | Network architecture of CLS.

th time period under environmental condition c, at current time t (i =t); the task is to predict the traffic flow of this moment by the historical traffic flow sequence with some prediction domain σ and time interval Δ. The formal expression is as follows:

$$\text{Historical traffic flow}: \left\{X_i^c \middle| i = t - n\Delta,\ t - (n-1)\Delta, \ldots, \text{t} - \Delta \text{and c} \in \vec{\boldsymbol{C}}\right\}, \tag{5}$$

where C means a set containing different environmental conditions.

$$\text{Predicted traffic flow}: \left\{X_i^c \middle| i = t + \Delta,\ t + 2\Delta, \ldots, \text{t} + m\Delta \text{ and } m\Delta < \sigma\right\}. \tag{6}$$

For example, when we consider $\Delta = 5$ minutes, n = 12, and σ = 3, it can be divided into 288 traffic flow values in 24 h of a single day, and the objective is to predict three traffic flow values in the future 15 min by using 12 traffic flow values in the past 60 min. After the environmental condition expressed as a feature vector $\vec{\boldsymbol{C}}$, we can combine the historical traffic flow and the environmental condition. Let $c \in \vec{\boldsymbol{C}}$ mean different environmental conditions (for example, if c_1 represents the weather condition, then c_1 = 0,1,2,3 ... means rainy, sunny, foggy, and so on); the traffic flow from time t–n to t can be represented as $X_i^{c_1} = [\, f_{t-n\Delta}^{c_1}, f_{t-(n-1)\Delta}^{c_1}, \ldots, f_{t-\Delta}^{c_1}\,]$, where f_t^c denotes the traffic flow value under environmental condition c_1. If we have k sets of environmental condition vectors, the combined historical traffic flow and the environmental condition can be represented by the matrix as follows:

$$\overrightarrow{\boldsymbol{X}_i^c} = \begin{bmatrix} X_{t-n\Delta}^c \\ \vdots \\ X_{t-\Delta}^c \end{bmatrix} = \begin{bmatrix} f_{t-n\Delta}^{c_1} & \cdots & f_{t-n\Delta}^{c_k} \\ \vdots & \ddots & \vdots \\ f_{t-\Delta}^{c_1} & \cdots & f_{t-\Delta}^{c_k} \end{bmatrix}. \tag{7}$$

As shown in **Figure 3**, the proposed CLSTM consists of an input feature transformation layer, a feature fusion layer, and a fully connected layer (FC layer). The traffic flow input is the time series vector $\vec{\boldsymbol{X}}_{\boldsymbol{i}}$, which contains the traffic flow value per Δ time. The traffic flow input is a 1 × n vector, and it feeds into a multilayer of a CNN layer and an LSTM network, which has been proposed for a variety of applications such as network fault prediction (Tan and Pan, 2019), gesture recognition (Zhang et al., 2018), and speech emotion recognition (Zhang et al., 2019) to obtain the short-term temporal feature of the traffic flow. The second input is a 1 × m vector $\vec{C}$ of the environmental condition, and it feeds into an m × 64 FC layer. The output shape of both components of the input feature transformation layer is a 1 × 64 vector. Finally, the feature fusion layer is followed by an FC layer, both of which are regression layers, to perform forecasting. The output shape of the predicted flow is 1 × m.

The loss function we selected as the RMSE is the square root of the ratio of the square of the deviation between the value and the actual value, divided by the number of observations. The RMSE used to measure the deviation between the observed value and the actual value is calculated as follows:

$$Loss = RMSE = \sqrt{\frac{1}{n}\sum\nolimits_{i=1}^{n}\left(y_i - y_i^{'}\right)^2}. \tag{8}$$

Besides the RMSE, we used another two functions—the mean of absolute error (MAE) and mean absolute percentage error (MAPE)—as the accuracy evaluation indicators for comparing these prediction algorithms (Ma et al., 2018; Weng et al., 2018; Xu et al., 2018; Chen C. et al., 2019; Chen F. et al., 2019; Wu et al., 2019) in order to ensure the robustness of the forecast algorithm. MAE, which means the average absolute error, is calculated as follows (in all the following formulas, n represents the sample size, y_i is the actual value, and $y_i^{'}$ is the predicted value):

$$MAE = \frac{1}{n}\sum\nolimits_{i=1}^{n}\left|y_i - y_i^{'}\right|. \tag{9}$$

The MAPE represents the average of the absolute values of relative percentage errors, which is calculated as follows:

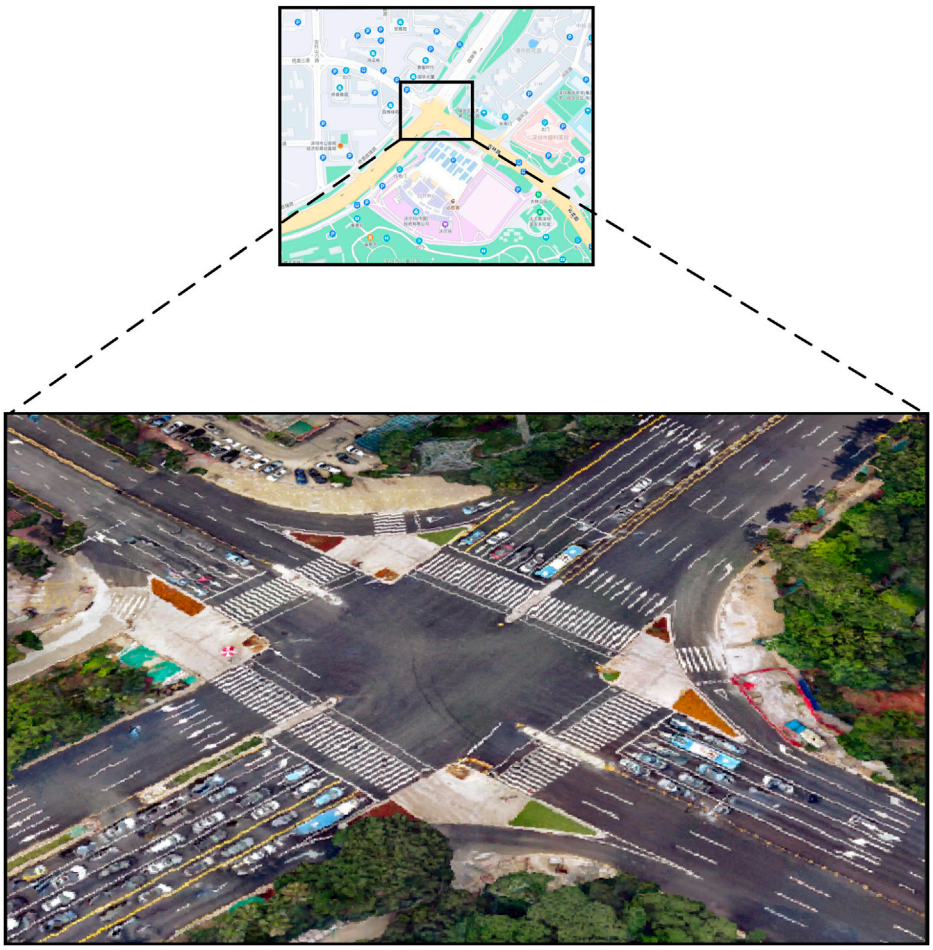

FIGURE 4 | Illustration of the study area.

$$MAPE = \frac{100\%}{n}\sum_{i=1}^{n}\left|\frac{y_i - y_i^{'}}{y_i}\right|. \quad (10)$$

3 RESULTS AND DISCUSSION

3.1 Data and Environment

In this section, we evaluated the performance of the proposed model by using a real-world dataset for object detection and short-term traffic flow prediction. The detailed hardware configuration of this experiment is as follows: the CPU of the computer is Intel (R) core (TM) i9-9900k, the CPU frequency is 3.60 GHz, the memory is 64G, the graphics card model is NVIDIA GeForce RTX 2080ti, and the graphics memory is 11G×2. Our application is deployed on the 64-bit operating system Ubuntu 16.04 with the deep learning frameworks of TensorFlow 1.13.1 and Keras 2.3.1 and the parallel computing framework of CUDA 10. The traffic data were collected at the intersection of Qiaoxiang and Nonglin Roads in Futian District, Shenzhen (**Figure 4**) between 1 June and 31 July 2021. The weather data come from the China National Meteorological Science Data Center.

3.2 Results for Multi-Target Tracking

The core idea of DCN-MultiNet-YOLO is separable convolution. The standard convolution is decomposed into a depth-wise convolution and a point-wise convolution, which play the role of filtering and linear combination, respectively, in order to reduce the number of parameters and calculation. As mentioned earlier, we used the DCN V2 convolution to expand the receptive domain that can improve the accuracy of the target detection model at the cost of slightly sacrificing the amount of parameters. As can be seen from **Table 1**, the parameter quantity of DCN-MultiNet-YOLO is only 0.48% more than that of MobileNet and 17% more than that of CSPDarknet. Meanwhile, in order to compare the training time of the algorithm, we set the size of the training batch to 32 and the total training cycle to 200. It is found that when MultiNet is used as the backbone, a single training cycle can cut the training time in half.

In order to verify the detection effect of different algorithms, the second experiment compares the AP results of all categories in the voc2007 + 2012 dataset, which implement the MobileNet and the CSPDarknet53 as backbones in the control group. **Figure 5** shows that compared with the YOLOv4 network, whose backbone network is MobileNet and CSPDarknet53, the mAP of DCN-MultiNet-YOLO increased by 13.19% and 6.63%, respectively.

TABLE 1 | Model parameters of different backbone networks.

	Non-trainable param (K)	Trainable param	Total param	Train time (min)
MobileNet	63	11,405K	11,468K	7
CSPDarknet	66	64,363K	64,429K	16
DCN-MultiNet	62	11,461K	11,523K	7

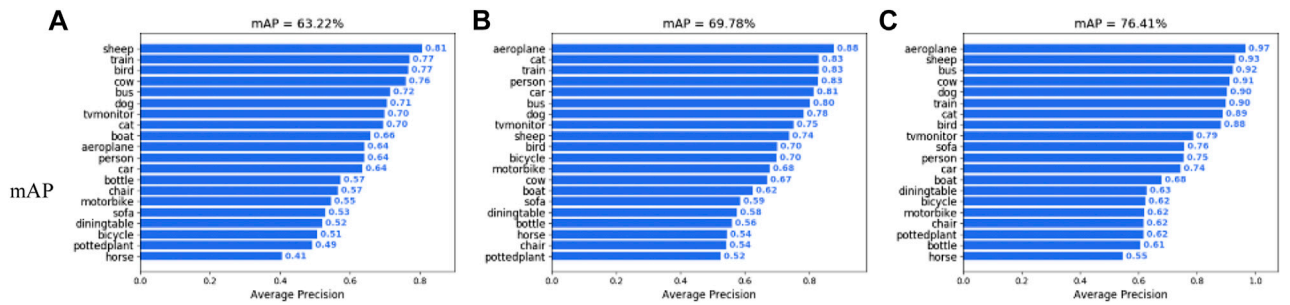

FIGURE 5 | AP values of different backbone networks: **(A)** MobileNet, **(B)** CSPDarknet, and **(C)** DCN-MultiNet-YOLO.

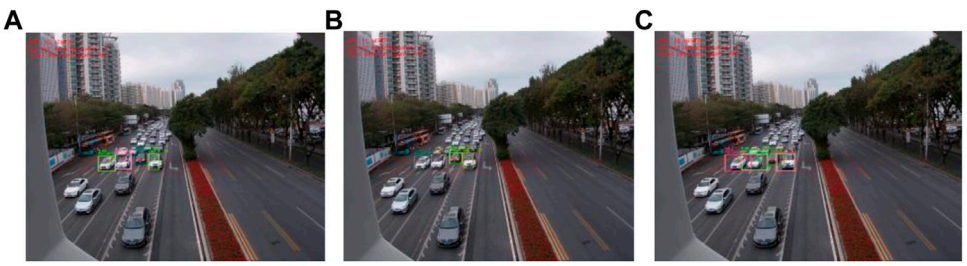

FIGURE 6 | Model test results of different backbone networks: **(A)** MobileNet, **(B)** CSPDarknet, and **(C)** DCN-MultiNet-YOLO.

TABLE 2 | Example of vehicle count statistics in each lane from 7 to 9 a.m., 1 June 2021.

	1	2	3	4	5	6	7	8	9	10	11	12	13	14	15	16	17	18	19	20	21	22	23
1	35	35	37	34	46	35	33	35	40	42	34	29	24	43	26	31	34	36	35	35	37	37	23
2	37	35	34	38	40	36	30	42	44	29	32	38	34	46	35	40	44	38	40	44	48	49	47
3	27	27	29	29	28	28	29	28	32	20	27	26	28	30	31	28	35	34	23	30	40	26	39
4	31	30	40	33	37	51	35	32	45	25	35	37	34	34	39	34	52	42	37	45	52	42	39
5	14	16	17	14	16	16	10	12	11	12	10	14	11	13	11	10	12	14	11	13	11	14	10
6	13	12	20	17	17	19	15	15	18	12	13	15	11	14	14	17	17	18	16	24	13	18	18
FPS	16	15	17	15	16	16	17	16	16	14	16	14	15	16	15	15	15	17	15	17	17	16	17

In **Figure 6**, we compared the results of object detection and lane vehicle count of different models. It should be noted that the detection frame rate is related to the currently detected number and training model. The higher the number of detected objects under the same model, the lower is the frame rate. It can be seen from **Figure 5** that DCN-MultiNet-YOLO has more current and total detection counts and faster real-time frame rates than that applied to MobileNet and CSPDarknet53 as the backbone in the network.

Finally, we obtained the traffic flow every 5 min in all directions of the Qiaoxiang–Nonglin road using DCN-MultiNet-YOLO. **Table 2** shows the example of the obtained traffic flow of six lanes from west to east 7:00 to 9:00 a.m. on 1 June 2021, in which the column numbers represent each 5-min time period during the morning peak hours, and row numbers represent different lanes.

3.3 Results for Short-Term Traffic Flow Prediction

Using the aforementioned object detection algorithm to make traffic statistics on the images of the Qiaoxiang–Nonglin intersection, we

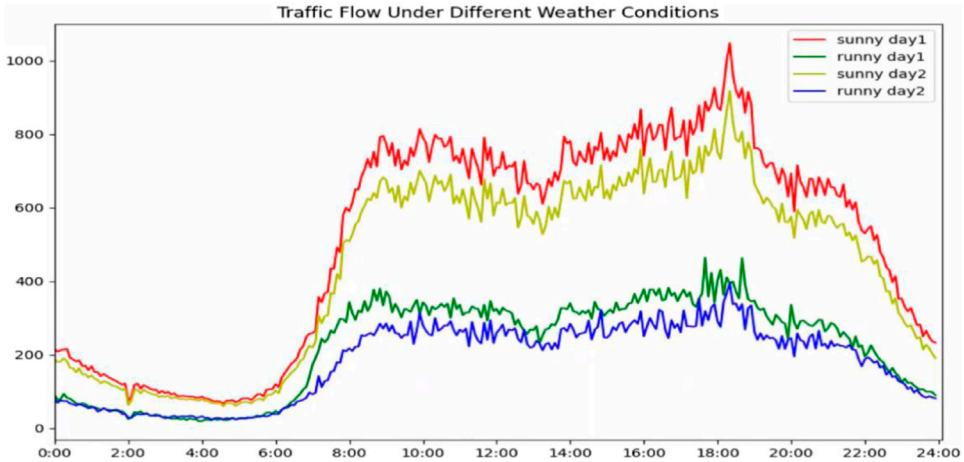

FIGURE 7 | Traffic flow under different weather conditions.

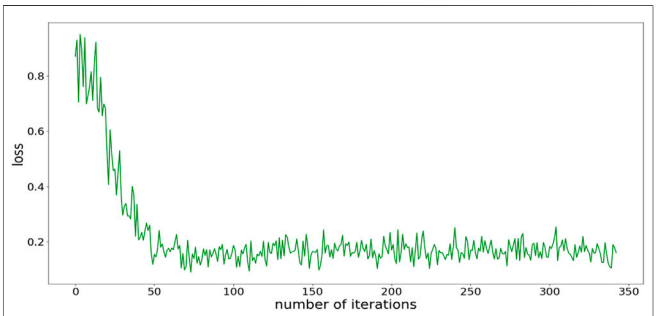

FIGURE 8 | Loss function curve of the algorithm.

TABLE 3 | Comparison of the prediction results of four models.

Network structure	Evaluation function	Weather conditions		
		Sunny	Cloudy	Rainy
KNN	RMSE	30.22	38.31	52.54
	MAE	23.57	31.11	38.39
	MAPE (%)	24.05	32.28	40.37
LSTM	RMSE	18.58	26.27	35.73
	MAE	12.97	18.65	25.82
	MAPE (%)	13.14	19.26	26.01
Cov-LSTM	RMSE	15.32	19.24	27.38
	MAE	12.06	16.72	19.35
	MAPE (%)	12.71	17.13	20.42
CLSTM	RMSE	15.74	16.78	18.31
	MAE	13.65	14.34	16.06
	MAPE (%)	12.91	15.19	16.85

Note: All the results are obtained by averaging on each day for the test dataset (about 10 days).

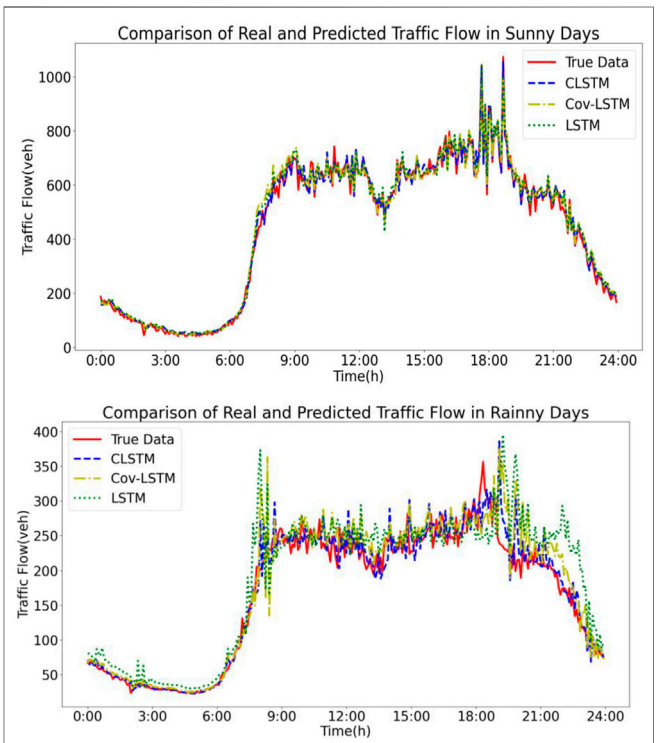

FIGURE 9 | Comparison of real and predicted traffic flows under different weather conditions.

can obtain the traffic statistics of the intersection for 2 months. We accumulated the traffic flow of three turns (left, right, and straight) in four directions (east, south, west, and north) every 5 min as a sample. After removing the abnormal data, a total of 5616 sample records were generated by using the traffic flow in 2 months. We used 85% of the aforementioned records as the training set and 15% as the test set. As shown in **Figure 7**, we first selected 4 days (two sunny days and two rainy days) to analyze the traffic data of the whole day. From the traffic flow data, we can draw the following conclusions: 1) the total traffic flow on rainy days is lower than that on sunny days. This is because the intersection is located in a busy section of Shenzhen, and the rainy days reduce the commuting ability of this road because many vehicles that would have taken this road chose other roads. 2)

We compared the correlation coefficient of the two sets of data and found that the correlation coefficient of the two groups of traffic flow data on sunny days is 0.935 and on rainy days it is 0.872, indicating that traffic changes are more random on rainy days, which makes it more difficult to predict.

It can be seen from **Figure 8** that the loss function of the algorithm decreases with the number of iterations. The loss function begins to converge after about 70 iterations and finally converges to about 0.16. The convergence of the algorithm proves that the traffic prediction method proposed in this article is feasible.

Two kinds of neural network structures—LSTM and Cov-LSTM (Liu et al., 2017)—are compared as benchmarks of the proposed network for prediction performance in this article. We also selected the KNN representative clustering algorithm to compare the accuracy of traffic prediction.

According to **Table 3**, on the sunny day, the CLSTM has RMSE, MAE, and MAPE values of 15.74, 13.65, and 12.91%, respectively, which are slightly higher than the values of Cov-LSTM of 15.32, 12.06, and 12.71% but lower than those of LSTM and KNN. On non-sunny days (cloudy and rainy days), the proposed module can achieve a smaller prediction error than the other module with all three metrics for all prediction horizons. On the cloudy day, it has RMSE, MAE, and MAPE values of 16.78, 14.34, and 15.19%, respectively, and 18.31, 16.06, and 16.85% on the rainy day. This is because the environmental conditions of the traffic flow are usually interwoven with each other, which can be captured more efficiently by the CLSTM module. The results prove the effectiveness of the proposed model.

Furthermore, we compared the prediction performance of both the benchmark neural network and CLSTM. Although the three network structures can eventually converge and overcome the long-term dependency of RNN, their performances are different. **Figure 9** illustrates performance comparison in terms of the predicted traffic volume from 0:00 a.m. to 12:00 p.m. for a 5-min prediction horizon. It can be seen that all three networks have relatively good prediction performance on sunny days. However, the prediction performance of the benchmark network on rainy days is not sufficient. In particular, in the evening and morning rush hours when there is a large fluctuation in traffic volume, the performance advantages of CLSTM are particularly prominent.

4 CONCLUSION

The grip of traffic flow patterns from multi-temporal images is essential to mitigating urban congestion and can assist in the construction of smart cities. In this article, we made use of 2-month traffic video data for traffic flow monitoring and prediction. We proposed 1) DCN-YOLO, a novel multi-target tracking and counting method for moving targets, which introduced the DCN V2 convolution into the YOLOv4 backbone network and replaced the original CSPDarknet network in order to solve the problem of limited detection accuracy of the MobileNet model. 2) CLSTM, a variant of the LSTM network, which takes the environmental conditions as the feature fusion layers for the short-term traffic flow prediction. Through the case study of one popular road junction in the metropolitan area, the results indicated the better performance of the proposed architecture, of which the mAP of the moving car detection with DCN-YOLO increased by 13.19%, and the prediction RMSE of the CLSTM decreased by 49.01% on rainy days.

Despite the strength of the proposed algorithms in this work, there is still room for improvement. With respect to object detection, it could be necessary to embed depth-wise separable convolution to reduce the number of CSPDarknet53 of the YOLOv4 network to fit for real-time operations at the mobile end. In terms of short-term traffic flow prediction, the current weather conditions can only be described as qualitative variables, such as sunny and rainy days, which limit the prediction accuracy to a certain extent. Future work can include more quantitative factors such as precipitation and air pressure. In addition to factors from the physical environment, human factors, such as driver behaviors under emergency events, can be considered to make the model closer to reality.

DATA AVAILABILITY STATEMENT

The original contributions presented in the study are included in the article/Supplementary Material, further inquiries can be directed to the corresponding author.

AUTHOR CONTRIBUTIONS

YZ conceived and designed the study and also provided funding; NW contributed to the study design, made improvements to the algorithm, and drafted the manuscript; XL contributed to the data acquisition and experimental study; and LX was involved in data acquisition and revision of the manuscript.

REFERENCES

Bochkovskiy, A., Wang, C. Y., and Liao, H. (2020). *YOLOv4: Optimal Speed and Accuracy of Object Detection*. doi:10.48550/arXiv.2004.10934

Chen, C., Cheng, R., and Ge, H. (2019). An Extended Car-Following Model Considering Driver's Sensory Memory and the Backward Looking Effect. *Physica A: Stat. Mech. its Appl.* 525, 278–289. doi:10.1016/j.physa.2019.03.099

Chen, F., Song, M., Ma, X., and Zhu, X. (2019). Assess the Impacts of Different Autonomous Trucks' Lateral Control Modes on Asphalt Pavement Performance. *Transportation Res. C: Emerging Tech.* 103, 17–29. doi:10.1016/j.trc.2019.04.001

Chen, X., and Chen, R. (2020). "A Review on Traffic Prediction Methods for Intelligent Transportation System in Smart Cities," in 2019 12th International Congress on Image and Signal Processing, BioMedical Engineering and Informatics (CISP-BMEI), Suzhou, China, 19-21 Oct. 2019 (IEEE). doi:10.1109/CISP-BMEI48845.2019.8965742

Dai, G., Ma, C., and Xu, X. (2019). Short-term Traffic Flow Prediction Method for Urban Road Sections Based on Space-Time Analysis and GRU. *IEEE Access* 7 (99), 143025–143035. doi:10.1109/ACCESS.2019.2941280(

Denimal, E., Marin, A., Guyot, S., Journaux, L., and Molin, P. (2017). Automatic Biological Cell Counting Using a Modified Gradient Hough Transform. *Microsc. Microanal* 23 (01), 11–21. doi:10.1017/S1431927616012617

Du, B., Peng, H., Wang, S., Bhuiyan, Z. A., Wang, L., Gong, Q., et al. (2020). Deep Irregular Convolutional Residual LSTM for Urban Traffic Passenger Flows Prediction. *IEEE Trans. Intell. Transportation Syst.* 21 (3), 972–985.

Fu, R., Zhang, Z., and Li, L. (2016). "Using LSTM and GRU Neural Network Methods for Traffic Flow Prediction," in 2016 31st Youth Academic Annual Conference of Chinese Association of Automation (YAC), Wuhan, China, 11-13 Nov. 2016 (IEEE). doi:10.1109/yac.2016.7804912

He, K., Gkioxari, G., Dollár, P., and Girshick, R. (2017). "Mask R-CNN," in 2017 IEEE International Conference on Computer Vision (ICCV), Venice, Italy, 22-29 Oct. 2017 (IEEE). doi:10.1109/ICCV.2017.322

He, K., Zhang, X., Ren, S., and Sun, J. (2016). "Deep Residual Learning for Image Recognition," in 2016 IEEE Conference on Computer Vision and Pattern Recognition (CVPR), Las Vegas, NV, USA, 27-30 June 2016 (IEEE). doi:10.1109/CVPR.2016.90

He, K., Zhang, X., Ren, S., and Sun, J. (2015). Spatial Pyramid Pooling in Deep Convolutional Networks for Visual Recognition. *IEEE Trans. Pattern Anal. Machine Intelligence* 37 (9), 1904–1916. doi:10.1109/TPAMI.2015.2389824

Khatoun, R., and Zeadally, S. (2016). Smart Cities. *Commun. ACM* 59 (8), 46–57. doi:10.1145/2858789

Khekare, G. S., and Sakhare, A. V. (2013). "A Smart City Framework for Intelligent Traffic System Using VANET," in 2013 International Mutli-Conference on Automation, Computing, Communication, Control and Compressed Sensing (iMac4s), Kottayam, India, 22-23 March 2013 (IEEE). doi:10.1109/imac4s.2013.6526427

Li, D., Miao, Z., Peng, F., Wang, L., Hao, Y., Wang, Z., et al. (2020). Automatic Counting Methods in Aquaculture: A Review. *J. World Aquaculture Soc.* 52. doi:10.1111/jwas.12745

Little, J., Kelson, M., and Gartner, N. (1981). MAXBAND: A Program for Setting Signals on Arteries and Triangular Networks. *Transportation Res. Rec. J. Transportation Res. Board* 795, 40–46.

Liu, S., and Huang, D. (2019). *Learning Spatial Fusion for Single-Shot Object Detection*. doi:10.48550/arXiv.1911.09516

Liu, Y., Zheng, H., Feng, X., and Chen, Z. (2017). "Short-term Traffic Flow Prediction with Conv-LSTM," in 2017 9th International Conference on Wireless Communications and Signal Processing (WCSP), Nanjing, China, 11-13 Oct. 2017 (IEEE). doi:10.1109/WCSP.2017.8171119

Ma, C., Dai, G., and Zhou, J. (2021). Short-Term Traffic Flow Prediction for Urban Road Sections Based on Time Series Analysis and LSTM_BILSTM Method. *IEEE Trans. Intell. Transport. Syst.* (99), 1–10. doi:10.1109/tits.2021.3055258

Ma, C., Hao, W., He, R., and Moghimi, B. (2018). A Multiobjective Route Robust Optimization Model and Algorithm for Hazmat Transportation. *Discrete Dyn. Nat. Soc.* 2018, 1–12. doi:10.1155/2018/2916391

Ma, X., Tao, Z., Wang, Y., Yu, H., and Wang, Y. (2015). Long Short-Term Memory Neural Network for Traffic Speed Prediction Using Remote Microwave Sensor Data. *Transportation Res. Part C: Emerging Tech.* 54, 187–197. doi:10.1016/j.trc.2015.03.014

Marais, J., Meurie, C., Attia, D., Ruichek, Y., and Flancquart, A. (2014). Toward Accurate Localization in Guided Transport: Combining GNSS Data and Imaging Information. *Transportation Res. Part C: Emerging Tech.* 43, 188–197. doi:10.1016/j.trc.2013.11.008

Mckenney, M., and Frey-Spurlock, C. (2018). "Aging in Place: Challenges for Smart & Resilient Communities," in SIGSPATIAL '18: 26th ACM SIGSPATIAL International Conference on Advances in Geographic Information Systems, November 2018, 1–2. doi:10.1145/3284566.3284567

Petkovics, Á., Simon, V., Gódor, I., and Böröcz, B. (2015). Crowdsensing Solutions in Smart Cities towards a Networked Society. *EAI Endorsed Trans. Internet Things* 1 (1), e6. doi:10.4108/eai.26-10-2015.150600

Raja, G., Ganapathisubramaniyan, A., Selvakumar, M. S., Ayyarappan, T., and Mahadevan, K. (2018). "Cognitive Intelligent Transportation System for Smart Cities," in 2018 Tenth International Conference on Advanced Computing (ICoAC), Chennai, India, 13-15 Dec. 2018 (IEEE). doi:10.1109/icoac44903.2018.8939091

Redmon, J., and Farhadi, A. (2018). *YOLOv3: An Incremental Improvement*. doi:10.48550/arXiv.1804.02767

Tan, Z., and Pan, P. (2019). "Network Fault Prediction Based on CNN-LSTM Hybrid Neural Network," in 2019 International Conference on Communications, Information System and Computer Engineering (CISCE), Haikou, China, 5-7 July 2019 (IEEE). doi:10.1109/cisce.2019.00113

Telang, S., Chel, A., Nemade, A., and Kaushik, G. (2021). "Intelligent Transport System for a Smart City," in *Security and Privacy Applications for Smart City Development*.

Weng, J., Du, G., Li, D., and Yua, Y. (2018). Time-varying Mixed Logit Model for Vehicle Merging Behavior in Work Zone Merging Areas. *Accid. Anal. Prev.* 117, 328–339. doi:10.1016/j.aap.2018.05.005

Wu, W., Liu, R., Jin, W., and Mac, M. (2019). Stochastic Bus Schedule Coordination Considering Demand Assignment and Rerouting of Passengers. *Transportation Res. B: Methodological* 121, 275–303.

Xu, X., Šarić, Ž., Zhu, F., and Babić, D. (2018). Accident Severity Levels and Traffic Signs Interactions in State Roads: a Seemingly Unrelated Regression Model in Unbalanced Panel Data Approach. *Accid. Anal. Prev.* 120, 122–129. doi:10.1016/j.aap.2018.07.037

Yoo, D., Park, S., Lee, J.-Y., Paek, A. S., and Kweon, I. S. (2016). "AttentionNet: Aggregating Weak Directions for Accurate Object Detection," in 2015 IEEE International Conference on Computer Vision (ICCV), Santiago, Chile, 7-13 Dec. 2015 (IEEE). doi:10.1109/iccv.2015.305

Zear, A., Singh, P. K., and Singh, Y. (2016). Intelligent Transport System: A Progressive Review. *Indian J. Sci. Technology* 9 (32), 1–8. doi:10.17485/ijst/2016/v9i32/100713

Zhang, L., Zhu, G., Mei, L., Shen, P., Shah, S. A. A., and Bennamoun, M. (2018). "Attention in Convolutional LSTM for Gesture Recognition," in Proceedings of the 32nd International Conference on Neural Information Processing Systems, 1957–1966.

Zhang, S., Zhao, X., and Tian, Q. (2019). Spontaneous Speech Emotion Recognition Using Multiscale Deep Convolutional LSTM. *IEEE Trans. Affective Comput.*, 1. doi:10.1109/TAFFC.2019.2947464

Zheng, H., Lin, F., Feng, X., and Chen, Y. (2021). A Hybrid Deep Learning Model with Attention-Based Conv-LSTM Networks for Short-Term Traffic Flow Prediction. *IEEE Trans. Intell. Transport. Syst.* 22 (11), 6910–6920. doi:10.1109/TITS.2020.2997352

Zheng, Y., Guo, R., Ma, D., Zhao, Z., and Li, X. (2020). A Novel Approach to Coordinating Green Wave System with Adaptation Evolutionary Strategy. *IEEE Access* 8, 214115–214127. doi:10.1109/ACCESS.2020.3037129

Zheng, Z., Chen, W., Wu, X., Chen, P. C. Y., and Liu, J. (2017). LSTM Network: a Deep Learning Approach for Short-Term Traffic Forecast. *Iet Intell. Transport Syst.* 11 (2), 68–75.

Zhou, Y., Ji, J., and Song, K. (2014). A Moving Target Detection Method Based on Improved Frame Difference Background Modeling. *Tocsj* 8 (1), 970–975. doi:10.2174/1874110x01408010970

Conflict of Interest: Author NW is employed by Guangzhou Wonping Info-Tech Co., Ltd.

The remaining authors declare that the research was conducted in the absence of any commercial or financial relationships that could be construed as a potential conflict of interest.

Publisher's Note: All claims expressed in this article are solely those of the authors and do not necessarily represent those of their affiliated organizations, or those of the publisher, the editors, and the reviewers. Any product that may be evaluated in this article, or claim that may be made by its manufacturer, is not guaranteed or endorsed by the publisher.

Copyright © 2022 Zheng, Li, Xu and Wen. This is an open-access article distributed under the terms of the Creative Commons Attribution License (CC BY). The use, distribution or reproduction in other forums is permitted, provided the original author(s) and the copyright owner(s) are credited and that the original publication in this journal is cited, in accordance with accepted academic practice. No use, distribution or reproduction is permitted which does not comply with these terms.

frontiers | Frontiers in Environmental Science

ORIGINAL RESEARCH
published: 13 May 2022
doi: 10.3389/fenvs.2022.864966

Road Safety Evaluation Framework for Accessing Park Green Space Using Active Travel

Yuanyuan Luo[1], Yanfang Liu[1], Lijun Xing[2], Nannan Wang[1] and Lei Rao[1]*

[1]School of Resource and Environmental Sciences, Wuhan University, Wuhan, China, [2]Faculty of Resources and Environmental Science, Hubei University, Wuhan, China

The COVID-19 pandemic has led to a burgeoning demand for active travel (walking or cycling), which is a healthy, pollution-free, and affordable daily transportation mode. Park green space (PGS), as an open natural landscape, have become a popular destination for active travel trips in metropolitan areas. Pedestrians and cyclists are often at high crash risk when exposed to complicated traffic environments in urban areas. Therefore, this study aims to propose a safety assessment framework for evaluating active travel traffic safety (ATTS) near PGS from the perspective of urban planning and exploring the effect of the point-of-interest (POI) aggregation phenomenon on ATTS. First, links between ATTS and the environment variables were investigated and integrated into the framework using the catastrophe model. Second, the relationship between the POI density and ATTS was investigated using three spatial regression models. Results in the Wuhan Metropolitan Area as a case study have shown that (1) the population density, road density, nighttime brightness, and vegetation situation near PGS have pronounced effects on ATTS; (2) pedestrians near PGS enjoy safer road facilities than cyclists. Active travel traffic near PGS requires more attention than non-park neighborhoods; (3) among four park categories, using active travel to access theme parks is the safest; and (4) SEM has the best fit for POI cluster research. Increases in leisure facility density and residence density may lead to deterioration and improvement in ATTS safety levels near PGSs, respectively. The safety framework can be applied in other regions because the selected environment indicators are common and accessible. The findings offer appropriate traffic planning strategies to improve the safety of active travel users when accessing PGS.

Keywords: active travel, urban green space, traffic safety, framework integration, spatial regression

OPEN ACCESS

Edited by:
Ying Jing,
Zhejiang University, China

Reviewed by:
Sanwei He,
Zhongnan University of Economics and Law, China
Shenjun Yao,
East China Normal University, China
Haoran Yang,
East China Normal University, China

****Correspondence:***
Yanfang Liu
yanfangliu88@163.com

Specialty section:
This article was submitted to Environmental Informatics and Remote Sensing, a section of the journal Frontiers in Environmental Science

Received: *29 January 2022*
Accepted: *12 April 2022*
Published: *13 May 2022*

Citation:
Luo Y, Liu Y, Xing L, Wang N and Rao L (2022) Road Safety Evaluation Framework for Accessing Park Green Space Using Active Travel. Front. Environ. Sci. 10:864966. doi: 10.3389/fenvs.2022.864966

1 INTRODUCTION

The importance of safety in urban transport and mobility has been recognized in achieving the globally discussed and accepted goals for human development (Poku-Boansi et al., 2019). Road traffic injuries are one of the top 10 causes of death in the world. The World Health Organization (WHO) reported that approximately 1.35 million people die in road traffic accidents every year, while 93% of global road deaths occur in middle- and low-income countries (World Health Organization, 2018). In China, vulnerable road users (i.e., pedestrians, motorcyclists, and pedal cyclists) accounted for more than 70% of the road traffic deaths between 2006 and 2016 (Wang et al., 2019). The crash risk of pedestrians, motorcyclists, and pedal cyclists in urban areas is often higher than that of vehicle users

due to their vulnerable characteristics when exposed to complicated traffic environments. However, in most Chinese cities, pedestrian and cyclist infrastructure and travel safety are yet to receive any major attention in terms of research, policies, and interventions. As the number of pedestrians and cyclists actively traveling increases, the risk of injury prompts the in-depth evaluation of route safety (Brown et al., 2017).

Park green space (PGS) plays a significant role in modern society, especially under giant working and psycho pressure (Ekkel and de Vries, 2017; Yang et al., 2019). Due to the purpose of health, most people choose a method of active travel (walk or cycle) to access park green spaces, which have been the main places for leisure and sports. Especially when residences are in the service range of PGS, they are willing to improve their physical activity, psychological restoration, and social contacts by access to PGS with active travel three to four times a week. Recent literature has studied various integrated indexes of walkability to PGS including safety, convenience, comfortability, and accessibility since the walk score was released (Lee and Hong, 2013; Lwin and Murayama, 2011; Xu et al., 2017). As residents access parks searching for recreation and relaxation, safety guarantees have an important influence on their decision (Wang et al., 2015). However, it is common to see many studies examine the methodology of the parks' internal safety evaluation by multi-criteria but fail to evaluate roadside safety facilities (Baran et al., 2018; Zavadskas et al., 2019). In addition, previous studies mainly conducted in developed Western countries; specialization in the safety index system is urgently needed for developing nations due to incomplete road facilities.

This study uses the Wuhan Metropolitan Area as an example and proposes the ATTS assessment framework based on road units, which includes safety assessment and sociodemographic factor analysis. The safety assessment uses the catastrophe model based on several environmental parameters. Sociodemographic factors were analyzed by converting POI density using kernel density estimation (KDE), followed by OLS, spatial error model (SEM), and spatial lag model (SLM) to explain the macroscopic distribution of AT accidents. We cannot be optimistic about ATTS because the safety situation is not fairly distributed within urban settings. The findings offer appropriate traffic planning strategies to improve the safety of active travel users.

This study contributes to the existing literature in various aspects: 1) an objective and systematic assessment framework for ATTS is first presented; 2) the correlation between various built environment parameters near PGS and active travel crash frequency is investigated; 3) the active travel safety status of roads near four types of parks is evaluated and; 4) the potential effects of the POI aggregation phenomenon near PGS reflected by the ATTS spatial distribution is explored.

The rest of this article is organized as follows: **Section 2** reviews the existing literature on the influencing factors of ATTS and presents an overview of the socioeconomic parameters that may affect safety inequity. The methodology and the materials adopted are discussed in **Section 3**. **Section 4** shows the results of the ATTS framework, which comprise the safety assessment and spatial regression. **Section 5** presents the research arguments and discusses the determinants of ATTS. Finally, in **Section 6**, our main conclusions are drawn, while future avenues for research are suggested.

2 LITERATURE REVIEW

2.1 Active Travel Accident Near PGSs

A large proportion of traffic fatalities occur inside urban and metropolitan areas, where the risk factors associated with congestion and high densities of vehicles and pedestrians coexist (Vorko-Jović et al., 2006; Dumbaugh and Rae, 2009). Traffic characteristics (such as traffic flow and speed) and road characteristics (such as road geometry and the quality of infrastructure) may affect road accidents (Ayati and Abbasi, 2011; Lord et al., 2005; Martin, 2002; Wang et al., 2009). The behaviors of vehicle drivers and pedestrians (e.g., driving speed and the use of seat belts) and the change in environmental variables (e.g., road conditions and traffic lights) have been investigated in a previous study related to urban accidents (Ramírez and Valencia, 2021). Walking and cycling have been examined separately in multiple studies at varying depths. Active travel consisting of both has become a trend. However, no studies have been conducted to examine road safety in the built environment for walking and cycling in a unified framework.

Neighborhoods near parks may represent a higher risk of collision injury or death because they attract more susceptible road users. Young energetic tourists and elderly residents may congregate in areas around parks. When it comes to transportation to parks, children prefer to use active transportation (Pont et al., 2009). The elderly are more likely to walk, rather than ride a bike to a local park (Duan et al., 2018). Therefore, active travelers in general are more susceptible in the absence of adequate infrastructure.

In the literature, the risk factors for pedestrian and cyclist–motor vehicle accidents have been mainly examined from the aspects of active travel users' characteristics, road conditions, and the environment surrounding the accident site. Children and old pedestrians are prone to motor vehicle accidents (O'Hern and Oxley, 2015; Poku-Boansi et al., 2019; Smith et al., 2020; Värnild et al., 2020; Yee et al., 2006). Road conditions, which comprise road network design and center turning lane settings, the number of traffic lanes, and road demarcation, are important risk factors for the occurrence of pedestrian and cyclist accidents (Shankar et al., 2003; Hess et al., 2004; Donroe et al., 2008). Environmental factors such as location, traffic volume, road lighting, and the time of the day may significantly affect the likelihood of pedestrian and cyclist accidents (Simončič, 2001; Shankar et al., 2003; Wier et al., 2009; Miranda-Moreno et al., 2011). The risk of pedestrian and cyclist injury is relatively high in areas with heavy traffic (Zhang et al., 2014). Findings indicate that pedestrian and cyclist injury or death may easily occur at intersections without traffic lights (Moudon et al., 2011; Hu et al., 2018).

The existing literature focuses on the effects of active travel users' personal characteristics, such as age, gender, and income, on ATTS. However, no studies have been conducted to compare

the variability and injury risk of active traffic accidents due to differences in the environment near various types of parks and explain the macroscopic distribution of active traffic accidents using a three-class spatial regression model. In addition, some specific ATTS risk factors such as road infrastructure (motorized and nonmotorized road facilities) and various urban traffic regulations (i.e., trunk roads, secondary trunk roads, and branch ways) should be taken into consideration.

2.2 Active Travel-Related Variables

This study on active travel-involved crashes covers a wide range of factors, which comprise the characteristics of road user behavior. Strong correlations between objective indicators of the built environment and traffic safety are well documented (Saha et al., 2020). Previous studies on the microlevel (road, segments, and intersections) examined the relationship between road safety and various parameters, such as built environment features (Clifton et al., 2009; Galanis et al., 2017). From the perspective of traffic safety, it is proposed that studying traffic characteristics, roadway characteristics, physical characteristics, and POI characteristics can help promote an understanding of the relationship between the built environment and active travel crashes.

Accidents usually occur when traffic moves. Therefore, investigating traffic characteristics to understand their influence on ATTS is significant (Golob and Recker, 2004; Lord et al., 2005). Increases in traffic volume are associated with an increase in the total crash frequency; hence, the effects of traffic exposure and land use characteristics are based on this (Wier et al., 2009; Lee et al., 2015). Various studies have associated greater traffic exposure with a higher frequency of accidents and accident severity (Abdel-Aty et al., 2013). For the improvement of ATTS, environmental indicators are also considered. Traffic calming is a significant transport intervention for population health, which decreases the negative influences of motor vehicles (Morrison et al., 2003; Pucher et al., 2010). Increasing the amount of walking and cycling is an effective way of reducing the chances of incurring injuries (Jacobsen, 2003).

Based on the engineering theory, roads play a significant role in road safety. Improved geometry design and infrastructure could help improve road safety, including ATTS (Noland, 2003; Noland and Oh, 2004). Among the road facilities, sidewalks are a major component of the transportation network and should provide pedestrians with safe, healthy, and attractive walking conditions (Aghaabbasi et al., 2018). The influence of environmental factors on walking, such as sidewalks, has contributed to the development of various measurements of the effects of environmental factors on walking but lacks the macro-level evaluation (Cunningham et al., 2005). Bicycle lanes may lessen the risks for bicycle riders by preventing crashes against motor vehicles, reducing the burden of traffic injuries, improving the sense of safety, and promoting greater participation in cycling. Bicycle lanes have several types: exclusive, shared, and parking lanes; marked wide curbside lanes; and curbside bicycle lanes. Among these types, only exclusive bicycle lanes are associated with decreased accidents, while greater separation provides better protection for cyclists and traffic (Morrison et al., 2019). Guardrails are installed as guides to safe crossing areas and prevent pedestrians from bursting into the road (Retting et al., 2003). In London, accidents at sites with guardrails are reportedly 2.5 times lower than those in areas without such facilities (Zheng et al., 2007). The study shows the importance of sidewalks, bicycle lanes, and guardrails in ATTS. The construction of pedestrian crossing facilities has become the main choice for reducing the negative effect of roads on pedestrians at the cost of crossing convenience. However, building these road facilities using observational and GIS measures requires investments in staff, training, data management, and high-quality data in numerous locations. Using street view can solve these problems (Brownson et al., 2009).

Physical environments exert influences that can facilitate or mitigate traffic safety. The correlation of nighttime brightness and vegetation with urban safety is generally assessed as a significant social humanities environment aspect. Street lighting is a necessary urban feature for improving the clarity when driving (Xu et al., 2018), while vegetation, as an along-street physical environment, may influence safety (Wolfe and Mennis, 2012; Fitzpatrick et al., 2014). Street lighting, walking and cycling paths, and street monitoring by buildings relate to personal safety when people actively travel (Administration, 1992). These two factors show various correlations with urban safety in various regions; thus, the effect of nighttime brightness and vegetation on active traffic safety and its intensity in Wuhan is explored in our study.

While POI data are not a typical factor used in traditional traffic accident analysis, it is specific to land use factors with precise location information (Jia et al., 2018). Previous studies have confirmed that the number, density, and distribution of POIs are significantly correlated with human–vehicle crashes (Kuo and Lord, 2021; Brühwiler et al., 2022; Zhu et al., 2022). Diverse POI types such as hospitals, markets, banks, hospitals, residential areas, and restaurants are often used as the main study subjects (Ng et al., 2002; Jia et al., 2018; Lee et al., 2018).

According to systematic reviews, the physical activities of adults, which include active travel, are affected by the safety environmental attributes from the physical and sociocultural perspectives (Wendel-Vos et al., 2007). However, their research mainly focuses on traffic control, natural monitoring, and concrete driving scene but lacks a general framework with strong application for evaluating the relationship between the built environment and road space.

2.3 Integration Method

The integration of transportation modes, which coordinates the harmony of transport modes, such as pedestrian, bicycle, and motor vehicle, is an important issue for urban transportation system safety (Saplıoğlu and Aydın, 2018). Obtaining the ATTS level involves a multi-attribute assessment, and combining indicators to form an effective safety assessment system is challenging. Various studies have focused on the integration method, including the traditional AHP (Żak and Kruszyński, 2015), the AHP with GIS (Saplıoğlu and Aydın, 2018; Zheng et al., 2019), and its hybrid approach based on SERVQUAL and fuzzy

TOPSIS (Awasthi et al., 2011; dos Santos et al., 2019; Vavrek and Chovancová, 2019). Quantitative studies on road safety facilities have focused on questionnaire preference surveys (Räsänen et al., 2007; Demiroz et al., 2015; Anciaes and Jones, 2018). For the aforementioned methodologies, an integrated level or index is formulated by assigning weights to the selected indicators via expert evaluation or interview questionnaires. This method is time-consuming and labor-intensive and has a certain degree of subjectivity. Traditional methods are criticized for incorporating inherent uncertainty and their inability to avoid subjectivity (Zhou et al., 2019).

Unlike the aforementioned methods with subjectivity and uncertainty, the catastrophe theory (CT) can explain the internal mechanism of all indicators' influences on ATTS. The CT has been used to simulate the sudden and inconsecutive phenomena in the natural world (Thom, 1976). According to the inactive importance of indicators, CT-integrated multiple assessments affect the safety of using active travel to green spaces without calculating the weight. The behavior that integrates indices from the bottom- to top-layer systems can be recognized as a steady construction within the catastrophe system. Small variations in the bottom-layer systems would lead to the destruction of the entire steady state (Su et al., 2011). Particularly, prior studies mainly focused on developed Western countries (e.g., the United States, Britain, and Japan); specialization in the safety index framework is urgently needed for developing nations owing to their insufficient road facilities.

The spatial clustering method for macroscopic traffic accident analysis based on POI data is used to identify traffic accident frequency distribution in areas with unreliable conventional traffic accidents and traffic data (Barua et al., 2015). Many researchers have performed crash hotspot identification on point data using various methods, such as crash frequency, crash rate, improvement potential, empirical Bayes (EB), and KDE (Montella, 2010; Yu et al., 2014). In several studies, the KDE correlated method is considered as the most promising method to describe the spatial patterns present in various parameters and adopted (Chainey and Ratcliffe, 2013). There is a lack of example studies using KDE to cluster line-like elements.

3 MATERIALS AND METHODS

3.1 Study Area

Wuhan, the most populated and fastest growing metropolitan, is the capital of Hubei Province in central China. Located in latitude 29°58′–31°22′N and longitude 113°41′–115°05′E, Wuhan comprises 16 administrative districts, including seven central urban districts, four functional districts, and five new urban districts. The latest government data, the statistical communique of the People's Republic of Wuhan on the 2018 National Economic and Social Development, shows its 81 integrated parks with a per capita area of 9.61 m^2/person. The present study uses the case of the Wuhan Metropolitan Area to introduce the ATTS assessment framework evaluating the road to green spaces and examine the effect of the POI aggregation phenomenon on ATTS (shown in **Figure 1**).

In this study, according to the Planning Report on the Green Space System in Wuhan from 2011 to 2020, parks are divided into four categories, with each park having its own serving scope and function: (a) urban parks are the main PGSs with various functions, such as recreation, sightseeing, ecological balance, and disaster shelter. Urban parks serve 2 km along the road network; (b) regional parks serve a smaller range of approximately 1 km along the road network than urban parks; (c) topic parks distribute areas into various specific themes, such as zoos and aquatic and cultural parks. Topic parks also serve 1 km along the road network; and (d) community parks cover an area of 2–5 ha and are combined with residential areas, ensuring that people can reach green spaces within 500 m. Residents in the urban center enjoy the functions of large-scale parks (urban, regional, and topic parks) more than those in the metropolitan fringes. Given the large-scale parks that cover a large area (urban, regional, and topic parks accounted for 43.2, 14.4, and 22.6% of the land, respectively), the services provided are very diverse.

3.2 ATTS Assessment Framework and Data Description

The factors of safety assessment are usually related to traffic, road, and physical characteristics (Golob and Recker, 2003; Wang et al., 2013). **Figure 2** shows the detailed aspects and data source of the ATTS assessment framework. The framework comprises two major parts: the first step is safety assessment and the second step is spatial regression. First, the safety assessment is performed using a catastrophe model to evaluate a total of 10 variables for traffic characteristics, road characteristics, and physical environment to obtain road-scale ATTS levels. The developed ATTS level brings a standardized measure of road active traffic safety to the field of transportation planning. The second is statistical modeling of POI and ATTS levels with one simple linear regression and two spatial models. This aims to estimate the properties and correlations of POI distributions with ATTS levels.

Wuhan Planning and Design Institute provides 2018 road network data, PGS data, traffic characteristic data, and crossing facilities spatial data for Wuhan. The PGS data comprise the spatial location, size, name, and function category, while the facilities data comprise footbridges and underpasses. Traffic characteristics data, which include population, road, and vehicle number data, are collected on 18 June 2018, in the middle of the year. The original data include all road categories. Thus, we included trunk roads, secondary trunk roads, and branch ways that allow for active travel routes within the green space service range. All fundamental data are transformed into the road level based on the visual interpretation of the street view and the grid processing. Given the unreliable small-scale spatial population data and the unavailability of economic data from the government, this study focuses on the POI density based on spatial analysis. The POI data are integrated with the traffic crash data to identify the varying land use and its effect on traffic safety. When assessing the POI density, the buffer

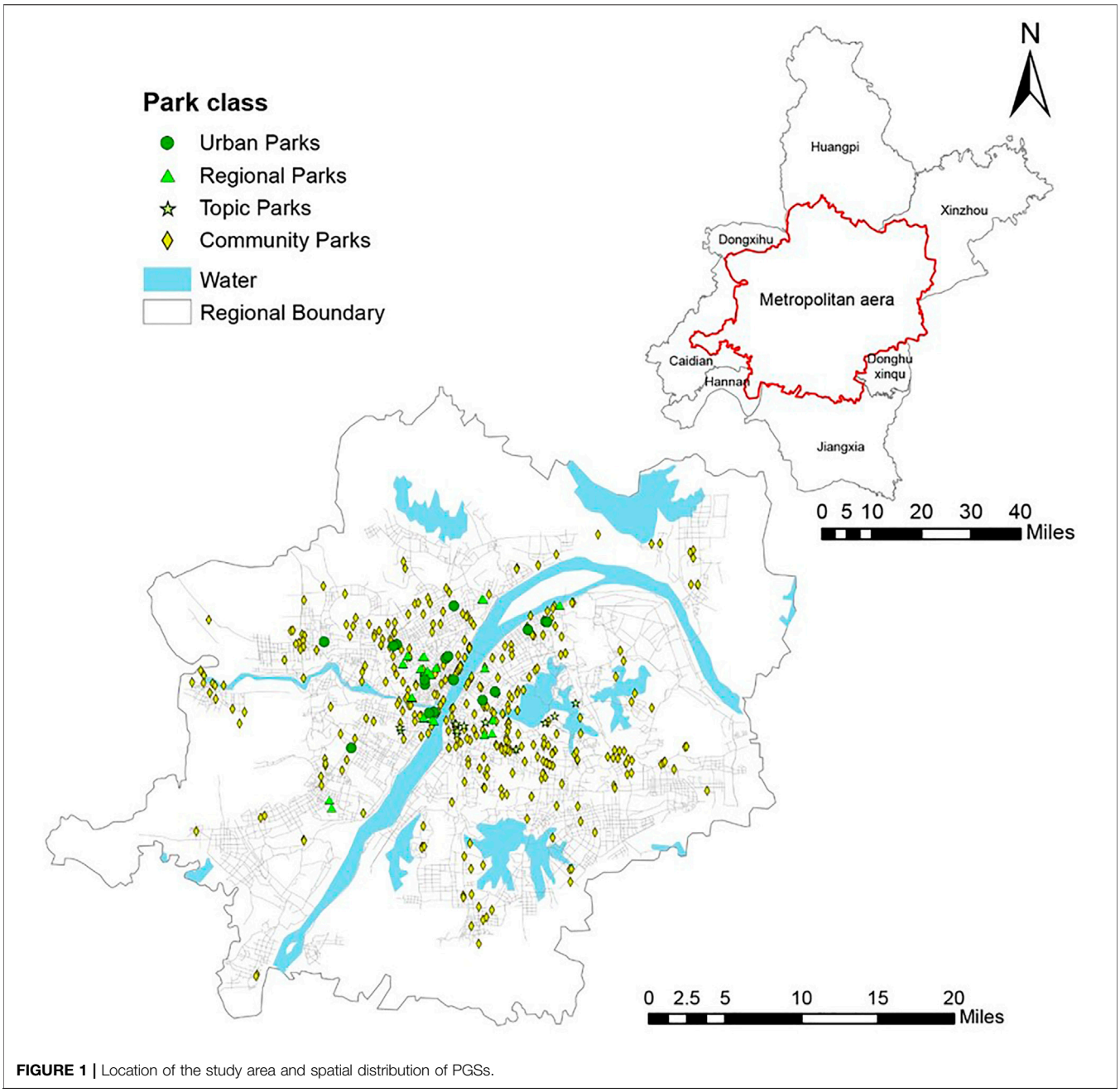

FIGURE 1 | Location of the study area and spatial distribution of PGSs.

range is set to 500 m with each road as a unit. **Table 1** presents the calculated road attributes.

3.3 Data Preprocessing

3.3.1 Crash Frequency Data

Given the limited police crash report records available in China, the study on ATTS remains largely insufficient. Previous studies used media data for crash information and relevant safety research (Yankson et al., 2010; Goddard et al., 2019). Similar to other types of crashes, walking- and cycling-related crashes with valuable injury information, such as gender, age, and severity, have been reported in the news many times (Yang et al., 2020). Such representative news reports provide useful information and have the potential to facilitate ATTS research.

This study took advantage of a Wuhan official news search engine (www.cjn.cn) to gather media-reported crash information and build a surrogate crash database for analytics. The keywords "road name + walking crash" (e.g., walking crash on the Hongshan Road) and "road name + cycling crash" (e.g., cycling crash on the Hongshan Road) were used to search news websites to determine the crash frequency of every road. The search period was from January 1 to 31 December 2018. This study only targeted crash reports containing essential

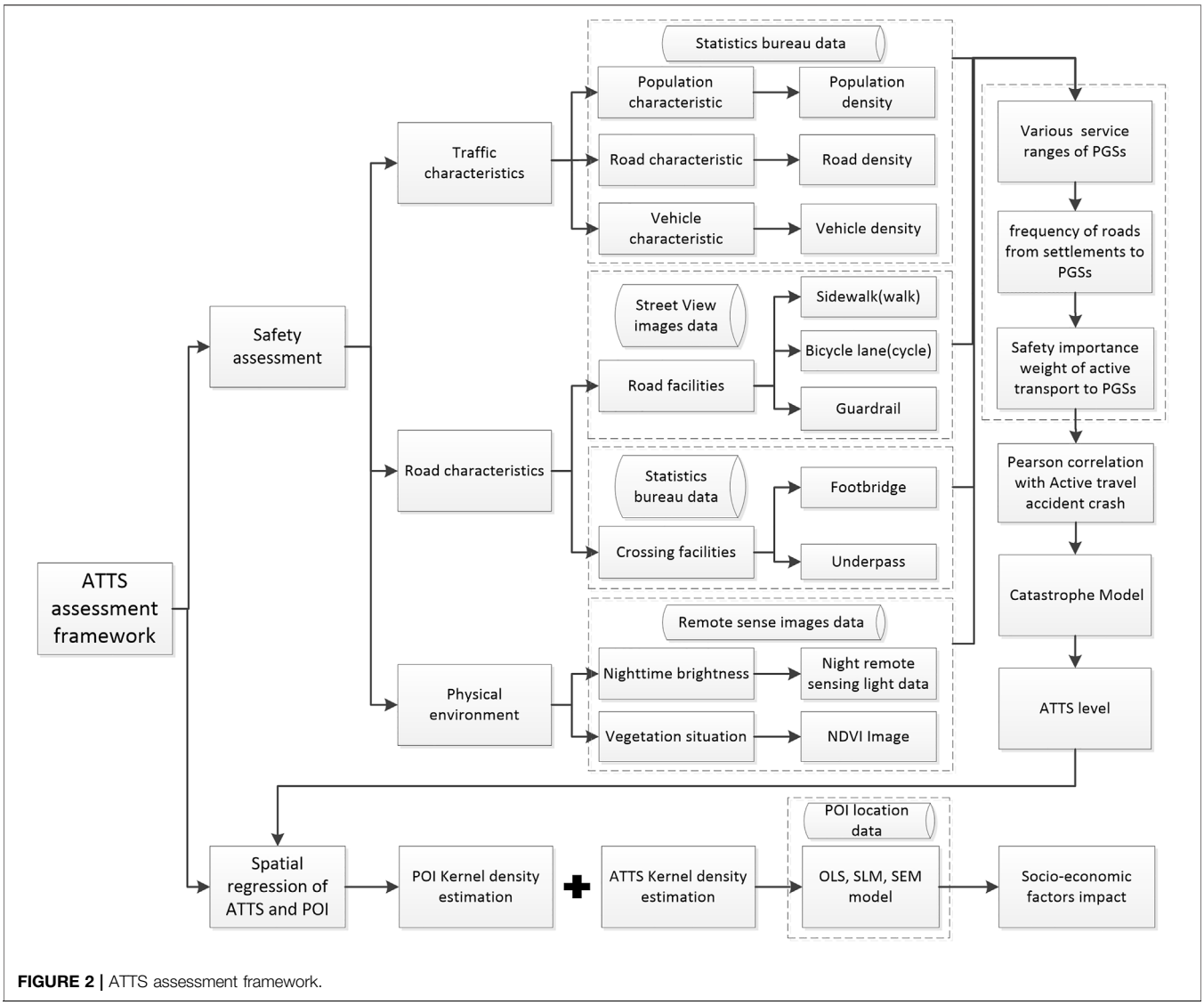

FIGURE 2 | ATTS assessment framework.

components, including the date, location, victim description, and crash facts (e.g., type). The collected text information may be duplicated and must be cross-checked. A total of 147 walking crashes and 179 cycling crashes were identified through the mining of news reports during the study period.

3.3.2 Street View Images

We acquired road auxiliary facility data, including sidewalks, guardrails, and bicycle lanes, through the Baidu Maps street view (BMSV) image data using the Baidu Maps API. Given that Google Maps is inaccessible, Baidu Maps is a good substitute. The BMSV documents imagery from 372 cities that covers more than 738,000 km and provides a 360° panorama of cities, streets, and other environments. The BMSV is a free and accessible online scenery map service for everyone. On the basis of the road location next to green spaces supplied by the road network data, we sent an HTTP request with coordinates and the uniform resource locator (URL) parameters of the target road position to obtain a static street view near the PGSs.

Given the complicated road conditions and varying types of facilities, we used visual interpretation to classify the level of road infrastructure. On the basis of the previous research and the local road facility construction criterion, the interpretation rule and a few examples are shown in **Table 2** and **Figure 3**.

This study obtained the crossing facility shapefiles in Wuhan from a local planning department. Thus, we considered crossing facilities as an indicator integrated into the evaluation framework. Footbridges and underpasses, as grade-separated facilities, tend to be safe when people face the risk of vehicle collisions on the road. The design specification of urban road traffic facilities (http://www.mohurd.gov.cn/wjfb/201908/t20190829_241614.html) states that crossing facilities should be set when the motor width exceeds 25 m. Therefore, not all road-crossing facilities are evaluated using the same criterion. Roads with insufficient widths are assessed as having average standards.

TABLE 1 | Data description.

Variable	Max	Min	Mean	Std
Built environment				
Population density (persons/km^2)	8265.3117	0	1677.8342	1553.7297
Road density (km/km^2)	10.2498	0	5.3728	4.9720
Vehicle density (vehicle/km^2)	241.53	0	47.2983	12.1059
Sidewalks	1	0	0.8217	0.3346
Bicycle lanes	1	0	0.1299	0.3228
Guardrails	1	0	0.2786	0.4108
Footbridges	1	0	0.9324	0.2510
Underpasses	1	0	0.9158	0.2777
Nighttime brightness	328288	0	54710.1426	35827.0661
Vegetation coverage	676067	17650	343484.436	91283.1690
POI density				
Restaurant density	59453.8144	0	4957.5599	8798.6139
Leisure facility density	1286.6212	1.4239	240.2072	212.1846
Hospital density	177.3928	0	12.5326	36.9121
Residence density	197.5652	0	43.4395	39.4975
School density	118.3315	0	9.4824	8.2576
Bank density	153.6234	0	22.2876	32.2345
Accidents				
Number of accidents correlated with walking	20.6	0	0.5998	1.5865
Number of accidents correlated with cycling	25.1	0	0.6334	1.9204

TABLE 2 | Visual interpretation judging criteria.

Road infrastructure	Good (1)	Medium (0.5)	Bad (0)
(a) Sidewalks	Wide	Narrow	Without
(b) Bicycle lanes	Individual	Mixed	Without
(c) Guardrails	Complete	Rough	Without

3.3.3 Remote Sense Images

3.3.3.1 Nighttime Light Imagery Data

Users can obtain the LJ-01 cloud-free nighttime light imagery data for free by logging in at http://www.hbeos.org.cn/, which is available for scientific research and teaching organizations. Removing noise from the LJ1-01 data is unnecessary because the negative pixels have already been removed (Zhang et al., 2019). According to a released report on LJ1-01, the images are geometrically corrected by the system. However, to investigate the street lighting condition accurately, the experimental images must be geometrically corrected corresponding to the actual road network, which can be recognized clearly with 130-m-resolution imagery. Thus, we collected approximately 30 ground control points in the road intersections. The images also require absolute radiation correction, while the conversion formula adopted is

$$L = DN^{3/2} \times 10^{-10}, \quad (1)$$

where L is the radiance value after absolute radiation correction in $W/(m^2 \times sr \times \mu m)$ and DN is the gray value of each pixel (Zhang et al., 2019). The extracted roads are used as the mask to obtain the nighttime light images from the region required by our experiment, which include the entire Wuhan city data set of LJ1-01 nighttime light images. The ultimate nighttime light imagery is shown in **Figure 4**.

3.3.3.2 NDVI Data

The NDVI derived from satellite imagery is a widely used index, which indicates the growth status and parameter of vegetation. In this study, the NDVI values from the 250-m monthly Terra MODIS NDVI (MOD13Q1) in June 2018 are unitless and ranged from −2000 to 10000. After the standardized process, with a scale factor of 0.0001, the range becomes 0–1.0. The high values indicate the increased concentration of green vegetation and bush density.

3.4 Catastrophe Model

The CT is a powerful mathematical tool for studying the evolution of the system order. This theory explains and predicts a sudden phenomenon in nature and society. Additionally, the CT has broad application prospects in mathematics, physics, biology, engineering technology, and social science. The system tends to achieve an ideal stable state or enter a defined state range when at rest, without external forces. Upon receiving external forces of change, the system initially attempts to absorb external pressure through reaction. If such forces of change are too strong to be fully absorbed, a catastrophic change occurs, and the system then enters a new stable state; otherwise, it would return to its original state. The return of the system to its original stable state through continuity is impossible. **Table 3** introduces the four primary catastrophe models required in the dimensions of the control parameters.

3.5 Kernel Density Estimation

Because the object units of our study are roads, the benefit of calculating the distance from each road to the hospital is tiny. Therefore, we calculated the density of POI around the roads. KDE is used to transform discrete check-in points with POIs into continuous surfaces that reflect their spatial density. By using the density method, an arbitrary spatial unit of analysis can be

FIGURE 3 | Interpretation of the street view (from left to right is good, medium, and bad). **(A)** Sidewalks, **(B)** bicycle lanes, and **(C)** guardrails.

defined that is homogenous for the entire area, which makes the comparison and ultimately classification possible (Jia et al., 2018). The KDE can be described by

$$f(s) = \sum_{i=1}^{n} \frac{1}{h^2} k\left(\frac{d_{is}}{h}\right), \tag{2}$$

TABLE 3 | Summary of possible catastrophe models

Category	Dimension of control parameter	Potential function	Bifurcation set	Normalization formula
Fold model	$f(x) = x^3 + ax$	$a = -3x^2$	$X_a = \sqrt{a}$	1
Cusp model	$f(x) = x^4 + ax^2 + bx$	$a = -6x^2$, $b = 8x^3$	$x_a = \sqrt{a}$, $x_b = \sqrt[3]{b}$	2
Swallowtail model	$f(x) = x^5 + ax^3 + bx^2 + cx$	$a = -6x^2$, $b = 8x^3$, $c = -3x^4$	$x_a = \sqrt{a}$, $x_b = \sqrt[3]{b}$, $x_c = \sqrt[4]{c}$	3
Butterfly model	$f(x) = x^6 + ax^4 + bx^3 + cx^2 + dx$	$a = -10^{x2}$, $b = 20x^3$, $c = -15x^4$, $d = 4x^5$	$x_a = \sqrt{a}$, $x_b = \sqrt[3]{b}$, $x_c = \sqrt[4]{c}$, $x_d = \sqrt[5]{d}$	4

FIGURE 4 | Clipped imagery of LJ-01 cloud-free nighttime light imagery data.

where $f(s)$ is the KDE function at location s, h denotes the bandwidth, d_{is} represents the distance from point i to s, and k is a space weight function. Previous studies indicated that the choice of k barely affects the results and that the threshold of the distance decay is important. In this study, the bandwidth ranging from 100 to 1000 m was tested. The optimum bandwidth was tested to be 500 m as it resulted in a density pattern that was neither excessively sharp nor excessively smooth.

3.6 Spatial Regression Models

General spatial models have the following relative forms (Griffith, 1988):

$$Y = \rho W_1 Y + X\beta + \mu, \tag{3}$$

$$\mu = \lambda W_2 \mu + \varepsilon where \varepsilon \sim MVN(0, \sigma^2 I_n), \tag{4}$$

where Y is the dependent variable, X is an $(n \times n)$ matrix of k explanatory variables, ρ and λ are spatial autoregressive coefficients, ρ is the intensity of the spatial dependence of sample observations, λ is the effect of the error of the dependent variable in the neighborhood on the observations in the region, W_1 and W_2 are $(n \times n)$ spatial weight matrices, μ is the unobserved error term that can incorporate spatial correlation through its first term, ε is an $(n \times 1)$ vector of unobserved error terms that are identically and independently distributed, MVN is the multivariate normal distribution, and I_n is the $(n \times n)$ identity matrix. In **Eq. 3**, the model becomes an SLM when W_2 is 0 and a SEM when W_1 is 0. This study uses the queen's method of the spatial contiguity matrix, which defines neighbors as sharing a common side or vertex with the region of interest.

4 RESULTS

4.1 Exploration of Factors Affecting ATTS

Pearson's correlation was used to test the correlation between the crash frequency and the built environment factors to indicate ATTS. The effects were negative when the coefficient was positive, and *vice versa*. Results show that population density has a positive impact on ATTS, and the coefficient is −0.182. This result indicates that individual risk may decline as the volume increases. Road density has a negative effect on ATTS, while the coefficient is 0.095. This result is consistent with the conclusions of previous studies (Kononov et al., 2008). The large number of roads indicates the existence of numerous intersections, which may easily lead to accidents. Road and crossing facilities, except footbridges, were found to have positive influences on ATTS. Among the road facilities, bicycle lanes are the most helpful in improving road safety, while the coefficient is −0.071 ($p < 0.01$), indicating the importance of maintenance in nonmotorized vehicle lanes due to their proximity to driveways and exposure to accidents. Street nighttime lighting was found to be an important factor that affects ATTS in parks, while the coefficient is −0.121. Improved street nighttime lighting significantly decreases ($p < 0.01$) the crash frequency because nighttime poses additional risks to pedestrians. However, these risks can be mitigated by lighting (Bernhardt and Kockelman, 2021). The abundance of vegetation can significantly decrease ($p < 0.01$) the crash frequency. Dense woods where trees isolate lanes and sidewalks can prevent accidents that cause injury. Kaplan (1987) also reported that vegetation may have mentally healing functions that could reduce the psychological harbinger of criminals. The Pearson coefficient results were used in the subsequent catastrophic model calculation.

4.2 Multi-Scale ATTS Analysis

Based on geospatial big data, we deciphered the ATTS security spatiality near parks by referring to other scholars using spatial statistics, segmented street analysis, sub-loop analysis, and sub-park types compared to not near parks (Xing et al., 2018; Jing et al., 2021).

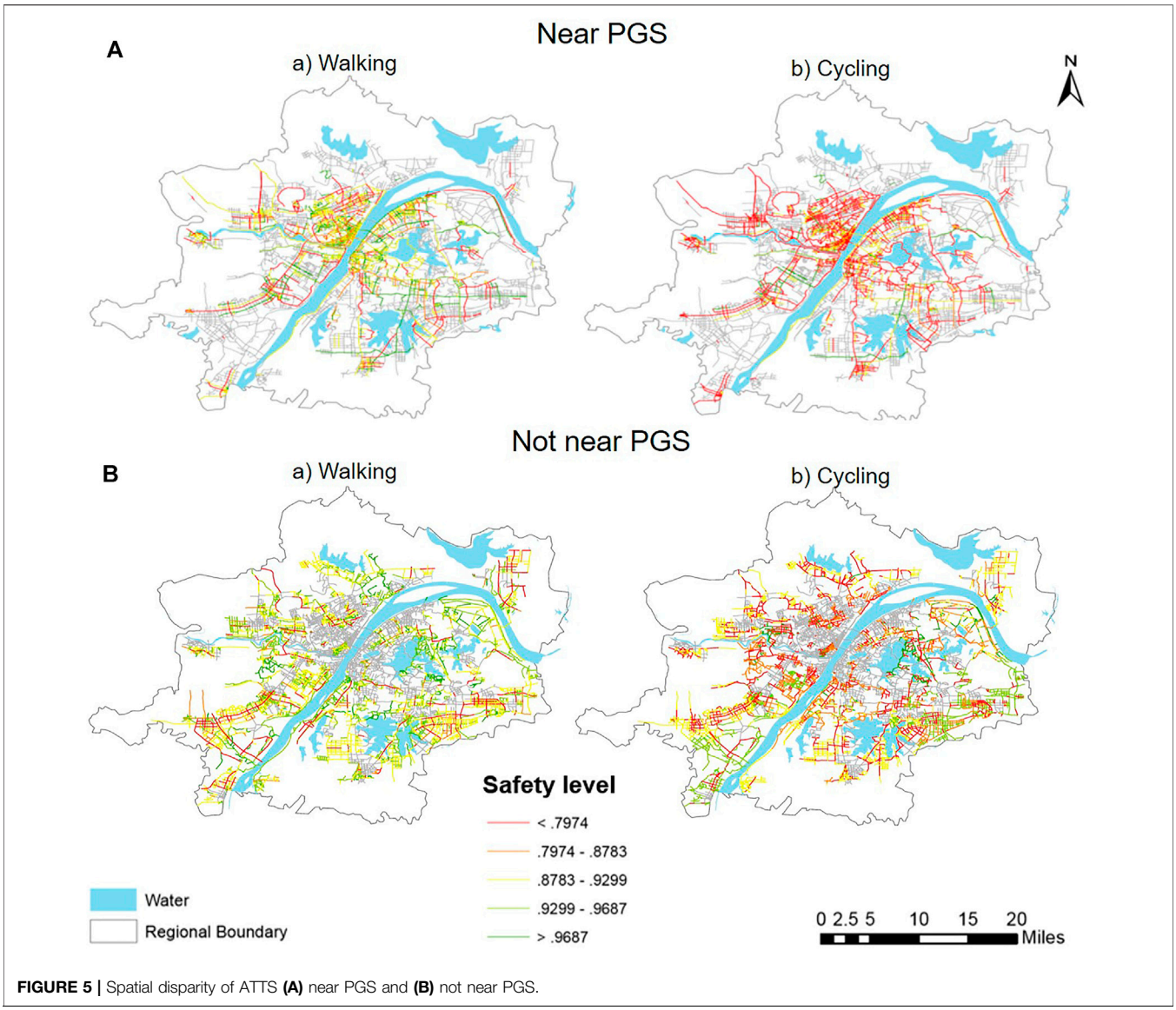

FIGURE 5 | Spatial disparity of ATTS **(A)** near PGS and **(B)** not near PGS.

TABLE 4 | ATTS-level percentage comparison

ATTS level	Near PGS		Not near PGS	
	Walking	Cycling	Walking	Cycling
Secure	14.52%	12.09%	18.47%	15.06%
Slight secure	21.82%	14.47%	26.52%	21.82%
Ordinary	25.71%	17.63%	24.92%	18.92%
Slight unsecure	19.21%	23.99%	16.62%	19.57%
Unsecure	18.74%	31.82%	13.47%	24.63%

4.2.1 Comparison Between ATTS Near PGS and Not Near PGS

Table 4 and **Figure 5** show the significant differences in walking and bicycling modes for roads near parks and non-park neighborhoods.

Roads near parks are concentrated in downtown areas, with higher road density along both sides of the river. The safety level of pedestrians is significantly better than that of cycling, while the difference probably stems mainly from the poorer construction of bike lanes. Roads that are relatively far from parks are mostly distributed along the metropolitan area. Safety levels of pedestrians are also significantly better than those of cycling. There is a general trend of higher to lower levels of pedestrian safety from the center of the metropolitan area outward, and vice versa, for cycling.

By contrast, ATTS levels on roads near non-parks are slightly better than those on roads near parks. Validating the conclusion we found that crash injuries may be higher near parks. The red-lined roads in **Figure 5** require urgent government consideration of safety matters related to their active traffic.

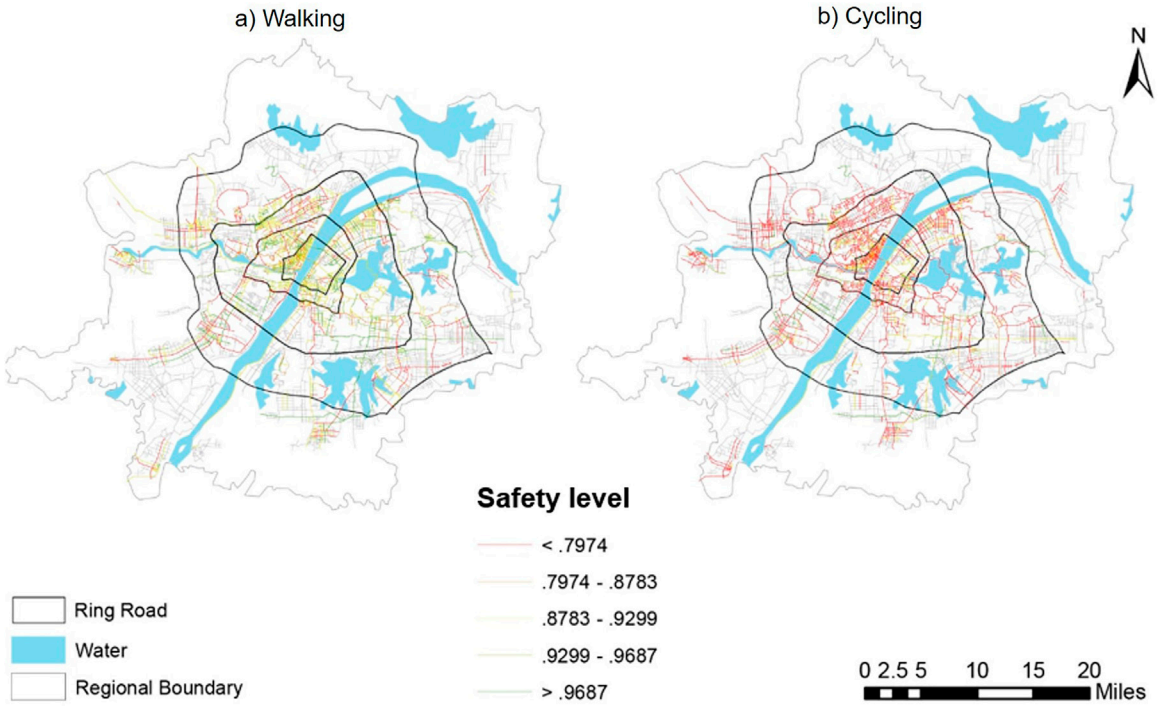

FIGURE 6 | Spatial disparity ATTS in the ring road level.

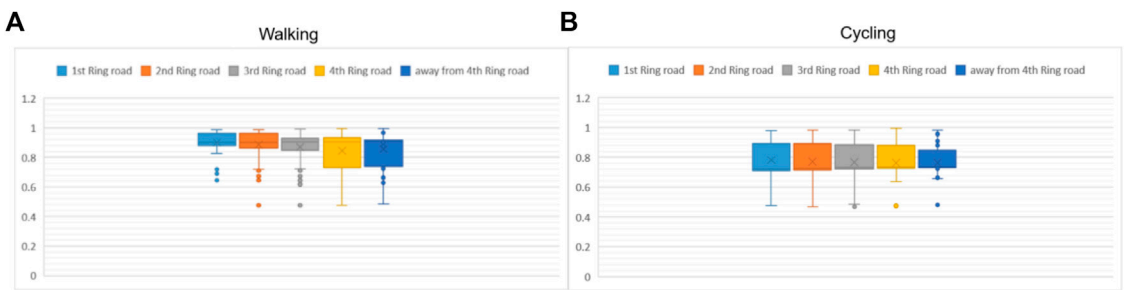

FIGURE 7 | Box plots for ATTS in the ring road level.

4.2.2 Ring Road-Level Analysis

Among 16 administrative districts, Hannan district and the Donghu New and High-Technology Development Zone have a good walking safety level for active travel (>0.8). The walking safety level (<0.2) in Hannan and Dongxihu districts is high. The safety result of active travel to parks is not determined by the district.

The evaluated safety levels are grouped according to road location and the four kinds of ring roads stated by the government (shown in **Figure 6**). **Figure 7** indicates the physical differences in the safety level of the ring roads in Wuhan using a box plot. Walking to parks on the first three ring roads has a safety level of 0.9. Away from the third ring road, the safety level shows a dispersed distribution, nearly without an outlier. The low quartile accounts for a relatively high proportion, indicating many citizens outside the third ring road walk to PGSs with a low safety. The mean safety level of cycling to parks is less than 0.8. Unlike that of walking, the cycling safety level does not decrease from the inside to the outside of the ring road. Therefore, nonmotorized vehicle lanes are ignored near downtown because the evolving traffic pressure of automobiles requires urgent consideration. Few road units could be evaluated due to the limited number of parks.

4.2.3 PGS-Level Analysis

The comparison among the four categories of parks indicates that the first three green spaces (urban, regional, and topic parks) generally aggregate in central districts in the form of parks and forests. Therefore, districts that have a socioeconomic advantage have more restricted access to green spaces and facilities for ATTS to PGSs (colored roads in **Figure 8**).

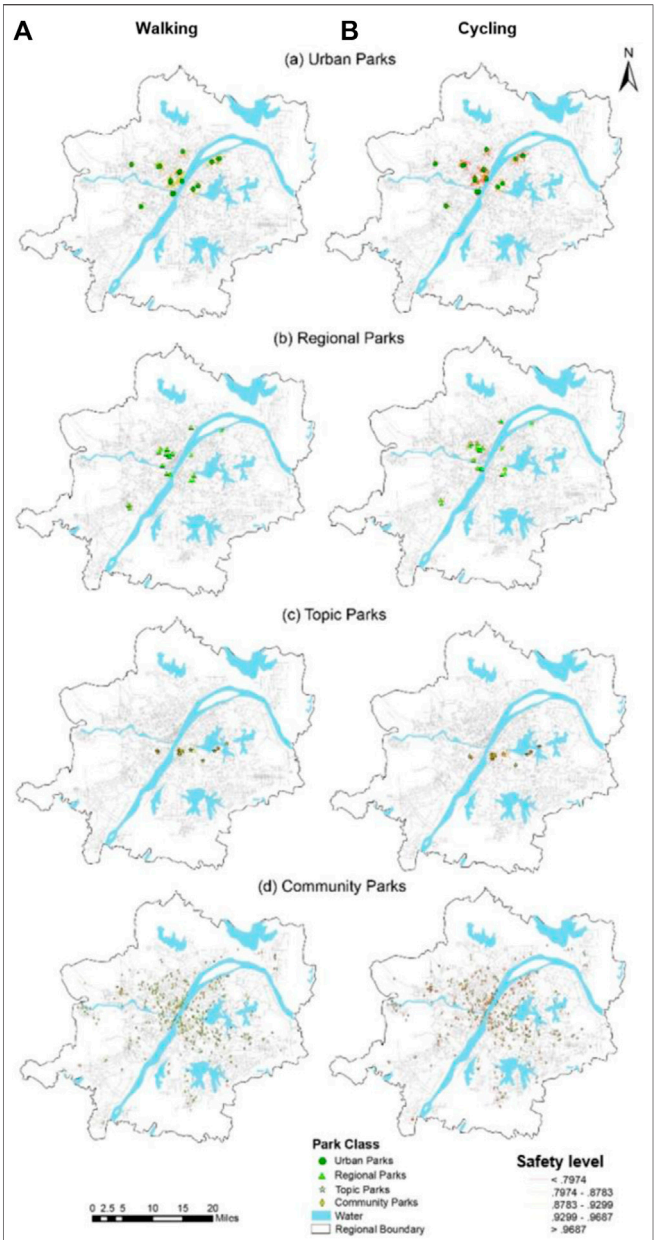

FIGURE 8 | Spatial disparity ATTS in the PGS level.

Figure 9 shows that both patterns of safety situations near urban parks, such as the highest-level park, are not ideal. However, compared with the other three park categories, access to topic parks is the safest because of its highest proportion of safety levels (including extremely secure, secure, and middle).

4.3 Spatial Regression of POI Cluster

4.3.1 Kernel Density Estimation Cluster Result

Clustered distributions have been shown to improve model validity more than non-clustered counts in spatial regression analysis (Jia et al., 2018). In this study, the natural break cluster-based KDE method (Barua et al., 2016; Jia et al., 2018) was applied to quantify the POI influencing factors of land use to evaluate the ATTS near PGSs in Wuhan. According to the natural break cluster flowchart in the previous study, the k-value was set to 6 to ensure that the dense and sparse areas are clearly divided into various classes. The POI KDE and ATTS level KDE with natural break cluster reclassification results are presented in **Figures 10**, **11**. The hotpots coded in deep purple and deep red represent high concentrations and are observed in densely populated areas. Different POI data show different features, which reflect the spatial diversity of POI and the land use characteristics for non-hot areas.

4.3.2 Model Validation

The spatial correlation and Lagrange multiplier (LM) were conducted for ATTS clusters before the spatial econometric models were applied (shown in **Table 5**). Moran's I index of ATTS clusters passed the significance test at the 0.01 level for walking and cycling. This indicates that the ATTS clusters are spatially correlated and require a spatial econometric model. Results show that the LM for both the lag and error test statistics of two patterns is highly significant, and the SEM values are larger than the SLM values, indicating a strong spatial dependence in the two cases. Robust LM for the SEM is significantly significant, while the SLM is not, indicating that the SEM is more applicable than the SLM for two patterns. Therefore, the SEM was chosen to further explore the POI metrics.

4.3.3 Spatial Regression Results

The comparison of the spatial analysis results of the three models shown in **Table 6** verifies that spatial regression outperforms traditional regression methods. The higher the log-likelihood of the model, the better the model fit; the lower AIC indicates a better model fit. Clearly, SEM parameters outperformed those of the other models. The SEM lambda coefficients with statistical significance, higher log-likelihood, and lower AIC indicate a better model fit. Therefore, SEM is the best choice for POI.

The SEM results were used to determine the regression results for ATTS safety levels and POI near the park. Regression coefficients for leisure facility and residence were significant. The leisure facility shows a significant negative correlation with the ATTS level near PGSs, indicating that an increase in the density of the leisure facility may lead to a decrease in the ATTS safety level near the park. Leisure facilities include entertainment venues such as Internet cafés, amusement parks, and bars, which gather more mobile people. The traffic flow of cars and people gathered nearby may have a negative effect on the ATTS through the roadway. Residence shows a significant positive correlation with the ATTS safety level near PGSs, indicating that a high density of residence enhances the ATTS safety level near the park. A residential area has a low transient population, and people often come from families. The presence of resident security guards at the entrances and exits of the neighborhoods promotes regular traffic order, wherein people are not at great risk.

The fit of the walking mode is better than the fit of the cycling mode. The variables that differed significantly between the two patterns were restaurant and school. Restaurants showed a more significant negative correlation with the level of cycling safety in PGS neighborhoods and a lower correlation with walking. This indicates that an increase in restaurant density leads to a decrease

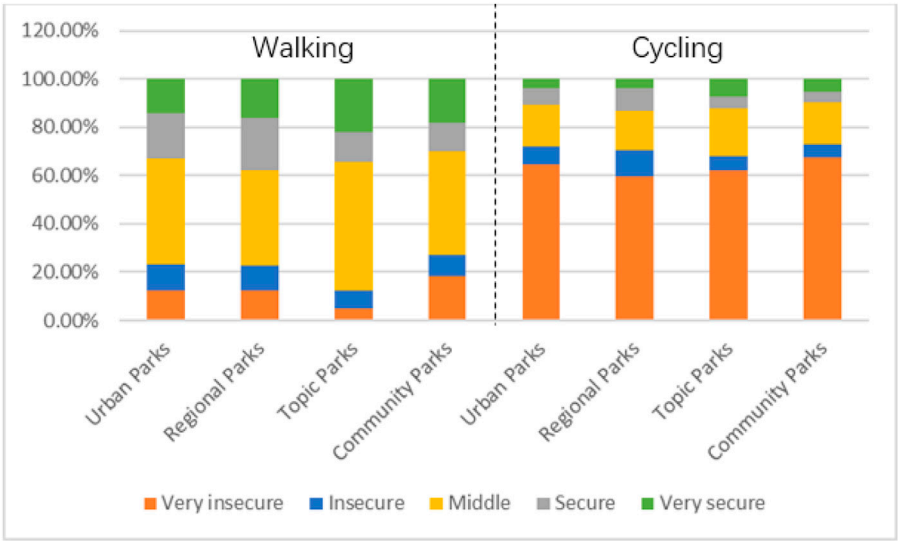

FIGURE 9 | Stacked diagram of ATTS situation proportion near different PGSs.

in the level of cycling safety near parks. This is related to the fact that restaurants often occupy common ground to expand their business area privately. Schools show a significant positive correlation with pedestrian safety near PGSs, and a low correlation with cycling. This indicates that the increased density of schools improves the level of pedestrian safety in the vicinity of PGSs. Traffic control and traffic speed reduction signs, which are common near schools, have a significant effect on pedestrian safety.

5 DISCUSSION

The requirements of transport networks accommodated the increasing number of advantages found in active travel. The evidence supporting the net positive health benefits of active travel has been well established (Mueller et al., 2015). Therefore, understanding the factors influencing ATTS is essential for offering a safe travel environment. Our study emphasizes the influences of built environment factors on ATTS and proposes an evaluation framework for ATTS near PGSs. We used the data on traffic, road, and physical characteristics to depict a comprehensive street space. Results show that various built environments have varying influences on ATTS. First, road and crossing facilities have positive influences on ATTS. This finding indicates that the provision of thorough auxiliary facilities at the road level helps increase ATTS. Among these road subsidiary factors, bicycle lanes are the most helpful for improving road safety. Results show the importance of maintaining nonmotorized vehicle lanes due to their proximity to driveways and exposure to crash-related factors. Furthermore, the effects of the other two built environment factors have pronounced effects on ATTS. These effects also presented distinct results from Western countries: nighttime brightness pronounces negative impacts on ATTS, whereas the vegetation situation has a positive influence. Consistent with previous studies, the driver's reaction capability is reduced, and the reaction time for operation is longer due to the complex and strong light environment at night (He et al., 2021). Roadside vegetation provides numerous environmental and psychological benefits to drivers (Fitzpatrick et al., 2014).

Given the rapid development of bike-sharing in China (Cao and Shen, 2019), a significant increase in cycling behavior is observed. However, the results of this study comparing walking and cycling modes of active travel demonstrate that pedestrians enjoy safer roadway facilities than cyclists. In addition, active travel traffic near PGS requires more attention than non-park neighborhoods. One reason for this is that bike lanes are also not as well constructed. A certain number of roads have no established bicycle lanes. The frequent occurrence of mixed use and occupied use is another important reason. The safety situation near topic parks outweighs that of other parks. This result shows that the safety service provided by urban parks, as the highest-level park in urban cities, does not correspond to their establishment level. Moreover, the comparison among common traffic boundaries in China shows that the safety situation of active travel to parks is not optimistic away from the third ring road (near suburbs).

The OLS, SLM, and SEM are used to investigate the correlation of ATTS with the POI aggregation phenomenon. With regard to the effects of POI aggregation on ATTS, specific land use has a great effect on ATTS. Our study revealed that the SEM has the best fit for the POI cluster, compared to OLS and SLM. Moreover, the fit of the walking pattern is better than the fit of the cycling pattern. Some specific POIs have profound effects on the spatial distribution of ATTS. Specifically, increases in the leisure facility density and residence density lead to deterioration and improvement in ATTS safety levels near PGSs, respectively. Increases in the restaurant density and school density worsen the level of cycling safety and enhance

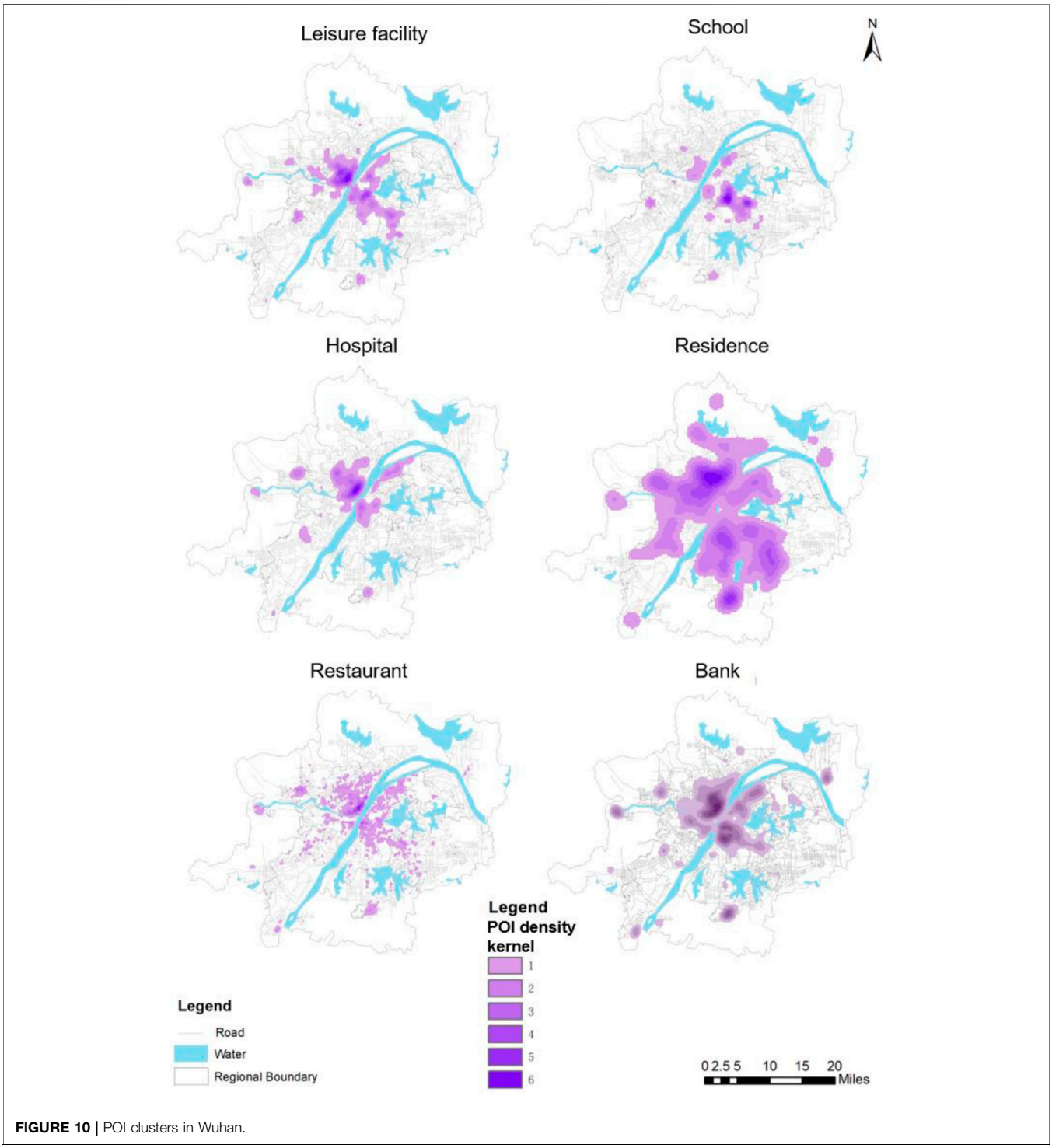

FIGURE 10 | POI clusters in Wuhan.

the level of walking safety near PGSs, respectively. Therefore, policy measures should focus on enhancing the active travel environment in areas with many recreational areas and restaurants. The results of the experiment combining all variables indicate the need to improve effective goal-oriented measures in mixed land uses when seeking equitable ATTS in a variety of settings.

This study proposes a new framework for the ATTS assessment framework. The extent to which people are threatened on their way to parks to experience healthy living is estimated. Our proposed assessment framework focuses on the safety of built environment parameters. In addition to the research area of accident (Gilstad-Hayden et al., 2015; Suk and Walter, 2019), we selected several hot factors in recent years,

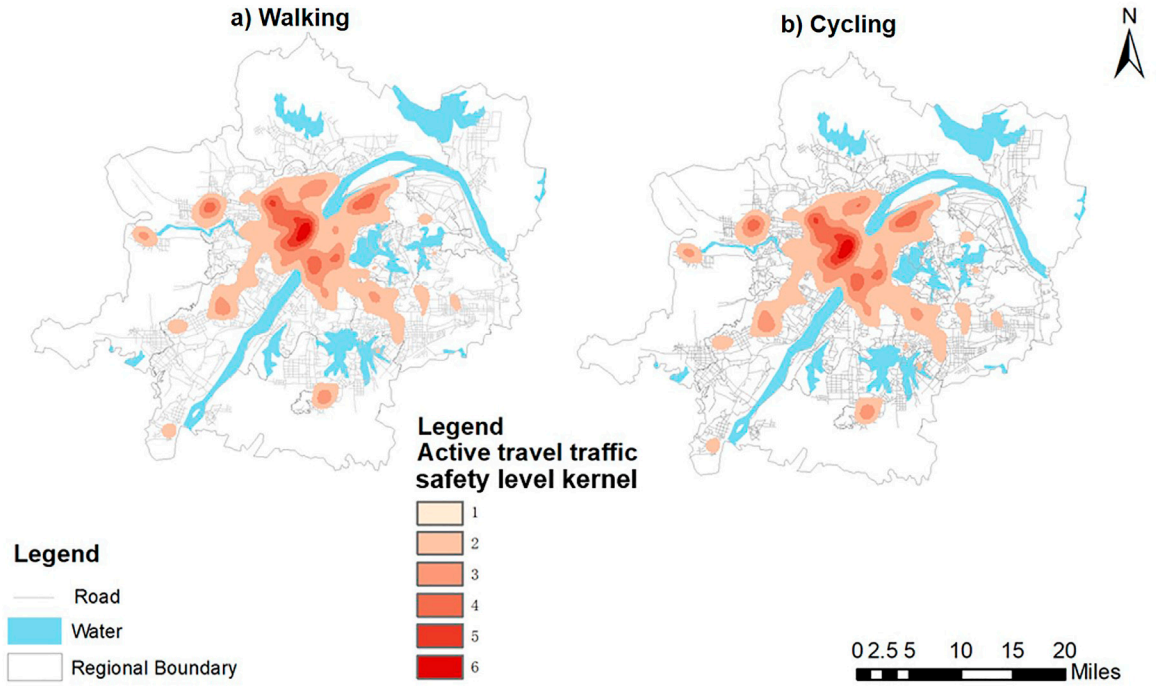

FIGURE 11 | ATTS clusters used in Wuhan.

TABLE 5 | Results of the Lagrange multiplier (LM) test for walking and cycling.

Test	Walking		Cycling	
	Value	p-value	Value	p-value
Moran's I	0.12	0.00	0.09	0.00
LM (SLM)	14.28	0.00	12.84	0.00
LM (SEM)	26.27	0.00	21.98	0.00
Robust LM (SLM)	1.03	0.72	0.67	0.69
Robust LM (SEM)	8.29	0.00	5.28	0.00

including nighttime brightness and vegetation situation. The proposed framework provides a rational estimation of the performance of ATTS before the occurrence of accidents. Given the site-specific data on roads, the proposed framework can provide concrete and insightful observations that may help in managing the safety of the built environment against hazardous conditions. Compared with other methods of active travel evaluation, our framework presented the following advantages:

1) Previous studies performed cross-sectional surveys by using the multivariate analysis of personal traits (Hansen et al., 2015; Fairnie et al., 2016; Brainard et al., 2019). In this study, a systematic citywide evaluation framework for ATTS was introduced, focusing on the safety effect of the environment parameters.
2) Evaluating the safety of accessibility to PGSs is important because people use active travel, instead of motorized transport when traveling (Jerrett et al., 2016). This study divided PGSs into various levels and estimated safety according to their serving ranges. This process verifies whether the safety levels of various parks correspond to their establishment levels.
3) The perspective of roads in this study differs from that of the segments and intersections presented in previous research (Flahaut, 2004; Barua et al., 2014). Planning administration can use the evaluation based on road units to recognize roads that require urgent repair accurately. The refinement of units can improve the practicality of this study.
4) The natural break cluster method is used to reclassify the kernel density, and the spatial analysis model is used to estimate the correlation of the POI aggregation phenomenon with active travel traffic safety. The exploration helps to obtain the prone areas of active travel traffic accidents according to the characteristics of POI aggregation for preventing accidents early.

This study has several limitations with regard to the framework of ATTS based on PGS classifications. First, this study focuses on the influence of the built environment but lacks in terms of the depiction of street moral character. Second, the definition of active travel used in this study only includes walking and cycling. Other transport modes, such as driving and riding public transport, also play significant roles in accessing PGSs (Xing et al., 2018) and cannot be ignored. Third, this study uses a subjective method to interpret the situation extracted from the street view images. Considerable manpower is required in dealing with original data. Processing greater volumes of data, such as entire city

TABLE 6 | Model performance and regression result of ATTS and POI density

Model	Variables	Walking	Cycling
OLS	Constant	0.814***	0.753***
	Restaurant density	0.02**	–0.101**
	Leisure facility density	–0.022***	–0.025***
	Hospital density	–0.128**	–0.130*
	Residence density	0.086**	0.089**
	School density	0.138*	0.021*
	Bank density	0.102*	0.052*
	Number of observations	5520	5520
	R^2	0.37	0.31
	Sum squared residual	7.63	10.61
	Log-likelihood (LIK)	5339.8	4561.3
	Akaike information criterion (AIC)	-9667.8	-8018.8
SEM	Constant	0.828 ***	0.762 ***
	Restaurant density	0.02 **	–0.118 **
	Leisure facility density	–0.020 ***	–0.019 ***
	Hospital density	–0.126 **	–0.126 **
	Residence density	0.072***	0.077***
	School density	0.133**	0.012 *
	Bank density	0.092**	0.036*
	Lambda (λ)	0.5541***	0.5646***
	Log-likelihood (LIK)	5345.4	4563.2
	Akaike information criterion (AIC)	-10674.7	-9157.6
SLM	Constant	0.373***	0.333***
	Restaurant density	0.013**	–0.112**
	Leisure facility density	–0.013***	–0.014***
	Hospital density	–0.117**	–0.117**
	Residence density	0.081*	0.084 *
	School density	0.125*	0.011*
	Bank density	0.089*	0.033
	Rho (ρ)	0.5421**	0.5591**
	Log-likelihood (LIK)	5336.6	4560.6
	Akaike information criterion (AIC)	-10655.1	-9103.2

*Levels of significance: ***, ** and * indicate significance at 1, 5, and 10% levels, respectively.*

roads, requires an automated method (Zhou et al., 2019), which is included in the agenda of subsequent study. Finally, the present POI variables are limited to six categories. The sociodemographic indicators (e.g., education, income, and age) (Su et al., 2019) should be considered in future research for exploring the inequity of ATTS distribution.

6 CONCLUSION

This study estimates the ATTS access to parks by using the proposed spatial assessment framework. The proposed framework highlights the importance of accounting for built environment factors in analyzing ATTS. Additionally, the correlation between POI aggregation and ATTS is explored, identifying the potential land use factors of the ATTS. The results in Wuhan confirmed that traffic, road and physical characteristics greatly affect ATTS, especially population density, road density, nighttime brightness, and vegetation situation. The spatial distribution of ATTS indicated that pedestrians enjoy safer road facilities than cyclists, and roads along the river have a high ATTS level in Wuhan. The spatial regression results urge the authorities to monitor the ATTS in areas with many leisure facilities and residences. Findings indicated that the provision of thorough auxiliary facilities at the road level helps increase the safety of access to PGSs. Furthermore, our proposed framework could be applied to other public facilities that attract active travel users (e.g., schools). The proposed framework offered appropriate traffic planning strategies to improve the safety and equity of ATTS users during their access to PGSs. Transport planners should pay more attention to roads near specific land uses. Improving the safety conditions of walking and cycling near PGSs is recommended to avoid safety inequality.

DATA AVAILABILITY STATEMENT

The original contributions presented in the study are included in the article/Supplementary Material, further inquiries can be directed to the corresponding author.

AUTHOR CONTRIBUTIONS

YYL: conceptualization, methodology, writing—original draft, formal analysis, and investigation. YFL: writing—review and editing, supervision, funding acquisition, and resource. LX: data duration, resource, and software. NW: validation, visualization, and software. LR: resources, visualization, and software.

FUNDING

This study was supported by the National Natural Science Foundation of China (Grant No: 41771432) and the Natural Science Foundation of Hubei Province (Grant No: 2020CFB483).

REFERENCES

Abdel-Aty, M., Lee, J., Siddiqui, C., and Choi, K. (2013). Geographical Unit Based Analysis in the Context of Transportation Safety Planning. *Transportation Res. A: Pol. Pract.* 49, 62–75. doi:10.1016/j.tra.2013.01.030

Administration, F. H. (1992). Bicycling and Walking Study Case Study No. 3: What Needs to Be Done to Promote Bicycling and Walking? Available at: https://trid.trb.org/view/386096.

Aghaabbasi, M., Moeinaddini, M., Zaly Shah, M., Asadi-Shekari, Z., and Arjomand Kermani, M. (2018). Evaluating the Capability of Walkability Audit Tools for Assessing Sidewalks. *Sustainable Cities Soc.* 37, 475–484. doi:10.1016/j.scs.2017.12.001

Anciaes, P. R., and Jones, P. (2018). Estimating Preferences for Different Types of Pedestrian Crossing Facilities. *Transportation Res. F: Traffic Psychol. Behav.* 52, 222–237. doi:10.1016/j.trf.2017.11.025

Awasthi, A., Chauhan, S. S., Omrani, H., and Panahi, A. (2011). A Hybrid Approach Based on SERVQUAL and Fuzzy TOPSIS for Evaluating

Transportation Service Quality. *Comput. Ind. Eng.* 61 (3), 637–646. doi:10.1016/j.cie.2011.04.019

Ayati, E., and Abbasi, E. (2011). Investigation on the Role of Traffic Volume in Accidents on Urban Highways. *J. Saf. Res.* 42 (3), 209–214. doi:10.1016/j.jsr.2011.03.006

Baran, P. K., Tabrizian, P., Zhai, Y., Smith, J. W., and Floyd, M. F. (2018). An Exploratory Study of Perceived Safety in a Neighborhood Park Using Immersive Virtual Environments. *Urban For. Urban Green.* 35, 72–81. doi:10.1016/j.ufug.2018.08.009

Barua, S., El-Basyouny, K., and Islam, M. T. (2014). A Full Bayesian Multivariate Count Data Model of Collision Severity with Spatial Correlation. *Analytic Methods Accid. Res.* 3-4, 28–43. doi:10.1016/j.amar.2014.09.001

Barua, S., El-Basyouny, K., and Islam, M. T. (2015). Effects of Spatial Correlation in Random Parameters Collision Count-Data Models. *Analytic Methods Accid. Res.* 5-6, 28–42. doi:10.1016/j.amar.2015.02.001

Barua, S., El-Basyouny, K., and Islam, M. T. (2016). Multivariate Random Parameters Collision Count Data Models with Spatial Heterogeneity. *Analytic Methods Accid. Res.* 9, 1–15. doi:10.1016/j.amar.2015.11.002

Bernhardt, M., and Kockelman, K. (2021). An Analysis of Pedestrian Crash Trends and Contributing Factors in Texas. *J. Transport Health* 22, 101090. doi:10.1016/j.jth.2021.101090

Brainard, J., Cooke, R., Lane, K., and Salter, C. (2019). Age, Sex and Other Correlates with Active Travel Walking and Cycling in England: Analysis of Responses to the Active Lives Survey 2016/17. *Prev. Med.* 123, 225–231. doi:10.1016/j.ypmed.2019.03.043

Brown, V., Moodie, M., and Carter, R. (2017). Evidence for Associations between Traffic Calming and Safety and Active Transport or Obesity: A Scoping Review. *J. Transport Health* 7, 23–37. doi:10.1016/j.jth.2017.02.011

Brownson, R. C., Hoehner, C. M., Day, K., Forsyth, A., and Sallis, J. F. (2009). Measuring the Built Environment for Physical Activity. *Am. J. Prev. Med.* 36 (4), S99–S123. e112. doi:10.1016/j.amepre.2009.01.005

Brühwiler, L., Fu, C., Huang, H., Longhi, L., and Weibel, R. (2022). Predicting Individuals' Car Accident Risk by Trajectory, Driving Events, and Geographical Context. *Comput. Environ. Urban Syst.* 93, 101760. doi:10.1016/j.compenvurbsys.2022.101760

Cao, Y., and Shen, D. (2019). Contribution of Shared Bikes to Carbon Dioxide Emission Reduction and the Economy in Beijing. *Sustainable Cities Soc.* 51, 101749. doi:10.1016/j.scs.2019.101749

Chainey, S., and Ratcliffe, J. (2013). Crime Mapping Case Studies. *Gis & Crime Mapping*. (2005). Hoboken: Wiley.

Clifton, K. J., Burnier, C. V., and Akar, G. (2009). Severity of Injury Resulting from Pedestrian-Vehicle Crashes: What Can We Learn from Examining the Built Environment? *Transportation Res. D: Transport Environ.* 14 (6), 425–436. doi:10.1016/j.trd.2009.01.001

Cunningham, G. O., Michael, Y. L., Farquhar, S. A., and Lapidus, J. (2005). Developing a Reliable Senior Walking Environmental Assessment Tool. *Am. J. Prev. Med.* 29 (3), 215–217. doi:10.1016/j.amepre.2005.05.002

Demiroz, Y. I., Onelcin, P., and Alver, Y. (2015). Illegal Road Crossing Behavior of Pedestrians at Overpass Locations: Factors Affecting gap Acceptance, Crossing Times and Overpass Use. *Accid. Anal. Prev.* 80, 220–228. doi:10.1016/j.aap.2015.04.018

Donroe, J., Tincopa, M., Gilman, R. H., Brugge, D., and Moore, D. A. J. (2008). Pedestrian Road Traffic Injuries in Urban Peruvian Children and Adolescents: Case Control Analyses of Personal and Environmental Risk Factors. *PLOS ONE* 3 (9), e3166. doi:10.1371/journal.pone.0003166

dos Santos, B. M., Godoy, L. P., and Campos, L. M. S. (2019). Performance Evaluation of green Suppliers Using Entropy-TOPSIS-F. *J. Clean. Prod.* 207, 498–509. doi:10.1016/j.jclepro.2018.09.235

Duan, Y., Wagner, P., Zhang, R., Wulff, H., and Brehm, W. (2018). Physical Activity Areas in Urban parks and Their Use by the Elderly from Two Cities in China and Germany. *Landscape Urban Plann.* 178, 261–269. doi:10.1016/j.landurbplan.2018.06.009

Dumbaugh, E., and Rae, R. (2009). Safe Urban Form: Revisiting the Relationship between Community Design and Traffic Safety. *J. Am. Plann. Assoc.* 75 (3), 309–329. doi:10.1080/01944360902950349

Ekkel, E. D., and de Vries, S. (2017). Nearby green Space and Human Health: Evaluating Accessibility Metrics. *Landscape Urban Plann.* 157, 214–220. doi:10.1016/j.landurbplan.2016.06.008

Fairnie, G. A., Wilby, D. J. R., and Saunders, L. E. (2016). Active Travel in London: The Role of Travel Survey Data in Describing Population Physical Activity. *J. Transport Health* 3 (2), 161–172. doi:10.1016/j.jth.2016.02.003

Fitzpatrick, C. D., Harrington, C. P., Knodler, M. A., and Romoser, M. R. E. (2014). The Influence of clear Zone Size and Roadside Vegetation on Driver Behavior. *J. Saf. Res.* 49, e1e91–104. doi:10.1016/j.jsr.2014.03.006

Flahaut, B. (2004). Impact of Infrastructure and Local Environment on Road Unsafety. *Accid. Anal. Prev.* 36 (6), 1055–1066. doi:10.1016/j.aap.2003.12.003

Galanis, A., Botzoris, G., and Eliou, N. (2017). Pedestrian Road Safety in Relation to Urban Road Type and Traffic Flow. *Transportation Res. Proced.* 24, 220–227. doi:10.1016/j.trpro.2017.05.111

Gilstad-Hayden, K., Wallace, L. R., Carroll-Scott, A., Meyer, S. R., Barbo, S., Murphy-Dunning, C., et al. (2015). Research Note: Greater Tree Canopy Cover Is Associated with Lower Rates of Both Violent and Property Crime in New Haven, CT. *Landscape Urban Plann.* 143, 248–253. doi:10.1016/j.landurbplan.2015.08.005

Goddard, T., Ralph, K., Thigpen, C. G., and Iacobucci, E. (2019). Does News Coverage of Traffic Crashes Affect Perceived Blame and Preferred Solutions? Evidence from an experiment. *Transportation Res. Interdiscip. Perspect.* 3, 100073. doi:10.1016/j.trip.2019.100073

Golob, T. F., and Recker, W. W. (2004). A Method for Relating Type of Crash to Traffic Flow Characteristics on Urban Freeways. *Transportation Res. Part A: Pol. Pract.* 38 (1), 53–80. doi:10.1016/j.tra.2003.08.002

Golob, T. F., and Recker, W. W. (2003). Relationships Among Urban Freeway Accidents, Traffic Flow, Weather, and Lighting Conditions. *J. Transp. Eng.* 129 (4), 342–353. doi:10.1061/(asce)0733-947x(2003)129:4(342)

Griffith, D. A. (1988). Spatial Econometrics: Methods and Models. *Econ. Geogr.* 65 (2), 160–162. doi:10.1007/978-94-015-7799-1

Hansen, A. Y., Umstattd Meyer, M. R., Lenardson, J. D., and Hartley, D. (2015). Built Environments and Active Living in Rural and Remote Areas: a Review of the Literature. *Curr. Obes. Rep.* 4 (4), 484–493. doi:10.1007/s13679-015-0180-9

He, Y., Zhang, X., Quan, L., Mi, R., Cui, Y., Xu, J., et al. (2021). Influence of Coloured Light Projected from Night-Time Excessive Luminance Outdoor LED Display Screens on Vehicle Driving Safety along Urban Roads. *Building Environ.* 188, 107448. doi:10.1016/j.buildenv.2020.107448

Hess, P., Moudon, A., and Matlick, J. (2004). Pedestrian Safety and Transit Corridors. *Jpt* 7, 73–93. doi:10.5038/2375-0901.7.2.5

Hu, Y., Zhang, Y., and Shelton, K. S. (2018). Where Are the Dangerous Intersections for Pedestrians and Cyclists: A Colocation-Based Approach. *Transportation Res. C: Emerging Tech.* 95, 431–441. doi:10.1016/j.trc.2018.07.030

Jacobsen, P. L. (2003). Safety in Numbers: More Walkers and Bicyclists, Safer Walking and Bicycling. *Inj. Prev.* 9 (3), 205–209. doi:10.1136/ip.9.3.205

Jerrett, M., Su, J. G., MacLeod, K. E., Hanning, C., Houston, D., and Wolch, J. (2016). Safe Routes to Play? Pedestrian and Bicyclist Crashes Near Parks in Los Angeles. *Environ. Res.* 151, 742–755. doi:10.1016/j.envres.2016.07.029

Jia, R., Khadka, A., and Kim, I. (2018). Traffic Crash Analysis with point-of-interest Spatial Clustering. *Accid. Anal. Prev.* 121, 223–230. doi:10.1016/j.aap.2018.09.018

Jing, Y., Ma, D., Liu, Y., Cui, J., Zhang, S., and Chen, Y. (2021). Decoding the Street-Based Spatiality of Urban Gyms: Implications for Healthy City Planning. *Land* 10 (2), 175. doi:10.3390/land10020175

Kaplan, S. (1987). Mental Fatigue and the Designed Environment. *Public environments [Press release]*. Abingdon: Taylor & Francis.

Kononov, J., Bailey, B., and Allery, B. K. (2008). Relationships between Safety and Both Congestion and Number of Lanes on Urban Freeways. *Transportation Res. Rec.* 2083 (1), 26–39. doi:10.3141/2083-04

Kuo, P.-F., and Lord, D. (2021). A Visual Approach for Defining the Spatial Relationships Among Crashes, Crimes, and Alcohol Retailers: Applying the Color Mixing Theorem to Define the Colocation Pattern of Multiple Variables. *Accid. Anal. Prev.* 154, 106062. doi:10.1016/j.aap.2021.106062

Lee, G., and Hong, I. (2013). Measuring Spatial Accessibility in the Context of Spatial Disparity between Demand and Supply of Urban Park Service. *Landscape Urban Plann.* 119, 85–90. doi:10.1016/j.landurbplan.2013.07.001

Lee, J., Abdel-Aty, M., and Jiang, X. (2015). Multivariate Crash Modeling for Motor Vehicle and Non-motorized Modes at the Macroscopic Level. *Accid. Anal. Prev.* 78, 146–154. doi:10.1016/j.aap.2015.03.003

Lee, J., Chae, J., Yoon, T., and Yang, H. (2018). Traffic Accident Severity Analysis with Rain-Related Factors Using Structural Equation Modeling - A Case Study of Seoul City. *Accid. Anal. Prev.* 112, 1–10. doi:10.1016/j.aap.2017.12.013

Lord, D., Manar, A., and Vizioli, A. (2005). Modeling Crash-Flow-Density and Crash-Flow-V/C Ratio Relationships for Rural and Urban Freeway Segments. *Accid. Anal. Prev.* 37 (1), 185–199. doi:10.1016/j.aap.2004.07.003

Lwin, K. K., and Murayama, Y. (2011). Modelling of Urban green Space Walkability: Eco-Friendly Walk Score Calculator. *Comput. Environ. Urban Syst.* 35 (5), 408–420. doi:10.1016/j.compenvurbsys.2011.05.002

Martin, J.-L. (2002). Relationship between Crash Rate and Hourly Traffic Flow on Interurban Motorways. *Accid. Anal. Prev.* 34 (5), 619–629. doi:10.1016/S0001-4575(01)00061-6

Miranda-Moreno, L. F., Morency, P., and El-Geneidy, A. M. (2011). The Link between Built Environment, Pedestrian Activity and Pedestrian-Vehicle Collision Occurrence at Signalized Intersections. *Accid. Anal. Prev.* 43 (5), 1624–1634. doi:10.1016/j.aap.2011.02.005

Montella, A. (2010). A Comparative Analysis of Hotspot Identification Methods. *Accid. Anal. Prev.* 42 (2), 571–581. doi:10.1016/j.aap.2009.09.025

Morrison, C. N., Thompson, J., Kondo, M. C., and Beck, B. (2019). On-road Bicycle Lane Types, Roadway Characteristics, and Risks for Bicycle Crashes. *Accid. Anal. Prev.* 123, 123–131. doi:10.1016/j.aap.2018.11.017

Morrison, D. S., Petticrew, M., and Thomson, H. (2003). What Are the Most Effective Ways of Improving Population Health through Transport Interventions? Evidence from Systematic Reviews. *J. Epidemiol. Community Health* 57 (5), 327–333. doi:10.1136/jech.57.5.327

Moudon, A. V., Lin, L., Jiao, J., Hurvitz, P., and Reeves, P. (2011). The Risk of Pedestrian Injury and Fatality in Collisions with Motor Vehicles, a Social Ecological Study of State Routes and City Streets in King County, Washington. *Accid. Anal. Prev.* 43 (1), 11–24. doi:10.1016/j.aap.2009.12.008

Mueller, N., Rojas-Rueda, D., Cole-Hunter, T., de Nazelle, A., Dons, E., Gerike, R., et al. (2015). Health Impact Assessment of Active Transportation: A Systematic Review. *Prev. Med.* 76, 103–114. doi:10.1016/j.ypmed.2015.04.010

Ng, K.-s., Hung, W.-t., and Wong, W.-g. (2002). An Algorithm for Assessing the Risk of Traffic Accident. *J. Saf. Res.* 33 (3), 387–410. doi:10.1016/S0022-4375(02)00033-6

Noland, R. B., and Oh, L. (2004). The Effect of Infrastructure and Demographic Change on Traffic-Related Fatalities and Crashes: a Case Study of Illinois County-Level Data. *Accid. Anal. Prev.* 36 (4), 525–532. doi:10.1016/S0001-4575(03)00058-7

Noland, R. B. (2003). Traffic Fatalities and Injuries: the Effect of Changes in Infrastructure and Other Trends. *Accid. Anal. Prev.* 35 (4), 599–611. doi:10.1016/S0001-4575(02)00040-4

O'Hern, S., and Oxley, J. (2015). Understanding Travel Patterns to Support Safe Active Transport for Older Adults. *J. Transport Health* 2 (1), 79–85. doi:10.1016/j.jth.2014.09.016

Poku-Boansi, M., Amoako, C., and Atuah, D. O. (2019). Urban Travel Patterns and Safety Among School Children Around Accra, Ghana. *J. Transport Health* 15, 100660. doi:10.1016/j.jth.2019.100660

Pont, K., Ziviani, J., Wadley, D., Bennett, S., and Abbott, R. (2009). Environmental Correlates of Children's Active Transportation: A Systematic Literature Review. *Health & Place* 15 (3), 849–862. doi:10.1016/j.healthplace.2009.02.002

Pucher, J., Buehler, R., Bassett, D. R., and Dannenberg, A. L. (2010). Walking and Cycling to Health: a Comparative Analysis of City, State, and International Data. *Am. J. Public Health* 100 (10), 1986–1992. doi:10.2105/AJPH.2009.189324

Ramírez, A. F., and Valencia, C. (2021). Spatiotemporal Correlation Study of Traffic Accidents with Fatalities and Injuries in Bogota (Colombia). *Accid. Anal. Prev.* 149, 105848. doi:10.1016/j.aap.2020.105848

Räsänen, M., Lajunen, T., Alticafarbay, F., and Aydin, C. (2007). Pedestrian Self-Reports of Factors Influencing the Use of Pedestrian Bridges. *Accid. Anal. Prev.* 39 (5), 969–973. doi:10.1016/j.aap.2007.01.004

Retting, R. A., Ferguson, S. A., and McCartt, A. T. (2003). A Review of Evidence-Based Traffic Engineering Measures Designed to Reduce Pedestrian-Motor Vehicle Crashes. *Am. J. Public Health* 93 (9), 1456–1463. doi:10.2105/AJPH.93.9.1456

Saha, D., Dumbaugh, E., and Merlin, L. A. (2020). A Conceptual Framework to Understand the Role of Built Environment on Traffic Safety. *J. Saf. Res.* 75, 41–50. doi:10.1016/j.jsr.2020.07.004

Saplıoğlu, M., and Aydın, M. M. (2018). Choosing Safe and Suitable Bicycle Routes to Integrate Cycling and Public Transport Systems. *J. Transport Health* 10, 236–252. doi:10.1016/j.jth.2018.05.011

Shankar, V. N., Ulfarsson, G. F., Pendyala, R. M., and Nebergall, M. B. (2003). Modeling Crashes Involving Pedestrians and Motorized Traffic. *Saf. Sci.* 41 (7), 627–640. doi:10.1016/S0925-7535(02)00017-6

Simončič, M. (2001). Road Accidents in Slovenia Involving a Pedestrian, Cyclist or Motorcyclist and a Car. *Accid. Anal. Prev.* 33 (2), 147–156. doi:10.1016/S0001-4575(00)00025-7

Smith, M., Hawley, G., Mackay, L., Hosking, J., Mackie, H., Ikeda, E., et al. (2020). Impact of Changing Road Infrastructure on Children's Active Travel: A Multi-Methods Study from Auckland, New Zealand. *J. Transport Health* 18, 100868. doi:10.1016/j.jth.2020.100868

Su, S., Li, D., Yu, X., Zhang, Z., Zhang, Q., Xiao, R., et al. (2011). Assessing Land Ecological Security in Shanghai (China) Based on Catastrophe Theory. *Stoch Environ. Res. Risk Assess.* 25 (6), 737–746. doi:10.1007/s00477-011-0457-9

Su, S., Zhou, H., Xu, M., Ru, H., Wang, W., and Weng, M. (2019). Auditing Street Walkability and Associated Social Inequalities for Planning Implications. *J. Transport Geogr.* 74, 62–76. doi:10.1016/j.jtrangeo.2018.11.003

Suk, J. Y., and Walter, R. J. (2019). New Nighttime Roadway Lighting Documentation Applied to Public Safety at Night: A Case Study in San Antonio, Texas. *Sustainable Cities Soc.* 46, 101459. doi:10.1016/j.scs.2019.101459

Thom, R. (1976). Structural Stability and Morphogenesis. *Pattern Recognition* 8 (1), 61. doi:10.1016/0031-3203(76)90030-3

Värnild, A., Tillgren, P., and Larm, P. (2020). What Types of Injuries Did Seriously Injured Pedestrians and Cyclists Receive in a Swedish Urban Region in the Time Period 2003-2017 when Vision Zero Was Implemented? *Public Health* 181, 59–64. doi:10.1016/j.puhe.2019.11.019

Vavrek, R., and Chovancová, J. (2019). Assessment of Economic and Environmental Energy Performance of EU Countries Using CV-TOPSIS Technique. *Ecol. Indicators* 106, 105519. doi:10.1016/j.ecolind.2019.105519

Vorko-Jović, A., Kern, J., and Biloglav, Z. (2006). Risk Factors in Urban Road Traffic Accidents. *J. Saf. Res.* 37 (1), 93–98. doi:10.1016/j.jsr.2005.08.009

Wang, C., Quddus, M. A., and Ison, S. G. (2013). The Effect of Traffic and Road Characteristics on Road Safety: A Review and Future Research Direction. *Saf. Sci.* 57, 264–275. doi:10.1016/j.ssci.2013.02.012

Wang, C., Quddus, M., and Ison, S. (2009). The Effects of Area-wide Road Speed and Curvature on Traffic Casualties in England. *J. Transport Geogr.* 17 (5), 385–395. doi:10.1016/j.jtrangeo.2008.06.003

Wang, D., Brown, G., Zhong, G., Liu, Y., and Mateo-Babiano, I. (2015). Factors Influencing Perceived Access to Urban parks: A Comparative Study of Brisbane (Australia) and Zhongshan (China). *Habitat Int.* 50, 335–346. doi:10.1016/j.habitatint.2015.08.032

Wang, L., Ning, P., Yin, P., Cheng, P., Schwebel, D. C., Liu, J., et al. (2019). Road Traffic Mortality in China: Analysis of National Surveillance Data from 2006 to 2016. *The Lancet Public Health* 4 (5), e245–e255. doi:10.1016/S2468-2667(19)30057-X

Wendel-Vos, W., Droomers, M., Kremers, S., Brug, J., and Van Lenthe, F. (2007). Potential Environmental Determinants of Physical Activity in Adults: a Systematic Review. *Obes. Rev.* 8 (5), 425–440. doi:10.1111/j.1467-789X.2007.00370.x

Wier, M., Weintraub, J., Humphreys, E. H., Seto, E., and Bhatia, R. (2009). An Area-Level Model of Vehicle-Pedestrian Injury Collisions with Implications for Land Use and Transportation Planning. *Accid. Anal. Prev.* 41 (1), 137–145. doi:10.1016/j.aap.2008.10.001

Wolfe, M. K., and Mennis, J. (2012). Does Vegetation Encourage or Suppress Urban Crime? Evidence from Philadelphia, PA. *Landscape Urban Plann.* 108 (2), 112–122. doi:10.1016/j.landurbplan.2012.08.006

World Health Organization (2018). *Global Status Report on Road Safety 2018*. WHO's Social Determinants of Health. Available at: https://www.who.int/publications/i/item/9789241565684.

Xing, L., Liu, Y., and Liu, X. (2018). Measuring Spatial Disparity in Accessibility with a Multi-Mode Method Based on Park green Spaces Classification in Wuhan, China. *Appl. Geogr.* 94, 251–261. doi:10.1016/j.apgeog.2018.03.014

Xu, M., Xin, J., Su, S., Weng, M., and Cai, Z. (2017). Social Inequalities of Park Accessibility in Shenzhen, China: The Role of Park Quality, Transport Modes, and Hierarchical Socioeconomic Characteristics. *J. Transport Geogr.* 62, 38–50. doi:10.1016/j.jtrangeo.2017.05.010

Xu, Y., Fu, C., Kennedy, E., Jiang, S., and Owusu-Agyemang, S. (2018). The Impact of Street Lights on Spatial-Temporal Patterns of Crime in Detroit, Michigan. *Cities* 79, 45–52. doi:10.1016/j.cities.2018.02.021

Yang, B.-Y., Markevych, I., Bloom, M. S., Heinrich, J., Guo, Y., Morawska, L., et al. (2019). Community Greenness, Blood Pressure, and Hypertension in Urban Dwellers: The 33 Communities Chinese Health Study. *Environ. Int.* 126, 727–734. doi:10.1016/j.envint.2019.02.068

Yang, H., Ma, Q., Wang, Z., Cai, Q., Xie, K., and Yang, D. (2020). Safety of Micro-mobility: Analysis of E-Scooter Crashes by Mining News Reports. *Accid. Anal. Prev.* 143, 105608. doi:10.1016/j.aap.2020.105608

Yankson, I. K., Browne, E. N. L., Tagbor, H., Donkor, P., Quansah, R., Asare, G. E., et al. (2010). Reporting on Road Traffic Injury: Content Analysis of Injuries and Prevention Opportunities in Ghanaian Newspapers. *Inj. Prev.* 16 (3), 194–197. doi:10.1136/ip.2009.024174

Yee, W. Y., Cameron, P. A., and Bailey, M. J. (2006). Road Traffic Injuries in the Elderly. *Emerg. Med. J.* 23 (1), 42–46. doi:10.1136/emj.2005.023754

Yu, H., Liu, P., Chen, J., and Wang, H. (2014). Comparative Analysis of the Spatial Analysis Methods for Hotspot Identification. *Accid. Anal. Prev.* 66, 80–88. doi:10.1016/j.aap.2014.01.017

Żak, J., and Kruszyński, M. (2015). Application of AHP and ELECTRE III/IV Methods to Multiple Level, Multiple Criteria Evaluation of Urban Transportation Projects. *Transportation Res. Proced.* 10, 820–830. doi:10.1016/j.trpro.2015.09.035

Zavadskas, E. K., Bausys, R., and Mazonaviciute, I. (2019). Safety Evaluation Methodology of Urban Public parks by Multi-Criteria Decision Making. *Landscape Urban Plann.* 189, 372–381. doi:10.1016/j.landurbplan.2019.05.014

Zhang, G., Guo, X., Li, D., and Jiang, B. (2019). Evaluating the Potential of LJ1-01 Nighttime Light Data for Modeling Socio-Economic Parameters. *Sensors* 19 (6), 1465. doi:10.3390/s19061465

Zhang, G., Yau, K. K. W., and Zhang, X. (2014). Analyzing Fault and Severity in Pedestrian-Motor Vehicle Accidents in China. *Accid. Anal. Prev.* 73, 141–150. doi:10.1016/j.aap.2014.08.018

Zheng, P., Hall, R. D., and McDonald, M. (2007). "Pedestrian Behaviour and Safety in the Presence of Guard Railing," in Proceedings of the 2nd International Conference on System Safety, London, UK, 22-24/10/07 (IET Digital Library), 141–146. Paper presented at the. Available at: https://eprints.soton.ac.uk/53077/. doi:10.1049/cp:20070455

Zheng, Y., Lan, S., Chen, W. Y., Chen, X., Xu, X., Chen, Y., et al. (2019). Visual Sensitivity versus Ecological Sensitivity: An Application of GIS in Urban forest park Planning. *Urban For. Urban Green.* 41, 139–149. doi:10.1016/j.ufug.2019.03.010

Zhou, H., He, S., Cai, Y., Wang, M., and Su, S. (2019). Social Inequalities in Neighborhood Visual Walkability: Using Street View Imagery and Deep Learning Technologies to Facilitate Healthy City Planning. *Sustainable Cities Soc.* 50, 101605. doi:10.1016/j.scs.2019.101605

Zhu, M., Li, H., Sze, N. N., and Ren, G. (2022). Exploring the Impacts of Street Layout on the Frequency of Pedestrian Crashes: A Micro-level Study. *J. Saf. Res.* doi:10.1016/j.jsr.2022.01.009

Conflict of Interest: The authors declare that the research was conducted in the absence of any commercial or financial relationships that could be construed as a potential conflict of interest.

Publisher's Note: All claims expressed in this article are solely those of the authors and do not necessarily represent those of their affiliated organizations, or those of the publisher, the editors, and the reviewers. Any product that may be evaluated in this article, or claim that may be made by its manufacturer, is not guaranteed or endorsed by the publisher.

Copyright © 2022 Luo, Liu, Xing, Wang and Rao. This is an open-access article distributed under the terms of the Creative Commons Attribution License (CC BY). The use, distribution or reproduction in other forums is permitted, provided the original author(s) and the copyright owner(s) are credited and that the original publication in this journal is cited, in accordance with accepted academic practice. No use, distribution or reproduction is permitted which does not comply with these terms.

frontiers | Frontiers in Environmental Science

ORIGINAL RESEARCH
published: 17 May 2022
doi: 10.3389/fenvs.2022.851321

Optimizing Leisure Agriculture by Analyzing Spatial Patterns and Tourists' Perceptions: Evidence From Wuhan, China

Chengcheng Wang[1], Shaohua Wu[1], Wei Yang[2], Haijun Bao[3], Jinxia Zhu[1] and Xia Wang[4]*

[1]Land and Urban-Rural Development Institute, Zhejiang University of Finance and Economics, Hangzhou, China, [2]School of Management Science and Real Estate, Chongqing University, Chongqing, China, [3]Spatial Planning and Design, Zhejiang University City College, Hangzhou, China, [4]School of Geography and Ocean Science, Nanjing University, Nanjing, China

Leisure agriculture can meet the leisure needs of residents and promote farmers' income, which is an important way to achieve rural revitalization. However, the unreasonable spatial patterns and weak competitiveness of leisure agriculture seriously restrict its sustainable development. This paper proposes a framework for optimizing leisure agriculture development, including spatial patterns analysis of leisure agriculture based on big data, quality analysis of leisure agriculture based on tourists' perceptions, and strategies for optimizing leisure agriculture based on spatial patterns and tourists' perceptions. Taking Wuhan city as an example, the results show that: 1) the main types of leisure agriculture are leisure farms, fishing, and picking gardens, showing an agglomerative distribution pattern; 2) considering tourists' emotional perceptions, most comments are positive, and leisure farms should enhance the tourist experience; 3) tourists' dissatisfaction mainly involves the environment, price, and travel, while product and service factors are relatively satisfactory; and 4) moderate agglomeration is beneficial to the quality of leisure agriculture, while excessive agglomeration has adverse effects. This study explores the development law of regional leisure agriculture, improves the relevant theoretical research system and methods, and provides decision-making references for promoting the development of leisure agriculture.

Keywords: leisure agriculture, spatial patterns, tourists' perceptions, quality evaluation, optimization strategy

OPEN ACCESS

Edited by:
Ding Ma,
Shenzhen University, China

Reviewed by:
Jun Yang,
Northeastern University, China
Kiriaki M. Keramitsoglou,
Democritus University of Thrace, Greece

****Correspondence:***
Haijun Bao
haijun_bao@126.com

Specialty section:
This article was submitted to Environmental Informatics and Remote Sensing, a section of the journal Frontiers in Environmental Science

Received: *09 January 2022*
Accepted: *11 March 2022*
Published: *17 May 2022*

Citation:
Wang C, Wu S, Yang W, Bao H, Zhu J and Wang X (2022) Optimizing Leisure Agriculture by Analyzing Spatial Patterns and Tourists' Perceptions: Evidence From Wuhan, China. Front. Environ. Sci. 10:851321. doi: 10.3389/fenvs.2022.851321

1 INTRODUCTION

In recent years, with the rapid development of industrialization and urbanization, urban residents' demands to live close to and access nature have been gradually increasing (Jing et al., 2018; Qiu et al., 2019). In the suburbs of some large cities, leisure agriculture has become a regular pastime for urban residents (Barbieri, 2020; Chase et al., 2018). Additionally, traditional agriculture is no longer the only economic force in most rural areas (Wu, 2018). The quality of rural areas attracts visitors and leads people to prefer a natural and harmonious lifestyle (Jacobsen and Tommervik, 2016). In places with rich natural resources and beautiful scenery, the development of tourism and the service industry is also very important.

The growing popularity of leisure agriculture has many positive effects. On one hand, it promotes the development of the agricultural and rural economy, including increasing the household incomes

of farmers, expanding employment capacity, and increasing tax revenue (Giaccio et al., 2018). On the other hand, leisure agriculture also provides an environment where urban residents can have a pleasant leisure experience and promotes people's physical and emotional health (Sgroi et al., 2018). More importantly, it promotes the development of agriculture from traditional to diversified models and creates new possibilities for the local economy (Su et al., 2019), which is an important path to realizing rural revitalization (Tao, 2019).

Driven by market demand, leisure agriculture in China is developing rapidly, showing strong vitality and growth prospects. However, such rapid development can create many problems related to the spatial patterns and quality of leisure agriculture in mainland China (Ren and Dong, 2016). In terms of spatial patterns, most businesses are small-scale operations and have poor planning practices. Industrial agglomeration of leisure agriculture can guide production factors to flow to rural areas, form agglomeration effects, and improve overall competitiveness, but excessive agglomeration can lead to vicious competition (Kim et al., 2021; Pejanović et al., 2017). Therefore, we need to scientifically measure the spatial patterns of leisure agriculture, explore the relationship between spatial patterns and quality and engage in detailed planning. Similarly, many leisure agriculture businesses are low quality and have single brands, weak core competitiveness, and other factors that prevent them from meeting the gradually diversifying and personalized tourism consumption needs, resulting in a decline in the number of tourists who visit the area (Guo and Lv, 2008). To date, the overall integration of leisure agriculture has not been accomplished, and there are no large-scale companies with high-quality multifunctional services. Therefore, it is important to optimize the development of leisure agriculture by combining the spatial patterns and quality improvement of leisure agriculture.

Scholars mostly use GIS spatial analysis to study patterns of leisure agriculture (Bajgier-Kowalska et al., 2017; Baležentis et al., 2012; Walford, 2001), and measurement indicators include the nearest-neighbor index, the geographic concentration index, the coefficient of variation, kernel density estimation, the spatial dispersion index, and the spatial distribution curve, among others (Chang et al., 2018; Liu et al., 2017; Xu et al., 2021). The measurement of leisure agriculture quality is based on the tourist satisfaction model and focuses on the evaluation of service quality (Liu and Yen, 2010; Reichel et al., 2000). The measurement index covers the product, environment, service, price, travel, and other aspects (Goossen and Langers, 2000; Zhao and Chang, 2014). A questionnaire is the most common method to obtain tourists' perceptions data (Dubois et al., 2017; Tew and Barbieri, 2012). The analyses in this field mainly adopt fuzzy comprehensive evaluation and factor analysis (Rozman et al., 2009). Development strategies of leisure agriculture have been offered from the perspectives of spatial distribution, tourists' motivation, and tourism development (Yang et al., 2016). The development of leisure agriculture should rely on the regional resource endowment, reasonably optimize the layout (Wu and Cai, 2006), enhance the tourism image (Ohe and Kurihara, 2013), improve tourist satisfaction (Choo and Petrick, 2014; Lee, 2012), focus on rural characteristics and rural value (Shen et al., 2019) and increase the participation of local residents (Xue and Kerstetter, 2019).

The existing research has the following shortcomings. First, evaluations of the tourist experience of leisure agriculture mostly draw on the evaluation tourists' experiences in scenic spots rather than their experiences with the specific characteristics of leisure agriculture. A scientific and reasonable quality evaluation model for leisure agriculture has not been formed. Second, most studies rely on statistical data from government departments or surveys with small samples, resulting in unrepresentative suggestions (Wu and Cheng, 2017). In contrast, multisource, large-sample, and multidimensional big data with geographical locations obtained from social media platforms provide new research means and observation perspectives to understand urban socioeconomic perceptions (Liu et al., 2015; Zhang et al., 2019). Using big data ensures that researchers possess a sufficient amount of data, reduces the cost of data collection, and can help scholars analyze people's perceptions (Li et al., 2018). Tourist evaluation data come from active volunteers, and this format more effectively captures participants' emotions. Analyzing these data facilitates large-scale regional, multi-perspective qualitative and quantitative research and aids in decision-making in resource allocation, planning, and quality improvement of leisure agriculture.

This paper aims to propose a quality assessment model for leisure agriculture and further explores optimization strategies for the development of leisure agriculture. The main contribution of the paper is to explore the optimization strategies of leisure agriculture by combining spatial patterns and tourists' perceptions. Through this approach, we can obtain a comprehensive understanding of the role of spatial patterns in the development of leisure agriculture and explore the sustainable development model of leisure agriculture. Furthermore, this study sheds light on the analysis of big data. China's experiences with leisure agriculture could provide valuable references for other developing countries. This study is structured as follows: (1) a spatial patterns analysis of leisure agriculture based on big data; (2) evaluations of leisure agriculture based on tourists' perceptions; (3) quality evaluation of leisure agriculture based on tourists' perceptions; and (4) optimization strategies for the development of leisure agriculture that combine spatial patterns and tourists' perceptions.

2 MATERIALS AND METHODS

2.1 Research Framework

The rapid development of the tourism industry has created an obvious industrial agglomeration phenomenon and trend in some regions (Chhetri et al., 2017). The concept of tourism agglomeration originated from economic geography and was introduced by Alfred Marshall. Tourism industry agglomeration is the concentration of tourism enterprises based on rich tourism resources in a certain geographical space (Estevão and Ferreira, 2012). Spatial agglomeration has two sides in tourism development (Lee et al., 2020; Novelli et al.,

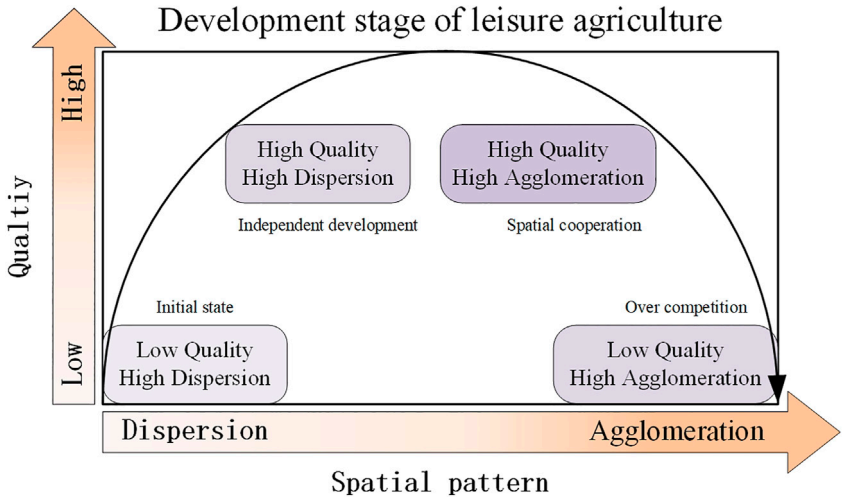

FIGURE 1 | Theoretical framework.

2006). On one hand, spatial agglomeration can enhance the competitiveness of enterprises (Chen et al., 2021), produce multiplier and external effects, promote the interaction and synergy between enterprises (Hawkins, 2004), and promote the sustainable development of tourism destinations (Benur and Bramwell, 2015). On the other hand, spatial agglomeration easily produces a substitution effect and vicious competition (Weidenfeld et al., 2011). The evaluation index of the quality of leisure agriculture usually comes from tourists' perceptions. Tourists' perceptions are tourists' understanding of tourism products and services. Leisure agriculture is an industry in which tourists are the main consumers, thus, their experiences are very important (Kastenholz et al., 2018; Volo, 2021). Regions with high tourists' evaluation can attract more visitors (Da Liang et al., 2020; Nazariadli et al., 2018).

At present, there is no consensus about the role of spatial agglomeration in the development of leisure agriculture. In other words, it is not clear whether the agglomeration pattern or the dispersion pattern is conducive to industrial development. **Figure 1** presents a theoretical framework for understanding spatial patterns and the quality of leisure agriculture. The framework helps identify strategies for leisure agriculture development. It is based on the two features of leisure agriculture products: the spatial patterns of leisure agriculture (from dispersion to agglomeration) and the quality of leisure agriculture (from low quality to high quality). As the spatial patterns of leisure agriculture change from dispersion to agglomeration, its quality also changes. There are four typical states, among which there are different transition states: low quality and high dispersion, high quality and high dispersion, high quality and high agglomeration, and low quality and high agglomeration. The category of low quality and high dispersion is usually the primary stage of leisure agriculture development, characterized by low quality and small scale. The category of high quality and high dispersion indicates that regional leisure agriculture presents a single point development mode, and the spatial distribution is dispersed. In this state, the leisure agriculture spots have no influence on each other, and the existence of high-quality leisure agriculture spots has not driven the development of other leisure agriculture in the region. The high-quality and high-agglomeration group is the "ideal type", which gives full play to the advantages of industrial agglomeration and spatial synergy, and forms a high-quality leisure agriculture agglomeration area with a scale effect within the region. Low quality and high agglomeration indicate that the agglomeration distribution of regional leisure agriculture does not promote high-quality development of the practice. This type of leisure agriculture may produce vicious competition and is considered to be large scale and of low quality.

2.2 Study Area

Wuhan is the central city in central China. In 2019, the city governed 13 districts with a permanent resident population of 11.212 million and an urbanization rate of 80.49%. Wuhan has the advantage of possessing agricultural resources, with 2,938.6 km^2 of cultivated land; it is known as a "land of fish and rice". Bodies of water occupy approximately one-quarter of the city's area, ranking Wuhan first in the country. Rich agricultural and water resources provide good opportunities for the development of leisure agriculture, including picking, fishing, recreation, and other practices. Furthermore, Wuhan is a national historical and cultural city. In 2019, there were 44 A-level scenic spots in Wuhan, and the tourism industry developed rapidly. The total number of tourists who visited the area during the year reached 318.98 million, and the total tourism income was 357.08 billion yuan. The rapid rise of the tourism industry has driven the development of the leisure agriculture market.

2.3 Data

The data for this study include the leisure agriculture database of user-generated content (UGC) and the administrative division

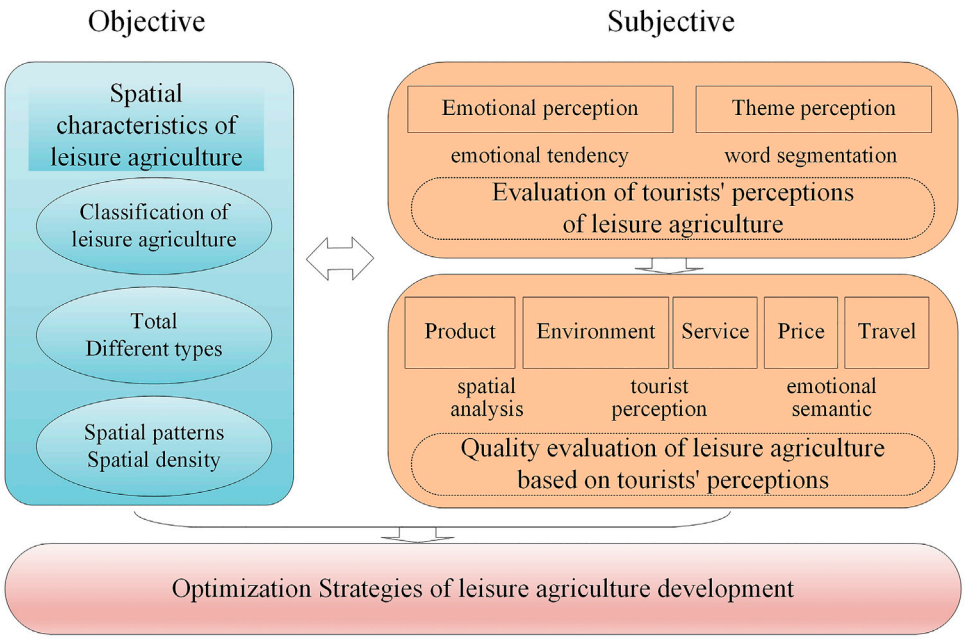

FIGURE 2 | Research process.

data of Wuhan in 2018. The leisure agriculture data were obtained from Dianping.com using a web crawler tool. These data include the latitude and longitude of leisure agriculture sites, comment information (comment text, comment time), basic information about the reviewers (gender, community level), and other factors. Dianping.com is a leading third-party consumer comment platform in China that began operating in April 2003 (Wu et al., 2015). Members can freely express their opinions about businesses and consumption experiences through the website, providing information for potential consumers. Public comment data identify the spatial location and attribute information of leisure agriculture businesses, with large coverage, high accuracy, and representativeness. ArcGIS was used for the spatial processing of information and to build a leisure agriculture database based on big data.

2.4 Methods

This paper constructs an optimization framework for the development of leisure agriculture using big data (**Figure 2**). First, we analyzed the spatial patterns characteristics of different types of leisure agriculture, which is an objective analysis. The types of leisure agriculture are divided according to differences in their function and scale (Busby and Rendle, 2000). The spatial characteristics need to identify the spatial patterns and density. GIS spatial analysis was used to analyze the agglomeration or dispersion characteristics of leisure agriculture. Second, this paper evaluates leisure agriculture tourists' perceptions from two perspectives: emotional perception and theme perception. The emotional tendency analysis module of the Baidu Ai platform was used to analyze the positive and negative emotions of tourists, and word segmentation analysis helped us explore the core issues of tourists' concerns (Wu, 2019). Then, we constructed a quality evaluation method for leisure agriculture based on tourists' perceptions, focusing on the product, environment, service, price, travel, and other factors. Finally, we explore the optimization strategies for leisure agriculture by combining spatial patterns and tourists' perceptions.

2.4.1 Analysis of the Spatial Characteristics of Leisure Agriculture

The spatial characteristics of leisure agriculture were measured in terms of the spatial pattern and density. Each measure is described here.

Average nearest neighbor

The average nearest neighbor index was used to analyze the spatial distribution of leisure agriculture after measuring the distance between each leisure agriculture as follows:

$$ANN = \frac{\overline{D_0}}{\overline{D_e}} = \frac{\sum_{i=1}^{n} d_i / n}{\sqrt{n/A}/2} \quad (1)$$

where $\overline{D_0}$ is the observed mean distance between each leisure agricultural point and its nearest neighbor, $\overline{D_e}$ is the expected mean distance for the features given in a random pattern; n corresponds to the total number of leisure agricultural points, and A is the area of the study area. If ANN is less than 1, the distribution of leisure agriculture points is considered clustered; if the index is greater than 1, the leisure agriculture points are considered dispersed.

Kernel density

A kernel density was used to measure the spatial density of leisure agriculture. The kernel density estimation calculation formula is:

TABLE 1 | Evaluation index of leisure agriculture quality.

Target layer	System layer (w_k)	Index layer (w_j)
Evaluation index of leisure agriculture quality	Product (0.3)	Quality (0.6667)
		Facilities (0.3333)
	Environment (0.2)	Scenery (0.2274)
		Health (0.4231)
		Space (0.1222)
		Environment (0.2274)
	Service (0.2)	Attitude (0.3333)
		Feeling (0.6667)
	Price (0.2)	Price (1.0000)
	Travel (0.1)	Traffic (0.5000)
		Position (0.5000)

$$f(x) = \frac{1}{nh}\sum_{i=1}^{n} k\left(\frac{x - x_i}{h}\right) \tag{2}$$

where $f(x)$ is the density estimation at the location (x), n is the number of leisure agriculture points, h is the bandwidth, k is the kernel function, and $(x - x_i)$ is the distance between location (x) and the location of the ith observation.

2.4.2 Evaluation of Tourists' Perceptions of Leisure Agriculture

This paper uses emotional tendency analysis to analyze the positive and negative emotions of tourists. We applied the emotional tendency analysis module of the Baidu Ai platform. The method automatically judges the emotional polarity category of the tourists' comments, and the corresponding confidence level is given. Emotional polarity is divided into positive, negative, and neutral. Emotional tendency analysis estimates the emotional tendency of text that contains subjective information, which helps users make decisions. Based on deep learning training, the system automatically learns deep semantic and syntactic features and has high generalization ability, which is highly effective, even for relatively long sentences (Yan et al., 2018).

Using word segmentation analysis, this paper explores the core issues of tourists' concerns and the advantages and disadvantages of current leisure agricultural products. It then analyzes the concerns of leisure agriculture tourists with different emotional tendencies. We use the Python Jieba cut to segment the tourists' comments. After excluding common pause words, we calculate statistics for the common words in the comment text and uncover the most important concerns of tourists about leisure agriculture. Then, based on emotional analysis, this paper uses word segmentation analysis to mine the advantages and dissatisfaction factors expressed by tourists.

2.4.3 Quality Evaluation of Leisure Agriculture Based on Tourists' Perceptions

We searched the comments offered by leisure agriculture tourists from the public comment websites. According to existing research and data availability (Rozman et al., 2009), the quality characteristics of leisure agriculture are divided into five dimensions: product (quality and facilities), environment (scenery, health, and space), service (attitude and feelings), price, and travel (traffic and location), as shown in **Table 1**. The emotional semantic dimensions of leisure agriculture were classified and scored to evaluate tourists' experiences of these different dimensions of leisure agriculture; on this basis, the weights of the dimensions were determined to comprehensively evaluate the quality of leisure agriculture. The specific steps were as follows:

Text preprocessing: This step involved sentence segmentation, tokenization, and removing stop words.

Extracting feature–opinion pairs: The assumption was that each sentence evaluated a dimension of the feature object, with direct links between opinion words (sentiment) and noun words (feature) in a clause.

Weight determination: The analytic hierarchy process was used to determine the weight.

Emotional score calculation: The emotional score was calculated using the polarity and degree of the emotion (Yang and Ai, 2018) as follows:

$$f_i = p_i \times d_i \tag{3}$$

where f_i is the emotional score of the segmented sentence i, p_i is the emotional polarity of the segmented sentence i, and d_i is the emotional degree of the segmented sentence i. Emotional polarity is classified as positive, neutral, or negative, expressed by 1, 0, and −1, respectively. The emotional degree is divided into three levels—strong, medium, and weak, expressed by 3, 2, and 1, respectively.

Score calculation by dimension: Considering that different sentences may evaluate the same features of leisure agriculture, feature sentences were combined according to the previously defined dimension feature dictionary. Through the calculation of each dimension score, all dimensions of leisure agriculture businesses were evaluated:

$$S_k = \sum_{j=1}^{b} \frac{1}{c_j} \sum_{i=1}^{c_j} f_i \cdot w_j \tag{4}$$

where S_k is the score of the kth dimension of the system layer, j is the dimension of the index layer, b is the number of index layers, c is the number of sentences after the jth dimension

TABLE 2 | Types and characteristics of leisure agriculture.

Type	Characteristics
Picking garden	Relying on orchards, vegetable gardens, melon gardens, flower beds, and so on, tourists can enjoy the scenery and work in the garden to experience rural life
Fishing	Relying on reservoirs, fish ponds, and other water bodies for fishing, boating, and other forms of entertainment on the water
Leisure farm	Can provide large-scale agricultural and recreational activities, fishing, and sightseeing. Provides comprehensive services, such as food, accommodation, travel, entertainment, shopping, and experiences
Agritainment	Can provide small-scale agricultural and recreational activities. Mainly takes farmers as the unit; includes farm food and agricultural products and farmers' life experiences and leisure activities
Planting and breeding	Nursery cultivation and animal husbandry
Agriculture technology	Relies on modern scientific and agricultural technology, high-tech agricultural demonstration parks, and agricultural companies

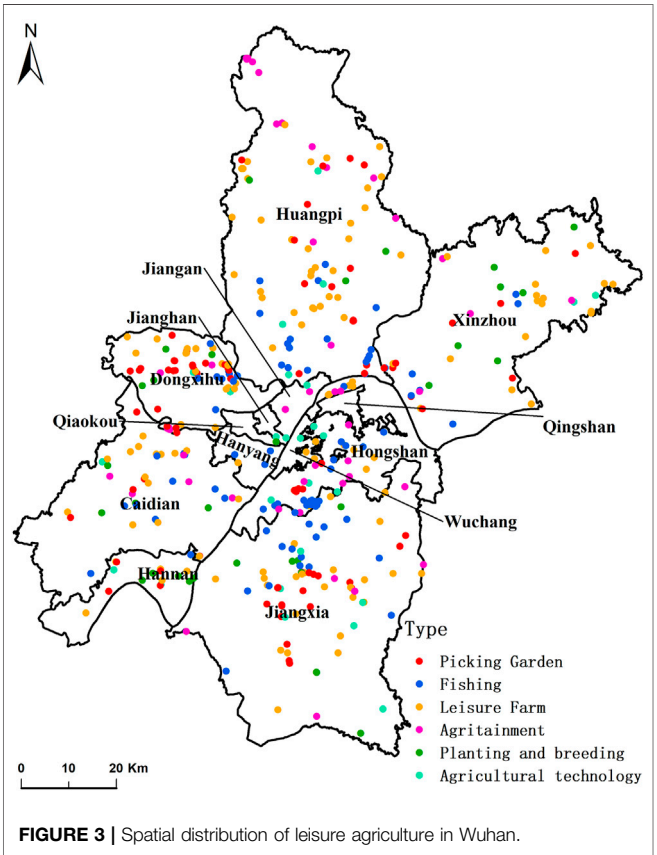

FIGURE 3 | Spatial distribution of leisure agriculture in Wuhan.

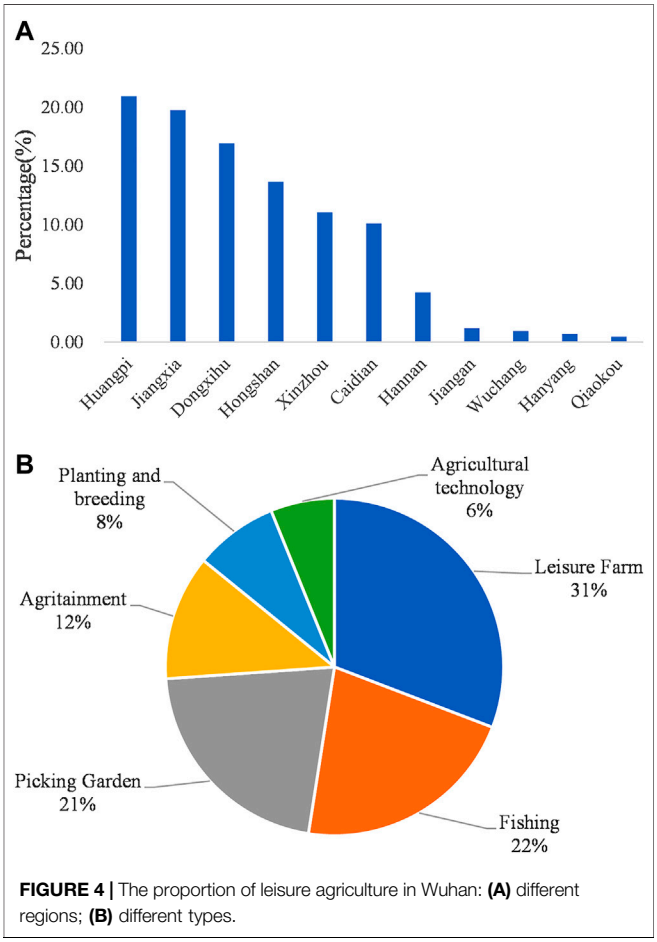

FIGURE 4 | The proportion of leisure agriculture in Wuhan: **(A)** different regions; **(B)** different types.

segmentation of the index layer, and w_j is the weight of the index layer.

Total quality score calculation:

$$Score = \sum_{k=1}^{a} S_k \cdot w_k \tag{5}$$

where *Score* is the total score for quality, k is the dimension of the system layer, a is the number of system layers, and w_k is the weight of the system layer.

Based on the multidimensional experience evaluations of tourists, this paper offers suggestions for the development of leisure agriculture in terms of products, environment, service, price, and travel, among others.

3 RESULTS

3.1 Analysis of Spatial Characteristics of Leisure Agriculture Based on Big Data

Based on the leisure agriculture data, using the method of text recognition, and combining the characteristics of the scale and function (Guo and Lv, 2008; Ren and Dong, 2016) of leisure agriculture businesses, the leisure agriculture activities were divided into six types (**Table 2**): picking garden, fishing, leisure farm, agritainment, planting and breeding, and agricultural technology.

TABLE 3 | Nearest-neighbor index of different types of leisure agriculture in Wuhan.

Types	Nearest neighbor index	Z value	P value	Average observation distance(m)	Expected average distance(m)	Layout pattern
All	0.6586	−13.4655	0.0000	1661.5626	2522.9710	cluster
Picking garden	0.6076	−7.1620	0.0000	2816.3698	4635.6083	cluster
Fishing	0.7973	−3.7199	0.0002	3207.5386	4023.1151	cluster
Leisure farm	0.8227	−3.8828	0.0001	3549.2054	4314.2367	cluster
Agritainment	0.8876	−1.5357	0.1246	6109.2066	6882.9010	random
Planting and breeding	0.9521	−0.5347	0.5928	7402.6166	7775.3470	random
Agricultural technology	0.9554	−0.4347	0.6638	8105.4862	8483.5288	random

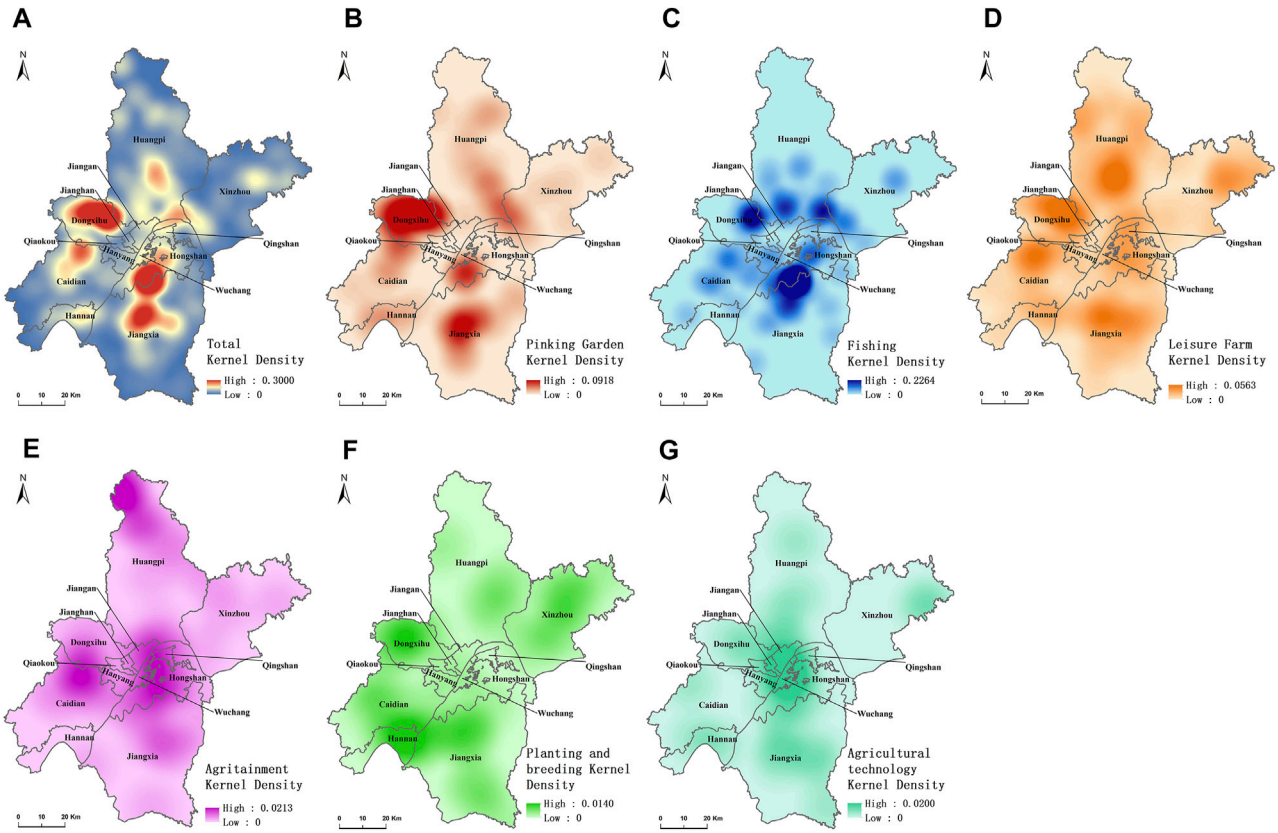

FIGURE 5 | The kernel density of leisure agriculture in Wuhan: **(A)** All types; **(B)** Picking Garden; **(C)** Fishing; **(D)** Leisure Farm; **(E)** Agritainment; **(F)** Planting and breeding; **(G)** Agricultural Technology.

The distribution of leisure agriculture (**Figure 3**) is found more in the outer suburbs than in the central city. Huangpi District accounts for the highest proportion (20.94%), followed by Jiangxia District (19.76%), Dongxihu District (16.94%), and Hongshan District, Caidian District, and Xinzhou District (each accounting for approximately 10%). Other districts have lower proportions. As shown in **Figure 4**, among the leisure agriculture businesses in Wuhan, the proportion of leisure farms is the highest (30.52%). Furthermore, the types of leisure agriculture are ranked in the following order: leisure farm, fishing, picking garden, agritainment, planting and breeding, and agricultural technology. This finding indicates that leisure farms and fishing are the most popular types of leisure agriculture among tourists in Wuhan.

The results of the nearest-neighbor index analysis of the types of leisure agriculture in Wuhan are shown in **Table 3**. The leisure agriculture in Wuhan is generally in the form of agglomeration. Specifically, picking gardens, fishing, and leisure farms have clustered distributions. Agritainment, planting and breeding, and agricultural technology show random distribution patterns.

There are obvious regional differences in the spatial distribution density of leisure agriculture in Wuhan (**Figure 5**). The areas with

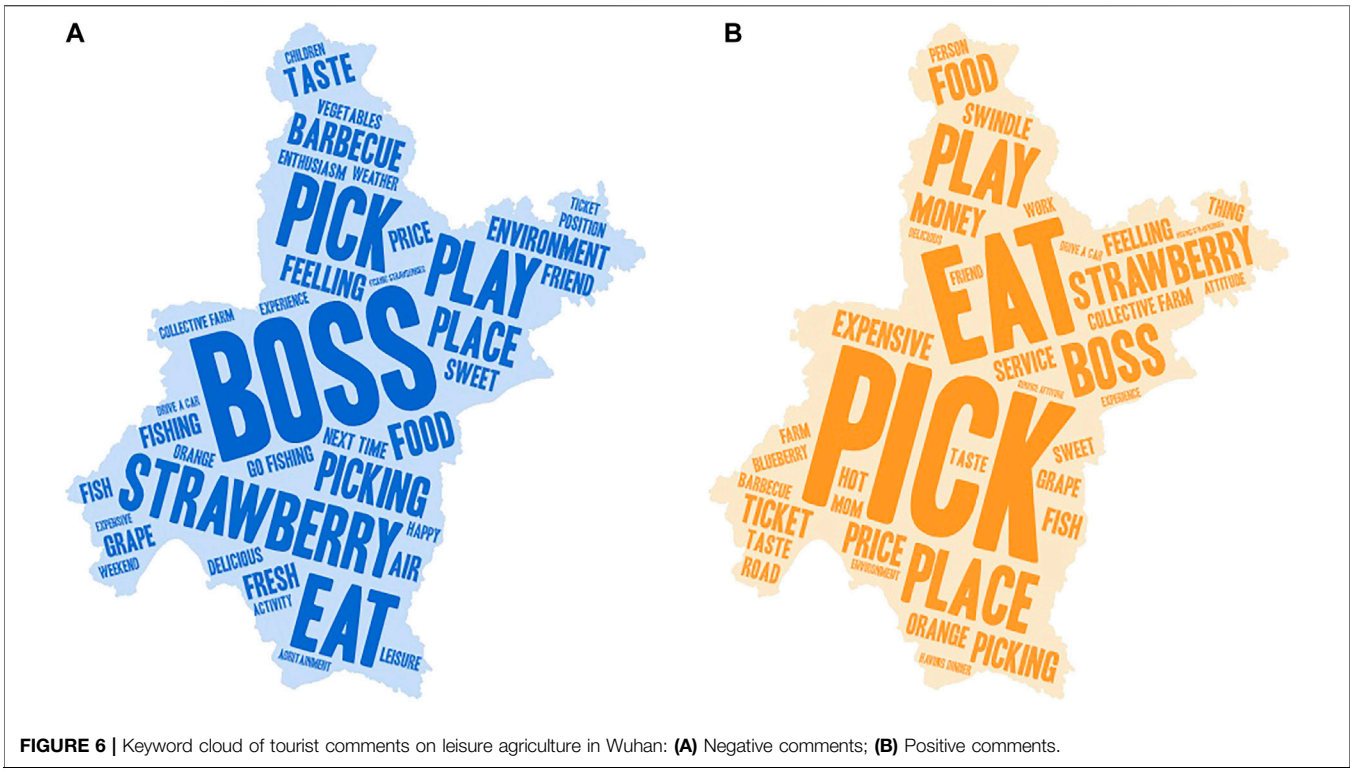

FIGURE 6 | Keyword cloud of tourist comments on leisure agriculture in Wuhan: **(A)** Negative comments; **(B)** Positive comments.

higher leisure agriculture density are mainly concentrated in central and southern Wuhan. The picking garden distribution is similar to that of leisure agriculture. Fishing is mainly distributed around the main urban area of Wuhan city, among which Liangzi Lake is the center of fishing activities. Leisure farms are distributed in almost all districts. Agritainment is mainly distributed in central and northern Wuhan, while the type of planting and breeding is concentrated in the outer suburbs. The distribution of agricultural technology is highly dependent on cities.

3.2 Evaluation of Tourists' Perceptions of Leisure Agriculture

The results (**Figure 6**) show that the overall comments on leisure agriculture in Wuhan are positive, with a positive comment rate of 79.60%, a neutral comment rate of 1.51%, and a negative comment rate of 18.89%. However, since the numbers of comments on agricultural technology and planting and breeding are small, the analyses of these categories are unreliable, so they are not considered. Evaluations of all types of leisure agriculture in Wuhan are positive. Specifically, fishing received the most positive feedback, and picking gardens received the fewest positive reactions. Likewise, in terms of negative evaluations, picking gardens had the highest number, while fishing had the lowest number. In the future, we should focus on the development of picking gardens as a form of leisure agriculture.

Through the word segmentation analysis, it can be seen that leisure agriculture tourists in Wuhan mainly focus on products, environment, service, price, and travel. In terms of "products", leisure agriculture activities mainly involve picking gardens and fishing, with "barbecue" and "vegetables" as the main characteristics. "Strawberry", "grape" and "orange" are the most frequently picked foods, and "taste", "sweet" and "fresh" are the important evaluation criteria. In terms of the "environment", tourists pay attention to the quality of "weather" and "air". "Farm" and "farmhouse" are the main locations for leisure agriculture in Wuhan. In terms of "service", the main factors that tourists pay attention to are "boss", "feeling" and "enthusiasm". Furthermore, "price", "ticket" and "expensive" are high-frequency words. Finally, in terms of "travel", location is the main concern for tourists.

Wuhan, as the capital of Hubei Province, has the leading economy in the province, and it features many scenic spots. Its leisure agriculture has garnered praise from users based on services, products, and the environment. However, it still has some problems. Tourists have mixed evaluations of products, prices, services, the environment, or travel experiences. Among them, "expensive", "ticket", "money", "buy", "price" and other words frequently appear in negative comments, which shows that the cost of visiting has affected the development of regional leisure agriculture and needs to be improved. In addition, the quality of services is also an important factor.

3.3 Quality Evaluation of Leisure Agriculture Based on Tourists' Perceptions

The spatial distribution of the leisure agriculture quality evaluation scores in Wuhan is shown in **Figure 7**. The score range is −3.00 to +3.00, and the scores are divided into four levels: level I [1.50 to 3.00], level II [0.00 to 1.50), level III [−1.50 to 0.00), and level IV (−3.00 to −1.50]. Among the 425 businesses, 126 have

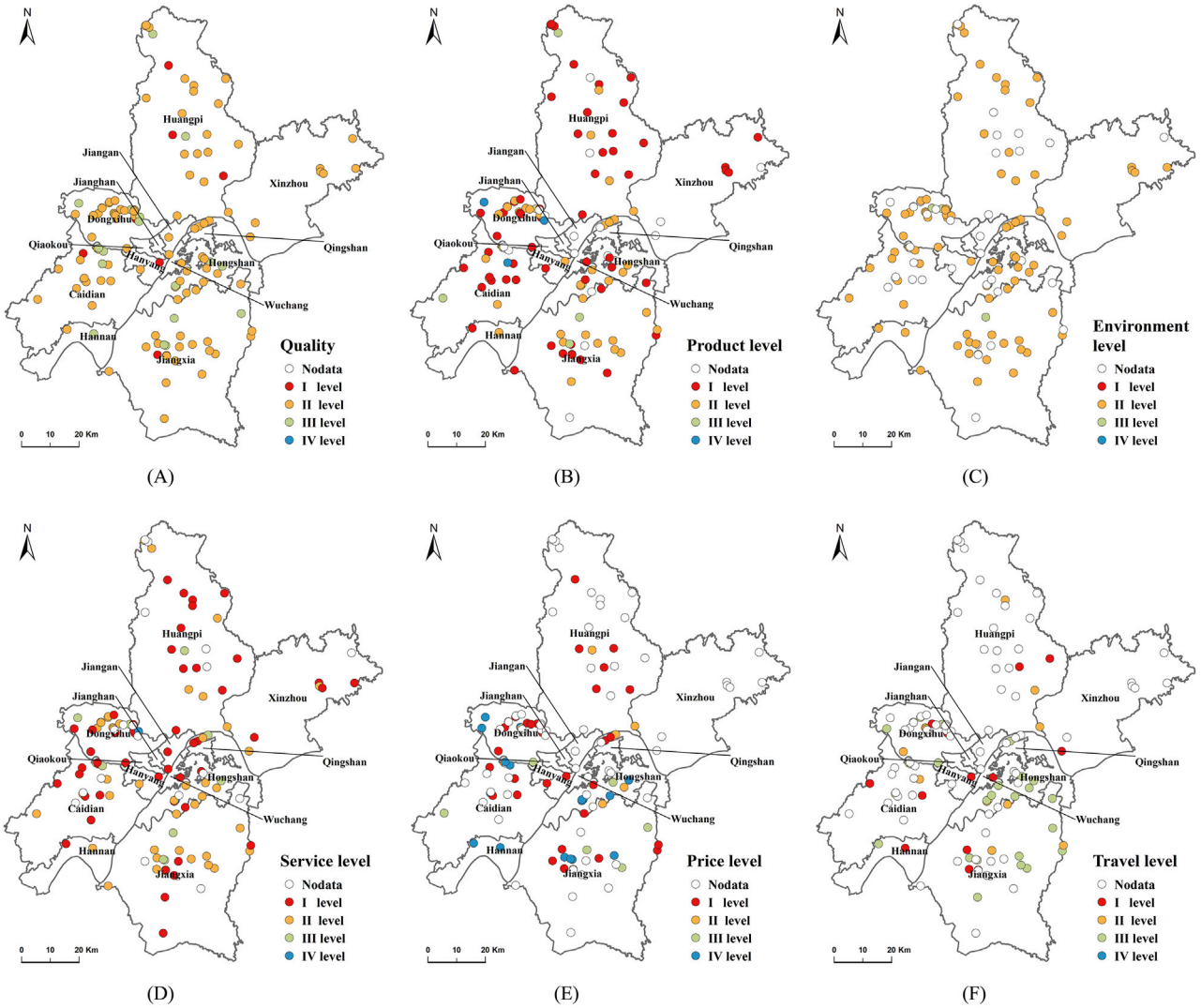

FIGURE 7 | Spatial distribution of the quality evaluation of leisure agriculture in Wuhan: **(A)** Overall quality; **(B)** Product level; **(C)** Environment level; **(D)** Service level; **(E)** Price level; **(F)** Travel level.

received comments. The total score is concentrated between −1.50 and +1.74, and most of the businesses are located in level II or level I. Among them, 18 businesses have ratings below 0, which is poor. In addition, high-quality leisure agriculture businesses are distributed in almost all districts, while low-quality leisure agriculture businesses are mainly located in central Wuhan. As shown in **Figure 7**, tourists' dissatisfaction is mainly due to environment, price, and travel factors, while product and service are relatively good.

The numbers of leisure agriculture businesses in product levels I–IV is 60, 38, 6, and 3, respectively. Product scores are concentrated in levels I and II. Businesses with higher scores are distributed in almost all districts, and the businesses with lower scores are mainly distributed in Dongxihu and Jiangxia District, which are located in central and southern Wuhan, respectively. The environmental scores are concentrated in level II, and the scores of most businesses are low. The numbers of leisure agriculture businesses with service scores in levels I–IV are 51, 45, 9, and 2, respectively, showing a concentration of scores in levels I and II. The spatial distribution characteristics of service scores are similar to those of product scores. The numbers of leisure agriculture businesses with price scores in levels I–IV are 32, 8, 7, and 17, respectively. The price scores are concentrated in levels I and IV, with serious differentiation. Businesses with lower scores are mainly distributed in central and southern Wuhan. Finally, the travel scores are distributed in levels II-IV. Businesses with lower scores are mainly distributed in Hongshan District and Jiangxia District, which are located in central and southern Wuhan, respectively.

3.4 Optimization Strategies for the Development of Leisure Agriculture

Considering the spatial patterns and quality of leisure agriculture, this paper proposes an optimization strategy for the sustainable

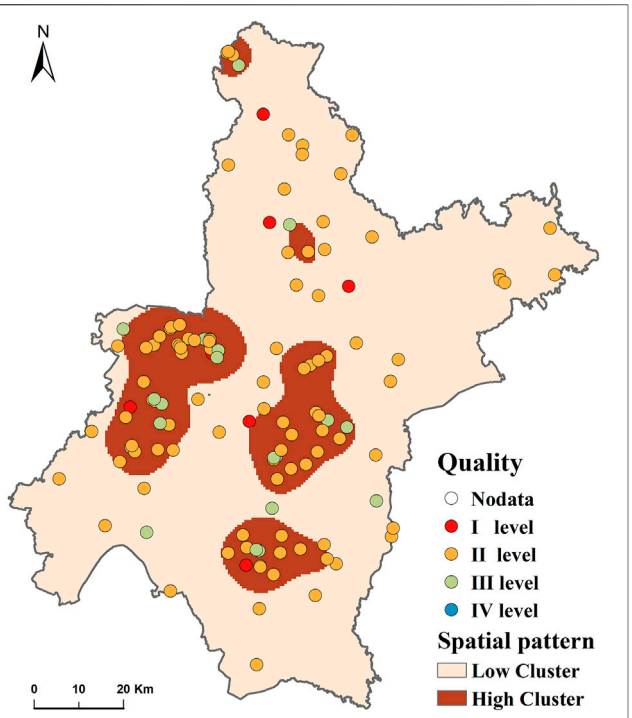

FIGURE 8 | Quality score and spatial kernel density distribution of leisure agriculture.

development of leisure agriculture. Taking Wuhan as an example, the kernel density of 126 leisure agriculture businesses with review data were overlaid with the quality of these businesses for analysis, and the results are shown in **Figure 8**. The findings indicate that overall leisure agriculture in Wuhan is in the form of agglomeration. The average leisure agriculture quality score is 0.6591, and most of the businesses are located in levels I and II. On the whole, leisure agriculture in Wuhan is characterized by high agglomeration and high quality. Moreover, using the natural breaks method, the core density of leisure agriculture can be divided into two types. The type with high core density is high agglomeration, and the other type is low agglomeration. The results show that the average quality score for the high-agglomeration group is 0.6285, which is lower than the average value for businesses in the whole city. This finding indicates that excessive agglomeration has a negative impact on the quality of leisure agriculture. One possible reason is the competition among the homogeneous leisure agriculture businesses. The average quality score of low-concentration businesses is 0.7072, which is higher than the average quality of businesses in the whole city. This finding suggests that the low-agglomeration pattern promotes the development of local leisure agriculture. Scientific planning is beneficial to the development of the leisure agriculture industry. It is necessary to improve the quality of leisure agriculture in highly clustered areas, avoid excessive competition among businesses in the same industry, promote the coordinated development of industries, and promote the industrial agglomeration effect.

From the perspective of development type, leisure farms are the most popular in Wuhan, followed by fishing, picking gardens, and agritainment. However, the activity that received the best tourist evaluations was fishing, followed by agritainment, leisure farms, and picking gardens. As the most widely distributed type of leisure agriculture in Wuhan, leisure farms should further improve the quality of businesses and enhance the experiences of tourists.

From the perspective of quality improvement suggestions, tourists' dissatisfaction mainly involves environment, price, and travel factors. Based on the analysis of the text of tourists' comments, the main environmental problems are poor scenery, small sites, and excessive dust, among others. We should pay attention to improving the environment of leisure agriculture businesses, selecting scenic areas when adding new businesses, and expanding business sites. The main price problems are high ticket prices and false advertising. Improvements include providing free tickets, allowing group purchases on websites, and offering discounts, among others. Travel problems mainly include inconvenient transportation, remote locations, and difficulty in finding the location. Attention should be given to increasing shop signage and offering timely telephone communication. The results suggest that the government should build roads to tourist destinations and establish public transportation or finance construction through other means. In addition, when planning new businesses, it is important to pay attention to factors such as traffic convenience and improve the comprehensive transportation system.

4 DISCUSSION

4.1 Research Findings Compared to Other Studies

Leisure agriculture has become one way to promote agricultural diversification and enhance urban-rural integration. Therefore, leisure agriculture is promoted by the Chinese government (Cui et al., 2021). This study explores the optimization strategies of leisure agriculture that combine spatial patterns and tourists' perceptions. Leisure agriculture is mostly distributed in peri-urban areas (Chang et al., 2018), which are exposed to urban pressures and land-use changes (Gao and Cheng, 2020; Zasada, 2011). Scientific spatial planning of leisure agriculture is conducive to considering the relationship between urban and rural areas. Leisure agriculture planning is mainly reflected in spatial patterns. The findings of this study regarding the agglomeration spatial patterns of leisure agriculture are consistent with multiple studies (Cui et al., 2021; Fanelli and Romagnoli, 2021; Van Sandt et al., 2018; Xiang et al., 2019), in which the authors suggest promoting the agglomeration of leisure agriculture. Our analysis has confirmed the generalizability of this view across Chinese cities. In addition, the matching relationship between the spatial patterns and the quality of leisure agriculture was analyzed. The results show that moderate agglomeration is beneficial to the quality of leisure agriculture, while excessive agglomeration has adverse effects. Leisure agriculture originated in developed countries, and gradually expanded from Europe to Japan, South Korea, Singapore, and other countries and regions in Asia. We suggest that this method be applied to the study of other cities to explore the relationship between the spatial patterns and quality of

leisure agriculture and to optimize the development of regional leisure agriculture. Through extensive empirical analysis, it will be possible to determine the best spatial pattern of leisure agriculture according to local conditions.

The improvement of leisure agriculture depends on the understanding of the roles of consumers, which takes consumers' preferences into consideration (Zasada, 2011). This study analyzes tourists' perceptions using big data, which helps to explore the core issues of tourists' concerns. A previous study found that leisure agriculture users pay attention to the requirements of diet, accommodation, and travel (Wu, 2019). We find that in addition to products and travel, the environment, service, and price are also important factors for leisure agriculture tourists in Wuhan. In addition, we evaluate the quality of leisure agriculture based on tourists' perceptions; this approach clearly identifies the characteristics of leisure agriculture quality and its spatial patterns. The research shows that tourists' dissatisfaction about leisure agriculture in Wuhan mainly results from the environment, price, and travel. This finding helps clarify the development focus of leisure agriculture in different regions and how scientific planning and management can be carried out. Moreover, these beneficial findings and discussions offer feasible suggestions for leisure agriculture development. In future development, on one hand, operators should ensure the richness of products, improve product quality, regularly maintain infrastructure, improve health and environmental conditions and service levels, and set reasonable consumer prices (Tsaur et al., 2016). On the other hand, the government and market should conduct reasonable layout planning for leisure agriculture while also scientifically managing customer complaints and improving comprehensive transportation (Liu et al., 2020).

4.2 Practical Implications

The study helps to provide recommendations for sustainable leisure agriculture: (1) The spatial disparity of leisure agriculture needs to be emphasized, and development guidance should consider local situations. Spatial analysis is recommended for integration into leisure agriculture policy-making. (2) Spatial planning needs to combine the spatial distributions and quality of leisure agriculture to promote agglomeration and avoid excessive competition. (3) The quality improvement of leisure agriculture should be guided by market demand, especially consumer demand. It is important to conduct quality evaluations of leisure agriculture, build high-quality brands and avoid homogeneous competitiveness. (4) Effective measures should be taken to strengthen the supporting facilities of public services and provide professional training for leisure agriculture practitioners.

4.3 Limitations and Prospects

First, due to limitations of the data collection, this study does not analyze the evolution of leisure agriculture from the perspective of spatiotemporal dynamic patterns. In the future, we will explore the spatiotemporal evolution of leisure agriculture to understand development trends and to offer development suggestions. Second, because of the low accuracy of the existing classification methods, this paper uses manual interpretation to judge the characteristics of leisure agriculture reviews. In later work, we plan to use natural language processing and machine learning to characterize tourists' experience evaluations and to improve the efficiency of these characterizations and the scientific rigor and accuracy of the method in later batch processing and comparative analyses between different cities.

5 CONCLUSIONS

This paper has constructed a framework for optimizing leisure agriculture using big data, taking Wuhan city as the case study for the analysis. The results show that the main types of leisure agriculture in Wuhan are leisure farms, fishing, and picking gardens, and the spatial pattern shows an agglomeration distribution. In planning the spatial distribution of leisure agriculture, attention should be given to appropriate agglomeration. As the most widely distributed type in Wuhan, leisure farms receive low tourist evaluation, so it is necessary to improve the quality of businesses and enhance tourists' experiences.

High-quality leisure agriculture businesses are distributed in almost all districts in Wuhan, while low-quality sources are mainly located in the central part of the city. Tourists' dissatisfaction with leisure agriculture mainly includes the environment, price, and travel factors, while products and services are relatively satisfactory. The sustainable development of leisure agriculture needs to take quality-building as the core, deeply tap into the regional industrial characteristics, and cultivate the competitiveness of leisure agriculture development. The purpose of this study was not only to guide the development of leisure agriculture in Wuhan, but also to explore tourist experiences and identify a suitable way forward for the development of leisure agriculture on a wider scale.

DATA AVAILABILITY STATEMENT

The original contributions presented in the study are included in the article/supplementary material, further inquiries can be directed to the corresponding author.

AUTHOR CONTRIBUTIONS

CW: Conceptualization, Methodology, Writing–original draft. SW: Methodology, Writing–review and editing. WY: Methodology, Software, Data curation. HB: Conceptualization, Writing–review and editing. JZ: Investigation, Data curation. XW: Writing–review and editing.

FUNDING

This work was supported by the Soft Science Program of Zhejiang Province (2022C35073), A Project supported by Scientific Research Fund of Zhejiang Provincial Education Department (Y202148202), Fundamental Research Funds for the Central Universities (2020CDJSK03XK06), and Natural science foundation of Zhejiang Province (LY20D010007).

REFERENCES

Bajgier-Kowalska, M., Tracz, M., and Uliszak, R. (2017). Modeling the State of Agritourism in the Malopolska Region of Poland. *Tour. Geogr.* 19 (3), 502–524. doi:10.1080/14616688.2017.1300935

Baležentis, T., Kriščiukaitienė, I., Baležentis, A., and Garland, R. (2012). Rural Tourism Development in Lithuania (2003-2010) - a Quantitative Analysis. *Tour. Manag. Perspect.* 2-3, 1–6. doi:10.1016/j.tmp.2012.01.001

Barbieri, C. (2020). Agritourism Research: A Perspective Article. *Tour. Rev.* 75 (1), 149–152. doi:10.1108/Tr-05-2019-0152

Benur, A. M., and Bramwell, B. (2015). Tourism Product Development and Product Diversification in Destinations. *Tour. Manag.* 50, 213–224. doi:10.1016/j.tourman.2015.02.005

Busby, G., and Rendle, S. (2000). The Transition from Tourism on Farms to Farm Tourism. *Tour. Manag.* 21 (6), 635–642. doi:10.1016/s0261-5177(00)00011-x

Chang, J., He, P., Gao, W. B., Guo, Y. H., Li, X., and Xi, X. D. (2018). Study on Spatial Distribution Characteristics of Leisure Agriculture in Chengdu. *Chin. J. Agric. Resour. Regional Plan.* 39, 206–214. (in Chinese). doi:10.7621/cjarrp.1005-9121.20180429

Chase, L. C., Stewart, M., Schilling, B., Smith, B., and Walk, M. (2018). Agritourism: Toward a Conceptual Framework for Industry Analysis. *J. Agric. Food Syst. Community Dev.* 8 (1), 13–19. doi:10.5304/jafscd.2018.081.016

Chen, Q. Y., Guan, X. H., and Huan, T.-C. (2021). The Spatial Agglomeration Productivity Premium of Hotel and Catering Enterprises. *Cities* 112. doi:10.1016/j.cities.2021.103113

Chhetri, A., Chhetri, P., Arrowsmith, C., and Corcoran, J. (2017). Modelling Tourism and Hospitality Employment Clusters: A Spatial Econometric Approach. *Tour. Geogr.* 19 (3), 398–424. doi:10.1080/14616688.2016.1253765

Choo, H., and Petrick, J. F. (2014). Social Interactions and Intentions to Revisit for Agritourism Service Encounters. *Tour. Manag.* 40, 372–381. doi:10.1016/j.tourman.2013.07.011

Cui, J. X., Li, R. H., Zhang, L. Y., and Jing, Y. (2021). Spatially Illustrating Leisure Agriculture: Empirical Evidence from Picking Orchards in China. *Land* 10 (6). doi:10.3390/land10060631

Da Liang, A. R., Nie, Y. Y., Chen, D. J., and Chen, P.-J. (2020). Case Studies on Co-branding and Farm Tourism: Best Match between Farm Image and Experience Activities. *J. Hosp. Tour. Manag.* 42, 107–118. doi:10.1016/j.jhtm.2019.11.009

Dubois, C., Cawley, M., and Schmitz, S. (2017). The Tourist on the Farm: A 'muddled' Image. *Tour. Manag.* 59, 298–311. doi:10.1016/j.tourman.2016.08.016

Estevão, C., and Ferreira, J. J. (2012). Tourism Cluster Positioning and Performance Evaluation: The Case of Portugal. *Tour. Econ.* 18 (4), 711–730. doi:10.5367/te.2012.0137

Fanelli, R. M., and Romagnoli, L. (2021). The Spatial Agglomeration of Italian Agritourism Farms. *Reg. Stud.* doi:10.1080/00343404.2021.1980523

Gao, C. L., and Cheng, L. (2020). Tourism-Driven Rural Spatial Restructuring in the Metropolitan Fringe: An Empirical Observation. *Land Use Policy* 95. doi:10.1016/j.landusepol.2020.104609

Giaccio, V., Giannelli, A., and Mastronardi, L. (2018). Explaining Determinants of Agri-Tourism Income: Evidence from Italy. *Tour. Rev.* 73 (2), 216–229. doi:10.1108/Tr-05-2017-0089

Goossen, M., and Langers, F. (2000). Assessing Quality of Rural Areas in the Netherlands: Finding the Most Important Indicators for Recreation. *Landsc. Urban Plan.* 46 (4), 241–251. doi:10.1016/S0169-2046(99)00058-4

Guo, H. C., and Lv, M. W. (2008). The Status Quo and Counter Measures of the Leisure Agriculture in China. *Econ. Geogr.* 28 (4). (in Chinese). doi:10.15957/j.cnki.jjdl.2008.04.032

Hawkins, D. E. (2004). A Protected Areas Ecotourism Competitive Cluster Approach to Catalyse Biodiversity Conservation and Economic Growth in Bulgaria. *J. Sustain. Tour.* 12 (3), 219–244. doi:10.1080/09669580408667235

Jacobsen, J. K. S., and Tømmervik, H. (2016). Leisure Traveller Perceptions of Iconic Coastal and Fjord Countryside Areas: Lush Naturalness or Remembrance of Agricultural Times Past? *Land Use Policy* 54, 38–46. doi:10.1016/j.landusepol.2016.01.013

Jing, Y., Liu, Y. L., Cai, E. X., Liu, Y., and Zhang, Y. (2018). Quantifying the Spatiality of Urban Leisure Venues in Wuhan, Central China - GIS-Based Spatial Pattern Metrics. *Sustain. Cities Soc.* 40, 638–647. doi:10.1016/j.scs.2018.05.015

Kastenholz, E., Carneiro, M. J., Marques, C. P., and Loureiro, S. M. C. (2018). The Dimensions of Rural Tourism Experience: Impacts on Arousal, Memory, and Satisfaction. *J. Travel & Tour. Mark.* 35 (2), 189–201. doi:10.1080/10548408.2017.1350617

Kim, Y. R., Williams, A. M., Park, S., and Chen, J. L. (2021). Spatial Spillovers of Agglomeration Economies and Productivity in the Tourism Industry: The Case of the Uk. *Tour. Manag.* 82. doi:10.1016/j.tourman.2020.104201

Lee, M.-S. (2012). An Analysis of the Critical Factors that Affect the Competitive Advantages and Developmental Strategies of Leisure Farms in Taiwan. *Agric. Econ. - Czech* 58 (10), 467–481. doi:10.17221/128/2011-AGRICECON

Lee, Y.-J. A., Jang, S., and Kim, J. (2020). Tourism Clusters and Peer-To-Peer Accommodation. *Ann. Tour. Res.* 83. doi:10.1016/j.annals.2020.102960

Li, J. J., Xu, L. Z., Tang, L., Wang, S. Y., and Li, L. (2018). Big Data in Tourism Research: A Literature Review. *Tour. Manag.* 68, 301–323. doi:10.1016/j.tourman.2018.03.009

Liu, C.-H., and Yen, L.-C. (2010). The Effects of Service Quality, Tourism Impact, and Tourist Satisfaction on Tourist Choice of Leisure Farming Types. *Afr. J. Bus. Manag.* 4 (8), 1529–1545. doi:10.5897/AJBM.9000578

Liu, C. Y., Dou, X. T., Li, J. F., and Cai, L. A. (2020). Analyzing Government Role in Rural Tourism Development: An Empirical Investigation from China. *J. Rural Stud.* 79, 177–188. doi:10.1016/j.jrurstud.2020.08.046

Liu, Y., Liu, X., Gao, S., Gong, L., Kang, C. G, Zhi, Y., et al. (2015). Social Sensing: A New Approach to Understanding Our Socioeconomic Environments. *Ann. Assoc. Am. Geogr.* 105 (3), 512–530. doi:10.1080/00045608.2015.1018773

Liu, Y. L., Jing, Y., Cai, E. X., Cui, J. X., Zhang, Y., and Chen, Y. Y. (2017). How Leisure Venues Are and Why? A Geospatial Perspective in Wuhan, Central China. *Sustainability* 9 (10), 1865. doi:10.3390/su9101865

Nazariadli, S., Morais, D. B., Barbieri, C., and Smith, J. W. (2018). Does Perception of Authenticity Attract Visitors to Agricultural Settings? *Tour. Recreat. Res.* 43 (1), 91–104. doi:10.1080/02508281.2017.1380144

Novelli, M., Schmitz, B., and Spencer, T. (2006). Networks, Clusters and Innovation in Tourism: A Uk Experience. *Tour. Manag.* 27 (6), 1141–1152. doi:10.1016/j.tourman.2005.11.011

Ohe, Y., and Kurihara, S. (2013). Evaluating the Complementary Relationship between Local Brand Farm Products and Rural Tourism: Evidence from Japan. *Tour. Manag.* 35, 278–283. doi:10.1016/j.tourman.2012.07.003

Pejanović, R., Demirović, D., Glavaš-Trbić, D., Maksimović, G., and Tomaš-Simin, M. (2017). Clusters as a Factor of Competitiveness of Rural Tourism Destinations in the Danube Region of the Republic of Serbia. *Tour. Econ.* 23 (2), 475–482. doi:10.5367/te.2015.0509

Qiu, S. C., Cai, L. P., Lehto, X. R., Huang, Z. J., Gordon, S., and Gartner, W. (2019). Reliving Self-Presentational Concerns in Rural Tourism. *Ann. Tour. Res.* 74, 56–67. doi:10.1016/j.annals.2018.10.005

Reichel, A., Lowengart, O., and Milman, A. (2000). Rural Tourism in Israel: Service Quality and Orientation. *Tour. Manag.* 21 (5), 451–459. doi:10.1016/s0261-5177(99)00099-0

Ren, K. R., and Dong, J. G. (2016). A Review of Leisure Agriculture. *Chin. J. Agric. Resour. Regional Plan.* 37 (3), 195–203. (in Chinese). doi:10.7621/cjarrp.1005-9121.20160334

Rozman, Č., Potočnik, M., Pažek, K., Borec, A., Majkovič, D., and Bohanec, M. (2009). A Multi-Criteria Assessment of Tourist Farm Service Quality. *Tour. Manag.* 30 (5), 629–637. doi:10.1016/j.tourman.2008.11.008

Sgroi, F., Donia, E., and Mineo, A. M. (2018). Agritourism and Local Development: A Methodology for Assessing the Role of Public Contributions in the Creation of Competitive Advantage. *Land Use Policy* 77, 676–682. doi:10.1016/j.landusepol.2018.06.021

Shen, S. Y., Wang, H., Quan, Q. H., and Xu, J. (2019). Rurality and Rural Tourism Development in China. *Tour. Manag. Perspect.* 30, 98–106. doi:10.1016/j.tmp.2019.02.006

Su, M. M., Wall, G., Wang, Y. A., and Jin, M. (2019). Livelihood Sustainability in a Rural Tourism Destination - Hetu Town, Anhui Province, China. *Tour. Manag.* 71, 272–281. doi:10.1016/j.tourman.2018.10.019

Tao, C. J. (2019). Development Efficiency of Leisure Agriculture Based on Dea Model in the Background of Rural Revitalization. *Rev. Cercet. Interv. Soc.* 67, 169–187. doi:10.33788/rcis.67.11

Tew, C., and Barbieri, C. (2012). The Perceived Benefits of Agritourism: The Provider's Perspective. *Tour. Manag.* 33 (1), 215–224. doi:10.1016/j.tourman.2011.02.005

Tsaur, S.-H., Yen, C.-H., and Ku, P.-S. (2016). An Evaluation Framework for the Sustainable Operation of Leisure Farms. *Leis. Stud.* 36 (6), 739–751. doi:10.1080/02614367.2016.1246589

Van Sandt, A., Low, S. A., and Thilmany, D. (2018). Exploring Regional Patterns of Agritourism in the U.S.: What's Driving Clusters of Enterprises? *Agric. Resour. Econom. Rev.* 47 (3), 592–609. doi:10.1017/age.2017.36

Volo, S. (2021). The Experience of Emotion: Directions for Tourism Design. *Ann. Tour. Res.* 86. doi:10.1016/j.annals.2020.103097

Walford, N. (2001). Patterns of Development in Tourist Accommodation Enterprises on Farms in England and Wales. *Appl. Geogr.* 21 (4), 331–345. doi:10.1016/S0143-6228(01)00010-8

Weidenfeld, A., Butler, R., and Williams, A. W. (2011). The Role of Clustering, Cooperation and Complementarities in the Visitor Attraction Sector. *Curr. Issues Tour.* 14 (7), 595–629. doi:10.1080/13683500.2010.517312

Wu, B. H., and Cai, L. P. A. (2006). Spatial Modeling Suburban Leisure in Shanghai. *Ann. Tour. Res.* 33 (1), 179–198. doi:10.1016/j.annals.2005.10.013

Wu, B. W. (2019). *A Study of Leisure Agricultural Districts and Development Strategy in Zhejiang Province Based on Big Data*. Hangzhou: Zhejiang University. (in Chinese).

Wu, C. H., Che, H., Chan, T. Y., and Lu, X. H. (2015). The Economic Value of Online Reviews. *Mark. Sci.* 34 (5), 739–754. doi:10.1287/mksc.2015.0926

Wu, H.-C., and Cheng, C.-C. (2017). What Drives Green Advocacy? A Case Study of Leisure Farms in Taiwan. *J. Hosp. Tour. Manag.* 33, 103–112. doi:10.1016/j.jhtm.2017.10.008

Wu, T.-c. (2018). Agriculture Tourism and the Transformation of Rural Countryside. *Tour. Geogr.* 20 (2), 354–357. doi:10.1080/14616688.2018.1434819

Xiang, Y., Chen, Y. J., Hou, Y. L., and Qu, B. X. (2019). Spatial Distribution and Influencing Factors of Leisure Agriculture: A Case from Hebei Province. *Sci. Geogr. Sin.* 39, 1806–1813. (in Chinese). doi:10.13249/j.cnki.sgs.2019.11.015

Xu, J., Yang, M. S., Hou, C. P., Lu, Z. L., and Liu, D. (2021). Distribution of Rural Tourism Development in Geographical Space: A Case Study of 323 Traditional Villages in Shaanxi, China. *Eur. J. Remote Sens.* 54, 318–333. doi:10.1080/22797254.2020.1788993

Xue, L., and Kerstetter, D. (2019). Rural Tourism and Livelihood Change: An Emic Perspective. *J. Hosp. Tour. Res.* 43 (3), 416–437. doi:10.1177/1096348018807289

Yan, Q., Zhou, S. M., and Wu, S. P. (2018). The Influences of Tourists' Emotions on the Selection of Electronic Word of Mouth Platforms. *Tour. Manag.* 66, 348–363. doi:10.1016/j.tourman.2017.12.015

Yang, W., and Ai, T. H. (2018). Poi Information Enhancement Using Crowdsourcing Vehicle Trace Data and Social Media Data: A Case Study of Gas Station. *ISPRS Int. J. Geo-Information* 7 (5), 178. doi:10.3390/ijgi7050178

Yang, Z. S., Hao, P., Liu, W. D., and Cai, J. M. (2016). Peri-Urban Agricultural Development in Beijing: Varied Forms, Innovative Practices and Policy Implications. *Habitat Int.* 56, 222–234. doi:10.1016/j.habitatint.2016.06.004

Zasada, I. (2011). Multifunctional Peri-Urban Agriculture-A Review of Societal Demands and the Provision of Goods and Services by Farming. *Land Use Policy* 28 (4), 639–648. doi:10.1016/j.landusepol.2011.01.008

Zhang, K., Chen, Y., and Li, C. L. (2019). Discovering the Tourists' Behaviors and Perceptions in a Tourism Destination by Analyzing Photos' Visual Content with a Computer Deep Learning Model: The Case of Beijing. *Tour. Manag.* 75, 595–608. doi:10.1016/j.tourman.2019.07.002

Zhao, S. H., and Chang, X. Y. (2014). Empirical Analysis on Tourist Satisfaction of Leisure Agriculture - Based on the Survey Data of Nanjing, Jiangsu Province. *Agric. Technol. Econ.*, 110–119. (in Chinese). doi:10.13246/j.cnki.jae.2014.04.013

Conflict of Interest: The authors declare that the research was conducted in the absence of any commercial or financial relationships that could be construed as a potential conflict of interest.

Publisher's Note: All claims expressed in this article are solely those of the authors and do not necessarily represent those of their affiliated organizations, or those of the publisher, the editors and the reviewers. Any product that may be evaluated in this article, or claim that may be made by its manufacturer, is not guaranteed or endorsed by the publisher.

Copyright © 2022 Wang, Wu, Yang, Bao, Zhu and Wang. This is an open-access article distributed under the terms of the Creative Commons Attribution License (CC BY). The use, distribution or reproduction in other forums is permitted, provided the original author(s) and the copyright owner(s) are credited and that the original publication in this journal is cited, in accordance with accepted academic practice. No use, distribution or reproduction is permitted which does not comply with these terms.

frontiers | Frontiers in Environmental Science

ORIGINAL RESEARCH
published: 24 June 2022
doi: 10.3389/fenvs.2022.909554

What Is the Impact of the Establishment of Natural Reserves on Rural Residential Land? An Empirical Study From Hunan Province, China

Yuanlai Wu[1], *Houtian Tang*[1], *Ping Jiang*[2]* *and Jinxiu Chen*[3]

[1]School of Public Administration, Central South University, Changsha, China, [2]School of Resource and Environmental Sciences, Wuhan University, Wuhan, China, [3]School of Public Administration, Guangxi University, Nanning, China

OPEN ACCESS

Edited by:
Jiaxing Cui,
Central China Normal University, China

Reviewed by:
Shuyao Wu,
Shandong University, China
Zhifang Wang,
Peking University, China
Yasi Tian,
Soochow University, China

***Correspondence:**
Ping Jiang
longkangkang@whu.edu.cn

Specialty section:
This article was submitted to Land Use Dynamics, a section of the journal Frontiers in Environmental Science

Received: 31 March 2022
Accepted: 06 May 2022
Published: 24 June 2022

Citation:
Wu Y, Tang H, Jiang P and Chen J (2022) What Is the Impact of the Establishment of Natural Reserves on Rural Residential Land? An Empirical Study From Hunan Province, China. Front. Environ. Sci. 10:909554. doi: 10.3389/fenvs.2022.909554

The rural residential land (RRL) in natural reserves has been deeply transformed due to the disturbance constrained by ecological protection policies. Exploring the distribution characteristics and driving factors of RRL in natural reserves and non-natural reserves will help to promote the governance of land space and alleviate the contradiction of land use. Therefore, taking 122 county-level administrative regions in Hunan Province as an example, this article analyzes and compares the spatiotemporal distribution characteristics of RRL in natural reserves and non-natural reserves by using land use change dynamics, nuclear density analysis, the transfer matrix model, and the ordinary least-squares model and explores how the establishment of natural reserves affects the RRL area change. The results show that (1) the overall RRL area in Hunan changed from 171,162.27 hm^2 in 2000 to 169,914.6 hm^2 in 2020, with a total reduction of 1,247.67 hm^2 and a decrease of 0.73%, and the distribution of the RRL area change presented a hot trend in the northeast and a cold trend in the southwest. (2) The occupation of urban construction land is the main reason for the reduction in RRL area, and the transformation of cultivated land and forestland into RRL is the main source of the increase in RRL area. (3) During 2000–2020, the overall RRL in natural reserves increased by 1,538.37 hm^2, with an increase of 0.11%, while the overall RRL in non-natural reserves decreased by 2,786.04 hm^2, with a decrease of 0.14%. (4) The establishment of natural reserves has a significant negative correlation with the area of RRL in 2000, 2010, and 2020, indicating that the establishment of natural reserves can limit the growth speed of the RRL area to a certain extent, but is affected by factors such as economic development and rural population growth; it cannot directly promote the overall reduction of RRL area. The results of this study can provide a reference for decision-making related to the spatial structure optimization of natural reserves and non-natural protected RRL and the coordinated development of urban and rural areas.

Keywords: rural residential land, natural reserves, driving factors, China, spatiotemporal variation characteristics

1 INTRODUCTION

The contrast between urban expansion and rural recession is becoming increasingly serious (Long et al., 2012; Bai et al., 2014; Liu and Li, 2017; Li K. et al., 2021). As a very important land use type in rural areas, rural residential land (RRL) is an important carrier of farmers' production and life (Chen et al., 2019; Yang R. et al., 2019). Since its emergence in the specific natural and cultural environment, it has been affected by the natural increase and decrease in the rural population and the slow growth of the rural economy (Qu et al., 2017). However, with the rapid development of rural economies around the world, the functions and layout of rural settlements have changed significantly and are evolving toward heterogeneity and non-simplification (Zhu et al., 2014; Li G. et al., 2020; Rosner and Wesołowska, 2020). Meanwhile, due to the interaction of historical origin, customs, resource endowment, transportation convenience, and other factors, the spatial layout of RRL is mostly formed by the independent selection and lack of unified planning (Shcherbina and Gorbenkova, 2019; Wang and Zhang, 2021). This continuous disorderly expansion also exacerbates the fragmentation of RRL (Li G. et al., 2020). During the early stages, developed countries such as South Korea and Germany were the first to realize the importance of spatial planning of rural settlements and conducted the consolidation movement of RRL, including the "New Village Movement" in South Korea (Suh, 2015) and the "Village Renewal" in Germany (Zasada and Piorr, 2015). Moreover, with the gradual prominence of the contradiction between man and land, developing countries such as China, Uzbekistan, and Myanmar have paid more attention to the spatial planning of RRL and have issued corresponding policies (Conrad et al., 2015; Hoffman-Hall et al., 2019; Zhou et al., 2021). However, unlike developed countries, developing countries have some disadvantages in experience, technology, and capital, which makes it difficult to realize the consolidation of RRL (Njoh, 2011; Trukhachev, 2015; Rosner and Wesołowska, 2020). Therefore, promoting RRL consolidation has always been a thorny problem faced by China and other countries lacking land resources, and it is of great significance to make the rational use of RRL and alleviate the contradiction between land supply and demand (Li et al., 2014; Kong et al., 2021).

In consideration of social and economic development, China's urban construction and development are relatively rapid, and relevant guidance planning and supporting infrastructure construction are also relatively abundant (Fernández, 2007; Guan et al., 2018; Li Y. et al., 2020). However, the construction and development of RRL lack planning guidance, which leads to the increasingly prominent phenomena of scattered layout, high degree of fragmentation, low utilization efficiency and serious illegal land occupation of RRL (You and Chen, 2019; Wen et al., 2020; Li J. et al., 2021). Moreover, it has further derived problems such as the extensive use of RRL, the lack of living infrastructure, and the fragile ecological environment, which have led to the continuous decline of rural development potential (Wu et al., 2017; Li Y. et al., 2018; Ristić et al., 2019). Nevertheless, with the improvement of rural residents' income level, lifestyle transformation, and rural cultural progress, rural residents have also put forward new requirements for production, living conditions, and environment quality (Zhou et al., 2020; Deng et al., 2021). Using the Hunan Province of China as an example, statistical yearbooks of the Hunan Provincial Bureau of Statistics, the urbanization rate increased from 29.75% in 2000 to 58.76% in 2020, with extremely rapid growth. In the context of rapid urbanization, the nonagricultural rural population has led to a significant reduction in the rural resident population; a large amount of rural construction land has been gradually abandoned and left idle, and the abandonment of houses in villages has become very serious, which further intensifies the sharp contradiction between the current tight supply of urban construction land and the idle waste of land resources in rural settlements (Li L. et al., 2020; Huang et al., 2020; Zhu et al., 2020).

Previous studies have conducted rich theoretical research and practical explorations of RRL (Linard et al., 2012; Phokaides, 2018; Li S. et al., 2021; Nandi and Mistri, 2022). Scholars generally believe that the spatial distribution and evolution of rural settlements are the result of the comprehensive action of physical and geographical conditions and socioeconomic development (Yu et al., 2018; Li G. et al., 2020). The scale, shape, distribution, and other characteristics of rural settlements are closely related to natural conditions such as landform, soil, hydrology, climate, and vegetation and are affected by factors such as government regulation, economic development, urbanization level, traffic conditions, and scientific and technological strength (Linard et al., 2012; Liu et al., 2016; Tu et al., 2018; Cyriac and Firoz, 2022). Meanwhile, in a short period of time, RRL changes are more affected by human factors (Wang and Zhang, 2021). Specifically, in the existing studies, the research contents of rural settlements are relatively diversified, mainly focusing on the characteristics of spatiotemporal evolution and its driving factors, spatial layout optimization, functions, etc., gradually enriching the content system of rural settlement research (Heng et al., 2021; Tan et al., 2021). Moreover, the research on RRL also presents different research scales, including mainly analyses of the overall evolution and driving mechanism of RRL at the macroscale, explorations of the structure, function, and spatial layout optimization of RRL, and the gradual transformation from the national and provincial macroscale to the shrinking of the county, town, and even village at the microscale (Li G. et al., 2018; Chirisa, 2021). In addition, the research methods on rural settlements are diverse, mainly involving multifactor comprehensive evaluation methods, spatial econometric analysis, spatial autocorrelation, geographic information systems, geographic detectors, and other methods and models, revealing the general or local characteristics of the research content of rural settlements (Yang et al., 2019a; Gosch et al., 2021; Kong et al., 2021).

However, only a few scholars have conducted research on RRL in the natural reserve. Among them, Yao and Xie (2016) believed that the scale of RRL in the natural reserve should be the smallest, while the scale of ecological land should be the largest. Abelairas-Etxebarria and Astorkiza (2012) compared the difference in land

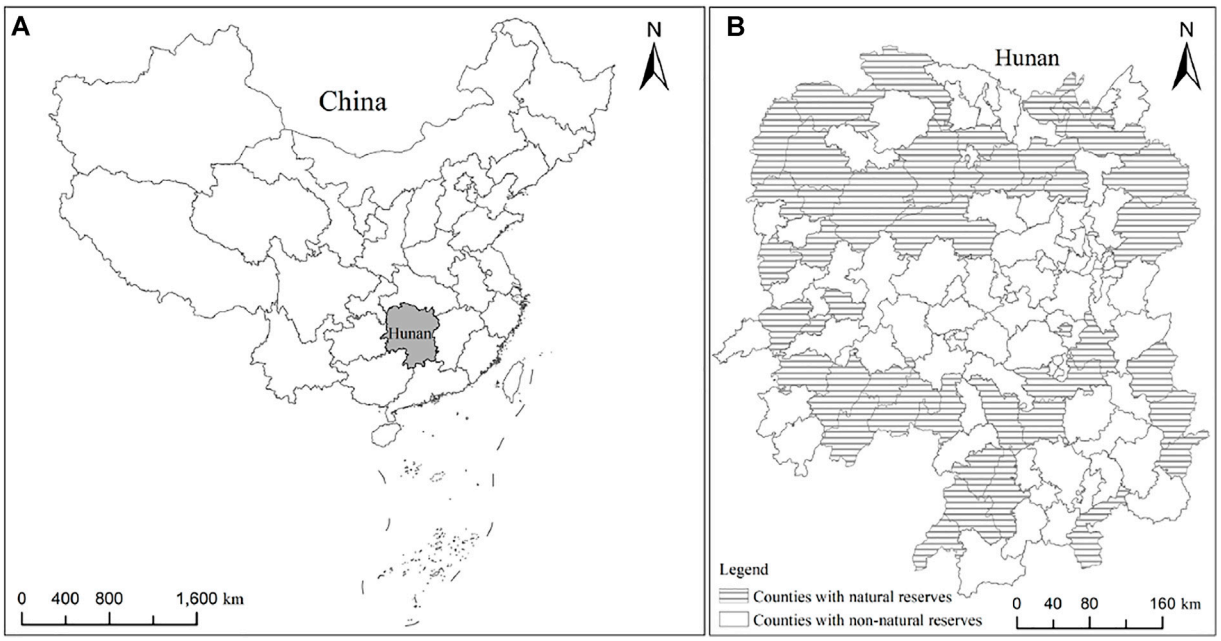

FIGURE 1 | Study area. [Panel **(A)**: geographical location of the Hunan Province in China. Panel **(B)**: geographical location of counties with natural reserves and non-natural reserves in Hunan Province in 2020].

prices within and outside the natural reserve and found that the policy of establishing a natural reserve has a highly restrictive effect on land transaction volume and land use change. Martín and Chehébar (2001) researched indigenous communities and RRL inhabited by migrant populations in the federal protected area system of Argentinian Patagonia and found that the growth of RRL directly threatened the ecological environment. Previous studies have neglected to explore and compare the spatiotemporal variation characteristics of RRL in natural reserves and non-natural reserves. As an area designated by relevant government departments to protect special ecosystems for scientific research, natural reserves have played an important role in soil and water conservation, environmental improvement, biodiversity protection, and ecological balance (Zhou and Chen, 2006; Yang et al., 2019b). In the natural reserve, to protect the ecological environment, the government has issued a variety of policies and measures to encourage the relocation of residents in the ecological reserve or limit the new expansion of existing rural settlements, which makes the rural settlements in the natural reserve form a completely different spatiotemporal evolution characteristic (Yu et al., 2018). Therefore, comparing the spatiotemporal evolution characteristics of RRL in the natural reserves and non-natural reserves can not only enrich the research topics related to RRL in the natural reserve but also provide policy suggestions for the management organization of the natural reserve to optimize and reduce the land use of RRL.

Therefore, we explore the differences in the spatiotemporal evolution characteristics, change intensity, and driving factors of RRL between natural reserves and non-natural reserves. Based on the relevant spatial and panel data of rural settlements in natural reserves and non-natural reserves of Hunan Province, China, and combined with the methods of land use dynamics, kernel density analysis, transfer matrix model, and ordinary least-squares model, this article intends to solve the following issues. (1) What are the overall spatiotemporal change characteristics of RRL in Hunan Province? (2) What are the spatiotemporal evolution characteristics of RRL in natural reserves and non-natural reserves? What is the difference? (3) What is the impact of the establishment of natural reserves on the spatiotemporal changes in RRL? Moreover, we believe that the results of this study can provide a decision-making reference for the spatial structure optimization of natural reserves and non-natural protected RRL and the coordinated development of urban and rural areas.

2 MATERIALS AND METHODS

2.1 Study Area

China's Hunan Province governs 14 prefecture-level cities (including autonomous prefectures), with a total of 122 county-level administrative regions (including county-level cities, districts, and autonomous counties, uniformly called counties), and is located in the middle reaches of the Yangtze River (**Figure 1**). Superior natural conditions have created the characteristics of rich animals and plant biodiversity and a beautiful natural landscape in Hunan Province (Ding et al., 2022; Fan et al., 2022). Provincial or national natural reserves in Hunan Province were distributed in 27, 42, and 44 counties in 2000, 2010, and 2020, respectively. By 2021, the permanent resident population of Hunan Province was 66.44 million, and the regional gross domestic product was 4,606.3 billion RMB. With the rapid development of the social economy, the disposable income of farmers has been significantly improved,

and its urbanization rate has increased from 29.75% in 2000 to 58.76% in 2020. However, due to the geographical conditions, the industrial structure and economic development of various regions in Hunan Province are quite different, resulting in the structure and functional space of RRL being significantly differentiated, which is mainly reflected in the scattered layout of RRL, a high degree of fragmentation, and obvious differences in hollowing (Tang et al., 2018; Han et al., 2021), especially in natural reserves and non-natural reserves. Therefore, this article selects Hunan Province with the characteristics of typical natural reserves and non-natural reserves as the research area, which has strong practical significance for the multifunctional promotion and coordinated optimization of RRL.

2.2 Data Sources

The land use data and the provincial, municipal, and county-level administrative division boundary data of Hunan in this article are from the Resource and Environmental Science and Data Center of the Institute of Geographical Sciences and Resources, Chinese Academy of Sciences (https://www.resdc.cn/). Among them, the land use data cover the three periods of 2000, 2010, and 2020, with a 30 m resolution. Using the reclassify function of ArcGIS10.5 software, the land types were reclassified into eight categories: cultivated land, forestland, grassland, water area, urban construction land, RRL, other construction land, and unused land; the area data of each land type were obtained. In addition, the rural population, economic, and social data involved in the study are mainly from the statistical yearbooks of the Hunan Provincial Bureau of Statistics (http://tjj.hunan.gov.cn/). On this basis, ArcGIS10.5 software is used to form the basic database for the study of RRL area change in Hunan Province through the spatial matching and link between attribute data and county-level administrative units, which lays the data foundation for this study.

2.3 Research Methods

2.3.1 Dynamic Degree of Land Use Change

The dynamic degree model of land use change is the quantitative change of a certain land use type in the study area during the study period (Stumpf et al., 2018). Through the dynamic degree of land use change, the area and change speed of various land types in the region at different time points can be obtained, the general change trend and structural evolution trend in different research periods can be grasped, and the core of the model is reflected by land use transfer flow (Gallant et al., 2004; Öztürk et al., 2013). This article uses this model to analyze the spatiotemporal changes in RRL in Hunan Province. The calculation formula is as follows:

$$K = \frac{U_b - U_a}{U_a} \times \frac{1}{T} \times 100\% \tag{1}$$

where K represents the dynamic degree of RRL change in the study period; U_a represents the initial value of the RRL area; U_b represents the final value of the RRL area; and T is the period time of the study.

2.3.2 Transfer Matrix Model

The transfer matrix model can effectively describe the structural characteristics and transformation direction of land use change in the study area and can also analyze the change characteristics of the spatial conflict level of various land types during different periods (Romero-Calcerrada and Perry, 2004; Xue et al., 2018). This article uses this model to analyze the direction and quantity of mutual transformation between RRL and other land use types in Hunan Province. The calculation formula is as follows:

$$T_{ij} = \begin{bmatrix} a_{11} & \cdots & a_{1n} \\ \vdots & \ddots & \vdots \\ a_{n1} & \cdots & a_{nn} \end{bmatrix} \tag{2}$$

where n represents the number of land use types; i and j represent the land use types at the beginning and end of the study periods, respectively; and T_{ij} represents the area converted from land use type i to land use type j during the study period.

2.3.3 Kernel Density Estimation Method

Kernel density estimation is a nonparametric calculation method that usually uses the built-in spatial analysis tool of ArcGIS10.5 software to define the nearest-neighbor object and realize the measurement of density distribution (Elgammal et al., 2002). At present, the kernel density estimation method has been applied to the study of spatial distribution patterns and change characteristics of various land use types (Gong et al., 2019). The higher the value of kernel density is, the greater the distribution density of RRL (Lin et al., 2022). This method mainly analyzes the spatiotemporal distribution pattern and change characteristics of RRL in natural reserves and non-natural reserves in Hunan Province. The calculation formula is as follows:

$$f_x = \frac{1}{nh} \sum_{i=1}^{n} k\left(\frac{x - x_i}{h}\right) \tag{3}$$

where f_x represents the estimated value of the kernel density of the RRL distribution; n represents the number of rural residential plots; h represents the bandwidth or smoothing parameter; k represents the kernel density function; and $x - x_i$ represents the distance between the measured x-th rural residential plot and the sample rural residential plot x_i.

2.3.4 Getis-Ord G_i^* Hot-Spot Analysis

Getis-Ord G_i^* hot-spot analysis is used to measure the spatial clustering intensity between each unit in the study area and its surrounding units. It mainly detects whether each geographical element belongs to a high-value or low-value aggregation mode in space by calculating the relationship between the geographical attributes of a location and the geographical attributes of its adjacent locations (Gao et al., 2019; Tan and Guan, 2021). This article uses this method to explore the degree of change and difference in RRL between natural reserves and non-natural reserves in Hunan Province. The calculation formula is as follows:

$$G_i^* = \frac{\sum_{j=1}^{n} w_{ij} X_j}{\sum_{j=1}^{n} X_j} \tag{4}$$

where G_i^* represents the statistical value of Getis-Ord; X_j represents the element attribute value of the j-th spatial unit; n represents the total number of rural settlements; and w_{ij} represents the spatial weight matrix. If the statistical value of G_i^* is positive and significant, it indicates that the value around the detected point is relatively high

TABLE 1 | Factors influencing RRL.

Target layer	Index layer	Calculation method (data source)	Variable type	Unit
Natural reserves	Whether there are natural reserves	List of natural reserves in Hunan Province (http://lyj.hunan.gov.cn/lyj/ztzl/gdzt/zrbhq/201512/t20151227_2587443.html)	D	—
Urban expansion	Per capita investment in fixed assets	Total investment in fixed assets/number of permanent residents	C	RMB
	Per capita investment in real estate development	Total investment in real estate development/number of permanent residents	C	RMB
	Urban construction land area	https://www.resdc.cn/	C	m^2
Economic growth	Per capita gross domestic product	Total regional gross domestic product/number of permanent residents	C	RMB
	The proportion of primary industry	Primary industry value/total regional gross domestic product	C	%
	Per capita fiscal expenditure	Total regional financial expenditure/number of permanent residents	C	RMB
Rural development	Per capita crop sowing area	The total sown area of crops/number of permanent residents	C	m^2
	Per capita cultivated land area	Total cultivated land area/number of permanent residents	C	m^2
	Per capita disposable income of farmers	Hunan statistical yearbook (http://tjj.hunan.gov.cn/)	C	RMB
	Rural resident population	Hunan statistical yearbook (http://tjj.hunan.gov.cn/)	C	People

Notes: D represents dichotomous, C represents continuous.

and belongs to a high-value spatial agglomeration (hot-spot area). If the statistical value of G_i^* is negative and significant, it indicates that the value around the detected point is relatively low and belongs to low-value spatial agglomeration (cold-spot area).

2.3.5 Ordinary Least-Squares Method

The ordinary least-squares method is used to evaluate the relationship between two or more element attributes. The principle of this method is to minimize the sum of squares of errors between the predicted value and the actual observed value of the regression empirical model (Sanchez, 2020; Liang and Qamruzzaman, 2022). This method is mainly used to explore the factors affecting the change in RRL. This article uses the change in the RRL area as the dependent variable and determines the model with better fitting through the forward stepwise regression method. The MNL-1 model only adds the influencing factors of the RRL area change, while the MNL-2 model adds the interactive term based on the MNL-1 model. The calculation formula is as follows:

$$Y_i = \beta_1 + \beta_2 X_{2i} + \beta_3 X_{3i} + \ldots + \beta_k X_{ki} + \varepsilon_i \quad (5)$$

The global parameter estimation vector can be obtained by using the ordinary least-squares model

$$\beta = \left(X^T X\right)^{-1} X^T Y \quad (6)$$

where β represents the parameter-estimated value vector influence coefficient; X represents the matrix composed of the observed values of the respective variables; Y represents the dependent variable; and ε_i is the random disturbance term.

2.4 Research Index System

The area change in RRL is closely related to natural, socioeconomic, land management, and other factors (Liu et al., 2013; Li G. et al., 2018, Li et al., 2020 G.). Based on the actual situation of Hunan Province and the availability of data, referring to previous research results (Zhou et al., 2013; Ristić et al., 2019; Wang and Zhang, 2021), and following the principles of scientificity and comprehensiveness, this article takes the area of RRL as a dependent variable. Meanwhile, four dimensions, including natural reserves, urban expansion, economic growth, and rural development situation, were selected, including 11 dependent variable indicators as the influencing factors of the change in the RRL area (**Table 1**).

First, due to the high intensity of environmental regulation policies within the scope of natural reserves (Zhou et al., 2014), the delimitation of natural reserves may have a significant impact on the change in RRL areas. The indicator of whether there are natural reserves set in this article only explores whether the county-level administrative units have provincial or national nature reserves.

Second, there is a certain contradiction between urban expansion and RRL because the rapid expansion of urban areas will accelerate the urbanization process of rural populations and may reduce the demand area of RRL (Liu et al., 2017; Yang et al., 2018). Therefore, the urban expansion dimension in this article includes three indicators: per capita investment in fixed assets, per capita investment in real estate development, and the urban construction land area. Among them, the per capita investment in fixed assets represents the local construction investment level, the per capita investment in real estate development represents the local investment level in urban housing construction, and the urban construction land area represents the actual situation of local urban expansion.

Third, rapid economic growth can increase the per capita gross domestic product, increase government fiscal expenditure, adjust the structure of local industries, promote the improvement of the speed of rural economic development, and affect the number of people engaged in agricultural production, resulting in affecting the change rate in the RRL area (Ma et al., 2018; Qu et al., 2021). Therefore, the economic growth dimension of this article also includes three indicators: per capita gross domestic product, the proportion of primary industry, and per capita fiscal expenditure. Among them, the per capita gross domestic product represents the economic development of the research county, the proportion of the primary industry represents the importance of the primary industry in the local industrial structure, and the per capita fiscal expenditure represents the fiscal expenditure capacity of the local government.

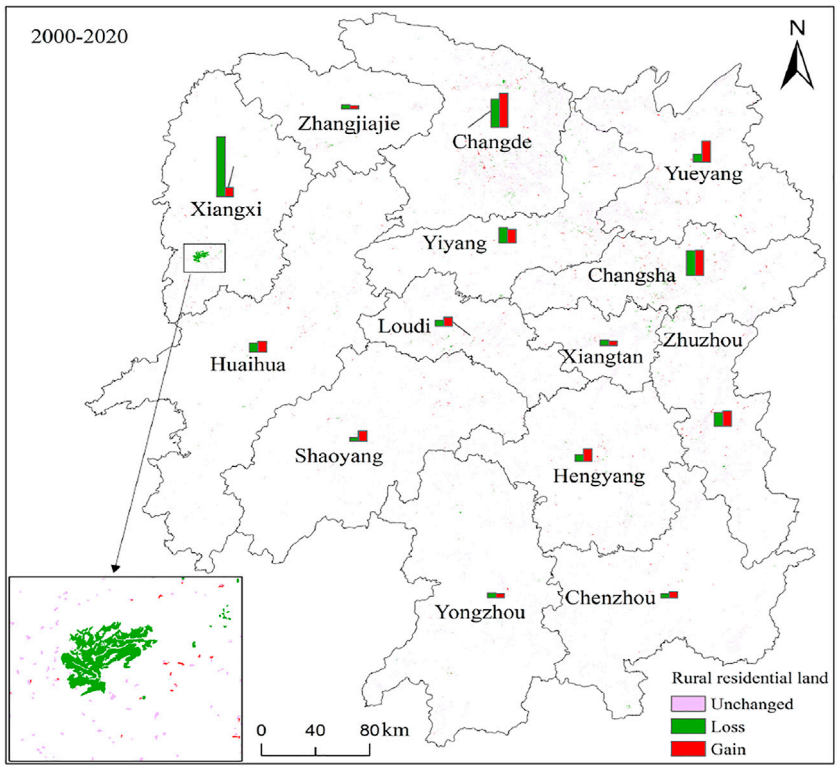

FIGURE 2 | Distribution of RRL change in 2000–2020.

Finally, there is a strong correlation between rural development and the change in the RRL area. Generally, areas with better rural development have greater population mobility, and farmers are more likely to change their place of residence due to work, transportation, and other factors (Sun et al., 2021). The dimensions of rural development in this article mainly include four indicators: per capita crop sowing area, per capita cultivated land area, per capita disposable income of farmers, and rural resident population. Among them, the per capita sown area of crops represents the agricultural planting status of the local rural surplus labor force, the per capita cultivated land area represents the cultivated land resources owned by local farmers to carry out basic agricultural production, the per capita disposable income of farmers represents the development degree of the local rural economy, and the rural resident population represents the number of people living in rural areas for a long time.

3 RESULTS

3.1 Change Characteristics of Rural Residential Land in Hunan Province

3.1.1 Spatiotemporal Characteristics of Rural Residential Land Change at the Macroscale

Based on the area change transfer matrix between RRL and other land types from 2000 to 2020 (**Supplementary Appendix**) and the spatiotemporal change distribution characteristic of RRL (**Figure 2**), the RRL area decreased from 171,162.27 hm^2 in 2000 to 169,914.60 hm^2 in 2020, with a total reduction of 1,247.67 hm^2 and a decrease of 0.73%. The reason can be found that in 2000–2020, although RRL occupied the largest area of cultivated land, the net occupied area of cultivated land was as high as 5,773.32 hm^2. However, due to a large number of RRLs occupied by urban and other construction lands, the RRL showed a downward trend from 2000 to 2020. This phenomenon can also be confirmed in **Figure 2**. The red spots (representing the gain of RRL) are significantly greater than the green spots (representing the loss of RRL). Specifically, the RRL area decreased by 5,165.10 hm^2 in 2000–2010; that is, the RRL area transferred out at this stage was greater than the area transferred in, while the RRL area increased by 3,917.43 hm^2 in 2010–2020. The main reason is that the urban expansion was relatively rapid, requiring higher amounts of urban construction land, resulting in a large amount of RRL occupied by urban construction land in 2000–2010. Moreover, due to the vigorous implementation of policies such as converting farmland to forestland during that time, some areas that reclaimed RRL were transferred to forestland. In 2010–2020, due to the stricter control over the expansion of urban construction land, the occupation of urban construction land to RRL was effectively alleviated. However, due to the reduction in the RRL area in 2000–2010 and the strong demand of farmers for RRL, a large amount of cultivated land and forestland around RRL was occupied. In addition, the distribution of RRL is too scattered, which is not obvious in **Figure 2**, but the

TABLE 2 | RRL change in prefecture-level cities from 2000 to 2020.

Cities	2000–2010		2010–2020		2000–2020	
	Area change (hm^2)	Change dynamics	Area change (hm^2)	Change dynamics	Area change (hm^2)	Change dynamics
Changsha	−28.62	−0.02%	87.39	0.07%	58.77	0.05%
Zhuzhou	−555.48	−0.45%	701.91	0.60%	146.43	0.12%
Xiangtan	−133.11	−0.24%	46.71	0.09%	−86.4	−0.16%
Hengyang	123.84	0.09%	381.51	0.29%	505.35	0.38%
Shaoyang	450.81	0.39%	137.97	0.12%	588.78	0.51%
Yueyang	552.51	0.34%	579.15	0.34%	1131.66	0.69%
Changde	−690.84	−0.26%	1186.92	0.46%	496.08	0.19%
Zhangjiajie	−115.29	−0.43%	37.26	0.15%	−78.03	−0.29%
Yiyang	−423.63	−0.35%	261	0.22%	−162.63	−0.13%
Chenzhou	−61.56	−0.04%	243.99	0.17%	182.43	0.13%
Yongzhou	−65.43	−0.04%	12.06	0.01%	−53.37	−0.03%
Huaihua	49.5	0.06%	110.61	0.12%	160.11	0.18%
Loudi	115.47	0.14%	165.33	0.20%	280.8	0.35%
Xiangxi	−4383.27	−4.12%	−34.38	−0.06%	−4417.65	−4.15%
Total	−5165.1	−0.30%	3917.43	0.24%	−1247.67	−0.07%

overall density is high in the northeast and low in the southwest. The reason for this scattered layout may be that northeastern Hunan is a traditional agricultural area with high residential density.

3.1.2 Spatiotemporal Characteristics of Rural Residential Land Change at the Microscale

By analyzing the changes in the RRL area in 14 prefecture-level cities in Hunan Province from 2000 to 2020 (**Table 2**), it can be found that the RRL area in different prefecture-level cities shows different changes, and the changes in RRL in the same prefecture-level city at different stages also show significant differences. It is worth noting that in 2000–2010 and 2010–2020, excluding the dynamic change degree of the RRL area in Xiangxi, which has been in a negative growth state, other prefecture-level cities showed an initial decreasing and then increasing or continuously increasing trend. Specifically, the reduction rate of the residential land area in Xiangxi in 2000–2020 is much higher than that in other prefecture-level cities, and the dynamic degree of the change of the RRL area in this prefecture in 2000–2010 indicates that the comprehensive improvement intensity of RRL in Xiangxi during 2000–2010 is high, which causes the area of RRL in this stage to show a significant trend of reduction. In addition, among the other 13 prefecture-level cities, the overall change dynamics of RRL in Xiangtan, Zhangjiajie, Yiyang, and Yongzhou showed negative growth in 2000–2020, indicating that the area of RRL in these cities decreased. In contrast, the dynamic change degree of the RRL area in Changsha, Zhuzhou, Hengyang, Shaoyang, Yueyang, Changde, Chenzhou, Huaihua, and Loudi positively increased and showed a small growth trend in 2000–2020.

The cold-spot and hot-spot analyses of RRL identify the spatial cluster distribution of high- and low-function values based on the spatial distribution of each function value domain. The hot-spot analysis tool in ArcGis10.5 software is used to identify the statistically significant distribution characteristics of cold and hot spots in the current situation and changes in the RRL area in 122 counties of Hunan Province. Among them, the value of G_i^* is divided into five categories using the natural break method in ArcGis10.5 software, which are named hot-spot, sub-hot-spot, insignificant, sub-cold-spot, and cold-spot from high to low (**Figure 3**). There was little difference in the distribution of cold and hot spots in the RRL area of 122 counties in Hunan Province in 2000, 2010, and 2020. The overall performance is that it is hot in the northeast and cold in the southwest. However, the three phases of data are mainly in areas with insignificant clustering characteristics. Specifically, the hot-spots are mainly distributed in the urban counties of Changsha, Changde, Yiyang, Yueyang, and Zhuzhou and the sub-hot-spots are mainly distributed in northern Changde, western Yueyang, and southern Zhuzhou, which shows that the RRL area in these areas increased faster and that farmers have a strong demand for RRL. The sub-cold-spot areas are mainly concentrated in eastern–western Hunan, eastern Huaihua, and northern Xiangtan. Cold-spot areas are mainly concentrated in western Huaihua and eastern Xiangtan, indicating that the RRL area in these areas decreased faster. In terms of the dynamic degree of change in the RRL area at each stage, the hot-spot and sub-hot-spot areas in 2000–2010 were mainly concentrated in the east of Shaoyang, the east and south of Hengyang, while they were mainly distributed in the middle of Changde, the southeast of Hengyang, and the middle of Zhuzhou in 2010–2020, indicating that the growth rate of the RRL area in Hunan Province showed significant differences in different periods. The cold-spot and sub-cold-spot areas were mainly concentrated in the east of Xiangtan, the middle of Changsha, the north of Zhuzhou, and the southwest of western Hunan in 2000–2010, while it was mainly concentrated in the southwest of western Hunan in 2010–2020, indicating that the decreasing trend of the RRL

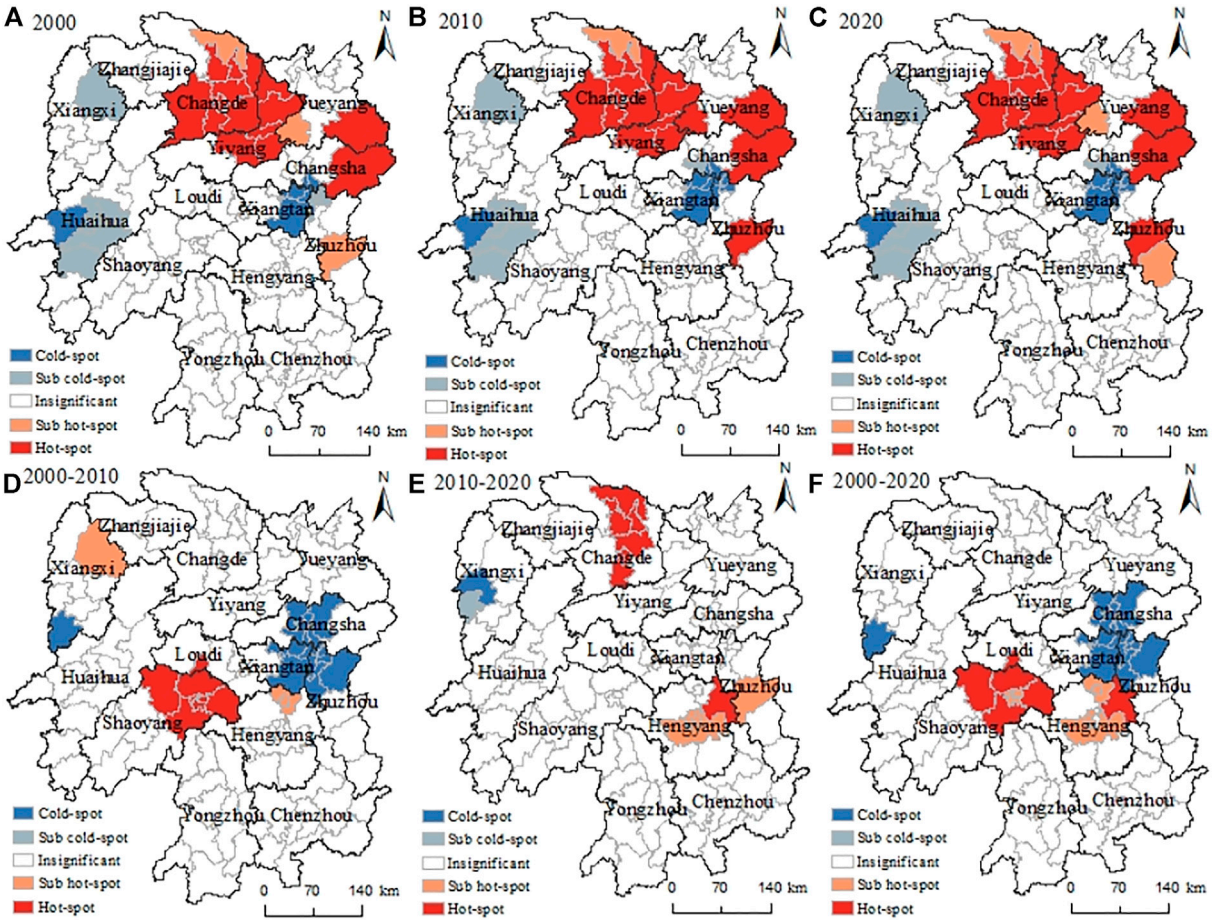

FIGURE 3 | Cold-spot and hot-spot distributions of the RRL area and change dynamics at the county level in Hunan Province from 2000 to 2020. [Panels **(A–C)** show the distribution of cold spots and hot spots in the current area of RRL in various counties of Hunan Province in 2000, 2010, and 2020, respectively. Panels **(D–F)** show the distribution of the change dynamics of RRL in various counties of Hunan Province in 2000–2010, 2010–2020, and 2000–2020, respectively.]

TABLE 3 | The overall change in the RRL area in natural reserves and non-natural reserves.

	2000–2010		2010–2020		2000–2020	
	Area change (hm^2)	Change dynamics	Area change (hm^2)	Change dynamics	Area change (hm^2)	Change dynamics
Natural reserves	−234.27	−0.03%	1709.46	0.25%	1538.37	0.11%
Non-natural reserves	−4930.83	−0.47%	2207.97	0.23%	−2786.04	−0.14%

area in Hunan Province gradually shifted from developed areas in the middle of the east to underdeveloped areas in the west.

3.2 Spatiotemporal Variation Characteristics of Rural Residential Land in Natural Reserves and Non-Natural Reserves

Table 3 shows that from 2000 to 2020, the RRL area in natural reserves and non-natural reserves decreased in 2000–2010 but increased in 2010–2020. It is worth noting that the overall area of RRL in natural reserves increased by 1,538.37 hm^2 in 2000–2020, with an increase of 0.11%, while the overall area of RRL in non-natural reserves decreased by 2,786.04 hm^2 in 2000–2020, with a decrease of 0.14%. According to the dynamic degree of change in the RRL area of counties in natural reserves and non-natural reserves in 2000–2010, 2010–2020, and 2000–2020, it was divided into five intervals by using the natural break method in ArcGIS 10.5 software (**Figures 4A–C**). Meanwhile, to intuitively express the change characteristics of the RRL area in counties of natural reserves and non-natural reserves, the kernel density of the RRL area change in counties of natural reserves and non-natural

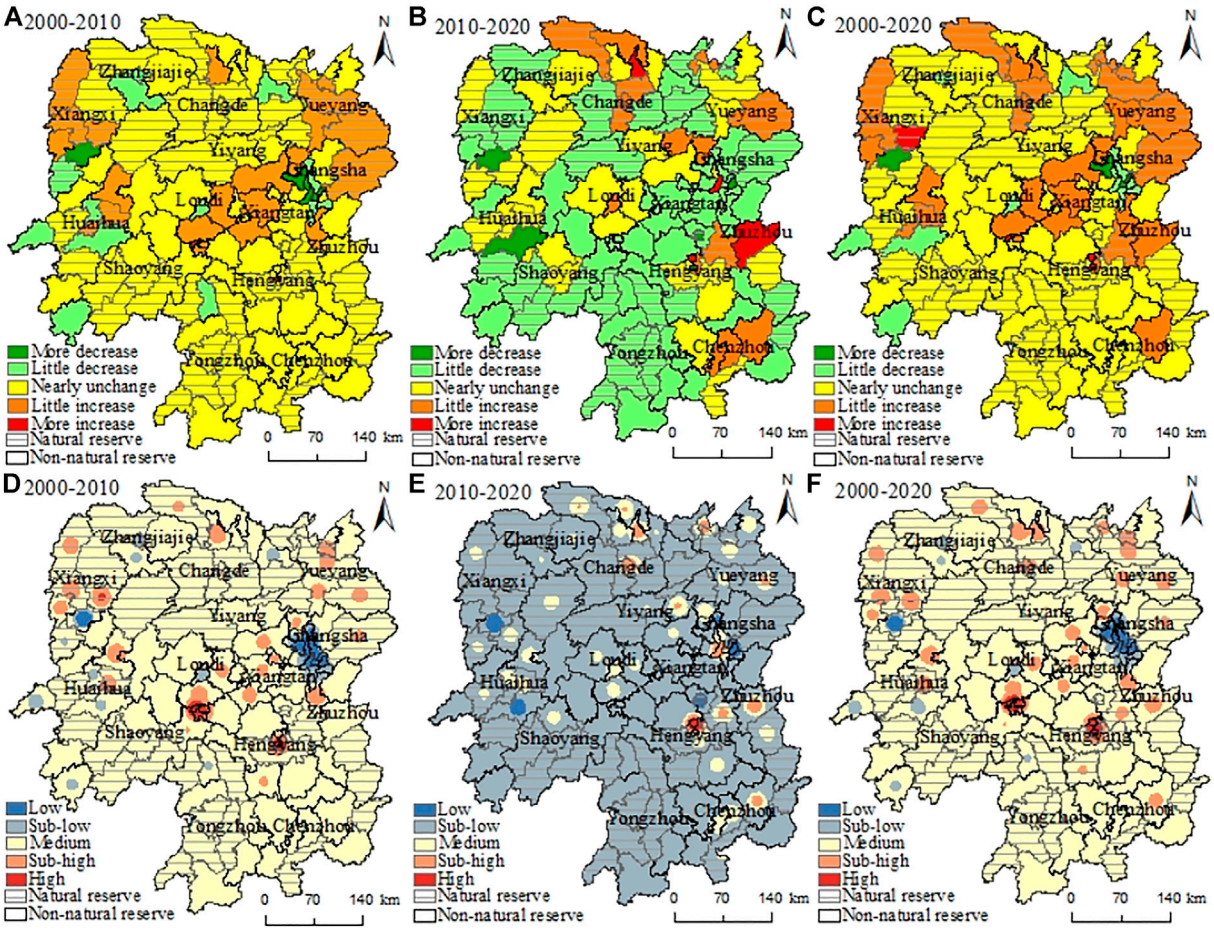

FIGURE 4 | The change dynamics and kernel density of the RRL area in natural reserves and non-natural reserves. [Panels **(A–C)** show the change dynamics of the RRL area in counties of natural reserves and non-natural reserves in 2000–2010, 2010–2020, and 2000–2020, respectively. Panels **(D–F)** show the kernel density of the RRL area change in counties of natural reserves and non-natural reserves in 2000–2010, 2010–2020, and 2000–2020, respectively.]

reserves in 2000–2010, 2010–2020, and 2000–2020 can be obtained by using the kernel density estimation method (**Figures 4D–F**). It can be found that the area and kernel density change of RRL in Hunan in 2000–2010 are very similar to that in 2000–2020, mainly concentrated in the non-natural reserves in the middle and the natural reserves in the northeast and northwest. We found that the growth of the RRL area in non-natural reserves is mainly affected by economic factors, while the growth of the RRL area in natural reserves is mainly affected by economic and policy factors. Furthermore, the area of RRL reduction is mainly concentrated in non-natural reserves, and the economic growth factor is the main factor of RRL change.

Moreover, it is also worth noting that from the change dynamics and kernel density of the RRL area in 2010–2020, the RRL area of non-natural reserves in Zhuzhou and Changde show a significant growth trend, while the counties with a small growth of the RRL area are mainly concentrated in the non-natural reserves in Chenzhou and Yiyang and the natural reserves in Changde and Yueyang. It can also be found that the counties with the increase in the RRL area in 2010–2020 are mainly concentrated in the plain areas with high economic development and dense populations in eastern and northern Hunan. In addition, the RRL area in most regions of Hunan has decreased slightly, while the RRL area in some non-natural reserves in Huaihua and Xiangxi has decreased significantly. Additionally, this study found that urbanization and the poverty alleviation and relocation policy are the main factors for the reduction of RRL in these regions.

3.3 Analysis of Driving Factors of Area Change in Rural Residential Land

Due to the different units and magnitudes of each index, the data are standardized to narrow the fluctuation range of the data to [0,1] to better show the changes to each index and the area of RRL in Hunan Province (Huyan and Li, 2021). Meanwhile, by analyzing the research data, we find that the dependent variable RRL in this article satisfies the normal distribution; the influencing factors are independent of each other as

TABLE 4 | Ordinary least-squares regression results of influencing factors of RRL.

Variable	2000		2010		2020	
	MNL-1	MNL-2	MNL-1	MNL-2	MNL-1	MNL-2
Constant	–0.188***	–0.161***	–0.142***	–0.122***	–0.107***	–0.131***
WNR	0.021	–0.348**	0.029**	–0.186***	0.021	–0.234***
PIFA	0.008	–0.008	0.081	0.091	0.081	0.104**
PIRED	–0.276***	0.136	–0.065	–0.024	–0.063	–0.074
UCLA	0.289***	0.172**	–0.086*	–0.063	–0.271***	–0.183**
PGDP	–0.104*	–0.066	0.011	0.034	–0.063	–0.031
PPI	0.057	0.022	–0.114***	–0.095*	–0.135**	–0.009
PFE	0.116	0.011	–0.005	–0.081	–0.011	–0.051
PCSA	0.045	0.165**	0.016	0.034	0.004	–0.091
PCLA	1.125***	1.026***	0.638***	0.641***	0.724***	0.791***
PDIF	0.081	0.084	0.009	–0.036	0.053*	0.071
RRP	0.404***	0.364***	0.552***	0.503***	0.661***	0.551***
PIFA * WNR		–0.484		0.254		0.202
PIRED * WNR		–0.159		–0.161		0.711***
UCLA * WNR		0.066		0.065		0.012
PGDP * WNR		0.568		–0.401		–0.713***
PPI * WNR		0.309*		–0.018		–0.167
PFE * WNR		1.218***		0.426***		1.219***
PCSA * WNR		–0.623***		0.007		0.271**
PCLA * WNR		0.917***		0.038		–0.071
PDIF * WNR		–0.396**		0.111		–0.128
RRP * WNR		0.551***		0.253***		0.493***
R-squared	0.861	0.914	0.917	0.933	0.891	0.926
Sig.	0.000	0.000	0.000	0.000	0.000	0.000
Number of samples	122	122	122	122	122	122

*Note: (1) ***, **, and * show statistical significance at the levels of 1%, 5%, and 10%, respectively. (2) WNR represents whether there are natural reserves, PIFA represents the per capita investment in fixed assets, PIRED represents the per capita investment in real estate development, UCLA represents the urban construction land area, PGDP represents the per capita gross domestic product, PPI represents the proportion of the primary industry, PFE represents the per capita fiscal expenditure, PCSA represents the per capita crop sowing area, PCLA represents the per capita cultivated land area, PDIF represents the per capita disposable income of farmers, and RRP represents the rural resident population.*

independent variables, and there is no multicollinearity problem, and there is a linear relationship between the dependent variable and the independent variable. Therefore, the research data in this article meet the requirements of using an ordinary least-squares model for analysis (Gómez et al., 2020).

The calculation results of the ordinary least-squares model (**Table 4**) show that the overall significance level of all models is within 1%. Compared with the R-squared values of various models in 2000, 2010, and 2020, it is found that the MNL-2 model has a better fitting and is more suitable for further research. Overall, the presence of natural reserves has a negative correlation with the area of RRL within the significance level of 5%, indicating that the delimitation of the natural reserve will limit the growth of the area of local RRL to a certain extent. The per capita cultivated land area and the rural resident population are significantly positive at the 1% level, indicating that with the growth of per capita cultivated land area and the rural resident population, the RRL area will also increase. It is worth noting that the urban construction land area did not show a significant correlation in 2010, while the proportion of the primary industry showed a significant negative correlation at the 10% level, indicating the growth of the urban construction land area after 2000. The area of RRL also showed a trend of initial growth and then decline. Meanwhile, the reduction of the proportion of the primary industry will promote the reduction of RRL areas. In addition, there is a significant positive correlation between the per capita crop sowing area in 2000 and the per capita investment in fixed assets in 2020 at the 5% level, indicating that the growth of the crop sowing area and fixed asset investment will also promote the growth of the RRL area.

From the overall results of the interaction analysis of influencing factors, the interaction items of whether there are natural reserves and per capita financial expenditure and whether there are natural reserves and rural resident population are significantly positive at the 5% level, indicating that with the government delimiting the natural reserve, the impact of financial expenditure and rural resident population on the change in the RRL area in the natural reserve will increase. In 2000, the interaction terms of whether there are natural reserves and the proportion of the primary industry and whether there are natural reserves and the per capita cultivated land area were significantly positive at the levels of 10% and 1%, respectively, indicating that the growth of the proportion of the primary industry and the per capita cultivated land area will lead to the growth of the RRL area of the natural reserve. This growth may be because the proportion of the primary industry and the growth of per capita cultivated land area will lead to an increase in rural population, while the growth of farmers' per capita disposable income will lead to the improvement of rural residents' consumption ability and accelerate the process of farmers' urbanization, which restricts the growth of the RRL area. Different from 2000 to 2020, the interaction between whether

there were natural reserves and the per capita crop sowing area in 2010 was not significant, while the per capita cultivated land area in 2010 greatly affected the change in the RRL area in the natural reserve. Moreover, it is worth noting that in 2020, the interaction term between whether there are natural reserves and per capita real estate development investment and whether there are natural reserves and per capita GDP is significant, indicating that the delimitation of natural reserves will enhance the impact of GDP on the growth of the RRL area and improve the impact of per capita real estate development investment.

4 DISCUSSION

4.1 The Distribution and Change in Rural Residential Land Show Differentiated Characteristics

The current RRL area showed a trend of hot in the northeast and cold in the southwest from 2000 to 2020. The hot spots were mainly concentrated in Changsha, Changde, Yueyang, and other cities, while the cold spots were concentrated in some counties of Xiangtan and Huaihua. Among them, economic development was the main factor affecting the increase in RRL (Fan et al., 2019). The difference is that the RRL area in Xiangxi decreased the most (4,417.65 hm^2). In addition to economic factors, the government's policy of poverty alleviation and relocation in other places also has an important impact. In addition, the change dynamics of RRL also show significant spatial differences. The RRL area is growing due to the constraints of economic development and the farmers' thought of "going home" in eastern Shaoyang and Hengyang. For the counties in the middle of Changsha, east of Xiangtan, and north of Zhuzhou, the demand for urban construction land increases due to the development of the Chang Zhu Tan metropolitan area, which leads to the occupation of RRL, resulting in a significant reduction in the area of RRL (He et al., 2019). Furthermore, we explore the change forms of transfer in and transfer out of RRL and find that the main reason for the reduction of RRL is the occupation of urban construction land, which is mainly caused by the strong demand for urban construction land with rapid urbanization. However, the increase in RRL mainly comes from the cultivated land and forestland around the original RRL. The main reason is that the occupied cultivated land and forestland close to the original RRL are more convenient to develop into new homesteads, and the protection intensity of cultivated land and forestland by the local government is not enough. Moreover, different from other countries and regions, the distribution and change in RRL in Hunan Province of China are not only related to the terrain and socioeconomic development but also closely related to the immigration and relocation policies implemented by the government (Liu et al., 2020).

4.2 The Growth of Rural Residential Land Area in Natural Reserves Is Higher Than That in Non-Natural Reserves

By analyzing the changes in the RRL area in natural reserves and non-natural reserves from 2000 to 2020, we found that the area of RRL in natural reserves increased by 1,538.37 hm^2, while the area of RRL in non-natural reserves decreased by 2,786.04 hm^2. Combined with the local social, economic, and policy constraints, it is found that to protect the healthy and sustainable development of the natural environment, the local government has formulated relatively strict land control policies for the natural reserve, limiting the speed of its socioeconomic development and urbanization, resulting in the urbanization development speed of the natural reserve being lower than that of the non-natural reserve. Therefore, the area of RRL in the non-natural reserve shows a significant reduction trend. It is worth noting that although the establishment of natural reserves is negatively correlated with the change of RRL, the RRL area in natural reserves is increasing. The main reason for this increase is that the growth of RRL is affected by many other factors, such as rural economic development and population growth, and the factor of whether there is a natural reserve cannot directly promote the overall reduction of the RRL area.

Meanwhile, some residents who moved to the urban areas did not change their registered residence. To enjoy the dividend policy brought by the establishment of natural reserves, the new rural settlements in the natural reserves were brought to the advantage by their registered residents in rural areas, which to a certain extent led to the increase of the RRL area in the natural reserves (Ristić et al., 2019). It is worth noting that the RRL area in wetland nature reserves, such as the East Dongting Lake National Nature Reserve in Yueyang, increased rapidly in 2000–2020. When analyzing the management policy of the natural reserve, it is found that the management department divides the wetland natural reserve into three levels: core area, test area, and buffer area. The core area is prohibited from development, the test area is moderately developed, and the buffer area is allowed to be fully developed. However, the test area and buffer area do not strictly restrict the expansion of RRL, which leads to the rapid growth of RRL in these areas to a certain extent (Xiao et al., 2021). Although the area of RRL in the natural reserve shows a trend of growth, through the analysis of the ordinary least-squares model, it is found that the presence of natural reserves has a significant negative correlation with the area of RRL, which also shows that the establishment of natural reserves still limits the growth rate of RRL to a certain extent.

4.3 Diversification of Factors Affecting the Change in Rural Residential Land

Although the spatial distribution change of RRL is the result of the joint action of natural, social, and economic factors (Liu et al., 2019), the establishment of natural reserves limits the change of RRL from the aspects of social economy and land management policies to a certain extent. Through the analysis of the ordinary least-squares model, it is found that the growth of per capita cultivated land area and rural resident population from 2000 to 2020 leads to a large

number of farmers living in rural areas, and more RRL is needed to build new houses. The growth of urban construction land area during the early stage has no direct impact on the growth of the RRL area, while the promotion of urbanization needs to absorb a large rural population, and this factor reduces the demand for the RRL area to a certain extent. In addition, the establishment of natural reserves will enhance the impact of government financial expenditure and rural resident population on RRL; that is, in natural reserves, more government financial expenditure and an increase in rural resident population will promote the growth of the RRL area. The per capita crop sowing area from 2000 to 2020 shows the influence of first limiting and then promoting the growth of the RRL area. The summary and analysis can divide the driving factors of RRL change in Hunan Province into three categories: endogenous demand for urbanization development, exogenous catalysis of unbalanced regional development, and policy resettlement measures (Yang et al., 2016). The establishment of natural reserves does not play a decisive role but regulates some factors affecting the change in RRL and then affects the change in the RRL area through the comprehensive action of multiple factors.

4.4 Research Contribution and Deficiency

The research contributions of this article are as follows: (1) based on the perspective of whether there are natural reserves, this article compares and analyzes the spatiotemporal change characteristics of RRL between natural reserves and non-natural reserves in Hunan Province; and (2) this article analyzes the influencing factors of the RRL area change and explores how the establishment of natural reserves affects RRL.

There are some deficiencies in this study. (1) Although this article selects 11 influencing factors based on the relevant literature and the actual conditions of RRL in Hunan Province, it does not involve the level of subjective factors such as farmers' will, which requires data to be obtained through field research. (2) Due to the weak protection and policy constraints of county-level natural reserves, this article only considers provincial and national nature reserves. (3) Since the research scale of this article is 122 county-level administrative regions in Hunan Province, the research results of this article may not apply to all regions of China but can provide some reference for regions with similar natural, social, and economic conditions.

5 CONCLUSION AND POLICY IMPLICATIONS

Based on the spatial and panel data of 122 county-level administrative regions in Hunan Province, this article analyzes the spatiotemporal distribution characteristics of RRL in natural reserves and non-natural reserves by using land use change dynamics, nuclear density analysis, transfer matrix modeling, and ordinary least-squares modeling and explores how the establishment of natural reserves affects RRL. The results show that (1) affected by rapid urbanization, the overall RRL area in Hunan shifted from 171,162.27 hm^2 in 2000 to 169,914.6 hm^2 in 2020, with a total reduction of 1,247.67 hm^2 and a decrease of 0.73%, and the distribution of the RRL area change presented a hot trend in the northeast and a cold trend in the southwest. (2) The spatial distribution of RRL has significant heterogeneity due to natural conditions. The traditional agricultural areas in the east and northeast of Hunan have high residential density and large land scale, while the RRL in the hills and mountainous areas in the west and southwest of Hunan has low aggregation degree and obvious sporadic distribution characteristics, and the RRL area in western Hunan shows a sharp reduction trend due to immigration policy. (3) The occupation of urban construction land is the main reason for the reduction in RRL area, and the transformation of cultivated land and forestland into RRL is the main source of the increase in the RRL area. (4) There are significant differences in the spatiotemporal variation characteristics of the RRL area between natural reserves and non-natural reserves. The RRL area mainly shows an increasing trend in natural reserves, while it mainly shows a decreasing trend in non-natural reserves. Furthermore, the growth of the RRL area is mainly concentrated in the non-natural reserves in central Hunan and the natural reserves in northeast and northwest China, while the non-natural reserves are the main areas where the RRL area decreases. (5) The establishment of natural reserves cannot directly promote the overall reduction of the RRL area. Although there is a significant negative correlation between the establishment of natural reserves and the area of RRL, the total area of RRL in the natural reserve still shows an increasing trend, indicating that the area of RRL is more affected by economic development, government financial expenditure, rural permanent population, etc. Meanwhile, the per capita cultivated land area and rural resident population promote the growth of the RRL area, while urban construction land initially limits and then promotes the growth of the RRL area from 2000 to 2020.

In addition, this article puts forward the following policy implications for the optimization of RRL in natural reserves. (1) The government should strengthen the planning and management of RRL in natural reserves and relocate RRL that are not suitable for living or have a fragile ecological environment. (2) The government can strictly restrict the construction of new RRL in the natural reserve and protect and merge the original RRL suitable for living in the natural reserve to strictly control the growth of RRL in the natural reserve. (3) If farmers have a high demand for RRL, the local government needs to protect and develop the natural reserve according to local conditions. For example, the construction of new RRL is prohibited in the core zone, and the area of RRL is strictly limited in the experimental zone and buffer zone. (4) The local government should also introduce relevant welfare policies to encourage residents in natural reserves to migrate to non-natural reserves and to reduce the area of RRL in natural reserves.

DATA AVAILABILITY STATEMENT

The original contributions presented in the study are included in the article/**Supplementary Material**; further inquiries can be directed to the corresponding author.

AUTHOR CONTRIBUTIONS

YW: Formal analysis, software, and writing—review and editing. HT: Conceptualization, formal analysis, data curation, software, visualization, and writing—original draft. PJ: Conceptualization, formal analysis, data curation, software, methodology, supervision, writing—review and editing, and funding acquisition. JC: Data curation. All authors contributed to this article and approved the submitted version.

FUNDING

This research was supported by the National Key Research and Development Program of China (2018YFD1100801).

SUPPLEMENTARY MATERIAL

The Supplementary Material for this article can be found online at: https://www.frontiersin.org/articles/10.3389/fenvs.2022.909554/full#supplementary-material

REFERENCES

Abelairas-Etxebarria, P., and Astorkiza, I. (2012). Farmland Prices and Land-Use Changes in Periurban Protected Natural Areas. *Land Use Policy* 29, 674–683. doi:10.1016/j.landusepol.2011.11.003

Bai, X., Shi, P., and Liu, Y. (2014). Society: Realizing China's Urban Dream. *Nature* 509, 158–160. doi:10.1038/509158a

Chen, Z., Liu, Y., Feng, W., Li, Y., and Li, L. (2019). Study on Spatial Tropism Distribution of Rural Settlements in the Loess Hilly and Gully Region Based on Natural Factors and Traffic Accessibility. *J. Rural Stud.* doi:10.1016/j.jrurstud.2019.02.014

Chirisa, I. (2021). Opportunities in Master and Local Planning for Resilient Rural Settlement in Zimbabwe. *J. Rural Stud.* 86, 97–105. doi:10.1016/j.jrurstud.2021.05.026

Conrad, C., Rudloff, M., Abdullaev, I., Thiel, M., Löw, F., and Lamers, J. P. A. (2015). Measuring Rural Settlement Expansion in Uzbekistan Using Remote Sensing to Support Spatial Planning. *Appl. Geogr.* 62, 29–43. doi:10.1016/j.apgeog.2015.03.017

Cyriac, S., and Firoz, M. (2022). Dichotomous Classification and Implications in Spatial Planning: A Case of the Rural-Urban Continuum Settlements of Kerala, India. *Land Use Policy* 114, 105992. doi:10.1016/j.landusepol.2022.105992

Deng, Z., Dai, L., Deng, L., and Peng, P. (2021). Analysis of Farmers' Perceptions and Behavioral Response to Rural Living Environment Renovation in a Major Rice-Producing Area: a Case of Dongting Lake Wetland, China. *Cienc. Rural.* 51, e20200847. doi:10.1590/0103-8478cr20200847

Ding, M., Liu, W., Xiao, L., Zhong, F., Lu, N., Zhang, J., et al. (2022). Construction and Optimization Strategy of Ecological Security Pattern in a Rapidly Urbanizing Region: A Case Study in Central-South China. *Ecol. Indic.* 136, 108604. doi:10.1016/j.ecolind.2022.108604

Elgammal, A., Duraiswami, R., Harwood, D., and Davis, L. S. (2002). Background and Foreground Modeling Using Nonparametric Kernel Density Estimation for Visual Surveillance. *Proc. IEEE* 90, 1151–1163. doi:10.1109/JPROC.2002.801448

Fan, J., Han, Q., Tan, S., and Li, J. (2022). Evaluation of Six Satellite-Based Soil Moisture Products Based on *In Situ* Measurements in Hunan Province, Central China. *Front. Environ. Sci.* 10, 1–12. doi:10.3389/fenvs.2022.829046

Fan, P., Ouyang, Z., Nguyen, D. D., Nguyen, T. T. H., Park, H., and Chen, J. (2019). Urbanization, Economic Development, Environmental and Social Changes in Transitional Economies: Vietnam after Doimoi. *Landsc. Urban Plan.* 187, 145–155. doi:10.1016/j.landurbplan.2018.10.014

Fernández, J. E. (2007). Resource Consumption of New Urban Construction in China. *J. Ind. Ecol.* 11, 99–115. doi:10.1162/jie.2007.1199

Gallant, A. L., Loveland, T. R., Sohl, T. L., and Napton, D. E. (2004). Using an Ecoregion Framework to Analyze Land-Cover and Land-Use Dynamics. *Environ. Manag.* 34 (Suppl. 1), S89–S110. doi:10.1007/s00267-003-0145-3

Gao, J., Liu, Y., Chen, J., and Cai, Y. (2019). Demystifying the Geography of Income Inequality in Rural China: A Transitional Framework. *J. Rural Stud.* doi:10.1016/j.jrurstud.2019.01.010

Gong, J., Jian, Y., Chen, W., Liu, Y., and Hu, Y. (2019). Transitions in Rural Settlements and Implications for Rural Revitalization in Guangdong Province. *J. Rural Stud.* doi:10.1016/j.jrurstud.2019.10.037

Gosch, M. S., Parente, L. L., Santos, C. O. d., Mesquita, V. V., and Ferreira, L. G. (2021). Landsat-based Assessment of the Quantitative and Qualitative Dynamics of the Pasture Areas in Rural Settlements in the Cerrado Biome, Brazil. *Appl. Geogr.* 136, 102585. doi:10.1016/j.apgeog.2021.102585

Guan, X., Wei, H., Lu, S., Dai, Q., and Su, H. (2018). Assessment on the Urbanization Strategy in China: Achievements, Challenges and Reflections. *Habitat Int.* 71, 97–109. doi:10.1016/j.habitatint.2017.11.009

Han, Z., Jiao, S., Zhang, X., Xie, F., Ran, J., Jin, R., et al. (2021). Seeking Sustainable Development Policies at the Municipal Level Based on the Triad of City, Economy and Environment: Evidence from Hunan Province, China. *J. Environ. Manag.* 290, 112554. doi:10.1016/j.jenvman.2021.112554

He, Y., Zhou, G., Tang, C., Fan, S., and Guo, X. (2019). The Spatial Organization Pattern of Urban-Rural Integration in Urban Agglomerations in China: An Agglomeration-Diffusion Analysis of the Population and Firms. *Habitat Int.* 87, 54–65. doi:10.1016/j.habitatint.2019.04.003

Heng, J., Wang, H., Fan, Y., Wang, Z., and Gao, Y. (2021). Simulation and Optimization of Urban–Rural Settlement Development from the Perspective of Production–Life–Ecology Space: A Case Study for Aksu City. *Sustainability* 13, 7452. doi:10.3390/su13137452

Hoffman-Hall, A., Loboda, T. V., Hall, J. V., Carroll, M. L., and Chen, D. (2019). Mapping Remote Rural Settlements at 30 M Spatial Resolution Using Geospatial Data-Fusion. *Remote Sens. Environ.* 233, 111386. doi:10.1016/j.rse.2019.111386

Huang, Q., Song, W., and Song, C. (2020). Consolidating the Layout of Rural Settlements Using System Dynamics and the Multi-Agent System. *J. Clean. Prod.* 274, 123150. doi:10.1016/j.jclepro.2020.123150

Huyan, W., and Li, J. (2021). Research on Rural Tourism Service Intellectualization Based on Neural Network Algorithm and Optimal Classification Decision Function. *J. Ambient. Intell. Hum. Comput.* doi:10.1007/s12652-021-03039-6

Kong, X., Liu, D., Tian, Y., and Liu, Y. (2021). Multi-objective Spatial Reconstruction of Rural Settlements Considering Intervillage Social Connections. *J. Rural Stud.* 84, 254–264. doi:10.1016/j.jrurstud.2019.02.028

Li, G., Jiang, C., Du, J., Jia, Y., and Bai, J. (2020a). Spatial Differentiation Characteristics of Internal Ecological Land Structure in Rural Settlements and its Response to Natural and Socio-Economic Conditions in the Central Plains, China. *Sci. Total Environ.* 709, 135932. doi:10.1016/j.scitotenv.2019.135932

Li, G., Jiang, G., Jiang, C., and Bai, J. (2018a). Differentiation of Spatial Morphology of Rural Settlements from an Ethnic Cultural Perspective on the Northeast Tibetan Plateau, China. *Habitat Int.* 79, 1–9. doi:10.1016/j.habitatint.2018.06.002

Li, J., Lo, K., Zhang, P., and Guo, M. (2021a). Reclaiming Small to Fill Large: A Novel Approach to Rural Residential Land Consolidation in China. *Land Use Policy* 109, 105706. doi:10.1016/j.landusepol.2021.105706

Li, K., Geng, H., Yue, L., Li, K., and Huang, L. (2021b). Spatial Differentiation Characteristics and Driving Mechanism of Rural Settlements Transformation

in the Metropolis: A Case Study of Pudong District, Shanghai. *Front. Environ. Sci.* 9, 1–16. doi:10.3389/fenvs.2021.755207

Li, L., Li, X., Hai, B., Wang, X., and Xu, J. (2020b). Evolution of Rural Settlement in an Inland Nonmetropolitan Region of China at a Time of Rapid Urbanisation: The Case of Gongyi. *J. Rural Stud.* 79, 45–56. doi:10.1016/j.jrurstud.2020.08.003

Li, S., Zhu, C., Lin, Y., Dong, B., Chen, B., Si, B., et al. (2021c). Conflicts between Agricultural and Ecological Functions and Their Driving Mechanisms in Agroforestry Ecotone Areas from the Perspective of Land Use Functions. *J. Clean. Prod.* 317, 128453. doi:10.1016/j.jclepro.2021.128453

Li, Y., Jia, L., Wu, W., Yan, J., and Liu, Y. (2018b). Urbanization for Rural Sustainability - Rethinking China's Urbanization Strategy. *J. Clean. Prod.* 178, 580–586. doi:10.1016/j.jclepro.2017.12.273

Li, Y., Kong, X., and Zhu, Z. (2020c). Multiscale Analysis of the Correlation Patterns between the Urban Population and Construction Land in China. *Sustain. Cities Soc.* 61, 102326. doi:10.1016/j.scs.2020.102326

Li, Y., Liu, Y., Long, H., and Cui, W. (2014). Community-based Rural Residential Land Consolidation and Allocation Can Help to Revitalize Hollowed Villages in Traditional Agricultural Areas of China: Evidence from Dancheng County, Henan Province. *Land Use Policy* 39, 188–198. doi:10.1016/j.landusepol.2014.02.016

Liang, Z., and Qamruzzaman, M. (2022). An Asymmetric Investigation of the Nexus between Economic Policy Uncertainty, Knowledge Spillover, Climate Change, and Green Economy: Evidence from BRIC Nations. *Front. Environ. Sci.* 9, 1–16. doi:10.3389/fenvs.2021.807424

Lin, H., Wang, H., Wang, J., Yin, J., and Yang, J. (2022). A Novel Ship Detection Method via Generalized Polarization Relative Entropy for PolSAR Images. *IEEE Geosci. Remote Sens. Lett.* 19, 1–5. doi:10.1109/LGRS.2020.3019196

Linard, C., Gilbert, M., Snow, R. W., Noor, A. M., and Tatem, A. J. (2012). Population Distribution, Settlement Patterns and Accessibility across Africa in 2010. *PLoS One* 7, e31743. doi:10.1371/journal.pone.0031743

Liu, M., Feng, X., Wang, S., and Qiu, H. (2020). China's poverty alleviation over the last 40 years: successes and challenges†. *Aust. J. Agric. Resour. Econ.* 64, 209–228. doi:10.1111/1467-8489.12353

Liu, W., Henneberry, S. R., Ni, J., Radmehr, R., and Wei, C. (2019). Socio-cultural Roots of Rural Settlement Dispersion in Sichuan Basin: The Perspective of Chinese Lineage. *Land Use Policy* 88, 104162. doi:10.1016/j.landusepol.2019.104162

Liu, Y., Kong, X., Liu, Y., and Chen, Y. (2013). Simulating the Conversion of Rural Settlements to Town Land Based on Multi-Agent Systems and Cellular Automata. *PLoS One* 8, e79300–14. doi:10.1371/journal.pone.0079300

Liu, Y., and Li, Y. (2017). Revitalize the World's Countryside. *Nature* 548, 275–277. doi:10.1038/548275a

Liu, Y., Yang, Y., Li, Y., and Li, J. (2017). Conversion from Rural Settlements and Arable Land under Rapid Urbanization in Beijing during 1985-2010. *J. Rural Stud.* 51, 141–150. doi:10.1016/j.jrurstud.2017.02.008

Liu, Y., Ye, Q., Li, J., Kong, X., and Jiao, L. (2016). Suitability Evaluation of Rural Settlements Based on Accessibility of Production and Living: A Case Study of Tingzu Town in Hubei Province of China. *Chin. Geogr. Sci.* 26, 550–565. doi:10.1007/s11769-015-0771-0

Long, H., Li, Y., Liu, Y., Woods, M., and Zou, J. (2012). Accelerated restructuring in rural China fueled by 'increasing vs. decreasing balance' land-use policy for dealing with hollowed villages. *Land Use Policy* 29, 11–22. doi:10.1016/j.landusepol.2011.04.003

Ma, W., Jiang, G., Wang, D., Li, W., Guo, H., and Zheng, Q. (2018). Rural Settlements Transition (RST) in a Suburban Area of Metropolis: Internal Structure Perspectives. *Sci. Total Environ.* 615, 672–680. doi:10.1016/j.scitotenv.2017.09.152

Martin, C. E., and Chehébar, C. (2001). The National Parks of Argentinian Patagonia - Management Policies for Conservation, Public Use, Rural Settlements, and Indigenous Communities. *J. Roy. Soc. New Zeal.* 31, 845–864. doi:10.1080/03014223.2001.9517680

Nandi, S., and Mistri, T. (2022). Transformation of Rural Settlement in Salanpur Community Development Block, West Bengal, India. *GeoJournal* 5, 214–221. doi:10.1007/s10708-021-10565-5

Njoh, A. J. (2011). Municipal Councils, International NGOs and Citizen Participation in Public Infrastructure Development in Rural Settlements in Cameroon. *Habitat Int.* 35, 101–110. doi:10.1016/j.habitatint.2010.04.001

Öztürk, M., Copty, N. K., and Saysel, A. K. (2013). Modeling the Impact of Land Use Change on the Hydrology of a Rural Watershed. *J. Hydrology* 497, 97–109. doi:10.1016/j.jhydrol.2013.05.022

Phokaides, P. (2018). Rural networks and planned communities: Doxiadis Associates' plans for rural settlements in post-independence Zambia. *J. Archit.* 23, 471–497. doi:10.1080/13602365.2018.1458044

Qu, Y., Jiang, G., Zhao, Q., Ma, W., Zhang, R., and Yang, Y. (2017). Geographic Identification, Spatial Differentiation, and Formation Mechanism of Multifunction of Rural Settlements: A Case Study of 804 Typical Villages in Shandong Province, China. *J. Clean. Prod.* 166, 1202–1215. doi:10.1016/j.jclepro.2017.08.120

Qu, Y., Jiang, G., Ma, W., and Li, Z. (2021). How Does the Rural Settlement Transition Contribute to Shaping Sustainable Rural Development? Evidence from Shandong, China. *J. Rural Stud.* 82, 279–293. doi:10.1016/j.jrurstud.2021.01.027

Ristić, D., Vukoičić, D., and Milinčić, M. (2019). Tourism and sustainable development of rural settlements in protected areas - Example NP Kopaonik (Serbia). *Land Use Policy* 89, 104231. doi:10.1016/j.landusepol.2019.104231

Romero-Calcerrada, R., and Perry, G. L. W. (2004). The role of land abandonment in landscape dynamics in the SPA 'Encinares del rı´o Alberche y Cofio, Central Spain, 1984-1999. *Landsc. Urban Plan.* 66, 217–232. doi:10.1016/S0169-2046(03)00112-9

Rosner, A., and Wesołowska, M. (2020). Deagrarianisation of the Economic Structure and the Evolution of Rural Settlement Patterns in Poland. *Land* 9, 523–619. doi:10.3390/land9120523

Gómez, R., Rodríguez Sánchez, A., García, C. G., and García Pérez, J. (2020). The VIF and MSE in Raise Regression. *Mathematics* 8, 605–628. doi:10.3390/math8040605

Sanchez, J. M. (2020). Linear Calibrations in Chromatography: The Incorrect Use of Ordinary Least Squares for Determinations at Low Levels, and the Need to Redefine the Limit of Quantification with This Regression Model. *J. Sep. Sci.* 43, 2708–2717. doi:10.1002/jssc.202000094

Shcherbina, E., and Gorbenkova, E. (2019). Factors Influencing the Rural Settlement Development. *IFAC-PapersOnLine* 52, 231–235. doi:10.1016/j.ifacol.2019.12.478

Stumpf, F., Keller, A., Schmidt, K., Mayr, A., Gubler, A., and Schaepman, M. (2018). Spatio-temporal Land Use Dynamics and Soil Organic Carbon in Swiss Agroecosystems. *Agric. Ecosyst. Environ.* 258, 129–142. doi:10.1016/j.agee.2018.02.012

Suh, J. (2015). Communitarian Cooperative Organic Rice Farming in Hongdong District, South Korea. *J. Rural Stud.* 37, 29–37. doi:10.1016/j.jrurstud.2014.11.009

Sun, P., Zhou, L., Ge, D., Lu, X., Sun, D., Lu, M., et al. (2021). How Does Spatial Governance Drive Rural Development in China's Farming Areas? *Habitat Int.* 109, 102320. doi:10.1016/j.habitatint.2021.102320

Tan, M. J., and Guan, C. (2021). Are People Happier in Locations of High Property Value? Spatial Temporal Analytics of Activity Frequency, Public Sentiment and Housing Price Using Twitter Data. *Appl. Geogr.* 132, 102474. doi:10.1016/j.apgeog.2021.102474

Tan, S., Zhang, M., Wang, A., and Ni, Q. (2021). Spatio-Temporal Evolution and Driving Factors of Rural Settlements in Low Hilly Region-A Case Study of 17 Cities in Hubei Province, China. *Int. J. Environ. Res. Public Health* 18, 2387–2418. doi:10.3390/ijerph18052387

Tang, C., He, Y., Zhou, G., Zeng, S., and Xiao, L. (2018). Optimizing the Spatial Organization of Rural Settlements Based on Life Quality. *J. Geogr. Sci.* 28, 685–704. doi:10.1007/s11442-018-1499-4

Trukhachev, A. (2015). Methodology for Evaluating the Rural Tourism Potentials: A Tool to Ensure Sustainable Development of Rural Settlements. *Sustainability* 7, 3052–3070. doi:10.3390/su7033052

Tu, S., Long, H., Zhang, Y., Ge, D., and Qu, Y. (2018). Rural Restructuring at Village Level under Rapid Urbanization in Metropolitan Suburbs of China and its Implications for Innovations in Land Use Policy. *Habitat Int.* 77, 143–152. doi:10.1016/j.habitatint.2017.12.001

Wang, J., and Zhang, Y. (2021). Analysis on the Evolution of Rural Settlement Pattern and its Influencing Factors in China from 1995 to 2015. *Land* 10, 1137. doi:10.3390/land10111137

Wen, Y., Zhang, Z., Liang, D., and Xu, Z. (2020). Rural Residential Land Transition in the Beijing-Tianjin-Hebei Region: Spatial-Temporal Patterns and Policy Implications. *Land Use Policy* 96, 104700. doi:10.1016/j.landusepol.2020.104700

Wu, Y., Shan, L., Guo, Z., and Peng, Y. (2017). Cultivated Land Protection Policies in China Facing 2030: Dynamic Balance System versus Basic Farmland Zoning. *Habitat Int.* 69, 126–138. doi:10.1016/j.habitatint.2017.09.002

Xiao, J., Watanabe, T., Lu, X., Chand, M. B., Umarhadi, D. A., Chen, X., et al. (2021). Integrating Land Use/land Cover Change with Change in Functional Zones' Boundary of the East Dongting Lake National Nature Reserve, China. *Phys. Chem. Earth, Parts A/B/C* 126, 103041. doi:10.1016/j.pce.2021.103041

Xue, J., Lyu, D., Wang, D., Wang, Y., Yin, D., Zhao, Z., et al. (2018). Assessment of Soil Erosion Dynamics Using the GIS-Based RUSLE Model: A Case Study of Wangjiagou Watershed from the Three Gorges Reservoir Region, Southwestern China. *Water* 10, 1817. doi:10.3390/w10121817

Yang, J., Song, C., Yang, Y., Xu, C., Guo, F., and Xie, L. (2019a). New Method for Landslide Susceptibility Mapping Supported by Spatial Logistic Regression and GeoDetector: A Case Study of Duwen Highway Basin, Sichuan Province, China. *Geomorphology* 324, 62–71. doi:10.1016/j.geomorph.2018.09.019

Yang, J., Yang, J., Luo, X., and Huang, C. (2019b). Impacts by Expansion of Human Settlements on Nature Reserves in China. *J. Environ. Manag.* 248, 109233. doi:10.1016/j.jenvman.2019.07.004

Yang, R., Xu, Q., and Long, H. (2016). Spatial Distribution Characteristics and Optimized Reconstruction Analysis of China's Rural Settlements during the Process of Rapid Urbanization. *J. Rural Stud.* 47, 413–424. doi:10.1016/j.jrurstud.2016.05.013

Yang, R., Xu, Q., Xu, X., and Chen, Y. (2019c). Rural Settlement Spatial Patterns and Effects: Road Traffic Accessibility and Geographic Factors in Guangdong Province, China. *J. Geogr. Sci.* 29, 213–230. doi:10.1007/s11442-019-1593-2

Yang, Y., Liu, Y., Li, Y., and Du, G. (2018). Quantifying Spatio-Temporal Patterns of Urban Expansion in Beijing during 1985-2013 with Rural-Urban Development Transformation. *Land Use Policy* 74, 220–230. doi:10.1016/j.landusepol.2017.07.004

Yao, G., and Xie, H. (2016). Rural Spatial Restructuring in Ecologically Fragile Mountainous Areas of Southern China: A Case Study of Changgang Town, Jiangxi Province. *J. Rural Stud.* 47, 435–448. doi:10.1016/j.jrurstud.2016.07.014

You, L., and Chen, C. (2019). Planning and Implementing Smart Shrinkage of Rural China: The Case of Chengdu's Rural Settlement Consolidation with SGME Model. *jrcp* 30, 62–75. doi:10.5614/jpwk.2019.30.1.5

Yu, Z., Xiao, L., Chen, X., He, Z., Guo, Q., and Vejre, H. (2018). Spatial Restructuring and Land Consolidation of Urban-Rural Settlement in Mountainous Areas Based on Ecological Niche Perspective. *J. Geogr. Sci.* 28, 131–151. doi:10.1007/s11442-018-1464-2

Zasada, I., and Piorr, A. (2015). The Role of Local Framework Conditions for the Adoption of Rural Development Policy: An Example of Diversification, Tourism Development and Village Renewal in Brandenburg, Germany. *Ecol. Indic.* 59, 82–93. doi:10.1016/j.ecolind.2015.02.002

Zhou, D., Wang, Z., Lassoie, J., Wang, X., and Sun, L. (2014). Changing Stakeholder Relationships in Nature Reserve Management: A Case Study on Snake Island-Laotie Mountain National Nature Reserve, Liaoning, china. *J. Environ. Manag.* 146, 292–302. doi:10.1016/j.jenvman.2014.07.018

Zhou, G., He, Y., Tang, C., Yu, T., Xiao, G., and Zhong, T. (2013). Dynamic Mechanism and Present Situation of Rural Settlement Evolution in China. *J. Geogr. Sci.* 23, 513–524. doi:10.1007/s11442-013-1025-7

Zhou, J., Hua, C., Wu, S., Wang, Z., and Wang, X. (2021). Sustainable Village Planning Indicator System in Rural Transformation: Application to Xufu Village in the Yangtze River Delta Region in China. *J. Urban Plann. Dev.* 147, 05021050. doi:10.1061/(asce)up.1943-5444.0000768

Zhou, W., and Chen, B. (2006). Biodiversity of Bitahai Nature Reserve in Yunnan Province, China. *Biodivers. Conserv.* 15, 839–853. doi:10.1007/s10531-004-1869-3

Zhou, Z., Liu, J., Zeng, H., Zhang, T., and Chen, X. (2020). How does soil pollution risk perception affect farmers' pro-environmental behavior? The role of income level. *J. Environ. Manag.* 270, 110806. doi:10.1016/j.jenvman.2020.110806

Zhu, F., Zhang, F., Li, C., and Zhu, T. (2014). Functional Transition of the Rural Settlement: Analysis of Land-Use Differentiation in a Transect of Beijing, China. *Habitat Int.* 41, 262–271. doi:10.1016/j.habitatint.2013.07.011

Zhu, S., Kong, X., and Jiang, P. (2020). Identification of the Human-Land Relationship Involved in the Urbanization of Rural Settlements in Wuhan City Circle, China. *J. Rural Stud.* 77, 75–83. doi:10.1016/j.jrurstud.2020.05.004

Conflict of Interest: The authors declare that the research was conducted in the absence of any commercial or financial relationships that could be construed as a potential conflict of interest.

Publisher's Note: All claims expressed in this article are solely those of the authors and do not necessarily represent those of their affiliated organizations, or those of the publisher, the editors, and the reviewers. Any product that may be evaluated in this article, or claim that may be made by its manufacturer, is not guaranteed or endorsed by the publisher.

Copyright © 2022 Wu, Tang, Jiang and Chen. This is an open-access article distributed under the terms of the Creative Commons Attribution License (CC BY). The use, distribution or reproduction in other forums is permitted, provided the original author(s) and the copyright owner(s) are credited and that the original publication in this journal is cited, in accordance with accepted academic practice. No use, distribution or reproduction is permitted which does not comply with these terms.

frontiers | Frontiers in Earth Science

ORIGINAL RESEARCH
published: 01 July 2022
doi: 10.3389/feart.2022.883779

Deep Semantic Segmentation for Rapid Extraction and Spatial-Temporal Expansion Variation Analysis of China's Urban Built-Up Areas

Maoyang Bai[1], *Shiqi Zhang*[1], *Xiao Wang*[1], *Yu Feng*[1], *Juan Wang*[2] *and Peihao Peng*[1,2]*

[1]College of Earth Sciences, Chengdu University of Technology, Chengdu, China, [2]College of Tourism and Urban-Rural Planning, Chengdu University of Technology, Chengdu, China

Changes in the spatial expansion of urban built-up areas are of great significance for the analysis of China's urbanization process and economic development. Nighttime light data can be used to extract urban built-up areas in a large-scale and long-time series. In this article, we introduced the UNet model, a semantic segmentation network, as a base architecture, added spatial attention and channel attention modules to the encoder part to improve the boundary integrity and semantic consistency of the change feature map, and constructed an urban built-up area extraction model—CBAM_UNet. Also, we used this model to extract urban built-up areas from 2012 to 2021 and analyzed the spatial and temporal expansion of China's urban built-up areas in terms of expansion speed, expansion intensity, expansion direction, and gravity center migration. In the last decade, the distribution pattern of urban built-up areas in China has gradually changed from "center" to "periphery-networked" distribution pattern. It reveals a trend from agglomeration to the dispersion of urban built-up areas in China. It provides a reference for China's urban process and its economic development.

Keywords: urban built-up areas, deep semantic segmentation network, CBAM_UNet, spatial and temporal expansion of China, center–periphery network

OPEN ACCESS

Edited by:
Ding Ma,
Shenzhen University, China

Reviewed by:
Milad Janalipour,
Ministry of Science, Research, and Technology, Iran
Minmin Li,
Shenzhen University, China

***Correspondence:**
Peihao Peng
peihaop@163.com

Specialty section:
This article was submitted to Environmental Informatics and Remote Sensing, a section of the journal Frontiers in Earth Science

Received: *25 February 2022*
Accepted: *25 May 2022*
Published: *01 July 2022*

Citation:
Bai M, Zhang S, Wang X, Feng Y, Wang J and Peng P (2022) Deep Semantic Segmentation for Rapid Extraction and Spatial-Temporal Expansion Variation Analysis of China's Urban Built-Up Areas. Front. Earth Sci. 10:883779. doi: 10.3389/feart.2022.883779

1 INTRODUCTION

In 2012, China's economy ushered the "New Normal" period. After experiencing rapid growth, China's economic growth rate began to slow down (Yang and Zhao, 2020; Yu et al., 2020). In 1966, J.R. Fridemna proposed the "center-periphery" theory, which emphasizes that regional economic growth must be accompanied by changes in the spatial structure of the economy and is mainly used as a theoretical model to explain the unbalanced development process between inter-regional or rural and urban areas (Liu et al., 2018). Urban built-up area expansion provides resources and capital for rapid industrialization and urbanization, thus promoting economic growth, which will drive the agglomeration of resources and labor, promoting the further expansion of urban built-up areas, but the expansion also brings various problems, such as endangering national food security and reducing biodiversity (Yue et al., 2014; Yang et al., 2020). Urban built-up areas are the most rapidly changing areas in China during the transition period, and the extent of urban built-up areas expansion affects the quality of urbanization and the process of sustainable development in China significantly (Liu

et al., 2016; Zhang et al., 2016; Li J. et al., 2017; Hu et al., 2018). Therefore, accurate spatial change in urban built-up areas is essential to detect the urbanization process and to analyze the driving factors of urban development and its impact on the environment in China.

The gradual development of the remote sensing technology and big data technology offers the possibility of rapidly extracting urban built-up areas (Zhang et al., 2018; Bramhe et al., 2020). In recent years, a large number of high-resolution (12–30 m) built-up area products have been released globally and regionally, such as Fine Resolution Observation and Monitoring of Global Land Cover (FROM-GLC) (Gong et al., 2013) and GlobeLand30 (Chen et al., 2015), which contains built-up areas as of 2010. Although these product data have high accuracy, due to the limitations of remote sensing image quality and launch time, most of them have only 1 year of built-up area data, and there is also the problem of confusion with the classification of bare land (Liu et al., 2019). The nighttime light data (NTL) can provide timely urbanization information, and it reflects the regional light intensity of the earth's surface at night and the weak light emitted from cities or even rural areas, traffic flow, etc. Therefore, it can also clearly distinguish urban and non-urban areas, and nighttime light data can frequently and quickly obtain information about the earth's surface at night. Simultaneously, it can largely avoid the spectral confusion of traditional multispectral remote sensing, so it is widely used in long time series urban monitoring research. In recent years, with the continuous enrichment of nighttime light remote sensing data products, especially the emergence of the new generation of nighttime light data NPP/VIIRS (National Polar-Orbiting Partnership's Visible Infrared Imaging Radiometer Suite), which has effectively improved the spatial resolution, temporal resolution, radiative resolution (Shi et al., 2014), and other deficiencies of DMSP/OLS (Defense Meteorological Satellite Program Operational Linescan System) nighttime light data, it expands the research direction and application fields of nighttime light data (Li and Zhou, 2017).

The data selection methods to extract urban built-up areas mainly include the following three ways: first, the nighttime light data were used alone. However, the lower spatial resolution and insufficient detailed information on urban built-up areas will lead to lower accuracy of the extraction (Zhang and Seto, 2013). Second, it extracted urban built-up areas by combining nighttime light data with statistical data, but statistical data are difficult to obtain and have low timeliness. Third, the method combined nighttime light data and remote sensing images to extract urban built-up areas, which is commonly used in small-scale extraction (Ma, 2018; He et al., 2020; Li et al., 2020), for example, combining the traditional remote sensing image Landsat with nighttime light data. However, the Landsat image has many bands, and extracting urban built-up areas on a large scale requires a large amount of data, resulting in a more complex and time-consuming experimental setup for extraction (Liu et al., 2021; Mithun et al., 2021). Lu et al. (2008) found that combining MODIS (moderate-resolution imaging spectroradiometer) and NDVI (Normalized Difference Vegetation Index) data with DMSP/OLS nighttime light data can improve the accuracy of urban built-up area extraction. In our experiment, a new generation of nighttime light data NPP/VIIRS combined with MODIS NDVI data was selected to explore a fast and accurate method to extract urban built-up areas on large-scale and long-time series. Also, there are three main methods to extract urban built-up areas from the aforementioned images. One is the threshold segmentation method, which relies on the determination of the best threshold for the data, and no systematic and effective threshold determination rules have been formed: the artificial threshold method has strong subjectivity, and the accuracy of extracting urban built-up areas is low through the cluster threshold method, and the mutation detection method is inefficient, and the accuracy stability is poor (Liu et al., 2019; Wang et al., 2021). The second is the pixel classification method. At present, machine learning methods such as K-means unsupervised classification (Ju et al., 2017) and support vector machines (SVMs) (Ma et al., 2017; Jiang C. et al., 2021) are mainly used. The traditional machine learning methods are relatively simple, but the feature learning ability is limited, resulting in lower accuracy. Deep learning can use deep-architecture neural networks (e.g., CNN) to automatically learn features from the input raw data and directly generate powerful deep features, making it rapidly developed in the field of target detection and scene classification (Tan et al., 2018, 2020; Sun et al., 2020). Fully convolutional neural networks are the cornerstone of deep learning in the image semantic segmentation field, and it replaces the last fully connected layer of the convolutional neural network with a convolutional layer, effectively implementing end-to-end training of the convolutional neural network for image semantic segmentation, but the disadvantage is that the translation invariance of the convolutional network does not consider useful global context information (Wang et al., 2018; Karim et al., 2019; Tan et al., 2019). The UNet model based on the encoder-decoder was proposed, which was widely used in medical images in the early days (Navab et al., 2015; Kaur et al., 2021; Zhou et al., 2021), and in recent years, it has also been performed prominently in the classification of remote sensing images. The model has a neural network with an encoder-decoder structure that first encodes features from the raw data using an encoder and then decodes the target result from the feature encoding using a decoder, while high-level and low-level image features are merged through skip connections to maximize the extraction of context information (Peng et al., 2019; Wu et al., 2021; Yang et al., 2021). The attention module was originally proposed to solve machine translation problems by automatically learning weights to capture the correlation between the hidden states of the encoder and the decoder, weighting the output of the encoder, and can achieve alignment between input and output while utilizing more context information about the original data, making it an integral part in the encoder-decoder structure (Zhu and Yang, 2018; Kearney et al., 2019; Yang et al., 2021).

Remote sensing data combined with deep learning can quickly extract urban built-up areas, which brings the possibility to measure the changes of urban built-up areas in both temporal and spatial dimensions. Previously, the existing urban expansion metrics mostly characterize the process and characteristics of

urban land expansion from a single "temporal" or "spatial" dimension. Among them, the "temporal" urban expansion metrics refer to the use of urban built-up area land scale, spatial form, and other characteristics of the temporal change, the intensity of change, which mainly includes the expansion intensity index, and the average annual expansion index. "Spatial" urban built-up area expansion metrics are measured from the geometry of urban built-up areas (graphical patterns, such as shape and area), which mainly include the expansion direction index, center of gravity offset index, and aggregation index (Liu et al., 2018); domestic scholars mainly study the expansion characteristics of urban built-up areas in central, eastern, and central-western China on a large scale; representative regions such as Yangtze River Delta, Pearl River Delta, Beijing, Tianjin, and Tang (Liu et al., 2000) on a medium scale; studies of large cities such as Beijing, Shanghai, and Guangzho (Liu et al., 2018; Li et al., 2021) on a small scale; less research on the expansion of construction land in small- and medium-sized cities (Jiang W. et al., 2021), and less quantitative analysis of spatial and temporal changes in the expansion of urban built-up areas in China. In this article, based on Google Earth Engine (GEE), using NPP/VIIRS nighttime light data and MOD13Q1 NDVI with the same spatial resolution, the UNet deep semantic segmentation neural network was selected, which added both spatial attention and channel attention modules in the encoder to improve the boundary integrity and semantic consistency of the change feature map. Then, a deep semantic segmentation model—CBAM_UNet was built and was trained and tuned by the Adam optimization algorithm and Dice Loss function to get the best parameters. With the proposed model, we could rapidly extract urban built-up areas on a large scale. So, we effectively and rapidly extracted China's urban built-up areas based on the CBAM_UNet model. Meanwhile, to deeply analyze the expansion of China's urban built-up areas during slow economic growth, NPP/VIIRS nighttime light data and MOD13Q1 NDVI data in 2012, 2015, 2018, and 2021 were selected to calculate China's urban built-up areas. We also analyzed the expansion characteristics of China's urban built-up areas through expansion speed, expansion intensity, expansion direction, and gravity center migration. Therefore, the proposed model—CBAM_UNet can provide a methodological guide for quickly obtaining the area of built-up areas, and the analysis results of the long-term spatial expansion of built-up areas can also provide a certain reference value for urban construction in China.

2 STUDY AREA AND DATASETS

2.1 Study Area

The study area is located in China (longitude 73°33'~135°05′ East, latitude 3°51'~53°33′ North). From 1980 to 2011 was a period of high economic growth in China: the average annual growth rate of GDP was 10.03%, and urban population had increased from 89.405 million to 354.256 million. Urban built-up areas of provinces were shown a typical center-periphery distribution, mostly concentrated around a pole, and the distribution of urban built-up areas in the coastal was concentrated around Beijing-Tianjin-Hebei urban agglomeration, Yangtze River Delta urban agglomerations, and Pearl River Delta urban agglomerations.

After 2012, China's economy had ushered in a period of slow growth with a focus on high-quality development. From 2012 to 2018, the average annual growth rate of GDP was 7.24%, and urban population had increased from 369.897 million to 427.300 million. Based on the period from the launch of VIIRS (2012) to the present, this experiment researched the changes in China's urban built-up area expansion after the slowdown of economic growth. These data come from the China Statistical Yearbook.

2.2 Datasets

2.2.1 Data Sources and Access

1) NTL data

We used VIIRS as the NTL data, derived from the National Geophysical Data Center (NGDC) of the National Oceanic and Atmospheric Administration (NOAA) and provided by the Suomi National Polar-orbiting Partnership (Suomi-NPP) Visible Infrared Imagining Radiometer Suite (VIIRS), with a spatial resolution of 742 m. In this experiment, monthly averaged radiometric composites images with the influence of stray light were removed and used. The aim was to avoid a large number of missing values in the summer at high latitudes in this image version (Li X. et al., 2017); the research period was chosen to be from January to March and from September to December for each year, with seven images per year.

2) Reference data

This experiment's remote sensing data are NDVI data, which are from MOD13A1, a 16-day synthetic product with a spatial resolution of 500 m. Meanwhile, to reduce the influence of cloud cover, we used maximum value composite (MVC) (Holben, 1986) to get the NDVI images for each year.

Also, the sample data are the 2020 WorldCover product from the European Space Agency (ESA), which provides a 10-m spatial resolution global land cover map based on Sentinel-1 and Sentinel-2 data, including 11 land cover categories, and we selected the "built-up" label as the sample data for the model input.

All data were acquired through Google Earth Engine (https://code.earthengine.google.com/, GEE).

2.2.2 Data Reprocessing

We used the threshold method for NTL data to remove the images' extraordinarily high and low values and the mean value method (Shi et al., 2014) to composite the annual images. In addition, we logarithmically transform the composite annual nighttime light images to reduce the influence of high values and enhance the homogeneity of the overall radiation value distribution in urban built-up areas.

All images were converted to Asia Lambert Conformal Conic projection, where both VIIRS and WorldCover images were resampled to 500 m spatial resolution by the nearest neighbor method to avoid decreasing in DN values of the images with

TABLE 1 | Dataset overview.

Dataset	Data type	Spatial resolution (m)	Resampled spatial resolution (m)	Year
VIIRS	NTL	742	500	2012, 2015, 2018
MOD13A1	NDVI	500	500	2020, 2021
WorldCover	LandCover	10	500	2020

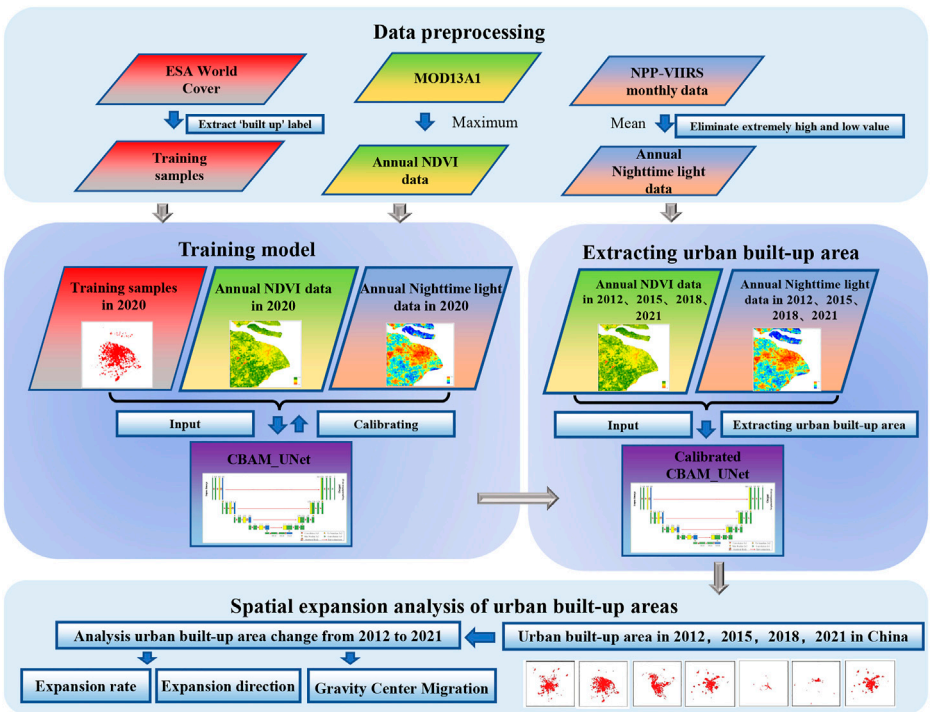

FIGURE 1 | Overview of the workflow.

increasing latitude (Elvidge et al., 2009) and ensure the spatial consistency across the datasets. In addition, based on WorldCover data, all data layers were geometrically rectified. An overview of the datasets is shown in **Table 1**.

3 METHODS

This experiment consists of extracting China's urban built-up areas and its spatial expansion analysis (**Figure 1**). The first part is the time-series urban built-up areas extraction. First, the NTL data and NDVI data in 2020 were chosen to build and train a deep semantic segmentation model for rapidly extracting China's urban built-up areas, and then input the NTL data and NDVI data in 2012, 2015, 2018, and 2021 into the calibrated model to extract China's urban built-up areas for the 4 years. The second part is to analyze the expansion speed, intensity, and direction of China's urban built-up areas and gravity center migration of urban construction based on the extracted time-series urban built-up areas.

3.1 Construction and Training for Urban Built-Up Area Extraction's Model

3.1.1 Developing CBAM_UNet

1) Standard UNet

The UNet is based on the fully convolutional neural network, which was first proposed for biomedical image segmentation, overcoming the difficulty of predicting boundaries with small training set images (Navab et al., 2015). It mainly consists of an encoder part and a decoder part. The encoder has four sub-modules: a convolutional layer and a pooling layer, making the image features progressively smaller and more abstract. The decoder corresponds to the encoder layer by layer. With the decoder deconvolution layer, the feature sizes were sequentially getting more extensive and using skip connections to connect and merge the decoder part deconvolution results in the output of the encoder part. Finally, the probability map is output through a 1 × 1 convolution layer.

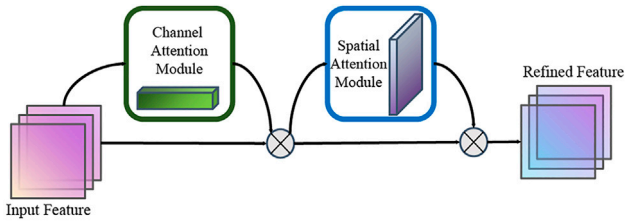

FIGURE 2 | Overview of CBAM. The module has two sequential submodules: channel and spatial (Woo et al., 2018).

The UNet model currently performs well in image segmentation due to its excellent model architecture. The combination of NTL data and NDVI used in this experiment has fewer bands, which was consistent with the medical image with fewer bands. In other words, this experiment can also be regarded as a problem of the image extraction with small training sets (urban built-up areas), so the model built in this experiment chose the UNet model as the base architecture.

2) Convolutional Block Attention Module

The attention module is a simulation of the human brain operation, which is designed to guide the deep neural network to focus on the features that are more relevant to the task. For the image classification task, the attention module combines the important features of the input image and the extracted feature spectrum, by combining the true value and the loss function, together with the backward propagation algorithm, to guide the network to automatically find the features that improve the task performance the most and assign a higher weight to that feature, thus improving the performance of the model.

Generally, the attention module mainly used by the neural network is divided into two categories: (1) soft attention, which assigns a weight between 0 and 1 to each input item, indicating the level of attention for each part. Soft attention is differentiable so that the attention weights can be obtained by forward and backward propagation (Xiao et al., 2015). However, since soft attention considers most of the information to different degrees, the amount of calculation is relatively large. (2) Hard attention, which assigns a weight of either 0 or 1 to each input item, is different from soft attention in that hard attention only considers which parts need attention and which parts do not. Hard attention is not differentiable, so the training process is usually carried out through reinforcement learning (Mnih et al., 2014). The advantage is that the time and computational cost can be reduced, but some information that should be attended to may be lost.

Convolutional block attention module (CBAM), as a lightweight attention module, belongs to soft attention and contains two sequential sub-modules: channel attention module (CAM) and spatial attention module (SAM), which build attention modules on channel and space, respectively (**Figure 2**) (Zhu and Yang, 2018).

CAM mainly focuses on "what" is meaningful in the input image (**Figure 3**). To compute channel attention efficiently, average-pooling and max-pooling are used to compress the spatial dimension of the input feature map, realizing the aggregation of spatial information. Then, the average pooled features and max pooled features are forward propagated into a shared multi-layer perceptron (MLP). Finally, the two output feature vectors are merged by element summation to obtain the channel attention map. The calculation formula of channel attention is shown in **Eq. 1**.

SAM is different from CAM in that it is more concerned with "where" being the more informative part, which complements channel attention (**Figure 3**). Average-pooling and max-pooling are first applied in the channel dimension, and the two-channel features are concatenated to compute spatial attention. A standard 7 × 7 convolutional layer then convolves the concatenated features to obtain the spatial attention map. The calculation formula of spatial attention is shown in **Eq. 2**.

$$\begin{aligned} M_c(F) &= \sigma\left(MLP\left(AvgPool(F)\right) + MLP\left(MaxPool(F)\right)\right) \\ &= \sigma\left(W_1\left(W_0\left(F^c_{avg}\right)\right) + W_1\left(W_0\left(F^c_{max}\right)\right)\right), \end{aligned} \tag{1}$$

$$\begin{aligned} M_s(F) &= \sigma\left(f^{7\times7}\left(\left[AvgPool(F); MaxPool(F)\right]\right)\right) \\ &= \sigma\left(f^{7\times7}\left(\left[F^s_{avg}; F^s_{max}\right]\right)\right), \end{aligned} \tag{2}$$

where $M_c(F)$ denotes channel attention map, and $M_s(F)$ denotes spatial attention map; σ denotes the sigmoid function, *MLP* denotes multi-layer perceptron and F denotes input features, F^c_{avg} and F^c_{max} denote average-pooled features and max-pooled features, respectively, W_0 and W_1 denote the *MLP* weights, $f^{7\times7}$ represents a convolution operation with the filter size of 7×7, F^s_{avg} and F^s_{max} denote average-pooled features and max-pooled features across the channel.

3) CBAM_UNet

In this experiment, we constructed a CBAM_UNet neural network for urban built-up areas extraction, which combined channel and spatial attention modules (**Figure 4**). The main structure of CBAM_UNet consists of two parts: the encoder and decoder. The encoder part, which extracted the features of the image layer by layer through convolution and pooling to obtain feature information, consists of four blocks, and each block was convolved twice with standard 3 × 3 convolution layer and batch normalization and activated by the ReLU function. The CBAM attention module was added before under-sampling the image. Each under-sampling doubled the number of feature channels while compressing the length and width of the image by half. Finally, the length and width of the input raw image were compressed from 128 × 128 to 8 × 8, and the number of feature channels was increased from 2 to 1024 through the entire encoder part.

The decoder part also consists of four blocks (this part follows the standard UNet), which were up-sampled by deconvolution to recover the original size of the image and output the segmentation result. It consists of eight 3 × 3 convolution layers, one 1 × 1 convolution layer, and four 2 × 2 up-sampling layers, with the feature channels, were reduced from 1024 to 2, all using ReLU as the activation finally got the classification results through the

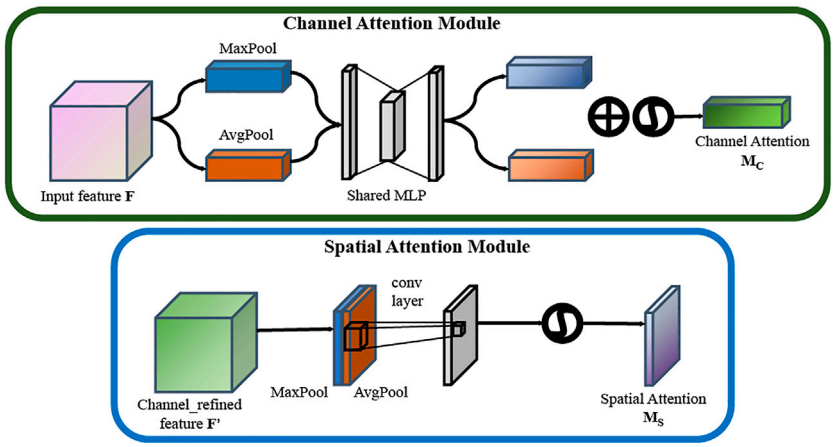

FIGURE 3 | Diagram of each attention sub-module (Woo et al., 2018).

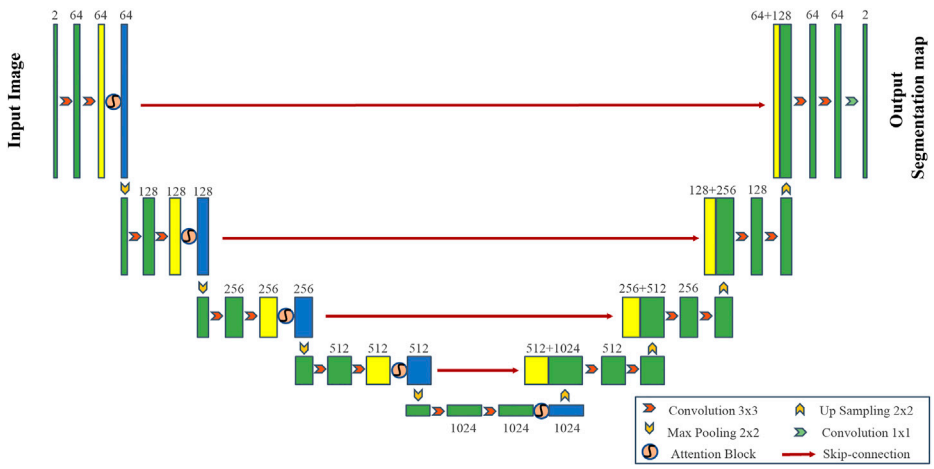

FIGURE 4 | CBAM_UNet architecture.

Sigmoid function. Since high-resolution feature information is often lost in up-sampling, the UNet did not directly up-sample high-level semantic features. It added skip connections to each block. There has the advantage of merging more low-level features into the up-sampling process, achieving feature fusion at different scales, improving the information during up-sampling, and complementing the contextual information of the input image. Ultimately, this multi-scale prediction is achieved, improving the segmentation's accuracy.

Therefore, the main difference is in the encoder part between the proposed model CBAM_UNet and the standard UNet structure, and we added the CBAM attention module before under-sampling the image.

3.1.2 Algorithm Implementation

The training part is mainly to train and calibrate the model, and its purpose is to obtain the optimal tuning model. Essentially, calibration uses an optimization algorithm to minimize the loss function by iteratively estimating the weights of the parameters. The process consists of determining the loss function, setting the optimization algorithm, and iterating parameters.

In semantic segmentation, choosing the appropriate loss function is crucial to the results of model training. Linear cross-entropy loss was mostly used as the loss function in binary image segmentation (Vi-de and Qing, 2004) and is shown in **Eq. 3**:

$$L = -\frac{1}{N}\sum_{i=1}^{N}[y_i \cdot \log(p_i) + (1 - y_i) \cdot \log(1 - p_i)], \qquad (3)$$

where y_i represents the label of sample, i and p_i indicate the probability that the sample i is predicted to be a positive class.

However, the linear cross-entropy loss function has an obvious disadvantage. When the quantity of positive samples is significantly less than that of negative samples, the results of

the model classification will be greatly biased toward the background. So we used Dice Loss, which was proposed to solve the problem of extremely unbalanced classification samples (Milletari et al., 2016). Dice Loss is a function based on the Dice coefficient and derived from binary classification. It is a measure of the overlapping part of two samples, with the measure ranging from 0 to 1. A dice coefficient equal to 1 means complete overlap. Dice Loss is defined as **Eq. 4**:

$$L = 1 - \frac{2\sum_{pixels} y_{true}\, y_{pred}}{\sum_{pixels}\left(y_{true}^2 + y_{prd}^2\right)}, \tag{4}$$

where y_{true} represents the label's value, and y_{pred} denotes the value obtained from the model.

In summary, the steps of model training are as follows:

1) We combined the preprocessed NPP-VIIRS NTL data and MOD13A1 NDVI data in 2020 into a two-band image data through band composited and selected the "built-up" label from WorldCover product in 2020 provided by ESA as the label data for the model input.
2) Clipping the sample datasets: The "fishnet" function in ArcGIS was used to clip both the composited two-band image data and the label data into 128 × 128 size images.
3) Splitting the sample datasets: 1294 images were randomly chosen as the training set, and the remaining 142 images were used as the validation set. Both sets were the input data of the model.
4) Model training process: The training set was input into the CBAM_UNet model, the loss values of the training data and label data were calculated through the Dice Loss function, and the model parameters were optimized by the Adam optimizer until the loss function was fitted (Kingma and Ba, 2015). The initial learning rate of the model was 1e-3, and the total number of iterations was 40 epochs.

3.1.3 Accuracy Evaluation

We introduced five accuracy evaluation indicators to verify the model's accuracy. These are precision (P), recall (R), F1-score (F1), mean of class-wise intersection over union (mIoU), and overall accuracy (OA). Among them, P evaluates the precision of the model: the larger value means there are fewer misclassified pixels. R evaluates the recall rate of the model: the larger the value is, the fewer omitted pixels are. F1 represents the harmonic mean of P and R, and it is a global indicator for evaluating the classification accuracy: the higher the value indicates, the more accurate the model is. Meanwhile, OA and mIoU show the model's overall performance: and their larger values reveal the better performance. OA is the ratio of the number that correctly classified category elements to the total number of categories. mIoU is obtained by calculating the ratio of the intersection and union of the two sets of the true values and the predicted values of each category, then averaging the results. Intersection over union (IOU) of urban built-up areas was not used in the evaluation indicators. Because the number of samples in urban built-up areas (foreground) and non-urban built-up areas (background) was extremely unbalanced, it leads to low IOU values in urban built-up areas. Therefore, it is reasonable to evaluate the accuracy of the extraction results of urban built-up areas by p value, R value, and F1, and to evaluate the model's overall accuracy by OA and mIOU. The calculation formula for each indicator is as follows:

$$P = \frac{TP}{TP + FP}, \tag{5}$$

$$R = \frac{TP}{TP + FN}, \tag{6}$$

$$F1 = \frac{2PR}{P + R}, \tag{7}$$

$$OA = \frac{TP + TN}{TP + TN + FP + FN}, \tag{8}$$

$$mIOU = \frac{1}{2}\left(\frac{TP}{TP + FP + FN} + \frac{TN}{TN + FN + FP}\right), \tag{9}$$

where *TP*, *FP*, *TN*, and *FN* denote the number of true positives, the number of false positives, the number of true negatives, and the number of false negatives.

Meanwhile, to verify the model's accuracy in extracting built-up areas from 2012 to 2021 without sample data, we introduced the "China Statistical Yearbook" (stats.gov.cn) issued by the National Bureau of Statistics to obtain the built-up area data in 2012, 2015, and 2018 (excluding Hong Kong, Macau, and Taiwan, but the data for 2021 have not yet been released), and the experimental model extraction results are compared.

3.1.4 Comparison With Other Methods

To verify the model accuracy of the proposed CBAM_UNet, we input the same sample data into the other three models, the standard U-Net, support vector machine (SVM), random forest (RF), and extracted urban built-up areas in China in 2020. Also, to ensure the objectivity of the result comparison, the loss function, optimizer, and training parameters of the basic UNet were the same as the method proposed in this article. SVM is a fast and reliable classification method for supervised learning. A given training data achieve classification by finding the maximum margin hyper-plane and using the cross-validation method to determine the penalty factor C and the parameter γ of the kernel function. RF is an ensemble learning algorithm based on a non-parametric regression algorithm, which is an ensemble classifier based on the decision tree. Parameters such as the number of decision trees, the maximum number of leaf nodes, and the minimum number of samples that can be divided by a node are optimized through the accuracy curve.

3.1.5 Experimental Setup

This experiment was carried out in a Windows10 environment, and the model was built by a deep learning framework—Pytorch. The software and hardware environments are shown in **Table 2**.

3.2 Extraction of Urban Built-Up Areas

We downloaded the NPP-VIIRS NTL and the MOD13A1 NDVI data from 2012 to 2021 through GEE (every 3 years). They were preprocessed as described earlier to composite the datasets for

TABLE 2 | Hardware and software parameters.

		Parameter configuration
Hardware	CPU	Intel(R) Core(TM) i7-10750H CPU @ 2.60 GHz 2.59 GHz
	Memory	16 GB
	Hard disk	1 TB
	GPU	NVIDIA GeForce RTX 2060 Video Memory: 6 GB CUDA Cores: 1920
Software	Operating system	Windows10
	Computing platform	CUDA11.2 + cudnn8.1.0
	Programming language	Python3.8
	Processing platform and framework	Image processing: ArcGIS10.8、Google Earth Engine Deep Learning: Pytorch 1.8.1

semantic segmentation. Then, we extracted China's urban built-up areas in 2012, 2015, 2018, and 2021 through the calibrated CBAM_UNet and analyzed the change in urban built-up areas during the study period.

3.3 Spatial Expansion Analysis Method

1) Expansion speed and intensity

Using the urban expansion speed and intensity as indicators to study the spatial and temporal characteristics of China's urban built-up areas expansion (Yin et al., 2021).

Urban expansion speed (**Eq. 10**): this indicates the growth of China's urban built-up areas.

Urban expansion intensity (**Eq. 11**): this indicates the rate of China's urban built-up areas in a period.

$$S = \frac{M_b - M_a}{T}, \tag{10}$$

$$P = \frac{M_b - M_a}{M_a} \times \frac{1}{T}, \tag{11}$$

where S indicates the expansion speed of urban built-up areas, P is the expansion intensity of urban built-up areas, T is the time interval and M_a and M_b indicate the area of early and late urban built-up areas.

2) Expansion directions

The direction of the country's urban expansion determines the development direction of the entire country to a certain extent and provides a reference value for the country's macro-management work. In this section, we used the geometric quadrant orientation method (Liu et al., 2021) to compare and analyze the expansion differences of urban built-up areas in different spatial orientations in each period, and different spatial orientations reflected the spatial characteristics of urban expansion, so the spatial form of China's urban built-up areas expansion can be described.

The area change of urban built-up areas in several regions of China during the study period was calculated by the geometric quadrant orientation method. The center was set at 34°32′27.00″N and 108°55′25.00″E. So China was divided into north (N), northeast (NE), east (E), southeast (SE), south (S), southwest (SW), west (W), and northwest (NW).

3) Gravity Center Migration

The change in the country's urban built-up areas' gravity center is a significant indicator (Liu et al., 2013; Zeng et al., 2015), which reflects the intensity and spatial characteristics of China's urban expansion and is also important for understanding the compactness of modern urban development. With the expansion of China's urban built-up areas, we calculated the coordinates of the gravity center and the migration distances of China's urban built-up areas in 2012, 2015, 2018, and 2021. As shown in **Eqs 12**, **13**:

$$X_t = \frac{\sum_{i=1}^{n} C_{ti} X_i}{\sum_{i=1}^{n} C_{ti}}, \tag{12}$$

$$Y_t = \frac{\sum_{i=1}^{n} C_{ti} Y_i}{\sum_{i=1}^{n} C_{ti}}, \tag{13}$$

where X_t denotes the longitude coordinate of the gravity center in year t, and Y_t denotes the latitude coordinate of the gravity center in year t. C_{ti} denotes the area of urban built-up areas patch i; X_i and Y_i denote the gravity center coordinates of patch i, respectively; n denotes the number of patches.

4 RESULTS AND ANALYSIS

4.1 Experimental Results and Analysis

4.1.1 Model Training and Built-Up Area Extraction Results in 2020

- Model training results

The learning rate is the hyperparameter of how the gradient of the loss function is used to adjust the network weights in the gradient descent method. A learning rate that is too large may cause the loss function to cross the global optimum directly; a learning rate that is too small will result in a slow change in the loss function, increase the convergence complexity of the network, and make it easy to get trapped in a local minimum. A suitable learning rate can reach the loss minimum faster, while ensuring that the converged loss value is the global optimal solution of the neural network. Therefore, the

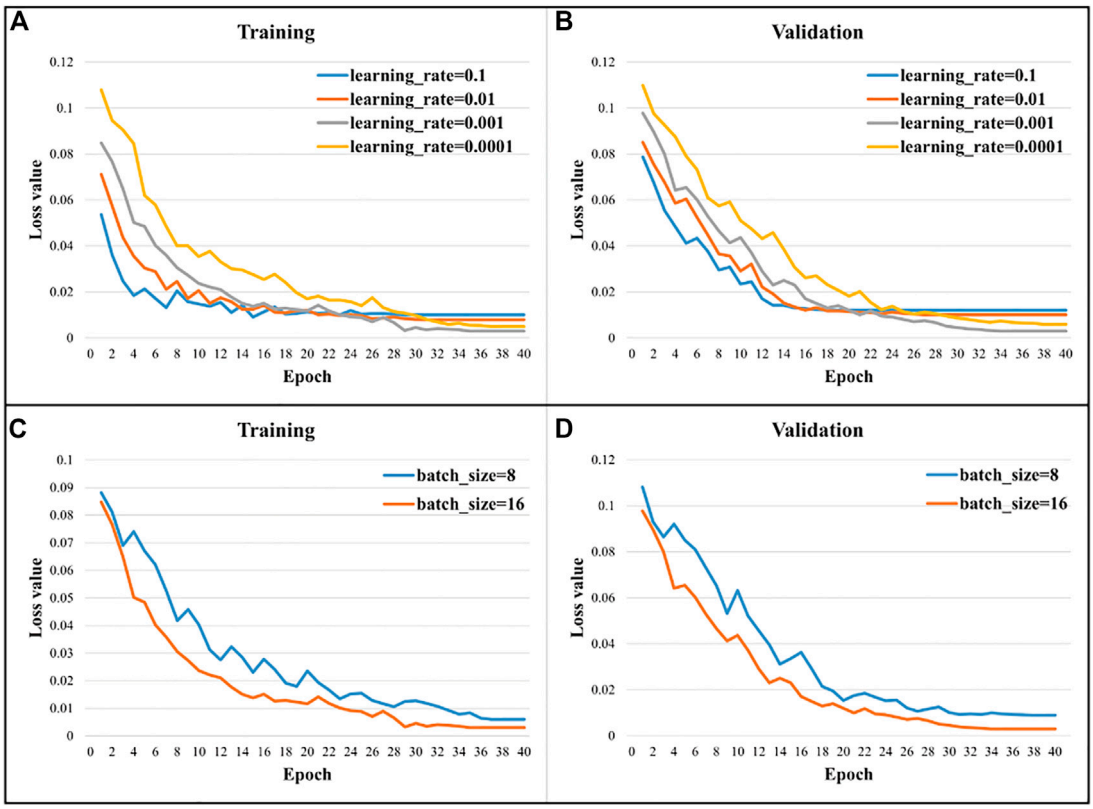

FIGURE 5 | Sensitivity analysis. **(A,B)** Loss value with different learning rates. **(C,D)** Loss value with different batch sizes.

learning rate in model training is an unavoidable and particularly important hyperparameter. This experiment uses the Adam optimizer to adjust the gradient adaptively, which effectively balances the influence generated by the learning rate. Four initial learning rates of 0.1, 0.01, 0.001, and 0.0001 were set for comparison, all with 40 training cycles and a batch size of 16. The batch size refers to the number of data samples crawled in one training, which will have an impact on the stability of the network model. In this experiment, two batch sizes of 8 and 16 are selected for training, considering the effect of computer memory. Their accuracy variations are shown in **Figure 5**.

As can be seen from **Figure 5**, the convergence speed of the CBAM_UNet model for extracting the built-up area is mainly influenced by the learning rate. During training, the convergence speed obtained for small learning rate (0.0001, 0.001) than large learning rate (0.1, 0.01) is smaller, but the converged loss value is lower than that of large learning rate, but the loss value of small learning rate 0.0001 is not as good as that of learning rate 0.001, indicating that learning rate 0.0001 is trapped in the local minimum, so the optimal initial learning rate for the proposed CBAM_UNet model training is 0.001. When the batch size is selected as 8, the network model still has large local fluctuations after leveling off, while the network model with batch size 16 has less fluctuation in classification accuracy after leveling off.

Based on the sensitivity test of the model, we can derive the sensitivity analysis of this experiment for model training: the optimal parameters for its hyperparameter learning rate and batch size are learning rate 0.001 and batch size 16. According to the hyperparameters, it can be concluded the extraction accuracy urban built-up area in 2020.

Among the 34 provinces, Shanghai has the highest F1 value of 0.8095, followed by Guangdong, Taiwan, and Beijing, all of which have F1 values greater than 0.70. Eighteen provinces have F1 values in the range of 0.60–0.70, including Jiangsu, Sichuan, and Fujian. The remaining 12 provinces have F1 values below 0.60. Overall, the image segmentation accuracy is higher in economically developed regions.

To compare the differences between the areas extracted by the four models and Ground Truth, we selected three cities with GDP greater than 1 in 2012: Beijing, Shanghai, Guangzhou, three cities with GDP between 0.1 and 1 in 2012: Chengdu, Zhengzhou, Changchun, and two cities with GDP less than 0.1 in 2012: Haikou, Xining, tracking their urban built-up area variation over the past decade. As shown in **Figure 6**.

We can see that for the eight cities, the area extracted by traditional machine learning algorithms is larger than that extracted by ground truth, especially SVM, which shows that traditional machine learning algorithms have more misclassifications and fewer wrong classification areas, which is consistent with our conclusion that the recall value of the classification accuracy is larger and the precision is smaller; for the deep learning model, the area extracted by the two models is smaller than the area extracted by the ground truth, which is also consistent with the precision value we obtained for

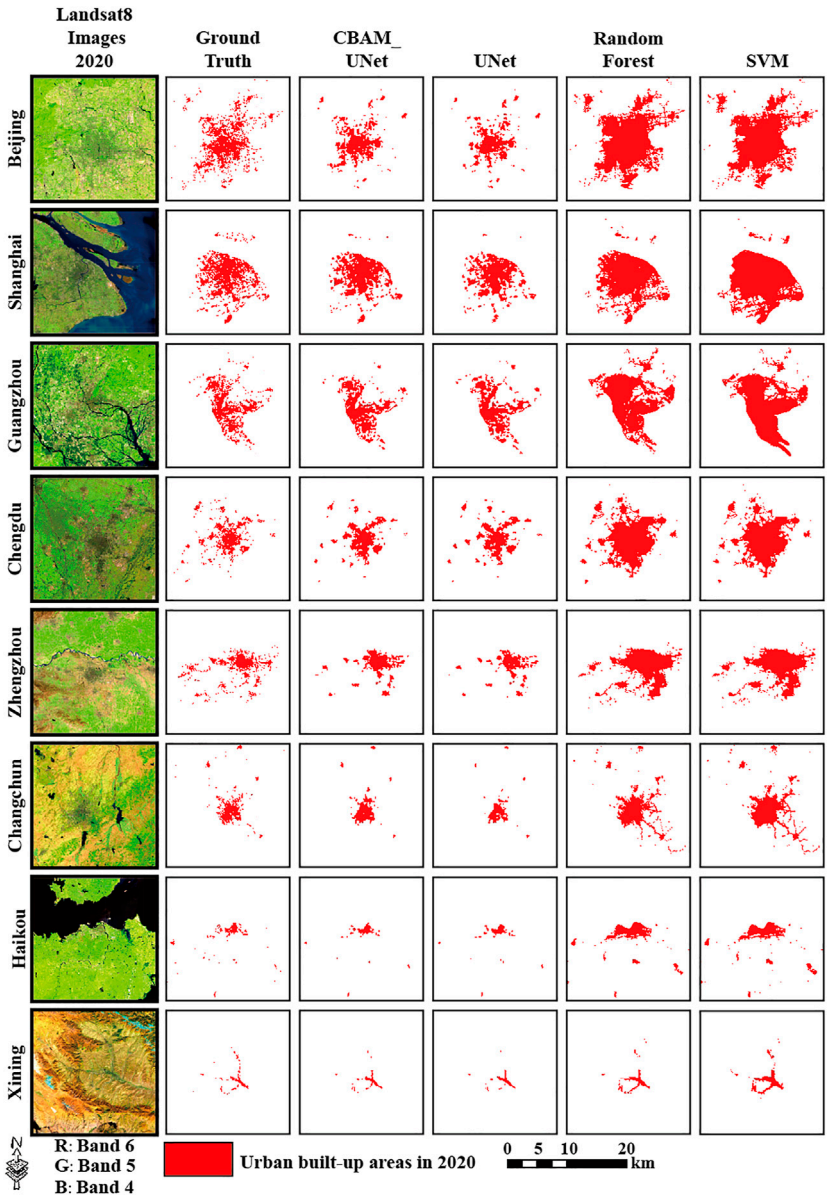

FIGURE 6 | Accuracy assessment using ground truth.

its classification accuracy greater than its recall value. Meanwhile, the area of our proposed CBAM_UNet model is the closest to the ground truth, which also shows that our model has higher accuracy.

Also, we validated the accuracy of the model in 34 provinces in China. Except CBAM_UNet proposed in this article, we also used standard UNet, RF, and SVM, three models to extract China's urban built-up areas in 2020. To ensure the objectivity of the result comparison, the loss function, optimizer, and training parameters of standard UNet were the same as the method proposed in this article. The various accuracy indicators proposed in the previous section were calculated by comparing the label data in 2020 with the image segmentation results obtained by the four models. The results are shown in **Table 3**.

As shown in **Table 3**, the average OA value of CBAM_UNet is 0.9969, *p* value is 0.7454, R value is 0.6016, F1 value is 0.6658, and mIoU value is 0.7480; the average OA value of UNet is 0.9969, *p* value is 0.7655, R value is 0.5512, F1 value is 0.6409, and mIoU value is 0.7342; the average OA value of RF is 0.9944, *p* value is 0.3573, R value is 0.8452, F1 value is 0.5023, and mIoU value is 0.6648; the average OA value of SVM is 0.9943, *p* value is 0.3542, R value is 0.8567, F1 value is 0.5012, and mIoU value is 0.6643. In the method proposed in this article, except the *p* value is slightly lower than the standard UNet (0.7655), the other four indicators are better than or equal to the standard UNet, RF, and SVM. Compared with traditional machine learning (RF and SVM), this model has a

TABLE 3 | Accuracy assessment of urban built-up area results.

Province	CBAM_UNet					UNet					RF					SVM				
	OA	Precision	Recall	F1	mIoU	OA	Precision	Recall	F1	mIoU	OA	Precision	Recall	F1	mIoU	OA	Precision	Recall	F1	mIoU
Heilongjiang	**0.9966**	0.8754	0.4468	**0.5917**	**0.7084**	0.9963	**0.9199**	0.3634	0.5210	0.6743	0.9933	0.4332	0.7217	0.5414	0.6822	0.9920	0.3911	**0.8058**	0.5266	0.6747
Xinjiang	**0.9990**	**0.6016**	0.4824	**0.5354**	**0.6823**	0.9989	0.5884	0.4762	0.5264	0.6781	0.9978	0.3127	0.6385	0.4198	0.6317	0.9971	0.2634	**0.7230**	0.3862	0.6182
Shanxi	0.9900	0.7312	0.5575	**0.6326**	**0.7263**	**0.9901**	**0.8031**	0.4786	0.5997	0.7092	0.9676	0.3040	**0.8436**	0.4469	0.6275	0.9702	0.3211	0.8277	0.4627	0.6354
Ningxia	0.9886	0.7073	0.4899	**0.5788**	**0.6979**	**0.9888**	**0.7335**	0.4725	0.5748	0.6960	0.9829	0.4720	0.6154	0.5343	0.6736	0.9783	0.3966	**0.6835**	0.5019	0.6566
Tibet	**0.9999**	0.4080	0.4090	**0.4085**	**0.6283**	**0.9999**	**0.4111**	0.3691	0.3890	0.6207	0.9997	0.1810	0.7880	0.2944	0.5861	0.9996	0.1465	**0.8628**	0.2505	0.5714
Shandong	**0.9559**	0.7953	0.5080	**0.6200**	**0.7017**	0.9525	**0.8572**	0.3960	0.5417	0.6613	0.9198	0.4612	**0.7860**	0.5813	0.6624	0.9241	0.4778	0.7689	0.5894	0.6688
Henan	0.9769	0.7372	0.5660	**0.6403**	**0.7237**	**0.9773**	**0.7998**	0.5020	0.6168	0.7114	0.9503	0.4071	0.8065	0.5411	0.6598	0.9496	0.4034	**0.8097**	0.5385	0.6582
Jiangsu	0.9445	0.7533	0.6236	**0.6823**	**0.7294**	**0.9459**	**0.7969**	0.5817	0.6725	0.7247	0.8529	0.3855	0.9095	0.5415	0.6051	0.8508	0.3832	**0.9218**	0.5413	0.6038
Anhui	0.9843	0.6629	0.6616	**0.6623**	**0.7395**	**0.9854**	**0.7245**	0.6039	0.6587	0.7382	0.9483	0.2955	**0.8792**	0.4423	0.6156	0.9521	0.3115	0.8725	0.4591	0.6245
Hubei	0.9891	0.6463	0.6077	**0.6264**	**0.7225**	**0.9897**	**0.6973**	0.5584	0.6202	0.7195	0.9709	0.3196	0.8311	0.4617	0.6353	0.9718	0.3277	**0.8327**	0.4703	0.6394
Zhejiang	0.9634	0.7111	0.6658	0.6877	0.7430	**0.9647**	**0.7325**	0.6556	**0.6919**	**0.7461**	0.8898	0.3466	0.9289	0.5048	0.6104	0.8857	0.3420	**0.9627**	0.5047	0.6081
Jiangxi	0.9904	0.6254	0.6069	**0.6160**	**0.7177**	**0.9908**	**0.6569**	0.5699	0.6103	0.7150	0.9794	0.3613	0.8250	0.5025	0.6573	0.9802	0.3717	**0.8269**	0.5129	0.6624
Hunan	**0.9926**	0.6595	0.6594	**0.6594**	**0.7422**	**0.9926**	**0.6763**	0.6189	0.6464	0.7350	0.9818	0.3627	**0.8756**	0.5129	0.6633	0.9821	0.3668	0.8737	0.5167	0.6652
Yunnan	**0.9970**	0.6828	0.6009	**0.6392**	**0.7334**	**0.9970**	**0.7021**	0.5749	0.6321	0.7296	0.9897	0.2845	0.8720	0.4290	0.6314	0.9895	0.2807	**0.8805**	0.4257	0.6299
Guizhou	**0.9947**	0.5070	0.4982	**0.5026**	**0.6651**	**0.9947**	**0.5131**	0.4512	0.4802	0.6553	0.9825	0.2210	0.8894	0.3540	0.5987	0.9813	0.2130	**0.9137**	0.3454	0.5950
Fujian	**0.9823**	**0.6515**	0.6073	**0.6286**	**0.7202**	0.9820	0.6449	0.6003	0.6218	0.7164	0.9441	0.3007	**0.9534**	0.4572	0.6196	0.9476	0.3142	0.9488	0.4721	0.6277
Guangxi	0.9940	0.6352	0.6418	**0.6385**	**0.7315**	**0.9942**	**0.6563**	0.6140	0.6344	0.7294	0.9839	0.3216	0.8649	0.4688	0.6450	0.9831	0.3119	**0.8800**	0.4606	0.6411
Guangdong	**0.9752**	**0.7653**	0.7521	**0.7586**	**0.7926**	0.9745	0.7481	0.7670	0.7574	0.7915	0.9156	0.3777	0.9667	0.5432	0.6420	0.9151	0.3774	**0.9764**	0.5444	0.6423
Hainan	**0.9914**	**0.7284**	0.5082	**0.5987**	**0.7093**	0.9910	0.7052	0.5020	0.5865	0.7030	0.9438	0.1740	0.9152	0.2924	0.5572	0.9455	0.1790	**0.9208**	0.2998	0.5606
Jilin	**0.9946**	0.8317	0.5465	**0.6595**	**0.7433**	0.9942	**0.8930**	0.4480	0.5966	0.7097	0.9879	0.4322	0.8247	0.5671	0.6918	0.9850	0.3779	**0.8658**	0.5262	0.6709
Liaoning	**0.9858**	0.8266	0.5110	**0.6316**	**0.7236**	0.9847	**0.8933**	0.4025	0.5549	0.6843	0.9707	0.4391	0.8443	0.5777	0.6881	0.9687	0.4224	**0.8612**	0.5668	0.6818
Tianjin	**0.9091**	0.7964	0.6171	**0.6954**	**0.7158**	0.9026	**0.8549**	0.5068	0.6364	0.6801	0.7742	0.4210	**0.9137**	0.5764	0.5690	0.7918	0.4418	0.9033	0.5933	0.5882
Qinghai	**0.9995**	0.6187	0.3703	**0.4633**	**0.6505**	**0.9995**	**0.6381**	0.3393	0.4430	0.6421	0.9991	0.2769	0.4924	0.3544	0.6072	0.9988	0.2422	**0.5697**	0.3398	0.6018
Gansu	0.9976	0.7017	0.4026	0.5116	0.6707	**0.9977**	**0.7132**	0.4156	**0.5252**	**0.6769**	0.9953	0.3583	0.6549	0.4632	0.6484	0.9948	0.3372	**0.7108**	0.4574	0.6457
Shaanxi	0.9931	0.6883	0.5997	**0.6410**	**0.7324**	**0.9933**	**0.7196**	0.5663	0.6338	0.7286	0.9805	0.3264	0.8538	0.4723	0.6447	0.9770	0.2925	**0.8828**	0.4394	0.6292
Neimenggu	**0.9985**	0.8084	0.4733	**0.5970**	**0.7120**	0.9984	**0.8643**	0.4042	0.5508	0.6893	0.9970	0.4154	0.6212	0.4979	0.6642	0.9968	0.3983	**0.7284**	0.5150	0.6718
Chongqing	**0.9895**	**0.5221**	0.6750	**0.5888**	**0.7033**	**0.9895**	0.5212	0.6711	0.5867	0.7023	0.9627	0.2240	0.9562	0.3630	0.5920	0.9636	0.2288	**0.9595**	0.3695	0.5949
Hebei	**0.9707**	0.8512	0.3965	**0.5410**	**0.6705**	0.9690	**0.9094**	0.3200	0.4734	0.6393	0.9500	0.4492	**0.6452**	0.5296	0.6544	0.9526	0.4678	0.6260	0.5355	0.6585
Shanghai	**0.8635**	0.8461	0.7759	**0.8095**	**0.7438**	0.8596	**0.8680**	0.7364	0.7968	0.7342	0.7624	0.6187	0.9500	0.7493	0.6154	0.6444	0.5127	**0.9847**	0.6743	0.4729
Beijing	**0.9305**	0.8530	0.6087	**0.7104**	**0.7374**	0.9292	**0.8870**	0.5669	0.6917	0.7259	0.8131	0.4262	**0.9664**	0.5915	0.6019	0.8204	0.4360	0.9629	0.6003	0.6106
Taiwan	**0.9694**	**0.7209**	0.7396	0.7302	0.7715	0.9693	0.7057	0.7760	**0.7391**	**0.7771**	0.7593	0.1886	0.9993	0.3173	0.4668	0.7612	0.1898	**0.9994**	0.3190	0.4684
Hong Kong	0.9404	0.8796	0.5250	0.6575	0.7133	**0.9463**	**0.9071**	0.5649	**0.6962**	**0.7384**	0.6804	0.2537	0.9960	0.4044	0.4475	0.4622	0.1682	**0.9980**	0.2879	0.2824
Macao	**0.8824**	**0.6500**	0.6300	**0.6398**	**0.6752**	0.8137	0.6231	0.5482	0.5833	0.4309	0.6311	0.0556	0.3000	0.0938	0.2317	0.3627	0.1333	**1.0000**	0.2353	0.2134
Sichuan	0.9963	0.6362	0.6763	0.6556	0.7420	**0.9964**	**0.6520**	0.6625	**0.6572**	**0.7429**	0.9856	0.2561	**0.9322**	0.4018	0.6185	0.9858	0.2579	0.9315	0.4040	0.6194
total	**0.9969**	0.7454	0.6016	**0.6658**	**0.7480**	**0.9969**	**0.7655**	0.5512	0.6409	0.7342	0.9944	0.3573	0.8452	0.5023	0.6648	0.9943	0.3542	**0.8567**	0.5012	0.6643

The bold values in table highlight the optimal values for each precision indicator when extracted from each province and for the total urban built-up areas.

TABLE 4 | Expansion of urban built-up areas in all provinces from 2012 to 2021.

Province	Urban built-up areas in 2012		Urban built-up areas in 2021		Urban built-up areas expansion from 2012 to 2021	
	Area (km^2)	Percentage (%)	Area (km^2)	Percentage (%)	Area (km^2)	Growth percentage (%)
Heilongjiang	1006.5	1.97	1225.25	1.57	218.75	0.81
Xinjiang	738.5	1.45	1497	1.92	758.5	2.80
Shanxi	1201.5	2.36	1761.25	2.26	559.75	2.07
Ningxia	326	0.64	496.5	0.64	170.5	0.63
Tibet	64.25	0.13	111.5	0.14	47.25	0.17
Shandong	3,868.75	7.59	6,208.25	7.95	2,339.5	8.64
Henan	2,659.25	5.22	4,295.25	5.50	1636	6.04
Jiangsu	5,399.5	10.59	7,072.25	9.06	1672.75	6.18
Anhui	1897.25	3.72	3,214.75	4.12	1317.5	4.87
Hubei	1391.25	2.73	2,492.25	3.19	1101	4.07
Zhejiang	3,346.25	6.56	5,288.25	6.78	1942	7.17
Jiangxi	970	1.90	2047	2.62	1077	3.98
Hunan	1258.75	2.47	2,249.75	2.88	991	3.66
Yunnan	946	1.86	1625.5	2.08	679.5	2.51
Guizhou	384.5	0.75	958.5	1.23	574	2.12
Fujian	1655.5	3.25	3,040	3.89	1384.5	5.11
Guangxi	998	1.96	2,212	2.83	1214	4.48
Guangdong	**7,174.5**	**14.07**	**10,221.25**	**13.10**	**3,046.75**	**11.25**
Hainan	241.25	0.47	387.25	0.50	146	0.54
Jilin	817.25	1.60	1061	1.36	243.75	0.90
Liaoning	1514.25	2.97	1881.5	2.41	367.25	1.36
Tianjin	1079	2.12	1266.25	1.62	187.25	0.69
Qinghai	141.25	0.28	208.25	0.27	67	0.25
Gansu	383	0.75	676.75	0.87	293.75	1.09
Shaanxi	1161	2.28	1724.75	2.21	563.75	2.08
Neimenggu	904	1.77	1457.25	1.87	553.25	2.04
Chongqing	664.5	1.30	1375.5	1.76	711	2.63
Hebei	1867.25	3.66	3,287	4.21	1419.75	5.24
Shanghai	1843.25	3.62	1953.5	2.50	110.25	0.41
Beijing	1194.75	2.34	1447.25	1.85	252.5	0.93
Taiwan	2,128.5	4.18	2,269.5	2.91	141	0.52
Hong Kong	83.25	0.16	83.75	0.11	0.5	0.00
Macao	12.5	0.02	14.5	0.02	2	0.01
Sichuan	1660.25	3.26	2,944	3.77	1283.75	4.74
Total	50,981.5	100.00	78,054.5	100.00	27,073	100.00

The bold values in table highlight the values with the largest area and percentage of urban built-up areas in 2012 and 2020 for each province and the values with the largest increase in urban built-up areas and percentage of built-up areas from 2012 to 2020.

reduction in R value, which means the omitted urban built-up areas have increased, but the significant improvement in p value is useful for analyzing the changes of urban built-up areas over a period. Excessive misclassification of RF and SVM models will lead to overestimating urban built-up areas each year, thus weakening inter-annual growth.

TABLE 5 | Comparison of extracted areas to statistical data.

Year	CBAM_UNet (km^2)	Statistical_data (km^2)	Relative error (%)
2012	48,757.25	45,565.90	7.00
2015	54,964.75	52,102.60	5.49
2018	66,446.50	58,455.70	13.67

4.1.2 The Extraction Results of Urban Built-Up Areas in China From 2012 to 2020

We used the calibrated model for extracting urban built-up areas, and the proposed built-up areas for 2012 to 2020 are shown in **Table 4** as follows.

On a province scale: Guangdong has the largest urban built-up areas, with 10,221.25 km^2 in 2021, making it the only province with over 10000 km^2, followed by Jiangsu, Shandong, and Zhejiang, which have urban built-up areas over 5000 km^2. Hong Kong and Macau have the smallest urban built-up areas, especially due to their small administrative districts. In addition, urban built-up areas of Tibet, Qinghai, Hainan, and Ningxia are less than 500 km^2, relatively smaller than other provinces.

From the above **Table 4**, it is worth noting that we can conclude that Guangdong, Shandong, Zhejiang, Jiangsu, and Henan have the largest growth area. Since 2011, these five provinces have introduced a series of policies that encourage farmers to buy houses in cities, providing preferential loans to promote the "citizenization" of migrant workers. The demand for

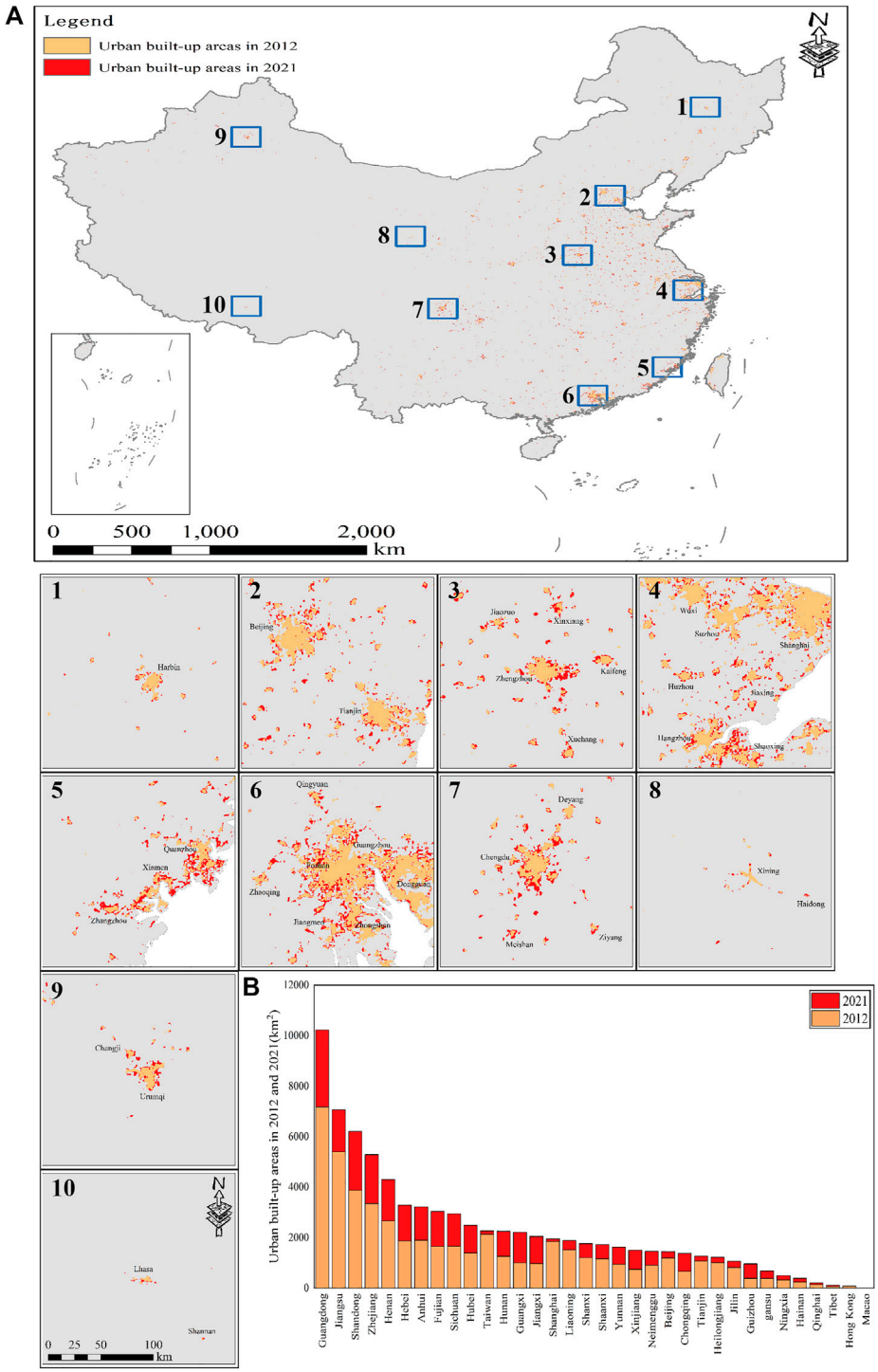

FIGURE 7 | Expansion of urban built-up areas in China from 2012 to 2021. **(A)** Expansion of urban built-up areas in some cities (including developed, moderately developed, and underdeveloped). **(B)** Urban built-up area expansion by provinces.

commercial housing in cities has increased, which has also led to the expansion of urban built-up areas. Therefore, the relationship between urban built-up area expansion and population geography is also particularly close.

On the other hand, we compared the built-up area extracted by the corrected CBAM_UNet with the built-up area data obtained from the National Bureau of Statistics' China Statistical Yearbook (stats.gov.cn) in 2012, 2015, and 2018 (excluding Hong Kong,

TABLE 6 | Expansion of China's urban built-up areas from 2012 to 2021.

Period	Expansion area (km^2)	Expansion speed (km^2/year)	Expansion intensity (%)
2012–2015	6,364.75	2,121.58	4.16
2015–2018	**11,562**	**3,854.00**	**6.72**
2018–2021	9,146.25	3,048.75	4.42
2012–2021	27,073	3,008.11	5.90

The bold values in table highlight the values with the largest increase in the Expansion area, Expansion speed, and Expansion intensity in the three periods.

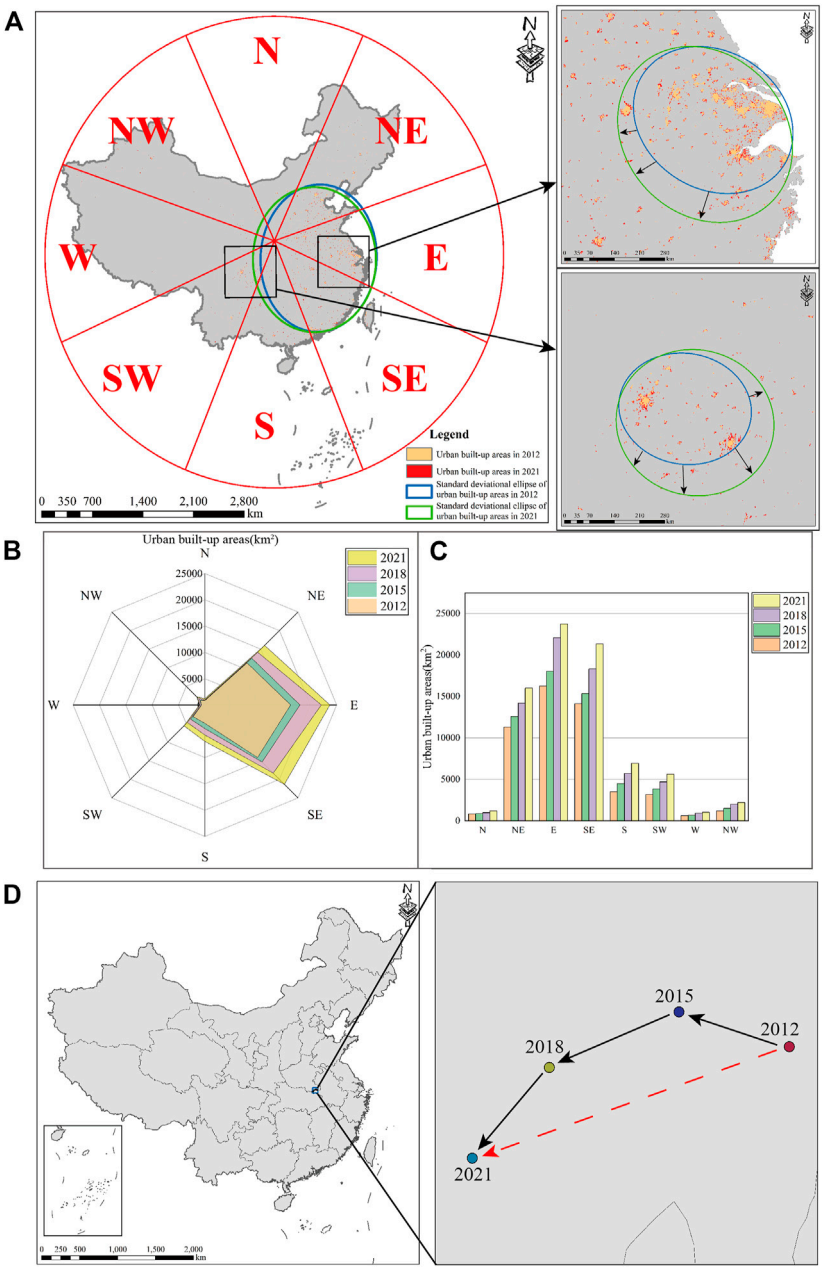

FIGURE 8 | (A–C) Expansion of urban built-up areas in all orientations from 2012 to 2021. **(D)** Gravity center migration of China's urban built-up areas, 2012–2021.

TABLE 7 | Urban built-up areas in all orientations from 2012 to 2021.

Orientation	2012	2015			2018			2021			Total changes	
	Area (km^2)	Area (km^2)	Growth area (km^2)	Growth rate (%)	Area (km^2)	Growth area (km^2)	Growth rate (%)	Area (km^2)	Growth area (km^2)	Growth rate (%)	Growth area (km^2)	Growth rate (%)
N	831.50	879.25	47.75	5.74	987.00	107.75	12.25	1206.25	219.25	**22.21**	374.75	45.07
NE	11,300.75	12,572.75	1272	11.26	14,171.50	1598.75	12.72	16,016.25	1844.75	13.02	4,715.5	41.73
E	**16,259.00**	**18,032.50**	**1773.5**	10.91	**22,092.00**	**4,059.5**	22.51	**23,719.00**	1627	7.36	**7,460**	45.88
SE	14,130.00	15,344.50	1214.5	8.60	18,324.00	2,979.5	19.42	21,327.00	**3,003**	16.39	7,197	50.93
S	3,491.50	4,496.00	1004.5	**28.77**	5,718.25	1222.25	27.19	6,931.75	1213.5	21.22	3,440.25	**98.53**
SW	3,166.75	3,834.25	667.5	21.08	4,706.25	872	22.74	5,618.75	912.5	19.39	2,452	77.43
W	618.25	684.50	66.25	10.72	926.50	242	**35.35**	1028.00	101.5	10.96	409.75	66.28
NW	1183.75	1502.50	318.75	26.93	1982.75	480.25	31.96	2,207.50	224.75	11.34	1023.75	86.48

The bold values in table highlight the maximum values of urban built-up areas, percentage and growth rate for each orientation in 2012, 2015, 2018, and 2021.

Macau, and Taiwan, and 2021 data not yet available); results are shown in **Table 5**.

By comparison, we can see that the area we extracted can achieve more than 85% accuracy without labels, proving that our model has strong generalization ability and can also ensure a certain accuracy. Then, we can also be seen that the area we extracted is generally larger than the area of the statistical yearbook, indicating that there is a certain misclassification in our model.

To more intuitively see the expansion in the built-up area from 2012 to 2020, we compared the urban built-up areas in 2012 with the urban built-up areas in 2021 and obtained the figure as shown in **Figure 7**.

During the study period, there were 12 provinces with a growth of urban built-up areas over 1000 km^2, and Guangdong has the most significant growth area, with an increase of 3,046.75 km^2, accounting for 11.25% of China's urban built-up areas growth. From a geographical point of view, these provinces are primarily found in the east and southeast of the country. There are nine provinces with the growth of urban built-up areas of less than 200 km^2, except for Tibet, Hainan, and Ningxia. The others are provinces with relatively developed economies and high-level of urbanization. Their limited constructible space leads to less growth (**Table 4**).

4.2 Spatial-Temporal Variation Analysis of China's Urban Built-Up Areas

4.2.1 Spatial Variation Analysis

- Expansion speed and intensity

China has experienced fast urbanization and economic growth in the past decade. Urban built-up areas had increased from 50,981.5 km^2 in 2012 to 78,054.5 km^2 in 2021, an increase of 27,073 km^2, increased by 53.10% (**Table 4**) and calculated the expansion speed and intensity of urban built-up areas by period (**Eqs 10,11**) . The expansion speed in 2015–2018 was higher than that of 2012–2015 and 2018–2021, indicating that the speed of urban construction in China had increased and then had slowed down in the past decade, and the expansion intensity also had changed, from 4.16% in 2012–2015 to 6.72% in 2015–2018, and then slowed down to 4.42%, but overall, China's urban built-up areas had consistently expanded at a high rate over the past 10 years (**Table 6**).

4.2.2 Temporal Variation Analysis

- Expansion Directions

The spatial quadrant orientation method was used to calculate the expansion in urban built-up areas of each region in China during the study period, with the center set at 34°32′27.00″N and 108°55′25.00″E. We divide China into north (N), northeast (NE), east (E), southeast (SE), south (S), southwest (SW), west (W), and northwest (NW) through eight quadrants (**Figure 8A**). The urban built-up area images in 2012, 2015, 2018, and 2021 were, respectively, divided into eight orientations through the spatial quadrant orientation method and counted the information of urban built-up areas of each quadrant in each (**Figures 8B,C**; **Table 7**).

The results show that in 2021, the E orientation has the largest urban built-up areas of all orientations, with areas of 23719 km^2. The W orientation has the smallest urban built-up areas of all orientations, only 1028 km^2.

During the study period, the E orientation urban built-up areas increased the most, from 16,259.00 km^2 in 2012 to 23,719.00 km^2 in 2021, an increase of 7460 km^2, increased by 45.88%. N orientation increased the least, by only 374.75 km^2, but with a growth rate of 45.07%. The fastest growth rate was in the S orientation, where urban built-up areas in 2021 have increased by 98.53% compared to 2012 and high during the study period (**Table 7**).

We can conclude that the distribution of urban built-up areas gradually showed a scattered trend. Jiangsu, Zhejiang, and Shanghai have formed a trend of group development with Anhui. Meanwhile, the urban built-up areas between Chengdu and Chongqing have gradually spread and connected. After 2018, the spread and integration in Chengdu and Chongqing have been further strengthened. At the same time, Henan, Anhui, and northern Jiangxi have gradually connected to Jiangsu, Zhejiang, and Shanghai.

To represent the expansion direction more intuitively, we used the standard ellipse difference to visualize the expansion direction according to the expansion area from 2012 to 2020. From **Figure 8A**, we can see that, generally, the distribution pattern of China's urban built-up areas has gradually migrated from the "center-periphery" distribution around the growth pole to a networked distribution pattern, showing a trend from agglomeration to dispersion, which is satisfied by the "center-periphery" theory proposed by J.R.

Fridemna: from the center of the North-South-Guangzhou triangle in 2012, we gradually migrated to the North-South-Guangzhou-Chengdu-Chongqing economic zone. At the same time, we selected regions from the North-South-Guangdong and Chengdu-Chongqing economic zones, respectively, and their local trends are also "center-periphery," which also satisfies the "center-periphery" theory proposed by J.R. Fridemna.

- Gravity Center Migration

We calculated the center of gravity for 2012–2020 based on the center of gravity migration index proposed earlier, as shown in **Figure 8D**.

As we can see, the gravity center of China's urban built-up areas has migrated to the southwest in the past decade, with a linear migration distance of 60.82 km, including 57.37 km to the west and 20.21 km to the south. The results show that China's support policies for the west impact the gravity center of urban built-up areas.

Generally, the analysis results show that China's urban built-up areas have been overgrowing in recent years, but the development in various orientations is quite different. The main growth orientations of urban built-up areas are E and SE; the sum of increased areas in these two orientations exceeds 50% of China's urban built-up areas, which are the two regions with the fastest urbanization in China. The increase in the urban built-up areas in W and N is less than 500 km^2, accounting for 1.51% and 1.38% of the increase in China's urban built-up areas, respectively. With a large disparity with other orientations, especially because there are fewer cities in these two orientations, but in terms of growth speed, these two orientations have grown fast. Overall, the degree of urbanization in the economically developed regions is higher, and the economically underdeveloped regions are currently chasing.

5 CONCLUSION

In this article, CBAM_UNet deep semantic segmentation network was built, which combined NTL data and NDVI data to realize the automatic extraction of long-time series in China's urban built-up areas and analyze the spatial and temporal expansion changes of China's urban built-up areas over the past 10 years. The results show the following:

1) We selected the UNet model in the field of biomedical segmentation and added the CBAM attention module into the encoder part of UNet to build CBAM_UNet; the model can merge multiple features. Then the NTL data were merged with NDVI data, and taking the 2020 WorldCover as the sample data, we assigned a semantic label to each pixel in the image, realizing end-to-end, pixel-level classification of remote sensing images. [not available in Crossref]
2) Compared with other models, CBAM_UNet shows higher accuracy, the F1 value is 0.6658, and the mIoU value is 0.7480. In addition, through the calibrated CBAM_UNet, the experiment automatically extracted China's urban built-up areas in 2012, 2015, 2018, and 2021, saving a lot of workforce and time. Thus, the model can realize the annual urban built-up areas extraction in China by combining annual NTL data and NDVI data, which provides a feasible method for long-time series change analysis. [not available in Crossref]
3) Based on urban built-up areas extracted from the calibrated CBAM_UNet model in 2012, 2015, 2018, and 2021, the spatial and temporal expansion of China's urban built-up areas was analyzed from four indicators: expansion speed, expansion intensity, expansion direction, and gravity center migration. China's urban built-up area expansion speed in 2015–2018 was higher than that of 2012–2015 and 2018–2021, indicating that China's urban construction speed increased first and then slowed down in the past decade; the expansion intensity increased from 4.16% in 2012–2015 to 6.72% in 2015–2018 and then slowed down to 4.42%. However, overall, China's urban built-up areas have consistently expanded at a high rate over the past 10 years. From the view of expansion direction: the E orientation urban built-up areas have increased the most, from 16,259.00 km2 in 2012 to 23,719.00 km2 in 2021, an increase of 7460 km2, increased by 45.88%. Urban built-up areas in the N orientation increased the least, by only 374.75 km^2, but with a growth rate of 45.07%. The gravity center of China's urban built-up areas migrated to the southwest, with a linear migration distance of 60.82 km, including 57.37 km to the west and 20.21 km to the south. The results show that China's support policies for the west impact the gravity center of urban built-up areas.

The CBAM_UNet model proposed in this experiment can quantitatively and accurately extract urban built-up areas in a long-time series. The findings of this article would help understand the spatial and temporal expansion of urban built-up areas. Such an understanding would help analyze China's urban development changes in the past 10 years in a relatively macroscopic manner and provide specific scientific decision-making for China's economic development.

DATA AVAILABILITY STATEMENT

The original contributions presented in the study are included in the article/supplementary material; further inquiries can be directed to the corresponding author.

AUTHOR CONTRIBUTIONS

MB contributed to the methodology, design of the study, and writing—original draft; SZ contributed to the methodology, writing, checking and editing, and project administration; XW contributed to the methodology and software usage; YF contributed to the data analysis; JW contributed to project administration; PP contributed to conception and funding acquisition.

FUNDING

The research was supported by The Second Tibetan Plateau Scientific Expedition and Research Program (STEP), China (No. 2019QZKK0301); the program of Census of Forest Germplasm

Resources in Chenghua District, Chengdu (No. 80303-AHL038); and the Second National Survey of Key Protected Wild Plant Resources–Special Survey of Orchidaceae in Sichuan Province (No. 80303-AZZ003).

REFERENCES

Bramhe, V. S., Ghosh, S. K., and Garg, P. K. (2020). Extraction of Built-Up Areas from Landsat-8 OLI Data Based on Spectral-Textural Information and Feature Selection Using Support Vector Machine Method. *Geocarto Int.* 35, 1067–1087. doi:10.1080/10106049.2019.1566406

Chen, J., Chen, J., Liao, A., Cao, X., Chen, L., Chen, X., et al. (2015). Global Land Cover Mapping at 30m Resolution: A POK-Based Operational Approach. *ISPRS J. Photogrammetry Remote Sens.* 103, 7–27. doi:10.1016/j.isprsjprs.2014.09.002

Elvidge, C., Ziskin, D., Baugh, K., Tuttle, B., Ghosh, T., Pack, D., et al. (2009). A Fifteen Year Record of Global Natural Gas Flaring Derived from Satellite Data. *Energies* 2, 595–622. doi:10.3390/en20300595

Gong, P., Wang, J., Yu, L., Zhao, Y., Zhao, Y., Liang, L., et al. (2013). Finer Resolution Observation and Monitoring of Global Land Cover: First Mapping Results with Landsat TM and ETM+ Data. *Int. J. Remote Sens.* 34, 2607–2654. doi:10.1080/01431161.2012.748992

He, X., Zhou, C., Zhang, J., and Yuan, X. (2020). Using Wavelet Transforms to Fuse Nighttime Light Data and POI Big Data to Extract Urban Built-Up Areas. *Remote Sens.* 12, 3887–3920. doi:10.3390/rs12233887

Holben, B. N. (1986). Characteristics of Maximum-Value Composite Images from Temporal AVHRR Data. *Int. J. Remote Sens.* 7, 1417–1434. doi:10.1080/01431168608948945

Hu, Y., Kong, X., Zheng, J., Sun, J., Wang, L., and Min, M. (2018). Urban Expansion and Farmland Loss in Beijing during 1980-2015. *Sustainability* 10, 3927–4020. doi:10.3390/su10113927

Jiang, C., Miao, Y., and Xi, Z. (2021a). A New Method of Extracting Built-Up Area Based on Multi-Source Remote Sensing Data: a Case Study of Baoding Central City, China. *Geocarto Int.* 0, 1–13. doi:10.1080/10106049.2021.1933214

Jiang, W., Li, T., Li, Q., Wu, S., Zhou, Y., and Lu, L. (2021b). Spatial and Temporal Characteristics of Urban Sprawl in Northern Anhui Based on Multi- Temporal Remote Sensing Images—A Case Study of Fuyang City , Anhui Province. *Resour. Dev. Markct* 37, 780. doi:10.3969/j.issn.1005-8141.2021.07.003

Ju, Y., Dronova, I., Ma, Q., and Zhang, X. (2017). Analysis of Urbanization Dynamics in Mainland China Using Pixel-Based Night-Time Light Trajectories from 1992 to 2013. *Int. J. Remote Sens.* 38, 6047–6072. doi:10.1080/01431161.2017.1302114

Karim, F., Majumdar, S., Darabi, H., and Harford, S. (2019). Multivariate LSTM-FCNs for Time Series Classification. *Neural Netw.* 116, 237–245. doi:10.1016/j.neunet.2019.04.014

Kaur, A., Kaur, L., and Singh, A. (2021). GA-UNet: UNet-Based Framework for Segmentation of 2D and 3D Medical Images Applicable on Heterogeneous Datasets, *Neural Comput. Applic* 33, 14991–15025. doi:10.1007/s00521-021-06134-z

Kearney, V., Chan, J. W., Wang, T., Perry, A., Yom, S. S., and Solberg, T. D. (2019). Attention-enabled 3D Boosted Convolutional Neural Networks for Semantic CT Segmentation Using Deep Supervision. *Phys. Med. Biol.* 64, 135001. doi:10.1088/1361-6560/ab2818

Kingma, D. P., and Ba, J. L. (2015). Adam: A Method for Stochastic Optimization. *3rd Int. Conf. Learn. Represent. ICLR 2015 - Conf. Track Proc.* 1–15.

Li, F., Yan, Q., Bian, Z., Liu, B., and Wu, Z. (2020). A Poi and Lst Adjusted Ntl Urban Index for Urban Built-Up Area Extraction. *Sensors* 20, 2918. doi:10.3390/s20102918

Li, J., Fang, W., Wang, T., Qureshi, S., Alatalo, J., and Bai, Y. (2017a). Correlations between Socioeconomic Drivers and Indicators of Urban Expansion: Evidence from the Heavily Urbanised Shanghai Metropolitan Area, China. *Sustainability* 9, 1199. doi:10.3390/su9071199

Li, M., Hu, B., and Ling, Z. (2021). Analysis of Spatial and Temporal Expansion Characteristics of Built-Up Area in Nanning City in Recent 30 Years. *Pop. Sci. Technol.* 24, 22

Li, X., Li, D., Xu, H., and Wu, C. (2017b). Intercalibration between DMSP/OLS and VIIRS Night-Time Light Images to Evaluate City Light Dynamics of Syria's Major Human Settlement during Syrian Civil War. *Int. J. Remote Sens.* 38, 5934–5951. doi:10.1080/01431161.2017.1331476

Li, X., and Zhou, Y. (2017). Urban Mapping Using DMSP/OLS Stable Night-Time Light: a Review. *Int. J. Remote Sens.* 38, 6030–6046. doi:10.1080/01431161.2016.1274451

Liu, C., Yang, K., Bennett, M. M., Guo, Z., Cheng, L., and Li, M. (2019). Automated Extraction of Built-Up Areas by Fusing VIIRS Nighttime Lights and Landsat-8 Data. *Remote Sens.* 11, 1571–1620. doi:10.3390/rs11131571

Liu, F., Zhang, Z., Shi, L., Zhao, X., Xu, J., Yi, L., et al. (2016). Urban Expansion in China and its Spatial-Temporal Differences over the Past Four Decades. *J. Geogr. Sci.* 26, 1477–1496. doi:10.1007/s11442-016-1339-3

Liu, J., Jiao, L., Dong, T., Xu, G., Zhang, B., and Yang, L. (2018). A Novel Measure Approach of Expansion Process of Urban Landscape:Multi-Order Adjacency Index. *Sci. Geogr. Sin.* 38, 1741–1749. doi:10.13249/j.cnki.sgs.2018.11.001

Liu, S., Wu, C., and Shen, H. (2000). A GIS Based Model of Urban Land Use Growth in Beijing. *Acta Geogr. Sin.* 55, 407

Liu, X., Dong, G., Wang, X., Xue, Z., Jiang, M., Lu, X., et al. (2013). Characterizing the Spatial Pattern of Marshlands in the Sanjiang Plain, Northeast China. *Ecol. Eng.* 53, 335–342. doi:10.1016/j.ecoleng.2012.12.071

Liu, Y., Zuo, R., and Dong, Y. (2021). Analysis of Temporal and Spatial Characteristics of Urban Expansion in Xiaonan District from 1990 to 2020 Using Time Series Landsat Imagery. *Remote Sens.* 13, 4299. doi:10.3390/rs13214299

Lu, D., Tian, H., Zhou, G., and Ge, H. (2008). Regional Mapping of Human Settlements in Southeastern China with Multisensor Remotely Sensed Data. *Remote Sens. Environ.* 112, 3668–3679. doi:10.1016/j.rse.2008.05.009

Ma, T. (2018). An Estimate of the Pixel-Level Connection between Visible Infrared Imaging Radiometer Suite Day/night Band (VIIRS DNB) Nighttime Lights and Land Features across China. *Remote Sens.* 10, 723–811. doi:10.3390/rs10050723

Ma, X., Tong, X., Liu, S., Luo, X., Xie, H., and Li, C. (2017). Optimized Sample Selection in SVM Classification by Combining with DMSP-OLS, Landsat NDVI and GlobeLand30 Products for Extracting Urban Built-Up Areas. *Remote Sens.* 9, 236. doi:10.3390/rs9030236

Milletari, F., Navab, N., and Ahmadi, S.-A. (2016). V-net: Fully Convolutional Neural Networks for Volumetric Medical Image Segmentation. *Proc. - 2016 4th Int. Conf. 3D Vis.* 3DV, 565–571. doi:10.1109/3DV.2016.79

Mithun, S., Sahana, M., Chattopadhyay, S., Johnson, B. A., Khedher, K. M., and Avtar, R. (2021). Monitoring Metropolitan Growth Dynamics for Achieving Sustainable Urbanization (Sdg 11.3) in kolkata Metropolitan Area, india. *Remote Sens.* 13, 4423. doi:10.3390/rs13214423

Mnih, V., Heess, N., Graves, A., and Kavukcuoglu, K. (2014). Recurrent Models of Visual Attention. *Adv. Neural Inf. Process. Syst.* 3, 2204

Navab, N., Hornegger, J., Wells, W. M., and Frangi, A. F. (2015). Medical Image Computing and Computer-Assisted Intervention - MICCAI 2015. *Lect. Notes Comput. Sci. Incl. Subser. Lect. Notes Artif. Intell. Lect. Notes Bioinforma.* 9351, 12–20. doi:10.1007/978-3-319-24574-4

Peng, D., Zhang, Y., and Guan, H. (2019). End-to-end Change Detection for High Resolution Satellite Images Using Improved UNet++. *Remote Sens.* 11, 1382. doi:10.3390/rs11111382

Shi, K., Yu, B., Huang, Y., Hu, Y., Yin, B., Chen, Z., et al. (2014). Evaluating the Ability of NPP-VIIRS Nighttime Light Data to Estimate the Gross Domestic Product and the Electric Power Consumption of China at Multiple Scales: A Comparison with DMSP-OLS Data. *Remote Sens.* 6, 1705–1724. doi:10.3390/rs6021705

Sun, J., Di, L., Sun, Z., Wang, J., and Wu, Y. (2020). Estimation of GDP Using Deep Learning with NPP-VIIRS Imagery and Land Cover Data at the County Level in CONUS. *IEEE J. Sel. Top. Appl. Earth Obs. Remote Sens.* 13, 1400–1415. doi:10.1109/JSTARS.2020.2983331

Tan, Y., Xiong, S., and Li, Y. (2018). Automatic Extraction of Built-Up Areas from Panchromatic and Multispectral Remote Sensing Images Using Double-Stream Deep Convolutional Neural Networks. *IEEE J. Sel. Top. Appl. Earth Obs. Remote Sens.* 11, 3988–4004. doi:10.1109/JSTARS.2018.2871046

Tan, Y., Xiong, S., Li, Z., Tian, J., and Li, Y. (2019). Accurate Detection of Built-Up Areas from High-Resolution Remote Sensing Imagery Using a Fully Convolutional Network. *Photogramm. Eng. Remote Sens.* 85, 737–752. doi:10.14358/PERS.85.10.737

Tan, Y., Xiong, S., and Yan, P. (2020). Multi-branch Convolutional Neural Network for Built-Up Area Extraction from Remote Sensing Image. *Neurocomputing* 396, 358–374. doi:10.1016/j.neucom.2018.09.106

Tianjun Xiao, T., Yichong Xu, Y., Kuiyuan Yang, K., Jiaxing Zhang, J., Yuxin Peng, Y., and Zhang, Z. (2015). The Application of Two-Level Attention Models in Deep Convolutional Neural Network for Fine-Grained Image Classification." in Proc. IEEE Comput. Soc. Conf. Comput. Vis. Pattern Recognit, 842–850. doi:10.1109/CVPR.2015.7298685

Wang, M., Song, Y., Wang, F., and Meng, Z. (2021). Boundary Extraction of Urban Built-Up Area Based on Luminance Value Correction of NTL Image. *IEEE J. Sel. Top. Appl. Earth Obs. Remote Sens.* 14, 7466–7477. doi:10.1109/JSTARS.2021.3098787

Wang, Q., Gao, J., and Yuan, Y. (2018). Embedding Structured Contour and Location Prior in Siamesed Fully Convolutional Networks for Road Detection. *IEEE Trans. Intell. Transp. Syst.* 19, 230–241. doi:10.1109/TITS.2017.2749964

Woo, S., Park, J., Lee, J.-Y., and Kweon, I. S. (2018). *CBAM: Convolutional Block Attention Module*. Cham: Springer, Vol. 1, 782–797. doi:10.1007/978-3-030-01234-2

Wu, F., Wang, C., Zhang, H., Li, J., Li, L., Chen, W., et al. (2021). Built-up Area Mapping in China from GF-3 SAR Imagery Based on the Framework of Deep Learning. *Remote Sens. Environ.* 262, 112515. doi:10.1016/j.rse.2021.112515

Yang, W., and Zhao, J. (2020). Study on China's Economic Development from the Perspective of Strong Sustainability. *Singap. Econ. Rev.* 65, 161–192. doi:10.1142/S021759081746002X

Yang, Y., Wang, D., Yan, Z., and Zhang, S. (2021). Delineating Urban Functional Zones Using U-Net Deep Learning: Case Study of Kuancheng District, Changchun, China. *Land* 10, 1266–1321. doi:10.3390/land10111266

Yang, Z., Xie, L., Sun, W., and Cheng, Z. (2020). Transitional Spatial Structure with Development of Economic Clusters: The Case of Beijing. *J. Urban Plann. Dev.* 146, 04020008. doi:10.1061/(asce)up.1943-5444.0000561

Yi-de Ma, M. A., Qing Liu, L. I. U., and Zhi-bai Quan, . 2004). Automated Image Segmentation Using Improved PCNN Model Based on Cross-Entropy," in Proceedings of 2004 International Symposium on Intelligent Multimedia, Video and Speech Processing, 2004. 743–746. doi:10.1109/ISIMP.2004.1434171

Yin, C. L., Meng, F., Guo, L., Zhang, Y. X., Zhao, Z., Xing, H. Q., et al. (2021). Extraction and Evolution Analysis of Urban Built-Up Areas in Beijing, 1984-2018. *Appl. Spat. Anal.* 14, 731–753. doi:10.1007/s12061-021-09374-7

Yu, G., He, D., Lin, W., Wu, Q., Xiao, J., Lei, X., et al. (2020). China's Spatial Economic Network and its Influencing Factors. *Complexity* 2020, 1–13. doi:10.1155/2020/6352021

Yue, W., Fan, P., Wei, Y. D., and Qi, J. (2014). Economic Development, Urban Expansion, and Sustainable Development in Shanghai. *Stoch. Environ. Res. Risk Assess.* 28, 783–799. doi:10.1007/s00477-012-0623-8

Zeng, C., Liu, Y., Stein, A., and Jiao, L. (2015). Characterization and Spatial Modeling of Urban Sprawl in the Wuhan Metropolitan Area, China. *Int. J. Appl. Earth Observation Geoinformation* 34, 10–24. doi:10.1016/j.jag.2014.06.012

Zhang, Q., and Seto, K. (2013). Can Night-Time Light Data Identify Typologies of Urbanization? A Global Assessment of Successes and Failures. *Remote Sens.* 5, 3476–3494. doi:10.3390/rs5073476

Zhang, X., Bai, Z., Fan, X., Lu, Y., Cao, Y., Zhao, Z., et al. (2016). Urban Expansion Process, Pattern, and Land Use Response in an Urban Mining Composited Zone from 1986 to 2013. *J. Urban Plann. Dev.* 142, 04016014. doi:10.1061/(asce)up.1943-5444.0000327

Zhang, Z., Liu, F., Zhao, X., Wang, X., Shi, L., Xu, J., et al. (2018). Urban Expansion in China Based on Remote Sensing Technology: A Review. *Chin. Geogr. Sci.* 28, 727–743. doi:10.1007/s11769-018-0988-9

Zhou, Y., Huang, W., Dong, P., Xia, Y., and Wang, S. (2021). D-UNet: A Dimension-Fusion U Shape Network for Chronic Stroke Lesion Segmentation. *IEEE/ACM Trans. Comput. Biol. Bioinf.* 18, 940–950. doi:10.1109/TCBB.2019.2939522

Zhu, L., and Yang, Y. (2018). *Cbam*. Springer International Publishing. doi:10.1007/978-3-030-01234-2

Conflict of Interest: The authors declare that the research was conducted in the absence of any commercial or financial relationships that could be construed as a potential conflict of interest.

Publisher's Note: All claims expressed in this article are solely those of the authors and do not necessarily represent those of their affiliated organizations, or those of the publisher, the editors, and the reviewers. Any product that may be evaluated in this article, or claim that may be made by its manufacturer, is not guaranteed or endorsed by the publisher.

Copyright © 2022 Bai, Zhang, Wang, Feng, Wang and Peng. This is an open-access article distributed under the terms of the Creative Commons Attribution License (CC BY). The use, distribution or reproduction in other forums is permitted, provided the original author(s) and the copyright owner(s) are credited and that the original publication in this journal is cited, in accordance with accepted academic practice. No use, distribution or reproduction is permitted which does not comply with these terms.

frontiers | Frontiers in Environmental Science

TYPE Original Research
PUBLISHED 08 August 2022
DOI 10.3389/fenvs.2022.932753

Check for updates

OPEN ACCESS

EDITED BY
Ying Jing,
Zhejiang University, China

REVIEWED BY
Liangzhi Li,
Chang'an University, China
Mengling Qiao,
The Chinese University of Hong Kong, China
Jiawei Zhu,
Central South University, China

*CORRESPONDENCE
Lijun Xing,
ljxing2019@hubu.edu.cn

SPECIALTY SECTION
This article was submitted to Environmental Informatics and Remote Sensing, a section of the journal Frontiers in Environmental Science

RECEIVED 30 April 2022
ACCEPTED 27 June 2022
PUBLISHED 08 August 2022

CITATION
Liu Y, Kuai X, Su F, Wang S, Wang K and Xing L (2022), Research on the spatiotemporal distribution and evolution of remote sensing: A data-driven analysis.
Front. Environ. Sci. 10:932753.
doi: 10.3389/fenvs.2022.932753

COPYRIGHT
© 2022 Liu, Kuai, Su, Wang, Wang and Xing. This is an open-access article distributed under the terms of the Creative Commons Attribution License (CC BY). The use, distribution or reproduction in other forums is permitted, provided the original author(s) and the copyright owner(s) are credited and that the original publication in this journal is cited, in accordance with accepted academic practice. No use, distribution or reproduction is permitted which does not comply with these terms.

Research on the spatiotemporal distribution and evolution of remote sensing: A data-driven analysis

Yu Liu[1], Xi Kuai[2,3], Fei Su[4], Shaochen Wang[5], Kaifeng Wang[1] and Lijun Xing[6]*

[1]Institute of Environment and Development, Guangdong Academy of Social Sciences, Guangzhou, China, [2]Shenzhen Key Laboratory of Spatial Information Smart Sensing and Services, Research Institute for Smart Cities, Shenzhen University, Shenzhen, China, [3]Peng Cheng Laboratory, Shenzhen, China, [4]School of Surveying and Geo-Informatics, Shandong Jianzhu University, Jinan, China, [5]School of Resource and Environmental Sciences, Wuhan University, Wuhan, China, [6]Key Laboratory of Regional Development and Environmental Response, Hubei University, Wuhan, China

The development of remote sensing technology largely reflects the scientific research level of a country or region. Given that the quantity and quality of research works are important indicators for scientific prowess evaluation, exploratory spatial data analysis and scientometric analysis of remote sensing work published from 2012 to 2021 were performed in this study, utilizing the Web of Sciences database. This study probed the spatial distribution and spatiotemporal evolution at the country/regional level to reveal the spatiotemporal characteristics of knowledge spillover in remote sensing. According to the results, the global spatial distribution of research output in remote sensing presented a significant dispersion; the United States and China were the most active countries. During the study period, *Transferring Deep Convolutional Neural Networks for the Scene Classification of High-Resolution Remote Sensing Imagery* was one of the most influential studies, both in the field of remote sensing and in the whole scientific community. With respect to the spatial evolution of research output in remote sensing, the gap between continents and the regional imbalance showed a downward trend, while Asia ranked first in the intracontinental disparity and Europe ranked last. For relevant countries/regions and institutions trying to optimize the spatial allocation of scientific and technological resources to narrow regional disparities, this study provides fundamental data and decision-making references.

KEYWORDS

remote sensing, spatiotemporal distribution, research paper, regional disparity, paper output

1 Introduction

Remote sensing is a technology used to observe and explore target objectives and natural phenomena over long distances (Weng, 2012; Han et al., 2014; Cheng et al., 2017). Remote sensing technology can be used to objectively and accurately obtain timely information about various targets. Over the past few decades, remote sensing has been utilized to observe natural resources and Earth's environment from multiple layers to collect data from areas of Earth to space for application in diverse fields, such as the atmosphere, ocean, resources, environment, economy, agriculture, forestry, urban areas, disaster rescue, and the military (Chen et al., 2006; Chang et al., 2011; Jewiss et al., 2020). Moreover, remote sensing is a new interdisciplinary subject that is integrated with surveying and mapping, space science, electronic science, geosciences, and computer science (Fuentes, 2006; Lary et al., 2016; Tapete, 2018). The development level of remote sensing represents the level of scientific research in a country/region (Soille and Pesaresi, 2002; Andrefouet and Riegl, 2004). Therefore, an increasing number of countries are investing increasing amounts of money and effort in remote sensing research.

Over the past decades, some countries/regions have been in leading positions in remote sensing-related research, and their research results have influenced the development trend of the industry (Kussul et al., 2017; Mikhaylov et al., 2021). Some countries/regions have come to the forefront and have become a new force in remote sensing-related research and are expanding their field. Other countries have turned from field leaders to followers for various reasons (Zhu et al., 2017; Goga et al., 2019). These phenomena reflect the change in scientific research power in remote sensing among countries and the changes in national scientific and technological strength (Nogueira et al., 2016; Zhang et al., 2016). An in-depth study of the phenomena is required not only for researchers to get a quick overview of the history and current situation of remote sensing research but also for related countries/regions to better predict the trend of remote sensing research development and then make remote sensing development plans that really meet their national conditions (Zou et al., 2015; Nogueira et al., 2016). However, the broadness of remote sensing research fields, the diversity of subfields, the differences in disciplinary backgrounds, and the limited personal energy of scholars make it quite difficult to systematically and comprehensively summarize the national/regional strength changes in remote sensing research without high-quality data sources and reliable quantitative analysis methods.

Fortunately, tens of thousands of remote sensing-related research works have been published by researchers in the past few decades. These research works are important carriers and the main transmitters for research achievement, providing information about the research history, current situation, and development trends of the realm and sub-realms (Guarino, 1995; Qiu and Shen, 2021). Previous studies show that the output and quality of research are important indicators to measure the level of national science and technology (Price, 1963; Bourdieu, 2004). Research work data are characterized by easy accessibility and massive volume. In addition, the existing academic databases have collated the research data so that researchers can easily access high-quality studies. On the other hand, quantitative analysis is a mathematical method in scientometrics to measure research results, describe the scientific system structure and analyze the inner operating mechanism of the scientific system. This method can be employed to reveal the spatial and temporal characteristics of scientific development and explore the quantitative regular characteristics of scientific activities in human society. And in the field of spatial data analysis, exploratory spatial data analysis methods have been introduced into fields such as library intelligence and scientometrics in recent years, demonstrating their applicability in the exploration of the spatial differences and evolution of research in related disciplines/fields. More importantly, according to recent studies, research on the spatial distribution of research output can not only help discover the spatial distribution of professional knowledge but also unearth the external causes of regional gaps in research output (Ma et al., 2019a).

In summary, based on the Web of Science (WoS) database, this study presents a study focusing on the output of research works in remote sensing at different levels, such as the distribution of, spatial differences in the aggregation of the global level, differential evolution, and polarization and spatial aggregation between different local areas. The results of this study can not only provide an important basis for related resource allocation and decisive references for scientific macro arrangement in relevant countries/regions, which is conducive to regional science development and thus reduce the regional gap in remote sensing fields. The rest of this study is organized as follows. Section 2 describes the data collection and preparation. Then, the research methodology and analysis of the experimental results are introduced. The conclusion is summarized in the final section.

2 Data collection

On the basis of a web development platform, the WoS is a large, comprehensive citation indexing database developed by Thomson Reuters. Through this database, users can retrieve information about literature in the natural sciences, social sciences, arts, and humanities (Mongeon and Paul-Hus, 2016). The WoS provides relatively complete bibliographic and citation information, including the title, author, abstract, keywords, date, author address, subject category, and reference list (Harzing and Alakangas, 2016). Importantly, bibliographic and citation data in the WoS can be downloaded to track the history and reveal the characteristics of a research field. Given the above, the WoS has been adopted as a data source for many scientometric studies.

The data used in this study were collected from the WoS to investigate the spatial distribution and evolution pattern of the research work output in remote sensing. The data acquisition process was as follows: First, the search function of the WoS database was utilized, and "remote sensing" was selected as the search term. Second, the publication time was set as 2012–2021 (download date: 2 November 2021), the literature type was set as "article," and the language category was set as English. Finally, 13,057 pieces of data were obtained after removing duplicate data.

3 Method

In this study, the standard deviation and coefficient of variation were used to measure the absolute and relative differences between countries/regions and the Gini coefficient was used to explore intra- and intercontinental differences. Exploratory spatial data analysis (ESDA) was performed to reveal the spatial and temporal characteristics of knowledge spillover in remote sensing fields.

3.1 Coefficient of variation

The standard deviation is the arithmetic square root of the variance, which is an absolute indicator of the degree of dispersion of each observation (Lee et al., 2015). The calculation formula is as follows:

$$S = \sqrt{\sum_{i=1}^{n} \frac{(x_i - \bar{x})^2}{n-1}}. \tag{1}$$

The coefficient of variation (CV) is the ratio of the standard deviation to the mean value, which is a relative index reflecting the dispersion of observed values (Shechtman, 2013). The mathematical expression is as follows:

$$CV = \frac{1}{\bar{x}} \sqrt{\sum_{i=1}^{n} \frac{(x_i - \bar{x})^2}{n-1}}, \tag{2}$$

where x_i is the output of remote sensing research in country/region i, $\bar{x}$ is the average output of remote sensing research, and n is the number of countries/regions.

3.2 Gini coefficient

The Gini coefficient is an index originally used in economics that is mainly used for income gap measurement. The value of the Gini coefficient is in the range of 0–1. The closer the value is to 1, the larger the income gap is, while the closer it is to 0, the smaller the gap is. The Gini coefficient has been widely used in fields such as medicine, geography, and computing (Chen et al., 1982). The Gini coefficient decomposition model was put forward by Dagum C in 1997; this model can describe the spatial differences of the remote sensing research output as a whole and quantify differences within and between regions compared with the ordinary Gini coefficient model (Dagum, 1997). The total Gini coefficient calculation formula is as follows:

$$G = \frac{\sum_{i=1}^{N}\sum_{j=1}^{N}\sum_{k=1}^{n_i}\sum_{h=1}^{n_j}\left|y_{ik} - y_{jh}\right|}{2n^2\bar{y}}, \tag{3}$$

where N is the number of continents and n is the number of countries/regions. n_i, n_j are the number of countries/regions in continents i and j, respectively; y_{ik} and y_{jh} are the output of remote sensing research in country/region k and country/region h in continents i and j, respectively; and $\bar{y}$ is the average output of remote sensing research.

According to the Gini coefficient decomposition model of Dagum C, the total Gini (G) can be decomposed as follows:

$$G = G_w + G_{nb} + G_t, \tag{4}$$

where G_w measures the contribution of differences in the number of remote sensing research within continents to the total Gini; G_{nb} measures the contribution of differences in the number of remote sensing research between continents to the total Gini; and G_t measures the contribution of the various intensity of the number of remote sensing research between continents to the total Gini. Among them, G_w, G_{nb}, and G_t are as follows:

$$G_w = \sum_{j=1}^{N} G_{jj} p_j s_j, \tag{5}$$

$$G_{nb} = \sum_{j=2}^{N}\sum_{h=1}^{j-1} G_{jh}\left(p_j s_h + p_h s_j\right) D_{jh}, \tag{6}$$

$$G_{nb} = \sum_{j=2}^{N}\sum_{h=1}^{j-1} G_{jh}\left(p_j s_h + p_h s_j\right)\left(1 - D_{jh}\right), \tag{7}$$

where G_{jj} is the Gini coefficient within the continent j; G_{jh} is the Gini coefficient between continent j and continent h; D_{jh} is the relative influence of remote sensing research output between continents j and h; $p_j = n_j/n$ is the ratio of the number of countries/regions in the continent j to the number of countries/regions in all continents; $S_j = n_j\bar{Y}_j/n\bar{y}$, $j = 1, 2, \ldots, N$; $\bar{Y}_j$ is the average output of remote sensing research in the continent j; and D_{jh} is the relative influence of the output of research in remote sensing between continent j and continent h.

$$G_{jj} = \frac{\sum_{i=1}^{n_j}\sum_{r=1}^{n_j}\left|y_{ji} - y_{jr}\right|}{2n_j^2\bar{Y}_j}, \tag{8}$$

$$G_{jj} = \frac{\sum_{i=1}^{n_j}\sum_{r=1}^{n_j}\left|y_{ji} - y_{jr}\right|}{n_j n_h\left(\bar{Y}_j + \bar{Y}_h\right)}, \tag{9}$$

$$D_{jh} = \frac{d_{jh} - p_{jh}}{d_{jh} + p_{jh}}, \tag{10}$$

where y_{ji} is the output of remote sensing research from a country i on the continent j; $\bar{Y}_j$ is the average output of remote sensing

research for all countries on the continent j; and n_j is the number of countries on the continent j; $p_j = n_j/n$ is the ratio of the number of countries/regions in the continent j to the number of countries/regions in all continents; d_{jh} is the mathematical expectation of the sum of samples satisfying $y_{jt} - y_{hr} > 0$ in continent j and continent h; p_{jh} is the mathematical expectation of the sum of samples satisfying $y_{hr} - y_{jt} > 0$ in continent h and continent j.

3.3 ESDA

ESDA is the application of exploratory data analysis (EDA) to spatial data analysis (SDA). It includes global spatial autocorrelation analysis and local spatial autocorrelation analysis. Different from global spatial autocorrelation describing the spatial aggregation degree of the research object in the whole research region (Griffith et al., 2003), local spatial autocorrelation describes the similarity between research objects, which can be used to measure the degree of local units obeying the whole (Flahaut et al., 2003; Jing et al., 2021). Generally, local spatial autocorrelation analysis can reveal the location of the research object that has local spatial autocorrelation when the global spatial autocorrelation is not significant. When the global spatial autocorrelation is significant, local spatial autocorrelation analysis can reveal the spatial heterogeneity of the study object.

3.3.1 Global spatial autocorrelation

In this study, the global *Moran's I* was used to measure the global spatial autocorrelation of the remote sensing research output. A global *Moran's I* value above 0 indicates a positive spatial correlation (i.e., spatial aggregation) in the research output, while a value below 0 indicates a negative spatial correlation (i.e., spatial dispersion). The research output in remote sensing is considered to have no spatial relevance when the global *Moran's I* value is equal to 0. The global spatial autocorrelation formula is as follows:

$$I = \frac{n\sum_{i=1}^{n}\sum_{j=1}^{n} w_{ij}(y_i - \bar{y})(y_j - \bar{y})}{\sum_{i=1}^{n}\sum_{j=1}^{n} w_{ij}\sum_{i=1}^{n}(y_j - \bar{y})^2} = \frac{\sum_{i=1}^{n}\sum_{j=1}^{n} w_{ij}(y_i - \bar{y})(y_j - \bar{y})}{S^2\sum_{i=1}^{n}\sum_{j=1}^{n} w_{ij}}, \quad (11)$$

$$S^2 = \frac{1}{n}\sum_{i=1}^{n}(y_i - \bar{y}), \quad (12)$$

where n indicates the number of countries/regions; y_i, y_j represent the research output in remote sensing in a country/region i and j, respectively; $\bar{y}$ is the average number of research in remote sensing and w_{ij} is the spatial weight between the ith country/region and the jth country/region. The value range is as follows:

TABLE 1 Classification of local spatial correlation.

Category	I	Z(I)
High–High	$0 < I \leq 1$	$1.96 < Z(I) < +\infty$
Low–Low	$0 < I \leq 1$	$-\infty < Z(I) < -1.96$
High–Low	$-1 \leq I < 0$	$-\infty < Z(I) < -1.96$
Low–High	$-1 \leq I < 0$	$1.96 < Z(I) < +\infty$

$$w_{ij} = \begin{cases} 1, & i \cap j \neq \varnothing \\ 0, & i \cap j = \varnothing \end{cases}. \quad (13)$$

3.3.2 Local spatial autocorrelation

Taking i as the country/region in the study area, the formula of the local *Moran's I* index I_i of country/region i is as follows:

$$I_i = \frac{(x_i - \bar{x})}{S^2}\sum_{j=1}^{n} w_{ij}(x_j - \bar{x}). \quad (14)$$

The formula for the significance level of the local *Moran's I* index I_i of country/region i is

$$Z(I_i) = \frac{I_i - E(I_i)}{\sqrt{\mathrm{VAR}(I_i)}}. \quad (15)$$

Under a certain significance level, the local spatial correlation can be classified into four types: High–High, Low–Low, High–Low, and Low–High by calculating the values with I and Z (I) (Table 1). Among them, both High–High and Low–Low indicate positive spatial correlation, implying large spatial similarity between neighboring countries/regions, i.e., spatial aggregation, while High–Low and Low–High indicate negative spatial correlation, implying large spatial differences between neighboring countries/regions, i.e., spatial dispersion.

4 Results

4.1 Overview

In this study, the national research production statistics are based on the country/region where the institutions are located, in which authors complete related research. In addition, many articles are finished under the international collaboration. In order to be consistent with existing related studies, we counted the collaborative articles for each involved country once. For example, if an article is completed by researchers from the United States, China, and the United Kingdom, this article will be counted for all three countries (Lin et al., 2016; Leung et al., 2017).

A total of 153 countries/regions published remote sensing studies during 2012–2021, 19 of which contributed only one

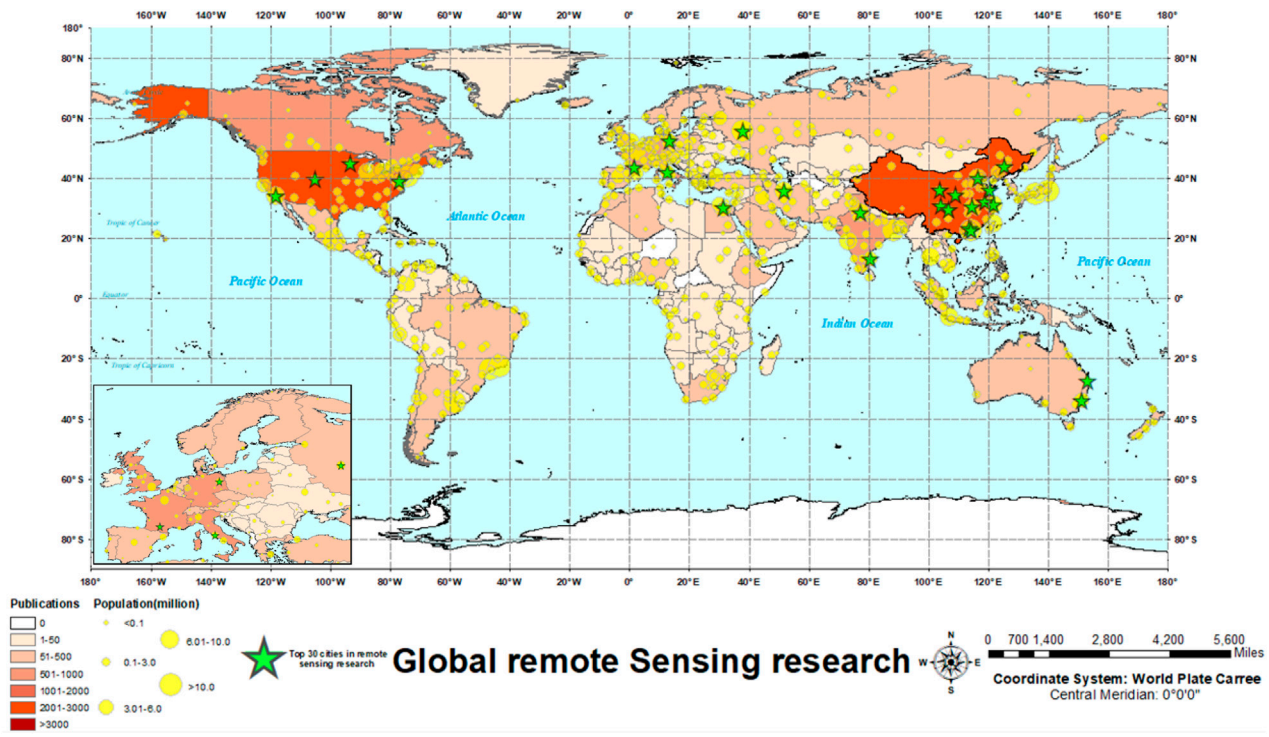

FIGURE 1
Geographic distribution of the global remote sensing research paper output.

(Figure 1). Figure 1 shows that the top 30 cities with high research output were those with large populations. The 10 most productive countries/regions contributed 68.78% of the total studies, with the United States and China being the two most active countries/regions in remote sensing research (Figure 1). China and the United States had the largest numbers of research publications, 5,389 and 2,649 research, respectively. Developed countries such as the United Kingdom, Italy, France, Canada, and Spain also had high output. Large emerging countries, including India (947), Brazil (331), Iran (310), and Egypt (260), have large populations or are large energy consumers. Articles from these countries mostly focused on society, the environment, and energy. To some extent, this indicates that the economic level plays a vital role in scientific input in remote sensing (Li et al., 2016; Lukac et al., 2016; Mikhaylov et al., 2021). Furthermore, for countries/regions with large populations, especially emerging developing countries/regions, new methods based on remote sensing technologies have been sought to solve social problems (such as traffic congestion, environmental pollution, etc.) caused by population growth or develop new technologies for energy surveys (for mineral exploration, etc.) to reduce costs and improve the efficiency of energy exploration (Duane et al., 2021; Chen et al., 2022; Wu et al., 2022).

4.2 Annual publication

Figure 2 describes the annual output of remote sensing research. In Figure 2, the total global citation score (TGCS) indicates the total citations of a remote sensing research by study in the whole database, representing the influence of that research on the academic community, while the total local citation score (TLCS) indicates the citations in the field of this study, which showcases its influence within the field. It can also be seen that 12,549 studies were produced in the field during 2012–2021. 2012 was the year with the lowest yield, with 709 published research, while 2021 had the highest yield, with the publication of 2,576 research. An average of 1,331.8 research was published per year, with an average of 2,105 citations per year (21,050 citations in total in research in the field). The total number of citations in the whole database reached 181,944, an average of 18,194.4 citations per year.

During 2012–2021, the first peaks of the TLCS and TGCS emerged in 2013. In 2013, the study *The detection of "hot regions" in the geography of science—A visualization approach by using density maps* and *Automatic landslide detection from remote-sensing imagery using a scene classification method based on BoVW and pLSA* had the highest TGCS and TLCS, respectively (Bornmann and

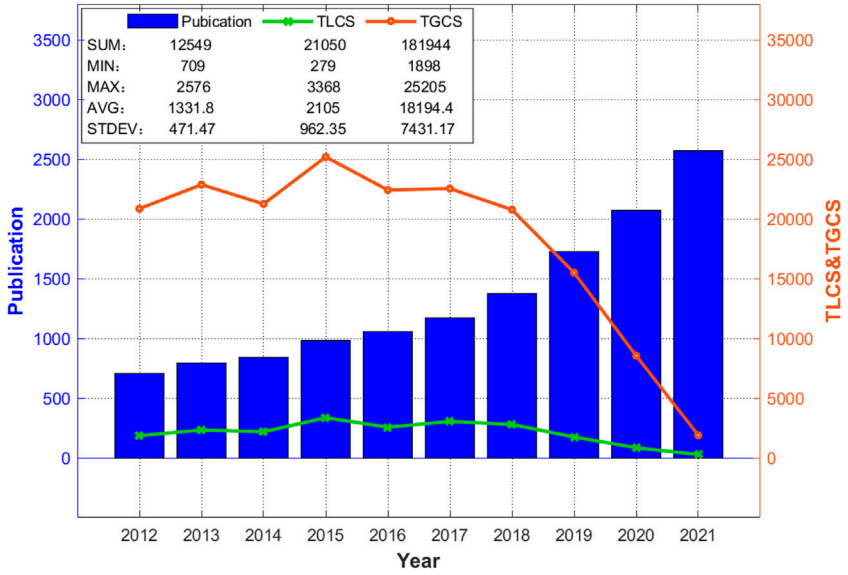

FIGURE 2
Temporal distribution of the output of remote sensing research from 2012 to 2021.

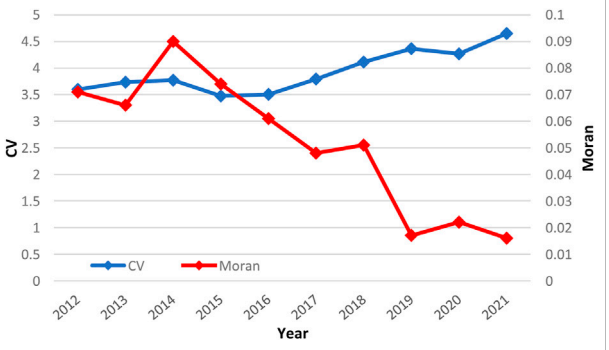

FIGURE 3
Line graph of the annual index change of remote sensing research output.

TABLE 2 Annual index of remote sensing research output.

Year	STDEV	CV	Moran
2012	24.1585	3.5976	0.071
2013	29.0000	3.7332	0.066
2014	31.1722	3.7716	0.090
2015	34.5797	3.4741	0.074
2016	37.1906	3.5033	0.061
2017	43.7571	3.7930	0.048
2018	57.4446	4.1129	0.051
2019	79.0978	4.3638	0.017
2020	91.7205	4.2680	0.022
2021	82.1665	4.6503	0.016

Waltman, 2011; Cheng et al., 2013). After a temporary rebound in 2014, the TGCS and TLCS reached the peak of their research duration in 2015 simultaneously, demonstrating that the academic achievements of this year attracted high attention from both the respective fields and the whole academic community (Figure 2). *Transferring deep convolutional neural networks for the scene classification of high-resolution remote sensing imagery* was the research with the highest TGCS and TLCS during 2012–2021 (Hu et al., 2015). After 2016, the TLCS and TGCS continuously declined; however, remote sensing research output displayed an upward trend. This result does not suggest that the research conducted after 2016 is not important or that the academic community has lost interest in remote sensing. It is more like a reflection of the delayed citation window effect (O'Leary et al., 2015; Chi, 2016; Gonzalez and Gonzalez, 2016; Hu et al., 2019), which means that it takes time from publication to citation (Campanario, 2011; Chi, 2016). In general, the citation of research is directly related to its publication time. The earlier the article is published, the more times it will be cited (Leung et al., 2017; Hu et al., 2019). Conversely, the research output in remote sensing has been increasing since 2016, which indicates that research in remote sensing has attracted ongoing attention from both its own field and the global community (Figure 2) (Weng, 2009; Zhuang et al., 2013).

TABLE 3 Gini coefficient and decomposition results of the output of remote sensing research.

		Year									
		2012	2013	2014	2015	2016	2017	2018	2019	2020	2021
Gini		0.8741	0.8733	0.8741	0.8503	0.8417	0.8495	0.8634	0.8588	0.8469	0.8519
Gini coefficient of intra-continental(G_w)	SA	0.8444	0.8000	0.8222	0.7667	0.7863	0.7846	0.8024	0.7152	0.7839	0.7969
	Oc	0.7467	0.7500	0.7070	0.7758	0.7524	0.7314	0.7536	0.7481	0.7297	0.7463
	NA	0.8587	0.8490	0.8366	0.8433	0.8440	0.8347	0.8402	0.8321	0.8263	0.8328
	Eur	0.6962	0.7150	0.7433	0.6815	0.6603	0.6805	0.6684	0.6875	0.6571	0.6588
	As	0.8796	0.8926	0.8812	0.8647	0.8623	0.8669	0.8972	0.8933	0.8809	0.8762
	Af	0.8865	0.8010	0.7615	0.7967	0.7273	0.7805	0.7093	0.7378	0.6946	0.7234
Gini coefficient of inter-continental (G_{nb})	SA–Oc	0.8737	0.8581	0.8260	0.8504	0.8521	0.8038	0.8672	0.8144	0.8308	0.8196
	SA–NA	0.9677	0.9632	0.9396	0.9538	0.9551	0.9444	0.9534	0.9239	0.9298	0.9265
	SA–Eur	0.8597	0.8468	0.8378	0.8199	0.8215	0.8237	0.8264	0.7884	0.7956	0.7858
	SA–As	0.9112	0.9090	0.8924	0.8796	0.8884	0.8903	0.9122	0.8860	0.9023	0.9010
	SA–Af	0.8956	0.8250	0.8708	0.8129	0.7884	0.8143	0.8062	0.7635	0.7799	0.8049
	Oc–NA	0.9118	0.9041	0.8755	0.9122	0.8937	0.9070	0.8768	0.8696	0.8553	0.8659
	Oc–Eur	0.7480	0.7660	0.7432	0.7749	0.7448	0.7499	0.7367	0.7518	0.7205	0.7330
	Oc–As	0.8554	0.8724	0.8480	0.8695	0.8519	0.8532	0.8743	0.8758	0.8568	0.8693
	Oc–Af	0.9438	0.9110	0.9320	0.9049	0.8797	0.8608	0.9091	0.8818	0.8688	0.8762
	NA–Eur	0.8915	0.8825	0.8741	0.8600	0.8598	0.8574	0.8632	0.8554	0.8383	0.8478
	NA–As	0.9198	0.9132	0.9052	0.9042	0.8993	0.8991	0.9125	0.9029	0.8892	0.8989
	NA–Af	0.9871	0.9802	0.9798	0.9760	0.9725	0.9688	0.9743	0.9567	0.9522	0.9615
	Eur–As	0.8194	0.8390	0.8442	0.8085	0.7985	0.8098	0.8344	0.8412	0.8192	0.8243
	Eur–Af	0.9341	0.8994	0.9297	0.8927	0.8641	0.8724	0.8776	0.8616	0.8365	0.8369
	As–Af	0.9541	0.9376	0.9414	0.9214	0.9095	0.9183	0.9339	0.9250	0.9223	0.9249

Notes: SA: South America; Oc: Oceania; NA: North America; Eur: Europe; As: Asian; Af: Africa.

10.3389/fenvs.2022.932753

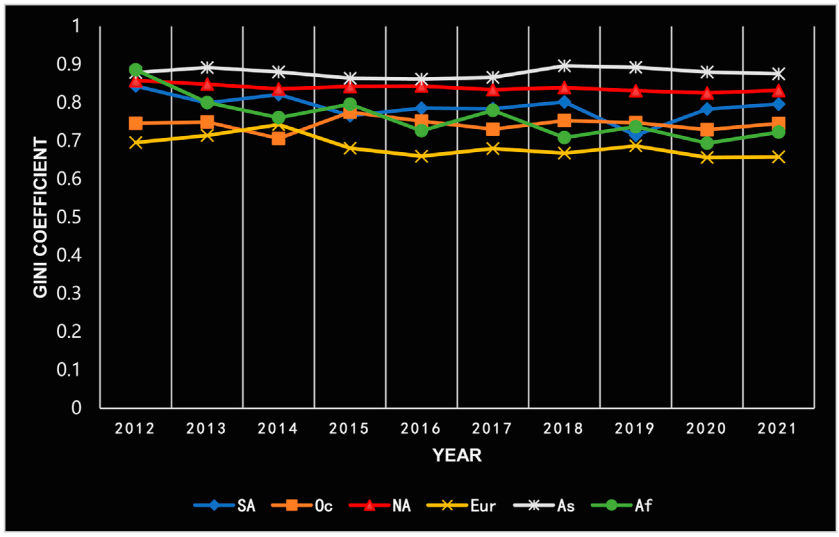

(Notes.: SA: South America; Oc: Oceania; NA: North America; Eur: Europe; As: Asian; Af: Afric)

FIGURE 4
Evolution of the intracontinental variation in the output of remote sensing research. (Notes.: SA: South America; Oc: Oceania; NA: North America; Eur: Europe; As: Asian; Af: Africa).

4.3 Spatial characteristics

The standard deviation of the research output in remote sensing has been on the rise from 2012 to 2021, and that in 2021 was 82.1665, which was 240.11% higher than that in 2012. In addition, its coefficient variation has been increasing significantly since 2012 (Figure 3), and it was 4.6503, 29.26% higher than that of 2012 (Table 2). This indicates a significant dispersion of research output in remote sensing during the time period, especially after 2017. One major reason is that the number of countries/regions involved in remote sensing increased yearly, and the annual research output of the original high-producing countries/regions increased quickly. In the initial stage, the publication of newly involved countries/regions is usually less than that of developed countries/regions, thus leading to an increase in the values of the standard deviation and coefficient of variation year by year. To a certain extent, this result reflects that remote sensing has attracted the attention of scholars in an increasing number of countries/regions (Zhuang et al., 2013; Schmitt et al., 2017; Morales-Barquero et al., 2019). However, it is worth noting that this phenomenon may lead to a decrease in the spatial aggregation of remote sensing studies (Zhuang et al., 2013; Ma et al., 2019b; Jin and Li, 2019; Xu and Yang, 2020).

During 2012–2021, the Moran index was above 0. There was a positive spatial correlation in the remote sensing research output, indicating spatial clustering in the sensing field, which is consistent with the conclusion of Figure 1. In addition, from 2012 to 2014, the Moran index increased and then decreased, which suggests the same trend of remote sensing research output agglomeration (Figure 3). After 2015, the Moran index continued to decline and fell to 0.016 in 2021, meaning that the research output was still spatially aggregated to a significantly lower degree than in the last 3 years. One important reason is that collaborative research before 2018 was mostly among countries/regions that are geographically close to each other or among institutions within countries/regions (Fuentes, 2006; Weng, 2012; Zhuang et al., 2013). After 2019, it became more international, involving more countries/regions and regions (Ma et al., 2019b; Morales-Barquero et al., 2019; Wu et al., 2022).

4.4 Spatial evolution

4.4.1 Regional differences

Based on the continental division of geography (Asia, Europe, Oceania, Africa, North America, and South America) and the Dagum C algorithm, this study calculated the Gini coefficients of six continents to analyze the intra and intercontinental differences in research output in remote sensing.

The Gini coefficient of the remote sensing research output decreased, and the smaller indicator shows the research convergence. In addition, the regional imbalance decreased (Table 3). As shown in Figure 4, the largest intracontinental disparity in remote sensing research output during 2012–2021 was observed in Asia (G_w was the largest), while Europe showed the smallest intracontinental disparity (G_w was the smallest), and North

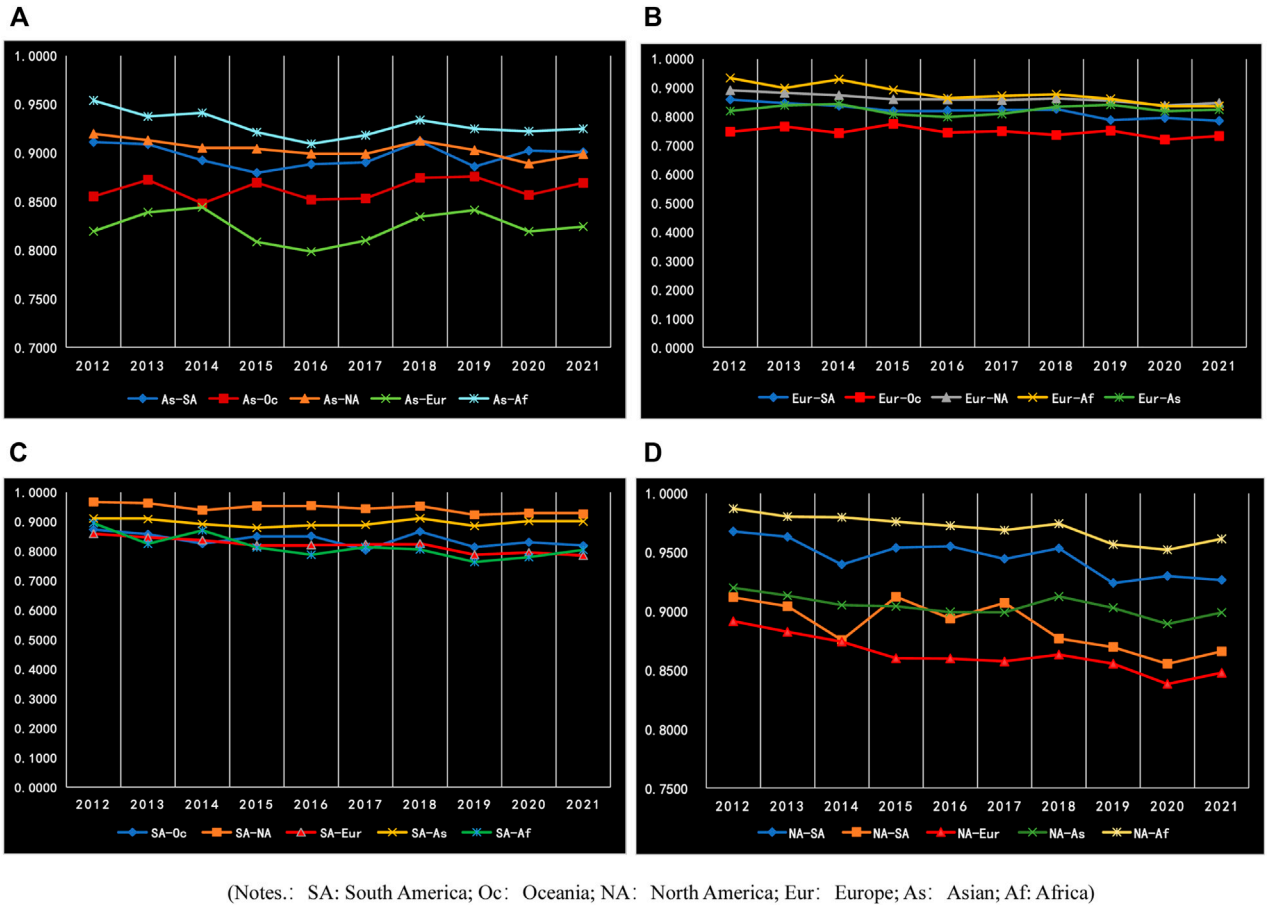

FIGURE 5
(A–D) respectively show the evolution of intercontinental differences in remote sensing research output between Asia, Europe, South America, and North America and other continents. (Notes.: SA: South America; Oc: Oceania; NA: North America; Eur: Europe; As: Asian; Af: Africa).

America was relatively stable, fluctuating at approximately 0.83. In Africa, the Gini coefficient of intracontinental differences decreased dramatically, indicating that the intracontinental differences in the research output on the continent have significantly declined.

Asia, the continent with the largest intracontinental disparity of research output in remote sensing fields, had the largest intercontinental Gini coefficient with Africa and the smallest with Europe (Figure 5A); Europe, the continent with the smallest intracontinental disparity, also had the largest with Africa and the smallest with Oceania (Figure 5B). In the Americas, South America had the largest intercontinental Gini coefficient with North America and the smallest with Africa (Figure 5C); North America had the largest with Africa and the smallest with Europe (Figure 5D). Overall, the intercontinental disparity is dropping. Taking 2012 as the base period, most of the six intercontinental Gini coefficients declined, with Europe-Africa decreasing the most (by 10.4%) and South America-Asia the least (by 1.11%). The regional differences in research output decreased.

4.4.2 Spatial patterns

Figure 6 shows the 30 countries/regions with the most active research output in remote sensing during 2012–2021. As shown in Figure 6, the number of involved Asian countries/regions increased from 6 to 10 in 2012, while the number of involved European countries/regions decreased from 16 to 12. In 2012, the United States was the largest country/region in terms of research output, with China, India, Germany, and the United Kingdom ranking 2–5. China became the country/region with the largest scientific research work output during 2013–2021, and India moved up to the top three after 2018.

The changes in quadrants in Figure 7 reflect the local spatial evolutionary characteristics of the output of research work related to remote sensing. Table 4 presents the countries/regions included in

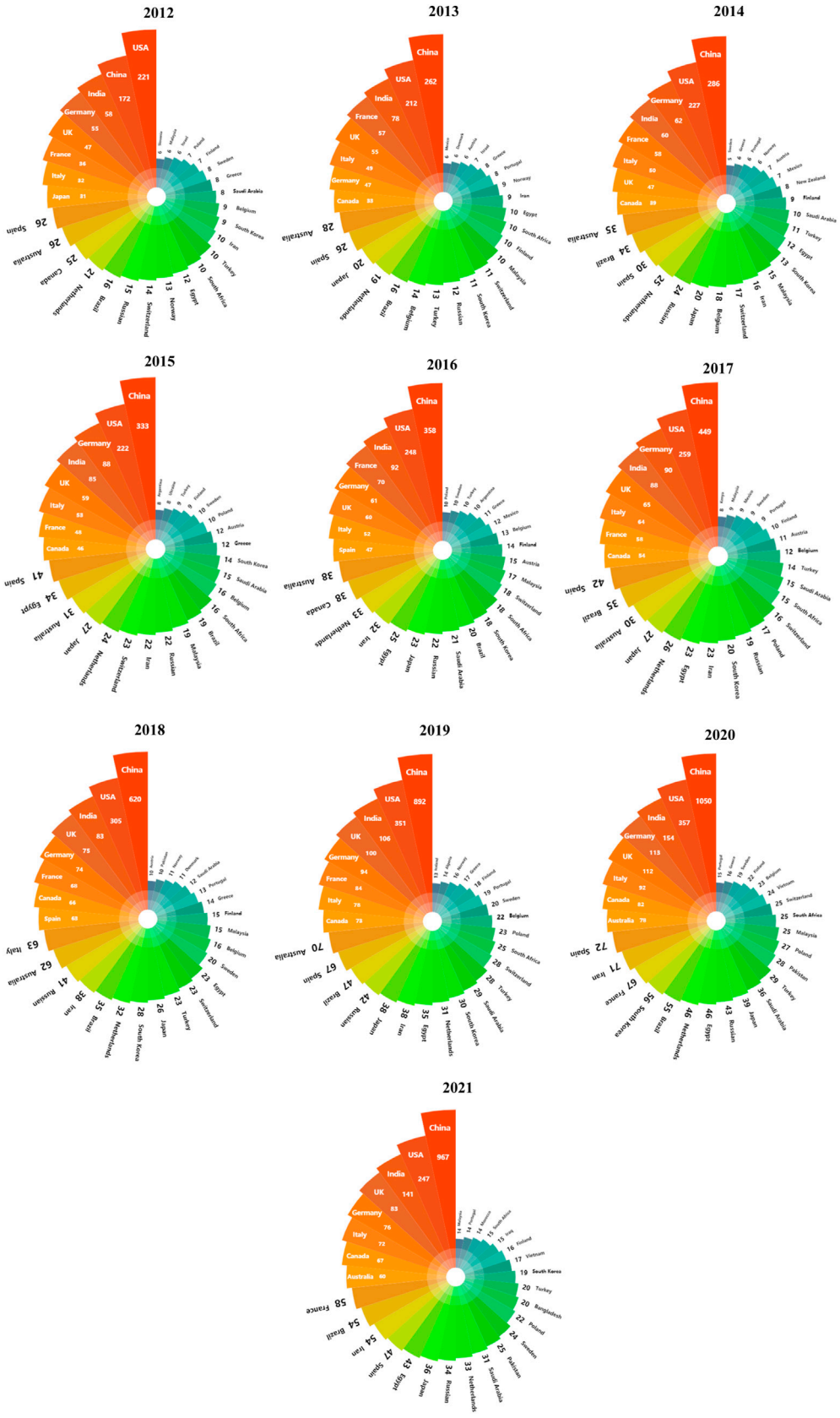

FIGURE 6
Top 30 countries with the most active output of remote sensing research.

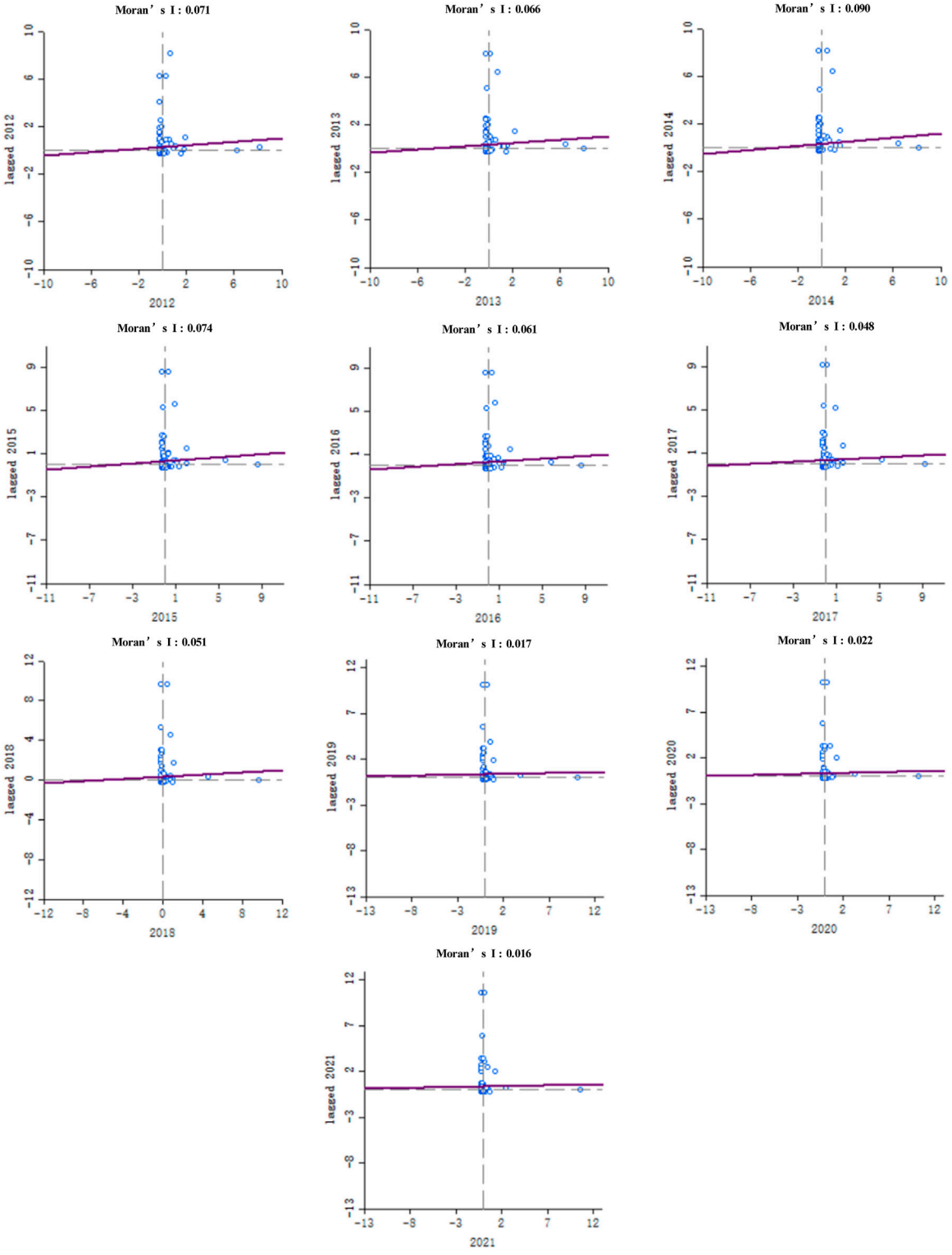

FIGURE 7
Scatterplot of the Moran index of the output of remote sensing research.

TABLE 4 Corresponding countries/regions of the Moran scatterplot for the output of remote sensing research.

	Year				
	2012	**2013**	**2014**	**2015**	**2016**
High–High	Canada Netherlands Russian	Canada India Russian Spain	Canada India Netherlands Russian Spain	Canada, India, Netherlands, and Russian	Canada, India, Russian, and Spain
Low–High	Afghanistan, Bangladesh, Denmark, Ireland, Kazakhstan, Kyrgyzstan, Luxembourg, Mexico, Mongolia, Myanmar, Nepal, Pakistan, and Viet Nam	Afghanistan, Bangladesh, Ireland, Kazakhstan, Kyrgyzstan, Laos, Luxembourg, Mexico, Mongolia, Myanmar, Nepal, Pakistan, and Viet Nam	Afghanistan, Denmark, French Guiana Ireland, Kazakhstan, Kyrgyzstan, Laos, Luxembourg, Mexico, Mongolia, Myanmar, Nepal, Pakistan, and Viet Nam	Afghanistan, Denmark, Ireland, Kazakhstan, Kyrgyzstan, Laos, Luxembourg, Mexico, Mongolia, Myanmar, Nepal, Pakistan, and Viet Nam	Afghanistan, Bangladesh, Denmark, Ireland, Kazakhstan, Kyrgyzstan, Laos, Luxembourg, Mexico, Mongolia, Myanmar, Nepal, Pakistan, and Viet Nam
Low–Low	Guinea, Mali, Democratic Republic of the Congo, and Zambia	Burkina Faso Cote D'ivoire, Guinea, and Tanzania	Burkina Faso Cote D'ivoire, Guinea, Mali, Tanzania, and Democratic Republic of the Congo	Angola Congo Cote D'ivoire, Guinea, Nigeria, Tanzania, Democratic Republic of the Congo, and Zambia	Angola Burkina Faso Cote D'ivoire, Ghana, Guinea, Liberia Mali, Tanzania, Democratic Republic of the Congo, and Zambia
High–Low	United Kingdom and South Africa	United Kingdom			
	Year				
	2017	**2018**	**2019**	**2020**	**2021**
High–High	Canada, India, Netherlands, and Russian	Canada, India, Netherlands, and Russian	Canada, India, Netherlands, and Russian	Canada, India, Pakistan, and Russian	Canada, India, Pakistan, and Russian
Low–High	Afghanistan Denmark Ireland Kazakhstan Kyrgyzstan Laos Luxembourg Mexico Mongolia Myanmar Nepal Pakistan Viet Nam	Afghanistan, Bangladesh, Denmark, Ireland, Kazakhstan, Kyrgyzstan, Laos, Luxembourg, Mexico, Mongolia, Myanmar, Nepal, Pakistan, and Viet Nam	Afghanistan, Denmark, Ireland, Kazakhstan, Kyrgyzstan, Laos, Luxembourg, Mexico, Mongolia, Myanmar, Nepal, Pakistan, and Viet Nam	Afghanistan, Bangladesh, Denmark, Ireland, Kazakhstan, Kyrgyzstan, Laos, Mexico, Mongolia, Myanmar, Nepal, Luxembourg, and Viet Nam	Afghanistan, Denmark, Ireland, Kazakhstan, Bangladesh, Kyrgyzstan, Laos, Mexico, Mongolia, Myanmar, Nepal, and Viet Nam
Low–Low	Angola, Burkina Faso, Guinea, Liberia Mali, Tanzania, Democratic Republic of the Congo, and Zambia	Angola, Congo, Guinea, Nigeria Tanzania, Democratic Republic of the Congo, and Zambia	Angola, Tanzania, Democratic Republic of the Congo, and Zambia	Angola, Burkina Faso, Congo, Cote D'ivoire, Guinea, Senegal Nigeria Tanzania, Democratic Republic of the Congo, and Zambia	Angola, Burkina Faso, Cote D'ivoire, Ghana, Guinea, Liberia Mali, Senegal, Tanzania, and Democratic Republic of the Congo
High–Low					

each quadrant in Figure 5. As seen from Table 4, a total of 6 countries/regions entered the high–high cluster from 2012 to 2021, with low–high, low–low, and high–low comprising 16, 12, and 2 countries, respectively. Moreover, two countries/regions (Canada and Russia) are in the High–High cluster, indicating that the outputs of research work related to remote sensing in these countries/regions and their neighboring countries/regions were at a relatively high level and stable. In addition, 9 countries/regions are in the low–high category. In general, the countries/regions located in each quadrant were relatively stable in the research period, and only a few countries/regions underwent quadrant location changes. For example, Pakistan moved from the second quadrant (low–high) to the first quadrant (high–high), which demonstrates the output of scientific research work in Pakistan and its neighboring countries/regions or regions improved.

TABLE 5 Top10 articles of remote sensing with the highest TLCS.

No.	Article	TLCS	TGCS	References
1.	Remote Sensing Image Scene Classification: Benchmark and State of the Art	258	616	Cheng et al. (2017)
2.	Learning Rotation-Invariant Convolutional Neural Networks for Object Detection in VHR Optical Remote Sensing Images	226	775	Cheng et al. (2016)
3.	Transferring Deep Convolutional Neural Networks for the Scene Classification of High-Resolution Remote Sensing Imagery	198	632	Hu et al. (2015)
4.	When Deep Learning Meets Metric Learning: Remote Sensing Image Scene Classification via Learning Discriminative CNNs	157	461	Cheng et al. (2018)
5.	Deep Learning for Remote Sensing Data A technical tutorial on the state of the art	143	863	Zhang et al. (2016)
6.	Towards better exploiting convolutional neural networks for remote sensing scene classification	139	433	Nogueira et al. (2016)
7.	Deep Learning in Remote Sensing: A Comprehensive Review and List of Resources	139	816	Zhu et al. (2017)
8.	Deep Learning Based Feature Selection for Remote Sensing Scene Classification	107	322	Zou et al. (2015)
9.	Object Detection in Optical Remote Sensing Images Based on Weakly Supervised Learning and High-Level Feature Learning	100	447	Han et al. (2014)
10.	Accurate Object Localization in Remote Sensing Images Based on Convolutional Neural Networks	99	222	Long et al. (2017)

5 Discussion

According to the previous analysis, the gap in the research work output regarding global remote sensing between the different continents decreased, and the spatial aggregation was obviously reduced. The top 10 countries/regions with the largest amount of published research were not the top 10 countries/regions with the largest gross domestic product (GDP). Similarly, the ranking of GDP was not consistent with the research output of the country/region. Meanwhile, almost all the top 30 cities with the largest research work output were among the top 30 in terms of urban populations; however, some cities with large populations like Tokyo and So Paulo fail to make top -30 listed countries with their research output. To some extent, although not decisively, regional economic development and the population have significant impacts on the output of research work in relevant fields of remote sensing (Li et al., 2016; Lukac et al., 2016; Ma et al., 2019a; Ma et al., 2019b).

During the past decade, the output of research work on remote sensing has increased sharply. With more countries/regions concerned about remote sensing and the wider geographic distribution of the nations, the most active countries/regions in the remote sensing research involved the main developed countries/regions as well as emerging developing countries/regions. Tables 5 and 6 show remote sensing research published from 2012 to 2021 with the top 10 TLCS and TGCS values. Most of the study with high TLCS and TGCS was published after 2016, representing the most cutting-edge studies on remote sensing. During this period, studies with a higher TGCS were published in 2013. Interestingly, the ranking of TLCS in Table 6 was not identical to that of TGCS. Generally, published research will be cited by work in this field first, and then cited by studies in other fields after a period of time. During this period, two situations may occur: first, the method or idea proposed in this study may be refuted or optimized by other research in this field

TABLE 6 Top 10 articles of remote sensing with the highest TGCS.

No.	Article	TLCS	TGCS	References
1.	Hyperspectral Remote Sensing Data Analysis and Future Challenges	40	908	Bioucas-Dias et al. (2013)
2.	Deep Learning for Remote Sensing Data A technical tutorial on the state of the art	143	863	Zhang et al. (2016)
3.	Deep Learning in Remote Sensing: A Comprehensive Review and List of Resources	139	816	Zhu et al. (2017)
4.	Learning Rotation-Invariant Convolutional Neural Networks for Object Detection in VHR Optical Remote Sensing Images	226	775	Cheng et al. (2016)
5.	Twenty 5 years of remote sensing in precision agriculture: Key advances and remaining knowledge gaps	50	705	Mulla, (2013)
6.	Transferring Deep Convolutional Neural Networks for the Scene Classification of High-Resolution Remote Sensing Imagery	198	632	Hu et al. (2015)
7.	Remote Sensing Image Scene Classification: Benchmark and State of the Art	258	616	Cheng et al. (2017)
8.	Remote sensing of impervious surfaces in the urban areas: Requirements, methods, and trends	62	601	Weng, (2012)
9.	Deep Learning Classification of Land Cover and Crop Types Using Remote Sensing Data	58	493	Kussul et al. (2017)
10.	Convolutional Neural Networks for Large-Scale Remote-Sensing Image Classification	90	465	Maggiori et al. (2017)

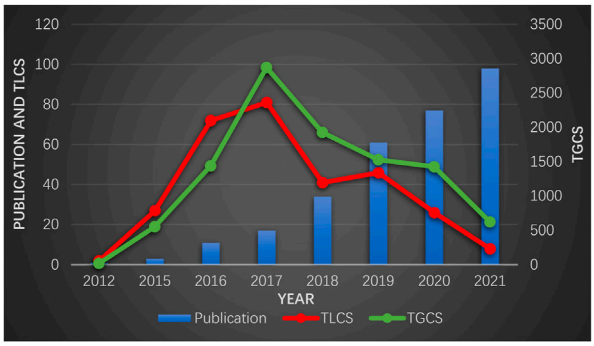

FIGURE 8
Annual yield of remote sensing research to deep learning.

but is being borrowed and used by other fields; therefore, this study gets a low TLCS ranking and a high TGCS ranking; second, the method or idea proposed in this study is only applicable to this field, so it is ranked high in TLCS but low in TGCS (Hu et al., 2019; Jin and Li, 2019).

As shown in Tables 5 and 6, there were five study associated with deep learning and focused on target detection, scene understanding, and autonomous exploration. Meanwhile, the number of remote sensing research related to in-depth learning increased from 3 in 2015 (accounting for 0.3% of the total number of research) to 98 in 2021 (5.43%), showing a significant upward trend (Figure 8). In recent years, with the soaring development of computer vision, such as image classification, target identification, and semantic segmentation, deep learning has been widely applied to remote sensing and has become an important innovation driver for remote sensing research (Zhang et al., 2016; Leung et al., 2017; Kozlowski et al., 2020).

The continental imbalance in the output of remote sensing research work decreased. The continental gap in output in Asia was the largest, while the gap in Europe was the smallest (Table 3; Figure 4). In Asia, there were nations with advanced academic institutions, talented scientific researchers, and large research work output as well as nations with unfavorable research conditions, few scientific researchers, and small study output (Klein et al., 2014; de Beurs et al., 2015; Vadrevu et al., 2019). Thus, the gap in research work output in Asia was larger than that in Europe (Goga et al., 2019; Chen et al., 2020; Mikhaylov et al., 2021). Moreover, the continental gap in Africa has obviously narrowed due to the increasing investment in scientific research in the current decade (Khechba et al., 2021; Mngadi et al., 2022; Sebola, 2022). Regarding the continental gap between Asia and other continents, the gap between Asia and Africa was the largest, and the gap between Asia and Europe was the smallest (Figure 5A), showing that the gap between the two continents with high research output was not large. The gaps between Europe and other continents were all smaller than those between Asia and other continents. In contrast, the gap between Europe and Africa was the largest (Figure 5B), suggesting a large imbalance between Africa and other continents with high research output, such as Asia and Europe.

With the development of communication technology, the cost of cross-regional cooperation decreased, thus promoting international cooperation (Figure 5). Recently, with the help of artificial intelligence, deep learning, and blockchain technologies, remote sensing has been widely and deeply applied to national defense, the economy, and people's daily lives (Zhu et al., 2017; Kocaman and Ozdemir, 2020; Jung et al., 2021). With an increasing number of countries/regions paying attention to remote sensing, some with lower output will become high-output countries/regions, and some less developed countries/regions will no longer have low output, so the spatial aggregation

of the professional research work on remote sensing will decrease.

Despite the above discoveries, due to the limitations of the data, there is an inevitable deficiency in the methodological universality of this exploratory research. Initially, because of data availability and the heterogeneity of the different databases, data from the WoS core database were used in this study. Although the data have high authority, its lack of comprehensiveness cannot be ignored. During the over 10-year research, the name of some institutions may have changed or even become defunct. Secondly, the same university, organization, and institution might be in different cities, so we decided to analyze the research output at the national level. Lastly, the weight impacts and author priority in the cooperation were not taken into account in the research output analyses. In future studies, we will improve the availability and scientific rigor of the results by considering the above limitations.

6 Conclusion

Based on 13,057 research articles included in the WoS from 2012–2021, this study probed the spatiotemporal distribution and evolutionary characteristics of research work output in remote sensing by utilizing scientometric and exploratory spatial analysis. The conclusions are as follows:

Over the last decade, the output of remote sensing research has increased significantly, and its spatial distribution presents a significant dispersion trend. Countries/regions actively participating in remote sensing research included both developed and emerging developing countries/regions, among which the United States and China were the most active. Although the regional economic level and population size play important roles in the remote sensing research work output, neither factor is a determinant. Nearly half of the top ten studies with the highest TGCS and TLCS values were related to deep learning, suggesting that deep learning technology will be one of the most important drivers of innovation in future remote sensing application models. The regional imbalance of the research work output in remote sensing generally dwindled. Although both Asia and Europe had the largest remote sensing research work output, the intracontinental disparity in Asia was the largest, and that in Europe was the smallest, which is related to uneven regional development. The continuous development of telecommunication and other technologies reduces the cost of cross-regional cooperation, and international cooperation in remote sensing has become more frequent. As a result, massive incorporation can bring new technologies and methods. Moreover, remote sensing technology has been widely applied to various fields, such as national defense and economics. More national attention has been given to remote sensing, resulting in mitigation of the clustering of research work output in remote sensing fields.

The results of this study can help countries/regions and institutions understand the overall situation of research output and the continental research gaps in remote sensing as well as improve understanding of the evolution trend of research output. By exploring the essential features of national/regional gaps, the results also serve as important sources of fundamental data and decision-making references for the spatial allocation optimization of scientific and technological resources and regional gap reduction. However, a few limitations and shortcomings should be noted, and future efforts are needed. 1) Although the adopted data source is sufficiently authoritative, it is relatively simplistic and not comprehensive. 2) Due to various reasons, the research work output in remote sensing fields was only analyzed at the national/regional scale, leading to a lack of universality of the conclusions. 3) The absence of weight calculation and priority analysis of institutional importance also affects the rigor of the results.

Data availability statement

Publicly available datasets were analyzed in this study. These data can be found at: Web of Science.

Author contributions

Conceptualization: YL, XK, and LX; software: FS and KW; visualization: YL and SW; writing—original draft preparation: YL and LX; and review and editing: SW, FS, and XK. All authors have read and agreed to the published version of the manuscript.

Funding

This work was supported by the Guangdong Planning Office of Philosophy and Social Science (GD21CTS01 and GD19CYJ04), National Natural Science Foundation of China (Grant No. 41901325), Guangdong Basic and Applied Basic Research Foundation (2022A1515010117 and 2021A1515011448), Open Fund of Key Laboratory of Urban Land Resources Monitoring and Simulation, Ministry of Land and Resources (KF-2021-06-123), and Natural Science Foundation of Hubei Province (2020CFB483).

Acknowledgments

The authors would like to thank the editors and the reviewers for their valuable comments and suggestions.

Conflict of interest

The authors declare that the research was conducted in the absence of any commercial or financial relationships that could be construed as a potential conflict of interest.

Publisher's note

All claims expressed in this article are solely those of the authors and do not necessarily represent those of their affiliated organizations, or those of the publisher, the editors, and the reviewers. Any product that may be evaluated in this article, or claim that may be made by its manufacturer, is not guaranteed or endorsed by the publisher.

References

Andrefouet, S., and Riegl, B. (2004). Remote sensing: A key tool for interdisciplinary assessment of coral reef processes. *Coral Reefs* 23, 1–4. doi:10.1007/s00338-003-0360-z

Bioucas-Dias, J. M., Plaza, A., Camps-Valls, G., Scheunders, P., Nasrabadi, N., Chanussot, J., et al. (2013). Hyperspectral remote sensing data analysis and future challenges. *IEEE Geosci. Remote Sens. Mag.* 1, 6–36. doi:10.1109/mgrs.2013.2244672

Bornmann, L., and Waltman, L. (2011). The detection of "hot regions" in the geography of science—a visualization approach by using density maps. *J. Inf.* 5, 547–553. doi:10.1016/j.joi.2011.04.006

Bourdieu, P. (2004). *Science of science and reflexivity*. Cambridge: Polity.

Campanario, J. M. (2011). Empirical study of journal impact factors obtained using the classical two-year citation window versus a five-year citation window. *Scientometrics* 87, 189–204. doi:10.1007/s11192-010-0334-1

Chang, A., Eo, Y., Kim, S., Kim, Y., and Kim, Y. (2011). Canopy-cover thematic-map generation for Military Map products using remote sensing data in inaccessible areas. *Landsc. Ecol. Eng.* 7, 263–274. doi:10.1007/s11355-010-0132-1

Chen, C.-N., Tsaur, T.-W., and Rhai, T.-S. (1982). The Gini coefficient and negative income. *Oxf. Econ. Pap.* 34, 473–478. doi:10.1093/oxfordjournals.oep.a041563

Chen, C. L., Qian, J., Chen, X., Hu, Z. Y., Sun, J. Y., Wei, S. J., et al. (2020). Geographic distribution of desert locusts in Africa, Asia and Europe using multiple sources of remote-sensing data. *Remote Sens.* 12, 3593. doi:10.3390/rs12213593

Chen, F. N., Zhang, Y., Zhang, J. C., Liu, L. M., and Wu, K. H. (2022). Rice false smut detection and prescription map generation in a complex planting environment, with mixed methods, based on near Earth remote sensing. *Remote Sens.* 14, 945. doi:10.3390/rs14040945

Chen, X. L., Zhao, H. M., Li, P. X., and Yin, Z. Y. (2006). Remote sensing image-based analysis of the relationship between urban heat island and land use/cover changes. *Remote Sens. Environ.* 104, 133–146. doi:10.1016/j.rse.2005.11.016

Cheng, G., Guo, L., Zhao, T. Y., Han, J. W., Li, H. H., Fang, J., et al. (2013). Automatic landslide detection from remote-sensing imagery using a scene classification method based on BoVW and pLSA. *Int. J. Remote Sens.* 34, 45–59. doi:10.1080/01431161.2012.705443

Cheng, G., Han, J., and Lu, X. (2017). Remote sensing image scene classification: Benchmark and state of the art. *Proc. IEEE* 105, 1865–1883. doi:10.1109/jproc.2017.2675998

Cheng, G., Yang, C., Yao, X., Guo, L., and Han, J. (2018). When deep learning meets metric learning: Remote sensing image scene classification via learning discriminative CNNs. *IEEE Trans. Geosci. Remote Sens.* 56, 2811–2821. doi:10.1109/tgrs.2017.2783902

Cheng, G., Zhou, P., and Han, J. (2016). Learning rotation-invariant convolutional neural networks for object detection in VHR optical remote sensing images. *IEEE Trans. Geosci. Remote Sens.* 54, 7405–7415. doi:10.1109/tgrs.2016.2601622

Chi, S. (2016). Differing disciplinary citation concentration patterns of book and journal literature? *J. Inf.* 10, 814–829. doi:10.1016/j.joi.2016.05.005

Dagum, C. A. (1997). A new approach to the decomposition of the Gini income inequality ratio. *Empir. Econ.* 22, 515–531. doi:10.1007/bf01205777

de Beurs, K. M., Henebry, G. M., Owsley, B. C., and Sokolik, I. (2015). Using multiple remote sensing perspectives to identify and attribute land surface dynamics in Central Asia 2001-2013. *Remote Sens. Environ.* 170, 48–61. doi:10.1016/j.rse.2015.08.018

Duane, D., Godo, O. R., and Makris, N. C. (2021). Quantification of wide-area Norwegian spring-spawning herring population density with Ocean acoustic waveguide remote sensing (OAWRS). *Remote Sens.* 13, 4546. doi:10.3390/rs13224546

Flahaut, B., Mouchart, M., San Martin, E., and Thomas, I. (2003). The local spatial autocorrelation and the kernel method for identifying black zones. *Accid. Analysis Prev.* 35, 991–1004. doi:10.1016/s0001-4575(02)00107-0

Fuentes, M. V. (2006). Remote sensing and climate data as a key for understanding fasciolosis transmission in the andes: Review and update of an ongoing interdisciplinary project. *Geospat. Health* 1, 59–70. doi:10.4081/gh.2006.281

Goga, T., Feranec, J., Bucha, T., Rusnak, M., Sackov, I., Barka, I., et al. (2019). A review of the application of remote sensing data for abandoned agricultural land identification with focus on central and eastern Europe. *Remote Sens.* 11, 2759. doi:10.3390/rs11232759

Gonzalez, M. I. D., and Gonzalez, P. D. (2016). Do fixed citation windows match impact maturation rates of scientific journals? *Investig. Bibl. Arch. Bibl. Inf.* 30, 73–89. doi:10.1016/j.ibbai.2016.02.004

Griffith, D. A., Wong, D. W. S., and Whitfield, T. (2003). Exploring relationships between the global and regional measures of spatial autocorrelation. *J. Regional Sci.* 43, 683–710. doi:10.1111/j.0022-4146.2003.00316.x

Guarino, N. (1995). Formal ontology, conceptual analysis and knowledge representation. *Int. J. Human-Computer Stud.* 43, 625–640. doi:10.1006/ijhc.1995.1066

Han, J., Zhang, D., Cheng, G., Guo, L., and Ren, J. (2014). Object detection in optical remote sensing images based on weakly supervised learning and high-level feature learning. *IEEE Trans. Geosci. Remote Sens.* 53, 3325–3337. doi:10.1109/tgrs.2014.2374218

Harzing, A. W., and Alakangas, S. (2016). Google scholar, scopus and the web of science: A longitudinal and cross-disciplinary comparison. *Scientometrics* 106, 787–804. doi:10.1007/s11192-015-1798-9

Hu, F., Xia, G. S., Hu, J. W., and Zhang, L. P. (2015). Transferring deep convolutional neural networks for the scene classification of high-resolution remote sensing imagery. *Remote Sens.* 7, 14680–14707. doi:10.3390/rs71114680

Hu, K., Liu, J., Li, B., Liu, L., Gharibzahedi, S., Su, Y., et al. (2019). Global research trends in food safety in agriculture and industry from 1991 to 2018: A data-driven analysis. *Trends Food Sci. Technol.* 85, 262–276. doi:10.1016/j.tifs.2019.01.011

Jewiss, J. L., Brown, M. E., and Escobar, V. M. Satellite remote sensing data for decision support in emerging agricultural economies: How satellite data can transform agricultural decision making perspectives. *IEEE Geosci. Remote Sens. Mag.* 2020, 8, 117–133. doi:10.1109/mgrs.2020.3023343

Jin, Y. R., and Li, X. (2019). Visualizing the Hotspots and emerging trends of Multimedia big data through scientometrics. *Multimed. Tools Appl.* 78, 1289–1313. doi:10.1007/s11042-018-6172-5

Jing, Y., Shu, J., Wang, R., and Zhang, X. (2021). Tempo-spatial variability of urban leisure functional zones: An analysis based on geo-big data. *Growth Change*, 52, 1852–1865. doi:10.1111/grow.12526

Jung, J. H., Maeda, M., Chang, A. J., Bhandari, M., Ashapure, A., Landivar-Bowles, J., et al. (2021). The potential of remote sensing and artificial intelligence as tools to improve the resilience of agriculture production systems. *Curr. Opin. Biotechnol.* 70, 15–22. doi:10.1016/j.copbio.2020.09.003

Khechba, K., Laamrani, A., Dhiba, D., Misbah, K., and Chehbouni, A. (2021). Monitoring and analyzing yield gap in Africa through soil attribute best management using remote sensing approaches: A review. *Remote Sens.* 13, 4602. doi:10.3390/rs13224602

Klein, I., Dietz, A. J., Gessner, U., Galayeva, A., Myrzakhmetov, A., Kuenzer, C., et al. (2014). Evaluation of seasonal water body extents in Central Asia over the past 27 years derived from medium-resolution remote sensing data. *Int. J. Appl. Earth Obs. Geoinf.* 26, 335–349. doi:10.1016/j.jag.2013.08.004

Kocaman, S., and Ozdemir, N. (2020). Improvement of disability rights via geographic information science. *Sustainability* 12, 5807. doi:10.3390/su12145807

Kozlowski, D., Dusdal, J., Pang, J., and Zilian, A. (2020). Semantic and relational spaces in science of science: Deep learning models for article vectorisation. *Scientometrics* 126, 5881–5910.

Kussul, N., Lavreniuk, M., Skakun, S., and Shelestov, A. (2017). Deep learning classification of land cover and crop types using remote sensing data. *IEEE Geosci. Remote Sens. Lett.* 14, 778–782. doi:10.1109/lgrs.2017.2681128

Lary, D. J., Alavi, A. H., Gandomi, A. H., and Walker, A. L. (2016). Machine learning in geosciences and remote sensing. *Geosci. Front.* 7, 3–10. doi:10.1016/j.gsf.2015.07.003

Lee, D. K., In, J., and Lee, S. (2015). Standard deviation and standard error of the mean. *Korean J. Anesthesiol.* 68, 220. doi:10.4097/kjae.2015.68.3.220

Leung, X. Y., Sun, J., and Bai, B. (2017). Bibliometrics of social media research: A co-citation and co-word analysis. *Int. J. Hosp. Manag.* 66, 35–45. doi:10.1016/j.ijhm.2017.06.012

Li, X. X., Li, W. W., Middel, A., Harlan, S. L., Brazel, A. J., Turner, B. L., et al. (2016). Remote sensing of the surface urban heat island and land architecture in Phoenix, Arizona: Combined effects of land composition and configuration and cadastral-demographic-economic factors. *Remote Sens. Environ.* 174, 233–243. doi:10.1016/j.rse.2015.12.022

Lin, L., Yu, L., Zhu, H., Shen, Y., Hang, S., Luo, H., et al. (2016). A bibliometric and visual analysis of global geo-ontology research. *Comput. Geosciences* 99, 1–8. doi:10.1016/j.cageo.2016.10.006

Long, Y., Gong, Y., Xiao, Z., and Liu, Q. (2017). Accurate object localization in remote sensing images based on convolutional neural networks. *IEEE Trans. Geosci. Remote Sens.* 55, 2486–2498. doi:10.1109/tgrs.2016.2645610

Lukac, N., Seme, S., Dezan, K., Zalik, B., and Stumberger, G. (2016). Economic and environmental assessment of rooftops regarding suitability for photovoltaic systems installation based on remote sensing data. *Energy* 107, 854–865. doi:10.1016/j.energy.2016.04.089

Ma, C., Li, G., Mao, J., and Gu, Y. (2019). Research on the spatial distribution of scientific research output: Taking the computer software and application field as an example. *Libr. Inf. Serv.* 63, 9.

Ma, Q., Li, Y., Chen, J., Li, X., Liu, B. Y., Li, J. Z., et al. (2019). "Undergraduate education of remote sensing science and technology in China: A case of study in jiangsu normal university[C]," in *IGARSS 2019—2019 IEEE International Geoscience and Remote Sensing Symposium*, Piscataway, NJ: IEEE, 2019.

Maggiori, E., Tarabalka, Y., Charpiat, G., and Alliez, P. (2017). Convolutional neural networks for large-scale remote-sensing image classification. *IEEE Trans. Geosci. Remote Sens.* 55, 645–657. doi:10.1109/tgrs.2016.2612821

Mikhaylov, A., Mikhaylova, A., Alsynbaev, K., Bryksin, V., and Hvaley, D. (2021). Remote-sensing technology in mapping socio-economic divergence of Europe. *Bull. Geogr. Ser.* 52, 69–84. doi:10.2478/bog-2021-0014

Mngadi, M., Odindi, J., Mutanga, O., and Sibanda, M. (2022). Quantitative remote sensing of forest ecosystem services in sub-saharan africa's urban landscapes: A review. *Environ. Monit. Assess.*, 194, 242. doi:10.1007/s10661-022-09904-x

Mongeon, P., and Paul-Hus, A. (2016). The journal coverage of web of science and scopus: A comparative analysis. *Scientometrics* 106, 213–228. doi:10.1007/s11192-015-1765-5

Morales-Barquero, L., Lyons, M. B., Phinn, S. R., and Roelfsema, C. M. (2019). Trends in remote sensing accuracy assessment approaches in the context of natural resources. *Remote Sens.* 11, 2305. doi:10.3390/rs11192305

Mulla, D. J. (2013). Twenty five years of remote sensing in precision agriculture: Key advances and remaining knowledge gaps. *Biosyst. Eng.* 114, 358–371. doi:10.1016/j.biosystemseng.2012.08.009

Nogueira, K., Penatti, O., and Santos, J. (2016). Towards better exploiting convolutional neural networks for remote sensing scene classification. *Pattern Recognit.* 61, 539–556. doi:10.1016/j.patcog.2016.07.001

O'Leary, J. D., Crawford, M. W., Jurczyk, E., and Buchan, A. (2015). Benchmarking bibliometrics in biomedical research: Research performance of the university of toronto's faculty of medicine, 2008–2012. *Scientometrics* 105, 311–321. doi:10.1007/s11192-015-1676-5

Price, D. J. d. S. (1963). "Little science, big science," in *Little science, Big science* (Columbia University Press). New York, New York, United States

Qiu, J., and Shen, C. (2021). Analysis of hot topics in domestic big data research based on LDA model. *J. Mod. Inf.* 41 (9), 22–31. doi:10.3969/j.issn.1008-0821.2021.09.003

Schmitt, M., Tupin, F., and Zhu, X. X. (2017). "Ieee. Fusion of sar and optical remote sensing data - challenges and recent trends," in Proceedings of the IEEE International Geoscience & Remote Sensing Symposium, Fort Worth, TX, Jul 23-28, 2017, 5458–5461.

Sebola, M. P. South (2022). South Africa's public higher education institutions, University research outputs, and contribution to national human capital. *Hum. Resour. Dev. Int.*, 1–15. doi:10.1080/13678868.2022.2047147

Shechtman, O. (2013). "The coefficient of variation as an index of measurement reliability," in *Methods of clinical epidemiology* (Springer), Berlin/Heidelberg, Germany, 39–49.

Soille, P., and Pesaresi, M. (2002). Advances in mathematical morphology applied to geoscience and remote sensing. *IEEE Trans. Geosci. Remote Sens.* 40, 2042–2055. doi:10.1109/tgrs.2002.804618

Tapete, D. (2018). Remote sensing and geosciences for archaeology. *Geosciences* 8, 41. doi:10.3390/geosciences8020041

Vadrevu, K. P., Dadhwal, V. K., Gutman, G., and Justice, C. (2019). Remote sensing of agriculture – South/Southeast Asia research initiative special issue. *Int. J. Remote Sens.* 40, 8071–8075. doi:10.1080/01431161.2019.1617507

Weng, Q. H. (2009). Thermal infrared remote sensing for urban climate and environmental studies: Methods, applications, and trends. *Isprs J. Photogrammetry Remote Sens.* 64, 335–344. doi:10.1016/j.isprsjprs.2009.03.007

Weng, Q. (2012). Remote sensing of impervious surfaces in the urban areas: Requirements, methods, and trends. *Remote Sens. Environ.* 117, 34–49. doi:10.1016/j.rse.2011.02.030

Wu, S. P., Gao, X., Lei, J. Q., Zhou, N., Guo, Z. K., Shang, B. J., et al. (2022). Ecological environment quality evaluation of the Sahel region in Africa based on remote sensing ecological index. *J. Arid. Land* 14, 14–33. doi:10.1007/s40333-022-0057-1

Xu, L., and Yang, J. (2020). Research on spatial-temporal distribution and evolution law of domestic journal paper output. *J. Mod. Inf.* 40, 9. doi:10.3969/j.issn.1008–0821.2020.04.015

Zhang, L., Zhang, L., and Du, B. (2016). Deep learning for remote sensing data: A technical tutorial on the state of the art. *IEEE Geoscience Remote Sens. Mag.* 4, 22–40. doi:10.1109/MGRS.2016.2540798

Zhu, X. X., Tuia, D., Mou, L., Xia, G. S., Zhang, L., Xu, F., et al. (2017). Deep learning in remote sensing: A comprehensive review and list of resources. *IEEE Geosci. Remote Sens. Mag.* 5, 8–36. doi:10.1109/mgrs.2017.2762307

Zhuang, Y. H., Liu, X. J., Nguyen, T., He, Q. Q., and Hong, S. (2013). Global remote sensing research trends during 1991-2010: A bibliometric analysis. *Scientometrics* 96, 203–219. doi:10.1007/s11192-012-0918-z

Zou, Q., Ni, L., Zhang, T., and Wang, Q. (2015). Deep learning based feature selection for remote sensing scene classification. *IEEE Geosci. Remote Sens. Lett.* 12, 2321–2325. doi:10.1109/lgrs.2015.2475299

frontiers | Frontiers in Environmental Science

TYPE Original Research
PUBLISHED 10 August 2022
DOI 10.3389/fenvs.2022.942577

Check for updates

OPEN ACCESS

EDITED BY
Jiaxing Cui,
Central China Normal University, China

REVIEWED BY
Qingsong He,
Huazhong University of Science and Technology, China
Jie Zeng,
China University of Geosciences Wuhan, China

*CORRESPONDENCE
Yang Zhang,
zhangyang2020@cdut.edu.cn

SPECIALTY SECTION
This article was submitted to Land Use Dynamics,
a section of the journal
Frontiers in Environmental Science

RECEIVED 12 May 2022
ACCEPTED 14 July 2022
PUBLISHED 10 August 2022

CITATION
Xia X, Zhang Y, Zhang Y and Rao T (2022), The spatial pattern and influence mechanism of urban vitality: A case study of Changsha, China.
Front. Environ. Sci. 10:942577.
doi: 10.3389/fenvs.2022.942577

COPYRIGHT
© 2022 Xia, Zhang, Zhang and Rao. This is an open-access article distributed under the terms of the Creative Commons Attribution License (CC BY). The use, distribution or reproduction in other forums is permitted, provided the original author(s) and the copyright owner(s) are credited and that the original publication in this journal is cited, in accordance with accepted academic practice. No use, distribution or reproduction is permitted which does not comply with these terms.

The spatial pattern and influence mechanism of urban vitality: A case study of Changsha, China

Xiaojiang Xia[1,2], Yang Zhang[1,2]*, Yue Zhang[1,2] and Tiechuan Rao[1,2]

[1]College of Tourism and Urban-Rural Planning, Chengdu University of Technology, Chengdu, China, [2]Research Center for Human Geography of Tibetan Plateau and Its Eastern Slope, Chengdu University of Technology, Chengdu, China

In the new era, the vitality of urban space is an important engine of urban development, and the improvement of urban space vitality is the core component of urban spatial structure optimization and space renewal. However, the availability of data is an important issue in the evaluation of urban space vitality, and continuous vitality monitoring of the entire city is difficult to achieve through traditional methods of field research and questionnaire interviews. Due to this challenge, the traditional vitality assessment methods have serious limitations in the analysis of vitality causes and the guidance of urban space development. Using mobile phone signaling data, this study takes Changsha City as an example to measure the urban spatial vitality and uses the SEM model to analyze how market intervention, traffic accessibility, and spatial characteristics affect the density and stability of urban spatial populations. The results show that the overall urban space vitality density and vitality stability demonstrates an obvious "center–periphery" pattern, and the vitality of the urban center area is in a "high density–low stability" state. The overall urban vitality density on rest days is slightly lower than that on weekdays, and the stability of vitality on rest days is significantly higher than that on weekdays. Market intervention and transportation accessibility support vitality density, but not vitality stability, and spatial characteristics are the opposite. The findings can provide insights relevant to urban spatial planning and design.

KEYWORDS

space vitality, spatial pattern, environmental influence, (MPSD) mobile phone signaling data, Changsha

1 Introduction

Since the implementation of the reform and opening-up policy, China has experienced unprecedented urbanization (Jin et al., 2017). Land-dominated urbanization (Zeng et al., 2018) has led to explosive growth of urban built-up areas (Huang et al., 2017). Many large cities have also entered a concentrated outbreak period of "urban diseases" (Hui et al., 2014) such as "ghost towns," "traffic congestion," and "environmental deterioration." Such rapid urban space expansion has concerned scholars about the creation of urban space vitality

(Batty, 2016). The government has also noticed the potential problems in the process of urbanization and has made urban physical examination and promotion of urban vitality an important strategic task for urban space development in the new era (Wang et al., 2022). At present, the development of urban space in China has fully entered the era of stock development, and the supply of new construction land in a large number of cities has been severely restricted (Xia et al., 2020; Dong et al., 2021). The development model of China's large cities has gradually shifted from incremental planning to stock planning (Xia et al., 2019). In this context, the academic community and the general public have generally recognized that using the huge stock space formed by rapid urbanization (Wang et al., 2017; He et al., 2018) to enhance the vitality of space is an important means to improve the quality of urban space and alleviate urban diseases. Therefore, an understanding of urban vitality is essential for cities to be vibrant and sustainable (Lang et al., 2016). The study of urban spatiotemporal vitality pattern provides a new way to alleviate the problems of blind urban expansion and resource allocation imbalance (Liu and Long, 2019). Moreover, analyzing the temporal and spatial laws of urban space vitality and its impact mechanism can effectively provide an important basis for enhancing urban space vitality and promoting high-quality development of urban space.

Since Jacobs proposed the concept of urban vitality, it has received extensive attention from multiple disciplines (Delclòs-Alió et al., 2019). The connotation and dimension of the concept of urban vitality are one of the important issues to be studied in urban planning disciplines (Pakoz and Isik, 2022). Urban vitality is the source and driving force of urban development, which directly affects urban development and the satisfaction of the urban population (Lan et al., 2020; Guo et al., 2022). Researchers generally believe that urban vitality reflects the interaction between various human activities and existing urban facilities, and plays a crucial role in promoting comprehensive, coordinated, and sustainable urban development (Wu. et al., 2018; Mouratidis and Poortinga, 2020). Urban vitality represents the level of human activities in different times and spaces of the city (Li et al., 2016; Li and Liu, 2016), and good urban vitality reflects the relationship between urban space and urban population. Human relationships also reflect the quality of urban space (Jin et al., 2017).

At present, academia has carried out numerous research works on the vitality of urban space. In terms of study area type, current research on urban vitality mainly focuses on urban parks (Zhu et al., 2020; Mu et al., 2021; Mushkani and Ono, 2021), commercial centers (Guo et al., 2022) and communities (Li et al., 2022), waterfront space (Liu et al., 2021; Niu et al., 2021), urban streets (Gehl et al., 2006), and other aspects of spatial vitality measurement and analysis of influencing factors. In addition, many scholars often use urban vitality to evaluate the quality of urban development (Lan et al., 2020; Jiang et al., 2022). In terms of data usage, availability of data used to be the primary issue for quantitative analysis of urban vitality (Sung and Lee, 2015; Ye et al., 2017). In recent years, the development of information and communication technology and perception technology has provided new data, methods, and research objects for urban vitality research (García-Palomares et al., 2018; Kim, 2018). A wealth of microscale geographic open data, including social media data, mobile phone trajectories, points of interest (POIs), night-lighting data (Zheng et al., 2017), location-based service data (Jin et al., 2017), and smart card records, can be used for quantitative and systematic studies of urban density and urban vitality (Liu et al., 2015; Xia et al., 2017; Wu and Niu, 2019; Tu et al., 2020). Compared with traditional census and survey data, these geotagged big data have a large sample size, high penetration rate, and strong timeliness, which have significant advantages for us to study urban vitality further (Ye et al., 2017; Wu, et al., 2018), thereby promoting the research paradigm shift of dynamic observation of static data analysis items (Liu and Long, 2019). In recent years, many studies have attempted to analyze spatial big data from different sources to explore urban vitality (Tang et al., 2018; Lu et al., 2019). For example, mobile phone signaling data (MPSD) can provide more objective and high-resolution data for urban spatial vitality research (Birenboim and Shoval, 2016; Chen and Akar, 2016; Delclòs-Alió et al., 2019). In terms of selection of influencing factors, in the evaluation of urban vitality at a regional or national level with cities as the basic units, socio-economic data are mainly selected as influencing factors. Examples of these socio-economic data are per capita gross domestic product and per capita fiscal revenue (Lan et al., 2020; Shi et al., 2021). In the research on the vitality of urban interior space, the selection of influencing factors is mainly based on public service facilities (education, entertainment facilities, etc.), landscape elements (human landscape elements, natural landscape elements), and traffic accessibility (subway, taxi) as the main body (Delclòs-Alió et al., 2019; Mouratidis and Poortinga, 2020; Li et al., 2021; Niu et al., 2021; Yue et al., 2021). In terms of research methods, global and local regression models (Fan et al., 2021), space syntax (Xu and Chen, 2021), and other methods are widely used. In recent years, structural equation model methods have been increasingly applied to urban space research for causal analysis, especially for latent variables that cannot be directly observed (Mouratidis and Poortinga, 2020; Liu et al., 2021).

In summary, in-depth research on urban vitality and its influencing factors can help shed light on the complex relationship between urban vitality and socio-economic order (Lang et al., 2016; Li et al., 2022). Moreover, it can

help urban planners and policymakers develop effective urban sustainability plans (Laman et al., 2019; Meng and Xing, 2019). Urban planners often expect to plan and build a space with high vitality, yet spaces with high vitality cannot be attributed to planning alone. The formation of spatial vitality is significantly affected by market economic activities. Therefore, planners trying to plan or update urban space to enhance urban vitality must master the status and influencing factors of urban space vitality. However, for urban planners, little research and discussion have been conducted on the spatial and temporal characteristics of the overall spatial vitality of a city, for example, what affects urban spatial vitality, and what factors are the most important. This involves many issues: how the vitality of urban space is affected by factors of the built environment and how to optimize the spatial structure on the overall scale of the city to enhance the vitality of space. In addition, current research mainly uses regression models to explain the impact of various environmental characteristics on the vitality of urban local areas or specific functional areas. Although this method can obtain the correlation and statistical significance between built environment elements and spatial vitality, it is difficult to use for establishing the causal relationship between variables and for analyzing the complex relationship between urban spatial vitality and influencing factors. In particular, factors such as spatial accessibility and market economic activities have an important impact on the vitality of urban space, but these variables cannot be directly observed. Traditionally, some distance factors such as the location and agglomeration of commercial facilities are often used to replace accessibility and market economic activities, but whether these indicators can be accurately measured has not been verified. In addition, compared with other emerging data, MPSD has obvious advantages in analyzing the vitality of urban space. On the one hand, MPSD is a direct response of individuals in urban populations with very high spatial resolution and smaller granularity. On the other hand, MPSD can have better timeliness, which is an important reason why many current research works use MPSD (De Nadai et al., 2016; Yue et al., 2016).

Therefore, this research will use MPSD data to measure the vitality of urban space, analyze the situation of urban space vitality, and use a structural equation model to analyze the causes of urban space vitality. We focus on the distribution pattern of urban spatial vitality in different times, the vitality persistence (vitality stability), and its relationship with the urban built environment. This study is organized as follows: the introduction section gives the background of this study and a descriptive literature review. The latter consists of a summary of the reviewed articles and examines the concept of urban vibrancy and related studies in MPSD. Section 2 explains the research methods, including the data and analytical methods used. Section 3 elaborates the analysis results. Section 4 discusses the findings from the viewpoint of urban planning practices. Section 5 concludes the study. Our study follows the trend of academic research and attempts to use advanced spatiotemporal analysis techniques to conduct an in-depth analysis of urban vitality to advance the scientific understanding of sustainable urban development.

2 Data and methodology

2.1 Study area

Changsha is the capital city of Hunan Province, an important central city in the middle reaches of the Yangtze River. The city was identified by the Chinese Central Government as an important political, economic, educational, cultural, and transportation center in the central region. With the continuous economic development of Changsha Zhuzhou and Xiangtan urban agglomerations and the continuous advancement of national strategies such as the rise of Central China, the middle reaches of the Yangtze River, the Yangtze River Economic Belt, and the “One Belt and One Road” initiative, the development of Changsha has ushered in a significant period of opportunity. Furthermore, its international status has been elevated. As China continues to shift its development focus to the central region, Changsha’s future becomes promising. Changsha is one of the most famous cities in China. The spatial behavior of urban people is typical, making it a good research area for urban vitality research (Figure 1).

Changsha City has six districts and three counties. The spatial activities of urban people mainly occur in the areas that have been built in the city. By comparing satellite maps and administrative boundary data, we selected Tianxing District, Yuelu District, Yuhua District, Kaifu District, most of Wangcheng District, Furong District, and part of Xingsha County as the study area (Table 1).

2.2 Data sources

This study used four types of data, namely, MPSD, POI data, road network data, and the administrative boundaries of the study area. First, the MPSD are obtained from Hunan Mobile Company. The data covered weekdays and weekends in July 2021 when weather conditions were good. In order to protect privacy, Hunan Mobile uses a 200 m × 200 m grid to count the number of people distributed in time and space. Mobile phone data depict the spatiotemporal characteristics of the activities of individuals (Qian et al., 2021). Several previous studies have proven that MPSD are effective in determining the temporal and spatial distribution of the

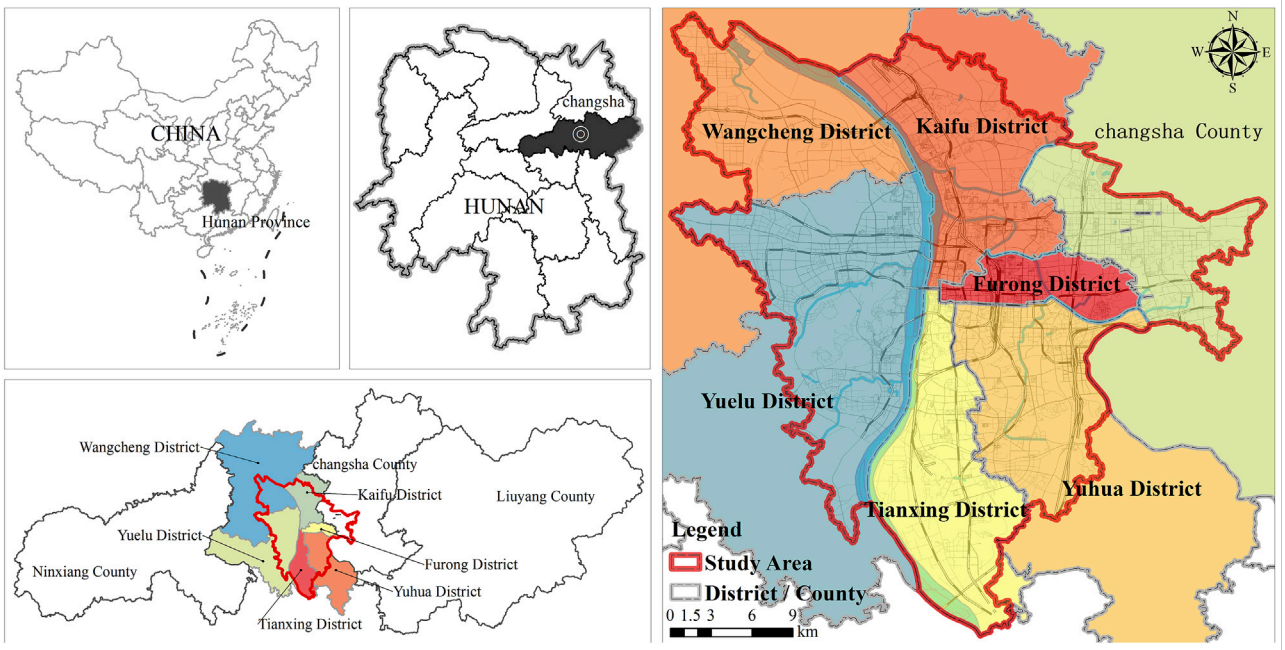

FIGURE 1
Research area.

TABLE 1 Detailed scope of the study area.

Study area	Include area only	Not included area
Yuelu District	All regions except exclude regions	Yuchangping Street, Lianhua Town, Hanpu Street, Xueshi Street, Zhongtang Village, Yujiang Village, Shuanghu Village, Baiquan Village, Xinghe Village, Lianhuashan Village, Taiping Village
Kaifu District	All regions except exclude regions	Hanhui Village, Shuangtang Village, Zhuan Village, Shulin Village, Shaping Village, Zhongshan Village, Xinyuan Village, Jinxia New Village, Tiansheng Community
Wangcheng District	Moon Island Street, Baishazhou Street, Daze Lake Street, Jinshanqiao Community, Jinping Community, Guifang Village, Gaochong Village, Renhe Community, Lianhu Community, Baifutang Community, Gaotang Community, Yujiapo Community	
Changsha County	Quantang Street, Langli Street, Xianglong Street, Xingsha Street, Longxiang Community, Huaxiang Village, Changlong Village, Longjing Community	
Yuhua District	All regions except exclude regions	Tiaoma Town
Tianxin District	All regions except exclude regions	Xuxing Village
Furong District	All areas	

urban population (Fan et al., 2018; Xiao et al., 2019; Yin et al., 2021). We selected hourly cell phone signal data from 9 a.m. to 9 p.m. for the following reasons. First, during the night period (21:00–06:00), urban residents are mainly concentrated in urban living spaces, and the usage of urban public space is small. Second, from 6:00 a.m. to 9:00 a.m., urban traffic commutes make the spatial activity highly dynamic and the response to the spatial vitality inaccurate.

The POI data in July 2021 were obtained from the online map service platform GAODE map (http://lbs.amap.com/) by calling the open API Python programming. Each POI data include name, address, longitude, and latitude. After data cleaning, coordinate transformation, and sorting, the effective data volume exceeded 300,000. On this basis, we established a database of different types of POI in the study area. The road network data which were used to extract the study area were obtained from the OpenStreetMap

TABLE 2 Vitality density formulas for weekdays and weekends.

Variables	Formula	Description
Weekday density	$D_{i,work} = \frac{\sum_{j=1}^{3}(\sum_{i=1}^{13} P_{i,jwork})}{S \times 13 \times 3}$.	$D_{i,work}$ is the weekday density. $P_{i,\ jwork}$ is the number of users in the ith hour on the jth working day.
Weekend density	$D_{i,rest} = \frac{\sum_{j=1}^{2}(\sum_{i=1}^{13} P_{i,jrest})}{S \times 13 \times 2}$.	$D_{i,work}$ is the weekend density. $P_{i,\ jrest}$ is the number of users in the ith hour on the jth weekends.

Notes: The research selects hourly MDSP, from 9 a.m. to 9 p.m.

TABLE 3 Vitality stability formulas for weekday and weekends.

Variables	Formula	Description
Weekday stability	$S_j = \sqrt{\frac{1}{13} \times \sum_{i=1}^{13}(D_{i,j} - \bar{D}_j)^2}$, $S_{work} = \frac{1}{2} \times \sum_{j=1}^{3} S_j$.	S_j is the standard deviation of user density on the jth day. $D_{i,j}$ is the user density on the jth day, ith hour of the ith block. $\bar{D}_j$ is the average user density on the jth day. S_{work} is the standard deviation of user density on Weekday.
Weekend stability	$S_j = \sqrt{\frac{1}{13} \times \sum_{i=1}^{13}(D_{i,j} - \bar{D}_j)^2}$, $S_{rest} = \frac{1}{2} \times \sum_{j=1}^{2} S_j$.	$S_{i,\ j}$ is the standard deviation of user density on the jth day of the ith block. $D_{i,j}$ is the user density on the kth day, ith hour of the ith block. $\bar{D}_j$ is the average user density on the kth day. S_{rest} is the standard deviation of user density on weekends of the ith block.
Dimensionless	$S'_k = \frac{S_k - S_{min}}{S_{max} - S_{min}}$.	S'_k is the stability index of the kth block, which is the value of the standard deviation index, which is standardized (dimensionless). S_k is the standard deviation of the kth block, S_{max} is the standard deviation maximum value among 1,475 blocks, and S_{min} is the standard deviation minimum value.

Notes: The research selects hourly MDSP, from 9 a.m. to 9 p.m.

(http://www.openstreetmap.org/). Changsha administrative division boundary data come from the Institute of Geography and Resources, Chinese Academy of Sciences.

2.3 Analysis framework and model construction

2.3.1 Characterization of urban space vitality density and its stability

2.3.1.1 Vitality density

Urban space vitality density refers to the intensity of crowd activities in the urban space at a certain moment, usually expressed by the ratio of the total population to the research unit area. The larger the index value, the stronger the vitality. This study is based on the general scale of urban block units in Changsha City, and the study unit is divided into 800 m × 800 m grids for analysis. Table 2 shows the formulas for calculating the space vitality density during the research period.

2.3.1.2 Vitality stability

Vitality stability refers to the degree of dynamic changes in the intensity of urban crowd activity during the overall study period, that is, the degree of dispersion of the intensity of urban crowd activity in a specific time period in the time dimension, which is usually measured by the standard deviation. The smaller the value, the more stable the vitality. For the convenience of follow-up statistics, we have carried out reverse normalization of this value, so that the larger the index after normalization, the stronger the stability of the indicated vitality. Table 3 shows the calculation formula of vitality stability.

2.3.2 Structural equation model approach

Since the development of the SEM model in the 1990s, it has promoted the research process in the fields of psychology, economics, sociology, and spatial planning (Halkos et al., 2021; Liu et al., 2021; Tong et al., 2021). The main advantage of using SEM over multivariate regression models and univariate regression is the opportunity to model complicated interrelationships among dependent and/or independent variables (Najaf et al., 2018). SEM can estimate direct effects, indirect effects, and total effects, which gives a deeper and more comprehensive insight into the links between variables than ordinary linear models (Tong et al., 2021). In addition, SEM can be applied to cope with the problem of endogeneity when it is caused by simultaneous causality (Jo and Jeon, 2021; Tong et al., 2021; Shami et al., 2022). In order to ensure the reliability of the SEM model, a large number of fitting parameters have been developed, including goodness-of-fit index (GFI), normed fit index (NFI), comparative fit index (CFI), and Tucker–Lewis

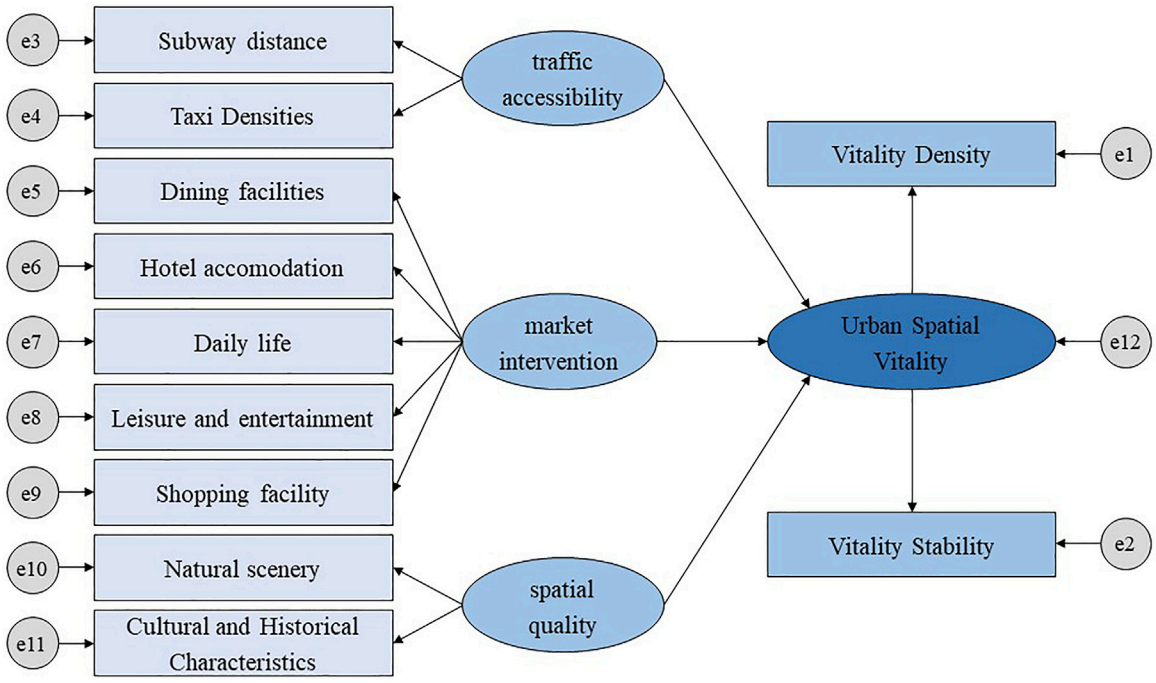

FIGURE 2
Conceptual structural model.

coefficient (TLI). On this basis, we choose the most commonly used indicators, namely, TLI, NFI, GFI, SRMR, and CFI to test SEM (Xie et al., 2020).

AMOS is an added SPSS module and is specifically used for SEM. Through AMOS, we can draw models graphically using simple drawing tools. AMOS performs the computations for SEM and displays the results quickly (Shami et al., 2022). These features provide great convenience for this research.

2.3.3 Construction of the theoretical model

Taking Changsha urban built-up area as a case study area, the structural equation model was elaborated and consists of a measurement model and a structural model (Figure 2). In previous urban population density studies, shopping facilities, catering facilities, entertainment facilities, hotel accommodation facilities, and daily life service facilities are widely used factors (Li et al., 2019; Yang et al., 2021; Chen et al., 2022; Li et al., 2022). Subway, taxis, and other modes of transportation, which are components of transportation accessibility, are almost mandatory factors in all studies on population density distribution and spatial vitality (Yue et al., 2021; Guo et al., 2022). Scholars have also adopted elements such as spatial landscape and cultural attractions (Lin et al., 2021; Niu et al., 2021; Xu and Chen, 2021). The spatial behavior and spatial flow of urban people mainly consider the influence of three aspects: the push end, the pull end, and the link channel between the two. The research on the vitality of urban space mainly considers the tension end and the link channel. The link channel refers to the accessibility of traffic, whereas the pull section refers to the spatial attribute that meets the public needs of the urban population. The functional attributes of public space come from two ways: one is the land-use attribute given by spatial planning, and the other is the dynamic and stable attribute formed by the continuous operation of the market economy. For the renewal of urban built-up areas, it is more reasonable to consider the dynamic and stable attributes generated by market operation, which is also the dynamic demand for urban space vitality. However, the spatial dynamism of government-led facilities such as educational facilities and medical facilities is moot. This type of facility is planned in accordance with the configuration standard of public service facilities, and it is not necessary to enhance the vitality of the space. Therefore, we choose the average vitality density and vitality stability of weekdays and weekends as endogenous variables. According to the attributes of urban space facilities, urban functional facilities are divided into three types of endogenous variables: market-led facilities, spatial quality, and traffic accessibility. A geographic information system will be an effective tool for visualizing the results. The following three hypotheses are proposed to verify the relationship between urban space vitality and built environment characteristics.

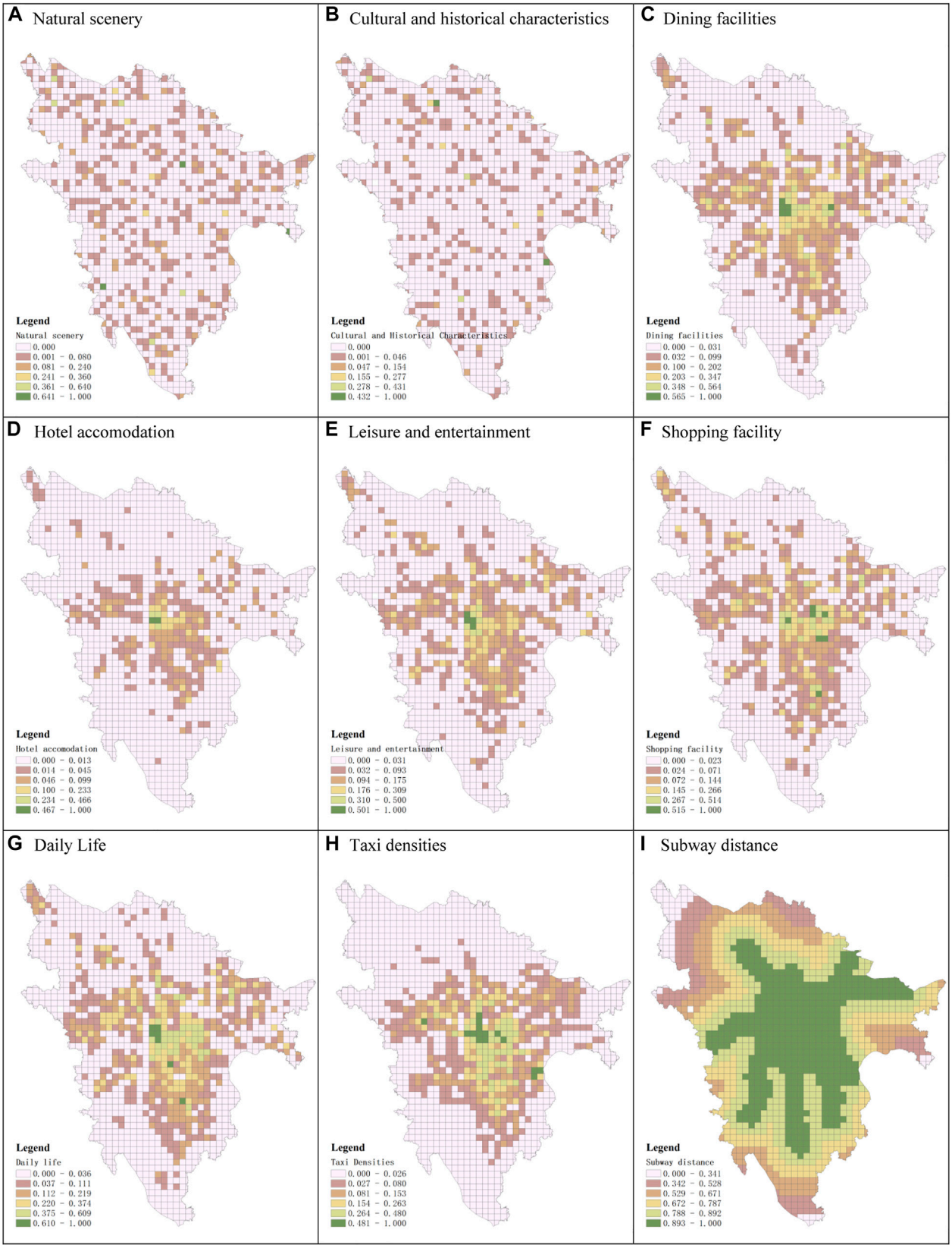

FIGURE 3
Spatial distribution of independent variables. **(A)** Natural scenery. **(B)** Cultural and historical characteristics. **(C)** Dining facilities. **(D)** Hotel accommodation. **(E)** Leisure and entertainment. **(F)** Shopping facility. **(G)** Daily life. **(H)** Taxi densities. **(I)** Subway distance.

H 1. The greater the density of market-led implementation, the more vibrant the urban space.
H 2. The greater the traffic accessibility, the more vibrant the urban space.
H 3. The better the quality of the space, the more vibrant the urban space.

2.3.4 Variable settings

2.3.4.1 Exogenous variable

The exogenous variables of this study are the functional characteristics of the urban built environment. Except for the parameter of traffic accessibility, which is the same as the index used by a large number of scholars, we have made innovations in other exogenous variables. According to the construction and use attributes of functional space, an environmental factor index system that is composed of market intervention facility, spatial quality, and traffic accessibility of the urban space has been constructed.

2.3.4.1.1 The impact of the market intervention facility. The implementation of a large number of commercial administrations in the city has fully considered the vitality of the urban space when selecting the site and has an impact on the vitality of the city. Among them, the layout and scale of commercial facilities, catering facilities and living service facilities are mainly determined by the market environment. Therefore, this study integrated the number of commercial facilities, catering facilities, living service facilities, leisure and entertainment facilities, and hotel accommodation facilities per unit area into the market intervention facility index system.

2.3.4.1.2 The impact of spatial quality. Whether the urban space has good natural scenery and cultural and historical characteristics are important parameters to measure the attractiveness of the space. The spatial quality of this research refers to scenic spots with natural landscape attributes and historical sites with cultural and historical attributes. It is quantified by spatial density.

2.3.4.1.3 The impact of traffic accessibility. Traffic accessibility refers to the convenience of transportation to a specific space in a city, and is used as a common indicator in the study of urban space vitality (Niu et al., 2021; Guo et al., 2022). Numerous scholars usually take the development of urban public transportation as an important parameter to measure traffic accessibility (Yang et al., 2021; Yue et al., 2021). Inspired by this convention, this study mainly used the number of taxis per unit area and the distance to nearby subway stations as indicators to measure traffic accessibility. The significance of urban bus stops is poor in the analysis process, so the factor of bus stops is not included in the model analysis. To ensure the convenience of data processing, the accessibility indicators are normalized (dimensionless). In addition, the distance from the subway station is reversely processed to ensure that the larger the value, the closer the distance to the subway station.

Figure 3 shows the spatial distribution of all these observed variables.

2.3.4.2 Endogenous variable

This research uses urban spatial vitality as an endogenous variable. Urban spatial vitality refers to the distribution of people in space and the balance of time dimensions. According to previous studies on urban space vitality (Li et al., 2020; Liu et al., 2021), this research takes vitality stability and vitality density as observed variables. Given the overall reverse difference between the vitality density and vitality stability of Changsha City, to ensure the stability of the model, the vitality density and vitality stability will be modeled separately. At the same time, the spatial vitality between weekdays and weekends has differences, so they are evaluated separately.

2.3.5 Reliability and validity testing

In order to ensure the validity of model fitting evaluation and hypothesis testing, this study conducted reliability and validity tests on variables. In this study, Cronbach's coefficient alpha (CCA) and composite reliability (CR) were used to test the reliability of the data, and the validity was assessed by calculating the mean variance (AVE). Both CCA and CR should be greater than 0.7, and AVE should be kept above 0.5 (Halkos et al., 2021; Liu et al., 2021). In this study, confirmatory factor analysis was used to measure the reliability and validity of the variables (Table 4). The analysis results show that the variables used in the study have good reliability and discriminant validity except for the assumption of spatial characteristics. Among them, the CCA value of spatial characteristic elements is slightly lower than the suggested value, because the spatial distribution of natural landscape and human landscape is often mutually exclusive. Moreover, the analysis unit of the study fails to include a wider range of spatial elements. Overall, the hypotheses and variables constructed by the study set the requirements for compound analysis.

3 Results and analysis

3.1 Spatial–temporal distribution of vitality

3.1.1 Spatial–temporal distribution of human vitality density

We divided the values of vitality density into 10 levels at natural breaks in classification (Jenks). Levels 1–10 represent density from low to high (Figure 4). The spatial vitality of urban crowds in Changsha shows a similar spatial pattern on both weekdays and rest days, that is, the central urban area is

TABLE 4 Reliability and validity of all variables (*N* = 1,475).

Latent variable	Observed variable	Mean	SD	CCA	CR	AVE
Vitality density	Weekday vitality density	0.081	0.096	0.984	0.99	0.981
	Weekend vitality density	0.069	0.082			
Vitality stability	Weekday vitality stability	0.891	0.125	0.726	0.918	0.871
	Weekend vitality stability	0.964	0.051			
A_market intervention	Shopping facility	0.045	0.086	0.929	0.958	0.835
	Dining facilities	0.061	0.103			
	Hotel accommodation	0.015	0.05			
	Daily life	0.081	0.123			
	Leisure and entertainment	0.047	0.078			
B_traffic accessibility	Subway distance	0.775	0.195	0.713	0.718	0.654
	Taxi densities	0.057	0.106			
C_spatial quality	Natural scenery	0.023	0.062	0.695	0.702	0.654
	Cultural and historical characteristics	0.008	0.043			

Notes: Total explained variance: 81.846%. Kaiser–Meyer–Olkin measure of sampling adequacy = 0.879.

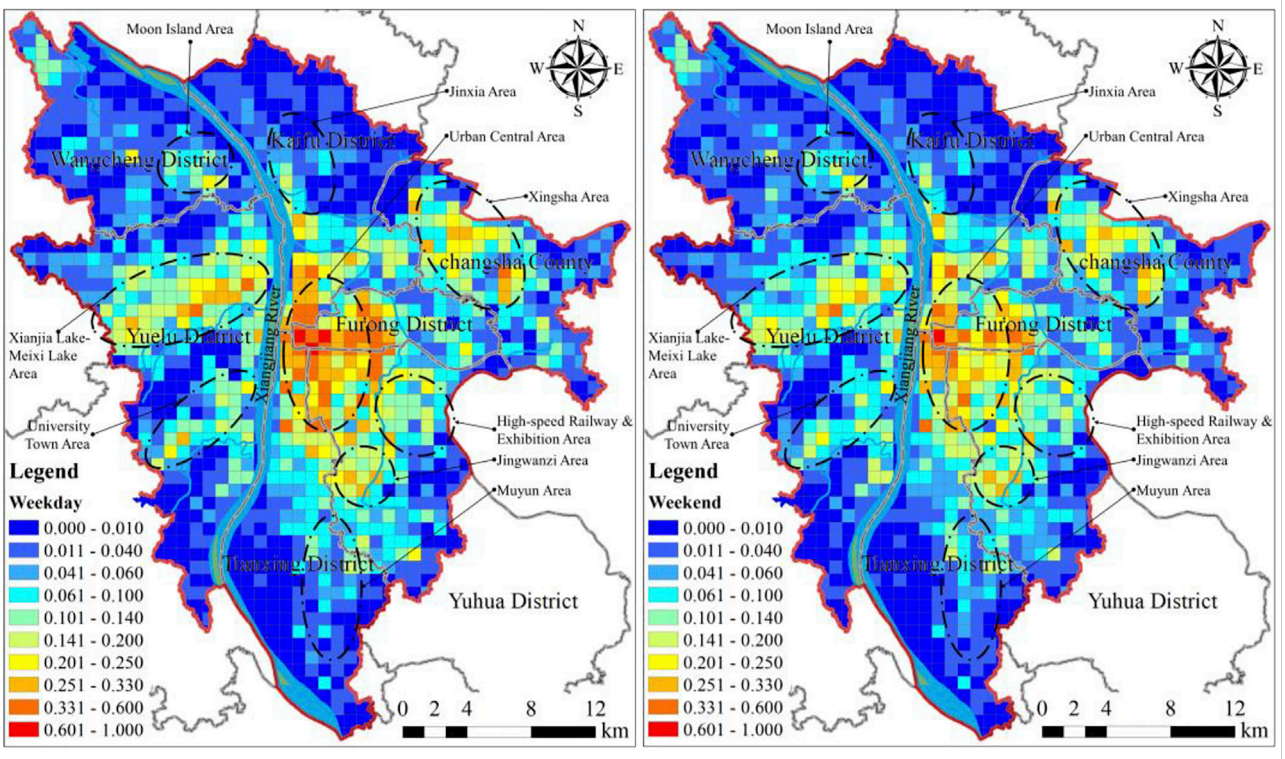

FIGURE 4
Weekday (left) and weekend (right) density of human activities.

a high-vitality density area, and the urban peripheral area is a low-vitality density area. In particular, the spatial vitality of urban crowds in Changsha can be divided into three-level areas. The first-level area is the city center area; the second-level area is the Xianjia Lake–Meixi Lake area, Xingsha area, and Jingwanzi area; and the third-level area is the Jinxia area, Moon Island area, high-speed railway, and exhibition area. In terms of the difference in vitality density between weekday and rest days, the changes in the urban center are the most significant. For rest days, the vitality density in the central

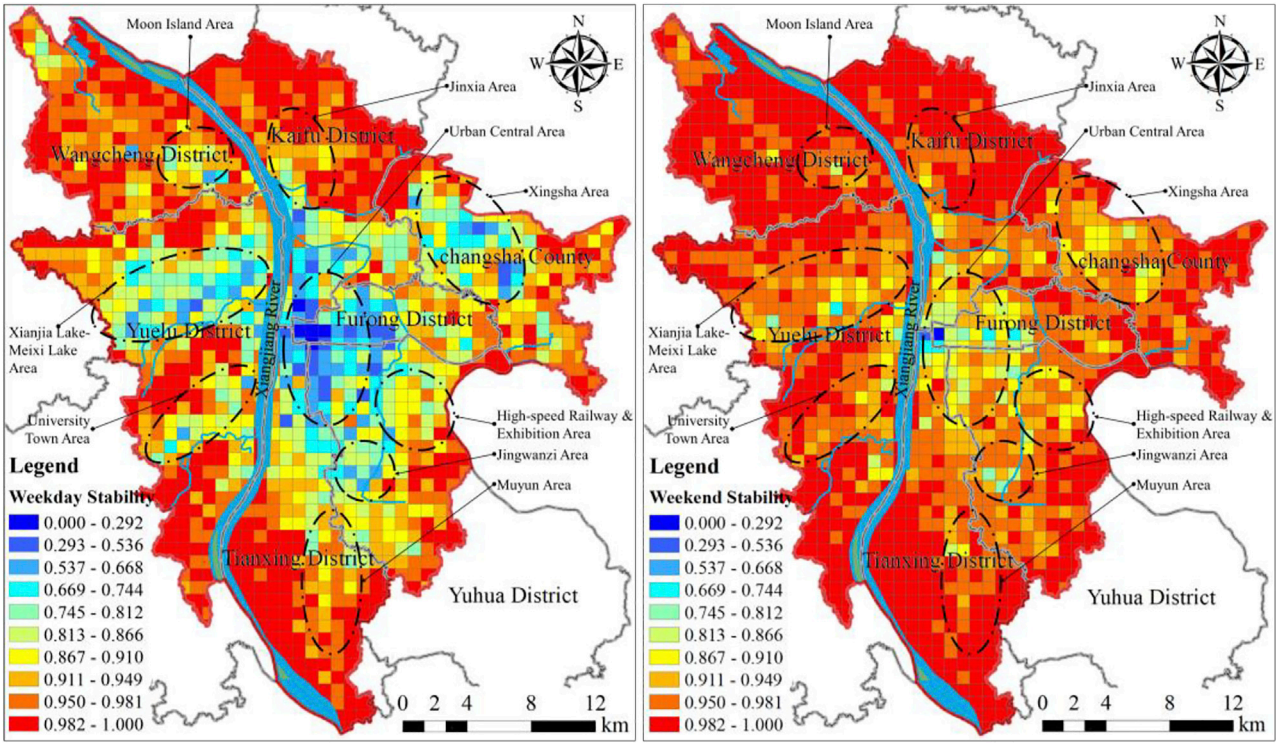

FIGURE 5
Weekday (left) and weekend (right) stability of human activities.

area of the city generally shows a downward trend, the range of high density is shrinking and the agglomeration intensity is increasing. It shows that the urban crowd gathers in the core area of the city center at a high density on rest days, and urban crowds do not tend to gather in urban areas on rest days.

3.1.2 Spatial–temporal distribution of human vitality stability

We divided values of vitality stability into 10 grades at natural breaks (Figure 5). The closer the color of the block is to red, the higher the stability; the closer to blue, the lower the stability. The overall stability of urban vitality and the density of urban vitality show a reverse pattern, that is, high-density areas show a state of low stability, and low-density areas are in a state of high stability. This result fully shows that the mobility of the urban population is significant. In particular, the stability of the city center is low. A significant difference exists in the stability of urban vitality on weekday and rest days. The stability of urban space vitality on rest days has been significantly improved, especially in the outer areas of the city center. Combined with the analysis of vitality density and vitality stability, the vitality density and vitality stability of the peripheral areas of the city center are both higher.

3.2 Analysis of environmental impacts on the vitality of urban spaces

The previous research results have shown that the urban spatial vitality density and stability of Changsha City generally present opposite spatial states. Therefore, to ensure the model analysis's accuracy, we separately carried out the model analysis of vitality density and stability. Model 1–model 4 depict the activity density of weekdays, vitality density of rest days, vitality stability of weekdays, and vitality stability of rest days, respectively. Table 5 shows the goodness-of-fit measures of the model, including GFI, CFI, NFI, TLI, and SRMR. All indices surpassed the recommended threshold for SEM, indicating a satisfactory level of goodness-of-fit.

3.2.1 The impact of traffic accessibility

The results of the model (Table 6) show that the direct impact of traffic accessibility on the vitality of urban space is 0.74 and 0.669 on weekdays and weekends, respectively. That is, the higher the transit accessibility of the waterfront open space, the higher the level of vitality. The effect of traffic accessibility on the stability of space vitality is the opposite, with −0.803 and −0.474 on weekdays and weekends, respectively. Moreover, the impact of traffic accessibility on weekdays is higher than that on rest days, the negative impact

TABLE 5 Model fit indicators.

	Model fit index	GFI	CFI	NFI	TLI	SRMR
	Recommended value	**>0.9**	**>0.9**	**>0.9**	**>0.9**	**<0.1**
Model 1	Weekday vitality density	0.937	0.971	0.969	0.955	0.023
Model 2	Weekend vitality density	0.939	0.983	0.982	0.974	0.024
Model 3	Weekday vitality stability	0.928	0.982	0.981	0.972	0.026
Model 4	Weekend vitality stability	0.914	0.973	0.972	0.958	0.028

TABLE 6 Hypotheses tests.

Model	Relationship	Influence coefficient	Standard error	Standard deviation	Result
Model 1	Market intervention→Weekday vitality density	0.295	0.114	3.401	Supported
	Traffic accessibility→Weekday vitality density	0.74	0.102	7.257	Supported
	Spatial quality→Weekday vitality density	−0.023	0.098	−1.017	Not supported
Model 2	Market intervention→Weekend vitality density	0.364	0.098	4.155	Supported
	Traffic accessibility→Weekend vitality density	0.669	0.084	6.636	Supported
	Spatial quality→Weekend vitality density	−0.025	0.083	−1.167	Not supported
Model 3	Market intervention→Weekday vitality stability	−0.211	0.17	−2.051	Not supported
	Traffic accessibility→Weekday vitality stability	−0.803	0.148	−6.754	Not supported
	Spatial quality→Weekday vitality stability	0.027	0.139	0.94	Supported
Model 4	Market intervention→Weekend vitality stability	−0.505	0.044	−7.718	Not supported
	Traffic accessibility→Weekend vitality stability	−0.474	0.037	−6.644	Not supported
	Spatial quality→Weekend vitality stability	0.026	0.058	1.184	Supported

of traffic accessibility on stability is weaker on weekends, and the positive impact on vitality density is also weaker.

This study is consistent with the view of traditional urban space vitality analysis that good transportation accessibility can increase the frequency of interaction between urban population and urban space, thereby enhancing the vitality of urban space (Delclòs-Alió and Miralles-Guasch, 2018; Niu et al., 2021; Yang et al., 2021). Some research results reveal the negative impact of transportation accessibility on urban vitality (Liu et al., 2021). This study also found that good transportation accessibility leads to a decrease in the stability of urban vitality.

3.2.2 The impact of market intervention facility

Market intervention factors have a positive impact on the vitality of urban space, and their impact factors are 0.295 and 0.364 on weekdays and weekends, respectively. Thus, market intervention factors have a greater impact on the vitality of urban space on weekends. People tend to patronize market intervention facilities on weekends, and their consumption behavior is also more intensive. The factors of market intervention have a negative impact on the stability of urban spatial vitality on weekdays and weekends, and the impact is greater on weekends. This result fully shows that the more concentrated urban market facilities, the more unstable the urban vitality, especially on weekends.

Five observed variables representing attributes of the market intervention were found to positively affect the vitality: shopping facility, dining facilities, hotel accommodation, daily life, and leisure and entertainment. The results of shopping facilities and dining facilities are in line with previous findings (Xia et al., 2020; Li et al., 2021).

3.2.3 The impact of spatial quality

The influence of spatial quality on the vitality density and vitality stability of urban space is small whether it is a weekday or a rest day. The direct impact of spatial quality on the vitality density of urban space is −0.023 and −0.025 on weekdays and weekends, respectively. The direct impact of spatial quality on the stability of urban space vitality is 0.027 and 0.026 on weekdays and weekends, respectively. Thus, the richer the urban spatial quality, the lower the urban vitality density, and the better the sustainability of crowd space agglomeration.

In general, the intensity of the influence of spatial elements on the urban spatial vitality density is in descending order: traffic accessibility, market intervention, and spatial characteristics. Among them, the influence of spatial characteristics is small. Spatial characteristics have similar effects on the stability of urban vitality during weekdays and weekends. The influence of traffic accessibility on the stability of urban spatial vitality on weekdays is greater than that on rest days, and the impact of market intervention factors on the stability of urban spatial vitality on weekdays is smaller than that on rest days.

4 Discussion

4.1 Comparison with existing research

The research results show that the vitality density and vitality stability of the urban population are in opposite states whether it is a work day or a rest day. The spatial distribution pattern of its vitality density is basically consistent with previous studies (Delclòs-Alió and Miralles-Guasch, 2018; Liu and Long, 2019; Guo et al., 2021), that is, the urban center area has a high-vitality density, and the vitality density of urban fringe areas continues to decrease. However, the opposite pattern characteristics of vitality density and vitality stability are different from the research results of Shanghai waterfront space (Liu et al., 2021). We comparatively analyzed the results of this study and found a significant difference between the vitality distribution status of city-wide regions and smaller regions. In a smaller area, high dynamism and high stability coexist, but this situation is almost non-existent on the overall scale of the city. This finding illustrates the value of studying the spatial dynamism of a city as a whole. The impact of urban transportation accessibility on urban vitality density is significant; and the better the accessibility, the greater the vitality density. This finding is consistent with other research results (Lu et al., 2019; Niu et al., 2021). However, the effect of traffic accessibility on the stability of urban vitality is the opposite. In particular, efficient urban traffic often leads to high-frequency flow of urban people, but it is not conducive to the continuous gathering of urban people in the same space. The impact of market-led facilities on the vitality of urban spaces is similar to that of urban transport accessibility.

4.2 Suggestions for urban space optimization

The study of urban spatial vitality patterns and influencing factors has important implications for urban spatial optimization and spatial structure adjustment. The urban spatial structure is the distribution state of different spatial attributes or spatial functions in the city, including the agglomeration and connection of spatial elements. From the perspective of attribute types, the spatial structure can be divided into the spatial structure of population distribution, green space structure, commercial spatial structure, and employment spatial structure (Wu and Plantinga, 2003; Gong et al., 2017; Mathey et al., 2021; Zhou, 2022). The agglomeration of public space and the connection between different agglomeration points have obvious interactive characteristics with the spatial agglomeration of urban people. This study clarifies the impact of different functional spaces on urban vitality, which has a good reference for urban space optimization and structural adjustment.

Research shows that the vitality and stability of urban space are affected by the elements of the urban built environment. In turn, the improvement of the vitality of urban public space will promote the optimization of urban space quality and its spatial structure. Urban transportation accessibility is the most critical factor affecting urban vitality, followed by market intervention attributes. The improvement in the stability of urban spatial vitality on weekends is mainly due to the decrease in the influence of traffic accessibility and the increase in the influence intensity of the elements of the market intervention attribute. Therefore, the adjustment of urban spatial structure should pay attention to the elements of urban traffic and market intervention attributes, and consider them together. The layout of facilities related to market intervention attributes should be increased in the periphery of the city center, especially the Jinxia area, Muyun area, University Town area and Moon Island area; in the Xianjiahu–Meixihu area and Xingsha area, short-distance traffic should be improved. The accessibility of the high-speed rail station, the exhibition area, and the Jingwanzi District to the city's central business district should be improved.

The elements of spatial characteristic attributes have a weak negative impact on the urban spatial vitality density, but at the same time, they have a weak positive impact on the vitality stability. This may have a strong relationship with the environmental quality, scale, and supporting facilities of urban natural and human landscapes. Therefore, urban spaces with spatial characteristics should be optimized through landscape planning, environmental improvement, and regional support.

4.3 Implications for urban renewal actions

The improvement of urban space vitality is one of the core purposes of urban renewal and stock planning. At present, China's urbanization process has entered the era of stock development. How to enhance the vitality of urban space through space optimization and create a city full of vitality is particularly urgent. Analyzing the spatial distribution of urban spatial vitality density and stability can provide important methods for urban physical examination and urban planning evaluation by ensuring that planners and policymakers can quickly and effectively identify urban-wide spatial vitality issues. The research analyzes the degree of influence of different influencing factors on the vitality of urban space, which provides a direct basis for the formulation of urban space development policy and space renewal. For

example, in the optimization of market-led facilities, market-led facilities must be given proper guidance through urban policies, taxation, space environment improvement, and other methods to promote their rational layout. Spatial quality is the only element that has a positive effect on the vitality and stability of urban space. Thus, the optimization of urban space should focus on the combined planning or adjustment of featured spaces and other types of urban spaces.

4.4 Limitations and uncertainty

The study analyzes the distribution pattern of urban spatial vitality density in different time periods and analyzes the urban vitality stability status on the basis of hourly changes in the urban population. Through SEM, the influencing factors of urban space vitality are discussed. The research provides a useful reference for urban spatial structure adjustment, stock planning and urban renewal, urban vitality enhancement, and spatial quality optimization.

However, similar to any empirical research, this study suffers from limitations. On the one hand, the research is insufficient in the analysis of urban function mixed feature intervention, micro-spatial features and design features, and spatial–temporal heterogeneity of influencing mechanisms. On the other hand, although an epidemic did not occur in the study area during the period selected in this study, the subsequent interference of the novel coronavirus disease (COVID-19) was insufficiently explained in this study. These shortcomings will be addressed through model optimization and feature mining, which we may explore in future research.

5 Conclusion

The purpose of this study was to analyze the distribution pattern of urban population in urban space at different time periods and to analyze the influencing factors of spatial vitality. The research uses MPSD to reveal the spatial vitality density and vitality stability of urban population on weekdays and rest days. On this basis, the influence mechanism of urban vitality density and vitality stability in different time periods was analyzed using the SEM model. The research provides a useful reference for urban space optimization and structural adjustment. The result shows

1) On the urban scale, the overall spatial vitality density and vitality stability show a reverse pattern, that is, the high-vitality density area presents a low-vitality stability state, and the low-vitality density area presents a low-vitality state. The city center area has the highest density of vitality due to the attraction of commercial centers. The city's vitality density continues to decline from the urban center to the urban periphery.
2) The overall urban vitality density on rest days is slightly lower than that on weekdays, and the stability of vitality on rest days is significantly higher than that on weekdays. Xianjia Lake–Meixi Lake area, Xingsha area, Jingwanzi area, and University Town area performed better in rest day vitality density and vitality stability.
3) According to the structural equation model hypothesis, each model supports two hypotheses and rejects one hypothesis. Urban transportation accessibility has the greatest impact on the city's vitality density at various time periods and the stability of the vitality on weekday, followed by market intervention facilities, and the least impact is on spatial characteristics. The impact of rest day traffic accessibility is slightly smaller than that of market intervention facilities. Urban transportation accessibility and market intervention facilities have a positive impact on urban vitality density and a negative impact on urban vitality stability. Spatial features are the opposite.

This study fully demonstrates a significant interaction between urban spatial vitality and vitality stability and the urban built environment. The adjustment of urban spatial structure should strengthen the coordination between the construction of urban transportation networks and the improvement of urban market intervention facilities to jointly promote the improvement of urban vitality and spatial quality. Taking Changsha City as an example, the study analyzes the spatial distribution pattern of spatial vitality density and vitality stability at the urban scale. The study uses MPSD and spatial facility location data. Considering that these types of data are easy to obtain, this method can inform other urban or regional studies. In addition, our research results provide a direct reference for the optimization of urban spatial environment. Particularly in the preliminary work of urban renewal and stock planning, it can play a key role, such as in the identification of urban problem spaces, the selection of renewal modes, and the cognition of spatial characteristics.

Data availability statement

The original contributions presented in the study are included in the article/Supplementary Material; further inquiries can be directed to the corresponding author.

Author contributions

XX: conceptualization, methodology, and formal analysis. YZ: conceptualization and methodology. YZ: data curation and

formal analysis. TR: writing—review and editing. YZ: writing—review and editing.

Funding

This work was financially supported by the Philosophy and Social Sciences Fund major projects in Sichuan Province, SC21EZD002, the Philosophy and Social Science Research Fund of the Chengdu University of Technology, YJ2021-QN007, and Open Foundation of the Research Center for Human Geography of Tibetan Plateau and Its Eastern Slope (Chengdu University of Technology), Grant number RWDL2021-YB010. Also, we want to thank the anonymous reviewers for their valuable suggestions and comments that contributed to improving the quality of the manuscript.

Conflict of interest

The authors declare that the research was conducted in the absence of any commercial or financial relationships that could be construed as a potential conflict of interest.

Publisher's note

All claims expressed in this article are solely those of the authors and do not necessarily represent those of their affiliated organizations, or those of the publisher, the editors, and the reviewers. Any product that may be evaluated in this article, or claim that may be made by its manufacturer, is not guaranteed or endorsed by the publisher.

References

Batty, M. (2016). Empty buildings, shrinking cities and ghost towns. *Environ. Plann. B. Plann. Des.* 43 (1), 3–6. doi:10.1177/0265813515619858

Birenboim, A., and Shoval, N. (2016). Mobility research in the age of the smartphone. *Ann. Am. Assoc. Geogr.* 06 (2), 293–291. doi:10.1080/00045608.2015.1100058

Chen, N., and Akar, G. (2016). Effects of neighborhood types & socio-demographics on activity space. *J. Transp. Geogr.* 54, 112–121. doi:10.1016/j.jtrangeo.2016.05.017

Chen, Z., Dong, B., Pei, Q., and Zhang, Z. (2022). The impacts of urban vitality and urban density on innovation: Evidence from China's Greater Bay Area. *Habitat Int.* 119, 102490. doi:10.1016/j.habitatint.2021.102490

De Nadai, M., Staiano, J., Larcher, R., Sebe, N., Quercia, D., and Lepri, B. (2016). "The death and life of great Italian cities: A mobile phone data perspective," in Proceedings of the 25th International Conference on World Wide Web, Montréal Québec Canada, April 11 - 15, 2016. Paper presented at the.

Delclòs-Alió, X., Gutiérrez, A., and Miralles-Guasch, C. (2019). The urban vitality conditions of Jane Jacobs in Barcelona: Residential and smartphone-based tracking measurements of the built environment in a Mediterranean metropolis. *Cities* 86, 220–228. doi:10.1016/j.cities.2018.09.021

Delclòs-Alió, X., and Miralles-Guasch, C. (2018). Looking at Barcelona through Jane Jacobs's eyes: Mapping the basic conditions for urban vitality in a Mediterranean conurbation. *Land Use Policy* 75, 505–517. doi:10.1016/j.landusepol.2018.04.026

Dong, Y.-H., Peng, F.-L., and Guo, T.-F. (2021). Quantitative assessment method on urban vitality of metro-led underground space based on multi-source data: A case study of Shanghai inner ring area. *Tunn. Undergr. Space Technol.* 116, 104108. doi:10.1016/j.tust.2021.104108

Fan, Z., Duan, J., Luo, M., Zhan, H., Liu, M., Peng, W., et al. (2021). How did built environment affect urban vitality in urban waterfronts? A case study in nanjing reach of Yangtze River. *ISPRS Int. J. Geoinf.* 10 (9), 611. doi:10.3390/ijgi10090611

Fan, Z., Pei, T., Ma, T., Du, Y., Song, C., Liu, Z., et al. (2018). Estimation of urban crowd flux based on mobile phone location data: A case study of beijing, China. *Comput. Environ. Urban Syst.* 69, 114–123. doi:10.1016/j.compenvurbsys.2018.01.005

García-Palomares, J. C., Salas-Olmedo, M. H., Moya-Gómez, B., Condeço-Melhorado, A., and Gutiérrez, J. (2018). City dynamics through Twitter: Relationships between land use and spatiotemporal demographics. *Cities* 72, 310–319. doi:10.1016/j.cities.2017.09.007

Gehl, J., Kaefer, L. J., and Reigstad, S. (2006). Close encounters with buildings. *Urban Des. Int.* 11 (1), 29–47. doi:10.1057/palgrave.udi.9000162

Gong, Y., Lin, Y., and Duan, Z. (2017). Exploring the spatiotemporal structure of dynamic urban space using metro smart card records. *Comput. Environ. Urban Syst.* 64, 169–183. doi:10.1016/j.compenvurbsys.2017.02.003

Guo, X., Chen, H., and Yang, X. (2021). An evaluation of street dynamic vitality and its influential factors based on multi-source big data. *ISPRS Int. J. Geoinf.* 10 (3), 143. doi:10.3390/ijgi10030143

Guo, X., Yang, Y., Cheng, Z., Wu, Q., Li, C., Lo, T., et al. (2022). Spatial social interaction: An explanatory framework of urban space vitality and its preliminary verification. *Cities* 121, 103487. doi:10.1016/j.cities.2021.103487

Halkos, G., Leonti, A., and Sardianou, E. (2021). Activities, motivations and satisfaction of urban parks visitors: A structural equation modeling analysis. *Econ. Anal. Policy* 70, 502–513. doi:10.1016/j.eap.2021.04.005

He, Q., He, W., Song, Y., Wu, J., Yin, C., Mou, Y., et al. (2018). The impact of urban growth patterns on urban vitality in newly built-up areas based on an association rules analysis using geographical 'big data. *Land Use Policy* 78, 726–738. doi:10.1016/j.landusepol.2018.07.020

Huang, D., Liu, Z., Zhao, X., and Zhao, P. (2017). Emerging polycentric megacity in China: An examination of employment subcenters and their influence on population distribution in Beijing. *Cities* 69, 36–45. doi:10.1016/j.cities.2017.05.013

Hui, C., Xianghui, W., Xiqiang, Z., and Shaoli, Z. (2014). "The evaluation of Chinese urban traffic management system Application based on intelligent traffic control technology," in Paper presented at the 2014 7th International Conference on Intelligent Computation Technology and Automation, Changsha, China, Oct. 25 2014 to Oct. 26 2014.

Jiang, Y., Han, Y., Liu, M., and Ye, Y. (2022). Street vitality and built environment features: A data-informed approach from fourteen Chinese cities. *Sustain. Cities Soc.* 79, 103724. doi:10.1016/j.scs.2022.103724

Jin, X., Long, Y., Sun, W., Lu, Y., Yang, X., Tang, J., et al. (2017). Evaluating cities' vitality and identifying ghost cities in China with emerging geographical data. *Cities* 63, 98–109. doi:10.1016/j.cities.2017.01.002

Jo, H. I., and Jeon, J. Y. (2021). Overall environmental assessment in urban parks: Modelling audio-visual interaction with a structural equation model based on soundscape and landscape indices. *Build. Environ.* 204, 108166. doi:10.1016/j.buildenv.2021.108166

Kim, Y.-L. (2018). Seoul's Wi-Fi hotspots: Wi-Fi access points as an indicator of urban vitality. *Comput. Environ. Urban Syst.* 72, 13–24. doi:10.1016/j.compenvurbsys.2018.06.004

Laman, H., Yasmin, S., and Eluru, N. (2019). Using location-based social network data for activity intensity analysis: A case study of New York city. *J. Transp. Land Use* 12 (1), 723–740. doi:10.5198/jtlu.2019.1470

Lan, F., Gong, X., Da, H., and Wen, H. (2020). How do population inflow and social infrastructure affect urban vitality? Evidence from 35 large- and medium-sized cities in China. *Cities* 100, 102454. doi:10.1016/j.cities.2019.102454

Lang, W., Chen, T., and Li, X. (2016). A new style of urbanization in China: Transformation of urban rural communities. *Habitat Int.* 55, 1–9. doi:10.1016/j.habitatint.2015.10.009

Li, F., Li, F., Li, S., and Long, Y. (2020). Deciphering the recreational use of urban parks: Experiments using multi-source big data for all Chinese cities. *Sci. Total Environ.* 701, 134896. doi:10.1016/j.scitotenv.2019.134896

Li, J., Li, J., Yuan, Y., and Li, G. (2019). Spatiotemporal distribution characteristics and mechanism analysis of urban population density: A case of xi'an, shaanxi, China. *Cities* 86, 62–70. doi:10.1016/j.cities.2018.12.008

Li, M., Shen, Z., and Hao, X. (2016). Revealing the relationship between spatio-temporal distribution of population and urban function with social media data. *Geojournal* 81 (6), 919–935. doi:10.1007/s10708-016-9738-7

Li, Q., Cui, C., Liu, F., Wu, Q., Run, Y., Han, Z., et al. (2021). Multidimensional urban vitality on streets: Spatial patterns and influence factor identification using multisource urban data. *ISPRS Int. J. Geoinf.* 11 (1), 2. doi:10.3390/ijgi11010002

Li, S.-m., and Liu, Y. (2016). The jobs-housing relationship and commuting in Guangzhou, China: Hukou and dual structure. *J. Transp. Geogr.* 54, 286–294. doi:10.1016/j.jtrangeo.2016.06.014

Li, X., Li, Y., Jia, T., Zhou, L., and Hijazi, I. H. (2022). The six dimensions of built environment on urban vitality: Fusion evidence from multi-source data. *Cities* 121, 103482. doi:10.1016/j.cities.2021.103482

Lin, Y., Shui, W., Li, Z., Huang, S., Wu, K., Sun, X., et al. (2021). Green space optimization for rural vitality: Insights for planning and policy. *Land Use Policy* 108, 105545. doi:10.1016/j.landusepol.2021.105545

Liu, S., Lai, S.-Q., Liu, C., and Jiang, L. (2021). What influenced the vitality of the waterfront open space? A case study of huangpu river in Shanghai, China. *Cities* 114, 103197. doi:10.1016/j.cities.2021.103197

Liu, X., Song, Y., Wu, K., Wang, J., Li, D., Long, Y., et al. (2015). Understanding urban China with open data. *Cities* 47, 53–61. doi:10.1016/j.cities.2015.03.006

Liu, S, and Long, Y. (2019). Urban vitality area identification and pattern analysis from the perspective of time and space fusion. *Sustainability* 11 (15), 4032. doi:10.3390/su11154032

Lu, S., Shi, C., and Yang, X. (2019). Impacts of built environment on urban vitality: Regression analyses of beijing and Chengdu, China. *Int. J. Environ. Res. Public Health* 16 (23), 4592. doi:10.3390/ijerph16234592

Mathey, J., Hennersdorf, J., Lehmann, I., and Wende, W. (2021)., 125. Germany, 107519. doi:10.1016/j.ecolind.2021.107519Qualifying the urban structure type approach for urban green space analysis – a case study of Dresden, Germany*Ecol. Indic.*

Meng, Y., and Xing, H. (2019). Exploring the relationship between landscape characteristics and urban vibrancy: A case study using morphology and review data. *Cities* 95, 102389. doi:10.1016/j.cities.2019.102389

Mouratidis, K., and Poortinga, W. (2020). Built environment, urban vitality and social cohesion: Do vibrant neighborhoods foster strong communities? *Landsc. Urban Plan.* 204, 103951. doi:10.1016/j.landurbplan.2020.103951

Mu, B., Liu, C., Mu, T., Xu, X., Tian, G., Zhang, Y., et al. (2021). Spatiotemporal fluctuations in urban park spatial vitality determined by on-site observation and behavior mapping: A case study of three parks in zhengzhou city, China. *Urban For. Urban Green.* 64, 127246. doi:10.1016/j.ufug.2021.127246

Mushkani, R. A., and Ono, H. (2021). The role of land use and vitality in fostering gender equality in urban public parks: The case of Kabul city, Afghanistan. *Habitat Int.* 118, 102462. doi:10.1016/j.habitatint.2021.102462

Najaf, P., Thill, J.-C., Zhang, W., and Fields, M. G. (2018). City-level urban form and traffic safety: A structural equation modeling analysis of direct and indirect effects. *J. Transp. Geogr.* 69, 257–270. doi:10.1016/j.jtrangeo.2018.05.003

Niu, Y., Mi, X., and Wang, Z. (2021). Vitality evaluation of the waterfront space in the ancient city of Suzhou. *Front. Archit. Res.* 10 (4), 729–740. doi:10.1016/j.foar.2021.07.001

Pakoz, M. Z., and Isik, M. (2022). Rethinking urban density, vitality and healthy environment in the post-pandemic city: The case of Istanbul. *Cities* 124, 103598. doi:10.1016/j.cities.2022.103598

Qian, C., Li, W., Duan, Z., Yang, D., and Ran, B. (2021). Using mobile phone data to determine spatial correlations between tourism facilities. *J. Transp. Geogr.* 92, 103018. doi:10.1016/j.jtrangeo.2021.103018

Shami, M. R., Rad, V. B., and Moinifar, M. (2022). The structural model of indicators for evaluating the quality of urban smart living. *Technol. Forecast. Soc. Change* 176, 121427. doi:10.1016/j.techfore.2021.121427

Shi, J., Miao, W., Si, H., and Liu, T. (2021). Urban vitality evaluation and spatial correlation research: A case study from Shanghai, China. *Land* 10 (11), 1195. doi:10.3390/land10111195

Sung, H., and Lee, S. (2015). Residential built environment and walking activity: Empirical evidence of Jane Jacobs' urban vitality. *Transp. Res. Part D Transp. Environ.* 41, 318–329. doi:10.1016/j.trd.2015.09.009

Tang, L., Lin, Y., Li, S., Li, S., Li, J., Ren, F., et al. (2018). Exploring the influence of urban form on urban vibrancy in shenzhen based on mobile phone data. *Sustainability* 10 (12), 4565. doi:10.3390/su10124565

Tong, D., Yuan, Y., and Wang, X. (2021). The coupled relationships between land development and land ownership at China's urban fringe: A structural equation modeling approach. *Land Use Policy* 100, 104925. doi:10.1016/j.landusepol.2020.104925

Tu, W., Zhu, T., Xia, J., Zhou, Y., Lai, Y., Jiang, J., et al. (2020). Portraying the spatial dynamics of urban vibrancy using multisource urban big data. *Comput. Environ. Urban Syst.* 80, 101428. doi:10.1016/j.compenvurbsys.2019.101428

Wang, M., Madden, M., and Liu, X. (2017). Exploring the relationship between urban forms and CO2 emissions in 104 Chinese cities. *J. Urban Plan. Dev.* 143 (4). doi:10.1061/(asce)up.1943-5444.0000400

Wang, X., Zhang, Y., Yu, D., Qi, J., and Li, S. (2022). Investigating the spatiotemporal pattern of urban vibrancy and its determinants: Spatial big data analyses in Beijing, China. *Land Use Policy* 119, 106162. doi:10.1016/j.landusepol.2022.106162

Wu, C., Ye, X., Ren, F., and Du, Q. (2018). Check-in behaviour and spatio-temporal vibrancy: An exploratory analysis in Shenzhen, China. *Cities* 77, 104–116. doi:10.1016/j.cities.2018.01.017

Wu, J., and Plantinga, A. J. (2003). The influence of public open space on urban spatial structure. *J. Environ. Econ. Manage.* 46 (2), 288–309. doi:10.1016/s0095-0696(03)00023-8

Wu, J., Ta, N., Song, Y., Lin, J., and Chai, Y. (2018). Urban form breeds neighborhood vibrancy: A case study using a GPS-based activity survey in suburban beijing. *Cities* 74, 100–108. doi:10.1016/j.cities.2017.11.008

Wu, W., and Niu, X. (2019). Influence of built environment on urban vitality: Case study of Shanghai using mobile phone location data. *J. Urban Plan. Dev.* 145 (3). doi:10.1061/(asce)up.1943-5444.0000513

Xia, C., Wang, H., Zhang, A., and Zhang, W. (2017). A high-performance cellular automata model for urban simulation based on vectorization and parallel computing technology. *Int. J. Geogr. Inf. Sci.* 32 (2), 399–424. doi:10.1080/13658816.2017.1390118

Xia, C., Yeh, A. G.-O., and Zhang, A. (2020). Analyzing spatial relationships between urban land use intensity and urban vitality at street block level: A case study of five Chinese megacities. *Landsc. Urban Plann.* 193, 103669. doi:10.1016/j.landurbplan.2019.103669

Xia, C., Zhang, A., Wang, H., Zhang, B., and Zhang, Y. (2019). Bidirectional urban flows in rapidly urbanizing metropolitan areas and their macro and micro impacts on urban growth: A case study of the Yangtze River middle reaches megalopolis, China. *Land Use Policy* 82, 158–168. doi:10.1016/j.landusepol.2018.12.007

Xiao, Y., Wang, D., and Fang, J. (2019). Exploring the disparities in park access through mobile phone data: Evidence from Shanghai, China. *Landsc. Urban Plan.* 181, 80–91. doi:10.1016/j.landurbplan.2018.09.013

Xie, M., Chen, J., Zhang, Q., Li, H., Fu, M., Breuste, J., et al. (2020). Dominant landscape indicators and their dominant areas influencing urban thermal environment based on structural equation model. *Ecol. Indic.* 111, 105992. doi:10.1016/j.ecolind.2019.105992

Xu, Y., and Chen, X. (2021). Quantitative analysis of spatial vitality and spatial characteristics of urban underground space (UUS) in metro area. *Tunn. Undergr. Space Technol.* 111, 103875. doi:10.1016/j.tust.2021.103875

Yang, J., Cao, J., and Zhou, Y. (2021). Elaborating non-linear associations and synergies of subway access and land uses with urban vitality in Shenzhen. *Transp. Res. Part A Policy Pract.* 144, 74–88. doi:10.1016/j.tra.2020.11.014

Ye, Y., Li, D., and Liu, X. (2017). How block density and typology affect urban vitality: An exploratory analysis in shenzhen, China. *Urban Geogr.* 39 (4), 631–652. doi:10.1080/02723638.2017.1381536

Yin, L., Lin, N., and Zhao, Z. (2021). Mining daily activity chains from large-scale mobile phone location data. *Cities* 109, 103013. doi:10.1016/j.cities.2020.103013

Yue, W., Chen, Y., Thy, P. T. M., Fan, P., Liu, Y., Zhang, W., et al. (2021). Identifying urban vitality in metropolitan areas of developing countries from a comparative perspective: Ho chi minh city versus Shanghai. *Sustain. Cities Soc.* 65, 102609. doi:10.1016/j.scs.2020.102609

Yue, Y., Zhuang, Y., Yeh, A. G. O., Xie, J.-Y., Ma, C.-L., Li, Q.-Q., et al. (2016). Measurements of POI-based mixed use and their relationships with neighbourhood vibrancy. *Int. J. Geogr. Inf. Sci.* 31 (4), 658–675. doi:10.1080/13658816.2016.1220561

Zeng, C., Song, Y., He, Q., and Shen, F. (2018). Spatially explicit assessment on urban vitality: Case studies in Chicago and Wuhan. *Sustain. Cities Soc.* 40, 296–306. doi:10.1016/j.scs.2018.04.021

Zheng, Q., Deng, J., Jiang, R., Wang, K., Xue, X., Lin, Y., et al. (2017). Monitoring and assessing "ghost cities" in Northeast China from the view of nighttime light remote sensing data. *Habitat Int.* 70, 34–42. doi:10.1016/j.habitatint.2017.10.005

Zhou, N. (2022). Research on urban spatial structure based on the dual constraints of geographic environment and POI big data. *J. King Saud Univ. - Sci.* 34 (3), 101887. doi:10.1016/j.jksus.2022.101887

Zhu, J., Lu, H., Zheng, T., Rong, Y., Wang, C., Zhang, W., et al. (2020). Vitality of urban parks and its influencing factors from the perspective of recreational service supply, demand, and spatial links. *Int. J. Environ. Res. Public Health* 17 (5), 1615. doi:10.3390/ijerph17051615

frontiers | Frontiers in Environmental Science

TYPE Original Research
PUBLISHED 16 August 2022
DOI 10.3389/fenvs.2022.962410

Check for updates

OPEN ACCESS

EDITED BY
Ying Jing,
Zhejiang University, China

REVIEWED BY
Xiping Yang,
Shaanxi Normal University, China
Yanwen Wang,
China University of Geosciences
Wuhan, China

*CORRESPONDENCE
Meng Huang,
huangm16@chinatelecom.cn

SPECIALTY SECTION
This article was submitted to Environmental Informatics and Remote Sensing,
a section of the journal
Frontiers in Environmental Science

RECEIVED 06 June 2022
ACCEPTED 07 July 2022
PUBLISHED 16 August 2022

CITATION
Huang M, Li X, Tu W and Yang M (2022), Multisource data integration for targeted bus exterior advertising. *Front. Environ. Sci.* 10:962410. doi: 10.3389/fenvs.2022.962410

COPYRIGHT
© 2022 Huang, Li, Tu and Yang. This is an open-access article distributed under the terms of the Creative Commons Attribution License (CC BY). The use, distribution or reproduction in other forums is permitted, provided the original author(s) and the copyright owner(s) are credited and that the original publication in this journal is cited, in accordance with accepted academic practice. No use, distribution or reproduction is permitted which does not comply with these terms.

Multisource data integration for targeted bus exterior advertising

Meng Huang[1]*, Xinchi Li[1], Wei Tu[2] and Mingchuan Yang[1]

[1]China Telecom Research Institute, Beijing, China, [2]Shenzhen Key Laboratory of Spatial Information Smart Sensing and Services and Research Institute of Smart Cities, School of Architecture and Urban Planning, Shenzhen University, Shenzhen, China

Bus exterior advertising plays a significant role in outdoor advertising, since it provides frequent exposure to a large number of residents. Traditional route selection methods are generally based on a rough estimation, for example, the number of total passengers of a bus route or the geographical features along the bus route. Targeted bus exterior advertising remains a challenge as little is known about the characteristics of the people along the bus route. In this study, we are aiming at determining a set of bus routes for a given ad category to maximize advertising effectiveness, by mining multiple data sources, including mobile phone data, bus GPS data, smart card data (SCD), and land use data. Specifically, we first estimated the distribution of potential target audiences using mobile phone data and land use data. Two optimization models are proposed considering different advertising requirements. For well-established brands that audiences are familiar with, a wide coverage-oriented bus route selection model is proposed to maximize the coverage of potential target audiences. For new brands that require a high level of exposure before they become recognizable, a deep coverage-oriented bus route selection model is proposed to maximize the total exposure times of the ads. Both models were demonstrated with a case study in Shenzhen, China to explicitly present the outcomes of the models and the differences between them. The calculation results show that the wide coverage-oriented model achieves an average of 84.8% improvement compared with baseline 1 which selects the bus routes with the most passengers, while an average of 9.2% improvement compared with baseline 2 which selects the bus route with the maximum coverage of the target area in reaching more potential target audiences. The exposure intensity of the deep coverage-oriented model is almost 3.7 times of the wide coverage-oriented model. The proposed models provide new options for advertisers to select a suitable advertising strategy according to their needs.

KEYWORDS

bus exterior advertising, mobile phone data, maximal coverage location problem, multiple coverage problem, targeted advertising

1 Introduction

According to a recent market report, Out-of-home (OOH) advertising is the only traditional media category that has shown consistent revenue growth, and the revenue is expected to grow by 4% each year (JCDecaux 2020). Outdoor advertising is still a highly competitive and effective way to reach potential consumers despite the emergence of many new media, e.g., online advertising. The most common form of outdoor advertising is billboards, but transit advertising is becoming more and more popular, especially in countries with high traffic and pedestrian densities. As an important subset of outdoor advertising, transit advertising contains static transit advertising (e.g., bus stop advertising) and moving transit advertising (e.g., bus interior advertising, bus exterior advertising) (Roux 2014). In this study, we focus on bus exterior advertising. Exterior advertisements can be displayed on the side, front, and rear of the bus, offering advertisers high exposure. In addition to the common outdoor advertising advantages, the mobility of the bus makes it possible to reach mass audiences with broad coverage and targeted capabilities.

While an advantage of transit advertising is the ability to provide exposure to a large number of people, some audiences may not be interested in the content of the ad, and therefore it will not very effective in reaching these people. Exist studies have demonstrated that targeted advertising is effective to attract audience' attention and increase the effectiveness of the advertising campaigns (Tam and Ho 2006; Tucker 2014). Hence, to launch a successful advertising campaign, the key is to maximize the ads' exposure to the audiences who may be interested in the ads. Bus exterior ads will target different audiences depending on the route it follows. The audience of bus exterior advertising includes pedestrians in the streets, bus riders, and people in nearby cars, which is almost the most complex audience component to measure (Małecki et al., 2019). Traditional methods usually simplified the number of audiences to the number of passengers taken by a bus (Zhang et al., 2017a; Zhang D. et al., 2017b). However, the traditional methods ignore the pedestrians, and people in nearby cars, who are also an important part of the audience. In addition, they did not consider the interests of the audiences and were unable to achieve targeted advertising. There are also some studies selecting bus routes based on functional regions or categories of POIs that a bus route covers (Zhang X. et al., 2017c). For example, clothing ads prefer to be placed on the bus routes passing through many department stores and clothing stores. This method only considers the geographical features along the bus route, ignoring the audience flow difference in different areas. In short, there is still a lack of effective methods for estimating the number of audiences who are interested in the content of the bus ads.

Different advertising campaigns often have various marketing strategies and priorities. Reach and frequency are two fundamental metrics when planning an advertising campaign. Reach is the number of target audiences that are potentially exposed to the ad campaign. Frequency is the number of times an audience is likely to be exposed to an ad during a marketing campaign (STRATEGUS 2022). For well-established brands, audiences are very familiar with these brands, fewer exposure times can still bring a successful outcome (Tellis 1988), so reach is the priority in this case. As a result, the goal of advertisers is to cover as many target audiences as possible. In this case, it's more suitable to choose longer bus routes as they can cover a larger area and more audiences. From the perspective of location theory, this problem can be solved based on the maximal covering location problem (MCLP). Church and ReVelle (1974) first proposed the MCLP, intending to maximize service coverage by a limited number of facilities, and it has achieved many successful applications, such as suggesting locations for health facilities (Bennett et al., 1982), ambulances (Saydam and McKnew 1985), urban fire stations (Murray 2013), and bike sharing stations (Xu et al., 2016). Different from the advertising strategies for well-established brands, new brands usually require a high level of exposure before they become recognizable and acceptable, because of consumer inertia and selective information processing (Tellis 1988). As a result, frequency is the priority in this case. The goal of advertisers is to achieve high exposure times for target audiences. In this case, it inclines to select shorter bus routes. The bus runs serval times a day along the fixed route, so bus exterior ads are exposed to the same area serval times a day. Different buses run different numbers of times a day due to different route lengths. Namely, different bus routes will have different exposure intensities to an area. Intuitively, shorter bus routes run more times a day and have higher exposure intensity to areas along the routes. When selecting a set of bus routes for advertising, the selected routes may overlap. If the travel demand between two bus stops on one bus route can be served by another bus route, it is defined as route overlapping (Deng and Yan 2019). The higher the degree of overlap, the more times an area is covered. From the perspective of location theory, this is a multiple coverage problem. Daskin and Stern (1981) developed the first model considering multiple coverages, which is regarded as an extension of the location set covering problem (LSCP) (Toregas et al., 1971). One of the objectives of this model is to maximize the number of times that demand is covered beyond a single facility. Then in 1986, an extension of the MCLP considering multiple coverages was proposed (Hogan and ReVelle 1986). This model is known as the backup coverage location problem (BCLP) to maximize both primary and secondary service coverage. Several other multiple coverage models have been proposed for ambulance service planning (Gendreau et al., 1997), cybersecurity planning (Zheng et al., 2019), and the recovery of infrastructure systems after disasters (Iloglu and Albert 2020).

Traditional outdoor advertising has mainly depended on demographic data (Cronin 2008), video data (Zhang et al.,

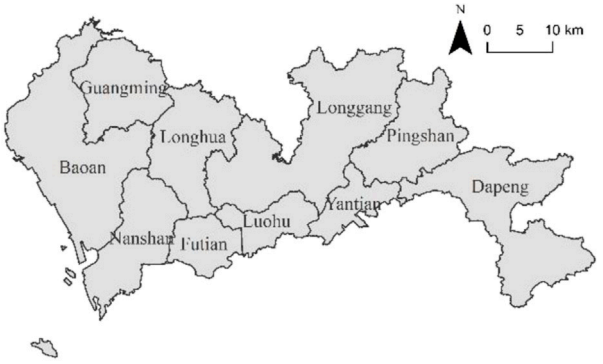

FIGURE 1
Study area of Shenzhen.

2012; Zhang et al., 2013) to estimate the number of audiences. Nowadays, an amount of geolocated data becomes available, such as GPS data, smart card data, and mobile phone data. They allow advertisers to understand their audiences better and provide possibilities to achieve targeted outdoor advertising. And there are a growing number of studies leveraging trajectory data for outdoor advertising in recent years. For example, Lai et al. (2017) have mined local interests from social media data and used them for targeted advertising in the subway stations. Wang et al. (2019) have inferred users' trip purposes, and traffic conditions based on vehicle trajectory data and used them to quantify advertisement influence spread. Lou et al. (2020) extracted potential customers' information from their vehicular trajectories and proposed an advertising strategy for roadside billboard advertising. Huang et al. (2021) have inferred audiences' interests from their mobile internet usage and then combined their trajectories from the mobile phone data to select the most promising place for advertising. But most existing studies focus on the general form of outdoor advertising, i.e., digital screens, and billboards. Limited efforts and attention are paid to the targeted bus exterior advertising by using trajectory data.

Different advertising campaigns often have different marketing strategies and different priorities. Established brands need only reminder advertising, while new brands need more exposure (Tellis 1988). However, to the best of our knowledge, no such studies have considered these two different advertising needs when selecting bus routes for advertising. In this study, we are aiming at determining a set of bus routes for a given ad category, which can maximize advertising effectiveness, by mining multiple data sources, including mobile phone data, SCD, bus GPS data, and land use data. Specifically, we first estimate the distribution of potential target audiences from mobile phone data and land use data. Then two optimization models are proposed considering different advertising needs.

TABLE 1 Sample records of mobile phone location data.

User ID	Date	Time	BaseID	Longitude	Latitude
58**	2012/**/**	07:32	11*	114.****	22.****
58**	2012/**/**	08:32	11*	114.****	22.****
76**	2012/**/**	09:27	12*	114.****	22.****

2 Study area and dataset

2.1 Study area

The investigated area of this study is the city of Shenzhen, China. Shenzhen is located in the Pearl River Delta, South China. It covers an area of approximately 2000 km^2 with 18 million people. After 40 years of rapid urbanization, Shenzhen has become one of the most developed and innovative cities in China. Currently, it encompasses 10 administrative districts (Figure 1). Among these districts, the south areas of Shenzhen, i.e., Luohu, Futian, and Nanshan districts, are concentrated with commercial, financial, and high-tech companies and are considered the central city, while the other districts include four suburban districts (Baoan, Longhua, Yantian, and Longgang), and three outer suburban districts (Pingshan, Guangming, and Dapeng). According to a recent survey, about 55.6% of passengers in Shenzhen have chosen to travel by bus due to its convenience and low fare of it (Yang et al., 2019b). Public transportation makes a significant contribution to people's daily commute in Shenzhen. The popularity of public transportation in Shenzhen makes it an ideal place for this study.

2.2 Dataset

Five types of data are utilized in this study, i.e. mobile phone location data, land use data, bus network data, bus GPS data, and smart card data. According to the role of the data, they can be classified into two categories. The first category is used to estimate the potential target audience distribution, including mobile phone location data and land use data. The other category is multi-source bus data, including bus network data, bus GPS data, and smart card data. These data are used to acquire some attributes of the bus routes, i.e. average number of running times per day, and average passenger number. If the timetable of the bus route is available, the advertisers don't have to use the bus GPS data to acquire the average number of running times per route. In practical application scenarios, the data to use depends on the precision requirements and the available dataset. A brief introduction of the dataset is given below.

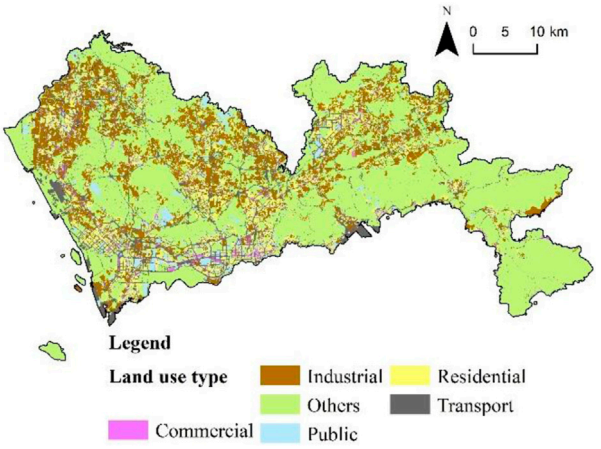

FIGURE 2
Land use in Shenzhen.

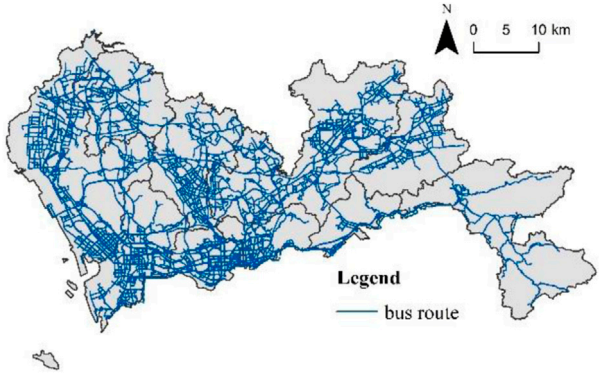

FIGURE 3
Spatial distribution of bus routes in Shenzhen.

2.2.1 Mobile phone location data

The mobile phone location data used in this study was acquired from a main mobile phone operator in China. About 16 million mobile phone users were collected in this dataset during a typical workday in 2012. The data was passively recorded, when a mobile phone user had a mobile phone activity, or active update, i.e., regular location updates and periodic location updates. In this dataset, the interval of the records is approximately 1 h. Table 1 shows examples of the data. Each record comprises an anonymous user ID, recording time, the ID of the mobile phone tower, and the latitude and longitude of the corresponding mobile phone tower. In total, there were 5,940 unique mobile phone towers in this dataset.

2.2.2 Land use data

The land use data of Shenzhen was obtained for the same year as the mobile phone location data. The dataset includes six land-use types (Figure 2), which are commercial (e.g., retail, wholesale), industrial (e.g., factories, industrial parks), residential, public (e.g., schools, hospitals), transport, and special lands (e.g., water bodies, green space) (Yang et al., 2019a).

2.2.3 Bus network data

The bus network data including bus stations and bus routes were acquired from the Gaode API. The Gaode map is the leading map service provider in China. As of September 2014, there were 874 bus routes and 51,606 bus stations in Shenzhen. Bus stops with the same name but belonging to different routes are merged into one-stop. Accordingly, a total of 4,602 bus stops were generated. The bus routes include the main-line routes, branch routes, express routes, and some special routes. Since we only consider bus routes that people usually take in their daily commute, these special routes such as peak-time routes, travel routes, and intercity bus routes are excluded. The remaining 794 routes are used as candidate routes for advertising, which is shown in Figure 3. The maximum length of the remaining routes is 101.5 km and the average length is 20.1 km.

2.2.4 Bus GPS data

The GPS trajectory data was collected from bus vehicles with GPS equipment reporting real-time location at certain intervals. The used dataset was provided by the transport operation command center (TOCC) of Shenzhen, from September 24 to September 30 in 2014. Each record includes the fields of vehicle id, time, longitude, latitude, speed, equipment status, etc. Due to data availability, there is a mismatch between the period of bus GPS data and the mobile phone data. However, as the effects of the two datasets are independent and we focus on the methodology in this study, we expect this mismatch will have a limited impact.

2.2.5 Smart card data

The SCD was also provided by TOCC and was in the same period as GPS data. The SCD is mixed with both metro and bus transactions. Transactions from the metro were ignored, since we only focus on bus exterior advertising. Passengers only need to tap smart cards for boarding in Shenzhen, so each SCD record only contains the user id, the boarding time, and the id of the bus boarded. Both the boarding and alighting stops cannot be derived directly.

3 Materials and methods

3.1 Overall framework

The framework of this study is shown in Figure 4. The study area was divided into grids. The mobile phone location data and

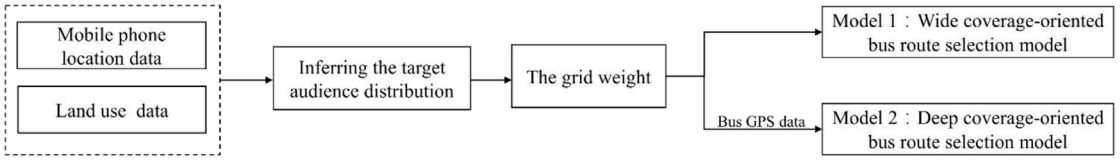

FIGURE 4
Framework of this study.

land use data were first used to estimate the potential target audience distribution (Section 3.2). Then the weight of each grid was defined by the number of potential target audiences inside. The targeted bus exterior advertising problem is formulated as a grid coverage problem. Considering different advertising needs, two models are proposed. Specifically, for well-established brands, a wide coverage-oriented bus route selection model is proposed to maximize the coverage of the potential target audience (Section 3.3). While for new brands or products, a deep coverage-oriented bus route selection model is proposed to maximize the total exposure times (Section 3.4).

3.2 Potential target audience distribution

Different from other facilities, such as hospitals and schools, the influence range of bus exterior advertising is not fixed. It depends on many factors, such as the size of the ad, traffic volume, and bus speed. For simplification, we divided the study area into grids of the same size and used the grids that the bus passes through as the influence range of bus exterior advertising.

The importance of each grid is based on the number of potential target audiences inside. Irrelevant audiences are ignored, since we aim to deliver ads to the audience with a strong preference for ads' contents. To achieve this goal, this study first identified the total audience inside each grid by using mobile phone location data. Then the interests of audiences were inferred by land-use data. Existing studies have already verified that a given land use type has a close relationship with the type of activity performed at that location (Widhalm et al., 2015; Tu et al., 2017). In this study, we used the type of land use where the audiences were located to infer their activities, thereby inferring the types of ads they might be interested in. For example, the people located in the educational land may be teachers and students conducting educational activities, so it is assumed that they are more likely to be interested in education-related ads. We assume that the land use category and the bus exterior ad category conform to the same set C. For instance, we may have C = {education, industry, transportation, . . .}. For a given advertising category, the corresponding target audiences are those located in the same category of land use. Each grid can be represented in the form below:

$$\{(c_1, \beta_{i1}), (c_2, \beta_{i2}), \ldots (c_n, \beta_{in})\} \quad (1)$$

Where c_n stands for the advertising category n, corresponding land use type n, β_{in} represents the number of target audiences of advertising category n in grid i.

Within each grid, we assume that people are uniformly distributed. Hence, the number of target audiences of each advertising category can be estimated based on the composition of the land use and total audiences in each grid, which can be formulated as:

$$\beta_{in} = \frac{A_{in}}{\sum_n A_{in}} \times pop_i \quad (2)$$

Where A_{in} is the area of land use category n in grid i, $\sum_n A_{in}$ is the total area of grid i, and pop_i is the total audiences in grid i.

3.3 Wide coverage-oriented bus route selection model

In this study, we divided the advertising campaigns into two categories. For the first category, the advertisers aim at covering as many target audiences as possible. The more eyes see their ads, the more potential to reach their goals. The cost of each bus route for advertising is assumed the same for simplification. Hence, for the first category campaign, the problem is to select a set of bus routes to place the ad of category n that can maximize the exposure to the target audiences. This problem can be solved based on the MCLP, which we term wide coverage-oriented bus route selection model in this study. The bus routes can be seen as facilities providing ad content as a service to people around them. The potential target audiences can be seen as the demands in the model that need to be covered. Each bus route's influence range is represented by the grids that the bus passes through. Once the audiences are located within the influence range, they are declared as covered. Each grid is weighted by the average number of target audiences inside to reflect its importance. Before introducing the mathematical formulation of this problem, consider the following notations:

i = index of demand grid where i = 1, 2, ...I.
j = *index of the potential facility* (i.e. bus route) where j = 1, 2, ...J
p = *number of facilities* (i.e.bus routes) to select
β_i = the weight of demand grid i determined by target audience flow
N_i = the set of the potential facilities capable of covering demand at i

$$x_j = \begin{cases} 1, \text{if bus route j is selected for advertising} \\ 0, \text{otherwise} \end{cases}$$

$$y_i = \begin{cases} 1, \text{ if demand at grid i is covered by at least one route} \\ 0, \text{ otherwise} \end{cases}$$

For a given advertising category, the model is stated as follows:

$$Maximize: \sum_{i \in I} \beta_i y_i \tag{3}$$

$$Subject\ to: \sum_{j \in N_j} x_j \geq y_i, \forall i \in I \tag{4}$$

$$\sum_{j \in J} x_j = p \tag{5}$$

$$x_j \in \{0, 1\}, , \forall j \in J \tag{6}$$

$$y_i \in \{0, 1\}, \forall i \in I \tag{7}$$

The objective of the model is to maximize the coverage of demands (i.e. target audiences). Eq. 4 tracks whether demand is covered by at least one selected route or not. Eq. 5 defines the number of routes to be selected is p. Eq. 6 indicates that a route is either selected or not. Eq. 7 indicates that a demand grid is either covered or not.

3.4 Deep coverage-oriented bus route selection model

For the second category of the campaign, the advertisers want to have high exposure or repetition times to target audiences to improve branding and increase consumer acceptance. This strategy is often used for new brands or products. For this category of campaign, every exposure is counted. The problem is to select a set of bus routes to place the ad of category n that would maximize the total exposure times to users who are interested in n. However, the relationship between ad repetition and an audience's reception of the ad is not monotonic. Ad effectiveness is believed to increase at low levels of repetition and then decrease as ad repetition increases (Berlyne 1970; Campbell and Keller 2003). Therefore, it is necessary to limit the maximum exposure times of ads to avoid adverse consequences caused by excessive exposure. For bus exterior ads, the multiple exposures for an area come from two parts, i.e. the overlapping of different routes and the multiple round trips of the bus in a day. To select a set of bus routes that can maximize the ad exposure times for a satisfactory ad influence, we propose a maximal multiple coverage model, which we term deep coverage-oriented bus route selection model.

Before continuing, it is necessary to consider the following notations:

z_i = the number of times grid i is covered;
α_j = the average running times of a bus of route j in a day;
$MaxEx$ = the maximum allowed coverage times to a grid

The maximum allowed exposure times of an ad to each grid is defined by *MaxEx*. *MaxEx* is pre-specified to avoid adverse consequences caused by excessive exposure. For example, setting $MaxEx = 2$ means that only primary and secondary coverage are considered and additional coverage is not taken into account.

Using the above notations, the model is defined as follows:

$$Maximize \sum_{i \in I} \beta_i z_i \tag{8}$$

$$Subject\ to: \sum_{j \in N_i} \alpha_j x_j \geq z_i, \ \forall i \in I \tag{9}$$

$$\sum_{j \in N_i} \alpha_j x_j \leq MaxEx, \forall j \in J \tag{10}$$

$$\sum_{j \in J} x_j = p \tag{11}$$

$$x_j \in \{0, 1\}, , \forall j \in J \tag{12}$$

$$z_i \geq 0 \text{ and } integer, \forall i \in I \tag{13}$$

The objective of the deep coverage-oriented bus route selection model is to maximize the total exposure times of the ads. Constraints Eq. 9 track whether demand is covered by at least one selected route or not. Constraints Eq. 10 specify an upper bound on the number of times each grid can be covered. Constraint Eq. 11 defines that the p bus routes are to be selected. Constraint Eq. 12 indicates that a route is either selected or not. Constraints Eq. 13 impose integer and non-negativity requirements on z_i.

In general, two strategies have been used to solve the above location optimization problem, exact methods, and heuristics. Exact methods, for example, enumeration, branch-and-bound, and linear programming, guarantee the optimal solutions. Some exact approaches have been incorporated into commercial packages such as CPLEX, and Gurobi (Mu and Tong 2020). However, for large-scale data, the computational effort increases dramatically, and solving these problems exactly can be difficult or impossible, so advanced heuristic methods such as genetic algorithms, and Tabu searches, become essential (Tu et al., 2014). Heuristic methods seek to obtain near-optimal solutions at relatively low computational cost and are suitable for large-sized problems (Tong and Murray 2017). The selection of the algorithm depends on the size of the problem, the efficiency and precision requirements of the problem.

4 Results

4.1 Distribution of potential target audience

As mentioned in Section 3.2, we first divided the study area into equal-size grids and used the grids that a bus passed

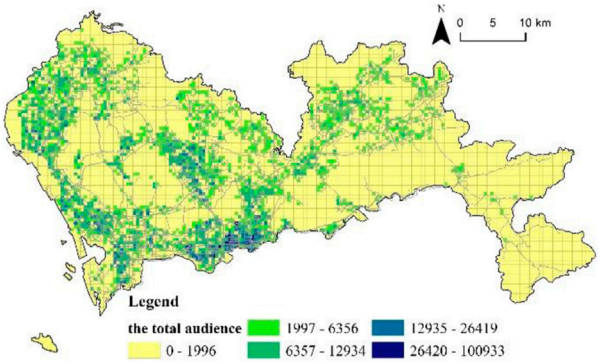

FIGURE 5
The distribution of total audience.

through as the influence range of bus exterior advertising for simplification. As to the grid size, we used 500 m × 500 m mesh grids based on related research (Yang et al., 2016). In total, there were 8,293 grids in the study area, and each grid was tagged with a unique Grid ID.

The mobile phone records were first mapped onto the grids based on the spatial relation of the grid and mobile phone tower. The operation time of Shenzhen's public transport was from 6: 00 a.m. to 11:00 p.m., so only the records during this period were considered. As the interval of this dataset was approximately 1 h, the number of distinct audiences in each grid per hour was acquired. Then the average audience volume of each grid during this period was calculated, which is shown in Figure 5. It is shown that the spatial distribution of the population in the study area was heterogeneous. People were concentrated in the central urban districts of Futian, Nanshan, and Luohu, while few people were located in Longgang, Pingshan, and Dapeng.

After obtaining the total audiences in each grid, the number of potential target audiences of each advertising category was calculated. We first overlapped the land use data with the grids to obtain the proportions of various land-use types in each grid. Then the number of target audiences of each advertising category was calculated based on Eq. 2. The results are shown in Figure 6. It indicates that the spatial distribution differs over different

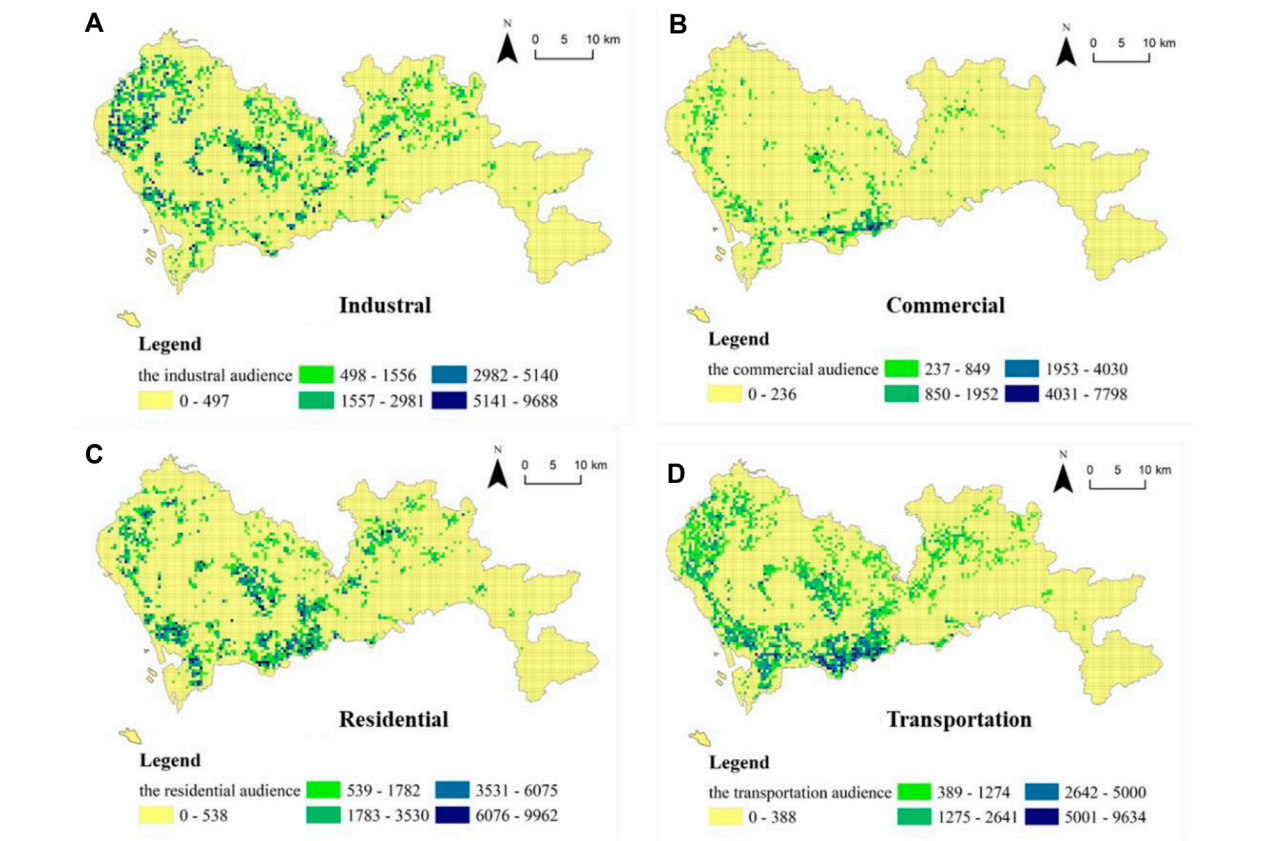

FIGURE 6
Potential target audience distribution for **(A)** Industral ads, **(B)** Commercial ads, **(C)** Residential ads, **(D)** Transportation ads.

audience categories. The industrial audiences were concentrated in Baoan, Longhua district, while target audiences of commercial ads were mainly located in Luohu, Futian district. The residential audiences and the transportation audiences were both densely located in Nanshan, Luohu, and Futian districts, but the distribution of transportation audiences was more uniform overall.

4.2 Model implementation and evaluation

To evaluate the effectiveness of the proposed bus route selection models (Section 3.3 and Section 3.4) respectively, we compared them with two commonly utilized methods:

(1) The first method selects the bus routes with the most passengers (Zhang et al., 2017a). This method is referred to as "baseline 1" hereafter.
(2) The second method selects the bus route with the maximum coverage of the target area, namely, the land use type of the area that matches the category of the ads (Zhang X. et al., 2017c). We denote this method as "baseline 2" hereafter.

The performance indicators to describe the effectiveness of a model include the coverages of the potential target audience and the average daily coverage times of each grid. The target audience within each covered grid was accumulated to acquire the total covered target audiences.

In summary, four models were involved in this study, namely, the two proposed models and two baselines. All the models were implemented in Python 2.7.2, using ArcPy for ArcGIS 10.1 and solved by Gurobi.

4.3 Evaluation of the wide coverage-oriented model

The first experiment was to compare the wide coverage-oriented bus route selection model with the two baselines. For each advertising category, namely, industrial, residential, commercial, and transportation, a fixed number of routes (p = 5) was selected. The target audience coverage results achieved by these three models were compared.

As mentioned in Section 2.2, bus passengers only need to tap smart cards for boarding in Shenzhen. Both the boarding and alighting stops cannot be derived directly. Before applying baseline 1, the bus ridership has to be extracted. In this study, each SCD record was first linked to the bus GPS trajectory based on the id of the bus. Then the boarding time was used to estimate the boarding location from the GPS trajectory. Following the direction of the bus route, the boarding location was assigned to the closest bus stop on the bus route. Accordingly, a total of 15,119,857 bus ridership were generated from bus SCD. Then

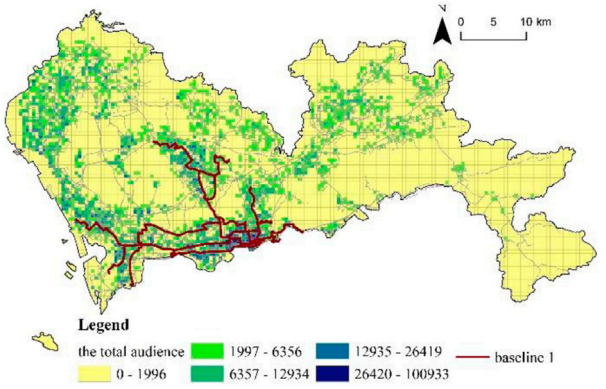

FIGURE 7
The selected routes of baseline 1.

baseline 1 selected bus routes with the most passengers, and the selected bus routes are shown in Figure 7. For different categories of ads, baseline 1 selected the same bus routes. Most of the selected bus routes were located in the Futian, Luohu, and Nanshan districts, which were the central part of Shenzhen. The average length of the selected bus route was 39.5 km.

For the wide coverage-oriented model and baseline 2, the selected routes of each category are shown in Figure 8. Table 2 summarizes the coverage values of the various methods for all the categories. Specifically, for industrial ads, the wide coverage-oriented model covered 24.1% of the target audience, which was the highest. Baseline 2 covered 23.4% of the target audience, while baseline 1 covered only 8.4% of the target audience. As to the spatial distribution of the routes, both the wide coverage-oriented model and baseline 2 selected routes concentrated in Baoan, Longgang, and Longhua districts, which have many factories and industrial parks. The average length of the selected routes of baseline 2 was 80.4 km and was the longest, while the average length of the wide coverage-oriented model was 59.7 km. These two methods have three shared routes. For commercial ads, the wide coverage-oriented model covered 41.1% of the target audience and the average length of the selected routes was 48.9 km. Most of the routes passed through Luohu, Futian districts, where there were many shopping centers and financial institutions. For residential ads, the wide coverage-oriented model still covered the highest proportion of target audiences, at 29.2%; followed by baseline 2, at 26.7%; baseline 1 at 18.0%. The average length of the selected bus routes of the wide coverage-oriented model was 56.0 km, passing through many large communities, such as Taoyuan Village, Taoyuan Ju, and Yitian Village. For transportation ads, the wide coverage-oriented model covered 29.4% of the target audience and was the highest. The selected routes passed through many transportation hubs such as Shenzhen East

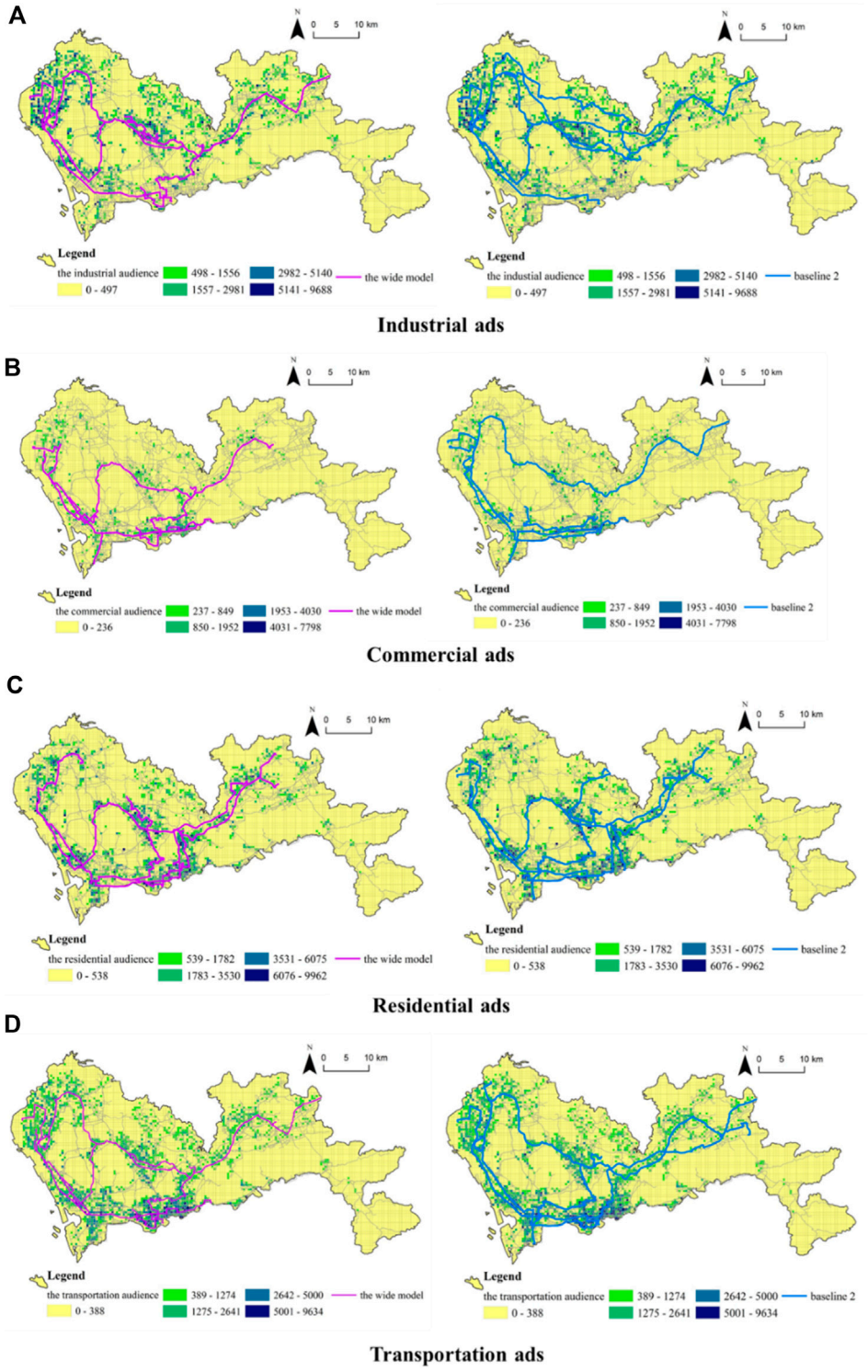

FIGURE 8
The selected bus routes of the wide coverage-oriented model and baseline 2 for **(A)** Industrial ads, **(B)** Commercial ads, **(C)** Residential ads, **(D)** Transportation ads.

TABLE 2 Evaluation of the wide coverage-oriented model.

The category of ads	Indicators	Wide coverage-oriented model	Baseline 1	Baseline 2
Industrial	The coverage of target audience	24.1%	8.4%	23.3%
	Covered grids	621	343	765
	Average length of the selected routes	59.7 km	39.5 km	80.4 km
Commercial	The coverage of target audience	41.1%	28.4%	37.2%
	Covered grids	517	343	587
	Average length of the selected routes	48.9 km	39.5 km	52.5 km
Residential	The coverage of target audience	29.2%	18.0%	26.7%
	Covered grids	613	343	661
	Average length of the selected routes	56.0 km	39.5 km	60.0 km
Transportation	The coverage of target audience	29.4%	19.9%	25.9%
	Covered grids	641	343	714
	Average length of the selected routes	65.5 km	39.5 km	63.9 km

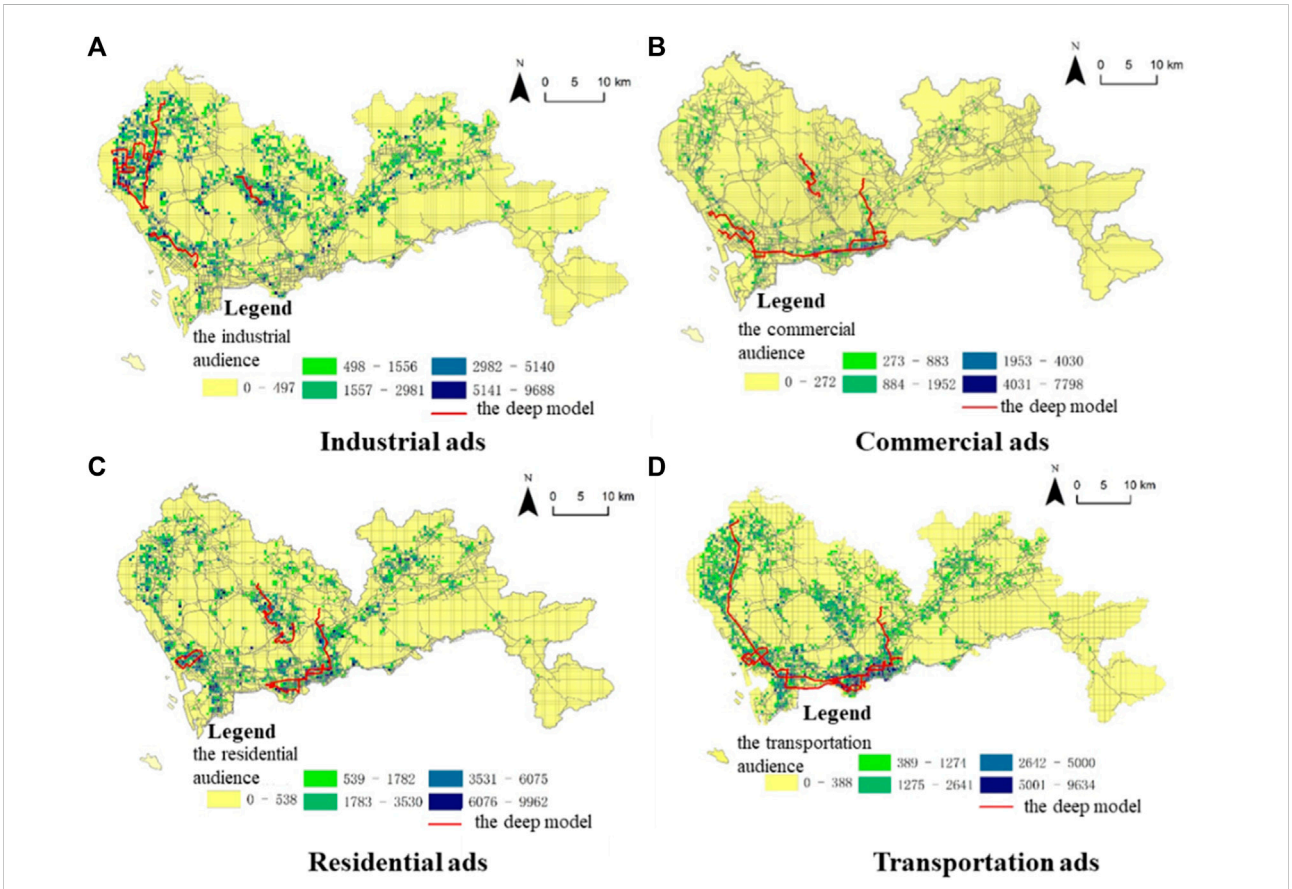

FIGURE 9
The selected bus routes of the deep coverage-oriented model for **(A)** Industrial ads, **(B)** Commercial ads, **(C)** Residential ads, **(D)** Transportation ads.

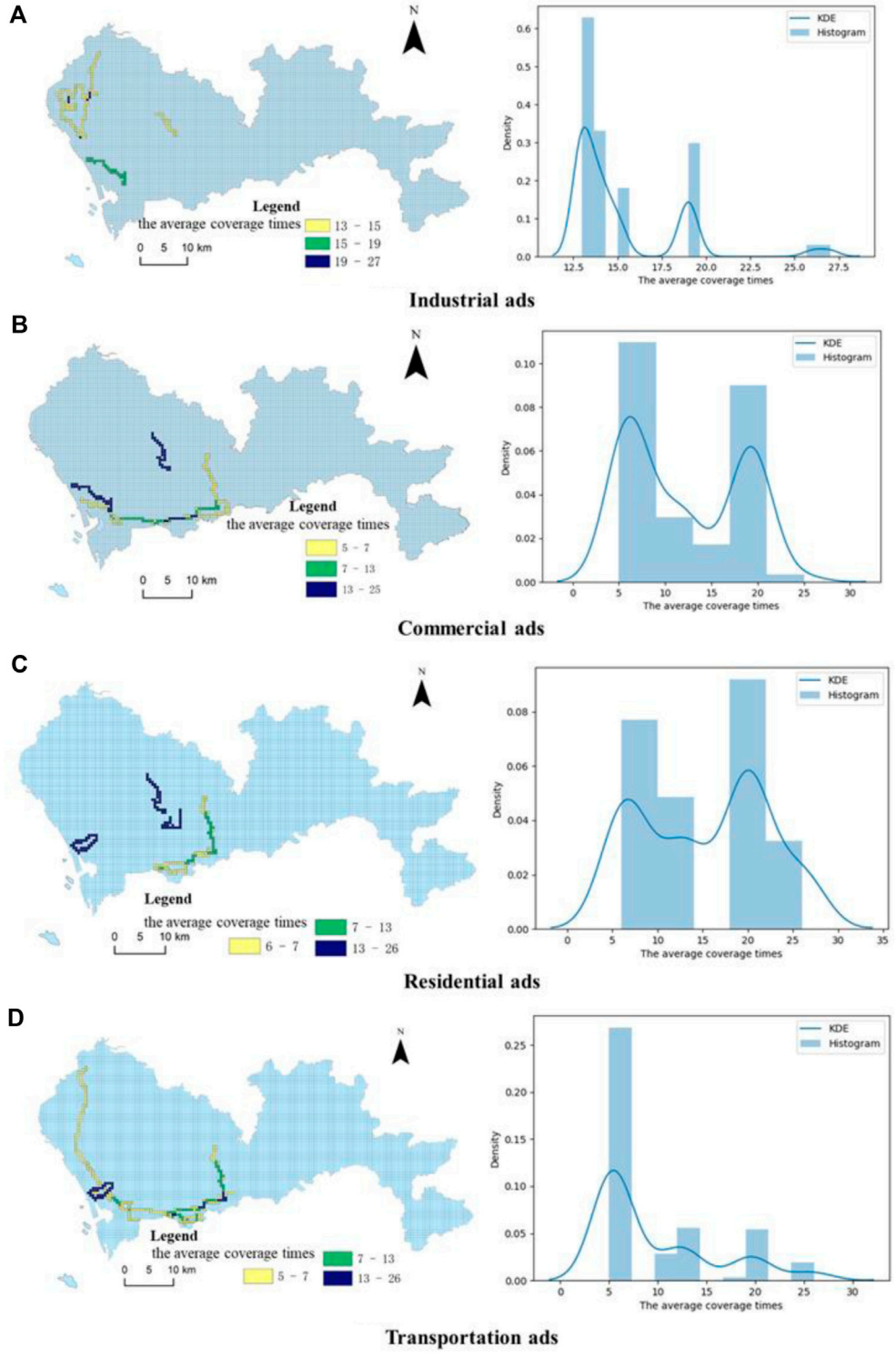

FIGURE 10
The average coverage times of each grid for **(A)** Industrial ads, **(B)** Commercial ads, **(C)** Residential ads, **(D)** Transportation ads.

TABLE 3 Evaluation of the deep coverage-oriented model.

The category of ads	Indicators	Deep coverage-oriented model	Wide coverage-oriented model
Industrial	The coverage of target audience	11.0%	24.1%
	Covered grids	191	621
	Average daily coverage times of a grid	15.2	3.5
	Average length of the selected routes	17.2 km	59.7 km
Commercial	The coverage of target audience	27.0%	41.1%
	Covered grids	219	517
	Average daily coverage times of a grid	12.1	3.3
	Average length of the selected routes	24.5 km	48.9 km
Residential	The coverage of target audience	14.4%	29.2%
	Covered grids	185	613
	Average daily coverage times of a grid	15.2	3.5
	Average length of the selected routes	18.7 km	56.0 km
Transportation	The coverage of target audience	17.6%	29.4%
	Covered grids	286	641
	Average daily coverage times of a grid	9.6	3.5
	Average length of the selected routes	33.3 km	65.5 km

Railway Station, Pingshan Railway Station, and Baoan Passenger Transport Center.

In summary, for all the categories, the wide coverage-oriented bus route selection model achieved the highest coverage results, followed by baseline 2 and then baseline 1. The wide coverage-oriented model achieved an average of 84.8% improvement compared with baseline 1, while an average of around 9.2% improvement compared with baseline 2 in reaching more target audience. Though the average length of the selected routes of the wide coverage-oriented model was not the longest, it has the ability to cover more target audiences.

4.4 Evaluation of the deep coverage-oriented model

The second experiment was to compare the deep coverage-oriented bus route selection model with the wide coverage-oriented model. For each advertising category, a fixed number of routes ($p = 5$) were selected. The *MaxEx* was set to 30. The number of the daily running times of each bus was inferred by matching the GPS coordinates of the bus to the stops along the bus route. Then the average number of running times of each bus route was calculated. The coverages of the target audience and the average daily coverage times of each grid were utilized as the performance indicators.

For all categories, the selected bus routes calculated by the deep coverage-oriented model are shown in Figure 9. The average coverage times of each grid and the corresponding histogram for all the categories of ads are shown in Figure 10. Table 3 summarizes the coverage values of the wide and deep coverage-oriented models for all the categories of ads. Specifically, for industrial ads, 80% of the selected routes were located in the Baoan district, which was the industrial center in Shenzhen with a high concentration of electronics factories. These routes passed through many industrial parks, such as Fuqiao industrial park, Haosi industrial park, and so on. As shown in Table 3, the selected routes of the deep coverage-oriented model were much shorter than those of the wide coverage-oriented model, but the average number of daily coverage times of a grid was 15.2, which was much higher than that of the wide coverage-oriented model. Most grids were covered between 13 and 15 times, and few grids have maximum coverage of 27 times due to route overlap. For commercial ads, the routes were mainly located in the Nanshan, Futian, and Luohu districts, passing through Shenzhen Stock Exchange, PICC Property Insurance, and other financial institutions. The average length of the selected routes was 24.5 km, which was much shorter than that of the wide coverage-oriented model. The deep coverage-oriented model covered 27% target audience, and each grid has an average of 12.1 times coverage. The grid coverage times were mainly concentrated in the two intervals of 5–7 and 19–20. For residential ads, the selected routes were distributed in the Futian, Luohu, Longhua, and Baoan districts, passing through many large residential areas. The average length of the selected routes was 18.7 km. Though this model only covered 14.4% of the target audience, the average coverage times of each grid was 15.2. The maximum grid coverage times was 26, located in Longhua district. For transportation ads, the average length of the selected routes was 33.3 km,

and 17.6% of the target audiences were covered. The average grid coverage times was 9.6, which was much higher than that of the wide coverage-oriented model. Most of the grids were covered in the range of 5–7 times and the maximum grid coverage times was 26.

In summary, for all the categories of ads, the deep coverage-oriented model achieved higher grid coverage times but lower target audience coverage compared with the wide coverage-oriented model. The average grid coverage times of the deep coverage-oriented model have been increased by an average of 3.7 times. This model can achieve high exposure intensity to areas along the bus routes.

5 Discussion and conclusion

Although bus exterior advertising plays a significant role in outdoor advertising, the analytical methods to optimize bus exterior advertising strategies are limited. Traditional methods are generally based on a rough estimation, for example, the number of total passengers of a bus route or the geographical features along the bus route. It remains a challenge to accurately select a bus route for targeted advertising.

In this study, we demonstrated how the geolocated data, i.e., mobile phone location data, and bus GPS data can be combined with location models to provide suggestions for the bus route selection for exterior advertising. The audience number along the bus route was first estimated by using mobile phone data. Then the category of ads that the audience may be interested in was inferred by using land-use data. Considering various advertising needs, two optimization models have been proposed. Specifically, for well-established brands, a wide coverage-oriented bus route selection model was proposed to maximize the coverage of the potential target audience. While for new brands or products, a deep coverage-oriented bus route selection model was proposed to maximize the total exposure times of the ads. Since untried new brands often require a high level of exposure before they become recognizable and acceptable.

A case study using mobile phone data, SCD, and bus GPS data in Shenzhen, China was adopted to evaluate the two proposed models and the differences between the two models were explicitly investigated. If the data of other cities are available, the proposed workflow and methods can also be applied. For the wide coverage-oriented model, it tended to choose longer routes. This model can achieve a higher proportion of audience coverage, but lower exposure intensity to the areas along the road. For the deep coverage-oriented model, it tended to select shorter routes with a high daily running times. Though this model covered fewer target audiences compared with the wide coverage-oriented model, the average grid coverage times of the deep coverage-oriented model have been increased by an average of 3.7 times. These two models have different priorities for selecting routes, and advertisers can choose the appropriate model according to their needs and marketing scenarios. We trust the proposed models can help advertising planners make better use of transit advertising.

There are also some limitations of this work. Firstly, the interests of the audience are now inferred by using land-use data due to the limited data. In the future, a more precise user interest profile can be constructed by integrating more data sources, such as social media data, mobile internet usage data. Secondly, the impact of traffic flow and travel speed on the exposure strength of ads is not considered in this study. Obviously, larger traffic flow and lower travel speed would increase the travel time of buses through the road. Therefore, the opportunity of the ad being viewed by the audience is also increased. The traffic condition mined from bus GPS data can further be incorporated into the models for more precise results. Thirdly, now the coverage requirements in the models come from an overall perspective, which may lead to unbalanced grid coverage, e.g., most ad exposures are concentrated in few grids. More specific and fine-grained coverage requirements in the time and space domain from the advertisers can be considered in the future, such as the coverage times per hour, to make ad exposure more reasonable and effective. Lastly, due to ability constraints, we evaluate our method by comparing it with two baselines in this study. It would be of great interest if a real advertising campaign can be launched in the future to evaluate our methods.

Data availability statement

The original contributions presented in the study are included in the article/supplementary material, further inquiries can be directed to the corresponding author.

Author contributions

MH: Conceptualization, Methodology, Writing the original draft. XL: Methodology, review and editing. WT: Data acquisition, review and editing. MY: Conceptualization, review and editing.

Conflict of interest

The authors declare that the research was conducted in the absence of any commercial or financial relationships that could be construed as a potential conflict of interest.

Publisher's note

All claims expressed in this article are solely those of the authors and do not necessarily represent those of their affiliated organizations, or those of the publisher, the editors and the reviewers. Any product that may be evaluated in this article, or claim that may be made by its manufacturer, is not guaranteed or endorsed by the publisher.

Reference

Bennett, V. L., Eaton, D. J., and Church, R. L. (1982). Selecting sites for rural health workers. *Soc. Sci. Med.* 16 (1), 63–72. doi:10.1016/0277-9536(82)90424-5

Berlyne, D. E. (1970). Novelty, complexity, and hedonic value. *Percept. Psychophys.* 8 (5), 279–286. doi:10.3758/bf03212593

Campbell, M. C., and Keller, K. L. (2003). Brand familiarity and advertising repetition effects. *J. Consumer Res.* 30 (2), 292–304. doi:10.1086/376800

Church, R., and ReVelle, C. (1974). *Papers of the regional science association*, 101–118.The maximal covering location problem

Cronin, A. M. (2008). Mobility and market research: Outdoor advertising and the commercial ontology of the city. *Mobilities* 3 (1), 95–115. doi:10.1080/17450100701797349

Daskin, M. S., and Stern, E. H. (1981). A hierarchical objective set covering model for emergency medical service vehicle deployment. *Transp. Sci.* 15 (2), 137–152. doi:10.1287/trsc.15.2.137

Deng, Y., and Yan, Y. (2019). Evaluating route and frequency design of bus lines based on data envelopment analysis with network epsilon-based measures. *J. Adv. Transp.*, 1–12. doi:10.1155/2019/5024253

Gendreau, M., Laporte, G., and Semet, F. (1997). Solving an ambulance location model by tabu search. *Locat. Sci.* 5 (2), 75–88. doi:10.1016/s0966-8349(97)00015-6

Hogan, K., and ReVelle, C. (1986). Concepts and applications of backup coverage. *Manag. Sci.* 32 (11), 1434–1444. doi:10.1287/mnsc.32.11.1434

Huang, M., Fang, Z., Weibel, R., Zhang, T., and Huang, H. (2021). Dynamic optimization models for displaying outdoor advertisement at the right time and place. *Int. J. Geogr. Inf. Sci.* 35 (6), 1179–1204. doi:10.1080/13658816.2020.1823396

Iloglu, S., and Albert, L. A. (2020). A maximal multiple coverage and network restoration problem for disaster recovery. *Operations Res. Perspect.* 7, 100132. doi:10.1016/j.orp.2019.100132

JCDecaux (2020). *Why advertise in out-of-home*. [online]. Available from: https://www.jcdecaux-cityscape.hk/hong-kong/media/why-advertise-ooh (Accessed 0430 2022, 2022).

Lou, K., Yang, Y., Wang, E., Liu, Z., Baker, T., and Bashir, A. K. (2020). Reinforcement learning based advertising strategy using crowdsensing vehicular data. *IEEE Trans. Intell. Transp. Syst.* 22 (7), 4635–4647. doi:10.1109/tits.2020.2991029

Małecki, K., Jankowski, J., and Szkwarkowski, M. (2019). Modelling the impact of transit media on information spreading in an urban space using cellular automata. *Symmetry* 11 (3), 428. doi:10.3390/sym11030428

Mu, W., and Tong, D. (2020). On solving large p-median problems. *Environ. Plan. B Urban Anal. City Sci.* 47 (6), 981–996. doi:10.1177/2399808319892598

Murray, A. T. (2013). Optimising the spatial location of urban fire stations. *Fire Saf. J.* 62, 64–71. doi:10.1016/j.firesaf.2013.03.002

Roux, T. (2014). The effectiveness of car advertising media: Perceptions of generation-Y consumers. *Mediterr. J. Soc. Sci.* 5 (20), 1877. doi:10.5901/mjss.2014.v5n20p1877

Saydam, C., and McKnew, M. (1985). Applications and implementation a separable programming approach to expected coverage: An application to ambulance location. *Decis. Sci.* 16 (4), 381–398. doi:10.1111/j.1540-5915.1985.tb01490.x

STRATEGUS (2022). *Reach vs frequency: Are you prioritizing the right metrics?* [online]. Available from: https://www.strategus.com/blog/reach-vs-frequency-prioritizing-the-right-metrics (Accessed 0217, 2022).

Tam, K. Y., and Ho, S. Y. (2006). Understanding the impact of web personalization on user information processing and decision outcomes. *MIS Q.* 30 (4), 865. doi:10.2307/25148757

Tellis, G. J. (1988). Advertising exposure, loyalty, and brand purchase: A two-stage model of choice. *J. Mark. Res.* 25 (2), 134. doi:10.2307/3172645

Tong, D., and Murray, A. T. (2017). "Location analysis: Developments on the horizon," in *Regional research Frontiers - vol. 2: Methodological advances, regional systems modeling and open sciences*. Editors R. Jackson and P. Schaeffer (Cham: Springer International Publishing), 193–208.

Toregas, C., Swain, R., ReVelle, C., and Bergman, L. (1971). The location of emergency service facilities. *Operations Res.* 19 (6), 1363–1373. doi:10.1287/opre.19.6.1363

Tu, W., Cao, J., Yue, Y., Shaw, S. L., Zhou, M., Wang, Z., et al. (2017). Coupling mobile phone and social media data: A new approach to understanding urban functions and diurnal patterns. *Int. J. Geogr. Inf. Sci.* 31 (12), 2331–2358. doi:10.1080/13658816.2017.1356464

Tu, W., Fang, Z., Li, Q., Shaw, S. L., and Chen, B. (2014). A bi-level Voronoi diagram-based metaheuristic for a large-scale multi-depot vehicle routing problem. *Transp. Res. Part E Logist. Transp. Rev.* 61, 84–97. doi:10.1016/j.tre.2013.11.003

Tucker, C. E. (2014). Social networks, personalized advertising, and privacy controls. *J. Mark. Res.* 51 (5), 546–562. doi:10.1509/jmr.10.0355

Widhalm, P., Yang, Y., Ulm, M., Athavale, S., and Gonzalez, M. C. (2015). Discovering urban activity patterns in cell phone data. *Transportation* 42 (4), 597–623. doi:10.1007/s11116-015-9598-x

Xu, Y., Shaw, S. L., Fang, Z., and Yin, L. (2016). Estimating potential demand of bicycle trips from mobile phone data—an anchor-point based approach. *ISPRS Int. J. Geoinf.* 5 (8), 131. doi:10.3390/ijgi5080131

Yang, X., Fang, Z., Xu, Y., Shaw, S. L., Zhao, Z., Yin, L., et al. (2016). Understanding spatiotemporal patterns of human convergence and divergence using mobile phone location data. *ISPRS Int. J. Geoinf.* 5 (10), 177. doi:10.3390/ijgi5100177

Yang, X., Fang, Z., Yin, L., Li, J., Lu, S., and Zhao, Z. (2019a). Revealing the relationship of human convergence–divergence patterns and land use: A case study on shenzhen city, China. *Cities* 95, 102384. doi:10.1016/j.cities.2019.06.015

Yang, X., Lu, S., Zhao, W., and Zhao, Z. (2019b). Exploring the characteristics of an intra-urban bus service network: A case study of shenzhen, China. *ISPRS Int. J. Geoinf.* 8 (11), 486. doi:10.3390/ijgi8110486

Zhang, C., Wang, H., and Xiong, H. (2017). An automatic approach for transit advertising in public transportation systems. In *IEEE international conference on data mining*, 181183–211188.

Zhang, D., Guo, L., Nie, L., Shao, J., Wu, S., and Shen, H. T. (2017b). Targeted advertising in public transportation systems with quantitative evaluation. *ACM Trans. Inf. Syst.* 35 (3), 1–29. doi:10.1145/3003725

Zhang, X. L., Weng, W. G., and Yuan, H. Y. (2012). Empirical study of crowd behavior during a real mass event. *J. Stat. Mech.* 2012 (08), P08012. doi:10.1088/1742-5468/2012/08/p08012

Zhang, X. L., Weng, W., Yuan, H., and Chen, J. (2013). Empirical study of a unidirectional dense crowd during a real mass event. *Phys. A Stat. Mech. its Appl.* 392 (12), 2781–2791. doi:10.1016/j.physa.2013.02.019

Zhang, X., Wan\g, Y., and Lv, P. (2017c). "Ibbas: A visual analytics system of large-scale traffic data for bus body advertising," in *2017 18th international conference on parallel and distributed computing, applications and technologies* (Taipei: PDCAT), 18-20, 67–74.

Zheng, K., Albert, L. A., Luedtke, J. R., and Towle, E. (2019). A budgeted maximum multiple coverage model for cybersecurity planning and management. *IISE Trans.* 51 (12), 1303–1317. doi:10.1080/24725854.2019.1584832

frontiers | Frontiers in Environmental Science

TYPE Original Research
PUBLISHED 06 September 2022
DOI 10.3389/fenvs.2022.993333

Check for updates

OPEN ACCESS

EDITED BY
Ying Jing,
Zhejiang University, China

REVIEWED BY
Huili Chen,
Loughborough University,
United Kingdom
Yuling Peng,
Wuhan Institute of Technology, China

*CORRESPONDENCE
Enxiang Cai,
caiex213@henau.edu.cn

SPECIALTY SECTION
This article was submitted to Environmental Informatics and Remote Sensing,
a section of the journal
Frontiers in Environmental Science

RECEIVED 13 July 2022
ACCEPTED 15 August 2022
PUBLISHED 06 September 2022

CITATION
Hou H, Zhang L, Bi H, He J, Cai E and Ren W (2022), Differential characteristics and driving forces of the spatial distribution of heritage trees in Luoyang, an ancient capital of China. *Front. Environ. Sci.* 10:993333. doi: 10.3389/fenvs.2022.993333

COPYRIGHT
© 2022 Hou, Zhang, Bi, He, Cai and Ren. This is an open-access article distributed under the terms of the Creative Commons Attribution License (CC BY). The use, distribution or reproduction in other forums is permitted, provided the original author(s) and the copyright owner(s) are credited and that the original publication in this journal is cited, in accordance with accepted academic practice. No use, distribution or reproduction is permitted which does not comply with these terms.

Differential characteristics and driving forces of the spatial distribution of heritage trees in Luoyang, an ancient capital of China

Heping Hou[1,2], Longchong Zhang[2], Huitao Bi[2], Jing He[2], Enxiang Cai[3]* and Wanqian Ren[2]

[1]Post-doctoral Research Station of Landscape Architecture, Henan Agricultural University, Zhengzhou, China, [2]College of Forestry, Henan Agricultural University, Zhengzhou, China, [3]School of Resources and Environment, Henan Agricultural University, Zhengzhou, China

Heritage trees have important historical, landscape, and ecological value. Exploring the spatial distribution pattern of heritage trees is of great importance to the construction of ecological civilization and the connotation of regional history and culture. This paper took 5,216 heritage trees in Luoyang, an ancient capital of China, as the research object and used geospatial analysis methods and a geographically weighted regression model to analyze the differences and driving forces of the spatial distribution of heritage trees. Results show that 1) the heritage trees in Luoyang were primarily *Gleditsia sinensis*, *Sophora japonica*, and *Platycladus orientalis*, and more than half of these trees were under 300 years old; 2) the high-density area formed a distribution pattern of "three cores, one ring, and two belts," and the distribution of heritage trees had a positive spatial autocorrelation; 3) different driving factors in different regions had complex influences on the spatial distribution of heritage trees, and the order of influence was as follows: area of forest and orchard land > elevation > number of POIs (points of interest) > distance to the nearest river > slope > number of immovable relics. The results could provide a comprehensive understanding of the spatial distribution of heritage trees to protect the ecological function of heritage trees and mine the cultural value of heritage trees.

KEYWORDS

spatial distribution, driving forces, heritage trees, geographically weighted regression, luoyang

1 Introduction

Heritage trees refer to trees with important ecological, historical, and cultural values preserved in history, and they are non-renewable resources formed by the combined effects of time and geography (Nolan et al., 2020). As an important part of the ecosystem, heritage trees provide not only habitats for animals and plants, but also production and

living materials for human beings (Wu et al., 2020; Gilhen-Baker et al., 2022). Moreover, some heritage trees retain valuable genes of endangered species; therefore, they are of great significance to biodiversity conservation (Spooner and Shoard, 2016). Meanwhile, heritage trees are the activation records of local ancient geography and climate change, (Lindenmayer et al., 2012; Huang et al., 2020; Nolan et al., 2020). Therefore, characteristics such as species, age, and location of heritage trees can provide important information for historical geographic studies (Atindehou et al., 2022). Heritage trees are also important urban landscapes. They not only beautify and improve the urban ecology through their rhizomes, trunks, flowers, and leaves (Lindenmayer, 2017), but also endow with certain cultural meanings, for example, *Cupressus funebris* and *Ginkgo biloba* trees were used as the materialization expression and inheritance of customs and cultural beliefs (Blicharska and Mikusinski, 2014; Liu et al., 2020). During industrialization and urbanization, historical cities, where heritage trees can be primarily found, had undergone major developmental transformation and landscape reconstruction, which has had a remarkable effect on the original living environment and distribution of heritage trees (Lindenmayer et al., 2012; Chen and Hua, 2017; Huang et al., 2022). Therefore, the protection of heritage trees is an urgent issue faced by historical cities. Exploring the spatial pattern of the distribution of heritage trees in historical cities and their influencing factors based on the "human–land relationship" in geography will provide comprehensive understanding of heritage trees and important reference significance for protecting heritage trees, thereby enhancing the cultural connotation of historical cities and developing tourism related to historical culture.

Scholars have conducted research on heritage trees from various topics. First, the definition and evaluation criteria for heritage trees vary worldwide (Spies, 2004). The United States and Europe have considered the size of heritage trees such as canopy and height, whereas China has emphasized the age and historical and cultural connotations of heritage trees (Lai et al., 2019). Second, despite different definitions of heritage trees, investigation and monitoring method have certain similarities; thus, sophisticated and intelligent techniques, including unmanned aerial vehicles, have been widely used (Singh et al., 2015; Qiu et al., 2018). Finally, biologists and foresters primarily aimed to explore rejuvenation and pest control; thus, they conducted research on specific tree species (Zhang et al., 2013; Takács et al., 2020). Some studies have indicated that heritage trees are closely associated with daily needs of local residents and their cultures and beliefs, and the direct or indirect historical and cultural value of heritage trees has been effectively excavated (Jordan et al., 2021; Cannon et al., 2022). Economic valuation of heritage trees provided an innovative perspective and dimension to quantify their value (Lin et al., 2020; Wyla & Ycc, 2022). With the improvement of economic development and the enhancement of heritage tree protection, relevant regulations and practical explorations of heritage tree protection have gradually emerged based on local conditions (Lindenmayer et al., 2014). In recent years, with the continuous investigation of heritage trees, the heritage tree information system has been gradually established and improved; therefore, a growing body of work has been carried out on reporting the spatial distribution of heritage trees. Based on different dimensions, the current studies can be roughly divided into three major categories: 1) With regard to the spatial distribution of heritage trees, existing research methods have gradually changed from simple mathematical statistics to spatial econometric analysis, but most studies have remained in the quantity statistics of heritage trees in different regions and administrative units (Asanok et al., 2021; Liu et al., 2022). Few in-depth analyses of the patterns, characteristics, and trends of the spatial distribution of heritage trees have been conducted, but such analyses are not conducive to the resource integration and planning of heritage trees. 2) The influencing factors of the distribution of heritage trees can be divided into two categories: natural and human factors. The former primarily includes latitude and longitude, topography (e.g., elevation, and slope) (Lindenmayer and Laurance, 2016; Wan et al., 2020), and climate (e.g., average annual temperature and average annual precipitation) (Liu et al., 2020; Li and Zhang, 2021). The latter can be measured by human activity intensity and urban development, such as population density and GDP per capita. Heritage trees are closely associated with historical figures, events, and buildings, which are an important part of local culture. In particular, some ancient capitals have glorious and profound historical culture, which are indispensable influencing factors of the spatial distribution of heritage trees (Badgujar et al., 2014; Ray et al., 2014). However, less concern was given to these important factors. 3) Regarding the relationship between influencing factors and the spatial distribution of heritage trees, most of the existing studies were carried out by qualitative induction or simple quantitative regression analysis (Zhang et al., 2017; Liu et al., 2019). Nevertheless, trees and their communities have certain spatial autocorrelation and heterogeneity (Wang et al., 2021). Therefore, various influencing factors of the distribution of heritage trees are spatially unbalanced. A geographically weighted regression (GWR) model is a typical local regression model, and the regression coefficient of its independent variable is not a global uniform value; it changes with the spatial position, indicating that different factors have different effects on the dependent variable because of different locations (Osborne and Suárez-Seoane, 2002; Foody, 2004). Therefore, GWR is suitable for the research of the influencing factors and their degree of influence on heritage trees distribution. GWR has been widely applied in various disciplines, including social economy, forestry, and ecological activities (Austin, 2007; Chen et al., 2021), but it is rarely seen in the research on the influencing factors of heritage tree distribution.

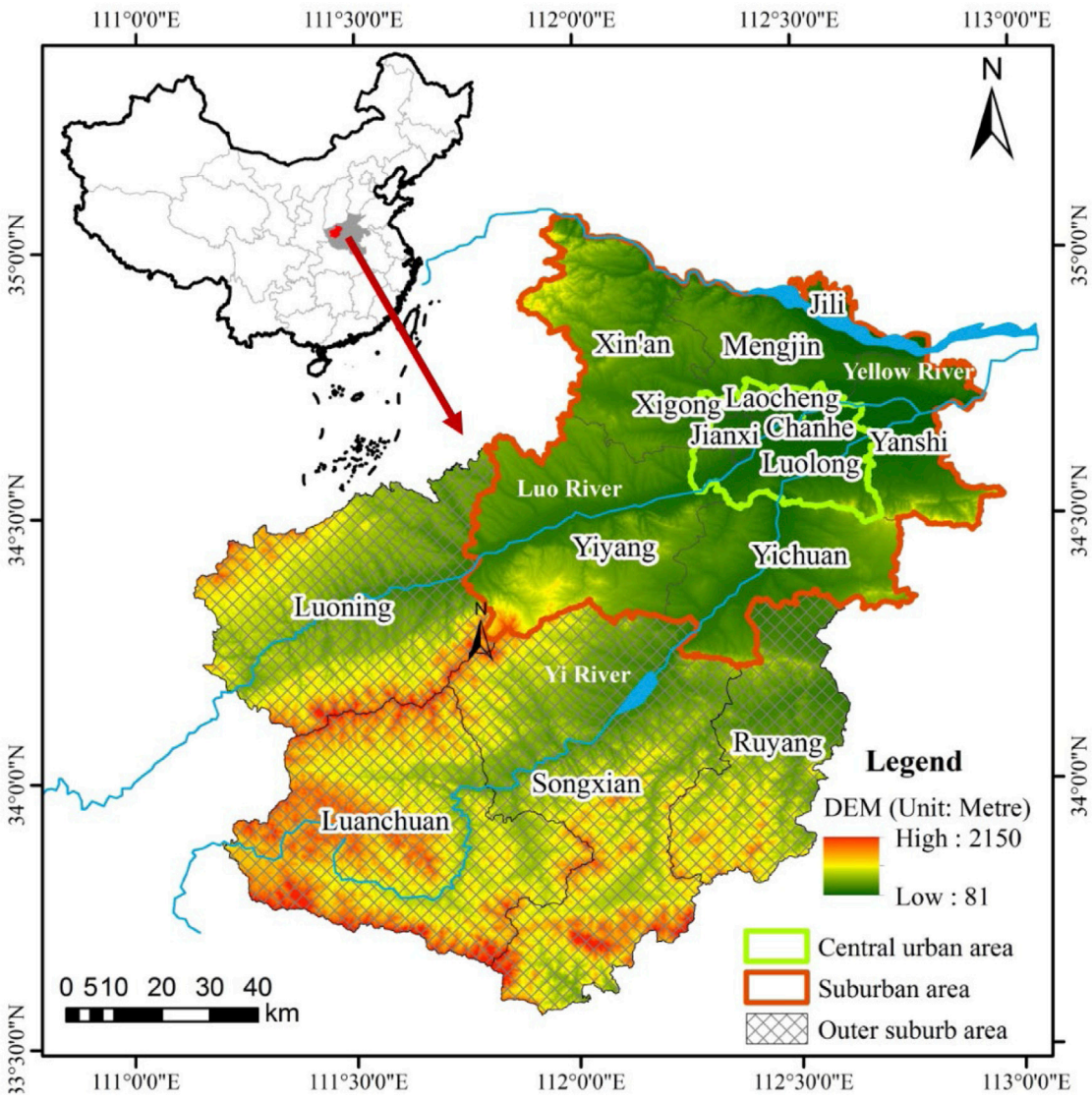

FIGURE 1
Location of luoyang in central China.

From the perspective of "human–land relationship", this paper focused on the multiple characteristics of heritage trees in nature, humanities, and geography. Taking 5,216 heritage trees in the ancient capital of Luoyang in central China as the research object, quantitative analysis was performed on their species composition and spatial distribution, and a GWR model was used to reveal the degree of influence and spatial variation of natural and human factors influencing the distribution of heritage trees. The exploration of the spatial patterns and influencing factors of the distribution of heritage trees in Luoyang will provide theoretical reference for scientifically protecting the ecological and cultural functions and effectively excavating the social and economic value of heritage trees.

2 Data and method

2.1 Study area

Luoyang covers 15,230 km^2 area, and it is located in the West of Henan Province in central China (34°32′–34°45′N, 112°16′–112°37′E). Luoyang has a complex and diverse topography. The terrain is high in the West and low in the East. It belongs to the warm temperate continental monsoon climate with four distinctive seasons, and it is rich in vegetation resources. The city covers a forest area of 6,929.65 km^2, with 45.5% forest coverage rate. Luoyang is a famous historical city, and it is one of the four ancient capitals of China (the other three

are Xi'an, Beijing, and Nanjing), with more than 5,000 years of civilization history, 4,000 years of urban history, and 1,500 years of capital history. In history, 13 ancient Chinese dynasties established their capitals in Luoyang. Luoyang has rich historical cultural landscapes, and it has five capital ruins and three world cultural heritage sites. It is a national famous historical cultural city and an excellent tourism city. Heritage trees were widely distributed in Luoyang, and they symbolize the long history of the ancient capital Luoyang.

In recent decades, Luoyang has witnessed rapid economic development as an important industrial base and tourism city in central China. In 2020, Luoyang's GDP was 544.71 billion yuan, ranking first among non-provincial capital cities in central China, with a population of 7.06 million. And an urbanization rate of 65.01%. In the past few decades, the urban population of Luoyang has increased from 19% in 1990 to 64% in 2020, experiencing rapid urbanization process. At present, Luoyang is a major city in the Yellow River Basin and a sub-center city of the Central Plains Urban Agglomeration. It has 15 administrative districts, which are divided into central urban areas (Laocheng, Chanhe, Luolong, Jianxi, and Xigong), suburbs (Yiyang, Xin'an, Mengjin, Yanshi, Jili, and Yichuan), and outer suburbs (Luoning, Luanchuan, Songxian, and Ruyang; Figure 1). Rapid urbanization has eroded the living environment of heritage trees and caused damage to the historical culture and urban landscape of Luoyang. Therefore, taking the heritage trees of Luoyang as the research object and excavating the degree and difference of the influence of natural and cultural factors on heritage trees is important for the protection of historical heritage and urban landscape of Luoyang.

2.2 Data sources

The data of heritage trees in Luoyang were obtained from the compilation of "Henan Ancient and Famous Trees" (Wang et al., 2010). Then, species, coordinates, tree age, and other information of heritage trees were collated and supplied in accordance with Cloud Platform for Forest Genetic Resources Information of Henan Province, in which the data were collected on the basis of provincial forest field surveys from 2016 to 2020 in Henan Province. The investigations of ancient trees were conducted in accordance with the Chinese government's national-level document "Technical Guidelines for the Document Establishment of a General Survey of National Ancient and Famous Trees" in 2001, which has been widely used in China (Li and Zhang, 2021). First, based on the coordinates and location description, heritage trees in Luoyang were selected as the study object. Furthermore, botanical names, taxonomic classifications, and species name of all heritage trees in Luoyang were identified following the Flora of China. For example, some heritage trees were recorded as *Huai* in Chinese; then based on their photos and morphological descriptions, they were corrected to *Guohuai*, which are *Sophora japonica* in terminology. Finally, four ancient trees were excluded because their ages were less than 100 years old. The slope and elevation data were obtained from the 30 m resolution data of the Digital Elevation Model (DEM) provided by Resource and Environment Science and Data Center in Chinese Academy of Science. River and land use data were extracted from the results of the annual survey of land use changes in Luoyang in 2020. The data of immovable relics were downloaded from the "Immovable Cultural Relics Data System" provided by Luoyang Municipal Bureau of Cultural Relics. The POI data reflects the spatial pattern of human–land relationship through the basic spatial information. Meanwhile, the POI data obtained through a unified platform, not only has the advantages of wide coverage, easy collection and centralized processing in quantities, but also can avoid data deviation caused by inconsistent data update time and recording standards. The POI data in December 2019 in Luoyang City were obtained through the application program interface embedded in the AutoNavi map navigation platform, and 291,539 POIs were obtained through deduplication and spatial registration. Each POI data included the name, longitude and latitude, address, type, telephone, administrative region and other information.

2.3 Methods

A geographic database of heritage trees in Luoyang was established using ArcGIS 10.2. The nearest neighbor index (NNI), kernel density analysis method, and exploratory spatial data analysis (ESDA) were used to study the distribution characteristics of heritage trees in Luoyang at different geographical scales. In addition, a GWR method was used to analyze the influencing factors of the spatial distribution of heritage trees.

2.3.1 Nearest neighbor index

The NNI method was used to investigate the spatial distribution types of heritage trees in Luoyang. In general, NNI was defined as the ratio of the actual nearest neighbor distance to the theoretical nearest neighbor distance (Lin and Chen, 2021), which was calculated as follows:

$$NNI = \sum_{i=1}^{n} \frac{min(d_{ij})}{n} \Big/ \left(\frac{1}{2}\sqrt{n/A}\right) \quad (1)$$

where d_{ij} refers to the actual distance between heritage trees; A refers to the total area of Luoyang, and n refers to the number of heritage trees. NNI>1 indicates that the heritage tree is uniformly distributed; NNI = 1 indicates random distribution, and NNI<1 indicates agglomerative distribution. The smaller the NNI value, the more agglomerated heritage trees were distributed.

2.3.2 Kernel density estimation

Kernel density estimation indicated the specific area where heritage trees gather and disperse (Sheather, 2004), which was calculated as follows:

$$f(x) = \frac{1}{nh}\sum_{i*1}^{n} K\left(\frac{x - x_i}{h}\right) \quad (2)$$

where *f(x)* refers to the kernel density value of heritage trees; *n* refers to the number of heritage trees; *h* refers to the bandwidth, which is the radius of the circle; *K* refers to the spatial weight function; $x–x_i$ refers to the estimated distance between two heritage trees.

2.3.3 Exploratory spatial data analysis

ESDA was used to analyze the spatial dependence and correlation of heritage trees. Global Moran's I index can be used to observe the spatial correlation of heritage trees in the whole study area based on their spatial locations. Local correlation index Getis-Ord G_i^* distinguished the spatial differentiation between cold and hot spots by detecting high-value and low-value agglomeration areas (Getis & Ord, 1992). The specific calculation formulas were as follows:

$$I = \frac{n}{s_0} \times \frac{\sum_{i-1}^{n}\sum_{j-1}^{n} W_{ij}(X_i - \bar{X})(X_{j-}\bar{X})}{\sum_{i-1}^{n}(X_i - \bar{X})^2} \quad (3)$$

$$G_i^*(d) = \frac{\sum_{j}^{n} W_{ij}(d)X_j}{\sum_{j}^{n} X_j} \quad (4)$$

$$Z(G_i^*) = \frac{G_i^* - E(G_i^*)}{\sqrt{Var(G_i^*)}} \quad (5)$$

where *n* refers to the number of heritage trees; X_i and X_j refer to the heritage tree of the *i*-th and *j*-th units, respectively; $\bar{X}$ is the mean value of heritage trees; W_{ij} is the spatial weight matrix, and S_0 is the sum of spatial weight matrices. $E(G_i^*)$ and $Var(G_i^*)$ are the variance and expectation of G_i^*, respectively. The value of Moran's I ranges from −1 to 1. Moran's I > 0 indicates a positive spatial correlation, whereas Moran's I < 0 indicates a negative spatial correlation. If the index is close to 0, then no spatial correlation is observed. The statistical significance of G_i^* (*d*) can be tested by standardized Z value. When Z > 0, the higher the Z value, the denser the aggregation of high values (hot spots); When Z < 0, the lower the Z value, the denser the aggregation of low value (cold spot).

2.3.4 Geographically weighted regression

The GWR model provided each spatial position with a regression coefficient, which was unattainable using the ordinary least squares (OLS) model. Regression analysis performed using the GWR model was used to select the center point and standard distance in each selected area to determine whether different regression coefficients can be acquired (Wang et al., 2021). Hence, the regression coefficient was not calculated using a constant value. Instead, the position function for each geographic location *i* was used to calculate the regression coefficient. Therefore, the spatial variation of influencing factors in different locations can be explored by applying GWR, and the results were more reliable. The Akaike information criterion (AIC) method was based on the concept of entropy and can obtain. Thus, in this study, the AIC was used to optimize the bandwidth (Chen et al., 2021). The GWR model formula was presented as follows:

$$y_i = \beta_0(u_i, v_i) + \sum_{k=1}^{n} \beta_k(u_i, v_i)x_{ik} + \varepsilon_i \quad (6)$$

where y_i refers to the $(n \times 1)$-dimensional explained variable; x_{ik} refers to the $(n \times k)$-dimensional explanatory variable matrix; β_k (u_i, v_i) refers to the regression coefficient of factor *k* at regression point *i*; *n* refers to the number of independent variables; (u_i, v_i) refers to the longitude and latitude coordinates of the *i*th observation point, and ε_i is the residual.

3 Results

3.1 Differential characteristics of heritage trees

3.1.1 Species characteristics of heritage trees

A total of 5,216 heritage trees were identified in Luoyang, belonging to 97 species, 70 genera, and 39 families. The number of species varied greatly. As shown in Table 1, the number of *Gleditsia sinensis* was the largest, with a total of 2,225 plants, accounting for 42.6% of the total, which was primarily distributed in Xin'an and Yichuan, followed by 940 *S. japonicas* and 423 *Platycladus orientalis*, accounting for 18% and 8.1%, respectively. These three dominant species of heritage trees in Luoyang had unique biological characteristics and economic and cultural values. On the one hand, these three species were all endemic to China. They were physiologically resistant to drought and frost without strict soil requirements. They had good shape, long lifespan, and fruiting period of hundreds of years. To date, as excellent greening trees, they were still found for urban landscape in China. On the other hand, their wood was hard and straight, and their leaves, flowers, fruits, seeds, skins, and thorns were important materials for traditional Chinese medicine and food. For example, the saponin horn produced by *G. sinensis* was the primary raw material for washing clothes and hair in the agricultural era, and the leaves, flowers, and seeds were edible and medicinal.

According to the "Technical Guidelines for the Document Establishment of a General Survey of National Ancient and Famous Trees," the heritage trees in Luoyang were divided into three categories based on their age (Table 2), namely,

TABLE 1 Statistics of the top 10 heritage tree species in Luoyang.

Name	Family	Genera	Number	Ratio/%	Distribution
Gleditsia sinensis	Leguminous	*Gleditsia*	2,225	42.66	Xin'an, Yichuan
Sophora japonica	Leguminous	*Sophora*	940	18.02	Yichuan, Yanshi
Platycladus orientalis	Cupressaceae	*Platycladus*	423	8.11	Yichuan, Mengjin
Diospyros kaki	Persimmonaceae	*Diospyros*	279	5.35	Yichuan, Mengjin
Pistacia chinensis	Anacardiaceae	*Pistacia*	277	5.31	Luoning, Songxian
Juglans regia	Jugaceae	Juglans	179	3.43	Luanchuan, Songxian
Ginkgo biloba	Ginkgoaceae	*Ginkgo*	178	3.41	Luanchuan, Songxian
Quercus variabilis	Fagaceae	*Quercus*	61	1.17	Luanchuan, Songxian
Quercus fabri	Fagaceae	*Quercus*	52	1.00	Luanchuan, Songxian
Cyclobalanopsis glauca	Fagaceae	*Cyclobalanopsis*	44	0.84	Luanchuan, Songxian

TABLE 2 Categories of heritage trees according to their age.

Types	Age	Number	Ratio(%)	Locations	Species
III	0–199a	1,695	32.50	Yichuan, Xin'an, Yiyang	▲, *Diospyros kaki*
	200–299a	1,258	24.12	Songxian, Yichuan, Yiyang	▲, *Juglans regia*
II	300–399a	938	17.98	Luoning, Songxian, Yiyang	▲, *Diospyros kaki*, *Pistacia chinensis*, *Quercus variabilis*
	400–499a	380	7.29	Luoning, Yichuan, Songxian	▲, *Pistacia chinensis*, *Diospyros kaki*, *Quercus fabri*
I	500–599a	398	7.63	Luoning, Songxian, Yichuan	▲, *Pistacia chinensis*, *Diospyros kaki*, *Quercus variabilis*
	600–999a	325	6.23	Songxian, Luoning, Ruyang	▲, *Ginkgo biloba*, *Pistacia chinensis*
	≥1000a	222	4.26	Songxian, Luoning, Mengjin	*Ginkgo biloba*, ▲

Notes: ▲ indicates the three dominant species: *G. sinensis*, *S. japonica*, and *P. orientalis*.

type I (age ≥500a), type II (300a ≤ age <500a), and type III (age <300a). Among these categories, the number of heritage trees for type I, II, and III was 723, 1,318, and 2,953, accounting for 13.86%, 25.27%, and 56.62%, respectively. The age of heritage in Luoyang presented a pyramid structure. With the increase of age, the number of heritage trees gradually decreased, and young trees had an absolute advantage. Among the dominant heritage trees, *G. sinensis* accounted for a larger proportion in type II and III, with an average age of only 215.67a, whereas *G. biloba* (with an average age of 1,052.74a), *P. orientalis* (with an average age of 463.21a), and *S. japonica* (with an average age of 408.77a) primarily belonged to type I because of their religious significance and folk beliefs.

3.1.2 Spatial characteristics of heritage trees

1) Regional differences in the distribution of heritage trees

Significant regional differences were found in the distribution of heritage trees (Figure 2). As the political, economic, and cultural center of Luoyang, the central urban area had a large population and high urbanization, but only 176 heritage trees were identified, accounting for 3.37%, with a low density of 0.22 trees/km^2. Suburbs had the most heritage trees (2,929), accounting for 56.15%, and the density was 0.55 trees/km^2. Suburbs were located along the Yellow River, Yi River, and Luo River, and they had a flat terrain and numerous national and provincial cultural relics, making it a gathering area of heritage trees in Luoyang. A total of 2,111 heritage trees were found in outer suburbs, accounting for 40.47%, and the density was 0.23 trees/km^2. The valley and hills in outer suburbs were alternately distributed, and heritage trees were relatively scattered, which were primarily distributed in bands along the river valleys.

The number of heritage trees in each county varied greatly (Table 3). Songxian, Yichuan, Luoning, Xin'an, Yiyang, and Mengjin were the top six counties with the highest number of heritage trees, ranging from 514 to 839, and the proportion exceeds 9.85%. The number of heritage trees in the central urban areas of Chanhe, Jianxi, Xigong, and Laocheng was less, ranging from 0 to 21. Therefore, the order of the number and density of

10.3389/fenvs.2022.993333

TABLE 3 Statistics of heritage trees in each county.

Regions	Counties	Number	Proportion (%)	Density (trees/km^2)
Central urban area	Luolong	142	2.72	0.24
	Chanhe	21	0.40	0.83
	Jianxi	9	0.17	0.11
	Xigong	4	0.08	0.08
	Laocheng	0	0.00	0.00
Suburbs areas	Xin'an	665	12.75	0.57
	Yiyang	639	12.25	0.40
	Mengjin	514	9.85	0.70
	Yanshi	293	5.62	0.44
	Ruyang	174	3.34	0.13
	Jili	1	0.02	0.01
Outer suburbs areas	Songxian	839	16.09	0.28
	Yichuan	817	15.66	0.77
	Luoning	720	13.80	0.31
	Luanchuan	378	7.25	0.15

heritage trees was inconsistent because of the large area difference among counties. Chanhe only had 21 heritage trees, but its density was the highest (0.83 trees/km^2) because of its small area. Songxian, Luoning, Luanchuan, and Ruyang had more heritage trees but less density. Among these counties, Songxian had the most existing heritage trees, but the density was only 0.28 trees/km^2. Mengjin and Yichuan had advantages in the number and density of heritage trees.

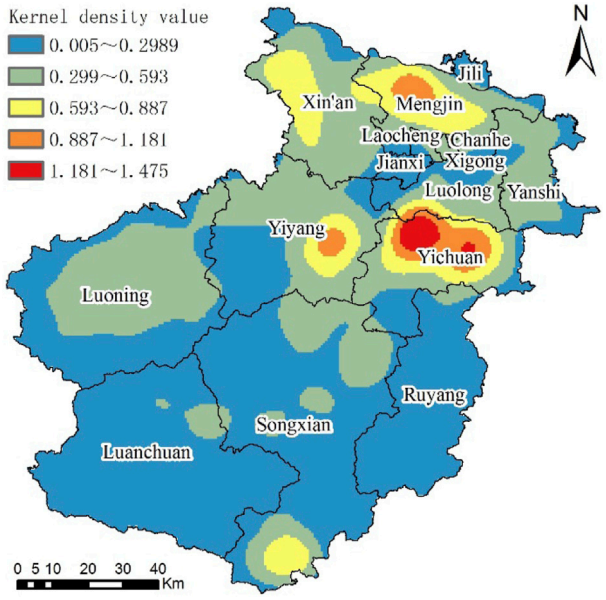

FIGURE 2
Kernel density estimation of heritage trees.

2) Spatial agglomeration characteristics of heritage trees

ArcGIS 10.2 was used to calculate the NNI of 5,216 heritage trees. After standardized statistics, the Z value was −103.74; the *p* value of the significance test was 0.00, and the confidence level was 99%, which indicated that the spatial distribution of heritage trees in Luoyang tended to agglomerate. The spatial aggregation characteristics of heritage trees were further analyzed by kernel density, and the study area was divided into the lowest density area, lower density area, medium-density area, higher-density area, and highest-density area by equal interval grading based on the kernel density value. The distribution of heritage trees in Luoyang presentd the aggregation characteristics of "three cores, one ring and two belts" (Figure 2). "Three cores" refered to the three typical highest density and higher density agglomeration areas along the Yi River in the north of Yichuan, along the Luo River in the southeast of Yiyang, and along the Yellow River in the middle-west of Mengjin Medium-density areas were distributed around the "three cores" in the Daimei Mountain area in the west of Xin'an and the Funiu Mountains in the south of Songxian, forming two relatively scattered agglomeration areas. "One ring" refered to the ring-shaped lower density agglomeration area formed around the central urban area of the Northern Luo River. The "two belts" refered to the two lower density areas formed along the Luo River in the Southwest and along the Yi River in the Southeast. The lower density area along the Luo

10.3389/fenvs.2022.993333

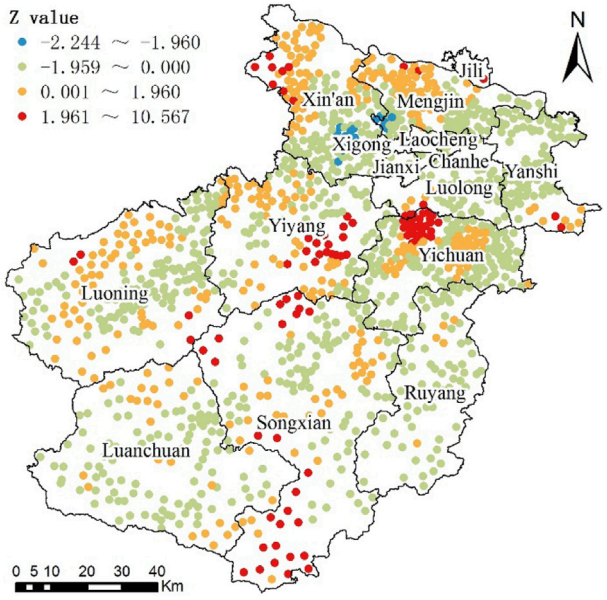

FIGURE 3
Classification of cold and hot spots for villages with heritage trees.

River was larger, and the lower density area of the Yi River was composed of scattered dots. Moreover, the nuclear density value was in the range of 0.30–0.59 trees/km^2. The lowest density area was widely distributed in Ruyang, Luanchuan, and Songxian in the south and central urban area in the North, with the lowest value of 0.0046 trees/km^2.

3) Spatial correlation characteristics of heritage trees

The estimated value of Global Moran's I of heritage trees in Luoyang was 0.0892 > 0, and the Z value of normal statistics was 16.17, which passed the 99% confidence test. This result showed that the distribution of heritage trees in Luoyang had positive spatial autocorrelation. 1,374 village-level units where the heritage trees were located were identified by cold and hot spots, and the local correlation index Getis-Ord G_i^* was calculated (Figure 3). Based on the Z value, four types of areas were divided into four categories, namely, cold spot (−2.244 to −1.960), sub-cold spot (−1.959 to 0), sub-hot spot (0.001–1.960), and hot spot (1.961–10.567). With regard to the number of villages, the hot spots and sub-hot spots, where the villages and their neighborhoods had more heritage trees, only contained 91 and 390 villages, respectively, whereas the number of sub-cold spots and cold spots, including villages and their surrounding villages with little heritage trees, were 876 and 17, respectively. With regard to regional distribution, hotspots and sub-hotspots were relatively concentrated in suburbs and primarily located in Yichuan, Yiyang, Mengjin, and the West of Xin'an; while the hotspot and sub-hotspots scattered in the outer suburbs. The distribution range of sub-cold spot villages were relatively wide, meanwhile, some were concentrated in the urban area and the surrounding suburbs. Cold spots included 11 villages gathering around the county seat of Xin'an and six villages near Luoyang Beijiao Airport. The distribution of cold and hot spots of heritage trees in Luoyang was uneven, the hot spot area and cold spot area were small but concentrated, whereas the sub-hot spot area and sub-cold spot area were large but scattered.

3.2 Driving force of the spatial distribution of heritage trees

3.2.1 Geographically weighted regression model

The spatial distribution difference of heritage trees in Luoyang results from the long-term comprehensive effect of local environment and culture. Based on previous studies and the actual situation of Luoyang, six quantifiable and accessible factors were selected from the two aspects of natural environment (elevation, slope, and water source) and human activities (historical and cultural aspects, land use, and economic intensity), and then taking 1,374 villages with heritage as statistical units, a GWR model was built to explore the driving force of the distribution of heritage trees. The interpretation and visualization of driving factors were shown in Table 4 and Figure 4.

A GWR model was constructed to analyze the driving force of the distribution of Luoyang heritage trees, and the regression coefficients of the selected driving factors were calculated (Table 5). The positive (negative) of the regression coefficient of each factor indicated the positive (negative) correlation between the distribution of Luoyang heritage trees and the driving factor. Greater absolute value of the regression coefficient indicated more significant influence of the factor on the distribution of Luoyang heritage trees. The maximum and minimum values of the regression coefficients of all driving factors were different, indicating that the driving factors of the spatial distribution of heritage trees in different regions were different (Figure 5). Based on the mean values of the regression coefficient, the results were obtained as follows: elevation, slope, and the area of forest and orchard land were positively correlated, whereas distance to the nearest river and number of POIs were negatively correlated; the relationship between the number of immovable relics and the spatial distribution of heritage trees was relatively weak. The degree of influence of the six factors on the distribution of heritage trees was in the following order according to the absolute value of their regression coefficients in the GWR model: area of forest and orchard > elevation > number of POIs > distance to the nearest river > slope > number of immovable relics.

TABLE 4 Driving factors and their interpretation.

Category	Factors	Symbol	Interpretation
Natural factors	Elevation	D_{ele}	The average altitude of the village
	Slope	D_{slo}	The average slope of the village
	Water sources	D_{riv}	Distance to the nearest river
Human factors	Historical culture	D_{rel}	Number of immovable relics
	Land use	D_{lan}	Area of forest and orchard land
	Economic intensity	D_{eco}	Number of POIs

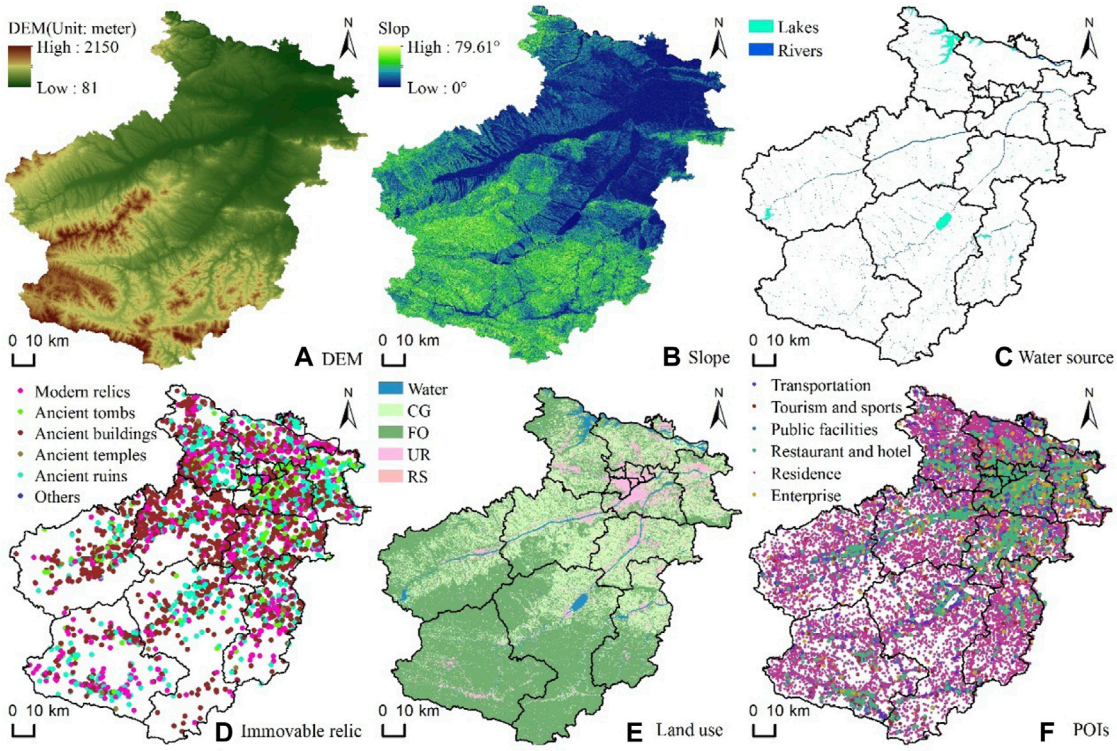

FIGURE 4
Visualization of driving factors: **(A)** DEM; **(B)** Slope; **(C)** Water source; **(D)** Immovable relic; **(E)** Land use; **(F)** POIs.

TABLE 5 Statistics of regression parameters of the GWR model.

Factors	Minimum	25% Quantile	Median	75% Quantile	Maximum	Mean
D_{ele}	−0.671	0.002	0.068	0.124	0.493	0.062
D_{slo}	−0.148	−0.014	0.005	0.037	0.651	0.021
D_{riv}	−2.794	−0.038	−0.011	0.019	0.274	−0.023
D_{rel}	−0.315	−0.063	−0.008	0.017	3.643	−0.012
D_{lan}	−0.377	0.069	0.187	0.621	2.635	0.412
D_{eco}	−12.648	−0.057	0.020	0.056	2.697	−0.051

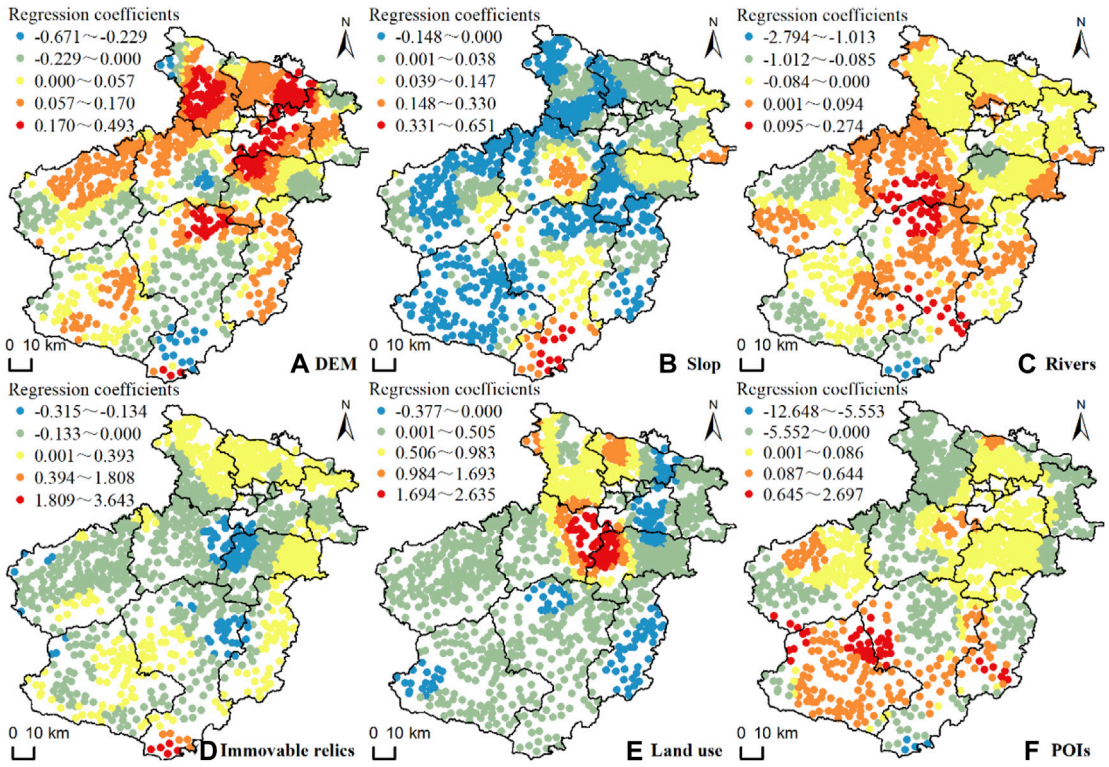

FIGURE 5
Spatial distribution of regression coefficients of driving factors in the GWR model: **(A)** DEM; **(B)** Slope; **(C)** Rivers; **(D)** Immovable relic; **(E)** Land use; **(F)** POIs.

3.2.2 Natural factors

1) Elevation

Heritage trees in Luoyang were distributed in the areas with elevation between 91 and 1,603 m, of which the areas with elevations of 200–500 m had the largest number of heritage trees (2,913), accounting for more than 40% of the total, followed by the areas with elevation ranging from 500 to 1,000 m (1,445 heritage trees), accounting for 27.70%. In flat areas with elevation of 93–200 m and mountainous areas with elevation of 1,000–1,603 m, the number of heritage trees decreased sharply, accounting for only 9.82% and 6.63%, respectively. The regression coefficient of D_{ele} in the GWR model ranged from −0.671 to 0.493, with a mean value of 0.062, which indicated that the influence of elevation on the spatial distribution of heritage trees was heterogeneous. The areas with high regression coefficient were primarily located in the plain area in the North and the valleys of the Yi River and Luo River in the South, which were concentrated in the central urban area, Mengjin, and Xin'an. In mountainous and hilly areas of Yiyang, Luoning, and Songxian, the regression coefficients of D_{ele} were negative, and the elevation was negatively correlated with the distribution of heritage trees. The minimum value of the regression coefficients were primarily concentrated in the mountainous area in the South of Songxian. More than 80% of the heritage trees in Luoyang were concentrated in hilly land because of the crisscross of river valleys, appropriate temperature, and convenient water source. The complex terrain was conducive to reducing the intensity of human activities and providing necessary conditions for the growth and protection of heritage trees.

2) Slop

The number of heritage trees in Luoyang increased initially and then decreased with the increase of slope (Figure 6). The regression coefficients of D_{slo} ranged from −0.148 to 0.651. The mean value of 0.021 and standard deviation of 0.069 indicated that the explanatory power of the slope to the distribution of heritage trees was weak, and the elasticity of the regression coefficients was small. The number of heritage trees in the areas with a slope ranging from 5° to 15° was the largest, accounting for more than 39.90%, followed by the areas with a slope ranging from 2° to 5°, accounting for 20.21%. The number of heritage trees in the area with a slope of >15° decreased sharply, whereas that in areas with steep slopes (35°–55°) only accounted for 3.60%.

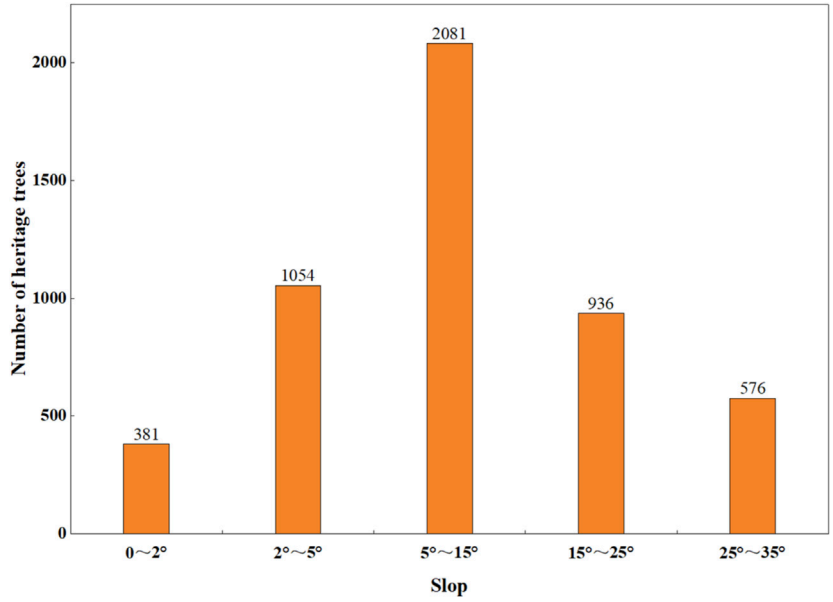

FIGURE 6
Number of heritage trees under different slopes.

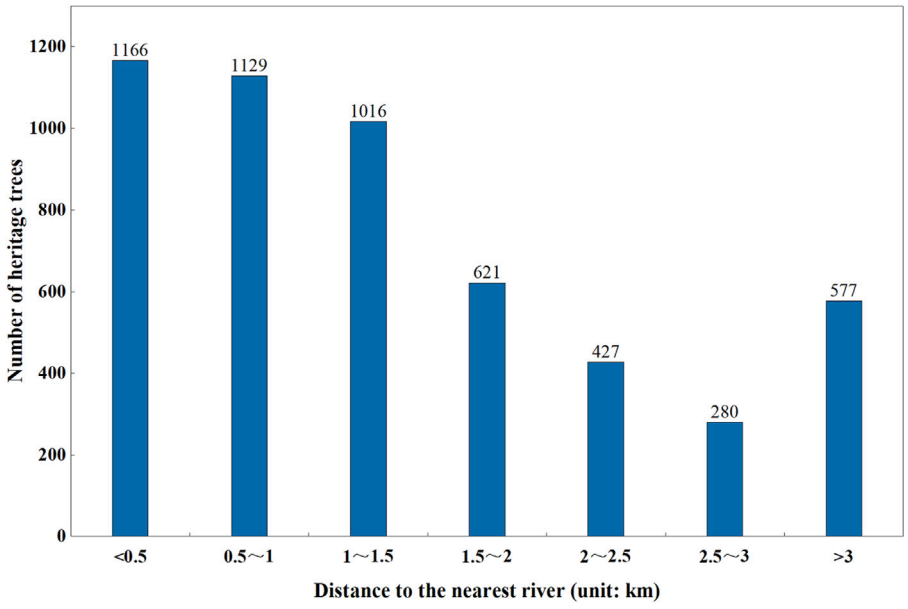

FIGURE 7
Number of heritage trees in different distances to the nearest river.

3) Water sources

Heritage trees in Luoyang had a near-water distribution, and they were primarily distributed along the banks of the Yellow River, Luo River, and Yi River. The regression coefficient of D_{riv} ranged from −2.794 to 0.274, with a mean value of −0.023 and standard deviation of 0.149. The number of heritage trees in Luoyang gradually decreased with the increase of the distance to

the river and showed a certain spatial heterogeneity. Heritage trees in areas less than 1.5 km away from the nearest river were the most concentrated, accounting for 63.48%. If the distance to the nearest river was greater than 1.5 km, then the number of heritage trees decreased significantly (Figure 7). In the northeastern of Luoyang, the river network was dense, and the terrain was flat. Historically, the rivers in this area were prone to floods during the flood season. Therefore, the distribution of heritage trees had a negative correlation with the distance to the river. The Southern region was the upper reaches of the Luo River and Yi River. The water volume of the rivers was small and unstable, and it was highly dependent on seasonal precipitation. Consequently, heritage trees in the Southern region were mostly distributed along the river to ensure sufficient water source.

3.2.3 Human factors

1) Historical culture

As a special ecological resource, heritage trees have a certain spatial relationship with relics, and the relationship between the two has an important effect on the protecting heritage trees and excavating the value of them. Using the spatial analysis function of ArcGIS 10.2, D_{rel} was calculated in the range of 0–8.42 km. A total of 4,121 heritage trees were primarily distributed within 2 km from the nearest river, accounting for 79.01%. The proportions of heritage trees in other three distances of 2–4 km, 4–6 km, and >6 km were 14.32%, 5.02%, and 1.65%, respectively. The GWR coefficient of D_{rel} (−0.315–3.643) and its mean value (−0.012) indicated that more negative relationship units were found than positive ones, indicating spatial heterogeneity. The river valleys and plains in Luoyang were concentrated areas of immovable relics. The number of immovable relics and the number of heritage trees had a negative spatial relationship because of frequent human activities, low vegetation coverage, and less stable environments suitable for the growth of heritage trees in these areas. The units with a positive relationship between immovable relics and heritage trees were primarily concentrated in the northeast of Luoyang, and these areas belonged to the mountainous area of Mangshan with many ancient ruins and tombs. Heritage trees, such as *P. orientalis*, were the important component of the ancient ruins and tombs to indicates longevity and permanence. In areas with complex terrain such as mountains and hills, immovable relics were scattered, and the distribution of heritage trees is “close to relics”.

2) Land use

Based on the suitability of the growth of heritage trees, the land in Luoyang was divided into five types: forest and orchard land (FO), cultivated land and grassland (CG), rural and square land (RS), urban construction and road land (UR), and waters. The spatial data of heritage trees and land use were superimposed to obtain the land use type where the heritage tree was located. The result showed that the heritage trees in Luoyang were primarily distributed in the land of FG and CG, accounting for 48.43% and 39.36%, respectively. Furthermore, GWR analysis was carried out on forest land and garden areas. Regression coefficients ranged from −0.377 to 2.635, with a mean value of 0.412 and standard deviation of 0.541. Compared with other driving factors, the factor of D_{lan} had the strongest explanatory power for the distribution of heritage trees. In addition, spatial differences were more significant, and most units had a positive relationship. In general, FO were the original growth sites of heritage trees, providing them with complete and stable growth environment, and they were the main land type of heritage tree distribution.

3) Economic intensity

POIs, as the information of human economic activities with spatial attributes, played an important innovative role in revealing the spatial pattern of heritage trees and the human–land relationship. The spatial distance and interaction between POIs and heritage tree were analyed to reveal the spatial heterogeneity of the effect of economic intensity on the distribution of heritage trees. First, by calculating the shortest distance between the heritage trees and POIs, the number of heritage trees gradually decreased with the increase of the distance from POIs. The shortest distance to POIs ranged from 0 to 2,538 m. The value of 56 heritage trees was 0 because most of them were located on POIs such as schools, temples, and addresses. The shortest distances form 75.82% of heritage trees to POIs were less than 600 m, and heritage trees farther from the POIs were primarily distributed in mountainous and hilly areas in the South. Second, the GWR coefficient of D_{eco} ranges from −12.648 to 2.697, with a mean value of −0.051 and standard deviation of 0.680, indicating that the number of POIs had a negative relationship with the distribution of heritage trees, and the spatial fluctuation of the regression coefficient was evident. In the northern of Luoyang where POIs were dense, the high-values of the regression coefficient were primarily concentrated in the central urban areas and its surroundings; in the Southern of Luoyang where POIs were relatively sparse, the high-values tended to be concentrated near main traffic roads and scenic spots. The heritage trees in the southern edge of Luoyang were negatively affected by the number of POIs, which indicated that many heritage trees were found but less POIs, and the economic development of this area was relatively slow.

4 Discussion

4.1 Spatial patterns and driving factors of heritage trees

A total of 5,216 heritage trees were found in Luoyang, which belonged to 39 families, 70 genera, and 97 species. The heritage

trees were numerous and widely distributed, showing a spatial distribution pattern of "three cores, one ring, and two belts." The spatial pattern of heritage trees resulted from the comprehensive effects of physical geography, historical culture, and socioeconomic. First, physical geography played a fundamental role in determining the variety and distribution pattern of heritage trees in Luoyang. Luoyang had a typical temperate monsoon climate, which was easy for the growth of broad–leaved tree species. Luoyang, located in the West of Henan, has interlaced landforms with mountains, rivers and hills, and the forest coverage was high. These natural conditions provided a relatively stable growth environment for heritage trees. Second, Luoyang was the ancient capital of 13 dynasties in China, and its profound history and culture had nurtured rich heritage tree resources. For example, a large number of long-aged *P. orientalis* and *G. biloba* were common in temples, ancient tombs, and relics. Furthermore, the intensity of economic activity sometimes dominated the survival of heritage trees. For example, the spatial distribution of heritage trees in the central urban area of Luoyang had an evident "hollow" phenomenon because of high-intensity economic activities. In recent years, the awareness of the public to protect heritage trees has gradually increased. Parks, green spaces, and scenic spots have been built around heritage trees, which not only provided suitable environment for heritage trees, but also enhanced the urban cultural heritage while beautifying the urban landscape.

In terms of the influencing factors of the spatial distribution of heritage trees in Luoyang, this study carries out quantitative measurement from six factors, such as elevation, slope, water source, historical cultural, land use, and economic intensity. Due to the limitations of the GWR model and the data acquisition of individual heritage trees, there was few indepth discussion on the impact of certain relatively stable factors (e.g., soil quality and specific growth environment) and accidental factors (e.g., geological disasters and historical events). With the improvement of acquisition technology of relevant data, further study will be carried out to improve the explanatory power of the spatial distribution of heritage trees and its influenced factors from the comprehensive perspective of geographical, cultural, ecological and other factors.

4.2 Effective protection and value mining of heritage trees

As non-renewable and irreplaceable natural and cultural resource, heritage trees are not only an important component of local biodiversity and excellent genetic resources, but also an active carrier of local history and culture. Heritage trees have laid a vital material foundation for Luoyang's ecological civilization construction and cultural prosperity. Therefore, taking measures is necessary to effectively protect heritage trees and reasonably excavate the value of heritage trees. The first measure is natural disaster prevention. A large number of heritage trees in Luoyang were distributed in low mountains and hilly areas, and it is necessary to prevent geological disasters such as landslides and debris flows that were prone to occur in the rainy season. In river alluvial plain areas, preventing the destruction of heritage trees by flood disasters is the primary focus. The second measure is to improve the growth environment of heritage trees. The conservation of heritage tree habitats in remote areas such as woodlands, gardens, and grasslands must be strengthened. It is also necessary to guide the public to actively protect heritage trees and prevent the growth space of heritage trees from being occupied by human activities in rural houses, urban blocks, and roads. Finally, reasonable development should be carried out on the premise of well-protected heritage trees. Diversified forms were encouraged to promote the history and culture loaded on heritage trees to transform "preserved" to "alive", which was conducive to cultivate regional cultural confidence. There were planty of historical and cultural relics in the urban area, but few heritage trees were preserved. Attention should be paid to supplement heritage tree reserve resources in scenic spots, parks, squares, universities and other places. The distribution of heritage trees was "close to relics" in areas with complex terrain such as mountains and hills where tourist attractions were mainly located. The tourism activities with the theme of ancient trees, as an important part of agricultural and eco-tourism, can meet people's increasing cultural and psychological needs (Cui et al., 2021). Therefor, Joint development of heritage trees and surrounding cultural relics and scenic spots should be carried out by sorting out the historical and cultural context and forming characteristic tourist routes to enhance the social and economic value of heritage trees.

5 Conclusion

Taking 5,216 heritage trees in Luoyang, the ancient capital in central China, as the research object, this study quantitatively explored the distribution pattern of heritage trees based on geospatial statistical methods, and a GWR model was used to analyze the driving degree and spatial heterogeneity of natural and human factors on the distribution of heritage trees. The results were intended to provide a comprehensive understanding of heritage trees to protect the ecological functions of heritage trees and mine the cultural value of heritage trees. The main conclusions were drawn as follows:

1) *G. sinensis*, *S. japonica*, and *P. orientalis* accounted for 68.7% of the heritage trees in Luoyang, which were related to their unique biological characteristics and economic and cultural values. With the increase of tree age, the number of heritage trees gradually decreased. *G. sinensis* accounted for a large proportion of the younger heritage trees, whereas the older heritage trees were mostly *G. biloba*, *P. orientalis*, and *S. japonica*.

2) The distribution of heritage trees in Luoyang varied greatly in space. Suburbs had the largest number and density of heritage trees, and they were the main gathering area for heritage trees. In the outer suburbs of Songxian, Luoning, Luanchuan, and Ruyang, their heritage trees were numerous but less dense. The distribution of heritage trees in Luoyang presentd the aggregation characteristics of "three cores, one ring and two belts", and it had positive spatial autocorrelation characteristics.
3) The GWR model was suitable for analyzing the influencing factors of spatial heterogeneity of heritage trees. The results showed that the influence of different factors on the distribution of heritage trees was spatially complex. The influence of driving factors on the distribution of heritage trees was in the following order: $D_{lan} > D_{ele} > D_{eco} > D_{riv} > D_{slo} > D_{rel}$. Elevation, slope, and area of forest and orchard were positively correlated with the spatial distribution of heritage trees, whereas the distance to the nearest river and POIs was negatively correlated with such factors. The influence of the number of immovable relics on the spatial distribution of heritage trees was relatively weak.

Data availability statement

The original contributions presented in the study are included in the article/Supplementary Material, further inquiries can be directed to the corresponding author.

Author contributions

HH: Conceptualization, methodology, software, investigation, formal analysis, writing—original draft; LZ: Visualization, investigation, writing—original draft; HB: Resources, supervision; JH: Software, validation; EC: Conceptualization, funding acquisition, resources, supervision, writing—review and editing; WR: Data curation.

Funding

This research was funded by the Henan Post Doctoral Research launch project in Henan Province (No. 247974), the Henan Philosophy and Social Science Planning Project (No. 2021BSH006), the National Natural Science Foundation of China (General Program, No. 42171058), the Humanities and Social Sciences Research Projects of Higher Education Institutions in Henan Province (No. 2021-ZZJH-160).

Conflict of interest

The authors declare that the research was conducted in the absence of any commercial or financial relationships that could be construed as a potential conflict of interest.

Publisher's note

All claims expressed in this article are solely those of the authors and do not necessarily represent those of their affiliated organizations, or those of the publisher, the editors and the reviewers. Any product that may be evaluated in this article, or claim that may be made by its manufacturer, is not guaranteed or endorsed by the publisher.

References

Asanok, L., Kamyo, T., Norsaengsri, M., Yotapakdee, T., and Navakam, S. (2021). Assessment of the diversity of large tree species in rapidly urbanizing areas along the chao phraya river rim, Central Thailand. *Sustain. (Basel, Switz.* 13 (18), 10342. doi:10.3390/su131810342

Atindehou, M. M. L., Avakoudjo, H. G. G., Idohou, R., Azihou, F. A., Assogbadjo, A. E., Adomou, A. C., et al. (2022). Old sacred trees as memories of the cultural landscapes of southern Benin (west africa). *Land* 11, 1–28. doi:10.3390/land11040478

Austin, M. (2007). Species distribution models and ecological theory: A critical assessment and some possible new approaches. *Ecol. Model.* 200 (1), 1–19. doi:10.1016/j.ecolmodel.2006.07.005

Badgujar, S. B., Patel, V. V., Bandivdekar, A. H., and Mahajan, R. T. (2014). Traditional uses, phytochemistry and pharmacology of Ficus carica: A review. *Pharm. Biol.* 52 (11), 1487–1503. doi:10.3109/13880209.2014.892515

Blicharskaand Mikusinski (2014). Incorporating social and cultural significance of large old trees in conservation policy. *Conserv. Biol.* 28 (6), 1558–1567. doi:10.1111/cobi.12341

Cannon, C. H., Piovesan, G., and Munné-Bosch, S. (2022). Old and ancient trees are life history lottery winners and vital evolutionary resources for long-term adaptive capacity. *Nat. Plants* 8 (2), 136–145. doi:10.1038/s41477-021-01088-5

Chen, K., Zhang, H., Zhang, B., and He, Y. (2021). [Spatial distribution of carbon storage in natural secondary forest based on geographically weighted regression expansion model. *Ying yong sheng tai xue bao = J. Appl. Ecol.* 32 (4), 1175–1183. doi:10.13287/j.1001-9332.202104.002

Chen, W. Y., and Hua, J. (2017). Heterogeneity in resident perceptions of a bio-cultural heritage in Hong Kong: A latent class factor analysis. *Ecosyst. Serv.* 24, 170–179. doi:10.1016/j.ecoser.2017.02.019

Cui, J., Li, R., Zhang, L., and Jing, Y. (2021). Spatially illustrating leisure agriculture: Empirical evidence from picking orchards in China. *Land* 10 (6), 631. doi:10.3390/land10060631

Foody, G. M. (2004). Spatial nonstationarity and scale-dependency in the relationship between species richness and environmental determinants for the sub-Saharan endemic avifauna. *Glob. Ecol. Biogeogr.* 13 (4), 315–320. doi:10.1111/j.1466-822x.2004.00097.x

Getis, A., and Ord, J. K. (1992). The analysis of spatial association by use of distance statistics. *Geogr. Anal.* 24 (3), 189–206. doi:10.1111/j.1538-4632.1992.tb00261.x

Gilhen-Baker, M., Roviello, V., Beresford-Kroeger, D., and Roviello, G. N. (2022). Old growth forests and large old trees as critical organisms connecting ecosystems and human health. A review. *Environ. Chem. Lett.* 20 (2), 1529–1538. doi:10.1007/s10311-021-01372-y

Huang, L., Jin, C., Zhen, M., Zhou, L., Qian, S., Jim, C. Y., et al. (2020). Biogeographic and anthropogenic factors shaping the distribution and species assemblage of heritage trees in China. *URBAN For. URBAN Green.* 50, 126652. doi:10.1016/j.ufug.2020.126652

Huang, S., Lee, J., and An, M. (2022). Socio-ecological restoration of cultural forests: The case of the Gyeongju historic areas in South Korea. *URBAN For. URBAN Green.* 69, 127516. doi:10.1016/j.ufug.2022.127516

Jordan, B., Julie, N., and Ken, L. (2021). Using traditional ecological knowledge to understand the diversity and abundance of culturally important trees. *J. Ethnobiol.* 41 (2), 209–228. doi:10.2993/0278-0771-41.2.209

Lai, P. Y., Jim, C. Y., Tang, G. D., Hong, W. J., and Zhang, H. (2019). Spatial differentiation of heritage trees in the rapidly-urbanizing city of Shenzhen, China. *Landsc. URBAN Plan.* 181, 148–156. doi:10.1016/j.landurbplan.2018.09.017

Li, K., and Zhang, G. (2021). Species diversity and distribution pattern of heritage trees in the rapidly-urbanizing Province of jiangsu, China. *Forests* 12 (11), 1543. doi:10.3390/f12111543

Lin, H., Chuang, Y., and Liu, W. (2020). Assessing the economic value of an iconic urban heritage tree. *For. POLICY Econ.* 118, 102216. doi:10.1016/j.forpol.2020.102216

Lin, X., and Chen, Q. (2021). Spatial characteristics and influencing factors of tourist towns in Fujian Province. *Sci. Geogr. Sin.* 41 (09), 1645–1653. doi:10.13249/j.cnki.sgs.2021.09.016

Lindenmayer, D. B. (2017). Conserving large old trees as small natural features. *Biol. Conserv.* 211, 51–59. doi:10.1016/j.biocon.2016.11.012

Lindenmayer, D. B., Laurance, W. F., and Franklin, J. F. (2012). Global decline in large old trees. *SCIENCE* 338 (6112), 1305–1306. doi:10.1126/science.1231070

Lindenmayer, D. B., Laurance, W. F., Franklin, J. F., Likens, G. E., Banks, S. C., Blanchard, W., et al. (2014). New policies for old trees: Averting a global crisis in a keystone ecological structure. *Conserv. Lett.* 7 (1), 61–69. doi:10.1111/conl.12013

Lindenmayer, D. B., and Laurance, W. F. (2016). The ecology, distribution, conservation and management of large old trees. *Biol. Rev.* 92 (3), 1434–1458. doi:10.1111/brv.12290

Liu, J., Jiang, R., and Zhang, G. (2020). Number and distribution of large old ginkgos in east China: Implications for regional conservation. *Nat. Conserv.* 42 (4), 71–87. doi:10.3897/natureconservation.42.59284

Liu, J., Lindenmayer, D. B., Yang, W., Ren, Y., Campbell, M. J., Wu, C., et al. (2019). Diversity and density patterns of large old trees in China. *Sci. TOTAL Environ.* 655, 255–262. doi:10.1016/j.scitotenv.2018.11.147

Liu, J., Xia, S., Zeng, D., Liu, C., Li, Y., Yang, W., et al. (2022). Age and spatial distribution of the world's oldest trees. *Conserv. Biol.* 36, e13907. doi:10.1111/cobi.13907

Nolan, V., Reader, T., Gilbert, F., and Atkinson, N. (2020). The ancient tree inventory: A summary of the results of a 15 year citizen science project recording ancient, veteran and notable trees across the UK. *Biodivers. Conserv.* 29 (2), 3103–3129. doi:10.1007/s10531-020-02033-2

Osborne, P. E., and Suárez-Seoane, S. (2002). Should data be partitioned spatially before building large-scale distribution models? *Ecol. Model.* 157 (2), 249–259. doi:10.1016/S0304-3800(02)00198-9

Qiu, Z., Feng, Z. K., Wang, M., Li, Z., and Lu, C. (2018). Application of UAV photogrammetric system for monitoring ancient tree communities in beijing. *Forests* 9 (12), 735. doi:10.3390/f9120735

Ray, R., Subash Chandran, M. D., and Ramachandra, T. V. (2014). Socio-cultural protection of endemic trees in humanised landscape. *Biodivers. Conserv.* 23 (8), 1977–1994. doi:10.1007/s10531-014-0699-1

Sheather, S. J. (2004). Density estimation. *Stat. Sci.* 19 (4), 588–597. doi:10.1214/088342304000000297

Singh, M., Evans, D., Tan, B. S., and Nin, C. S. (2015). Mapping and characterizing selected canopy tree species at the angkor world heritage site in Cambodia using aerial data. *PLoS One* 10 (4), e0121558. doi:10.1371/journal.pone.0121558

Spies, T. A. (2004). Ecological concepts and diversity of old-growth forests. *J. For.* 102 (3), 14–20. doi:10.1093/jof/102.3.14

Spooner, P. G., and Shoard, J. (2016). Using historic maps and citizen science to investigate the abundance and condition of survey reference 'blaze' trees. *Aust. J. Bot.* 64 (5), 377–388. doi:10.1071/bt16054

Takács, M., Szénási, Á., and Malatinszky, Á. (2020). Polypores, Agrobacterium and ivy damage on Hungarian ancient trees. *Nat. Conserv.* 40 (2), 1–38. doi:10.3897/natureconservation.40.51633

Wan, J., Li, Q., Wei, G., Yin, G., Wei, D., Song, Z., et al. (2020). The effects of the human footprint and soil properties on the habitat suitability of large old trees in alpine urban and periurban areas. *URBAN For. URBAN Green.* 47, 126520. doi:10.1016/j.ufug.2019.126520

Wang, J., Du, H., Li, X., Mao, F., Zhang, M., Liu, E., et al. (2021). Remote sensing estimation of bamboo forest aboveground biomass based on geographically weighted regression. *Remote Sens.* 13, 2962. doi:10.3390/rs13152962

Wang, Z., Zhang, S., and Song, M. (2010). Ancient – famous trees in henan Province. 17, 111. doi:10.1007/s13596-017-0286-6

Wu, C., Jiang, B., Yuan, W., Shen, A., Yang, S., Yao, S., et al. (2020). On the management of large-diameter trees in China's forests. *Forests* 11, 111. doi:10.3390/f11010111

Wyla, B., and Ycc, B. (2022). To exclude or not to exclude? The effect of protest responses on the economic value of an iconic urban heritage tree. *URBAN For. URBAN Green.* 71, 127551. doi:10.1016/j.ufug.2022.127551

Zhang, H., Lai, P. Y., and Jim, C. Y. (2017). Species diversity and spatial pattern of old and precious trees in Macau. *Landsc. Urban Plan.* 162, 56–67. doi:10.1016/j.landurbplan.2017.02.002

Zhang, Z., Yang, X., and Liu, J. (2013). Distribution and rejuvenation technology of ancient and famous tree in beijing. *Vegetos- Inter. Jour. Plnt. Rese.* 26 (1), 188–195. doi:10.5958/j.2229-4473.26.1.027

frontiers | Frontiers in Earth Science

TYPE Perspective
PUBLISHED 06 September 2022
DOI 10.3389/feart.2022.966907

Check for updates

OPEN ACCESS

EDITED BY
Jiaxing Cui,
Central China Normal University, China

REVIEWED BY
Qingsong He,
Huazhong University of Science and Technology, China
Xiaomin Lu,
Lanzhou Jiaotong University, China
Enxiang Cai,
Henan Agricultural University, China

*CORRESPONDENCE
Wei Zhu,
zhuwgiser@whu.edu.cn

SPECIALTY SECTION
This article was submitted to Environmental Informatics and Remote Sensing,
a section of the journal
Frontiers in Earth Science

RECEIVED 11 June 2022
ACCEPTED 08 August 2022
PUBLISHED 06 September 2022

CITATION
Zhang Y, Chen Y, Zhu W, Wang W and Zhang Q (2022), The topological structure of urban roads and its relation with human activities at the street-based community level.
Front. Earth Sci. 10:966907.
doi: 10.3389/feart.2022.966907

COPYRIGHT
© 2022 Zhang, Chen, Zhu, Wang and Zhang. This is an open-access article distributed under the terms of the Creative Commons Attribution License (CC BY). The use, distribution or reproduction in other forums is permitted, provided the original author(s) and the copyright owner(s) are credited and that the original publication in this journal is cited, in accordance with accepted academic practice. No use, distribution or reproduction is permitted which does not comply with these terms.

The topological structure of urban roads and its relation with human activities at the street-based community level

Yan Zhang[1], Yebin Chen[2], Wei Zhu[3]*, Wenwen Wang[1] and Qian Zhang[1]

[1]School of Land Engineering, Chang'an University, Xi'an, China, [2]School of Architecture and Urban Planning, Shenzhen University, Shenzhen, China, [3]School of Resource and Environmental Sciences, Wuhan University, Wuhan, China

The topological structure of the underlying streets can help us better understand urban space and human activities therein. As human urban movements are inherently heterogenous in space and statistics, whether or not the network of streets holds a similar degree of heterogeneity worth being investigated. Relying on the graph theory and complex-network thinking, we adopted the street segment analysis-based methods and computed segment-based topological metrics in the downtown of two major cities in China: Beijing and Shanghai. More specifically, we used Flickr photo location data as a proxy of human urban activities and counted the movement flow at levels of both street-based communities and street segments. We measured the heterogeneity of each segment-based metric *via* the extent of being long-tailed in the rank-size distribution (long-tailedness). We found that segment-based betweenness was most long-tailed and was the best metric for capturing human activities within each community and that neither segment-based degree nor can closeness show a similar extent of long-tailedness and can have a good correlation with the segment-based flow. These findings point to the insight that the positive relationship between street structure and human activities is significantly shaped by their shared heterogeneous nature.

KEYWORDS

topological analysis, segment analysis, long-tailed distribution, heterogeneity, urban roads

1 Introduction

The past decade in China witnesses a significant rural-urban transition. With more than sixty percent of the total population living in cities, people are confronting a series of urban issues. In the meantime, the advancement of information and communication technology leads more and more people to conduct activities in a hybrid physical-virtual urban space (Shaw and Yu 2009), from which we can easily acquire a massive amount of fined-grained, widely-covered, spatio-temporal data–so-called urban big data (Mayer-Schonberger and Cukier 2013). Big data makes it possible for us to foster a quantitative

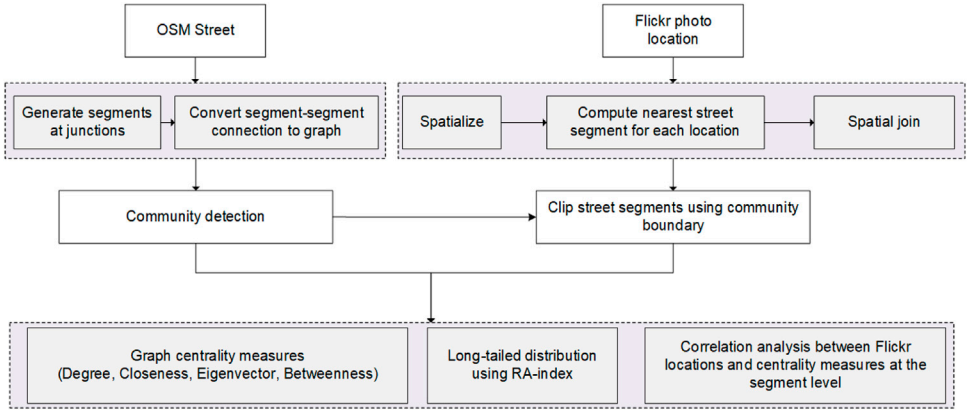

FIGURE 1
The methodological framework of this study.

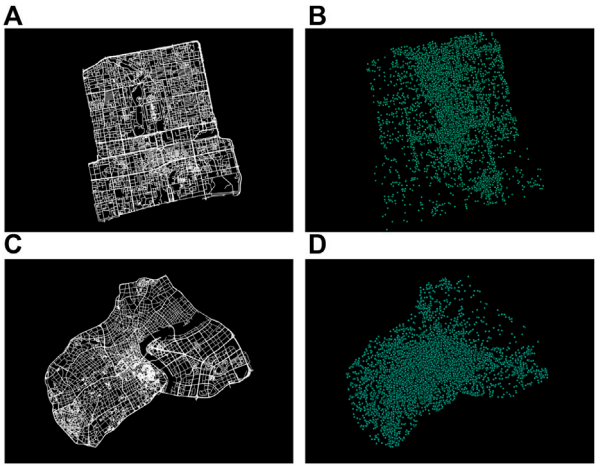

FIGURE 2
(Color online) The spatial distribution of processed geo-tagged photos in the study areas and the underlying street networks in the centermost region of Beijing **(A,B)** and Shanghai **(C,D)**.

understanding of how people live, work, and move in the urban area and, more importantly, to offer us a greater chance to explore the factors behind (Zheng et al., 2014). Among those factors, urban space or built environment is probably the first and foremost because it underlies and works as a primary constraint of our physical activities or movements (such as vehicles must run along the street). In this regard, the understanding of the urban structure and its relation to human activities becoming more urgent and important, as authorities and policymakers are actively seeking solutions for better urban and transport planning to related issues including energy, environment, and sustainability (Batty 2007; Batty 2013).

The urban spatial network has long been used for effectively characterizing the urban structure and its underlying dynamics (Zhong et al., 2014). Street network is one of the most prominent network types. On the one hand, the human movements on the streets in a two-dimensional geographical information system (GIS) can be abstracted as moving points along road center lines, in which we can count the number of points on each line as street-based movement flow. On another, the network of streets naturally allows us to store and model the street topology for investigating the underlying structure of urban space, represented by a dual graph consisting of nodes as streets themselves and links as intersections. Moreover, the correlation between the flow and those structural properties can further lead us to apprehend the relationship between urban form and function (Hillier and Lida 2005). It is commonly accepted that the very topology attained from the street segments has the potential to well correlate with human street movements. In the literature, street topological properties exhibit complex-network characteristics such as scale-free (Barabasi and Albert, 1999; García-Pérez et al., 2018). This indicates that a great heterogeneity of street-street connections that leads to the street network consists of compartments or communities wherein the streets are denser than the ones outside (Newman 2003). However, there were rare studies investigating human activities at the street community level. Supported by Flickr data that are with finer spatial and temporal granularities, it is plausible to adopt street communities as the unit to conduct correlation analysis between human activities and a more refined urban space.

In this article, we study the relationship between the street topological properties and human activities represented by location-based social media (LBSM). As one major kind of urban big data, LBSM data record massive geo-related information from millions of users and works as a good proxy of conventional data for exploring the geographic space and human activities therein. Rooted in complex-network thinking and graph theory, we adopt the street

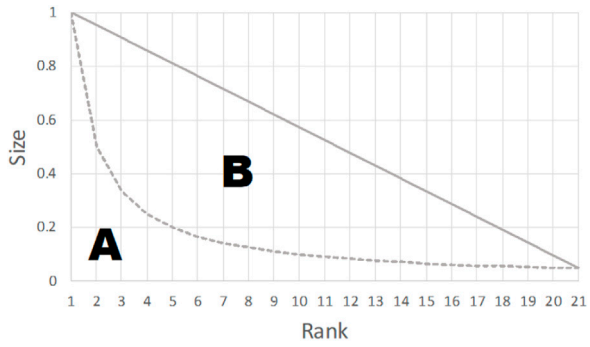

FIGURE 3
The illustration of the RA-index using a rank-size plot.

community as a unit for analysis and seek the correlation between different types of topological metrics of street segments within each community and related movement flow counted by Flickr points along the segments. The contribution of this study is three-fold: 1) We apply RA-index to measure the heterogeneity or long-tainedness of the spatial distribution of Flickr photos, not only at the community level but also at the street segment level; 2) At the segment level, only betweenness has a moderate correlation with a number of Flickr locations, others do not have at all. 3) A further investigation of statistical distribution of all these metrics suggests that only betweenness metrics exhibit a similar profile to that of Flickr locations. This explains why betweenness can better capture human activities and this knowledge could help us in some urban applications such as traffic prediction and route planning.

The remainder of this paper proceeds as follows. Section 2 introduces the datasets and methods. Section 3 presents the visualization and statistical results regarding the topological analysis of the street network, the imbalance distribution of photo locations at the community and street levels, and the correlation between the two. Section 4 discusses and concludes the results and points to the future research direction.

2 Methodology

2.1 Data and data processing

The framework of this study is presented in Figure 1. We focused on the centermost area of Beijing and Shanghai bounded by the inner ring road for this study. Respectively (Figure 2). The area includes two highly developed districts such as Dongcheng in Beijing and Pudong in Shanghai, both of which attract massive amounts of human activities. We wrote a simple script to clip out the Flickr data downloaded from the Yahoo database. As Figure 2 shows, there were 73,276 and 92,479 records in downtown Beijing and downtown Shanghai, respectively, including Photo ID, user ID, timestamp, and XY coordinates. We also followed a previous study (Wu et al., 2014) and cleaned the data by removing photo duplicates (same user sent at same time and location) and those photos sent by robots. The cleaned data contained 19,970 photo locations for Beijing and 24,589 for Shanghai. The street network was downloaded directly from OpenStreetMap. We further used the *Near* function to assign each location to the nearest street segment and eventually counted how many photo locations were assigned to a single segment as the segment-based flow.

2.2 Topological properties for characterizing a street network structure

We built the dual graph $G(V, E)$ of the obtained street networks in two cities, in which V stands for the set of nodes $\{v_1, v_2 \ldots\}$, and E is a set of edges or links among the nodes. Before that, we processed the original street data in ArcMap to ensure the right polyline topology, where the intersection can only occur in case of three or more segments. The resulting number of street segments in Beijing and Shanghai were respectively 13,709 and 23,583. The dual graph of segment-segment topology was based on their intersection relationship and had 30,260 and 65,377 edges. The constructed graph was undirected and unweighted. To characterize a street network, this study used the following topological metrics for each segment:

Degree centrality, as denoted in Eq. 1, the degree of a node is based on how many links connect to that node.

$$D(v_i) = \frac{d(v_i)}{\sum_{v_i \in V} d(v_i)} \tag{1}$$

Closeness centrality, refers to the topological distance of a node to every other node in a network, which is denoted by Eq. 2, which $d(v_i, v_j)$ is the shortest distance between a node v_i and v_j.

$$C(v_i) = \frac{1}{\sum_{j-1}^{g} d(v_i, v_j)} \tag{2}$$

Eigenvector centrality, makes use of the centrality of a node's neighbor to determine the centrality for that node. The eigenvector centrality for a node v_i can be described as Eq. 3.

$$E(v_i) = \frac{1}{\lambda} \sum_{j \in G} a_{v,j} v_i \tag{3}$$

Betweenness centrality measures how big a role a node v_k plays as a bridge in a network. Described as Eq. 4, the betweenness score of v_k is calculated by the ratio of the number of shortest paths between any two nodes v_i, v_j passing through v_k.

$$B(v_k) = \sum_{v_i, v_j \in V} \frac{\sigma(v_i, v_j | v_k)}{\sigma(v_i, v_j)} \tag{4}$$

TABLE 1 The statistics of derived street communities in downtowns Beijing and Shanghai. (Note: #, number; Comm, Communities; Mod, Modularity score; MaxSeg, the maximum number of segments within a community; MaxPhotos, maximum unique photo locations within a community).

	#Comm	Mod	#MaxSeg	#MinSeg	#MaxPhotos	#MinPhotos
Beijing	52	0.944	481	52	2116	8
Shanghai	58	0.937	797	34	2274	1

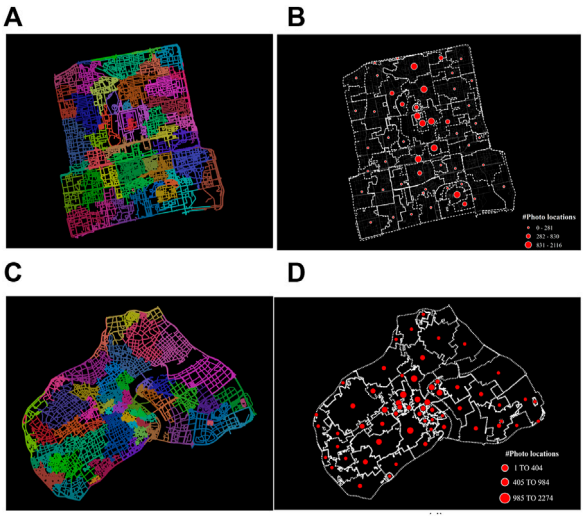

FIGURE 4
(Color online): The layout of detected street communities in the downtown area of Beijing and Shanghai **(A,C)**, each of which is with a number of Flickr points that are mapped using dot size **(B,C)**.

Like many other real-world networks, a street network consists of many independent compartments, forming a community structure. This way we can naturally divide a large street network group by group for a better understanding of the structure of the streets. To assess the goodness of a community structure, modularity is often used, denoted by Eq. 5:

$$Q = \frac{1}{2m}\sum_{i,j}\left(A_{ij} - \frac{k_i k_j}{2m}\right)\delta\left(c_i, c_j\right) \tag{5}$$

in which $A_{i,j}$ refers to weights between nodes (v_i, v_j), c_i, c_j are community indexes, $\delta(c_i, c_j) = 1$ denotes they belong to one community if not, it equals to 0. The detection of communities for a large network requires some efficient algorithms. This study uses the Louvain method (Blondel et al., 2008) for the community detection of the street network. With the street segments being represented as nodes, and the intersection relationship being represented as binary edges, the community detection algorithms can divide the segment-segment network into communities, within which these segments interact with each other more strongly than ones outside the subgroup. To determine the best community detection result, this algorithm joins individual nodes into communities progressively until the modularity score no longer increases.

2.3 RA-index for measuring the long-tailedness of topological metrics

Commonly, human urban activities are substantially heterogeneous (e.g., Brockmann et al., 2006; Gonzalez et al., 2008), manifested mathematically as a right skew in the probability distribution or a long tail in rank-size distribution. The skewness or long-tailedness in the distribution can also be understood as data imbalance or unevenness since data with this such kind of distribution contain only a few large values but numerous small values, that is, large-to-small ratios are disproportional (e.g., 80/20 rather than 50/50). In recent years, the ratio (RA-index; Gao et al., 2016) is widely used to quantify the extent of a data being long-tailed distribution (Ma et al., 2020). To calculate RA-index, we first rank all values in the data set from the largest to the smallest (a rank-size plot). The RA-index value, as Eq. 6 denotes, equals the ratio between the areas of two polygons A and B divided by the line connected with the largest and smallest values (Figure 3). The value range of the RA-index is between 0 and 1. The smaller the RA-index value, the more long-tailed or right-skewed the data is. This study would compute the RA-index on every type of segment-based measure, as well as the segment-based movement flow.

$$\mathrm{RA} = \frac{S_A}{S_A + S_B} \tag{6}$$

Where S_A and S_B represent respectively the area of two parts of the triangle divided by the rank-size distribution line.

3 Results

3.1 Detected communities and related statistics

We firstly partitioned the network graph into several communities. As Table 1 presents, the statistical results of the two downtown areas were similar. As the case with Shanghai, the derived 58 communities with the highest modularity score of 0.937. The size (number of street

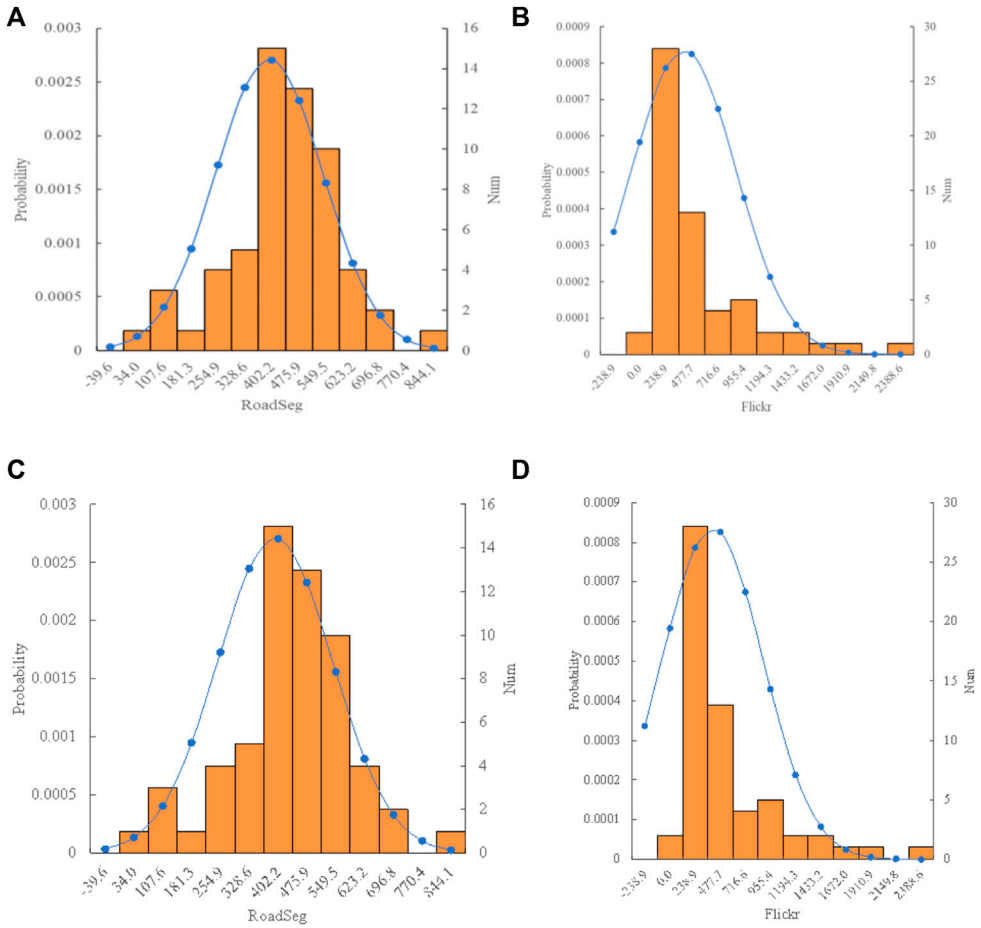

FIGURE 5
(Color online): The probability statistical distribution of #street segments and #Flickr locations within each community [Note: # = number, #road segments for each community obey a normal distribution **(A,C)**, while # Flickr photos exhibit in a right-skewed or long-tailed manner **(B,D)**].

TABLE 2 The average community-based RA-index values for several photo locations and each of the centrality measures.

	#Photo	Betweenness	Closeness	Degree	Eigenvector
Shanghai	0.04	0.12	0.75	0.79	0.72
Beijing	0.06	0.14	0.76	0.75	0.66

segments) of each community ranges from 34 to 797 (Table 1). As can be seen from Figure 4A,C, at the center of the study area, numerous small-sized communities were concentrated, whereas bigger ones were surrounded layer by layer. On the other hand, the number of geotagged Flickr photos within each street community gave another story. Figure 4B,D showed that smaller communities at the center tended to possess a considerably large amount of photo locations (2274 at most in one community; Table 1), indicative of the area of interest in the downtown area, while much fewer photo locations resided in larger communities at the periphery. From a statistical point of view, the number of segments contained in each community follows a normal-like distribution, that is, the big-to-small ratio regarding the number of street segments for each community was proportional, that is, around the average value. The statistical distribution for photo locations within each street community was, therefore, quite disproportional (right-skewed) and was with an RA-index of 0.04, suggesting a

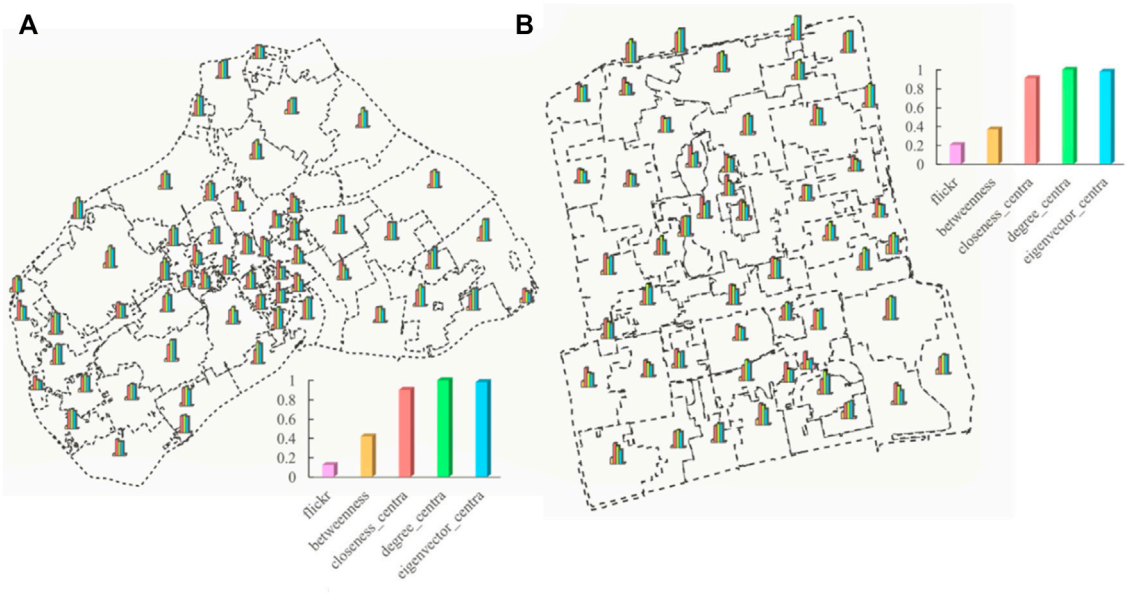

FIGURE 6
(Color online): The bar chart view of RA-index values on five metrics at the community level (Note: Data with an RA-index closer to 0 is prone to be highly right-skewed. Thus, across four types of centrality measures, the extent of imbalance distribution of betweenness is the closest to that of #photo locations, followed, in order, by degree, closeness, and eigenvector).

highly imbalanced distribution, both in space and statistics, of human activities in social media (Figures 4, 5).

3.2 Correlation within each community

We computed four types of centrality measures for each street segment, that is, betweenness, closeness, degree, and eigenvector. Within each derived street community, we further extracted the contained street segments and then examined the extent of imbalance distribution across four topological parameters as well as the number of photo locations (Table 2). It is very interesting to note that the distribution of photo locations at the street segment level was very uneven too, for most of the RA-index values were less than 0.1, similar to what has been distributed over different street communities. On the other hand, the centrality measures behaved quite differently. Figure 6 provides an overview of the RA-index for each metric at the community level, from which we can see a remarkable consistency between several photo locations and betweenness, while the other three centrality measures appeared several times bigger (above 0.7).

We correlated each segment-based topological metric with the corresponding amount of photo location. The range of correlation for all metrics was in general (−0.21, 0.39) in Shanghai (Figure 6a) and (−0.18, 0.48) in Beijing (Figure 6b). Taking examples of the top 10 popular communities for both cities shown in Figure 7, the correlation results vary from community to community and demonstrate, by and large, a consistent pattern with the RA-index values, that is, metrics with a smaller RA-index was inclined to have a larger correlation result (e.g., betweenness). In contrast, a lack of correlation or negative correlation can be found in some communities where metrics with a large RA-index value (e.g., degree and closeness). In this regard, betweenness outperforms other structural properties regarding the capture of human activities at the community level (e.g., the strongest correlations in 5 communities out of the top 10 communities in Shanghai; Figure 7A), as it conforms to the imbalanced spatial distribution of photo locations. Furthermore, to confirm the above result about the presence or absence of correlations, we mapped street segments within one of the most popular communities (Figures 7A, B). For example, we selected one community in Shanghai with 1,545 geo-tagged photos over 580 street segments, the visualization uses a color scheme from blue (lowest) to red (highest) showing high/low correspondence between different measures and human activities.

4 Discussion

The street network is a *de facto* complex network, in which the connections among streets are distributed rather unevenly (Newman 2003). In other words, the connections in some parts

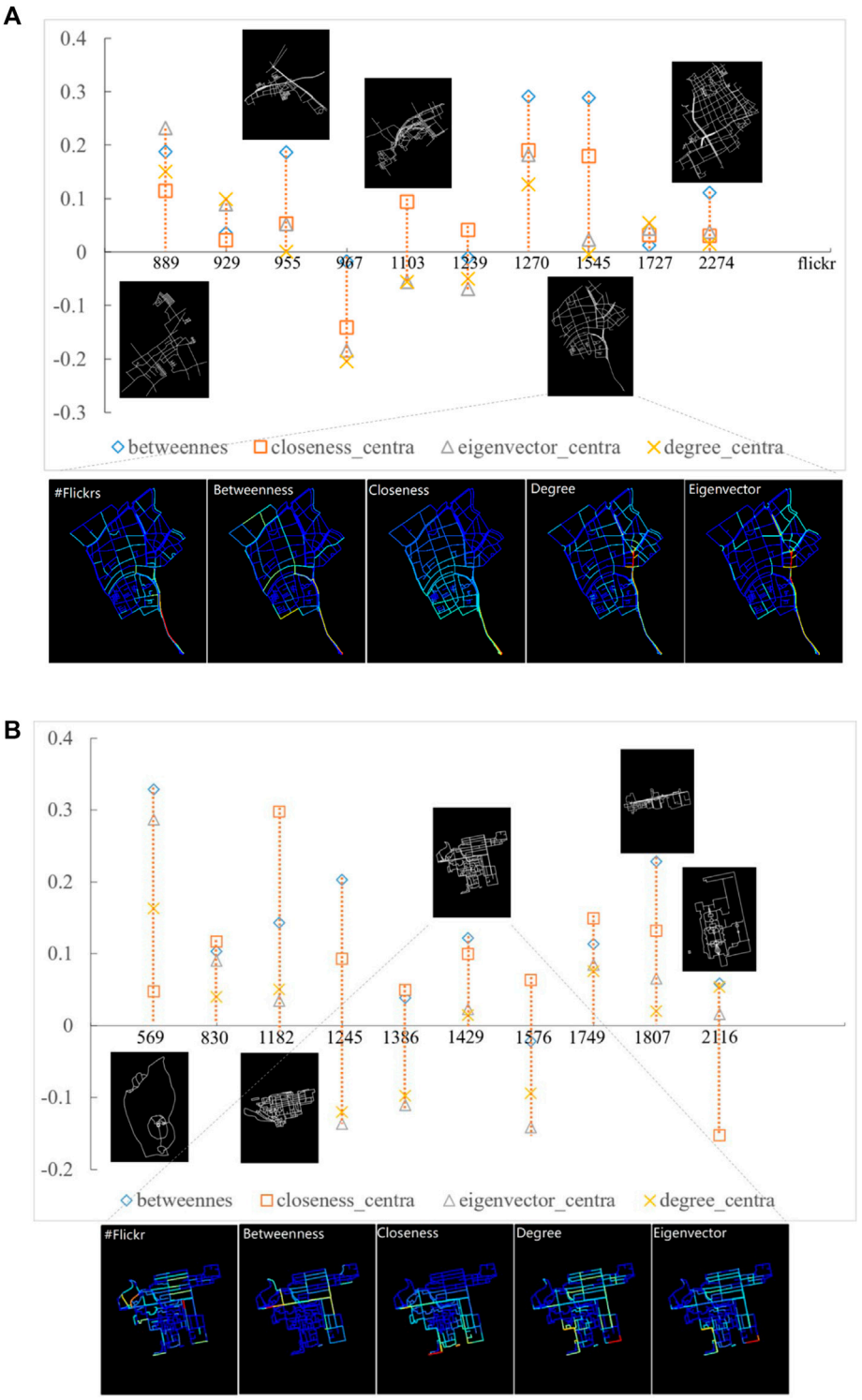

FIGURE 7
(Color online) The segment-based metric-flow correlation results between four types of topological parameters, respectively, and several photo locations in the top 10 popular communities and the street network in one of the selected 10 communities, rendered using different types of segment-based measures, respectively in Shanghai **(A)** and Beijing **(B)**. (Note: The betweenness value shows the strongest uniformity with the number of photos, either spatially or statistically, and thus has a better correlation than other metrics).

of the network are dense while in other parts are quite sparse. This leads us to decompose such a network into communities within which the streets interact more intensively than the ones outside. It should be noted that the detected communities work effectively as alternative space partitioning units that are emerged from the bottom-up rather than traditional ones from the top-down such as equal-sized grids that neglect the essentials of the underlying spatial environment. This is very much in line with the Flickr data used in this study which is also collected in a bottom-up manner and with an unbalanced spatial distribution. Although Flickr is not as popular as Weibo and Wechat in China, we chose the centermost part of the two largest Chinese metropolises where the places are relative with very dense photo locations to ensure the Flickr data can reflect greatly the activity level. In doing so, we managed to conduct an in-depth investigation of the interplay between urban spatial structure and human activities.

From a statistical viewpoint, the unevenness can be characterized as a right-skewed or long-tailed distribution. In the study, it is interesting to stress that such an uneven spatial distribution of Flickr photo locations at two levels: across communities and within a single community, represented by the RA-index value being smaller than or equal to 0.1. From one community to another, the different amount of photo locations can reflect the varying popularity degrees of a place. Such a variation also appears from the street to street within a community. The result showed that the minimum RA-index value for the number of photo locations distributed across streets is 0.02, indicating an extremely imbalanced pattern of far more rarely-visited streets than frequently-visited ones. What is more, some of the calculated segment-based structural parameters exhibited a similar statistical pattern such as betweenness whose RA-index largely resonates one of photo locations in most cases (also shown in Figure 6B).

The correlation test further revealed that betweenness was the best segment-based topological metric for capturing human activities at the community level. Other metrics like degree or closeness were with larger RA-index values and thus were hard to have a moderate metric-flow correlation. The primary reason could be that the betweenness is a more global measure (Freeman 1979) and its calculation takes account of not only the immediate intersected streets (neighbors) of a street, but also neighbors' neighbors, and so on. On the contrary, the degree of closeness centrality considers only the local neighbors of a street. As a street segment usually intersects immediately with only 3 or 4 segments, the segment-based degrees within a community would not differ too much from one another, thereby leading to a larger RA-index value or a more proportional distribution (e.g., 50/50 rather than 20/80).

The similar community-based statistics in the two cities above help us better understand the interplay between the complex or heterogenous street structure and human check-in activities. As confirmed in many urban literatures, although one has his/her own choice or behavior while moving, the collective movements are greatly influenced by the underlying spatial environment such as the network of streets (e.g., Hillier 2012) and can, to a certain extent, captured by the structural properties (network metrics). Moreover, based on the detected long-tailed distribution on both the betweenness metric and the number of photo locations along streets within each community, we further identify that the heterogeneity of urban space may work as an effective means of characterizing group-level human activities.

5 Conclusion

The relationship between the urban environment and human activities therein is one of the cores in urban science. The present study makes use of the street network in the downtown two metropolitan areas Beijing and Shanghai and decodes the urban morphology from the perspective of the street communities, from which we can further understand a city's configurational and functional complexity regarding the imbalanced distribution of street topological parameters and human check-in activities. Despite previous studies had pointed out a positive correlation between street topological properties and people movement flow, our experiment further contributes to the literature that one of the reasons behind the positive correlation is the shared heterogeneous or imbalanced nature held by both street structure and human activities. Future work will involve more metropolises worldwide for an international outlook and develop agent-based simulation using street networks as the computation environment for deeper insights into urban structure and its complex dynamics.

Data availability statement

Publicly available datasets were analyzed in this study. This data can be found here: https://www.openstreetmap.org/.

Author contributions

Conceptualization, YZ, and WZ; data curation, YZ.and QZ; formal analysis, YZ, and YC; funding acquisition, YZ; methodology, WZ, and YC; supervision, YC, and WZ; visualization, WW and QZ; writing—original draft, YZ, and WZ; writing—review and editing, YC. All authors have read and agreed to the published version of the manuscript.

Funding

This research was funded by the Technology Innovation Leading Program of Shaanxi (Grant No. 2022ZDLSF07-05), and

the Open Fund of the Key Laboratory of Urban Land Resources Monitoring and Simulation, MNR (Grant No. KF-2018-03-016).

Conflict of interest

The authors declare that the research was conducted in the absence of any commercial or financial relationships that could be construed as a potential conflict of interest.

Publisher's note

All claims expressed in this article are solely those of the authors and do not necessarily represent those of their affiliated organizations, or those of the publisher, the editors, and the reviewers. Any product that may be evaluated in this article, or claim that may be made by its manufacturer, is not guaranteed or endorsed by the publisher.

References

Barabási, A. L., and Albert, R. (1999). Emergence of scaling in random networks. *Science* 286 (5439), 509–512. doi:10.1126/science.286.5439.509

Batty, M. (2007). *Cities and Complexity: Understanding cities with cellular automata, agent-based models, and fractals*. Cambridge, Massachusetts: MIT Press.

Batty, M. (2013). *The new science of cities*. Cambridge, Massachusetts: MIT Press.

Blondel, V. D., Jean-Loup, G., Renaud, L., and Etienne, L. (2008). Fast unfolding of communities in large networks. *J. Stat. Mech.* 10, P10008. doi:10.1088/1742-5468/2008/10/p10008

Brockmann, D., Hufnage, L., and Geisel, T. (2006). The scaling laws of human travel. *Nature* 439, 462–465. doi:10.1038/nature04292

Freeman, L. C. (1979). Centrality in social networks: conceptual clarification. *Soc. Netw.* 1, 215–239. doi:10.1016/0378-8733(78)90021-7

Gao, P. C., Liu, Z., Tian, K., and Liu, G. (2016). Characterizing traffic conditions from the perspective of spatial-temporal heterogeneity. *ISPRS Int. J. Geoinf.* 5 (3), 34. doi:10.3390/ijgi5030034

García-Pérez, G., Boguñá, M., and Serrano, M. Á. (2018). Multiscale unfolding of real networks by geometric renormalization. *Nat. Phys.* 14 (6), 583–589. doi:10.1038/s41567-018-0072-5

Gonzalez, M., Hidalgo, C. A., and Barabási, A. L. (2008). Understanding individual human mobility patterns. *Nature* 453, 779–782. doi:10.1038/nature06958

Hillier, B. (2012). Studying cities to learn about minds: some possible implications of space syntax for spatial cognition. *Environ. Plann. B. Plann. Des.* 39 (1), 12–32. doi:10.1068/b34047t

Hillier, B., and Lida, S. (2005). "Network and psychological effects," in *International Conference on Spatial Information Theory*. (Berlin, Heidelberg: Springer), 475–490

Ma, D., Guo, R., Zheng, Y., Zhao, Z., He, F., and Zhu, W. (2020). Understanding Chinese urban form: The universal fractal pattern of street networks over 298 cities. *ISPRS Int. J. Geoinf.* 9 (4), 192. doi:10.3390/ijgi9040192

Mayer-Schonberger, V., and Cukier, K. (2013). *Big data: A revolution that will transform how we live, work, and think*. New York: Eamon Dolan/Houghton Mifflin Harcourt.

Newman, M. E. J. (2003). The structure and function of complex networks. *SIAM Rev. Soc. Ind. Appl. Math.* 45 (2), 167–256. doi:10.1137/s003614450342480

Shaw, S. L., and Yu, H. (2009). A GIS-based time-geographic approach of studying individual activities and interactions in a hybrid physical–virtual space. *J. Transp. Geogr.* 17 (2), 141–149. doi:10.1016/j.jtrangeo.2008.11.012

Wu, L., Zhi, Y., Sui, Z., and Liu, Y. (2014). Intra-urban human mobility and activity transition: Evidence from social media check-in data. *PloS one* 9 (5), e97010. doi:10.1371/journal.pone.0097010

Zheng, Y., Capra, L., Wolfson, O., and Yang, H. (2014). Urban computing: Concepts, methodologies, and applications. *ACM Trans. Intell. Syst. Technol.* 5 (31–38), 155. doi:10.1145/2629592

Zhong, C., Arisona, S. M., Huang, X., Batty, M., and Schmitt, G. (2014). Detecting the dynamics of urban structure through spatial network analysis. *Int. J. Geogr. Inf. Sci.* 28 (11), 2178–2199. doi:10.1080/13658816.2014.914521

frontiers | Frontiers in Environmental Science

TYPE Original Research
PUBLISHED 09 September 2022
DOI 10.3389/fenvs.2022.994860

Check for updates

OPEN ACCESS

EDITED BY
Ehsan Elahi,
Shandong University of Technology, China

REVIEWED BY
Baishu Guo,
China University of Geosciences Wuhan, China
Decai Tang,
Nanjing University of Information Science and Technology, China

*CORRESPONDENCE
Ying Jing,
y.crystal@nit.zju.edu.cn

SPECIALTY SECTION
This article was submitted to Land Use Dynamics, a section of the journal Frontiers in Environmental Science

RECEIVED 15 July 2022
ACCEPTED 15 August 2022
PUBLISHED 09 September 2022

CITATION
Zhang Y, Jin X, Li M, Liu R and Jing Y (2022), Evaluating civil aviation airport competitiveness in the Yangtze River Economic Belt of China: A lens of spatial-temporal evolution. *Front. Environ. Sci.* 10:994860. doi: 10.3389/fenvs.2022.994860

COPYRIGHT
© 2022 Zhang, Jin, Li, Liu and Jing. This is an open-access article distributed under the terms of the Creative Commons Attribution License (CC BY). The use, distribution or reproduction in other forums is permitted, provided the original author(s) and the copyright owner(s) are credited and that the original publication in this journal is cited, in accordance with accepted academic practice. No use, distribution or reproduction is permitted which does not comply with these terms.

Evaluating civil aviation airport competitiveness in the Yangtze River Economic Belt of China: A lens of spatial-temporal evolution

Yang Zhang[1,2], Xue Jin[3], Meng Li[2], Rongtian Liu[1,2] and Ying Jing[4]*

[1]School of Economics and Management, Xi'an Aeronautical University, Xi'an, Shaanxi, China, [2]General Aviation Industry Research Center, Xi'an Aeronautical University, Xi'an, Shaanxi, China, [3]School of Economics and Management, Chang'an University, Xi'an, Shaanxi, China, [4]Business School, NingboTech University, Ningbo, Zhejiang, China

The civil aviation industry plays an important role in advancing interregional socio-economic development. Investigating the competitiveness of civil aviation airports (CAAs) from the tempo-spatial change perspective aids in the optimization of airport layout towards balanced and coordinated regional development. This research assesses the overall competitiveness of 86 CAAs in 11 provinces or provincial-level municipalities of the Yangtze River Economic Belt (YREB) from 2009 to 2019 by the entropy weight approach, then characterizes their spatial-temporal evolution via Moran index of spatial auto-correlation analysis, and finally explores their dynamic changing tendency of the spatial variability based on Theil index measurement and decomposition. The findings are concluded: 1) From 2009 to 2019, the overall competitiveness of civil aviation airports is dramatically improved and an evidently hierarchical system is formed at the provincial level, with the spatial pattern of "strong in the east and west, weak in the middle". 2) The global Moran indexes of civil aviation airport competitiveness in 2009, 2014, and 2019 are negative, indicating that superior and inferior airports are likely to be spatially clustered. 3) The local Moran Indexes show that the spatial agglomerations of civil aviation airports tend to be more evident in the recent decade. The high-high competitiveness clusters lie in the Yangtze River Delta Economic Zone for the long run, transforming from "Shanghai-Hangzhou" high-competitiveness pole to "Shanghai-Hangzhou-Nanjing" and further extending to central Jiangsu. Civil aviation airports in provincial capitals and secondary cities have formed clusters of high-low competitiveness. Moreover, clusters of low-low competitiveness stretch from the Yunnan-Guizhou Plateau to cities in the middle reaches of the Yangtze River. 4) The interprovincial Theil indexes of civil aviation airport competitiveness fluctuate, with the discrepancy increasing and then decreasing.

KEYWORDS

civil aviation airport, competitiveness evaluation, spatial analysis, dynamic evolution, the Yangtze River Economic Belt

Introduction

Background

Since the founding of the People's Republic of China in 1949, China's civil aviation industry (CCAI) has been developing rapidly and playing a key role in the national economic system. In particular, market-oriented construction since the reform and opening-up in 1978 has brought new opportunities to CCAI. This has made CCAI achieve rapid development in many aspects, such as air transportation, fleet size, regulation construction, route layout, etc. As an essential node of civil aviation, the airport is the key carrier of the structure and function of the civil aviation network, the window of a country for international exchange and cooperation, and an essential bridge for a regional economy to participate in international labor division. After more than 40 years of growth since the reform and opening up, CCAI has become the world's second largest air transportation system after the United States (Liang et al., 2016). To better meet the needs of China's socio-economic development, how to further accelerate airport construction and optimize airport layout has become a vital issue in the development of CCAI. Airport competitiveness is a quantitative standard of the overall capability of airports, which reflects the ability of airports to reasonably integrate and optimize the use of internal and external resources facing market competition. It is also an important indicator to measure the prospects of airports and formulate scientific tactics for the development of airports (Wen et al., 2022). On this basis, exploring the competitiveness and spatial-temporal evolution of airports enables aviation authorities to understand airports' strengths and weaknesses, formulate scientific development strategies, improve their advantages continuously, optimize airport layout, strengthen airport operation and management, and promote the development of regional economy and civil aviation industry.

The Yangtze River Economic Belt (YREB) is a vital national strategic development region in China (Liu and Xia, 2020; Yu et al., 2020; Peng and Xu, 2021). As an international economic region connecting home and abroad, YREB plays an essential role in coordinating both regions along the Yangtze River and part of coastal border regions in China (Zhang et al., 2021). At the 2020 Symposium on Promoting the Development of the YREB, China's General Secretary Jinping Xi pointed out that the transport system, especially the air transport network, is a significant driving force in creating a new height for the opening-up of YREB (Lu et al., 2022). Moreover, the air transportation network contributes to inland opening, regional coordination, and high-quality integration development of the Yangtze River Economic Belt (YREB) and the Belt and Road Initiative (BRI). On this basis, building a well-developed aviation network has become one of the critical tasks of constructing a comprehensive three-dimensional transport system in YREB (Pei et al., 2021). As the fundamental component of an air carrier, the airport provides site support. The airport acts as a center for passengers' transit, departure, and arrival in the air transportation network. Due to the geographically strategic position, YREB promotes the synergistic development among the cities in its upper, middle, and lower reaches by exploring the spatial-temporal patterns of civil aviation airports (CAAs).

Literature review

The airport competitiveness evaluation facilitates optimizing the spatial layout of airport clusters in YREB (Zhang et al., 2022). Previous studies on evaluating airport competitiveness have mostly been conducted from a global, national, or single airport perspective (Zeng et al., 2012; Cui et al., 2013; Jiang et al., 2013; Spaina et al., 2014; Ishizuka, 2014; Cui et al., 2017; Tang and Li, 2019; Wei et al., 2019; Choi, 2020; Liang et al., 2020; Moura et al., 2020; Qin, 2020; He et al., 2021). Some scholars explored the competitiveness of airports by various econometric methods such as factor analysis, principal component analysis, hierarchical analysis, DEA, fuzzy comprehensive evaluation, and entropy weight method, emphasizing the symbiosis between transportation and economic development and the importance of hub airports for local and regional economic development (MacKinnon et al., 2008; Liang et al., 2016). Previous studies related to airport competitiveness focus on three major aspects: 1) designing the evaluation index system (Zeng et al., 2012; Tang and Li, 2019; Qin, 2020); 2) empirical evaluation of single airport competitiveness (Jiang et al., 2013; Luo et al., 2020; He et al., 2021) and 3) influence factors or formation mechanism (Ishizuka, 2014; Choi, 2020; Moura et al., 2020).

In designing the evaluation index system of airport competitiveness, Sarkis (2000) used data envelopment analysis to assess the operations of 44 major U.S. airports based on four resource input indicators (i.e., airport operating costs, the population of airport employees, gates, and runways) and five output indicators (i.e., operating revenues, passenger traffic, commercial and general aviation movements, and total cargo traffic efficiency). Based on big system cybernetics, Zhang et al. (2012) construct an evaluation index system (e.g., passenger throughput, number of navigable cities, geographical location, and airspace conditions) for regional multi-airport coordinated development in the Yangtze River Delta region. Chao and Yu, 2013 developed a quantitative evaluation model to analyze the air cargo competitiveness of 10 major airports in Asia-Pacific from different dimensions (air carrier capacity, airport facilities and operations, and economic development). Liang et al. (2016) designed a systematic evaluation method to evaluate the competitiveness of 42 airports in China by the entropy weight, grey correlation, principal component, and cluster analysis by constructing 30 airport competitiveness evaluation indexes from two dimensions: airport development and location

conditions with 30 indexes concerning seven significant factors (i.e., facility construction, operation scale, management efficiency, urban passenger and cargo distribution, urban traffic development, geographic condition, and government support). The above evaluation index systems provide a reference for constructing the evaluation index of CAAs competitiveness in YREB.

In empirically evaluating the competitiveness of each airport, Park (1997) assessed the geographical characteristics, access systems, environmental impacts, airline operating conditions, regional development, availability of planning implementation, socio-economic impacts, and airport charges of eight major airports in East Asia by a fuzzy language approach. Wu and Wu (2005) established an AHP evaluation system to compare the strengths and weaknesses of the five major airports in Asia-Pacific and proposed some improvement measures for Shanghai Pudong Airport. Cui et al. 2013a proposed the IDCQGA-BP algorithm to evaluate the competitiveness of eight airports in the Yangtze River Delta from 2011 to 2015. Huynh et al. (2020) measure the efficiency of major airports in Southeast Asia to compare and analyze the competitiveness of these airports in regional development through a two-stage method. Sydorenko et al. (2021) assess the competitiveness of the production infrastructure of international airports in the global aviation market by the comprehensive situational model. The main purpose of creating and implementing an evaluation system is to facilitate the successful implementation of the competitiveness management functions of the production infrastructure of international airports in the global aviation market.

In analyzing the influencing factors of airport competitiveness, Pels et al. (2003) constructed nested logit models to study competition among airports in the San Francisco Bay Area and revealed that access time is vital in competition among airports in this region. McLay and Reynolds, 2006 studied the economic impact caused by the new initiative of introducing terminal competition at Dublin Airport. In addition to being closely related to the regional economy, geographic and demographic factors, market structure, social factors, and air transport market maturity are also important factors closely related to airport development (Demirsoy, 2012). Zietsman and Vanderschuren (2014) surveyed the airport development stakeholders and found that socio-economic development, urban planning, transportation improvement and efficiency, environmental protection, and financial capacity all influenced airport development and operations, with socio-economic development as the most influential factor. Cui et al. 2013b, 2016) constructed an index system of airport competitiveness from four aspects (i.e., regional development, production factors, demand conditions, and supporting industries) and studied the dynamic formation mechanism of airport competitiveness based on 25 airports in China from 2006 to 2010 by structural equation modelling and system dynamics methods and found that the two most important factors affecting airport competitiveness, namely, airport investment and urban research development investment.

Based on the above analysis, for the airport competitiveness evaluation, scholars have chosen various methods and a sound index system. These studies basically cover the operational scale, connectivity, service quality level, operation management, economic efficiency, and development environment of airports and provide some theoretical references. However, the current relevant research also has certain shortcomings. Firstly, in the comprehensive empirical evaluation of airport competitiveness, more attention is paid to all airports within countries or large hub airports in geographically adjacent areas. Rare research is conducted on the airport competitiveness in important economic regions within one country, e.g., the YREB in China. Secondly, studies on the evaluation of airport competitiveness or its influencing factors are mainly carried out from the time scale, which can only clarify the level of competition and positive and negative influencing factors of airports within a specific time range. Still, they cannot meet the needs of coordinated development, mutual promotion of airports in a certain area, and balanced airport layout. The spatial autocorrelation approach helps to solve the above problems and has been widely used in various research fields to explore the dynamic characteristics of regional differences and spatial structures (Liu et al., 2017; Jin et al., 2018; Jing et al., 2018; Cui et al., 2021; Zhang et al., 2021). Compared with traditional data ranking of different airports' competitiveness on the time scale, spatial auto-correlation analysis reveals the regional structure of spatial variables. It is an important indicator to test whether the attribute values of a certain element are correlated with the attribute values of its adjacent spatial units (Zhao et al., 2012; Darand et al., 2017; Hu et al., 2020; Chen., 2021). Adopting spatial auto-correlation analysis in evaluating airport competitiveness helps observe the interdependence of all airports in YREB in a specific spatial range; meanwhile, it can explore the interaction of a single airport with other airports within a certain spatial unit. Although it has advantages in regional airport coordination and layout optimization, few studies on the competitiveness analysis of CAAs have adopted this method. Therefore, this paper aims to comprehensively evaluate the competitiveness of civil aviation airports (CAAs) in the Yangtze River Economic Belt (YREB) from the lens of tempo-spatial dynamics towards the orderly and coordinated development in YREB.

Methodology

Study site

The Yangtze River has a total length of 6,300 km and a watershed area of 180 km^2, accounting for about 1/5 of the country's total area. With various terrain types (i.e., plateaus,

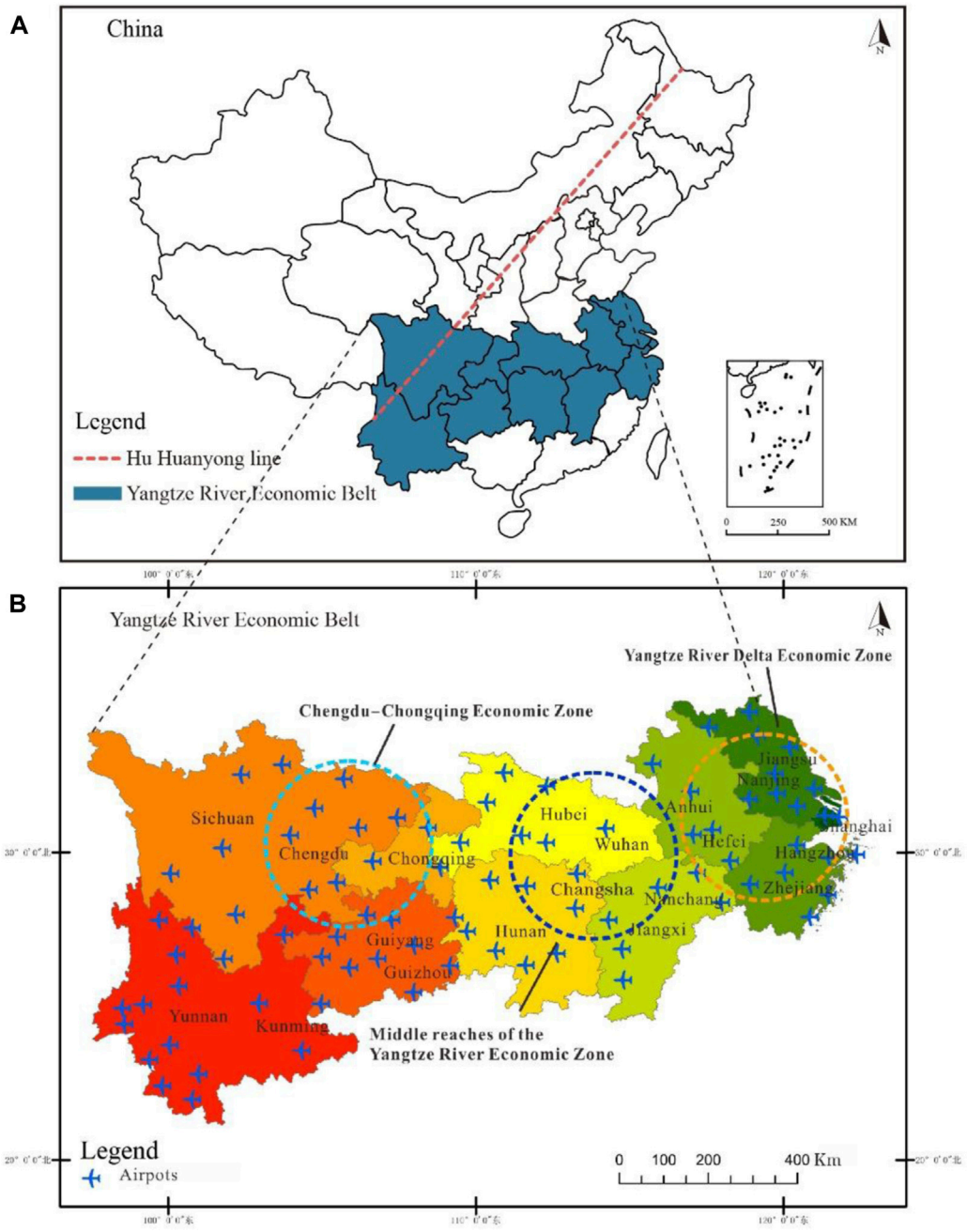

FIGURE 1
Study site.: (A) China; (B) the Yangtze River Economic Belt.

mountains, rivers, lakes, and basins), it runs through most of China's eastern, central and western regions, spanning the subregions of Three Gradient Terrains of China (TGTC). The Yangtze River flows from upstream to downstream through the Qinghai-Tibet Plateau, the Yunnan-Guizhou Plateau, the Sichuan Basin, and the middle and lower reaches of the Yangtze River Plain, creating various natural sceneries with mountains, seashores, rivers, canyons, and lakes, etc. As a significant national strategic development region, the YREB promotes the coordinated development of East, Central, and West China. This area stretches from Shanghai in East China to Yunnan in West China, connecting 43 cities in 11 provinces or provincial-level municipalities along the Yangtze River (except Qinghai and Tibet), with 1,482,300 km^2, accounting for 15.44%

TABLE 1 Provincial ranking of the CAAs comprehensive index in YREB.

Province	2009		2014		2019		Ranking
	Comprehensive index	Mean	Comprehensive index	Mean	Comprehensive index	Mean	
Shanghai	0.72823	0.36412	1.06303	0.53152	3.36367	1.12122	1
Chongqing	0.36095	0.18047	0.43678	0.14559	1.60404	0.53468	2
Zhejiang	0.78825	0.11261	0.79342	0.13224	2.47602	0.35372	3
Hubei	0.32664	0.08166	0.42688	0.08538	1.51204	0.30241	4
Jiangsu	0.42565	0.06081	0.66467	0.07385	2.84322	0.31591	5
Sichuan	0.61812	0.05619	0.79503	0.06625	2.30525	0.1921	6
Yunnan	0.82412	0.06868	0.66413	0.05534	2.27733	0.15182	7
Hunan	0.09959	0.01992	0.37624	0.06271	1.32705	0.16588	8
Anhui	0.12312	0.03078	0.20119	0.04024	0.67859	0.13572	9
Jiangxi	0.11475	0.02295	0.15496	0.03099	0.73765	0.12294	10
Guizhou	0.19697	0.03283	0.31683	0.0288	1.12012	0.11201	11

of the national territorial area. According to the *Statistical Communiqué of the People's Republic of China on the 2021 National Economic and Social Development* released by China's National Bureau of Statistics and the statistical communiqué of the 11 provinces or provincial-level municipalities in YREB, China's GDP was 114.37 trillion yuan, while the regional GDP of YREB reached 53.02 trillion yuan in 2021, nearly half of China's total economy. YREB is the region with the fastest economic development and the area with the highest potential for future economic growth in China. With the implementation of the national strategy of developing YREB, the region has been given the new strategic mission of being the main battlefield of ecological priority and green development, the main artery of smoothing domestic and international circulation, and the main force of leading high-quality economic development.

YREB contains three major economic zones, namely the Yangtze River Delta Economic Zone (Shanghai, Zhejiang, Anhui, Jiangsu), the Middle Yangtze River Economic Zone (Hubei, Hunan, Jiangxi), and the Chengdu-Chongqing Economic Zone (Sichuan, Chongqing, Yunnan, Guizhou), shown in Figure 1. The above three economic zones are developed areas in China with a large population, rich tourism resources, and frequent internal and international exchanges contributing to the rapid development of transportation in YREB. At the same time, transportation is also a vital factor in promoting the regional economy. As China's opening-up highland, YREB's civil aviation transportation is playing a power source, which is mutually promotive with regional development (Sun et al., 2018). By the end of 2019, a total of 86 CAAs were opened in this study area, accounting for 36.1% of the national CAAs, which completed 567 million passenger trips, 7,956,400 tons of cargo and mail throughput, and 4,780,400 landings and takeoffs. Concerning the spatial distribution density at the city level, the average number of airports in the upstream, midstream, and downstream cities are respectively 0.83, 0.56, and 0.39, with the upstream region taking the lead. However, concerning airport hierarchy, 14 of 28 high-level airports in the YREB are located in the Yangtze River Delta Zone, accounting for 60.9% of the total number, while airports in the middle and upper reaches of YREB are 6 and 8, accounting for 37.5 and 20.5% respectively. The Yangtze River Delta Zone has an outstanding advantage in airport quality (Bian et al., 2020).

Data resources

This study targets 86 CAAs in 11 provinces or provincial-level municipalities of YREB. ArcGIS 10.6 is used to draw the spatial structure map required for the study, whose base map data are selected from the National Basic Geographic Database of the National Basic Geographic Information Center of the Ministry of Natural Resources. In this study, nine specific indexes were selected, namely, the passenger throughput, cargo and mail throughput, takeoffs and landing movements, the number of international routes, the number of domestic routes, the number of navigable cities, the grade of airports, the area of terminal buildings and the number of airplane slots. The data of passenger throughput, cargo, and mail throughput, and landing and takeoff sorties are obtained from the Production Bulletin of Civil Aviation Airports in 2011, 2016, and 2020; the data of international and domestic routes indicators are obtained from the official websites of CAAs; and the data of takeoffs and landing movements, the number of navigable cities, the grade of airports, the area of terminal buildings and the number of airplane slots are from Baidu encyclopedia website.

Methodology

The spatial-temporal patterns of 86 airports' competitiveness in YREB are studied by the following methods.

The entropy weighting method

The entropy weighting method is an objective assignment method to determine the weight of indicators (Stoyanets et al., 2020). To reflect the competitiveness level of CAAs in YREB, the raw data are processed by deviation standardization. Then the index weights are determined with the entropy weighting method to obtain a comprehensive index of CAAs' competitiveness (Xiong and Wang, 2018; Liang et al., 2019; Wang et al., 2020; Liu et al., 2021; Pan et al., 2021). The first step is the dimensionless processing of data. Because the nine indicators selected in the study are consistent with the meaning of the competitiveness representation of CAAs. All of them are positive indicators, and Equations 1, 2 are used to standardize the data.

$$X'_{ij} = \frac{X_{ij} - min\, X_{ij}}{max\, X_{ij} - min\, X_j} \tag{1}$$

$$X'_{ij} = \frac{max\, X_{ij} - X_{ij}}{max\, X_{ij} - min\, X_j} \tag{2}$$

In the above Equations X_{ij} denotes the statistical value of the index of the j criterion level; $\max X_{ij}$ and $\min X_{ij}$ respectively represent the maximum and minimum values of the j index X'_{ij} represents the standardized value.

The second step is to calculate the indicators after standardization to derive the comprehensive index of each indicator in the comprehensive benefit evaluation. The specific equations are as follows.

$$H_i = -\frac{1}{\ln\,(n)} \sum_{j=1}^{n} p_{ij} \ln\left(p_{ij}\right) \tag{3}$$

$$W_1 = \frac{1 - H_i}{\sum (1 - H_i)} \tag{4}$$

In Equation 3, n represents the number of CAAs; p_{ij} means the proportion of each indicator to the total number of indicators; In Equation 3 and Equation 4, H_i and W_1 refer to the entropy value and entropy weight, respectively. The size of the entropy is between 0–1.

Spatial autocorrelation analysis

Spatial autocorrelation analysis is a quantitative description of the state of spatial association of geographical data between things. The result is either correlated, random, or insignificant by calculating spatial autocorrelation indices (Liu et al., 2017; Chen, 2021).

This study chooses the global Moran index and local LISA to measure the spatial agglomeration characteristics of CAAs. The global spatial auto-correlation mainly tests the overall spatial correlation of all CAAs in YREB. In contrast, the local LISA mainly tests a single CAA's local spatial distribution correlation and agglomeration. The equations are as follows (Jin et al., 2018; Carracedo, 2021; Kim and Song, 2021).

$$I = \frac{\sum_{i=1}^{n} \sum_{i=1}^{n} W_{ij} (x_i - \bar{x}) \left(x_j - \bar{x}\right)}{S^2 S_0} \tag{5}$$

$$I = \frac{(x_i - \bar{x})}{S^2} \sum_j W_{ij} (x_i - \bar{x}) \tag{6}$$

In Equation 5, x_i is the value of the variable at the location or region i. $\bar{x}$ is the mean value of the variable. S^2 is the variance of the variable. S_0 is the sum of the spatial weights of all variables. n is the total number of observed variables and the total number of regions or locations to which the observations correspond. W_{ij} is an element in the space weight matrix W, which refers to the space weight between the region or the location i or j and the space between them. Set $W_{ij} = 1$ if the space unit i is adjacent to the space unit j, otherwise, $W_{ij} = 0$. In Equation 6, x_i is the attribute value of space unit i; $\bar{x}$ is the mean value of x_i ; S is the variance; w is the matrix of space weight; w_{ij} is the degree of influence between space unit i and j.

Theil index

The Theil index, also known as the Theil coefficient or short for Theil, was first proposed by Theil and Henri in 1967. It is often used to quantitatively describe the equilibrium of economic development and income distribution (Klophaus and Lauth, 2022). Though both Theil index and local spatial autocorrelation can reflect inter-regional disparity, their differences exist. First, the local spatial autocorrelation analysis characterizes the disparity at the spatial scale, while Thiel index presents the disparity from a statistical view. Second, the former focuses on the competitiveness differences of 86 specific airports in YREB from a micro perspective, while the latter focus on the competitiveness differences at a macro level, that is, among the three major economic zones (i.e., the Yangtze River Delta Economic Zone, the Middle Yangtze River Economic Zone, and the Chengdu-Chongqing Economic Zone). Therefore, this research selects the Theil index to measure the difference in the CAAs' competitiveness in YREB. The equations are as follows.

$$T_b = \sum_i \frac{I_i}{I} \times ln\left(\frac{\frac{I_i}{I}}{\frac{N_i}{N}}\right) \tag{7}$$

$$T_w = \sum_i \left(\frac{I_i}{I}\right) \times T_{wi} \tag{8}$$

$$T_p = \sum_i \sum_j \frac{I_{ij}}{I} \times ln\left(\frac{\frac{I_{ij}}{I}}{\frac{N_{ij}}{N}}\right) \tag{9}$$

In Equations 7–9, I_i/I represents the ratio of the composite index sum within a region to the composite index sum within all areas. N_i/N represents the ratio of the number of airports in a

region to the number of airports in all regions. I_{ij} represents the composite index of province *j* in region *i*. N_{ij} represents the number of airports in province *j* in region *i*. T_b, T_w, and T_P represent the Thayer index of inter-regional differences, intra-regional differences, and overall inter-provincial differences.

Results

Comprehensive evaluation of CAAs' competitiveness in YREB

Provincial-level CAAs' competitiveness hierarchy

After specifying the weights, the comprehensive index of CAAs' competitiveness in YREB is calculated by the entropy weighting method. As shown in Table 1 and Figure 2, the sum of the comprehensive evaluation indexes in 2009, 2014, and 2019 are 4.88, 5.89, and 20.245, respectively. The comprehensive competitiveness of CAAs in YREB has increased significantly in the past 10 years. It is also found that in the comprehensive index of airport competitiveness of both the overall region of the Yangtze River Economic Belt and each single airport, the growth rate of competitiveness from 2009 to 2014 is much smaller than that from 2014 to 2019. The growth rate in the first 5 years is less than 50%, and the growth rate in the next 5 years is more than two times. The reason is that, on the one hand, due to the difficulty and periodicity of airport construction, there are fewer major changes in the short term, but more significant changes in the long term; on the other hand, the development plan for YREB has evolved from "promotion" to "in-depth promotion" and then to "comprehensive promotion" at the three symposiums on the development of the YREB held by China's General Secretary Xi Jinping in 2016, 2018 and 2020 respectively. Such high-level progressive planning has brought more political benefits and better development prospects. As shown in Figure 2, the competitiveness layout of CAAs in YREB is featured as "strong in the east and west, weak in the middle" (Jin et al., 2018). The coastal cities in YREB have the most competitive CAAs, consolidating the leading position of the Yangtze River Delta airport cluster. In 2019, the Yangtze River Delta region possesses seven 10-million-passenger-throughput airports (i.e., Shanghai Pudong, Shanghai Hongqiao, Nanjing Lukou, Hangzhou Xiaoshan, Hefei Xinqiao, Wenzhou Longwan, and Ningbo Lishe International Airports), completing a total of 248 million passenger throughput which is much higher than the second-placed Beijing-Tianjin-Hebei airport cluster of 145 million passengers. In terms of future development, metropolitan areas will become the main form of city cluster competition and cooperation. In addition, airport cluster competition and cooperation will expand from central cities and single airports to metropolitan area airport systems, which features a highly mature stage of development of city clusters and airport clusters. Sichuan and Yunnan CAAs in the upstream are the second most competitive. Benefiting from the well-developed domestic route network and the rich tourism resources in the southwest, Sichuan and Yunnan airports in the upstream region are the second most competitive. By 2019, the Chengdu-Chongqing airport cluster had become the following "potential stock" after the three world-class airport clusters in Beijing-Tianjin-Hebei, Yangtze River Delta, and Guangdong-Hong Kong-Macao. Although the overall competitiveness of the airport in the central region is the weakest, it plays the role of linking the east with the west as well as communicating between the north and the south. The airport development of the central region is expected to boost by building a "dual hub" system for passengers and cargo, relying on the original characteristics of air cargo.

The CAAs in YREB has formed a relatively distinct hierarchical structure at both provincial and municipal level. First, the comprehensive competitiveness of CAAs in Shanghai and Zhejiang has long been in the lead. The huge demand for civil aviation carriers is indispensable from solid economic strength, superior foreign trade location, and the high consumption level of residents. Second, the overall competitiveness of Sichuan, Jiangsu, and Yunnan is also high, but the trends in the decade vary. CAAs in Yunnan occupied a prominent position because other transport modes were initially restricted due to the complex and rugged geographical conditions. However, with economic development and technological breakthroughs, the competitiveness of CAAs is gradually weakening as other transportation modes are improving. Jiangsu is located on the eastern coast, with a superior location adjacent to Shanghai, with a substantial economic radiating effect.

Moreover, the expansion of airports such as Nanjing Lukou Airport has laid the foundation for domestic and foreign trade and an open economy. Therefore, its comprehensive competition has increased significantly, which is second subsequent to Shanghai in 2019. Furthermore, Sichuan has been in a steady development stage for a long time since 2009. Third, the competitiveness of CAAs in Chongqing, Hubei, Guizhou, and Hunan is at a medium-to-low level. Except for Hunan, the improvement of capacity supply due to the conversion, expansion, and construction of Changsha Huanghua and other provincial airports has prompted its development and competitiveness within 1 decade. Although the overall competitiveness of other three provinces has improved, the regional rankings are stable. Fourth, Jiangxi and Anhui have always been most disadvantaged concerning the comprehensive competitiveness of CAAs in the YREB.

Single CAA competitiveness spatialization in YREB

Figure 3 shows the comprehensive index of CAAs in 2009, 2014, and 2019, respectively. Each dot represents one single CAA.

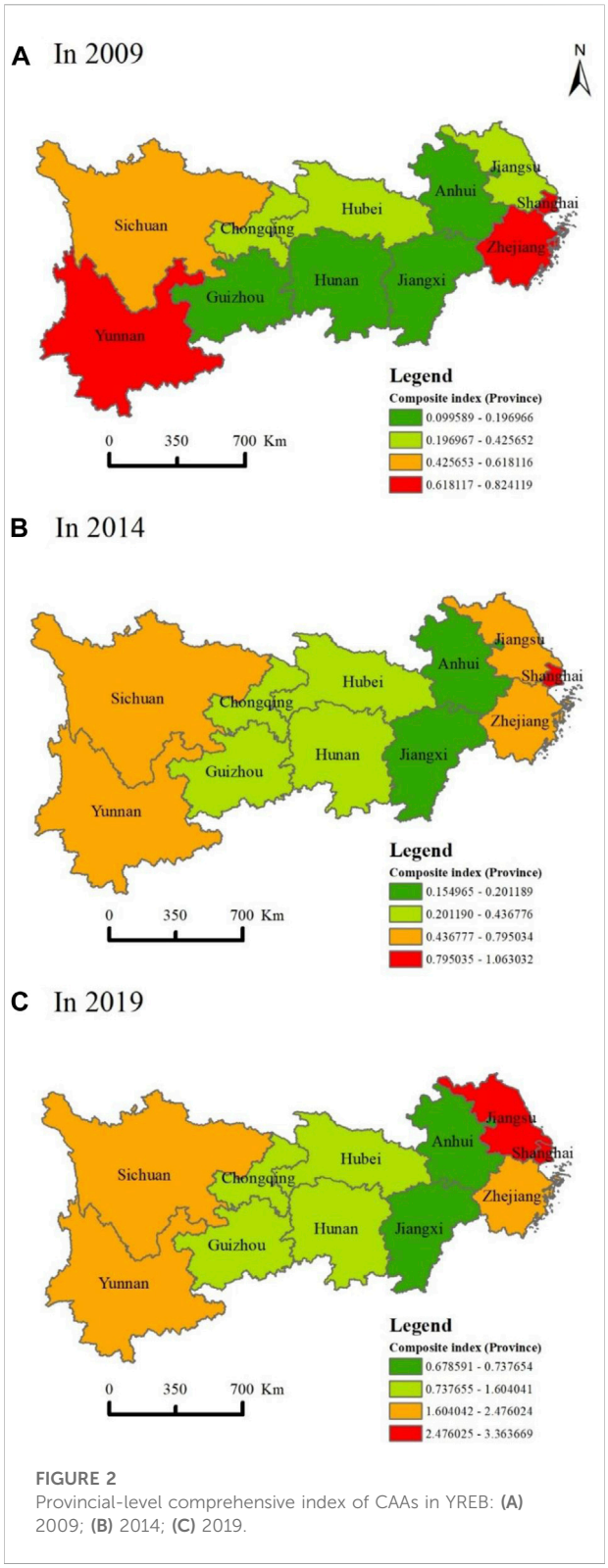

FIGURE 2
Provincial-level comprehensive index of CAAs in YREB: **(A)** 2009; **(B)** 2014; **(C)** 2019.

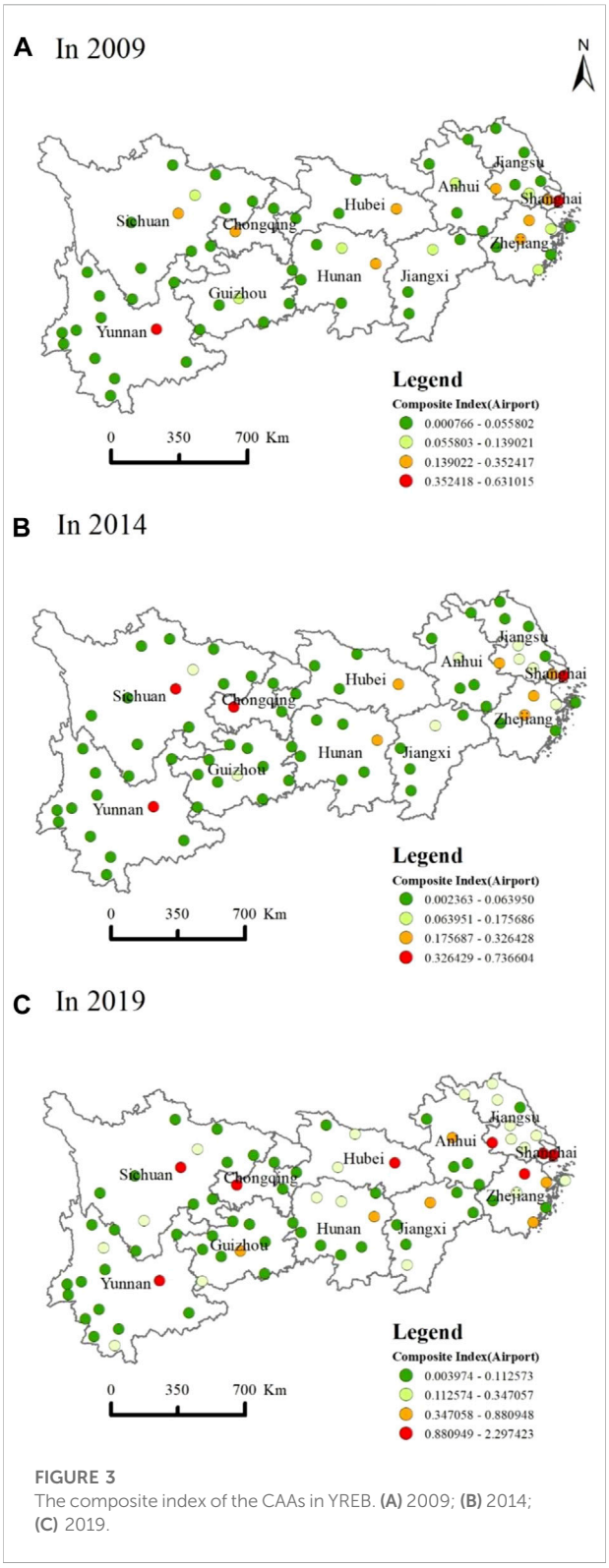

FIGURE 3
The composite index of the CAAs in YREB. **(A)** 2009; **(B)** 2014; **(C)** 2019.

Different colors indicate the competitiveness level of airports. From high to low, competitiveness is reflected as red-orange-light green-dark green. It can be seen that, with the total index of each CAA increasing in the past 10 years, the competitiveness has been significantly enhanced. The airport cluster in the downstream Yangtze River Delta region is characterized by high-high

competitiveness. The competitiveness of airports in the midstream cities develops to middle-to-high competitiveness. Among the upstream cities, the competitiveness of airports in Chengdu, Chongqing, and Kunming is high. In contrast, the competitiveness of other airports is still weak.

In 2009, Shanghai Pudong International Airport and Kunming Changshui International Airport were the most competitive in 2009, followed by Chongqing Jiangbei, Chengdu Shuangliu, Wuhan Tianhe, and Changsha Huanghua International Airports in the middle and lower reaches. Most of the other airports were at a weak level of competitiveness. In 2014, the competitiveness of CAAs in the Chengdu-Chongqing city cluster in the upper reaches of the Yangtze River has been significantly improved, which can be seen in the transformation of Chengdu Shuangliu and Chongqing Jiangbei International Airport into red circles. Benefiting from the developed service industry and strong foreign trade demand boosted by the integration strategy of Chengdu and Chongqing, the competitiveness of the midstream city cluster has increased exponentially. But the overall color field shows that the single airport competitiveness still has much room for improvement. In 2019, the comprehensive index value of each airport expands, and the competitiveness of regional airports continues to enhance. Compared with 2014, three more red dots are added in 2019, including Nanjing Lukou International Airport, Hangzhou Xiaoshan International Airport, and Wuhan Tianhe International Airport. The former two make it more remarkable in terms of clusters of highly competitive airports in the downstream Yangtze River Delta region. The latter is located in the middle of the area, east of the Hu Huanyong Line, with a large regional flow of passengers. The regional airport, Wuhan Tianhe International Airport, has undergone rapid development, boosted by the strategy for the rise of the central region.

Temporal-spatial characteristics of CAAs in YREB

Analysis of global spatial autocorrelation

Based on the overall index data of CAAs in the YREB in 2009, 2014, and 2019, the univariate Moran's I module of GeoDa spatial analysis is used to calculate the global Moran index for quantifying the spatial correlation of each CAA development in YREB. Table 2 shows that the absolute value of Z is greater than 1.96 at the significance level of 0.05 (by 95% confidence test), indicating a significant autocorrelation of spatial elements.

The global Moran indexes of civil CAAs in YREB for 2009, 2014, and 2019 are -0.018, -0.012, and -0.01. The result indicates a negative spatial autocorrelation in CAAs' development strength. That is, airports with superior strength and weaker strength are more likely to gather in space. The reason is that China's airports can be divided into three main categories: hub, trunk, and feeder. There will be one or two hub airports with solid strength in a particular region, where several weak trunk airports and feeder airports are distributed. And they are spatially clustered.

TABLE 2 Global moran index of CAA competitiveness in the YREB.

Year	Moran index	SD	P	Z
2009	−0.018	0.0842	0.0572	1.9019
2014	−0.012	0.0691	0.0002	3.7496
2019	−0.011	0.0789	0.0001	3.9933

Analysis of local spatial autocorrelation

Figure 4 spatializes the local spatial autocorrelation analysis of civil aviation airports in YREB. The Local Moran's I module of the ArcGIS 10.6 is used to calculate the local LISA index in 2009, 2014, and 2019. The improvement of the overall competitiveness index of CAAs in YREB from 2009 to 2019 has facilitated the trend of local spatial clustering in the region. The cluster of high-high competitiveness has been in the Yangtze River Delta Economic Zone for a long time. It has changed from the "Shanghai-Hangzhou", a highly competitive development pole, to "Shanghai-Hangzhou-Nanjing" and extends to central Jiangsu Province. The airports of provincial capitals and secondary cities form clustered areas of high-low competitiveness, indicating that the provincial capital city airports are the provincial core area of competitiveness development. The clustered area of low-low competitiveness covers the Yunnan-Guizhou Plateau to cities of the middle reaches, which shows that the CAAs' competitiveness in YREB still needs to be improved through certain spatial planning strategies.

In 2009, 82.8% of the CAAs showed an insignificant spatial cluster. Four of the airports form a cluster area with high-high competitiveness, namely Shanghai Pudong International Airport, Shanghai Hongqiao International Airport, Hangzhou Xiaoshan International Airport, and Yiwu Airport. Six CAAs, all located in provincial capitals, form a cluster of high-low competitiveness. Compared with other provincial airports, these are featured with high level, good accessibility, strong distribution capacity, well-connected cities, and wide radiation range, forming the competitiveness center of the lagging area. Though Nantong Xingdong Airport has surpassed more than 70% of the airports in the region, it is a weak unit in an area with solid regional competitiveness due to its geographical constraints and its adjacent location to clusters of high-high competitiveness, namely, Shanghai, Zhejiang, and Jiangsu. In 2014 the high-high, high-low, and low-high clusters remain the same with more airports covered. A cluster of high-high competitiveness has formed a "Shanghai-Hangzhou" highly competitive developing pole. The low-high cluster includes Zhoushan Putuoshan airport. Average CAAs in Yunnan and Guizhou have formed a cluster of low-low competitiveness, a contiguous lagging place in the competitiveness ranking within the region. In 2019, 80.5% of

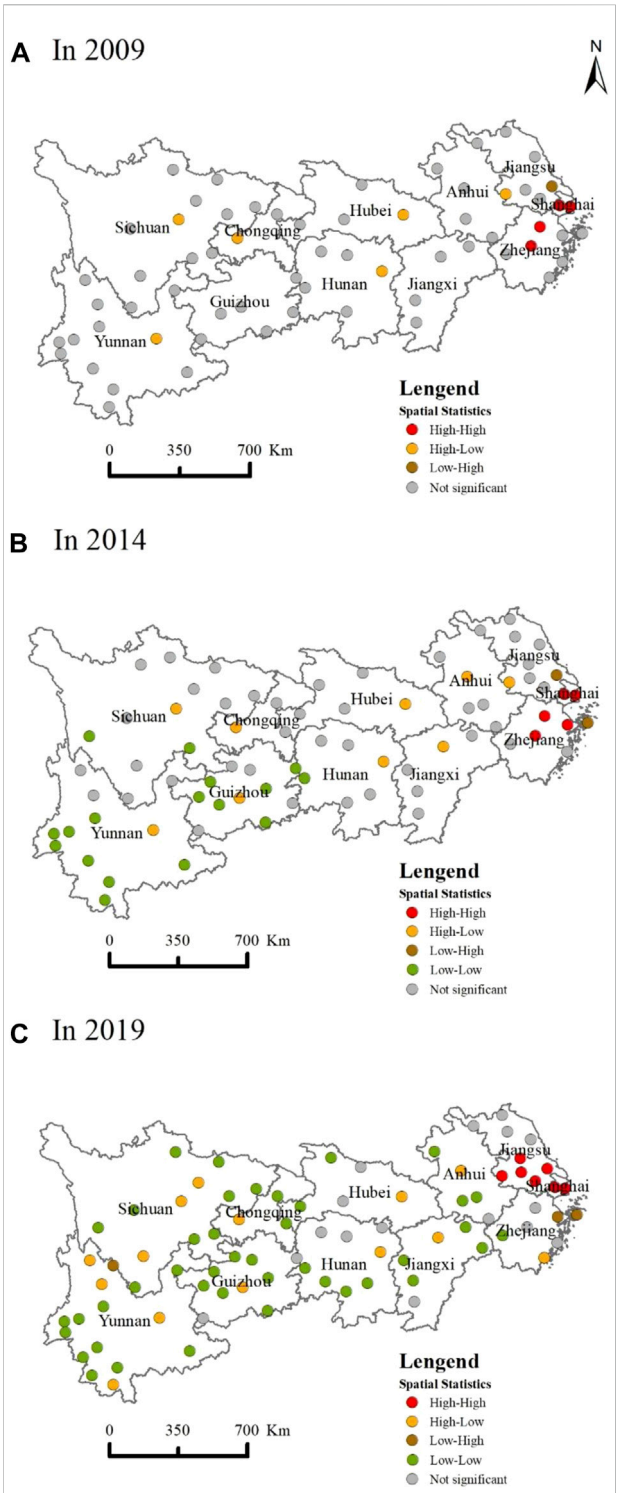

FIGURE 4
Local clustering characteristics of CAAs in YREB: **(A)** 2009; **(B)** 2014; **(C)** 2019.

the airports are locally clustered in terms of the competitiveness. The cluster of high-high competitiveness takes Shanghai as the center to link Hangzhou and gradually spreads to the middle of Jiangsu Province, forming a "Shanghai-Hangzhou-Nanjing" high-competitive developing pole, covering Nantong Xingdong International Airport. Fourteen CAAs form a cluster of high-low competitiveness, indicating a backward unit in the competitiveness ranking of CAAs in YREB. In addition to the provincial capital airports with clustering capacity, airports adjacent to the provincial capital airport, airports with a particular trading strength and source market stand out from the local spatial competitiveness ranking. There are two clusters of low-low competitiveness: Ningbo Lishe International Airport, Zhoushan Putuoshan Airport, and Ninglang Luguhu Airport. Therefore, clustered areas of low-low competitiveness spread from the airport in the upper reaches to the airports in the middle and lower reaches, forming a contiguous lagging area.

Analysis of competitiveness difference of CAAs based on theil index

To further explore the interregional difference and temporal evolution of CAA competitiveness in YREB by the Theil index, this study takes provinces and economic zones as research units. Table 3 shows the inter-regional, intra-regional, and overall inter-provincial differences among CAAs in the three major zones of YREB in 2009, 2014, and 2019.

Taking the YREB as a whole, the total inter-provincial differences show a fluctuating trend, with the overall difference first expanding and then shrinking. The increase in inter-provincial differences from 2009 to 2014 is due to the rapid development of the international and regional leading airports in YREB, while other feeder airports are still lagging. In addition, the inconsistency of airport development in the region caused by the incompatible number of airports with the regional economic growth sharpens the disparity in competitiveness. The narrowing of inter-provincial differences from 2014 to 2019 is due to the gradual development of feeder airports in YREB and the strong follow-up momentum, narrowing the gap between the leading regional and feeder airports. The variation trend of inter-regional and intra-regional differences in the Theil index is consistent with the overall competitiveness gap (i.e., expanding before shrinking). The change of inter-regional differences is because the three major regions show a chronological sequence of development in the past decade, the Yangtze River Delta progressed first, the Midstream Economic Zone, and the Middle and Upper Reach of Economic Zone followed. The inter-regional change is because each region has provinces with precedence in development over other provinces within 10 years.

Specific to the three major zones, the Theil index of the competitiveness of CAAs in the Yangtze River Delta Economic Zone is the largest, which is the dominating factor affecting regional differences, followed by the Middle and Upper Reaches of the Yangtze Economic Belt. A stepped competitiveness difference has formed with Shanghai in the lead, followed by

TABLE 3 Theil index measurement and contribution rate decomposition.

Year	Inter-regional difference	Intra-regional difference	Three regions			Total inter-provincial difference
			The delta	The midstream	The middle and upper streams	
2009	−0.1190	0.1644	0.2961	0.1925	0.1021	0.2497
2014	0.1649	0.2284	0.3795	0.0696	0.1112	0.2947
2019	0.0064	0.1727	0.3161	0.0656	0.1190	0.2752

Jiangsu and Zhejiang with a large gap compared with Shanghai. Anhui is the weakest in competitiveness. The competitiveness difference between airports in the middle and upper reaches of YREB is the slightest because Hubei, Hunan, and Jiangxi airports are weak in terms of overall competitiveness.

In general, there are differences in the CAA competitiveness of YREB in 2009, 2014, and 2019. And the competitive differences exist both in the three major zones, namely, the Yangtze River Delta Economic Zone, the Midstream YREB, and the Upper and Middle YREB. From the perspective of overall trends, the inter-provincial and inter-zonal differences in the CAA competitiveness of the YREB show a fluctuating trend, with the level of differences first expanding and then narrowing. From the inter-provincial and zonal perspectives, the difference in the CAA competitiveness has developed from inter-provincial hierarchical differences to inter-regional differences. For the contribution of the three major zones, regional differences are mainly manifested in the Yangtze River Delta Economic Zone, followed by the Middle and Upper Yangtze Economic Zone, and finally the Midstream Yangtze Economic Zone.

Discussion

Research findings

This study comprehensively evaluates the competitiveness of CAAs at the provincial level of YREB and spatializes their spatio-temporal evolution in 2009, 2014, and 2019. The research findings are as follows.

1) From 2009 to 2019, the comprehensive competitiveness of CAAs in YREB has increased remarkably, showing a distribution characteristic of "strong in east and west, weak in central". The provincial-level distribution of the civil CAAs competitiveness in YREB has formed a relatively distinct hierarchical system. Shanghai and Zhejiang are in the first tier, with Sichuan, Jiangsu, and Yunnan in the second tier, Chongqing, Hubei, Guizhou, and Hunan in the third, and Jiangxi and Anhui in the fourth tier. In terms of single airports, the competitiveness in central cities per province has increased the most. The airports in the downstream Yangtze River Delta region are highly clustered, and the competitiveness of airports in midstream city clusters develops to medium-to-high intensity. The upstream city clusters have Chengdu and Chongqing as the core of high competitiveness of CAAs, while the competitiveness of other airports in this region is still weak.
2) The global Moran Index shows spatial auto-correlation of CAAs in YREB is negative in 2009, 2014, and 2019. That is, highly competitive airports and uncompetitive airports are more likely to be spatially clustered. At the same time, the local Moran index shows that the local spatial cluster in the region from 2009 to 2019 has become more and more distinct. The clustered area of high-high competitiveness has been located in the Yangtze River Delta Economic Zone for a long time, converging from the "Shanghai-Hangzhou" high-competitive development pole to "Shanghai-Hangzhou-Nanjing" and further extends to central Jiangsu Province. The provincial capitals CACs and sub-city airports form a clustered area of high-low competitiveness; clustered areas of low-low competitiveness spread from the Yunnan-Guizhou Plateau to urban cities in the middle reaches of the Yangtze River.
3) From 2009 to 2019, spatial heterogeneity exists in terms of the competitiveness of CAAs at the provincial level in YREB among the three major zones (i.e., the Yangtze River Delta Economic Zone, the Midstream Yangtze River Economic Zone, and the Upper Middle Yangtze River Economic Zone). In terms of the overall evolution trend, the Thiel index shows fluctuations, namely, increasing first and then decreasing. The Yangtze River Delta Economic Zone is the dominating region affecting the level of spatial heterogeneity. From the inter-provincial and inter-zonal perspectives, the differences in the CAAs competitiveness develop from an inter-provincial hierarchical difference to an inter-regional integration.

Research strengths and limitations

Theoretically, this study comprehensively evaluates the competitiveness of CAAs in YREB. Methodologically, this

research applies the classic tempo-spatial analytical method to spatialize the spatial-temporal pattern of CAAs. Practically, the study site is enriched in YREB. The limitations of this study are: 1) all data adopted are second-hand, which tends to be with low timeliness; 2) The research objects are airports in YREB and a larger spatial scale could better reflect the spatial distributional regularities, e.g., in the whole China. More case studies (e.g., other regions in China or other countries) should be considered to verify or discover more regularities. 3) This study involves the decade 2009–2019 and did not consider the impact of COVID-19 which erupted in 2020.4) The time span is 5 years, namely 2009, 2014, and 2019. A yearly analysis needs further exploring. Taking the impact of COVID-19 into consideration, the following research will explore airports' competitiveness evolution at multiple spatial scales, e.g., in other regions of China or even around the world over a longer period. Based on analyzing the mechanisms behind the evolution and the interactions of various influencing factors, the following research aims to improve airport competitiveness evaluation by involving more factors from a systematic perspective in further studies.

Policy implications

Based on investigating the competitiveness and spatial interdependence of CAAs in YREB, it is found that there is an unbalanced layout of competitiveness at multiple spatial scales, namely, the zonal spatial scale, the provincial scale, and the single airport scale. Therefore, it is necessary to make the competitive strategies of CAAs from different spatial dimensions for building a hierarchical CAAs system with a reasonable layout and excellent functions towards maximizing the competitive advantages of airport clusters in the YREB.

First of all, for the three zones in the upper, middle, and lower reaches of the YREB, the Yangtze River Delta Economic Zone is the leading region affecting the spatial heterogeneity of airport competitiveness, and it should play its leading role in the development of CAAs in the entire YREB, and continue to promote the effect of domestic and international dual circulation on trade, economic development, international exchange, and cooperation. Specifically, airports in the upper reach region should seize the development opportunity of the "Chengdu-Chongqing" city cluster, and progress the construction of regional and feeder airports to achieve better integration into the synergistic regional development. Relying on the original air cargo, airports in the middle reach should build a "dual hub" system of air passengers and cargo based on its natural geographical location of linking the east and the west, communicating with the north and the south to boost its development. Secondly, at the provincial spatial scale in the YREB, airports in the central cities and featured cities with rich tourism resources play a crucial role in improving the competitiveness of airports in the whole province. Eleven provinces or provincial-level municipalities in the YREB should grasp the trend of expanding airport cluster competition and cooperation from central cities and single airports to metropolitan area airports system and take airports with strong competitiveness in the province as the core to drive the airports in the adjacent geographic areas. Alternatively, the airports in the vicinity of the central cities should develop joint provincial cooperation to build a metropolitan area airport cluster. Under solid competition in the domestic aviation market, expanding international airline markets will promote the metropolitan airport cluster to be a "stabilizer" and "builder" of the aviation market order. In terms of each single airport in the YREB, evaluating the competitiveness of CAAs facilities the application of specific policies, and hierarchical development of airports.

The last but not the least, as the international hub airports and domestic backbone airports are at the core of the three zones of the YREB, they should actively adapt to the new development pattern that mainly relies on the domestic cycle and mutually promotes the domestic and international dual cycle, emphasizing regional synergy and epidemic prevention and control. For regional medium-sized and feeder airports that are less competitive, clearer development goals are needed, for example, taking advantage of their spatial dependence on strong airports to take over the overcapacity. Moreover, breakthroughs in regional medium-sized and feeder airports can be made by improving their capacity and differentiating competition with distinctive services, brand building, and active market development.

Conclusion

The development of civil aviation airports (CAAs) affects the advancement of the regional economy to a certain extent. Exploring the competitiveness and spatial-temporal imbalance of CAAs in the Yangtze River Economic Belt (YREB) is conducive to optimizing the airport layout and promoting the coordinated development of urban agglomerations along the YREB. To fill the research gap of lacking the tempo-spatial insights into the CAAs' competitiveness, this research maps the dynamic changes of 86 CAAs' competitiveness in YREB based on the competitiveness evaluation by the entropy weight approach, spatial auto-correlation analytical technique and Theil index measurement respectively. This research is concluded that: 1) The comprehensive competitiveness of CAAs in the Yangtze River Economic Belt increased significantly from 2009 to 2019, showing that provinces in East and West China are more competitive in terms of airports competitiveness compared with provinces in Central China. 2) Superior and inferior airports are likely to be spatially clustered. Moreover, CAAs in provincial capitals and secondary cities form high-low cluster areas. 3) From 2009 to 2019, spatial differences in CAA competitiveness exist, among provinces of the Yangtze River Economic Belt, or within the three major zones (i.e., the Yangtze

River Delta Economic Zone, the middle reaches of the Yangtze River Economic Zone, and the middle and upper reaches of the Yangtze River economic zone). 4) The interprovincial civil aviation airport competitiveness fluctuates, with the discrepancy increasing and then decreasing. This research benefits the spatial planning of civil aviation airports in the Yangtze River Economic Belt.

Data availability statement

The datasets presented in this study are available from the corresponding author upon request.

Author contributions

YZ conceptualization, methodology, writing original draft preparation; RL software, validation and visualization; XJ resources, data collection, formal analysis and investigation; ML writing, reviewing and editing; YJ supervision and project administration. All authors have read and agreed to the published version of the manuscript.

Acknowledgments

Shaanxi Provincial Soft Science Research Program (Grant 2020KRM068); Shaanxi Provincial Research Project on Major Theoretical and Practical Issues in Philosophy and Social Sciences (Grant 2021ND0193).

Conflict of interest

The authors declare that the research was conducted in the absence of any commercial or financial relationships that could be construed as a potential conflict of interest.

Publisher's note

All claims expressed in this article are solely those of the authors and do not necessarily represent those of their affiliated organizations, or those of the publisher, the editors and the reviewers. Any product that may be evaluated in this article, or claim that may be made by its manufacturer, is not guaranteed or endorsed by the publisher.

References

Bian, H. Y., Gao, J., Wu, J. G., Sun, X., and Du, Y. (2020). Hierarchical analysis of landscape urbanization and its impacts on regional sustainability: A case study of the Yangtze River economic Belt of China. *J. Clean. Prod.* 279, 123267. doi:10.1016/j.jclepro.2020.123267

Carracedo, P., and Debon, A. (2021). Spatiotemporal econometrics models for old age mortality in europe. *Mathematics* 9, 1061. doi:10.3390/math9091061

Chao, C. C., and Yu, P. C. (2013). Quantitative evaluation model of air cargo competitiveness and comparative analysis of major Asia-Pacific airports. *Transp. Policy* 30 (30), 318–326. doi:10.1016/j.tranpol.2013.10.001

Chen, Y. G. (2021). An analytical process of spatial autocorrelation functions based on Moran's index. *Plos One* 16 (4), e0249589. doi:10.1371/journal.pone.0249589

Choi, M. S. (2020). A study on the development and priority analysis of the evaluation index for local airport competitiveness. *Int. J. Tour. Hosp. Res.* 34 (8), 117–130. doi:10.21298/IJTHR.2020.8.34.8.117

Cui, J. X., Li, R. H., Zhang, L. Y., and Jing, Y. (2021). Spatially illustrating leisure agriculture: Empirical evidence from picking orchards in China. *Land* 10 (6), 631. doi:10.3390/land10060631

Cui, Q., Kuang, H. B., and Li, Y. (2013a). The evaluation of dynamic airport competitiveness based on IDCQGA-BP algorithm, 1–8. doi:10.1155/2013/309750

Cui, Q., Kuang, H. B., Wu, C. Y., and Li, Y. (2013b). Dynamic formation mechanism of airport competitiveness: The case of China. *Transp. Res. Part A Policy Pract.* 47 (1), 10–18. doi:10.1016/j.tra.2012.10.021

Cui, Q., Wei, Y. M., Li, Y., and Li, W. X. (2016). Exploring the differences in the airport competitiveness formation mechanism: Evidence from 45 Chinese airports during 2010–2014. *Transp. B Transp. Dyn.* 5, 325–341. doi:10.1080/21680566.2016.1216811

Cui, Q., Wei, Y. M., Li, Y., and Li, W. X. (2017). Exploring the differences in the airport competitiveness formation mechanism: Evidence from 45 Chinese airports during 2010–2014. *Transp. B Transp. Dyn.* 5 (3), 325–341. doi:10.1080/21680566.2016.1216811

Darand, M., Dostkamyan, M., and Rehmanic, M. I. A. (2017). Spatial autocorrelation analysis of extreme precipitation in Iran. *Russ. Meteorol. Hydrol.* 42 (6), 415–424. doi:10.3103/S1068373917060073

Spina, L. D., Scrivo, R., Ventura, C., and Viglianisi, A. (2014). The culture of evaluation to improve the airport competitiveness of the metropolitan city of the strait: Analysis of alternative scenarios of connection. *Adv. Mater. Res.*, 1065–1069. doi:10.4028/www.scientific.net/AMR.1065-1069.3381

Demirsoy, C. (2012). *Analysis of stimulated domestic air transport demand in Turkey*. Rotterdam: Erasmus University.

He, J. L., Wei, M. H., Yu, H., Yuan, J., and Chen, Y. (2021). Evaluating the rail-based multimodal freight transportation after HSR entry in Yangtze River Delta economics zone. *Sci. Program.* 2021, 1–14. doi:10.1155/2021/5530343

Hu, L., Chun, Y. W., and Griffith, D. A. (2020). Uncovering a positive and negative spatial autocorrelation mixture pattern: A spatial analysis of breast cancer incidences in broward county, Florida, 2000-2010. *J. Geogr. Syst.* 22 (3), 291–308. doi:10.1007/s10109-020-00323-5

Huynh, T. M., Kim, G., and Ha, H. K. (2020). Comparative analysis of efficiency for major Southeast Asia airports: A two-stage approach. *J. Air Transp. Manag.* 89, 101898. doi:10.1016/j.jairtraman.2020.101898

Ishizuka, Y. (2014). Efforts to the tourism-oriented country and strengthening of international competitiveness of airport in Singapore. *JAFIT Int. Tour. Rev.* 21, 159–165. doi:10.24526/jafit.21.0_159

Jiang, Y., Wang, L., Jiang, X., and Lu, J. (2013). Spatial-temporal evolution of multi-airports' homogenization in China Yangtze River Delta. *Procedia - Soc. Behav. Sci.* 96, 1402–1411. doi:10.1016/j.sbspro.2013.08.159

Jin, G., Deng, X., Zhao, X., Guo, B., and Yang, J. (2018). Spatiotemporal patterns in urbanization efficiency within the Yangtze River economic Belt between 2005 and 2014. *J. Geogr. Sci.* 28 (8), 1113–1126. doi:10.1007/s11442-018-1545-2

Jing, Y., Liu, Y., Cai, E., and Zhang, Y. (2018). Quantifying the spatiality of urban leisure venues in Wuhan, Central China – GIS-based spatial pattern metrics. *Sustain. Cities Soc.* 40, 638–647. doi:10.1016/j.scs.2018.05.015

Kim, D., and Song, I. (2021). Predicting model improvement by accounting for spatial autocorrelation: A socioeconomic perspective. *Prof. Geogr.* 73 (1), 131–149. doi:10.1080/00330124.2020.1812408

Klophaus, R., and Lauth, G. J. (2022). Monetary mapping of the climate footprint of air travel to a single airport. *J. Air Transp. Manag.* 5 (2), 102204. doi:10.1016/j.jairtraman.2022.102204

Liang, X. B., Liang, W., Zhang, L. B., and Guo, X. Y. (2019). Risk assessment for long-distance gas pipelines in coal mine gobs based on structure entropy weight method and multi-step backward cloud transformation algorithm based on sampling with replacement. *J. Clean. Prod.* 227, 218–228. doi:10.1016/j.jclepro.2019.04.133

Liang, X. Z., Lai, K. K., Liu, J., Qiao, H., Yin, H. X., et al. (2016). Study on the multilayer airport system in China based on evaluation of airport competitiveness. *Manag. Rev.* 28 (12), 116–126. doi:10.14120/j.cnki.cn11-5057/f.2016.12.010

Liu, X., Guo, P., Yue, X., Zhong, S., and Cao, X. (2021). Urban transition in China: Examining the coordination between urbanization and the eco-environment using a multi-model evaluation method. *Ecol. Indic.* 130 (1), 108056. doi:10.1016/j.ecolind.2021.108056

Liu, X. J., Xia, S. Y., Yang, Y., Wu, J. f., Zhou, Y. N., and Ren, Y. W. (2020). Spatiotemporal dynamics and impacts of socioeconomic and natural conditions on PM2.5 in the Yangtze River Economic Belt. *Environ. Pollut.* 263, 114569. doi:10.1016/j.envpol.2020.114569

Liu, Y. L., Jing, Y., Cai, E. X., Cui, J., Zhang, Y., and Chen, Y. (2017). How leisure venues are and why? A geospatial perspective in wuhan, central China. *Sustainability* 9, 1865. doi:10.3390/su9101865

Lu, Y. N., Li, X. P., and Li, K. X. (2022). *Promoting the high-quality development of the Yangtze River Economic Belt the People's daily*, cited from, Available at: http://politics.people.com.cn/n1/2022/0612/c1001-32444082.html (Accessed on July 1, 2022).

Luo, J., Chen, S., Sun, X., Zhu, Y., and Chen, G. (2020). Analysis of city centrality based on entropy weight topsis and population mobility: A case study of cities in the Yangtze River economic Belt. *J. Geogr. Sci.* 30 (4), 515–534. doi:10.1007/s11442-020-1740-9

Wen, J., Xu, Z. H., and Luo, X. Y. (2022). Evaluation and Empirical Study on competitiveness of Regional Airport Cluster. *Aeronautical Computing Technique* 51 (05), 10–14. doi:10.3969/j.issn.1671-654X.2021.05.003

MacKinnon, D., Pirie, G., Gather, M., Knowles, R. D., and Shaw, J. (2008). "Transport and economic development," in *Docherty I. Transport geographies: Mobilities, flows and spaces* (Malden: Blackwell Publishing).

McLay, P., and Reynolds, F. A. (2006). Competition between airport terminals: The issues facing Dublin airport. *Transp. Res. Part A Policy Pract.* 40 (2), 181–203. doi:10.1016/j.tra.2005.06.002

Moura, F. H. S. D., Caetano, M., and Severino, M. R. (2020). Airport competitiveness analysis from aircraft and passenger movement. *J. Transp. Logist.*, 143–157. doi:10.26650/JTL.2020.0015

Pan, Z., He, J., Liu, D., Wang, J., and Guo, X. (2021). Ecosystem health assessment based on ecological integrity and ecosystem services demand in the middle reaches of the Yangtze River Economic Belt, China. *Sci. Total Environ.* 774 (7724), 144837. doi:10.1016/j.scitotenv.2020.144837

Park, Y. (1997). Application of a fuzzy linguistic approach to analyse Asian airports' competitiveness. *Transp. Plan. Technol.* 20 (4), 291–309. doi:10.1080/03081069708717595

Pei, T. A., Wu, H. Q., Yang, T. T., Jiang, F., Zhang, W., Zhu, Z., et al. (2021). Evaluation of urban water ecological civilization: A case study of three urban agglomerations in the Yangtze River economic Belt, China. *Ecol. Indic.* 123, 107351. doi:10.1016/j.ecolind.2021.107351

Pels, E., Nijkamp, P., and Rietveld, P. (2003). Access to and competition between airports: A case study for the san Francisco Bay area. *Transp. Res. Part A Policy Pract.* 37 (1), 71–83. doi:10.1016/S0965-8564(02)00007-1

Peng, M., Xu, H., Qu, C., Xu, J., Chen, L., Duan, L., et al. (2021). Understanding China's largest sustainability experiment: Atmospheric and climate governance in the Yangtze River Economic Belt as a lens. *J. Clean. Prod.* 290, 125760. doi:10.1016/j.jclepro.2020.125760

Qin, G. (2020). An empirical study on the impact of Yangtze River Delta airport cluster on regional economy. *Open J. Transp. Technol.* 09 (6), 464–475. doi:10.12677/ojtt.2020.96056

Sarkis, J. (2000). An analysis of the operational efficiency of major airports in the United States. *J. Operations Manag.* 18 (3), 335–351. doi:10.1016/S0272-6963(99)00032-7

Stoyanets, N., Hu, Z. T., Chen, J. M., and Niu, L. C. (2020). Managing sustainability development of the agricultural sphere based on the entropy weight TOPSIS model. *Int. J. Technol. Manag. Sustain. Dev.* 19 (3), 263–278. doi:10.1386/TMSD_00026_1

Sun, C., Chen, L., and Tian, Y. (2018). Study on the urban state carrying capacity for unbalanced sustainable development regions: Evidence from the Yangtze River economic Belt. *Ecol. Indic.* 89 (JUN), 150–158. doi:10.1016/j.ecolind.2018.02.011

Sydorenko, K., Sydorenko, O., Lozhachevska, O., and Pashchenko, O. (2021). Competitiveness of international airports production infrastructure in global air transportation market: Comprehensive situational model. *Asian Acad. Manag. J.* 26 (2), 173–195. doi:10.21315/aamj2021.26.2.8

Tang, D., and Li, Z. J. (2019). Relevance analysis of sustainable development of Yangtze River Economic Belt based on spatial structure[J]. *J. Audit Econ.* 16 (17), 3076. doi:10.3390/ijerph16173076

Wang, C. Y., Xu, M., Olsson, G., and Liu, Y. (2020). Characterizing of water-energy-emission nexus of coal-fired power industry using entropy weighting method. *Resour. Conserv. Recycl.* 161, 104991. doi:10.1016/j.resconrec.2020.104991

Wei, Y. E., Hong, J., and Park, D. (2019). Evaluating the competitiveness for major international airports in northeast Asia. *KSCE J. Civ. Eng.* 23 (2), 844–849. doi:10.1007/s12205-018-0254-9

Wu, X. Y., and Wu, K. Y. (2005). Study on the competency of Shanghai Pudong airport in Asia- pacific ocean with AHP. *Logist. Technol.* 9, 203–206. doi:10.3969/j.issn.1005-152X.2005.09.068

Xiong, N. X., and Wang, Y. M. (2018). Multiple attribute decision method based on improved fuzzy entropy and evidential reasoning. *J. Comput. Appl.* 38 (10), 2803–2808. doi:10.11772/j.issn.1001-9081.2018030677

Yu, Y., Zhang, N., and Kim, J. D. (2020). Impact of urbanization on energy demand: An empirical study of the Yangtze River Economic Belt in China. *Energy Policy* 139, 111354. doi:10.1016/j.enpol.2020.111354

Zeng, J., Wang, C., Song, D., and Sun, G. (2012). Evolution of industrial structure in airport economic zone: Taking hub airports in the Yangtze River Delta as examples. *Prog. Geogr.* 31 (12). doi:10.11820/dlkxjz.2012.12.014

Zhang, X., Du, Q., Xu, Z. L., and Tao, H. Q. (2012). "Construction of evaluation index system of regional multi-airport coordinated development in the Yangtze River Delta region," in Proceeding 7th International Conference on Computing and Convergence Technology, 3 - 5 December 2012 (ICCCT), 338–341.

Zhang, Z., Ou, G., Elshkaki, A., and Liu, R. (2022). Evaluation of regional carrying capacity under economic-social-resource-environment complex system: A case study of the Yangtze River Economic Belt. *Sustainability* 14, 7117. doi:10.3390/su14127117

Zhang, Z. X., Yu, Y., Wang, D., Kharrazi, A., Ren, H., Zhou, W., et al. (2021). Socio-economic drivers of rising CO_2 emissions at the sectoral and sub-regional levels in the Yangtze River Economic Belt. *J. Environ. Manag.* 290, 112617. doi:10.1016/j.jenvman.2021.112617

Zhao, X. F., Huang, X. J., and Liu, Y. B. (2012). Spatial autocorrelation analysis of Chinese inter-provincial industrial chemical oxygen demand discharge. *Int. J. Environ. Res. Public Health* 9 (6), 2031–2044. doi:10.3390/ijerph9062031

Zietsman, D., and Vanderschuren, M. (2014). Analytic hierarchy process assessment for potential multi-airport systems-the case of cape town. *J. Air Transp. Manag.* 36 (1), 41–49. doi:10.1016/j.jairtraman.2013.12.004

frontiers | Frontiers in Environmental Science

TYPE Original Research
PUBLISHED 28 September 2022
DOI 10.3389/fenvs.2022.999124

Check for updates

OPEN ACCESS

EDITED BY
Ying Jing,
Zhejiang University, China

REVIEWED BY
Peng Cheng,
Wuhan University, China
Guo Long,
Huazhong Agricultural University, China

*CORRESPONDENCE
Shaokun Wei,
weishaokun@ccud.org.cn;

SPECIALTY SECTION
This article was submitted to Environmental Informatics and Remote Sensing,
a section of the journal
Frontiers in Environmental Science

RECEIVED 20 July 2022
ACCEPTED 25 August 2022
PUBLISHED 28 September 2022

CITATION
Zhang Y, Yang Y, Wei S, Ma Z, Tian M, Sun M and Nie J (2022), Research on spatial structure and resilience of complex urban network: A case study of Jing-Jin-Ji Urban Agglomeration.
Front. Environ. Sci. 10:999124.
doi: 10.3389/fenvs.2022.999124

COPYRIGHT
© 2022 Zhang, Yang, Wei, Ma, Tian, Sun and Nie. This is an open-access article distributed under the terms of the Creative Commons Attribution License (CC BY). The use, distribution or reproduction in other forums is permitted, provided the original author(s) and the copyright owner(s) are credited and that the original publication in this journal is cited, in accordance with accepted academic practice. No use, distribution or reproduction is permitted which does not comply with these terms.

Research on spatial structure and resilience of complex urban network: A case study of Jing-Jin-Ji Urban Agglomeration

Yang Zhang[1,2], Yang Yang[1,2], Shaokun Wei[3]*, Zijun Ma[1,2], Miao Tian[1,2], Meng Sun[1,2] and Jiabin Nie[1,2]

[1]College of Urban Economics and Public Administration, Capital University of Economics and Business, Beijing, China, [2]Beijing Key Laboratory of Megaregions Sustainable Development Modelling, Beijing, China, [3]China Center for Urban Development, Beijing, China

With the long-term impact of economic globalization, the accelerated cross-border flow of resource elements between cities is increasingly important for the development of urban regions. In this context, the central place theory, which emphasizes the vertical hierarchical relationship between cities, has obvious limitations in interpreting urban interaction. This paper takes the Beijing Tianjin Hebei Urban Agglomeration (including Beijing, Tianjin. and 11 prefecture-level cities in Hebei Province) as the research object, constructs three complex networks of economy, information, and economic information coupling connection, and analyzes the resilience of the network structure. The research results show that: 1) The spatial distribution of the three network structures of Jing-Jin-Ji Urban Agglomeration presents a spatial pattern with Beijing as the core and radiating outward. 2) In terms of weighted degree distribution, Beijing, as an arrow city, has strong competitiveness in the economy and information network, but the hierarchy of cities with balanced information economy development is low. 3) In terms of weighted degree correlation, among the three networks, the cities with a high weighted degree prefer to connect with cities with a low weighted degree, and the mismatch is ranked as information network > information economy coupling network > economic connection network. 4) In terms of network transmission, information network > economy connection network > information economy coupling network, and Beijing and Tianjin have a greater impact. The above results have strong guidance and practical significance for the formulation and adjustment of territorial spatial planning and regional optimization.

KEYWORDS

urban network, Resilience, Coupling, complex network, Jing-Jin-Ji (3J) region

1 Introduction

1.1 Background

Modern cities are regarded as resources and springboards to connect and participate in the global economy. They are laboratories of globalization in space, economy, society, culture, and environment. Urban revitalization and growth coexist with urban stagnation and recession. Driven by globalization and the revolution of information technology, many cities have separated from the track of national economic development and connected into horizontal economic networks, thus reshaping and process of globalization (Cohen, 2001; Hanssens et al., 2013; Pereira and Derudder, 2010). Since the 1960', the research on world urban has experienced three stages: world urban research with "attributes but no relationship," world urban research in the network society, and world urban network research. In the first two stages, node cities are studied based on urban attribute data, and little attention is paid to the relationship between cities (Yang et al., 2011).

1.2 Literature review

(1) In terms of urban network construction, the current research mainly includes the following progress: Gordon, (2010) studied networks of cities in the world rather than "world cityness." The study offered a "Southern" perspective on world city research, and it included places not ordinarily considered. Also, fourteen years of sample data on cross-border, intercity airline traffic were used as time-series relational information. The data reflect the links between the two principal cities of South Africa and other cities in Africa and beyond. Pereira and Derudder, (2010) believed that using air passenger flow data to measure and evaluate the world urban system is an effective method. Vinciguerra et al. (2010) modeled the evolution of infrastructure networks as a preferential attachment process. The average path length and average clustering coefficient of the observed network were successfully simulated. Arthur, (2010) employed techniques developed for the analysis of networks to evaluate more than 6,300 cities that are linked together by such firms in terms of their point centrality. Meanwhile, they adopted the block modeling technique to evaluate the positions occupied by these cities and the roles they play in the system. Hanssens et al. (2013) of the POLYMET project group built the Belgian city network in central Belgium. They used the office location of high-end producer services as the node of the network to measure the degree of network development with the multi-center index. Liu et al. (2014) explored the temporal evolution of cities and firms in a two-mode intercity corporate network formed by 50 leading advanced producer service firms across 154 cities for the years 2000 and 2010. In addition, from the perspective of spatial differences, the urban network structure was built with efficiency indicators such as urbanization efficiency, technological innovation efficiency, and green efficiency (Xing et al., 2018; Jing and Zhao, 2018), as well as city scale indicators such as night light data and urban construction land (Li et al., 2018; Yang et al., 2020). Moreover, based on the Baidu Index and other aspects, the urban service industry, transportation, logistics enterprises, economy, information, and other networks were established (Jabareen., 2013; Polèse., 2015). Frost and Podkorytova, (2018) adopted the interlocking network model proposed by the Globalization and World Cities research (GaWC) to the regional level to uncover the interurban relations, which focuses on the analysis of intraregional spatial patterns of globalization.

(2) In the research of urban network structure and network resilience

"Inclusive, safe, and resilient sustainable cities" is an important topic of sustainable development in 2030 of the United Nations (Pizzo, 2015). "Resilient cities" has become a goal of urban construction in China, and the research on the influencing factors of resilient cities has been carried out from the following aspects. Suzanne et al. studied urban resilience from economic, social, institutional, and other factors, and they believed that collaborative management and decentralization are two institutional management factors that can strengthen urban resilience (Hallie et al., 2017). Chad et al. (2018) studied the impact of disaster disturbance on urban resilience. They pointed out that urban resilience is affected by natural disasters such as climate change, natural disasters, resource crises, human disturbances, and human pressure. David et al. (2019) studied the impact of infrastructure on urban resilience, and the study suggested that the impact of an urban environment on urban resilience was mainly reflected in infrastructure, ecological environment, and other factors. Currently, there are two main directions in the study of urban network structure and network resilience.

I. In the evaluation of network structure resilience

At present, there is no unified method for evaluating network structure resilience. In English, both toughness and elasticity are translated as resilience, which refers to the stability and resilience of the system to maintain its original state under external impact. According to the concept of "structure determines function principle," by taking the network as a physical phenomenon, the network topology parameters based on complex network theory are considered to have a key impact on resilience (Bombelli et al., 2020; Dixit et al., 2020). Vijaya et al. (2020) found that the enterprise supply chain network with the lowest

density and centrality and the largest connectivity and network size has the highest resilience.

II. In terms of the resilience evaluation system

Hudec et al. (2018) investigated the differences in urban resilience in Slovakia in response to the financial crisis from three dimensions and 12 indicators of economic, social, and community management capabilities. Moser et al. (2019) constructed an index system from the perspective of nature, society, politics, human resources, economy, and capital. Noura et al. (2020) pointed out that urban resilience is determined by physical, ecological, and socio-economic factors. Cutter et al. (2014) selected 27 regional resilience evaluation indicators from the five dimensions of society, economy, infrastructure, institutions, and environment.

1.3 Research questions

With the rapid development of economy, science, and technology, the links between cities are increasingly closer. Among them, economic ties and information attention are more powerful, which indicates the degree of communication between cities. The resilience of the urban network indicates the ability of the urban network to maintain normal operations of the city under the impact. This is a scientific question worth investigation. Therefore, it is significant to study the resilience of complex urban networks for normal operations of the regional space. Meanwhile, based on the construction of the urban network, the resilience of the urban network needs to be reasonably evaluated, and optimization suggestions should be given according to the results.

By summarizing the existing research and taking the Jing-Jin-Ji Urban Agglomeration as an example, this paper constructs the information connection network, economic connection network, and information economy coupling network based on the Baidu search index and socioeconomic data. Then, the information and economic coupling degree of Jing-Jin-Ji are evaluated, and the resilience of the network is optimized from the perspective of matching and transmission. The study results provide a theoretical basis for enhancing the connectivity of cities in the economic network and information network of the Jing-Jin-Ji Urban Agglomeration and the stability of urban operation and development.

2 Study area, data, and method

2.1 Study area

The Jing-Jin-Ji region is located in the north of North China Plain, north of Zhanghe River, with Yanshan mountain on its back, the Bohai Sea in the East, Taihang Mountain in the west, Shandong and Henan provinces in the southeast and south, Taihang Mountain in the west, Shanxi Province and Inner Mongolia Autonomous Region in the Northwest and North, and Liaoning Province in the northeast. The region includes two municipalities under the central government of Beijing and Tianjin and 13 cities in Hebei Province, including Baoding, Tangshan, Langfang, Shi Jiazhuang, Qin Huangdao, Zhang Jiakou, Chengde, Cangzhou, Hengshui, Xingtai, and Handan (Figure 1).

2.2 Research data

In the study of urban network characteristics, cities are regarded as nodes in the network. The Baidu search index between cities is used to characterize the information flow in the network nodes. With the help of the Baidu index platform, a Baidu search index with one city as the scope and another city as the keyword is established to obtain the information connection between cities. For example, to obtain the contact information between Beijing and Tianjin, the Baidu search index of Beijing to Tianjin for a certain period of time can be obtained by taking Tianjin as the keyword and Beijing as the range. This study uses the Baidu search index between two cities in the Jing-Jin-Ji region in 2018 to build a 13 * 13 intercity contact matrix for studying the characteristics of the urban network in the Jing-Jin-Ji region.

Meanwhile, the shortest road distance between two cities is used in the process of calculating economic ties, and the data are borrowed from the Gaode map. The statistical data used in this study include the number of permanent residents and the GDP data of 13 cities in Beijing, Tianjin, and Hebei at the end of 2018, which are derived from the 18-years statistical yearbook of each city.

2.3 Research methods and models

2.3.1 Construction of the urban network structure and the network characteristics

By reading the current literature and the sorted information flow intensity, economic connection intensity, and information economy coupling connection intensity, the information, economy, and information economy coupling connection networks are constructed by using the gephi network analysis tool and ArcGIS spatial analysis software. Then, the attribute characteristics of various networks in spatial pattern and centrality are analyzed.

(1) Information contact network (Xiong et al., 2013; Jiang et al., 2015.)

In the calculation of information flow intensity, the intensity of information flow between two cities is expressed by the

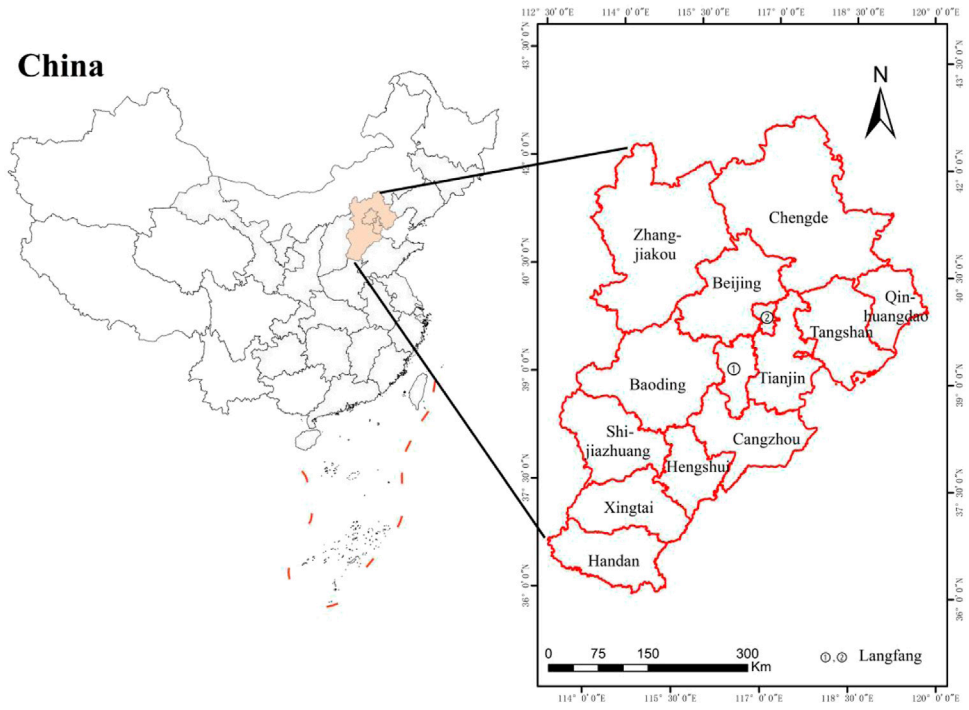

FIGURE 1
Study area.

product of mutual attention between city A and city B, and the formula is as follows

$$R_k = A_b{}^*B_a \quad (1)$$

where, R_k is the information flow intensity between cities A and B ; A_b is the attention of city B to city A; B_a is the attention of city A to city B. Based on the intensity of information flow, this study constructs and analyzes the information connection network between 13 cities in Beijing, Tianjin, and Hebei, and evaluates the resilience of the information network structure.

(2) Economic connection network (Niu et al., 1998; Wang et al., 2006)

The gravity model is a common method for the calculation of absolute economic connection quantity, and it is used in this study to measure the economic connection strength between Beijing, Tianjin, and Hebei. The calculation formula is shown as follows:

$$R_{ij} = \left(\sqrt{P_iG_i} * \sqrt{P_jG_j}\right) \Big/ D_{ij}^2 \quad (2)$$

where R_{ij} is the economic connection strength between regions i and j; P_i is the population of area i and j; G_i and G_j are the GDP of regions i and j; D_{ij} is the shortest path between i and j based on the road network.

(3) Information economy coupling network

The construction of an information economy coupling network is based on the coupling coordination model, which is an important index for representing the interconnection and interaction degree between two or more systems. The information connection strength and economic connection strength are coupled, and the coupling value is used as the connection strength between the information economy coupling network. The calculation formula is:

$$C = 2^* \sqrt{\frac{U1^*U2}{(U1 + U2)^2}} \quad (3)$$

where C represents coupling degree; $U1$ and U 2 represent the comprehensive scores of the information network system and economic network system respectively. If $U1 < U$ 2, the information network system is lagging; if U 1 $> U$ 2, the economic network system is lagging; if $U1 = U$ 2, the information network system and economic network system are synchronous. To further distinguish the coordination and interaction degree between the two types of systems, the coupling coordination degree needs to be introduced for evaluation. The calculation formula is:

TABLE 1 Classification standard of coupling coordination degree.

D-value interval of coupling coordination degree	Coordination level	Coupling coordination degree
(0.0–0.1)	1	Extreme disorder
[0.1–0.2)	2	Severe imbalance
[0.2–0.3)	3	Moderate disorder
[0.3–0.4)	4	Mild disorder
[0.4–0.5)	5	Verge of disorder
[0.5–0.6)	6	Reluctantly coordinate
[0.6–0.7)	7	Primary coordination
[0.7–0.8)	8	Intermediate coordination
[0.8–0.9)	9	Good coordination
[0.9–1.0)	10	High quality coordination

$$D = \sqrt{C \times T} \tag{4}$$

$$T = \alpha^{*}U1 + \beta^{*}U2 \tag{5}$$

where D stands for the coupling of co-scheduling; T is the coordination index; α and β represent the weight. This study believes that the weight of information network connection strength is equal to that of economic network connection strength. Also, the degree of coupling and coordination reflects the synergy of the overall development of the two urban networks. Thus, the types of coupling and coordination are divided. The evaluation criteria are presented in Table 1. The range of D value of coupling coordination degree is (0–1). The larger the D value, the higher the coordination level, and the more coordinated the coupling coordination degree.

(4) Degree centrality

Degree centrality reflects the interaction between a node and other nodes. It is an important expression of the interconnection relationship between cities. The greater the degree of a node, the higher the degree of centrality of the node, and the more important it is in the network (Lin et al., 2019). The calculation formula of degree centrality is shown as follows:

$$C_D(i) = \frac{Ki}{N-1} \tag{6}$$

where C_D is the degree centrality of node *i*, I is the degree of node *i*, and *N* is the number of nodes in the network.

2.3.2 Measurement and optimization of network structure resilience

By summarizing the existing literature, this paper selects the attribute characteristics of hierarchy matching and transmission in the interruption scenario, measures, analyzes, and evaluates the structural resilience of the three networks, and proposes optimization countermeasures and suggestions on this basis.

(1) Hierarchical——weighting degree and weighting degree distribution

Weighting degree: The weight of the network edge is included in the hierarchical calculation, which is expressed by weighting degree and weighting degree distribution. In an undirected graph, the degree represents the number of edges directly connected to a node, while the weighting degree describes the sum of the weights of the edges directly connected to a node, that is, the sum of the connection strength. The greater the value of the weighting degree, the stronger the connection between the node and other nodes.

Weighting degree distribution: the probability distribution or frequency distribution of the weighting degree of all nodes in the network can reflect the macrostructure characteristics of the network. The greater the slope, the more significant the hierarchy (Crespo et al., 2013).

$$W_m = C*\left(W_m^{*}\right)^{a} \tag{7}$$

where W_m is the weighting degree of city m, i.e., the sum of the weights of the edges directly connected to node m; W_m^{*} is the ranking of the weighted degree of city m in the network; *C* is a constant, and a represents the slope of the weighted degree distribution curve.

(2) Matching——neighbor average weighting and degree correlation.

Neighbor weighted average: In the network, each node has a certain number of adjacent nodes (V*i*) directly connected with the node. The average degree of all adjacent nodes directly connected to node *i* is calculated as:

$$\bar{k} = \frac{1}{k}\sum_{j \in Vi} kj \tag{8}$$

where k_j represents the degree of adjacent node j of node i; Vi represents the set of all adjacent nodes j of node i.

Weighted degree correlation: In the network, each node has a certain number of adjacent nodes directly connected with the node. If the weighted degree is positive and the correlation coefficient is positive, the network has the same matching result. If the positive correlation coefficient of the weighted degree is negative, the network is considered mismatched.

$$\bar{W} = \frac{1}{K_{\mathrm{m}}} \sum_{\mathrm{i} \epsilon G_{\mathrm{m}}} \mathrm{wi} \tag{9}$$

where Wm is the average of the weighted degrees of all adjacent nodes directly connected to node m, i.e., the weighted average degree of neighbors; Wi is the weighting degree of adjacent node i directly connected to the city; Km is the degree of city m, and Gm is the collection of all adjacent nodes in the city.

$$\mathrm{W_m} = \mathrm{D} * \left(\mathrm{W_m^*}\right)^{\mathrm{b}} \tag{10}$$

where D is a constant, and b is the weighted correlation coefficient.

(3) Transmissibility—network efficiency

Network efficiency: it refers to the efficiency of element flow between nodes in the network. The greater the value, the better the transmission of the network (Huang and Hu, 2014)

$$\mathrm{E} = \frac{1}{\mathrm{N}(\mathrm{N}-1)} \sum_{\mathrm{i} \neq \mathrm{j} \epsilon \mathrm{G}} \frac{1}{D_{ij}} \tag{11}$$

where E is the network efficiency, D_{ij} is the length of all shortest paths from node i to node j, and G is the set of nodes in the network after removing a node.

3 The construction of intercity connection network and the characteristics of cyberspace

3.1 Spatial pattern of the intercity connection network

Based on the intensity of information flow, economic connection, and information economy coupling among 13 cities in Beijing, Tianjin, and Hebei, the information connection network, economic connection network, and information economy coupling network are visualized respectively. The natural fracture method is used to classify the constructed network. Each network is divided into five levels, and the network connection is visualized. The construction results of the three types of contact networks are shown in Figure 2.

The information contact network in Figure 2A reflects the mutual search attention of cities. There are 13 nodes and 156 connecting lines in the network. Among the cities at the first level (254,340–1105094), only Beijing and Tianjin show strong information connection strength. This indicates that the information connection between Beijing and Tianjin is strong in the Jing-Jin-Ji Urban Agglomeration network, but there is no attention intensity at the first level to Hebei. The information connection network at the second level (184,437–254,340) presents a network structure centered on Beijing and radiating outward in a spatial structure. Beijing has strong economic concerns with Tianjin, Shi Jiazhuang, Tangshan, Qin Huangdao, Baoding, Zhang Jiakou, Langfang, and Handan. However, except Beijing, the links between cities do not appear at the second level, indicating that the links in the information network group are relatively single. In terms of the structural point, the attention links between cities other than Beijing should be strengthened. At the third level, the urban links with the intensity of information contact between (86,445–152250) mainly include Beijing and Chengde, Cangzhou, and Xingtai, Tianjin-Shi Jiazhuang and Tianjin-Tangshan, and Baoding and Shi Jiazhuang. The information attention among cities at the fourth level of contact intensity (43,512–82,416) mainly appears among cities other than Beijing: in addition to the connection between Beijing and Hengshui, Tianjin, Shi Jiazhuang, Tangshan, Qin Huangdao, Baoding, Zhang Jiakou, Cangzhou, Langfang, Xingtai, Hengshui, and Handan are compared with the first, second. In terms of the intensity of information connection at the three levels, the connection between prefecture-level cities is the closet at the fourth level. The information contact intensity of cities located at the fifth level (6,798–35,478) is the highest among the five categories, which accounts for about two-thirds of the information contact network, indicating that the attention intensity of information between most cities is still relatively weak. The fifth-level network has a hollow network structure in the periphery of the whole Jing-Jin-Ji Urban Agglomeration.

The economic connection network in Figure 2B reflects the overall pattern of economic connection strength between cities, including 13 nodes and 156 connecting lines. Compared with the information network, the location of each node and the distance between nodes in the economic network have a greater impact on the strength of economic ties between cities. Similarly, this study divides the economic ties into the following five levels by using the natural fracture method. The cities at the first level (3,548.826223–4,311.141520) are Beijing-Tianjin and Beijing -Langfang. In the whole Jing-Jin-Ji Urban Agglomeration, there is no strong connection between Tianjin and Langfang, and the economic connectivity between the two cities is still a certain distance from that of Beijing, At the first level, the spatial structure of the economic network is only two rays with Beijing as the endpoint. The cities at the second level of the economic network (873.828960–1463.976270) except Beijing and Tangshan, Handan and Xingtai, Tangshan, Cangzhou, and Langfang all take Tianjin as the center, showing a radial

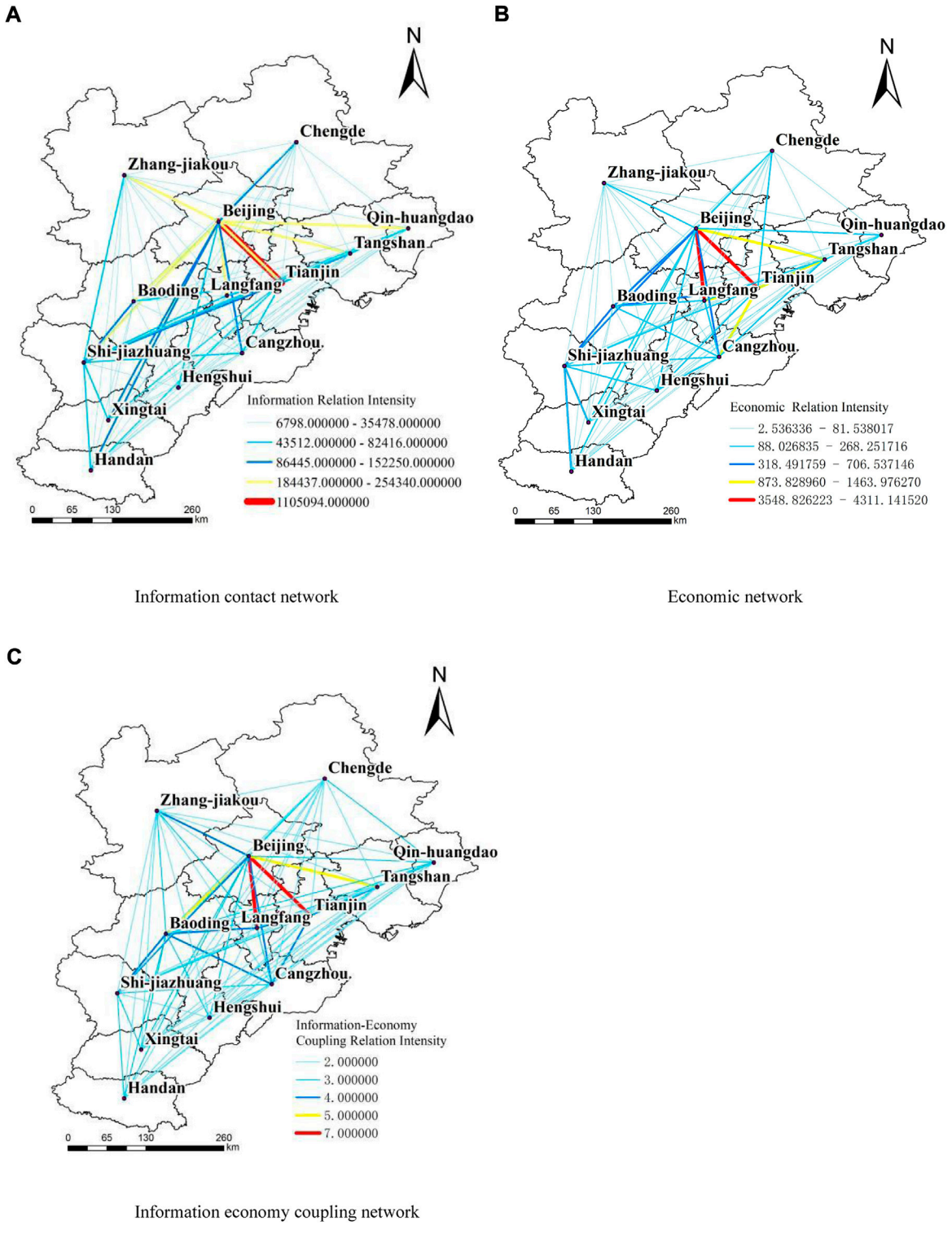

FIGURE 2
Spatial pattern of urban networks.

shape. At the third level of the economic connection network (318.491759–706.537146), the city connections include Beijing - Baoding, Beijing - Cangzhou, Tianjin—Baoding, Xingtai - Shi Jiazhuang, and Shi Jiazhuang - Handan. The links between the prefecture-level cities in Hebei are gradually increasing. At the fourth level of the economic network (88.026835–268.251716),

each city is involved. Whether it is Beijing, Tianjin, or the prefecture-level cities in Hebei, the economic connection is more widely distributed in space than that at the first, second, and third levels. The number of cities at the fifth level (2.536336–81.538017) is similar to that in the information connection network. This is the level with the largest number of inter-city connections, which accounts for two-thirds of the network connections. However, unlike the information connection network space, the economic network is not hollow at the fifth level, and Beijing still has economic connections with other cities. This shows that from the perspective of the economic network built by the gravity model, Beijing, as the center of the urban agglomeration, is generally weak in the strength of economic links with other cities relative to the strength of information links, but the links between the cities on the fifth level of the two networks are the strongest, so there is a certain space for network optimization.

Figure 2C shows the information economy coupling network obtained by coupling the information connection network and the economic connection network. It reflects the coordination and matching of information and economic connections between cities, including 13 nodes and 156 connections. Combined with the coupling degree classification standard, this paper analyzes whether the coupling links in different information economic networks are coordinated, and adopts the natural fracture method to divide the calculation results into the following five levels. The coupling value of the information economy coupling network at the first level is 7. The network spatial structure at this level is similar to that of the economic connection network. The connection between Beijing Tianjin and Beijing Langfang has reached primary coordination, which reflects that the overall information connection strength and economic connection strength of the Jing-Jin-Ji Urban Agglomeration has not reached good coordination. The three cities of Beijing, Tianjin, and Langfang are most closely connected in the middle of the urban agglomeration, and they only achieve primary coordination. This indicates that the overall information and economic connection of the Jing-Jin-Ji Urban Agglomeration are unbalanced, and there is still a lot of room for improvement in the coordinated development of the two networks. The cities with a coupling coordination degree of 5 at the second level are Beijing and Tangshan, Beijing and Baoding, and the coupling coordination degree of information economic ties is nearly imbalanced. The value of the information economy connection coupling network at the third level is 4, which shows a slight imbalance. In terms of spatial structure, in the whole information economy coordination network, the cities outside Beijing, Tianjin, and Hebei such as Chengde, Handan, Qin Huangdao, Hengshui, and Xingtai do not appear at this level. Generally, there are more connections between cities near the center of urban agglomeration at this level. The coordination intensity of information economy coupling between cities at the fourth level is 3, which shows a moderate imbalance. Compared with the links at the third level, the links between cities at this level are significantly increased. The coupling strength of the fifth level is 2, and the links between cities are the most at this level, which shows a serious imbalance. From the perspective of coordinated development, the development of economic ties lags that of information links, resulting in the level of coordination in the whole information economic ties coupling network. Though Beijing Tianjin and Beijing Langfang reach the level of primary coordination, none of them reach the coordination level.

3.2 Central characteristics

Presents the calculated center value of point degree for the cities at four levels of the three networks.

Point degree centrality reflects the ability of network nodes to directly mobilize network resources and information (Wang et al., 2006), and its ability is positively correlated with the value. The results of point degree centrality are shown in Figure 3 and Table 2. It can be seen that the degree of centrality of the economic connection network is higher than that of the information connection network and information economy coupling connection network. There are four cities with a degree center value of economic connection network above 0.58, which accounts for 30.8% of the total cities, indicating that about one-third of the cities can directly mobilize the economic resources between cities. Compared with the other two networks, the lowest value has only one point, and the centrality is less than 0.1 (Figure 3B). There are three points with a degree centrality of above 0.67 in the information contact network, which accounts for 25% of the total number of cities, but the value is higher than that of the economic contact network, and the point degree center value of the two cities is lower than 0.1 (Figure 3A). The degree center centrality of the information economic connection coupling network is generally low. Only one city (i.e., Beijing) has a degree centrality value of 1, and Baoding and Tianjin have a degree centrality value of 0.5 (Figure 3C), indicating that only the above three cities can directly adjust the resources of surrounding cities under the condition of coordinated economic and information development. The coupling degree centrality values of other cities are less than 0.34, There are even four cities with a point degree centrality of 0, and these cities cannot mobilize resources among other cities at all.

4 Resilience of urban network structure

For the three networks of information, economy, and information economy coupling constructed above, the

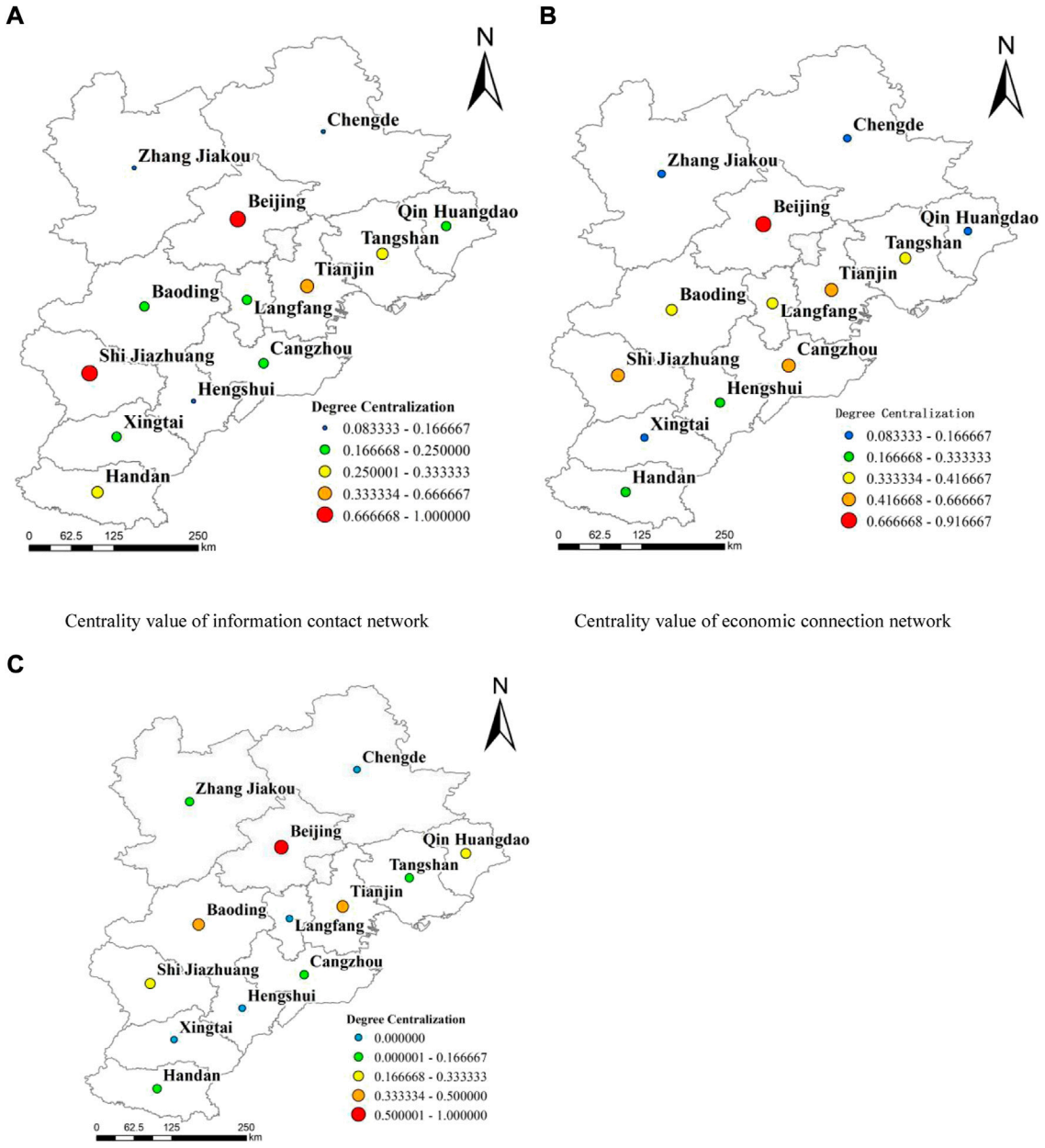

FIGURE 3
The spatial distribution of degree centrality.

resilience of the network structure is measured and analyzed in terms of hierarchy and matching at the individual and regional levels respectively. Then, the overall transmission and diversity of the network structure under a node interruption scenario are simulated and evaluated.

4.1 Network hierarchy

4.1.1 Weighting degree

The network weighting degree reflects the degree of correlation between urban nodes and the strength of complex correlation, as well as the strength of network connection. Based

TABLE 2 Centrality value.

	City	Economic rational degree centralization	Information rational degree centralization	Information-economic coupling rational degree centralization
1	Beijing	0.917	1	1
2	Tianjin	0.667	0.667	0.500
3	Shi Jiazhuang	0.583	0.833	0.333
4	Tangshan	0.417	0.333	0.083
5	Qin Huangdao	0.167	0.250	0.250
6	Handan	0.250	0.333	0.167
7	Xingtai	0.167	0.250	0.000
8	Baoding	0.417	0.250	0.500
9	Zhang Jiakou	0.083	0.167	0.083
10	Chengde	0.167	0.083	0.000
11	Langfang	0.417	0.250	0.083
12	Hengshui	0.333	0.083	0.000
13	Cangzhou	0.583	0.250	0.000

on network weighting degree, this paper measures the correlation strength of urban nodes and the hierarchical resilience of the network and uses the natural fracture method to divide the weighting degrees of the three types of networks into five levels respectively. The results are illustrated in Figure 4.

In terms of degree centrality, Shi Jiazhuang, at the first level of degree centrality (high-value area), is located at the second level of the weighting degree, and only Beijing is located at the first level in the Jing-Jin-Ji Urban Agglomeration. This indicates that Beijing, as the capital, not only has a strong connection with other cities in the Jing-Jin-Ji Urban Agglomeration in terms of information connection. By considering the ability to directly mobilize the surrounding resources, the cities at the second and third levels of weighting show a strip distribution from east to west in space. Specifically, Tianjin at the second level is the central node of the strip, and it connects the cities at both ends and plays an important role in an undertaking; The cities at the fourth and fifth levels are mainly distributed on the north and south edges of the Jing-Jin-Ji Urban Agglomeration, with a weak correlation with other cities. Overall, the urban development of the information contact network is relatively homogeneous. If there is a failure in any city except Beijing and Tianjin, the failure or even loss of any node will have a limited impact on the normal operation of the network function (Figure 4A).

Compared with degree centrality, Langfang city and Tianjin city are less located at the first level of degree centrality, indicating that in the Jing-Jin-Ji Urban Agglomeration, Beijing not only has a strong correlation with the surrounding cities but also can directly mobilize the economic resources of the surrounding cities. The cities at the second level of degree distribution are mainly located in the east of the Jing-Jin-Ji Urban Agglomeration. The cities at the third level are mainly located in the south of the Jing-Jin-Ji Urban Agglomeration. The city at the fourth level is only Cangzhou, and the city at the fifth level is located in the north of the Jing-Jin-Ji Urban Agglomeration. Cities at all levels in the economic connection network are roughly distributed in blocks. High-level cities are generally located in the middle east of the Jing-Jin-Ji Urban Agglomeration, and low-level cities are distributed in the north, while high-level cities in the west and south show a semi-surrounded structure. Compared with the information connection network, the hierarchy of the economic connection network is more obvious, its "robustness" has a certain decline compared with the information network, and its "vulnerability" is stronger. Once there is a problem in a high-level city, it will have a great impact on the whole economic connection network, and the network is more prone to failure (Figure 4B).

Compared with the degree of centrality and centrality of the information economy coupling network, high-level cities are the same, and the number of cities at the third level increases. The cities at the fourth and fifth levels are mainly distributed in the south of the urban network. The high-level cities are a city belt running through Beijing, Tianjin, and Hebei, and these cities are at the east-west of the urban agglomeration. Most of the cities at the fourth and fifth levels are in the north, and the cities with balanced information and economy and high external contact intensity in the Jing-Jin-Ji Urban Agglomeration are still concentrated in Beijing (Figure 4C).

4.1.2 Weighted degree distribution

The weighting degrees of all urban nodes in the three types of networks are ranked, and the power curve is drawn to analyze the overall hierarchical structure resilience of the network. The results are shown in Figure 5. The slope a of the weighted degree distribution curve of the three types of

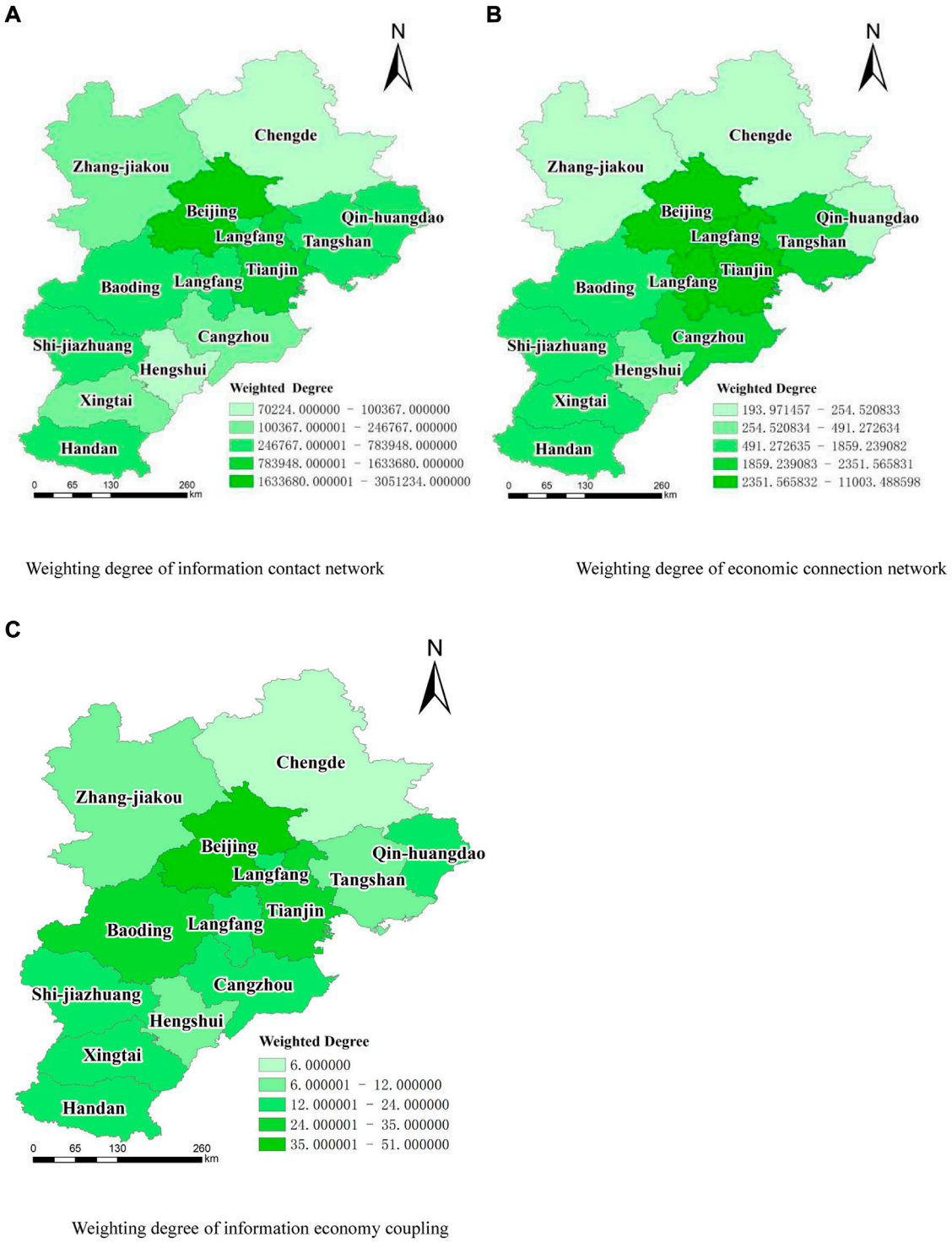

FIGURE 4
Spatial distribution of network weighting degree.

networks is large, and | a | is between 0.7 and 1.6, indicating that the hierarchy of the networks is significant. The | a | of information, economy, and coupling network is 1.289, 1.59, and 0.711 respectively, indicating that the hierarchical difference between the three networks is obvious (Figures 5A–C). The economic connection network has the

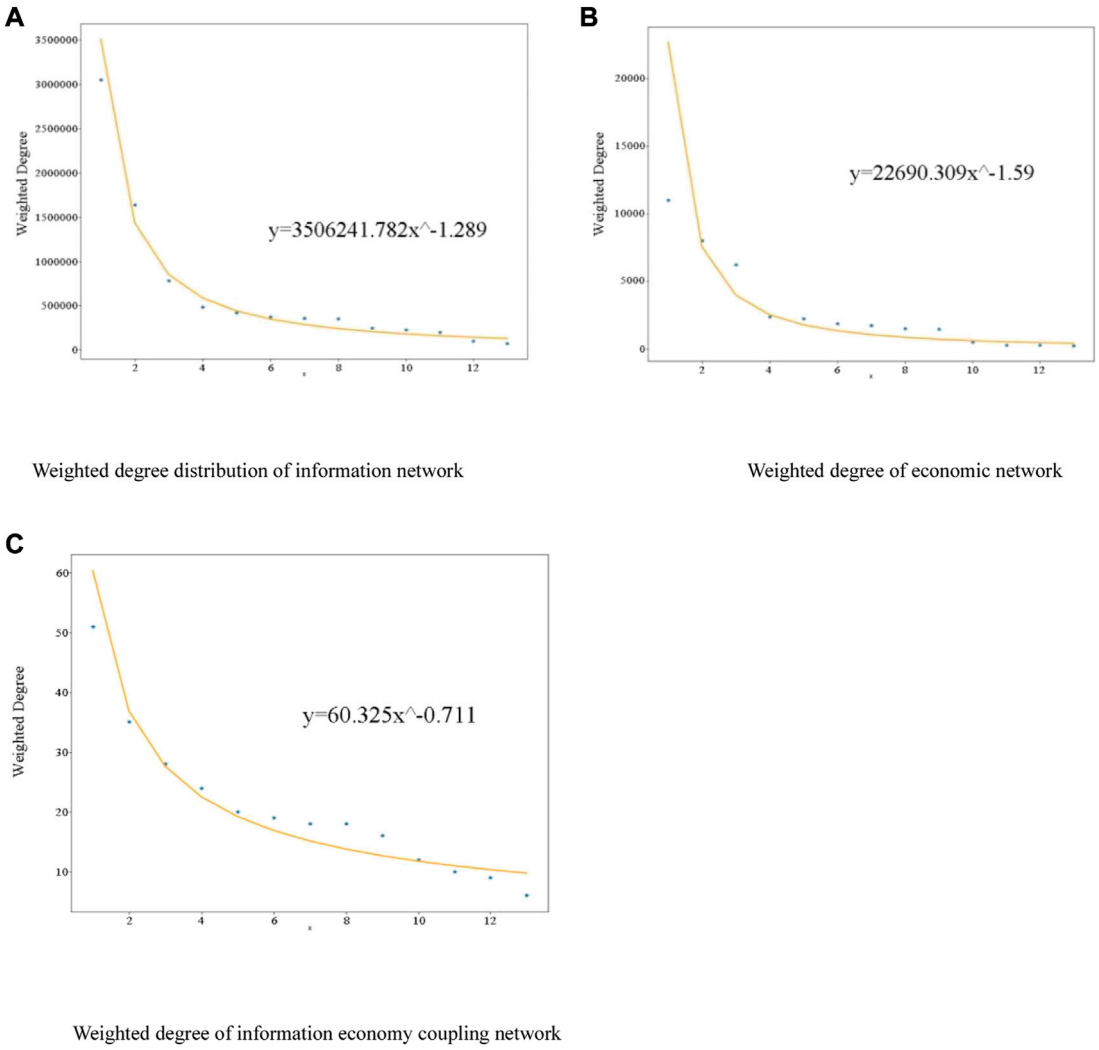

FIGURE 5
Weighted degree distribution of networks.

highest hierarchy, and the hierarchical structure between the cities is the most obvious. Besides, there is a strong core city, which is consistent with the spatial distribution of weighting degree. The information connection network ranks second. Although there are high-level cities in Beijing and Tianjin, their spatial distribution is relatively scattered, i.e., in addition to Beijing and Tianjin, the homogenization phenomenon of other cities is obvious. Compared with the economic network, the number of high-level cities in the information economy coupling network is smaller; the hierarchy is the lowest, and its spatial distribution is more scattered, mainly in low-level cities. Therefore, the information economy coupling network has the lowest hierarchy. It shows that there are still great differences in the hierarchy between the information economy coupling network and the single factor network.

4.2 Network matching

Matching is used to describe the correlation between nodes in the network. If a node with a medium value tends to contact the node with a high value, the network is said to be matched; otherwise, it is mismatched (Batty, 2009; Crespo et al., 2013). If a city tends to develop together with cities of the same level and status, the network has the same matching. The same matching network is easy to be affected by factors such as solidified contact path and closed structure so that it has low innovation and information permeability. When it is affected by the outside world, its recession risk is difficult to be avoided. Therefore, the resilience of network structure is relatively low. If the relationship between cities exists across different levels, cultural backgrounds, and economic differences, the network is considered to have

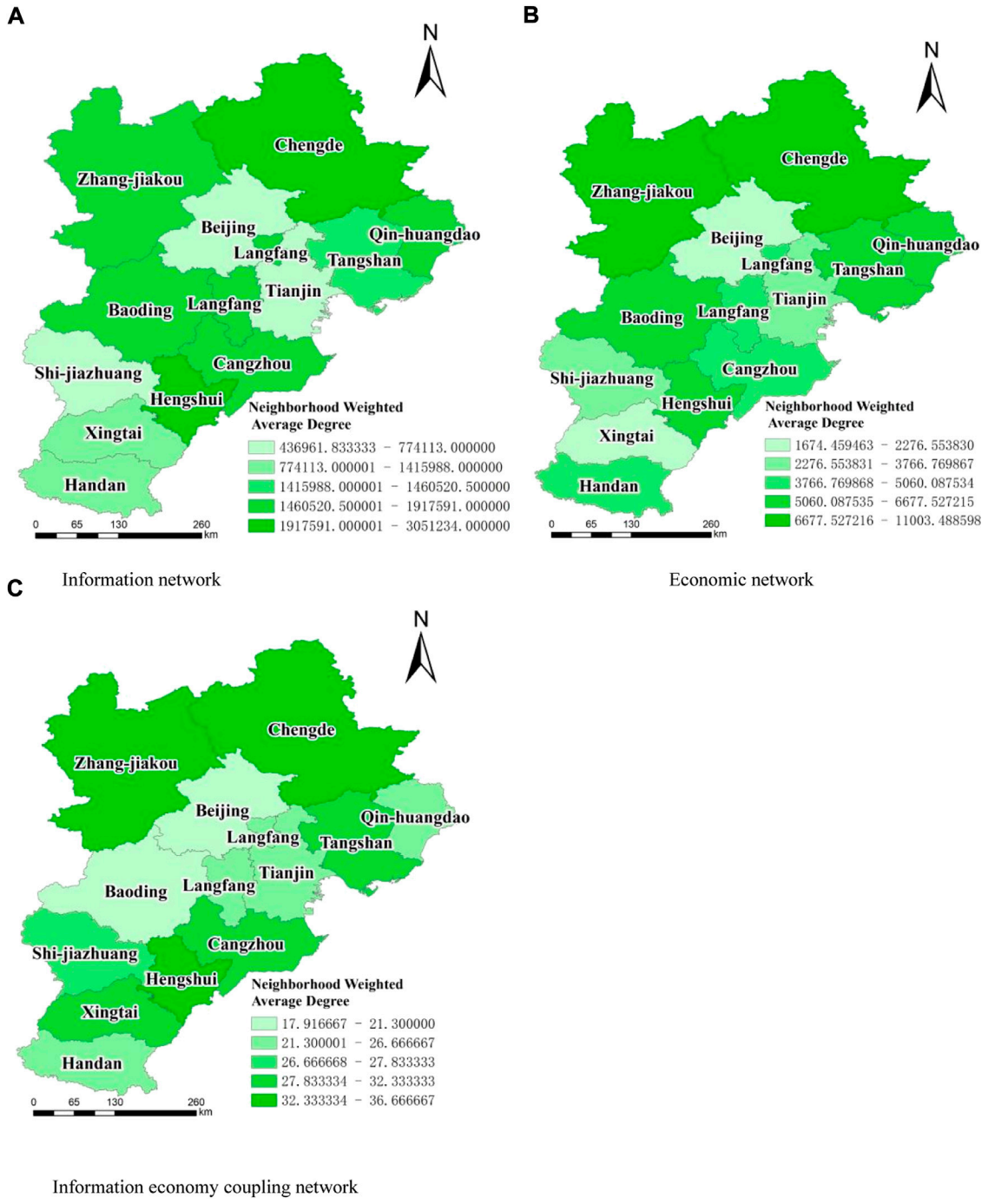

FIGURE 6
Spatial distribution of neighborhood weighted average degree.

allogeneic. Due to its heterogeneity and openness, the allogeneic network can show a certain resistance and adaptability in the face of regional risks. Therefore, the network structure has a higher resilience.

4.2.1 Neighbor weighted average

The weighted average of neighbors reflects the connection between a node and its neighbor nodes. In this study, the weighted average degree of neighbors is used to measure the

preference attachment and network matching resilience of urban nodes. The weighted average degree of the neighbors of three types of network city nodes is graded, and the spatial pattern is shown in Figure 6 by using the natural fracture method.

Compared with other networks, the information network has the largest number of cities with a weighted average degree of neighbors at the fifth level. Spatially, the neighbors in the cities with a high weighting degree have a low weighted average degree, and there are node cities with low weighting degree around them, indicating that the cities with a high weighting degree in the information network are generally connected with nodes with a low weighting degree. In this way, high-weighted cities can better exchange information with their surrounding cities (Figure 6A).

In the economic connection network, although the cities with the weighted average degree of neighbors at the fifth level only include Beijing and Xingtai, with Beijing and Xingtai as the center, they are surrounded by cities with a low weighting degree and form a surrounding structure around high weighting degree. In terms of spatial distribution, the two cities with a high weighting degree do not gather. It can better connect and drive the surrounding cities with a low weighting degree, which is conducive to the rapid development of the global network structure (Figure 6B).

In the information economy coupling connection network, the city nodes with a high weighting value are located at the fourth and fifth levels, indicating that the node cities with a high central value and balanced development of information connection and economic connection strength play an important role in driving the balanced development of economic and information connection of the surrounding cities. Such node cities have a great impact on the circulation and dissemination of elements of the network, and we should strengthen the interaction ability with high-weighted nodes (Figure 6C).

4.2.2 Weighted degree correlation

In this study, weighted degree association is employed to further describe the matching of the three networks. If the weighted average degree of neighbors increases with the weighting degree, the network has the same matching, i.e., the weighted degree is positively correlated; If the weighted average degree of neighbors decreases with the increase of weighting degree, the network is considered to have mismatching, i.e., the weighted degree correlation index is negative.

The weighted degree correlation results are shown in Figure 7. The weighted degree correlation coefficients of the three networks are 0.502, −0.266, and −0.328, respectively. The weighted degree correlation coefficients B are less than 0, and the coefficients of the three networks are quite different, which indicates that the cities with a high weighting degree in the three networks prefer to connect with the cities with a low weighting degree, i.e., the networks have different matching. Meanwhile, it also shows that the three types of networks have different matching connections.

It can be seen that the weighted degree correlation coefficient of the information connection network is the largest, and the slope of the weighted degree correlation curve is the steepest. That is, the mismatch phenomenon in the network is obvious, and the network connection paths are diversified. This indicates that the core cities with high weighting in the Jing-Jin-Ji Urban Agglomeration not only connect with cities with the same development and comprehensive level but also tend to connect with cities with certain differences in development level. This network mismatch can make the core cities in the Jing-Jin-Ji Urban Agglomeration promote the development of relatively backward cities and strengthen the intensity of information exchange between cities at different levels. From the perspective of structural resilience, combined with the above network hierarchy analysis, it is known that although the information connection network has a high hierarchy, except for Beijing and Tianjin, the distribution of cities at other levels is relatively scattered and homogeneous. In addition, the mismatch phenomenon can weaken the potential crises such as path dependence and regional locking caused by high-level and strengthen the efficient connection and close connection between core city nodes and edge nodes. The occurrence of external interference is conducive to the adaptive adjustment of the network structure. Meanwhile, the network has an obvious mismatch so that the urban agglomeration structure can change from vertical tree growth to horizontal network spread, thus realizing diversified development and regional risk reduction and improving the resilience of the urban network structure. (Figure 7A).

The degree correlation coefficient of the economic connection network is only −0.266. Compared with the degree correlation coefficient of the information connection network and the information economy coupling connection network, there is no strong mismatch. Combined with the analysis results of the network level, the hierarchy of the economic connection network is the highest, but there is a gap between the mismatch and the information connection network, indicating that there is certain path dependence in the economic connection network. Meanwhile, compared with the core cities with a high development level of information networks, they prefer connection. The connection between core cities and general cities and marginal cities is relatively low in the network, which intensifies the closeness of the economic network to a certain extent. Besides, compared with the information connection network, the higher level and lower mismatch of the economic network make the resilience of the economic connection network lower than that of the information connection network. This is not conducive to the resistance and resilience of regional economic flow to disasters (Figure 7B).

The degree correlation coefficient of the information economic connection coupling network is −0.328, which is greater than that of the economic network but less than that of the information network. Combined with the above weighted degree distribution analysis results, the hierarchy of the coupling network is the lowest among the three networks. The low-level

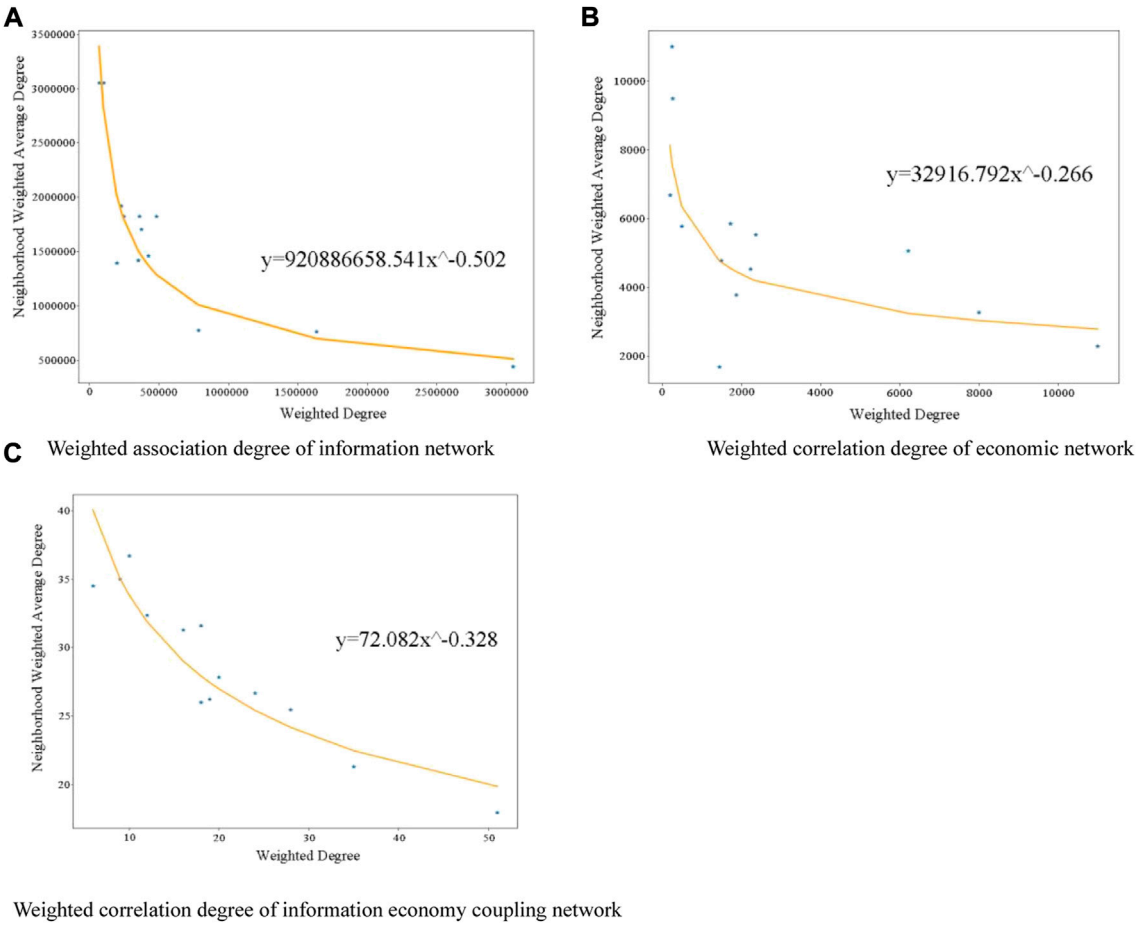

FIGURE 7
Weighted degree correlation of networks.

resilience of the network structure shows that the distribution of the information economy network cities is relatively homogeneous. In addition, the core cities between networks prefer to connect with general cities and marginal cities, and the connection paths between cities are diversified. Although the arrow ability of highly balanced cities is not very prominent, the "robustness" of the network structure of the information economy coupling network is high. In this case, the node failure of the high equilibrium city has no great impact on the balance of the overall Jing-Jin-Ji Urban Network, and the "vulnerability" of the city is low (Figure 7C).

4.3 Transmissibility of network structure in interrupt scenario

In this study, network efficiency is used to measure the transportability of information, economy, and coupled information-economy coupling networks, which reflects the diffusion ability of elements in the network. When the transportability of the network is high, it indicates that the transmission and exchange of elements between the nodes of the network can be faster, which helps to promote inter-city learning, innovation, communication, etc. Also, it can enhance the resistance of the network in the face of external shocks and make the network highly resilient. The results of the spatial distribution of network transmission after the failure of different nodes are shown in Figure 8, and the network transmission after the failure of different nodes in the 13 cities of the Jing-Jin-Ji Urban Agglomeration of the three networks are ranked, and the result is shown in Table 3.

The transferability of the information linkage network is between (0.1538–0.2334), which is slightly lower than that of the economic linkage network (0.1784–0.0.2521) and the coupled information-economic linkage network (0.1934–0.2607), indicating the lowest transfer efficiency among cities of the information network. Combined with the centrality characteristics, Beijing and Shi Jiazhuang have a higher degree

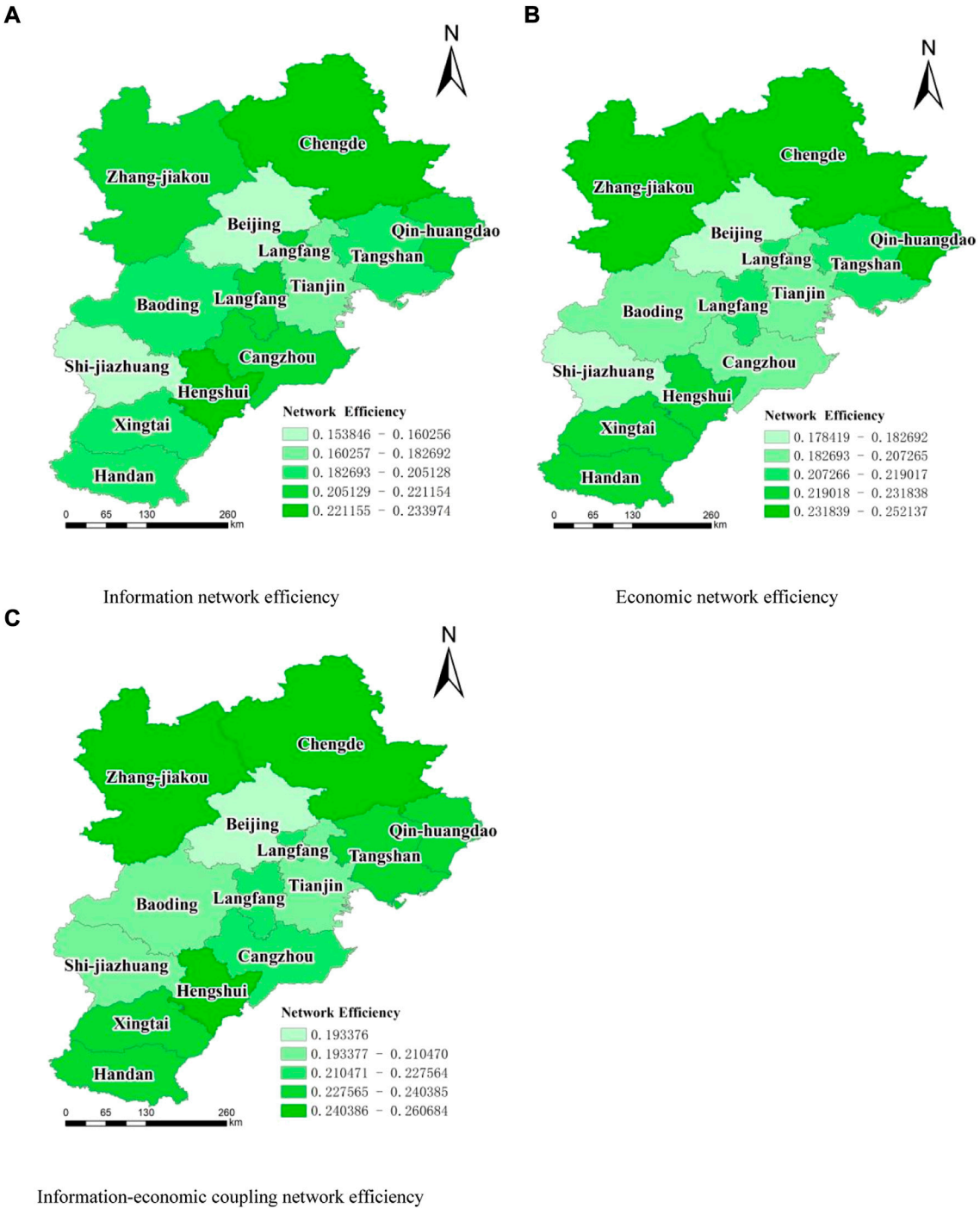

FIGURE 8
Spatial pattern of network transmission after the failure of different nodes.

of centrality, and they have the greatest impact on the transmission effect of the information network. Meanwhile, the network efficiency decreases to 0.1538 and 0.1826 after the failure of two nodes in Beijing and Shi Jiazhuang, which has a greater impact on the transmission type of the city network (Figure 8A).

Beijing has the highest moderate central value of the economic connection network, and it has the greatest impact

TABLE 3 Network transmission ranking.

Rank	City	Information rational network efficiency	City	Economic network efficiency	City	Information-economic coupling rational network efficiency
1.0000	Beijing	0.1538	Beijing	0.1784	Beijing	0.1934
2.0000	Shi Jiazhuang	0.1603	Shi Jiazhuang	0.1827	Tianjin	0.2062
3.0000	Tianjin	0.1827	Cangzhou	0.1998	Baoding	0.2062
4.0000	Baoding	0.1955	Tianjin	0.2009	Shi Jiazhuang	0.2105
5.0000	Tangshan	0.2019	Baoding	0.2073	Langfang	0.2222
6.0000	Handan	0.2019	Tangshan	0.2126	Cangzhou	0.2276
7.0000	Xingtai	0.2051	Langfang	0.2190	Handan	0.2340
8.0000	Cangzhou	0.2115	Hengshui	0.2265	Tangshan	0.2382
9.0000	Langfang	0.2115	Handan	0.2286	Qin Huangdao	0.2382
10.0000	Qin Huangdao	0.2212	Xingtai	0.2318	Xingtai	0.2404
11.0000	Zhang Jiakou	0.2212	Chengde	0.2425	Zhang Jiakou	0.2521
12.0000	Chengde	0.2340	Qin Huangdao	0.2457	Hengshui	0.2575
13.0000	Hengshui	0.2340	Zhang Jiakou	0.2521	Chengde	0.2607

on network transmission. After the node fails, the network transmission efficiency decreases to 0.1784. Secondly, the city with a greater impact is Shi Jiazhuang. When the network node is interrupted, the network transmission efficiency is reduced to 0.1827. Besides, Zhang Jiakou, Chengde, and Qin Huangdao are the cities that have the least impact on the economic connection network and have smaller central values of the same degree. The failure of the three cities has little impact on the whole network, and the network efficiency decreases to 0.2425, 0.2457, and 0.2521 respectively (Figure 8B).

Compared with the information and economic connection network, the information economy coupling connection network has higher transmission efficiency. When the node is interrupted, this network has higher network efficiency and resilience than the other two networks. Beijing, which has the largest degree center value, also has the greatest impact on the network. When the nodes in Beijing are disconnected, the network efficiency drops to 0.1934. The top cities include Hengshui, Zhang Jiakou, and Chengde, and these cities have the least impact on the network efficiency of the information coupling network after failure (Figure 8C).

From the perspective of the spatial distribution of the three networks around Beijing, the transmission failure of the three networks is decreasing.

5 Conclusion

With the long-term impact of economic globalization, the ability of regional space to handle the impact and restore, maintain, or improve the characteristics and functions of the original system is crucial. As a new form of regional expression, building a complex urban network and evaluating the resilience of urban network structure is significant to promoting regional sustainable development. A safe urban development environment can promote the prosperity and vitality of the city. Based on the Baidu search index and social statistics, this paper constructs the information, economy, and information economy coupling network respectively. Then, the strength and centrality of network connection are analyzed, and the transmission of urban individuals and regional whole in hierarchy matching are measured and analyzed. The results show that:

1 The spatial distribution of economy, information, and economic information coupling network of the Jing-Jin-Ji Urban Agglomeration shows a spatial pattern with Beijing as the core and radiating outward. In the three networks, the connection strength is concentrated between Beijing, Tianjin, and Langfang, and mainly between Beijing-Tianjin and Beijing-Langfang. The connection strength between Tianjin and Langfang is relatively weak; Besides, due to the selection of the model, the information intensity between cities is not affected by distance, so the information connection intensity between cities is closer than the economic connection intensity, but the information connection intensity between developed cities is higher. Moreover, due to the influence of distance, the economic connection strength between cities is generally weaker than the information connection strength. Therefore, in the information economy coupling connection network, only Beijing-Tianjin and Beijing-Langfang are at the level of preliminary coordination. The overall coordination of the information economy network is poor. There is an imbalance in the strength of economic and information links.

2 From the perspective of the weighted degree distribution, the three networks are ranked as economic network > information network > information economy coupling network. The higher hierarchy of the economic and information networks will bring arrow cities with strong competitiveness to these two types of networks. The absolute core is Beijing, followed by Tianjin, Langfang, Cangzhou, and Tangshan. However, with a higher hierarchy, we should always be concerned with the impact and digestion ability of high-level networks in case of core node failure. The cities with balanced development of information economy are at a low level, and the core cities with balanced development have a low driving ability, but the resilience of the network is relatively good.

3 From the perspective of weighted correlation, the high-weighted cities in the three networks prefer to connect with the cities with a low weighting, that is, the network has different matching. The information network has the highest mismatch, followed by the information economy coupling network, and finally the economic connection network. Such nodes have a great impact on the circulation and dissemination of elements of the network. We should pay attention to strengthening the interaction ability with high-weighted nodes.

4 The transmission of the three connection network structures is in the order of information > economy > coupling network. Based on the results of centrality, hierarchy, matching, and transmission, Beijing and Tianjin have a great impact on the transmission of information and economic networks, and Beijing has the greatest impact on the coupling network.

6 Optimization suggestions

In the face of the overall economic downturn and the increasingly fierce competition and fluctuations in various fields of society, the stability, coordination, and sustainability of urban network operation and the ability to recover in time in the face of shocks are significant. Based on the three networks constructed, aiming at the three perspectives of network hierarchy, matching, and transmission, and starting from the resilience of the urban network structure, the urban network institutions are adjusted to strengthen the resilience of the network.

Hierarchical aspects. We should further strengthen the link between high-level cities and low-level cities. Combined with the work of non-capital function relief, we should radiate the functions of Beijing as a core city and strengthen the role of xiong'an new area. Meanwhile, we need to take xiong'an new area as an important starting point, revitalize the entire Beijing Tianjin Hebei Urban Network, flatten the network structure, pay attention to the radiation effect on low-value nodes, and strengthen the supporting role of each node of the urban network.

Matching. We should further improve and build the traffic road network to give full play to the role of core cities, drive the development of marginal cities, and strive to break the barriers of administrative boundaries. Meanwhile, the construction and improvement of the traffic network can further alleviate the excessive accumulation of resources in core cities so that cities on the edge of Beijing Tianjin Hebei can also access good technology and information resources. The outline of the 14th five-year plan mentions three circles, namely, the living circle 50 km away from Beijing. We need to focus on strengthening regional cooperation around Beijing, developing regional express lines, strengthening public service supporting facilities, and achieving the effect of urbanization within 100 km of the functional circle of xiong'an and Tianjin. Xiong'an new area is a concentrated carrier of Beijing's non-capital functions, and it is 150 km from Chengde, Tangshan, Cangzhou, Baoding, and Zhangjiakou, belonging to the industrial circle. We should make full use of the planning outline to strengthen the vulnerable nodes of the urban network and improve the resilience of the network.

In terms of network transmission, we should take Beijing as the center to radiate the driving ability of Beijing's core cities to the outside through scientific and technological innovation, cultural transmission, and other approaches, thus strengthening the driving ability and stability of Beijing's core nodes. Secondly, we can drive the cities on the edge of the Beijing Tianjin Hebei Urban Network with the help of the collaborative mechanism formed by transportation, industry, and ecological environment construction, thus improving the network transmission efficiency of the overall network and the network resilience of the Beijing Tianjin Hebei Urban Network.

Data availability statement

The original contributions presented in the study are included in the article/supplementary material, further inquiries can be directed to the corresponding authors.

Author contributions

YZ proposed the overall research program and the technical route, YY wrote and proofread the manuscript. SW was responsible for the communication and editing, and other academics did the data analysis.

Funding

This research was supported by the Major projects of National Social Science Fund (ID:20ZDA086), Fundamental Research Funds for the Capital University of Economics and

Business (ID: QNTD202009 and QNTD202209), Major project of Beijing Social Science Foundation (19ZDA03).

Conflict of interest

The authors declare that the research was conducted in the absence of any commercial or financial relationships that could be construed as a potential conflict of interest.

Publisher's note

All claims expressed in this article are solely those of the authors and do not necessarily represent those of their affiliated organizations, or those of the publisher, the editors and the reviewers. Any product that may be evaluated in this article, or claim that may be made by its manufacturer, is not guaranteed or endorsed by the publisher.

References

Arthur, S., Beckfield, J., and Sprague-Jones, J. (2010). Intercity relations and globalisation: The evolution of the global urban hierarchy, 1981—2007. *Urban Stud.* 47 (9), 1899–1923. doi:10.1177/0042098010372679

Batty, M. (2009). "Cities as complex systems: Scaling, interaction, networks, dynamics and urban morphologies," in *Encyclopedia of complexity and systems science*. Editor R. A. Meyers (Springer), 1041–1071.

Bombelli, A., Santos, B. F., and Tavasszy, L. (2020). Analysis of the air cargo transport network using a complex network theory perspective. *Transp. Res. Part E Logist. Transp. Rev.* 138 (C), 101959. doi:10.1016/j.tre.2020.101959

Chad, S., Sarah, W., Laura, D. V., Zuniga-Teran, A., Gerlak, A. K., Schoeman, Y., et al. (2018). Contributions of green infrastructure to enhancing urban resilience. *Environ. Syst. Decis.* 38 (8), 330–338. doi:10.1007/s10669-018-9702-9

Cohen, M. (2001). Urban assistance and the material world: Learning by doing at the world bank. *Environ. Urbanization* 13 (1), 37–60. doi:10.1177/095624780101300104

Crespo, J., Suire, R., and Vicente, J. (2013). Lock-in or lock-out? How structural properties of knowledge networks affect regional resilience? *J. Econ. Geogr.* 14 (01), 199–219. doi:10.1093/jeg/lbt006

Cutter, S. L., Kevin, D. A., and Christopher, T. E. (2014). The geographies of community disaster resilience. *Glob. Environ. Change* 24 (11), 65–77. doi:10.1016/j.gloenvcha.2014.08.005

David, R., Pavel, S., and Martin, H. (2019). Complex approach to assessing resilience of critical infrastructure elements[J]. *Int. J. Crit. Infrastructure Prot.* 25 (3), 125–138. doi:10.1016/j.ijcip.2019.03.003

Dixit, V., Verma, P., and Tiwari, M. K. (2020). Assessment of pre and post-disaster supply chain resilience based on network structural parameters with CVaR as a risk measure. *Int. J. Prod. Econ.* 227 (C), 107655. doi:10.1016/j.ijpe.2020.107655

Frost, I., and Podkorytova, M. (2018). Former soviet cities in globalization: An intraregional perspective on interurban relations through networks of global service firms. *Eurasian Geogr. Econ.* 59 (1), 98–125. doi:10.1080/15387216.2018.1506995

Gordon, P. (2010). Trajectories of North—south city inter-relations: Johannesburg and cape town, 1994—2007[J]. *Urban Stud.* 47 (9), 1985–2002. doi:10.1177/0042098010372681

Hallie, Eakin, Bojorquez-Tapia, L. A., Janssen, M. A., Georgescu, M., Manuel-Navarrete, D., Vivoni, E. R., et al. (2017). Opinion: Urban resilience efforts must consider social and political forces.[J]. *Proc. Natl. Acad. Sci. U. S. A.* 114 (2), 186–189. doi:10.1073/pnas.1620081114

Hanssens, H., Derudder, B., and Witlox, S. V. A. F. (2013). Assessing the functional polycentricity of the mega-city-region of central Belgium based on advanced producer service transaction links. *Reg. Stud.* 48 (12), 1939–1953. doi:10.1080/00343404.2012.759650

Huang, C. C., and Hu, B. (2014). Simulation modeling and analysis of the group relationship's resilience. *Chin. J. Manag. Sci.* 22 (S1), 686–690.

Hudec, O., Reggiani, A., and ŠiserováM, M. S. (2018). Resilience capacity and vulnerability:A joint analysis with reference to Slovak urban districts. *Cities* 73 (3), 24–35. doi:10.1016/j.cities.2017.10.004

Jabareen, Y. (2013). Planning the resilient city: Concepts and strategies for coping with climate change and environmental risk. *Cities* 31 (2), 220–229. doi:10.1016/j.cities.2012.05.004

Jiang, D. L., Sun, Y., Ren, H., Chen, Y. Y., and Zhang, Z. K. (2015). Analyses on the city network characteristics of middle Yangtze urban agglomeration based on Baidu index. *Resour. Environ. Yangtze Basin* 24 (10), 1654–1664.

Jin, G., Deng, X. Z., Zhao, X. D., Guo, B., and Yang, J. (2018). Spatiotemporal patterns in urbanization efficiency within the yangtze river economic belt between 2005 and 2014. *J. Geogr. Sci.* 28 (8), 1113–1126. doi:10.1007/s11442-018-1545-2

Li, Y., Shao, H., Jiang, N., Shi, G., and Cheng, X. (2018). The evolution of the urban spatial pattern in the yangtze river economic belt: Based on multi-source Remote sensing data. *Sustainability* 10 (8), 2733–2753. doi:10.3390/su10082733

Lin, P. F., Weng, J. C., Fu, Y., and Yin, B. C. (2019). Structure characteristics of rail transit weighted network based on smart card data. *J. Jilin Univ. Eng. Technol. Ed.* 50 (03), 1–7.

Liu, X., Derudder, B., Witlox, F., and Hoyler, M. (2014). Cities as networks within networks of cities: The evolution of the city/firm-duality in the world city network, 2000-2010. *Tijdschr. Econ. Soc. Geogr.* 105 (4), 465–482. doi:10.1111/tesg.12097

Moser, S., Meerow, S., Arnott, J., and Jack-Scott, E. (2019). The turbulent world of resilience:Interpretations and themes for transdisciplinary dialog[J]. *Clim. Change* (1), 1–20. doi:10.1007/s10584-018-2358-0

Niu, H. N., Meng, Q. M., Hu, Q. C., and Chen, Y. C. (1998). Economic relation analysis between regions and Gansu province and their surrounding areas. *Econ. Geogr.* 18 (03), 51–56.

Noura, A., Talalal, Al-A., Mohamed, H., Ahsan, R., and Alrubkhi, A. (2020). Changing urban ecology a challenge for coastal urban resilience:A study on Muscat [J]. *Environ. Urbanization ASIA* 2 (1), 10–28. doi:10.1177/0975425320906307

Pereira, R. A. O., and Derudder, B. (2010). Determinants of dynamics in the world city network, 2000-2004. *Urban Stud.* 47 (9), 1949–1967. doi:10.1177/0042098010372678

Pizzo, B. (2015). Problematizing resilience: Implications for planning theory and practice[J]. *Cities* 43, 133–140. doi:10.1016/j.cities.2014.11.015

Polèse, M. (2015). *The resilient city: On the determinants of successful urban economies.*

Vinciguerra, S., Frenken, K., and Valente, M. (2010). The geography of internet infrastructure: An evolutionary simulation approach based on preferential attachment. *Urban Stud.* 47 (9), 1969–1984. doi:10.1177/0042098010372685

Vijaya, Dixit, Priyanka, Verma, and Manoj Kumar, Tiwari (2020). Assessment of pre and post-disastersupply chain resilience based on network structural parameters with CVaR as a riskmeasure[J]. *International Journal of Production Economics* 227, 107655–107655. doi:10.1016/j.ijpe.2020.107655

Wang, X., Wu, D. T., and Wang, H. Q. (2006). An attempt to calculate economic links between cities. *Urban Stud.* 03, 55–59.

Xing, Z. C., Wang, J. G., and Zhang, J. (2018). Total-factor ecological efficiency and productivity in yangtze river economic belt, China: A non-parametric distance function approach. *J. Clean. Prod.* 200, 844–857. doi:10.1016/j.jclepro.2018.08.015

Xiong, L. F., Zhen, F., Wang, B., and Xi, G. L. (2013). The research of the Yangtze River delta core area's city network characteristics based on Baidu index. *Econ. Geogr.* 33 (07), 67–73.

Yang, Y., Leng, B., Tan, Y., and Arthur, S. A. (2011). Re-view on world city studies and their implications in urban systems. *Geogr. Res.* 30 (6), 1009–1020. doi:10.11821/yj2011060005

Yang, Z., Lin, A., He, L., Zhou, Z., and Yuan, M. (2020). Spatiotemporal dynamics and driving forces of urban land-use expansion: A case study of the yangtze river economic belt, China. *Remote Sens.* 12 (2), 287. doi:10.3390/rs12020287

frontiers | Frontiers in Ecology and Evolution

TYPE Original Research
PUBLISHED 01 November 2022
DOI 10.3389/fevo.2022.962299

Check for updates

OPEN ACCESS

EDITED BY
Ding Ma,
Shenzhen University, China

REVIEWED BY
Prof-Maged Marghany,
Syiah Kuala University, Indonesia
Janaka Bamunawala,
University of Moratuwa, Sri Lanka

*CORRESPONDENCE
Yuhan Shao
shaoyuhan@tongji.edu.cn

SPECIALTY SECTION
This article was submitted to Environmental Informatics and Remote Sensing, a section of the journal Frontiers in Ecology and Evolution

RECEIVED 06 June 2022
ACCEPTED 06 October 2022
PUBLISHED 01 November 2022

CITATION
Yin Y, Shao Y, Lu H and Han Y (2022) Environmental drivers of the vital urban coastal zones: An explorative case study based on the data-driven multi-method approach. *Front. Ecol. Evol.* 10:962299. doi: 10.3389/fevo.2022.962299

COPYRIGHT
© 2022 Yin, Shao, Lu and Han. This is an open-access article distributed under the terms of the Creative Commons Attribution License (CC BY). The use, distribution or reproduction in other forums is permitted, provided the original author(s) and the copyright owner(s) are credited and that the original publication in this journal is cited, in accordance with accepted academic practice. No use, distribution or reproduction is permitted which does not comply with these terms.

Environmental drivers of the vital urban coastal zones: An explorative case study based on the data-driven multi-method approach

Yuting Yin[1], Yuhan Shao[1]*, Huilin Lu[1] and Yun Han[2]

[1]Department of Landscape, College of Architecture and Urban Planning, Tongji University, Shanghai, China, [2]Department of Urban Planning and Design, College of Architecture, The University of Hong Kong, Hong Kong, Hong Kong SAR, China

Success in delivering dynamic urban coastal zones is considered essential, as it brings enormous opportunities to the social, economic, ecological, and cultural development of the cities in addition to benefitting the coastal zones. However, the environmental drivers contributing to urban coastal zone vitality remain uncertain due to unclarified spatial boundaries and the influences of diverse characteristics from surrounding contexts. This study aims at exploring environmental drivers that can vitalize urban coastal zones and can inform an effective way to instruct design procedures. It sets out from clarifying the spatial boundaries of urban coastal zones and emphasizing the mutual connections among its spatial components. A data-driven multi-method approach is used to analyze spatial forms, traffic organizations, land uses, landscape characteristics, and coastal functions of the eight typical coastal cases selected in different countries. Results suggested that six typical coastal zone types can be classified based on landscape characteristics and coastal functions, while the other vitality-related aspects, spatial forms, traffic organizations, and land uses are analyzed to imply design requirements for each type. It is found that requirements on vitality-related aspects of the six types evidently vary with the coastal functions, but there are similarities among the types with similar landscape characteristics.

KEYWORDS

urban coastal zone vitality, environmental drivers, typology, design implications, data-driven analysis

Introduction

The coastal zone is where the terrestrial environment mutually influences marine environments (Carter, 2013). In response to global issues related to coastlines, relevant studies mostly contribute to projecting sea-level rise, mitigating storm hazards (Godschalk et al., 1989), monitoring shoreline erosion (Maged et al., 2010; Marghany, 2014), controlling waste disposal into coastal environments (Council, 1993), exploitation of coastal energy (Gill, 2005), and adapting climate change. Besides sustainable and ecological considerations, the coastal zones are also in possess of huge construction and

development potentials—especially those located within urban areas to deliver dynamics to the coastal zones, as well as to bring enormous opportunities for the social, economic, ecological, and cultural development of the cities (Martínez et al., 2007; Barragán and De Andrés, 2015).

Nevertheless, the current environmental drivers contributing to the vitality of urban coastal zones remain uncertain, not only because the spatial boundary of urban coastal zones under urban design context has not been clarified and united but also the importance of urban coastal zones as social-spatial edges influencing both hinterlands and sea areas has not been fully understood. This study proposes that the delivery of urban coastal zone vitality should consider the waterfronts, the connected hinterlands, and the inshore sea areas as a whole; more importantly, emphasis should be placed on their mutual connections. A data-driven multi-method approach is used to explore environmental drivers in relation to the vitality of coastal cases selected in countries with evidently different geographical, landscape, morphological, and spatial attributes. Vitality contributors are then concluded on a typological basis of classifying urban coastal zones according to their contextual characteristics, and design instructions were then proposed accordingly.

The vitality of urban coastal zones

When coastal zones traverse cities, they usually trigger a highly concentrated area of local population and economy—areas with the most concentrated contradictions between land and marine development (Papatheochari and Coccossis, 2019). However, as a result of the different paths in coastal zone research, there is currently a lack of consistent spatial definitions in planning and management implementations. Marine-centered coastal zone planning tends to define rigid protection areas from the perspective of ecological protection (Duck, 2012) with scarce planning guidelines and instructions for the waterfronts and hinterlands; land-focused coastal zone planning mainly responds to local development requirements and merely considers the sea as a landscape resource (Ioppolo and Saija, 2013). No efficient way has been proposed to reflect the proper positioning and importance of urban coastal zones to facilitate local vitality and effectively connect hinterlands with the sea. To design dynamic urban coastal zones, it is crucial to begin with the planning and design perspective of exploring the definition of urban coastal zones and the social-spatial connections between its components must be investigated.

Coastal zone vitality is a design arena emerging only recently with the increasing emphasis on coastal development, but another similar concept, waterfront vitality, has long been regarded as an important planning focus in urban areas (Wakefield, 2007). The classic vitality theory formed by Jacobs (1961), Lynch (1984), and Gehl (1987) claimed three important factors determining urban vitality—people, activity, and space (Li et al., 2022). And spatial affordance under this context is revealed by the opportunities to attract different types of people to participate in different activities at different times of the day (Li et al., 2016). Thus, the vitality of waterfront areas can also be reflected through the interactions between human activities and physical environments (Li et al., 2022). Existing evidence has confirmed the effects of spatial form, traffic organization, landscape, cultural characteristics, and land uses on waterfront vitality (Norcliffe et al., 1996; Da and Xu, 2016). With respect to spatial form, block sizes (Sha et al., 2014), building densities (Bunce, 2011), and other textural attributes are found to be relevant; road networks with higher levels of integration (Wang F. et al., 2020), accessibility (Othman et al., 2021) and intersection density (Yang et al., 2018) are also positively related to waterfront vitality. In terms of the land use aspect, the mixed levels of land use (Lehrer and Laidley, 2008) and specific functions such as commercial activities (Hagerman, 2007) are proved to be influential, while vitality-related landscape characteristics include: openness (Sairinen and Kumpulainen, 2006), aesthetic and cultural value (Hurley, 2006), and the number and quality of landmarks (Gotham, 2002).

Many attempts have been made to explore how vitality can be generated within waterfront areas through planning and design interventions. These primarily fall into two categories. The first is the use of qualitative methods such as questionnaires (Woo et al., 2017), activity notations (Latip et al., 2012), and behavior mapping (Mansournia et al., 2016) to observe and compare the distribution of human activities and physical environment attributes across different sites. For example, Unt and Bell (Unt and Bell, 2014) used site observations and behavior mapping to compare waterfront spatial usage before and after small design interventions. Another approach is the use of quantitative methods; this normally involves the collection and analysis of data describing waterfront characteristics (Romero et al., 2016). The advancement of information technology in recent years—particularly the widely used big data and the advancement of location-based services—has provided technical support for extensive and in-depth investigations of the spatial-temporal characteristics of people and activities within urban waterfront areas. These newly emerged methods have been used by many researchers to measure the vitality of waterfront public spaces and disclose the relationships between environmental characteristics and spatial vitality (Liu et al., 2021; Niu et al., 2021). Yu et al. (2019) proved that there is a high spatial coupling between spaces with high levels of vitality and actual aggregation of activities using the open-sourced big data of streetscape images. Besides, there are also studies utilizing geographical information systems (GISs) to classify and identify coastal zones based on high-precision satellite maps (Balasubramanian et al., 2022; Thirumurthy et al., 2022).

Though efforts have been made to investigate the geospatial (i.e., locations (Yang and Shao, 2018), traffic connections

(Wang F. et al., 2020), spatial compositions (Delclòs-Alió and Miralles-Guasch, 2018), and social dimensions such as symbolic identities (Hurley, 2006), human activities (Hoyle, 1999), and functions (Latip et al., 2012) that lead to the vitality of urban waterfronts, they can provide limited implications to coastal zones because no specific standard has been set to indicate the form such coastal zones should take. Urban coastal zone vitality cannot be achieved with the same methods used for waterfront vitality design due to their apparent differences. First, urban coastlines can be far longer than riversides and lakesides, and their characteristics may vary with the different contexts surrounding them. Thus, the successful experience of delivering one dynamic coastal zone cannot be applied to others without the support of the typological research basis and design implications summarized accordingly. Moreover, studies based on qualitative methods are limited in their exploration of vitality dimensions and sample sizes, while the data-based quantitative analysis approaches often ignore the role of local contexts in influencing coastal zone vitality. Therefore, practical instructions for designing vital urban coastal zones can hardly be developed without an analytical framework that is founded on typological thinking and integrates both qualitative and quantitative aspects.

This study, therefore, intends to formalize the concept of urban coastal zone vitality starting with clarifying its spatial components and emphasizing their interactive influences. The descriptive statistics analysis was used together with the case study to identify relevant environmental cues from urban coastal zone case studies selected in different countries since they are efficient in handling both qualitative and quantitative data. A qualitative analysis of landscape characteristics and coastal function aspects was first conducted to classify urban coastal zones, while a quantitative analysis of spatial form, traffic organization, and land use aspects was implemented to disclose the causes of coastal zone vitality. This study then explored design implications to inform how vitality can be delivered, while remaining responsive to local contexts for each coastal zone type and also adaptable to other urban coastal zones with similar characteristics.

Materials and methods

Selecting urban coastal zones cases

Two rounds of the case study selection process were conducted. The first round involved locating potential coastal zone cases through an extensive search of design and travel websites, design review articles, and related books. A total of 15 constructed coastal zone design case studies were identified and presented to a group of 10 expert researchers specializing in landscape, urban design, and architecture. Selection was based on the following review criteria: (1) the selected cases should be known for their vitality, attractiveness, and high visitor rates; (2) the selected case study areas should be fully constructed and developed with similar levels of prosperity in the hinterlands; and (3) the selected cases should have diverse coastal characteristics containing as many landscape and function types as possible. As a result, eight coastal zones with different orientations toward the sea were selected for further analysis, including Vancouver, Chicago, Toronto, Barcelona, Zhuhai, Qingdao, Shenzhen, Haikou, and Dalian (Figure 1).

Determining coastal zone vitality indicators

Eleven indicators were selected from existing theoretical and empirical literature on waterfront vitality, coastal zone qualities, and the overlaps between environmental vitality and urban coastal zones; the definition (Table 1) and calculation formula of each indicator were also referred from previous studies. Among these, seven indicators measure quantitative vitality aspects of the selected coastal zone cases, including spatial forms, traffic organizations, and land use conditions, while the other four describe the landscape and functional attributes from a qualitative perspective.

Analyzing coastal zone vitality indicators

Quantitative indicators analysis methods

The quantitative attributes related to urban coastal zone vitality include spatial form, traffic organization, and land uses. Quantitative data were mostly retrieved from national statistics and Google dataset updated around the year 2019 (Table 2). The result for each quantitative indicator was calculated and visualized using the ArcGIS platform to reveal the coastal zone characteristics.

The aspect of spatial form is described with three indicators—development density, building density, and building heights—and can be calculated using the three-dimensional spatial data. Building density and development intensity reveal the spatial utilization in horizontal and vertical directions, respectively (Hoppenbrouwer and Louw, 2005). An appropriate level of building density and development intensity can bring vitality to the coastal zone by shaping the interface of public spaces to attract social activities (Liu et al., 2021). Mathematically, the ***development density*** [refer to Eq. (1)], ***building density*** [refer to Eq. (2)], and ***building height*** [refer to Eq. (3)] can be defined as follows:

$$FAR = Sgf \div S \quad (1)$$

Where,

FAR: the development density of the coastal zone

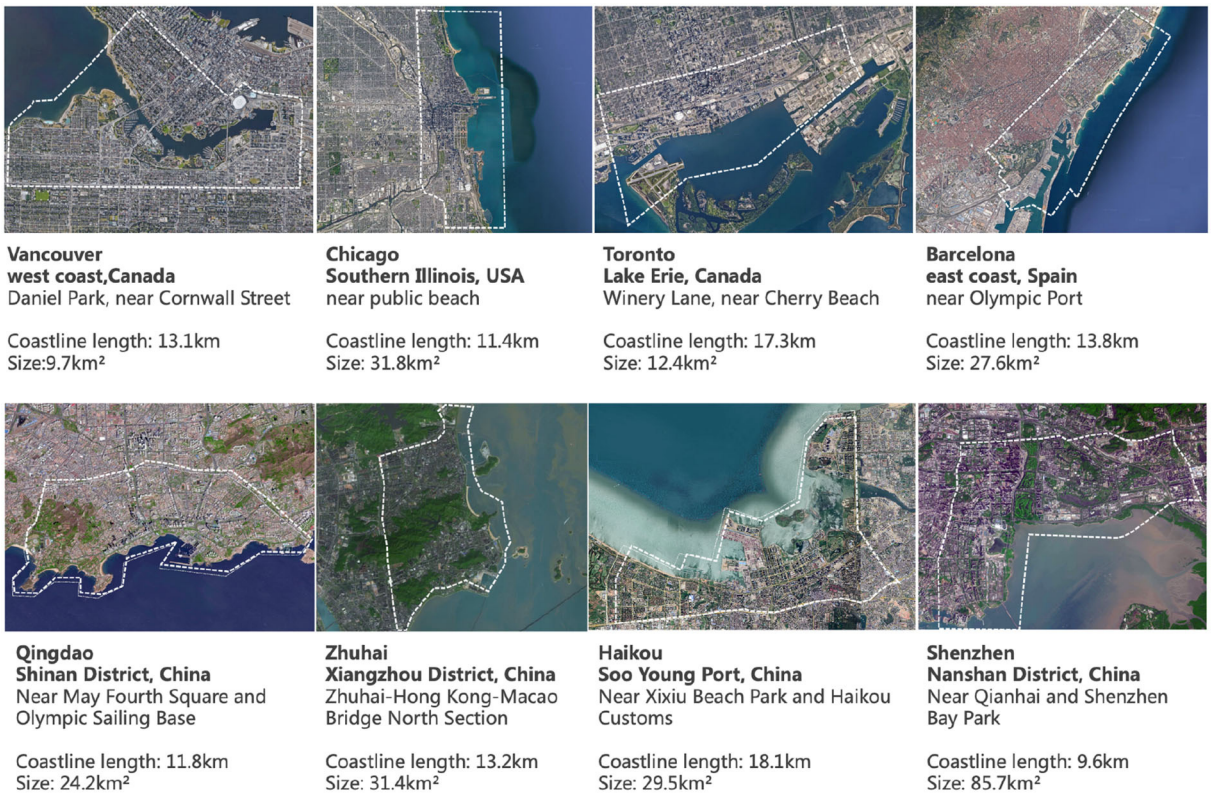

FIGURE 1
Site conditions of the eight selected coastal zone cases.

Sgf: the total floor acreage of buildings in the coastal zone
S: the total acreage of the coastal zone

$$BCR = Sba \div S \tag{2}$$

Where,

BCR: the average building density of the coastal zone
Sba: the vertical projection acreage of buildings in the coastal zone
S: the total acreage of the coastal zone

$$H = H_{avg} \tag{3}$$

Where,

H: the building height
H_{avg}: the average height of buildings within the block

The aspect of traffic organization encompasses the density of road networks and intersections and the sizes of street blocks. Road network density, intersection density, and block size can efficiently indicate whether the local traffic organization supports the effective development of coastal zones. Road network density illustrates the level of accessibility within the area and to other districts (Wang M. et al., 2020); the intersection density and block size are normally used to show how welcoming this area are to pedestrians (Jin et al., 2017) and how the spatial connectivity is handled in the coastal zone, respectively (Boulos, 2016). Based on the road network data obtained from Google Open Street Map, typology networks were built for the eight case studies to perform a large-scale calculation on urban road network indicators. Among which, ***road network density*** [refer to Eq. (4)], ***intersection density*** [refer to Eq. (5)], and ***block size*** [refer to Eq. (6)] are defined as below:

$$D = L \div A \tag{4}$$

Where,

D: the road network density
L: the total length of the road network, including the trunk roads, the collector roads, and the branch roads
A: the total land acreage of the coastal zone

$$I = R_i \div A \tag{5}$$

Where,

I: the intersection density
R_i: the number of intersections
A: the total land acreage of the coastal zone

$$L = L_{avg} \tag{6}$$

TABLE 1 Environmental indicators related to urban coastal zone vitality.

	Vitality-related Aspects	Indicator	Definition	Unit	Sources
Quantitative Analysis Indicators	Spatial form	Development density	The proportion of constructed or developed area to the total area.	km^2/km^2	Desfor and Jørgensen, 2004; Long and Huang, 2019
		Building density	Ratio of total floor area to street block area.	km^2/km^2	
	Traffic organization	Road network density	The length of road network to the acreage of the area.	km/km^2	Sairinen and Kumpulainen, 2006; Li et al., 2020; Othman et al., 2021
		Intersection density	The number of road intersections.	per km^2	
		Block size	The average size of street blocks.	ha	
	Land use	Functional diversity	The number of subdivided land units for mixed uses.	/	Im and Choi, 2019
		Proportion of specific functions	The proportion of certain types (such as commercial activities) of land use function.	/	
Qualitative Analysis Indicators	Landscape characteristic	Waterfront features	The natural characteristics of the waterfront area.	/	Hurley, 2006; Xie and Gu, 2015; Da and Xu, 2016
		Local identities	Sense of place, local cultural, historic spirit.	/	
	Costal function	Waterfront functions	Functional composition of the coastal zone.	/	
		Hinterland functions	Functional composition of the connected hinterlands.	/	

Where,

L: the block size

L_{avg}: the land acreage of block

The aspect of land use is described with functional diversity and specific functions. Twelve points of interests (PoIs) categories were obtained from the Google dataset, including: transportation, healthcare, sports leisure, life convenience, culture and education, shopping and dining, hotels, the scenic spot, commercial housing, finance and insurance, government agencies, and business companies. These were then sorted into four major categories including employment, living, recreation, and transportation, and then visually mapped accordingly. The mix-used functions that reflect the type of diverse facilities and the proportion of each type of facility concurrently were calculated through the entropy value (Jiang et al., 2022). PoIs with specific functions, such as catering services (Liu et al., 2018) and sport leisure facilities (Mu et al., 2021) that can contribute to spatial vitality, were also calculated. Hence, ***functional diversity*** [refer to Eq. (6)] and ***proportion of specific functions*** [refer to Eq. (7)] are defined as follows:

$$FM = -\sum (Pi \times InPi) / L \tag{7}$$

Where,

i =1, ..., n

FM: the functional diversity

n: the number of PoIs categories within a block in the coastal zone

Pi: the proportion of the i type of PoIs

L: the length of the block

$$BUM = -(\sum pi \times In(pi)) \div In(n) \tag{8}$$

where,

BUM: the proportion of specific functions

n: the number of PoIs categories within a block in the coastal zone

TABLE 2 Quantitative indicators and their related data sources.

Vitality-related quantitative aspects	Indicator	Target data	Data sources
Spatial form	Development density	Building data	Building data in Chinese cities: Beijingcitylab.com Building data in other cities: Github.com/Microsoft/USBuildingFootprints
	Building density		
Traffic organization	Road network density	Road network data	Openstreetmap.org
	Intersection density		
	Block size	Block data (clipped by road network)	
Land use	Functional diversity	Point of interest data (PoIs)	PoIs in Chinese cities: Lbs.amap.com PoIs in other cities: Foursqure.com/products/places-api
	Proportion of specific functions		
	Hinterland functions		

Pi: the proportion of the *i* type of PoIs.

Qualitative indicator analysis methods

Four qualitative indicators, waterfront features, local identities, waterfront functions, and hinterland functions, responsible for coastal zone vitality were analyzed for two purposes. The first was to classify urban coastal zones so that the underlying reason for bringing vitality could be explored and the design implications could be developed on a typological basis. Among the four indicators, the functions of the waterfront areas should be regarded as the results of the waterfront features and hinterland functions. Also, local identities are represented by diverse historical and cultural resources which can hardly be set as a classification standard.

Therefore, waterfront features and hinterland functions are used as criteria for categorizing coastal zone types, while local identity and waterfront functions are analyzed together with quantitative indicators to develop design instructions on delivering vitality for each type. The same group of experts previously noted conducted traditional design analysis on the eight case study sites through photos, online materials, and open-sourced records to discuss qualitative results on the four vitality-related indicators.

Results

Coastal zone vitality presented by qualitative and quantitative indicators

Descriptive analysis of qualitative indicators

The eight cases are coastal cities located between latitudes 20 and 50°N. Among these, Vancouver is the political, cultural, tourism, and transportation center of western Canada and has a waterfront characterized by public spaces, such as beaches and squares, and the hinterland functions are mainly residences and business offices. Chicago has a coastline toward the east with waterfront leisure space composed of beaches and green spaces, with evident industrial cultural characteristics. Its hinterland has commerce and office buildings, as well as residences and industrial facilities. Toronto, a Northwest coast city of Canada, waterfront partly retains the reefs as the dominant natural features, while the rest of the waterfront largely handles public life with squares; hinterland functions are composed of commerce, business, and industries. Barcelona has a coastal zone dominated by ports and beaches, and its hinterland functions are mainly for living and commercial purposes.

Four Chinese cases are mainly coastal cities in its eastern region. Among these, Qingdao is in the southeast of the Shandong Peninsula, bordering the Yellow Sea on its east and south sides. Its coastal zone is mostly composed of beaches, ports, and reefs, and the hinterland functions include residences and commerce. Shenzhen and Zhuhai are coastal cities located in the south of Guangdong province, adjacent to the South China Sea. The waterfront of Shenzhen is dominated by greenways, reefs, and beaches, and its hinterland functions include business, industries, and residences. In Zhuhai, reefs and beaches are the major characteristics of the waterfront, with residence and office buildings as hinterland compositions. Haikou is in the northern part of Hainan Island, close to the South China Sea, and its waterfront contains green spaces, ports, beaches, and reefs. The major hinterland functions of Haikou are living and services, with a limited proportion of commerce and business.

Qualitative analysis results on the eight coastal cases are shown in Figure 2.

FIGURE 2
Qualitative analysis on the eight case study sites. ("▬ ▬ ▬" means reef, "▬ ▬ ▬" means port, "▬ ▬ ▬" means square/trail, "▬ ▬ ▬" means green spaces, "▬ ▬ ▬" means beach, "▬" means living and services, "▬" means industries and production, and "▬" means commercial, cultural, and tourism).

Descriptive analysis of quantitative indicators

Numerous evidence suggests that an appropriate level of development density can facilitate urban vitality (Dovey and Pafka, 2014). A low level of development density has difficulty in supporting the aggregation of urban functions (Jiao, 2015) and the organization of multi-mode public transportation (Gharaibeh et al., 2022); this could impede commercial and social activities. People are also unlikely to use coastal zones when development density is too high, since the densified population and the oppressive building heights would negatively influence their perceived sense of comfort (Lan et al., 2021).

Figure 3 illustrates the development density analysis results of the eight case study sites. It is reflected that the overall mean density of the eight case study sites is relatively low, with a range between 1.0 and 4.0 km^2/km^2. Shenzhen has the highest development density (8.5 km^2/km^2), and the lowest is Toronto (1.2 km^2/km^2). The plot ratios of certain individual plots in Chicago are high, but the overall mean value still stays at a low level (1.8 km^2/km^2).

The vitality indicator of building density describes the spatial form aspect that can reveal the accessibility and availability of open spaces within the coastal zone (Ye et al., 2018). Building density should also be maintained at a moderate level to provide sufficient opportunities for the survival and lushness of open spaces, as well as to provide spaces for the elaborate design of surrounding landscapes. However, a too low or too high level of building density may either lead to unnecessary waste of land uses or uncomfortable human perception (Chen et al., 2022b). The analysis of the eight case study sites found that the building density of Barcelona (0.9 km^2/km^2) is the highest and Haikou (0.2 km^2/km^2) is the lowest, with the average density of all eight sites staying between 0.25 and 0.4 km^2/km^2 (Figure 4).

Among the three traffic organization indicators, a high level of road network and intersection density has been proven to be positively related to spatial vitality (Long et al., 2019). Figure 5 indicates the road network density analysis results with an average appeared to be 13.0–18.0 km/km^2. The road network density of Barcelona and Chicago reaches over 22.0 km/km^2, but the highest density in Chinese sites is only 17.5 km/km^2 (Qingdao). The site with the lowest road network density among all case study sites is Shenzhen (8.5 km/km^2). As for the intersection density results presented in Figure 6, Toronto (105.0 per km^2) ranks as the highest, while Shenzhen (9.5 per km^2) and Chicago (10.0 per km^2) have the fewest intersections within the coastal zones. The mean intersection density of the eight sites is 20.0–55.0 per km^2.

Small size (around 25.0 ha) of street blocks is widely encouraged (Ewing et al., 2016), since existing evidence indicates blocks at this scale can effectively improve local vitality by enhancing spatial connections (Zhang et al., 2021), encouraging social life at street edges (Yin and Wang, 2016), promoting mixed land uses (Long et al., 2019), and providing comfortable walking experiences (Hassan and Elkhateeb, 2021). Results show that all eight case study sites have block sizes under 25.0 ha, with an average of less than 3.0 ha (Figure 7). Chinese coastal zones have relatively larger block sizes compared to the others, especially in Shenzhen (12.5 ha) and Haikou (11.0 ha; Figure 7).

Functional diversities and the proportion of specific functions were used to indicate the land use aspect of coastal vitality. A moderate level of mixed functions in a

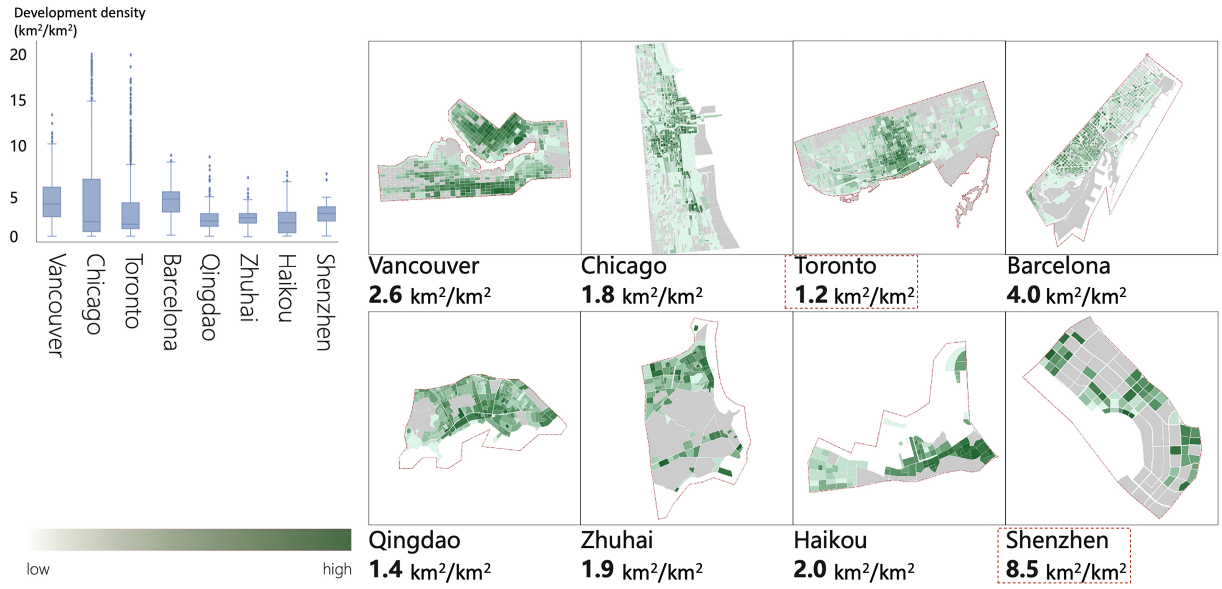

FIGURE 3
Development density analysis of the eight case study sites.

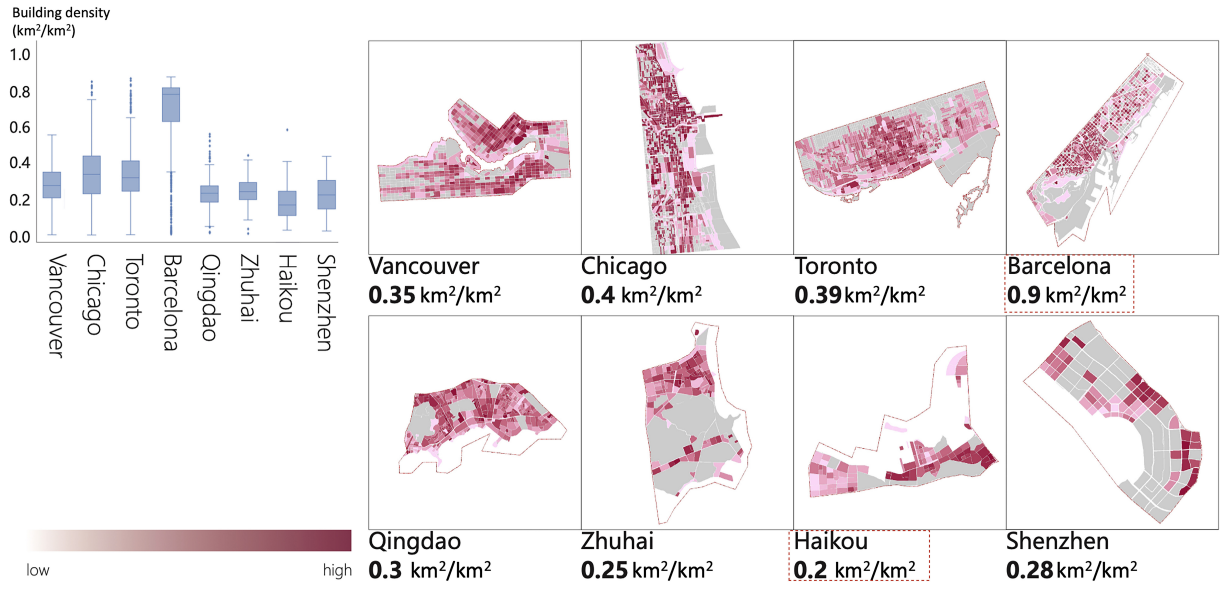

FIGURE 4
Building density analysis of eight case study sites.

block can provide residents with convenient life services and encourage walking activities to enhance the vitality within the area (Im and Choi, 2019). Results in Figure 8 suggested that the overall functional mixing value of Barcelona ranks highest (7.7%), followed by Chicago (7.3%), Qingdao (7.2%), and Zhuhai (6.8%). Functional diversities of the other four sites, however, are relatively low, with an average value between 3.0 and 8.0% (Figure 8). Another indicator in this aspect, the proportion of specific functions, is used to reflect the main functional attributes of blocks (Chen et al., 2022a). The analysis results reveal that most blocks within coastal zones of Vancouver, Chicago, Toronto, and

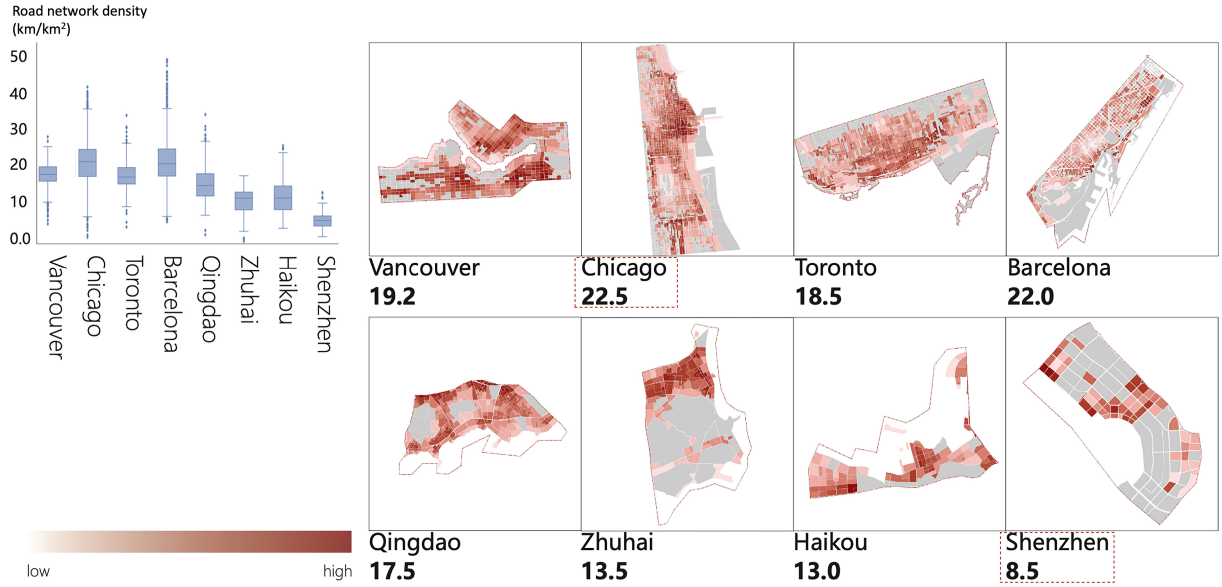

FIGURE 5
Road network density analysis of eight case study sites.

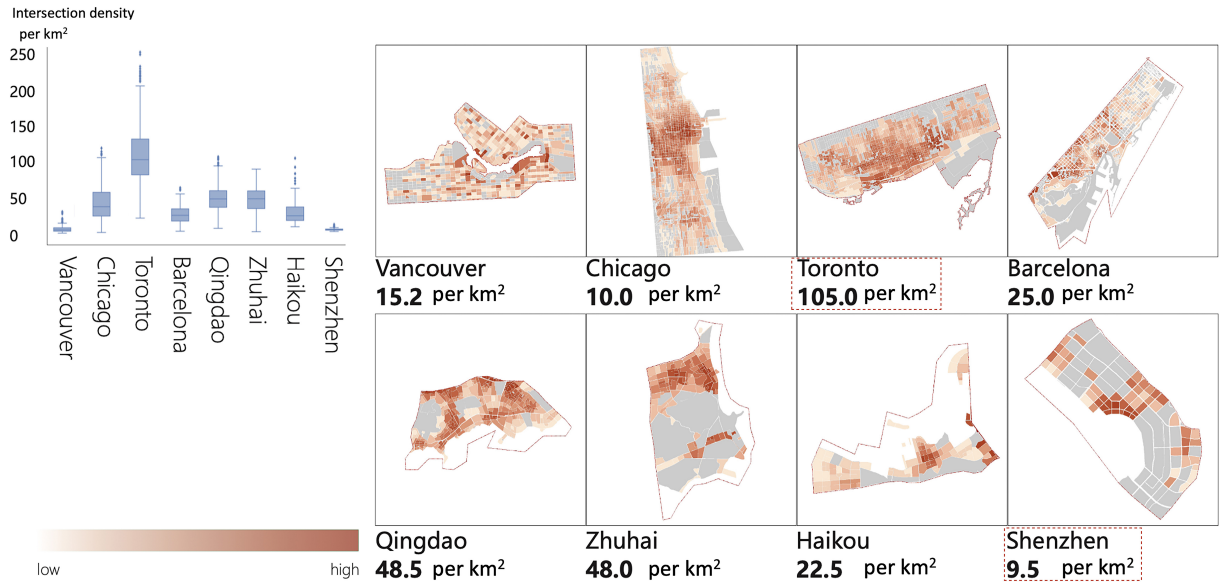

FIGURE 6
Intersection density analysis of the eight case study sites.

Barcelona are dominated by residences and corresponding living and service functions, while in Qingdao, Shenzhen, and Haikou, the proportion of employment functions is distinctly higher than residential and recreational functions (Figure 9).

Quantitative analysis results of the selected eight case study coastal zones are summarized in Table 3.

Classifying urban coastal zones based on qualitative analysis results

Urban coastal zones have different landscape characteristics due to their different contexts, such as geographical locations, climates, topography, and geomorphology. Waterfront features of the case study sites can be divided into soft and hard types;

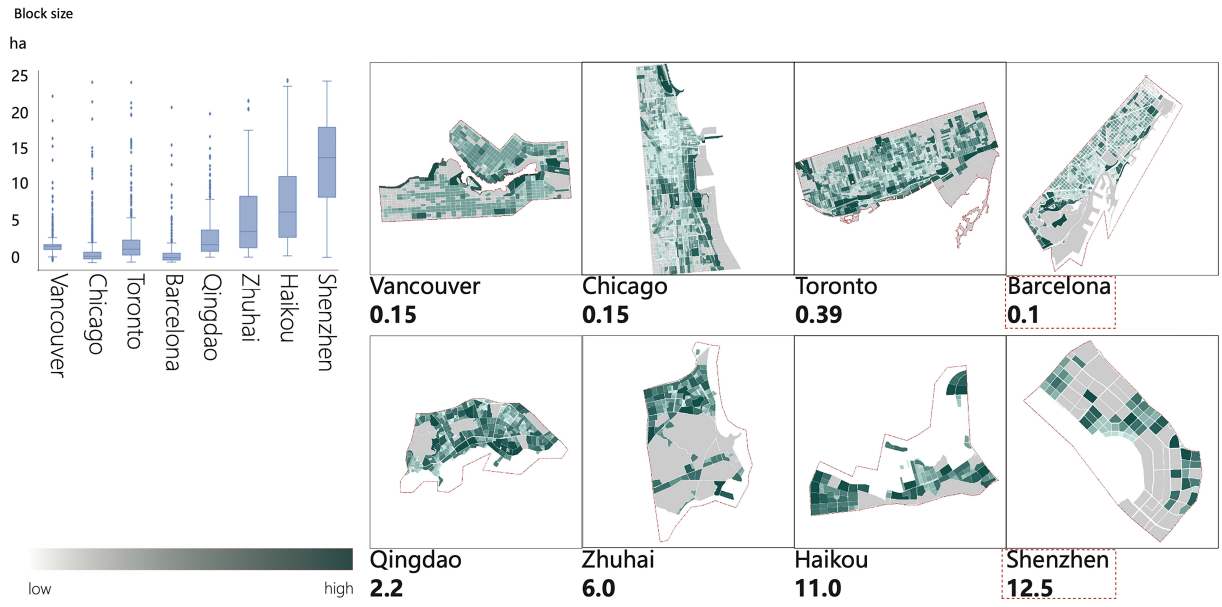

FIGURE 7
Block size analysis of the eight case study sites.

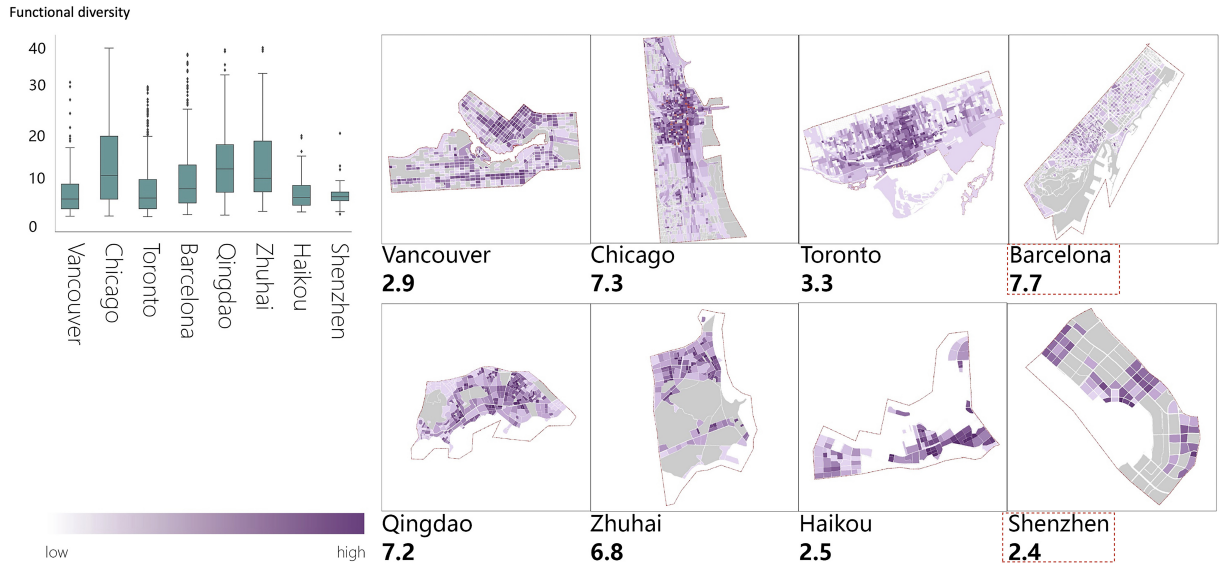

FIGURE 8
Functional diversities in the eight case study sites.

the soft types are those dominated by natural elements like beaches and green spaces, while the hard types are mainly dominated by ports, roads, squares, or reefs. Within hinterland functions, there are three basic types include living and services, industries and production, and commercial, cultural, and tourism. Through the combinative considerations of waterfront features and hinterland functions, urban coastal zones are classified into six major types (Figure 10); a hard waterfront with living and services as the major hinterland functions (H1), a hard waterfront with industries and production as the major hinterland functions (H2), a hard waterfront with commercial, cultural and tourism as the major hinterland functions (H3), a soft waterfront with living and services as the major hinterland functions (S1), a soft waterfront with industries and production

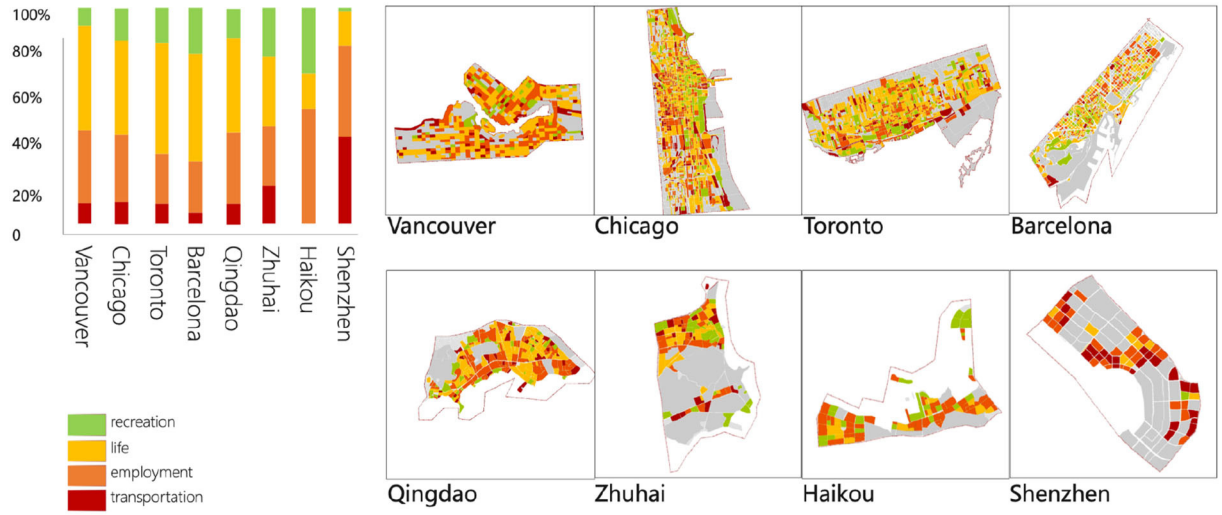

FIGURE 9
The proportion of specific functions in the eight case study sites.

TABLE 3 The summary of quantitative analysis results of the selected eight case study coastal zones.

	Vancouver	Chicago	Toronto	Barcelona	Qingdao	Zhuhai	Haikou	Shenzhen
Development density (km^2/km^2)	2.6	1.8	1.2	4.0	1.4	1.9	2.0	8.5
Building density (km^2/km^2)	0.4	0.4	0.4	0.9	0.9	0.3	0.2	0.3
Block size (ha)	0.2	0.2	0.4	0.1	2.2	6.0	11.0	12.5
Road network density (km/km^2)	19.2	22.5	18.5	22.0	17.5	13.5	13.0	8.5
Intersection density (per km^2)	15.2	10.0	105.0	25.0	48.5	48.0	22.5	9.5
Functional diversity (%)	2.9	7.3	3.3	7.7	7.2	6.8	2.5	2.4

as the major hinterland functions (S2), and a soft waterfront with commercial, cultural and tourism as the major hinterland functions (S3). The classification results of the selected eight coastal study sites are summarized in Table 4.

Design implications for vital urban coastal zones

The results of the quantitative and qualitative analysis disclosed the environmental drives of urban coastal zone vitality (Table 5), which informed a way to develop design implications, respectively, for the six coastal types.

The H1 type is coastal zones with hard waterfront characteristics, such as reefs, ports, and squares, and hinterland functions are mostly composed of living and services. Green spaces and squares that can manage public life are recommended as the major waterfront functions. For this type of coastal zones, a relatively wide range of development density of 1.0–6.0 km^2/km^2 is allowed for delivering vitality but building density should be controlled within 0.2–0.4 km^2/km^2. Road network density and intersection density can also be flexible in the design requirements. Results indicate that 12.0–20.0 km/km^2 of road network density and a range of 15.0–50.0 per km^2 intersection density are beneficial to promote local vitality for this type. The block size in this coastal zone is encouraged to be around 1.0–3.5 ha, and functional diversity is encouraged to be within 2.2%—8.2%.

The H2 type is coastal zones characterized by hard waterfronts with industries and production as the major hinterland functions. The waterfronts can contain public spaces, and ports and other industrial heritages should be kept as landmarks. Research findings suggest development density should be controlled at under 1.8 km^2/km^2, and the building density should be between 0.2 and 0.3 km^2/km^2 to enhance the vitality of coastal zones. The control over intersection density can be loose (15.0–65.0 per km^2), but a higher level of road network density (10.0–15.0 km/km^2) is suggested. The acreage of block sizes between 3.0 and 8.0 ha and a low level of functional

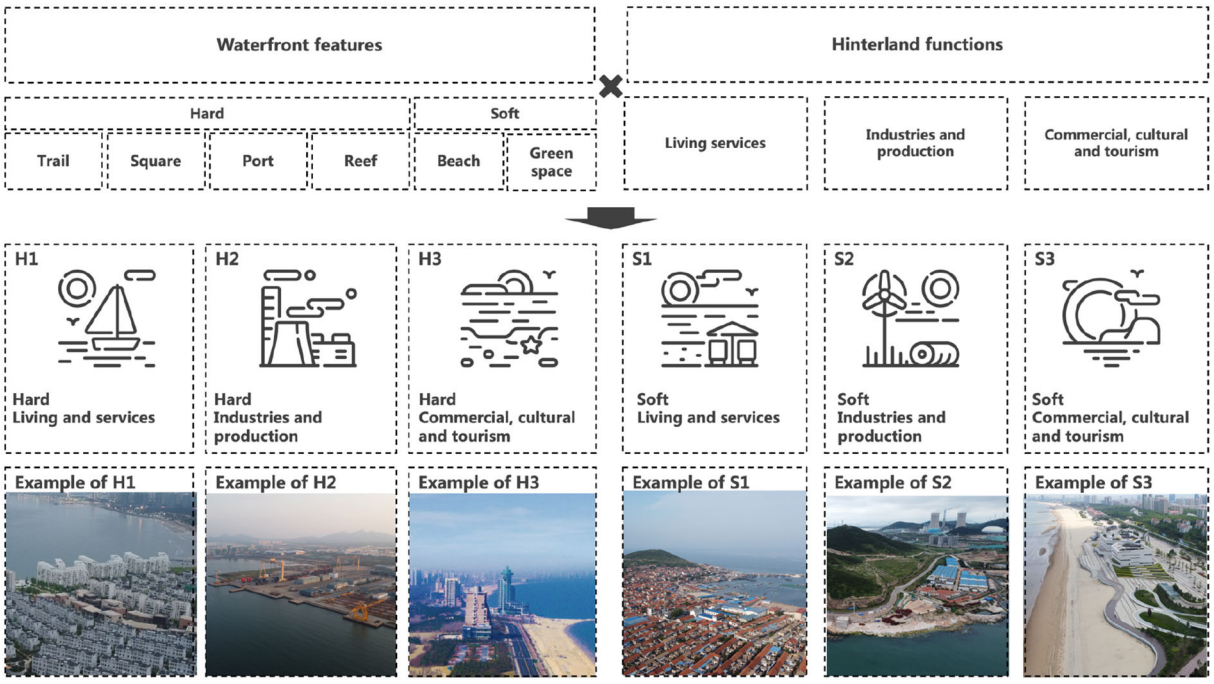

FIGURE 10
The classification results of urban coastal zones. The illustration photos were taken by the author.

diversity (1.2%−2.6%) for each block are regarded as conducive to coastal vitality as well.

The H3, the last type with hard waterfronts, has commercial, cultural, and tourism as the dominant hinterland functions and should develop local history and culture as its coastal zone identity to provide tourist attractions. According to the results, both indicators of the spatial form aspect should be controlled at a high level, with development density between 3.0 and 8.0 km^2/km^2 and building density between 0.3 and 0.8 km^2/km^2. These two have the highest ranges of design requirements among the six coastal zone types. As for the traffic organization, road network density is suggested within 18.0–27.0 km/km^2 and the block size between 0.5 and 2.5 ha. There is also a loose range of requirements for the indicators of intersection density (15.0–55.0 per km^2) and functional diversity (1.5–7.9%).

The S1 type refers to coastal zones with soft waterfronts, such as wetlands, green spaces, and beaches, with residential and services as hinterland functions. The waterfronts should be characterized by public spaces, such as green spaces and squares, to provide a perception of leisure to local residents. Building density (0.2–0.3 km^2/km^2) and development density (0.5–3.0 km^2/km^2) should be low to encourage the aggregation of high-quality residential neighborhoods. The size of blocks, therefore, can be relatively large (2.0–8.0 ha). A moderate level of intersection density (10.0–30.0 per km^2) and a low level of road network density (8.0–14.0 km/km^2) are needed to bring vitality to this coastal zone type. Functional diversity is suggested to be within 1.2–9.4%.

The S2 type is coastal zones with soft waterfront characteristics; the hinterland functions are primarily composed of industries and production. Its industrial heritage can be regenerated into public spaces and can also serve as landmarks. The maximum that development density can reach is 2.0 km^2/km^2 but building density should be controlled under 0.4 km^2/km^2. Intersection density (15.0–45.0 per km^2) and road network density (9.0–16.0 km/km^2) should be at a moderate level, while the block can have a larger size with a range between 2.0 and 9.0 ha. Functional diversity between 6.0 and 9.2% is concluded from the analysis as being beneficial to deliver coastal vitality.

The S3 is the last type with the coastal zones characterized by the soft waterfront. It has commercial, cultural, and tourism as the major hinterland functions. Local historical and cultural characteristics should be emphasized along the corridors connecting the hinterland and the waterfront to lead tourists to a full exploration of the coastal zone. This type has the widest range for building density (0.2–0.8 km^2/km^2) among all six types, and development density is suggested to be between 0.5 and 5.5 km^2/km^2. Road network density (12.0–24.0 km/km^2) and intersection density (20.0–55.0 per

10.3389/fevo.2022.962299

TABLE 4 The classification results of the selected eight coastal zones.

Sites	Landscape characteristics	Waterfront type	Hinterland functions	Coastal types	Analysis illustrations
Vancouver	Square/trail	Hard	Commercial, cultural and tourism	H3	
			Living and services	H1	
	Beach	Soft	Commercial, cultural and tourism	S3	
			Living and services	S1	
Chicago	Beach	Soft	Living and services	S1	
	Green space		Commercial, cultural and tourism	S3	
			Industries and production	S2	
	Port	Hard	Commercial, cultural and tourism	H3	
Toronto	Port	Hard	Industries and production	H2	
	Square/trail		Commercial, cultural and tourism	H3	
Barcelona	Port	Hard	Commercial, cultural and tourism	H3	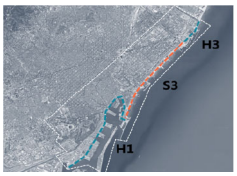
			Living and services	H1	
	Beach	Soft	Commercial, cultural and tourism	S3	
Qingdao	Beach	Soft	Living and services	S1	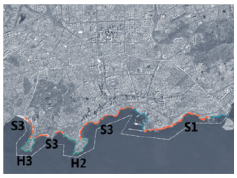
			Commercial, cultural and tourism	S3	
	Reef	Hard	Industries and production	H2	
			Commercial, cultural and tourism	H3	
Zhuhai	Reef	Hard	Living and services	H1	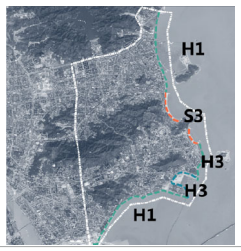
			Living and services	H3	
	Port		Living and services	H3	
	Beach	Soft	Commercial, cultural and tourism	S3	
Haikou	Reef	Hard	Living and services	H1	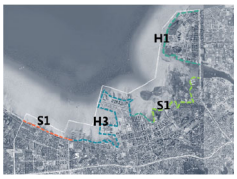
			Commercial, cultural and tourism	H3	
	Green space	Soft	Living and services	S1	
	Beach		Living and services	S1	
Shenzhen	Reef	Hard	Commercial, cultural and tourism	H3	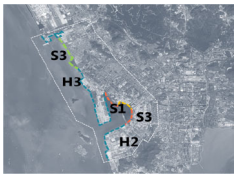
	Reef		Industries and production	H2	
	Beach	Soft	Commercial, cultural and tourism	S3	
			Living and services	S1	
	Green space		Commercial, cultural and tourism	S3	

"▬▬▬" means reef, "▬▬▬" means port, "▬▬▬" means square/trail, "▬▬▬" means green spaces, and "▬▬▬" means beach.

TABLE 5 Environmental drivers of coastal vitality based on typological analysis.

Types	H1	H2	H3	S1	S2	S3
Waterfront features	Hard waterfront			Soft waterfront		
Hinterland functions	Living and services	Industries and production	Commercial, cultural and tourism	Living and services	Industries and production	Commercial, cultural and tourism
Waterfront functions	Green spaces, squares	Port, green spaces, squares	Port	Wetlands, beaches, parks		
Local identities	Public life	Industrial heritage	Historical and cultural	Public life	Industrial heritage	Historical and cultural
Building density (km^2/km^2)	0.2–0.4	0.2–0.3	0.3–0.8	0.2–0.3	0–0.4	0.2–0.8
Development Density (km^2/km^2)	1.0–6.0	0–1.8	3.0–8.0	0.5–3.0	0–2.0	0.5–5.5
Block size (ha)	1.0–3.5	3.0–8.0	0.5–2.5	2.0–8.0	2.0–9.0	0–3.5
Intersection density (per km^2)	15.0–50.0	15.0–65.0	15.0–55.0	10.0–30.0	15.0–45.0	20.0–55.0
Road network density (km/km^2)	12.0–20.0	10.0–15.0	18.0–27.0	8.0–14.0	9.0–16.0	12.0–24.0
Functional diversity (%)	2.2–8.2	1.2–2.6	1.5–7.9	1.2–9.4	6.0–9.2	2.3–8.8
Proportion of specific functions (%)						
Employment	35.5	25.0	31.0	28.0	12.8	33.0
Living	32.7	16.7	32.3	22.0	33.3	30.7
Recreation	17.8	0.0	23.4	28.0	23.1	24.7
Transportation	14.0	58.3	13.3	22.0	30.8	11.6

km^2) should be controlled at a moderate level, while small block sizes (0–3.5 ha) are encouraged for this type. As for functional diversity, there is a relatively wide range of requirements 2.3–8.8%.

The comparison of the six types of urban coastal zones shows that waterfront functions and local identities should be in line with waterfront features and hinterland functions to facilitate coastal zone vitality. The range of the quantitative vitality indicators of the six coastal zone types also varies evidently with the hinterland functions, but there are similarities in vitality design control among the types with similar waterfront features. For example, the types of H3 and S3 both have the widest and highest ranges of development and building density. Similarities are also observed between H2 and S2 in terms of almost all vitality indicators, and the block sizes of these two types cover the widest and highest ranges. As for the H1 and S1 with hinterland functions of living and services, they have similar recommended design requirements on the indicators of building densities and block sizes. The most evident difference that is observed between coastal zones with similar hinterland functions is in functional diversity in H2 and S2; H2 has a range of 1.2–2.6%, while S2 is between 6.0 and 9.2%.

Discussion and conclusion

This study explores environmental drivers to deliver urban coastal zone vitality by analyzing the eight coastal zone cases. Eleven indicators were identified from the literature as being influential to coastal zone vitality, including development density, building density, road network density, intersection density, block size, functional diversity, proportion of specific functions, waterfront features, local identities, waterfront functions, and hinterland functions. In general, spatial form, function, and consistency between them are the key determinants of urban coastal zone vitality.

Six urban coastal zone types were classified based on their waterfront features and hinterland functions. Results suggested that coastal types with similar hinterland functions have similar characteristics of building density, block size, road network density, and functional diversity, while development density and intersection density are more likely to be affected by waterfront features. In the respect of spatial form, costal zones with hinterland functions of commercial, cultural, and tourism require a relatively high level of building and development density to provide sufficient human activities (Desfor and Jørgensen, 2004), as well as the small size of blocks to increase

walkability (Sha et al., 2014). A relatively loose spatial form with a low level of building and development density and medium size of building blocks can be more favorable when coastal zone vitality needs to be balanced with other quality of life, for example, living and production. A high level of road network density and intersection density is also necessary for coastal zone vitality, especially for the type with commercial, cultural, and tourism as hinterland functions. This can possibly be explained by their positive relationship with walkability and connectivity (Li et al., 2020). In addition, the importance of functional diversity to urban vitality has been confirmed in this and existing studies (Im and Choi, 2019), though there are no differences in design constraints found for different coastal zone types.

Though research findings appear to be conclusive, there are limitations that exist in this research design and analysis. First, only eight coastal zone design case studies were selected to control their construction levels, locations, orientations, the scales of hinterlands, and the lengths of the coastal zones. The number of case studies is also constrained by the lack of an efficient way, and the case study selection since, to date, there are still no consistent definitions of urban coastal zone vitality. Though the emerging deep learning algorithms provided bases for large-scale image analysis, they have their shortages in identifying qualitative attributes and their application is also limited greatly by the generality of training datasets. With the development of artificial intelligence, the continuous accumulation of basic datasets as well as the vitality contributors disclosed in this study, they can together be used in evaluating the vitality of worldwide urban coastal zones and then, in turn, refine the definition and the contributors. Also, research outcomes may also be affected by the accuracy of the obtained data since for most potential indicators; Google is the only data source involved. Besides, a part of the quantitative data was retrieved from open-sourced government websites of different counties and the investigation years were slightly different—this could also bias the analysis results. The use of multiple data sources and robustness tests in future similar studies can help reduce data errors, though data collection standards may differ across platforms.

To conclude, this study set out from clarifying the social-spatial boundary of urban coastal zones and proposed a typological basis for future relevant research. Through a data-based case study analysis, a comprehensive perspective of understanding how urban coastal zone vitality was developed. Research outcomes provide cues for designing dynamic urban coastal zones that can be straightforwardly relevant to environmental planning and design aspects and are responsive and adaptable to local contexts. More importantly, they can be applied to coastal zones with similar characteristics or within the same categories, and thus, have practical values in promoting coastal city development strategies.

Data availability statement

Publicly available datasets were analyzed in this study. This data can be found at: [Beijingcitylab.com][Github.com/Microsoft/USBuildingFootprints][https://Openstreetmap.org][Lbs.amap.com][Foursqure.com/products/places-api][Ditu.amap.com][Gditu.net].

Author contributions

YY and YS: conceptualization, methodology, validation, resources, and writing—review and editing. YH and HL: software, investigation, and visualization. YY, YH, and HL: formal analysis. YY: data curation and writing—original draft preparation. YS: supervision, project administration, and funding acquisition. All authors contributed to the article and approved the submitted version.

Funding

This research was funded by the Nature Science Foundation of China: 51808393; Shanghai Post-doctoral Excellence Program: 2021357; Restorative Urbanism Research Center (RURC), Joint Laboratory for International Cooperation on Eco-Urban Design, Tongji University (CAUP-UD-06).

Conflict of interest

The authors declare that the research was conducted in the absence of any commercial or financial relationships that could be construed as a potential conflict of interest.

Publisher's note

All claims expressed in this article are solely those of the authors and do not necessarily represent those of their affiliated organizations, or those of the publisher, the editors and the reviewers. Any product that may be evaluated in this article, or claim that may be made by its manufacturer, is not guaranteed or endorsed by the publisher.

References

Balasubramanian, G., Suresh, S., Goswami, S., and Swaminathan, B. and Pereira, G. F. (2022). Delineation of sensitive coastal zone of northern Ramanathapuram coast, Tamilnadu, India, using a GIS approach. *Geodesy Geodynam.* 13, 456–463. doi: 10.1016/j.geog.2022.03.004

Barragán, J. M., and De Andrés, M. (2015). Analysis and trends of the world's coastal cities and agglomerations. *Ocean Coastal Manage.* 114, 11–20. doi: 10.1016/j.ocecoaman.2015.06.004

Boulos, J. (2016). Sustainable development of coastal cities-proposal of a modelling framework to achieve sustainable city-port connectivity. *Proc. Soc. Behav. Sci.* 216, 974–985. doi: 10.1016/j.sbspro.2015.12.094

Bunce, S. (2011). *Public-Private Sector Alliances in Sustainable Waterfront Revitalization: Policy, Planning, and Design in the West Don Lands.* Toronto: University of Toronto Press, 287–304.

Carter, R. W. G. (2013). *Coastal Environments: An Introduction to the Physical, Ecological, and Cultural Systems of Coastlines.* Amsterdam: Elsevier Science.

Chen, Y., Yang, J., Yang, R., and Xiao, X. and Xia, J. (2022a). Contribution of urban functional zones to the spatial distribution of urban thermal environment. *Building Environ.* 216, 109000. doi: 10.1016/j.buildenv.2022.109000

Chen, Z., Dong, B., and Pei, Q. and Zhang, Z. (2022b). The impacts of urban vitality and urban density on innovation: evidence from China's Greater Bay Area. *Habitat Int.* 119, 102490. doi: 10.1016/j.habitatint.2021.102490

Council, N. R. (1993). *Managing Waste Water in Coastal Urban Areas.* Washington, DC: National Academies Press.

Da, T., and Xu, Y. (2016). Evaluation on connectivity of urban waterfront redevelopment under hesitant fuzzy linguistic environment. *Ocean Coastal Manage.* 132, 101–110. doi: 10.1016/j.ocecoaman.2016.08.014

Delclòs-Alió, X., and Miralles-Guasch, C. (2018). Looking at Barcelona through Jane Jacobs's eyes: mapping the basic conditions for urban vitality in a Mediterranean conurbation. *Land Use Policy* 75, 505–517. doi: 10.1016/j.landusepol.2018.04.026

Desfor, G., and Jørgensen, J. (2004). Flexible urban governance. The case of Copenhagen's recent waterfront development. *Eur. Plann. Stu.* 12, 479–496. doi: 10.1080/0965431042000212740

Dovey, K., and Pafka, E. (2014). The urban density assemblage: modelling multiple measures. *Urban Design Int.* 19, 66–76. doi: 10.1057/udi.2013.13

Duck, R. W. (2012). Marine spatial planning: managing a dynamic environment. *J. Environ. Policy Plan.* 14, 67–79. doi: 10.1080/1523908X.2012.664406

Ewing, R., Hajrasouliha, A., Neckerman, K. M., and Purciel-Hill, M., and Greene, W. (2016). Streetscape features related to pedestrian activity. *J. Plan. Educ. Res.* 36, 5–15. doi: 10.1177/0739456X15591585

Gehl, J. (1987). *Life Between Buildings.* New York: Van Nostrand Reinhold.

Gharaibeh, A. A., Tawil, H. S., and Alomari, A. H. (2022). Developing an indicative spatial accessibility analysis tool for urban public transportation system. *Case Studies Trans. Policy* 10, 175–186. doi: 10.1016/j.cstp.2021.11.015

Gill, A. B. (2005). Offshore renewable energy: Ecological implications of generating electricity in the coastal zone. *J. Appl. Ecol.* 42, 605–615. doi: 10.1111/j.1365-2664.2005.01060.x

Godschalk, D. R., and Brower, D. J., and Beatley, T. (1989). *Catastrophic Coastal Storms: Hazard Mitigation and Development Management.* Durham, NC: Duke University Press.

Gotham, K. F. (2002). Marketing mardi gras: commodification, spectacle and the political economy of tourism in New Orleans. *Urban Stu.* 39, 1735–1756. doi: 10.1080/0042098022000002939

Hagerman, C. (2007). Shaping neighborhoods and nature: urban political ecologies of urban waterfront transformations in Portland, Oregon. *Cities* 24, 285–297. doi: 10.1016/j.cities.2006.12.003

Hassan, D. K., and Elkhateeb, A. (2021). Walking experience: exploring the trilateral interrelation of walkability, temporal perception, and urban ambiance. *Front. Architec. Res.* 10, 516–539. doi: 10.1016/j.foar.2021.02.004

Hoppenbrouwer, E., and Louw, E. (2005). Mixed-use development: theory and practice in Amsterdam's eastern docklands. *Eur. Plann. Stu.* 13, 967–983. doi: 10.1080/09654310500242048

Hoyle, B. (1999). Scale and sustainability: the role of community groups in Canadian port-city waterfront change. *J. Trans. Geograph.* 7, 65–78. doi: 10.1016/S0966-6923(98)00030-1

Hurley, A. (2006). Narrating the urban waterfront: the role of public history in community revitalization. *Pub. Histor.* 28, 19–50. doi: 10.1525/tph.2006.28.4.19

Im, H. N., and Choi, C. G. (2019). The hidden side of the entropy-based land-use mix index: Clarifying the relationship between pedestrian volume and land-use mix. *Urban Stud.* 56, 1865–1881. doi: 10.1177/0042098018763319

Ioppolo, G., and Saija, G. and Salomon, E. R. (2013). From coastal management to environmental management: the sustainable eco-tourism program for the mid-western coast of Sardinia (Italy). *Land Use Policy* 31, 460–471. doi: 10.1016/j.landusepol.2012.08.010

Jacobs, J. (1961). *The Death and Life of Great American Cities.* New York, NY: Modern Library.

Jiang, Y., Han, Y., Liu, M., and Ye, Y. (2022). Street vitality and built environment features: A data-informed approach from fourteen chinese cities. *Sustain. Cities. Soc.* 79, 103724. doi: 10.1016/j.scs.2022.103724

Jiao, L. (2015). Urban land density function: a new method to characterize urban expansion. *Landscape Urban Plan.* 139, 26–39. doi: 10.1016/j.landurbplan.2015.02.017

Jin, X., Long, Y., Sun, W., Lu, Y., and Yang, X., and Tang, J. (2017). Evaluating cities' vitality and identifying ghost cities in China with emerging geographical data. *Cities* 63, 98–109. doi: 10.1016/j.cities.2017.01.002

Lan, H., and Lau, K. L., Shi, Y., and Ren, C. (2021). Improved urban heat island mitigation using bioclimatic redevelopment along an urban waterfront at Victoria Dockside, Hong Kong. *Sust. Cities Soc.* 74, 103172. doi: 10.1016/j.scs.2021.103172

Latip, N. S. A., and Shamsudin, S., and Liew, M. S. (2012). Functional dimension at 'Kuala Lumpur Waterfront'. *Proc. Soc. Behav. Sci.* 49, 147–155. doi: 10.1016/j.sbspro.2012.07.013

Lehrer, U., and Laidley, J. (2008). Old mega-projects newly packaged? Waterfront redevelopment in Toronto. *Int. J. Urban Reg. Res.* 32, 786–803. doi: 10.1111/j.1468-2427.2008.00830.x

Li, M., and Shen, Z., and Hao, X. (2016). Revealing the relationship between spatio-temporal distribution of population and urban function with social media data. *Geo J.* 81, 919–935. doi: 10.1007/s10708-016-9738-7

Li, S., Wu, C., Lin, Y., Li, Z., and Du, Q. (2020). Urban morphology promotes urban vibrancy from the spatiotemporal and synergetic perspectives: a case study using multisource data in Shenzhen, China. *Sustainability* 12, 4829. doi: 10.3390/su12124829

Li, X., Li, Y., Jia, T., Zhou, L., and Hijazi, I. H. (2022). The six dimensions of built environment on urban vitality: fusion evidence from multi-source data. *Cities* 121, 103482. doi: 10.1016/j.cities.2021.103482

Liu, S., Lai, S. Q., Liu, C., and Jiang, L. (2021). What influenced the vitality of the waterfront open space? A case study of Huangpu River in Shanghai, China. *Cities* 114, 103197. doi: 10.1016/j.cities.2021.103197

Liu, X., Zhu, Z., Jin, L., Wang, L., and Huang, C. (2018). Measuring patterns and mechanism of greenway use–A case from Guangzhou, China. *Urban Forestry Urban Greening* 34, 55–63. doi: 10.1016/j.ufug.2018.06.003

Long, Y., and Huang, C. (2019). Does block size matter? The impact of urban design on economic vitality for Chinese cities. *Environ. Plann. B Urban Anal. City Sci.* 46, 406–422. doi: 10.1177/2399808317715640

Long, Y., Huang, C. J. E., Analytics, P. B. U., and Science, C. (2019). Does block size matter? The impact of urban design on economic vitality for Chinese cities. *Environ. Plan. B Urban Anal. City Sci.* 46, 406–422. doi: 10.1177/2399808317715

Lynch, K. (1984). *Good City Form.* Cambridge, MA: MIT Press.

Maged, M., Zurina, S., and Mazlan, H. (2010). Mapping coastal geomorphology changes using synthetic aperture radar data. *Int. J. Phys. Sci.* 5, 1890–1896.

Mansournia, S., Gharaei, F., and Bahrami, B. (2016). Behavior mapping, an approach to assessment of urban spaces responsiveness. case study: recreational space of zrêbar lake Waterfront, Marivan, Kurdistan. *Motaleate Shahri* 5, 77–90.

Marghany, M. (2014). Simulation of three-dimensional of coastal erosion using differential interferometric synthetic aperture radar. *Global NEST Journal,* 16, 80–86. doi: 10.30955/gnj.001055

Martínez, M. L., Intralawan, A., Vázquez, G., Pérez-Maqueo, O., Sutton, P., and Landgrave, R. (2007). The coasts of our world: Ecological, economic and social importance. *Ecol. Econ.* 63, 254–272. doi: 10.1016/j.ecolecon.2006.10.022

Mu, B., Liu, C., Mu, T., Xu, X., Tian, G., Zhang, Y., et al. (2021). Spatiotemporal fluctuations in urban park spatial vitality determined by on-site observation and behavior mapping: a case study of three parks in Zhengzhou City, China. *Urban Forestry Urban Greening* 64, 127246. doi: 10.1016/j.ufug.2021.127246

Niu, Y., Mi, X., and Wang, Z. (2021). Vitality evaluation of the waterfront space in the ancient city of Suzhou. *Front. Architec. Res.* 10, 729–740. doi: 10.1016/j.foar.2021.07.001

Norcliffe, G., Bassett, K., and Hoare, T. (1996). The emergence of postmodernism on the urban waterfront: geographical perspectives on changing relationships. *J. Transp. Geograph.* 4, 123–134. doi: 10.1016/0966-6923(96)00005-1

Othman, A., Al-Hagla, K., and Hasan, A. E. (2021). The impact of attributes of waterfront accessibility on human well-being: Alexandria Governorate as a case study. *Ain Shams Eng. J.* 12, 1033–1047. doi: 10.1016/j.asej.2020.08.018

Papatheochari, T., and Coccossis, H. (2019). Development of a waterfront regeneration tool to support local decision making in the context of integrated coastal zone management. *Ocean Coastal Manage.* 169, 284–295. doi: 10.1016/j.ocecoaman.2018.12.013

Romero, V. P., Maffei, L., Brambilla, G., and Ciaburro, G. (2016). Modelling the soundscape quality of urban waterfronts by artificial neural networks. *App. Acoust.* 111, 121–128. doi: 10.1016/j.apacoust.2016.04.019

Sairinen, R., and Kumpulainen, S. (2006). Assessing social impacts in urban waterfront regeneration. *Environ. Impact Assessment Rev.* 26, 120–135. doi: 10.1016/j.eiar.2005.05.003

Sha, Y., Wu, J., Ji, Y., and Chan, S. L. T. and Lim, W. Q. (2014). *Xuhui Waterfront Area: Urban Restructuring for Quality Waterfront Working and Living. Shanghai Urbanism at the Medium Scale*. Berlin: Springer.

Thirumurthy, S., Jayanthi, M., Samynathan, M., Duraisamy, M., Kabiraj, S., and Anbazhahan, N. (2022). Multi-criteria coastal environmental vulnerability assessment using analytic hierarchy process based uncertainty analysis integrated into GIS. *J. Environ. Manage.* 313, 114941. doi: 10.1016/j.jenvman.2022.114941

Unt, A. L., and Bell, S. (2014). The impact of small-scale design interventions on the behaviour patterns of the users of an urban wasteland. *Urban Forestry Urban Green.* 13, 121–135. doi: 10.1016/j.ufug.2013.10.008

Wakefield, S. (2007). Great expectations: waterfront redevelopment and the hamilton harbour waterfront trail. *Cities* 24, 298–310. doi: 10.1016/j.cities.2006.11.001

Wang, F., Zhao, M. X., and Meng, Q. L. (2020). Analysis of the vitality measurement and correlation factors of urban waterfront space. *IOP Conf. Series Earth Environ. Sci.* 612, 012013. doi: 10.1088/1755-1315/612/1/012013

Wang, M., Chen, Z., Mu, L., and Zhang, X. (2020). Road network structure and ride-sharing accessibility: A network science perspective. *Comput. Environ. Urban Syst.* 80, 101430. doi: 10.1016/j.compenvurbsys.2019.101430

Woo, S. W., Omran, A., Lee, C. L., and Hanafi, M. H. (2017). The impacts of the waterfront development in Iskandar Malaysia. *Environ. Dev. Sust.* 19, 1293–1306. doi: 10.1007/s10668-016-9798-3

Xie, P. F., and Gu, K. (2015). The changing urban morphology: waterfront redevelopment and event tourism in New Zealand. *Tour. Manage. Persp.* 15, 105–114. doi: 10.1016/j.tmp.2015.05.001

Yang, C., and Shao, B. (2018). Influence of waterfront public space elements on lingering vitality and strategies: taking two typical waterfronts along Huangpu River, Shanghai as examples. *Urban. Archit* 4, 40–47.

Yang, C., Shi, M., and Geng, H. (2018). Study on the pedestrian accessibility of waterfront area based on an understanding of urban fabric level: taking the estuary area of Suzhou River in Shanghai as an example. *City Planning Rev.* 42, 104–114.

Ye, Y., Li, D., and Liu, X. (2018). How block density and typology affect urban vitality: an exploratory analysis in Shenzhen, China. *Urban Geograph.* 39, 631–652. doi: 10.1080/02723638.2017.1381536

Yin, L., and Wang, Z. (2016). Measuring visual enclosure for street walkability: using machine learning algorithms and google street view imagery. *App. Geograph.* 76, 147–153. doi: 10.1016/j.apgeog.2016.09.024

Yu, Y., Zhaoxi, Z., Xiaohu, Z., and Wei, Z. (2019). Human-scale measurement of street space quality—a large-scale, high-accuracy evaluation framework combining street view data and new analytical techniques. *Urban Plannin Int.* 34, 18–27. doi: 10.22217/upi.2018.490

Zhang, L., Zhang, R., and Yin, B. (2021). The impact of the built-up environment of streets on pedestrian activities in the historical area. *Alexandria Eng. J.* 60, 285–300. doi: 10.1016/j.aej.2020.08.008

frontiers | Frontiers in Environmental Science

TYPE Original Research
PUBLISHED 08 November 2022
DOI 10.3389/fenvs.2022.1048378

Check for updates

OPEN ACCESS

EDITED BY
Ying Jing,
Zhejiang University, China

REVIEWED BY
Lijun Xing,
Hubei University, China
Gui Jin,
China University of Geosciences
Wuhan, China

*CORRESPONDENCE
Xingping Wang,
wxpsx@seu.edu.cn

SPECIALTY SECTION
This article was submitted to Environmental Informatics and Remote Sensing,
a section of the journal
Frontiers in Environmental Science

RECEIVED 19 September 2022
ACCEPTED 24 October 2022
PUBLISHED 08 November 2022

CITATION
Zhang Y, Wang X, Ji M, Chen Y and Yan F (2022), Evaluating the barrier of typical production factor flow in the Chengdu-Chongqing Urban Agglomeration based on multi-source big data.
Front. Environ. Sci. 10:1048378.
doi: 10.3389/fenvs.2022.1048378

COPYRIGHT
© 2022 Zhang, Wang, Ji, Chen and Yan. This is an open-access article distributed under the terms of the Creative Commons Attribution License (CC BY). The use, distribution or reproduction in other forums is permitted, provided the original author(s) and the copyright owner(s) are credited and that the original publication in this journal is cited, in accordance with accepted academic practice. No use, distribution or reproduction is permitted which does not comply with these terms.

Evaluating the barrier of typical production factor flow in the Chengdu-Chongqing Urban Agglomeration based on multi-source big data

Yang Zhang[1,2,3], Xingping Wang[1]*, Mengrong Ji[2], Yulu Chen[4] and Feng Yan[4]

[1]School of Architecture, Southeast University, Nanjing, China, [2]College of Tourism and Urban-Rural Planning, Chengdu University of Technology, Chengdu, China, [3]Key Laboratory of Spatial Intelligent Planning Technology, Ministry of Natural Resources of the People's Republic of China, Shanghai, China, [4]Chengdu Economic Development Academy, Chengdu, China

Promoting the free flow of production factors and improving the efficiency of resource allocation is a necessary requirement for China to achieve high-quality development. Therefore, it is significant to evaluate the barrier of production factors flow and analyze its influencing factors. This study, based on the flow space theory, takes the Chengdu-Chongqing urban agglomeration as an example, constructs the factor flow barrier index (FFBI) with multi-source big data (Baidu Migration data, investment data of listed companies and patent transfer data) and statistical data to evaluate the barriers of three typical product factors flow (labor flow, technology flow and capital flow). Moreover, quadratic assignment procedure regression model is used to analyze how system, economic, society, culture, policy and facility factors affect the barrier of the three typical production factors flow. The results demonstrate that: 1) The intensity of the three typical production factors flow of Chengdu-Chongqing are the highest, and the intensity of three typical production factors flow between the two cities and other cities are higher than that between other 14 cities. 2) In 120 city pairs, 87, 100 and 106 city pairs have positive FFBI of labor flow, capital flow and technology flow, respectively. The FFBI of Chongqing between other cities are mostly positive, indicating the three typical production factors flow are hindered to some extent. Labor flow is less hindered than capital flow and technology flow. 3) Administrative division relationships and administrative level differences have important impact on the barriers of the three typical production factors flow. City pairs belonging to different provincial administrative regions or within the same administrative level have larger FFBI. The barrier of labor and capital are positively affected by the transportation cost and the similarity of the industrial structure, respectively. The framework and findings are of great significance for revealing the formation mechanism of the barrier of production factors flow and provide some guidance for promoting the free flow of production factors and forming a new pattern of high-quality development in the Chengdu-Chongqing Urban Agglomeration.

KEYWORDS

production factor flow, flow space theory, improved gravity model, quadratic assignment procedure, chengdu-chongqing urban agglomeration

1 Introduction

Benefiting from economic globalization and China's reform and opening-up policy, China has experienced rapid economic growth in the past 4 decades. In 2021, China's GDP reaches US$17.7 trillion, accounting for over 18% of the global economy. However, the trend of anti-globalization has appeared since the 2008 financial crisis, influencing the way and efficiency of global resource allocation and changing the world economic pattern (Andreas et al., 2020; Duan and Jiang, 2021). To this end, the Chinese government proposes to build a new development pattern with the domestic cycle as the main body and the domestic and international dual cycles promoting each other ("dual circulation" development pattern), and takes high-quality development as the goal of economic development. It is foreseeable that China's economic development will put more emphasis on efficiency, coordination and comprehensiveness in the future. Improving resource allocation efficiency can directly improve total factor productivity, which is considered to be the most important driving force for high-quality development (Xu et al., 2022).

Production factors are the source and basis of social production, which generally consist of six important components: natural resources, capital, labor, technology, management and information (Feldstein and Horioka, 1979; Li and Miao, 2017; Wu et al., 2017). Generally speaking, the stronger the ability of the region to gather production factors, the greater the development potential. Production factors are scarce and profit-oriented, which will produce cross-regional flow under the guidance of the market (Guo and Zhang, 2017). When production factors cannot flow freely, economic cooperation between regions is reduced and more duplicative industries are built, thereby reducing overall economic efficiency (Wang and Yang, 2021). Promoting the free flow of production factors is an important way to improve resource allocation and realize the integrated development of the regional economy (Walz, 1997; Chu et al., 2018; Chen, 2020; Yang et al., 2022). Therefore, promoting the free flow of production factors is an important starting point to achieve high-quality development for China. According to the Outline of the 14th Five-Year Plan (2021–2025) for National Economic and Social Development and Vision 2035 of the People's Republic of China, promoting the smooth flow of resources is one of the key tasks to build the "dual circulation" development pattern. To deepen the reform of market-based allocation and promote the independent and orderly flow of production factors, the "Opinions on building a more perfect institutional mechanism for the market-oriented allocation of factors" was proposed by China government. However, due to institutional mechanisms and other reasons, there are still some obstacles that affect the flow of production factors, especially in the western regions where the level of social and economic development is relatively backward (Fan, 2022).

The Chengdu-Chongqing urban agglomeration is the region with the highest development level and greatest development potential in western China. It stretches across the two provincial administrative regions of Sichuan and Chongqing and has a population of more than 95 million. In 2021, the GDP of the Chengdu-Chongqing urban agglomeration has exceeded US$1 trillion, accounting for 30.8% of the western regions. However, compared with the eastern coastal regions, the Chengdu-Chongqing urban agglomeration is still characterized with low flow intensity of production factors and insufficient coordination of regional development (Shi and Pan, 2021). Taking the Chengdu-Chongqing urban agglomeration as the study area, this study evaluates and analyzes the barriers to the three typical and representative production factors, labor, capital and technology.

The contributions of this study are as follows. First, unlike most current studies focusing on the intensity of production factors flow, this study focuses on the barriers of production factors flow. Second, this paper constructs the factor flow barrier index (FFBI), which can quantitatively evaluate the factor flow barrier. Finally, the quadratic assignment procedure (QAP) regression model is used to analyze the causes of the barriers of labor, capital and technology flow. This article endeavors to provide a better understanding of the barrier of production factors flow, which is of great significance to the high-quality development of economy in China.

The remainder of this paper is organized as follows. The literature on production factors flow is reviewed in Section 2. The research methods, including the study area, data and analytical methods are explained in Section 3. Section 4 elaborates the analysis of the strength and barrier of typical production factors flow. Section 5 concludes the research findings and suggests avenues of future research.

2 Literature review

With the improvement of transportation and communication facilities and the deepening of social, economic and cultural exchanges, the flow of people, materials, information and other elements between regions is accelerated, which attracts the attention of researchers (Mitchelson and Wheeler, 1994; Karemera et al., 2000; Dash and Rae, 2016). (Castells 1996) proposed the concept of flow space and considered flows to be real relational data that can

reflect interactions between cities. The spatial agglomeration and diffusion of factors caused by the flow of various factors profoundly shape the regional spatial structure (Moll et al., 2017). Among these factors, the flow of production factors such as labor, capital, technology and information is positively correlated with resource allocation efficiency and is considered to be an important factor affecting economic growth and regional coordinated development, drawing widespread attention under the background of high-quality development (Yin et al., 2021; Zhou et al., 2022).

Since the spatial immobility of natural resource factors and the difficulty in quantifying flow intensity of management and information factors, existing studies mainly focus on the three production factors of labor, capital, and technology and explore the flow intensity of these production factors (Ben David, 2010; Zhou et al., 2019; Ding and Sui, 2021). At present, there are two kinds of methods to measure the flow intensity of production factors. The first method is to use gravity model, breaking point model and potential model to simulate the flow intensity of production factors based on the relevant statistics (Wang et al., 2017; Zheng et al., 2020). For example, Lottum and Marks (2011) applied gravity model to estimate the interprovincial migration in Indonesia. Niu et al. (2018) used improved breaking point model to estimate the flow intensity of people and applied to the urban hinterland range division. This method only considers the size of relevant statistical indicators and the geographic distance between cities when simulating the intensity of factors flow, often deviates with the data of the actual survey (Jung, et al., 2008), which can be considered as an effective measure under natural conditions. Another method is to use multi-source big data to measure the flow intensity of factors or substitute them with parameters (Wang et al., 2017). For example, (Li et al., 2022), measured the intensity of people flow in Northeast China based on Tencent location big data. (Jin et al., 2018). fetched transaction records from Jingdong Mall website to reflect the intensity of provincial capital flow. (He et al., 2022). used patent transfer data and venture capital data between cities to analyze the intensity of production factors flow in Beijing-Tianjin-Hebei region. With the development of information technology, this method has become the main method to measure the intensity of factors flow. Relatively speaking, evaluating the barrier of production factor flow is of greater significance in promoting the free flow of production factors. However, few studies addressing the evaluation methods for the barrier production factor flow.

Many studies have focused on the influence factors that affect the production factors flow (Young, 2000; Xie and Lin, 2016). Geographical distance, economic development, innovation environment and administrative level are considered to be the main factors affecting the intensity of production factors flow (Torre, 2008; Gao et al., 2021; Gui et al., 2021). QAP regression model, Geodetector and Tobit model are commonly used to identify influence factors affecting the intensity of production factors flow. For example, using Tobit regression model, (Wang et al., 2022), concluded that factors such as city administrative level and inter-city innovation cooperation have significant effects on patent transfer in Northeast China. In the existing research on the reasons for the formation of production factors flow obstacles, it is generally believed that the institutional differences between cities and local protectionism brought about by administrative division are the fundamental reasons for restricting the free flow of production factors (Zhang et al., 2018; Dong and Chi, 2020). However, the above conclusions lack the support of quantitative models, and few studies have paid attention to the influence of cultural differences, planning guidance and other factors on the barriers of production factors flow.

To sum up, although the existing research has carried out many fruitful explorations on production factors flow, there are still some shortcomings. First, the existing studies mostly focus on the measurement of the intensity of a single production factor flow, so it is difficult to reflect the intensity of production factors flow between cities as a whole. Second, it ignores the quantitative measurement of barriers to production factors flow, which is very important for evaluating the efficiency of resource allocation. Finally, few studies have used quantitative models to analyze the multifaceted factors that cause the barriers of production factors flow and their mechanisms. Therefore, for the three production factors of labor, capital, and technology, this paper attempts to establish a quantitative method to measure the barrier of production factor flow and use quantitative models to identify influence factors that affect the barriers of different production factors flow.

3 Data and methodology

3.1 Study area

The Chengdu-Chongqing urban agglomeration is seated in Sichuan Province and Chongqing City in Southwest China. Surrounded by mountains, it is a relatively independent economic zone (Figure 1). The Chengdu-Chongqing urban agglomeration covers an area of 185,000 square kilometers and consists of two central cities, Chengdu and Chongqing, and other 14 cities (Zigong, Luzhou, Deyang, Mianyang, Suining, Neijiang, Leshan, Nanchong, Meishan, Yibin, Guangan, Dazhou, Yaan, Ziyang), among which, Chongqing is one of the four municipalities directly under the Central Government in China, Chengdu is the capital of Sichuan Province, and other 14 cities are all prefecture-level cities under the jurisdiction of Sichuan Province. Since ancient times, this area has fertile land and abundant products, which gave birth to the Bashu culture with the Ba culture and Shu culture as the main body. In 2021, the per capita GDP has exceeded US$10,000, which is quite close to the average level in China.

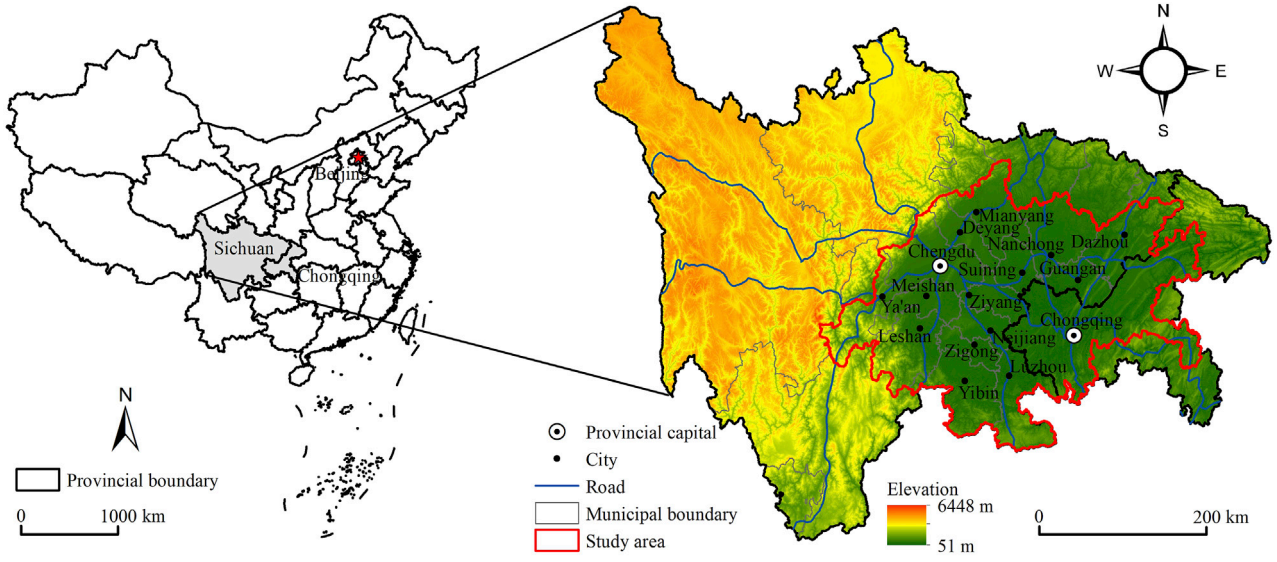

FIGURE 1
Study area.

In 2021, the Central Committee of the Communist Party of China and the State Council officially issued the "Outline of the Construction Plan for the Chengdu-Chongqing Economic Circle", focusing on promoting the Chengdu-Chongqing urban agglomeration to become a growth pole for China's high-quality development in the future. In recent years, cooperation between cities in the Chengdu-Chongqing urban agglomeration has become more intensive, and the intensity of production factors flow has tended to increase. In order to give full play to the leading role of Chengdu and Chongqing in the development of surrounding areas, the Sichuan Provincial People's Government and the Chongqing Municipal People's Government have issued the "Chengdu Metropolitan Circle Development Plan" and "Chongqing Metropolitan Circle Development Plan".

3.2 Data sources

Three types of big data, including Baidu Migration data, enterprise investment capital data and patent transfer data are used in this study. Among them, Baidu Migration is a mobile app based on big data system recording movements of mobile phone users and is commonly used for population and labor mobility research (Zhan et al., 2020). This paper screens out the population flow data between cities in the Chengdu-Chongqing urban agglomeration from January 1 to 14, 2020, fully considering working days, rest days and holidays population inflows and outflows. Enterprise investment capital data comes from the Qixinbao website (https://www.qixin.com/). By screening the location of investing companies and invested companies, we build a 16 × 16 matrix of mutual investment between cities in 2020. Similarly, patent transfer data is obtained in a similar manner, and its source website is inCopat (https://www.incopat.com/).

In addition, this paper also cites a number of statistical indicators, such as GDP, per capita GDP, urbanization rate, gross deposits of financial institutions, and the number of patent authorizations, mainly from the "Sichuan Statistical Yearbook 2021" and "Chongqing Statistical Yearbook 2021".

3.3 Empirical model

A research framework is developed in this study to achieve the research objectives. Firstly, based on multi-source big data and statistical data, the intensity of three kinds of production factors flow is respectively measured by parametric substitution and improved gravity model. Secondly, the factor flow barrier index (FFBI) is established to evaluate the barriers of production factors flow. Finally, the QAP regression model is used to analyze the factors affecting FFBI.

3.3.1 Measuring the intensity of production factor flow

This paper utilizes population migration data to reflect the intensity of labor mobility due to the difficulty in obtaining the amount of labor transfer. Patent transfer and enterprise investment are the main forms of capital and technology flow, so the data of patent transfer and enterprise investment amount can be used to represent the intensity of capital and technology

TABLE 1 Formulas for calculating the intensity of production factors flow.

Variables	Formula	Description
The intensity of labor flow	$L_{ij} = L_{i,j} + L_{j,i}$	L_{ij} is the calculated intensity of labor flow. $L_{i,j}$ and $L_{j,i}$ are the number of population flowing from city i to city j and from city j to city i, respectively
The intensity of capital flow	$C_{ij} = C_{i,j} + C_{j,i}$	C_{ij} is the calculated intensity of capital flow. $C_{i,j}$ and $C_{j,i}$ are the total investment flowing from city i to city j and from city j to city i, respectively
The intensity of technology flow	$T_{ij} = T_{i,j} + T_{j,i}$	T_{ij} is the calculated intensity of technology flow. $T_{i,j}$ and $T_{j,i}$ are the number of patents transferred from city i to city j and from city j to city i, respectively

TABLE 2 Formulas for estimating the intensity of production factors flow.

Variables	Formula	Description
The intensity of labor flow	$L'_{ij} = \frac{L_i \times L_j}{D_{ij}}$	L'_{ij} is the estimated intensity of labor flow, L_i and L_j are the total population of city i and city j, respectively. D_{ij} is the geographical distance between cities i and j
The intensity of capital flow	$C'_{ij} = \frac{C_i \times C_j}{D_{ij}}$	C'_{ij} is the estimated intensity of labor flow, C_i and C_j are the total deposits of financial institutions of city i and city j, respectively. D_{ij} is the geographical distance between cities i and j
The intensity of technology flow	$T'_{ij} = \frac{T_i \times T_j}{D_{ij}}$	T'_{ij} is the estimated intensity of labor flow, T_i and L_j are the total amount of patent authorization of city i and city j, respectively. D_{ij} is the geographical distance between cities i and j

flow between cities. Table 1 shows the formulas for calculating the flow intensity of three kinds of production factors.

In addition, the improved gravity model is applied to estimate the intensity of production factors flow under natural conditions. Gravity model is a theoretical model proposed based on the law of universal gravitation to measure the strength of the connection between regions (Tinbergen, 1966; Daniel, 2006). Scholars usually use some aggregate indicators instead of mass to improve the traditional gravitational model and apply it to the study of distance decay effects and spatial interactions (Atif et al., 2016; Saleh et al., 2019). This study takes the total population, the total deposits of financial institutions, and the total amount of patent authorization as the total scale of labor, capital, and technology in gravity model, respectively. Table 2 shows the formulas for estimating the intensity of three kinds of production factors flow.

3.3.2 Evaluating the barrier of production factor flow

The intensity of production factor flow calculated using multi-source big data is often different from that estimated based on improved gravity models. These intensity difference can reflect the degree of deviation between the intensity of the real factor flow and that under natural conditions, which can be evaluated by FFBI. The calculation formula of FFBI is as follows:

$$\boldsymbol{FFBI_{ij}} = \mathbf{1} - \frac{\boldsymbol{I_{ij}}}{\sum_{i=1,j=1}^{16} \boldsymbol{I_{ij}}} \div \frac{\boldsymbol{I'_{ij}}}{\sum_{i=1,j=1}^{16} \boldsymbol{I'_{ij}}}$$

Where $\boldsymbol{FFBI_{ij}}$ is the FFBI between city i and city j. $\boldsymbol{I_{ij}}$ is the calculated intensity of a production factor flow. $\boldsymbol{J_{ij}}$ is the estimated intensity of a production factor flow. Using this formula, the FFBI of labor, capital, and technology flows between the 16 cities in the Chengdu-Chongqing urban agglomeration can be calculated. If $\boldsymbol{FFBI_{ij}}$ is a positive value, it means that there is an obstacle to the flow of factor between cities i and j. The larger the value of $\boldsymbol{FFBI_{ij}}$, the stronger the obstacle. If $\boldsymbol{FFBI_{ij}}$ is a negative value, it means that there is a promotion effect on the flow of factor between cities i and j. The larger the value of $\boldsymbol{FFBI_{ij}}$, the stronger the promotion effect. If $\boldsymbol{FFBI_{ij}}$ is equal to 0, it means that the flow of elements between cities i and j is close to the natural state.

3.3.3 QAP regression model

QAP is a resampling-based method that has been widely used in measuring "relationships" in relational data, which can avoid the collinearity problem caused by relational data regression (Liu, 2007; Ju and Sohn, 2015; Lee et al., 2016). QAP analysis can be divided into QAP correlation analysis and QAP regression model. QAP correlation analysis compares the lattice values corresponding to two or more square matrices to give the correlation coefficients between the matrices, and conducts non-parametric tests on the coefficients (Zhang et al., 2020; Li et al., 2021). Based on the permutation of matrix data, QAP regression model studies the regression relationship between multiple matrices and one matrix, and at the same time evaluates the significance of R-squared (Cranmer et al., 2017; Chong et al., 2018). In recent years, the model has been introduced by some scholars into the study of production factors flow (Wang et al., 2021).

TABLE 3 Definition of explanatory variables.

Aspect	Variables name	Abbreviation	Definition
System	Administrative division relationship	ADR	If two cities belong to the same provincial-level administrative region, then ADR = 0; Otherwise, ADR = 1
	Administrative level differences	ALD	If two cities have the same administrative level, ALD = 0; Otherwise, ALD = 1
Economic	Difference in per capita GDP	D_GDP	Difference between GDP per capita of two cities
Society	Difference in urbanization rate	D_UA	Difference between urbanization rates of two cities
Culture	Whether belong to the same cultural division	CD	If two cities belong to the same cultural zone, then CD = 0; Otherwise, CD = 1
Policy	Whether belong to the same metropolitan area	MA	If two cities belong to the same metropolitan area, then CD = 0; Otherwise, CD = 1
Facility	Minimum driving time	MDT	The minimum travel time by car between two cities

Based on the QAP model, this paper reveals the determinants of the barrier of three kinds of production factors flow from the perspectives of system, economy, society, culture, policy and facility, to better explain the mechanism of FFBI. Among these perspectives, the system mainly considers administrative divisions and administrative levels. In the economic aspect, the difference of per capita GDP is selected as a representative variable. Since the urban-rural dual structure is an important feature of Chinese society, the model selects the difference in the urbanization rate as a social variable. In terms of culture, the main consideration is that the Chengdu-Chongqing urban agglomeration can be divided into the Ba cultural area (Chongqing, Nanchong, Guangan and Dazhou) and the Shu cultural area (Chengdu, Zigong, Luzhou, Deyang, Mianyang, Suining, Neijiang, Leshan, Meishan, Yibin, Yaan, Ziyang) in space. Planning can reflect policies that guide the development of space, and cities in the same metropolitan area tend to be more closely linked. The planning scope of Chengdu Metropolitan Circle includes Chengdu, Deyang, Meishan and Ziyang. And the planning scope of Chongqing Metropolitan Circle includes Chongqing and Guangan. In terms of facility, the shortest car travel time is mainly used as a variable to measure the convenience of transportation facilities. The definition of variables is as Table 3. Based on the above process, the study establishes seven 16 × 16 independent variable matrices.

4 Results and analysis

4.1 The intensity of production factors flow

4.1.1 The intensity of production factors flow calculated by multi-sources big data

Using natural breaks in ArcGIS, we divided the intensity of three typical production factors flow calculated by multi-sources big data into five grades (the lowest, lower, medium, higher and the highest). The colors from blue to red indicate the intensity from low to high (Figure 2). In terms of labor flow, the factors flow intensity of Chongqing-Chengdu, Chengdu-Deyang and Chengdu-Meishan are at the highest level; the factors flow intensity of Chongqing-Guangan, Chengdu-Ziyang and Chengdu-Nanchong are at higher level. Chengdu-Suining has the highest capital flow intensity. Chongqing-Chengdu, Chengdu-Leshan, Chengdu-Deyang and Chengdu-Mianyang are at the second level. Chongqing-Chengdu and Chengdu-Deyang are at the highest level of technology flow intensity. after these are Chengdu-Meishan and Chengdu-Suining. It shows that Chongqing and Chengdu are the two core cities in the Chengdu-Chongqing urban agglomeration, playing important dominant roles in the three typical production factors flow network, and Chengdu plays an even bigger role than Chongqing. The intensity of labor, capital and technology flow between other 14 cities are all medium or below.

4.1.2 The intensity of production factors flow estimated by improved gravity model

We also divided the intensity of three typical production factors flow estimated by improved gravity model into five levels at natural breaks (Figure 3). Whether it is labor mobility, capital mobility or technological mobility, Chongqing-Chengdu has the highest intensity of factors flow. Chongqing and Chengdu are at the centre of the production factors flow network with the most intensive flows with other cities. For example, the intensity of labor flow and capital flow of Chengdu-Deyang, Chengdu-Mianyang, Chengdu-Meishan are at the highest level. The intensity of technology flow of Chengdu-Deyang and Chengdu-Mianyang are at higher level. The intensity of labor flow of Chongqing-Luzhou, Chongqing-Nanchong, Chongqing-Guangan, Chongqing-Dazhou are also at higher level. Except for Deyang-Mianyang, the intensity of labor, capital and technology flow between other 14 cities are all medium or below.

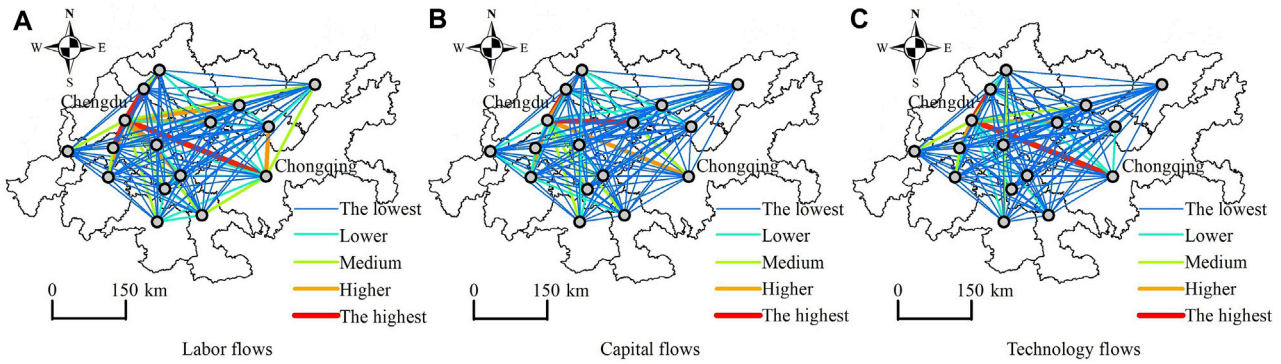

FIGURE 2
The intensity of labor, capital and technology flow calculated by multi-sources big data.

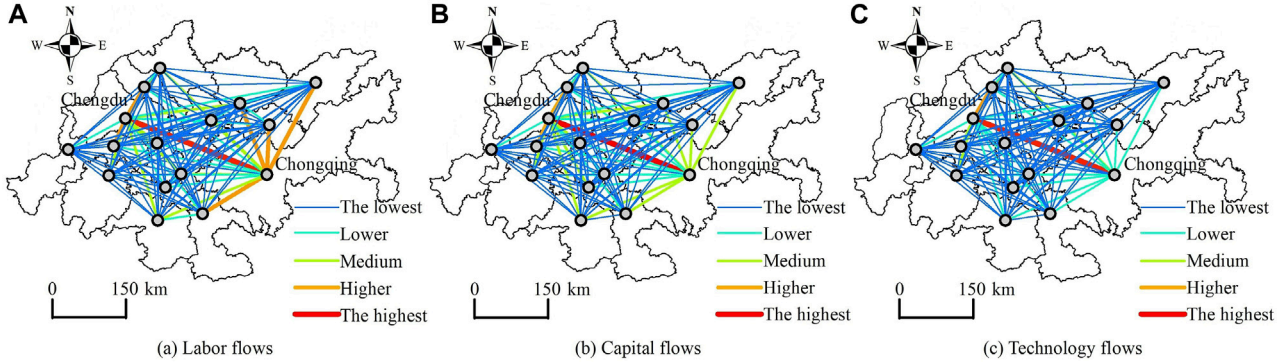

FIGURE 3
The intensity of labor, capital and technology flow estimated by improved gravity model.

4.2 The barrier of production factors flow

Figure 4 illustrates the FFBI of labor, capital and technology flow between 16 cities in the Chengdu-Chongqing urban agglomeration. The colors of line and grid from green to red indicate the FFBI from negative to positive, reflecting the production factors flow from being promoted to being hindered.

4.2.1 The barrier of labor flow

As shown in Figure 4A, the FFBI of labor flow between Chongqing and other cities are all positive, showing that the labor flow between Chongqing and other cities are hindered. Except for Chongqing, the FFBI of labor flow of the city pairs composed by Chengdu and other 14 cities are negative, indicating that labor flow between Chengdu and other 14 cities are promoted to a certain extent. Another observable spatial pattern is that the FFBI of labor flow is smaller between closed cities. For example, the FFBI of Chongqing-Guangan, Chongqing-Dazhou, Choingqing-Ziyang and Chongqing-Luzhou are smaller, indicating the impediment of labor flow between Chongqing and these neighboring cities are relatively small.

4.2.2 The barrier of capital flow

Unlike labor flow, the FFBI of capital flow of Chongqing-Suining is negative. That is to say, the capital flow of the city pairs composed by Chongqing and other cities are not all hindered. The positive and negative FFBI values of the city pairs composed by Chengdu and other cities are almost equal. Among the city pairs consist of Leshan, there are over five ones where capital flow is facilitated. Notably, the FFBI of capital flow between Ziyang and other cities are all positive, showing that the capital flow between Ziyang and other cities are all hindered, which is similar with the capital flow between Nanchong and other cities. Overall, the laws of capital flow are more complex than labor flow, and not much related to spatial proximity (Figure 4B).

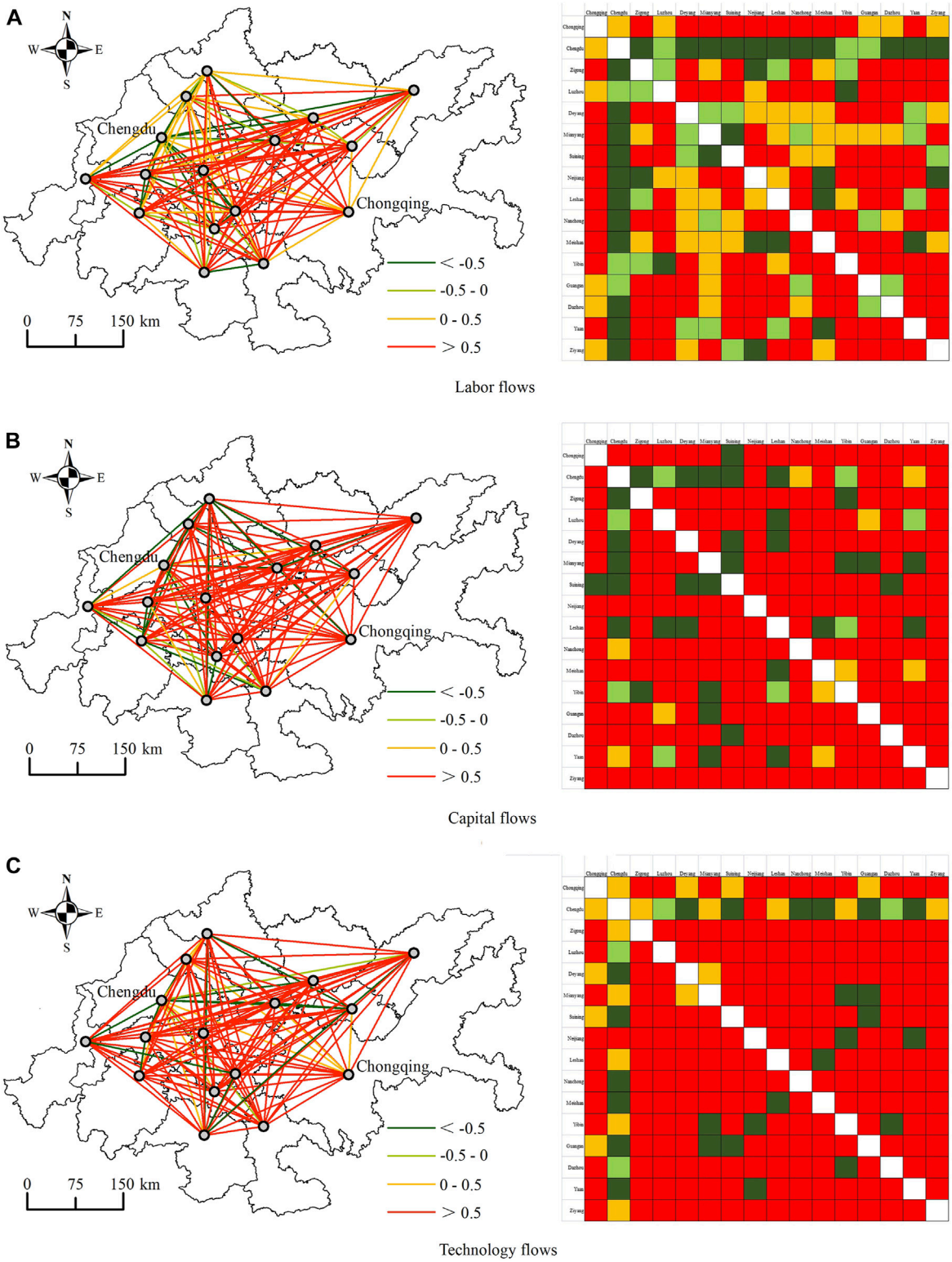

FIGURE 4
The FFBI of labor, capital and technology flow.

TABLE 4 QAP regression Model on the FFBI of three typical production factors flow.

Aspect	Variable	Labor flow		Capital flow		Technology flow	
		Standardized coefficient	*p*-Value	Standardized coefficient	*p*-Value	Standardized coefficient	*p*-Value
System	ADR	0.576**	0.000	0.281**	0.044	0.157*	0.071
	ALD	-0.820**	0.000	-0.520**	0.023	-0.294*	0.092
Economy	D_GDP	-0.098	0.142	-0.077	0.291	-0.005	0.494
Society	D_UA	0.182	0.132	0.366*	0.087	0.212	0.189
Culture	CD	0.083	0.145	0.015	0.464	0.110	0.156
Policy	MA	0.080	0.106	0.081	0.202	0.006	0.597
Facility	MDT	0.408**	0.000	0.125	0.173	-0.083	0.237
R^2		0.595	0.071	0.028			

*, ** represent a significance level of 10% and 5%, respectively.

4.2.3 The barrier of technology flow

As shown in Figure 4C, the FFBI of technology flow of the city pairs involving Chongqing, Zigong, Ziyang are all positive, showing that the technology flows of these city pairs are hindered. The positive and negative FFBI values of the city pairs composed by Chengdu and other cities are almost equal. Among the city pairs involving Yibin and Guangan, the technology flow of three city pairs are facilitated. The FFBI of technology flow of Chengdu-Deyang and Chengdu-Luzhou is the only negative values in the city pairs involving Luzhou and Deyang, respectively.

4.3 Determinants of the barrier of typical production factors flow

By importing the multidimensional independent variable matrices into the QAP regression model, and then having performed 2000 times of matrix random permutations to estimate the standard errors, the regression results are obtained. Table 4 reports the results of the QAP regression model. The model fitting result varies from 0.028 to 0.595, and the variables can better explain the difference of the FFBI of labor flow between cities than that of capital and technology flow.

In terms of labor flow, there are three variables that have an impact on the FFBI between cities at a significance level of 5%, they are ADR, ALD of system and MDT of facility, among which ADR has a positive impact on the barrier of labor flow. In other words, since Chongqing and other cities belong to different provincial administrative regions, the intensity of labor flow between Chongqing and other cities are hindered to a certain extent. However, ALD has a negative impact on the barrier of labor flow, indicating that cities at same administrative levels have larger FFBI of labor flow. MDT exerts positive impact on the barrier of labor flow. That is to say, the higher the cost of travel time between two cities, the greater the impediment to labor flow.

As for the FFBI of capital flow, factors related to system and society do exert influence. City pairs belonging to different provincial administrative regions or within the same administrative level have larger FFBI of capital flow, capital flows are more hindered. D_UA of society has a positive impact on the barrier of capital at a significance level of 10%, indicating capital flow between cities with large urbanization level gaps is more hindered.

The regression results also show that ADR and ALD of system are the two factors affecting the barrier of technology flow at a significance level of 10%. Similar to labor and capital flow, city pairs belonging to different provincial administrative regions but within the same administrative level have larger FFBI of technology flow.

5 Discussion

5.1 Comparison among the barriers of the three typical production factors flow

In 120 city pairs of the Chengdu-Chongqing urban agglomeration, 87, 100 and 106 city pairs have positive FFBI of labor flow, capital flow and technology flow, respectively. The results show that the three typical production factors flow between most cities are hindered to a certain extent and only a small number of production factors flow between cities are facilitated. For these city pairs, the FFBI of capital flow and technology flow are also greater than that of labor mobility. Thus, labor flow is less hindered than capital and technology flow. Another notable phenomenon is that the FFBI of labor flow are relatively lower in city pairs consisting of neighboring cities, but the barriers of capital flow and technology between two cities are not related to their spatial proximity obviously.

ADR, ALD of system have similar effects on the FFBI of the three typical production factors flow, indicating that

administrative division hinders the three typical production factors flow in the Chengdu-Chongqing urban agglomeration, and the Chengdu-Chongqing urban agglomeration is still in the stage of production factors agglomerated to high-level administrative cities (Chongqing and Chengdu). The difference is that time and space compression brought by informatization makes the capital and technology flow no longer subject to spatial distance, which is the reason why the low significance of the MDT factor. The difference in urbanization rate reflects the proportion of non-agricultural production population between cities is similar, and the industrial structure is more similar, which is an important factor affecting capital flow. In addition, D_GDP of economic and CD of culture have no significant impact on the FFBI of the three typical production factors flow, indicating that differences in economic development levels and cultural are not obstacles to the three typical production factors flow in the Chengdu-Chongqing urban agglomeration. Although "Chengdu Metropolitan Circle Development Plan" and "Chongqing Metropolitan Circle Development Plan" have been formulated in the past 2 years, the effect of MA on the barrier of the three typical production factors flow is not obvious, indicating these two plans have not guided the free flow of production factors due to their short implementation time.

5.2 Research and policy implications

The concept of high-quality put forward by Chinese government emphasizes the high efficiency and coordination of development. Promoting the free flow of production factors helps to improve the efficiency and fairness of resource allocation, which is the key to high-quality development. Compared with most existing studies focusing on the flow intensity of production factors, this study further explores the barriers of three typical production factors flow and their influencing factors, which is a more direct support for the research on high-quality development paths. Calculating and estimating the intensity of production factors flow by multi-source big data and improved gravity model, based on which the FFBI is established to evaluated the barrier of labor flow, capital flow and technology flow. Moreover, three QAP regression models are established to identify the factors that determine the barriers of three typical production factors flow. This study provides a methodological reference for factors flow related research.

In addition, the analysis of determinants of labor flow, capital flow and technology flow in the Chengdu-Chongqing urban agglomeration highlights some implications that could assist governments in evidence-based policymaking and policy outputs. Institutional reforms such as exploring the mode of moderate separation of administrative regions and economic regions and cultivating sub-central cities are very necessary, which will effectively break the barriers of the three typical production factors. In order to promote the free flow of labor, expressway network should be further optimized and strengthened, especially the traffic lines between major cities of Sichuan province and Chongqing. In addition, in order to form the situation of coordinated industrial development and efficient capital flow, unified industrial planning of the Chengdu-Chongqing urban agglomeration should be compiled.

5.3 Limitations and uncertainty

This research also has several limitations, which also suggests avenues for further research. One limitation relates to the accuracy of using FFBI to evaluate the barrier of production factors flow. The improved gravity model used in this study mainly draws on previous studies (Wu et al., 2017), and its estimation of the intensity of the three production factors flow under natural conditions has not been fully verified, which may affect the evaluation results of factors flow barriers to some extent. The second concern is related to the representativeness of the multi-source big data used to calculate the intensity of three typical production factors flow. For instance, Baidu Migration data mainly reflects population flow (Zhang et al., 2021), including not only labor flow data, but also population flow for other purposes such as tourism flow. Thirdly, our research evaluates the barrier of labor, capital and technology flow by FFBI, insufficient attention goes to other production factors such as natural resources, management and data for some reason. These shortcomings will be addressed through model optimization and data source supplement, which we may explore in future research to establish a more comprehensive understanding of production factors flow.

6 Conclusion

In the analysis of the Chengdu-Chongqing urban agglomeration, three meta-findings about the barriers of three typical production factors flow stand out. First, although there are differences in the intensity of three typical production flow measured by different methods, Chongqing and Chengdu are at the centre of the three typical production factors flow network with the most intensive flows with other cities, but the intensity of labor, capital and technology flow between other 14 cities are all relatively weak. Second, the three typical production factors flow between most cities are hindered to a certain extent and only a small number of production factors flow between cities are facilitated. Labor flow is less hindered than capital and technology flow. The barriers of three typical production

factors flow between Chongqing and other cities are nearly all hindered. And third, administrative division hinders the three typical production factors flow in the Chengdu-Chongqing urban agglomeration. Chengdu and Chongqing, as two cities with high administrative level, their production factors flow with other cities are facilitated. In addition, the barrier of labor and capital flow are positively affected by the transportation cost and the similarity of the industrial structure, respectively.

This study aims to describe the barriers of three typical product factors flow (labor flow, technology flow and capital flow) by FFBI and identify the influence factors by QAP regression model, which help to expand the current research dimension of production factor flow. Understanding the differences in influence factors of the barriers of the three typical production factors flow is greatly beneficial for regional and urban planners to make breakthroughs in the development path of the integration mechanism of urban agglomeration. Administrative division is the key to the barriers of the three typical production factors flow in the Chengdu-Chongqing urban agglomeration, and we should be aware of the difference of other influence factors between the three typical production flow and aim at the target in promoting the free and orderly flow of production factors (Li et al., 2021).

Data availability statement

The original contributions presented in the study are included in the article/supplementary material further inquiries can be directed to the corresponding author.

Author contributions

YZ: conceptualization, methodology, writing. XW: review and editing. ML: data curation, methodology. YC: writing—review and editing. FY: data curation.

Funding

This work was financially supported by the Philosophy and Social Science Research Fund of Project funded by China Postdoctoral Science Foundation (2021M700760) and the Chengdu University of Technology (Grant no. YJ2021-QN007).

Conflict of interest

The authors declare that the research was conducted in the absence of any commercial or financial relationships that could be construed as a potential conflict of interest.

Publisher's note

All claims expressed in this article are solely those of the authors and do not necessarily represent those of their affiliated organizations, or those of the publisher, the editors and the reviewers. Any product that may be evaluated in this article, or claim that may be made by its manufacturer, is not guaranteed or endorsed by the publisher.

References

Andreas, D., Jappe, E., and Arlo, P. (2020). Global value chains, the anti-globalization backlash, and EU trade policy: A research agenda. *J. Eur. Public Policy* 27 (6), 944–956. doi:10.1080/13501763.2019.1619802

Atif, R. M., Haiyun, L., and Mahmood, H. (2016). Pakistan's agricultural exports, determinants and its potential: An application of stochastic frontier gravity model. *J. Int. Trade Econ. Dev.* 26 (3), 257–276. doi:10.1080/09638199.2016.1243724

Ben David, N. (2010). A technique for gradual identification of labor market flows. *Comput. Econ.* 36 (4), 341–364. doi:10.1007/s10614-010-9221-3

Castells, M. (1996). *Rise of the network society: The information age: Economy, society and culture*. London: Blackwell.

Chen, M. (2020). Economic spatial connection and evolution trend of national urban agglomeration:take Harbin-Changchun Urban Agglomeration as an example. *Econ. Geogr.* 40 (5), 99–105. doi:10.15957/j.cnki.jjdl.2020.05.011

Chong, Z., Qin, C., and Pan, S. (2018). The evolution of the belt and road trade network and its determinant factors. *Emerg. Mark. Finance Trade* 55 (14), 3166–3177. doi:10.1080/1540496X.2018.1513836

Chu, Z., Liu, C., Li, G., and Guan, K. (2018). Sustainable development of the economic Circle around beijing: A view of regional economic disparity. *Sustainability* 10, 3691. doi:10.3390/su10103691

Cranmer, S. J., Leifeld, P., McClurg, S. D., and Rolfe, M. (2017). Navigating the range of statistical tools for inferential network analysis. *Am. J. Political Sci.* 61 (1), 237–251. doi:10.1111/ajps.12263

Daniel, G. (2006). On the empirics of market Integration in ECOWAS. *J. Policy Reform* 9 (4), 289–303. doi:10.1080/13841280601124955

Dash, N. G., and Rae, A. (2016). An economic geography of the United States: From commutes to megaregions. *Plos One* 11 (11), e0166083. doi:10.1371/journal.pone.0166083

Ding, X., and Sui, L. (2021). The complexity of global capital flows: Evidence from G20 countries. *Discrete Dyn. Nat. Soc.* 2021 (2), 1–15. doi:10.1155/2021/1162155

Dong, X., and Chi, R. (2020). Characteristics of the temporal and spatial pattern of the economic disparity and convergence between different regions in China. *Econ. Geogr.* 40 (10), 11–21. doi:10.15957/j.cnki.jjdl.2020.10.002

Duan, Y., and Jiang, X. (2021). Pollution haven or pollution halo? A Re-evaluation on the role of multinational enterprises in global CO2 emissions. *Energy Econ.* 97, 105181. doi:10.1016/j.eneco.2021.105181

Fan, H. (2022). Vigorously promote high-quality economic development in Western region: Preface to "research report on the high-quality development of western China's economy (2021). *Reg. Econ. Rev.* 01, 9–15. doi:10.14017/j.cnki.2095-5766.2022.0002

Feldstein, M., and Horioka, C. (1979). *Domestic savings and international capital flows*. Cambridge, Massachusetts: National Bureau of Economic Research, Inc. NBER Working Paper No. w0310.

Gao, P., He, D., Ning, Y., and Han, M. (2021). Spatio-temporal dynamics and factors of urban investment linkage level in the Yangtze River Delta. *Geogr. Res.* 40 (10), 2760–2779. doi:10.11821/dlyj020200453

Gui, Q., Du, D., Liu, C., Xu, W., Hou, C., Jiao, M., et al. (2021). Structural characteristics and influencing factors of the global inter-city knowledge flows network. *Geogr. Res.* 40 (05), 1320–1337. doi:10.11821/dlyj020200443

Guo, Q., and Zhang, Z. (2017). Spatial-temporal evolution of factors aggregating ability in urban agglomeration in the middle reaches of the Yangtze River. *Acta Geogr. Sin.* 72 (10), 1746–1761. doi:10.11821/dlxb201710002

He, C., Ren, Z., and Wang, W. (2022). Dual circulation" and Beijing-Tianjin-Hebei high-quality coordinated development: From the division in the value chain and factor mobility perspective. *Acta Geogr. Sin.* 77 (6), 1339–1358. doi:10.11821/dlxb202206004

Jin, B., Yan, L., Sha, J., and Yao, Z. (2018). The spatial difference of the intensity of information and capital flow in Chinese provincial region: A case study of mobile phone transactions in jingdong Mall in 2015. *Sci. Geogr. Sin.* 38 (2), 223–232. doi:10.13249/j.cnki.sgs.2018.02.008

Ju, Y., and Sohn, S. Y. (2015). Identifying patterns in rare Earth element patents based on text and data mining. *Sci. Int. J. All Quantitative Aspects Sci. Sci. Policy* 102 (1), 389–410. doi:10.1007/s11192-014-1382-8

Jung, W. S., Wang, F., and Stanley, E. (2008). Gravity model in the Korean highway. *Europhys. Lett.* 81 (4), 48005–5. doi:10.1209/0295-5075/81/48005

Karemera, D., Oguledo, V. I., and Davis, B. (2000). A gravity model analysis of international migration to North America. *Appl. Econ.* 32 (13), 1745–1755. doi:10.1080/000368400421093

Lee, W. J., Lee, W. K., and Sohn, S. Y. (2016). Patent network analysis and quadratic assignment procedures to identify the convergence of robot technologies. *PLoS ONE* 11 (10), e0165091. doi:10.1371/journal.pone.0165091

Li, J., and Miao, C. (2017). Impact of population flow on regional economic disparities in the Yangtze River economic belt[J]. *Acta Geogr. Sin.* 72 (2), 197–212. doi:10.11821/dlxb201702002

Li, Y., Zhang, Y., Lee, V., and Li, J. (2021). Structural characteristics and determinants of an international green technological collaboration network. *J. Clean. Prod.* 324, 129258. doi:10.1016/j.jclepro.2021.129258

Li, Z., Wang, S., Cheng, L., Shi, X., Guan, H., and Shu, C. (2022). Differences and relationship between population flow and transportation networks in North-east China. *Prog. Geogr.* 41 (6), 985–998. doi:10.18306/dlkxjz.2022.06.004

Liu, J., Corredig, M., and Alexander, M. (2007). QAP: A unique method of measuring "relationships" in relational data. *Colloids Surf. B Biointerfaces* 27 (4), 164–170. doi:10.1016/j.colsurfb.2007.05.004

Lottum, J. V., and Marks, D. (2011). The determinants of internal migration in a developing country: Quantitative evidence for Indonesia, 1930–2000. *Appl. Econ.* 44, 4485–4494. doi:10.1080/00036846.2011.591735

Mitchelson, R. L., and Wheeler, J. O. (1994). The flow of information in a global economy: The role of the American urban system in 1990. *Ann. Assoc. Am. Geogr.* 84 (1), 87–107. doi:10.1111/j.1467-8306.1994.tb01730.x

Moll, B., Townsend, R. M., and Zhorin, V. (2017). Economic development, flow of funds, and the equilibrium interaction of financial frictions. *Proc. Natl. Acad. Sci. U. S. A.* 114 (24), 6176–6184. doi:10.1073/pnas.1707055114

Niu, X., Wang, Y., and Ding, L. (2018). Delimitation of city hinterland in regional urban system: Measurement and validation. *City Plan. Rev.* 42 (12), 15–22. doi:10.11819/cpr20181203a

Saleh, S., Lu, Q., and Sokvibol, K. (2019). Determinants of exports in China's meat industry: A gravity model analysis. *Emerg. Mark. Finance Trade* 55 (11), 2544–2565. doi:10.1080/1540496X.2019.1578647

Shi, Y., and Pan, Z. (2021). The spatial structural features and spatial pattern optimization of Chengdu-Chongqing Urban Agglomeration. *Macroecon. Manag.* 07, 21–27. doi:10.19709/j.cnki.11-3199/f.2021.07.007

Tinbergen, J. (1966). Shaping the world economy: Suggestions for an international economic policy. *Econ. J.* 76 (301), 92–95. doi:10.2307/2229041

Torre, A. (2008). On the role played by temporary geographical proximity in knowledge transmission. *Reg. Stud.* 42 (6), 869–889. doi:10.1080/00343400801922814

Walz, U. (1997). Dynamic effects of economic integration: A survey. *Open Econ. Rev.* 8, 309–326. doi:10.1023/a:1008298900468

Wang, W., and Yang, D. (2021). Factor flow and total factor productivity: Based on spatial DCubin model. *Science-technology Manag.* 23 (6), 12–20. doi:10.16315/j.stm.2021.06.003

Wang, Y., Niu, X., and Meng, X. (2017). Research progress of regional spatial structure under the perspective of space of flow. *Urban Plan. Int.* 32 (06), 27–33. doi:10.22217/upi.2017.012

Wang, Y., Wang, H., Zhang, B., and Huang, X. (2021). Analysis on the network structure of urban agglomeration and its influencing factors based on the perspective of multi-dimensional feature flow: Taking wuhan urban agglomeration as an example. *Econ. Geogr.* 41 (6), 68–76. doi:10.15957/j.cnki.jjdl.2021.06.008

Wang, J., Du, F., Jing, Y., and Du, D. (2022). Spatial-industry paths of technology transfer: An empirical study of Northeast China. *Resour. Sci.* 44 (2), 365–374. doi:10.18402/resci.2022.02.12

Wu, P., Zhu, X., and Wang, W. (2017). A study on the impact of inter-city industrial linkages on economic output among ten megalopolises of yangtze river economic belt: Based on the inter industryinput-output gravity model. *Urban Stud.* 24 (7), 49–55. doi:10.3969/j.issn.1006-3862.2017.07.007

Xie, P., and Lin, Z. (2016). Local protectionism, factor prices distortion and resources misallocation: Empidical evidence from A-share listed companies. *Finance Trade Econ.* 37 (02), 71–84. doi:10.19795/j.cnki.cn11-1166/f.2016.02.006

Xu, W., Yi, J., and Cheng, J. (2022). The heterogeneity of high-quality economic development in China's mining cities: A meta frontier function. *Int. J. Environ. Res. Public Health* 19 (11), 6374. doi:10.3390/ijerph19116374

Yang, H., Tong, Q., and Zhao, P. (2022). Study on the impact of the Beijing–Shanghai high-speed railway on regional economic equity based on economic performance. *Ann. Reg. Sci.* 68, 229–253. doi:10.1007/s00168-021-01077-8

Yin, J., Liu, H., Shi, P., and Zhang, W. (2021). Exploring coupling relationship between urban connection and high-quality development using the case of Lanzhou-Xining Urban Agglomeration. *Complexity* 2021, 1–12. doi:10.1155/2021/9933582

Young, A. (2000). The razor's edge: Distortions and incremental reform in the People's republic of China. *Q. J. Econ.* 115 (4), 1091–1135. doi:10.1162/003355300555024

Zhan, C., Tse, C. K., Fu, Y., Lai, Z., and Zhang, H. (2020). Modeling and prediction of the 2019 coronavirus disease spreading in China incorporating human migration data. *Plos One* 15 (10), e0241171. doi:10.1371/journal.pone.0241171

Zhang, Z., Wu, D., and Zhou, S. (2018). Production factor mobility, rgional coordination and integration and economic growth. *J. Industrial Technol. Econ.* 37 (11), 58–66. doi:10.3969/j.issn.1004-910X.2018.11.008

Zhang, W., Zhuang, X., Lu, Y., and Wang, J. (2020). Spatial linkage of volatility spillovers and its explanation across G20 stock markets: A network framework. *Int. Rev. Financial Analysis* 71, 101454. doi:10.1016/j.irfa.2020.101454

Zhang, X., Han, H., Tang, Y., and Luo, G. (2021). Research on the characteristics of urban network structure in China based on baidu migration data. *J. Geo-information Sci.* 23 (10), 1798–1808. doi:10.12082/dqxxkx.2021.210223

Zheng, L., Long, F., and Zhang, S. (2020). Comparison of the spaces of call and traffic flows: An empirical study of Qianzhong urban region, China. *Cities* 107, 102927. doi:10.1016/j.cities.2020.102927

Zhou, B., Wang, N., Zhang, Z., Liu, W., Lu, W., Xu, R., et al. (2022). Research on the Spatial-temporal differentiation and path analysis of China's provincial regions' high-quality economic development. *Sustainability* 14, 6348. doi:10.3390/su14106348

Zhou, C., Zeng, G., and Shang, Y. (2019). Progress and prospect of research on innovation networks:A perspective from evolutionary economic geography. *Econ. Geogr.* 39 (5), 27–36. doi:10.15957/j.cnki.jjdl.2019.05.004

frontiers | Frontiers in Environmental Science

TYPE Original Research
PUBLISHED 11 November 2022
DOI 10.3389/fenvs.2022.1056854

Check for updates

OPEN ACCESS

EDITED BY
Ding Ma,
Shenzhen University, China

REVIEWED BY
Li Peng,
Sichuan Normal University, China
Chun Li,
Yunnan University, China

*CORRESPONDENCE
Huiting Chen,
huiting_chen@whu.edu.cn

SPECIALTY SECTION
This article was submitted to Environmental Informatics and Remote Sensing, a section of the journal Frontiers in Environmental Science

RECEIVED 29 September 2022
ACCEPTED 26 October 2022
PUBLISHED 11 November 2022

CITATION
Liu Y, Zhang H, Chen H and Chen C (2022), Flood impact on urban roads and commuting: A case study of Wuhan, China.
Front. Environ. Sci. 10:1056854.
doi: 10.3389/fenvs.2022.1056854

COPYRIGHT
© 2022 Liu, Zhang, Chen and Chen. This is an open-access article distributed under the terms of the Creative Commons Attribution License (CC BY). The use, distribution or reproduction in other forums is permitted, provided the original author(s) and the copyright owner(s) are credited and that the original publication in this journal is cited, in accordance with accepted academic practice. No use, distribution or reproduction is permitted which does not comply with these terms.

Flood impact on urban roads and commuting: A case study of Wuhan, China

Yaolin Liu[1,2,3], Hongxin Zhang[1], Huiting Chen[1]* and Cuizhen Chen[4]

[1]School of Resource and Environmental Sciences, Wuhan University, Wuhan, China, [2]Key Laboratory of Geographic Information System, Ministry of Education, Wuhan University, Wuhan, China, [3]Collaborative Innovation Center for Geospatial Information Technology, Wuhan University, Wuhan, China, [4]Wuhan Institute of Water Science Researching in Hubei Province, Wuhan, China

Rainfall events have become more frequent and more serious, leading to rampant floods. Floods in urban areas greatly impair the serviceability of the transport system and cause disruption to commuting. However, little is known about the commute response under various rainfall scenarios in developing country cities despite the uncertainty of climate change. A high-resolution flood modeling module and a commute simulation module were integrated to examine the impact on commuting under floods. Flood maps under three rainfall scenarios with increasing rainfall intensity and duration were obtained, and road vulnerability was assessed considering the speed drop. We innovatively employed location-based service big data to perform commute simulation under floods based on the shortest time cost principle. The results show that a large amount of passable but affected commuters become disconnected commuters as the rainfall intensity increases. Also, commute loss of each traffic zone would not increase linearly, which means that the emphasis and strategy of disaster prevention and mitigation are not the same in different rainfall scenarios. We integrated hot spots of flood exposure, road vulnerability, and commuting loss and found that there was inconsistent spatial distribution between the three indicators. This indicates that areas need to take different measures according to the local damage characteristics. This work studied the relationship between severe weather conditions and commuting activity performance at the city level and has important practical guiding significance for building resilient cities.

KEYWORDS

urban flood, flood mapping, road vulnerability, commute simulation, location-based service (LBS) data

1 Introduction

Under the backdrop of climate change and its uncertainty, studies predict that future rainfall intensity and frequency would continue to increase (Kendon et al., 2012; Birch, 2014). With dense population and economic activities, cities have high land-use density and high proportion of impervious cover area. Moreover, due to the promotion of

intensive and economical land use, increasing underground space mining and other construction activities have further greatly changed the urban built environment (Zhang et al., 2019). These changes, coupled with inadequate response by drainage facilities, eventually led to floods. Due to the high-intensity utilization of urban space, road and drainage systems have become two highly overlapped systems related to surface floods. When the drainage system is insufficient or poorly managed to accommodate the runoff caused by high-intensity rainwater, the road system would be the first to be directly affected (Singh et al., 2018; Yang et al., 2019). Flood damage to road systems will hinder urban traffic and greatly weaken the service capacity of urban transport systems (Fu et al., 2014; Borowska-Stefańska and Wiśniewski, 2018). To mitigate the impact of flood disruptions, it is necessary to obtain knowledge of traffic response in flood scenarios. Flood response is often passive and lacks proactive preventive research in many cities of developing countries. Also, many researchers have studied coastal cities to explore the impact of floods on urban commuting (Keeler et al., 2018; Kasmalkar et al., 2020a). However, there are few case studies exploring traffic response under floods in inland cities. Therefore, it is very urgent to evaluate urban road vulnerability and traffic response of inland cities in developing countries under floods caused by bad weather.

A recent literature suggests that road vulnerability in bad weather is receiving increasing attention. A more commonly accepted definition of road network vulnerability is the "susceptibility" or "sensitivity" of road networks to disruptions (Berdica, 2002). According to different research interests of the research field, the value dimensions of performance indicators to reveal road vulnerability are different (Jenelius et al., 2006; Balijepalli and Oppong, 2014; El-Rashidy and Grant-Muller, 2014; Mattsson and Jenelius, 2015). Many scholars in the field of transportation networks focused on measuring the impact of local road failure on the overall road network system from a global perspective (Demirel et al., 2015; Casali and Heinimann, 2019). Scholars who focus on spatial justice tend to reveal local road damage in spatial units or at the scale of road sections (Liu et al., 2021). Many researchers often use critical thresholds based on the work of Shah et al. (2021) to determine whether a road section can work. Roads that flooded deep below the threshold are considered normal, while roads that flooded above the threshold are removed during road network modeling (Chen et al., 2015; Jie et al., 2016; Coles et al., 2017). This binary assumption means that the impact on the specific service performance of roads is ignored. Because flooded roads do not necessarily mean complete failure, it is possible for them to travel at a lower speed. Liu et al. (2021) used the actual monitoring data to distinguish between smooth or congested or severely congested roads and to measure road vulnerability in floods, which also means that road damage within the same threshold is seen as homogenized. Speed, as an important service performance of road infrastructure, is an important measure under disturbance, but has not been given sufficient attention in the current road vulnerability research. Pregnolato et al. (2017) simulated the relationship between flood depth and the vehicle speed and plotted the relationship. The characterization of this relationship opens up the space for discussion of the speed impact details of flooded roads. Using this equation, the reduction of network speed during floods can be calculated. This study will also use the depth speed curve to further modify the speed of flooded roads to simulate residents' routes based on the shortest travel time rule to explore commuting responses in flood scenarios.

So far, traffic response, especially the commuting theme under floods, has attracted the attention of many scholars and accumulated a large amount of contributions. Popular topics for commuting exposure in floods mainly include the accessibility assessment between regions, prediction of the amount of impassable commuters, and the estimation of increased commuting time costs and their economic costs (Aghababaei et al., 2021; Borowska-Stefańska and Wiśniewski, 2018; Debionne et al., 2016; Hauer et al., 2021a; Liu et al., 2021). Some studies have found knowledge of local commuting disruption and road performance under flood events by analyzing the actual traffic data during floods (Chung, 2012; Liu et al., 2021). The advantage of this data-driven method is that the results are credible. However, due to the limited financial and monitoring resources, it is difficult for most cities to collect spatiotemporal commuting behavior data in real disasters. Therefore, it is necessary to grasp the knowledge of commuting response in flood events in advance through simulation methods. In addition, the uncertainty of climate change also makes it necessary to know in advance under various rainfall scenarios. The development of hydrological models makes it possible to simulate urban waterlogging with high precision. Integrating the flood simulation module and the commuting simulation module that can be flexibly applied to various flood scenarios, to measure the commuting impact under flood events, is the common method used in many studies (Kasmalkar et al., 2020b; Tsang and Scott, 2020; Hauer et al., 2021a).

As for commuting simulation, it is important to accurately clarify the commuting demands of residents. The commonly used method is the four-step traffic assignment method, including trip generation, trip distribution, modal split, and traffic assignment (Sharma and Chandel, 2020). A commuting survey sampling dataset was also employed to determine travel OD demand (He et al., 2021a). Many studies employed the gravity model and the Monte Carlo method through demographic data and other spatial data of employment to estimate travel OD (Hu and Downs, 2019; Liu et al., 2021). Although this method can be verified by statistical data to some extent, it is still not the real commuting OD of urban residents but only a proxy indicator for commuting OD demand. With the

development of information technology, geographic commuting big data have gradually been applied to urban studies (Zhao and Cao, 2020; An et al., 2022). Many Internet companies have the ability to collect location-based services' request information received from various applications loaded on residents' electronic devices, and the location of urban residents' homes and workplaces can be calculated by clustering methods such as the density-based spatial clustering of applications with noise (DBSCAN) method (Wang et al., 2021). This kind of emerging data can greatly help to promote commuting simulation under floods. However, as far as we know, it is rare to see research that incorporates this commuting big data into the hazard field to guide analysis and decision-making. This study obtained flood maps under various rainfall scenarios using a high-precision hydrological model and attempted to use Baidu location-based service (LBS) commuting big data to predict commuting responses under floods, providing spatial information about commuting disruptions, thereby contributing to the literature.

This study has three main objectives: 1) to determine road vulnerability under multiple rainfall scenarios in combination with the impact of floods on road speed; 2) to predict and quantify the commute loss under different flood events; and 3) to explore the spatial hot spot patterns of flood exposure, road vulnerability, and commute loss. This study integrates flood modeling and spatial analysis to understand the commuting response under different flood events, aiming to provide a decision-making basis for disaster prevention and mitigation, urban planning, and commuting resilience promotion.

The remainder of this article is organized as follows. Section 2 introduces the context of the study area, Wuhan City, the experimental data and main methods including flood modeling and commute simulation, and the hot spot analysis methods used to explore the spatial patterns of flood exposure, road vulnerability, and commuter impact. In Section 3, the results of flood exposure are presented first, followed by the description of road vulnerability and commuting loss. Also, we integrated the hot spot analysis results of these three indicators and explained the similarities and differences of spatial high-value/low-value aggregation patterns. Section 4 is the discussion, focusing on the theoretical value and application value of this study and the limitation and the future direction. This article concludes with Section 5.

2 Materials and methods

2.1 Study area description

Wuhan, as the capital of Hubei Province, is an important industrial area, educational base, and transportation center in China, located between 113°41′E-115°05′E and 29°58′N-31°22′N. The terrain in the central urban area of Wuhan is low and flat, with an average elevation of about 24 m, which is lower than the average flood level of the Yangtze River (25.56 m, monitoring data from 1865 to 2013). Therefore, Wuhan is often threatened by floods in rainy seasons and has experienced frequent rainstorms and waterlogging disasters in recent years (Liu et al., 2021). On 18 June 2011, the maximum 24-h rainfall in Wuhan reached 200.5 mm, and 88 locations in the urban area were flooded. On 7 July 2013, the maximum rainfall was increased to 258.5 mm. In June 2016, Wuhan suffered the most severe flood disaster since 1998. The maximum rainfall in a single day reached 582.5 mm, which paralyzed the traffic, and nearly 200 major roads in the city were impassable (Zhiqiang, 2016).

The central urban area of Wuhan was adopted as the study area in this work, circled by the Third Ring Road, and we took the traffic analysis zone (TAZ) as the smallest research unit (Figure 1). TAZ was a commonly used research unit in the current commuting analysis. We divided the TAZs based on the road network data provided by Wuhan Geomatics Institute and adjusted it according to the Wuhan Urban Planning Unit. Finally, we obtained 512 TAZs in central Wuhan with an average area of 0.91 km^2.

2.2 Data acquisition and processing

The data used in this article are mainly used to support hydrological simulation and commuting simulation. The types and sources are shown in Table 1. The flood hydrological simulation module mainly uses vector data including land use data, digital elevation model data (DEM), drainage network facilities data, and building data. The urban building data are derived from the basic geographical conditions monitoring data of Wuhan City in 2018, and the resolution of digital elevation model (DEM) data is 10 m.

In the commuting simulation process, commuting OD data come from location-based service (LBS) data collected by Baidu whose base station records the user's location point every 5s, and the positioning accuracy in the main city of Wuhan is 50 m. In this study, we collected all of the location records during 21 working days of June 2018. First, we merged all location records into one dataset and then adopted the density-based spatial clustering of applications with noise (DBSCAN) to cluster the location points. If the clusters with large number point of night time (21:00-8:00) were located in residence land, then its geometric center was defined as the user's residence location. In the same way, clusters' center of daytime (9:00-17:00) with work land type was defined as the workplace. When the user stayed at home, his dwell points stayed around the residence. When he began to commute, the acquisition time of the first moving points was the start time. Similarly, the acquisition time of the last moving points near the workplace was the end time. Meanwhile, his commuting trajectory was also recorded so that the commuting distance, time, and speed can be calculated.

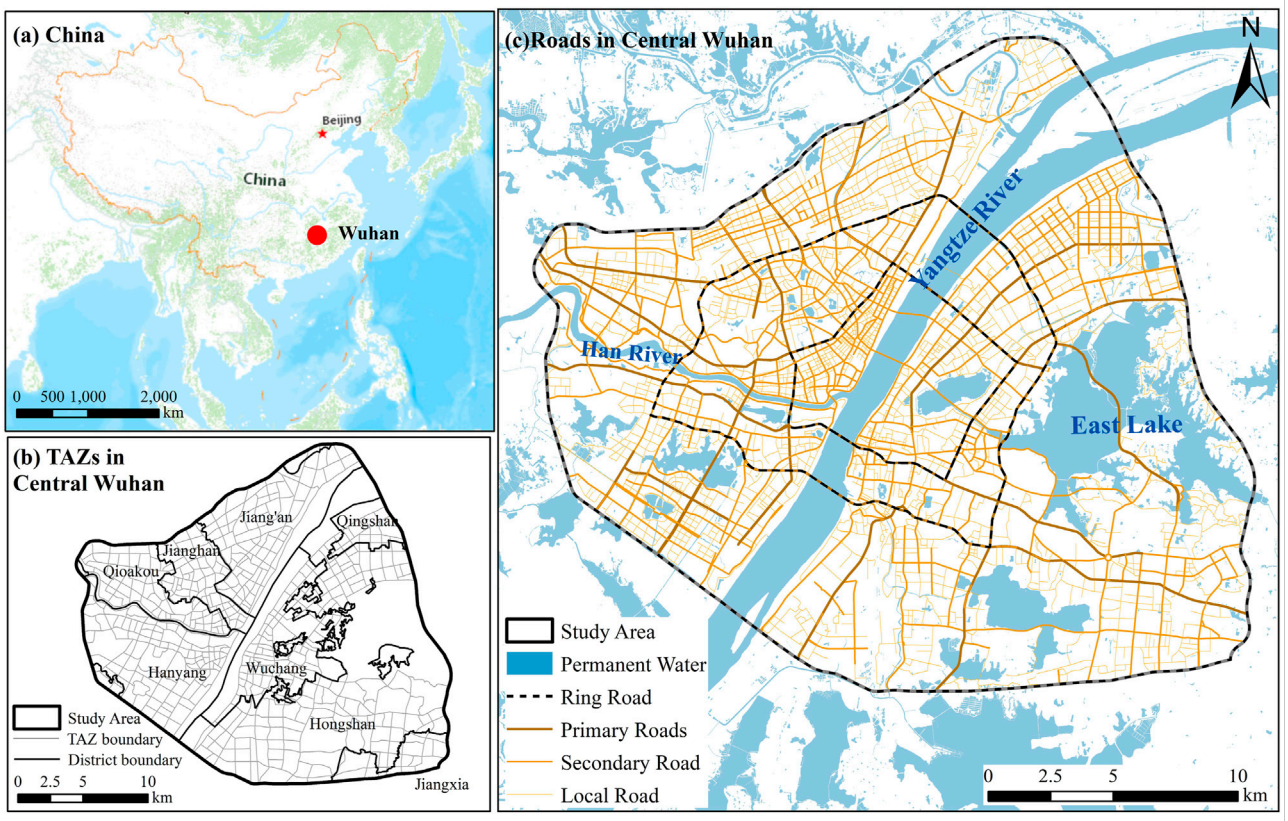

FIGURE 1
Location of the study area: **(A)** Wuhan's location in China; **(B)** Traffic analysis zones in Central Wuhan; **(C)** Roads in Central Wuhan.

TABLE 1 Names and sources of study data.

Analysis module	Data name	Data source	Resolution
Flood modeling	Land use data	Hubei Provincial Department of Natural Resources	1 m
	Digital elevation model (DEM) data	Wuhan Institute of Water Science Researching in Hubei Province	10 m
	Drainage facilities data	Wuhan Institute of Water Science Researching in Hubei Province	10 m
	Urban building data	Wuhan Geomatics Institute	10 m
Commute simulation	Commuting OD data	Wuhan Geomatics Institute	50 m
	Transport network data	Wuhan Geomatics Institute	10 m
	Traffic speed data	Amap (http://ditu.amap.com/)	—

Finally, more than 840,000 commuting OD data were identified in central Wuhan with attributes of the user's residence, employment location, and commuting trajectory characteristics (including commuting distance, time, and speed). Furthermore, the transport network data were also obtained from the General Survey and Monitoring of Geography and National Conditions in 2018, which includes attributes of road types, speed limits, and road width. The traffic speed data were crawled from Amap (http://ditu.amap.com/) based on the Python program, and the data acquisition time is from 5 April to 11 April 2021.

2.3 Flood modeling

To capture the flood inundation situation of the area under a set of rainfall scenarios, we used a hydrodynamic model to perform hazard simulation instead of directly using flooding

TABLE 2 Rainfall intensity of the simulated design rainfall scenarios with reference to Planning and Design Standards of Wuhan Drainage and Waterlogging Prevention System (HubeiBureauofQualityandTechnicalSupervision, 2013).

Scenario	Recurrence interval (year)	Rainfall (mm)	Duration (h)
A	10	205	24
B	30	273	24
C	50	303	24

events records, which cannot satisfy the data demand of continuous rainfall intensity sequence. The Wallingford Software model for integrated catchment management (ICM6.5) is employed in this study to produce outputs for each time step of the simulation to give flood depths and velocities. ICM6.5, integrating shallow drainage pipe network and river channels, can construct one-dimensional and two-dimensional water conservancy models of urban waterlogging for comprehensive drainage simulation at high resolution (Sidek et al., 2021). This study used the Chicago rainfall pattern and considered rainfall intensity uniform across the model domain. The rainfall series considered is summarized in Table 2. In this study, we choose 10-year, 30-year, and 50-year floods to perform hazard modeling, considering the local climate condition in Wuhan. The degree of the most severe flood disaster in Wuhan recently (in 2016) was basically close to a 50-year flood (People's Government of Hubei Province, 2016), and the common rainfall intensity in summer is similar to that of a 10-year flood. We add a 30-year flood between them in order to set a continuous sequence.

The process of flood modeling during rainfall consists of three main steps (Chen et al., 2016).

(1) Model building. Data of drainage facilities responsible for rainwater discharge functions, including rainwater pipe networks, drainage ports, pumping stations, and storage lakes, were imported into InfoWorks ICM6.5, which was commonly used in flood modeling (Sidek et al., 2021). The catchment area was divided based on the terrain and image data, and runoff generation parameters were determined through the analysis of the underlying surface. The SWMM (storm water management model) nonlinear reservoir method (Xiong and Melching, 2005) (i.e., using the finite difference method to approximate the continuous equation and the Manning equations) was used to simulate the surface confluence process of subcatchment areas divided in the runoff generation model.
(2) Model calibration and validation. We selected the actual measurement data and facility operating condition data in the water system during heavy rain from 12:00 on 30 June 2016 to 12:00 on 14 July 2016 to calibrate and check the model. The maximum rainfall in this field on the 7th day is 582.5 mm (Wuhan National Meteorological Station), which is the highest weekly rainfall since the meteorological record of Wuhan City. After one-dimensional and two-dimensional calibrations, the simulated water level and the monitored water level of each monitoring station are evaluated using the NSE (Nash–Sutcliffe coefficient) (Moriasi et al., 2007). The closer the NSE to 1, the smaller the deviation between the simulated value and the measured value, and the better the simulation effect. NSE <0 means that the simulation reliability is low, NSE >0.5 means that the simulation result has good credibility, and NSE ≥0.65 means the simulation result is very good and has high credibility. The results of comparative analysis of calculated values of the main lake nodes (see Supplementary Appendix SA1) show that the overall agreement between the model simulation results and the measured data after verification is good.
(3) Model calculation. For a given scenario of rainfall, water depth and velocity were calculated dynamically throughout the simulation period and reported at each time step as each subcatchment area (divided based on the terrain and image data). However, with the huge amount of computation, caution must be applied, the maximum inundation depth instead of the dynamic changes during the entire process was selected for subsequent road network analysis to reduce the calculating burden. This is reasonable in this study as residents are inclined to make driving decisions based on the most severe submergence of road sections out of caution.

2.4 Commute simulation under floods

In order to compare the discrepancy between residents' commuting distance and time under different scenarios, it is necessary to distribute the commuting routes of every OD pair. The simulation process is divided into three steps.

(1) OD pairs filtering and road network processing. Different from the normal scenario, it is vital to consider the impact of floods on the road under flood scenarios. When the flooded depth exceeds 30 cm, the air intake of the vehicle will be submerged, which will seriously affect the performance of the vehicle (Shah et al., 2021). Therefore, the OD pairs and roads located in areas with flood depth more than 30 cm

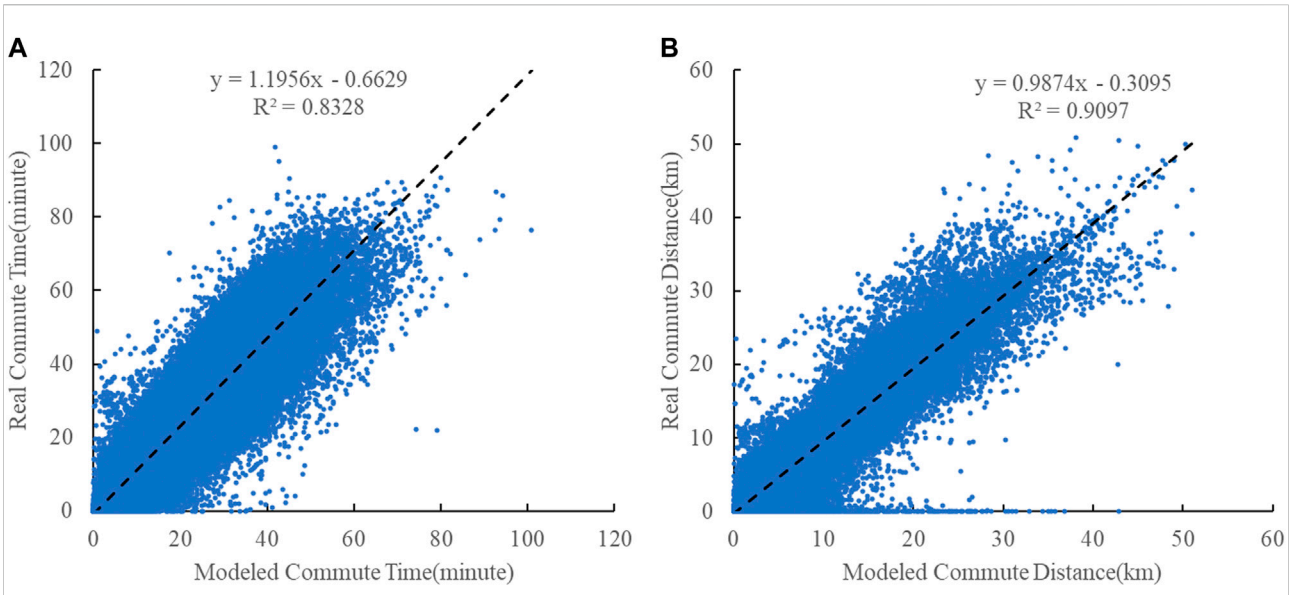

FIGURE 2
Results verification: modeled commute time **(A)** and modeled commute distance **(B)**.

have been removed. Moreover, although roads with a water depth of less than 30 cm can pass normally, the speed of vehicles on this road will be limited. Pregnolato et al. (2017) proposed a function that described the relationship between the maximum vehicle speed and water depth under flood scenarios (Eq. 1):

$$v(w) = 0.0009w^2 - 0.5529w + 86.9448 \quad (1)$$

where the speed $v(w)$ is the limited maximum speed and w ($0 < w < 300$ mm) is the depth of water. It should be noted that commute simulations in normal scenarios can skip this step.

(2) Shortest path distributing. Based on the OD pairs' location and the construction of road network, commute route distributions were implemented with ArcMap10.5 software by the extensions module "network analyst." Assuming that the commuters tend to take the least-time-cost path, we applied the new route option in the network analyst to assign commute paths between origins and destinations with the objective of minimizing time cost. Each path's commute distance and time can also be calculated.

(3) Results verification. We compared our simulation results under normal scenario to real commute time and distance in original OD pair records of the LBS data. The Pearson correlation coefficient (CORREL) and root mean square error (RMSE) were used as evaluation indices. Figure 2 shows the fitting curves of the modeled and real commute time and distance. The modeled results are highly consistent with the real commute time and distance. The modeled time and real time have a Pearson correlation coefficient of 0.913** ($p < 0.01$) and a root mean square error of 0.12, while the distance has a Pearson correlation coefficient of 0.958**($p < 0.01$) and a root mean square error of 1.79.

2.5 Hot spot analysis

Hot spot analysis (Getis-Ord Gi*) can be calculated by ArcGIS software to obtain the spatial distribution of high-value and low-value elements and clustering situation. The Z score of the calculation result represents the multiple of standard deviation, which can reflect the dispersion degree of the dataset. A highly affected cluster area by flood surrounding a highly affected area is called a hot-spot cluster. On the contrary, the less affected area surrounded by a clustered area of low value is called a cold spot clustered area (CAO et al., 2020). In this work, Getis-Ord Gi* local statistics was used to identify statistically significant hot spots and cold spots of TAZs affected by floods. The calculation formula is shown in Eqs 2–4.

$$G_i = \frac{\sum_{i=1}^{n} z_{hi}k_i - \bar{X}\sum_{i=1}^{n} z_{hi}}{S\sqrt{\frac{n\sum_{i=1}^{n} z_{hi}^2 - \left(\sum_{i=1}^{n} z_{hi}\right)^2}{n-1}}} \quad (2)$$

$$\bar{X} = \frac{\sum_{i=1}^{n} k_i}{n} \quad (3)$$

$$S = \sqrt{\frac{\sum_{i=1}^{n} k_i^2}{n} - \bar{X}^2} \quad (4)$$

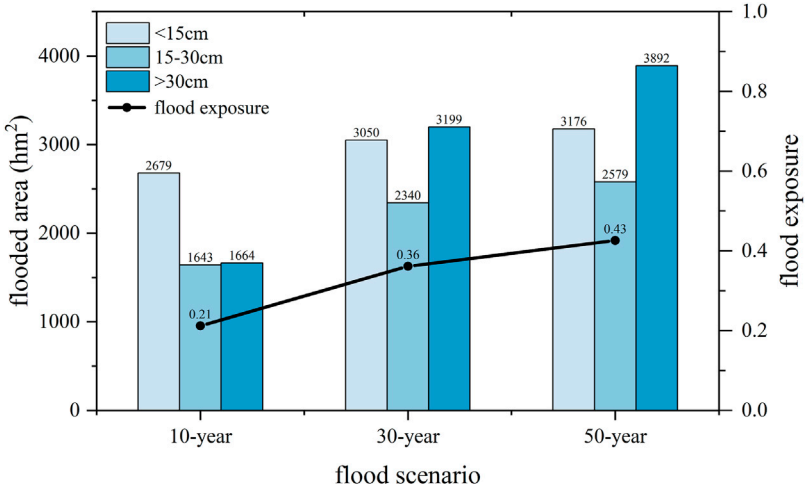

FIGURE 3
Characterization of the flood area and flood exposure.

where G_i is the Z score of output result; k_i is th statistic index of TAZ i; z_{hi} is the spatial weight between TAZ h and i; n is the total amount of TAZ; X is the average of statistical index; S is the standard deviation.

3 Results

3.1 Flood modeling and exposure mapping

Taking the traffic analysis zones as the analysis unit, we counted the flood area at different depths under the three rainfall scenarios (Figure 3), including less than 15 cm, 15–30 cm, and more than 30 cm, respectively. The results revealed that water area of depth less than 15 cm increased the smallest, only from 2,679 to 3,176 ha, while water area of depth greater than 30 cm increased the most of 2,228 ha. We use an indicator of flood exposure to represent the comprehensive hazard degree. The space of the traffic analysis zones (TAZs) that bears the disaster was homogenized, while the degree of flood disaster is considered and divided into three types including less than 15 cm, 15–30 cm, and more than 30 cm. Then, AHP (analytic hierarchy process) (Saaty, 1980) was adopted to derive the severity weight of the three types of flood depths (see Supplementary Appendix SA2 for the weight results). The flooded area of each traffic zone was multiplied by the weight to obtain the flood exposure, and subsequently, the product results were summarized and shown at the scale of the traffic analysis zones. As the intensity of flood increases, flood exposure of a 30-year flood became approximately 1.7 times that of a 10-year flood, and flood exposure of 50-year flood became more than twice the 10-year flood exposure.

Figure 4 shows the spatial distribution of flood exposure under three flood scenarios, and we put the spatial distribution map of flood area under three rainfall scenarios in Supplementary Appendix SA1). Under the 10-year flood scenario, flood exposure of the whole area is relatively light, and only three TAZs have more than 18.84 ha of standing water. With the increase in rainfall intensity, areas seriously flooded began to increase. Large patches of standing water emerged in Qiaokou District and Jianghan District in the northwest. The terrain in this area is relatively low and flat, combined with many buildings, wide impervious surface, and poor drainage capacity, resulting in serious water accumulation. Also, there was serious water accumulation around East Lake, Shahu Lake, South Lake, and other lakes. This may be due to the generally low terrain around the lake. If the water storage capacity of the lake exceeds a certain limit, it is prone to overflow when urban waterlogging occurs; therefore, the areas around the lake are easily affected.

3.2 Vulnerability assessment of road networks

Figure 5 shows the proportion of flooded road length under different floods. In a 10-year flood, 10.53% of the roads are flooded, and this ratio increases to 13.63% in a 50-year flood. Among the flooded roads, flooded roads of 15–30 cm depth accounted for the highest proportion and increased the most with the increase in flood intensity, which increased twice by 123.19 km from a 10-year flood to a 50-year flood. Flooded roads of depth more than 30 cm, or failed impassable roads, also increase in length as the flood intensity increases. The impassable road in the 10-year flood is 2.35 km, which increases to 3.92 km

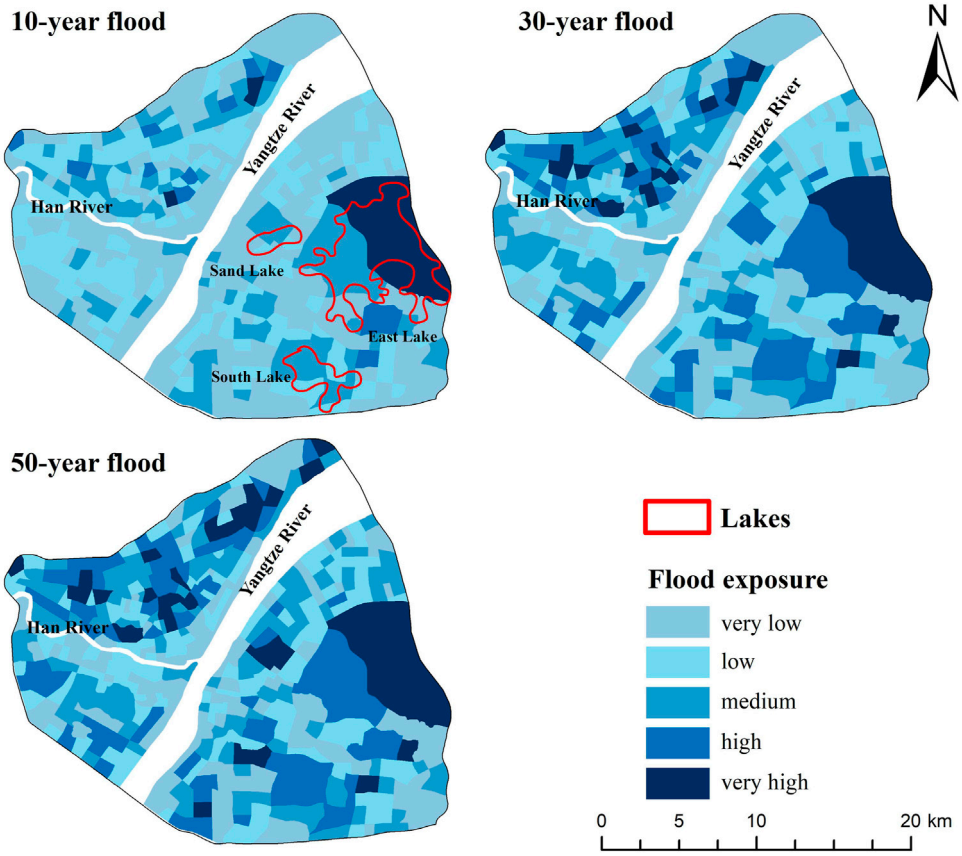

FIGURE 4
Spatial distribution of flood exposure under three flood scenarios in traffic analysis zones.

in the 30-year flood and finally to 11.99 km in the 50-year flood, more than five times that in the 10-year flood.

The first line of Figure 6 shows the distribution of the roads affected by standing water under each flood scenario within the Third Ring. It can be seen that the distribution pattern of the affected roads is consistent with the standing water, and the declined velocity of the road in the area with severe stagnation is relatively high. Specifically, affected roads were mainly present in Jiang'an District, Jianghan District, and Jiangdi Street of Hanyang District in the northwest, as well as the area around East Lake. In terms of the changes in roads velocity under three scenarios, the speed reduction in the 10-year scenario is relatively small, generally within 1–10 km/h. With the increase in flood intensity, the speed limit gradually increases. In the 50-year scenario, roads with a velocity decline of more than 30 km/h becomes the major part.

According to the declined velocity of the road, we further classified the affected roads into three types. The roads with a decrease in travel speed of 1–10 km/h were divided into low-declined type, the roads with a decrease of 11–30 km/h were divided into medium-declined type, and the decrease of more than 30 km/h were divided into high-declined type. Then, the proportion of the roads in three types is calculated. The second line of Figure 6 shows the length ratio of the three declined types in each TAZ. The area A in Figure 6 located in Jiangdi Street and the area D located in the north of Jiyuqiao Street both have a high level of road speed reduction under the three flood scenarios. Almost all flooded roads in the two areas experienced a speed drop of more than 30 km/h. The surroundings of area A are all highlands; therefore, the accumulated water is easy to converge to area A. Area D is located between Sand Lake and the Yangtze River, therefore more vulnerable to floods. The declined level of road speed in area B shows a trend from low to medium to high. It can be seen that the drop in the road travel speed is also increasing with the increase in flood intensity in this area. Area C is the area with more serious flood exposure under the flood scenario, but the main speed drop level of the traffic area is relatively low. Even in the 50-year flood, the main type seemed to be medium, and only a few regions showed high level. This may be because the area belongs to the central business district of Wuhan City. The traffic in this area is relatively congested, and the road speed is low under normal times, basically around 30 km/h.

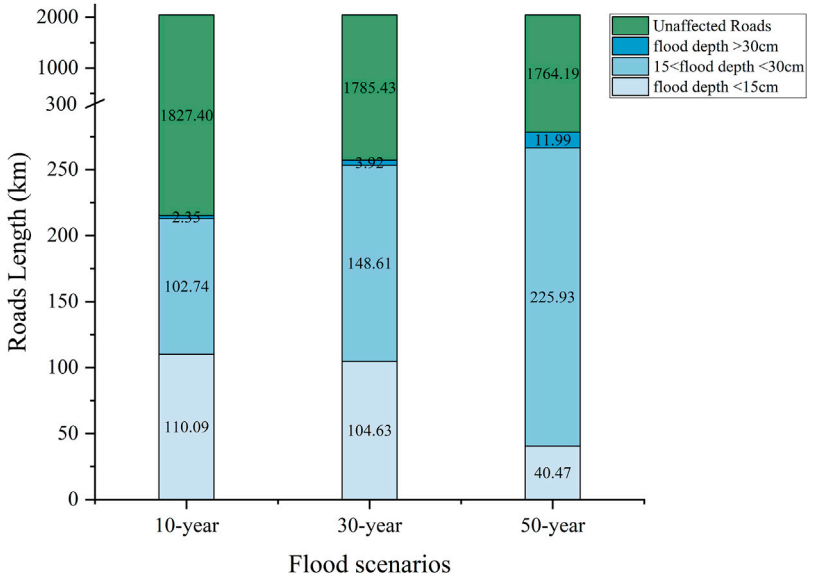

FIGURE 5
Characterization of the flooded road under three flood scenarios.

The impact of floods on the transport network within a traffic zone includes not only the declined velocity of affected roads but also the length of roads affected. Therefore, we measure the vulnerability of the road network in terms of both the length of the affected roads and the declined velocity (Formula 1).

Roads vulnerability = Affected length of roads × Declined velocity.

The third line of Figure 6 shows the distribution of road vulnerability at the scale of the traffic analysis zones in each scenario. The road vulnerability level is generally low in the 10-year flood. Only the southern Jiangdi Street, the northwestern Hanxing Street and Changfeng Street, and the eastern East Lake Scenic Area Streets showed a higher level. When the flood intensity increased to 30-year and 50-year return period, the road vulnerability level increased significantly, showing a spatial pattern of contiguous distribution of high-level vulnerable traffic analysis zones.

3.3 Analysis of commute condition under floods

The commuting loss caused by flood is mainly seen in two aspects, including commuting trip cancellation and increased commuting time. Under floods, all commuting trips can be divided into three categories: disconnected, passable but affected, and unaffected. Figure 7 shows the statistical results of the three commuting types under three flood scenarios. The horizontal axis in the figure represents the commuting distance in the normal scenario, with a distance interval of 5 km. The left ordinate represents the proportion of the three types, and the right ordinate represents the number of commuters of a certain commuting distance type.

Figure 7 shows that it is dominated by short-distance commuters in the study area. Commuting trips within 0–10 km account for the vast majority, and the number of commuting trip gradually decreases with the increase in travel distance. Among the three types, unaffected commuters account for the highest proportion in the commuting distance of 0–5 km under floods, indicating that short-distance commuters are less vulnerable to floods than long-distance commuters. When commuting distances are between 30 and 40 km, commuters are more likely to be disconnected. Also, the proportion and number of passable commuters in all distance intervals are the largest in the 10-year flood, and about 80% of commuting trips can be completed. In the 30-year flood, the order of the number of the three types is passable but affected commuters > disconnected commuters > unaffected commuters. With the increase in flood intensity, the proportion of disconnected commuters increases gradually, and the proportion of passable but affected commuters and disconnected commuters decrease gradually. In the 50-year flood, the proportion of disconnected commuters exceeds that of passable but affected commuters.

The cumulative distribution function of commute distance in Figure 8A shows that the slope decreases as the commute distance increases. The proportion of long-distance commuters decreases as the commute distance increases, with more than 50% of commuting distance below 10 km. Moreover,

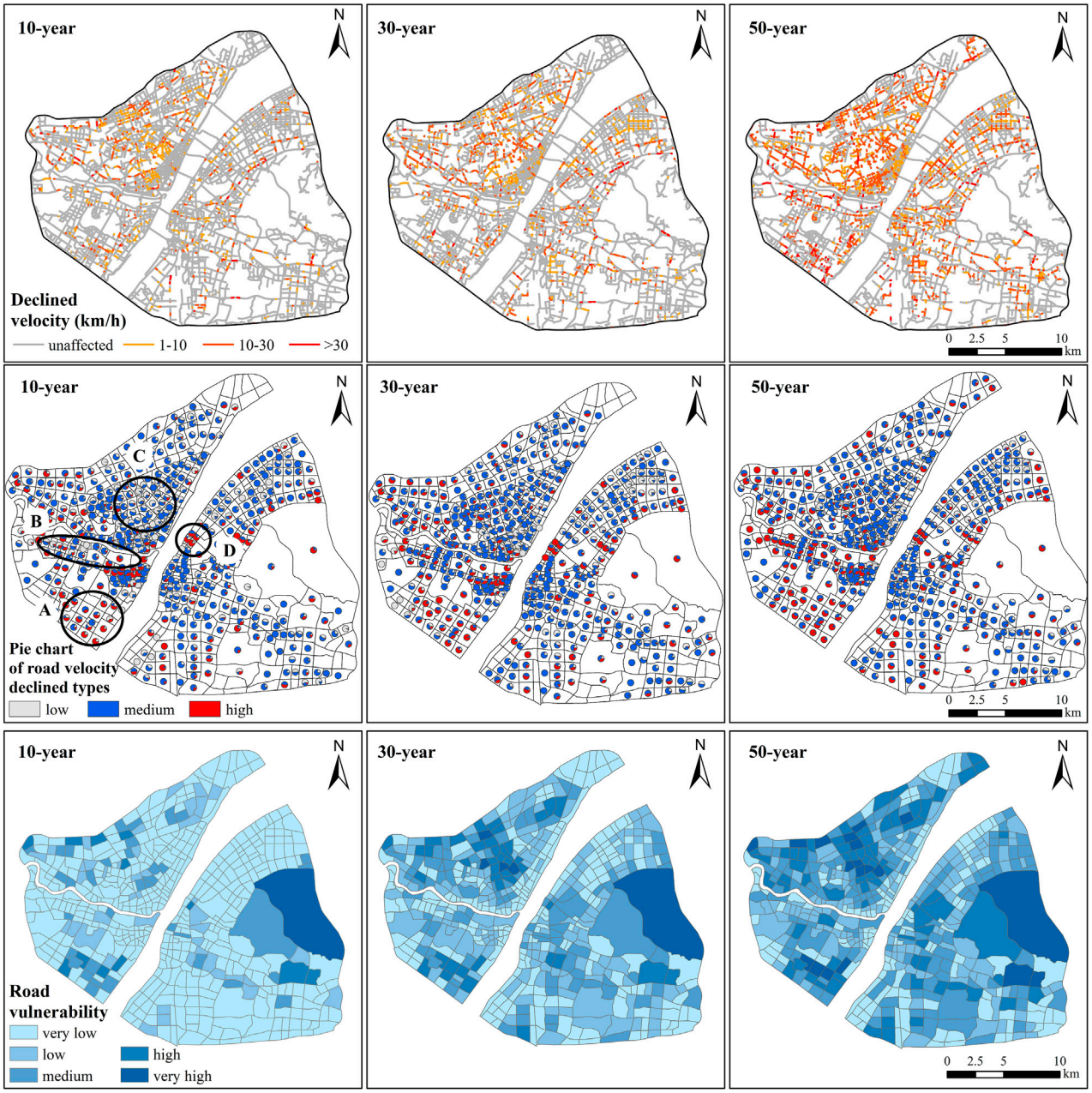

FIGURE 6
Vulnerability results of roads in traffic analysis zones.

the greater the flood intensity, the greater is the proportion of short-distance commuters. Within 2 km commuting distance, the proportion in a 50-year flood is the highest, followed by the 30-year, and then the 10-year flood. When the distance exceeds 10 km, the cumulative probability of the four scenarios is reversed. The cumulative probability under the normal scenario is the highest, followed by the 10-year flood, the 30-year flood, and the minimum is the 50-year flood. This indicates that long-distance commuters are more vulnerable to flood disruption, while short-distance commuters are less vulnerable. In addition, the increase in flood intensity also leads to an increase in the commuting distance. The cumulative function of commuting in a baseline scenario reaches saturation at about 25 km, while the longest commuting distance in the 50-year flood has reached 80 km.

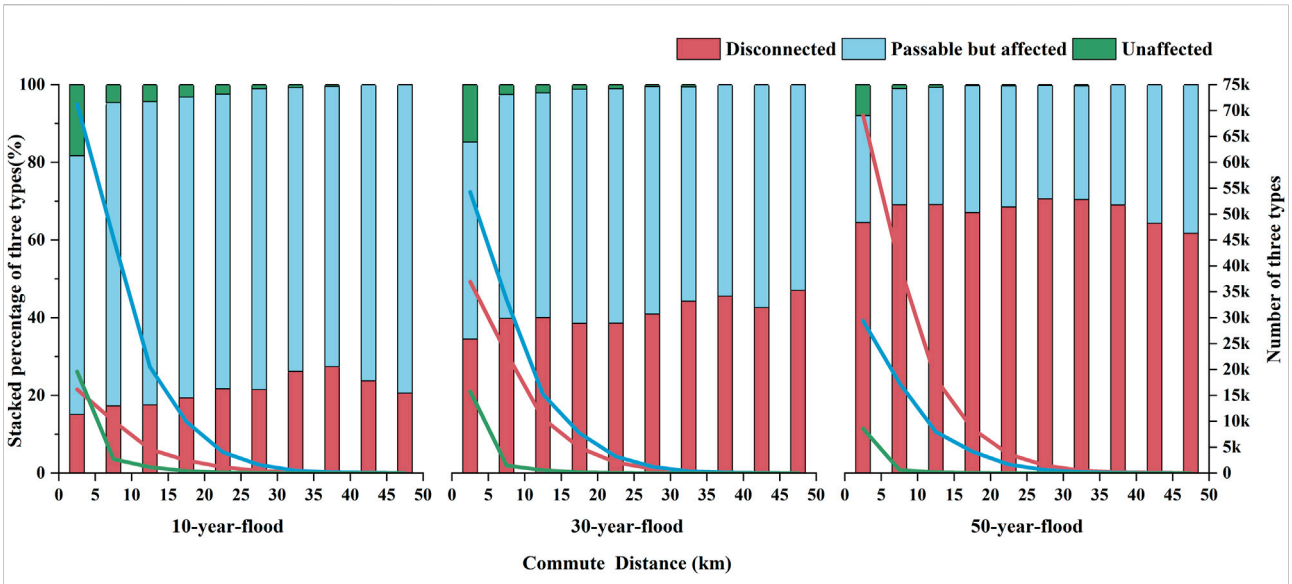

FIGURE 7
Structural analysis of commuters under three flood scenarios.

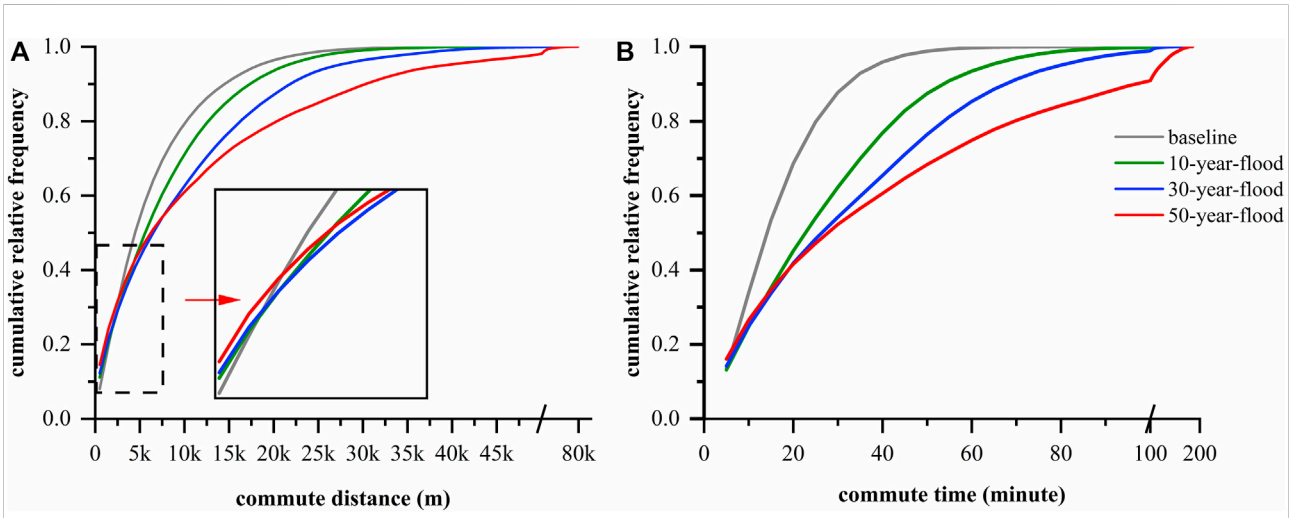

FIGURE 8
Cumulative function distribution of commuting travel distance **(A)** and commuting travel time **(B)** under floods.

The results of the commuting time cumulative function (Figure 8B) are similar to the characteristics of the commuting distance cumulative function. In the baseline scenario, more than 50% of the commuting time is less than 15 min, while this value reaches 40 min in the 50-year flood. The greater the flood intensity, the greater is the proportion of short-time commuters. Commuting trips within 20 min account for the highest proportion in the 50-year flood, followed by the 30-year flood, and then the 10-year flood. When the commuting time exceeds 20 min, the proportion order changes that cumulative probability in the 10-year ranks first, followed by that in the 30-year flood, and then that in the 50-year flood. In the baseline scenario, the travel time is less than 1 h, while the maximum commuting time reaches 3 h in the 50-year flood.

Comparing the commuting distance cumulative function diagram and the commuting time cumulative function diagram, it can be seen that the slope difference of the commuting time cumulative function in the baseline scenario

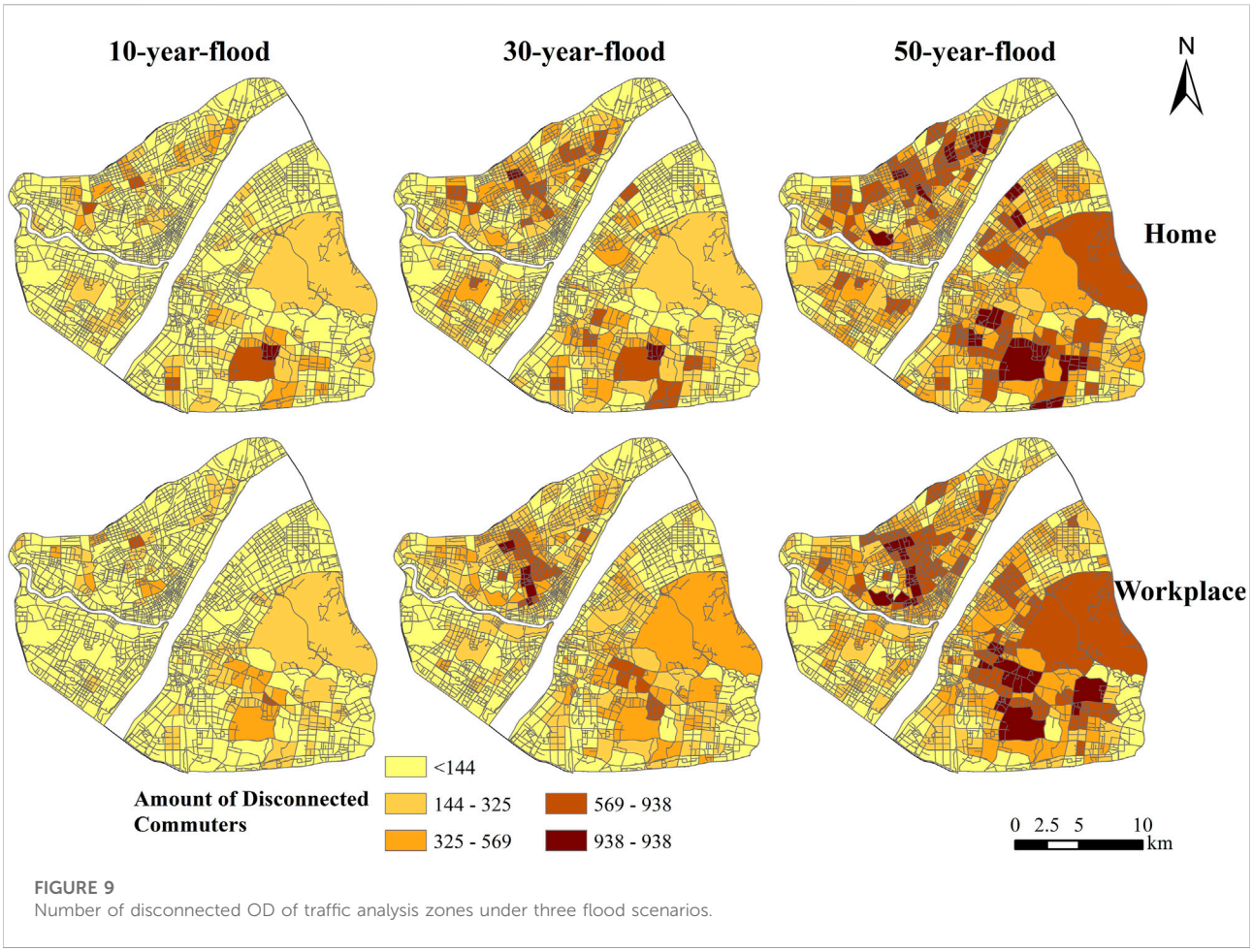

FIGURE 9
Number of disconnected OD of traffic analysis zones under three flood scenarios.

and three flood scenarios is greater, while the difference between the commuting distance cumulative functions is more moderate. This shows that there are differences in the results of time-cost and distance-cost indicators, and the increase in time is greater than the increase in distance, which is consistent with the research results of Pyatkova et al. (2019). A study had also pointed out that the time cost was more suitable for measuring the delay of the urban network, and the distance cost is more suitable for sparse road network (Balijepalli and Oppong, 2014).

Our model divides into two ways in which floods have impacts on commuting. One is to characterize the number of unsatisfied OD, including the disconnected commuters due to flooded homes or workplaces and necessary roads failure. The other is to measure the cost of extended commuting time due to floods. In order to better demonstrate the impact on commuting from floods, we equate each unsatisfied OD with an 8-h extended travel time (the same as the legal working time in China) and then normalize the comprehensive commuting loss. The results were displayed at the traffic analysis zones scale, in which home and workplace of the commute OD pairs were located.

The top three panels of Figure 9 aggregate the disconnected commuters by their home traffic analysis zones, while the bottom three panels aggregate the disconnected commuters by their workplace traffic analysis zones. Figures 10, 11 show the results of extended time and comprehensive commute loss in the same way.

The magnitude of the disconnected OD increases with flood intensity, as seen in Figure 9. A large number of residents were unable to accomplish the commuting under the 50-year flood. The highest values of the disconnected commuters by their workplace traffic analysis zones were more concentrated in urban center than that by their home traffic analysis zones.

The distribution of extended time is quite different from that of the disconnected OD (Figure 10). With the increase in flood intensity, the extent of extension time did not significantly deepen. This may be because when the flood intensity increases, delayed trips in the previous state transformed to disconnected trips so that the extended time of almost all traffic analysis zones does not increase globally. High values of extended time by their home traffic analysis zones are mainly concentrated in the junction areas of Shizishan Street, Luonan

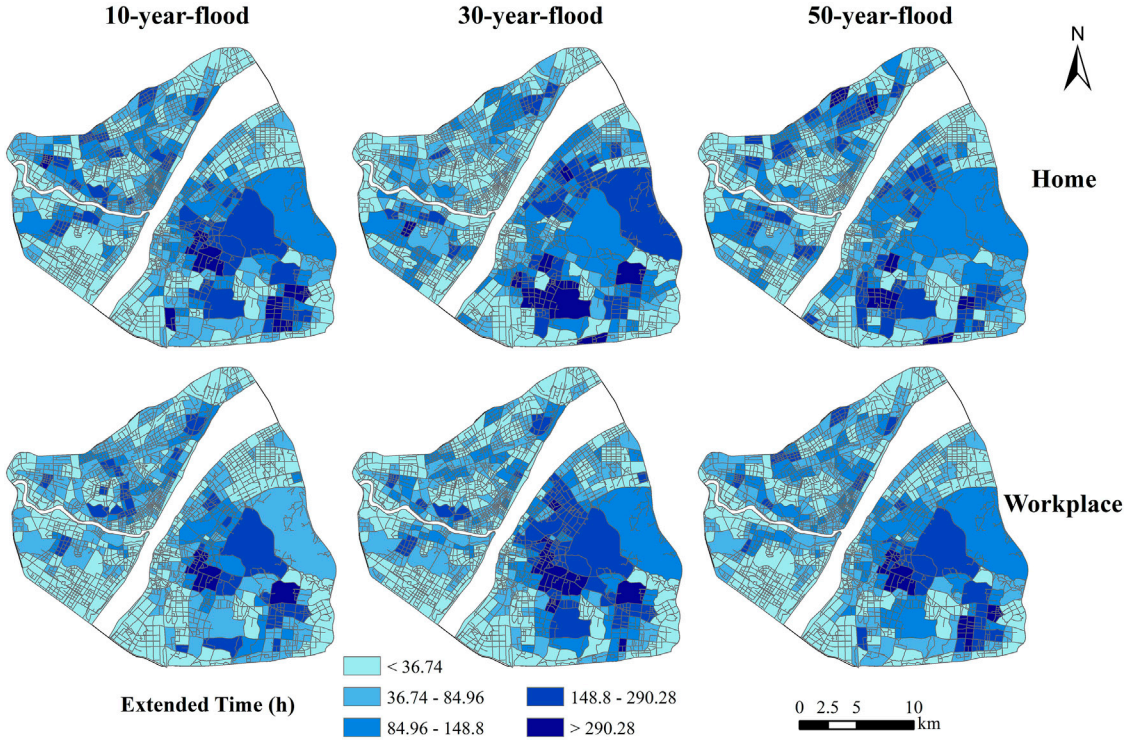

FIGURE 10
Extended time of traffic analysis zones under three flood scenarios.

Street, and Hongshan Street, while high values of that by their workplace traffic analysis zones were more north-distributed, mainly in the junction areas of Zhongnan Road Street, Shuiguo Lake Street, and Luonan Street.

The distribution of comprehensive commuting loss is more consistent with the distribution of disconnected OD, as seen in Figure 11. Areas with a huge commute loss under floods are still concentrated in the Qiaokou–Jianghan–Jiang' an areas in the northwestern and the Guanshan Street in the southeastern. These two areas should be the key areas for the allocation of flood control and disaster prevention resources.

3.4 Comparison of flood exposure, road vulnerability, and commuting loss hot spots

We normalized these three indicators including flood exposure, road vulnerability, and commute loss to see and compare their changes under three flood scenarios, as shown in Figure 12. All of the three indicators increase with the increase of flood intensity, but the magnitude of the variation is different. In the 10-year flood, the normalized value of flood exposure is the largest, followed by road vulnerability, and then commuting loss. From the 10-year flood to the 30-year flood, the order of the three indicators has not changed, but the increase in commuting loss is higher than the other two indicators. The normalized value of commuting loss is the highest in the 50-year flood, followed by road vulnerability, and then flood exposure.

The hot spot analysis tool is employed to analyze flood exposure, road vulnerability, and commuting loss, and the high–high adjacent (99% confidence hot spot clustering) and low–low adjacent (99% confidence cold spot clustering) are extracted for visualization, as shown in Figure 13.

Flood exposure mainly shows high-value aggregation in Qiaokou District and Jianghan District in the northwest, and low-value aggregation in the southern bank of the Hanjiang River and the southern bank of the Yangtze River at the junction of the Hanjiang River and the Yangtze River (Lu et al., 2021). As for road vulnerability, there are two high-value aggregations; one is located in Qiaokou District and Jianghan District in the northwest, which is consistent with the distribution of flood exposure hot spots. It can be seen that there is a high-value aggregation area of flood exposure, road vulnerability, and commuting loss under the 30-year flood and 50-year flood in the northwest. This is mainly due to the serious damage to the road network caused by the contiguous flood, which makes the commuting of residents in the area seriously damaged. Another

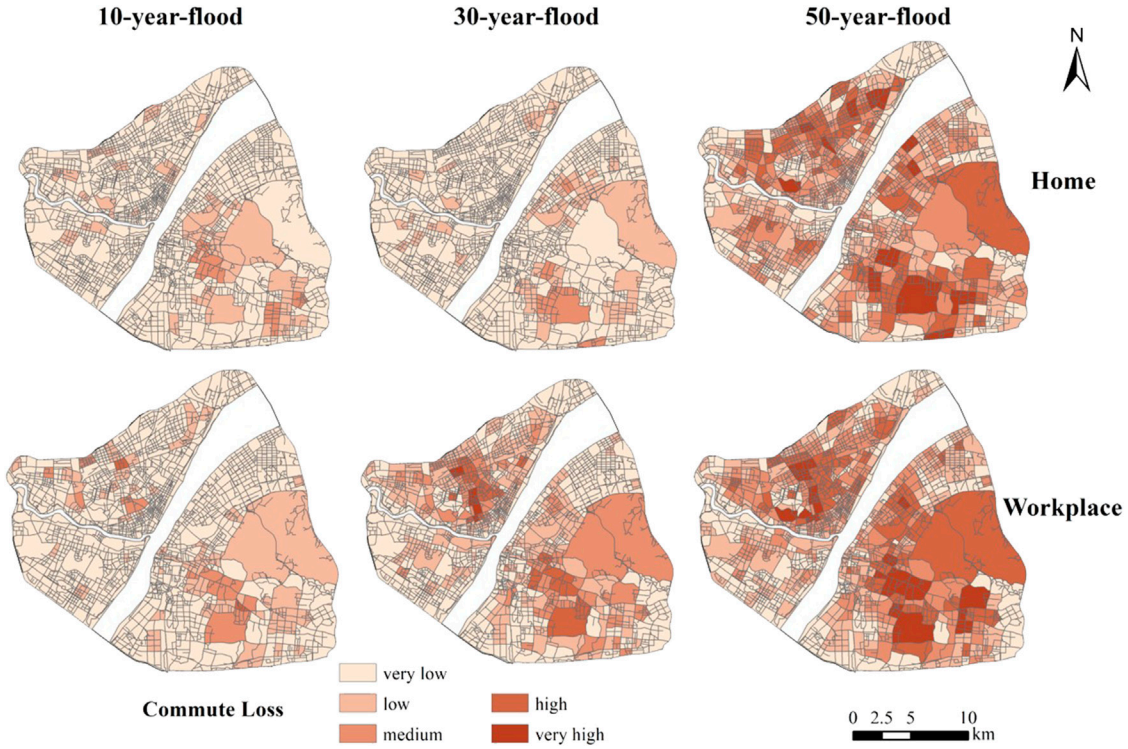

FIGURE 11
Comprehensive commute loss of traffic analysis zones under three flood scenarios.

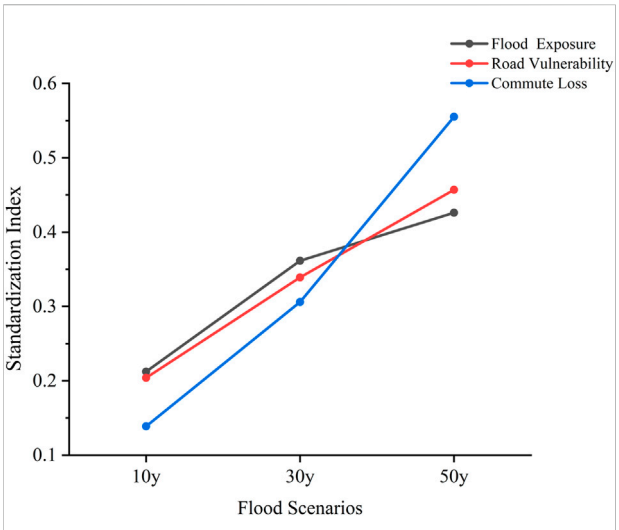

FIGURE 12
Normalized curves of flood exposure, road vulnerability, and commute loss under three floods.

high-value area of road vulnerability is located in the Jiangdi Subdistrict Office in the southwest of the study area. The road speed in this area was relatively fast in the baseline scenario, and the occurrence of floods greatly limits the speed of the original road speed, resulting in a high-value concentration of road vulnerability. The low-value aggregation area of road vulnerability is distributed at the junction of Qingshan District and Wuchang District in the northeast of the study area.

The hot spots of commuting loss show two agglomeration areas in the study area. One is distributed in the northwest, which coincides with flood exposure and road vulnerability. The other high-value agglomeration area is located in the Luonan Street and Hongshan Street office area in the southeast, which is not a high-value aggregation of flood exposure and road vulnerability. Due to the poor connectivity of the road network caused by its geographical isolation, small flood disturbances can make particularly high commuting losses in this area. The cold spot aggregation area of commuting loss shows a large distribution difference under the three floods, mainly the global commuting pattern would be affected under different floods. In the 10-year flood, the low-value aggregation area is mainly located at the junction of Hongshan District and Qingshan District in the northeast, while located at the junction of the Hanjiang River and the Yangtze River in the 30-year flood, and the intersection of the two rivers in the central region and Yongfeng Street in the west in the 50-year flood.

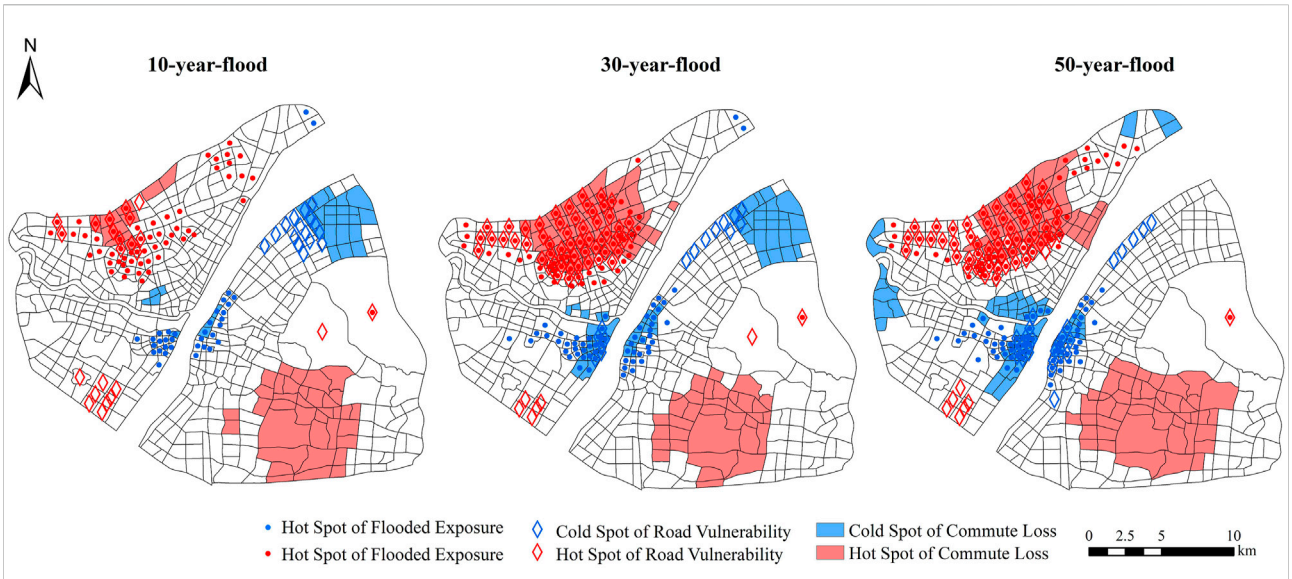

FIGURE 13
Getis-Ord Gi* results of flood exposure, road vulnerability, and commuting loss under three flood scenarios.

4 Discussion

In the context of climate change, regional and global floods are becoming more and more frequent (Birch, 2014). Although the road network construction in various cities is still constantly improving and the government is also continuously increasing investment in the construction of drainage facilities, there is still a growing trend of flood damage to the road network. China's urbanization process is still advancing. As the capital city of central China, Wuhan's population concentration in urban areas has gradually increased, making floods have a great impact on commuting as a necessary transportation activity (Liu et al., 2021). Measuring flood exposure, road network vulnerability, and commuting loss (People'SGovernmentofHubeiProvince, 2016) is critical to building resilient cities. This is an important contribution of our research. At present, there is a certain foundation for the combination of a hydrological model and a spatial analysis tool to explore the commuting risk under flood (Tsang and Scott, 2020). We integrated flood modeling and transportation network and further discussed the flood exposure and commuting loss under various rainfall scenarios based on commuting simulation. As opposed to a large number of studies using survey data or statistical data to calculate the amount of commuting activities (Borowska-Stefańska et al., 2018; Hu and Downs, 2019; Liu et al., 2021; Sharma and Chandel, 2020), we innovatively employed Baidu's commuting big data in this field. Baidu's commuting big data have a high data granularity. By actually monitoring the actual commuting activities of residents, it can accurately indicate the commuting demands of each resident (An et al., 2022). It is difficult to conduct a large-scale survey of commuting activities under floods. Knowing the accurate origin and destination of residents is an important guarantee for commuting simulation. In addition, we took into consideration the speed decline in the measurement of road vulnerability based on the flood depth-speed influence curve (Pregnolato et al., 2017). It is worth mentioning that this is not a monitored road decline rate, but the predicted road speed decline based on flood exposure results.

Studying the relationship between severe weather conditions and transportation system performance at the city level has important practical guiding significance for building sustainable cities (Hauer et al., 2021b). First of all, flood exposure under different scenarios can help guide the investment and improvement of drainage facilities. The road vulnerability assessment results identified vulnerable road sections under flood pressure, enabling decision makers to determine the order of priority interventions. The commuting loss results show that long-distance commuters are more vulnerable to flooding than short-distance commuters. In addition, the spatial distribution of commuting losses was shown in the form of traffic analysis zones, which helps to understand the response of urban commuting during floods and design adaptation and resilience strategies. Through the simple normalization of the three indicators, we found that when the flood intensity increased from a 30-year return period to a 50-year return period, the increase in commuter losses far exceeded the increase in flood exposure and road vulnerability. Also, the damage degree of each traffic zone will not increase linearly with the increase in flood intensity. In areas that are not severely damaged in a former less severe flood, it is highly likely that the damage will increase sharply as the flood intensity increases. The emphasis and strategy of disaster

prevention and mitigation are not the same in different rainfall scenarios (Liu et al., 2021); therefore, it is very important to conduct an assessment under various rainfall scenarios.

The hot spot analysis of these three indicators, through the identification of high-concentration areas, clarifies which places are urgent to be equipped with resources (He et al., 2021b). Second, by comprehensively combining the results of flood exposure, road vulnerability, and commuting loss hot spot analysis, some enlightening conclusions are also obtained by exploring the correlation factors and possible causes of overlap and difference. The northwest of the study area is the overlapping area of flood exposure, road vulnerability, and commuter loss, which is also the key area of flood resistance and mitigation in the future. For the nonoverlapping areas of the three indicators, different measures should be taken according to the local damage characteristics. A hot spot of commuting loss but not the other two indicator was found in the southwest, mainly due to the defect of the road network caused by the geographical barrier of Wuhan (Liu et al., 2021), which makes small flood disturbance also have a great impact on commuting. In order to improve the traffic resilience under floods, urban decision-makers should give priority to improving the road network construction in the region to make it more resilient.

Despite the comprehensive findings, this research has several limitations. First of all, in order to reduce the computational burden, we only selected the maximum flood depth when calculating flood exposure and did not discuss the entire flood process. Also, our commuting simulation has only been tested in the baseline scenario. Due to the lack of actual commuting behavior during the flood period, the reroute results during the flood period were not actually validated but were consistent with the previous Wuhan City studies (Liu et al., 2021; Liu et al., 2021). Because this study focuses on exploring the response of traffic network and commuting under floods, we only made the exploration at the traffic analysis zones scale. In order to provide suggestions for disaster prevention and mitigation, traffic management and urban planning, the research scale can be further increased in the future, including the planning unit scale and the catchment scale that can reflect the topographic characteristics.

5 Conclusion

This article integrated the flood modeling module and the commute simulation module to obtain knowledge about commute response under three rainfall scenarios, including a 10-year flood, a 30-year flood, and a 50-year flood. High-resolution flood maps were obtained through the hydrological model considering the condition of drainage facilities. Road vulnerability was assessed at the scale of road sections and traffic analysis zones (TAZs). We considered the declined speed based on the correlation between flood depth and travel speed, therefore, a targeted adaptation plan can be designed to manage them and promote the transport resilience. In the process of commute simulation, we introduced the Baidu location-based service (LBS) data to get the accurate location of residents' homes and workplaces, and modified the normal commuting speed based on the calculated speed under floods to reroute residents' commute trips. The results in Wuhan showed that short-distance commutes are less vulnerable to floods than long-distance commutes. In the 50-year flood, the proportion of disconnected commuters exceeds that of passable but affected commuters. There are differences in the results of time-cost and distance-cost indicators, and the increase in time is greater than the increase in distance. When the flood intensity increased, delayed trips in the previous state transformed into disconnected trips, so the extended time of almost all traffic analysis zones (TAZs) did not increase globally, while a number of disconnected commuters did. The hot spot analysis tool is employed to analyze flood exposure, road vulnerability, and commuting loss and we finally integrated them. Spatial distribution inconsistency of hot spots for flood exposure, road vulnerability, and commute loss was identified, and these areas need to take different measures according to the local damage characteristics. This article examined road vulnerability and commute loss under floods, which can provide a decision-making basis for disaster prevention and mitigation, emergency management, and urban planning in the context of climate change.

Data availability statement

The data analyzed in this study are subject to the following licenses/restrictions. The original data are confidential and we have signed a confidentiality agreement with the data holder for scientific analysis only. Requests to access these datasets should be directed to huiting_chen@whu.edu.cn.

Author contributions

YL: conceptualization, writing—reviewing and editing, and supervision. HZ: methodology, writing—reviewing and editing, visualization, and validation. HC: conceptualization, methodology, writing—original draft, and software. CC: methodology, software, and visualization.

Funding

This research was financially supported by the National Key Research and Development Program of China (No. 2017YFB0503601).

Conflict of interest

The authors declare that the research was conducted in the absence of any commercial or financial relationships that could be construed as a potential conflict of interest.

Publisher's note

All claims expressed in this article are solely those of the authors and do not necessarily represent those of their affiliated organizations, or those of the publisher, the editors, and the reviewers. Any product that may be evaluated in this article, or claim that may be made by its manufacturer, is not guaranteed or endorsed by the publisher.

Supplementary material

The supplementary material for this article can be found online at: https://www.frontiersin.org/articles/10.3389/fenvs.2022.1056854/full#supplementary-material

References

Aghababaei, M. T. S., Costello, S. B., and Ranjitkar, P. (2021). Measures to evaluate post-disaster trip resilience on road networks. *J. Transp. Geogr.* 95, 103154. doi:10.1016/j.jtrangeo.2021.103154

An, R., Wu, Z., Tong, Z., Qin, S., Zhu, Y., and Liu, Y. (2022). How the built environment promotes public transportation in Wuhan: A multiscale geographically weighted regression analysis. *Travel Behav. Soc.* 29, 186–199. doi:10.1016/j.tbs.2022.06.011

Balijepalli, C., and Oppong, O. (2014). Measuring vulnerability of road network considering the extent of serviceability of critical road links in urban areas. *J. Transp. Geogr.* 39, 145–155. doi:10.1016/j.jtrangeo.2014.06.025

Berdica, K. (2002). An introduction to road vulnerability: What has been done, is done and should be done. *Transp. Policy* 9 (2), 117–127. doi:10.1016/S0967-070X(02)00011-2

Birch, E. L. (2014). A Review of " climate change 2014: Impacts, adaptation, and vulnerability " and " climate change 2014: Mitigation of climate change. *J. Am. Plan. Assoc.* 80 (2), 184–185. doi:10.1080/01944363.2014.954464

Borowska-Stefańska, M., Domagalski, A., and Wiśniewski, S. (2018). Changes concerning commute traffic distribution on a road network following the occurrence of a natural disaster – the example of a flood in the Mazovian Voivodeship (Eastern Poland). *Transp. Res. Part D Transp. Environ.* 65, 116–137. doi:10.1016/j.trd.2018.08.008

Borowska-Stefańska, M., and Wiśniewski, S. (2018). Changes in transport accessibility as a result of flooding: A case study of the Mazovia Province (eastern Poland). *Environ. hazards* 17 (1), 56–83. doi:10.1080/17477891.2017.1343177

Cao, Y., Cao, Y., Li, G., Tian, Y., Fang, X., Li, Y., et al. (2020). Linking ecosystem services trade-offs, bundles and hotspot identification with cropland management in the coastal Hangzhou Bay area of China. *LAND USE POLICY* 97, 104689. doi:10.1016/j.landusepol.2020.104689

Casali, Y., and Heinimann, H. R. (2019). A topological characterization of flooding impacts on the Zurich road network. *PLoS One* 14 (7), e0220338. doi:10.1371/journal.pone.0220338

Chen, C., Jiang, J., and Li, M. (2016). Jiyu SHUILIMOXING DE QINGSHAN HAOMIANSHIFANQU PAISHUI FANGLAO FENGXIAN PINGGU. *CHINA WATER& WASTEWATER* 17, 105–108. doi:10.19853/j.zgjsps.1000-4602.2016.17.023

Chen, X., Lu, Q., Peng, Z., and Ash, J. E. (2015). Analysis of transportation network vulnerability under flooding disasters. *Transp. Res. Rec.* 2532 (1), 37–44. doi:10.3141/2532-05

Chung, Y. (2012). Assessment of non-recurrent congestion caused by precipitation using archived weather and traffic flow data. *Transp. Policy* 19 (1), 167–173. doi:10.1016/j.tranpol.2011.10.001

Coles, D., Yu, D., Wilby, R. L., Green, D., and Herring, Z. (2017). Beyond 'flood hotspots': Modelling emergency service accessibility during flooding in York, UK. *J. HYDROLOGY* 546, 419–436. doi:10.1016/j.jhydrol.2016.12.013

Debionne, S., Ruin, I., Shabou, S., Lutoff, C., and Creutin, J. (2016). Assessment of commuters' daily exposure to flash flooding over the roads of the Gard region, France. *J. HYDROLOGY* 541, 636–648. doi:10.1016/j.jhydrol.2016.01.064

Demirel, H., Kompil, M., and Nemry, F. (2015). A framework to analyze the vulnerability of European road networks due to Sea-Level Rise (SLR) and sea storm surges. *Transp. Res. Part A Policy Pract.* 81, 62–76. doi:10.1016/j.tra.2015.05.002

El-Rashidy, R. A., and Grant-Muller, S. M. (2014). An assessment method for highway network vulnerability. *J. Transp. Geogr.* 34, 34–43. doi:10.1016/j.jtrangeo.2013.10.017

Fu, G., Dawson, R., Khoury, M., and Bullock, S. (2014). Interdependent networks: Vulnerability analysis and strategies to limit cascading failure. *Eur. Phys. J. B* 87 (7), 148. doi:10.1140/epjb/e2014-40876-y

Hauer, M., Mueller, V., Sheriff, G., and Zhong, Q. (2021a). More than a nuisance: Measuring how sea level rise delays commuters in Miami, FL. *Environ. Res. Lett.* 16 (6), 064041. doi:10.1088/1748-9326/abfd5c

Hauer, M., Mueller, V., Sheriff, G., and Zhong, Q. (2021b). More than a nuisance: Measuring how sea level rise delays commuters in Miami, FL. *Environ. Res. Lett.* 16 (6), 064041. doi:10.1088/1748-9326/abfd5c

He, Y., Thies, S., Avner, P., and Rentschler, J. (2021a). Flood impacts on urban transit and accessibility—a case study of Kinshasa. *Transp. Res. Part D Transp. Environ.* 96, 102889. doi:10.1016/j.trd.2021.102889

He, Y., Thies, S., Avner, P., and Rentschler, J. (2021b). Flood impacts on urban transit and accessibility—a case study of Kinshasa. *Transp. Res. Part D Transp. Environ.* 96, 102889. doi:10.1016/j.trd.2021.102889

Hu, Y., and Downs, J. (2019). Measuring and visualizing place-based space-time job accessibility. *J. Transp. Geogr.* 74, 278–288. doi:10.1016/j.jtrangeo.2018.12.002

Hubei, F. (2013). Planning and design standards of Wuhan drainage and waterlogging prevention. *System*. Available at: http://gtghj.wuhan.gov.cn/UploadFile/20131030025327433.pdf.

Jenelius, E., Petersen, T., and Mattsson, L. (2006). Importance and exposure in road network vulnerability analysis. *Transp. Res. Part A Policy Pract.* 40 (7), 537–560. doi:10.1016/j.tra.2005.11.003

Jie, Y., Yu, D., Zhane, Y., Min, L., and Qing, H. (2016). Evaluating the impact and risk of pluvial flash flood on intra-urban road network; a case study in the city center of Shanghai, China. *J. hydrology (Amsterdam)* 537, 138–145. doi:10.1016/j.jhydrol.2016.03.037

Kasmalkar, I. G., Serafin, K. A., Miao, Y., Bick, I. A., Ortolano, L., Ouyang, D., et al. (2020a). *When floods hit the road: Resilience to flood-related traffic disruption in the San Francisco Bay Area and beyond*, 6. doi:10.1126/sciadv.aba2423

Kasmalkar, I. G., Serafin, K. A., Miao, Y., Bick, I. A., Ortolano, L., Ouyang, D., et al. (2020b). When floods hit the road: Resilience to flood-related traffic disruption in the San Francisco Bay Area and beyond. *Sci. Adv.* 6 (32), a2423. doi:10.1126/sciadv.aba2423

Keeler, A. G., McNamara, D. E., and Irish, J. L. (2018). Responding to sea level rise: Does short-Term risk reduction Inhibit Successful long-Term adaptation? *Earth's. Future* 6 (4), 618–621. doi:10.1002/2018EF000828

Kendon, E. J., Roberts, N. M., Senior, C. A., and Roberts, M. J. (2012). Realism of rainfall in a very high-resolution regional climate model. *J. Clim.* 25 (17), 5791–5806. doi:10.1175/JCLI-D-11-00562.1

Liu, J., Shi, Z., and Tan, X. (2021). Measuring the dynamic evolution of road network vulnerability to floods: A case study of Wuhan, China. *Travel Behav. Soc.* 23, 13–24. doi:10.1016/j.tbs.2020.10.009

Lu, X., Yang, S., Ye, T., An, R., and Chen, C. (2021). A new approach to estimating flood-affected populations by combining mobility patterns with multi-source data: A case study of Wuhan, China. *Int. J. Disaster Risk Reduct.* 55, 102106. doi:10.1016/j.ijdrr.2021.102106

Mattsson, L., and Jenelius, E. (2015). Vulnerability and resilience of transport systems – a discussion of recent research. *Transp. Res. Part A Policy Pract.* 81, 16–34. doi:10.1016/j.tra.2015.06.002

Moriasi, D. N., Arnold, J. G., Van Liew, M. W., Bingner, R. L., Harmel, R. D., and Veith, T. L. (2007). Model evaluation GUIDELINES for SYSTEMATIC QUANTIFICATION OF accuracy IN WATERSHED simulations. *Trans. ASABE* 50 (3), 885–900. doi:10.13031/2013.23153

People'SgovernmentofHubeiProvince (2016). As at 10 : 00 on july 6. *Wuhan. ' s Wkly. rainfall Exceed. its Hist. maximum*, 23. Available at: http://www.hubei.gov.cn/zwgk/bmdt/201607/t20160706_860661.shtml.

Pregnolato, M., Ford, A., Wilkinson, S. M., and Dawson, R. J. (2017). The impact of flooding on road transport: A depth-disruption function. *Transp. Res. Part D Transp. Environ.* 55, 67–81. doi:10.1016/j.trd.2017.06.020

Pyatkova, K., Chen, A. S., Butler, D., Vojinović, Z., and Djordjević, S. (2019). Assessing the knock-on effects of flooding on road transportation. *J. Environ. Manag.* 244, 48–60. doi:10.1016/j.jenvman.2019.05.013

Saaty, T. L. (1980). The analytic hierarchy process: Planning, priority setting, resource allocation. *Eur. J. Oper. Res.* 9, 97–98. doi:10.1016/0377-2217(82)90022-4

Shah, S. M. H., Mustaffa, Z., Martinez-Gomariz, E., Kim, D. K., and Yusof, K. W. (2021). Criterion of vehicle instability in floodwaters: Past, present and future. *Int. J. river basin Manag.* 19 (1), 1–23. doi:10.1080/15715124.2019.1566240

Sharma, I., and Chandel, M. K. (2020). Impact of past rainfall events on the urban transport sector of the Mumbai Metropolitan region: Current and future Projections under BAU scenario. *Transp. Dev. Econ.* 6 (2), 13. doi:10.1007/s40890-020-00104-1

Sidek, L. M., Jaafar, A. S., Majid, W. H. A. W., Basri, H., Marufuzzaman, M., Fared, M. M., et al. (2021). High-resolution hydrological-Hydraulic modeling of urban floods using InfoWorks ICM. *Sustainability* 13 (18), 10259. doi:10.3390/su131810259

Singh, P., Sinha, V. S. P., Vijhani, A., and Pahuja, N. (2018). Vulnerability assessment of urban road network from urban flood. *Int. J. Disaster Risk Reduct.* 28, 237–250. doi:10.1016/j.ijdrr.2018.03.017

Tsang, M., and Scott, D. M. (2020). An integrated approach to modeling the impact of floods on emergency services: A case study of Calgary, Alberta. *J. Transp. Geogr.* 86, 102774. doi:10.1016/j.jtrangeo.2020.102774

Wang, J., Qin, S., Xiang, W., Kan, C., and Yan, H. (2021). Tongqin Tezheng Shuju Queding Fangfa, Zhuangzhi, Dianzi Shebei and Cunchu Jiezhi *No. 202110501129.0*.

Zhiqiang, L. (2016). Experts Interpret the Causes of frequent Flood in Wuhan. *BeijingNews*. Retreved Sep 20 from http://www.xinhuanet.com//politics/2016-07/07/c_129123063.htm.

Xiong, Y., and Melching, C. (20052005). Comparison of Kinematic-Wave and nonlinear reservoir routing of urban Watershed runoff. *J. Hydrol. Eng.* 10 (24), 39–49. 10:1(39). doi:10.1061/(asce)1084-0699(2005)10:1(39)

Yang, Y., Ng, S. T., Zhou, S., Xu, F. J., and Li, H. (2019). A physics-based framework for analyzing the resilience of interdependent civil infrastructure systems: A climatic extreme event case in Hong Kong. *Sustain. Cities Soc.* 47, 101485. doi:10.1016/j.scs.2019.101485

Zhang, Y., Liu, Y., Jin, M., Jing, Y., Liu, Y., Liu, Y., et al. (2019). Monitoring land Subsidence in Wuhan city (China) using the SBAS-InSAR method with Radarsat-2 Imagery data. *Sensors (Basel)* 19 (3), 743. doi:10.3390/s19030743

Zhao, P., and Cao, Y. (2020). Commuting inequity and its determinants in Shanghai: New findings from big-data analytics. *Transp. Policy* 92, 20–37. doi:10.1016/j.tranpol.2020.03.006

frontiers | Frontiers in Environmental Science

TYPE Methods
PUBLISHED 28 November 2022
DOI 10.3389/fenvs.2022.1055807

Check for updates

OPEN ACCESS

EDITED BY
Jiaxing Cui,
Central China Normal University, China

REVIEWED BY
Jiqiang Niu,
Xinyang Normal University, China
Xiaojian Wei,
East China University of Technology, China

*CORRESPONDENCE
Qing He,
qhe@gzu.edu.cn
Liu Yang,
lyang3@gzu.edu.cn

SPECIALTY SECTION
This article was submitted to Environmental Informatics and Remote Sensing, a section of the journal Frontiers in Environmental Science

RECEIVED 28 September 2022
ACCEPTED 01 November 2022
PUBLISHED 28 November 2022

CITATION
Yang Y, He Q and Yang L (2022), UAV trajectory planning based on an improved sparrow optimization algorithm with multi-strategy integration. *Front. Environ. Sci.* 10:1055807. doi: 10.3389/fenvs.2022.1055807

COPYRIGHT
© 2022 Yang, He and Yang. This is an open-access article distributed under the terms of the Creative Commons Attribution License (CC BY). The use, distribution or reproduction in other forums is permitted, provided the original author(s) and the copyright owner(s) are credited and that the original publication in this journal is cited, in accordance with accepted academic practice. No use, distribution or reproduction is permitted which does not comply with these terms.

UAV trajectory planning based on an improved sparrow optimization algorithm with multi-strategy integration

Yu Yang[1], Qing He[1]* and Liu Yang[2]*

[1]College of Big Data and Information Engineering, Guizhou University, Guiyang, China, [2]School of Public Administration, Guizhou University, Guiyang, China

Real-time monitoring of urban high-altitude data is an important goal in the construction and development of smart cities today. However, with the development of modern cities, the monitoring space becomes complicated and narrow because of the different building heights and no-fly zones, which makes UAV trajectory planning more difficult. In this paper, a multi-strategy sparrow search algorithm (MSSA) is proposed to solve the UAV trajectory planning problem in a three-dimensional environment. The algorithm aims to minimize the flight distance and maximize the use efficiency of the UAV. First, the improved algorithm employed a reverse-learning strategy based on the law of refraction to improve the search range and enhance the optimization performance. Second, we introduced a random step size generated by Levy flight into the position update strategy of the participant. The algorithm accuracy and speed of convergence were improved by the randomness feature. Finally, the algorithm incorporated the Cauchy mutation to improve the scout position, which enhanced its ability to jump out of the local optimum of the algorithm. Sixteen benchmark test functions, Wilcoxon rank sum test, and 30 CEC2014 test function optimization results demonstrated that MSSA had better optimization accuracy, convergence speed, and robustness than the comparison algorithms. In addition, the proposed algorithm was applied to the UAV trajectory planning problem in different complex 3D environments. The results confirmed that the MSSA outperformed the other algorithms in complex 3D trajectory planning problems.

KEYWORDS

smart cities, trajectory planning, improved sparrow search algorithm, UAV, three-dimensional

Introduction

With the continuous development of information technology and smart cities (Van Steen and Leiba, 2018), UAV technology plays an important role in urban emergencies and transportation networks. Due to their usefulness, reliability, safety, and relatively low cost (Rodríguez et al., 2021), UAVs (commonly referred to as drones) have become an indispensable part of the operations of a smart city. In research on UAV technology,

trajectory planning is the key to the whole system. The main technical difficulty is to find a feasible way to avoid obstacles when the starting and ending points are known (Zhao et al., 2018). At present, many cities around the world are facing the problem of traffic congestion. In particular, there are periodic or sudden increases in the number of vehicles during peak hours, large events, construction work or accidents. In an emergency, the use of drones can assist traffic police in implementing security in smart cities, and rapid deployment can collect real-time information (Qadir, 2021). However, due to the complexity of the flight environment in modern urban spaces, UAV monitoring tasks are becoming more and more difficult (Mohamed, 2020). Therefore, how to outfit a UAV so that it can find a flight path that avoids obstacles but still maintains the shortest distance to the destination is a main focus of today's UAV research.

The process of UAV trajectory planning is a combinatorial optimization problem. Currently, UAVs have a low efficiency in completing tasks in complex areas because of the large scale of the mathematical model and its high computational complexity. The complexity and difficulty of real-world optimization problems continue to increase, as they are subject to strong constraints and require long computation times, non-convexity, and wide search space (Shin and Bang, 2020). Path length is the primary factor to be considered in engineering scenarios, and optimizing path is of great research significance for improving flight efficiency. Path optimization aims to maximize the execution efficiency of the UAV within permissible limits. The methods for deducing the optimal power flow in trajectory planning can be divided into traditional optimization algorithms and metaheuristic algorithms. Traditional optimization algorithms mainly include the gradient descent method Salgado et al., 1990), the Newton method (Tinney ea al., 1967), linear programming (Olofsson et al., 1995), and the interior point method (Momoh, 1999). These algorithms are characterized by their use of the objective function to solve the first- or second-order gradient of control variables. Traditional optimization algorithms are generally trapped in local optima; hence, the optimization results depend greatly on the initial value in solving large-scale problems. In recent years, researchers have proposed many metaheuristic algorithms by simulating various biological behaviors and physical phenomena in nature. The metaheuristic algorithms commonly include Archimedes optimization algorithm (AOA) (Hashim ea al., 2021), the tunicate swarm algorithm (TSA) (Kaur et al., 2020), Aquila optimization (AO) (Abualigah et al., 2021), Harris hawks optimization(HHO) (Heidari et al., 2019), ant colony optimization (ACO) (Zhang et al., 2015), grey wolf optimizer (GWO) (Mirjalili et al., 2014), differential evolution (DE) (Price, 2013), and particle swarm optimization (PSO) (Marini and Walczak, 2015).

Metaheuristic algorithms are widely used to solve problems related to power system optimization because of their simple structure, few adjustment parameters, and lack of need for gradient information. Wen et al. (2022) proposed a novel heuristic algorithm based on a three-dimensional (3D) UAV deployment scheme that could be used by a number of covered users without increasing the number of UAVs. Fan et al. (2022b) proposed an improved RRT algorithm based on the process of extending the random tree, and introduced ACO to make the planning path asymptotically optimal. Jia et al. (2022) described a UAV path coverage algorithm based on a 'greedy' strategy and ACO (Zhang et al., 2015) to minimize flight time and maximize coverage. Shin and Bang (2022) offered an improved PSO algorithm for path optimization. Belge et al. (2022) developed a new UAV trajectory planning algorithm for optimal path planning and tracking using HHO and GWO. Zhang et al. (2021) proposed an adaptive convergence factor adjustment strategy and an adaptive weight factor to update the individual's position based on GWO. Zhang et al. (2015) created an improved constrained DE algorithm to generate an optimal feasible route. Chang et al. (2021) introduced Q-learning to improve the dynamic window algorithm and increase its success rate for path planning in an unknown mountainous environment. However, the calculations necessary to use this algorithm are more complex, and beyond the low computational power of the UAV; the local

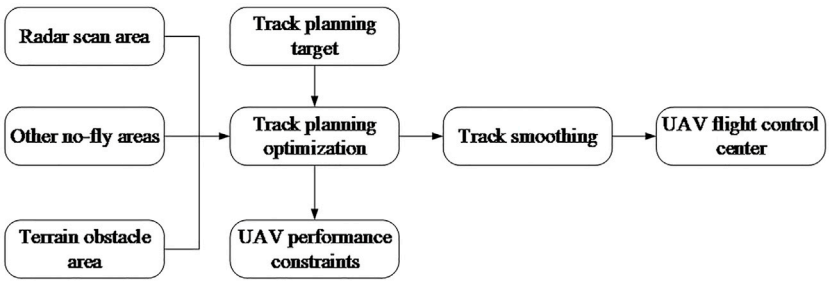

FIGURE 1
Flow chart of the trajectory planning system.

path planning strategy is not applicable to global optimization.

The sparrow search algorithm (SSA), a swarm intelligence optimization algorithm proposed by Xue and Shen (2020), combines simplicity with flexibility. It is very effective for solving highly nonlinear, multi-variate, and multimodal function optimization problems. Many researchers have studied the SSA algorithm and confirmed that it outperforms the GWO, PSO (Poli et al., 2007), and GA (Whitley, 1994) in solving numerous types of optimization problems. The SSA has been used in many other fields. Wu et al. (2021) reported the application of GGSC-SSA to solve the traveling salesman problem (TSP); Fan et al. (2022a) even utilized SSA to improve the quality of medical images; but few published reports exist on the application of SSA to UAV trajectory planning. Here we propose a new metaheuristic optimization algorithm based on the SSA and referred to as MSSA. Since the B-spline curve cannot guarantee absolute accuracy of the interpolation points (Thompson and Patel, 1987), we used the cubic spline interpolation method to smooth the path. First, we established a 3D environmental model for UAV trajectory planning that included reference terrain, obstacle areas, and threat areas. Second, a comprehensive cost evaluation model of UAV flight was proposed as the objective function. The path was smoothed by the method of cubic spline interpolation to obtain an optimal trajectory. Lastly, we analyzed the results and verified the effectiveness and feasibility of the proposed algorithm in planning the UAV's trajectory in the 3D model.

Study area and environment modelling

Overview of the study area

With the leapfrog development of information science, various new technologies employing AI for advanced communication and control have been put forward, many of which have been applied in UAV operating systems, providing a foundation for the rapid deployment of UAVs for numerous uses. At present, UAVs have become an important accessory for air power in the military, which can perform battlefield reconnaissance, supply delivery missions, and enemy target strikes. In addition to military applications, civilian applications of UAVs have also been accelerating in a number of areas, including traffic supervision, disaster relief, inspections, and scientific data gathering. The UAV trajectory problem is a multi-constraint combinatorial optimization problem. Due to the size of the mathematical model and the complexity of the calculation, a suitable cost function and an effective trajectory planning method are both crucial to the efficient implementation of UAVs.

Description of trajectory planning

Finding an optimal path using planning algorithms is the main goal of UAV trajectory planning, and this path must meet performance indicators and overcome limitations. The UAV may encounter several hurdles throughout this trajectory planning process, including terrain threats, fire, no-fly zones, and performance limitations imposed by the equipment itself (Bagherian and Alos, 2015). For testing of this algorithm, we held the UAV's speed constant and kept track of the distribution of the mission environment's peaks and no-fly zones to make the computation model simpler. The challenge of trajectory planning was changed into a static space routing mission problem. The trajectory planning system is depicted in Figure 1. Figure 1 illustrates the components of the UAV trajectory planning process, which included environmental modelling, cost function definition, track optimization, and track smoothing. Our goal in this study was to establish an optimal flight path before the UAV flight mission. By sending the algorithm's best path data to the UAV's flight master control system, the flight trajectory planning will be accomplished successfully.

Task environment modelling

According to the 3D space environment there were significant changes in altitude and terrain complexity along the route (Dübel and Schumann, 2017), and the flight path may be categorized into areas of plains, mountainous regions, and hilly areas. A large number of complex factors need to be considered if the flight must pass through a mountainous or hilly area. The UAV needs to adjust the travel direction and the flight altitude continuously in those complex environments, and trajectory planning must be carried out in 3D space. In this study, we developed two distinct settings for UAV trajectory planning and used a function simulation approach to characterize landform properties. Eq. 1 displays the function expression:

$$z(x, y) = \sin(y + a) + b\sin(x) + c\cos\left(d\sqrt{y^2 + x^2}\right) + e\cos(y) + f\sin\left(f\sqrt{y^2 + x^2}\right) + g\cos(y) \quad (1)$$

where (x, y) is the point coordinate of the terrain projected onto the horizontal plane and z is the height of the corresponding point coordinate on the Z axis. In Eq. 1, a, b, c, d, e, f, g, and h are constant coefficients, and the different topography features can be obtained by changing the size of the constant coefficients in the modelling process. In this test flight, we simulated the geographical environment, such as mountains and hills, by superimposing the mountain model on the base terrain. The

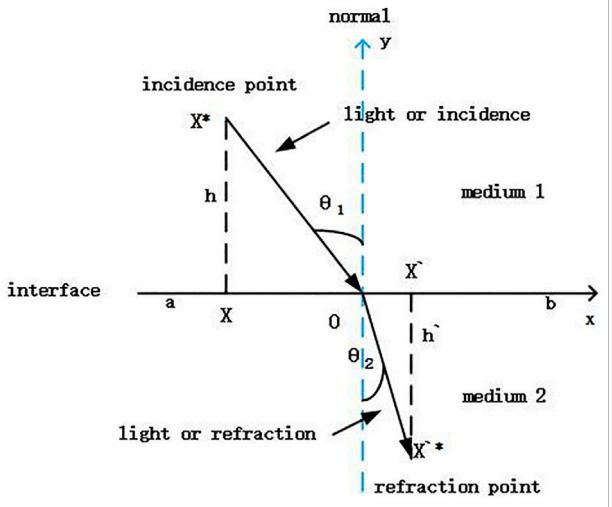

FIGURE 2
Refraction-learning process in one-dimensional space.

mathematical expression of the topography model is shown in Eq. 2:

$$h(x,y) = \sum_i h_i \exp\left[-\frac{(x_i - x_{oi})^2}{a_i^2} - \frac{(y_i - y_{oi})^2}{b_i^2} \right] + h_o \quad (2)$$

In Eq. 2, h_o and h_i represent the height of the reference terrain and the ith peak, respectively, (x_{oi}, y_{oi}) represent the central coordinate position of the ith peak, and a_i and b_i are the slopes of the ith mountain along the X and Y axes, respectively. The peaks can show different length and width characteristics by adjusting the value of those parameters. We can obtain Eq. 3 from Eqs 1, 2:

$$Z(x,y) = \max[z(x,y), h(x,y)] \quad (3)$$

In practical situations, UAVs frequently encounter areas with tall buildings and trees that threaten flight safety, or no-fly areas where UAVs have to avoid obstacles. Therefore, we included a certain number of threat areas in the UAV trajectory plan to judge the obstacle avoidance performance of the algorithm. Graphically, we represented a danger area as a cylinder with a radius of R to simplify the model. The center position of each cylinder affords the greatest threat to the UAV, and the threat decreases from the center to the outside.

UAV track planning modeling

When completing challenging jobs, the UAV trajectory planner must take into consideration the inherent performance restrictions of the drone based on environmental modeling. The final results produced by the algorithm can be made to comply with the specifications and guarantee that the intended flight route is valid with a suitable design of the trajectory evaluation function. We devised a sophisticated track evaluation algorithm to plan the UAV trajectory based on real circumstances. The indicators that most affected the performance of the UAV included track length, flight height, minimum step size, corner cost, and maximum climb angle.

Trajectory planning is inseparable from searching for the shortest path because the length of the track is very important for successful trajectory planning. Obviously, the shortest route can save on fuel and time and reduce the chance occurrence of unknown threats. We defined the path as the value of the distance from the starting to the ending point. Suppose a complete route has n nodes, the distance between the ith and the $i+1$-th waypoint is expressed as l_i, the coordinates of these two flight points are expressed as (x_i, y_i, z_i) and $(x_{i+1}, y_{i+1}, z_{i+1})$, denoted the two points as $g(i)$ and $g(i+1)$, respectively. The trajectory needs to satisfy the following conditions in Eq. 4:

$$\begin{cases} li = \left\| g(i+1) - g(i) \right\|_2 \\ L_{\text{path}} = \sum_{i=1}^{n-1} l_i \end{cases} \quad (4)$$

The UAV will run the risk of crashing or being shot down if it is unable to avoid obstacles or flying into a hazard region, which is indicated by the L_{path} being $L_{path} = \infty$. Because infinite functions are challenging to depict in real-world situations, we deal with them in a penalizing approach. The UAV should fly as low as it can in the real world to avoid potential radar detection. However, it is crucial to choose a steady flight altitude because a low flight altitude would increase the probability of the UAV colliding with trees, mountains, or the ground. The flying altitude should not change much because a constant altitude eases the strain on the control system and conserves fuel. To make the UAV flight safer, the flight height model given in Eq. 5:

$$\begin{cases} h_{\text{height}} = \sqrt{\frac{1}{n}\sum_{i=0}^{n-1} (z(i) - \bar{z})^2} \\ \bar{z} = \frac{1}{n}\sum_{i=0}^{n-1} z(i) \end{cases} \quad (5)$$

The maneuverability of a UAV is limited by its corner cost function. During the flight of the UAV trajectory planning, the turning angle should not be greater than the preset maximum turning angle, because of the turning angle size will affect the flight stability. In this paper, we set the maximum turning angle to φ and the current turning angle to θ, and a_i is the vector of the ith route segment. The corner formula is shown in Eq. 6:

$$\begin{cases} \cos\theta = \frac{a_i^T a_{i+1}}{|a_i||a_{i+1}|} \\ J_{turn} = \sum_{i=1}^{n} \left(\cos(\Phi - \cos\theta)\right) \end{cases} \quad (6)$$

In Eq. 6, $|a|$ represents the length of the vector a. Through the description of the above three aspects, we established the cost function of UAV trajectory planning as follows in Eq. 7:

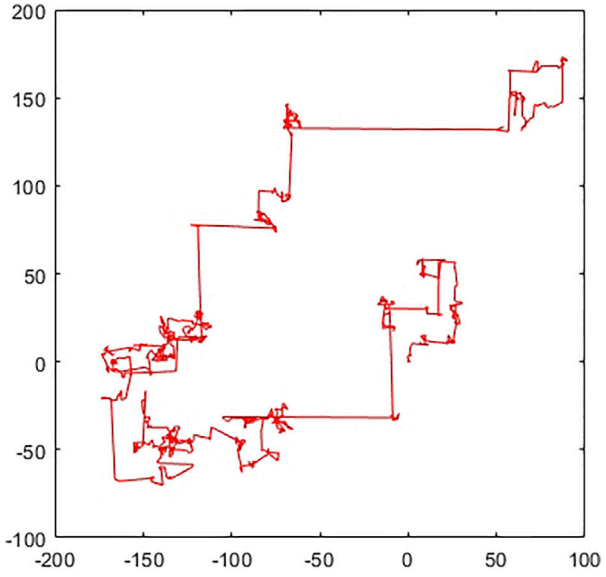

FIGURE 3
Step size of 100 Levy flights.

$$J_{cost} = w_1 L_{path} + w_2 h_{height} + w_3 J_{turn} \tag{7}$$

J_{cost} is the total cost function, and in the parameters w_i, $i = 1$, 2, 3 represent the weight of each cost function and satisfy the conditions of Eq. 8:

$$\begin{cases} w_i \geq 0 \\ \sum_{i=1}^{3} w_i = 1 \end{cases} \tag{8}$$

We obtained a track consisting of line segments by processing the total cost function effectively. However, the resulting track is only theoretically feasible, it is necessary to smooth the track to meet the actual situation. In this paper, cubic spline interpolation is used to smooth the UAV trajectory because the B-spline curve cannot guarantee the absolute accuracy of the interpolation points.

Sparrow search algorithm

The sparrow search algorithm is a new type of swarm intelligence optimization algorithm inspired by the feeding behavior of sparrows in nature. During the food search process, the sparrow population is divided into two roles: discoverer and follower. Discoverers generally make up 10%–20% of the population and lead the other individuals in the search for food. The discoverers have a high fitness and ability to expand the search range, while the remaining sparrows follow the discoverers to the destination. The population requires a particular number of sparrows to work as scouts and issue warnings to remind the populace that they can take action in time when the adversaries attack to escape the threat of natural enemies. The location update formula for the discoverer is as follows in Eq. 9:

$$x_{id}^{t+1} = \begin{cases} x_{i,j}^{t} \cdot \exp\left(\frac{-h}{\alpha \cdot T}\right) & if\ R_2 < ST \\ x_{i,j}^{t} + Q \cdot L & if\ R_2 > ST \end{cases} \tag{9}$$

In Eq. 9, h represents the current number of iterations and T is the maximum number of iterations. The value of $x_{i,j}$ denotes the current position of the ith sparrow in the jth dimension. The term, α, is a random number between 0 and 1, and Q is a random value obeying a standard normal distribution. L represents a 1×D matrix with all elements 1, alarm value $R_2 \in [0,1]$, and safety value $ST \in [0.5,1]$.

When $R_2 < ST$, it indicates that the surrounding environment is currently in a safe state, and the discoverers can search for food on a wide scale. If $R_2 > ST$, it means that there may be natural enemies in the surrounding environment, and the discoverers will quickly lead the population from the current position to avoid predators. Followers update their position according to their fitness ranking, and the positional update is described in Eq. 10:

$$x_{i,j}^{T+1} = \begin{cases} Q \cdot \exp\left(-\frac{x_{worst}^{T} - x_{i,j}^{T}}{i^2}\right) & if\ i > \frac{n}{2} \\ x_{p}^{T+1} + \left|x_{x,j}^{T} - x_{p}^{T+1}\right| \cdot A^{+} \cdot L & otherwise \end{cases} \tag{10}$$

In Eq. 10, xt w and x_{t+1} p represent the global worst position of the population at the tth iteration and the global optimal position of the population at the $t+1$-th iteration, respectively. A is a matrix of $1 \times D$ in which an element is only -1 or +1, with $A^{+} = A^{T}(AA^{T})^{-1}$. When $i > n/2$, it indicates that the ith participant is in a hungry state with poor fitness. In order to obtain higher energy, the participant needed to fly farther to find food. If $i < n/2$, the ith follower will find a random location near the current optimal position x_p to forage. The location of the scouter has been updated as shown in Eq. 11:

$$x_{i,j}^{T+1} = \begin{cases} x_{i,j}^{T} + Q \cdot \left|x_{i,j}^{T} - x_{best}^{T}\right| & f_i \neq f_g \\ x_{i,j}^{T} + K \frac{x_{i,j}^{T} - x_{worst}^{T}}{(f_i - f_w) + \varepsilon} & f_i = f_g \end{cases} \tag{11}$$

where K is a step coefficient, which is a random number in [-1, 1], and K represents the moving direction of the sparrows. Q is a value close to infinitesimal, which exists to avoid the denominator being zero. f_i represents the fitness values of the ith sparrows, f_g and f_w are the global optimal fitness and global worst fitness values within the current search scope, respectively, ε is the smallest real number, preventing the occurrence of 0 in the denominator. Individual sparrows face danger at the edge and approach the globally optimal sparrow

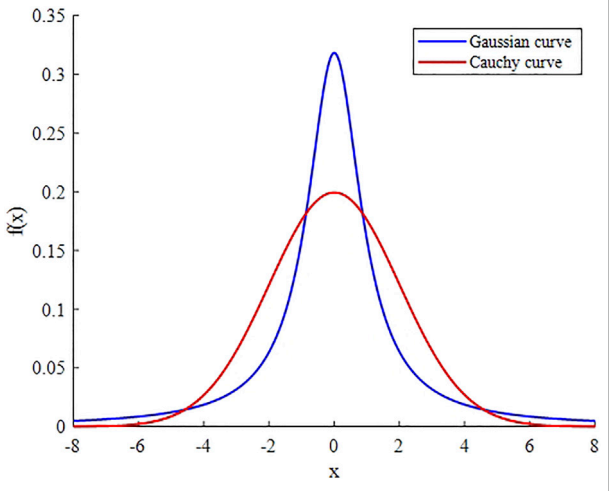

FIGURE 4
Gaussian curve and Cauchy curve distribution diagram.

when $f_i \neq f_g$. The individual sparrows in the center of the group can randomly walk among other individuals when $f_i = f_g$. This setup aims to avoid too many individuals reaching a local optimum, where the algorithm stops iterating and falls into a local optimum.

Multi-strategy sparrow search algorithm

The original SSA algorithm used a simple random function to generate the initial population, which cannot guarantee the diversity of the population and the stability of the algorithm. In the sparrow population, the foraging ability of the discoverers determines the foraging direction and foraging area of the population and also indicates the quality of the solution found by the algorithm. The formula for updating the discoverers' positions is one of the key formulas in the SSA. In the later iterations of the SSA, the sparrow population gradually approaches to the optimal individual, which leads to a lack of population diversity and a tendency toward premature convergence of the algorithm. In the SSA, it can be seen from Eq. 9 that each dimension of the individual discoverer decreases when $R2<ST$. This leads to a decrease in the population diversity of the algorithm in its later iterations and a lack of convergence accuracy. In the iterative process of the algorithm, the location update of sparrows mainly depends on the information exchanged among individuals, which easily produces population aggregation and leads to a lack of diversity. Then, according to Eq. 10, a large number of followers will flood into the search area around the finder. When they perceive that the finder has searched for a better food location, the high population density around the finder educes the diversity of population positions and easily falls into a local optimum. In summary, we propose three corresponding improvement strategies for the original SSA algorithm, which is prone to local optimal values and insufficient convergence accuracy. The specific strategies are discussed below.

Reverse learning strategy based on the law of refraction

For the SSA in the finder stage, with the continuous expansion of the search range, a broad and flexible search mechanism is the key to guiding the entire sparrow population to find food and avoid danger. When $R2 < ST$, the discoverer individuals of each dimension decrease. To better realize the leading role of the discoverer, this paper proposes a reverse learning strategy based on the law of refraction. We calculate the reverse solution of the candidate solution and select the better solution to continue the iterative calculation to effectively enhance the diversity of the algorithm and help the algorithm jump out of the local extreme value space.

As shown in Figure 2, O is the center point of $[a, b]$, $x \in [a, b]$; the global optimal individual X takes O as the center point to find its corresponding reverse individual X', where a represents the upper bound and b represents the lower bound. It can be derived from the law of refraction shown in Eq. 12:

$$\gamma = \frac{\sin\theta_1}{\sin\theta_2} = \frac{((a+b)/2 - x)/h}{(x' - (a+b)/2)/h'} \tag{12}$$

Assuming the scaling factor $\eta = h/h'$, the mathematical model of the reverse individual X' can be obtained by deriving Eq. 12 as shown in Eq. 13:

$$x' = \frac{(a+b)}{2} + \frac{(a+b)}{(2\eta\gamma)} - \frac{x}{\eta\gamma} \tag{13}$$

Extend Eq. 13 to n-dimensional space to obtain:

$$x_j' = \frac{(a_j + b_j)}{2} + \frac{(a_j + b_j)}{(2\eta\gamma)} - \frac{x_j}{\eta\gamma} \tag{14}$$

In this formula, a_j and b_j represent the jth dimensional vector of the upper bound and the jth dimensional vector of the lower bound, respectively; x_j and x' j represent the jth dimensional vector of X and x', respectively. Refraction reverse learning is performed on the optimal solution in the population, and each dimension value is mapped to the solution space to obtain a reverse solution, which not only avoids the interference between various dimensions but also expands the search range of the algorithm.

TABLE 1 Introduction to benchmark functions.

Fun no.	Name	Function type	Range	Dim	Optimal value
f_1	Sphere	Single-modal	[-100,100]	30/200/500	0
f_2	Schwefel's problem 2.22	Single-modal	[-10,10]	30/200/500	0
f_3	Schwefel's problem 1.2	Single-modal	[-100,100]	30/200/500	0
f_4	Schwefel's problem 2.21	Single-modal	[-100,100]	30/200/500	0
f_5	sum spare	Single-modal	[-10,10]	30/200/500	0
f_6	Zakharov	Single-modal	[-5,10]	30/200/500	0
f_7	Generalized Schwefel's problem 2.26	Multi-modal	[-500,500]	30/200/500	-12569.5
f_8	Generalized Rastrigin's function	Multi-modal	[-5.12,5.12]	30/200/500	0
f_9	Ackley's Function	Multi-modal	[-32,32]	30/200/500	0
f_{10}	Ceneralized Criewank function	Multi-modal	[-600,600]	30/200/500	0
f_{11}	Apline	Multi-modal	[-10,10]	30/200/500	0
f_{12}	Ceneralized penalized function 2	Fixed multi-modal	[-50,50]	30/200/500	0
f_{13}	Shekell's foxholes function	Fixed multi-modal	[-65,65]	30/200/500	1
f_{14}	Hatman's function 1	Fixed multi-modal	[0,1]	30/200/500	-3.86
f_{15}	Hatman's function 2	Fixed multi-modal	[0,1]	30/200/500	-3.32
f_{16}	Eggcrate	Fixed multi-modal	[-2π,2π]	30/200/500	0

Follower position update strategy based on Levy flight

Although the reverse learning strategy of the refraction law can help the algorithm to jump out of the local optimal value and improve the solution accuracy of the algorithm, it cannot expand the search range of the original population in the optimization process. Therefore, we introduced the Levy flight strategy to expand the follower's optimal range.

According to Eq. 10, a large number of followers in SSA will flood into the search area around the discoverers when they perceive that the finder has searched for a better food location, which has obvious convergence and makes the population density of the search area too high around the discoverers. This situation will reduce the diversity of population positions and easily fall into a local optimum. In this paper, the random step size s generated by Levy's flight is introduced into the follower's location update strategy, and the uncertainty of Levy's flight direction and step size is used to enhance the multiplicity of follower's search direction, thus improving the diversity of population locations and avoiding the search from falling into local optimal value. The random step size s of the Levy flight can be calculated by Eq. 15, and the result is shown in Figure 3:

$$\begin{cases} s = \mu/|v|^{1/\beta}, \beta = 3/2 \\ \mu \sim N\left(0, \sigma_\mu^2\right), v \sim N\left(0, \sigma_v^2\right) \\ \sigma_\mu = \left\{ \dfrac{\Phi(1+\beta)\sin(\pi\beta/2)}{\beta \cdot \Phi[(1+\beta)/2] \cdot 2^{(\beta-1)/2}} \right\}^{1/\beta}, \sigma_v = 1 \end{cases} \tag{15}$$

Figure 3 shows that Levy flight shuttles each other due to short and long distance searches, producing random steps s with no definite direction or size. By introducing the Levy flight strategy, followers can both roughly search over a large range and finely search over a small range as they approach the discoverer, which can effectively avoid convergence and enhance the diversity of population locations. The formula for updating the position of the follower was changed from Eqs 10–16 with the addition of the Levy flight strategy:

$$x_{i,j}^{t+1} = \begin{cases} Q \cdot \exp\left(\dfrac{x_w^t - x_{i,j}^t}{i^2}\right) & if\ i > \dfrac{n}{2} \\ x_p^{t+1} + s \cdot \left|x_{x,j}^t - x_p^{t+1}\right| A^+ \cdot L & otherwise \end{cases} \tag{16}$$

According to Formula 10, it can be seen that the individual with lower fitness value as a follower will reset the solution to a number near 1 after updating according to the formula, which is more effective for some objective functions whose optimal convergence solution is near 1 or 0. However, in practical engineering applications, the sparrows generally fly to places with lower fitness values on the whole. At the same time, the sparrow individuals with moderate fitness values are directly replaced by the current best individual. Although the convergence speed is improved to a certain extent, it will waste the search area of this part of the sparrow population and reduce the search accuracy. Comprehensively comparing the characteristics of the individual fitness values of followers, sparrows with moderate fitness values search in the direction of the best sparrow individual according to the current search area, while sparrow individuals with low fitness value fly to search

TABLE 2 Comparison of optimization results of different improvement strategies for SSA.

Fun no.	Algorithm	Optimal	Worst	Mean	Standard
f_1	SSA	0.00E+00	1.03E-50	3.44E-52	1.89E-51
	SSA1	0.00E+00	0.00E+00	0.00E+00	0.00E+00
	SSA2	0.00E+00	0.00E+00	0.00E+00	0.00E+00
	SSA3	0.00E+00	1.32E-65	4.45E-67	2.41E-66
	MSSA	0.00E+00	0.00E+00	0.00E+00	0.00E+00
f_2	SSA	0.00E+00	2.28E-21	7.59E-23	4.16E-22
	SSA1	0.00E+00	0.00E+00	0.00E+00	0.00E+00
	SSA2	0.00E+00	5.82E-272	3.09E-273	0.00E+00
	SSA3	0.00E+00	5.56E-30	1.89E-31	1.01E-30
	MSSA	0.00E+00	0.00E+00	0.00E+00	0.00E+00
f_3	SSA	0.00E+00	4.72E-63	1.61E-64	8.62E-64
	SSA1	0.00E+00	0.00E+00	0.00E+00	0.00E+00
	SSA2	0.00E+00	0.00E+00	0.00E+00	0.00E+00
	SSA3	0.00E+00	2.48E-50	8.28E-52	4.53E-51
	MSSA	0.00E+00	0.00E+00	0.00E+00	0.00E+00
f_4	SSA	0.00E+00	1.09E-23	3.65E-25	2.00E-24
	SSA1	0.00E+00	0.00E+00	0.00E+00	0.00E+00
	SSA2	7.88E-306	1.30E-258	4.35E-260	0.00E+00
	SSA3	0.00E+00	2.20E-25	8.76E-27	4.06E-26
	MSSA	0.00E+00	0.00E+00	0.00E+00	0.00E+00
f_5	SSA	0.00E+00	1.47E-37	4.89E-39	2.68E-38
	SSA1	0.00E+00	0.00E+00	0.00E+00	0.00E+00
	SSA2	0.00E+00	0.00E+00	0.00E+00	0.00E+00
	SSA3	0.00E+00	6.54E-44	2.18E-45	1.19E-44
	MSSA	0.00E+00	0.00E+00	0.00E+00	0.00E+00
f_6	SSA	0.00E+00	5.29E-37	2.25E-38	9.93E-38
	SSA1	0.00E+00	5.65E-35	1.88E-36	1.03E-35
	SSA2	0.00E+00	0.00E+00	0.00E+00	0.00E+00
	SSA3	0.00E+00	2.79E-46	9.29E-48	5.09E-47
	MSSA	0.00E+00	0.00E+00	0.00E+00	0.00E+00
f_7	SSA	-1.26E+04	-4.77E+03	-1.14E+04	1.92E+03
	SSA1	-1.26E+04	-4.13E+03	-1.02E+04	2.49E+03
	SSA2	-1.26E+04	-7.95E+03	-1.20E+04	9.45E+02
	SSA3	-1.13E+04	-3.96E+03	-9.30E+03	1.75E+03
	MSSA	-1.26E+04	-1.26E+04	-1.26E+04	2.03E-01
f_8	SSA	0.00E+00	0.00E+00	0.00E+00	0.00E+00
	SSA1	0.00E+00	0.00E+00	0.00E+00	0.00E+00
	SSA2	0.00E+00	0.00E+00	0.00E+00	0.00E+00
	SSA3	0.00E+00	0.00E+00	0.00E+00	0.00E+00
	MSSA	0.00E+00	0.00E+00	0.00E+00	0.00E+00
F_9	SSA	8.88E-16	8.88E-16	8.88E-16	0.00E+00
	SSA1	8.88E-16	8.88E-16	8.88E-16	0.00E+00
	SSA2	8.88E-16	8.88E-16	8.88E-16	0.00E+00
	SSA3	8.88E-16	8.88E-16	8.88E-16	0.00E+00
	MSSA	8.88E-16	8.88E-16	8.88E-16	0.00E+00
f_{10}	SSA	0.00E+00	0.00E+00	0.00E+00	0.00E+00
	SSA1	0.00E+00	0.00E+00	0.00E+00	0.00E+00
	SSA2	0.00E+00	0.00E+00	0.00E+00	0.00E+00

(Continued on following page)

TABLE 2 (*Continued*) Comparison of optimization results of different improvement strategies for SSA.

Fun no.	Algorithm	Optimal	Worst	Mean	Standard
	SSA3	0.00E+00	0.00E+00	0.00E+00	0.00E+00
	MSSA	0.00E+00	0.00E+00	0.00E+00	0.00E+00
f_{11}	SSA	0.00E+00	5.04E-19	1.68E-20	9.21E-20
	SSA1	0.00E+00	0.00E+00	0.00E+00	0.00E+00
	SSA2	0.00E+00	1.73E-261	5.78E-263	0.00E+00
	SSA3	0.00E+00	1.72E-23	5.74E-25	3.14E-24
	MSSA	0.00E+00	0.00E+00	0.00E+00	0.00E+00
f_{12}	SSA	-1.03E+00	1.88E-121	-9.63E-01	2.62E-01
	SSA1	-1.03E+00	0.00E+00	-9.28E-01	3.15E-01
	SSA2	-1.03E+00	-1.03E+00	-1.03E+00	2.32E-11
	SSA3	-1.03E+00	-1.03E+00	-1.03E+00	6.45E-05
	MSSA	-1.03E+00	-1.03E+00	-1.03E+00	1.47E-05
f_{13}	SSA	3.98E-01	3.98E-01	3.98E-01	3.15E-05
	SSA1	3.98E-01	8.45E-01	4.13E-01	8.16E-02
	SSA2	3.98E-01	3.98E-01	3.98E-01	5.35E-07
	SSA3	3.98E-01	6.42E-01	4.23E-01	6.90E-02
	MSSA	3.98E-01	3.98E-01	3.98E-01	7.41E-05
f_{14}	SSA	-3.86E+00	-3.09E+00	-3.75E+00	2.00E-01
	SSA1	-3.86E+00	-3.60E+00	-3.82E+00	5.91E-02
	SSA2	-3.86E+00	-3.09E+00	-3.81E+00	1.96E-01
	SSA3	-3.86E+00	-3.01E+00	-3.65E+00	2.03E-01
	MSSA	-3.86E+00	-3.86E+00	-3.86E+00	2.10E-03
f_{15}	SSA	-3.24E+00	-1.40E+00	-2.96E+00	3.62E-01
	SSA1	-3.30E+00	-2.82E+00	-3.10E+00	1.31E-01
	SSA2	-3.32E+00	-3.03E+00	-3.25E+00	9.02E-02
	SSA3	-3.17E+00	-1.17E+00	-2.65E+00	5.33E-01
	MSSA	-3.32E+00	-3.03E+00	-3.23E+00	9.01E-02
f_{16}	SSA	0.00E+00	1.63E-33	5.53E-35	2.97E-34
	SSA1	0.00E+00	0.00E+00	0.00E+00	0.00E+00
	SSA2	0.00E+00	0.00E+00	0.00E+00	0.00E+00
	SSA3	0.00E+00	4.17E-52	1.39E-53	7.62E-53
	MSSA	0.00E+00	0.00E+00	0.00E+00	0.00E+00

near the best position of the finder. The positions updated by Levy flight of the follower is changed from Eqs 16, 17:

$$x_{i,j}^{t+1} = \begin{cases} x_p^{t+1} + s \cdot \left| x_{x,j}^t - x_p^{t+1} \right| & if\ i > \frac{n}{2} \\ x_p^{t+1} + s \cdot \left| x_{x,j}^t - x_p^{t+1} \right| \cdot A^+ \cdot L & otherwise \end{cases} \tag{17}$$

Scouter position update strategy based on improved Cauchy mutations

In the SSA, the scouters enhance the global exploration ability of the algorithm to some extent, and the ability to jump out of the local optimal value is stronger if the number of scouters is a high percentage of the whole sparrow population. However, the random selection of scouters limits the more active sparrow individuals. The mechanism of fixing the number of scouter in the sparrow optimization algorithm slows down the optimization accuracy and convergence speed to a certain extent. Therefore, the improved scouter formula proposed in this paper on the original Eq. 11 is as follows:

$$x_{i,j}^{t+1} = \begin{cases} x_{i,j}^t + Q \cdot \left| x_{i,j}^t - x_{b,j}^t \right| & f_i \neq f_g \\ x_{b,j}^t + Q \cdot \left| x_w^t - x_{b,j}^t \right| & f_i = f_g \end{cases} \tag{18}$$

Because the sparrow optimization algorithm easily falls into a local optimum, the peak value of the Cauchy distribution function at the origin is small, but the distribution at both ends is relatively long. Because the range of the Cauchy

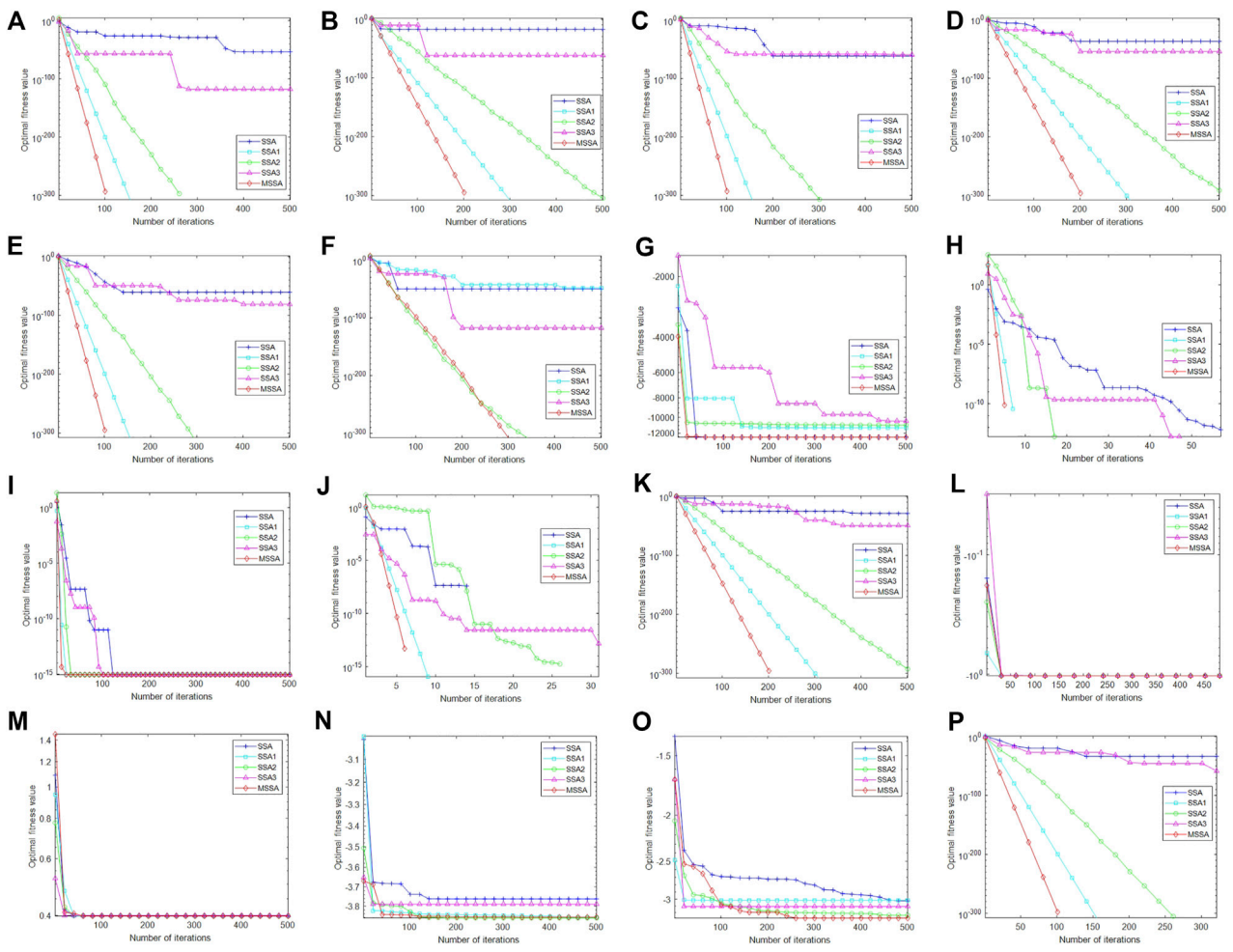

FIGURE 5
Mean convergence curve of the benchmark function. **(A)** f_1 mean convergence curve. **(B)** f2 mean convergence curve. **(C)** f3 mean convergence curve. **(D)** f4 mean convergence curve. **(E)** f5 mean convergence curve. **(F)** f6 mean convergence curve. **(G)** f7 mean convergence curve. **(H)** f8 mean convergence curve. **(I)** f9 mean convergence curve. **(J)** f10 mean convergence curve. **(K)** f11 mean convergence curve. **(L)** f12 mean convergence curve. **(M)** f13 mean convergence curve. **(N)** f14 mean convergence curve. **(O)** f15 mean convergence curve. **(P)** f_{16} mean convergence curve.

distribution function is relatively wide, it is easier to jump out of the local optimum by using the distribution at both ends of the Cauchy variation (Li et al., 2017). We used the Cauchy mutation to generate larger disturbances near the currently mutated sparrow individual to improve the local search ability of the algorithm and expand the search space of the algorithm. The standard Cauchy distribution function formula is as follows:

$$f_c(x) = \frac{1}{\pi}\left(\frac{\gamma}{(x-x_0)^2+\gamma^2}\right) - \infty < x < \infty \tag{19}$$

If the random variable x of the Cauchy distribution obeys the position parameter of x_0 and the scale parameter of γ, it is recorded as Cauchy(γ, x_0). When the special case of $\gamma = 1$ and $x_0 = 0$, it becomes the standard Cauchy distribution function, and the corresponding cumulative distribution function is shown in Eq. 20:

$$F_c(x) = \frac{1}{2} + \frac{1}{\pi}\arctan\left(\frac{x-x_0}{\gamma}\right) \tag{20}$$

There are two main differences because the density function of the Cauchy distribution is similar to the Gaussian density function. On the one hand, the Cauchy distribution in the vertical direction is slightly smaller than the Gaussian distribution. On the other hand, the closer the Cauchy distribution is to the horizontal axis in the horizontal direction, the slower the change, so the Cauchy distribution can be regarded as infinite.

The comparison of the two distributions is shown in Figure 4. The Cauchy distribution and the Gaussian distribution have

TABLE 3 Comparison with the results of five metaheuristic algorithms.

Fun no.	Name	30 *dim*		200 *dim*		500 *dim*	
		Mean	SD	Mean	SD	Mean	SD
f_1	SSA[26]	1.28E-52	6.76E-52	5.12E-40	2.80E-39	4.12E-64	2.25E-63
	GWO[16]	2.12E-27	3.08E-27	1.17E-07	7.25E-08	1.66E-03	5.71E-04
	WOA[34]	2.21E-73	9.78E-73	4.55E-67	2.49E-66	2.68E-71	9.22E-71
	TSA[12]	1.91E-21	7.58E-21	3.64E-06	3.57E-06	2.77E-02	1.82E-02
	EO[35]	2.48E-41	3.99E-41	1.44E-25	2.04E-25	1.11E-22	1.64E-22
	MSSA	0.00E+00	0.00E+00	0.00E+00	0.00E+00	0.00E+00	0.00E+00
f_2	SSA[26]	3.12E-20	1.71E-19	3.18E-19	1.74E-18	1.89E-26	1.04E-25
	GWO[16]	1.18E-16	9.88E-17	3.26E-05	7.11E-06	1.21E-02	2.11E-03
	WOA[34]	3.09E-51	1.09E-50	6.10E-49	2.18E-48	6.87E-49	3.18E-48
	TSA[12]	9.65E-14	1.78E-13	5.24E-05	3.37E-05	6.84E-03	4.31E-03
	EO[35]	5.63E-24	4.83E-24	1.56E-15	8.88E-16	8.77E-14	6.13E-14
	MSSA	0.00E+00	0.00E+00	0.00E+00	0.00E+00	0.00E+00	0.00E+00
f_3	SSA[26]	7.58E-49	3.99E-48	1.04E-42	5.70E-42	2.66E-56	1.46E-55
	GWO[16]	1.79E-05	4.40E-05	2.02E+04	8.92E+03	3.22E+05	8.03E+04
	WOA[34]	4.52E+04	1.34E+04	5.17E+06	1.56E+06	3.02E+07	1.04E+07
	TSA[12]	1.22E-03	5.79E-03	1.72E+05	4.14E+04	1.42E+06	2.42E+05
	EO[35]	4.95E-09	5.06E-10	7.62E+02	1.53E+03	2.95E+04	3.08E+04
	MSSA	0.00E+00	0.00E+00	0.00E+00	0.00E+00	0.00E+00	0.00E+00
f_4	SSA[26]	7.37E-20	4.04E-19	1.41E-23	7.74E-23	3.32E-34	1.82E-33
	GWO[16]	9.14E-07	6.67E-07	2.38E+01	7.22E+00	6.40E+01	5.40E+00
	WOA[34]	5.07E+01	2.83E+01	7.59E+01	2.58E+01	8.04E+01	2.32E+01
	TSA[12]	4.57E-01	6.01E-01	9.39E+01	4.14E+00	9.91E+01	3.10E-01
	EO[35]	5.06E-10	9.39E-10	2.23E+01	2.48E+01	6.81E+01	1.59E+01
	MSSA	0.00E+00	0.00E+00	0.00E+00	0.00E+00	0.00E+00	0.00E+00
f_5	SSA[26]	1.72E-51	9.40E-51	4.54E-49	2.49E-48	8.45E-50	4.63E-49
	GWO[16]	4.03E-29	5.75E-29	1.68E-08	8.39E-09	8.45E-04	2.78E-04
	WOA[34]	1.56E-72	8.53E-72	3.49E-71	1.19E-70	1.70E-68	6.15E-68
	TSA[12]	3.22E-23	3.46E-23	1.07E-06	1.60E-06	1.32E-02	1.52E-02
	EO[35]	1.90E-42	3.16E-42	4.63E-26	1.30E-25	9.77E-23	9.61E-23
	MSSA	0.00E+00	0.00E+00	0.00E+00	0.00E+00	0.00E+00	0.00E+00
f_6	SSA[26]	1.93E-38	1.06E-37	3.33E-40	1.82E-39	1.38E-29	7.56E-29
	GWO[16]	2.59E-07	7.08E-07	9.92E+02	2.21E+02	3.88E+03	5.58E+02
	WOA[34]	4.98E+02	1.34E+02	3.33E+03	3.94E+02	8.03E+03	1.06E+03
	TSA[12]	2.79E-10	3.32E-10	5.03E+02	1.04E+02	1.93E+03	3.31E+02
	EO[35]	1.46E-05	3.12E-05	9.35E+02	3.08E+02	3.08E+03	9.19E+02
	MSSA	0.00E+00	0.00E+00	0.00E+00	0.00E+00	0.00E+00	0.00E+00
f_7	SSA[26]	-1.13E+04	1.90E+03	-7.62E+04	8.05E+03	-1.84E+05	2.15E+04
	GWO[16]	-6.15E+03	8.82E+02	-2.70E+04	6.46E+03	-5.67E+04	9.18E+03
	WOA[34]	-1.05E+04	1.79E+03	-6.86E+04	1.12E+04	-1.75E+05	2.84E+04
	TSA[12]	-5.96E+03	5.65E+02	-1.94E+04	1.19E+03	-3.09E+04	1.95E+03
	EO[35]	-8.85E+03	6.65E+02	-4.26E+04	2.74E+03	-7.41E+04	4.79E+03
	MSSA	-1.26E+04	9.57E-02	-8.38E+04	1.95E-01	-2.09E+05	1.12E+00
f_8	SSA[26]	0.00E+00	0.00E+00	0.00E+00	0.00E+00	0.00E+00	0.00E+00
	GWO[16]	2.30E+00	2.95E+00	2.55E+01	1.45E+01	7.42E+01	2.30E+01
	WOA[34]	0.00E+00	0.00E+00	1.52E-14	8.30E-14	3.03E-14	1.66E-13
	TSA[12]	1.82E+02	3.73E+01	2.19E+03	2.31E+02	5.89E+03	5.98E+02

(Continued on following page)

TABLE 3 (*Continued*) Comparison with the results of five metaheuristic algorithms.

Fun no.	Name	30 *dim*		200 *dim*		500 *dim*	
		Mean	SD	Mean	SD	Mean	SD
	EO[35]	0.00E+00	0.00E+00	1.52E-14	5.77E-14	6.06E-14	2.31E-13
	MSSA	0.00E+00	0.00E+00	0.00E+00	0.00E+00	0.00E+00	0.00E+00
f_9	SSA[26]	8.88E-16	0.00E+00	8.88E-16	0.00E+00	8.88E-16	0.00E+00
	GWO[16]	1.11E-13	1.57E-14	2.42E-05	6.94E-06	1.95E-03	3.93E-04
	WOA[34]	5.27E-15	2.02E-15	5.27E-15	2.41E-15	3.85E-15	2.48E-15
	TSA[12]	1.87E+00	1.57E+00	2.72E-04	1.74E-04	1.06E-02	5.51E-03
	EO[35]	8.70E-15	2.17E-15	9.49E-14	2.87E-14	4.85E-13	2.46E-13
	MSSA	8.88E-16	0.00E+00	8.88E-16	0.00E+00	8.88E-16	0.00E+00
f_{10}	SSA[26]	0.00E+00	0.00E+00	0.00E+00	0.00E+00	0.00E+00	0.00E+00
	GWO[16]	4.22E-03	1.01E-02	6.69E-03	1.43E-02	6.75E-03	2.50E-02
	WOA[34]	0.00E+00	0.00E+00	0.00E+00	0.00E+00	3.70E-18	2.03E-17
	TSA[12]	1.39E-02	1.98E-02	2.63E-02	5.94E-02	3.74E-02	7.96E-02
	EO[35]	0.00E+00	0.00E+00	0.00E+00	0.00E+00	1.11E-03	6.07E-03
	MSSA	0.00E+00	0.00E+00	0.00E+00	0.00E+00	0.00E+00	0.00E+00
f_{11}	SSA[26]	1.95E-33	1.06E-32	7.03E-24	3.20E-23	5.12E-20	2.81E-19
	GWO[16]	4.46E-04	6.57E-04	1.30E-02	3.27E-03	6.83E-02	1.38E-02
	WOA[34]	2.53E-43	1.38E-42	1.20E-49	4.86E-49	2.45E-50	7.46E-50
	TSA[12]	2.58E+01	6.50E+00	3.50E+02	4.66E+01	8.75E+02	1.96E+02
	EO[35]	1.41E-07	7.17E-07	1.23E-15	5.16E-15	1.19E-14	5.56E-15
	MSSA	0.00E+00	0.00E+00	0.00E+00	0.00E+00	0.00E+00	0.00E+00
f_{12}	SSA[26]	-1.03E+00	2.40E-07	-1.01E+00	1.45E-01	-8.60E-01	3.91E-01
	GWO[16]	-1.03E+00	1.82E-08	-1.03E+00	1.03E-08	-1.03E+00	6.06E-09
	WOA[34]	-1.03E+00	6.71E-10	-1.03E+00	6.26E-09	-1.03E+00	6.69E-10
	TSA[12]	-1.03E+00	8.02E-03	-1.03E+00	1.09E-02	-1.03E+00	5.77E-03
	EO[35]	-1.03E+00	6.39E-16	-1.03E+00	6.18E-16	-1.03E+00	6.39E-16
	MSSA	-1.03E+00	1.46E-05	-1.03E+00	1.31E-05	-1.03E+00	1.46E-05
f_{13}	SSA[26]	3.98E-01	8.02E-06	3.98E-01	9.38E-06	3.98E-01	5.02E-06
	GWO[16]	3.98E-01	3.88E-05	3.98E-01	1.32E-06	3.98E-01	1.27E-04
	WOA[34]	3.98E-01	4.45E-05	3.98E-01	9.77E-06	3.98E-01	8.92E-06
	TSA[12]	3.98E-01	9.97E-05	3.98E-01	3.50E-05	3.98E-01	8.92E-05
	EO[35]	3.98E-01	0.00E+00	3.98E-01	0.00E+00	3.98E-01	0.00E+00
	MSSA	3.98E-01	9.24E-05	3.98E-01	5.85E-05	3.98E-01	6.99E-05
f_{14}	SSA[26]	-3.81E+00	6.70E-02	-3.76E+00	1.95E-01	-3.80E+00	1.47E-01
	GWO[16]	-3.86E+00	2.46E-03	-3.86E+00	2.60E-03	-3.86E+00	1.64E-03
	WOA[34]	-3.85E+00	1.92E-02	-3.86E+00	6.28E-03	-3.86E+00	1.07E-02
	TSA[12]	-3.86E+00	1.43E-03	-3.86E+00	1.41E-03	-3.86E+00	1.10E-04
	EO[35]	-3.86E+00	1.44E-03	-3.86E+00	2.49E-15	-3.86E+00	2.49E-15
	MSSA	-3.86E+00	2.03E-02	-3.86E+00	6.59E-03	-3.86E+00	4.01E-03
f_{15}	SSA[26]	-3.05E+00	2.17E-01	-2.96E+00	4.63E-01	-2.91E+00	3.37E-01
	GWO[16]	-3.25E+00	7.06E-02	-3.24E+00	7.51E-02	-3.27E+00	6.64E-02
	WOA[34]	-3.25E+00	9.10E-02	-3.20E+00	1.26E-01	-3.26E+00	8.98E-02
	TSA[12]	-3.24E+00	1.26E-01	-3.26E+00	7.44E-02	-3.25E+00	1.04E-01
	EO[35]	-3.24E+00	6.99E-02	-3.28E+00	5.85E-02	-3.25E+00	6.92E-02
	MSSA	-3.21E+00	8.80E-02	-3.24E+00	7.45E-02	-3.21E+00	9.89E-02
f_{16}	SSA[26]	4.77E-40	2.61E-39	1.48E-59	8.09E-59	3.49E-64	1.91E-63
	GWO[16]	9.42E-207	0.00E+00	8.88E-205	0.00E+00	1.00E-210	0.00E+00

(Continued on following page)

TABLE 3 (*Continued*) Comparison with the results of five metaheuristic algorithms.

Fun no.	Name	30 *dim*		200 *dim*		500 *dim*	
		Mean	SD	Mean	SD	Mean	SD
	WOA[34]	4.18E-111	2.29E-110	4.90E-106	2.68E-105	1.38E-109	7.56E-109
	TSA[12]	6.90E-95	3.78E-94	1.47E-94	8.04E-94	7.55E-105	4.13E-104
	EO[35]	3.42E-205	0.00E+00	4.86E-213	0.00E+00	4.10E-208	0.00E+00
	MSSA	0.00E+00	0.00E+00	0.00E+00	0.00E+00	0.00E+00	0.00E+00

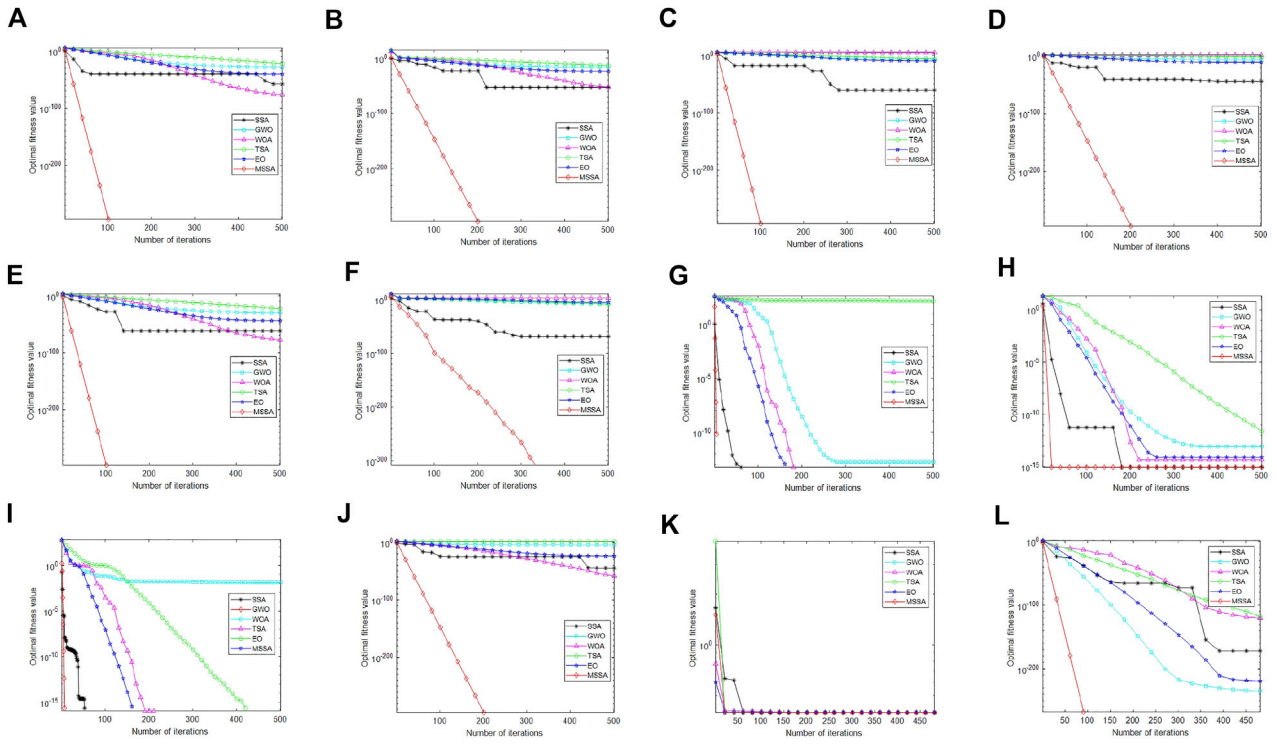

FIGURE 6
Comparison of optimization of each algorithm. **(A)** f1 mean convergence curve. **(B)** f2 mean convergence curve. **(C)** f3 mean convergence curve. **(D)** f4 mean convergence curve. **(E)** f5 mean convergence curve. **(F)** f6 mean convergence curve. **(G)** f8 mean convergence curve. **(H)** f9 mean convergence curve. **(I)** f10 mean convergence curve. **(J)** f11 mean convergence curve. **(K)** f13 mean convergence curve. **(L)** f_{16} mean convergence curve.

certain similarities and their own characteristics. The Cauchy distribution has a wider range than the Gaussian distribution. The Cauchy distribution easily generates a random number far from the origin, which means that the sparrow individual after Cauchy mutation has a higher probability of jumping out of the local optimal area. In addition, the peak value of the Cauchy distribution function is lower than that of the Gaussian distribution, which can shorten the search time of the mutated sparrow individuals around the neighborhood. Therefore, this paper integrates the Cauchy mutation to improve the scouter position update strategy, increases the diversity of the population and improves the ability of the algorithm to jump out of the local optimum. The position update formula is as follows:

$$x_{i,j}^{t+1} = x_{best}^{t} + x_{i,j}^{t} \cdot Cauchy\,(0,1) \tag{21}$$

Eqs 9–11, derived from the original work of SSA, specify how the sparrow is updated and construct the basic flow of the

TABLE 4 Wilcoxon rank sum test results.

Fun. No	SSA(p_1)	GWO(p_2)	WOA(p_3)	TSA(p_4)	EO(p_5)
f_1	1.31×10^{-07}	1.21 × 10–12	1.21 × 10–12	1.21 × 10–12	1.21 × 10–12
f_2	1.93×10^{-10}	1.21 × 10–12	1.21 × 10–12	1.21 × 10–12	1.21 × 10–12
f_3	1.70×10^{-08}	1.21 × 10–12	1.21 × 10–12	1.21 × 10–12	1.21 × 10–12
f_4	1.66×10^{-11}	1.21 × 10–12	1.21 × 10–12	1.21 × 10–12	1.21 × 10–12
f_5	1.31×10^{-07}	1.21 × 10–12	1.21 × 10–12	1.21 × 10–12	1.21 × 10–12
f_6	1.70×10^{-08}	1.21 × 10–12	1.21 × 10–12	1.21 × 10–12	1.21 × 10–12
f_7	2.15×10^{-10}	3.02 × 10–11	3.34 × 10–11	3.02 × 10–11	3.02 × 10–11
f_8	NaN	1.17 × 10–12	NaN	1.21 × 10–12	NaN
f_9	NaN	1.15 × 10–12	3.06 × 10–09	1.21 × 10–12	3.13 × 10–12
f_{10}	NaN	6.62 × 10–04	3.04 × 10–01	8.86 × 10–07	NaN
f_{11}	1.93×10^{-10}	1.21 × 10–12	1.21 × 10–12	1.21 × 10–12	1.21 × 10–12
f_{12}	3.34×10^{-11}	3.02 × 10–11	3.02 × 10–11	2.13 × 10–05	6.32 × 10–12
f_{13}	3.83×10^{-06}	1.07 × 10–09	5.00 × 10–09	8.31 × 10–03	1.21 × 10–11
f_{14}	6.41×10^{-01}	3.77 × 10–04	5.59 × 10–01	5.53 × 10–08	1.72 × 10–12
f_{15}	1.03×10^{-06}	9.79 × 10–05	6.55 × 10–04	3.34 × 10–03	3.06 × 10–11
f_{16}	1.31×10^{-07}	1.21 × 10–12	1.21 × 10–12	1.21 × 10–12	1.21 × 10–12
+/ = /-	13/3/3	16/0/0	15/1/1	16/0/0	14/2/2

algorithm. Based on the idealization and feasibility of the above model, the basic steps of the improved SSA can be summarized in the pseudo-code shown in Algorithm 1.

Simulation experiments of MSSA

Experimental environment parameters and test functions

The computer configuration used in the simulation experiment is Intel Core i7-6700HQ, the main frequency is 2.60 GHz, 8 GB memory, 64 bit operating system, and the computing environment is MATLAB 2019(b). We compare the SSA, GWO, WOA (Mirjalili and Lewis, 2016), TSA, and EO (Faramarzi et al., 2020) with MSSA. The basic parameters of the algorithms were set to the same value, including population size $N = 30$, the maximum number of iterations $T_{max} = 500$. The test function dimensions were divided into low-dimensional ($d = 30$) and high-dimensional ($d = 200$ and $d = 500$).

To test the optimization performance of the MSSA algorithm, 16 benchmark functions with different characteristics used in the literature were selected for the function optimization test. The selected test functions were divided into three categories. The first category was the single-modal test function, f_1-f_6, which is mainly used to evaluate the optimization accuracy and convergence speed of the algorithm. The second type is the multi-modal test function, f_7-f_{11}, which is used to test the exploration ability of the algorithm and the ability to jump out of the local optimal value. The third type is the fixed multi-modal test function, f_{12}-f_{16}. This paper used the 16 benchmark functions to evaluate the comprehensive ability of the algorithm. The detailed description and related information are shown in Table 1.

Comparing MSSA with various improvement strategies

Optimization performance experiment

To fully verify the optimization effect of the proposed improved strategy, we denoted the three improvement strategies as SSA1, SSA2, and SSA3, and compare them with SSA and MSSA. Each algorithm was independently run 30 times on 16 benchmark functions, and the optimal value, worst value, mean value, and standard value were recorded. The optimal value and the worst value reflected the single optimization ability of the algorithm, the average value reflected the convergence accuracy, and the standard deviation reflected the stability and robustness of the algorithm. Parameters were uniformly set as follows: population size $N = 30$, search space dimension dim = 30, and maximum number of iterations, $T_{max} = 500$. The results of experimental optimization are shown in Table 2:

Table 2 shows that for the single-modal test functions, f_1-f_6, MSSA can find the theoretical optimal value, illustrating that the stability is strong. At the same time, SSA1 can reach the theoretical optimal value and the more stable standard, showing that the introduction of the lens imaging learning strategy helps the algorithm to jump out of the local optimal

TABLE 5 Part of the CEC2014 function.

Fun no.	Dim	Function type	Range	Optimal
CEC01	30	UN	[-100,100]	100
CEC02	30	UN	[-100,100]	200
CEC03	30	UN	[-100,100]	300
CEC04	30	MF	[-100,100]	400
CEC05	30	MF	[-100,100]	500
CEC06	30	MF	[-100,100]	600
CEC07	30	MF	[-100,100]	700
CEC08	30	MF	[-100,100]	800
CEC09	30	MF	[-100,100]	900
CEC10	30	MF	[-100,100]	1000
CEC11	30	MF	[-100,100]	1100
CEC12	30	MF	[-100,100]	1200
CEC13	30	MF	[-100,100]	1300
CEC14	30	MF	[-100,100]	1400
CEC15	30	MF	[-100,100]	1500
CEC16	30	MF	[-100,100]	1600
CEC17	30	HF	[-100,100]	1700
CEC18	30	HF	[-100,100]	1800
CEC19	30	HF	[-100,100]	1900
CEC20	30	HF	[-100,100]	2000
CEC21	30	HF	[-100,100]	2100
CEC22	30	HF	[-100,100]	2200
CEC23	30	HF	[-100,100]	2300
CEC24	30	HF	[-100,100]	2400
CEC25	30	CF	[-100,100]	2500
CEC26	30	CF	[-100,100]	2600
CEC27	30	CF	[-100,100]	2700
CEC28	30	CF	[-100,100]	2800
CEC29	30	CF	[-100,100]	2900
CEC30	30	CF	[-100,100]	3000

value. SSA2 can reach the optimal theoretical value in f_1, f_2, f_5, and f_6, indicating that adding Levy flight can help the population to deeply mine the global optimal values and improve the global search ability of the algorithm. For the multi-modal test functions, f_7-f_{11}, there are a large number of local extremes distributed in their solution space, and it is difficult for the algorithm to perform global optimization. The MSSA and other comparative algorithms fall into local optimal solutions when solving function f_9. But MSSA has higher convergence accuracy and stability in other test functions, and the standards are more stable than other algorithms.

For the fixed multi-modal functions, f_{12}-f_{16}, MSSA can find the theoretical optimal value, and the stability is extremely strong and the standard value is lower than SSA1, SSA2, and SSA3, indicating that MSSA has stronger stability and robustness.

Convergence curve experiment

We used the average convergence curve to reflect the dynamic convergence characteristics of the MSSA in this paper. We make the algorithm run 30 times independently under the population size N = 30, maximum number of iterations T_{max} = 500, and the search dimension dim = 30. Figure 5 presents the average convergence curves of the 16 benchmark functions.

Figure 5 shows that the MSSA has a higher optimization accuracy solution rate and faster convergence speed in f_1-f_5 than under the same number of iterations. The values of f_7-f_{11} and f_{16} show that the MSSA is able to guarantee the exploration ability and illustrate that the MSSA can ensure the development ability without losing the population diversity and optimization stability. For f_6 and f_{12}-f_{14}, the MSSA can converge to the optimal value faster in the later stages, which indicates that adopting the three strategies can help the algorithm jump out of the local optimal value effectively. In general, the MSSA average convergence curve is below the four comparison algorithms and takes fewer iterations to reach the theoretical optimal. From Table 2 and Figure 5, the result illustrates that the MSSA has higher convergence accuracy, convergence speed, stronger stability, and better robustness. The experimental results verify the effectiveness of the proposed algorithm and achieve the purpose of improving the standard SSA.

Comparing MSSA with other algorithms

Optimization performance experiment

To further test the optimization characteristics of the MSSA algorithm for the benchmark function, this paper chose the standard SSA, GWO, WOA, TSA, EO, and MSSA to compare for optimization performance. For each benchmark function, the search dimension is set to dim = 30/200/500, the maximum number of iterations T_{max} = 500 and the population size is N = 30. The test functions of Table 1 are used to perform the optimization comparison test, and each algorithm is run 30 times independently. The comparison results are shown in Table 3:

As seen from Table 3, the solution rate of MSSA can reach 100% when solving for the single-modal test function, f_1-f_6, which indicates that MSSA has good optimization accuracy and robustness. For the multi-modal test function, f_7-f_{11}, MSSA can find the theoretical optimal value. For the fixed multi-modal test function, f_{12}-f_{16}, the MSSA solution results are very close to or equal to the theoretical optimal value. As the dimension of the search space increases from 30 to 200 and 500 dimensions, the search accuracy and stability of the algorithm decrease because the optimization process requires more computations, but MSSA still has the highest optimization accuracy. This illustrates that the MSSA has a significant

TABLE 6 CEC2014 function optimization comparison.

No.	SSA		GWO		WOA		TSA		EO		MSSA	
	Mean	SD	Mean	SD	Mean	SD	Mean	SD	Mean	SD	Mean	Std
CEC01	9.554E+08	2.631E+08	1.098E+08	8.610E+07	2.175E+08	1.105E+08	4.116E+08	2.529E+08	1.607E+07	7.842E+06	7.625E+08	2.612E+08
CEC02	7.477E+10	8.241E+09	3.206E+09	2.525E+09	6.849E+09	2.531E+09	3.020E+10	1.016E+10	1.450E+05	1.666E+05	5.933E+10	8.122E+09
CEC03	8.759E+04	3.076E+03	5.134E+04	1.349E+04	1.364E+05	7.675E+04	5.817E+04	1.096E+04	2.289E+04	1.232E+04	8.518E+04	4.116E+03
CEC04	1.369E+04	3.074E+03	6.920E+02	8.595E+01	1.350E+03	3.125E+02	3.325E+03	2.152E+03	5.261E+02	3.970E+01	9.841E+03	2.116E+03
CEC05	5.212E+02	9.680E-02	5.211E+02	7.219E-02	5.209E+02	1.063E-01	5.211E+02	7.515E-02	5.210E+02	8.605E-02	5.210E+02	7.811E-02
CEC06	6.432E+02	2.736E+00	6.169E+02	2.231E+00	6.388E+02	3.369E+00	6.331E+02	3.501E+00	6.112E+02	2.621E+00	6.405E+02	2.563E+00
CEC07	1.258E+03	1.513E+02	7.296E+02	2.719E+01	7.462E+02	1.945E+01	9.799E+02	8.968E+01	7.002E+02	1.168E-01	1.105E+03	9.123E+01
CEC08	1.134E+03	2.557E+01	9.024E+02	3.450E+01	1.052E+03	5.699E+01	1.072E+03	3.917E+01	8.621E+02	1.661E+01	1.099E+03	3.076E+01
CEC09	1.280E+03	3.438E+01	1.023E+03	3.495E+01	1.218E+03	5.999E+01	1.228E+03	4.629E+01	1.004E+03	2.524E+01	1.226E+03	2.770E+01
CEC10	8.566E+03	6.372E+02	3.904E+03	1.268E+03	6.099E+03	9.402E+02	6.759E+03	8.883E+02	3.408E+03	6.872E+02	7.815E+03	5.461E+02
CEC11	8.764E+03	6.220E+02	5.338E+03	1.774E+03	7.636E+03	4.399E+02	7.387E+03	6.106E+02	5.206E+03	7.782E+02	8.437E+03	5.112E+02
CEC12	1.204E+03	1.267E+00	1.203E+03	1.223E+00	1.202E+03	5.587E-01	1.203E+03	4.669E-01	1.202E+03	5.199E-01	1.203E+03	6.070E-01
CEC13	1.308E+03	9.376E-01	1.301E+03	2.225E-01	1.302E+03	9.442E-01	1.304E+03	7.534E-01	1.300E+03	1.018E-01	1.307E+03	7.269E-01
CEC14	1.608E+03	3.762E+01	1.406E+03	7.359E+00	1.420E+03	1.042E+01	1.505E+03	2.852E+01	1.400E+03	1.942E-01	1.578E+03	2.299E+01
CEC15	1.105E+05	4.523E+04	1.804E+03	5.126E+02	2.550E+03	1.105E+03	2.256E+04	3.623E+04	1.510E+03	2.472E+00	5.588E+04	2.556E+04
CEC16	1.613E+03	3.680E-01	1.612E+03	4.505E-01	1.613E+03	4.879E-01	1.613E+03	3.369E-01	1.612E+03	6.038E-01	1.613E+03	2.314E-01
CEC17	1.063E+08	9.442E+07	3.127E+06	2.652E+06	2.355E+07	1.383E+07	1.336E+07	1.277E+07	1.116E+06	7.946E+05	9.002E+07	5.939E+07
CEC18	3.101E+09	2.708E+09	2.865E+07	3.139E+07	6.831E+06	6.326E+06	6.929E+08	1.498E+09	6.086E+03	1.168E+04	1.666E+09	1.164E+09
CEC19	2.377E+03	1.769E+02	1.959E+03	2.991E+01	2.020E+03	6.305E+01	2.090E+03	9.015E+01	1.915E+03	1.975E+01	2.230E+03	1.034E+02
CEC20	6.555E+05	1.016E+06	3.720E+04	1.914E+04	1.578E+05	1.533E+05	7.574E+04	5.123E+04	2.100E+04	9.639E+03	2.980E+05	2.909E+05
CEC21	5.064E+07	4.092E+07	2.340E+06	3.394E+06	1.183E+07	9.843E+06	6.214E+06	6.954E+06	5.188E+05	3.946E+05	3.479E+07	3.409E+07
CEC22	5.127E+03	1.861E+03	2.708E+03	1.610E+02	3.238E+03	2.960E+02	3.487E+03	8.483E+02	2.608E+03	2.130E+02	4.939E+03	5.236E+03
CEC23	2.500E+03	0.000E+00	2.641E+03	1.343E+01	2.715E+03	3.445E+01	2.740E+03	9.350E+01	2.615E+03	1.493E-01	2.500E+03	0.000E+00
CEC24	2.600E+03	0.000E+00	2.600E+03	3.613E-02	2.610E+03	6.295E+00	2.610E+03	2.017E+01	2.600E+03	7.775E-03	2.600E+03	0.000E+00
CEC25	2.700E+03	0.000E+00	2.713E+03	5.881E+00	2.718E+03	2.124E+01	2.730E+03	1.082E+01	2.701E+03	2.503E+00	2.700E+03	0.000E+00
CEC26	2.769E+03	4.420E+01	2.747E+03	5.048E+01	2.717E+03	3.770E+01	2.806E+03	6.982E+01	2.727E+03	4.479E+01	2.766E+03	4.594E+01
CEC27	2.900E+03	0.000E+00	3.422E+03	1.145E+02	3.924E+03	3.295E+02	3.867E+03	2.875E+02	3.282E+03	1.095E+02	2.900E+03	0.000E+00
CEC28	3.000E+03	0.000E+00	4.327E+03	5.250E+02	5.274E+03	7.162E+02	7.836E+03	9.600E+02	3.777E+03	1.204E+02	3.000E+03	0.000E+00
CEC29	3.100E+03	0.000E+00	3.670E+06	5.556E+06	1.800E+07	1.944E+07	8.854E+07	7.142E+07	3.425E+06	4.721E+06	3.100E+03	0.000E+00
CEC30	3.200E+03	0.000E+00	9.243E+04	6.681E+04	5.368E+05	3.128E+05	6.287E+05	3.630E+05	1.109E+04	7.519E+03	3.200E+03	0.000E+00

competitive advantage and stability in solving high-dimensional and complex optimization problems.

High-dimensional convergence curve experiment

To compare the optimization performance of the MSSA and other algorithms, we selected SSA, GWO, WOA, TSA, EO, and MSSA for high-dimensional function optimization comparison. This paper used the 12 representative benchmark functions given in Table 1, the dimension dim = 500, and the maximum number of iterations, T_{max} = 500. The high-dimensional optimization curve of each algorithm is shown in Figures 6A–L. The convergence accuracy and speed of the MSSA were significantly higher than those of the other algorithms, which indicate that the multi-strategy can effectively prevent the algorithm from falling into local optima. The results of the optimization curve illustrated that for the single-modal test functions, f_1-f_6, the multi-modal functions test functions, f_8, f_{10}, f_{11}, and the fixed multi-modal function, f_{16}, MSSA can find the optimal value faster with fewer iterations and higher convergence accuracy. For the multi-modal function, f_9, the optimal value of MSSA was similar to several other contrast functions, but the MSSA converged much faster. For the fixed multi-modal function, f_{13}, MSSA fell into a local optimum similar to the five compared algorithms, but it still could find the theoretical optimum; thus, MSSA has significant advantages over the other algorithms.

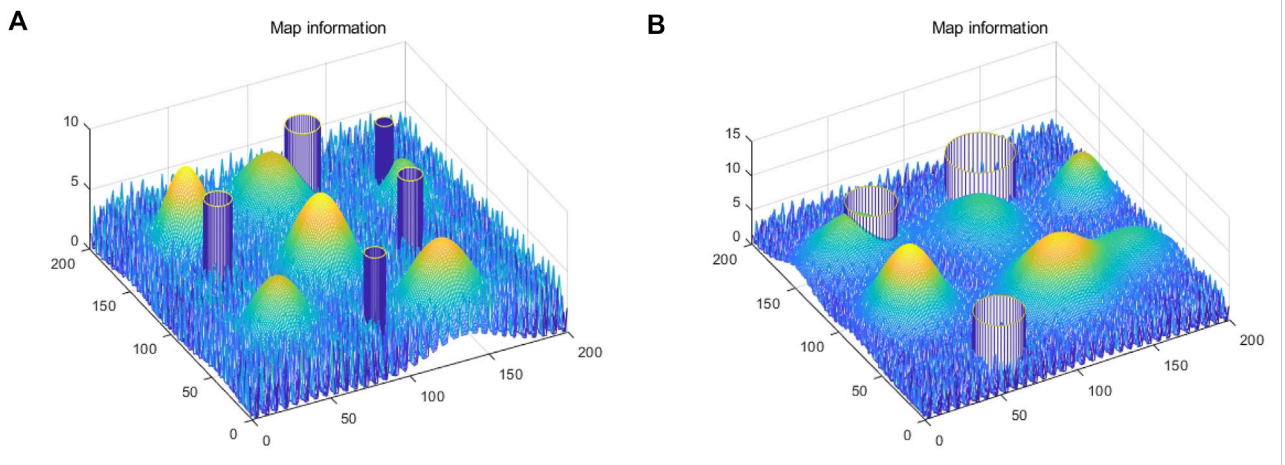

FIGURE 7
3D map model information of two environments. **(A)** 3D map of environment 1. **(B)** 3D map of environment 2.

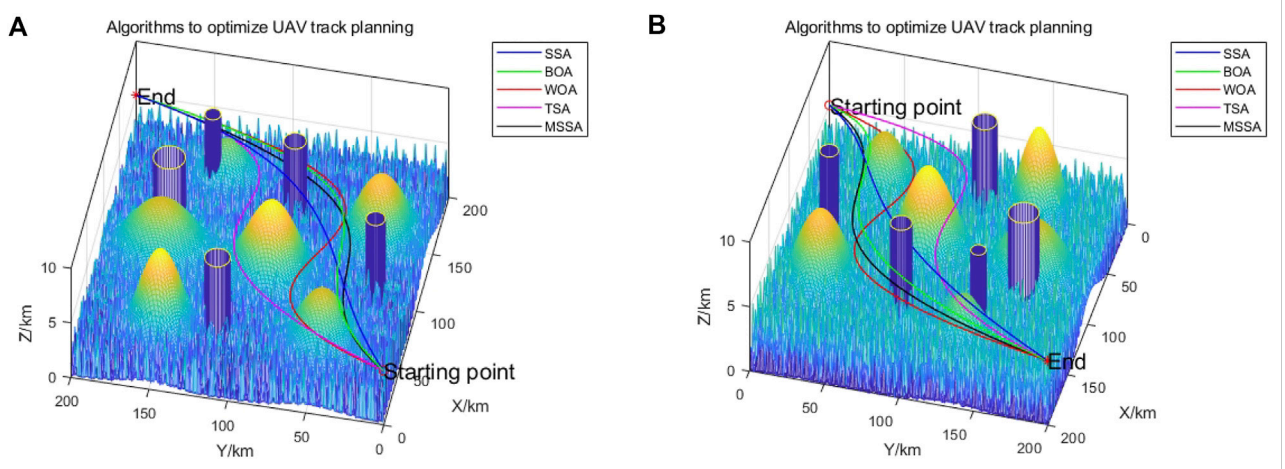

FIGURE 8
Simulation results of 3D trajectory planning in environment 1 from two different views.

Wilcoxon rank-sum test experiment

In general, only the mean and standard deviation are used for data analysis. The Wilcoxon rank-sum test is a non-parametric test method for the mean that is not limited by the overall distribution and has a wide range of applications (Derrac, J. et al., 2011). To more comprehensively analyze the performance difference between the MSSA and other algorithms, we selected the running results of MSSA and five comparison algorithms in sixteen test functions to conduct the Wilcoxon rank sum test. The p value can be considered to reject the null hypothesis when $p < 5\%$, indicating that there is a significant difference in the test results. *NaN* indicates that there are no data to compare with the algorithm, +, =, and - indicate that the MSSA algorithm's optimization performance is better than, equal to, and worse than the compared algorithms, respectively. The results of the Wilcoxon rank sum test are shown in Table 4:

As seen from Table 4, the MSSA p value of the Wilcoxon rank sum test is less than 5%. The experimental results indicate that there is a significant difference between the MSSA and the other five algorithms, and the MSSA is significantly better than the others, further reflecting the robustness of the MSSA.

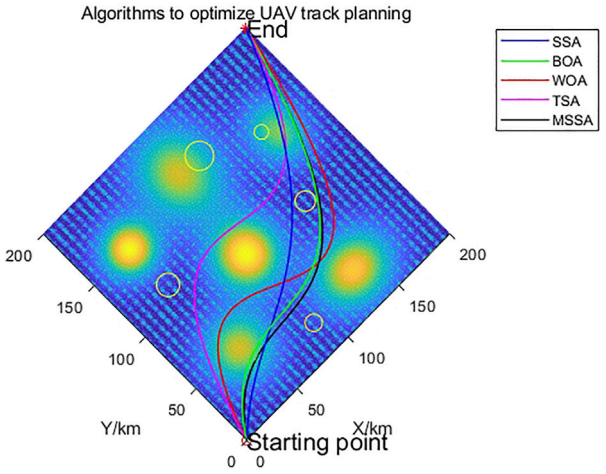

FIGURE 9
Comparison of 2D track planning in environment 1.

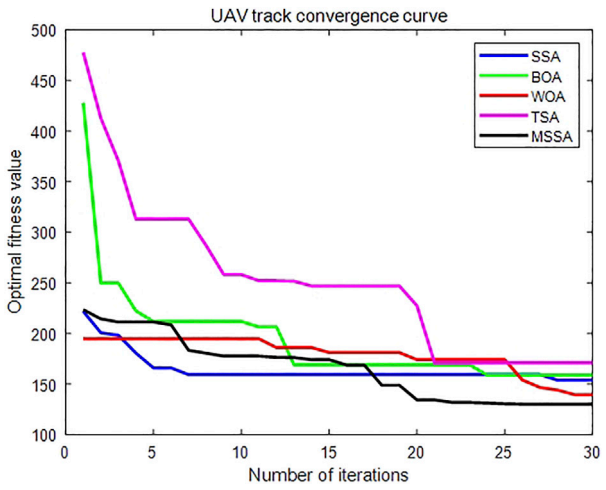

FIGURE 10
Convergence diagram of track cost function in environment 1.

CEC2014 test functions experiment

Most of the CEC2014 test functions (Tejani, 2018) are composed of the weights of multiple basic optimizations test functions, which makes the characteristics of the test functions more complex. In this paper, the proposed MSSA was tested against these complex test functions. On the one hand, these functions can effectively reflect the superior performance of MSSA for optimization of a complex function. On the other hand, the combinatorial optimization of multiple test functions reflects the applicability of SMSA to different complex optimization problems. To further test the performance of MSSA, this paper chose the CEC2014 single objective optimization function for solution analysis, including unit-modal, multi-modal, Hybrid, and composition type functions. Table 5 shows the relevant information of CEC2014 functions. This study compared the MSSA with five algorithms, including SSA, GWO, WOA, TSA, and EO. To ensure fairness of the algorithm comparison, the maximum number of iterations, T_{max} = 1000, the population size was N = 30, and the dimension, dim = 30, were set to the same values in each algorithm, which were run 30 times independently, and the mean and standard deviation were recorded. The results are shown in Table 6.

The algorithm initialization phase:
1. T: the maximum iterations;
2. Dd: the number of discovers;
3. Sd: the number of scouters;
4. R_2: the alarm value;
5. n: the number of sparrows;
6. Perform sparrow population position initialization;

The algorithm iterates the search phase:
7. **while** $t < T_{max}$;
8. Ranking of individual fitness values to find the best and worst individuals;
9. $R_2 = rand\ (1)$;
10. **for** $i = 1 : Dd$;
11. Using Eq. 14 update the sparrow's location;
12. **end for**;
13. **for** $i = 1 : (Dd+1)$;
14. Using Eq. 17 update the sparrow's location;
15. **end for**;
16. for i = 1 : Sd;
17. Using Eq. 21 update the sparrow's location;
18. **end for**;
19. Get the current optimal position;
20. $t = t+1$;
21. end while;
22. Output global optimum;

Algorithm 1. The framework of the MSSA.

Table 6 shows that MSSA was better than SSA on 22 test functions, including CEC01, CEC02, CEC03, CEC04, CEC05, CEC06, CEC07, CEC08, CEC09, CEC10, CEC11, CEC12, CEC13, CEC14, CEC15, CEC17, CEC18, CEC19, CEC20, CEC21, CEC22, and CEC26. MSSA can find values close to SSA on CEC16, CEC23, CEC24, CEC25, CEC26, CEC28, CEC29, and CEC30. In terms of standard deviation, MSSA is better than SSA, GWO, and TSA on most test functions. It is worth noting that MSSA is better than SSA in the remaining 25 test functions except CEC03, CEC05, CEC16, CEC22, and CEC26. Generally,

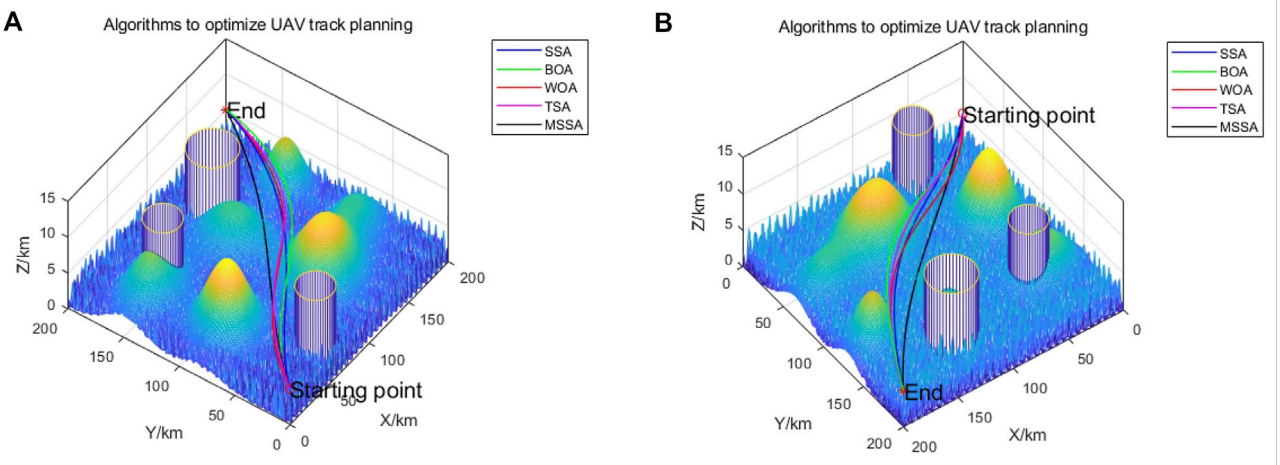

FIGURE 11
Simulation results of 3D trajectory planning in environment 2 from two different views.

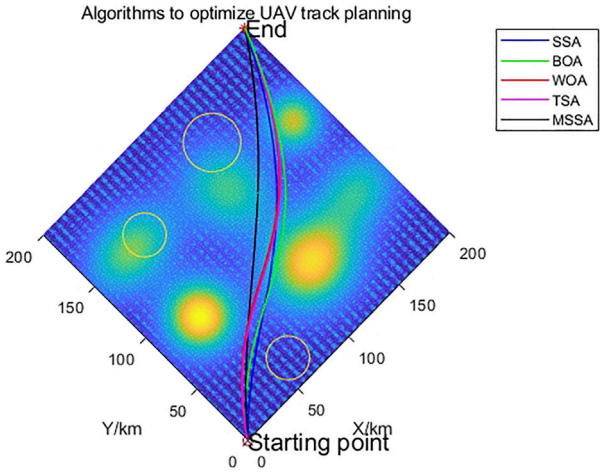

FIGURE 12
Comparison of 2D track planning in environment 2.

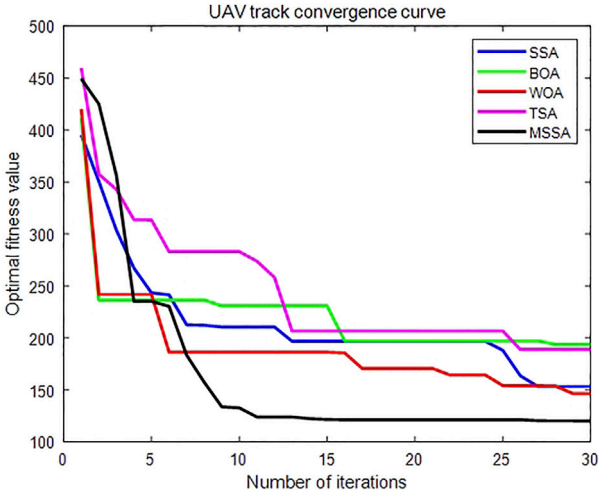

FIGURE 13
Convergence diagram of track cost function in environment 2.

the proposed algorithm has more prominent advantages in the CEC2014 test function compared with the other eight algorithms.

UAV trajectory planning based on MSSA

In this section, we established two mathematical models of trajectory planning constraints in MATLAB and simulation experiments were carried out in a 3-D environment. This experiment combines the content of the above sections, and we conducted simulation experiments on UAV trajectory planning in two challenging mission environments. We compared MSSA with the SSA, BOA, WOA, and TSA to verify the performance improvement of the MSSA in the trajectory planning problem.

Experimental simulation parameters

The first step in UAV trajectory planning was to initialize the relevant parameters. The basic parameters of SSA before and after the improvement were set as follows: the population size was $N = 50$, the maximum number of iterations was $T_{max} = 30$,

TABLE 7 Experimental data of environment 1.

No.	SSA	BOA	WOA	TSA	MSSA
1	221.9858	428.1988	194.8475	477.7604	223.6669
2	200.8703	249.9676	194.8475	412.8379	214.5968
3	198.3777	249.9676	194.8475	370.6239	211.5184
4	180.7114	222.4805	194.8475	313.0749	211.5184
5	166.1277	211.9584	194.8475	313.0749	211.5184
6	166.1277	211.9584	194.8475	313.0749	208.6994
7	159.4911	211.9584	194.8475	313.0749	183.4661
8	159.4911	211.9584	194.8475	286.9255	180.6388
9	159.4911	211.9584	194.8475	258.2724	177.8031
10	159.4911	211.9584	194.8475	258.2724	177.8031
11	159.4911	206.6703	194.8475	252.3117	177.8031
12	159.4911	206.6703	186.2235	252.3117	176.5868
13	159.4911	169.1189	186.2235	251.7576	176.4338
14	159.4911	169.1189	186.2235	247.0899	174.2706
15	159.4911	169.1189	181.2497	247.0899	174.2706
16	159.4911	169.1189	181.2497	247.0899	168.9351
17	159.4911	169.1189	181.2497	247.0899	168.9351
18	159.4911	169.1189	181.2497	247.0899	148.9273
19	159.4911	169.1189	181.2497	247.0899	148.9273
20	159.4911	169.1189	174.2521	171.1681	134.4919
21	159.4911	169.1189	174.2521	171.1681	134.4919
22	159.4911	169.1189	174.2521	171.1681	132.033
23	159.4911	169.1189	174.2521	171.1681	132.033
24	159.4911	158.9664	174.2521	171.1681	131.4209
25	159.4911	158.9664	174.2521	171.1681	130.6637
26	159.4911	158.9664	154.1683	171.1681	130.3178
27	159.4911	158.9664	146.8336	171.1681	130.3178
28	154.0068	158.9664	144.2572	171.1681	130.3178
29	154.0068	158.9664	139.5953	171.1681	130.3178
30	154.0068	158.9664	139.5953	171.1681	130.26

TABLE 8 Experimental data of environment 2.

No.	SSA	BOA	WOA	TSA	MSSA
1	395.4108	411.9735	420.1169	459.6827	449.4203
2	350.7416	236.5109	241.8295	357.607	425.1031
3	303.5717	236.5109	241.8295	342.8342	356.2115
4	267.1788	236.5109	241.8295	313.7257	235.2283
5	243.3833	236.5109	241.8295	313.5049	235.2283
6	241.4834	236.5109	186.2959	283.0012	230.3628
7	212.6503	236.5109	186.2959	283.0012	183.3411
8	212.1987	236.5109	186.2959	283.0012	157.4026
9	210.5834	230.8149	186.2959	283.0012	133.7521
10	210.5834	230.8149	186.2959	283.0012	132.6643
11	210.5834	230.8149	186.2959	273.8353	123.9401
12	210.5834	230.8149	186.2959	258.2411	123.9401
13	196.827	230.8149	186.2959	206.6917	123.9401
14	196.827	230.8149	186.2959	206.6917	122.3308
15	196.827	230.8149	186.2959	206.6917	121.5816
16	196.827	197.1322	185.5324	206.6917	121.3304
17	196.827	197.1322	170.6196	206.6917	121.3304
18	196.827	197.1322	170.6196	206.6917	121.3304
19	196.827	197.1322	170.6196	206.6917	121.3304
20	196.827	197.1322	170.6196	206.6917	121.3304
21	196.827	197.1322	170.6196	206.6917	121.3304
22	196.827	197.1322	164.3505	206.6917	121.3304
23	196.827	197.1322	164.3505	206.6917	121.3304
24	196.827	197.1322	164.3505	206.6917	121.3304
25	188.1075	197.1322	154.1458	206.6917	121.3304
26	163.5779	197.1322	153.9173	188.88	121.3304
27	153.2322	197.1322	153.9173	188.88	120.4412
28	153.2322	193.691	153.7423	188.88	120.3047
29	153.2322	193.691	146.4014	188.88	120.2426
30	153.2322	193.691	146.4014	188.88	120.1591

the proportion of discoverers was set to 20%, the scouter is 10%, and the alert threshold is set to 0.7.

To compare the performance of MSSA in the trajectory planning problem, we used two different map models as the task environment for simulation experiments. We built the three-dimensional environment and superimposed the threat area on it to make the model closer to the real environment. The area sizes of the two environments were 200×200×10 and 200×200×15 respectively. The start and end coordinates were set as S = (0, 0, 5) and E = (200, 200, 5). The height of the no-fly zone in the two environments was uniformly set at 10, the radius are R_1 = [10; 8; 6; 7; 5] and R_2 = [20; 15; 15]. The center coordinates were T_1 = [115,161; 50,150; 90,20; 175,70] and T_2 = [128,161; 50,150; 60,20]. The coordinates of the center of the mountain area were A_1 = [48,41; 90,90; 162,96; 134,165; 30,135; 150,35] and A_2 = [83,37; 149,36; 131,113; 54,118; 66,176; 131,178]. The heights were H_1 = [7; 9;7; 6;6; 9] and H_2 = [12; 8;7; 11; 6;9]. Slopes along the X axis direction were a_1 = [25; 25; 35; 25; 25; 20] and a_2 = [25; 25; 35; 30; 25; 20], and slopes along the Y axis direction were b_1 = [25; 25; 30; 20; 30; 20] and b_2 = [25; 35; 30; 35; 30; 20]. The 3-D environmental models are shown in Figure 7.

Convergence curve experiment

The trajectory simulation results of the two mission environments are shown in Figures 8 and 11, respectively. The two-dimensional trajectory planning results can be seen in Figures 9 and 12, respectively. The convergence graphs of the track cost function are in Figures 10 and 13, respectively. Figures 8 and 9 show that the five algorithms can both avoid the no-fly area from starting point to the target point in the environment. However, SSA, WOA, BOA, and TSA have large fluctuations. At the same time, the path is far away from the mountain peak and the no-fly area in the 2-D environment. This indicates that the algorithm falls into a local

TABLE 9 Statistical data of experimental results in environment 1.

Algorithm name	Optimal value	Worst value	Mean value
SSA	154.0068	221.9858	164.8511
BOA	158.9664	428.1988	193.6259
WOA	139.5953	194.8475	179.2734
TSA	171.1681	477.7604	247.9587
MSSA	130.26	223.6669	165.4328

TABLE 10 Statistical data of experimental results in environment 2.

Algorithm name	Optimal value	Worst value	Mean value
SSA	153.2322	395.4108	213.1830
BOA	193.691	411.9735	220.9971
WOA	146.4014	420.1169	189.6867
TSA	188.88	459.6827	245.5276
MSSA	120.1591	449.4203	165.6743

optimum when planning the trajectory. It is worth noting that the trajectory planned by MSSA is more stable, the fluctuation range is moderate, the trajectory is relatively stable, and it maintains a safe distance from the mountain and the threat area.

In Figure 10, the SSA converges from the seventh iteration to the 27th iteration, indicating that the original SSA algorithm fell into a local optimum during the iteration. The values of BOA and TSA decreased rapidly at the beginning of the iterations, but fell into a local optimum many times in the later stage. In contrast, MSSA found the optimal value and jumped out of the local optima many times, which resulted in an ideal cost function value, thus demonstrating that MSSA can better avoid falling into local optima and find the best path.

Figures 11, 12 show that in the second task environment, the trajectories planned by the four comparison algorithms fluctuated greatly, which confirms the poor solution quality and insufficiency of these algorithms in complex trajectory planning. The MSSA is more stable, and it can be clearly seen that the path planned by the MSSA is the shortest. Figure 13 shows that MSSA's optimal fitness values are lower than those of the comparison algorithms in the 8th iteration, and the local optimal value is still continuously removed at the end of the iteration. This shows that the trajectory cost function obtained by MSSA is smaller and the comprehensive performance index is better.

Optimization performance experiment

To more objectively compare the performance of the MSSA with that of the other four algorithms in trajectory planning, this experiment used five algorithms to conduct 30 repeated experiments in two task environments. The population size was N = 30, and the maximum number of iterations was T_{max} = 30. The experimental results are shown in Tables 7 and 8. The statistical results of the experimental data are shown in Tables 9 and 10. The performance of each algorithm was evaluated by comparing the optimal value, worst value, average value, and standard deviation of the track cost function values obtained.

From Tables 9, 10, MSSA has obvious advantages in the performance of the UAV trajectory planning problem in the two environments. In the first environment, although MSSA is not the fastest in convergence, it did find the best value. In the second environment, MSSA was not only faster in convergence speed but also found the best value. The optimal values showed that the cost value of the MSSA for acquiring tracks was lower than that of the SSA, BOA, WOA, and TSA, illustrating that the MSSA had a stronger global search ability and higher convergence accuracy. The MSSA had a lower value than the other four algorithms on average, indicating that the MSSA had better trajectory planning quality and higher solution stability. In summary, the three improvement mechanisms proposed in this paper can effectively improve the algorithm global search ability, convergence accuracy, convergence speed and stability in terms of trajectory planning. The MSSA can balance the global search ability and local development ability of the algorithm and has excellent performance in solving complex multi-constraint combinatorial optimization problems such as UAV 3D trajectory planning. Thus, the trajectory planned by MSSA can meet the follow-up flight requirements for the UAV.

Discussion

As one of the key technologies of the UAV autonomous control system, flight path planning is a hot research area in current information science. The UAV trajectory planning problem in a 3-D environment is complicated, computationally intensive and has many local optimal solutions, which poses great challenges to the performance of optimization algorithms. Based on analysis of the path planning problem and swarm intelligence algorithm, a new sparrow algorithm was proposed. First, the algorithm adopted a reverse learning strategy based on the law of refraction, enhanced the diversity of the algorithm, and improved the optimization accuracy of the algorithm. Second, the random step size of Levy's flight boosted the local search capability of the algorithm. Lastly, the MSSA combined the fusion Cauchy mutation to increase the ability of the algorithm to jump out of local optima. We performed multiple ablation experiments in sixteen benchmark test functions with different characteristics. In the comparison of optimization performance of various improvement strategies and MSSA convergence experiments, the results indicated that Levy flight could help the population to deeply mine the global optimal values and improve the global search ability of the algorithm, proving that MSSA had greater stability and robustness than SSA.

In the comparison of convergence performance and high-dimensional performance with other algorithms, the results illustrated that MSSA had a significant competitive advantage and stability in solving complex, high-dimensional optimization problems. In addition, the Wilcoxon rank sum test and 30 CEC2014 complex functions were tested, and the results were compared with other metaheuristic algorithms and improved algorithms. The experimental results demonstrated that the improved MSSA algorithm had better stability, convergence accuracy, and optimization performance than other algorithms. Despite the significantly better performance demonstrated in this paper, the algorithm strategy could still be further improved. In subsequent work, refinements to the improved MSSA will be compared and analyzed with other advanced optimization algorithms to further improve the global search ability and local development ability of the algorithm.

Conclusion

An improved sparrow search optimization technique termed MSSA was proposed to increase the effectiveness of UAV trajectory planning in a three-dimensional environment. UAV trajectory planning simulation experiments were carried out in two different established three-dimensional geographic environments. The results showed that the path length of the obtained trajectory was considerably shorter while satisfying the constraints, further proving the feasibility and applicability of the proposed MSSA for trajectory planning in a three-dimensional environment. However, in this paper, the UAV simulation was simplified to a particle and a fixed flight speed was preset for solving the UAV path planning problem. In subsequent work, a more realistic UAV dynamics model should be established, and the flight restrictions of the UAV should be further studied. The UAV trajectory planning problem can be solved using the enhanced MSSA algorithm in subsequent work to significantly enhance the performance of complex environment trajectory planning from a variety of perspectives.

Data availability statement

The original contributions presented in the study are included in the article/Supplementary Material, further inquiries can be directed to the corresponding authors.

Author contributions

QH and LY provided the idea of the article. YY wrote the article. YY derived the formula for the trajectory planning in the article. QH and LY were responsible for checking and improving the language in the article, and QH and LY provided all of the research funding.

Funding

The research was funded by the National Natural Science Foundation of China "Research on the Evidence Chain Construction from the Analysis of the Investigation Documents (No. 62166006)", the National Natural Science Foundation of China "Rural spatial restructuring in poverty-stricken mountainous areas of Guizhou based on spatial equity: A case study of Dianqiangui Rocky Desertification Area (No. 41861038)", and Guizhou Provincial Science and Technology Projects (Guizhou Science Foundation-ZK [2021] General 335).

Conflict of interest

The authors declare that the research was conducted in the absence of any commercial or financial relationships that could be construed as a potential conflict of interest.

Publisher's note

All claims expressed in this article are solely those of the authors and do not necessarily represent those of their affiliated organizations, or those of the publisher, the editors and the reviewers. Any product that may be evaluated in this article, or claim that may be made by its manufacturer, is not guaranteed or endorsed by the publisher.

References

Abualigah, L., Yousri, D., Abd Elaziz, M., Ewees, A. A., Al-qaness, M. A. A., and Gandomi, A. H. (2021). Aquila optimizer: A novel meta-heuristic optimization algorithm. *Comput. Industrial Eng.* 157, 107250. doi:10.1016/j.cie.2021.107250

Bagherian, M., and Alos, A. (2015). 3D UAV trajectory planning using evolutionary algorithms: A comparison study. *Aeronaut. J.* 119 (1220), 1271–1285. doi:10.1017/S0001924000011246

Belge, E., Altanof, A., and Hacıoğlu, L. (2022). Metaheuristic optimization-based path planning and tracking of quadcopter for payload hold-release mission. *Electronics* 11 (8), 1208. doi:10.3390/electronics11081208

Chang, L., Shan, L., Jiang, C., and Dai, Y. (2021). Reinforcement based mobile robot path planning with improved dynamic window approach in unknown environment. *Auton. Robots* 45 (1), 51–76. doi:10.1007/s10514-020-09947-4

Derrac, J., Garcia, S., Molina, D., and Herrera, F. (2011). A practical tutorial on the use of nonparametric statistical tests as a methodology for comparing evolutionary and swarm intelligence algorithms. *Swarm Evol. Comput.* 1 (1), 3–18. doi:10.1016/j.swevo.2011.02.002

Dübel, S., and Schumann, H. (2017). Visualization of features in 3D terrain. *ISPRS Int. J. Geoinf.* 6 (11), 357. doi:10.3390/ijgi6110357

Fan, X., Sun, Z., Tian, E., Yin, Z., and Cao, G. (2022a). Medical image contrast enhancement based on improved sparrow search algorithm. *Int. J. Imaging Syst. Technol.* 123–23. doi:10.1002/ima.22794

Faramarzi, A., Heidarinejad, M., Stephens, B., and Mirjalili, S. (2020). Equilibrium optimizer: A novel optimization algorithm. *Knowledge-Based Syst.* 191, 105190. doi:10.1016/j.knosys.2019.105190

Hashim, F. A., Hussain, K., Houssein, E. H., Mabrouk, M. S., and Al-Atabany, W. (2021). Archimedes optimization algorithm: A new metaheuristic algorithm for solving optimization problems. *Appl. Intell. (Dordr).* 51 (3), 1531–1551. doi:10.1007/s10489-020-01893-z

Heidari, A. A., Mirjalili, S., Faris, H., Aljarah, H., Mafarja, M., and Chen, H. (2019). Harris hawks optimization: Algorithm and applications. *Future gener. Comput. Syst.* 97, 849–872. doi:10.1016/j.future.2019.02.028

Jia, Y., Zhou, S., Zeng, Q., Li, C., Chen, D., Zhang, K., et al. (2022). The UAV path coverage algorithm based on the greedy strategy and ant colony optimization. *Electronics* 11 (17), 2667. doi:10.3390/electronics11172667

Kaur, S., Awasthi, L. K., Sangal, A. L., and Dhiman, G. (2020). Tunicate swarm algorithm: A new bio-inspired based metaheuristic paradigm for global optimization. *Eng. Appl. Artif. Intell.* 90, 103541. doi:10.1016/j.engappai.2020.103541

Li, C., Zhang, N., Lai, X., Lai, X., Zhou, J., and Xu, Y. (2017). Design of a fractional-order PID controller for a pumped storage unit using a gravitational search algorithm based on the Cauchy and Gaussian mutation. *Inf. Sci.* 396, 162–181. doi:10.1016/j.ins.2017.02.026

Marini, F., and Walczak, B. (2015). Particle swarm optimization (PSO). A tutorial. *Chemom. Intelligent Laboratory Syst.* 149, 153–165. doi:10.1016/j.chemolab.2015.08.020

Mirjalili, S., and Lewis, A. (2016). The whale optimization algorithm. *Adv. Eng. Softw.* 95, 51–67. doi:10.1016/j.advengsoft.2016.01.008

Mirjalili, S., Mirjalili, S., and Lewis, A. (2014). Grey wolf optimizer. *Adv. Eng. Softw.* 69, 46–61. doi:10.1016/j.advengsoft.2013.12.007

Mohamed, N., Al-Jaroodi, I., Idries, A., and Mohammed, F. (2020). Unmanned aerial vehicles applications in future smart cities. *Technol. Forecast. Soc. Change* 153, 119293. doi:10.1016/j.techfore.2018.05.004

Momoh, J. A., Adapa, R., and El-Hawary, M. E. (1999). A review of selected optimal power ftow literature to 1993 Part I: Non linear and quadratic programming approaches. *IEEE Trans. Power Syst.* 14 (1), 96–104. doi:10.1109/59.744492

Olofsson, M., Andersson, G., and Söder, L. (1995). Linear programming based optimal power flow using second order sensitivities. *IEEE Trans. Power Syst.* 10 (3), 1691–1697. doi:10.1109/59.466472

Poli, R., Kennedy, J., and Blackwell, T. (2007). Particle swarm optimization. *Swarm Intell.* 1 (1), 33–57. doi:10.1007/s11721-007-0002-0

Price, K. V. "Differential evolution vs. the functions of the 2/sup nd/ICEO," in Proceedings of the 1997 IEEE International Conference on Evolutionary Computation (ICEC '97), 153–157. April 1997 Indianapolis, IN, USA doi:10.1109/ICEC.1997.592287

Qadir, Z., Ullah, F., Munawar, H. S., and Al-Turjman, F. (2015). Addressing disasters in smart cities through UAVs path planning and 5G communications: A systematic review. *Comput. Commun.* 168, 114–135. doi:10.1016/j.comcom.2021.01.003

Salgado, R., Brameller, A., and Aitchison, P. (1990). Optimal power flow solutions using the gradient projection method. Part 1. Theoretical basis. *IEE Proc. C Gener. Transm. Distrib. UK.* 137 (6), 424–428. doi:10.1049/ip-c.1990.0057

Shin, J., and Bang, H. (2020). UAV path planning under dynamic threats using an improved PSO algorithm. *Int. J. Aerosp. Eng.* 2020, 1–17. doi:10.1155/2020/8820284

Tejani, G. G., Savsani, V. J., Patel, V. K., and Mirjalili, S. (2018). Truss optimization with natural frequency bounds using improved symbiotic organisms search. *Knowl. Based. Syst.* 143, 162–178. doi:10.1016/j.knosys.2017.12.012

Thompson, S. E., and Patel, R. V. (1987). Formulation of joint trajectories for industrial robots using B-splines. *IEEE Trans. Ind. Electron.* 34 (2), 192–199. doi:10.1109/tie.1987.350954

Tinney, W. F., Member, S., and Hart, C. E. (1967). Power flow solution by Newton's method. *IEEE Trans. Power Apparatus Syst.* PAS-86(86), 1449–1460. doi:10.1109/TPAS.1967.291823

Van Steen, M., and Leiba, B. (2018). Smart cities. *IEEE Internet Comput.* 23 (1), 7–8. doi:10.1109/MIC.2018.2887182

Videras Rodríguez, M., Melgar, S. G., Cordero, A. S., and Márquez, J. M. A. (2021). A critical review of unmanned aerial vehicles (UAVs) use in architecture and urbanism: Scientometric and bibliometric analysis. *Appl. Sci. (Basel).* 11 (21), 9966. doi:10.3390/app11219966

Wen, X., Ruan, Y., Li, Y., Xia, H., Zhang, R., Wang, C., et al. (2022). Improved genetic algorithm based 3-D deployment of UAVs. *J. Commun. Netw.* 24 (2), 223–231. doi:10.23919/JCN.2022.000014

Whitley, D. (1994). A genetic algorithm tutorial. *Stat. Comput.* 4 (2), 65–98. doi:10.1007/BF00175354

Wu, C., Fu, X., Pei, J., and Dong, Z. (2021). A novel sparrow search algorithm for the traveling salesman problem. *IEEE Access* 9, 153456–153471. doi:10.1109/ACCESS.2021.3128433

Xue, J., and Shen, B. (2020). A novel swarm intelligence optimization approach: Sparrow search algorithm. *Syst. Sci. Control Eng.* 8 (1), 22–34. doi:10.1080/21642583.2019.1708830

Zhang, D., Xian, Y., Li, J., Lei, G., and Cang, Y. "UAV path planning based on chaos ant colony algorithm[C]," in Proceedings of the International Conference on Computer Science & Mechanical Automation (IEEE), 81–85. doi:10.1109/CSMA.2015.23October 2015 Hangzhou, China .

Zhang, W., Zhang, S., Wu, F., and Wang, Y. (2021). Path planning of UAV based on improved adaptive Grey wolf optimization algorithm. *IEEE Access* 9, 89400–89411. doi:10.1109/ACCESS.2021.3090776

Zhang, X., and Duan, H. (2015). An improved constrained differential evolution algorithm for unmanned aerial vehicle global route planning. *Appl. Soft Comput.* 26, 270–284. doi:10.1016/j.asoc.2014.09.046

Zhao, Y, J., Zheng, Z., and Liu, Y. (2018). Survey on computational-intelligence-based UAV path planning. *Knowl. Based. Syst.* 158, 54–64. doi:10.1016/j.knosys.2018.05.033

Fan, Y., Fang, X., Gao, F., Zhou, X., Li, H., Jin, H., and Song, Y., (2022b). Obstacle Avoidance Path Planning for UAV Based on Improved RRT Algorithm. *Discrete Dynamics in Nature and Society*. 2022, 1, 9. doi:10.1155/2022/4544499

frontiers | Frontiers in Environmental Science

TYPE Original Research
PUBLISHED 30 November 2022
DOI 10.3389/fenvs.2022.1049187

Check for updates

OPEN ACCESS

EDITED BY
Ying Jing,
Zhejiang University, China

REVIEWED BY
Wende Li,
Lanzhou Jiaotong University, China
Quanjing Wang,
Zhengzhou University, China

*CORRESPONDENCE
Yanwen Wang,
wensomone@163.com
Shuwang Yang,
yswang998@163.com

SPECIALTY SECTION
This article was submitted to Land Use Dynamics,
a section of the journal
Frontiers in Environmental Science

RECEIVED 20 September 2022
ACCEPTED 24 October 2022
PUBLISHED 30 November 2022

CITATION
Yang J, Wang Y, Zhang H, Su Y, Wu X, Yan S and Yang S (2022), Impact of socio-economic and environmental factors on livestock production in Kyrgyzstan.
Front. Environ. Sci. 10:1049187.
doi: 10.3389/fenvs.2022.1049187

COPYRIGHT
© 2022 Yang, Wang, Zhang, Su, Wu, Yan and Yang. This is an open-access article distributed under the terms of the Creative Commons Attribution License (CC BY). The use, distribution or reproduction in other forums is permitted, provided the original author(s) and the copyright owner(s) are credited and that the original publication in this journal is cited, in accordance with accepted academic practice. No use, distribution or reproduction is permitted which does not comply with these terms.

Impact of socio-economic and environmental factors on livestock production in Kyrgyzstan

Jiamiao Yang[1,2], Yanwen Wang[1,2]*, Hao Zhang[1,2], Yuming Su[3], Xiaoyang Wu[1], Shuqi Yan[4] and Shuwang Yang[1,2]*

[1]School of Economics and Management, China University of Geosciences, Wuhan, China, [2]Research Center of Resource and Environmental Economics, China University of Geosciences, Wuhan, China, [3]School of Resource and Environmental Sciences, Wuhan University, Wuhan, China, [4]School of Interpreting and Translation Studies, Guangdong University of Foreign Studies, Guangzhou, China

Livestock husbandry is a key indicator of economic development, environmental protection, and food security in the world, which is vulnerable to environmental changes and economic shocks. In our study on Kyrgyzstan, we quantified the effects of socio-economic and environmental factors on the dynamics of livestock sales, self-consumption, and inventory from 2006 to 2020 using a two-period livestock production model and spatial panel model. The results showed that from 2006 to 2020, more than 50% livestock were stocked annually, which means that herders in Kyrgyzstan preferred to preserve their animals as assets to deal with unknown risks. Additionally, to gain greater profit, Kyrgyz herdsmen would expand or downsize their livestock business, tailor self-consumption, and manage inventory based on the livestock market price, loan on livestock, non-herding income, and its current stock. Our study found that the development of animal husbandry in seven oblasts of Kyrgyzstan had spatial spillover effects, which indicated that the dynamics of the animal husbandry market and environment not only affected the scale of local animal husbandry but also had an important impact on adjacent oblasts. Our research contributes to ensuring the income for herdsmen and the sustainable development of animal husbandry, thereby promoting high-quality economic development in developing countries with animal husbandry as a pillar industry.

KEYWORDS

livestock husbandry, Kyrgyzstan, herders, grasslands, spatial spillover effects

1 Introduction

Livestock is an important component of global agriculture and economy, and it plays a vital role in improving food security, promoting adjustment of the agricultural structure, and realizing comprehensive utilization of resources (Han et al., 2020; Wei and Zhen, 2020). With continuous population growth and increased demand for living, the global production of meat was predicted to increase from 229 million tons in 1999 to 465 million

tons in 2050, which was a huge challenge for livestock production (FAO, 2006; Gerber and Steinfeld, 2008). To improve the livelihoods of people and promote sustainable social, economic, and environmental development in the world, the United Nations formally adopted the Sustainable Development Goals (SDGs) in 2015 (WHO, 2015; Arora and Mishra, 2019; Rosati and Faria, 2019). This proposal encouraged member countries to jointly explore the sustainable and efficient animal husbandry production system to provide nutritional food for residents, which could contribute to SDG1 (no poverty), SDG2 (zero hunger), SDG3 (good health and well-being), SDG12 (responsible consumption and production), and SDG17 (partnerships for the goals) (Breeman et al., 2015; Varijakshapanicker et al., 2019; Mehrabi et al., 2020). To reach the growing demand for livestock in the coming decades, a sustainable balance between domestic products and imports must be maintained. This provided an opportunity for countries to export livestock products, livestock equipment, and breeding technology to expand the scale of livestock in countries with appropriate land resources (Gerosa and Skoet, 2012; Lan et al., 2021). Although the temporal and spatial details of grazing practices were quite different among countries, the combination of mobile animal husbandry and low-investment crop cultivation was still the main mode of production in developing countries with animal husbandry as the economic pillar (Koocheki and Gliessman, 2005). Developing with the experiences of environmental changes and natural disasters, nomadic animal husbandry was a long-term cultural choice for herdsman families (Zhang et al., 2007). For nomadic society, livestock was the foundation for herders' living, which provided food, housing construction materials, and transportation, as well other goods and services by exchange (Kerven et al., 2011; Sagynbekova, 2017; Xu et al., 2019; Haghiyan et al., 2022). However, under modern pressures, such as population growth, in-country migration, rapid urbanization, increasing demand for livestock products, land use change, and climate change, it seemed to pose a severe challenge for the sustainability of husbandry production (Tessema et al., 2014; Abay and Jensen, 2020; Raji et al., 2022; Wafula et al., 2022).

As arable land was scarce and grasslands covered about 56% of the total land in an arid climate, pastoralism became the main economic pillar in Kyrgyzstan, which made a significant contribution to the nation's economy with livestock production accounting for over 19.33% of the national GDP (NSCKR, 2020). Being well-known for the ridges and isolated valleys of the Tian Shan Mountains, Kyrgyzstan has a tradition of high spatial mobility, and nomadic civilization has become a part of the cultural symbol of Kyrgyzstan (Ludi, 2003). Local nomadic herders usually graze in mountain pastures in summer, but low temperatures in winter and unpredictable climate disasters force them to graze in lower altitudes (Borchardt et al., 2011). During Soviet times, formerly autonomous grazing was replaced by state-owned farms (sovkhozes) and collective farms (kolkhozes); thus, herders were forced to form collectives and settle, and the quantity of livestock increased drastically (Hoppe et al., 2018). The collapse of the Soviet Union led to the dissolution of the livestock markets and production-supporting services and resulted in a reduction in livestock quantity by nearly 60% in Kyrgyzstan (Iñiguez, 2004; Agadjanian and Gorina, 2019). Due to state-owned farms dismantling, many collectives broke up into individual households for lacking investment capital and comprehensive agricultural knowledge, which further led to a decrease in livestock productivity (Hauck et al., 2016). Additionally, with increasing unemployment, rural households had to focus on private subsistence agriculture. To meet the market demands for meat, dairy production, and livestock services, the livestock numbers began to increase again in 2000 (de la Martiniere, 2012), and animal husbandry was still an important source of income at the household level in Kyrgyzstan.

Due to relatively weak adaptability, high production environment risk, and low elasticity, livestock is one of the most vulnerable industries to climate and society fluctuations (Megersa et al., 2014). To avoid potential shocks on the sustainable development of husbandry, recent studies have been attempting to explore the patterns of livestock dynamics through theoretical models and field surveys. Tessema et al. (2014) reviewed and quantified global studies on the sustainable development of animal husbandry over the past decades and confirmed the sustainability of animal husbandry systems, which relied on herders' adaptability to unpredictable environments, grazing mobility, and institutional support. Grounded on a household survey of herders in southern Ethiopia, a study showed that adjusting the composition of herds was a vital adaptive strategy to cope with climate change and poor pasture conditions (Megersa et al., 2014). In volatile environments, interactions among biophysical, economic, and institutional factors promoted livestock migration for better feed resources. According to satellite imagery and interviews with herders of Kazakhstan, Robinson et al. (2016) indicated that the effects of economic and institutional factors on livestock migration and distribution were increasing. Combining the equilibrium replacement model of livestock products with the inventory relation, Ge and Kinnucan (2018) found that good weather conditions would reduce the number of goats but raise the number of cattle and sheep. In the market, higher prices had negative impact on the cattle inventory, while higher feed costs had positive impact on the stock of cattle and sheep in the Inner Mongolia Autonomous Region of China. Based on spatial autocorrelation analysis, standard deviation ellipse, and the spatial Durbin model (SDM), Han et al. (2020) found that there were significant positive spatial autocorrelation characteristics in China's husbandry industry. The result revealed that high-productivity land for grazing, people's income and living standard, and mechanization level could promote the development of animal husbandry in China.

Since the influencing factors of livestock dynamics and their interaction are complex, many researches have begun to assess and quantify internal mechanisms and impacts. Climate change, especially heat stress, could directly affect the metabolism and nutrient absorption of livestock, indirectly affect food intake, immune system, and feed supply, and ultimately affect livestock production (Baumgard et al., 2012). Wolfenson and Roth (2019) found that hot summer conditions could hinder the reproduction of cows, leading to a significant decline in worldwide pregnancy rates. In addition to climate factors, some scholars found that socio-economic factors also had the impact on the livestock scale. Based on the socio-economic and livestock quantity data over the past 40 years in Xilinguole of China, Jiang et al. (2019) revealed that the land use policy was negatively correlated with the change in livestock numbers, and the larger population of herders had significant and positive effects on the quantity of sheep and goats. Liang et al. (2021) found that population distribution would directly affect the quantity and structure of livestock consumption, and the total livestock consumption in Kazakhstan increased gradually from north to south. Xu et al. (2019) pointed out that Mongolian herdsmen would adjust their herd size according to market factors such as current and expected prices, alternative food prices, and debts. Although previous studies had focused on livestock dynamic analysis in general, few research studies had quantified the impact by integrated factors on the livestock scale, especially in the Central Asia arid region.

The main aims of this paper are to 1) assess the dynamic patterns of the livestock scale in Kyrgyzstan from 2006 to 2020; 2) quantify the impact of socio-economic and environmental factors on the scale of livestock; and 3) explore sustainable strategies for the high-quality development of animal husbandry and income security for herdsmen. To achieve the research objectives, we referred to the two-period livestock production model to determine the potential factors affecting the livestock scale. Then, we used the spatial panel model to quantify the spatial effects of different factors on the scale of livestock. Finally, we discussed the potential impact on livestock by different influencing factors. This study not only quantified the influencing mechanism of the animal husbandry scale in Kyrgyzstan but also explored effective paths for the sustainable development of local animal husbandry and income security for herdsmen. Our results could provide an important practical experience for high-quality economic development of countries in arid regions with animal husbandry as the economic pillar.

2 Materials and methods

2.1 Study area

Kyrgyzstan, a landlocked mountainous country of Central Asia located in the Tian Shan Mountains and Pamir-Alay mountain range, is bordered by Kazakhstan to the north, China to the east, and bounded by Uzbekistan and Tajikistan to the south and west (Figure 1A). The land area of Kyrgyzstan is about 199,951 km^2, including seven oblasts (provinces) and two municipalities. With 94% of the territory lying above 1,000 m, grasslands are the main land cover type (Figure 1B). Taking up 56% of the land, grasslands are one of the most vital natural resources of Kyrgyzstan (Wang et al., 2020). Due to uneven seasonal precipitation, the average annual precipitation in Kyrgyzstan is only 200–800 mm, making it a typically arid country (Liang et al., 2021). July and August are the hottest months of the year. In winter, the temperatures are the lowest in mountain valleys and depressions due to the terrain (Beer et al., 2008).

Kyrgyzstan is a low-income country with 6.59 million people. The per capita gross national income is about 1,170 USD, and more than 63% of residents live in rural areas (World Bank, 2020). Linking Eurasia and the Middle East, Kyrgyzstan is located in a key position for international trade with economies like Russia, the United Kingdom, and China. During the Soviet Union period, the main agricultural economic activities of Kyrgyzstan were controlled by state farms, which were the important livestock and agricultural suppliers of the Soviet Union. After Kyrgyzstan gained its independence in 1991, the planned economy transformed into a market economy, the state farms were demolished, and land and livestock were privatized (Dabrowski et al., 1995).

2.2 Data resources

In this study, environmental and socio-economic data in each oblast level from 2006 to 2020 were collected. Socio-economic data including GDP, population, income, livestock number (cattle, cows, sheep, goats, and horses) were obtained from the National Statistical Committee of the Kyrgyz Republic (NSCKR, http://www.stat.kg/en/). The agricultural loan data for herds were obtained from the Food and Agriculture Organization of the United Nations (FAOSTAT, https://www.fao.org/faostat/en/#home). Compared with other indexes displaying the static cover conditions of grasslands, net primary productivity (NPP) can dynamically reflect the condition of grassland production for livestock feeding in a certain period. To calculate the grassland NPP value of Kyrgyzstan from 2006 to 2020, the 1-km spatial resolution global MODIS NPP product MOD17A3 was acquired from the NASA MODIS Land Science Team website (https://modis.gsfc.nasa.gov/). The temperature and precipitation data were obtained from the NASA MODIS Land Science Team website (https://modis.gsfc.nasa.gov/), and the land cover data were obtained from the MODIS Terra–Aqua Combined Land Cover product MCD12Q1 (https://modisland.gsfc.nasa.gov/landcover.html).

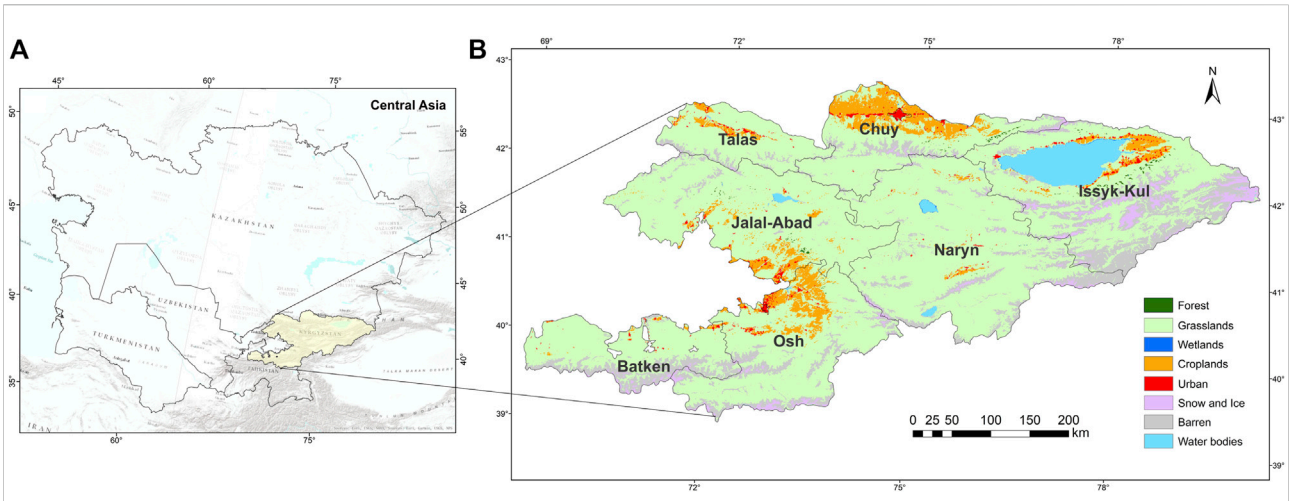

FIGURE 1
Location of the study area **(A)** and the distribution of the different land cover types in Kyrgyzstan **(B)**. The terrain map of this study region was from ESRI, USGS, and NOAA. Land cover data were obtained from the MODIS Terra–Aqua Combined Land Cover product MCD12Q1 (https://modisland.gsfc.nasa.gov/landcover.html).

2.3 Methods

To explore the dynamics of livestock production and driving factors in Kyrgyzstan from 2006 to 2020 under the changing socio-economic and environmental conditions, we first standardized and analyzed the environmental and socio-economic data and investigated the migration trajectory of the spatial gravity center of animal husbandry. Second, we used the two-period livestock production model to describe the livestock production cycle in Kyrgyzstan and introduced herders' preferences as part of the mechanism of livestock production to indicate the characteristics of livestock production dynamics. Finally, based on the calculation of global Moran's index and a series of tests for spatial model selection, we applied the spatial econometric model and panel data to quantify the driving factors of livestock production dynamics in Kyrgyzstan (Supplementary Figure S1).

2.3.1 Statistical processing

In this study, we selected an oblast scale to detect dynamic livestock sales, self-consumption, and inventory based on the environment and socio-economic data. In order to directly compare the data of past decades, all the monetary data in the socio-economic category were converted to the 2006 constant dollar using the consumer price index (CPI), which could eliminate the impact of inflation:

$$Real\ price = nominal\ price/CPI\,. \tag{1}$$

As different animals would have different sale prices and costs, large animals like horses and cattle were standardized to a national sheep unit in a way that one large animal equaled four sheep (Wang et al., 2020). In addition, we used logarithms to standardize the data with different dimensions.

In order to obtain the annual data of precipitation and temperature, we interpolated the original monthly data, then generated the grating image, and used the linear regression analysis based on the least square method. All the environmental data were processed using ArcGIS V10.3. We further carried out descriptive statistics based on the environment and socio-economic data using STATA 16, and the brief statistical description of each variable is given in Supplementary Table S1, which would be employed in the livestock production model to quantify the driving factors of livestock production in Kyrgyzstan.

2.3.2 Spatial gravity center of animal husbandry

Based on the geometric center of each oblast, we described the migration trajectory of livestock husbandry by calculating the weighted average center of gravity:

$$\bar{X}_t = \sum_{i=1}^{N} \frac{Z_{it} X_i}{\sum_{i=1}^{N} Z_{it}},\ \bar{Y}_t = \sum_{i=1}^{N} \frac{Z_{it} Y_i}{\sum_{i=1}^{N} Z_{it}}, \tag{2}$$

where X_i and Y_i are the longitude and latitude of the geometric center of the *ith* oblast, respectively. Z_{it} represents the quantity of the livestock sold, consumed, or stocked by the *ith* oblast in the *tth* year and N is the number of oblasts in Kyrgyzstan. Therefore, $(\bar{X}_t, \bar{Y}_t)$ could intuitively reflect the change path of national livestock sales, self-consumption, and inventory layout.

2.3.3 Two-period livestock production model

The livestock scale not only responded to the current environment and socio-economic conditions but was also strongly associated with herders' preferences on the production cycle, which could affect the herders' livestock scale (Rae and Zhang, 2009; Swanepoel et al., 2010). To simplify the production cycle of livestock, we used the two-period livestock production model (Xu et al., 2019) to quantify the dynamics of livestock and its influencing factors from 2006 to 2020 in each oblast of Kyrgyzstan. The original two-stage model was used to solve the problems of resource consumption and stock in agricultural production systems like fisheries and forestry (Packalen et al., 2009; Munavar et al., 2016). This two-period livestock production model (Xu et al., 2019) took herders' preferences of consuming or saving livestock as part of the mechanism of livestock dynamics and then categorized the production cycle into two periods: "present" and "future." In the present period, herders usually made decisions on livestock sales and self-consumption according to past market information and expectations for future markets. Then, the remaining livestock would become the initial stock for the second period, and Xu et al. (2019) postulated that herders would sell and consume the rest of the livestock at the end of the second period. Based on the assumption, the conceptual model is as follows:

$$U = (1-\alpha)\left[u(c_1)+\beta\cdot u(c_2)\right]+\alpha\left[g(x_{12})+\beta\cdot g(x_{22})\right], \quad (3)$$

where U is the utility of a herder and α is a parameter that measures the relative utility weight between sale and self-consumption. c_1, c_2 denote the consumption of the present and future, respectively, and β is the time preference rate of a herder. $u(x)$ and $g(x)$ are the utility function of sale and self-consumption, respectively, x_{12} is the quantity of herder's self-consumption in the first period, and x_{22} is the quantity of herder's self-consumption in the second period.

The price of livestock production was the most vital signal for herders to adjust their livestock scale (Bakucs et al., 2014), and the variation in the interest rate was an important form to embody the risk of livestock production (Meuwissen et al., 2001). To simulate the scenarios of the livestock market, Xu et al. (2019) brought the price and interest rate into the two-period livestock production model, which could reflect the fluctuation of the market condition. Economic production is essentially the product of the interaction of social resources, which is confirmed through the calculation and analysis of Eq. 3. Xu et al. (2019) detected that the dynamic changes of livestock would be influenced by socio-economic variables (household education, income, and livestock price) and environmental variables (annual precipitation and temperature).

The two-period production model has been widely used in the estimation of agricultural production efficiency, especially in arid and semi-arid areas with scarce production resources, single economic activities, and fragile environmental conditions. These regions need to constantly balance the consumption and inventory

TABLE 1 Specific description of the variables in this study.

Variable	Meaning	Unit
Preci	Annual precipitation	mm
Temp	Annual temperature	°C
NPP	Net primary productivity of grassland in each oblast	$gCm^{-2}\ yr^{-1}$
Q_{sale}	Quantity of livestock sold by herders	Per head
$Q_{self\text{-}consumption}$	Quantity of livestock consumed by herders	Per head
Q_t	Quantity of livestock inventory at the end of this year	Per head
Q_{t-1}	Quantity of livestock inventory at the end of the previous year	Per head
P_t	Livestock price of this year	Dollar/head
P_{t+1}	Livestock price of the next year	Dollar/head
m_t	Non-herding income of this year	Dollar
m_{t-1}	Non-herding income of the previous year	Dollar
Edu	Number of people graduating from high schools	Thousand Capita
Rural	Number of rural populations	Thousand Capita
Husgrp	Output of animal husbandry in each oblast	Dollar
Lorate	Ratio of loan to income (it reflects the difficulty for borrowing; a higher ratio means loans are easier to borrow)	—
Rurate	Ratio of rural residents to total population in each oblast	—
a_0, b_0, and c_0	Constant term	—
a_1~a_7	Correlation coefficients in Eq. 4	—
b_1~b_6	Correlation coefficients in Eq. 5	—
c_1~c_{11}	Correlation coefficients in Eq. 6	—
ε_0, f_0, and e_0	Random error term	—

of resources to maximize the output (Kimhi, 2006; Asfaw et al., 2010; Ma et al., 2018). Therefore, we ran three regressions to quantify the influencing factors of livestock change in Kyrgyzstan:

$$ln(Q_{Sale}) = a_0 + a_1 \cdot ln(P_t) + a_2 \cdot ln(P_{t+1}) + a_3 \cdot Lorate + a_4 \cdot ln(m_t) + a_5 \cdot ln(m_{t-1}) + a_6 \cdot ln(Q_t) + a_7 \cdot ln(Rural) + \varepsilon_0, \quad (4)$$

$$ln\left(Q_{self-consumption}\right) = b_0 + b_1 \cdot ln(P_t) + b_2 \cdot ln(P_{t+1}) + b_3 \cdot Lorate + b_4 \cdot ln(m_t) + b_5 \cdot ln(m_{t-1}) + b_6 \cdot ln(Q_t) + f_0, \quad (5)$$

$$ln(Q_t) = c_0 + c_1 \cdot ln(P_t) + c_2 \cdot ln(P_{t+1}) + c_3 \cdot Lorate + c_4 \cdot ln(Q_{t-1}) + c_5 \cdot ln(m_t) + c_6 \cdot ln(Preci) + c_7 \cdot Temp + c_8 \cdot ln(NPP) + c_9 \cdot Rurate + c_{10} \cdot ln(Husgrp) + c_{11} \cdot Edu + e_0. \quad (6)$$

All the aforementioned variables and their description are as follows (Table 1):

2.3.4 Spatial regression analysis

In order to explore the spatial correlation characteristics of the livestock scale in seven oblasts of Kyrgyzstan, we used the spatial regression model to quantify the driving factors based on global Moran's I analysis.

Compared with the normal linear regression model, the spatial regression model can accurately identify the spatial effects in a dataset (Anselin, 2003; Tirkaso and Hailu, 2022). Common spatial econometric models contain three basic forms, namely, the spatial lag model (SLM), spatial error model (SEM), and spatial Durbin model (LeSage and Pace, 2010). The specific descriptions of these models are given in Supplementary Material. Through a series of tests like the Lagrange multiplier (LM) test, likelihood ratio (LR) test, and Wald test, we took seven oblasts of Kyrgyzstan as spatial analysis units and selected the SLM and SDM to explore the dynamics of the animal husbandry number and its spatial effects on Kyrgyzstan from 2006 to 2020.

3 Results

3.1 Variation in livestock sales, self-consumption, and inventory

From 2006 to 2020, livestock sales of Kyrgyzstan increased overall, and a two-fold increase in obvious fluctuations appeared during this time. As shown in Figure 2A, the scale of national sales surged in 2006 and reached the first peak of 5.59 million heads in 2007. After the first peak, the national sales plummeted to an all-time low with 4.63 million heads in 2009 and then recovered and displayed a "U-shaped" curve. Since 2011, more

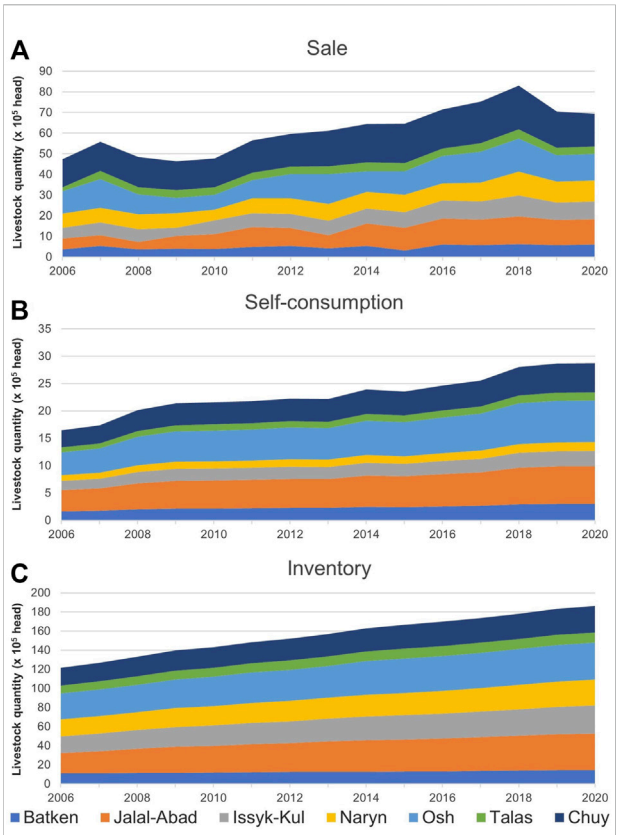

FIGURE 2
Variation in livestock quantity in each oblast of Kyrgyzstan from 2006 to 2020: **(A)** livestock quantity of sales; **(B)** livestock quantity of herders' self-consumption; and **(C)** livestock quantity of inventory.

than 5 million heads of livestock have been sold each year, and sales got the second peak of 8.29 million heads in 2018. It is obvious that Chuy Oblast had the largest actual covered area as shown in Figure 2A, which shows that Chuy Oblast sold the most livestock in Kyrgyzstan. The data series of livestock sales for Issyk-Kul, Naryn, and Chuy Oblast were relatively stable. By contrast, Batken, Jalal-Abad, Osh, and Talas Oblast had significant changes in covered areas, which means that the proportion of livestock sales in these oblasts was changed. Among these oblasts, Jalal-Abad Oblast had the largest annual growth rate of livestock sales with 9.66%, and its covered area kept increasing.

Figure 2B shows that the dynamic change of national livestock self-consumption could be divided into three periods (i.e., 2006–2007, 2008–2018, and 2019–2020). After a slight increase in 2007, livestock consumption in the country scale increased by over 16% in 2008. Since then, more than 2 million heads of livestock have been consumed annually by Kyrgyz nationals. From 2008 to 2018, the national livestock consumption grew steadily. After 2018, the livestock self-

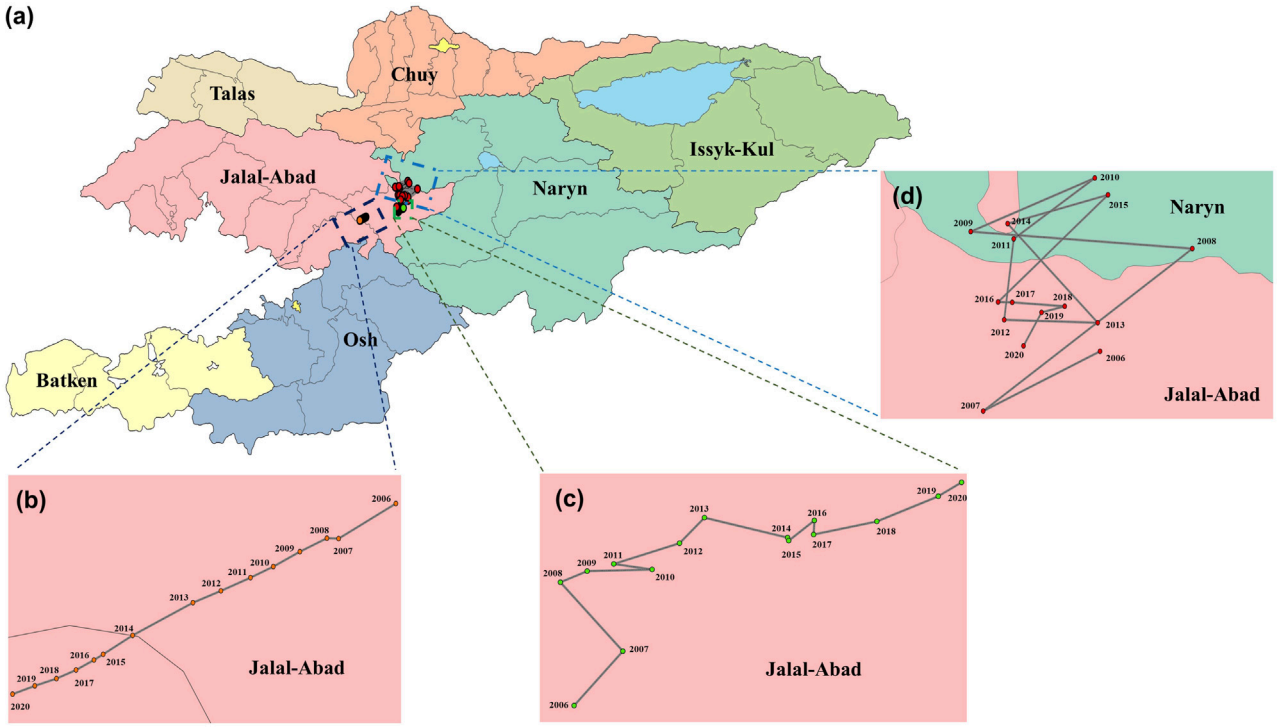

FIGURE 3
Dynamic changes in the distribution and evolution of the livestock scale in Kyrgyzstan from 2006 to 2020: **(A)** spatial distribution of the center of gravity for animal husbandry; **(B)** moving track of the center of gravity for livestock self-consumption; **(C)** moving track of the center of gravity for livestock inventory; and **(D)** moving track of the center of gravity for livestock sale.

consumption remained stable, which was contrary to the trend in sales. The consumption of livestock was mainly concentrated in Osh, Jalal-Abad, and Chuy Oblast, and the cumulative proportion of livestock consumed in these oblasts was more than 66%.

Different from the variation in livestock sales and self-consumption, the livestock inventory maintained a steady upward trend, with the number increasing over 50% in the past decade (Figure 2C). At the same time, the quantity of the livestock inventory was much larger than that of sales and self-consumption. In 2020, there were 18,622,750 heads of livestock stocked in Kyrgyzstan, while the livestock sales were only 6,940,200 heads, and herder families consumed 2,874,370 heads. The amount of inventory reached nearly 2 times of the sum of sales and self-consumption.

3.2 The shifting center of gravity for the livestock scale

Figure 3 and Table 2 show the shifting center of gravity, moving distance and direction of livestock sales, self-consumption, and inventory between 2006 and 2020 in Kyrgyzstan. It is obvious that the annual moving distance of livestock sales was much longer than self-consumption and inventory, and the center of gravity for livestock scales mainly occurred in Jalal-Abad and Naryn Oblast.

The moving track of the center of gravity for livestock self-consumption (Figure 3B) shows that the center continued to shift from northeast to southwest between 2006 and 2020. On the contrary, the center of livestock inventory has been moving to the northeast (Figure 3C). Though the shifting route looks relatively chaotic, it is not hard to find that the livestock sale center of Kyrgyzstan was spiraling northwestward (Figure 3D). Also, the center of gravity for livestock sales moved dramatically in 2008, 2009, and 2016, respectively.

3.3 Variation in different livestock stock

From 2006 to 2020, the quantity of cattle, cows, sheep and goats, and horses had a stable increase (Figure 4). Among the aforementioned livestock, cattle increased by 3 million heads, which was the largest. Although the number of sheep and goats increased more than horses, the variation in sheep and goats showed a convex curve, indicating a slowdown in growth from 4.42% in 2006 to 0.24% in 2020. On the contrary, the trend of horse numbers showed a concave curve, and the growth rate increased from 0.70% in 2006 to 3.27% in 2020.

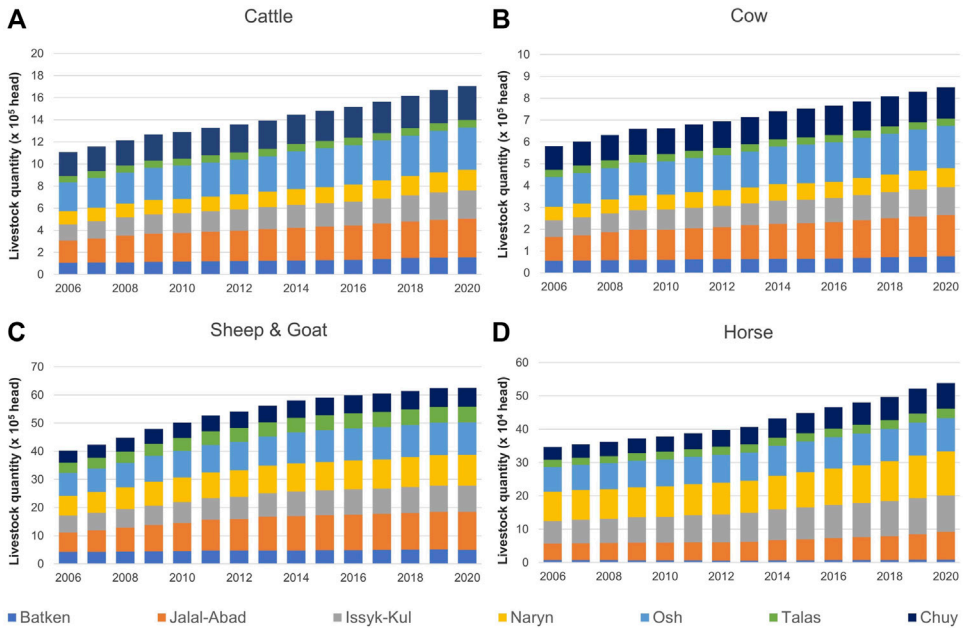

FIGURE 4
Dynamic changes in different livestock stock in each oblast of Kyrgyzstan from 2006 to 2020: **(A)** annual stock numbers of cattle; **(B)** annual stock numbers of cows; **(C)** annual stock numbers of sheep and goats; and **(D)** annual stock numbers of horses.

At the oblast level, Jalal-Abad Oblast had the highest increase in the livestock scale from 2006 to 2020, with the quantity of sheep and goats, cows, cattle, and horses increased by 95.01%, 73.82%, 74.74%, and 69.87%, respectively. For cattle and cows, Osh and Jalal-Abad Oblast showed an increase of more than 42% of the whole country, and the proportion was dynamically increasing (Figures 4A,B). The largest quantity of horses occurred in Naryn Oblast, with the proportion to the total horse number reached about 25%. At the same time, Issyk-Kul and Chuy Oblast greatly expanded the horse scale, where the quantity increased by 69.87% and 97.20%, respectively, and Batken Oblast showed the smallest increase in horse numbers with 3.56% (Figure 4D).

3.4 Results of spatial regression analysis of livestock quantity

According to the estimation of global Moran's I from 2006 to 2020, the results all showed a significant positive correlation at the 1% level, which indicates that there is a significant spatial correlation among the livestock scale in the seven oblasts of Kyrgyzstan (Supplementary Table S2). To avoid overfitting, we examined the variance inflation factors (VIFs) of each explanatory variable and dependent variable. The result showed that there was no multicollinearity problem between the variables (Supplementary Tables S3–S5). To select an appropriate spatial model to detect the driving factors of livestock production dynamics in Kyrgyzstan, we applied a series of tests including LM, LR, and the Wald test. The results given in Supplementary Table S6 show that the spatial lag model could be used to quantify the driving factors of livestock sales and self-consumption, and the spatial Durbin model suited better for analyzing the dynamics of livestock inventory and its influencing factors.

3.4.1 The driving factors of livestock sales

As shown in Table 3, the livestock price, the ratio of loan to income, non-herding income, livestock inventory, and rural population all exerted significant impact on livestock sales. The livestock sales were mainly affected by the ratio of loan to income and livestock price herders expected for the next year; in particular, the livestock prices of the present and next years could have opposite effects on sales. Though the effects of the present livestock price were not significant, the increase in the present price may lead to a reduction in livestock sales. For the price expected for the next year, each 1% price increase would promote livestock sales by 2.987 units. As a key indicator which would influence livestock sales, a higher ratio of loan to income could encourage local herders to sell more livestock, which has significantly negative spatial spillover effects on livestock sale markets in adjacent oblasts.

TABLE 2 Center of gravity for livestock scale in Kyrgyzstan from 2006 to 2020.

Year	Sale				Self-consumption				Inventory			
	Longitude	Latitude	Distance (mile)	Direction	Longitude	Latitude	Distance (mile)	Direction	Longitude	Latitude	Distance (mile)	Direction
2006	74.17	41.48	—	—	73.66	41.33	—	—	74.05	41.37	—	—
2007	74.03	41.42	8.45	Southwest	73.64	41.32	0.71	Southwest	74.06	41.38	0.72	Northeast
2008	74.28	41.58	17.31	Northeast	73.64	41.32	0.12	Northwest	74.05	41.39	0.92	Northwest
2009	74.01	41.60	14.02	Northwest	73.64	41.32	0.32	Southwest	74.05	41.39	0.26	Northeast
2010	74.16	41.65	8.65	Northeast	73.63	41.32	0.32	Southwest	74.06	41.39	0.55	Northeast
2011	74.06	41.59	6.62	Southwest	73.63	41.31	0.27	Southwest	74.05	41.40	0.33	Northwest
2012	74.05	41.51	5.60	Southwest	73.62	41.31	0.34	Southwest	74.06	41.40	0.60	Northeast
2013	74.17	41.51	5.91	Southeast	73.62	41.31	0.32	Southwest	74.07	41.40	0.35	Northeast
2014	74.06	41.60	8.88	Northwest	73.60	41.31	0.72	Southwest	74.08	41.40	0.74	Southeast
2015	74.18	41.63	6.63	Northeast	73.60	41.30	0.37	Southwest	74.08	41.40	0.03	Southeast
2016	74.05	41.53	10.13	Southwest	73.60	41.30	0.12	Southwest	74.09	41.40	0.31	Northeast
2017	74.06	41.53	0.89	Southeast	73.59	41.30	0.22	Southwest	74.09	41.40	0.15	Southwest
2018	74.13	41.52	3.32	Southeast	73.59	41.30	0.23	Southwest	74.10	41.40	0.55	Northeast
2019	74.10	41.52	1.53	Southwest	73.58	41.30	0.24	Southwest	74.11	41.41	0.59	Northeast
2020	74.08	41.48	2.57	Southwest	73.58	41.30	0.25	Southwest	74.11	41.41	0.25	Northeast

10.3389/fenvs.2022.1049187

TABLE 3 Effect of explanatory variables on livestock sales.

Variable	Main	Direct effect	Indirect effect	Total effect
Price $_{t}$	−1.572	−1.613	0.503	−1.110
	(1.25)	(1.36)	(0.48)	(0.93)
Price $_{t+1}$	2.987**	3.079**	−0.946*	2.133**
	(1.32)	(1.43)	(0.55)	(1.01)
Lorate	13.570***	14.830***	−4.441**	10.390***
	(4.98)	(4.94)	(1.88)	(3.89)
m $_{t-1}$	−0.100**	−0.107**	0.032**	−0.075**
	(0.04)	(0.04)	(0.02)	(0.03)
m $_{t}$	0.003	0.003	−0.001	0.001
	(0.04)	(0.04)	(0.01)	(0.03)
Q $_{t}$	0.597***	0.638***	−0.195***	0.443***
	(0.09)	(0.10)	(0.07)	(0.08)
Rural	0.270***	0.280***	−0.081**	0.199**
	(0.10)	(0.10)	(0.03)	(0.09)
R-squared	0.604			

Note: ***, **, and * represent that the statistics are significant at the 1%, 5%, and 10% levels, respectively.

3.4.2 The driving factors of livestock self-consumption

According to Table 4, all the variation in the livestock price of the next year, the ratio of loan to income, previous non-herding income, and current livestock inventory would have significant effects on herders' self-consumption. Among them, a higher ratio of loan to income was the primary signal for herders to increase their self-consumption, while the main factor restraining consumption was the higher livestock prices expected for the next year. With other conditions unchanged, every 1% increase in the ratio of loan to income would cause extra 14.620 units of livestock to be consumed. Different from the impact exerted on livestock sales, both the livestock price of the present year and next year had negative spatial spillover effects on livestock quantity for self-consumption.

3.4.3 The driving factors of livestock inventory

As shown in Table 5, the value of R-squared was 0.858, which showed that this model had good explanatory significance. It was observed that the livestock inventory in Kyrgyzstan was mainly influenced by the variation in current non-herding income, previous inventory, the number of educated people, the proportion of rural residents to regional population, and the regional output of animal husbandry. More previous inventory

TABLE 4 Effect of explanatory variables on livestock self-consumption.

Variable	Main	Direct effect	Indirect effect	Total effect
Price $_{t}$	−0.177	−0.140	0.041	−0.099
	(1.21)	(1.28)	(0.35)	(0.96)
Price $_{t+1}$	−5.481***	−5.729***	1.410**	−4.319***
	(1.20)	(1.27)	(0.63)	(1.09)
Lorate	14.620***	15.600***	−3.652**	11.950***
	(4.87)	(4.69)	(1.52)	(4.40)
m $_{t-1}$	0.097**	0.100**	−0.024*	0.076**
	(0.04)	(0.04)	(0.01)	(0.03)
m $_{t}$	0.024	0.025	−0.006	0.020
	(0.04)	(0.04)	(0.01)	(0.03)
Q $_{t}$	0.585***	0.613***	−0.144***	0.469***
	(0.10)	(0.09)	(0.05)	(0.12)
R-squared	0.546			

Note: ***, **, and * represent that the statistics are significant at the 1%, 5%, and 10% levels, respectively.

TABLE 5 Effect of explanatory variables on livestock inventory.

Variable	Main	Direct effect	Indirect effect	Total effect
Price $_t$	−0.037	−0.028	−0.107	−0.135
	(0.05)	(0.05)	(0.10)	(0.11)
Price $_{t+1}$	0.081	0.089*	−0.147*	−0.058
	(0.05)	(0.05)	(0.09)	(0.11)
Lorate	0.238	0.226	0.565	0.790
	(0.26)	(0.26)	(0.52)	(0.49)
Q $_{t-1}$	0.891***	0.906***	−0.192***	0.714***
	(0.04)	(0.04)	(0.07)	(0.09)
Temp	−0.002	−0.001	−0.014	−0.015
	(0.00)	(0.00)	(0.01)	(0.01)
Preci	0.003	0.008	−0.060**	−0.052**
	(0.01)	(0.01)	(0.03)	(0.03)
NPP	−0.020	−0.013	−0.085*	−0.099**
	(0.02)	(0.02)	(0.05)	(0.05)
m $_t$	−0.005**	−0.004**	−0.004	−0.008***
	(0.00)	(0.00)	(0.00)	(0.00)
Rurate	2.255***	2.026***	3.558***	5.584***
	(0.58)	(0.56)	(1.25)	(1.49)
Husgrp	−0.046**	−0.054***	0.113***	0.059
	(0.02)	(0.02)	(0.04)	(0.04)
Edu	0.003*	0.003*	0.001	0.004
	(0.00)	(0.00)	(0.00)	(0.00)
R-squared	0.858			

Note: ***, **, and * represent that the statistics are significant at the 1%, 5%, and 10% levels, respectively.

and educated people would have significant and positive spatial spillover effects on livestock inventory. Meanwhile, with other conditions unchanged, every 1% increase in the proportion of the rural population could facilitate the local livestock inventory expansion by 2.026 units and encourage the herders in adjacent oblasts to increase their livestock scale by 3.558 units.

The changes in the environment also had influences on livestock quantity. It was found that higher precipitation and grassland productivity could have significant and negative spatial spillover effects on neighboring livestock inventory. Each 1% increase in precipitation and grassland NPP could lead to an overall reduction by 0.052 and 0.099 units of livestock scale in the seven oblasts of Kyrgyzstan, respectively.

4 Discussion

This study quantified the dynamics of livestock scale and then assessed the effects of environmental and socio-economic factors on livestock sale, self-consumption, and inventory. Results showed that the quantity of livestock in Kyrgyzstan increased overall from 2006 to 2020 (Figure 4), and there were different patterns among the livestock distribution and variations in different oblasts (Figures 3, 4). Based on the spatial regression analysis, we found that multiple variables had effects on livestock quantity (Tables 3–5). All the livestock sales, self-consumption, and inventory were significantly influenced by the variation in livestock price, the ratio of loan to income, and non-herding income at different levels. The higher proportion of rural residents to regional population would have significant and positive impact on self-consumption and inventory, respectively. In addition to the socio-economic factors, the fluctuation of precipitation and grassland NPP also affected the number of livestock inventory.

4.1 The effects of environmental and socio-economic factors on livestock quantity

Our regression analysis showed that a higher non-herding income could encourage herders to consume more livestock, and the higher ratio of loan to income would also promote local herders to sell and consume more livestock (Tables 4, 5). In Kyrgyzstan, most households made a living with employment income, savings and loan, social grants, and income from animal husbandry (Wang et al., 2016; Sagynbekova, 2017). The direct contribution of livestock to the total income of household

families was limited, and many people diversified their income by international or internal labor migration (Schoch et al., 2010; Pica-Ciamarra et al., 2015). Previous studies reported that non-herding income accounted for about 38% of the total household income in the rural areas of developing countries (Ragie et al., 2020). Regional economic development provided non-agricultural employment opportunities for farmers and promoted the off-farm income for farmers. This caused strong and direct shock on animal husbandry, and even the negative effects were shown on adjacent areas (Wang et al., 2016). Meanwhile, due to more non-agricultural employment opportunities emerging and higher non-herding income increasing, pastoralists might gradually reduce their livestock scale. Kyrgyzstan's economy and people's living standards were changed greatly after the collapse of the Soviet Union, and Kyrgyzstan was classified as a lower-middle income country by the World Bank (World Bank, 2016). In order to improve people's living and production standards, microfinance was introduced in Kyrgyzstan as a poverty reduction tool. Lacking funds and technology to achieve self-sufficiency in production, the majority of Kyrgyz pastoralists would be more inclined to allocate most of the loans to scale up livestock production and compress production cycles to gain more profits (Ksoll et al., 2016; Angioloni et al., 2018). Herders also tend to purchase more food or consume more livestock to enhance living standards when they receive extra loans (Aldashev, 2019). Therefore, a higher ratio of loan to income may support Kyrgyz herders to sell and consume more livestock.

Market price was one of the most important signals that affect herders' choices for adjusting the livestock scale. Rucker et al. (1984) indicated that the change of the present price could have opposite effects on producers' decisions, bringing about herders' different responses to the market situation (Pica-Ciamarra et al., 2015). Higher market price could encourage producers to sell more livestock immediately to deal with important expenditures like living or medical costs (Megersa et al., 2014). On the other hand, producers would expect a more satisfactory price in the future and expand their stock for higher speculative profit (Ge and Kinnucan, 2018; Xu et al., 2019). Lacking more attractive and optional investment opportunities, livestock were often taken as main assets and buffer stocks in Kyrgyzstan (Munavar et al., 2016). However, only the wealthier large-herd owners could take risks and regard livestock inventory as investment for a longer term, while most livestock production came from small herders, who were more vulnerable to climate and economic fluctuation in Kyrgyzstan (de la Martiniere, 2012; Sabyrbekov, 2019). Munavar et al. (2016) defined herders with large livestock and no grazing services as large-herd owners, and small herders were those who offered grazing services to obtain seasonal income (Steimann, 2012). For small herders, pressure for longer-term feed costs and climate uncertainty would weaken their profitability (Brookfield, 1991; Biglari et al., 2019). The 2008 global financial crisis caused the surge of energy and food prices in Kyrgyzstan (Ruziev and Majidov, 2013). The attractive prices promoted herders to reduce livestock sales for saving capital to deal with uncertainty and wait for better sale opportunities. This was consistent with Figure 2A. As long as the livestock price reaches herders' anticipation, they prefer to sell more livestock.

Research results showed that more precipitation and higher grassland NPP could lead herders to reduce their livestock number in neighboring oblasts. The livestock scale was vulnerable to feed production, which depended on climate and environmental conditions (Jaber et al., 2016; Karimi et al., 2018). Insufficient precipitation, shortage of water resources, and poor water infrastructure would reduce grassland productivity, which directly affects the feed price and impacts the cost of animal husbandry and its size (Sagynbekova, 2017; Chen et al., 2020; Umuhoza et al., 2021; Kadupitiya et al., 2022). Pastures with more precipitation benefit for grassland productivity in Kyrgyzstan (Wang et al., 2020), which could offer abundant and high-quality feed for livestock and greatly promote the development of animal husbandry. In addition to the climate factors, human activities could also contribute to the recovery of grassland productivity. To ensure the sustainability of pastures, the Kyrgyzstan government established a series of policies and laws for pasture management after the country gained independence. As a result, more than 40% of grasslands recovered significantly under the joint efforts of the government and local people from 2000 to 2014 (Wang et al., 2020). The grassland restoration caused by anthropogenic activities mainly occurred in Osh, Naryn, Issyk-Kul, and southern Jalal-Abad Oblasts, which would attract more herders to migrate and graze in these regions. It is found that the center of gravity for livestock inventory in Kyrgyzstan shifted from southern Jalal-Abad to the northeast of Kyrgyzstan (Figure 3C).

As shown in Table 5, higher grassland NPP and more precipitation in pastures had significant spatial spillover effects, which might attract herders to migrate and graze from other regions (Opiyo et al., 2011). Lacking sufficient funds and anti-risk ability for long-distance migration, small herdsmen often grazed in pastures near villages, even if the feed resources were inadequate (Rahimon, 2012; Steimann, 2012). With the gradual improvement and stringency of policies of pasture management, small herders with little access to high-quality resources will be increasingly restricted (Crewett, 2012). In contrast, wealthier herders generally possessed significant power, sufficient funds, and livestock management expertise to migrate and privileges to graze on more productive pastures (Sagynbekova, 2017; Kasymov and Thiel, 2019).

4.2 Implication policy

The livestock system is extremely complex and influenced by different factors. To achieve sustainable development of animal

husbandry, Kyrgyzstan needs innovative combinations of system, policy, and technology. First, it is vital for the government to develop more flexible financial policies to directly ease the cost pressure on pastoralist families. In many countries, microfinance is regarded as an important approach to increase the flow of capital (Hossain, 1988; Hartarska and Nadolnyak, 2008; Kabir et al., 2017), which is an effective short-term method to help herdsmen overcome climate disasters such as drought or snowstorms, and has been advocated by governments and international organizations (Turner and Williams, 2002; Ouma et al., 2011; Addison and Brown, 2014). Meanwhile, the government could steer domestic investment and foreign capital in animal husbandry by reducing the tax rate of animal husbandry and increasing production subsidies for animal husbandry enterprises (Upton, 2004; Dovie et al., 2006; Zeleke et al., 2021). Second, national and local managers need to explore a new animal husbandry production system, which could improve the adaptability and reproductive efficiency of livestock under fluctuated environments. This system includes the techniques of feed and nutrition, genetics and breeding, disease prevention, and environmental management and then adopts different technical combinations for different production systems (Zhao et al., 2018; Enahoro et al., 2019). Third, pasture management should be transformed from unidirectional to multiple forms and make herders become the common managers. Providing alternative and cognitive frameworks, as well as appealing for actions, could be a more effective way to enhance herders' self-concept and produce positive outcomes (Cohen, 2001; Korman, 2012). For example, pasture managers could provide local herders with jobs like paid environmental monitors and data collectors, so herders can obtain extra income and be encouraged to co-create pasture conservation initiatives (Levine et al., 2017). Furthermore, it is worthwhile to explore the policies of livestock international trade, which conduces to promoting national economic development. The local livestock industry could be supported by raising import taxes, which could help to protect the market for domestic livestock production and ensure an income for local herdsmen (Jaber et al., 2016). For livestock export, developed countries follow strict food safety and quality standards to meet the international health standards. The Kyrgyzstan government should ensure the production and export of animal husbandry by actively complying with various health measures and actively exploring the market potential of importing countries with huge demand for livestock products (Kumar, 2010).

4.3 Innovation and contribution

Some previous studies have indicated that social economic factors played a dominant role in husbandry development of arid and semi-arid areas (Ge and Kinnucan, 2018; Xu et al., 2019; Wei and Zhen, 2020). The results provided more diversified practical proof for the dynamics of livestock scale and introduced a more flexible environmental index to strengthen the assessment of environmental effects on livestock quantity in Kyrgyzstan. This study also offered a new perspective for research studies on livestock change in arid and semi-arid areas and proposed significant measures for developing husbandry economy under the context of high quality and sustainable development of the national economy for developing countries. The approach we used was widely applicable in identifying the impact of climate change and socio-economic changes on the dynamics of livestock in arid and semi-arid areas and determined the spatial effects of socio-economic factors and environmental factors. This research not only provided new evidence for the efficient development of animal husbandry in Kyrgyzstan under environmental policies and financial regulation but also proposed a theoretical and practical basis for other Central Asian countries to maintain husbandry and national economy sustainability.

4.4 Limitation and uncertainty

In this study, the two-period livestock production model divided the operation of the livestock market into two stages, introduced the herdsmen's speculative behavior as a weight to the model, and revealed the specific influencing factors of livestock quantity change (Xu et al., 2019). However, this model algorithm has not been verified by a wide range of cases yet, and its control variables may be incomplete. In addition to the variables mentioned in this study, four other variables (i.e., abundance of feed resources, proportion of productive land area, the improvement of agricultural productivity, and mechanization level) had direct and positive effects on the grass-feeding livestock breeding industry (Wang et al., 2016), but the urbanization level and climatic changes had obvious negative effects (Peng et al., 2005; Munavar et al., 2016). Therefore, the accuracy of our model and variable selection may have a certain degree of limitation.

The analysis of livestock variation was also limited by data uncertainties as the dataset did not reflect the specific condition of the household unit. The livestock sales, self-consumption, and inventory could be significantly influenced by the household size and livestock structure (Xu et al., 2019; Wei and Zhen, 2020). In this study, the variables were based on provincial statistics, which represented the provincial average condition. Although the official data could objectively reflect the real condition of husbandry in the seven oblasts of Kyrgyzstan, the household data based on a field survey were deficient, which could not reflect the production capacity and income levels of different families and pastures. Future studies should focus on accessing and quantifying how the environmental and financial policies have affected the development of husbandry in Kyrgyzstan. This is a very promising direction for future policy approaches, especially in light of the multiple pressures anticipated from agricultural investment under China's Belt and Road Initiative.

5 Conclusion

We used the two-period livestock production model and spatial panel econometric model to estimate the dynamics of livestock quantity change and its influencing factors from 2006 to 2020 in Kyrgyzstan. Our results showed that the quantity of livestock increased overall, and the quantity of livestock for inventory was far more than sales and self-consumption. In addition, market price, non-herding income, and current livestock inventory were the dominant socio-economic factors contributing to dynamic changes in livestock sales, self-consumption, and inventory, and the higher proportion of rural residents and education level could support herders to expand their livestock scale. The results provided an effective way to not only guarantee the herders' livelihood and realize the sustainable development of animal husbandry but also promote high-quality economic development for Kyrgyzstan. In a broader sense, our findings have greatly advanced the understanding of sustainable development of a grassland ecosystem and animal husbandry economy in arid and semi-arid regions.

Data availability statement

The datasets presented in this study can be found in online repositories. The names of the repository/repositories and accession number(s) can be found in the article/ Supplementary Material.

Author contributions

JY and YW designed the study and planned the analysis; JY prepared the basic data; JY, HZ, and XW conducted the data analysis; JY drafted the manuscript; YW, JY, YS, SY, and SY revised the manuscript. All authors contributed critically to the drafts and approved the final version of the manuscript.

Funding

This work was supported by the National Natural Science Foundation of China (grant number 72074198).

Conflict of interest

The authors declare that the research was conducted in the absence of any commercial or financial relationships that could be construed as a potential conflict of interest.

Publisher's note

All claims expressed in this article are solely those of the authors and do not necessarily represent those of their affiliated organizations, or those of the publisher, the editors, and the reviewers. Any product that may be evaluated in this article, or claim that may be made by its manufacturer, is not guaranteed or endorsed by the publisher.

Supplementary material

The Supplementary Material for this article can be found online at: https://www.frontiersin.org/articles/10.3389/fenvs.2022.1049187/full#supplementary-material

References

Abay, K. A., and Jensen, N. D. (2020). Access to markets, weather risk, and livestock production decisions: Evidence from Ethiopia. *Agric. Econ.* 51, 577–593. doi:10.1111/agec.12573

Addison, J., and Brown, C. (2014). A multi-scaled analysis of the effect of climate, commodity prices and risk on the livelihoods of Mongolian pastoralists. *J. Arid Environ.* 109, 54–64. doi:10.1016/j.jaridenv.2014.05.010

Agadjanian, V., and Gorina, E. (2019). Economic swings, political instability and migration in Kyrgyzstan. *Eur. J. Popul.* 35, 285–304. doi:10.1007/s10680-018-9482-4

Aldashev, A. (2019). Social norms, status spending and household debt: Evidence from Kyrgyzstan. Available at: https://mpra.ub.uni-muenchen.de/id/eprint/91363.

Angioloni, S., Kudabaev, Z., Ames, G. C. W., and Wetzstein, M. (2018). Household allocation of microfinance credit in Kyrgyzstan. *Post-Communist Econ.* 30, 78–98. doi:10.1080/14631377.2017.1361691

Anselin, L. (2003). Spatial externalities, spatial multipliers, and spatial econometrics. *Int. regional Sci. Rev.* 26, 153–166. doi:10.1177/0160017602250972

Arora, N. K., and Mishra, I. (2019). United nations sustainable development goals 2030 and environmental sustainability: Race against time. *Environ. Sustain.* 2, 339–342. doi:10.1007/s42398-019-00092-y

Asfaw, S., Mithofer, D., and Waibel, H. (2010). Agrifood supply chain, private-sector standards, and farmers' health: Evidence from Kenya. *Agric. Econ.* 41, 251–263. doi:10.1111/j.1574-0862.2010.00443.x

Bakucs, Z., Falkowski, J., and Ferto, I. (2014). Does market structure influence price transmission in the agro-food sector? A meta-analysis perspective. *J. Agric. Econ.* 65, 1–25. doi:10.1111/1477-9552.12042

Baumgard, L. H., Rhoads, R. P., Rhoads, M. L., Gabler, N. K., Ross, J. W., Keating, A. F., et al. (2012). "Impact of climate change on livestock production," in *Environmental stress and amelioration in livestock production* (Berlin, Heidelberg: Springer).

Beer, R., Kaiser, F., Schmidt, K., Ammann, B., Carraro, G., Grisa, E., et al. (2008). Vegetation history of the walnut forests in Kyrgyzstan (central Asia): Natural or anthropogenic origin? *Quat. Sci. Rev.* 27, 621–632. doi:10.1016/j.quascirev.2007.11.012

Biglari, T., Maleksaeidi, H., Eskandari, F., and Jalali, M. (2019). Livestock insurance as a mechanism for household resilience of livestock herders to climate change: Evidence from Iran. *Land Use Policy* 87, 104043. doi:10.1016/j.landusepol.2019.104043

Borchardt, P., Schickhoff, U., Scheitweiler, S., and Kulikov, M. (2011). Mountain pastures and grasslands in the SW Tien Shan, Kyrgyzstan — floristic patterns, environmental gradients, phytogeography, and grazing impact. *J. Mt. Sci.* 8, 363–373. doi:10.1007/s11629-011-2121-8

Breeman, G., Dijkman, J., and Termeer, C. (2015). Enhancing food security through a multi-stakeholder process: The global agenda for sustainable livestock. *Food Sec.* 7, 425–435. doi:10.1007/s12571-015-0430-4

Brookfield, D. (1991). Structural relationships in UK store livestock markets. *J. Agric. Econ.* 42, 11–20. doi:10.1111/j.1477-9552.1991.tb00328.x

Chen, T., Tang, G., Yuan, Y., Guo, H., Xu, Z., Jiang, G., et al. (2020). Unraveling the relative impacts of climate change and human activities on grassland productivity in Central Asia over last three decades. *Sci. Total Environ.* 743, 140649. doi:10.1016/j.scitotenv.2020.140649

Cohen, S. (2001). *States of denial: Knowing about atrocities and suffering*. New York, United States: John Wiley & Sons, 177–183.

Crewett, W. (2012). Improving the sustainability of pasture use in Kyrgyzstan. *Mt. Res. Dev.* 32, 267–274. doi:10.1659/mrd-journal-d-11-00128.1

Dabrowski, M., Jermakowicz, W., Pańków, J., Kloc, K., and Antczak, R. (1995). Economic reforms in Kyrgyzstan. *Communist Econ. Econ. Transformation* 7, 269–297. doi:10.1080/14631379508427825

de la Martiniere, R. (2012). Rural livelihood trajectories around a "bull market" in Kyrgyzstan studying agropastoral change at the household level through farming system modeling. *Mt. Res. Dev.* 32, 337–344. doi:10.1659/mrd-journal-d-11-00098.1

Dovie, D. B. K., Shackleton, C. M., and Witkowski, E. T. F. (2006). Valuation of communal area livestock benefits, rural livelihoods and related policy issues. *Land Use Policy* 23, 260–271. doi:10.1016/j.landusepol.2004.08.004

Enahoro, D., Mason-D'Croz, D., Mul, M., Rich, K. M., Robinson, T. P., Thornton, P., et al. (2019). Supporting sustainable expansion of livestock production in South Asia and Sub-Saharan Africa: Scenario analysis of investment options. *Glob. Food Secur.* 20, 114–121. doi:10.1016/j.gfs.2019.01.001

FAO (2006). *World agriculture: Towards 2030/2050, interim report*. Rome, Italy: FAO.

Ge, W., and Kinnucan, H. (2018). Dynamic analysis of the livestock inventory in Inner Mongolia. *China Agric. Econ. Rev.* 10, 498–515. doi:10.1108/caer-02-2017-0015

Gerber, P. J., and Steinfeld, H. (2008). "Worldwide growth of animal production and environmental consequences," in *Trace elements in animal production systems*. Editors P. Schlegel, S. Durosoy, and A. W. Jongbloed (Wageningen, Netherlands: Wageningen Academic), 21–32.

Gerosa, S., and Skoet, J. (2012). Milk availability: Trends in production and demand and medium-term outlook. *Agrifood Econ.* ESA Working Papers. doi:10.22004/ag.econ.289000

Haghiyan, I., Mofidi-Chelan, M., Azadi, H., Nejatiyanpour, E., Motamedi, J., Sheidai-Karkaj, E., et al. (2022). Evaluating economic and ecological management to determine the economic size of pastoral units for different climatic zones in the northeast of Iran. *J. Environ. Manag.* 301, 113766. doi:10.1016/j.jenvman.2021.113766

Han, C. J., Wang, G. G., Zhang, Y. X., Song, L. L., and Zhu, L. Z. (2020). Analysis of the temporal and spatial evolution characteristics and influencing factors of China's herbivorous animal husbandry industry. *Plos One* 15, e0237827. doi:10.1371/journal.pone.0237827

Hartarska, V., and Nadolnyak, D. (2008). An impact analysis of microfinance in Bosnia and Herzegovina. *World Dev.* 36, 2605–2619. doi:10.1016/j.worlddev.2008.01.015

Hauck, M., Artykbaeva, G. T., Zozulya, T. N., and Dulamsuren, C. (2016). Pastoral livestock husbandry and rural livelihoods in the forest-steppe of east Kazakhstan. *J. Arid Environ.* 133, 102–111. doi:10.1016/j.jaridenv.2016.05.009

Hoppe, F., Schickhoff, U., and Oldeland, J. (2018). Plant species diversity of pastures in the Naryn Oblast (Kyrgyzstan). *DIE ERDE-Journal Geogr. Soc. Berlin* 149, 214–226. doi:10.12854/erde-2018-384

Hossain, M. (1988). *Credit for alleviation of rural poverty: The Grameen Bank in Bangladesh*. Washington, D.C., USA: Intl Food Policy Res Inst. 65.

Iñiguez, L. (2004). Goats in resource-poor systems in the dry environments of west Asia, central Asia and the inter-andean valleys. *Small Ruminant Res.* 51, 137–144. doi:10.1016/j.smallrumres.2003.08.014

Jaber, L. S., Diehl, K. E., and Hamadeh, S. K. (2016). Livestock and food security in the arab region: Policy framework. *Food Sec.* 8, 899–908. doi:10.1007/s12571-016-0608-4

Jiang, Y., Zhang, Q., Niu, J., and Wu, J. (2019). Pastoral population growth and land use policy has significantly impacted livestock structure in inner Mongolia-A case study in the xilinhot region. *Sustainability* 11, 7208. doi:10.3390/su11247208

Kabir, M. J., Alauddin, M., and Crimp, S. (2017). Farm-level adaptation to climate change in Western Bangladesh: An analysis of adaptation dynamics, profitability and risks. *Land Use Policy* 64, 212–224. doi:10.1016/j.landusepol.2017.02.026

Kadupitiya, H. K., Madushan, R. N. D., Gunawardhane, D., Sirisena, D., Rathnayake, U., Dissanayaka, D., et al. (2022). Mapping productivity-related spatial characteristics in rice-based cropping systems in Sri Lanka. *J. Geovis. Spat. Anal.* 6, 26. doi:10.1007/s41651-022-00122-0

Kang, Y. Q., Zhao, T., and Yang, Y. Y. (2016). Environmental kuznets curve for CO2 emissions in China: A spatial panel data approach. *Ecol. Indic.* 63, 231–239. doi:10.1016/j.ecolind.2015.12.011

Karimi, V., Karami, E., and Keshavarz, M. (2018). Vulnerability and adaptation of livestock producers to climate variability and change. *Rangel. Ecol. Manag.* 71, 175–184. doi:10.1016/j.rama.2017.09.006

Kasymov, U., and Thiel, A. (2019). Understanding the role of power in changes to pastoral institutions in Kyrgyzstan. *Int. J. Commons* 13, 931–948. doi:10.5334/ijc.870

Kerven, C., Steimann, B., Ashley, L., Dear, C., and Rahim, I. (2011). *Pastoralism and farming in central asia's mountains: A research review*. Bishkek, Kyrgyzstan: University of Central Asia. MSRC background paper. 1.

Kimhi, A. (2006). Plot size and maize productivity in Zambia: Is there an inverse relationship? *Agric. Econ.* 35, 1–9. doi:10.1111/j.1574-0862.2006.00133.x

Koocheki, A., and Gliessman, S. R. (2005). Pastoral nomadism, a sustainable system for grazing land management in arid areas. *J. Sustain. Agric.* 25, 113–131. doi:10.1300/j064v25n04_09

Korman, A. K. (2012). "Self-enhancement and self-protection: Toward a theory of work motivation," in *Work motivation in the context of a globalizing economy* (United Kingdom: Psychology Press), 127–136.

Ksoll, C., Lilleør, H. B., Lønborg, J. H., and Rasmussen, O. D. (2016). Impact of village savings and loan associations: Evidence from a cluster randomized trial. *J. Dev. Econ.* 120, 70–85. doi:10.1016/j.jdeveco.2015.12.003

Kumar, A. (2010). Exports of livestock products from India: Performance, competitiveness and determinants. *Agric. Econ. Res. Rev.* 23, 57–68. doi:10.22004/ag.econ.92095

Lan, X., Zhang, Q., Xue, H. L., Liang, H. G., Wang, B. J., and Wang, W. J. (2021). Linking sustainable livelihoods with sustainable grassland use and conservation: A case study from rural households in a semi-arid grassland area, China. *Land Use Policy* 101, 105186. doi:10.1016/j.landusepol.2020.105186

LeSage, J. P., and Pace, R. K. (2010). "Spatial econometric models," in *Handbook of applied spatial analysis* (Berlin, Heidelberg: Springer), 355–376.

Levine, J., Isaeva, A., Eddy, I., Foggin, M., Gergel, S., Hagerman, S., et al. (2017). A cognitive approach to the post-soviet central asian pasture puzzle: New data from Kyrgyzstan. *Reg. Environ. Change* 17, 941–947. doi:10.1007/s10113-017-1122-8

Liang, L., Zhang, F., and Qin, K. (2021). Assessing the vulnerability of agricultural systems to drought in Kyrgyzstan. *Water* 13, 3117. doi:10.3390/w13213117

Ludi, E. (2003). Sustainable pasture management in Kyrgyzstan and Tajikistan: Development needs and recommendations. *Mt. Res. Dev.* 23, 119–123. doi:10.1659/0276-4741(2003)023[0119:spmika]2.0.co;2

Ma, W. L., Renwick, A., and Grafton, Q. (2018). Farm machinery use, off-farm employment and farm performance in China. *Aust. J. Agric. Resour. Econ.* 62, 279–298. doi:10.1111/1467-8489.12249

Megersa, B., Markemann, A., Angassa, A., Ogutu, J. O., Piepho, H. P., and Valle Zárate, A. (2014). Livestock diversification: An adaptive strategy to climate and rangeland ecosystem changes in southern Ethiopia. *Hum. Ecol.* 42, 509–520. doi:10.1007/s10745-014-9668-2

Mehrabi, Z., Gill, M., Wijk, M. V., Herrero, M., and Ramankutty, N. (2020). Livestock policy for sustainable development. *Nat. Food* 1, 160–165. doi:10.1038/s43016-020-0042-9

Meuwissen, M. P. M., Huirne, R. B. M., and Hardaker, J. B. (2001). Risk and risk management: An empirical analysis of Dutch livestock farmers. *Livest. Prod. Sci.* 69, 43–53. doi:10.1016/s0301-6226(00)00247-5

Munavar, Z., Nicole, W. M., and Dietrich, D. (2016). Farmers' decision-making and land use changes in Kyrgyz agropastoral systems. *Mt. Res. Dev.* 36, 506–517. doi:10.1659/mrd-journal-d-16-00030.1

NSCKR (2020). National statistical committee of the Kyrgyz republic. Available at: http://www.stat.kg/en/.

Opiyo, F. E., Mureithi, S. M., and Ngugi, R. K. (2011). The influence of water availability on pastoralist's resource use in Mwingi and Kitui districts in Kenya. *J. Hum. Ecol.* 35, 43–52. doi:10.1080/09709274.2011.11906389

Ouma, R., Mude, A., and Van De Steeg, J. (2011). Dealing with climate-related risks: Some pioneering ideas for enhanced pastoral risk management in africa. *Exp. Agric.* 47, 375–393. doi:10.1017/s0014479710000888

Packalen, P., Suvanto, A., and Maltamo, M. (2009). A two stage method to estimate species-specific growing stock. *Photogramm. Eng. remote Sens.* 75, 1451–1460. doi:10.14358/pers.75.12.1451

Peng, X., Marchant, M. A., Qin, X. D., and Zhuang, J. (2005). Chinese consumers' preferences for livestock products. *Int. Food Agribus. Manag. Rev.* 8, 62–76. doi:10.22004/ag.econ.8134

Pica-Ciamarra, U., Tasciotti, L., Otte, J., and Zezza, A. (2015). Livestock in the household economy: Cross-country evidence from microeconomic data. *Dev. Policy Rev.* 33, 61–81. doi:10.1111/dpr.12092

Rae, A. N., and Zhang, X. (2009). China's booming livestock industry: Household income, specialization, and exit. *Agric. Econ.* 40, 603–616. doi:10.1111/j.1574-0862.2009.00402.x

Ragie, F. H., Olivier, D. W., Hunter, L. M., Erasmus, B. F. N., Vogel, C., Collinson, M., et al. (2020). A portfolio perspective of rural livelihoods in Bushbuckridge, South Africa. *S. Afr. J. Sci.* 116, 98–105. doi:10.17159/sajs.2020/7522

Rahimon, R. M. (2012). "Evolution of land use in pastoral culture in Central Asia with special reference to Kyrgyzstan and Kazakhstan," in *Rangeland stewardship in central Asia* (Dordrecht: Springer).

Raji, S. A., Odunuga, S., and Fasona, M. (2022). Spatially explicit scenario analysis of habitat quality in a tropical semi-arid zone: Case study of the sokoto-rima basin. *J. Geovis. Spat. Anal.* 6, 11. doi:10.1007/s41651-022-00106-0

Robinson, S., Kerven, C., Behnke, R., Kushenov, K., and Milner-Gulland, E. J. (2016). The changing role of bio-physical and socio-economic drivers in determining livestock distributions: A historical perspective from Kazakhstan. *Agric. Syst.* 143, 169–182. doi:10.1016/j.agsy.2015.12.018

Rosati, F., and Faria, L. G. (2019). Addressing the SDGs in sustainability reports: The relationship with institutional factors. *J. Clean. Prod.* 215, 1312–1326. doi:10.1016/j.jclepro.2018.12.107

Rucker, R. R., Burt, O. R., and LaFrance, J. T. (1984). An econometric model of cattle inventories. *Am. J. Agric. Econ.* 66, 131–144. doi:10.2307/1241030

Ruziev, K., and Majidov, T. (2013). Differing effects of the global financial crisis on the central asian countries: Kazakhstan, the Kyrgyz republic and Uzbekistan. *Europe-Asia Stud.* 65, 682–716. doi:10.1080/09668136.2013.766044

Sabyrbekov, R. (2019). Income diversification strategies among pastoralists in Central Asia: Findings from Kyrgyzstan. *Pastoralism* 9, 14. doi:10.1186/s13570-019-0152-x

Sagynbekova, L. (2017). Environment, rural livelihoods, and labor migration: A case study in Central Kyrgyzstan. *Mt. Res. Dev.* 37, 456–463. doi:10.1659/mrd-journal-d-17-00029.1

Schoch, N., Steimann, B., and Thieme, S. (2010). Migration and animal husbandry: Competing or complementary livelihood strategies. Evidence from Kyrgyzstan. *Nat. Resour. Forum* 34, 211–221. doi:10.1111/j.1477-8947.2010.01306.x

Steimann, B. (2012). "Conflicting strategies for contested resources: Pastoralists' responses to uncertainty in post-socialist rural Kyrgyzstan," in *Pastoral practices in high Asia* (Dordrecht: Springer).

Swanepoel, F., Stroebel, A., and Moyo, S. (2010). *The role of livestock in developing communities: Enhancing multifunctionality*. Johannesburg, South Africa: UJ Press.

Tessema, W. K., Ingenbleek, P. T. M., and van Trijp, H. C. M. (2014). Pastoralism, sustainability, and marketing. A review. *Agron. Sustain. Dev.* 34, 75–92. doi:10.1007/s13593-013-0167-4

Tirkaso, W., and Hailu, A. (2022). Does neighborhood matter? Spatial proximity and farmers' technical efficiency. *Agric. Econ.* 53, 374–386. doi:10.1111/agec.12702

Turner, M. D., and Williams, T. O. (2002). Livestock market dynamics and local vulnerabilities in the sahel. *World Dev.* 30, 683–705. doi:10.1016/s0305-750x(01)00133-4

Umuhoza, J., Jiapaer, G., Yin, H., Mind'je, R., Gasirabo, A., Nzabarinda, V., et al. (2021). The analysis of grassland carrying capacity and its impact factors in typical mountain areas in Central Asia-A case of Kyrgyzstan and Tajikistan. *Ecol. Indic.* 131, 108129. doi:10.1016/j.ecolind.2021.108129

Upton, M. (2004). The role of livestock in economic development and poverty reduction, PPLPI Working Paper No. 10.

Varijakshapanicker, P., Mckune, S., Miller, L., Hendrickx, S., Balehegn, M., Dahl, G. E., et al. (2019). Sustainable livestock systems to improve human health, nutrition, and economic status. *Anim. Front.* 9, 39–50. doi:10.1093/af/vfz041

Wafula, W. M., Wasonga, O. V., Koech, O. K., and Kibet, S. (2022). Factors influencing migration and settlement of pastoralists in Nairobi City, Kenya. *Pastoralism* 12, 2. doi:10.1186/s13570-021-00204-6

Wang, G. G., Wang, M. L., Wang, J. M., Yang, C., and Liu, Y. F. (2016). Characteristics and influencing factors of grass-feeding livestock breeding in China: An economic geographical perspective. *J. Geogr. Sci.* 26, 501–512. doi:10.1007/s11442-016-1282-3

Wang, Y., Yue, H., Peng, Q., He, C., Hong, S., and Bryan, B. A. (2020). Recent responses of grassland net primary productivity to climatic and anthropogenic factors in Kyrgyzstan. *Land Degrad. Dev.* 31, 2490–2506. doi:10.1002/ldr.3623

Wei, Y., and Zhen, L. (2020). The dynamics of livestock and its influencing factors on the Mongolian Plateau. *Environ. Dev.* 34, 100518. doi:10.1016/j.envdev.2020.100518

WHO (2015). *Health in 2015: From MDGs, millennium development goals to SDGs, sustainable development goals*. Geneva: WHO Press.

Wolfenson, D., and Roth, Z. (2019). Impact of heat stress on cow reproduction and fertility. *Anim. Front.* 9, 32–38. doi:10.1093/af/vfy027

World Bank (2016). Country and lending group. Available at: https://data.worldbank.org/about/country-and-lending-groups#Lower_middle_income (Accessed March 10, 2022).

World Bank (2020). Data worldbank. Available at: https://data.worldbank.org/country/kyrgyz-republic?view=chart (Accessed March 10, 2022).

Xu, Y., Zhang, Y., Chen, J., and John, R. (2019). Livestock dynamics under changing economy and climate in Mongolia. *Land Use Policy* 88, 104120. doi:10.1016/j.landusepol.2019.104120

Zeleke, F., Kassie, G. T., Haji, J., and Legesse, B. (2021). Would market sheds improve market participation and earnings of small ruminant keepers? Evidence from Ethiopia. *J. Agric. Econ.* 72, 470–485. doi:10.1111/1477-9552.12411

Zhang, M. A., Borjigin, E., and Zhang, H. (2007). Mongolian nomadic culture and ecological culture: On the ecological reconstruction in the agro-pastoral mosaic zone in Northern China. *Ecol. Econ.* 62, 19–26. doi:10.1016/j.ecolecon.2006.11.005

Zhao, X., Zhao, L., Li, Q., Chen, H., Zhou, H., Xu, S., et al. (2018). Using balance of seasonal herbage supply and demand to inform sustainable grassland management on the Qinghai-Tibetan Plateau. *Front. Agric. Sci. Eng.* 5, 1–8. doi:10.15302/j-fase-2018203

frontiers | Frontiers in Environmental Science

TYPE Original Research
PUBLISHED 04 January 2023
DOI 10.3389/fenvs.2022.1056042

Check for updates

OPEN ACCESS

EDITED BY
Yiyun Chen,
Wuhan University, China

REVIEWED BY
Chenxi Li,
Xi'an University of Architecture and Technology, China
Tianyu Lv,
Huazhong Agricultural University, China

*CORRESPONDENCE
Can Li,
lican3008@126.com
Zhongjiang Feng,
fengzhongjiang@163.com
Xiaomiao Feng,
fengxm0310@126.com

SPECIALTY SECTION
This article was submitted to Environmental Informatics and Remote Sensing,
a section of the journal
Frontiers in Environmental Science

RECEIVED 28 September 2022
ACCEPTED 05 December 2022
PUBLISHED 04 January 2023

CITATION
Li C, Wei W, Duan Y, Feng Z, Feng X, Zhu C and An P (2023), Exploration of the regional correlation and network structure characteristics of land prices: A case study of Hebei, China.
Front. Environ. Sci. 10:1056042.
doi: 10.3389/fenvs.2022.1056042

COPYRIGHT
© 2023 Li, Wei, Duan, Feng, Feng, Zhu and An. This is an open-access article distributed under the terms of the Creative Commons Attribution License (CC BY). The use, distribution or reproduction in other forums is permitted, provided the original author(s) and the copyright owner(s) are credited and that the original publication in this journal is cited, in accordance with accepted academic practice. No use, distribution or reproduction is permitted which does not comply with these terms.

Exploration of the regional correlation and network structure characteristics of land prices: A case study of Hebei, China

Can Li[1,2]*, Wei Wei[3], Yajing Duan[4], Zhongjiang Feng[1,2]*, Xiaomiao Feng[5]*, Chenming Zhu[1] and Pengfei An[1]

[1]School of Geographical Sciences, Hebei Normal University, Shijiazhuang, China, [2]Hebei Key Laboratory of Environmental Change and Ecological Construction, Shijiazhuang, China, [3]Chengde No. 2 High School, Chengde, China, [4]Shijiazhuang Public Resources Trading and Service Center, Shijiazhuang, China, [5]College of Resources and Environment, Shijiazhuang University, Shijiazhuang, China

It is important to explore the correlation characteristics of land markets among cities in order to promote coordinated developments. Based on the residential land prices in 168 counties in Hebei Province, this study used spatial econometric models and social network analysis to analyze the regional correlation effect and network structure evolution characteristics of residential land prices. The results indicated that: 1) the regional residential land price level has significant global spatial autocorrelation and local autocorrelation. High-High clusters were concentrated in cities around Beijing and Tianjin and provincial capitals, while Low-Low clusters were mostly distributed in central and southern Hebei. 2) The direct effect and spillover effect of influencing factors of residential land price were significantly different. The residents' purchasing power, the socioeconomic level, and the land resources had significant impacts on the residential land price of the county itself, while the level of infrastructure and the policy environment had significant impacts on the residential land price of neighboring counties. 3) The degree centrality and betweenness centrality of residential land price in central counties of Hebei Province was generally high, showing a trend of agglomeration. However, the peripheral cities of Hebei Province lacked important central nodes in the network structure. From 2013 to 2020, increasing numbers of counties had shown the transmission function of "bridge," and the balance of land price in the whole region had been constantly improved. The study found that the regional residential land price itself had spatial autocorrelation, and the spillover effect of its related factors was also the driving force that affects the transmission and diffusion of land price between counties. The change in the spatial network of county residential land price was primarily manifested in the transmission process starting from the central cities. The tightness of the spatial network was related to the number and distribution of central nodes. Hebei Province should focus on cultivating urban central nodes with development potential in marginal areas, create more land market growth poles according to local conditions, and accelerate the

integration of land factor markets in Beijing, Tianjin, and Hebei to achieve healthy and balanced development of residential land prices. This study made up for the shortcomings of previous studies on land price correlations. The combination of correlation feature analysis and spatial network structure analysis was more helpful to reveal the characteristics of regional land price development, and the results could provide a reference for the formulation of urban land market regulation policies.

KEYWORDS

regional correlation effect, spatial network structure, social network analysis, residential land price, spatial econometric model

1 Introduction

The land price is an important manifestation of the relationship between land supply and demand that reflects the interaction between land resources, the surrounding socioeconomic conditions and the ecological environment (Huang and Du, 2021), (Glumac et al., 2019). The land price provides feedback for the operation of the land market and plays an important role in the optimal allocation of land resources (Huang et al., 2022). The residential land price is a key part of the price of housing, and it is closely related to the operating mechanism of the real estate market, the level of urbanization, the degree of social and economic development, and the level of people's livelihood (Davis and Palumbo, 2008). Influenced by regional economic and natural endowment differences, urban residential land prices show strong regional heterogeneity. However, due to the existence of capital flow, population migration, economic cooperation, and other functions between cities, residential land prices will naturally produce spatial correlation in theory. The so-called spatial correlation of urban residential land price refers to the manifestation of the interaction between urban residential land price and its influencing factors in space. Due to the difference of land price level, there are also differences in the spatial connection of land prices among cities, thus forming several urban agglomeration collectives. There is attraction within the urban agglomeration that can generate a networked spatial structure and enhance the cohesion so as to optimize the allocation of land elements and promote the development of each city within the urban agglomeration (Liang et al., 2015).

In recent years, most studies on land prices has focused on the driving mechanisms of influencing factors and the spatio-temporal differentiation characteristics of land prices. The research on influencing factors has involved the identification and quantification of factors. Some studies have constructed a multi-factor land price characterization system and revealed the comprehensive driving mechanisms of multi-factor land prices. Brano formed a set of characteristic variables that can explain the price of land in Luxembourg, including Accessibility, Proximity, Physical, Legal, Social, and Economic factors (Glumac et al., 2019). Song Jianan constructed a characteristic system of urban residential land prices in China comprising four variables: land supply and demand, economic level, social level, and policy impact (Song et al., 2011a). Han Juan constructed a characteristic system of urban residential land prices in China by choosing three variables: urban location, development potential, and socioeconomic level (Han et al., 2017). Some studies have investigated the mechanism of certain factors on land price such as population structure and distribution (Song et al., 2022), regional environment (Zhu et al., 2018), urban traffic conditions (Shen and Karimi, 2017), (Sohn, 2014), and national land policy (Gyourko and Jacob, 2021), (Liu et al., 2022). The research on the spatio-temporal differentiation characteristics of land price has included the exploration of the non-stationarity in time and heterogeneity in space of land prices and the associated influencing factors. Relevant results have confirmed that plot ratio, public facilities, population, and environmental factors have different effects on land price in different regions (Kheir and Boris, 2016). The impact of natural facilities and educational facilities on the surrounding land price would gradually increase over time, while the impact of commercial facilities and public transport would continue to decline (Zhang et al., 2021). The above achievements have provided a good foundation for the research on spatial correlation of land prices and the spatial network structure.

In studies of the spatial correlation effect on residential land prices, researchers have explored the characteristics of spatial correlation of land prices and analyzed the influencing factors of the spatial correlation effect. The current studies have generally focused on a single city or several adjacent cities in a region. It is believed that the urban land price is rising rapidly in the time dimension while showing relevance in the spatial dimension (Griffin et al., 2015). Most researchers have attributed the factors of land price correlation to geographical proximity and have concluded that the closer the geographical distance, the stronger the land price correlation between cities (Harris et al., 2013), (Zhan et al., 2011). Geographic proximity creates conditions for spatial correlation of land prices between neighboring cities, but for distant cities, the impact of geographic proximity decreases with the increase of spatial distance (Zhou and Tang, 2019). For land prices, the spillover effect is an important factor that leads to the land price correlations between neighboring cities. The

spillover effect is reflected in the price transmission between geographical neighboring regions. The land price fluctuation in neighboring regions will have a significant impact on the local land price (Zhou and Tang, 2019). This rule applies not only to land prices but also to housing prices, which had been confirmed in city agglomerations in different countries such as the United Kingdom (Meen, 1999), the United States (Stephen, 1999), Australia (Tu, 2000) and China (Wang et al., 2016), (Zhang et al., 2015), (Liu and Chen, 2013). In addition to land price itself, frequent interactions of land price related factors between cities could also lead to land price related effects. Land price related factors such as urban traffic conditions (Okamoto and Sato, 2021), (Niu et al., 2021), administrative proximity (Zeng, 2019), and regulatory policies (Zheng et al., 2021) could link land price fluctuations by promoting the full flow of resources and information elements between regions. The government should implement land policy according to the distribution and flow of land elements and improve and adjust the land supply and demand structure in order to promote the stable and healthy operation of the local housing market (Tsai, 2018). The influence mechanism of land price related factors on land price correlation has become a trend in land price spatial correlation research, but there are few relevant achievements at present.

In terms of the research on the spatial network structure of residential land price, with the accelerated flow of elements between cities, studies no longer limit their research perspective to the spatial distribution pattern of residential land prices, but focus more on the spatial network structure between cities because of the relationship between regional residential land prices, focusing on the formation process and drivers of the spatial network structure of residential land prices. Relevant results have shown that the number of spillover relationships between real estate prices in most cities far exceeded the number of neighboring cities, indicating that the real estate linkage between multiple cities had broken through the "neighborhood effect" in the simple geographical sense and presented a complex network structure (Huang et al., 2009), (Zhang and Lin, 2015). The rapid progress of market integration and informatization has strengthened the long-distance transmission of resources and information and the ability to trade goods and personnel. This increases the closeness of the connection between residential land prices in different cities and makes the network characteristics more prominent (Gan and Huo, 2016). As to the reasons for the formation of the spatial network structure of land prices, most researchers believe that the spatial transmission of real estate prices has a certain regularity, and the land prices in some areas would lead to changes in the surrounding areas after the first price change. Family migration, wealth transfer, spatial arbitrage, and other factors as well as market heterogeneity factors such as regional land market development level and public expectations were the main reasons for the emergence of land price spatial networks (Elias, 2006). Some researchers also believe that the "ripple effect" of land price is related to the definition of geographical regions, and the mode of land price transmission was clear only between continuous geographical regions (Pollakowski and Ray, 1997), (Wang et al., 2008). With the frequent flow of factors among cities and the increasingly close cooperation relationships, the closeness of social and economic development levels, resource endowment, and infrastructure construction determine the form and characteristics of urban land price related networks and also affect the position and role of each city in the land price transmission process (Zhou et al., 2020).

In terms of research methods, exploratory spatial data analysis, spatial econometric models (Juethe and Pede, 2011), Geographically Weighted Regression models (Harris et al., 2013), (Nilsson, 2014) and hedonic price models (Zhu et al., 2014) are widely used in the research on spatial correlation effects and driving factors of residential land prices. These methods play important roles in analyzing the spatial differentiation characteristics of residential land prices. Spatial econometric models are used to study the spatial correlation and heterogeneity of economic phenomena. These models pay more attention to the spatial relationships between things, and they have advantages in finding the mechanism of the influence of land price-related factors on land price correlation (Cheng et al., 2020). Social network analysis methods are generally used to discuss the network types and development laws in urban industrial development (Fu, 2021), tourism economic development (Gan et al., 2021), ecological efficiency (Xu et al., 2020), land use efficiency (Xia et al., 2020), spatial planning (Bacău et al., 2020) and other fields in the region, while application to research on real estate prices is relatively rare. In recent years, only a few researchers have used the social network analysis methods to investigate the network structure characteristics of real estate price linkage between cities. However, these studies have verified the applicability of social network analysis methods in the real estate market, and they could provide data support and a theoretical basis for different cities to formulate targeted regulatory policies.

To sum up, most studies have confirmed that urban land prices generally have regional correlation effects and network morphological characteristics that can achieve optimal allocation of land resources to a large extent. However, there are two aspects worth further exploration: First, the existing studies often discuss the conduction and correlation of land price itself, ignoring the spatial correlation effect of land price-related factors (Peng et al., 2019), (Hu et al., 2016), (Griffin et al., 2015), and thus the influence mechanism of related factors on land price correlation needs further exploration. Second, there are few studies on the combination of regional residential land price correlation effect and spatial network structure. Most studies have focused on the analysis of land price correlations between cities, primarily considering the geographical "neighborhood" effect or "regional" effect, factors with which it is difficult to grasp

the overall characteristics of land price linkage. The analysis of the correlation effect of regional residential land prices and the spatial network structure is more helpful to comprehensively reveal the regional local and overall residential land price development characteristics. Three, most of the current studies have focused on urban scale residential land price correlation characteristics, while few studies have focused on the county scale. The correlation characteristics of land prices at different scales may be different. The study of small-scale unit land prices is more conducive to the government being able to formulate effective regulation policies. The spatial effect of residential land prices at the county level needs to be explored.

In recent years, the process of urbanization in China has accelerated significantly, and the demand for land has increased. The residential land market is becoming more competitive (Jiang et al., 2021). Hebei Province, which is the main region used to relieve Beijing's non-capital functions, is accelerating the integration of its land market. The complementary characteristics of land resources between regions are becoming more prominent (Ma et al., 2020), and the cross-border exchanges in land markets between regions are also increasing (Wang et al., 2020). In China, the rational use of land resources is the key to promoting industrial transfer from Beijing and Tianjin (Luo et al., 2021). However, it is unknown whether correlations exist among the elements of land resources in Hebei or how to coordinate the development of the inter-city residential land markets. These questions need to be answered.

The present study considered 168 counties in Hebei Province as the research object. We used the spatial econometric model to analyze the regional correlation effect of residential land prices in the region and used social network analysis methods to explore the structural characteristics of the overall regional residential land price network. This study explains the influence mechanisms of relevant factors on spatial correlation of residential land prices through the estimation results of direct and spillover effects, examines the status and role of each county in the residential land price linkage network through the measurement results of degree centrality and intermediary centrality, and depicts the overall network structure characteristics of residential land price linkage through the measurement results of network density, and agglomeration subgroups. This study answers the following three questions. What factors affect the linkage of residential land prices in different regions? What is the position and role of local residential land prices in this linkage network? What are the characteristics of the network structure of the linkage of land prices in different regions? Based on the answers to the above questions, the study has important theoretical significance and application value to improve the accuracy of residential land price regulation policy and build a coordinated regulation mechanism of cross-regional land markets.

2 Research area, data, and methods

2.1 Research area

The total area of Hebei Province is 188,000 km^2, accounting for 1.96% of China's total area. It is the only province in the country with plateaus, plains, mountains, hills, lakes, and seashores. Hebei Province includes Shijiazhuang, Baoding, Langfang, Tangshan, Cangzhou, Handan, Xingtai, Chengde, Zhangjiakou and Hengshui, 11 prefecture-level cities and 168 county-level administrative units. In 2020, the GDP of Hebei Province was 3620.69 billion yuan. Tangshan, Shijiazhuang, and Cangzhou ranked the top three contributors to GDP, with 721.09 billion yuan, accounting for 19.9%, 16.4%, and 10.2% respectively. The *per capita* GDP of Hebei Province was 48,564 yuan, a year-on-year growth rate of 4.78%. The permanent population of Hebei Province was 74.6384 million, accounting for 5.28% of the national population. Shijiazhuang had the highest population with 10.6471 million people. The population of Hebei Province is concentrated in the central and southern plains, and the population in the northern mountainous areas is sparsely distributed. Differences in the economic level and population density among cities contribute to the unbalanced nature of urban land prices. In 2020, the average residential land price in Hebei Province was 5278 yuan/m^2, with significant regional differences. The average residential land prices in Tangshan, Langfang and Baoding were high, at 8668 yuan, 6675 yuan, and 6580 yuan/m^2, respectively. In 2020, there was an investment of 581.7 billion yuan to increase the transportation volume in Hebei Province, a rise of 3.4%. Hebei Province had 7941 km of railways and 204,737 km of highways, forming a modern comprehensive transportation system with multiple modes of transportation. Hebei Province had an annual passenger volume of 182 million and a freight volume of 2.478 billion tons in terms of external connections. There are close economic ties between cities in Hebei Province, and these are increasing in the current social and economic conditions (Figure 1).

2.2 Materials and methods

This study applied spatial autocorrelation analysis, spatial econometric modelling, and social network analysis. Spatial autocorrelation analysis is the core content of spatial correlation analysis and is also an important prerequisite for spatial econometric analysis. Spatial autocorrelation analysis determines whether residential land prices are spatially relevant by measuring the degree of spatial correlation and difference, and the analysis can identify the regional

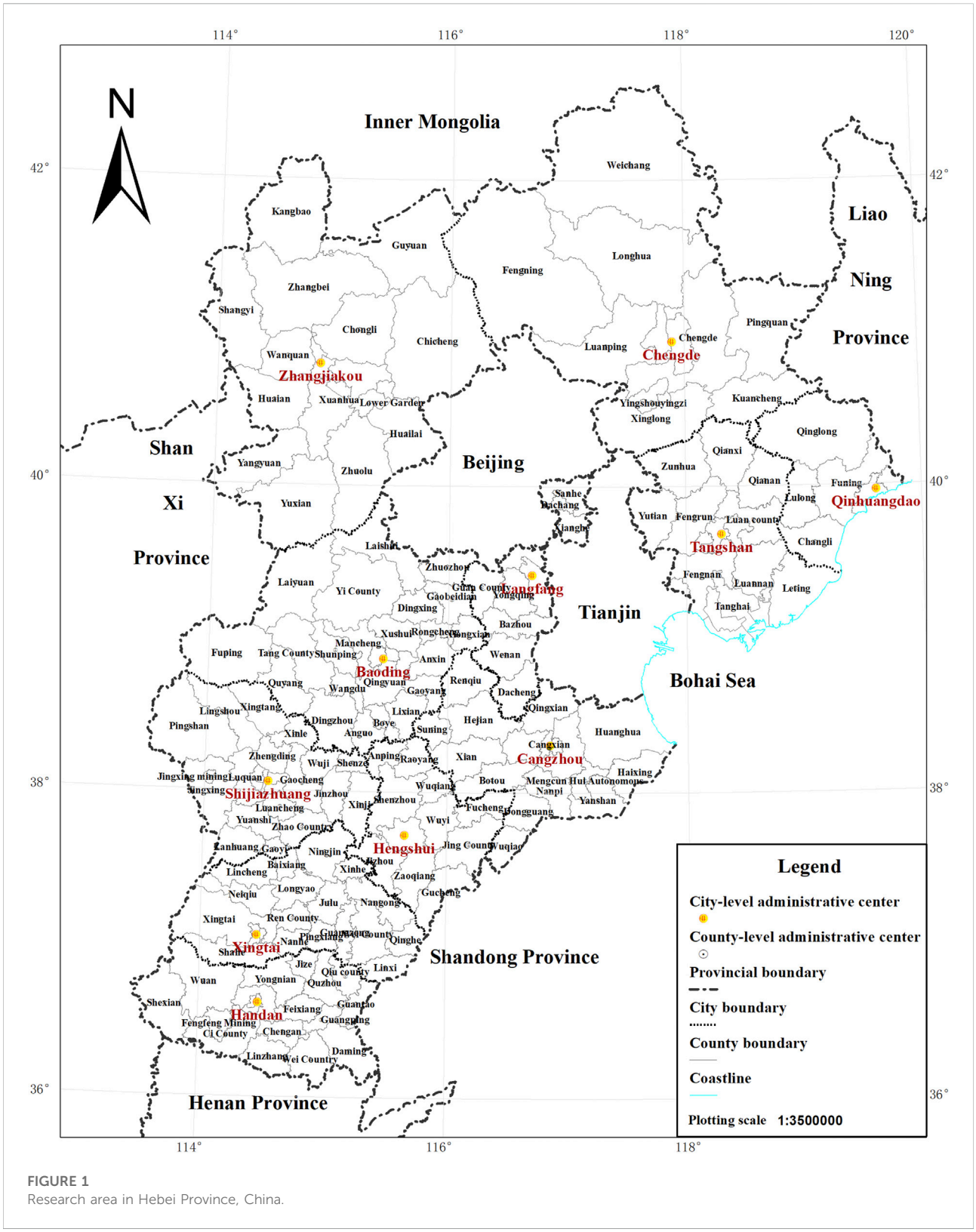

FIGURE 1
Research area in Hebei Province, China.

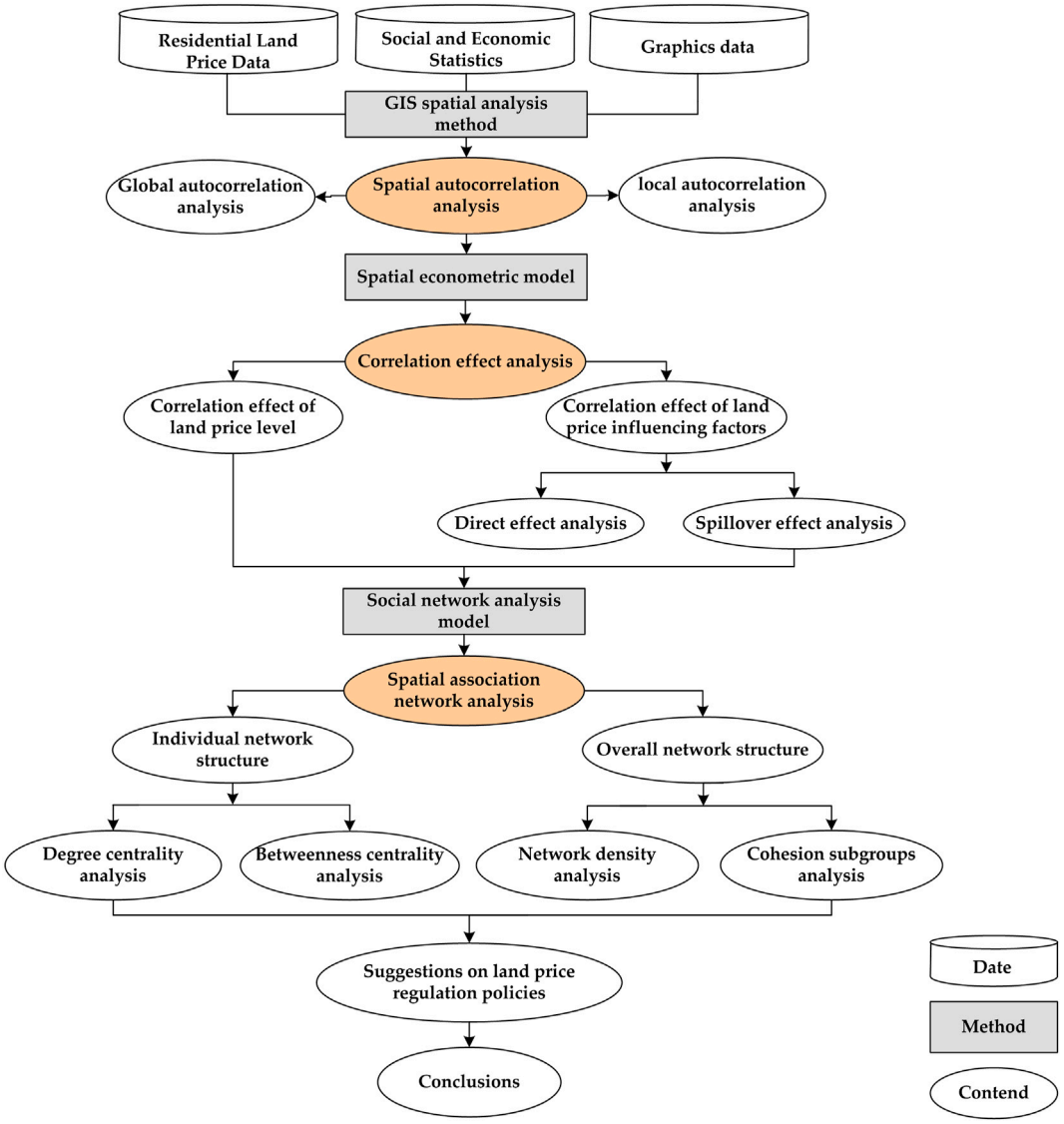

FIGURE 2
Flow chart of the study.

correlation characteristics of residential land prices at different levels. Spatial econometric analysis pays more attention to the spatial relationship between things and can further identify the impact mechanism of relevant factors on the spatial correlation of residential land prices and reveal the regional correlation characteristics of land price driving factors. Social network analysis can clarify the status and role of each region in the land price linkage network and depict the overall network structure characteristics of residential land price linkage. The combination of spatial autocorrelation analysis, spatial econometric analysis, and social network analysis is helpful to fully reveal the regional local and overall land price development characteristics. A flow chart of the study is presented in Figure 2.

2.3 Data and pre-processing

2.3.1 Residential land price data

This study took 168 county-level administrative units in Hebei Province as the research object. The research time span was from 2013 to 2020. The data included residential land transaction data and socio-economic data for each county in Hebei Province. The transaction data of residential land is obtained through China Land Market Network (https://www.landchina.com/#/), and the websites of natural resource bureaus of various cities, and field research. The transaction data of residential land included information such as the name, location, land use, area, land use period, land source, land

TABLE 1 Data source overview.

Data name	Main contents	Main source	Quantity obtained
Residential land transaction data	Name, location, land use, area, land use period, land source, land supply method, transaction price, plot ratio, and contract signing date	1. China Land Market Network (https://www.landchina.com/#/)	Data of 168 counties from 2013 to 2020, a total of 14,460 residential land transaction data
		2. The websites of natural resource bureaus of various cities	
Socio-economic data	New residential building area、*per capita* disposable income、Resident deposit savings、Average salary of employees、Urban road area *per capita*、Population density、Urbanization rate、Tax	1. China Urban Statistical Yearbook	Data of 168 counties from 2013 to 2020, a total of 10,752 indicators data
		2. Hebei Economic Yearbook	
		3. Hebei Urban Construction Statistics Annual Report	
		4. Hebei Statistical Yearbook	

TABLE 2 Descriptive statistics for variables related to spatial analysis.

Variable types	Variable name	Symbol	Average	Standard deviation	Maximum	Minimum	Define
Explained variable	Residential land price	P	7.35	0.68	9.78	5.25	Total transaction price/Total transaction area, unit: yuan per square meter
Land resources	New residential building area	X1	8.46	0.57	9.90	6.10	Unit: hectare
Residents' purchasing power	*per capita* disposable income	X2	10.13	0.24	10.7	9.23	Unit: Yuan per person
Socioeconomic level	Resident deposit savings	X3	51.06	19.95	100	12.44	Unit: million
	Average salary of employees	X4	10.81	0.28	11.62	10.12	Unit: yuan
Infrastructure	Urban road area *per capita*	X5	3.60	1.11	7.05	0.70	Unit: hectare
Population size	Population density	X6	7.87	0.59	9.24	5.72	Regional resident population/Built-up area, unit: people per square kilometer
Urban development level	Urbanization rate	X7	10.90	0.73	13.23	8.90	Unit: Number of households
Policy environment	Tax	X8	11.47	1.01	14.00	8.65	Unit: million

Note: Statistical results of all variables except the unit of % are logarithmic.

supply method, transaction price, plot ratio, and contract signing date. Socio-economic data included Per capital disposable income, Resident deposit savings, Average salary of employees, Population density, Urbanization rate, *etc.* which were derived from Various statistical yearbooks of Hebei Province from 2013 to 2020. The transaction data of residential land was mainly used to calculate the residential land price in different years in each county, and the socio-economic data was mainly used to build the indicator system of influencing factors of residential land price. See Table 1 for data source overview.

2.3.2 Social and economic data

To ensure the accuracy of model estimation and objectively reflect the relationship between residential land prices in the region, research on the regional correlation effect of residential land prices needs to consider both the single interaction of residential land prices between cities, and also other variables that affect residential land prices. According to the principles of regional differences, operability, and comparability (Liu et al., 2019), (Song et al., 2011b), (Lesage and Pace, 2009), we selected eight land price influencing factors, including land resources,

TABLE 3 Test results of KMO and Bartlett.

Kaiser–Meyer–Olkin measure of sampling adequacy		.852
Bartlett's sphericity test	Approximate chi-square	2631.346
	Df	200
	Sig	.000

TABLE 4 Reliability statistics results.

Variable	Cronbach's alpha	Number
X1- X8	0.945	8

residents' purchasing power, socioeconomic level, infrastructure, population size, urban development level, and the policy environment based on existing achievements. The data for these indicators were derived from China Urban Statistical Yearbook, Hebei Economic Yearbook, Hebei Urban Construction Statistics Annual Report, and the Statistical Yearbook of Cities in Hebei Province. To reduce the influence of strong fluctuations in the data, the natural logarithm of the original data of all variables was calculated (Table 2).

In order to ensure the scientific rationality of the survey data, we used the relevant research methods of Chenxi Li et al. (2021) to verify and analyze the quality of the survey data, including data validity test and reliability analysis.

Validity analysis mainly includes content validity and structure validity. The scientificity of the indicator types used in this study had been verified by relevant literatures. The data were from the land market transaction data published by the government and the publicly issued yearbook data. Combined with the theoretical elements of the literature and the realistic elements of the data source, the content validity of the data meets the requirements. Structural validity refers to the corresponding relationship between the framework and the measured value, usually using exploratory factor analysis. In this study, KMO and Bartlett's sphericity test were used to measure the correctness of the selected measurement variables. The KMO value calculated by SPSS statistics is 0.852, greater than 0.7, Bartlett's approximate chi square value is 2631.346, and the Sig. value is .000, less than .05 (Table 3). This showed that the research data is effective and suitable for subsequent spatial autocorrelation analysis and spatial econometric analysis.

Among the reliability analysis methods, Cronbach analysis is the most widely used measurement method, which directly used the reliability coefficient value(α) to describe the level of reliability. In order to further test the authenticity and credibility of the data, this study used Cronbach reliability analysis method to measure the reliability level of the data. If the coefficient of Cronbach's $\alpha \geqq 0.7$, it indicates that the data reliability is acceptable, and the larger the reliability coefficient value, the better (Feng and Tian, 2011), (Chai et al., 2019). Calculated by SPSS statistics, the coefficient of Cronbach's α of the total amount table was 0.956, which met the standard. This proved the reliability of the study data (Table 4).

2.4 Methods

2.4.1 Inspection method

2.4.1.1 Spatial autocorrelation

Moran's I was used to test the global spatial autocorrelation of residential land prices and provide a basis for the selection of subsequent spatial econometric models. The value range of Moran's I was [−1, 1]. If the Moran's I value was greater than 0, it meant that the residential land price showed a positive spatial correlation. When the index was closer to 1, there was a closer relationship between residential land prices among counties. If the Moran's I was equal to 0, it means that there was no spatial autocorrelation for residential land prices. If the Moran's I was less than 0, it indicated that there was a negative spatial correlation between residential land prices. When the Moran's I was close to −1, there was a greater difference in residential land prices among counties. The calculation formula is as follows:

$$I = \frac{\sum_{i=1}^{n}\sum_{j=1}^{n} W_{ij}\left(X_i - \bar{X}\right)\left(X_j - \bar{X}\right)}{S^2 \sum_{i=1}^{n}\sum_{j=1}^{n} W_{ij}},\ S^2 = \frac{1}{n}\sum_{i}^{n}\left(X_i - \bar{X}\right) \quad (1)$$

where I is the global Moran's index; X_i and X_j are the residential land prices of county i and j; n is the number of counties and districts; W_{ij} is the spatial weight matrix of county i and j; $\bar{X}$ is the average residential land price in the counties and districts of Hebei Province.

To further identify the spatial agglomeration characteristics of residential land prices among local counties and districts, this study used local Moran's I to measure the correlation between the residential land price in a county and in its neighboring counties. The value range of the local Moran's I_i was [−1, 1]. If Moran's I_i was greater than 0, it meant that the residential land price was spatially positively correlated, e.g., the residential land price between counties and districts had a "High–High" or "Low–Low" cluster phenomenon. If the Moran's I_i was equal to 0, it meant that there was no spatial autocorrelation for residential land prices. If the Moran's I_i was less than 0, it

meant that the residential land price was negatively correlated with space, and there was a "High–Low" or "Low–High" cluster phenomenon.

$$I_i = \frac{\sum_{j \neq i}^{n} W_{ij}(X_i - \bar{X})(X_j - \bar{X})}{\frac{1}{n}\sum(X_i - \bar{X})^2} \quad (2)$$

where I_i is the local Moran's I of county i; X_i and X_j are the residential land prices of counties i and j; n is the number of counties; W_{ij} is the spatial weight matrix of counties i and j; $\bar{X}$ is the average of residential land prices in counties and districts of Hebei Province.

2.4.1.2 Basic regression test

Before the quantitative regression of county residential land prices, this study considered whether there were certain constraints between the assumed factors. The three main test methods for econometric models are the Lagrange multiplier (LM) test, Wald test, and likelihood ratio (LR) test. These three methods were used to test whether the constraints we set were established, and methods were tested in turn. The LM test was used to assess whether there was a serial correlation in the residual series of the model. It can supplement the Moran's I estimation results and improve the accuracy of the spatial dependence estimation of the residential land price model. The LM statistic is defined as:

$$LM = \hat{\lambda}'\left[Var(\hat{\lambda})\right]^{-1}\hat{\lambda} \xrightarrow{d} \chi^2(K) \quad (3)$$

where λ is the Lagrange multiplier vector; $Var(\hat{\lambda})$ is a covariance matrix; K is the number of constraints (the number of explanatory variables); $\hat{\lambda} \xrightarrow{d} \chi^2$ means that the sample follows a normal distribution.

The Wald test and LR test were used to select and determine the applicable form of the specific spatial econometric model. In the Wald test, if the p-value of the Wald-lag test was significant, and the p-value of the Wald-error test was not significant, the Spatial Lag Model (SLM) was applicable. If the p-value of the Wald-lag test was not significant, and the p-value of the Wald-error test was significant, the Spatial Error Model (SEM) model was applicable. If the p-values of both the Wald-error test and the Wald-error test were significant, then the Spatial Dubin Model (SDM) model was used. The Wald statistic is defined as:

$$Wald = (\hat{\beta}_U - \hat{\beta}_R)'\left[Var(\hat{\beta}_U)\right]^{-1}(\hat{\beta}_U - \beta_0) \xrightarrow{d} \chi^2(K) \quad (4)$$

Where $\hat{\beta}_U$ represents an unconstrained estimator; $\hat{\beta}_R$ represents a constrained estimator; β_0 means known parameters.

In the LR test, if the p-value of the LR-lag test was significant, but the p-value of the LR-error test was not significant, then the SLM model was applicable. If the p-value of the LR-lag test was not significant, but the p-value of the LR-error test was significant, then the SEM model was applicable. If the p-value of both the LR-lag test and the LR-error test were significant, then the SDM model was used. The LR statistic is defined as:

$$LR = -2\ln\left[\frac{L(\hat{\beta}_R)}{L(\hat{\beta}_U)}\right] = 2\left[\ln L(\hat{\beta}_R)\right] \xrightarrow{d} \chi^2(K) \quad (5)$$

where $L(\hat{\beta}_U)$ represents the unconstrained likelihood function maximum; $L(\hat{\beta}_R)$ represents the constrained likelihood function maximum.

After determining the specific form of the model, we needed to analyze its internal effect dimensions. We selected a fixed effect and a random effect using the Hausman test. If the p-value of the Hausman test was high, the fixed effect model was used, otherwise the random effect was used. The Hausman statistic is defined as:

$$(\hat{\beta}_{FE} - \hat{\beta}_{RE})'\left[Var(\hat{\beta}_{FE}) - Var(\hat{\beta}_{RE})\right](\hat{\beta}_{FE} - \hat{\beta}_{RE}) \xrightarrow{d} \chi^2(K) \quad (6)$$

where $\hat{\beta}_{FE}$ is the fixed effects estimator; $\hat{\beta}_{RE}$ is the random effects estimator.

2.4.2 Spatial econometric model

In theory, the frequent interaction of land price related factors between cities leads to the correlation of land price. The change of related factors of land price in any region will not only affect its land price level, but also affect the land price level of the region with spatial correlation. Spatial econometric model is introduced in this study to explore the direct and indirect effects of related factors on residential land prices in various regions, and to reveal the influencing mechanism of related factors on the correlation of land prices. The spatial econometric model incorporated spatial effects into the model, which addressed the spatial dependence problem in the traditional linear regression model and measured the interaction between various factors that influenced the residential land price in counties and districts. The spatial Durbin model is a generalized form of the spatial econometric model, containing both endogenous interaction effects (WY) and exogenous interaction effects (WX). The spatial Durbin model was able to explore the regional correlation effect of the residential land price and the correlation path of each influencing factor from the dimensions of the intrinsic direct effect and the extrinsic spillover effect in the application process. The calculation is as follows:

$$Y_{it} = c + \rho W Y_{it} + \alpha X_{it-1} + \beta W X_{it-1} + \varepsilon_{it} \quad (7)$$

where Y_{it} is the explained variable (residential land price); X is the explanatory variable matrix (the influencing factors of residential land prices); ρ, α, β are the coefficients to be estimated; ε is the residual; i is the county, t is the year; W is the spatial weight matrix. The test of a correlation effect on residential land prices

between counties and districts was whether the coefficient ρ in the model was significant. If ρ was significant, this meant that the residential land price of a county was affected by other counties and districts, and there was a correlation effect. If ρ was not significant, this meant that the residential land price in a county was not affected by other counties and districts, and there was no correlation effect.

In the model, the parameter estimation results of each influencing factor cannot directly characterize the specific correlation path of the residential land price. Therefore, on the basis of the research of LeSage (Fu, 2021) and others, this study used partial differential decomposition to decompose the impact of various influencing factors on residential land prices into direct effects and spillover effects. The expression is adjusted as follows:

$$Y = (I - \rho W)^{-1}(\alpha X + \beta W X) + (I - \rho W)^{-1}\varepsilon \tag{8}$$

transform the expression:

$$Y = \sum_{r=1}^{k} S_r(W) X_r + V(W)\varepsilon \tag{9}$$

$$V(W) = (I - \rho W)^{-1} = I + \rho W + \rho^2 W^2 + \rho^3 W^3 + \ldots \text{ is space multiplier matrix} \tag{10}$$

$$S_r(W) = V(W)(I\alpha_r + \beta_r) \tag{11}$$

The matrix form is as follows:

$$\begin{bmatrix} Y1 \\ Y2 \\ Y3 \\ Y4 \end{bmatrix} = \sum_{r=1}^{k} \begin{bmatrix} S_r(W)_{11} & S_r(W)_{12} & \cdots & S_r(W)_{1n} \\ S_r(W)_{21} & S_r(W)_{22} & \cdots & S_r(W)_{2n} \\ & \vdots & & \\ S_r(W)_{n1} & S_r(W)_{n2} & \cdots & S_r(W)_{nn} \end{bmatrix} \begin{bmatrix} X_{1r} \\ X_{2r} \\ \vdots \\ X_{nr} \end{bmatrix} + V(W)\varepsilon \tag{12}$$

where $S_r(W)_{ij}$ represents the ith and jth factors in $S_r(W)$, and $V(W)_i$ represents the ith row in $V(W)$, and thus the expression is as follows:

$$Y_i = \sum_{i=1}^{k} \left[S_r(W)_{i1} + S_r(W)_{i2} X_{2r} + \cdots S_r(W)_{in} X_{nr} \right] + V(W)_i \varepsilon \tag{13}$$

where the diagonal mean $S_r(W)_{ii}$ represents the direct effect value, indicating that the change of the influencing factor r of a county will play an elastic role in the local residential land price. The non-diagonal mean $S_r(W)_{ij}$ represents the indirect effect value, indicating that the change of the influencing factor r of one county will have an overflow effect on the residential land price in other counties in the region. The mean value of the matrix row (column) $S_r(W)$ represents the comprehensive value of the spatial effect, representing the degree to which a county influencing factor affects the total residential land price in the area.

2.4.3 Social network analysis

The current study formed a county-level association network system of residential land prices by connecting the residential land price nodes in the counties of Hebei Province. By observing the characteristics of network centrality, network density, and agglomerated subgroups, we were able to analyze the organizational structure characteristics of the regional residential land price spatial network in Hebei Province. This analysis helped to identify the role and status of residential land prices in each county in the network structure, the degree of connection, and the characteristics of regional subgroups.

2.4.3.1 Network centrality calculation method

Network centrality is an important indicator to measure the degree of centralization of residential land price nodes. Network centrality can be divided into point degree centrality, closeness centrality and betweenness centrality.

Point degree centrality represents the influence and competitiveness of a land price node. Counties with higher centrality have a higher land price influence. The expression is as follows:

$$C_{RD}(i) = \frac{C_{AD}(i)}{n-1} \tag{14}$$

where $C_{RD}(i)$ is the relative degree centrality of city i; $C_{AD}(i)$ is the absolute degree centrality of city i, and n is the number of other cities connected to city i in the network.

Betweenness centrality represents the degree of connection between residential land price nodes. It is used to measure the ability of a land price node to be unaffected by other nodes. When the degree of the node is higher, it has a stronger ability to transmit and control information, and a higher degree of linkage to the spatial network. The expression is as follows:

$$C_{RBi} = \frac{2C_{ABi}}{n^2 - 3n + 2} = \frac{2\sum_{j}^{n}\sum_{k}^{n} b_{jk}(i)}{n^2 - 3n + 2} \tag{15}$$

where C_{RBi} is the relative betweenness centrality of city i; C_{ABi} is the absolute betweenness centrality of city i.

2.4.3.2 Network density calculation method

Network density was used to measure the degree of connection between all nodes in the network structure, which showed the cohesion of the spatial network. It could comprehensively reflect the impact of the residential land price spatial network on each land price node and the closeness of the communication between each node. When the network density value was high, there was a greater effect of the spatial network on the land price nodes, there was a higher degree of interaction between the land price nodes, and

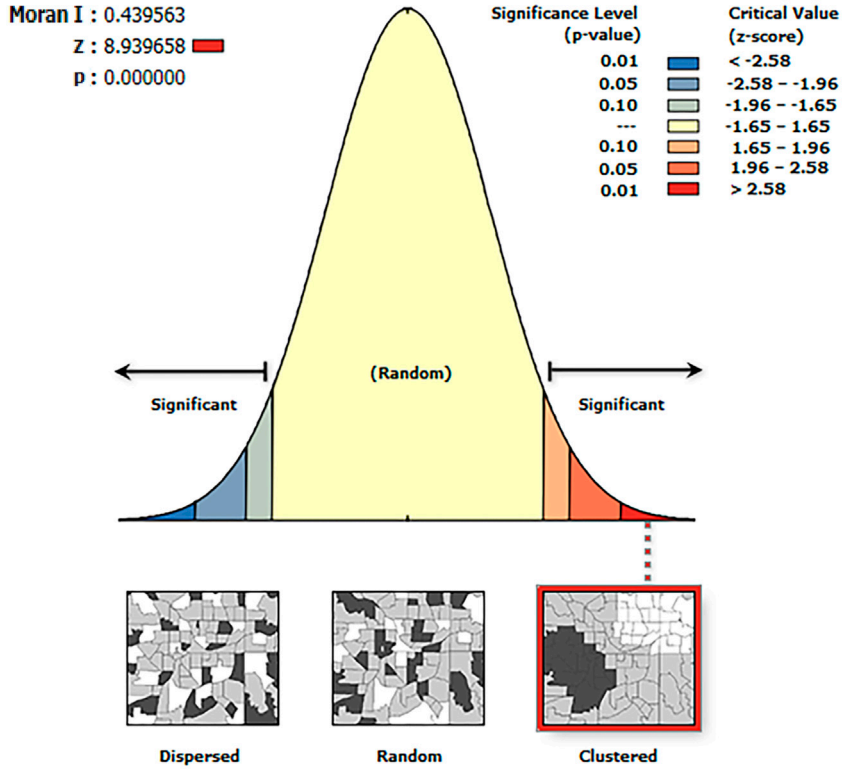

FIGURE 3
Moran's I of residential land prices.

the space was more closely related. The expression is as follows:

$$D = \sum_{i=1}^{k}\sum_{j=1}^{k}\frac{d(m_i, m_j)}{k(k-1)} \quad (16)$$

where D is the network density, k is the number of nodes in the network structure (168 counties in Hebei Province); $d(m_i,m_j)$ is the relationship between m_i and m_j. If there was an association between county i and county j, then $d(m_i,m_j)$ was 1, otherwise it was 0.

2.4.3.3 Cohesive subgroup calculation method

Cohesive subgroup analysis was used to identify small urban land price groups in the residential land price spatial network by simplifying the complex land price network. We could identify the number of agglomerated subgroups and the members of land price nodes within different subgroups through data analysis. This was able to show how subgroups were related, how they were connected, and how they were organized. We used UCINET software and CONCOR to carry out the calculation and analysis of cohesive subgroups.

3 Results

3.1 Spatial autocorrelation results

This study used ArcGIS10.2 software to calculate Moran's I (Figure 3). The global Moran's I index was 0.44, and the Z value was 8.94, exceeding the test threshold of 2.58, and the p-value passed the 1% significance test. It showed that the spatial distribution of the residential land price in the region had a strong global autocorrelation. Geoda was used to generate the LISA aggregation map (Figure 4). The results showed that the spatial distribution of residential land price in the region also had significant local autocorrelation characteristics. High-High clusters were mainly concentrated in cities around Beijing and Tianjin and provincial capitals and were distributed in 14 counties including Dachang and Xianghe in Langfang, Mancheng in Baoding, and Gaocheng in Shijiazhuang. The Low-Low clusters were mostly distributed on the southern and central Hebei, involving 20 counties. Therefore, it could be judged that the data set of this study could further carry out spatial correlation effect analysis.

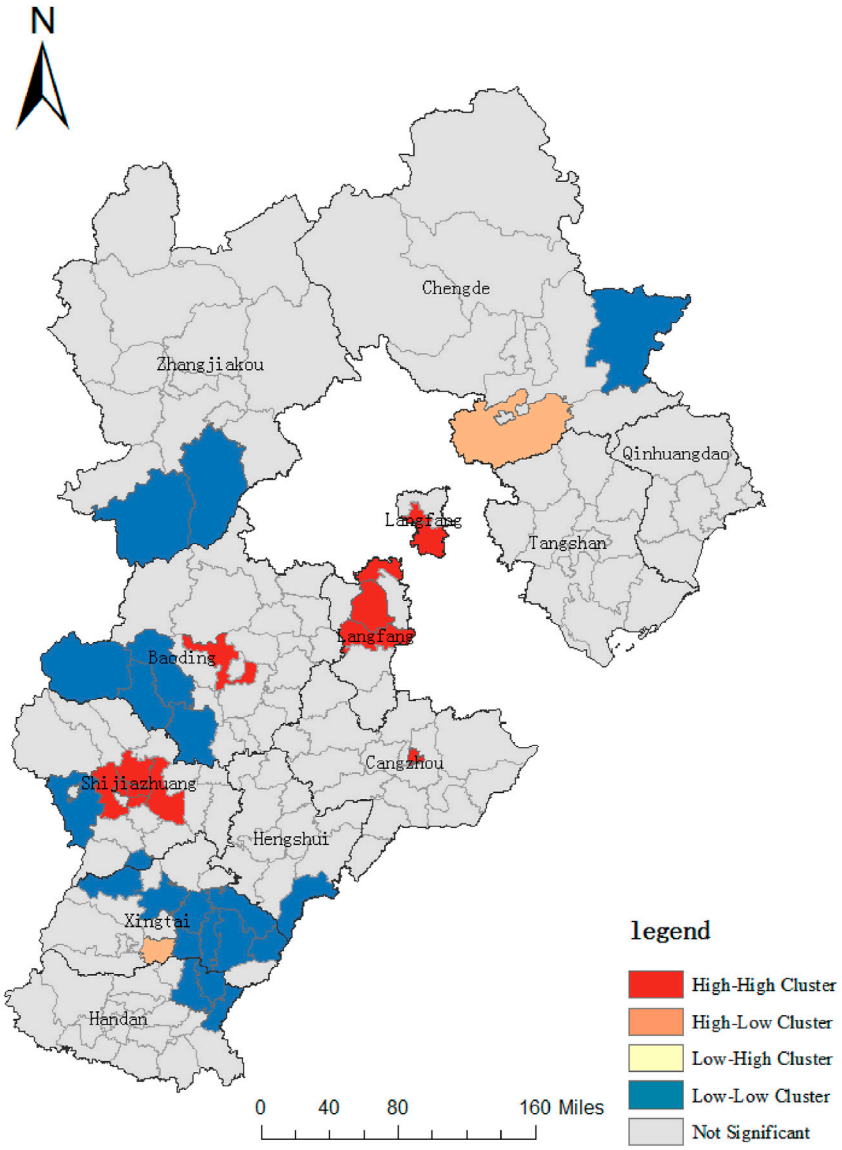

FIGURE 4
LISA cluster map of Hebei.

3.2 Spatial econometric results

3.2.1 Basic regression

The spatial econometric correlation analysis referred to the research process established by Anselin (Anselin et al., 1996). First, a series of regression tests was carried out on the residential land price, which was used to select and determine the applicable model for specific spatial measurement. The test results are shown in Table 5. 1) The LM spatial dependence test showed that: LM-Lag, LM-Error and their robustness tests passed the significance test at the levels of 5%, 1%, 1%, and 1% in turn, which indicates that the data in this study were suitable for use in the spatial econometric model for parameter estimation. 2) Both the Wald test and the LR test passed the 1% significance level test, and it was determined that the specific form of the spatial panel model was the Spatial Durbin model. 3) The Hausman test had a value of 38.13, which met the 1% significance level and showed that the spatial Durbin model under fixed effects was the most suitable choice to analyze the regional correlation effect of residential land prices between counties and districts in Hebei Province.

TABLE 5 Series of test results of spatial Econometric model.

	Test	Statistics
Spatial dependence test	LM Lag	6.347**
	LM Error	11.939***
	Robust LM Lag	8.734***
	Robust LM Error	14.325***
Wald test	Wald test (SAR)	21.36***
	Wald test (SEM)	22.00***
LR test	LR test (SAR)	21.18***
	LR test (SEM)	22.12***
Hausman test		38.13***

Note: *, **, *** indicate that the significance test was passed at the 10%, 5%, and 1% levels.

TABLE 6 Estimation results of spatial Durbin model.

Variable name	Coefficient	Variable name	Coefficient
W·lnP	0.158***	—	—
$LnX1_{it-1}$	0.063***	$LnX5_{it-1}$	−0.027
$LnX2_{it-1}$	0.587***	$LnX6_{it-1}$	0.045*
$LnX3_{it-1}$	0.134***	$LnX7_{it-1}$	0.008***
$LnX4_{it-1}$	0.324***	$LnX8_{it-1}$	0.039

Note: 1) *, **, ***, respectively, indicate that the significance test was passed at the level of 10%, 5% and 1%. 2) W · lnP is the spatial lag coefficient of residential land price; lnX represents the total impact of variable x on residential land price.

3.2.2 Spatial Durbin model estimation

After logarithmic processing of all research data, this study used the STATA spatial measurement tool to estimate the results, as shown in Table 6.

The spatial lag coefficient of the residential land price was 0.158, and it passed the significance test at the level of 1%. This result indicated that the residential land price in Hebei Province had a significant positive spatial correlation effect in geographical space. The changes in residential land prices in adjacent counties had interactive linkage and radiation effects, which were manifested in the form of synchronized increases and decreases.

Among the total effects of the different variables on the residential land price, Residents' purchasing power, Social and economic level, Land resources, and Urban development level variables had a positive impact on the residential land price at the 1% significance level. Every 1% increase in the Per capita disposable income increased the residential land price by .587%. Every 1% increase in Average salary of employees increased the residential land price by .324%. Every 1% increase in Resident deposit Savings increased the residential land price by .134%. Every 1% increase in New residential building area increased the residential land price by .063%, and every 1% increase in Urbanization rate increased the residential land price .008%. The variable of population size also had a positive impact on the residential land price at the 10% significance level. Every 1% increase in population density increased the residential land price by .045%.

3.2.3 Decomposition of the spatial correlation effect

The spatial Durbin model included the residential land price and the spatial lag terms of each variable. To further test the specific influence of each variable on the spatial effect of residential land price, this study used a partial differential solution to decompose the spatial effect of each variable and analyze the internal transmission mechanism of each variable's impact on the residential land price as a direct effect and a spillover effect. The direct effect represented the contribution of each variable to the residential land price within the county, and the spillover effect represented the contribution of each variable of the residential land price within the county to the residential land price in neighboring counties. The results are shown in Table 7.

TABLE 7 Estimation of the direct effect and spillover effect of the spatial econometric model.

Variable	Direct effect	Spillover effect
$lnX1_{it-1}$	.066***	.072**
$lnX2_{it-1}$	.585***	−.231
$lnX3_{it-1}$	.131***	−.137**
$lnX4_{it-1}$	.352***	.899***
$lnX5_{it-1}$	−.019	.243**
$lnX6_{it-1}$	.046*	−.055
$lnX7_{it-1}$	.008***	.003
$lnX8_{it-1}$	−0.037	.088*

Note: *, **,***, respectively, indicated that that the significance test was passed at the level of 10%, 5% and 1%.

3.2.3.1 Direct effect

Residents' purchasing power, Socio-economic level, Land resources, Population size and Urban development level all had a direct impact on residential land price within the county to varying degrees. The direct influence of each variable was in the order of Per capita disposable income >Average salary of employees > Residents' deposit savings > New residential building area > Population density > Urbanization rate. The *per capita* urban road area and taxation both showed negative effects, but these were not significant. The *per capita* disposable income had the greatest influence on residential land prices in the county, at the 1% significance level, every 1% increase raised the residential land price in the county by .585%. The urbanization rate had the lowest degree of influence, at the 1% significance level, every 1% increase raised the residential land price by .008%.

3.2.3.2 Spillover effect

Socio-economic level, Infrastructure, Policy environment all had an indirect impact on the residential land price of neighboring counties to varying degrees. The contribution of each variable to the spatial spillover effect of residential land prices in neighboring counties was in the order of Average salary of employees > Per capita road area > Residents' deposit savings# > Tax > New residential building area (# indicates a negative impact). The *per capita* disposable income and Population density had a negative effect, and the Urbanization rate had a positive effect, but none of these were significant. The average salary of employees was the most significant factor affecting the residential land price in neighboring counties. At the 1% significance level, every 1% increase in the average salary of employees increased the residential land price in neighboring counties by .899%. The contribution of the newly added residential building area to the residential land price in the neighboring counties was relatively low, but also showed a positive impact. Every 1% increase raised the residential land price in the neighboring counties by .072%.

3.3 Spatial association network measure

3.3.1 Individual network structure

The evolution of the individual network structure was dominated by the centrality characteristics. Centrality analysis mainly measured the role and dominance of node cities in the spatial network. Owing to the differences in economic level and resource conditions of cities, as well as the influence of traffic conditions and geographical location, node cities had different roles in the spatial network. The analysis of the individual network structure clarified the position of each network node city in the overall network. This study used UCINET to calculate the degree centrality and betweenness centrality of 168 counties and districts in Hebei Province in 2013 and 2020.

3.3.1.1 Degree centrality

As shown in Figure 5; Table 8, in 2013, the high-value areas of degree centrality were mainly distributed in the center of Hebei Province, with values of 115 in Qiaoxi of Shijiazhuang, 93 in Yuhua of Shijiazhuang, and 92 in Chang'an of Shijiazhuang; In 2020, the central high-value areas expanded to the surrounding areas, mainly in the central and southern parts of Hebei Province, in which Anci of Langfang reached 108, Yunhe of Cangzhou reached 104, and Zhengding of Shijiazhuang reached 96. From 2013 to 2020, the average degree centrality of residential land price in Hebei Province increased from 37.988 to 41.321, showing an overall upward trend. The high-value degree of centrality areas gradually became clustered in the central region, including Chang'an and Yuhua of Shijiazhuang, Jingxiu of Baoding, and Guangyang of Langfang. The average degree centrality of each node county expanded, and more counties played a growing role in the spatial network of residential land prices.

3.3.1.2 Betweenness centrality

As shown in Figure 6; Table 8, in 2013, the high-value areas of betweenness centrality were scattered in the central part of Hebei Province, including values of 2547.85 in Qiaoxi of Shijiazhuang,

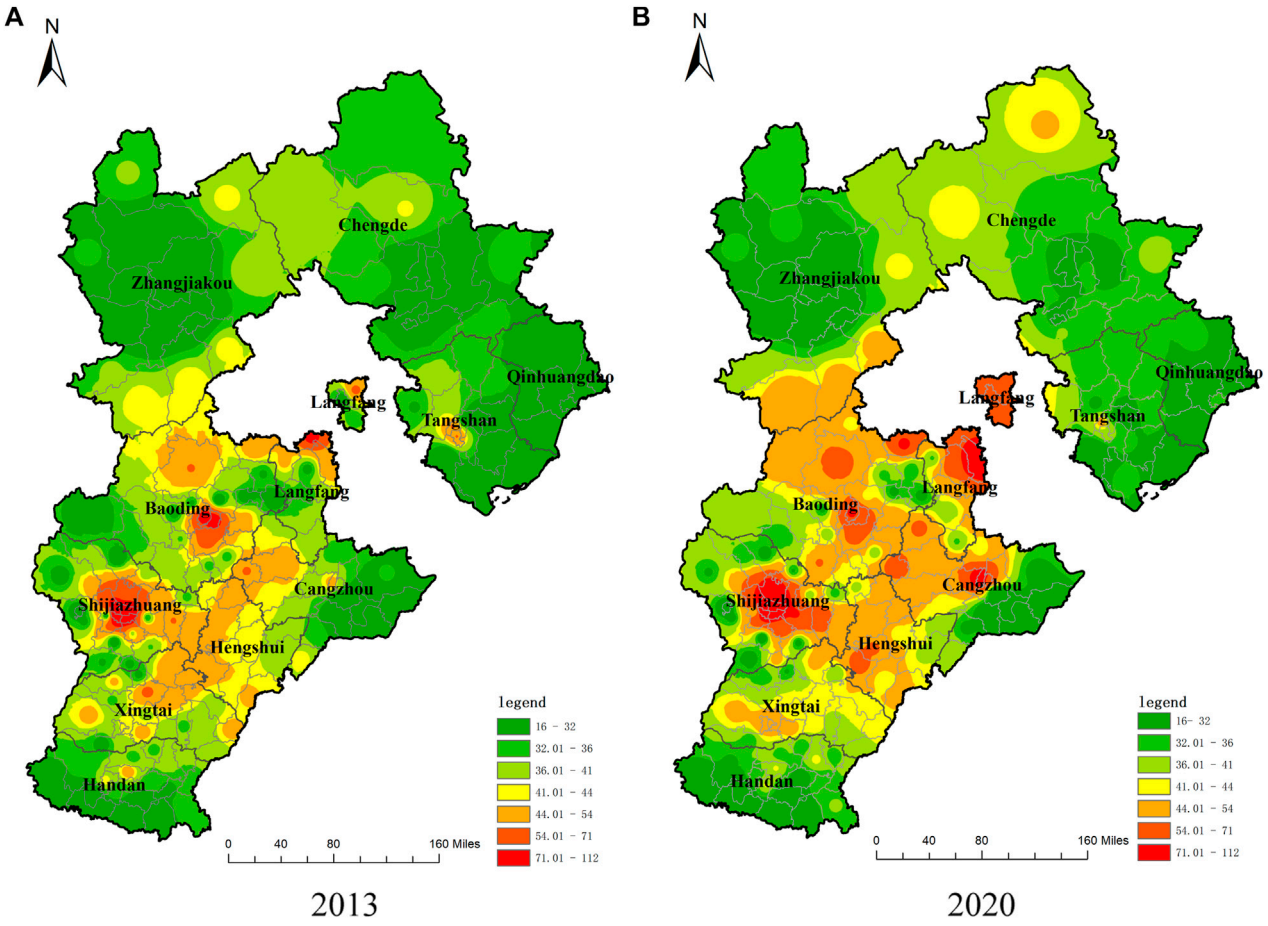

FIGURE 5
Map of the degree centrality of residential land prices in the counties of Hebei.

TABLE 8 Average value table of residential land price centrality in Hebei Province.

	2013	2014	2015	2016	2017	2018	2019	2020
Degree centrality	37.988	39.488	39.631	39.971	40.298	40.892	41.417	41.321
Betweenness centrality	313.917	322.399	317.458	320.083	321.839	318.279	322.685	326.845

1041.007 in Guangyang of Langfang, and 730.411 in Lianchi of Baoding. In 2020, the high-value areas of betweenness centrality expanded to the periphery, concentrated in the central and coastal areas of Hebei Province, with a small area in the north of the region. The highest values were in Yunhe of Cangzhou at 1684.134, Anci of Langfang at 1274.999, and Qiaoxi of Shijiazhuang at 768.572. From 2013 to 2020, the average value of betweenness centrality rose from 313.917 to 326.845, although the change trend showed a fluctuating distribution. The number of cities in the high-value areas increased, mainly in the central part of Hebei Province, and their role as "bridges" in the network structure was clear.

3.3.2 Overall network structure

3.3.2.1 Network density

Network density was used to measure tightness of the overall spatial network structure of residential land prices in Hebei Province. A high-density network will have a greater impact on the counties and districts in the region, and the flow of resource elements will be more active. As shown in Figure 7, from

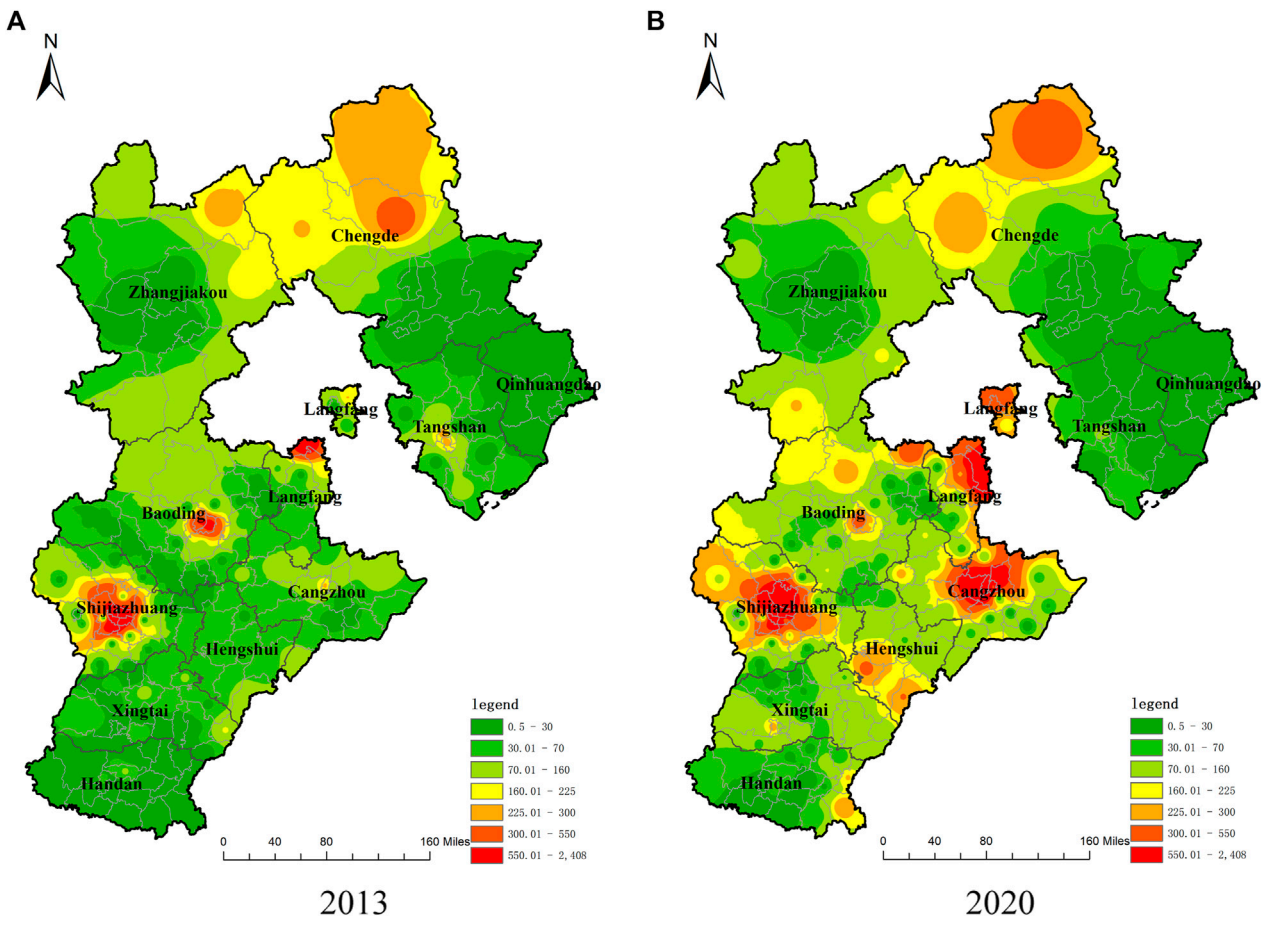

FIGURE 6
Betweenness centrality change map of residential land prices in Hebei province.

a numerical point of view, the network density value of residential land price in Hebei Province was low overall. From 2013 to 2020, the network density ranged between .1614 and .1663, indicating that the spatial network connection of residential land prices in the counties and districts of Hebei Province was weak. Over time, the network density value showed an upward trend, increasing from .1614 in 2013 to .1663 in 2020. This indicated that since 2013, the links among residential land price activities between counties and districts in Hebei Province had gradually increased. The network correlation coefficient reflected the robustness and vulnerability of the spatial network itself. The number of network relationships increased from 4527 in 2013–4665 in 2020, and the network structure gradually became more robust.

3.3.2.2 Cohesion subgroups

This study divided four agglomerate subgroups with the help of social network analysis tools. Agglomerate subgroups have distinct hierarchical structure and significant geographical proximity, as shown in Figure 8. The number of counties and role attributes included in the subgroups are shown in Table 9. The number of association relationships between county nodes within the four subgroups was high. The correlation coefficients of subgroup1 to subgroup4 were 830, 884, 893, and 683, respectively. The number of internal county nodes was 43, 41, 48, and 36, respectively. Owing to the change in the relationship among residential land prices between counties, the counties included in the subgroup also changed. The strength of the relationship between the sending and receiving counties in subgroup1 was 1402 and 1290, and the ratio of the expected to actual internal relationship was .25 and .64. The strength of the relationship between the sending and receiving counties in subgroup3 was 1408 and 1312, and the ratio of the expected to actual internal relationship was .28 and .68. Both subgroup1 and subgroup3 reflected the fact that the actual internal relationship ratio was greater than the expected internal relationship ratio, the ratio of the sending to receiving relationship was the ratio of the sending to receiving relationship

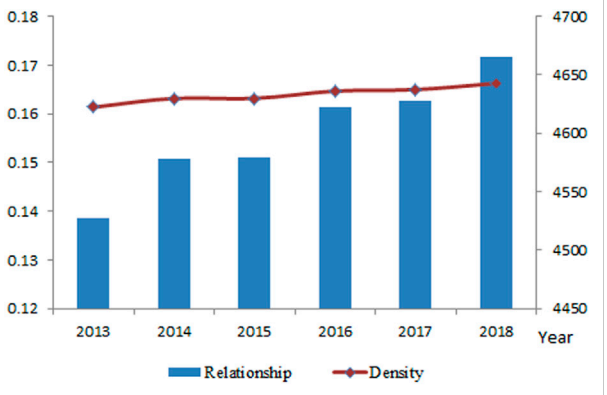

FIGURE 7
Spatial network density and changes in the correlation coefficient.

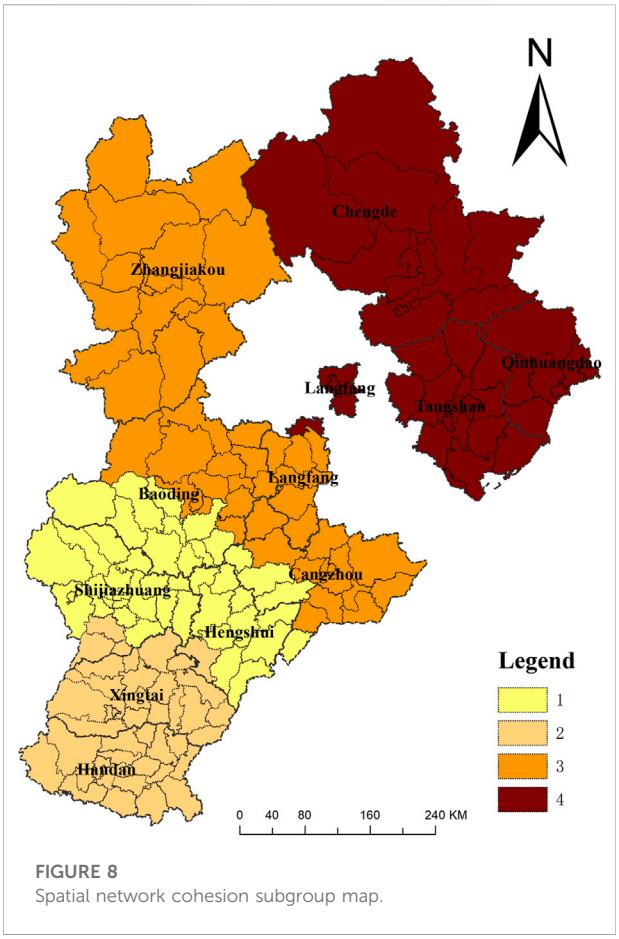

FIGURE 8
Spatial network cohesion subgroup map.

was more than 1. Therefore, both subgroup 1 and 3 reflected counties that showed a mutual spillover effect in the residential land price space network, and they played both an external connection role for other subgroups in the residential land price network. The intensity of the correlation between the sending and receiving association of subgroup2 was 1005 and 1211, and the ratio of the expected to actual internal relationship was .24 and .73. The intensity of the correlation between the sending and receiving association of subgroup 4 was 850 and 852, and the ratio of the expected to actual internal relationship was .21 and .80. Subgroups 2 and 4 reflected the fact that the ratio of the sending to receiving relationship was the ratio of the sending to receiving relationship was less than 1. Therefore, both subgroup 2 and subgroup 4 were net beneficiary counties, receiving a higher proportion of the radiation effect of residential land prices.

4 Discussion

4.1 Spatial autocorrelation analysis

There was a significant spatial autocorrelation between counties in Hebei Province. The change of the residential land price within a county was not only constrained by the existing local conditions, but also by the land price of adjacent counties. Owing to the influence of various factors such as resource endowment, policy measures, and facility conditions, there was a distinct spatial heterogeneity in residential land prices among counties. High–High clusters involved five counties in Langfang, two counties in Baoding, one county in Cangzhou, and six counties in Shijiazhuang. Most of the High–High cluster counties in Langfang, Baoding and Cangzhou were adjacent to Beijing and Tianjin, with pronounced regional advantages. These cities were within a 1 h radius of Beijing and Tianjin, and they had strong economic influence from Beijing and Tianjin. They also received policy dividends from the provincial capital city; the land transfer price was higher; they were closely connected with surrounding counties, and there was a significant spatial correlation effect. High-High cluster counties in Shijiazhuang were mostly downtown counties. Shijiazhuang is the political, economic, scientific, technological, financial, cultural, and information center of Hebei Province and is also an important central city in the Beijing-Tianjin-Hebei region of China. After years of development, Shijiazhuang has accumulated significant advantages. In 2020, Shijiazhuang had a permanent population of 11.24 million, ranking first in the province, with a GDP of 593.51 billion yuan, ranking third in the province. The large population, abundant capital, convenient transportation system, and complete infrastructure allowed the real estate market in this area to develop to a high degree, and the residential land price in the central area formed a “convex area.” Low-Low cluster counties involved one county in Chengde, two counties in Zhangjiakou, three counties in Baoding, two counties in Shijiazhuang, one county in Hengshui, eight counties in Xingtai, and three counties in Handan. Low-Low cluster counties in Chengde, Zhangjiakou, Baoding and Shijiazhuang were mostly located in

TABLE 9 The relationship and role of subgroups in the residential land price spatial network.

	Subgroup1	Subgroup2	Subgroup3	Subgroup4	Number of cities
Subgroup1	830	120	337	3	43
Subgroup2	311	884	16	0	41
Subgroup3	254	1	893	164	48
Subgrou4	7	0	162	683	36
	Expected internal relationship ratio	Actual internal relationship ratio	Strength of the connection	Strength of the received contact	Partition role
Subgroup1	.25	.64	1402	1290	Overflowing each other
Subgroup2	.24	.73	1005	1211	Net beneficiary
Subgroup3	.28	.68	1408	1312	Overflowing each other
subgroup4	.21	.80	850	852	Net beneficiary

the ecological conservation areas of Yanshan and Taihang Mountains. These counties were located in mountains and hills, and the complex terrain conditions restricted the urban construction and development to a certain extent. The disadvantages of inconvenient transportation, low land grade, and weak urban competitiveness finally led to low activity of the real estate market and low overall residential land prices. Low-Low cluster counties in Hengshui, Xingtai, and Handan were located in the plain area of southern Hebei Province. Most of these counties were poor, with weak resources and technical strengths. They were far from the city centers and had weak radiation and driving effects from developed counties. Low economic level and location disadvantage were the main reasons for the slow development of the real estate market and low residential land prices in these counties.

4.2 Spatial correlation effect analysis

Owing to the existence of spatial correlation, the influencing factors of residential land price also showed a significant spatial effect. However, there were important differences among the influencing factors on the residential land price and its spatial correlation effect. The direct effect and spillover effect reflected the internal mechanism of different influencing factors on the residential land price, which were important in analyzing the trend of the housing land market.

4.2.1 Factors and mechanism affecting the land price of the county itself

According to the results, the *per capita* disposable income, average salary of employees, resident deposit savings, new residential building area, and population density indicators had a significant positive impact on residential land prices in the region, of which *per capita* disposable income had the largest impact on residential land prices. This conclusion was similar to the research results of ZHOU (Zhou et al., 2019). ①The *per capita* disposable income reflected the purchasing power of residents, while the average salary of employees and resident deposit savings reflected the living standard of residents. The stronger the residents' purchasing power and living standard, the stronger the residents' demand for real estate (including rigid demand and improvement demand) and the greater the competition in land transactions, which led to the rise of residential land prices. In addition, the above three indicators reflected the social and economic development level of a region from the perspective of residents' living conditions. Higher social and economic development level is usually accompanied by higher local financial income, more rapid urban development, and greater real estate development investment scale that are the main reasons for the positive interaction between these three indicators and residential land prices. ②The driving effect of new residential building on residential land prices was related to the dependence of local governments on land finance in recent years. The increase of residential building area means the increase of residential land. In theory, the increase of residential land can effectively meet the vigorous demand for real estate, alleviate the contradiction between supply and demand, and thus play a role in restraining or stabilizing land prices. However, in recent years the "land finance" model has been an important means for Chinese local governments to accumulate urban capital and promote urbanization and economic development. In this mode, the increase of residential land could meet the capital needs of local governments for infrastructure and public facilities

construction, stimulate infrastructure construction, improve urban environment, and also increased the competition of real estate developers for land purchase and the expectations of consumers for housing purchase, which would drive the increase of land transfer prices. ③The driving effect of population density on residential land price was the specific performance of market supply and demand mechanisms. The population density reflected the relationship between the land quantity and the potential land demand of the population. The coordinated development of residential land and population change could stabilize the land price. In a certain period of time, the increase in population density would bring about an imbalance between supply and demand, leading to an increase in housing demand and thus driving up land prices.

4.2.2 Factors and mechanisms affecting land prices in neighboring counties

According to the results, the average salary of employees, urban road area per capital, taxes, and new residential building area had significant positive spillover effects on residential land prices in nearby areas, among which the average salary of employees had the greatest impact. However, residents' deposit savings had a significant negative spillover effect on residential land prices in nearby areas. ①Higher average salaries of employees could not only increase residents' local demand for housing but also increase residents' desire to buy houses in nearby areas. Especially under the background of strict regulation and control policies in some cities, developers were willing to bid for land at a higher price in anticipation of the flow of housing demand sand thus the land price in nearby areas would rise. ②With the improvement of traffic facilities and convenience, people had more ways of commuting, shorter commuting times, and wider choice of residence. People tended to consider neighboring regions with better living environments and infrastructure, and this increased the demand for residential land in surrounding counties to a certain extent and promoted the rise of residential land prices. ③Taxes were closely related to residents' living pressures, and an increase in residents' living pressures directly affected the choice of real estate. When the real estate price within a particular county was relatively high, the availability of housing land in surrounding counties with a relatively low residential land price was able to ease the pressures of life, thereby driving an increase in the residential land prices in the surrounding counties. ④Increased areas of new housing also drove the residential land prices in the surrounding areas. The reason might be that under the background of cooperation and competition between counties, the increase of new residential building area had a certain "demonstration effect". The increase of residential building area in a certain county might prompt the neighboring county governments to take similar actions, increase the supply of residential land, and thereby increased the pace of real estate development. Therefore, when the real estate development in some counties was strong, it would spill over to the neighboring counties through the expectation of the market development, causing the residential land prices in the neighboring areas to rise. ⑤Residents' deposit savings had a certain degree of inhibition on neighboring areas. Different from the *per capita* disposable income, the increase of residents' deposit savings indicated the decline of residents' consumption ability, and the residents' enthusiasm for purchasing or consuming in other places was reduced when the local living conditions were met; this reduced the pace of the real estate market in nearby areas to a certain extent, thus playing a role in curbing the rise of residential land prices.

4.3 Spatial association network analysis

4.3.1 Characteristics of individual network structure

After decomposing the spatial effect of the residential land price, it was found that the counties were connected through a number of influencing factors. This expanded the linkage in the residential land price among different counties and formed a closely related spatial network. Counties differed in geographical location, economic level, and resource conditions, and they played different roles in the allocation of land resources over the entire region.

Counties with a high degree centrality had a strong radiation and guidance role in the spatial network owing to their advantages of location and development level. These counties could achieve coordination and interaction with other county nodes and easily attract the inflow of economic and resource factors from surrounding counties. The inflow of economic and resource elements from the surrounding counties showed the Matthew effect of accumulated advantage. In 2013, the central high-value counties were mainly distributed in the central urban areas of Langfang, Shijiazhuang, and Baoding. Counties of Langfang and Baoding made full use of resources from the integration of Beijing-Tianjin-Hebei by virtue of its proximity to Beijing and Tianjin and thus developed rapidly. Shijiazhuang, as the capital of Hebei Province, played the role of "the third pole" in the coordinated development of Beijing, Tianjin, and Hebei. According to the data of China Land Price Information Service Platform, in 2013 the residential land prices of Langfang, Shijiazhuang and Baoding were 3059 yuan/m^2, 2245 yuan/m^2 and 2441 yuan/m^2 respectively, prices that were among the top cities in Hebei Province. Under the effect of price leverage, the surrounding labor, capital, and other land production factors of these three cities were concentrated in the center of the city. The good scale efficiency had promoted them to form the economic development pole and land price radiation center in Hebei Province. With the in-depth implementation of the coordinated development of Beijing, Tianjin, and Hebei, Beijing's industrial transfer had promoted the economic

development and residential land prices of Cangzhou, Hengshui, Xingtai and other cities in central Hebei Province. The data showed that from 2013 to 2020, the GDP growth rates of Cangzhou and Hengshui were 31.58% and 51.85% respectively, and the residential land price growth rates were 9.12% and 9.62% respectively, both of which were in the forefront of Hebei Province. The rapid economic growth had promoted the development of the land market, and these two cities had gradually formed a secondary radiation center of land prices in central Hebei Province. From the perspective of the distribution pattern of central high-value counties, the spatial network structure of residential land price in Hebei Province had gradually evolved from the decentralized central nodes dominated by Langfang, Shijiazhuang, and Baoding central areas in 2013 to a network-like central node group dominated by Langfang, Shijiazhuang, Baoding, Cangzhou, and Hengshui central areas in 2020. The change in the spatial network was manifested in the conduction process starting from the central city, a pattern that conformed to the central characteristics of the ripple effect. Under the radiation of the above urban centers, more counties had gradually played leading roles in the residential land price spatial network. The peripheral cities of Hebei Province lacked important central nodes in the network structure, and there were distance barriers from important central nodes. For example, Kangbao of Zhangjiakou, located in the northern part of Hebei Province, was at the edge of the spatial network, far from important economic centers, and it lacked central city nodes to participate in the connection. It was weakly driven by the radiation of cities with a high level of development, and the speed of reflection and regulation of land price information was slow.

The betweenness centrality of residential land prices in Hebei Province also rose overall, and the connection between counties was gradually smooth. Similar to the distribution pattern of degree centrality, the counties with high betweenness centrality were largely distributed in Shijiazhuang, Baoding, and Langfang in 2013. These counties not only had a strong ability to mobilize the land production factors of their own counties in the network structure but also showed a strong "bridge" role with high transmission capacity, becoming important media driving the connection between counties. In 2020, the structure of the spatial network changed from a single center with a scattered distribution to a multi-intermediary center with a centralized distribution. Two secondary intermediary centers of the network formed in Cangzhou central urban area and Hengshui central urban area. From 2013 to 2020, the number of counties with betweenness centrality above 300 increased from 7 to 14. More counties played important roles in land price transmission. Land prices between counties became more closely related. Superior geographical location and convenient transportation provided better conditions for the contact and cooperation between counties and in the middle of Hebei Province. Influenced by the Beijing Tianjin radiation, Langfang's socio-economic and land market changes were more sensitive, and it had become an important city node to transmit Beijing radiation and guide land price changes in Baoding and surrounding counties. Cangzhou had the regional advantage of being close to Tianjin and had become an important city node to transmit Tianjin's radiation and guide the land price of surrounding counties. As the city with the strongest economic strength and the most mature land market in Hengshui's surrounding cities, Shijiazhuang naturally became the most attractive city for Hengshui's land prices. The present study found that in the spatial connection network structure of land prices in central Hebei, Shijiazhuang, Hengshui, and Cangzhou, the three central node cities were basically consistent with the Shijiazhuang-Hengshui-Cangzhou-Huanghua port intercity railway station cities currently planned and constructed in Hebei Province. This indicated that the results were in line with the current planning of the Chinese government on road network construction and promoting the coordinated development of Beijing-Tianjin-Hebei urban agglomeration industries.

4.3.2 Overall network structure characteristics

The spatial network density of residential land prices in the counties and districts of Hebei Province slowly increased from 0.1614 in 2013 to 0.1663 in 2020. The overall network structure had some weak connection characteristics, and there was still room for improvement in the degree of spatial correlation. The transmission role of node cities in the process of spatial network development constantly increased. The number of network associations increased to 4,665 in 2020, reaching a peak, and the closeness of connections between cities was still improving. The increase of network density value year by year benefited from the evolution of land price multi-core structure. The spatial correlation network of residential land price in Hebei Province gradually evolved from the initial three core to five core driven evolution, and the position of the five core growth poles tended to be stable. In particular, the formation of Cangzhou and Hengshui, two intermediary central nodes, had gradually changed the relationship between counties in the province from unbalanced to relatively balanced. This trend was conducive to the full flow of land resource elements in the network and the benign interaction between different nodes. The increase in the number of network relations reflected the stability and reconstruction of the overall network structure. With the changes in the land market level, industrial development, and policy mechanism of each city, Hebei Province is likely to realize the new pattern of reconstruction and optimization, and the spatial network connection and interaction of residential land prices in the region may be more frequent.

The distribution of subgroups had a strong correlation with the geographical location and policy environment of each county. The counties with similar geographical location and policy

environment had frequent economic exchanges, and the residential land markets had close exchanges and cooperation that made it easier to combine into urban subgroups. Subgroup 1 was composed of Shijiazhuang and Hengshui counties, as well as the southern counties of Baoding and Cangzhou. Subgroup 3 was composed of Zhangjiakou counties, including the counties in the north of Baoding and Cangzhou and the counties in the south of Langfang. Subgroups 1 and 3 occupied the core position in the network. The land market environment of counties included in these two subgroups was superior. They were not only closely related internally but also displayed strong spillover effects, and they had close external communication with other subgroups. However, the close relationship between counties in subgroup 1 was weaker than that in subgroup 3, and thus it was necessary for subgroup 1 to accelerate its development and promote the coordinated improvement of economic strength and network status. Subgroup 2 was composed of Xingtai and Handan counties and also included a few counties in the south of Shijiazhuang and Hengshui. Subgroup 4 comprised Chengde, Qinhuangdao, and Tangshan counties, including the counties in the north of Langfang. Subgroups 2 and 4 played the role of edge subgroups. Their internal structure was relatively loose, and their interactions with other subgroups were insufficient, and thus the network edge risk was high. On the one hand, the diffusion effect of land factor marketization in Xingtai, Handan, Chengde, Qinhuangdao, Tangshan, and other cities was weaker than its siphon effect. On the other hand, these two subgroups lacked important central nodes and were spatially separated from the existing central nodes. Therefore, it was necessary to accelerate the cultivation and construction of more growth poles in subgroups 2 and 4, promote the orderly development of the land market pattern of the residential land price spatial correlation network in Hebei Province, and enhance the dual driving role of the center and the network.

4.4 Advice

Accurately identifying the correlation characteristics of urban residential land prices in the region will help improve the pertinence of regulatory measures. According to the research results, we put forward suggestions on regional land price regulation measures from three aspects:

First, we should explore the market regulation policy of differentiated residential land and build a city cluster with coordinated land price development. In view of the unbalanced development of residential land prices in Hebei Province, the government should consider the economic development status, functional positioning, leading industries, and land price differences of each city and customize development strategies for each city. For the central cities (Langfang, Shijiazhuang, and Baoding) with rapidly rising land prices, we can adjust and control the land demand by rationally allocating new construction land, activating the use of idle land, and optimizing the financial credit policy for residential land to ensure the healthy and stable development of the residential land market. For marginal cities (Chengde, Zhangjiakou, Qinhuangdao, and Handan) and mountainous counties where land prices are rising slowly, we should give full play to the advantages of ecological resources, improve the income level of residents by vigorously developing distinctive economies, strengthen economic cooperation among counties by improving transportation networks, and guide superior real estate enterprises and high-end technical talents to settle in through policies such as taxation, finance, and talent incentive plans to realize the balanced development of residential land prices in central cities.

Second, we should accelerate the optimization of residential land price network structure and strengthen the role of the network. On the one hand, we can further enhance the core leading function of the leadership subgroups in the network and enhance its radiation effect through the external transfer of the existing central city land elements. Subgroup 1 and Subgroup 3 should give play to their interconnection advantages and continue to build Cangzhou and Hengshui as two intermediary centers, actively playing the role of outward connection while undertaking Beijing's industrial transfer and driving the development of marginal subgroups by establishing long-term cooperation mechanisms such as talent exchange and industrial coordination. On the other hand, edge subgroups should strengthen external connections, focus on cultivating potential network centers, and reduce network edge risks. Subgroup 2 focuses on cultivating Xingtai as the intermediary center, creating a "Shijiazhuang-Xingtai-Handan" connecting channel to radiate around the counties; Subgroup 4 focuses on the construction and cultivation of Tangshan as the intermediary center and creates a "Qinhuangdao-Tangshan-Chengde" connecting channel to radiate to surrounding counties. By creating more growth poles, we will promote the orderly development of the network pattern and the communication ability between subgroups.

Third, Hebei Province should not only promote the network of the internal land market of the urban agglomeration but also actively build the external network of coordinated development. This province can play an important role in the national important strategy of "Beijing-Tianjin-Hebei coordinated development." On the one hand, more dense transportation lines should be built within Hebei Province, making it easier to connect the weak areas with the core cities. We can try to make the marginal cities such as Zhangjiakou, Chengde, Qinhuangdao, Handan, Beijing, and Tianjin have greater contact. On the other hand, we can accelerate the integration of the Beijing-Tianjin-Hebei land factor market. In the process of formulating the land space planning, the three areas of Beijing, Tianjin, and Hebei should break the situation of separate administration to organically connect the resources and guide reasonable competition among the cities by perfecting the construction of

the land price information network platform in order to realize the coordinated and healthy development of the land market.

5 Conclusion

By exploring the spatial correlation effect of residential land prices in counties of Hebei Province and the characteristics of spatial network structure, this study reached the following conclusions:

1) There was a significant spatial correlation effect of residential land prices between counties in Hebei Province. First, the regional residential land price level has significant global spatial autocorrelation and local autocorrelation. High-High clusters were mainly concentrated in cities around Beijing and Tianjin and provincial capitals, while Low-Low clusters were mostly distributed on the central and southern Hebei. Second, the residential land price changes in adjacent counties will produce interactive linkage, which is manifested in the form of simultaneous increase and decrease. The residents' purchasing power, the socioeconomic level, and the land resources have a significant impact on the residential land price of the county itself, while the level of infrastructure, and the policy environment have a significant impact on the residential land price of neighboring counties.
2) The centrality of residential land price in central counties of Hebei Province was generally high, and showed a trend of agglomeration. The spatial network characteristics of residential land prices were mainly manifested in the conduction process starting from the central county, which conformed to the centrality characteristics of the ripple pattern. However, the peripheral cities of Hebei Province lacked important central nodes in the network structure, and the risk of land price development marginalization was high. The betweenness centrality of residential land prices in counties around Beijing and Tianjin and provincial capital cities was generally high. The betweenness centrality of counties had evolved into a multi-core structure. More and more counties showed the role of "bridges" with transmission characteristics, and the balance of the entire regional land price network had been constantly improved.
3) The spatial network connection of residential land prices in the counties of Hebei Province was weak, but the network density was slowly increasing, and there was a large space to improve the tightness of spatial connection. The counties in Hebei Province can be divided into four subgroups, among which the residential land prices of provincial capital cities and surrounding counties (subgroup1), southern Hebei counties (subgroup2), and counties around Beijing and Tianjin (subgroup3) had a good interaction relationship. The residential land prices of subgroup1 and 3 played an important role in conducting the spatial network, while subgroup 2 and 4 had less interaction with other subgroups. The government departments should implement the integrated development strategy based on the overall functional orientation of Hebei, the development foundation and potential of each city, and realize the coordinated development of the whole region.

There may be a major limitations in this study. Due to the lack of data, this study did not consider the two cities of Beijing and Tianjin, and only focused on Hebei Province. The higher land price level and stronger economic radiation capacity in Beijing and Tianjin may have an impact on the structure of residential land price network in Hebei Province. The study in the Beijing-Tianjin-Hebei region may make the conclusion more scientific and valid, which is also the direction of the authors' follow-up research.

Data availability statement

Publicly available datasets were analyzed in this study. This data can be found here: http://landchina.mlr.gov.cn/.

Author contributions

Conceptualization and writing: CL and ZF; methodology and software: WW; data acquisition: CZ and PA; and analysis and interpretation of data: YD. All authors contributed to the article and approved the submitted version.

Funding

This research was funded by Chinese National Science Foundation (No. 41471090), Hebei Province National Science Foundation (No. H16028), Science Foundation of Hebei Normal University (No. L2021B29).

Conflict of interest

The authors declare that the research was conducted in the absence of any commercial or financial relationships that could be construed as a potential conflict of interest.

Publisher's note

All claims expressed in this article are solely those of the authors and do not necessarily represent those of their affiliated organizations, or those of the publisher, the editors and the reviewers. Any product that may be evaluated in this article, or claim that may be made by its manufacturer, is not guaranteed or endorsed by the publisher.

References

Anselin, L., Bera Anil, K., Raymond, F., and Yoon, M. J. (1996). Simple diagnostic tests for spatial dependence. *Regional Sci. urban Econ.* 26 (1), 77–104. doi:10.1016/0166-0462(95)02111-6

Bacău, S., Grădinaru, S. R., and Hersperger, A. M. (2020). Spatial plans as relational data: Using social network analysis to assess consistency among Bucharest's planning instruments. *Land Use Policy* 92, 104484. doi:10.1016/j.landusepol.2020.104484

Chai, N., Stevens, R., Fang, X., Mao, C., and Wang, D. (2019). The impact of compensation upon urban village residents satisfaction with the land expropriation process. *China. Int. J. Law Built Environ.* 11, 186–216. doi:10.1108/JPPEL-03-2019-0011

Cheng, D., Jing, L., and Peng, S. (2020). Research on the test and model of trans-regional interaction among urban housing price. *Constr. Econ.* 41 (04), 101–105. doi:10.14181/j.cnki.1002-851x.202004101

Davis, M. A., and Palumbo, M. (2008). The price of residential land in large US cities. *SSRN J.* 63 (1), 352–384. doi:10.2139/ssrn.943771

Elias, O. (2006). The diffusion of housing price movements from center to surrounding areas. *J. Hous. Res.* 15 (1), 3–28. doi:10.1080/10835547.2004.12091958

Feng, J. L., and Tian, P. C. (2011). Validity analysis of maximum entropy distribution based on different moment constraints for wind energy assessment. *Energy* 36, 1820–1826. doi:10.1016/j.energy.2010.11.033

Fu, N. (2021). Innovation efficiency and the spatial correlation network characteristics of intelligent-manufacturing enterprises. *Complexity* 2021, 1–15. doi:10.1155/2021/4299045

Gan, C., Voda, M., Wang, K., Chen, L., and Ye, J. (2021). Spatial network structure of the tourism economy in urban agglomeration: A social network analysis. *J. Hosp. Tour. Manag.* 47, 124–133. doi:10.1016/j.jhtm.2021.03.009

Gan, W., and Huo, X. (2016). Study on the measures of land factor market integration in beijing Tianjin hebei—from the perspective of supply side structural reform. *People's Trib.* 14, 215–217. doi:10.16619/j.cnki.rmlt.2016.14.070

Glumac, B., Herrera-Gomez, M., and Licheron, J. (2019). A hedonic urban land price index. *Land Use Policy* 81, 802–812. doi:10.1016/j.landusepol.2018.11.032

Griffin, T., Gregg, I., and Mark, T. (2015). How spatially clustered are state-level farmland values? *J. ASFMRA* 2015, 103–112. doi:10.22004/ag.econ.235188

Gyourko, J., and Jacob, K. (2021). The impact of local residential land use restrictions on land values across and within single family housing markets. *J. Urban Econ.* 126, 103374. doi:10.1016/j.jue.2021.103374

Han, J., Jin, X., Zhang, Z., Sun, W., Xu, X., and Zhou, Y. (2017). Development characteristics and FactorsAnalysis of residential land price in China. *Sci. Geogr. Sin.* 37 (04), 573–584. doi:10.13249/j.cnki.sgs.2017.04.011

Harris, R., Dong, G., and Zhang, W. (2013). Using contextualized geographically weighted R egression to model the spatial heterogeneity of land prices in beijing, China. *Trans. GIS* 17, 901–919. doi:10.1111/tgis.12020

Hu, S., Yang, S., Li, W., Zhang, C., and Xu, F. (2016). Spatially non-stationary relationships between urban residential land price and impact factors in Wuhan city, China. *Appl. Geogr.* 68, 48–56. doi:10.1016/j.apgeog.2016.01.006

Huang, Z., and Du, X. (2021). How does high-speed rail affect land value? Evidence from China. *Land Use Policy* 101, 105068–8. doi:10.1016/j.landusepol.2020.105068

Huang, F., Zhou, J., Li, Z., and Hou, T. (2009). Relationships effect among housing prices of Chinese big cities based on cointegration and vector error correction model. *China Manag. Stud.* 4 (2), 122–142.

Huang, Z., Li, S., and Du, X. (2022). Spatial-temporal pattern and influence mechanism of urban land prices under the integrated development of the yangtze river delta. *China Land Sci.* 36 (02), 53–62. doi:10.11994/zgtdkx.20220117.095034

Jiang, R., George, C., and Lin, S. (2021). Placing China's land marketization: The state, market, and the changing geography of land use in Chinese cities. *Land Use Policy* 103, 105293. doi:10.1016/j.landusepol.2021.105293

Juethe, T. H., and Pede, V. O. (2011). Regional housing price cycles: A spatio-temporal analysis using us state-level data. *Reg. Stud.* 45 (5), 563–574. doi:10.1080/00343400903497897

Kheir, N., and Boris, A. P. (2016). Economic, demographic and environmental factors affecting urban land prices in the Arab sector in Israel. *Land Use Policy* 50, 518–527. doi:10.1016/j.landusepol.2015.08.031

Lesage, J. P., and Pace, P. K. (2009). *Introduction to spatial economics [M]*. Boca Raton: Press Taylor and Francis Group, 66–71.

Li, C., Wu, J., Xi, Z., and Zhang, W. (2021). Farmers' satisfaction with land expropriation system reform: A case study in China. *Land* 10, 1353. doi:10.3390/land10121353

Liang, J., Wen, S., and Fang, J. (2015). The spatial economic association of city agglomeration on CAFTA based on the perspective of social network analysis. *Sci. Geogr. Sin.* 35 (05), 521–528. doi:10.13249/j.cnki.sgs.2015.05.002

Liu, H., Yuan, M., and Ma, J. (2019). Spatial distribution of influence factors of residential land price in Cangzhou city based on GWR model. *IOP Conf. Ser. Earth Environ. Sci.* 332 (2), 022032. doi:10.1088/1755-1315/332/2/022032

Liu, Y., Gao, H., Cai, J., Lu, Y., and Fan, Z. (2022). Urbanization path, housing price and land finance: International experience and China's facts. *Land Use Policy* 113, 105866. doi:10.1016/j.landusepol.2021.105866

Liu, Z., and Chen, Z. (2013). Spatial correlation, influencing factors and pass-through effect of urban housing prices: An empirical research based on regional market relation. *J. Shanghai Univ. Finance Econ.* 15 (05), 81–88. doi:10.16538/j.cnki.jsufe.2013.05.007

Luo, Y., Zhou, D., Tian, Y., and Jiang, G. (2021). Spatial and temporal characteristics of different types of pollution-intensive industries in the Beijing-Tianjin-Hebei region in China by using land use data. *J. Clean. Prod.* 329, 129601. doi:10.1016/j.jclepro.2021.129601

Ma, W., Jiang, G., Chen, Y., Qu, Y., Zhou, T., and Li, W. (2020). How feasible is regional integration for reconciling land use conflicts across the urban–rural interface? Evidence from beijing–tianjin–hebei metropolitan region in China. *Land Use Policy* 92, 104433. doi:10.1016/j.landusepol.2019.104433

Meen, G. (1999). Regional house prices and the ripple effect: A new interpretation. *Hous. Stud.* 14 (6), 733–753. doi:10.1080/02673039982524

Nilsson, P. (2014). Natural amenities in urban space: A geographically weighted regression approach. *Landsc. Urban Plan.* 121, 45–54. doi:10.1016/j.landurbplan.2013.08.017

Niu, F., Xin, Z., and Sun, D. (2021). Urban land use effects of high-speed railway network in China: A spatial spillover perspective. *Land Use Policy* 105, 105417. doi:10.1016/j.landusepol.2021.105417

Okamoto, C., and Sato, Y. (2021). Impacts of high-speed rail construction on land prices in urban agglomerations: Evidence from Kyushu in Japan. *J. Asian Econ.* 76, 101364. doi:10.1016/j.asieco.2021.101364

Peng, S-H., Jing, L-L., Zhang, M, Cheng, D-P., and Wu, Q. (2019). Study on the mode and spillover effect of interaction influence of local government land transfer. *China Population, Resources and Environment.* 29 (08), 156–167.

Pollakowski, H. O., and Ray, T. S. (1997). Housing price diffusion patterns at different aggregation levels: An examination of housing market efficiency. *J. Hous. Res.* 8 (1), 107–124. Available at: https://www.jstor.org/stable/24833634.

Shen, Y., and Karimi, K. (2017). The economic value of streets: Mix-scale spatio-functional interaction and housing price patterns. *Appl. Geogr.* 79, 187–202. doi:10.1016/j.apgeog.2016.12.012

Sohn, K. (2014). Identifying the impact on land prices of replacing at-grade or elevated railways with underground subways in the seoul metropolitan area. *Urban Stud.* 51 (1), 44–62. doi:10.1177/0042098013484543

Song, J., Jin, X., Tang, J., Zhang, Z., Ding, N., Zhao, J., et al. (2011). Analysis of influencing factors for urban land price and its changing trend in China in recent years. *Acta Geogr. Sin.* 66 (08), 1045–1054. doi:10.11821/xb201108004

Song, J., Jin, X., and Tang, J. (2011). Analysis of influencing factors or urban land price and its changing trend in China in recent years. *Acta Geogr. Sin.* 66 (08), 1045–1054. doi:10.1007/s12182-011-0124-2

Song, M., Xie, Q., and Chen, J. (2022). Effects of government competition on land prices under opening up conditions: A case study of the huaihe river ecological economic belt. *Land Use Policy* 113, 105875. doi:10.1016/j.landusepol.2021.105875

Stephen, M. (1999). A simple error correction model of house prices. *J. Hous. Econ.* 8 (01), 27–62. doi:10.1006/jhec.1999.0240

Tsai, I-C. (2018). Housing price convergence, transportation infrastructure and dynamic regional population relocation. *Habitat Int.* 79, 61–73. doi:10.1016/j.habitatint.2018.07.004

Tu, Y. (2000). Segmentation of Australian housing markets: 1989–98. *J. Prop. Res.* 17 (4), 311–327. doi:10.1080/09599910010001420

Wang, S., Yang, Z., and Liu, H. (2008). An empirical study on the interaction of urban housing prices in China's regional market. *Res. Financial Issues* (06), 122–129. doi:10.19654/j.cnki.cjwtyj.2008.06.020

Wang, S., Wang, Y., Lin, X., and Zhang, H. (2016). Spatial differentiation patterns and influencing mechanism of housing prices in China: Based on data of 2872 counties. *Acta Geogr. Sin.* 71 (08), 1329–1342. doi:10.11821/dlxb201608004

Wang, C., Liu, H., and Zhang, M. (2020). Exploring the mechanism of border effect on urban land expansion: A case study of beijing-tianjin-hebei region in China. *Land Use Policy* 92, 104424. doi:10.1016/j.landusepol.2019.104424

Xia, H., Li, C., Zhou, D., Zhang, Y., and Xu, J. (2020). Peasant households' land use decision-making analysis using social network analysis: A case of tantou village, China. *J. Rural Stud.* 80, 452–468. doi:10.1016/j.jrurstud.2020.10.023

Xu, J., Huang, D., He, Z., and Zhu, Y. (2020). Research on the structural features and influential factors of the spatial network of China's regional ecological efficiency spillover. *Sustainability* 12, 3137. doi:10.3390/su12083137

Zeng, C. (2019). Spatial spillover effect on land conveyance fee—a multi-scheme investigation in wuhan agglomeration. *Land Use Policy* 89, 104196. doi:10.1016/j.landusepol.2019.104196

Zhan, H., Zhan, H., and Wu, Q. (2011). Spatial autocorrelation analysis of urban land price in jiangsu province. *Statistics Decis.* (20), 102–104. doi:10.13546/j.cnki.tjyjc.2011.20.040

Zhang, Q., Wang, X-Z., and Wang, C-Z. (2015). On spillover effect of Chinese Cities'House price fluctuation- based on DCC-MVGARCH model. *J. Tibet Univ.* 30 (04), 187–194. doi:10.16249/j.cnki.1005-5738.2015.04.029

Zhang, P., Hu, S., Li, W., Zhang, C., Yang, S., and Qu, S. (2021). Modeling fine-scale residential land price distribution: An experimental study using open data and machine learning. *Appl. Geogr.* 129, 102442. doi:10.1016/j.apgeog.2021.102442

Zhang, X., and Lin, R. (2015). Empirical study of short- term ripple effect of China's urban housing price. *Finance Econ.* (09), 132–140.

Zheng, X., Chen, X., and Yuan, Z. (2021). Exploring the spatial spillover effect of home purchase restrictions on residential land prices based on the difference-in-differences approach: Evidence from 195 Chinese cities. *Land Use Policy* 102, 105236. doi:10.1016/j.landusepol.2020.105236

Zhou, Y., and Tang, N. (2019). Effects of spillover effect and comparison effect on spatial correlation of urban land price. *Geogr. Geo-Information Sci.* 35 (02), 111–119. doi:10.3969/j.issn.1672-0504.2019.02.017

Zhou, Z-P., Qin, Z-Y., Zhao, S., and Chai, D. (2019). The spatial pattern, evolution characteristics and inflfluencing factors of land share in housing price in China: A spatial econometric analysis of 35 large and medium-size cities. *China Land Sci.* 33 (01), 40–48. doi:10.11994/zgtdkx.20181218.144450

Zhou, Y., Tang, N., and Wang, W. (2020). Influence of multidimensional closeness on strength and centrality of urban land price spatial correlation network. *Areal Res. Dev.* 39 (03), 65–69+82.

Zhu, C., Tang, Y., and Wu, Q. (2014). A study on the influence factors of the residential land price based on hedonic price model: Taking nanjing city as an example. *Areal Res. Dev.* 33 (03), 156–160.

Zhu, J-W., Chen, B., Lu, P., Liu, J. L., and Tang, G. (2018). Impact of urban water system treatment on the surrounding residential land price. *Arab. J. Geosci.* 11, 6. doi:10.1007/s12517-017-3341-1

frontiers | Frontiers in Environmental Science

TYPE Original Research
PUBLISHED 10 January 2023
DOI 10.3389/fenvs.2022.1030796

Check for updates

OPEN ACCESS

EDITED BY
Ying Jing,
Zhejiang University, China

REVIEWED BY
Märit Jansson,
Swedish University of Agricultural Sciences, Sweden
Voltaire Alvarado Peterson,
University of Concepcion, Chile
Lijun Xing,
Hubei University, China

*CORRESPONDENCE
Shuna Xu,
xusn1027@aliyun.com

SPECIALTY SECTION
This article was submitted to Land Use Dynamics, a section of the journal Frontiers in Environmental Science

RECEIVED 29 August 2022
ACCEPTED 19 December 2022
PUBLISHED 10 January 2023

CITATION
Xu S and Wang Y (2023), Influence of spatial scale on the study of access fairness of urban park green space.
Front. Environ. Sci. 10:1030796.
doi: 10.3389/fenvs.2022.1030796

COPYRIGHT
© 2023 Xu and Wang. This is an open-access article distributed under the terms of the Creative Commons Attribution License (CC BY). The use, distribution or reproduction in other forums is permitted, provided the original author(s) and the copyright owner(s) are credited and that the original publication in this journal is cited, in accordance with accepted academic practice. No use, distribution or reproduction is permitted which does not comply with these terms.

Influence of spatial scale on the study of access fairness of urban park green space

Shuna Xu* and Yinzhen Wang

College of Urban and Environmental Sciences, Xuchang University, Xuchang, Henan, China

Park green space is an important ecological factor of the urban built-up environment, and it plays an increasingly important role in improving human welfare and the quality of urban life. Accessibility analysis of urban park green space is an issue of social equity and environmental justice that has received widespread attention. The accessibility of a city's park green space must be evaluated under the correct scale and resolution before it can be applied to urban green space planning. To measure the impact of different research scales on accessibility, Weidu District of Xuchang City, Henan Province, China, was taken as the experimental area. The Gaussian-based two-step floating catchment area method was used to compare and analyze the accessibility differences under three scales: subdistrict, community, and residential quarter. The influence of the source and destination point modes on accessibility was analyzed at the residential quarter scale. Results show that the accessibility of park green space at the subdistrict scale is different from that at the community and residential quarter scales in terms of spatial distribution characteristics and quantitative relationship. The accessibility of the geometric center mode and the entrance and exit mode at the residential quarter scale is similar in overall distribution and different in local quantity. Overall, the accessibility of the park green space at the residential quarter scale under the entrance and exit mode and the spatial fairness of visiting the park green space are better than that under the geometric mode. Therefore, accessibility analysis of park green space should be performed cautiously when taking the aggregation unit as the basic research unit. The accessibility of the aggregation unit is not the statistical summary of its subunits, especially when the area of the aggregation unit is far larger than the walking range of residents, and is thus likely to lead to wrong conclusions. Accessibility analysis should be conducted on the finest scale possible rather than the aggregation scale and use true distance rather than the centroid-to-centroid surrogate to obtain reliable results for further guiding urban green space planning.

KEYWORDS

park green space, accessibility, spatial fairness, Gaussian-based two-step floating catchment area method, urban green space planning

1 Introduction

The World Urban Report 2020 (Knudsen et al., 2020) shows through detailed demonstration that urbanization will continue to be the driving force of global growth. In the next 10 years, the proportion of the urban population in the global population will increase from 56.2% at present to 60.4% in 2030. While providing convenience for people's lives, high urbanization also brings a series of environmental pressures, such as the urban heat island effect and air pollution. Research shows that a causal relationship exists between the increase in lung

cancer, cardiopulmonary disease, pediatric asthma, and urban air pollution (Larondelle and Lauf, 2016). As an important ecological factor of the urban built environment, park green space plays an important role in improving human wellbeing and urban life quality by improving the ecological environment, increasing sports activities and social interaction within the neighborhood, and improving people's ability to participate in society (Hunter et al., 2019). Wang and Lan (2019) showed that the quantity, quality, and accessibility indicators of urban park green space have a significant negative correlation with the incidence rate of cardiopathy, chronic pneumonia, and hypertension. People often engage in outdoor entertainment activities in the natural environment near their residence, which can not only increase their health and happiness but also help them cope better with work pressure, mental fatigue, and depression (Buchecker and Degenhardt, 2015; Kondo et al., 2018; Hunter et al., 2019; Wang and Lan, 2019). Therefore, by providing accessible, attractive, well-maintained green spaces with room for socialization and encouraging people to use it, urban green spaces can effectively promote the physical and mental health of urban residents (Hunter et al., 2015; Kruize et al., 2019).

However, providing adequate park green spaces is challenging because housing, retail, and commercial developments, and transport infrastructure are all competing for limited space (Hunter et al., 2019). In most cases, park green spaces are not evenly distributed in the space within the cities (You, 2016). Unfair access to park green space may lead to environmental injustice, which can be accompanied by social stratification and housing segregation (Xiao et al., 2019). Thus, analyzing the spatial distribution characteristics of urban park green space accessibility is of great significance in promoting the fair and reasonable layout of urban park green space and improving the overall happiness of urban residents. Access to park green space is referred to as "accessibility," which is a key factor that affects the selection and use frequency of park green space (Žlender and Ward Thompson, 2016; Agimass et al., 2018; Mears et al., 2019; Tardieu and Tuffery, 2019; Zhang and Tan, 2019; Tu et al., 2020). Two kinds of accessibility measure methods exist. Place-based accessibility measures examine the proximity to desired activity locations from key locations in an individual's daily life, such as the home or workplace. People-based accessibility measures rely on detailed observations of an individual's activity schedule and space-time constraints (Neutens et al., 2010). Place-based accessibility is affected by the size and location of residential and recreational areas, the road network between them, and the mode of travel. Two main methods can be used for early place-based accessibility analysis: the travel cost and gravity model methods. The travel cost method determines the nearest park green space from the residential area according to the principle of minimum cost (distance, time, and money) (e.g., Ala-Hulkko et al., 2016; Wüstemann et al., 2017). Information such as the number of people living in the area and the scale of the park green space is not considered. The gravity model method assumes that spatial interaction decreases with the increase in the spatial distance between the residence and the destination. The gravity model is used to measure the attraction of each park green space to a certain residence and adds these attractions to obtain the accessibility of the park green space of the residence (e.g., Lee and Hong, 2013; Xiao et al., 2017). This method considers the distance between residence and park green space, number, and scale of the park green space. However, the influence of the size of the resident population is ignored. In view of the shortcomings of the above two methods, the two-step floating catchment area method (Radke and Mu, 2000), its improved version (the enhanced two-step floating catchment area method; Luo and Qi, 2009), and the Gaussian-based two-step floating catchment area method (Dai, 2011) have been increasingly used in the accessibility analysis of park green space (e.g., Shen et al., 2017; Wei, 2017; Li et al., 2019). The two-step floating catchment area method calculates the ease with which each resident can reach the park green space according to the population of the residence and the area of the park green space and their spatial distribution characteristics and path distances.

At present, place-based accessibility analysis of park green space is mostly based on administrative division units (e.g., You, 2016; Shen et al., 2017; Wei, 2017; Li et al., 2019; Wang and Lan, 2019; Hu et al., 2020; Shi et al., 2020; Zhang et al., 2022) or grid units (e.g., Ala-Hulkko et al., 2016; Xing et al., 2018; Guo et al., 2019; Shi et al., 2020) to analyze the spatial distribution characteristics, time-varying characteristics, and the correlation between accessibility and population, and socioeconomic indicators, and then analyze the spatial and social fairness of the urban green space distribution. These methods take the geometric center of the aggregation area as the source point and the geometric center of the park green space as the destination point to calculate the accessibility of the park green space of each research unit at a specific spatial scale. Spatial aggregation can affect the results of accessibility analysis (Miller, 2016). A major difference exists between the source and destination points here, and the actual origins and destinations of travelers in reality, bringing great uncertainty to the final accessibility results. Ahuja et al. (2021) pointed out the problem of mismatch between zone and movement scales in place-based accessibility analysis. This type of research is lacking in operability to guide the practice of urban green space planning (Liu et al., 2020). Tan and Samsudin (2017) studied the scale effect of the spatial fairness of urban park green space and found that the unfairness at the small scale was more intense than that at the large scale. They also emphasized the need to guide urban park planning at the neighborhood scale.

What impact will different research scales have on the accessibility analysis of urban park green space, and would different location selection methods of source and destination points have a significant impact on the accessibility results? In view of this problem, this paper takes Weidu District of Xuchang City as the experimental area and analyzes the spatial distribution characteristics of urban park green space accessibility and their relationship at three scales, namely, subdistrict (the fourth-level administrative division in China), community (the fifth-level administrative division in China), and residential quarter (the most basic population gathering area in the city). In China, the first two administrative division scales are frequently used as basic units for the accessibility analysis of urban park green space. A subdistrict consists of several communities, while a community consists of several residential quarters. At the residential quarter scale, the differences and relations between the two modes of accessibility are compared and analyzed, with one taking the geometric centers of the residential quarter and the park green space as the source and destination points (geometric center mode), and the other taking the entrance and exit of the two as the source and destination points (entrance and exit mode). The possible problems in the analysis of different research scales and accessibility modes are summarized to determine the research scale and method suitable for guiding the practice of urban green space planning.

2 Method and material

2.1 Method

2.1.1 Accessibility model

The accessibility model is used to analyze the access of residents to the park green space (accessibility). On the basis of the spatial location, scale, and road network of the park green space and the residence area, the Gaussian-based two-step floating catchment area method (Dai, 2011) is used to calculate the accessibility of each residence. The process is divided into two steps.

In the first step, for each park green space j, path distance threshold d_0 is given to form its spatial service range. For the population of each residence place k falling within its service range, the Gaussian equation is used to assign the corresponding weight according to the distance from the park green space. Then, the weighted sum is derived to obtain the potential users of park green space j. Next, the size of the green space is divided by the number of potential users to obtain supply and demand ratio R_j (m^2/person).

$$R_j = \frac{S_j}{\sum_{k\in\{d_{kj}\le d_0\}} G(d_{kj}, d_0) P_k} \tag{1}$$

where P_k is the population of residence place k within the service scope of green park j ($d_{kj} \le d_0$); d_{kj} is the distance from the geometric center (or entrance) of residence place k to the geometric center (or entrance) of park green space j; S_j is the scale of park green space j, which is expressed by the area; and $G(d_{kj}, d_0)$ is a Gaussian equation that considers the space friction problem. The calculation method is shown in Eq. 2.

$$G(d_{kj}, d_0) = \begin{cases} \dfrac{e^{-\left(\frac{1}{2}\right)\times\left(\frac{d_{kj}}{d_0}\right)^2} - e^{-\left(\frac{1}{2}\right)}}{1 - e^{-\left(\frac{1}{2}\right)}}, & if \quad d_{kj} \le d_0 \\ 0, & if \quad d_{kj} > d_0 \end{cases} \tag{2}$$

In the second step, for each residence place i, given path distance threshold d_0, the reachable range is formed. Similarly, the supply ratio (R_l) of each park green space l within the reachable range is weighted by the Gaussian equation. Then, the weighted sum of these supply ratios is used to obtain the park green space accessibility (A_i) for each residence place i. The size of A_i indicates the *per capita* occupancy of the urban park green space in each residence place within its reach, given in m^2/person.

$$A_i = \sum_{l\in\{d_{il}\le d_0\}} G(d_{il}, d_0) R_l \tag{3}$$

where l refers to all the park green spaces within the accessible space of residence place i ($d_{il} \le d_0$). Considering that the recreational activities of the residents who visit the park green space are mainly walking and cycling, distance threshold d_0 is set to 1,000 m, that is, approximately 10–15 min' walk. This threshold is determined for two reasons. First, 1,000 m (or 10–15 min) is an acceptable walking distance for residents to visit the park green space (You, 2016; Žlender and Ward Thompson, 2016; Guo et al., 2019; Nesbitt et al., 2019; Tu et al., 2020). In addition, the Gaussian-based two-step floating catchment area method itself accounts for the travel friction effect. Thus, a longer distance threshold can reduce the number of residential areas that have zero accessibility.

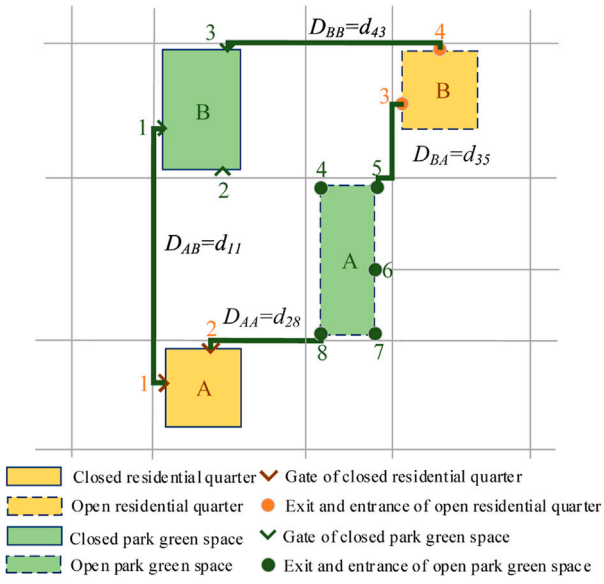

FIGURE 1
Schematic of the distance between residential quarter and park green space in entrance and exit mode.

2.1.2 Location of source and destination points

In the accessibility analysis of urban park green space, given that the residence place and the park green space are both polygons, the points that can represent them must be taken as the source (starting) and destination (end) points, respectively. In this study, two methods are used to select the source and destination points. First, the geometric centers of the subdistrict, community, and residential quarter areas are used as the source points and the geometric centers of the park green space are used as the destination points. Then, the distance between the source and destination points is the path distance between the two geometric centers (geometric center mode). Second, at the residential quarter scale, the entrance and exit positions are used as the source points, and the entrance and exit positions of the park green space are used as the destination points. Urban residential quarters are mainly closed, with one or more gates as entrances and exits. Some open urban villages have no gates. Thus, one or more intersections of urban roads with the main road through urban villages are selected as entrances and exits. Parks are also divided into two categories: closed walled parks with their gates as exits, and open park green space without enclosures, with the first place along each road from each direction to it serving as the entrances. Given that the residential quarter and the park green space may have more than one entrance and exit, multiple paths from the residential quarter to the park green space may exist. According to the principle of the best path, the shortest path distance is selected as the distance between the residential quarter and the park green space (entrance and exit mode), as shown in Figure 1.

2.2 Material

2.2.1 Experimental area

Weidu District of Xuchang City, located in the middle of Henan Province has a long history. The district is an important birthplace of Chinese culture and has a beautiful environment. Weidu is known as

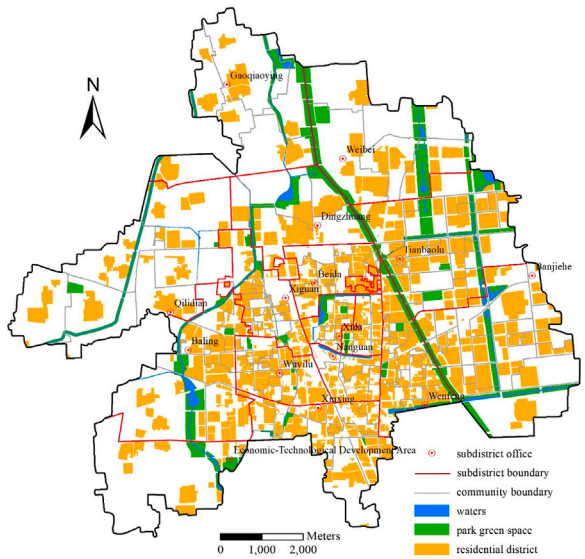

FIGURE 2
Distribution of subdistrict, community, and residential quarter and parks in the study area.

the "National Ecological Garden City," which is the highest comprehensive award in the field of urban construction in China. The district now has 16 subdistricts (including one economic and technological development zone) with a total area of 97 km^2. In 2020, the permanent resident population was 598,600, and the gross domestic product is CNY 42.11 billion (Chen and Cui, 2021).

Weidu District belongs to the warm temperate monsoon zone with a mild climate. The annual average temperature is 14.7°C, the number of hours of sunshine is 2,280 h, the annual precipitation is 579 mm, and the frost-free period is 217 days. The district is located in the hinterland of the Central Plains, which has a flat terrain. The terrain inclines from northwest to southeast. In the west are gentle low hills with alluvial deposits in front of mountains, with the highest elevation of 95 m. The rest of the area is part of the Huanghuai alluvial plain, with the lowest elevation of 65 m. The river is part of the Yinghe River system of the Huaihe River Basin (Weidu District government, 2020).

Weidu District has 115 park and green spaces within 1 km, covering a total area of about 1,179 ha and mainly composed of riverside parks and leisure squares. In recent years, Xuchang City has implemented the river lake water system connection project in the central urban area. The newly built urban park green spaces are arranged along the water system, forming a connected open green leisure space without walls, as shown in Figure 2.

2.2.2 Data sources

The data sources include subdistrict boundaries, community boundaries, the spatial distribution data of residential quarters, the population of residential quarters, urban road networks, and park green spaces. The subdistrict boundary data were obtained from the Yearbook of Weidu District, People's Government of Weidu District Xuchang City, 2018. The community boundary data mainly came from the subdistrict-by-subdistrict field survey and some from the Xuchang Natural Resources and Planning Bureau. The spatial distribution data of residential quarters, urban road networks, and park green spaces were obtained from QuickBird images (.5 m panchromatic image and 2 m multispectral image) of the study area in 2014, and an unmanned aerial vehicle was used to update the data of the urban fringe to the end of 2020. Given the difficulty of obtaining the population data of the residential quarter scale in the study area, the number of residential buildings is used to replace the population. The number of residential buildings is obtained from three sources: the real estate service platform HomeLink (https://xc.lianjia.com/), the planning permission document of the Xuchang Natural Resources and Planning Bureau (http://zrzyhghj.xuchang.gov.cn/), and field surveys. The total number of residential buildings in the subdistrict and community levels is obtained through zonal statistics (Xu et al., 2017). Therefore, the result of this study is the accessibility situation of park green space when the occupancy rate reaches 100%. In addition, to avoid the boundary effect, we buffered the study area outward by 1 km during data processing. Accessibility analysis is implemented using ArcGIS10.7 and MATLAB R2015a.

3 Results

3.1 Accessibility difference under different research scales

The accessibility of the park green space at the subdistrict, community, and residential quarter scales is shown in Figures 3A–C, respectively. The source points are the geometric centers of the subdistrict, community, and residential quarter areas, and the destination points are the geometric centers of the park green space. The statistics of accessibility at different scales are shown in Table 1.

From the spatial distribution perspective, the subdistrict scale shows completely different characteristics from the other two scales. At the subdistrict scale, the accessibility of park green space is slightly higher in the east-west central region than in the other regions and low in the south and north regions. At the community and residential quarter scales, the distribution characteristics are similar, that is, the accessibility in the east and midwest regions is higher than that in the other regions.

From the quantitative relationship among different scales, the accessibility on the subdistrict scale is generally low. The accessibility in 5 of the 16 subdistricts is 0, indicating that residents in these 5 subdistricts have no park green space to visit within the 1,000 m distance threshold, the average value is 5.59 m^2/household, and the median value is only 1.73 m^2/household. The accessibility at the subdistrict scale cannot reflect the comprehensive situation of the communities and residential quarters under its jurisdiction. For example, the accessibility of Gaoqiaoying subdistrict in the north is 0; among the six communities under its jurisdiction, the accessibility of the Banqiao community is as high as 1745.30 m^2/household and that of the Daluozhuang community is as high as 694.85 m^2/household, respectively, ranking first and second in accessibility at the community scale. The accessibility of Weibei subdistrict in the northeast is 0; among the five communities under its jurisdiction, the accessibility of the Guolou community is 566.24 m^2/household, and that of the Jinwan and Wangzhuang communities are 59.98 and 15.09 m^2/household, respectively. The accessibility of Banjiehe subdistrict in the southeast is 0, but at the community scale, 14 of the 19 communities under its jurisdiction are far greater than 0. The accessibility of Beida subdistrict

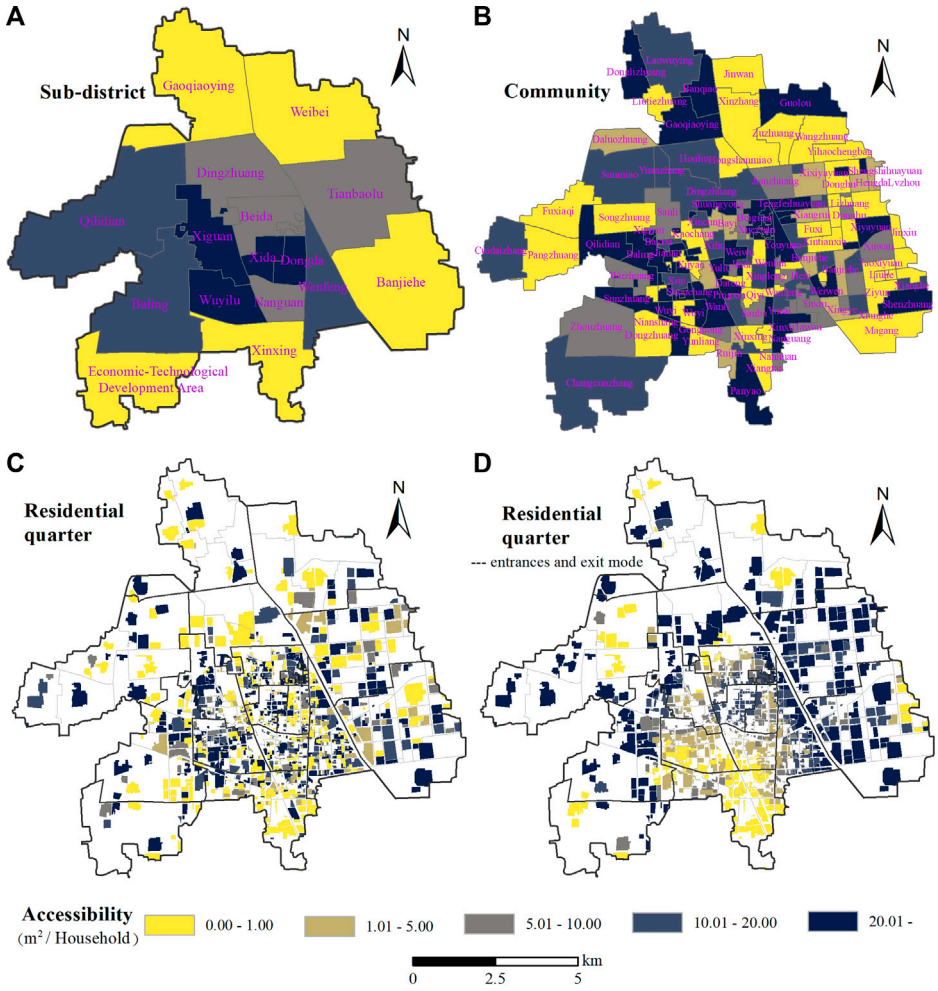

FIGURE 3
Figures **(A–C)** show the accessibility of the park green space at the subdistrict, community, and residential quarter scales under the geometric center mode. Figure **(D)** shows the accessibility at the residential quarter scale under the entrance and exit mode.

TABLE 1 Accessibility statistics under different research scales (m²/household).

Level / Statistics	Minimum	Maximum	Mean	Median	Standard deviation
Subdistrict	0	32.31	5.59	1.73	8.52
Community	0	1745.3	50.95	6.29	187.22
Residential quarter (geometry centers)	0	1624.3	17.36	4.41	72.12
Residential quarter (entrance and exits)	0	1326.7	17.04	6.84	55.49

in the center of the study area is 0, but the accessibility of 4 of the 6 communities under its jurisdiction are greater than 0.

To compare the relationship of accessibility between different scales in a statistical sense, the subdistrict and community scale accessibilities summarized by the residential quarter are obtained by weighted averaging the accessibility at the residential quarter scale according to the population (number of households). Weighted averaging the accessibility at the community scale according to the population (number of households) obtains the overall subdistrict scale accessibility of the community. The Spearman's correlation coefficient between original accessibility and aggregate accessibility at the subdistrict and community scales is shown in Table 2. No significant correlation exists between the accessibility at the subdistrict scale and the two kinds of accessibility obtained by the weighted aggregation of the communities and the residential quarters, respectively. However, a significant correlation exists between the latter two, indicating a significant difference between the accessibility at the subdistrict

TABLE 2 Spearman's correlation coefficient (*p*-value) between accessibility at subdistrict and community scales, and the corresponding weighted summary results.

		Accessibility	Accessibility summarized by communities	Accessibility summarized by residential quarters
Subdistrict scale (n = 16)	Accessibility		.167 (.536)	−0.015 (.956)
	Accessibility summarized by communities			0.647** (.007)
	Accessibility summarized by residential quarters			
Community scale (n = 123)		Accessibility		Accessibility summarized by residential quarters
	Accessibility			0.618** (.000)
	Accessibility summarized by residential quarters			

**The correlation is significant at the .01 level (double tailed)

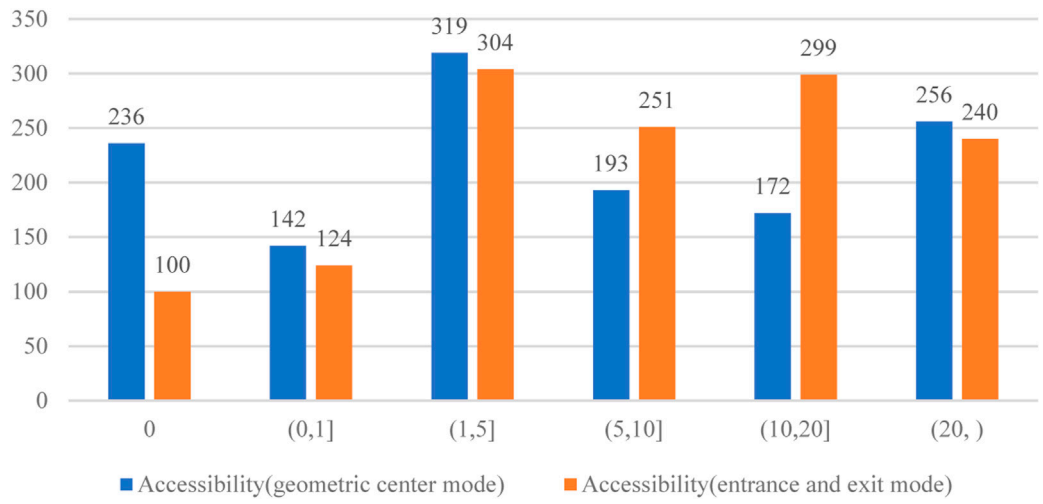

FIGURE 4
Statistical chart of two accessibility levels at the scale of residential area.

scale and the community and residential quarter scales. The latter two have similar spatial distribution characteristics, which is also confirmed by the significant correlation between the accessibility at the community scale and the accessibility summarized by the residential quarters.

3.2 Accessibility difference of different source and destination points under the same research scale

The accessibility at the residential quarter scale is presented in Figure 3C, which shows that the geometric centers of the residential area and the park green space are taken as the source and destination points (geometric center mode), respectively. Figure 3D shows the entrances and exits of the residential quarter and the park green space as the source and destination points (entrance and exit mode), respectively.

From the spatial distribution perspective, overall similarities and local differences between the two accessibility modes can be observed. Overall, the south-central regions have poor accessibility, whereas the surrounding residential areas have good accessibility. This rule is obvious in the entrance and exit mode. Locally, the former has more residential quarters with poor accessibility than the latter. For example, the residential quarters with poor accessibility distributed at the edge of the study area shown in Figure 3C correspond to the high accessibility shown in Figure 3D).

From the statistical relationship between the two modes, the Spearman's correlation coefficient is .730 (p = .000, n = 1,318), indicating a significant sequential correlation between the two modes and confirming their overall similar characteristics. The hierarchical statistical diagram of accessibility under the two modes is shown in Figure 4. Under the geometric center mode, many residential quarters have very low and high accessibility values, and the accessibility among different residential quarters changes greatly, indicating the poor spatial fairness of the park green space. However,

in the entrance and exit mode, few residential quarters have very low or very high accessibility values, while many residential quarters have medium accessibility, and the accessibility changes are small, that is, the spatial fairness of park green space access is good. This finding can also be confirmed from Table 1.

To sum up, in addition to the overall similarity, the two accessibility modes also have the following differences: 1) In the geometric center mode, the accessibility of 236 residential quarters is 0, indicating that they have no park green space to access within the 1 km distance threshold. In the entrance and exit mode, the number of residential quarters with accessibility of 0 is reduced to 100. 2) In the entrance and exit mode, the accessibility of 720 residential quarters is greater than that of the geometric center mode, that of 498 residential quarters is less than that of the geometric center mode, and the accessibility of 100 residential quarters is unchanged (0 in both modes). 3) Under the entrance and exit mode, the accessibility difference between residential quarters is small, indicating that the fairness of accessing the park green space is good, while the accessibility difference between residential quarters under the geometric center mode is large, which corresponds to strong spatial unfairness.

4 Discussion

4.1 Analysis of the influence of research scale on accessibility

Accessibility reflects the utilization possibilities of the park green space from a population perspective (Ala-Hulkko et al., 2016). In the Gaussian-based two-step floating catchment area method, the factors that affect the accessibility of urban park green space mainly include the number and spatial distribution of population, the number and spatial distribution of park green spaces, and the road network. The space range of the park green space is unchanged, while the population aggregation can be based on different scales. The impact of scale on accessibility is mainly manifested in two aspects: One is the scale effect caused by different levels of population spatial aggregation, and the other is the distance error between the residential area and the park green space. Spatial aggregation can affect the results of an accessibility analysis, with the results varying simply by changing the level of spatial aggregation (Miller, 2016). This is known as the scale effect in the modifiable areal unit problem. This study compares the accessibility results of the park green space under three spatial scales. The residential quarter is the most basic population gathering area of the city, while the community and subdistrict are the aggregation-level units. The population area and the park green space show a discrete or adjacent polygon distribution in space. In each polygon, the points that can represent the location of the population gathering area and the park green space are selected as the source and destination points in the accessibility analysis. No real starting point exists in the population aggregation-level units; it is often replaced by its geometric center. The area of the research unit affects the accessibility, and the uncertainty increases with the area. The accessibility on the subdistrict scale in the study area is generally low, which is different from the other two scales. The accessibility of 5 subdistricts is 0. One of the most important factors is that the area of the study unit is extremely large. The smallest subdistrict area spans 1.18 km^2, the largest subdistrict area is 12.53 km^2, and the average value is 5.72 km^2. When the subdistrict area is more than 4 km^2 and the path distance threshold is set to 1 km, the subdistrict has difficulty accessing the park green space outside its jurisdiction. The park inside the subdistrict must also be arranged near the geometric center point. And the road network has to be smooth. Otherwise, the subdistrict has no park green space to access, such as Gaoqiaoying subdistrict. Weibei subdistrict and the economic and technological development zone have many park green spaces. However, because they are far away from the geometric center and/or have a poor road network, their park green space accessibility is 0. Therefore, smaller zones or "homogeneous zones" are preferred in accessibility analysis (Riva et al., 2009; Ahuja et al., 2021). In our research, the residential quarter is the smallest and relatively homogeneous research unit because the house price and residents' socioeconomic characteristics of the same residential quarter are relatively similar.

When the geometric centers are used as the source and destination points, the geometric center is connected to the nearest road when calculating the path distance between the source and destination points, with the vertical intersection between them taken as the starting and end points. The geometric centers of the polygons are affected by their location, shape, and area. Without changing the number and distribution of the population, changing the shape of the population gathering area and its aggregation unit is likely to change the position of its geometric center. The distributions of the population in urban space and the urban road network are uneven. There is a certain randomness in terms of which road the geometric center is closest to. Moreover, given that the acceptable path distance for walking to the park green space is mostly within 1 km, the error of this path distance is sufficient to bring uncertainty to the accessibility analysis results. Therefore, using true distance between zones rather than the centroid-to-centroid surrogate can reduce the impact of scale on accessibility calculation (Miller, 2016). However, as communities and subdistrict are population aggregation units, there is no real starting point, and distance error is inevitable. On the scale of residential quarters, they have real starting points (gates), and the distance error can be avoided.

4.2 Analysis of the influence of the location of source point and destination point on accessibility

The location of different source and destination points affects the accessibility by affecting the path distance between them. Place-based accessibility measures depend strongly on how distance is measured (Ahuja et al., 2021). In particular, the activities of visiting park and green space by walking in cities are highly sensitive to distance (Grahn et al., 2003). In the same research scale, the path distances between different source and destination points also vary, resulting in different accessibility results. In the geometric center mode, the system is associated with the geometric center with the nearest road and takes the vertical intersection of the geometric center and the nearest road as the starting and end points. The starting and end points are often not the location of the entrance and the exit. Therefore, certain differences in the distance between the two paths exist, thereby affecting the final accessibility. The distance difference between the two paths is also affected by the area of the residential quarter. Given that the area of the residential quarter is generally small relative to the distance threshold (the average value is .02 km^2), a

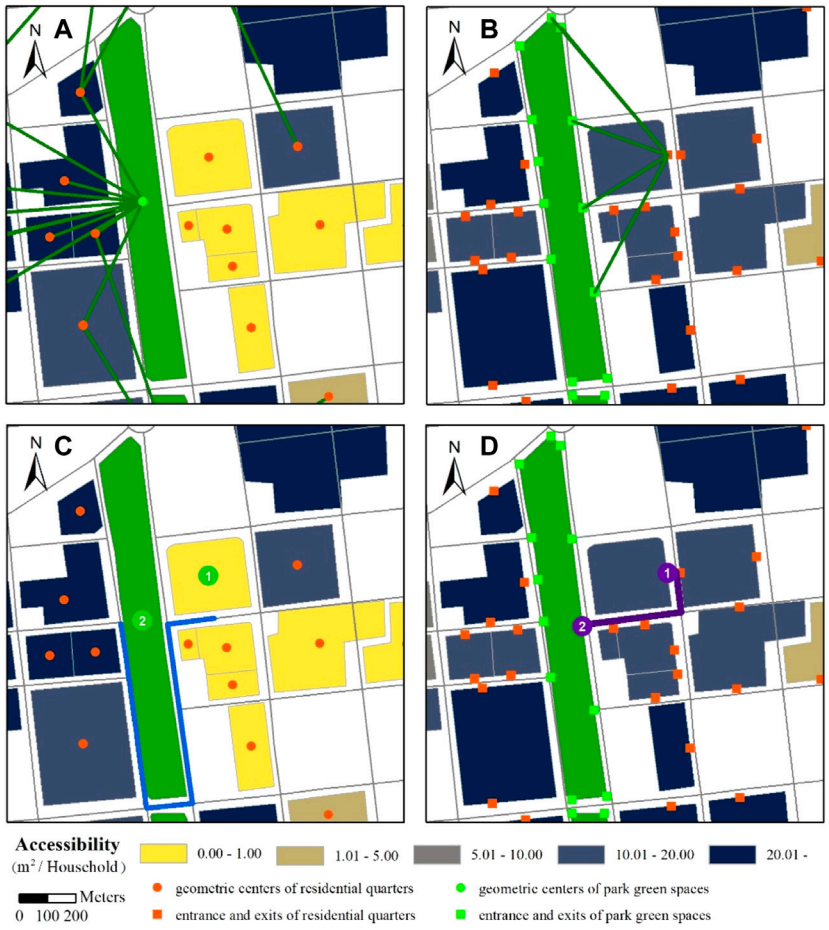

FIGURE 5
Figures **(A, C)** show the pathdistance between residential quarter and park green space under geometric center mode. Figures **(B, D)** show the path distance between them in the entrance and exit mode.

significant correlation exists between the accessibility under the two different source and destination point modes, and the spatial distribution characteristics of the accessibility are similar, but significant differences in local areas exist. The main reasons are as follows.

First, the geometric center mode will lead to the error of the path distance between the residential quarter and the park green space. Usually, the residential quarter and the park green space have more than one entrance and exit. Open and fenceless park green spaces have even more entrances and exits. Thus, multiple paths are available from the residential quarter to the park green space. According to the principle that human activities always tend to select the spatial location with the best effect according to certain goals, one of the shortest routes is selected as the path distance between the two. Therefore, the distance between the residential quarter and the park green space in the entrance and exit mode is usually shorter than that in the geometric center mode. As a result, the accessibility of most residential areas in the entrance and exit mode is higher than that in the geometric center mode. However, some residential quarters in the entrance and exit mode are less accessible than those in the geometric center mode. The main reason for this condition is that under a certain distance threshold (1 km here), many residential quarters can access the park green space under the entrance and exit mode (the number of residential communities with accessibility of 0 under the entrance and exit mode is greatly reduced), resulting in the increased service population of the corresponding park green space. Accordingly, the accessibility of the residential quarter that is near the park green space with a very high accessibility is reduced. The residential quarter with constant accessibility (equal to 0) is far from the park green space, and the path distance under both modes is greater than the distance threshold.

Second, in some special but not unusual cases, the geometric center mode will lead to the path distance mistake, and the final accessibility result is far from the actual situation. For example, the seven residential communities in the southeast of the Banjiehe subdistrict (yellow polygon in Figure 5A) are very near the park green space, but their accessibility is 0 under the geometric center mode, which obviously does not conform to the actual situation. The main reason for this phenomenon is that the geometric center of the park green space is near the road on the west side, so the end point is located on its west road. When the residents in the residential quarter located in the east of the park want to visit the park, they must go around the end point on the west side, thereby greatly increasing the path distance. When the path distance exceeds the threshold of 1 km, the accessibility of the residential quarter is 0, as shown in Figure 5C. In the entrance and exit mode, the entrance and the exit are located on

the road, and the above problems do not exist (Figure 5B). The residential quarter in the figure has one entrance and exit, and the open park green space without walls has multiple entrances and exits. After calculation, the path distance from the entrance and exit of the residential quarter to the five entrances and exits of the park is less than 1 km, and the shortest one is taken as the path distance between the two (Figure 5D). Therefore, the accessibility of these seven residential areas in the entrance and exit mode is greater than 0, which is in line with the reality.

4.3 Enlightenment to urban green space planning

In view of the accessibility of park green space and the resulting spatial fairness, different conclusions may be obtained under different research scales. Therefore, the following three ideas are proposed for urban green space planning.

First, the evaluation and planning of urban green space should be conducted at a suitable scale. Activities such as visiting parks and green space are considered ecosystem cultural services. The assessment of urban ecosystem services under the correct scale and resolution is the premise of the application to urban planning practice (Cortinovis and Geneletti, 2018). Assessing under an inappropriate scale may even have a negative impact (Larondelle and Lauf., 2016). For recreational activities that involve walking as the main travel mode, the activity range is relatively small. When the basic research unit is far larger than the activity range, the risk of drawing a wrong conclusion is great. For example, the accessibility of the park green space calculated at the subdistrict scale in this study is far lower than that in the actual situation. The spatial distribution characteristics of the accessibility obtained at the community scale and the residential quarter scale are similar, but significant differences in numerical values exist. Therefore, the larger aggregation unit is unsuitable for the basic unit of accessibility analysis. The smaller aggregation unit can be used to analyze the overall characteristics of accessibility distribution, but the value will have certain errors. Therefore, a better approach would be to undertake accessibility analysis at the finest possible spatial scales (Mears et al., 2019). All kinds of life behaviors of urban residents are carried out around the residential quarters. Accordingly, the accessibility of park green space must be analyzed and urban green space planning must be guided by taking the residential quarter as the basic unit.

Second, the evaluation and planning of urban green space should not ignore the impact of details. A better approach would be to use the true distance between zones rather than the centroid-to-centroid surrogate (Miller, 2016). To our knowledge, place-based accessibility analysis is mostly based on the spatial aggregation level: administrative division units (e.g., You, 2016; Shen et al., 2017; Wei, 2017; Li et al., 2019; Wang and Lan, 2019; Hu et al., 2020; Shi et al., 2020; Zhang et al., 2022) or grid units (e.g., Ala-Hulkko et al., 2016; Xing et al., 2018; Guo et al., 2019; Shi et al., 2020), on which scale centroid-to-centroid surrogate is inevitable. When evaluating the accessibility of park green space and the fairness of its spatial distribution under the residential quarter scale, two different accessibility modes will lead to the difference in the path distance between the residential quarter and the park green space. This difference often increases with the area of the residential quarter and the park green space, thus increasing the difference in accessibility. In some cases, the accessibility results under the two modes are different. The accessibility difference between residential quarters under the geometric center mode is relatively large, corresponding to the relatively high spatial unfairness of accessing park green space, while the accessibility difference between residential quarters under the entrance and exit mode is relatively small, corresponding to a relatively low spatial unfairness of accessing park green space. For recreational activities that require people to reach the green space for experiential interaction to benefit, the consistency of the source and destination points with the reality will directly affect the scientificity and accuracy of the evaluation results and further affect the subsequent green space planning and optimization. For example, in the geometric center mode, the real situation of some residential quarters with low accessibility or even 0 is not the case but is caused by the calculation mode. Therefore, taking the entrance and exit of the residential quarter and the park green space as the source and destination points conforms to the daily activities of the residents. Without changing the existing population and the distribution status of the park green space, the accessibility of the park green space can be improved by optimizing the entrance and exit positions of the residential quarter and the park green space. For residential quarters with limited access to park green space, the park green space can be visited by increasing the entrance and exit of residential quarters, increasing the entrance and exit of park green space, or changing the closed park green space into an open one.

Third, the conclusions on the fairness of people with different social and economic backgrounds visiting the park green space obtained by taking the aggregation area as the research unit should be treated with caution. The accessibility analysis results are often further related to the population, social economy, and other factors in the study area, influencing the conclusion as to whether the access enjoyed by people with different social and economic backgrounds to the park green space is unfair. When this activity is performed on the aggregation area, the conclusions are often uncertain because the accessibility of the aggregation area is not obtained through simple summary statistics of the sub-areas, such as the population and other factors. Shen et al. (2017) analyzed the correlation between the accessibility of public green space and socioeconomic factors in downtown Shanghai on the basis of the subdistrict scale. The results show that the accessibility of public green spaces is related to social status and family composition. Married couples who have children have high accessibility, whereas the elderly and the unemployed population have low accessibility. However, Xiao et al. (2017) conducted a study based on the community scale in the same research area and found that the low-income groups in Shanghai are not at a disadvantage in terms of entering urban parks. In addition to the research scales, the two studies adopted different accessibility methods and indicators of social and economic factors.

4.4 Limitations and prospects

The first limitation of this study is the determination of distance threshold. At present, the distance threshold values that were used include 300 m (Schipperijn et al., 2010a; Mears et al., 2019), 400 m (Tan and Samsudin, 2017; Wei, 2017), 500 m (Wüstemann et al., 2017), 600 m (Schipperijn et al., 2010b), 800 m (Wei, 2017), 1,000 m (You, 2016; Nesbitt et al., 2019; Tu et al., 2020), 1,200 m (Shen et al., 2017), 1,600 m (Xiao et al., 2017), or 10–20 min' walking distance

(Guo et al., 2019) and 15 min' walking distance (Žlender and Ward Thompson, 2016). Given that the Gaussian-based two-step floating catchment area method itself accounts for the travel friction effect and a longer distance threshold can reduce the number of residential areas with zero accessibility, a distance threshold of 1 km was determined in this study. Because of the space limitation, this study did not compare the impact of scale on accessibility under other distance thresholds. From the results of this study, we can infer that the influence of scale on accessibility increases with the decrease in the distance threshold. In addition, although not the focus of this study, given the difficulty of obtaining the permanent population data of each residential quarter in this study, the number of building households is used to replace the number of population, that is, with the assumption that the occupancy rate of each residential quarter is 100% and each household has the same population, the final accessibility results may have a certain deviation. Finally, this feature is also a common disadvantage of all place-based accessibility measures that assume that the residential area is the most relevant area that affects residents' behavior, thus facing the well-known problem of ecological fallacy, which involves erroneously ascribing attributes of an aggregate unit to individuals (Kwan and Hong, 2009). With the development of location-aware technologies, people-based accessibility research is no longer difficult. Place-based measures should be enhanced and complemented with people-based measures that are more sensitive to individual activity patterns and accessibility in space and time (Miller, 2016).

5 Conclusion

Accessibility analysis is one of the important methods of testing the rationality and fairness of spatial distribution and an important reference for the optimization of urban park green spaces. This analysis is the premise of application to urban green space planning to evaluate the accessibility of a city's park green space under the correct scale and resolution. To measure the impact of research scale on accessibility, on the basis of the Gaussian-based two-step floating catchment area method, this paper compares and analyzes the accessibility characteristics of urban park green space under three spatial scales, namely, the subdistrict, community, and residential quarter scales, under the 1 km walking distance threshold in the research area. The influence of the two source and destination points modes on accessibility is analyzed at the residential quarter scale. The following conclusions can be drawn from the analysis:

(1) Accessibility analysis of park green space should be performed cautiously when the aggregation unit is taken as the basic research unit. The accessibility of the aggregation unit is not the statistical summary of its subunits, especially when the area of the aggregation unit is generally larger than the walking range of residents, and is thus likely to lead to wrong conclusions. In accessibility analysis, two types of polygon (i.e., population aggregation unit and park green space) must be abstracted into two types of points (i.e., source and destination points). A large area of the polygon corresponds to less representativeness of the points and to greater uncertainty.
(2) When the finest urban population gathering area (residential quarter here) is taken as the research unit, the consistency of the source and destination points with the reality will directly affect the scientificity and accuracy of the evaluation results. The accessibility values of the two different source and destination point modes in the study area are similar in overall distribution and different in local quantity. Overall, the accessibility of the park green space in the residential quarter under the entrance and exit mode is better than that under the geometric mode, and the accessibility difference between the residential quarters is small, that is, the spatial fairness of visiting the park green space is good. The main reason for this finding is that under the entrance and exit mode, residential quarters and parks often have more than one entrance and exit, so residents have multiple paths to choose from. In some cases, the geometric center mode will cause the path distance to be completely inconsistent with the reality, resulting in incorrect accessibility results.
(3) Place-based accessibility analysis should be conducted on the finest scale possible rather than the aggregation scale. Moreover, a better approach is to use true distance rather than the centroid-to-centroid surrogate between the source and destination points. Only when the research scale and distance measure match the daily travel of residents in reality can reliable accessibility be obtained, which is also an important prerequisite for further guiding urban green space planning.

Data availability statement

The original contributions presented in the study are included in the article/supplementary material, further inquiries can be directed to the corresponding author.

Author contributions

SX proposed the original idea, designed the experiment, and wrote the draft. YW processed the basic data. Both of them read and revised this article, and approved the final manuscript.

Funding

The work was supported by the National Natural Science Foundation of China (NSFC) (Grant No. 42001265).

Conflict of interest

The authors declare that the research was conducted in the absence of any commercial or financial relationships that could be construed as a potential conflict of interest.

Publisher's note

All claims expressed in this article are solely those of the authors and do not necessarily represent those of their affiliated organizations, or those of the publisher, the editors and the reviewers. Any product that may be evaluated in this article, or claim that may be made by its manufacturer, is not guaranteed or endorsed by the publisher.

References

Agimass, F., Lundhede, T., Panduro, T. E., and Jacobsen, J. B. (2018). The choice of forest site for recreation: A revealed preference analysis using spatial data. *Ecosyst. Serv.* 31, 445–454. doi:10.1016/j.ecoser.2017.11.016

Ahuja, R., and Tiwari, G. (2021). Evolving term "accessibility" in spatial systems: Contextual evaluation of indicators. *Transp. policy* 113, 4–11. doi:10.1016/j.tranpol.2021.03.006

Ala-Hulkko, T., Kotavaara, O., Alahuhta, J., Helle, P., and Hjort, J. (2016). Introducing accessibility analysis in mapping cultural ecosystem services. *Ecol. Indic.* 66, 416–427. doi:10.1016/j.ecolind.2016.02.013

Buchecker, M., and Degenhardt, B. (2015). The effects of urban inhabitants' nearby outdoor recreation on their well-being and their psychological resilience. *J. Outdoor Recreat. Tour.* 10, 55–62. doi:10.1016/j.jort.2015.06.007

Chen, H., and Cui, G. (2021). Ecosystem services in urban plans: What is there, and what is still needed for better decisions. *Land Use Policy* 70, 298–312. doi:10.1016/j.landusepol.2017.10.017

Cortinovis, C., and Geneletti, D. (2018). Ecosystem services in urban plans: What is there, and what is still needed for better decisions. *Land Use Policy* 70, 298–312. doi:10.1016/j.landusepol.2017.10.017

Dai, D. (2011). Racial/ethnic and socioeconomic disparities in urban green space accessibility: Where to intervene? *Landsc. Urban Plan.* 102 (4), 234–244. doi:10.1016/j.landurbplan.2011.05.002

Grahn, P., and Stigsdotter, U. A. (2003). Landscape planning and stress. *Urban For. Urban Green.* 2 (1), 1–18. doi:10.1078/1618-8667-00019

Guo, S., Song, C., Pei, T., Liu, Y., Ma, T., Du, Y., et al. (2019). Accessibility to urban parks for elderly residents: Perspectives from mobile phone data. *Landsc. Urban Plan.* 191, 103642. doi:10.1016/j.landurbplan.2019.103642

Hu, S., Song, W., Li, C., and Lu, J. (2020). A multi-mode Gaussian-based two-step floating catchment area method for measuring accessibility of urban parks. *Cities* 105, 102815. doi:10.1016/j.cities.2020.102815

Hunter, R. F., Christian, H., Veitch, J., Astell-Burt, T., Hipp, J. A., and Schipperijn, J. (2015). The impact of interventions to promote physical activity in urban green space: A systematic review and recommendations for future research. *Soc. Sci. Med.* 124, 246–256. doi:10.1016/j.socscimed.2014.11.051

Hunter, R. F., Cleland, C., Cleary, A., Droomers, M., Wheeler, B. W., Sinnett, D., et al. (2019). Environmental, health, wellbeing, social and equity effects of urban green space interventions: A meta-narrative evidence synthesis. *Environ. Int.* 130, 104923. doi:10.1016/j.envint.2019.104923

Knudsen, C., Moreno, E., Arimah, B., Otieno, R. O., and Ogunsanya, O. (2020). *World cities Report 2020: The value of sustainable urbanization*. United Nations: United Nations Human Settlements Programme.

Kondo, M. C., Fluehr, J. M., McKeon, T., and Branas, C. C. (2018). Urban green space and its impact on human health. *Int. J. Environ. Res. Public Health* 15 (3), 445. doi:10.3390/ijerph15030445

Kruize, H., van der Vliet, N., Staatsen, B., Bell, R., Chiabai, A., Muinos, G., et al. (2019). Urban green space: Creating a triple win for environmental sustainability, health, and health equity through behavior change. *Int. J. Environ. Res. Public Health* 16 (22), 4403. doi:10.3390/ijerph16224403

Kwan, M. P., and Hong, I. (2009). From place-based to people-based exposure measures. *Soc. Sci. Med.* 69, 1311–1313. doi:10.1016/j.socscimed.2009.07.013

Larondelle, N., and Lauf, S. (2016). Balancing demand and supply of multiple urban ecosystem services on different spatial scales. *Ecosyst. Serv.* 22, 18–31. doi:10.1016/j.ecoser.2016.09.008

Lee, G., and Hong, I. (2013). Measuring spatial accessibility in the context of spatial disparity between demand and supply of urban park service. *Landsc. Urban Plan.* 69119 (9), 131185–131390. doi:10.1016/j.socscimed.2009.07.013

Li, L., Du, Q., Ren, F., and Ma, X. (2019). Assessing spatial accessibility to hierarchical urban parks by multi-types of travel distance in shenzhen, China. *Int. J. Environ. Res. Public Health* 16 (6), 1038. doi:10.3390/ijerph16061038

Liu, H., Remme, R. P., Hamel, P., Nong, H., and Ren, H. (2020). Supply and demand assessment of urban recreation service and its implication for greenspace planning-A case study on Guangzhou. *Landsc. Urban Plan.* 203, 103898. doi:10.1016/j.landurbplan.2020.103898

Luo, W., and Qi, Y. (2009). An enhanced two-step floating catchment area (E2SFCA) method for measuring spatial accessibility to primary care physicians. *Health & Place* 15 (4), 1100–1107. doi:10.1016/j.healthplace.2009.06.002

Mears, M., Brindley, P., Maheswaran, R., and Jorgensen, A. (2019). Understanding the socioeconomic equity of publicly accessible greenspace distribution: The example of Sheffield, UK. *Geoforum* 103, 126–137. doi:10.1016/j.geoforum.2019.04.016

Miller, H. J. (2016). "Place-based versus people-based accessibility," in *Access to destinations* (Bingley: Emerald Group Publishing Limited), 63–89.

Nesbitt, L., Meitner, M. J., Girling, C., Sheppard, S. R. J., and Lu, Y. (2019). Who has access to urban vegetation? A spatial analysis of distributional green equity in 10 us cities. *Landsc. Urban Plan.* 181, 51–79. doi:10.1016/j.landurbplan.2018.08.007

Neutens, T., Schwanen, T., Witlox, F., and De Maeyer, P. (2010). Equity of urban service delivery: A Comparison of different accessibility measures. *Environ. Plan. A* 42 (7), 1613–1635. doi:10.1068/a4230

People's Government of Weidu District Xuchang City (2022). Entering Weidu 6.1. AvaliableAt: http://www.weidu.gov.cn/zjwd/walkIntoWD.html#page1.

Radke, J., and Mu, L. (2000). Spatial decompositions, modeling and mapping service regions to predict access to social programs. *Ann. GIS* 6 (2), 105–112. doi:10.1080/10824000009480538

Riva, M., Gauvin, L., Apparicio, P., and Brodeur, J. M. (2009). Disentangling the relative influence of built and socioeconomic environments on walking: The contribution of areas homogenous along exposures of interest. *Soc. Sci. Med.* 69 (9), 1296–1305. doi:10.1016/j.socscimed.2009.07.019

Schipperijn, J., Ekholm, O., Stigsdotter, U. K., Toftager, M., Bentsen, P., Kamper-Jørgensen, F., et al. (2010a). Factors influencing the use of green space: Results from a Danish national representative survey. *Landsc. Urban Plan.* 95 (3), 130–137. doi:10.1016/j.landurbplan.2009.12.010

Schipperijn, J., Stigsdotter, U. K., Randrup, T. B., and Troelsen, J. (2010b). Influences on the use of urban green space – a case study in Odense, Denmark. *Urban For. Urban Green.* 9 (1), 25–32. doi:10.1016/j.ufug.2009.09.002

Shen, Y., Sun, F., and Che, Y. (2017). Public green spaces and human wellbeing: Mapping the spatial inequity and mismatching status of public green space in the Central City of Shanghai. *Urban For. Urban Green.* 27, 59–68. doi:10.1016/j.ufug.2017.06.018

Shi, L., Halik, Ü., Abliz, A., Mamat, Z., and Welp, M. (2020). Urban green space accessibility and distribution equity in an arid oasis city: Urumqi, China. *Forests* 11 (6), 690. doi:10.3390/f11060690

Tan, P. Y., and Samsudin, R. (2017). Effects of spatial scale on assessment of spatial equity of urban park provision. *Landsc. Urban Plan.* 158, 139–154. doi:10.1016/j.landurbplan.2016.11.001

Tardieu, L., and Tuffery, L. (2019). From supply to demand factors: What are the determinants of attractiveness for outdoor recreation? *Ecol. Econ.* 161, 163–175. doi:10.1016/j.ecolecon.2019.03.022

Tu, X., Huang, G., Wu, J., and Guo, X. (2020). How do travel distance and park size influence urban park visits? *Urban For. Urban Green.* 52, 126689. doi:10.1016/j.ufug.2020.126689

Wang, Q., and Lan, Z. (2019). Park green spaces, public health and social inequalities: Understanding the interrelationships for policy implications. *Land Use Policy* 83, 66–74. doi:10.1016/j.landusepol.2019.01.026

Wei, F. (2017). Greener urbanization? Changing accessibility to parks in China. *Landsc. Urban Plan.* 157, 542–552. doi:10.1016/j.landurbplan.2016.09.004

Wüstemann, H., Kalisch, D., and Kolbe, J. (2017). Access to urban green space and environmental inequalities in Germany. *Landsc. Urban Plan.* 164, 124–131. doi:10.1016/j.landurbplan.2017.04.002

Xiao, Y., Wang, D., and Fang, J. (2019). Exploring the disparities in park access through mobile phone data: Evidence from Shanghai, China. *Landsc. Urban Plan.* 181, 80–91. doi:10.1016/j.landurbplan.2018.09.013

Xiao, Y., Wang, Z., Li, Z., and Tang, Z. (2017). An assessment of urban park access in Shanghai – implications for the social equity in urban China. *Landsc. Urban Plan.* 157, 383–393. doi:10.1016/j.landurbplan.2016.08.007

Xing, L., Liu, Y., Liu, X., Wei, X., and Mao, Y. (2018). Spatio-temporal disparity between demand and supply of park green space service in urban area of Wuhan from 2000 to 2014. *Habitat Int.* 71, 49–59. doi:10.1016/j.habitatint.2017.11.002

Xu, S., Liu, Y., Wang, X., and Zhang, G. (2017). Scale effect on spatial patterns of ecosystem services and associations among them in semi-arid area: A case study in ningxia hui autonomous region, China. *Sci. Total Environ.* 598, 297–306. doi:10.1016/j.scitotenv.2017.04.009

You, H. (2016). Characterizing the inequalities in urban public green space provision in Shenzhen, China. *Habitat Int.* 56, 176–180. doi:10.1016/j.habitatint.2016.05.006

Zhang, J., and Tan, P. Y. (2019). Demand for parks and perceived accessibility as key determinants of urban park use behavior. *Urban For. Urban Green.* 44, 126420. doi:10.1016/j.ufug.2019.126420

Zhang, S., Yu, P., Chen, Y., Jing, Y., and Zeng, F. (2022). Accessibility of park green space in wuhan, China: Implications for spatial equity in the post-COVID-19 era. *Int. J. Environ. Res. Public Health* 19 (9), 5440. doi:10.3390/ijerph19095440

Žlender, V., and Ward Thompson, C. (2017). Accessibility and use of peri-urban green space for inner-city dwellers: A comparative study. *Landsc. Urban Plan.* 165, 193–205. doi:10.1016/j.landurbplan.2016.06.011

frontiers | Frontiers in Environmental Science

TYPE Original Research
PUBLISHED 23 January 2023
DOI 10.3389/fenvs.2023.1055100

Check for updates

OPEN ACCESS

EDITED BY
Ying Jing,
Zhejiang University, China

REVIEWED BY
Hao Jiang,
Guangzhou Institute of Geography, China
Qingsong He,
Huazhong University of Science and Technology, China
Jinzhu Wang,
Deakin University, Australia

*CORRESPONDENCE
Song Hong,
songhongpku@126.com

SPECIALTY SECTION
This article was submitted to Land Use Dynamics, a section of the journal Frontiers in Environmental Science

RECEIVED 27 September 2022
ACCEPTED 06 January 2023
PUBLISHED 23 January 2023

CITATION
Huang C, Hong S, Niu X, Wu Q, Zhong Y, Yang H and Zhang H (2023), Mapping of nighttime light trends and refugee population changes in Ukraine during the Russian–Ukrainian War.
Front. Environ. Sci. 11:1055100.
doi: 10.3389/fenvs.2023.1055100

COPYRIGHT
© 2023 Huang, Hong, Niu, Wu, Zhong, Yang and Zhang. This is an open-access article distributed under the terms of the Creative Commons Attribution License (CC BY). The use, distribution or reproduction in other forums is permitted, provided the original author(s) and the copyright owner(s) are credited and that the original publication in this journal is cited, in accordance with accepted academic practice. No use, distribution or reproduction is permitted which does not comply with these terms.

Mapping of nighttime light trends and refugee population changes in Ukraine during the Russian–Ukrainian War

Chaoqing Huang[1], Song Hong[1]*, Xiaoxiao Niu[1], Qian Wu[1], Yanmei Zhong[1], Huan Yang[1] and Haoran Zhang[2]

[1]Key Laboratory of Geographic Information System, Ministry of Education, School of Resources and Environmental Sciences, Wuhan University, Wuhan, China, [2]Department of Geography, University of Washington, Seattle, WA, United States

The nighttime lights accurately and coherently depict how humans live. This study uses nighttime light measurements to quantify changes in nighttime lighting and refugee population in Ukraine before and after the war. We combined the Theil–Sen estimator with the M-K test to explore the trends of nighttime light. In addition, we constructed a linear model using nighttime light data and a portion of the UNHCR refugee data. Our results reveal that 1 week after the start of the Russo-Ukrainian War, the nighttime light area and the average nighttime light DN value in Ukraine exhibited a steep decline of about 50 percent. Our findings showed taht refugee population changes calculated through models and nighttime light data were mostly consistent with UNHCR data. We thought that the nighttime light data might be used directly to dynamically estimate changes in the refugee movement throughout the war. Nighttime light changes has significant implications for international humanitarian assistance and post-war reconstruction.

KEYWORDS

nighttime lights, Russian–Ukrainian War, refugee population, mapping, spatio–temporal

1 Introduction

The Russian–Ukrainian War is one of the worst conflicts of the 21st century. Since the commencement of the conflict on February 24, Russia and Ukraine, particularly the Ukrainian populace, have sustained significant losses (Aljazeera, 2022; BBC, 2022; CBC, 2022; Guardian, 2022; NPR, 2022; UN News, 2022). Currently, the fight is increasing and expanding. Both countries, particularly Ukraine, will incur more losses if the crisis persists. Under the current circumstances, it is vital to conduct a scientific assessment of the refugee population, which will draw the world's attention to this unfortunate conflict and persuade the parties to continue peace discussions *via* the influence of public media. Simultaneously, it is crucial to create a scientific basis for international assistance to Ukraine and, more importantly, to build post-war domestic reconstruction indicators for Ukraine.

There are now multiple sources for the dynamic estimation of the Ukrainian domestic refugee population during the Russian–Ukrainian War, including reports from the Ukrainian government, western media, and the United Nations Refugee Agency. Using nighttime lights and remote sensing data to assess the war's dynamics is a practical and efficient method. The US Defense Meteorological Satellite Program (DMSP) developed the Operational Linescan System (OLS) in the twentieth century. The original goal of the system was to remotely measure the faint reflection of moonlight by clouds at night to obtain the inversion of nighttime meteorological data. However, OLS can catch

city lights sensitively in conditions of a clear night sky, which has spurred the development of nighttime light remote sensing (Croft, 1978; Deren and Xi, 2015). Numerous researchers have adopted this approach because of the extensive utility of nighttime light remote sensing in studies of global and regional urbanization, population change, and economic activity. Through literature reviews, some researchers have summarized the applications of nighttime light data from various industries in studies of the nature and society. In addition, they have voiced concerns about the limitations and difficulties of nighttime lighting data and have made proposals for its development and improvement (Zhao et al., 2019). Many studies have examined the origin, data platform, application orientation, and remote sensing nighttime light data development trends. Nighttime light data were analyzed to assess the potential for data mining from new data sources, knowledge discovery, ground observations, and geographical conditions, i.e., global situation monitoring (Deren and Xi, 2015).

Numerous nighttime light remote sensing applications have been devised and applied in studies of urbanization, population change, economic activity, conflict assessment, greenhouse gas emissions, and the environment. The possible impact of soil resources on construction lands can be evaluated using the DMSP/OLS nighttime light image dataset in conjunction with census data and soil map data (Imhoff et al., 1997). They used DMSP/OLS multi-temporal nighttime light data in urban development for iterative unsupervised classifications. The data then permitted the construction of maps of regional and urban dynamic changes (Zhang and Seto, 2011; Stokes and Seto, 2019; Liu et al., 2012). The inversion of nighttime light data on regional urbanization and economic growth is a mature topic of the study. Using multi-year nighttime light images in conjunction with urban street network data to capture the urban form and features of different regions has enabled a spatial–temporal analysis of urban expansion (Duque et al., 2019). The nighttime light data produced by the Visible Infrared Imaging Radiometer Suite (VIIRS) carried out by the Suomi National Polar-orbiting Partnership (S-NPP) satellite, when combined with local economic data and modeled with quadratic polynomials, allow the relationship between city-level gross domestic product (GDP) distribution characteristics and landform types to be investigated (Zhao et al., 2017). The study of the population distribution using the data on nighttime lights dates back to the 1990s. Using DMSP/OLS image composite data and high-resolution census data to perform comparative research, the regularity of image-valued areas and population residential areas can be determined (Sutton et al., 1997; Lo, 2001). Additionally, nighttime light data can be utilized to gauge social and economic growth (Chen and Nordhaus, 2011; Shi et al., 2014; Wu and Wang, 2019). Using nighttime light data to dynamically assess war-torn and underdeveloped countries can determine the status and development of post-war rehabilitation work and serve as a significant source of data for tracking humanitarian crises in the destination country. Furthermore, this analysis provides scientific evidence for the following recuperation and development of local economic activities (Li et al., 2017; Li et al., 2018). Social and productive human activities accompany the nighttime illumination. When losses are inflicted by war or natural catastrophes, a quantitative framework can be developed, and multi-temporal nighttime light data can be used to quantify the extent of the damage to economic activities rapidly. Also, the nighttime light data can even provide scientific information for recovery and post-disaster reconstruction (Qiang et al., 2020).

In exploring the application scope of the aforementioned nighttime light data, we discovered that nighttime lights are relatively mature in their ability to reflect the population and social activities. The aforementioned research focused primarily on the inversion, reasoning, and historical nighttime light data analysis. Most of the timescales were for years or months, which was reasonable for the long history of a region or country. Despite the significant changes in some areas in a short time, there are few research results on whether nighttime lights can induce inversion. In addition, the existing rules between nighttime lights and population activities, economic activities, and production activities reflect additional studies regarding the use of nighttime lights and the inversion of human social activities. However, further research was required for other levels, including emergency and the tendency of emergency inversion. In this study, we analyzed nighttime light data using empirical models and combined them with the Office of the UN High Commissioner for Refugees (UNHCR) data to develop a logistic regression model to explain population changes. Before and after the war, a quantitative analysis of dynamic spatial–temporal changes in nighttime lights and the refugee population was carried out. Ultimately, we aimed to evaluate the effectiveness of these new methods for exploring dynamic nighttime lights and refugee population changes during the war.

2 Data and methodology

2.1 Study area

Ukraine is situated in Eastern Europe, with the Black Sea to its south, the Russian Federation to its east, Belarus to its north, and Poland, Slovakia, Hungary, and Romania to its west. With a population of 41.17 million people, the country is geographically located at the intersection of the European Union and the Commonwealth of Independent States (excluding Crimea). Ukraine's administrative division consists of 24 regions (Figure 1), one autonomous republic, and two municipalities (UNdata, 2022). On 24 February 2022, conflict broke out between Russia and Ukraine on the grounds of the "demilitarization and de-Nazification", and the conflict officially turned into a full-scale war on that date (CNN, 2022a; CNN, 2022b; TASS, 2022).

We intended to perform a dynamic assessment of war damages in Ukraine, and our study area encompassed the entirety of Ukraine. Considering that the conflict significantly impacted the capital, Kyiv, we chose Kyiv as a specific research objective in this study to clarify the impact before and after the war. The Crimea region was excluded from the study due to the absence of demographic statistics for these areas.

2.2 Data sources

Nighttime light data were obtained from the Day–Night Band (DNB) sensor of the VIIRS onboard the S-NPP and Joint Polar Satellite System (JPSS) satellite platforms (NASA-Suomi NPP, 2022). The DNB's ultra-sensitive performance in low-light conditions marks a major improvement in the resolution and calibration over Defense Weather Satellite Program (DMSP)-generated nighttime light images from the previous generation (Román et al., 2018). The DNB sensor delivers global nighttime visible light

FIGURE 1
Study area.

data and daily measurements of near-infrared (NIR) data suited for Earth system science applications (UNdata, 2022). The Black Marble product kit (VNP46) comprises the Daily Atmosphere Sensor Top (TOA) nighttime light (NTL) product (VNP46A1) and the Daily Moonlight-adjusted nighttime light product (VNP46) (VNP46A2). Compared to VNP46A1, VNP46A2 can more realistically reverse the anthropogenic light sources on the Earth's surface. VNP46A2 utilizes all high-quality, cloud-free, atmospheric, terrain, vegetation, snow, lunar, and stray nighttime light-corrected DN values to estimate nighttime lights and have other inherent surface optical properties (Román et al., 2018; Román et al., 2019; Román et al., 2020; Román et al., 2021). Additionally, the Black Marble product kit (VNP46) comprises the Moonlight adjustable nighttime light product (VNP46A3) and the Annual Light adjustable nighttime light product (VNP46) (VNP46A4). VNP46A3 and VNP46A4 are the abbreviated names for the third and fourth nighttime light (NTL) products, respectively, in the Black Marble suite. VNP46A3 and VNP46A4 provide monthly and yearly composites derived from daily atmospherical and lunar bi-directional reflectance distribution function (BRDF)-corrected NTL radiance to eliminate the influence of artifacts and biases. This study utilized the VNP46A2 data series (NASA-VNP46A2, 2022; NASA- VNP46A4, 2022).

The United Nations High Commissioner for Refugees (UNHCR) is a global organization dedicated to saving lives, protecting rights, and building a better future for refugees, forcibly displaced communities, and stateless people. The UNHCR provides data on refugee population border crossings from Ukraine during the war and offers daily information on the influx and departure of refugees into and out of Ukraine (https://data.unhcr.org/en/situations/ukraine). The time and location of the fight between the Russian and Ukrainian soldiers were obtained from the website global conflict tracker, an interactive guide to ongoing conflicts of concern to the United States, including background information and resources (https://www.cfr.org/global-conflict-tracker).

2.3 Data preprocessing

For the nighttime light data on VNP46A2 and VNP46A4, we initially employed a Python encoding technique to obtain the 'gap-filled BRDF-corrected DNB NTL' and 'Temporal Radiance Composite Using All Observations During Snow-free Period' layers, respectively. Then, using visual contrast interpretation, we found the dates for which complete data were available in the daily Ukrainian night light data. Finally, these data were converted into a raster format with a unit of nWatts/cm/sr, and the georeference coordinate was WGS 1984. Moreover, we compiled daily values of VNP46A2 into weekly and monthly data (Román et al., 2020). Then, 10 weeks before (16 December 2021 to 23 February 2022) and after (24 February 2022 to 2 May 2022) the beginning of the Russian–Ukrainian War, the

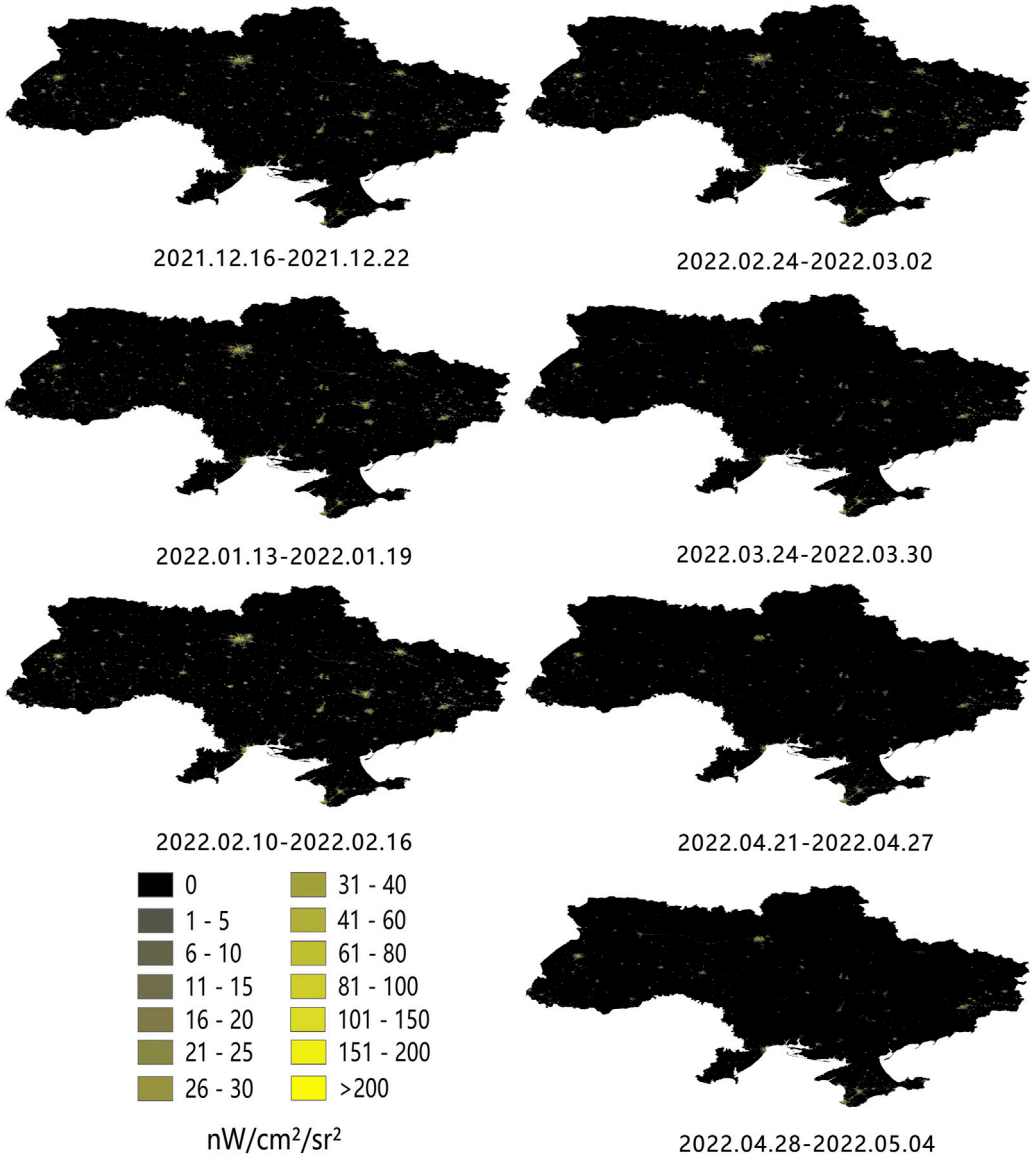

FIGURE 2
Ukrainian nighttime light spatial changes from 16 December 2021 to 2 May 2022.

obtained nighttime light images were combined. Additionally, we collected nighttime light data (VNP46A4) from 2012 to 2021 for a long-term nighttime light trend analysis.

On the auxiliary data side, we used Python encoding to convert the obtained UNHCR data from XML to CSV, making it easier to analyze. In addition, we utilized visual interpretation to track sites of daily battles in the Russian–Ukrainian War and used GIS tools to organize the time and position of the matches mentioned previously into data tables.

2.4 Methodology

2.4.1 Calculation of the total nighttime lights DN value

In this study, we employed the digital number value (DN value) of nighttime lights, which referred to the digital grayscale reflection of the brightness of surface nighttime lights on the image grid. The nighttime light DN value is usually a comprehensive indicator of a region's socioeconomic development level. A higher DN value suggests a higher degree of regional development and *vice versa*. We introduced a yearly average DN value of nighttime lights, the sum of the daily average DN values of nighttime lights in the area. The changes in the yearly average DN values of the annual nighttime lights can be used to characterize the evolution of an area over several years (Chen et al., 2003; Zhuo et al., 2003). The average DN value of nighttime lights is expressed as follows:

$$NTL_{total} = \sum_{i=1}^{DN_M} DN_i \times n_i, \quad (1)$$

where DN_i and n_i represent the i th grayscale pixel value and the number of pixels in the administrative unit, respectively. Also, M

represents the total number of pixels in the interval [1, DN_M] in the administrative unit. In this study, weekly nighttime light data were composited by daily nighttime light data.

2.4.2 Analysis of the trend of nighttime lights

We used the Theil–Sen estimator and the M-K test to calculate the trend of changes in image DN values during peacetime and war in Ukraine. The Theil–Sen estimator is a robust linear regression method that selects the median slope across all lines using two-dimensional sample pairs. Compared to the trend analysis based on the least squares method, the Theil–Sen estimator can avoid the lack of time series data and the influence of data distribution on the analysis results, eliminate the interference of outliers on the time series, and be used to identify trends in the univariate time series (Burn and Elnur, 2002; Wang et al., 2020).

$$Q = median\frac{NTL_j - NTL_i}{j - i} \quad 1 < i < j < n. \tag{2}$$

In the formula, *median* represents the median value of the slopes, i and j are the time series numbers, and NTL_i and NTL_j are image DN values of the time series in the i th week and the j th week, respectively. The slope Q is greater than 0, indicating an upward trend; when Q is less than 0, it shows a downtrend trend. The M-K test does not require samples to follow a certain distribution, which can eliminate a few outliers and is suitable for non-normally distributed data. The inspection process is as follows:

$$\tau = \sum_{i=1}^{n-1}\sum_{j=i+1}^{n} sign\left(NTL_j - NTL_i NTL_j - NTL_i\right), and$$
$$sign\left(NTL_j - NTL_i\right) = \begin{Bmatrix} 1 NTL_j - NTL_i > 0 \\ 0 NTL_j - NTL_i = 0 \\ -1 NTL_j - NTL_i < 0 \end{Bmatrix}. \tag{3}$$

The statistics for constructing trend analysis tests are as follows:

$$U_{MK} = \begin{Bmatrix} \frac{\tau - 1}{[Var(\tau)]^{\frac{1}{2}}} & \tau > 0 \\ 0 & \tau = 0 \\ \frac{\tau + 1}{[Var(\tau)]^{\frac{1}{2}}} & \tau < 0 \end{Bmatrix}, \tag{4}$$

$$Var(\tau) = \frac{n(n-1)(2n+5)}{18}. \tag{5}$$

In the formula, NTL_i and NTL_j are the image DN values in the i th week and the j th week, respectively, and n represents the time series length; *sign* is a symbolic function. At a given significance level α, when $|U_{MK}| > u_{1-\alpha/2}$, it means that the study sequence significantly changes at the α level.

Due to the unstable and complicated changes in all aspects of society throughout the war, months may not be the optimum unit of time to describe variations in nighttime lights, population, and economic activities. For analysis purposes, we composited the daily nighttime light data into weekly data. We selected the period between 16 December 2021 and 4 May 2022, 10 weeks before and 10 weeks after the start of the war, for a total of 20 weeks of nighttime light data. In addition, we combined the daily nighttime light data based on an analysis of the nighttime light change trend to compare the trend of the nighttime light 10 weeks from the start of the war (2022.2.24 to 2022.5.4) with nighttime light trends during peacetime for 10 weeks (2021.12.16 to 2021.2.23).

2.4.3 Verification of the reliability of the nighttime light-driven model

This study used the Nash–Sutcliffe efficiency index (NSE) and R square (R^2) to verify the model's reliability. The NSE is a widely used and potentially reliable statistic for assessing the model's goodness of fit (Schaefli and Gupta, 2007; Moriasi et al., 2007). R^2 indicates the degree to which the data fit the regression model (the goodness of fit). The data on Ukrainian nighttime lights and refugee population from 24 February 2022 (the beginning of the war) to 2 May 2022 were processed by a statistical distribution fitting and was confirmed to satisfy a normal distribution. Then, for modeling purposes, we utilized the Ukrainian domestic nighttime light data and refugee population data for this period. In addition, we used 50% of the nighttime light data and refugee population data for modeling analyses and the remaining 50% for model accuracy verification.

$$NSE = 1 - \frac{\sum_{i=1}^{n}(Q_{mi} - Q_{oi})^2}{\sum_{i=1}^{n}(Q_{oi} - \overline{Q_o})^2}, \tag{10}$$

$$R^2 = \frac{\left[\sum_{i=1}^{n}(Q_{oi} - \overline{Q_o})(Q_{mi} - \overline{Q_m})\right]^2}{\sum_{i=1}^{n}(Q_{oi} - \overline{Q_o})^2 \sum_{i=1}^{n}(Q_{mi} - \overline{Q_m})^2}. \tag{11}$$

In the formula, Q_{mi} is the total nighttime light DN value calculated by the model on i th night; Q_{oi} is the actual total nighttime light DN value on i th night; $\overline{Q_o}$ refers to an average value of the actual total nighttime light DN value at night.

The variation range of the NSE is from −∞ to 1. When the NSE calculation result is 1, the observed value is the same as the simulated value; if the NSE is between 0.5 and 1, it means that the model result is acceptable, and when the NSE result is less than 0, it is considered that the model reliability is poor. R^2 represents the correlation between the simulated value of the model and the measured value. The closer the value is to 1, the better the simulation effect.

3 Results

3.1 Nighttime light trends in Ukraine

Figure 2 depicts the nighttime light area and DN value distribution in Ukraine in the 10 weeks before and after the outbreak of the Russian–Ukrainian War (16 December 2021 to 4 May 2022). Ten weeks before the start of the war, the nighttime lights in Ukraine were stable on a national scale. The range of nighttime lights fluctuated but altered little. In the first week following the outbreak of war, the national nighttime light area was reduced by 50% (Figure 3A) (24 February 2022 to 2 March 2022). In the following weeks, the national nighttime light area hovered at 50% of its pre-war level (3 March 2022 to 4 May 2022). The fifth week following the start of the conflict was the darkest in Ukraine, and the nighttime light area was almost 75% smaller than that before the war, indicating that the war caused significant damage to Ukraine in a short amount of time. In addition, after the start of the conflict, the average nighttime light DN value, maximum nighttime light DN value, and total nighttime light DN value decreased dramatically throughout the country (Figures 3A, B). In Ukraine, the highest nighttime light DN value and total nighttime light DN value were lowered by more than 90% than the week before and after the war. The change in nighttime lights

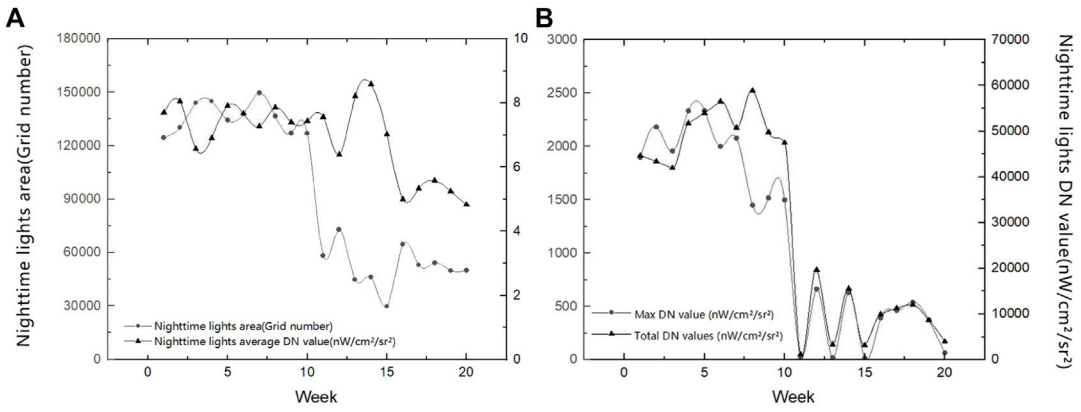

FIGURE 3
Weekly nighttime lights area trends **(A)** and nighttime lights DN value changes **(B)** in Ukraine from 16 December 2021 to 2 May 2022.

demonstrated that the conflict affected the quantity and quality of nighttime lights in Ukraine.

The changing map of nighttime lights provided a more concrete depiction of the oblast- and city-scale destruction wrought by the war in Ukraine. Based on the area of nighttime lights and the average DN value, we discovered that all oblasts had a substantial decline in the area and DN value during the first week of the war. In the weeks that followed, the nighttime lights exhibited low-value fluctuations much below pre-war values (Figure 4). From a spatial perspective, the city and oblast with the greatest reduction in the nighttime light area were the capital Kyiv (Figure 5), Cherkasy oblast in the center, Kyiv oblast, Donetsk oblast, Sumy oblast, and Ternopil oblast in the west, and these oblasts and cities had 50% fewer nighttime lights than before the war. In addition, the average nighttime light DN value changed, which indicates the quality of nighttime lights varied dramatically by oblasts, decreasing significantly in Donetsk and Sum oblasts in the east and Ternopil Oblast in the west. However, certain oblasts, including Luhansk, Zakarpattia, and Kherson, experienced few modifications, which might be because nighttime lights in these places did not meet high standards before the war.

Changes in the nighttime light area and nighttime light DN value indicated a gradual disappearance from the city's periphery to the center of the town. The DN value of the city's central district's nighttime lights decreased from a high value to a low value (Figure 5). Changes in the city's nighttime lights revealed the war's spatial–temporal impact on the operation and vibrancy of the city.

In addition, to scientifically reflect the changes in nighttime lights in Ukraine during the Russian–Ukrainian War, we presented the nighttime light data from consecutive years in peacetime and conducted trend analyses in conjunction with nighttime light data of the war. We performed a trend analysis on the monthly nighttime light data from 2012 to 2021 (combined daily data) and wartime nighttime light data. We discovered that the nighttime light area of the entire nation had fallen marginally, particularly in the central and eastern parts. During the 10 years between 2012 and 2021, the DN value of nighttime lights increased or decreased dramatically in some regions (Figure 6A). During the conflict period from February 24th to 2 May 2022, however, the nighttime light area across the nation reduced drastically and on a wide scale. Similarly, the light intensity gradually decreased (Figure 6B).

Since nighttime lights did not fluctuate significantly during times of peace, we investigated the short-term trend of nighttime lights in the country using data from 10 weeks before and after the start of the conflict. Using the Theil–Sen estimator and the M-K test, the trend of DN values at the pixel scale was analyzed. We found a significant reduction in the nighttime light DN value, which accounted for 5.24%, the severely reduced nighttime lights accounted for 15.17%, and only 0.45% of the region grew enormously. The remaining areas, which comprised 79.14%, exhibited little change (Figure 7).

From February 24 to May 2, nighttime lights showed a noticeable reduction, particularly in the capital Kyiv and built-up areas around it. Other oblasts, particularly Kharkiv and Donetsk in the east, saw a decrease in nighttime lights. The middle and western regions, where fighting and strife were less frequent and severe, had a less significant impact on nighttime lights than the eastern region. In addition, there was the periodic dimming of nighttime lights in areas where there was no fighting, which may have been caused by a power supply gap or artificial dimming.

3.2 Refugee population trends in Ukraine

We examined both variables based on the preceding findings, which indicated a general downward tendency in nighttime light changes in Ukraine and an upward trend in the UNHCR-registered refugee population data throughout the same period. The refugee population dataset registered by the UNHCR corresponded to a normal distribution, with a strong association coefficient (−0.89) with nighttime lights of Ukraine for the same period, as determined by the statistical distribution fitting. Then, we fit the data on nighttime lights and refugee populations. We analyzed the data trend changes using linear, polynomial, exponential, and S-shaped functions and determined that the S-shaped function was the most acceptable match. After multiple attempts, we decided that the logistic equation employed for the fit was the most appropriate in terms of the goodness-of-fit and statistical significance. As depicted in Figure 8A, the logistic equation was utilized to fit nighttime light data and refugee population registration data in order to generate a model for the final calculation of the registered refugee population using the total nighttime light DN value. The model was expressed as y =

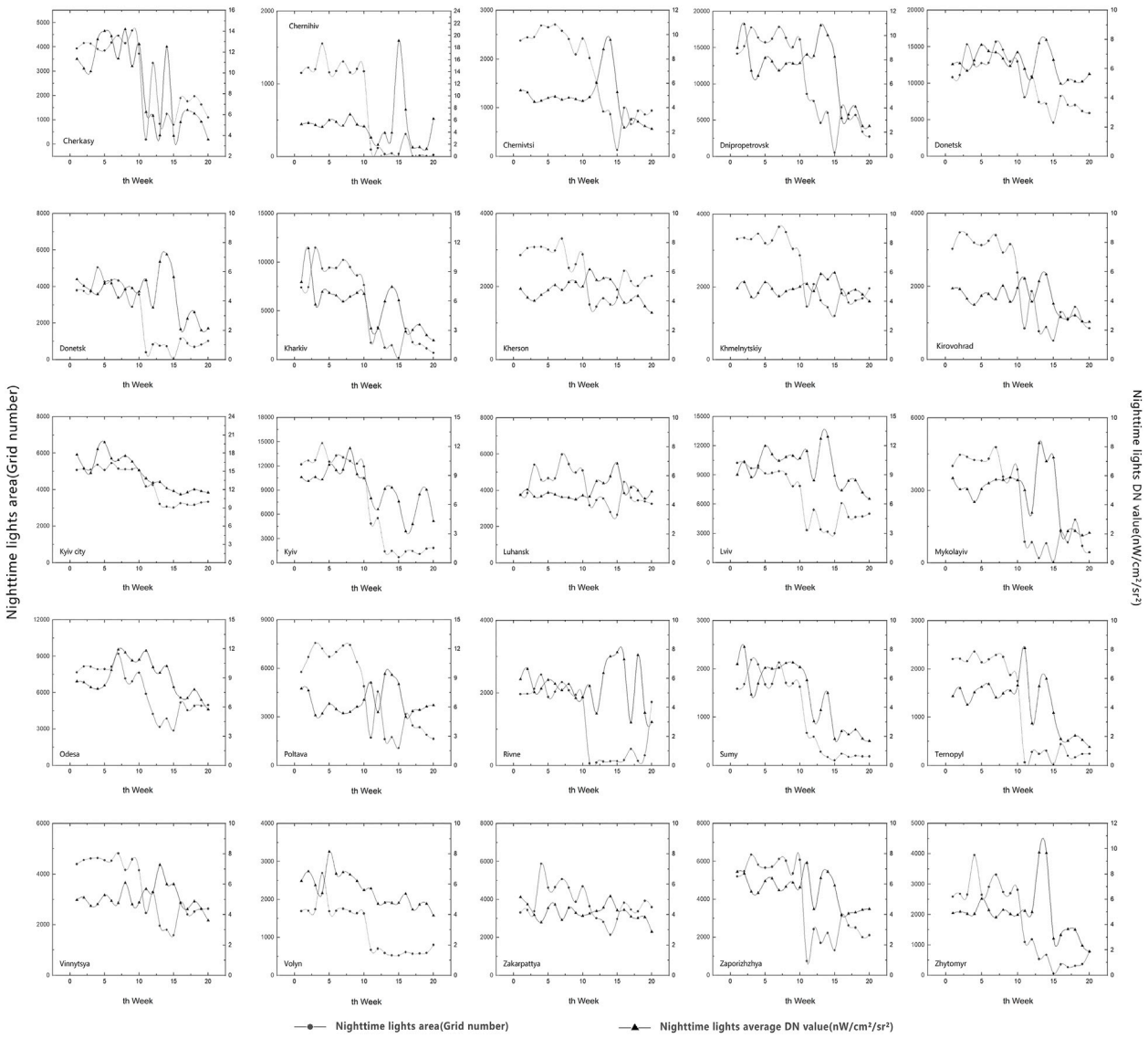

FIGURE 4
Weekly analysis of nighttime light trends in all oblasts of Ukraine (2021.12.16–2022.5.2).

3684039.53/{1 + exp[−1.19E-5*(x-584851.5)]}, where y was the refugee population registered on a specific day; x was the total nighttime light DN value of the Ukrainian nightlight on the same day; the goodness-of-fit of the model was 0.69, and the model was significant at the level of 0.05. In addition, the NSE of the model reached 0.78, indicating that the reliability of the model was acceptable and that the simulated values of the model were well correlated with the observed values. The comparison between the simulated and observed results is shown in Figure 8B.

From the aforementioned results, we found that the decrease in the total nighttime light DN value was mainly due to the decline in the area of nighttime lights and the reduction in the average nighttime light DN value. We utilized the daily nighttime light area and the average nighttime light DN value to examine the association between refugee population levels and nighttime lights. The correlation coefficient between the registered refugee population and area of nighttime lights was −0.52, and the correlation relationship with the average DN value of nighttime lights was −0.53. However, because the total nighttime light DN value is a product of the average DN value and area, we concluded that the effect of the location of nighttime lights and the average nighttime light DN value on the change in the refugee population were almost the same. Based on this consideration, we classify the changes in the DN value and nighttime light area before and after the conflict by Jenks Natural Breaks Classification (Chen et al., 2013); the classification situation is depicted in Table 1.

From Table 1, we calculated the weekly change in the refugee population after the war began, as depicted in Figure 9. After the war started, the refugee population increased significantly in the 2nd, 5th, and 8th weeks and increased slightly in the 1st, 3rd, 6th, and 9th weeks. The 4th and 7th weeks saw minimal variations from the previous week. The refugee population demonstrates a cyclical variation over 3 weeks, with a “low-high-low” trend, as depicted in Figure 8.

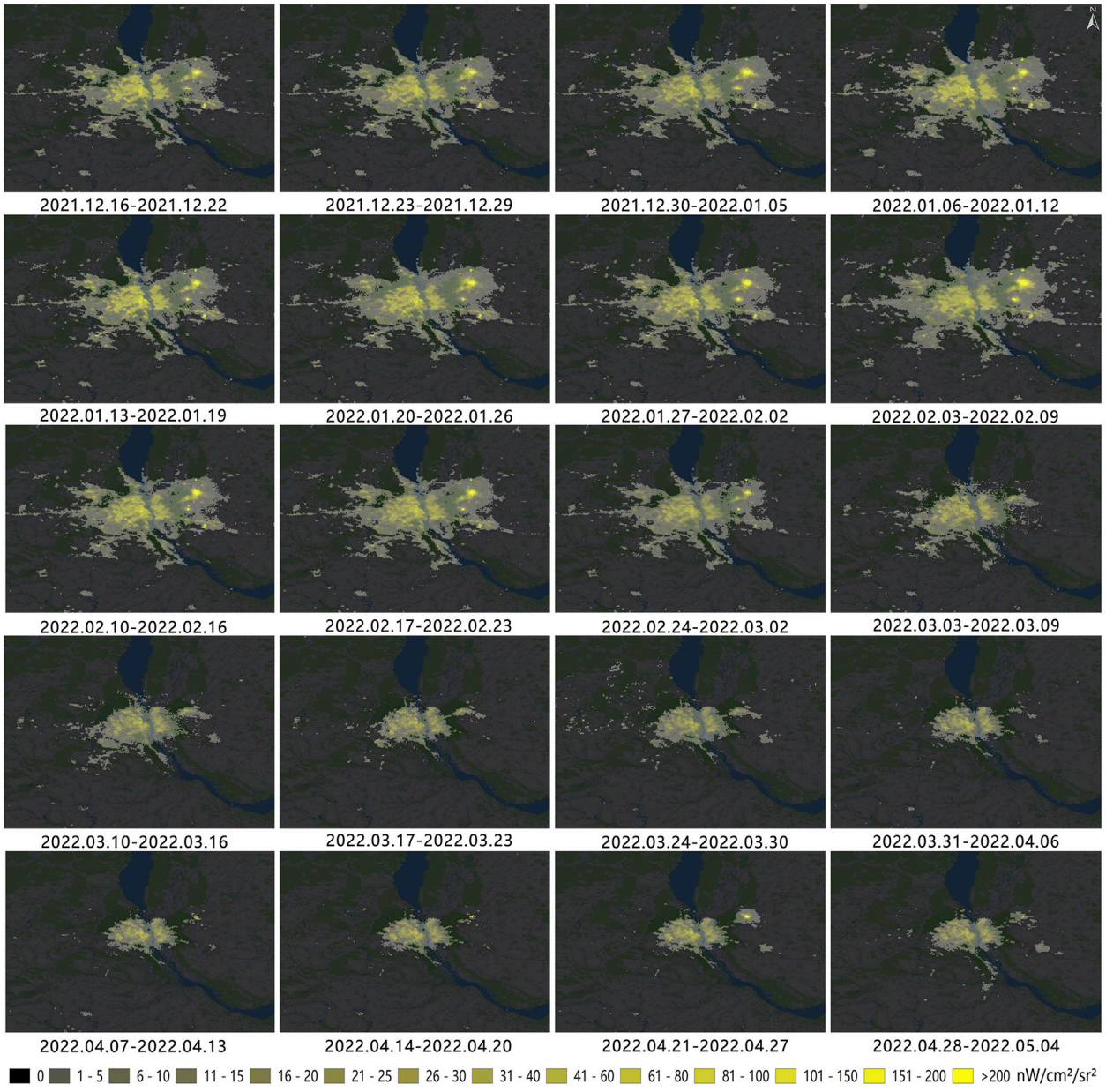

FIGURE 5
Weekly Kyiv city nighttime light spatial change from 16 December 2021 to 2 May 2022.

4 Discussion

4.1 Relationship between nighttime lights and conflicts

Based on the aforementioned analytical findings, it is certain that war conflicts have contributed to the decline of the light. Consequently, we considered analyzing and discussing nightlights and frequency of military conflicts throughout the same period. However, we compared the total intensity of nighttime lights and frequency of national disputes using a time series. We found that when the number of conflicts decreased, the fluctuation degree of the overall nighttime light intensity gradually reduced. Yet, the two trends were not entirely congruent (Figure 10), considering that the disappearance of nighttime lights was varied. The times of wars and conflicts were only a vague concept. It was challenging to gather and quantify additional information, such as the scope of disputes, their severity, their duration, and their subsequent consequences. Changing the number of conflicts made it impossible to adequately assess the relationship between the two variables.

Although it was difficult to quantify the precise relationship between nighttime lights and the number of conflicts, the overall trend was consistent. As a result, we would continue our discussion based on the general trend relationship between the two concepts. We considered that as the war proceeded, the country's nighttime lights would grow dimmer, symbolizing the immense damage caused by the conflict. Furthermore, across the nation, the frequency of conflict was not connected with the disappearance of the total nighttime light DN

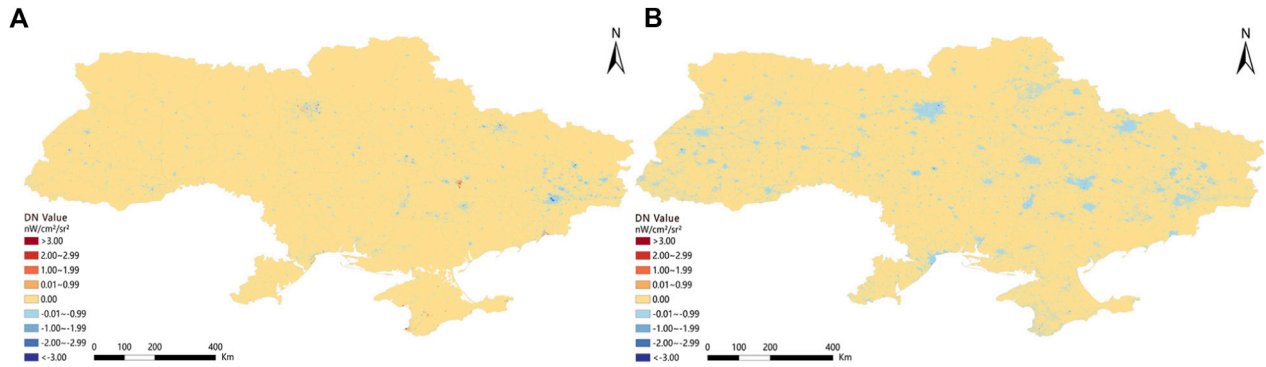

FIGURE 6
Comparison of the nighttime light DN value and area change from 2012 to 2021 **(A)** and from February 24 to 2 May 2022 **(B)**.

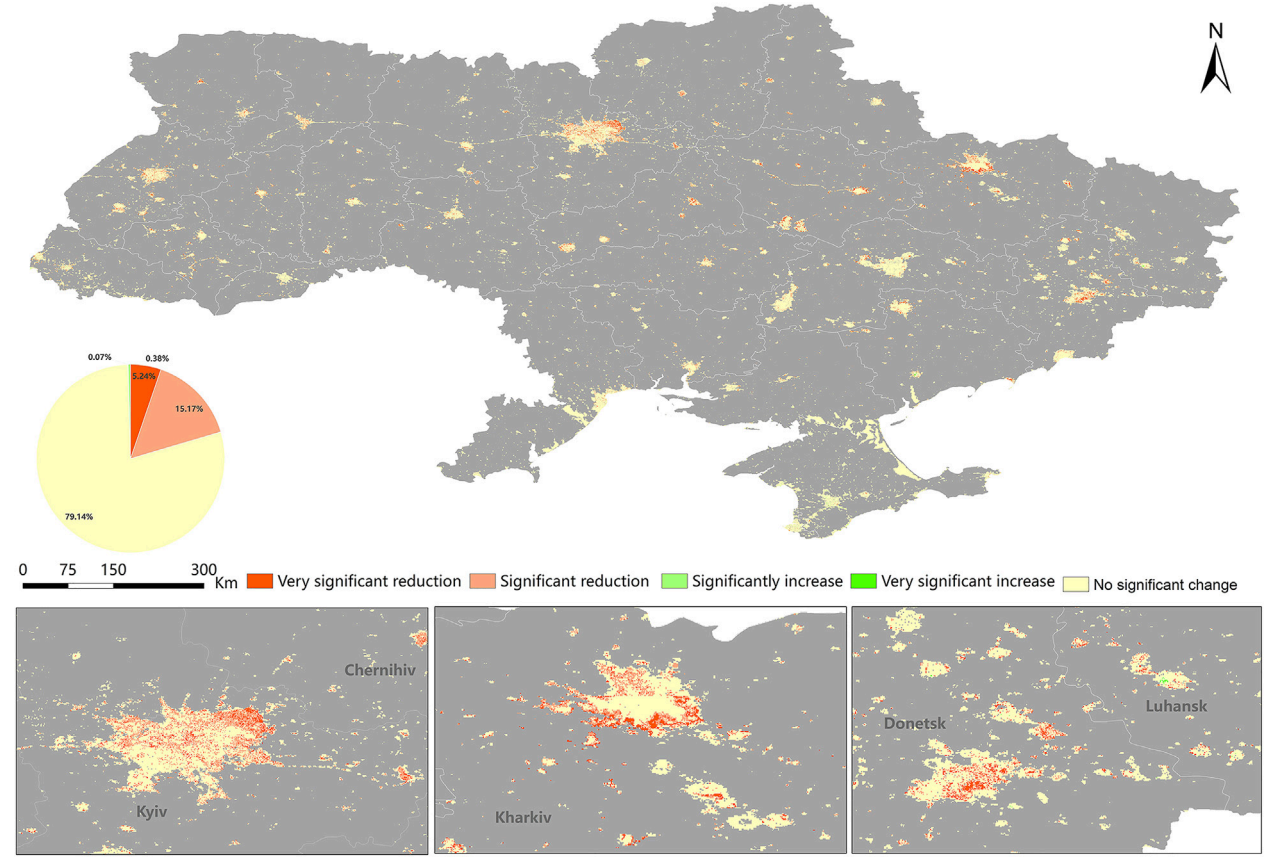

FIGURE 7
Nighttime light trends in Ukraine from 16 December 2021 to 2 May 2022.

value, indicating that observing the nighttime light conditions was not an effective way to determine the conflict situation in the area. Nonetheless, hostilities may erupt on other battlefields or at different scales, and the statistical analysis results may be vastly different; hence, the inferences require additional research. These estimates are useful as reference values and can be used to compare war losses, but more supplementary data are necessary to determine the extent of war damage.

4.2 Relationship between nighttime lights and refugees

Almost no research has been conducted on the correlation between nighttime lights and the movement of war refugees. Actual and reliable statistics are used to determine whether nighttime lights reflect the trend of the refugee population. This study's data were derived from the United Nations Refugee Agency's daily statistics to depict the refugee population's

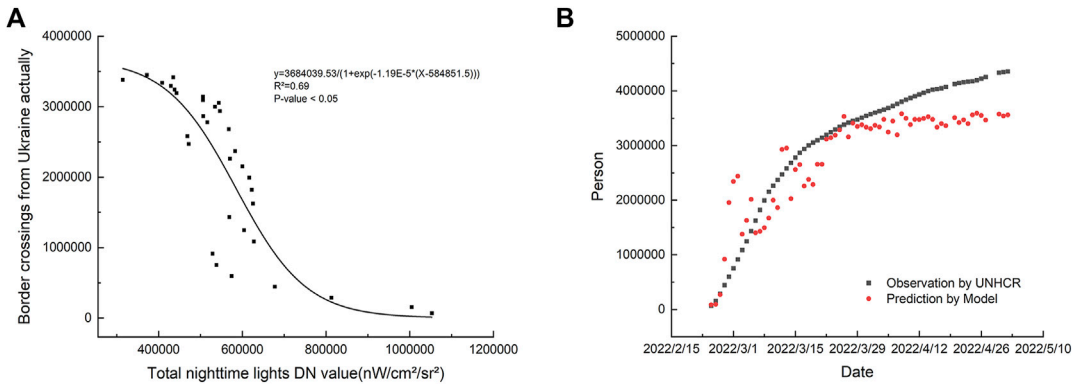

FIGURE 8
Relation between the refugee population and the total nighttime light DN value **(A)**; validation of the model of migration and nighttime lights using the UNHCR data **(B)**.

TABLE 1 Classification of changes in the refugee population.

NTL area change grid number	NTL average DN value change nW/cm^2/sr^2	Change in the value
>50000	>1	No significant change
>50000	<1	Slight increase
<50000	>1	Slight increase
<50000	<1	Significant increase

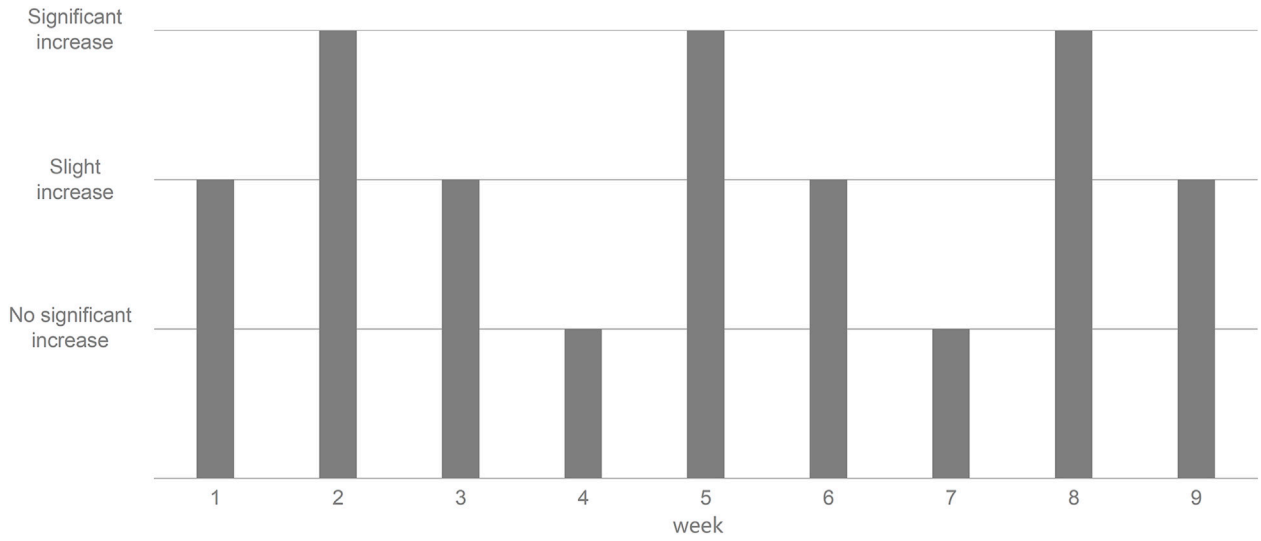

FIGURE 9
Trends in the refugee population by the grade within 9 weeks after the beginning of the war.

flow accurately. We eventually evaluated and adopted the logistic equation to construct the model of nighttime lights and refugee population fluctuations. Due to the high upper limit of nighttime light data, the changes were quite adaptable. However, the refugee population will not continue to expand indefinitely. Consequently, as the total nighttime light DN value grows in a linear regression equation, the convergence is problematic and the model fails. A more precise expression, such as the logarithm or multiple linear regression equation, is required for a broader perspective. Still, more supplementary data may be necessary to develop these equations and confirm the model's validity. This study employed a brief and continuous training data time series. The relationship between the refugee population and nighttime light data in Ukraine is reasonably basic

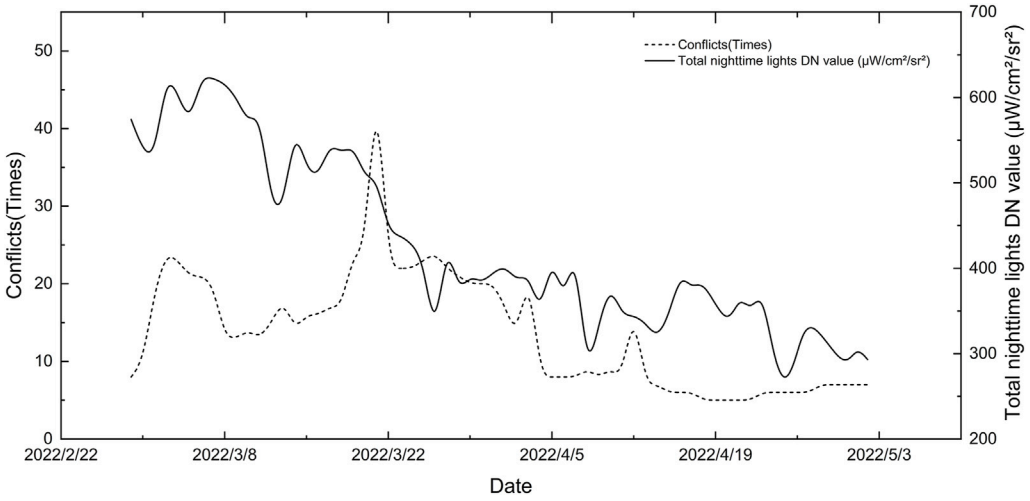

FIGURE 10
Conflicts and total nighttime light DN values in Ukraine during the war period.

and linear. It is impossible to estimate how long the current war situation in local conflicts will persist. However, based on the actual refugee population statistics and nighttime light inversion, the regression model developed for this study can achieve the research objectives.

We discussed the two situations according to the changing trend of nighttime lights and the refugee population, suppose the war continues in its current state. In this instance, the nighttime light area of Ukraine will continue to diminish in the original region, as will the average DN value of nighttime lights. According to our research, the fading of nighttime lights indicates a progressive transition from the city's periphery to its center. The average DN value of the city center's evening lighting gradually declines. Based on nighttime lights and the refugee population model, our analysis reveals that the refugee population continues to grow, with the majority originating from urban areas. However, it is based on the assumption that the war commences or concludes. In that circumstance, the refugee population and nighttime lights will depict a different state. Then, this study's refugee population calculation model driven by nighttime light data may no longer be applicable.

4.3 A depiction of the war by nighttime lights

The nighttime light is an inversion of the behavior and scope of human activity, just as a war is an abnormal and unpredictable act initiated by humans. Consequently, a relationship exists between the two. Li used the DMSP/OLS and VIIRS monthly composites to illustrate the variations in nighttime lights in Syria and Iraq during the war (Li et al., 2017; Li et al., 2018). The study indicates a rule that the war quickly destroys a country's nighttime lights, but post-war reconstruction allows nighttime lights to return gradually. As detailed previously, this circumstance also occurred in Ukraine, although the war between Russia and Ukraine remains in a stalemate. Furthermore, our simulations show that more nighttime lights in Ukraine will disappear as the war continues. Whether in Ukraine, Syria, or Iraq, the fact that the war may quickly extinguish nighttime lights holds true. The disappearance of nighttime lights also indicates changes in the spatial and temporal dimensions of the war. The timescale of nighttime lights employed by Li et al. in the Iraqi and Syrian wars was a month. In contrast, we used a week, which more accurately reflects the severity and brutality of the war and sensitivity of nighttime lights to the war. Furthermore, modeling, which employs weekly nighttime light data and refugee populations, followed by simulations of refugee population movements, can provide timely humanitarian assistance under specific circumstances and on finer timescales. Overall, nighttime lights offer an approximation of the extent and course of the war's impacts, but they are insufficient to adequately depict their particulars.

5 Conclusion

In this study, the refugee population and multi-day nighttime light data were used for mathematical modeling, and then, daily nighttime light data were compiled and analyzed. Before and after the beginning of the Russian–Ukrainian War, nighttime lights in Ukraine changed, and the refugee population changed as follows:

1) In the first week following the start of the war, the nighttime light area and average nighttime light DN value in Ukraine exhibited a sharp downward trend. The rate of decline then slowed. The changes in nighttime lights were especially pronounced in and around Kyiv and the northern and eastern regions.
2) During the first week, the refugee population in Ukraine increased the most, followed by a gradual decrease. After the start of the war, the refugee population shifted cyclically, exhibiting a "low–high–low" pattern. From the central and eastern regions poured an influx of displaced people. If the war continues, the number of refugees will continue to rise.
3) Following the outbreak of war, the Ukrainian state and society suffered a sudden decline, which was reflected in the alteration of nighttime lights. Affected by the transit time and other ground factors, night lights may not always reflect the actual status of the population and society; hence, assessing war losses based on nighttime lights may necessitate additional supplementary data for an accurate assessment.

Using nighttime light data to model the dynamic estimation of the changes in the refugee population of Ukraine during the war is crucial for calculating human losses in Ukraine and the subsequent supply of international humanitarian aid and post-war rehabilitation under the current war conditions.

Data availability statement

Publicly available datasets were analyzed in this study. These data can be found at: https://ladsweb.modaps.eosdis.nasa.gov/missions-and-measurements/products/VNP46A4/.

Author contributions

SH and CH conceived and supervised the research topic. CH and SH proposed the methods. CH and HZ processed the data. CH, HY, and YZ analyzed the results. CH, HY, XN, and QW wrote the manuscript.

Funding

This work was supported by the Project of Philosophy and Social Science Research of Colleges and Universities in Hubei Province (grant number 21G010).

Acknowledgments

The authors would like to thank the staff and scientists at NASA for providing the VIIRS–NPP data. The authors would like to appreciate the UNHCR and the Organization of the Global Conflict Tracker. They would also like to thank Liyuan Wei, Tingting Cui, and Lu Yang for providing some ideas about nighttime lights.

Conflict of interest

The authors declare that the research was conducted in the absence of any commercial or financial relationships that could be construed as a potential conflict of interest.

Publisher's note

All claims expressed in this article are solely those of the authors and do not necessarily represent those of their affiliated organizations, or those of the publisher, the editors, and the reviewers. Any product that may be evaluated in this article, or claim that may be made by its manufacturer, is not guaranteed or endorsed by the publisher.

References

Aljazeera (2022). Ukraine latest updates: UN says 6.5m displaced inside Ukraine. Available from: https://www.aljazeera.com/news/2022/3/17/un-says-more-than-700-civilians-killed-ukraine-liveblog (Accessed 04 10, 22).

BBC (2022). Broadcasting company. Available from: https://www.bbc.com/news/world-europe-60506682 (Accessed 03 01, 22).

Burn, D. H., and Elnur, M. H. (2002). Detection of hydrologic trends and variability. *J. Hydrology* 255 (1/4), 107–122. doi:10.1016/s0022-1694(01)00514-5

CBC (2022). UN says Ukraine's civilian deaths are being underestimated and the true number may never be known. Available from: https://www.cbc.ca/news/politics/civilian-deaths-ukraine-accurate-numbers-1.6404174. (accessed 04.03.22).

Chen, J., Yang, S. T., Li, H. W., Zhang, B., and Lv, J. R. (2013). Research on geographical environment unit division based on the method of natural Breaks (Jenks). *Spat. Inf. Sci.* 3, 47–50. doi:10.5194/isprsarchives-xl-4-w3-47-2013

Chen, J., Zhuo, L., Shi, P.-J., and Toshiaki, I. (2003). The study on urbanization process in China based on DMSP/OLS data: Development of a light index for urbanization level estimation. *J. REMOTE SENSING-BEIJING-* 7, 168–175.

Chen, X., and Nordhaus, W. D. (2011). Using luminosity data as a proxy for economic statistics. *Proc. Natl. Acad. Sci. U. S. A.* 108, 8589–8594. doi:10.1073/pnas.1017031108

CNN (2022a). CNN(Ukraine-satellite-images). Available from: https://edition.cnn.com/interactive/2022/03/world/ukraine-satellite-images/ (Accessed 03 01, 22).

CNN (2022b). What does putin want in Ukraine? The conflict explained. Available from: https://edition.cnn.com/2022/02/24/europe/ukraine-russia-conflict-explainer-2-cmd-intl/index.html (Accessed 04 28, 22).

Croft, T. A. (1978). Nighttime images of the Earth from space. *Sci. Am.* 239, 86–98. doi:10.1038/scientificamerican0778-86

Deren, L., and Xi, L. (2015). An overview on data mining of nighttime light remote sensing. *Acta Geod. Cartogr. Sinica* 44 (6), 591–601. doi:10.11947/j.AGCS.2015.20150149

Duque, J. C., Lozano-Gracia, N., Patino, J. E., Restrepo, P., and Velasquez, W. A. (2019). Spatiotemporal dynamics of urban growth in Latin American cities: An analysis using nighttime light imagery. *Landsc. Urban Plan.* 191, 103640. doi:10.1016/j.landurbplan.2019.103640

Guardian (2022). Ukraine economy to shrink by almost half this year, World Bank forecasts. Available from: https://www.theguardian.com/business/2022/apr/10/ukraine-economy-gdp-russia-invasion-world-bank-forecast (Accessed 03 23, 22).

Imhoff, M. L., Lawrence, W. T., Elvidge, C. D., Paul, T., Levine, E., and Privalsky, M. V. (1997). Using nighttime DMSP/OLS images of city lights to estimate the impact of urban land use on soil resources in the United States. *Remote Sens. Environ.* 59, 105–117. doi:10.1016/s0034-4257(96)00110-1

Li, X., Li, D. R., Xu, H. M., and Wu, C. Q. (2017). Intercalibration between DMSP/OLS and VIIRS nighttime light images to evaluate city light dynamics of Syria's major human settlement during Syrian Civil War. *Int. J. Remote Sens.* 38, 5934–5951. doi:10.1080/01431161.2017.1331476

Li, X., Liu, S. S., Jendryke, M., Li, D. R., and Wu, C. Q. (2018). Night-time light dynamics during the Iraqi civil war. *Remote Sens.* 10, 858. doi:10.3390/rs10060858

Liu, Z. F., He, C. Y., Zhang, Q. F., Huang, Q. X., and Yang, Y. (2012). Extracting the dynamics of urban expansion in China using DMSP-OLS nighttime light data from 1992 to 2008. *Landsc. Urban Plan.* 106, 62–72. doi:10.1016/j.landurbplan.2012.02.013

Lo, C. P. (2001). Modeling the population of China using DMSP operational linescan system nighttime data. *Photogrammetric Eng. Remote Sens.* 67, 1037–1047.

Moriasi, D. N., Arnold, J. G., Van Liew, M. W., Bingner, R. L., Harmel, R. D., and Veith, T. L. (2007). Model evaluation guidelines for systematic quantification of accuracy in watershed simulations. *Trans. ASABE* 50.3, 885–900. doi:10.13031/2013.23153

NASA-Suomi NPP (2022). Suomi NPP. Available from: https://www.nasa.gov/mission_pages/NPP/main/index.html (Accessed 04 08, 22).

NASA-VNP46A2 (2022). VNP46A2. Available from: https://ladsweb.modaps.eosdis.nasa.gov/missions-and-measurements/products/VNP46A2/ (Accessed 04 30, 22).

NASA-VNP46A4 (2022). VNP46A4. Available from: https://ladsweb.modaps.eosdis.nasa.gov/missions-and-measurements/products/VNP46A4/ (Accessed 04 08, 22).

NPR (2022). Russia's war could shrink the Ukrainian economy by 45% this year, the World Bank says.Available from: https://www.npr.org/2022/04/11/1092032051/russia-war-shrink-ukraine–economy-world-bank (Accessed 04 11, 22).

Qiang, Y., Huang, Q. X., and Xu, J. W. (2020). Observing community resilience from space: Using nighttime lights to model economic disturbance and recovery pattern in natural disaster. *Sustain. Cities Soc.* 57, 102115. doi:10.1016/j.scs.2020.102115

Román, M. O., Wang, Z., Shrestha, R., Yao, T., and Kalb, V. (2019). *Black Marble user guide version 1.0.* Washington, DC, USA: NASA.

Román, M. O., Wang, Z., Shrestha, R., Yao, T., and Kalb, V. (2020). *Black Marble user guide version 1.1.* Washington, DC, USA: NASA.

Román, M. O., Wang, Z., Shrestha, R., Yao, T., and Kalb, V. (2021). *Black Marble user guide version 1.2.* Washington, DC, USA: NASA.

Román, M. O., Wang, Z., Sun, Q., Kalb, V., Miller, S. D., Molthan, A., et al. (2018). NASA's Black Marble nighttime lights product suite. *Remote Sens. Environ.* 210, 113–143. doi:10.1016/j.rse.2018.03.017

Schaefli, B., and Gupta, H. V. (2007). Do Nash values have value? *Hydrol. Process.* 21, 2075–2080. doi:10.1002/hyp.6825

Shi, K. F., Yu, B. L., Huang, Y. X., Hu, Y. J., Yin, B., Chen, Z. Q., et al. (2014). Evaluating the ability of NPP-VIIRS nighttime light data to estimate the gross domestic product and the electric power consumption of China at multiple scales: A comparison with DMSP-OLS data. *Remote Sens.* 6, 1705–1724. doi:10.3390/rs6021705

Stokes, E. C., and Seto, K. C. (2019). Characterizing urban infrastructural transitions for the Sustainable Development Goals using multi-temporal land, population, and nighttime light data. *Remote Sens. Environ.* 234, 111430. doi:10.1016/j.rse.2019.111430

Sutton, P., Roberts, C., Elvidge, C., and Meij, H. (1997). A comparison of nighttime satellite imagery and population density for the continental United States. *Photogrammetric Eng. Remote Sens.* 63, 1303–1313.

TASS(MILITARY OPERATION IN UKRAINE) (2022). Putin declares beginning of military operation in Ukraine. Available from: https://tass.com/politics/1409329 (Accessed 02 24, 22).

UN News (2022). Ukraine. Available from: https://news.un.org/en/focus/ukraine (Accessed 04 05, 22).

UNdata (2022). Ukraine–Country profile. Available from: http://data.un.org/Search.aspx?q=ukraine (Accessed 04 26, 22).

Wang, Y. W., Yue, H. B., Peng, Q., He, C., Hong, S., and Bryan, B. A. (2020). Recent responses of grassland net primary productivity to climatic and anthropogenic factors in Kyrgyzstan. *Land Degrad. Dev.* 31, 2490–2506. doi:10.1002/ldr.3623

Wu, K., and Wang, X. N. (2019). Aligning pixel values of DMSP and VIIRS nighttime light images to evaluate urban dynamics. *Remote Sens.* 11, 1463. doi:10.3390/rs11121463

Zhang, Q. L., and Seto, K. C. (2011). Mapping urbanization dynamics at regional and global scales using multi-temporal DMSP/OLS nighttime light data. *Remote Sens. Environ.* 115, 2320–2329. doi:10.1016/j.rse.2011.04.032

Zhao, M., Cheng, W. M., Zhou, C. H., Li, M. C., Wang, N., and Liu, Q. Y. (2017). GDP spatialization and economic differences in south China based on NPP-VIIRS nighttime light imagery. *Remote Sens.* 9, 673. doi:10.3390/rs9070673

Zhao, M., Zhou, Y. Y., Li, X. C., Cao, W. T., He, C. Y., Yu, B. L., et al. (2019). Applications of satellite remote sensing of nighttime light observations: Advances, challenges, and perspectives. *Remote Sens.* 11, 1971. doi:10.3390/rs11171971

Zhuo, L., Shi, P., and Chen, J. (2003). Application of compound night light index derived from DMSP/OLS data to urbanization analysis in China in the 1990s. *ACTA Geogr. SINICA-CHINESE EDITION-* 58, 893–902.

frontiers | Frontiers in Environmental Science

TYPE Original Research
PUBLISHED 26 January 2023
DOI 10.3389/fenvs.2023.1057812

Check for updates

OPEN ACCESS

EDITED BY
Salvador García-Ayllón Veintimilla,
Technical University of cartagena, Spain

REVIEWED BY
Qingsong He,
Huazhong University of Science and Technology, China
Jun Liu,
Beijing Jiaotong University, China

*CORRESPONDENCE
Yanfang Liu,
yfliu610@yeah.net

SPECIALTY SECTION
This article was submitted to Land Use Dynamics, a section of the journal Frontiers in Environmental Science

RECEIVED 30 September 2022
ACCEPTED 16 January 2023
PUBLISHED 26 January 2023

CITATION
Zhang G, Liu Y, Jing Y, Chen H, Wang Y and Wang Z (2023), Unraveling the supply-service relationship between high-speed railway and conventional railway: A temporal perspective.
Front. Environ. Sci. 11:1057812.
doi: 10.3389/fenvs.2023.1057812

COPYRIGHT
© 2023 Zhang, Liu, Jing, Chen, Wang and Wang. This is an open-access article distributed under the terms of the Creative Commons Attribution License (CC BY). The use, distribution or reproduction in other forums is permitted, provided the original author(s) and the copyright owner(s) are credited and that the original publication in this journal is cited, in accordance with accepted academic practice. No use, distribution or reproduction is permitted which does not comply with these terms.

Unraveling the supply-service relationship between high-speed railway and conventional railway: A temporal perspective

Guangxia Zhang[1], Yanfang Liu[1,2]*, Ying Jing[3], Huiting Chen[1], Yiheng Wang[1] and Zhengyu Wang[1]

[1]School of Resource and Environmental Sciences, Wuhan University, Wuhan, China, [2]Key Laboratory of Geographic Information System, Ministry of Education, Wuhan University, Wuhan, China, [3]Business School, NingboTech University, Ningbo, China

With the rapid development of high-speed railway (HSR), many scholars have studied the competition between HSR and aviation or inter-city coach, but few studies have discussed the supply-service relationship within the railway system. This paper explores the competition and cooperation between HSR and conventional railway (CR) at the city-pair level of 39 core cities in China from the temporal perspective. Comprehensive considering the departure time and arrival time between city pairs as the representation of train service quality, we find that the proportion of superior quality service of high-speed train (HST) is far higher than that of conventional train (CT). However, the time slots representing the competition degree show that CR with fewer superior quality trains is easier to be replaced than HSR. The supply-service relationships of the railway system indicate that HSR has become the main transportation mode between core cities, and the CR, as an auxiliary transportation, shows a certain complementary effect in the temporal perspective. Spatially, HSR and CR services are more likely to generate temporal competition on the mainline, but temporal complementarity between city pairs on non-arterial lines. This study can provide inspiration for regional spatial planning by better understanding the operation strategy of railway passenger transport system.

KEYWORDS

intercity competition modes, supply service quality, substitutability degree, highspeed railway, conventional railway

Highlights

- A new method to identify the supply service relationship between high speed railway (HSR) and conventional railway (CR) is proposed.
- We propose a method to divide train service quality based on time availability.
- We find the characteristics of quantity and quality of HSR and CR are very different.
- The supply service relationship between HSR and CR shows that they have cooperation potential in terms of time.

1 Introduction

As a physical connection between cities, railway is one of the most important basic conditions for urban development. High-speed railway (HSR), as the most significant technological breakthrough of railway system since 1964, has greatly shortened the intercity

travel time (Spiekermann and Wegener, 1994; Shaw, Fang, Lu, and Tao, 2014). Because of its high accessibility and high frequency, HSR generates substitution effect by attracting passengers from other transport modes, which leading to a reallocation of the passenger market (Lee and Chang, 2006; Zhang et al., 2018; Wang et al., 2020b; Yang et al., 2018a). For example, China has built the world's largest HSR network after more than 10 years of rapid development, making the proportion of railway passenger traffic in 2020 to be 4.4 times that in 2010. In addition, HSR also reduces CO_2 emissions and haze pollution by influencing the intercity traffic patterns (Jiang et al., 2021; Li et al., 2022). However, the high construction and operation costs of HSR cannot be ignored by government departments and urban planners. Therefore, exploring the competition and cooperation between HSR and other intercity traffic modes is an important research issue for regional sustainable development and transportation optimization.

The impacts of HSR on air travel have been analyzed in many countries due to the high speed characteristics of two transport modes (Dobruszkes et al., 2014; Castillo-Manzano et al., 2015; Delaplace and Dobruszkes, 2015; Zhang et al., 2018). In recent years, the impacts of HSR on the railway system have gradually attracted the attention of scholars. For example, the change of passenger flow indicates that the development of HSR has a strong substitution effect on conventional railway (CR) in China due to the time-saving advantages of HSR (Cheng and Chen, 2021). But CR is still the best choice for cities with lower population density and poor socioeconomic performance (Shaw et al., 2014). Recent studies have shown the importance of cooperation between HSR and CR in improving travel efficiency and achieving spatial and social equity (Zhang. H et al., 2020; Huang and Zong, 2022). However, although some studies have compared the similarity and difference of the spatial pattern between HSR and CR from accessibility or network structure (Zhang. H et al., 2020; Huang and Zong, 2022), the exploration from the time dimension has not yet been seen. Therefore, it is necessary to deeply study the operation strategy of railway passenger transportation system from the perspective of time.

Traditionally, the schedules reflect the operation and management strategy of public transport supplier (Burghouwt and de Wit, 2005; Dobruszkes, 2011; Huang and Wang, 2017), which scholars have used to conduct a large number of empirical studies. For example, while there is potential temporal competition between China's HSR and airlines, the two have complementary spatial and temporal effects in resisting different types of hazards (Wang et al., 2020b; Li and Rong, 2022). In the railway system, train schedules show that the service intensity of HSR and CR are complementary in terms of spatial distribution (Huang and Zong, 2022). Railway departments operate more frequent high-speed trains (HST) during the peak hours of passenger travel (Wang et al., 2020b), but the characteristics of time slot between HST and conventional trains (CT) have not yet received attentions. To fill this gap, this paper explores the supply-service relationship between HSR and CR at the city-pair level based on train schedules, in order to better understand the competition and cooperation strategy of railway system. In addition, this paper measures the service quality level by comprehensively considering the departure time and arrival time of trains to distinguish the homogeneous train service in previous studies. And we assume that the smaller the time slot of departure time, the greater the degree of competition between HST and CT in the same city pair.

As the HSR is mainly designed to connect large cities, in general, core cities benefit more from HSR than peripheral cities (Levinson, 2012; An et al., 2022). In addition, studies have shown that the core layer is the densest cluster in the railway network structure (Zhang. H et al., 2020), carrying most of the traffic flow (Huang and Zong, 2022). Therefore, we attempt to enrich the research on HSR and CR supply-service relationships among core cities, and take 39 core cities with high administrative level or high population in China as research objects. Under the study objectives above, this paper 1) analyzed the distribution characteristics of service intensity of the HST and CT between core city-pairs, 2) distinguished the service quality types of HST and CT which determined by both departure time and arrival time, and 3) measured the level of substitutability between HST and CT from time slot perspectives. Furthermore, according to the quantity and quality of trains, the improved classification method identifies relationships between HSR and CR at the city-pair level, including single mode dominant type, cooperation complementary type and competition type.

The structure of this paper is as follows: Section 2 reviews the existing researches on the relationship between HSR and other transportation modes; Section 3 introduces the development of HSR in China and the research methods in this paper. Section 4 presents the results; Section 5 discusses the policy implications of the relationship between the two rail services; and Section 6 draws conclusions.

2 Literature review

The emergence of HSR has directly shortened the space-time distance, and indirectly changed the intercity travel mode. Empirical studies in many countries show that the construction of HSR can significantly improve the accessibility between cities (Shaw et al., 2014; Wang, 2018; Weng et al., 2020), making some governments strive for HSR stops. Due to differences in geographic regions and population sizes, the impacts of HSR development on economic growth are uneven (Guo et al., 2020; Jiao et al., 2020; Zhang. F, et al., 2020). With the advantages of low price compared with air and time saving compared with CR, HSR has led to the redistribution of market share by attracting passengers from other transportation modes (González-Savignat, 2004; Lee and Chang, 2006; Yang et al., 2018a). In addition, studies have shown that HSR has become an important tool to promote regional integration by providing convenient intercity travel services, which in turn will generate new intercity transportation needs (Cascetta and Coppola, 2015). For example, due to the high housing prices in Beijing and the convenient HSR services with surrounding small cities, a number of passengers have taken HST as their daily commuter. However, HSR is not always the best choice for low-density and economically underdeveloped areas due to the huge cost of construction and operation.

Many studies have explored the competitiveness of intercity transport from different perspectives, including individual trips, changes in passenger traffic, and provision of services. For individuals, although the influence degree of each factor varies depending on the travel distance, transportation mode choice is the result of the combination of transportation mode attributes, travel attributes, and individual passenger attributes (Castillo-Manzano et al., 2015; Lee et al., 2016; Li. X. W et al., 2021). Specifically, passengers with higher education levels, higher income levels, or

business trips are more likely to choose comfortable and time-saving transportation modes, such as HSR and airline. While passengers who are concerned about travel costs and are not time-sensitive are more likely to choose CR or intercity coach (Wang et al., 2017; Zhou et al., 2019). In terms of passenger traffic, HSR is more competitive in cities with better social economy, regardless of whether it is compared to airline or CR (Yang et al., 2018a; Yang et al., 2018b; Cheng and Chen, 2021). Empirical evidence shows that HSR is the most competitive compared to airline when the travel distance is within 500–800 km (Chen, 2017). In China, the substitution effect of HSR on CR varies spatially in different corridors (Huang and Zong, 2022). In terms of supply, the frequency change in the time dimension and the travel time change in the space dimension of HSR have a significant impact on air passenger flow (Yang et al., 2018a). Considering the high cost of HSR, railway operators need to adjust the service frequency of HSR to cover the cost.

In addition to competition, HSR has great demand and potential for cooperation with other transportation modes, including multimodal combined transport and complementation. From the perspective of individual travel, the combined of multiple transportation modes can significantly improve the accessibility and transportation efficiency of the whole journey chain. For example, integrated railway stations can realize rapid transfer between HST and CT, which significantly improve the efficiency of the railway system (Zhang. H et al., 2020). In addition, the effective connections between HSR and urban public transport can significantly shorten the total travel time (Huang and Zong, 2021), making up for the lack that HSR stations are far away from urban centers (Wang et al., 2013; Diao et al., 2017). Therefore, the travel efficiency will be further improved with the construction of comprehensive stations that can serve multiple transportation modes. In terms of spatial cooperation and complementarity, HST services in China are more concentrated in regions with better socio-economic performance, while CT services are better at providing more extensive geographical coverage (Huang and Zong, 2022). As for temporal coordination and complementation, HST and air services coordinate and facilitate round-trip travel. Further, the space-time complementary effect of multiple traffic modes can improve the robustness against different types of hazards (Li and Rong, 2022).

In recent years, the importance of HSR services has been recognized, and many scholars have shifted from location-based network structures to timetable-based service characteristics. On one hand, location-based reachability often overestimates the results due to ignoring the intensity differences of services between nodes (Moyano et al., 2018). On the other hand, location-based evaluations only reveal the potential of transport network configuration, which cannot reflect the actual operational characteristics of traffic facilities. Fortunately, the availabilities of more and more operation schedules make it possible for scholars to explore transportation services from the perspective of suppliers. For example, small cities in Europe and China are underserved by HSR due to insufficient potential markets (Moyano and Dobruszkes, 2017; Huang and Zong, 2022). In addition, traffic dispatching not only affects the competition of multimodal transport (Dobruszkes et al., 2014; Castillo-Manzano et al., 2015; Lee et al., 2016; Broman and Eliasson, 2017), but also affects the time competition across transport modes (Espinosa-Aranda et al., 2015). Previous studies have investigated the competition between HSR and flights between cities by using the time window method, which only considered the departure time (Wang et al., 2020b).

To sum up, the introduction of HSR will have great impacts on the market share and service supply of other transportation modes. Therefore, exploring the competition and cooperation among different transportation modes is of great significance for optimizing transportation services. Existing studies have carried out a lot of researches on the relationship between HSR and airline, while the relationship between HSR and CR in the railway system has not received enough attentions. Although scholars have explored the spatial distribution of HSR and CR, they are limited to differences in spatial network structure and spatial service distribution. The relationship between these two transport services has not been analyzed from the perspective of time. Therefore, we interpreted the competition and collaboration between HSR and CR supply services from a time perspective. This study not only enriches the empirical research of comparative analysis of different intercity traffic, but also has important significance for optimizing the railway service system.

3 Background and methods

3.1 Development of Chinese railways

Since the reform and opening up from 1978, in order to better serve the development of urbanization, China's traditional railway lines have rapidly formed the main trunk lines shown in Figure 1A. China released the HSR construction plan in 2004 (revised in 2016), and opened the first high standard HSR line between Beijing and Tianjin in 2008. In order to relieve the pressure on CR from the growing passenger demand, the Chinese government usually arranged HSR lines to be parallel to the existing CR lines (Figure 1B). The construction of China's HSR network is long-term and balanced, and the opened lines gradually expand from large cities to small and medium-sized cities and inland areas (Perl and Goetz, 2015; Xu et al., 2018). At present, "the four-horizontal and four-vertical HSR trunk lines" have been put into operation, and "the eight-horizontal and eight-vertical HSR lines" are also being gradually opened. The latest research shows that China's train service presents a complex hierarchical network (Xin and Niu, 2022), and core cities have a large number of HST services and CT services at the same time (Huang and Zong, 2022). Therefore, this paper takes cities with high administrative level or urban permanent population larger than one million in mainland China as core cities, including 39 cities in Figure 1, which is the research object of this paper.

As shown in Table 1, there are seven types of train number initials in the train timetable. The minimum planned running speed of the train prefixed with C\D\G is 200 km/h, which is called HST in this paper. CT include four types of railway trains, but the maximum speed is only 160 km/h. The Chinese government regards HSR as an important tool to improve railway transport capacity (Wu et al., 2014). Therefore, the number of HST in service is increasing year by year, while the number of CT is experiencing a gradual decline. G-type trains are the most in operation between core cities, and HST accounts for three-quarters of the total trains (Table 1).

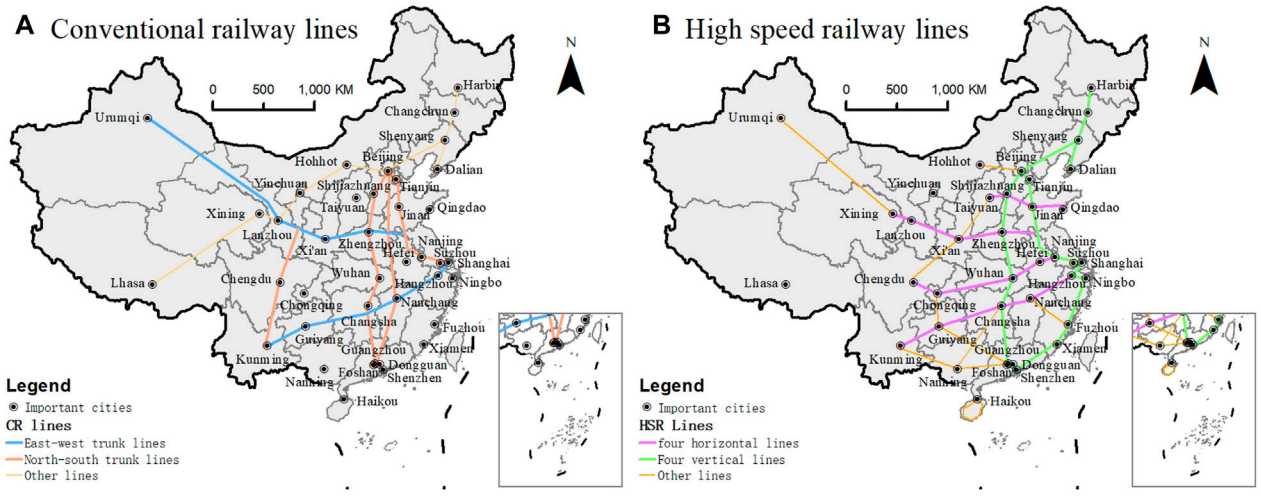

FIGURE 1
Spatial distribution of CR lines **(A)** and HSR lines **(B)** in operation in 2020.

TABLE 1 Classification of train types.

Train prefix	G-	D-	C-	Z-	T-	K-	Pure number
Max speed	350	300/250	250/200	160	140	120	100
Train type	HST	HST	HST	CT	CT	CT	CT
Trains Number	2,383	1,158	565	189	121	932	62

3.2 Data and network construction

Since the railway timetable is adjusted at a certain time, and the schedule of 1 day is fixed for a period of time, we obtained the domestic railway timetable of September 2020 (http://www.12306.com), which can represent the daily dynamics of intercity railway service arrangement. The location of the railway station was found on Baidu map (https://map.baidu.com). Geographic vector data obtained from 14 million basic topographic maps, including national boundaries in China. The administrative location coordinates of core cities selected are also from Baidu map, which is used to calculate the distance between cities.

The train schedule directly reflects the connections between stations. We first used the P-space model to build the connection networks of HSR and CR. Subsequently, we simplified the station connection network to the city connection network according to the station attribution. We noticed that some cities may have more than one railway station. For example, Wuhan has three railway stops: Wuhan Station, Wuchang Station and Hankou Station. In the process of simplifying the network, we ignored the connection between stations in the same city, and considered the connection between multiple stations of the same train between two cities as only one connection. We defined city pairs with only one service as OnlyHSR/OnlyCR city pairs, while city pairs with both HST and CT services are defined as overlapping city pairs. For actual travel, passengers need to choose a way of overlapping city pairs according to their own conditions. Therefore, it is necessary to further explore whether these two railway services are competitive or complementary in overlapping city pairs from a temporal perspective.

3.3 Methods

3.3.1 Supply service intensity

The supply service intensity is measured by the train frequency widely used in current research (Jiao et al., 2017; Wang et al., 2020b). For a city pair, the obtained supply service intensity is the number of trains between the departure city and the arrival city in 1 day, which can be obtained from the train schedule. For a city, we no longer emphasized the directionality of service supply, and measured the service intensity with the sum of the train frequency of the city as the departure endpoint and the arrival endpoint, as shown below.

$$T_i = \sum_{j=1,j\neq i}^{n} L_{ij} + \sum_{j=1,j\neq i}^{n} L_{ji} \quad (1)$$

Where T_i represents the total intensity of supply services obtained by city i, and the higher the value, the more important the status of city i in the network. L_{ij} represents the frequency of trains which taking city i as the departure city and city j as the arriving city, and L_{ji} is the opposite. The total number of nodes in the service network is n, that is, the 39 selected core cities. In addition, we use relative strength (Limtanakool et al., 2007; Yang et al., 2019) to compare the spatial differences of supply services, as shown below:

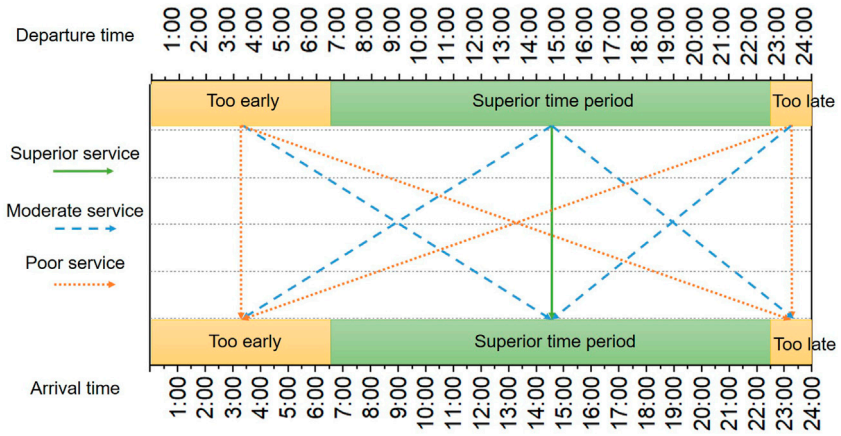

FIGURE 2
Classification methods of railway service quality.

$$RSL_{ij} = \frac{L_{ij}}{\left(\frac{\sum_{j=1}^{n} L_{ij}}{n}\right)} \quad (2)$$

$$RST_i = \frac{T_i}{\left(\frac{\sum_{j=1}^{n} T_i}{n}\right)} \quad (3)$$

Where RSL_{ij} is the ratio of the supply service intensity of a city pair to the average intensity of all city pairs in the same network. RST_i is the supply service intensity of a city, and its calculation method is consistent with RSL_{ij}. If the relative intensity is greater than 1, it means that the supply service intensity of the city pair or the city is higher than the average level.

3.3.2 Definition of supply service quality

This paper defines the service quality of trains from the perspective of time, which is different from that characterized by topology and number of trains (Zhang. F et al., 2020). Railway scheduling determines the availability of train services in terms of time, which in turn influences passenger travel mode choices (Dobruszkes et al., 2014; Castillo-Manzano et al., 2015; Lee et al., 2016). Many empirical studies of door to door full journey show that the time spent before and after the train can not be ignored. Therefore, we believe that the time when passengers can connect with public transport is the superior time period of trains. In China, although the service time of bus or subway varies slightly in different cities or seasons, we find that it is usually between 6:30–22:30. Therefore, we defined this time period as superior service time.

This study defined the service quality provided by the train based on the departure time and arrival time. As shown in Figure 2, the color of the arrow represents the service quality types. Specifically, if the time of train T1 in departure city i and destination city j are both within the superior time period, it is considered that T1 provides superior service for city pair ij. If only the departure time or the arrival time is within the superior time period, it is considered as a moderate service, including 4 situations. If the departure time and arrival time are both not within the superior time period, it is considered to be a poor service, which also includes 4 situations. It is worth noting that the stopping time of a train at different stations varies, which may lead to differences in the quality service provided by the same train between different city pairs.

3.3.3 Measures of substitutable index

Broman and Eliasson (2017) proposed that the competition took place between trains with similar departure times. In this paper, considering the quality of train services, it is recognized that only superior train services can compete (Borenstein and Netz, 1999). Put forward an index to quantify the time difference, the Time Difference Index (TDI), which refers to the absolute difference between the departure times of two transportation modes. For example, if an HST is scheduled at 8:00 a.m. and a CT is scheduled at 22:00 p.m., in this case, the TDI value is equal to 14. Since we define the superior service time as 6:30 to 22:30, the maximum TDI is 16 h. Superior overlapping city pairs, that is, city pairs with both superior quality CT and HST, are the objects that need to measure TDI. We calculate the TDIs between all superior HSTs and CTs in the same city, and calculate their average and minimum values, as shown in the following formula.

$$TDI_{ave} = \frac{\sum_{m=1}^{M}\sum_{n=1}^{N}\left|T_{HST,m} - T_{CT,n}\right|}{MN} \quad (4)$$

$$TDI_{min} = \min_{M,N}\left|T_{HST,m} - T_{CT,n}\right| \quad (5)$$

Where TDI_{ave} and TDI_{min} represent the average and minimum values of all TDIs in the same city, respectively. $T_{HST,m}$ and $T_{CT,n}$ represent the departure time of the *m*th superior HST and the *n*th superior CT of the city pair, respectively. The service frequencies of the superior HST and superior CT of this city pair are M and N, respectively. In general, the smaller the TDI_{ave}, the closer the departure times between HST and CT for this city pair. A larger TDI_{min} means that the schedules for HST and CT are less likely to overlap.

Some studies have suggested that different transportation modes with TDI less than 1 h are substitutable (Wang et al., 2020b). According to this scheme, we regard HST and CT services with TDI less than 1 h as mutually replaceable, and count the frequencies of HST and CT that can be replaced according to the city pair, as shown below.

$$RN_{ij,m,n} = \begin{cases} 1, \left|T_{HST,m} - T_{CT,n}\right| \le t \\ 0, \left|T_{HST,m} - T_{CT,n}\right| > t \end{cases} \quad (6)$$

$$RN_{ij}^{HST} = \left|\left\{m \middle| RN_{ij,m,n} = 1, 1 \le m \le M, 1 \le n \le N\right\}\right| \quad (7)$$

$$RN_{ij}^{CT} = \left|\left\{n \middle| RN_{ij,m,n} = 1, 1 \le m \le M, 1 \le n \le N\right\}\right| \quad (8)$$

$$RI_{ij} = \sqrt{\left(\frac{RN_{ij}^{HST}}{Q_{ij}^{HST}} * \frac{RN_{ij}^{CT}}{Q_{ij}^{CT}}\right)} \quad (9)$$

Where $RN_{ij,m,n}$ indicates whether the *m*th HST or the *n*th CT in city pair ij has a CT/HST that can be replaced, and t represents the radius of the time window, which is set as 1 in this paper. RN_{ij}^{HST} and RN_{ij}^{CT} represent the number of replaceable HST trains and CT trains for city pair ij, respectively. RI_i represents the comprehensive substitutability of the two services for city pair ij. The larger the value, the higher the probability that the HST and CT services on the city pair can be replaced, and the more intense the competition between the two railway services. Q_{ij}^{HST} and Q_{ij}^{CT} represent the number of superior HST and superior CT service trains for city pair ij, respectively.

3.3.4 Classification of relationship types

Some studies have explored the relationship between different transportation modes, including spatial relationship or temporal relationship (Wang et al., 2020b; Huang and Zong, 2022). For the relationship types, it is generally considered that they can be classified as single transportation mode dominant, multi-modal coordination and complementary type, and multi-modal competition type. However, there is no consensus on the specific method of classifying relationship types, which needs to vary depending on the indicators measured in the study. Therefore, according to the general cognition, this paper divides the relationship between HSR and CR into the above three types. By referring to relevant studies (Wang et al., 2020b) and combining with the specific indicators measured in this paper, we propose a method to classify the supply-service relationship between HSR and CR at the city-pair level from the temporal perspective, as shown below. It is worth noting that the classification of relationship types is only for overlapping city pairs with superior HST and superior CT at the same time.

The first step can distinguish the dominant type of single railway model. For some city pairs, the number of superior HST in a day may be significantly larger or smaller than that of CT, indicating that intercity travel is dominated by a single train mode. Taking into account the Pareto principle (Craft and Leake, 2002), we defined HST as dominant when HST accounts for more than 80% of the total superior service for a city pair. On the contrary, the city pair is considered to be the CT dominant type when the proportion of superior CT exceeds 80% of the total superior services. It is possible that the city pairs with different single-model dominant have very different characteristics, which is why rail providers use different approaches to primarily serve them.

The second step distinguished is the type of coordination complementarity. Coordination complementarity as defined in existing studies implies the integration or maximization of benefits between different transportation modes (Givoni and Banister, 2006; Jiang and Zhang, 2014; Xia and Zhang, 2017). However, the coordination complementarity defined in this paper is for the TDI of departure time between HST and CT in a city pair. If the minimum TDI is large, it means that the train can serve passengers at different times for 1 day, which meeting the travel needs of different travel periods. Based on the thinking of time slot in previous studies (Wang et al., 2020b), we also divided city pairs with TDImin greater than 4 h into coordination complementary types.

In the third step, the competition types of the two railway services are divided. The competition in this paper is defined from the perspective of passengers. If the time slot of HST and CT in the same city pair is small, passengers need to consider choosing one, in which case there is competition between the two rail services. For different city pairs, we note the significant differences in the degree of competitions. Therefore, we further divided the competition into full competition, partial competition and slight competition according to the minimum TDI and substitutability index measured in 3.3.3. In this process, the substitutable index is graded based on a three-point scale, as shown in the following 3 steps. 1) Full competition: TDImin is within 1 h, and the substitutable index is greater than 0.67. Not only the departure times of HST and CT between these city pairs are close, but also the frequency of substitutable trains is high; 2) Partial competition: TDImin is within 1 h, and the substitutable index is between 0.33–0.67 or TDImin is greater than 1 h but less than 2 h, indicating that the degree of competition between HST and CT of these city pairs is moderate; 3) Slight competition: TDImin is within 1 h, but the substitutable index is less than 0.33 or TDImin is greater than 2 h but less than 4 h, which means that there is less competition between HST and CT for these city pairs.

4 Results

4.1 Distribution of supply service intensity

As shown in Figure 3A, B, the HSR network has higher service intensity and CR network covers a wider space. CR network serves 1,137 city pairs among all core cities, while HSR network only includes 810 city pairs. The HSR network mainly connects cities in the southeast of Hu Huanyong Line, with a daily average frequency of 19.96. The CR network has a long distance feature, which makes the average distance between city pairs reach 1276.22 km. But 76.67% of the city pairs have a relative strength lower than 1. Generally speaking, the service intensity of the two networks are both limited by the distance. The greater the distance between cities, the lower the service intensity. However, there are city pairs with large distance but high service intensity in both networks. For example, the distance between Urumqi and Xi'an in CR network exceeds 2,100 km, while there are still 16 traditional trains every day. And the distance between Beijing and Shanghai in the HSRnetwork is close to 1,100 km, while there are nearly 50 high-speed trains every day.

The relative service intensity of HSR is more advantageous in the south, while CR is more advantageous in the north. As shown in Figure 3C, there are 412 OnlyCR city pairs, but their relative strength is relatively low, and only 2 city pairs have RSL exceeding 2. Some OnlyHSR city pairs have higher RSL, with Fujian-Xiamen having the highest value, close to 5. For overlapping city pairs, the relative intensity of the two services varies greatly, with 76.41% of them having higher CR service intensity. According to the spatial distribution of service intensity, we found that the high CR

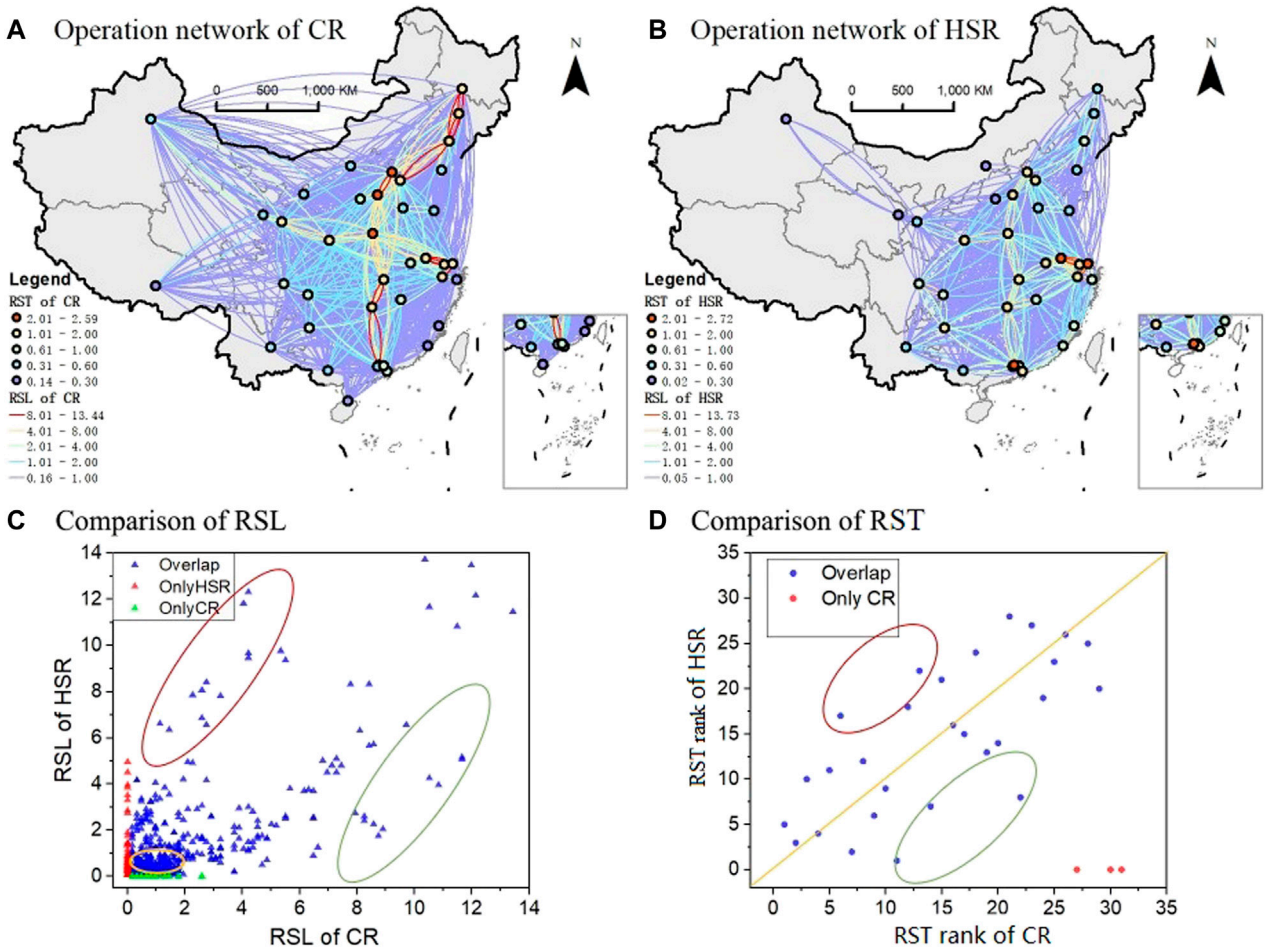

FIGURE 3
The spatial distribution of service intensity in CR network **(A)** and HSR network **(B)**, and the comparison of RSL **(C)** and RST rank **(D)** between the two railway modes.

service city pairs represented by the green circles are generally located in the northern region, while the high HSR service city pairs represented by the red circles are generally located in the southern region. In addition, some cities have very low HSR and CR frequencies (shown by the yellow circles), indicating that these two services work together to meet the transportation needs of these city pairs.

For cities, the daily train service intensity of the two networks is very different. On the whole, the average daily train frequency of each city in CR network is 359.74, while the value of HSR is as high as 872.92. Specifically, in CR network, the values of relative service intensity in Zhengzhou, Beijing and Shijiazhuang are greater than 2. In the HSRnetwork, the service intensity values of Nanjing, Shanghai and Guangzhou are more than twice the average. As shown in Figure 3D, compared with the CR network, the relative intensity of cities in the HSR network are quite different, with the most significant increase in Hefei and Nanjing (green circle), while the most significant decrease in Shenyang and Lanzhou (red circle). This means that the two rail service levels are spatially unbalanced. Some cities represented by the Yangtze River Delta region have better HSR services, while some cities represented by the three northeastern provinces have more advantages in CR services.

4.2 Time based quality of HST and CT services

The time structure of train operation reflects the quality characteristics of supply service. The daily departure and arrival rhythm of trains in HSR and CR networks are quite different.We aggregated the number of departing and arriving HST(CT) per hour in a day from the train schedule, as shown in Figures 4A, B. In HSR network, the trend of departure and arrival rhythm changes with time is the same, but the changing time nodes are different. The number of HST departures and arrivals both surged from 6 a.m, and the peak numbers were almost the same. The peak time of HST departure is 9: 00 a.m. to 17:00 p.m., while the peak time of HST arrival is 14:00 p.m. to 22:00 p.m. The intersection of the two curves shows that the number of HST departures is greater than the number of arrivals before 12: 00 during the day, while the opposite is true after 17:00 p.m. In CR network, the departure number of CTs wavelike rises with time, while the arrival number of CTs has the opposite trend. Unlike the HSR network, CT has more arrivals than departures before 12:00 a.m. This means that the service time of HSTs and CTs is different in a day, and they are complementary to each other to a certain extent.

Considering the departure time and arrival time of trains between city pairs, as shown in Figures 4C, D, the service levels of different train types are very different. In the HSR network, G-type service is the

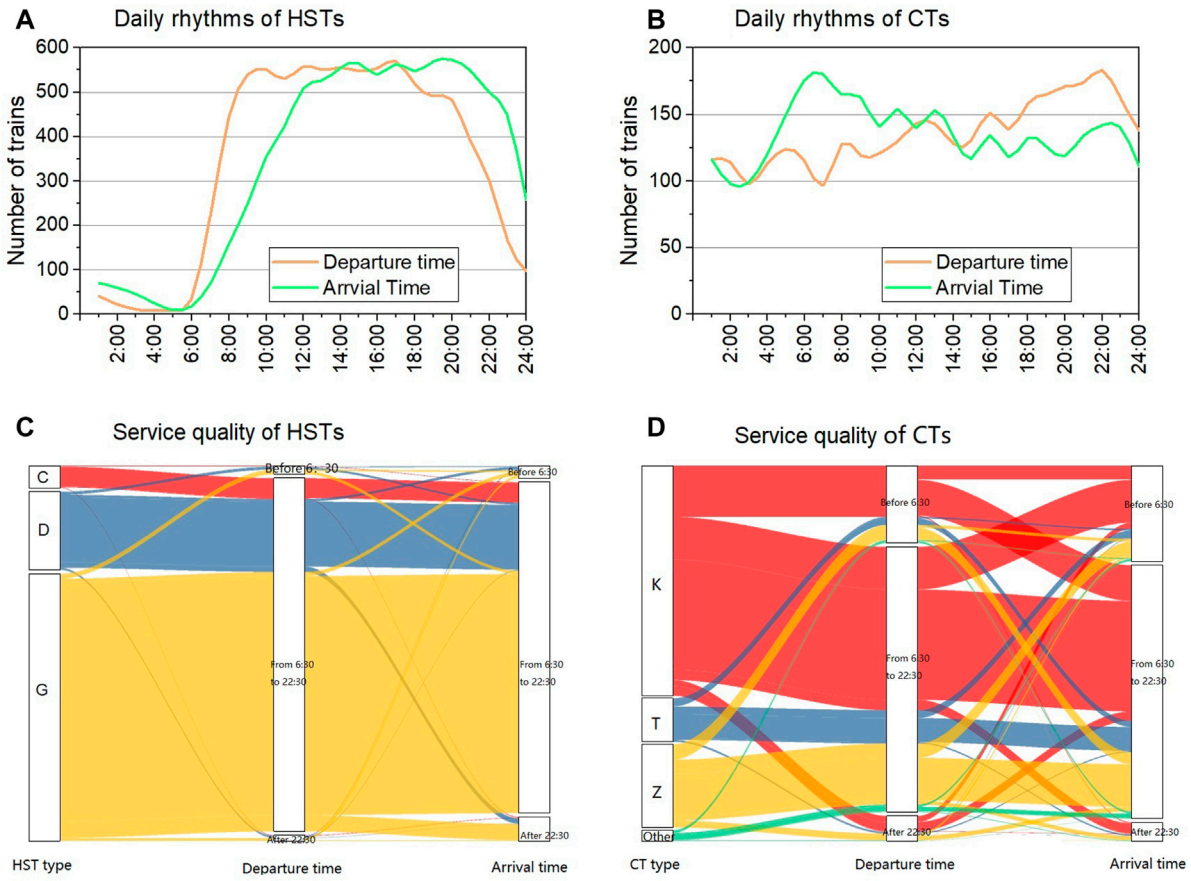

FIGURE 4
Daily rhythme of HSTs **(A)** and CTs **(B)** and the service quality of HSTs **(C)** and CTs **(D)** for overlapping city pairs.

largest, accounting for 72.75%, and C-type service only accounts for 5.92%. However, the superior service proportion of G-type and C-type are both about 90%, while that of D-type is only 82.85%. In the CR network, K-type trains serve the most, accounting for 62.74%, followed by Z-type trains. Type T has the best service quality, with superior services accounting for 55.01%. Other-types trains are not only the least in number but also the worst in service. In general, the service quality of HST is much higher than that of CT. As there are few high-speed trains running at night, most HST departure and arrival times are located in superior service areas, making the proportion of superior service as high as 88.33%. The superior service rate of CTs is only 51.08%, which means that only half of CTs can provide convenient boarding and alighting services for passengers. However, for price-conscious passengers, HST's superior service is not attractive. Therefore, although the quantity and quality of CT services are not dominant, it still has the potential to replace HST to a certain extent.

For city pairs, the distribution of superior services in HST and CT is very different. Figures 5A, B show the change in the number and quality of services for city pairs with distance. In the HSR network, the superior service rates of most city pairs are distributed on both sides of the average, which means that the average can reflect the overall situation. Most of the city pairs with RSL greater than 1 have a higher proportion of superior service rates than the average, which means that these city pairs with greater service intensity also have higher service quality. In addition, citie pairs with low service intensity also have the possibility of high service quality. In the CR network, the city pairs with superior ratios of 0 and 1 account for 15.39% and 33.25%, respectively, so that the average value cannot represent the general value. The proportion of superior ratios in cities with greater service intensity is widely distributed with RSL. For example, the superior CT ratio between Beijing and Shijiazhuang is as high as 63.89%, while the value between Tianjin and Shenyang is only 11.11%. We noticed that although some city pairs are close in distance, their service intensity and superior ratio are very small.

For cities, as shown in Figures 5C, D, the proportion of superior ratios in the HSR network decreases slightly with the increase of RSL, but this trend is more obvious in the CR network. However, the proportion of HST and CT superior rates have nothing to do with the size of the urban resident population. Cities are divided into 4 types based on RSL and average quality rate. In the HSR network, among the super cities, Shenzhen and Tianjin belong to high quantity and high quality, while Chengdu and Chongqing belong to low quantity and low quality. Suzhou, Hefei and Shijiazhuang, which belong to big cities, also belong to high quantity and high quality. In the CR network, although the central provincial capital cities of Zhengzhou, Wuhan and Changsha have greater service intensity, the superior service rates of them are lower than 40%. This means that these cities have a large number of trains passing by due to their

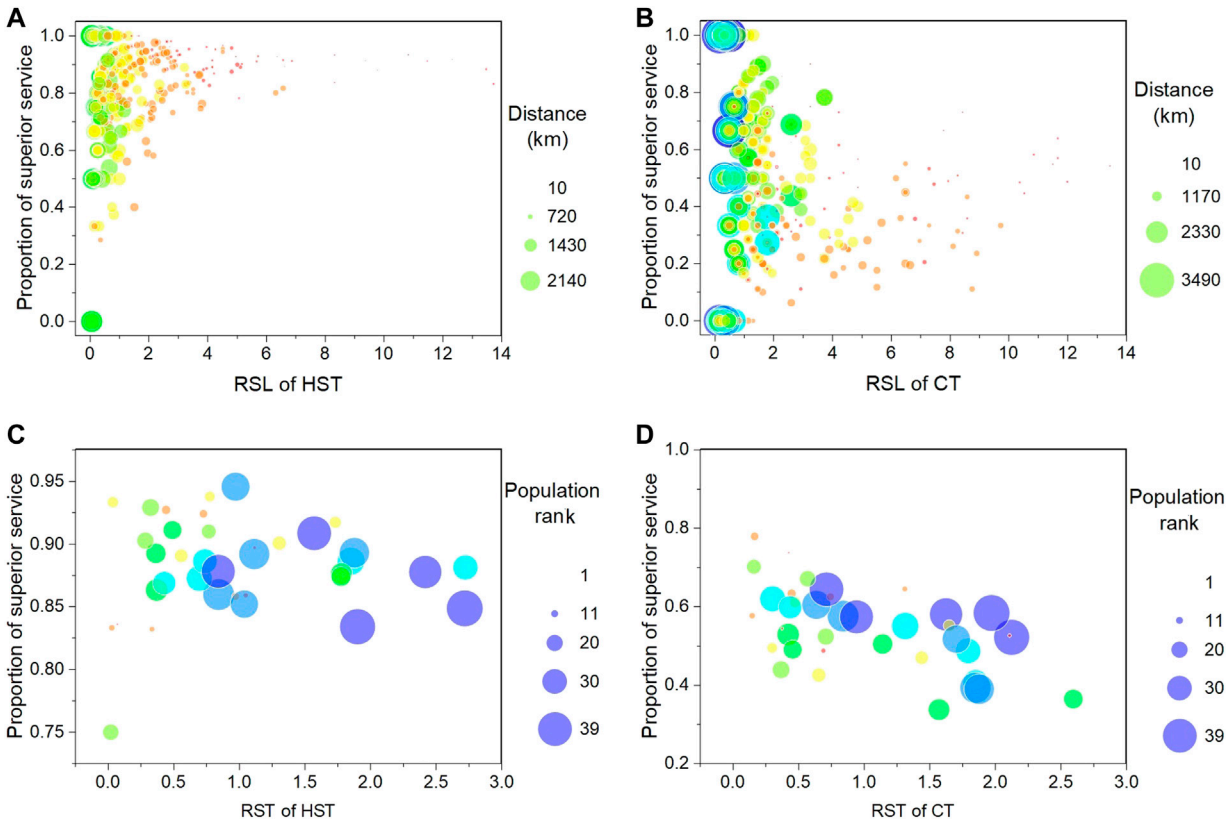

FIGURE 5
Distribution characteristics of HST superior service **(A)** and CT superior service **(B)** with RSL at city pair level, and the distribution characteristics of HST superior service **(C)** and CT superior service **(D)** with RST at city level.

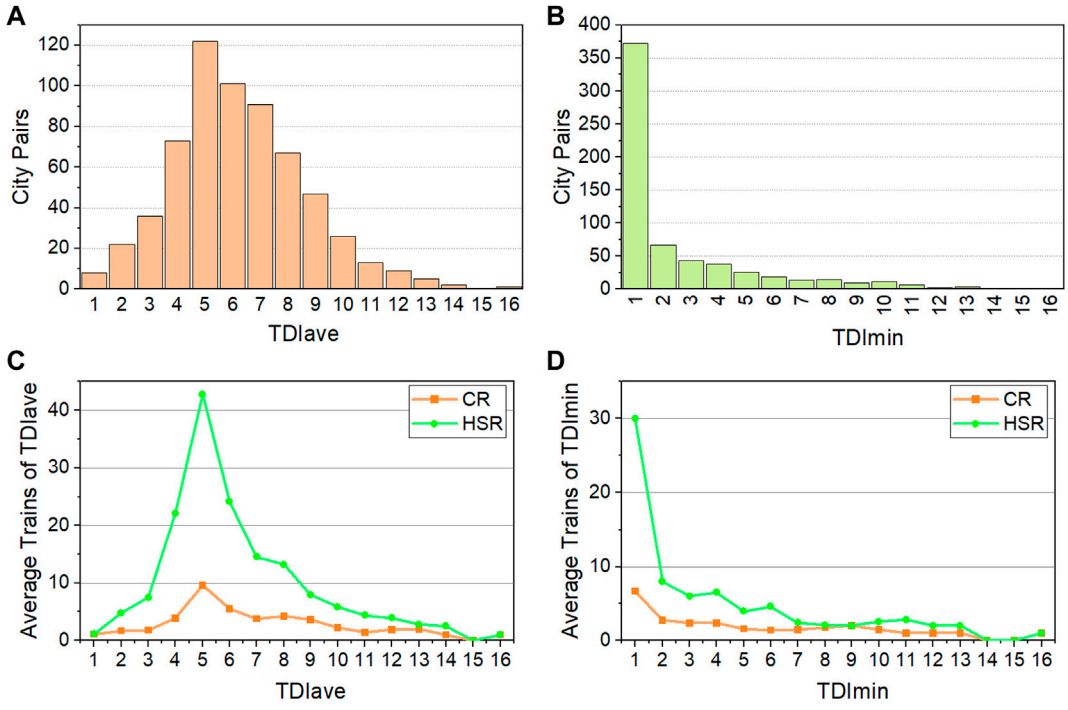

FIGURE 6
Number distribution characteristic of city pairs of TDIave **(A)** and TDImin **(B)**, and the average number of trains of TDIave **(C)** and TDImin **(D)**.

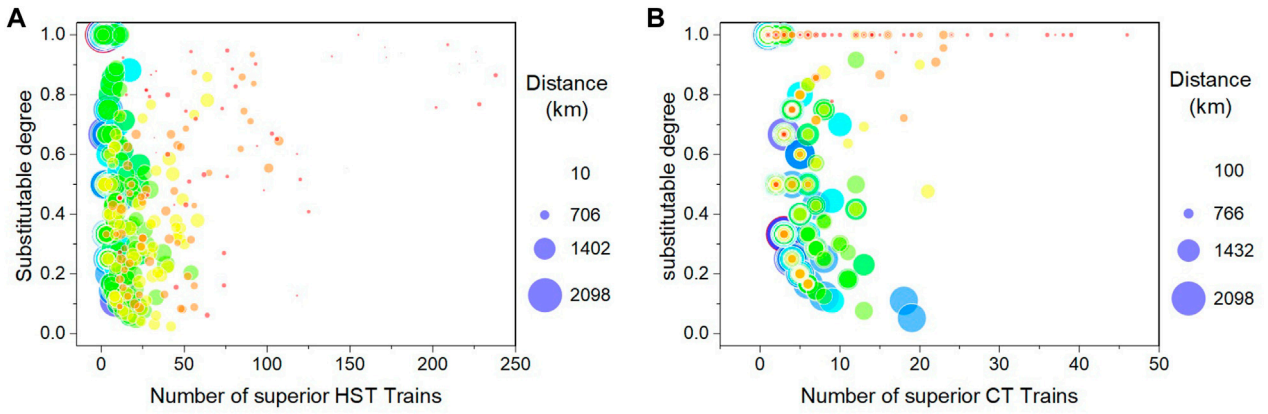

FIGURE 7
Distribution characteristics of substitutable degree of superior HST **(A)** and superior CT **(B)**.

superior geographical location, but the departure or arrival times of these trains are mostly during non-quality service time periods.

4.3 Interchangeability of superior HSTs and CTs

This paper assumes that competition only occurs between premium HST and CT services, that is, non-premium services with similar departure times cannot substitute for premium services. We calculate the time difference index between superior HST and CT services for the same city pair, for a total of 624 city pairs. Figure 6A shows that the number of city pairs in the hourly interval of TDIave follows a normal distribution. The number of city pairs with TDIave between 4 and 8 account for 72.87%, and these cities have a higher number of superior HST and CT services (Figure 6C). This is because the train departure times of high-frequency city pairs are widely distributed in the superior time, resulting in a large time slot difference between HST and CT. For city pairs with fewer train frequencies, if the TDIave is very small, the departure time of HST and CT is relatively concentrated, which will lead to greater competition. Conversely, if TDIave is very large, it indicates that the departure times of HST and CT are very scattered, and the two services have complementary effects in time.

Different from TDIave, Figure 6B shows an exponential distribution of the number of city pairs per hour in TDImin.The proportion of city pairs with CT services before or within 1 h after HST departure accounted for 59.71%. This suggests that superior HST services in these city pairs are at risk of being replaced by CT services at least once. The average superior HST and CT services of city pairs with a TDImin of more than 4 h did not exceed 5 trains (Figure 6D), indicating that the two rail services play a coordinating and complementary role in the connection between these city pairs. Combined with Figure 3, we found that the endpoints of a few city pairs with TDImin over 10 h are not on the same trunk line, such as Nanning-Hefei, Guangzhou-Jinan, Changsha-Taiyuan and Tianjin-Lanzhou. In addition, the departure time of the railway service between these city pairs follows the mode of "HST in the morning, CT in the evening".In general, HST and CT services are more likely to generate temporal substitutability on trunk lines and temporal complementarity between non-trunk city pairs.

We further analyze the substitutability degree between superior HST and CT services in city pairs with TDImin less than 1 h. There are 372 city pairs, and they have 89.21% superior HST services and 82.44% superior CT services, respectively. Overall, 59.01% of these HST services can be replaced, while up to 74.05% of these CT services are at risk of being replaced. For city pairs, the degree of mutual substitution between HST and CT services varies with the number of services and the distance between city pairs. As shown in Figure 7A, the substitutability of most city pairs with more than 150 superior HST services exceeds 80%, indicating that these city pairs have fierce competition for HST and CT. In addition, distant city pairs generally have lower quality HST services, but the substitution degree of them widely distributed between 0 and 1. As shown in Figure 7B, there are 147 city pairs facing HST competition for all superior CT services, accounting for 39.52% of the potential competing pairs. They include not only short-distance high-CT service city pairs, such as Beijing-Shijiazhuang, but also long-distance low-CT service city pairs, such as Fuzhou-Xi'an. Only a few city pairs with high CT service have low substitutability, such as Lanzhou-Urumqi.

4.4 Types of supply-service relationships of HSTs and CTs

According to the classification framework of 3.3.4, we obtain the relationship types of HST and CT for 624 overlapping superior city pairs, and the results are summarized in Table 2. Specifically, HST services dominate 34.67% of the city pairs, significantly higher than the number of city pairs dominated by CT services. The proportion of city pairs with complementary coordination between HST and CT is 13.48%. In addition, 9.47% of the city pairs have fierce competition between HST and CT services, and the city pairs with partial and slight competition both account for about 20%. Figure 8 shows the characteristics and spatial distribution of the three types of service relationship patterns.

TABLE 2 Summary of supply-service relationship of superior overlapping cities.

City pair types	Counts	Percent (%)	Distance (km)	Superior HSTs/Day	Superior CTs/Day
HST dominant	216	34.67	698.73	5.34	43.50
CT dominant	15	2.41	1417.38	6.87	1.27
Coordination and cooperation	84	13.48	1216.75	1.61	1.94
Full competition	59	9.47	880.69	10.36	21.90
Partial competition	131	21.03	1138.50	4.27	7.39
slightly competition	118	18.94	1137.35	3.87	5.65

4.4.1 City pairs dominated by a single service

As shown in Figures 8A, B, the spatial distribution of HST-dominated and CT-dominated city pairs is very different. Spatially, the city pairs dominated by HST are mainly concentrated between cities along the eastern coast, southwest and the Yangtze River Economic Belt. The average distance of these city pairs is the smallest, only 698.73 km, and the average superior superior HST reaches 43.50 frequencies per day. The C-type HSR provides high-frequency connections between urban agglomerations. Typical city pairs are Beijing-Tianjin in the Beijing-Tianjin-Hebei region, Shanghai-Nanjing in the Yangtze River Delta, and Guangzhou-Shenzhen in the Pearl River Delta. A few CT-dominated city pairs are characterized by long distances and low frequencies, with an average distance of 1417.38 km. Except for Urumqi-Lanzhou, the frequency of superior CT per day in other cities does not exceed 8. Typical city pairs are Tianjin-Guangzhou and Lanzhou-Guangzhou in the north-south direction, Shanghai-Nanning and Shanghai-Lanzhou in the east-west direction. We note that more than half of the CT-dominant city pairs have Lanzhou as the endpoint.

4.4.2 Complementary coordination city-pairs

As shown in Figure 8C, the spatial range of coordinated complementary city pairs is relatively wide, and also has the characteristics of long distances. While the average premium HST and CT for these city pairs were particularly low, the difference in departure times for both rail services was more than 4 h. Typical city pairs include Beijing-Lanzhou, Fuzhou-Chengdu, and Nanjing-Changchun. For individuals, travelers in competing city pairs may have different transportation options in the same time period, while travelers in coordinated and complementary city pairs have more choices of departure time within a day. This shows the importance of considering the time factor when analyzing the competition of different transportation modes, otherwise it would be impossible to distinguish between low-frequency competition and coordination and complementarity. For low-frequency competitive city pairs, the railway department should coordinate the departure times of the two railway services as much as possible when the train services remain unchanged. For low-frequency coordinated and complementary city pairs, the primary consideration is to increase train frequency.

4.4.3 Competitive city-pairs

About half of the citie pairs have competitive relationship between HSR and CR, and their competitive degree and spatial distribution are very different. As shown in Figure 8D, the city pairs with full competition are generally medium distance, with an average of 880.69 km, and the average number of high quality HST is about twice that of CT. Among them, a few city pairs are not only close to each other but also have high train service frequency, such as those located in northeast China and the Beijing-Tianjin-Hebei region. In addition, as a transit hub between northwest China and central and eastern China, Xi'an -Lanzhou city pair is also in full competition with high frequency. Partially and slightly competitive city pairs were generally long distance (Figures 8E, F), but the average distance was lower than that of coordinately coupled and CT-dominated city pairs. In addition, the high quality train frequency of partially competitive city pairs is higher than that of slightly competitive city pairs, and the average number of high quality HST of both two types is only slightly higher than that of CT. However, there are some differences in the spatial distribution of these two types of competition. Partially competitive city pairs generally end up with cities in the central and western regions, especially Beijing, Tianjin, Shijiazhuang and Zhengzhou. The slightly competitive city pairs generally end in cities in the northern region, and some of them have higher train frequency. Furthermore, those cities with low frequency and low level of competition have potential coordination and cooperation relations.

5 Discussion

This paper explores the relationship of supply services between HSR and CR from a temporal perspective, extending the study of railway systems from spatial to spatiotemporal perspective. The results show that China's HSR and CR services are spatially and temporally differentiated, and have shown a certain complementary pattern, but the two still have great potential for cooperation. Specifically, we divide the service quality of HST and CT from the perspective of time, which makes up for the lack of homogeneity of trains in different city pairs. Since most of the HST departure and arrival times are in the superior time period, the proportion of superior service is as high as 88.33%, while that of CT is only 51.08%. This means that the previous measure that only used train frequency to express strength has overestimated the CR level of some cities to a certain extent. For example, Zhengzhou, due to its superior geographical location, has the most CTs services every day, but only 37.00% of them are provided with superior services. Further, we found, HST and CT also have high-frequency competition and low-frequency competition, similar to the competition of HST and air (Wang et al., 2020b). In addition, HST and

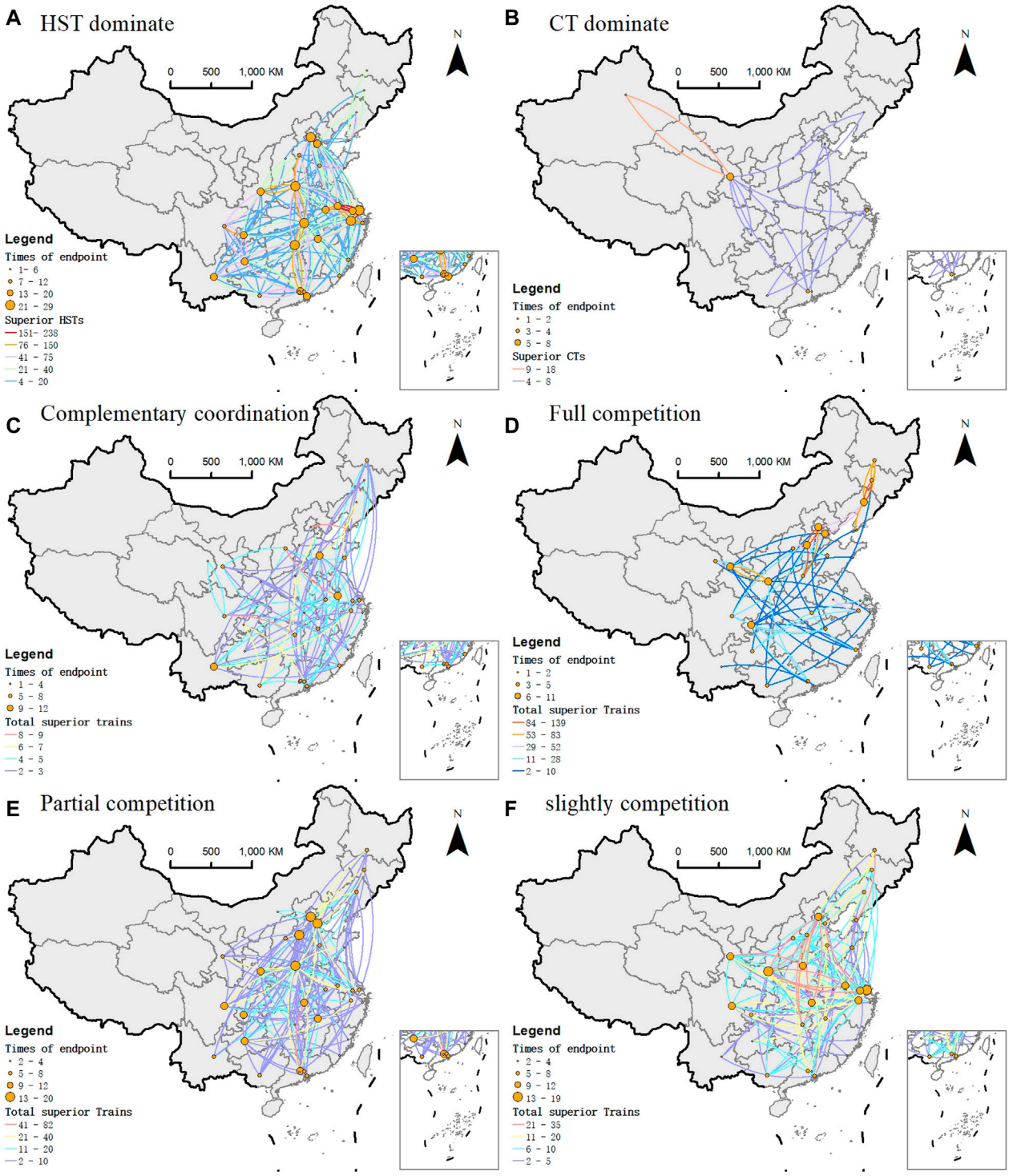

FIGURE 8
Spatial distribution of relationship types between HSR and CR: **(A)** HST dominated city pairs; **(B)** CT dominated city pairs; **(C)** Coordinated complementary city pairs; **(D)** Fully competitive city pairs; **(E)** Partially competitive city pairs; **(F)** Slightly competitive city pairs.

CT have cooperation potential not only in space (Huang and Zong, 2022), but also in time. This shows the importance of considering the time factor when analyzing the relationship between services of different transport modes.

Although the route length of HSR in China's railway system is still lower than that of CR, the service provided by HSR is much higher than that of CR in terms of quantity and quality. Therefore, China has entered the era of HSR, which is inseparable from the multi-faceted policy support of the government (Li. H et al., 2021). On the one hand, HST's high-intensity service provides convenient conditions for passengers to travel, gradually changing the public's perception of travel difficulties (Lee and Chang, 2006; Delaplace and Dobruszkes,

2015; Wei et al., 2017). As a result, more and more passengers choose HST as their first choice for travel, and new travel behaviors are constantly being born (Wang et al., 2019). On the other hand, HSR provides opportunities for economic interaction between core cities and provides transportation conditions for the creation of a unified national economic market. At the same time, the HSR service of core cities to surrounding small cities provides a guarantee for regional integration.

For HSR, the current challenges come from two aspects. On the one hand, due to the continuous impact of COVID-19, the government's control of travel behavior has greatly reduced intercity interaction (Cai et al., 2021). For example, in the first half of 2022, the net profit of Beijing-Shanghai Railway, which was the most profitable in the past, has lost 1.028 billion yuan, a year-on-year decrease of 137%. Another challenge comes from the fact that most of the HSR stations are built far away from the city center, and the HSR stations have insufficient driving force for the city. However, with the country's strict control of urban expansion, it is difficult to realize the original intention of allowing HSR to drive urban development.

For CR in the HSR era, the impact is self-evident, but there are still two opportunities. On the one hand, opportunities come from low- and middle-income groups, i.e., price-sensitive but time-insensitive travelers (Lee and Chang, 2006; Delaplace and Dobruszkes, 2015; Wei et al., 2017). It is necessary to make full use of CT's features of night operation and low price to open more trains with "starting at night and arriving at morning." So as to provide comfortable and affordable services for long-distance cities, especially core cities of non-trunk lines. On the other hand, opportunities come from cities with small population and underdeveloped economy. From the perspective of social equity, it is also necessary to open HST in these cities. However, due to the high operation and maintenance costs of HSR, these cities have limited access to HST services (Moyano and Dobruszkes, 2017). Therefore, for cities that have opened HSR, the CT service should be staggered by more than 4 h from the HST service as much as possible. For city pairs without direct HSR, CR service should improve service quality on the basis of satisfying service quantity.

Our findings have policy implications for the sustainable development of both rail systems and cities. First, the method of exploring the service relationship considering the quantity and quality of trains can provide inspiration for the railway department to improve the policy. Secondly, the results of this paper determine the different modes of HST and CT supply service relationship between core cities, which can provide some support for railway dispatching optimization. For example, in the highly competitive market, the railway department should pay more attention to the service quality of HST and CT. In addition, the city pairs with low frequency competition can be transformed into coordinated city pairs by optimizing train dispatching. Third, this paper reveals the advantages and disadvantages of the core cities in different aspects of railway services, which helps to determine the city's position and formulate development strategies. For example, although CR services have certain advantages in the three northeastern provinces, their proportion of superior services is lower than the average of all cities.

6 Conclusion

The rapid development of HSR not only shortens the time and space distance, but also affects the market share of other intercity transportation. As the future development direction of integrated transportation network, in-depth study of the competition and cooperation mode between HSR and other modes is a very important research issue for regional development and transportation optimization. Previous studies mostly analyzed the similarities and differences of different transportation modes from a spatial perspective, while the research on the relationship between multiple transportation modes from a time perspective was insufficient. This paper takes China's core cities as the research object, and interprets the relationship between HSR and CR supply services from the perspective of time and space, so as to better understand the operation strategy of the railway passenger transport system. Specifically, the HSR network has higher service intensity and is more advantageous in the south, and the CR network covers a wider range of space and has an advantage in the north. Due to the fact that there are few high-speed trains at night, the proportion of HST superior services is as high as 88.33%. And only half of the CTs can provide passengers with superior pick-up and drop-off at the same time. Additionally, 59.01% of HST services can be replaced, while up to 74.05% of CT services are at risk of being replaced. Spatially, HST and CT services are more likely to generate temporal substitution on the mainline and temporal complementarity between city pairs on the non-mainline.

In conclusion, based on the difference in operating time between HST and CT, we found that in addition to being competitive, they are complementary in terms of time to a certain extent. What we emphasize is the importance of time competition and cooperation between the two railway supply services to ease the pressure on passenger flow and achieve social equity. However, our study has at least two limitations. On the one hand, due to the availability of data, we cannot obtain the exact number of seats purchased between city pairs. In this study, we considered the train capacity of different trains and the same train in different city pairs to be homogeneous. At present, the allocation of seat tickets in China is dynamic, and more trains can represent more actual seats to a certain extent. Therefore, the limitations of the data do not affect the validity of our conclusions. On the other hand, we assume that passenger preferences in different cities are consistent, that is, the demands for HST and CT are the same. Due to the differences in the economies of different regions, the proportions of time-sensitive and price-sensitive passengers are actually different. To understand the supply relationship between the two railway modes from the perspective of passengers, a large-scale survey is needed to distinguish passenger preferences in different regions, so as to better realize the rational allocation of HST and CT services. In short, our research only discusses the time differences and similarities between HSR and CR in China from the perspective of suppliers. In short, our study only explores the differences and similarities of train services between HSR and CR in China from a temporal perspective. Due to China's vast geographical scope and differences in economic development, it is necessary to conduct in-depth research on the relationship between HSR and CR from different perspectives and data.

Data availability statement

The original contributions presented in the study are included in the article/Supplementary Material, further inquiries can be directed to the corresponding author.

Author contributions

GZ: conceptualization, methodology, writing—original draft, visualization. YL: conceptualization, writing—reviewing and editing, supervision. YJ: conceptualization, writing—reviewing and editing. HC: methodology, writing-reviewing and editing. YW: writing-reviewing and editing, visualization. ZW: writing—reviewing and editing, methodology.

Funding

This research was financially supported by the Key Program of National Natural Science Foundation of China (No. 42230107).

Conflict of interest

The authors declare that the research was conducted in the absence of any commercial or financial relationships that could be construed as a potential conflict of interest.

Publisher's note

All claims expressed in this article are solely those of the authors and do not necessarily represent those of their affiliated organizations, or those of the publisher, the editors and the reviewers. Any product that may be evaluated in this article, or claim that may be made by its manufacturer, is not guaranteed or endorsed by the publisher.

References

An, Y., Wei, Y. D., Yuan, F., and Chen, W. (2022). Impacts of high-speed rails on urban networks and regional development: A study of the Yangtze River Delta, China. *Int. J. Sustain. Transp.* 16 (6), 483–495. doi:10.1080/15568318.2021.1897909

Borenstein, S., and Netz, J. (1999). Why do all the flights leave at 8 am?: Competition and departure-time differentiation in airline markets. *Int. J. industrial Organ.* 17 (5), 611–640. doi:10.1016/s0167-7187(97)00058-1

Broman, E., and Eliasson, J. (2017). Market dynamics in on-rail competition. *19th Euro Work. Group Transp. Meet. (Ewgt2016)* 22, 232–244. doi:10.1016/j.trpro.2017.03.030

Burghouwt, G., and de Wit, J. (2005). Temporal configurations of European airline networks. *J. Air Transp. Manag.* 11 (3), 185–198. doi:10.1016/j.jairtraman.2004.08.003

Cai, M., Guy, C., Héroux, M., Lichtfouse, E., and An, C. (2021). The impact of successive COVID-19 lockdowns on people mobility, lockdown efficiency, and municipal solid waste. *Environ. Chem. Lett.* 19 (6), 3959–3965. doi:10.1007/s10311-021-01290-z

Cascetta, E., and Coppola, P. (2015). New high-speed rail lines and market competition short-term effects on services and demand in Italy. *Transp. Res. Rec.* 2475 (2475), 8–15. doi:10.3141/2475-02

Castillo-Manzano, J. I., Pozo-Barajas, R., and Trapero, J. R. (2015). Measuring the substitution effects between High Speed Rail and air transport in Spain. *J. Transp. Geogr.* 43, 59–65. doi:10.1016/j.jtrangeo.2015.01.008

Chen, Z. H. (2017). Impacts of high-speed rail on domestic air transportation in China. *J. Transp. Geogr.* 62, 184–196. doi:10.1016/j.jtrangeo.2017.04.002

Cheng, J. M., and Chen, Z. H. (2021). Impact of high-speed rail on the operational capacity of conventional rail in China. *Transp. Policy* 110, 354–367. doi:10.1016/j.tranpol.2021.06.016

Craft, R. C., and Leake, C. (2002). The Pareto principle in organizational decision making. *Manag. Decis.* 40, 729–733. doi:10.1108/00251740210437699

Delaplace, M., and Dobruszkes, F. (2015). From low-cost airlines to low-cost high-speed rail? The French case. *Transp. Policy* 38, 73–85. doi:10.1016/j.tranpol.2014.12.006

Diao, M., Zhu, Y., and Zhu, J. R. (2017). Intra-city access to inter-city transport nodes: The implications of high-speed-rail station locations for the urban development of Chinese cities. *Urban Stud.* 54 (10), 2249–2267. doi:10.1177/0042098016646686

Dobruszkes, F., Dehon, C., and Givoni, M. (2014). Does European high-speed rail affect the current level of air services? An EU-wide analysis. *Transp. Res. Part A Policy Pract.* 69, 461–475. doi:10.1016/j.tra.2014.09.004

Dobruszkes, F. (2011). High-speed rail and air transport competition in western Europe: A supply-oriented perspective. *Transp. Policy* 18 (6), 870–879. doi:10.1016/j.tranpol.2011.06.002

Espinosa-Aranda, J. L., Garcia-Rodenas, R., Ramirez-Flores, M. D., Lopez-Garcia, M. L., and Angulo, E. (2015). High-speed railway scheduling based on user preferences. *Eur. J. Operational Res.* 246 (3), 772–786. doi:10.1016/j.ejor.2015.05.052

Givoni, M., and Banister, D. (2006). Airline and railway integration. *Transp. Policy* 13 (5), 386–397. doi:10.1016/j.tranpol.2006.02.001

González-Savignat, M. (2004). Will the high-speed train compete against the private vehicle? *Transp. Rev.* 24 (3), 293–316. doi:10.1080/0144164032000083103

Guo, Y., Li, B., and Han, Y. (2020). Dynamic network coupling between high-speed rail development and urban growth in emerging economies: Evidence from China. *Cities* 105, 102845. doi:10.1016/j.cities.2020.102845

Huang, J., and Wang, J. E. (2017). A comparison of indirect connectivity in Chinese airport hubs: 2010 vs. 2015. *J. Air Transp. Manag.* 65, 29–39. doi:10.1016/j.jairtraman.2017.07.002

Huang, Y., and Zong, H. (2021). Has high-speed railway promoted spatial equity at different levels? A case study of inland mountainous area of China. *Cities* 110, 103076. doi:10.1016/j.cities.2020.103076

Huang, Y., and Zong, H. M. (2022). The intercity railway connections in China: A comparative analysis of high-speed train and conventional train services. *Transp. Policy* 120, 89–103. doi:10.1016/j.tranpol.2022.02.007

Jiang, C. M., Wan, Y. L., Yang, H. J., and Zhang, A. M. (2021). Impacts of high-speed rail projects on CO2 emissions due to modal interactions: A review. *Transp. Res. Part D-Transport Environ.* 100, 103081. doi:10.1016/j.trd.2021.103081

Jiang, C., and Zhang, A. (2014). Effects of high-speed rail and airline cooperation under hub airport capacity constraint. *Transp. Res. Part B Methodol.* 60, 33–49. doi:10.1016/j.trb.2013.12.002

Jiao, J. J., Wang, J. E., Zhang, F. N., Jin, F. J., and Liu, W. (2020). Roles of accessibility, connectivity and spatial interdependence in realizing the economic impact of high-speed rail: Evidence from China. *Transp. Policy* 91, 1–15. doi:10.1016/j.tranpol.2020.03.001

Jiao, J., Wang, J., and Jin, F. (2017). Impacts of high-speed rail lines on the city network in China. *J. Transp. Geogr.* 60, 257–266. doi:10.1016/j.jtrangeo.2017.03.010

Lee, J. H., and Chang, J. S. (2006). Effects of high-speed rail service on shares of intercity passenger ridership in South Korea. *Railways*, 1943, 31–42. doi:10.1177/0361198106194300105

Lee, J. K., Yoo, K. E., and Song, K. H. (2016). A study on travelers' transport mode choice behavior using the mixed logit model: A case study of the seoul-jeju route. *J. Air Transp. Manag.* 56, 131–137. doi:10.1016/j.jairtraman.2016.04.020

Levinson, D. M. (2012). Accessibility impacts of high-speed rail. *J. Transp. Geogr.* 22, 288–291. doi:10.1016/j.jtrangeo.2012.01.029

Li, C., Lin, T., Zhang, Z., Xu, D., Huang, L., and Bai, W. (2022). Can transportation infrastructure reduce haze pollution in China? *Environ. Sci. Pollut. Res.* 29 (11), 15564–15581. doi:10.1007/s11356-021-16902-y

Li, H. C., Wang, K., Yu, K. M., and Zhang, A. M. (2020). Are conventional train passengers underserved after entry of high-speed rail?-Evidence from Chinese intercity markets. *Transp. Policy* 95, 1–9. doi:10.1016/j.tranpol.2020.05.017

Li, H., Dong, X. C., Jiang, Q. Z., and Dong, K. Y. (2021). Policy analysis for high-speed rail in China: Evolution, evaluation, and expectation. *Transp. Policy* 106, 37–53. doi:10.1016/j.tranpol.2021.03.019

Li, T., and Rong, L. L. (2022). Spatiotemporally complementary effect of high-speed rail network on robustness of aviation network. *Transp. Res. Part a-Policy Pract.* 155, 95–114. doi:10.1016/j.tra.2021.10.020

Li, X. W., Ma, R. Y., Guo, Y. Y., Wang, W., Yan, B., and Chen, J. (2021). Investigation of factors and their dynamic effects on intercity travel modes competition. *Travel Behav. Soc.* 23, 166–176. doi:10.1016/j.tbs.2021.01.003

Limtanakool, N., Dijst, M., and Schwanen, T. (2007). A theoretical framework and methodology for characterising national urban systems on the basis of flows of people: Empirical evidence for France and Germany. *Urban Stud.* 44 (11), 2123–2145. doi:10.1080/00420980701518990

Moyano, A., and Dobruszkes, F. (2017). Mind the services! High-speed rail cities bypassed by high-speed trains. *Case Stud. Transp. Policy* 5 (4), 537–548. doi:10.1016/j.cstp.2017.07.005

Moyano, A., Martinez, H. S., and Coronado, J. M. (2018). From network to services: A comparative accessibility analysis of the Spanish high-speed rail system. *Transp. Policy* 63, 51–60. doi:10.1016/j.tranpol.2017.11.007

Perl, A. D., and Goetz, A. R. (2015). Corridors, hybrids and networks: Three global development strategies for high speed rail. *J. Transp. Geogr.* 42, 134–144. doi:10.1016/j.jtrangeo.2014.07.006

Shaw, S. L., Fang, Z. X., Lu, S. W., and Tao, R. (2014). Impacts of high speed rail on railroad network accessibility in China. *J. Transp. Geogr.* 40, 112–122. doi:10.1016/j.jtrangeo.2014.03.010

Spiekermann, K., and Wegener, M. (1994). The shrinking continent - new time-space maps of Europe. *Environ. Plan. B-Planning Des.*, 21(6), 653–673. doi:10.1068/b210653

Sun, J. Y. (2015). Clustered airline flight scheduling: Evidence from airline deregulation in Korea. *J. Air Transp. Manag.* 42, 85–94. doi:10.1016/j.jairtraman.2014.09.004

Wang, F., Wei, X. J., Liu, J., He, L. Y., and Gao, M. N. (2019). Impact of high-speed rail on population mobility and urbanisation: A case study on Yangtze River Delta urban agglomeration, China. *Transp. Res. Part a-Policy Pract.* 127, 99–114. doi:10.1016/j.tra.2019.06.018

Wang, J., Du, D., and Huang, J. (2020a). Inter-city connections in China: High-speed train vs. inter-city coach. *J. Transp. Geogr.* 82, 102619. doi:10.1016/j.jtrangeo.2019.102619

Wang, J. E., Huang, J., and Jing, Y. (2020b). Competition between high-speed trains and air travel in China: From a spatial to spatiotemporal perspective. *Transp. Res. Part a-Policy Pract.* 133, 62–78. doi:10.1016/j.tra.2019.12.030

Wang, J. J., Xu, J., and He, J. F. (2013). Spatial impacts of high-speed railways in China: A total-travel-time approach. *Environ. Plan. a-Economy Space* 45 (9), 2261–2280. doi:10.1068/a45289

Wang, L. (2018). High-speed rail services development and regional accessibility restructuring in megaregions: A case of the Yangtze River Delta, China. *Transp. Policy* 72, 34–44. doi:10.1016/j.tranpol.2018.09.015

Wang, Y., Yan, X. D., Zhou, Y., and Xue, Q. W. (2017). Influencing mechanism of potential factors on passengers' long-distance travel mode choices based on structural equation modeling. *Sustainability* 9 (11), 1943. doi:10.3390/su9111943

Wei, S., Yuan, J., Qiu, Y., Luan, X., Han, S., Zhou, W., et al. (2017). Exploring the potential of open big data from ticketing websites to characterize travel patterns within the Chinese high-speed rail system. *Plos One* 12 (6), e0178023. doi:10.1371/journal.pone.0178023

Weng, J., Zhu, X. L., and Li, X. (2020). Impact of high-speed rail on destination accessibility: A case study of China. *J. China Tour. Res.* 16 (4), 494–509. doi:10.1080/19388160.2019.1709937

Wu, J. H., Nash, C., and Wang, D. (2014). Is high speed rail an appropriate solution to China's rail capacity problems? *J. Transp. Geogr.* 40, 100–111. doi:10.1016/j.jtrangeo.2014.05.004

Xia, W., and Zhang, A. (2017). Air and high-speed rail transport integration on profits and welfare: Effects of air-rail connecting time. *J. Air Transp. Manag.* 65, 181–190. doi:10.1016/j.jairtraman.2017.06.008

Xin, Z., and Niu, F. (2022). Structure and robustness of China's railway transport network. *Transp. Lett.*, 1–11. doi:10.1080/19427867.2022.2053280

Xu, W. T., Zhou, J. P., and Qiu, G. (2018). China's high-speed rail network construction and planning over time: A network analysis. *J. Transp. Geogr.* 70, 40–54. doi:10.1016/j.jtrangeo.2018.05.017

Yang, H., Dijst, M., Witte, P., van Ginkel, H., and Wang, J. e. (2019). Comparing passenger flow and time schedule data to analyse High-Speed Railways and urban networks in China. *Urban Stud.* 56 (6), 1267–1287. doi:10.1177/0042098018761498

Yang, H. R., Burghouwt, G., Wang, J. E., Boonekamp, T., and Dijst, M. (2018a). The implications of high-speed railways on air passenger flows in China. *Appl. Geogr.* 97, 1–9. doi:10.1016/j.apgeog.2018.05.006

Yang, H. R., Dobruszkes, F., Wang, J. E., Dijst, M., and Witte, P. (2018b). Comparing China's urban systems in high-speed railway and airline networks. *J. Transp. Geogr.* 68, 233–244. doi:10.1016/j.jtrangeo.2018.03.015

Zhang, F., Graham, D. J., and Wong, M. S. C. (2018). Quantifying the substitutability and complementarity between high-speed rail and air transport. *Transp. Res. Part A Policy Pract.* 118, 191–215. doi:10.1016/j.tra.2018.08.004

Zhang, F., Yang, Z., Jiao, J., Liu, W., and Wu, W. (2020). The effects of high-speed rail development on regional equity in China. *Transp. Res. Part A Policy Pract.* 141, 180–202. doi:10.1016/j.tra.2020.09.013

Zhang, H., Cui, H. D., Wang, W., and Song, W. B. (2020). Properties of Chinese railway network: Multilayer structures based on timetable data. *Phys. a-Statistical Mech. Its Appl.* 560, 125184. doi:10.1016/j.physa.2020.125184

Zhou, Y., An, Z. W., and Wang, H. X. (2019). "On the passenger travel behavior of high-speed railway in China-with beijing-shanghai high-speed railway channel as an example," in Transportation Research Congress 2017: Sustainable, Smart, and Resilient Transportation, Beijing, China, May 23–25, 2017.

Frontiers in
Environmental Science

Explores the anthropogenic impact on our natural world

An innovative journal that advances knowledge of the natural world and its intersections with human society. It supports the formulation of policies that lead to a more inhabitable and sustainable world.

Discover the latest Research Topics

See more →

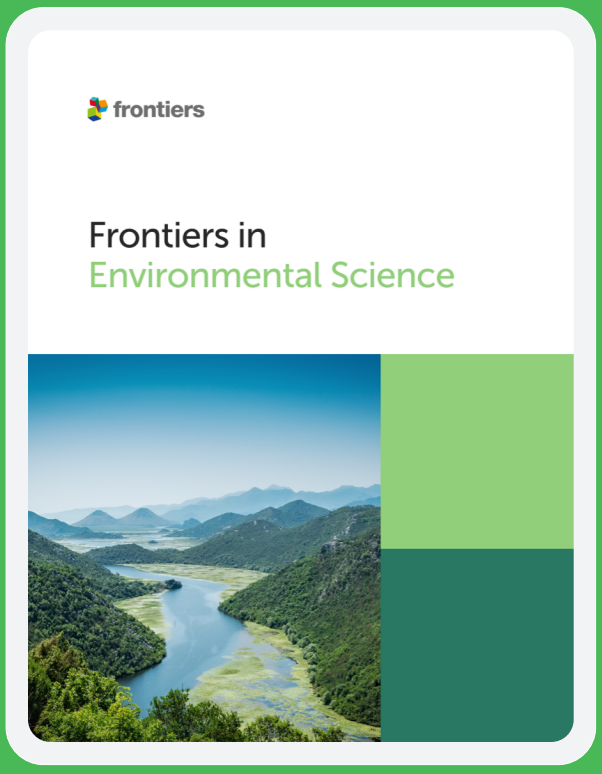

Frontiers

Avenue du Tribunal-Fédéral 34
1005 Lausanne, Switzerland
frontiersin.org

Contact us

+41 (0)21 510 17 00
frontiersin.org/about/contact